Studies in Computational Intelligence 635

Sundarapandian Vaidyanathan
Christos Volos *Editors*

Advances and Applications in Nonlinear Control Systems

Springer

Studies in Computational Intelligence

Volume 635

Series editor

Janusz Kacprzyk, Polish Academy of Sciences, Warsaw, Poland
e-mail: kacprzyk@ibspan.waw.pl

About this Series

The series "Studies in Computational Intelligence" (SCI) publishes new developments and advances in the various areas of computational intelligence—quickly and with a high quality. The intent is to cover the theory, applications, and design methods of computational intelligence, as embedded in the fields of engineering, computer science, physics and life sciences, as well as the methodologies behind them. The series contains monographs, lecture notes and edited volumes in computational intelligence spanning the areas of neural networks, connectionist systems, genetic algorithms, evolutionary computation, artificial intelligence, cellular automata, self-organizing systems, soft computing, fuzzy systems, and hybrid intelligent systems. Of particular value to both the contributors and the readership are the short publication timeframe and the worldwide distribution, which enable both wide and rapid dissemination of research output.

More information about this series at http://www.springer.com/series/7092

Sundarapandian Vaidyanathan
Christos Volos
Editors

Advances and Applications in Nonlinear Control Systems

Springer

Editors
Sundarapandian Vaidyanathan
Research and Development Centre
Vel Tech University
Chennai
India

Christos Volos
Department of Physics
Aristotle University of Thessaloniki
Thessaloniki
Greece

ISSN 1860-949X ISSN 1860-9503 (electronic)
Studies in Computational Intelligence
ISBN 978-3-319-30167-9 ISBN 978-3-319-30169-3 (eBook)
DOI 10.1007/978-3-319-30169-3

Library of Congress Control Number: 2016932741

Printed on acid-free paper

This Springer imprint is published by Springer Nature
The registered company is Springer International Publishing AG Switzerland

Preface

About the Subject

Control theory is a multidisciplinary branch of engineering that concerns with the behavior of dynamical systems with inputs (or controls) and seeks to modify the outputs by changes in the inputs using feedback. Linear control theory applies to systems made of linear devices and they obey the superposition principle. For linear control systems, the output of the device is proportional to the input. Nonlinear control theory covers a wider class of systems which do not obey the superposition principle. As most real-world control systems are nonlinear, nonlinear control theory has great applications for real-world control systems. Nonlinear control systems are often governed by nonlinear differential equations and many mathematical techniques have been developed to analyze these systems such as Lyapunov stability theory, limit cycle theory, Poincaré maps, bifurcation theory, chaos theory, and describing functions. In the recent decades, soft computing techniques such as neural networks, fuzzy logic, and evolutionary algorithms have been also successfully applied to analyze and apply nonlinear control theory for many multidisciplinary applications. In the recent decades, advanced techniques such as sliding mode control, fuzzy-based sliding mode control, backstepping control, and adaptive control have been also applied for control systems design. Control systems design has applications in several branches of engineering such as mechanical engineering, aeronautical engineering, electrical engineering, communications engineering, robotics, biomedical instrumentation, etc.

About the Book

The new Springer book, *Advances and Applications in Nonlinear Control Systems,* consists of 30 contributed chapters by subject experts who are specialized in the various topics addressed in this book. The special chapters have been brought out in this book after a rigorous review process in the broad areas of modeling and

applications of nonlinear control systems. Special importance was given to chapters offering practical solutions and novel methods for the recent research problems in the modeling and applications of nonlinear control systems.

This book discusses trends and applications of nonlinear control systems in science and engineering.

Objectives of the Book

This volume presents a selected collection of contributions on a focused treatment of recent advances and applications in nonlinear control systems. The book also discusses multidisciplinary applications in control engineering, computer science, and information technology. These are among those multidisciplinary applications where computational intelligence has excellent potentials for use. Both novice and expert readers should find this book a useful reference in the field of nonlinear control systems.

Organization of the Book

This well-structured book consists of 30 full chapters.

Book Features

- The book chapters deal with the recent research problems in the areas of nonlinear control systems.
- The book chapters contain a good literature survey with a long list of references.
- The book chapters are well written with a good exposition of the research problem, methodology, and block diagrams.
- The book chapters are lucidly illustrated with numerical examples and simulations.
- The book chapters discuss details of engineering applications and future research areas.

Audience

The book is primarily meant for researchers from academia and industry, who are working in the research areas—control engineering, electrical engineering, computer science, and information technology. The book can also be used at the graduate or advanced undergraduate level as a textbook or major reference for courses such as control systems, nonlinear dynamical systems, mathematical modeling, computational science, numerical simulation, and many others.

Acknowledgments

As the editors, we hope that the chapters in this well-structured book will stimulate further research in control systems, computational intelligence, and chaos theory, and utilize them in real-world applications.

We hope sincerely that this book, covering so many different topics, will be very useful for all readers.

We would like to thank all the reviewers for their diligence in reviewing the chapters.

Special thanks go to Springer, especially the book editorial team.

Sundarapandian Vaidyanathan
Christos Volos

Contents

Kinematic Control of a Robot by Using a Non-autonomous Chaotic System

Ch.K. Volos, D.A. Prousalis, S. Vaidyanathan, V.-T. Pham, J.M. Munoz-Pacheco and E. Tlelo-Cuautle

Abstract In this chapter, a new navigation strategy by designing a path planning generator, which ensures chaotic motion to an autonomous robot, has been investigated. This new technique is implemented by using the well-known from the nonlinear theory Poincaré map, which is produced by a non-autonomous chaotic system. For this reason one of the most studied non-autonomous systems, the Duffing—van der Pol system has been chosen, presenting suitable results. The path planning generator produces an unpredictable trajectory by converting the chaotic strange attractor, produced by system's Poincaré map, into the robot's "random" trajectory in a chosen workspace. As a consequence the autonomous robot covers the whole workspace with unpredictable way. The simulation results verify that the proposed generator achieves the aforementioned goal. So, with this work, new perspectives on use of non-autonomous chaotic systems in robotic applications are opened.

Ch.K. Volos (✉) · D.A. Prousalis
Physics Department, Aristotle University of Thessaloniki, Thessaloniki GR-54124, Greece
e-mail: volos@physics.auth.gr

D.A. Prousalis
e-mail: dprou@physics.auth.gr

S. Vaidyanathan
Research and Development Centre, Vel Tech University, Avadi,
Chennai 600062, Tamil Nadu, India
e-mail: sundarvtu@gmail.com

V.-T. Pham
School of Electronics and Telecommunications, Hanoi University of Science
and Technology, 01 Dai Co Viet, Hanoi, Vietnam
e-mail: pvt3010@gmail.com

J.M. Munoz-Pacheco
Electronics Department, Autonomous University of Puebla (BUAP), Puebla 72570, Mexico
e-mail: jesusm.pacheco@correo.buap.mx

E. Tlelo-Cuautle
Department of Electronics, INAOE, Tonantzintla Puebla 72840, Mexico
e-mail: etlelo@inaoep.mx

S. Vaidyanathan and C. Volos (eds.), *Advances and Applications in Nonlinear Control Systems*, Studies in Computational Intelligence 635,
DOI 10.1007/978-3-319-30169-3_1

Keywords Chaos · Non-autonomous dynamical system · Duffing—van der pol system · Poincaré map · Autonomous robot · Path planning generator · Terrrain coverage

1 Introduction

In the last decade the subject of robotics and especially the design of motion controllers for autonomous robots has become a very promising research field. This occurs because there is a tension, in many difficult or dangerous tasks, of human to be replaced by robots. In general, the great advantage of an autonomous robot is that performs a task without the continuous human supervision. Terrain exploration for searching for explosives [54], complete coverage of a terrain (like floor-cleaning robots) [15, 50], transportation [58], search and rescue of human victims on disaster places [59], fire fighting devices [61], map buildings [62] and surveillance or patrolling of terrains for intrusion [6, 10, 33, 36, 39, 40, 42] are some of the civil or military tasks, where autonomous robots can be very useful.

In the procedure of design and development of autonomous robots, the key issues are the locomotion, the sensing and the localization. However, the most challenging issue is the choice of the navigation strategy, which can be defined as the set of various techniques that allow a robot to autonomously decide where to move in the workspace in order to accomplish a given task [53]. Also, the navigation strategies have a remarkable influence over the performance of the task execution and significant contribution in building the robot's autonomy. Many interesting navigation techniques depending on the application have been proposed so far, but the issue continues to preoccupy the scientific community.

Covering all the possible classes of problems related with navigation strategies, such as the exploration of an initially unknown workspace or the patrolling of a known environment, the key-point is the robot's motion planning for the complete and fast workspace scanning. For accomplishing these requirements, a robot that is capable of crossing every region, covering systematically the entire workspace, should be designed. An obvious solution is a systematic scan by using parallel straight trajectories. Nevertheless, this approach could be easily understood, for example by an intruder in the case of a patrolling mission. Therefore, the unpredictability of the robot's trajectory is also a crucial factor for the success of such autonomous robot's tasks. Another, interesting feature that the navigation strategy should perform is not only the unpredictability but also the fast scanning of the entire workspace. So, the aforementioned features are the subjects of study among the researchers for selecting the most suitable autonomous robotic system.

In this direction, Nakamura and Sekiguchi in 2001, proposed a strategy to solve the above mentioned problem based on chaotic systems [47]. In that work the chaotic behavior of the Arnold dynamical system is imparted to the robot's motion control. Since then a great number of relative research works in the field of autonomous robots have been presented, because the chaotic motion guarantees the scanning

of the whole workspace without a terrain map or motion plan. Lorenz dynamical system [11, 37], Standard or Taylor–Chirikov map [38–40] , Chua circuit [54, 72], and double-scroll systems [63, 69–71] are some of the chaotic systems which have also been used for this purpose.

As it is known, the rich dynamic behavior of nonlinear systems and especially the chaotic phenomena which that system produces, makes these systems suitable candidates for using in several disciplines including meteorology, physics, economics, biology, philosophy [1, 2, 14, 19] and also in diverse engineering applications such as communications [18, 45, 55], cryptography [44, 46, 67, 68], random bits generators [78] and neuronal networks [12]. This was the starting point of inducing chaotic behavior to robotic systems. This goal is achieved by designing controllers, which ensure chaotic motion producing by a nonlinear circuit or by programming a microcontroller.

In more details, chaos theory studies the behavior of dynamical systems that are highly sensitive on initial conditions, an effect which is popularly referred to as the "*Butterfly Effect*". This means, that small differences in initial conditions, such as those due to rounding errors in numerical computation, yield widely diverging outcomes for such dynamical systems, rendering long-term prediction impossible in general. This happens even though these systems are deterministic, meaning that their future behavior is fully determined by their initial conditions, with no random elements involved. In other words, the deterministic nature of these systems does not make them predictable.

Until now, the great majority of the proposed chaotic motion controllers are based on autonomous nonlinear dynamical systems, in order to use the independence of these systems to external sources. However, in the present work, the robot's motion controller is based on a path planning generator, which is designed by using a non-autonomous dynamical system. For ridding from the system the influence of the external source and increasing the unpredictability of the proposed controller, the Poincaré section for sampling the chaotic signal has been used.

The proposed path planning generator produces an unpredictable trajectory by imparting the chaotic behavior of the system to the robot's motion. This occurs by converting the Poincaré map of the chaotic system into a sequence of planned target locations. As a consequence the autonomous robot can cover the whole workspace with unpredictable way, presenting satisfactory results in regard to other similar works.

This chapter is organized as follows. In Sect. 2 the features of chaotic systems and especially the description of the Duffing—van der Pol system, which is the key-point in this work, are given. The adopted robot's chaotic path planning generator is described in Sect. 3. The simulation results of the proposed autonomous robot's trajectory and its analysis are presented in Sect. 4. Finally, Sect. 5 includes the conclusion remarks of this work.

2 The Duffing—van der Pol System

In literature, chaos refers to some dynamical phenomena considered to be complex and unpredictable. Henry Poincaré was the first that observed this kind of dynamical behavior at the end of the 19th century [52], however chaos theory begins to take form in the second half of the 20th century after observations of the evolution of different physical systems [30, 34]. These systems revealed that despite of the knowledge of their evolution rules and initial conditions, their future seemed to be arbitrary and unpredictable. That opened quite a revolution in modern physics, terminating with Laplace's ideas of causal determinism [29].

Today chaos theory has been changed in a catholic model of study of many phenomena in weather and climate [30], population growth in ecology [41], economy [28], to mention only a few examples. Chaos has also been observed in the laboratory in a number of systems such as electrical circuits [66], lasers [7], chemical reactions [13], fluid dynamics [3], mechanical systems, and magneto-mechanical devices [43]. So, chaos theory provides the means to explain various phenomena in nature and makes use of chaotic dynamical systems in many different scientific fields.

A nonlinear dynamical system, from a mathematical viewpoint, in order to be considered as chaotic, must fulfill the following three conditions [21].

- It must be topologically mixing,
- Its chaotic orbits must be dense and
- It must be very sensitive on initial conditions.

The term topologically mixing means that the chaotic dynamical system, especially the chaotic designated area of the trajectory will eventually cover part of any particular region. This is a very crucial feature for the design of robots motion's controllers. Also, as it is mentioned, the chaotic orbits have to be dense if it comes arbitrarily close to any point in the domain. Finally, the most important feature of chaotic systems, as it is referred in the previous section, is the sensitivity on initial conditions. This means that a small variation on a system's initial conditions will produce a totally different chaotic trajectory.

In this chapter, a very well-known representative of the class of non-autonomous dynamical systems has been chosen. This is the second order nonlinear, non-autonomous Duffing—van der Pol system [65], which is described by the following set of differential equations (1).

$$\begin{cases} \dot{x} = y \\ \dot{y} = \mu\left(1 - x^2\right) y - x^3 + B\cos\left(\omega t\right) \end{cases} \tag{1}$$

This system is called Duffing—van der Pol, because it contains in the second equation the term, $\mu(1 - x^2)y$, which is a characteristic feature of the van der Pol oscillator

$$\frac{dx^2}{dt^2} - \mu\left(1 - x^2\right)\frac{dx}{dt} + x = 0, \quad (\mu > 0) \tag{2}$$

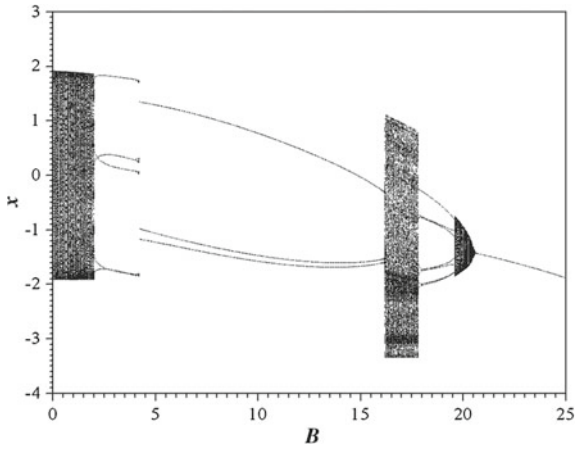

Fig. 1 Bifurcation diagram of x versus B, *for* $\mu = 0.2$ *and* $\omega = 4$

and the cubic term x^3 of Duffing's equation

$$\frac{dx^2}{dt^2} + a\frac{dx}{dt} + bx + cx^3 = F\cos(\omega t) \tag{3}$$

The dynamic behavior of the Duffing—van der Pol system is investigated numerically by employing the fourth order Runge–Kutta algorithm. The system's rich dynamical behavior is revealed in Fig. 1, which shows the bifurcation diagram of x versus the parameter B, for $\omega = 4$, while $\mu = 0.2$. Periodic and chaotic regions alternate as the parameter B increases while interesting dynamical phenomena, such as a route to chaos, through a quasi-periodic region, and crisis phenomena (i.e. boundary crisis), are also displayed. This richness of system's dynamic behavior makes the proposed non-autonomous system a suitable candidate for use in this work [9].

As it will be discussed in the next Section, the heart of the proposed robot's controller is the Poincaré map named by Henri Poincaré. This map is the intersection of an orbit in the state space of a continuous dynamical system with a certain lower dimensional subspace, called the Poincaré cross-section, transversal to the flow of the system. So, in this case, the Poincaré map is produced by using the Poincaré cross-section which is defined by

$$\sum = \left\{(x, y, \theta = \omega t_N) \in R^2 \times S^1\right\} \tag{4}$$

where $t_N = NT + t_0$ is the sampling time, t_0 the initial time determining the location of the Poincaré cross-section on which the coordinates (x, y) of the attractors are expressed and $T = 2\pi/\omega$ is the period of the voltage source.

In Figs. 2, 3 and 4 three characteristic Poincaré maps for various values of the parameter B of the bifurcation diagram of Fig. 1, in the case of $\mu = 0.2$ and $\omega = 4$, are displayed. From this figure the great utility of the Poincaré map can be seen, since for different system's dynamic behavior the Poincaré map has a totally different form. As it is known, the various forms of the Poincaré map depending on system's dynamic behavior are:

- Discrete number of points for Periodic behavior.
- Closed curve for Quasi-periodic behavior.
- Strange attractor for Chaotic behavior.

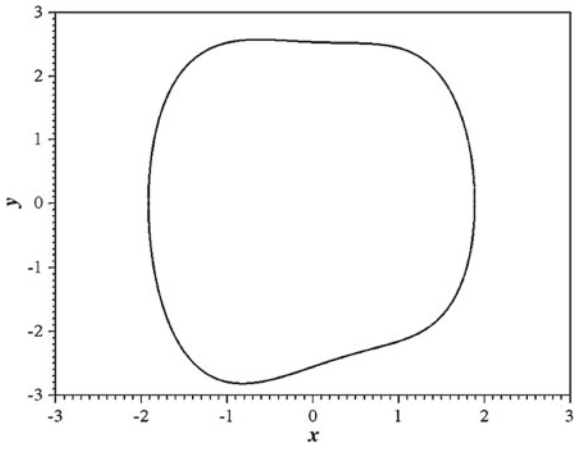

Fig. 2 Poincaré map of y versus x, for $\mu = 0.2$, $\omega = 4$ and $B = 1$ (quasi-periodic behavior)

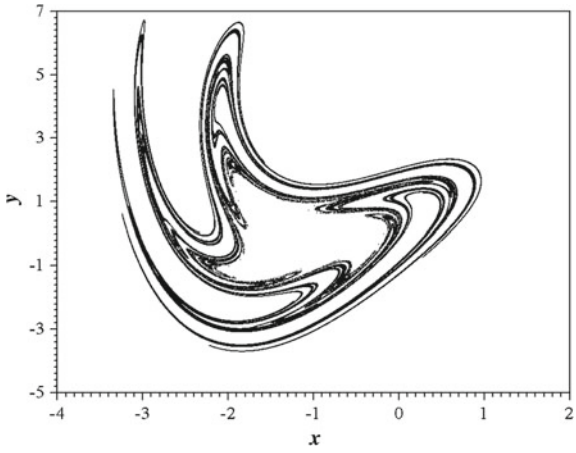

Fig. 3 Poincaré map of y versus x, for $\mu = 0.2$, $\omega = 4$ and B = 17 (chaotic behavior)

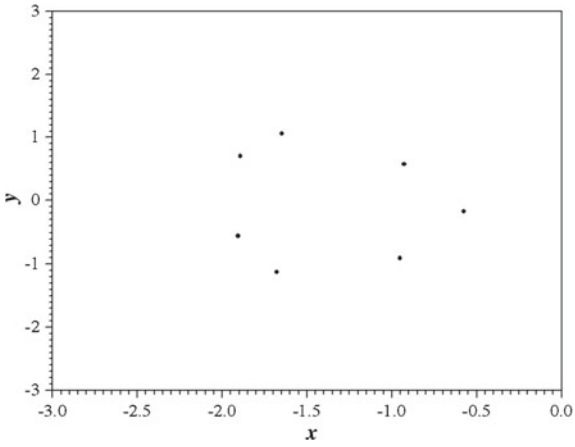

Fig. 4 Poincaré map of y versus x, for $\mu = 0.2$, $\omega = 4$ and B = 19 (periodic behavior)

3 The Chaotic Path Planning Generator

In this Section the path planning generator, which is the heart of the autonomous robot, is presented. The specific proposal is based on a novel chaotic random number generator. This generator produces a trajectory in a workspace, which is the result of a sequence of planned target locations.

One of the methods to obtain aperiodic sequences is to use chaos which is defined as "random" phenomenon generated by simple deterministic systems. Until now there have been reported in literature many works on random number generation based on chaos by using either continuous chaotic systems or discrete [4, 5, 14, 16, 17, 22, 24, 26, 27, 31, 32, 49, 56, 57, 64, 67, 68, 73, 74, 77, 78].

In the first case, continuous chaotic systems are used while in the second case various discrete-time chaotic systems realized by analog circuits are also used as random number generators, to generate aperiodic random number sequences. However, it is difficult to generate random sequences with good statistical properties due to nonidealities of analog circuit elements and inevitable noise [23, 64]. Thus, there have also been several works on post-processing of the chaos-based random numbers [51, 60].

The proposed random number generator, which has been used in this work, is based on a non-autonomous continuous chaotic system. So, for this reason, the values of system's parameters were selected so that the system is in chaotic state. In Figs. 5 and 6 the phase portrait and the respective Poincaré map for a chosen set of system's parameters are shown.

In more details, the proposed chaotic random number generator produced a sequence of planned target locations following the procedure.

Step 1: The number of cells, in which the workspace has been divided, is specified. In this work a square workspace with dimensions $M = 30 \times 30 = 900$ in normalized unit cells, is chosen.

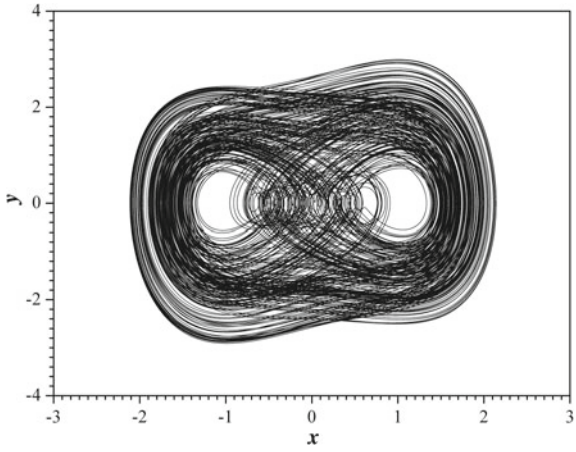

Fig. 5 Phase portrait of y versus x, for $\mu = 0.2$, $B = 1.175$ and $\omega = 0.92$

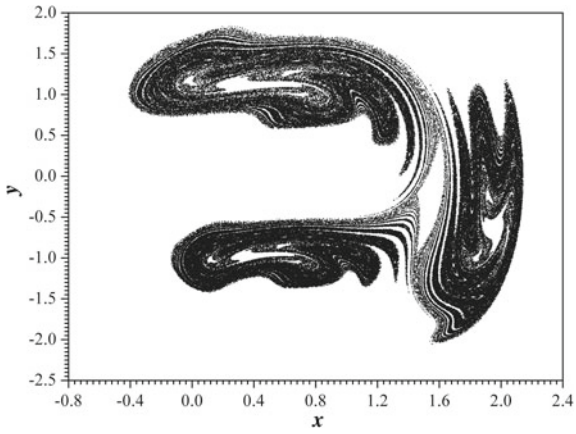

Fig. 6 Poincaré map of y versus x, for $\mu = 0.2$, $B = 1.175$ and $\omega = 0.92$

Step 2: An area of the Poincaré map, that is dense in points, is selected. This happens because the point's density on the Poincaré map will guarantee the coverage of the whole robot's workspace. In Fig. 7, the selected area of the Poincaré map ($x \in [1.834, 2.044]$, $y \in [-0.249, 0.407]$) in the red box for the chosen set of parameters ($\mu = 0.2$, $B = 1.175$ and $\omega = 0.92$) and initial conditions $(x_0, y_0) = (1, 1)$, is presented.

Step 3: The selected area in the Poincaré map is divided in the same unit cells as the workspace in Step 1. As it is shown in Fig. 7, all the cells of the selected area have been visited by the system. This is an essential condition for the success of robot's mission.

Step 4: Each time that a point in one of the cells of the selected area is produced in the Poincaré map, a target point in the coordination format $(x, y) = (0, 0)$, …, (30, 30) is also produced.

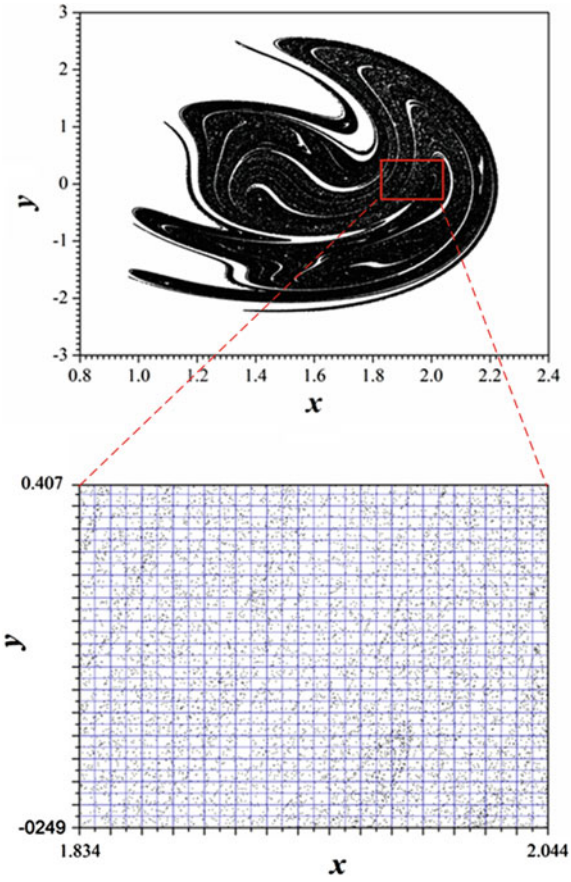

Fig. 7 The chaotic attractor from the Poincaré map of y versus x, for $\mu = 0.2$, $B = 1.175$ and $\omega = 0.92$, as well as the chosen area ($x \in [1.834, 2.044]$, $y \in [-0.249, 0.407]$) for using in the chaotic path planning generator

With the aforementioned procedure a sequence of target points in the robot's workspace is produced.

4 Simulation Results

In literature there has been presented a great number of works on kinematic control of chaotic robots, which is based mainly on a typical differential motion with two degrees of freedom, composed by two active, parallel, and independent wheels and a third passive wheel. However, the proposed, in this work, robot's path planning generator represents an interesting compromise of simplicity between control and implementation. So, it could be adopted by many commercial robotic models, because the proposed kinematic control model is very easy to be implemented not only in differential motion robots (Fig. 8), in which the robot rotates around itself

Fig. 8 The mobile robot Khepera

followed by a linear displacement directly to the next position, but also in humanoid robots (Fig. 9), which will have a rapid growth of interest in the upcoming decade.

Also, in the real world, robots move in spaces with boundaries like walls or obstacles. Furthermore, many robots have sensors, like sonar or infrared devices, which provide the capability to detect the presence of obstacles or even more the recognition of the searched objects or intruders. In this work, for a better understanding of the behavior of the robot's chaotic motion generator, we do not care about the kind of robot (mobile or humanoid) and we assume that the robot works in a smooth state space with boundaries and without any sensor.

Fig. 9 The humanoid robot Kondo KHR-2HV

So, in this Section the proposed robot's kinematic control was numerically simulated and the results are presented in details. For this reason the workspace coverage, using the well-known coverage rate (C), which represents the effectiveness, as the amount of the total surface covered by the robot, is used. The coverage rate (C) is given by the following equation

$$C = \frac{1}{M} \sum_{i=1}^{M} I(i) \tag{5}$$

where, $I(i)$ is the coverage situation for each cell [8]. This is defined by the following equation

$$I(i) = \begin{cases} 1, \text{ when the cell } i \text{ is covered} \\ \\ 0, \text{ when the cell } i \text{ is not covered} \end{cases} \tag{6}$$

where, $i = 1, 2, \ldots, M$. The robot's workplace, as it is mentioned, is supposed to be a square terrain with dimensions $M = 30 \times 30 = 900$ in normalized unit cells. Furthermore, a second interesting evaluation criterion is the coverage time of the system, which is the total time for the system to cover the entire terrain.

The simulation starts from an arbitrary initial position, as the chosen $(x_0, y_0) = (15, 15)$ in this work, which does not play any crucial role in coverage rate because the robot follows a specific sequence of target points. Following the procedure, which was explained in details in the previous Section, produces this sequence.

In order to accomplish the goal of complete terrain coverage, the robot must move in every region, covering systematically the entire workspace. The results for the first 5,000 of the produced target points are shown in Figs. 10, 11 and 12. Especially, in Fig. 10 the distribution of the target points over the entire terrain can be observed. So, the number of the 5,000 target points is enough to cover almost all the workspace (only 12 cells have not been visited). A more descriptive diagram, of the chaotic robot's behavior, is Fig. 11. In this figure a colour scale map of the terrain's cells versus the times of visiting is shown. The majority of the cells have been visited from 0 to 10 times in those 5,000 iterations. As a conclusion we may note the almost uniform distribution of the visiting times on the robot's workplace.

Also, in Fig. 12 the trajectory of the chaotic mobile robot, with the adopted discontinuous motion control, for the specific number of planned points (5,000) is shown. A very important feature is raised from this plot. The robot, when is moving from one target point to the next, visits other terrain's cell, possibly many times with different direction. As a consequence all the cells have been visited by the robot. This feature is crucial, especially, in a patrolling mission.

In Fig. 13, the coverage rate versus the number of target points, for the robot with the proposed chaotic motion generator, is shown, starting from the above mentioned, initial position. From this diagram the coverage of almost the entire terrain

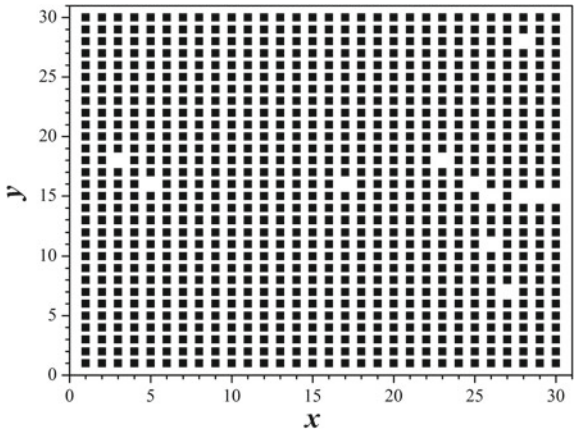

Fig. 10 Workspace coverage using the robot with proposed chaotic path-planning generator, for the first 5,000 target points

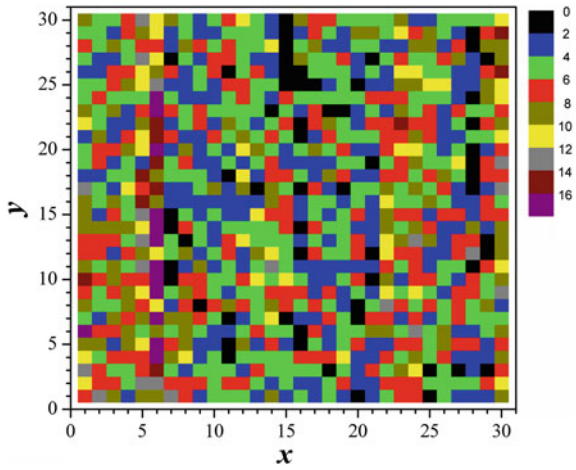

Fig. 11 Colour scale map of the workspace's cells versus the time of visiting

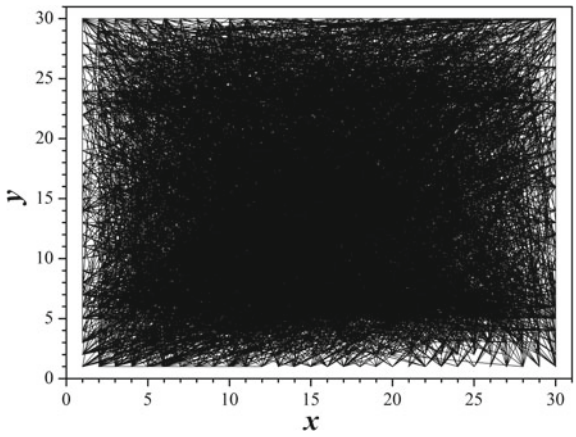

Fig. 12 The robot's trajectory evolution, after 5,000 path planned points, with the adopted path planning controller

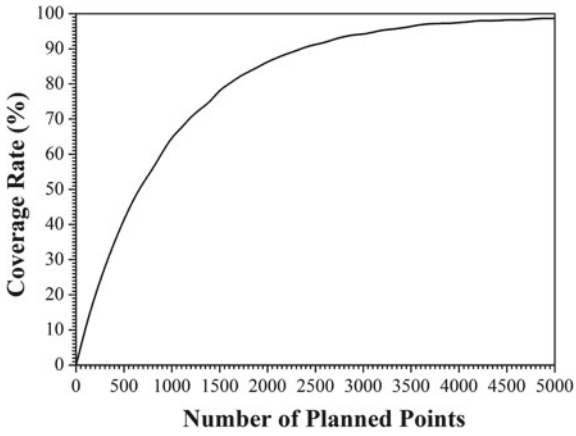

Fig. 13 Coverage rate versus the number of planned points, for the robot with the proposed chaotic path-planning generator, for 5,000 planned points

is confirmed. Furthermore, the curve in Fig. 13 has an exponential form which is confirmed by the fitting procedure with Origin. This fitting led to the conclusion that the produced curve satisfies the following exponential function

$$y = y_0 - Ae^{R_0 x} \tag{7}$$

where, $y_0 = 98.95123$, $A = 97.46218$ and $R_0 = -0.00103$ with R-Square equal to 0.99972.

Finally, in comparison with other similar works [39, 40, 69, 71, 72, 75, 76], this one shows very satisfactory results concerning the coverage rate and the scanning time. So, the above mentioned simulation results confirmed that the proposed chaotic robot satisfies the three basic requirements of autonomous robot's motion, the unpredictability of the trajectory, the complete and fast scanning of robot's workplace by following an exponential function.

5 Conclusion

In this chapter, a chaotic path planning generator for autonomous robots, mobile or humanoid, is presented. This generator is based on a controller that defines the position goal in each step by imparting the chaotic behavior.

Validation tests based on numerical simulations of the robot's motion control, confirm that the proposed method can obtain very satisfactory results in regard to unpredictability and fast scanning of the robot's workplace. So, the proposed approach has several interesting features and advantages.

As it is mentioned, this strategy ensures high unpredictability of robot trajectories, resembling a non-planned motion from external observer's point of view. The complete and fast scanning of the terrain is confirmed from the simulation results.

It is also important to mention, that the proposed strategy has an advantage over a randomly planned motion, which is the deterministic nature of the chaotic control law.

The proposed robot with the above mentioned features, such as unpredictability and fast scanning of workplace, may have many interesting applications in various, industrial, civil and military activities. Floor-cleaning devices and military autonomous robots for surveillance, patrolling or terrain exploration for explosives may be some of the proposed chaotic robot applications.

Finally, the results of this chapter ensure that the application of chaotic systems, in solutions for autonomous robots control strategies represents a very interesting task for researchers of both scientific fields. Furthermore, the simulation results of the proposed robot's motion show that such strategy can be easily applied in real robotic systems, many of which are commercially available. So, as a future work, an experimental realization of the proposed motion controller will be studied.

References

1. Azar AT, Vaidyanathan S (2015) Chaos modelling and control systems design, studies in computational intelligence. Springer, New York
2. Azar AT, Vaidyanathan S (2015) Computational intelligence applications in modelling and control studies in computational intelligence. Springer, New York
3. Baker GL (1996) Chaotic dynamics: an introduction. Cambridge University Press, Cambridge
4. Bernardini R, Cortelazzo G (2001) Tools for designing chaotic systems for secure random number generation. IEEE Trans Circ Syst 48(5):552–564
5. Bernstein GM, Lieberman MA (1990) Secure random number generation using chaotic circuits. IEEE Trans Circ Syst 37(9):1157–1164
6. Capezio F, Sgorbissa A, Zaccaria R (2005) GPS-based localization for a surveillance UGV in outdoor areas. 5th IEEE International workshop on robot motion and control. Dymaczewo, Poland, pp 157–162
7. Casperson LW (1988) Gas laser instabilities and their interpretation. In: Proceedings of the NATO advanced study institute Springer, pp 83–98
8. Choset S (2006) Coverage for robotics-a survey of recent results. Ann Math Artif Intel 31:113–126
9. Chudzik A, Perlikowski P, Stefanski A, Kapitaniak T (2011) Multistability and rare attractors in van der Pol-Duffing oscillator. Int J Bifurc Chaos 21(07):1907–1912
10. Corbett DR, Gage DW, Hackett DD (2011) Robotic communications and surveillance-the darpa landroids program. Lect Notes Comput Sci 7106(2011):749758
11. Curiac DI, Volosencu C (2009) Developing 2D trajectories for monitoring an area with two points of interest. In: 10th WSEAS international conference on automation and information, pp 366–369
12. Ebner M, Hameroff S (2011). Computational modelling of robust figure/ground separation. In: 3rd international conference on biocomputational systems and biotechnologies, pp 67–72
13. Field RJ, Györgyi L (1993) Chaos in chemistry and biochemistry. World Scientific Publishing, Singapore
14. Fu SM, Chen ZY, Zhou YA (2004) Chaos based random number generators. Comput Res Dev 41:749–754
15. Gao X, Li K, Wang Y, Men G, Zhou D, Kikuchi K (2007) A floor cleaning robot using Swedish wheels. IEEE international conference on robotics and biomimetics, (ROBIO 2007). Sanya, China, pp 2069–2073

16. Gentle JE (2003) Random number generation and monte carlo method. Springer, New York
17. Gerosa A, Bernardini R, Pietri S (2001) A fully integrated chaotic system for the generation of truly random numbers. IEEE Trans Circ Syst I 49(7):993–1000
18. Gomez-Pavon LC, Munoz-Pacheco JM, Luis-Ramos A (2015) Synchronous chaos generation in an Er3+-doped fiber laser system. IEEE Photon J (Published online). doi:10.1109/JPHOT.2015.2419073
19. Grebogi C, Yorke J (1997) The impact of chaos on science and society. University Press, United Nations
20. Gustafson H, Dawson HE, Nielsen L, Caelli W (1994) A computer package for measuring the strength of encryption algorithms. J Comput Secur 13:687–697
21. Hasselblatt B, Katok A (2003) A first course in dynamics: With a panorama of recent developments. Cambridge University Press, Cambridge
22. Huaping L, Wang S, Gang H (2004) Pseudo-random number generator based on coupled map lattices. Int J Mod Phys B 18:2409–2414
23. Kennedy MP, Rovatti R, Setti G (2000) Chaotic electronics in telecommunications. CRC Press, Florida
24. Knuth D (1998) The art of computer programming: semiemperical algorithms. Reading, Addison Wesley, Massachusetts
25. Kocarev L (2001) Chaos-based cryptography: a brief overview. IEEE Circ Syst Mag 1:6–21
26. Kohda T, Tsuneda A (1997) Statistics of chaotic binary sequences. IEEE Trans Inform Theory 43(1):104–112
27. Kolesov VV, Belyaev RV, Voronov GM (2001) Digital random-number generator based on the chaotic signal algorithm. J Commun Technol Electron 46:1258–1263
28. Kyrtsou C, Vorlow C (2005) Complex dynamics in macroeconomics: a novel approach. Diebolt C, Kyrtsou C (ed) In: New trends in macroeconomics. pp 223–245, ISBN-13: 978-3-540-21448-9, Springer, Berlin
29. Laplace PS (1825) Traité du Mécanique Céleste. Oeuvres complétes de Laplace, Gauthier-Villars, Paris
30. Lorenz EN (1963) Deterministic non-periodic flow. J Atm Sci 20:130–141
31. Li S, Mou X, Cai Y (2001) Pseudo-random bit generator based on coupled chaotic systems and its application in stream-ciphers cryptography. Progress in cryptology-INDOCRYPT 2001. Lect Notes Comput Sci 2247:316–329
32. Li K, Soh YC, Li ZG (2003) Chaotic cryptosystem with high sensitivity to parameter mismatch. IEEE Trans Circ Syst I: Fund Theory Appl 50:579–583
33. Luo RC, Lin TY, Su KL (2009) Multisensor based security robot system for intelligent building. Robot Auton Syst 57:330–338
34. Mandelbrot B (1977) The fractal geometry of nature. Freeman Company, New York
35. Marsaglia G (1995) DIEHARD Statistical Tests. http://stst.fsu.edu/pub/diehard
36. Marslanda S, Nehmzowb U (2005) On-line novelty detection for autonomous mobile robots. Robot Auton Syst 51:191–206
37. Martins-Filho LS, Machado RF, Rocha R, Vale VS (2004) Commanding mobile robots with chaos. Symp Ser Mech 1:40–46
38. Martins-Filho LS, Macau EEN, Rocha R, Machado RF, Hirano LA (2005) Kinematic control of mobile robots to produce chaotic trajectories. In: 18th international congress of mechanical engineering, Ouro Preto
39. Martins-Filho LS, Macau EEN (2007) Studies in computational intelligence. Trajectory planning for surveillance missions of mobile robotsSpringer, Heidelberg, pp 109–117
40. Martins-Filho LS, Macau EEN (2007) Patrol mobile robots and chaotic trajectories. Math Probl Eng 2007:1
41. May RM (1976) Theoretical ecology: principles and applications. Saunders Company, Philadelphia
42. MobileRobots Inc. (2006) Patrol brochure. Amherst. http://www.MobileRobots.com/
43. Moon FC (1987) Chaotic vibrations: an introduction for applied scientists and engineers. Wiley, New Jersey

44. Munoz-Pacheco JM, Tlelo-Cuautle E, Flores-Tiro E, Trejo-Guerra R (2014) Experimental synchronization of two integrated multi-scroll chaotic oscillators. J Appl Res Technol 12(3):459–470
45. Munoz-Pacheco JM, Tlelo-Cuautle E, Toxqui-Toxqui I, Sanchez-Lopez C, Trejo-Guerra R (2014) Frequency limitations in generating multi-scroll chaotic attractors using CFOAs. Int J Electron 101(11):1559–1569
46. Munoz-Pacheco JM, Zambrano-Serrano E, Felix-Beltran OG, Gomez-Pavon LC, Luis-Ramos A (2012) Synchronization of PWL function-based 2D and 3D multi-scroll chaotic systems. Nonlinear Dyn 70(2):1633–1643
47. Nakamura Y, Sekiguchi A (2001) The chaotic mobile robot. IEEE Trans Robot Autom 17(6):898–904
48. NIST (2001) Security Requirements for Cryptographic Modules. FIPS PUB 140–2. http://csrc.nist.gov/publications/fips/fips140-2/fips1402.pdf
49. Oishi S, Inoue H (1982) Pseudo-random number generators and chaos. Trans Inst Electron Commun Eng Jpn E 65:534–541
50. Palacin J, Salse JA, Valganon I, Clua X (2004) Building a mobile robot for a floor-cleaning operation in domestic environments. IEEE Trans Instrum Meas 53:1418–1424
51. Pareschi F, Rovatti R, Setti G (2006) Simple and effective post-processing stage for random stream generated by a chaos-based RNG. Int Symp Nonlinear Theory Appl 2006:383–386
52. Poincare JH (1890) Sur le probleme des trois corps et les equations de la dynamique. Divergence des series de M. Lindstedt. Acta Mathematica 13:1–270
53. Siegwart R, Nourbakhsh IR, Scaramuzza D (2011) Introduction to autonomous mobile robots, 2nd edn. Massachusetts Institute of Technology, Massachusetts
54. Sooraksa P, Klomkarn K (2010) No-CPU chaotic robots: from classroom to commerce. IEEE Circuits Syst Mag 10:46–53
55. Stavrinides SG, Anagnostopoulos AN, Miliou AN, Valaristos A, Magafas L, Kosmatopoulos K, Papaioannou S (2009) Digital chaotic synchronized communication system. J Eng Sci Technol Rev 2:82–86
56. Stojanovski T, Kocarev L (2001) Chaos-based random number generators-part I: analysis. IEEE Trans Circuit Syst I: Fund Theory Appl 48(3):281–288
57. Stojanovski T, Pihl J, Kocarev L (2001) Chaos-based random number generators-Part II: practical realizations. IEEE Trans Circ Syst I: Fund Theory Appl 48(3):382–385
58. Suh JH, Lee YJ, Lee KS (2005) Object transportation control of cooperative AGV systems based on virtual passivity decentralized control algorithm. J Mech Sci Technol 19:1720–1730
59. Tadokoro S (2010) Rescue robotics. Springer, Berlin
60. Tang KW, Tang W (2006) A low cost chaos-based random number generator realized in 8-bit precision environment. Int Symp Nonlinear Theory Appl 2006:395–398
61. Tavera MJM, Dutra MS, Diaz EYV, Lengerke O (2009) Implementation of chaotic behaviour on a fire fighting robot. In: 20th international congress of mechanical engineering, Gramado, Brazil
62. Thrun S (2002) Robotic mapping: a survey. In: Lakemeyer G, Nebel B (ed.), Exploring artificial intelligence in the new millenium, pp 1–35
63. Tlelo-Cuautle E, Ramos-Lopez HC, Sanchez-Sanchez M, Pano-Azucena AD, Sanchez-Gaspariano LA, Nuñez-Perez JC, Camas-Anzueto JL (2014) Application of a chaotic oscillator in an autonomous mobile robot. J Electr Eng-Elektrotechnický Casopis 65(3):157–162
64. Tsuneda A, Eguchi K, Inoue T (1999) Design of chaotic binary sequences with good statistical properties based on piecewise linear into maps. In: 7th international conference on microelectronics for neural, Fuzzy and bio-Inspired systems, pp 261–266
65. Ueda Y, Akamatsu N (1981) Chaotically transitional phenomena in the forced negative-resistance oscillator. IEEE Trans Circuit Syst CAS-28:217–224
66. van der Pol B, Van der Mark J (1927) Frequency demultiplication. Nature 120:363–364
67. Volos ChK, Kyprianidis IM, Stouboulos IN (2006) Experimental demonstration of a chaotic cryptographic scheme. WSEAS Trans Circuit Syst 5:1654–1661

68. Volos ChK, Kyprianidis IM, Stouboulos IN (2010) Fingerprint images encryption process based on a chaotic true random bits generator. Int J Multimed Intell Secur 1:320–335
69. Volos ChK, Kyprianidis IM, Stouboulos IN (2012) Motion control of robots using a chaotic truly random bits generator. J Eng Sci Technol Rev 5(2):6–11
70. Volos ChK, Bardis N, Kyprianidis IM, Stouboulos IN (2012) Motion control of a mobile robot based on double-scroll chaotic circuits. WSEAS Trans Syst 11(9):479–488
71. Volos ChK, Kyprianidis IM, Stouboulos IN (2012) A chaotic path planning generator for autonomous mobile robots. Robot Auton Syst 60:651–656
72. Volos ChK (2013) Motion direction control of a robot based on chaotic synchronization phenomena. J Autom Mob Robot Intell Syst 7(2):64–69
73. Volos ChK, Kyprianidis IM, Stouboulos IN (2013) Image encryption process based on chaotic synchronization phenomena. Signal Process 93:1328–1340
74. Volos ChK (2013) Chaotic random bit generator realized with a microcontroller. J Comput Model 3(4):115–136
75. Volos ChK, Kyprianidis IM, Stouboulos IN, Stavrinides SG, Anagnostopoulos AN (2013) An autonomous mobile robot guided by a chaotic true random bits generator. Chaos and complex systems, Springer, Berlin
76. Volos ChK, Kyprianidis IM, Stouboulos IN (2013) Experimental investigation on coverage performance of a chaotic autonomous mobile robot. Robot Auton Syst 60:1314–1322
77. Wei J, Liao X, Wong K, Xiang T (2006) A new chaotic cryptosystem. Chaos Soliton Fractal 30:1143–1152
78. Yalcin ME, Suykens JAK, Vandewalle J (2004) True random bit generation from a double scroll attractor. IEEE Trans Circuit Syst I 51(7):1395–1404

Nonlinear Observer Design for Chaotic Systems

Sundarapandian Vaidyanathan

Abstract This work investigates the nonlinear observer design for chaotic systems. Explicitly, we have applied Sundarapandian's theorem (2002) for local exponential observer design for nonlinear systems to design nonlinear observers for chaotic systems with a single stable equilibrium point, viz. Wei-Wang system (2013) and Kingni-Jafari system (2014). MATLAB simulations are provided to illustrate the phase portraits and nonlinear observer design for the Wei-Wang and Kingni-Jafari chaotic systems.

Keywords Nonlinear observers · Exponential observers · Observability · Chaotic systems

1 Introduction

The observer design problem is to estimate the state of a control system when only the plant output and control input are available for measurement. The problem of designing observers for linear control systems was first introduced and fully solved by Luenberger [21]. The problem of designing observers for nonlinear control systems was proposed by Thau [59]. Over the past three decades, several techniques have been developed in the control systems literature to the construction of observers for nonlinear control systems [5].

A necessary condition for the existence of a local exponential observer for nonlinear control systems was obtained by Xia and Gao [99]. On the other hand, sufficient conditions for nonlinear observers have been derived in the control literature from an impressive variety of points of view. Kou ey al. [14] derived sufficient conditions for the existence of local exponential observers using Lyapunov-like method. In [11, 15, 16, 98], suitable coordinate transformations were found under which a nonlin-

S. Vaidyanathan (✉)
Research and Development Centre, Vel Tech University, Avadi, Chennai 600062, Tamil Nadu, India
e-mail: sundarvtu@gmail.com

S. Vaidyanathan and C. Volos (eds.), *Advances and Applications in Nonlinear Control Systems*, Studies in Computational Intelligence 635,
DOI 10.1007/978-3-319-30169-3_2

ear control systems is transferred into a canonical form, where the observer design is carried out. In [61], Tsinias derived sufficient Lyapunov-like conditions for the existence of local asymptotic observers for nonlinear systems. A harmonic analysis method was proposed in [8] for the synthesis of nonlinear observers.

A characterization of local exponential observers for nonlinear control systems was first obtained by Sundarapandian [38]. In [38], necessary and sufficient conditions were obtained for exponential observers for Lyapunov stable continuous-time nonlinear systems and an exponential observer design was provided by Sundarapandian which generalizes the linear observer design of Luenberger [21] for linear control systems. In [41], Sundarapandian obtained necessary and sufficient conditions for exponential observers for Lyapunov stable discrete-time nonlinear systems and also provided a formula for designing exponential observers for Lyapunov stable discrete-time nonlinear systems. In [37], Sundarapandian derived new results for the global observer design for nonlinear control systems.

The concept of nonlinear observers for nonlinear control systems was also extended in many ways. In [39, 40], Sundarapandian derived new results characterizing local exponential observers for nonlinear bifurcating systems. In [42, 43, 48, 49], Sundarapandian derived new results for the exponential observer design for a general class of nonlinear systems with real parametric uncertainty. In [44–47], Sundarapandian derived new results and characterizations for general observers for nonlinear systems.

Chaotic systems are defined as nonlinear dynamical systems which are sensitive to initial conditions, topologically mixing and with dense periodic orbits. Sensitivity to initial conditions of chaotic systems is popularly known as the *butterfly effect*. Small changes in an initial state will make a very large difference in the behavior of the system at future states. Chaotic behaviour was suspected well over hundred years ago in the study of three bodies problem by Henri Poincaré [4], but chaos was experimentally established by Lorenz [19] only a few decades ago in the study of 3-D weather models.

Some classical paradigms of 3-D chaotic systems in the literature are Rössler system [30], ACT system [1], Sprott systems [36], Chen system [9], Lü system [20], Liu system [18], Cai system [6], Chen-Lee system [10], Tigan system [60], etc.

Many new chaotic systems have been discovered in the recent years such as Zhou system [100], Zhu system [101], Li system [17], Wei-Yang system [97], Sundarapandian systems [51, 56], Vaidyanathan systems [68, 69, 71–74, 76, 78, 81, 92, 95], Pehlivan system [24], etc.

Synchronization of chaotic systems is a phenomenon that occurs when two or more chaotic systems are coupled or when a chaotic system drives another chaotic system. Because of the butterfly effect which causes exponential divergence of the trajectories of two identical chaotic systems started with nearly the same initial conditions, the synchronization of chaotic systems is a challenging research problem in the chaos literature [2, 3].

Major works on synchronization of chaotic systems deal with the complete synchronization of a pair of chaotic systems called the *master* and *slave* systems. The design goal of the complete synchronization is to apply the output of the master

system to control the slave system so that the output of the slave system tracks the output of the master system asymptotically with time.

Pecora and Carroll pioneered the research on synchronization of chaotic systems with their seminal papers [7, 23]. The active control method [12, 31, 32, 50, 55, 62, 66, 83, 84, 87] is typically used when the system parameters are available for measurement. Adaptive control method [33–35, 52–54, 64, 70, 77, 82, 85, 86, 91, 94] is typically used when some or all the system parameters are not available for measurement and estimates for the uncertain parameters of the systems.

Backstepping control method [25–29, 58, 88, 93] is also used for the synchronization of chaotic systems, which is a recursive method for stabilizing the origin of a control system in strict-feedback form. Another popular method for the synchronization of chaotic systems is the sliding mode control method [57, 63, 65, 67, 75, 79, 80, 89, 90], which is a nonlinear control method that alters the dynamics of a nonlinear system by application of a discontinuous control signal that forces the system to "slide" along a cross-section of the system's normal behavior.

The control and synchronization of chaotic systems is based on the full knowledge of the states of the systems. When some of the chaotic systems are not available for measurement, exponential observer design for chaotic systems can be used in lieu of the states of the systems Thus, observer design for chaotic systems has important applications in the control literature.

This work is organized as follows. Section 2 reviews the definition and results of local exponential observers for nonlinear systems. Section 3 details the dynamic analysis and phase portraits of the Wei-Wang chaotic system [96]. Section 4 details the nonlinear observer design for the Wei-Wang chaotic system. Section 5 details the dynamic analysis and phase portraits of the Kingni-Jafari chaotic system [13]. Section 6 details the nonlinear observer design for the Kingni-Jafari chaotic system. Section 7 provides the conclusions of this work.

2 Review of Nonlinear Observer Design for Nonlinear Systems

By the concept of a *state observer* for a nonlinear system, it is meant that from the observation of certain states of the system considered as *outputs* or *indicators*, it is desired to estimate the state of the whole system as a function of time. Mathematically, observers for nonlinear systems are defined as follows.

Consider the nonlinear system described by

$$\dot{x} = f(x) \tag{1a}$$

$$y = h(x) \tag{1b}$$

where $x \in \mathbf{R}^n$ is the *state* and $y \in \mathbf{R}^p$ is the *output*.

It is assumed that $f : \mathbf{R}^n \to \mathbf{R}^n$, $h : \mathbf{R}^n \to \mathbf{R}^p$ are C^1 mappings and for some $x^\star \in \mathbf{R}^n$, the following hold:

$$f(x^\star) = 0, \quad h(x^\star) = 0 \tag{2}$$

Remark 1 We note that the solutions $x^\star$ of $f(x) = 0$ are called the *equilibrium points* of the plant dynamics (1a). Also, the assumption $h(x^\star) = 0$ holds without any loss of generality. Indeed, if $h(x^\star) \neq 0$, then we may define a new output function as

$$\psi(x) = h(x) - h(x^\star) \tag{3}$$

and it is easy to see that $\psi(x^\star) = 0$. ■

The linearization of the nonlinear system (1a) and (1b) at $x = x^\star$ is given by

$$\dot{x} = Ax \tag{4a}$$
$$y = Cx \tag{4b}$$

where

$$A = \left[\frac{\partial f}{\partial x}\right]_{x=x^\star} \quad \text{and} \quad C = \left[\frac{\partial h}{\partial x}\right]_{x=x^\star} \tag{5}$$

Definition 1 ([38]) A C^1 dynamical system defined by

$$\dot{z} = g(z, y), \quad (z \in \mathbf{R}^n) \tag{6}$$

is called a **local asymptotic** (respectively, **exponential**) **observer** for the nonlinear system (1a)–(1b) if the following two requirements are satisfied:

(i) If $z(0) = x(0)$, then $z(t) = x(t)$, for all $t \geq 0$.
(ii) There exists a neighbourhood V of the equilibrium $x^\star$ of $\mathbf{R}^n$ such that for all $z(0), x(0) \in V$, the estimation error

$$e(t) = z(t) - x(t) \tag{7}$$

decays asymptotically (respectively, exponentially) to zero as $t \to \infty$. ■

Theorem 1 ([38]) *Suppose that the nonlinear system dynamics (1a) is Lyapunov stable at the equilibrium $x = x^\star$ and that there exists a matrix K such that $A - KC$ is Hurwitz. Then the dynamical system defined by*

$$\dot{z} = f(z) + K[y - h(z)] \tag{8}$$

is a local exponential observer for the nonlinear system (1a)–(1b). ■

Remark 2 The estimation error is governed by the dynamics

$$\dot{e} = f(x+e) - f(x) - K[h(x+e) - h(x)] \tag{9}$$

Linearizing the error dynamics (9) at $x = x^\star$, we get the linear system

$$\dot{e} = Ee, \quad \text{where } E = A - KC \tag{10}$$

If (C, A) is observable, then the eigenvalues of $E = A - KC$ can be arbitrarily placed in the complex plane [22] and thus a local exponential observer of the form (8) can always be found such that the transient response of the error decays quickly with any desired speed of convergence. ■

3 Dynamic Analysis of the Wei-Wang Chaotic System

The Wei-Wang chaotic system [96] is described by the 3-D dynamics

$$\begin{aligned} \dot{x}_1 &= ax_1 + x_2x_3 \\ \dot{x}_2 &= -x_2 + x_1^2 \\ \dot{x}_3 &= 1 - 4x_1 \end{aligned} \tag{11}$$

where a is a constant, positive parameter.

The system (11) exhibits a chaotic attractor when $a = 0.03$.

For numerical simulations, we take the initial conditions as

$$x_1(0) = -0.6, \quad x_2(0) = 0.9, \quad x_3(0) = -1.7 \tag{12}$$

Figure 1 shows the 3-D phase portrait of the Wei-Wang chaotic system (11). Figures 2, 3, and 4 show the 2-D projections of the Wei-Wang chaotic system (11) on the (x_1, x_2), (x_2, x_3) and (x_1, x_3) coordinate planes respectively.

It is known that the Wei-Wang chaotic system (11) has a stable equilibrium at

$$x^\star = \begin{bmatrix} -0.6 \\ 0.9 \\ -1.7 \end{bmatrix} \tag{13}$$

Also, the Lyapunov exponents of the Wei-Wang chaotic system (11) for the parameter value $a = 0.03$ and for the initial values (12) are numerically found as

$$L_1 = 0.0340, \quad L_2 = 0, \quad L_3 = -1.0002 \tag{14}$$

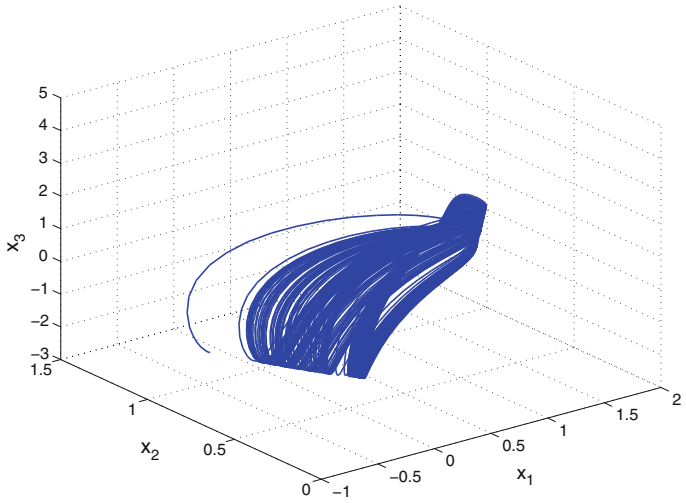

Fig. 1 3-D phase portrait of the Wei-Wang chaotic system

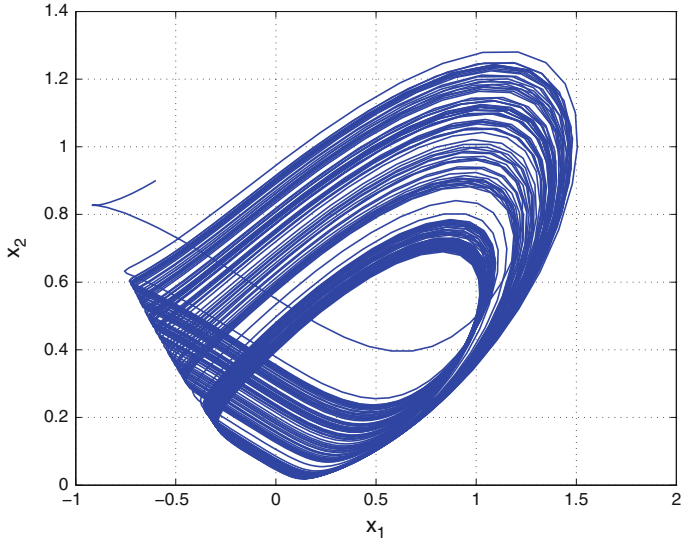

Fig. 2 2-D projection of the Wei-Wang chaotic system on the (x_1, x_2) plane

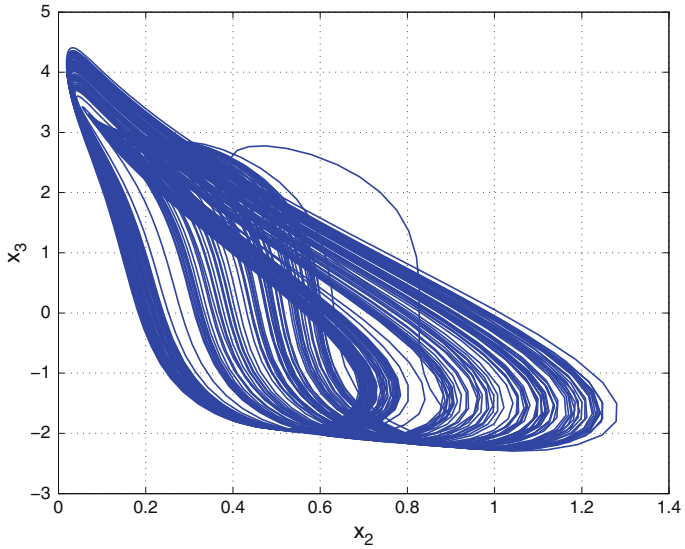

Fig. 3 2-D projection of the Wei-Wang chaotic system on the (x_2, x_3) plane

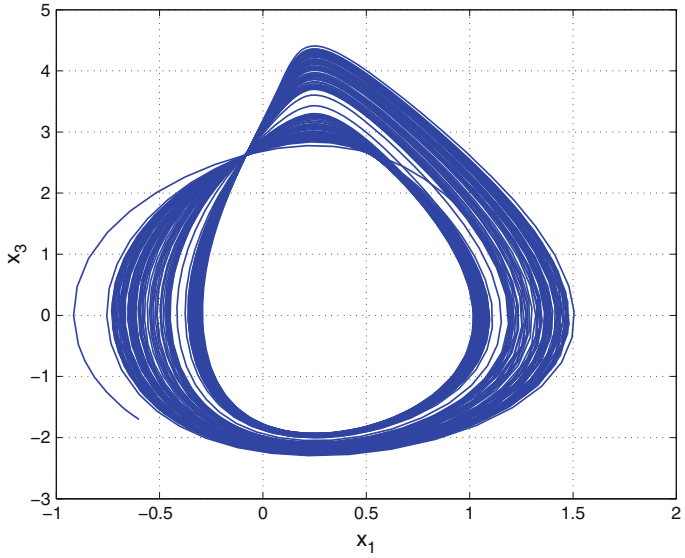

Fig. 4 2-D projection of the Wei-Wang chaotic system on the (x_1, x_3) plane

Thus, the Kaplan–Yorke dimension of the Wei-Wang chaotic system (11) is found as

$$D_{KY} = 2 + \frac{L_1 + L_2}{|L_3|} = 2.0340 \tag{15}$$

4 Nonlinear Observer Design for the Wei-Wang Chaotic System

This section investigates the problem of nonlinear observer design for the Wei-Wang chaotic system described by the dynamics

$$\begin{aligned} \dot{x}_1 &= ax_1 + x_2x_3 \\ \dot{x}_2 &= -x_2 + x_1^2 \\ \dot{x}_3 &= 1 - 4x_1 \end{aligned} \tag{16}$$

where a is a positive parameter.

The system (16) is chaotic when $a = 0.03$. In the chaotic case, the system (16) has a stable equilibrium point

$$x^\star = \begin{bmatrix} -0.6 \\ 0.9 \\ -1.7 \end{bmatrix} \tag{17}$$

We consider the output function as

$$y = x_1 \tag{18}$$

The linearization of the plant dynamics (16) at $x = x^\star$ is given by

$$A = \frac{\partial f}{\partial x}(x^\star) = \begin{bmatrix} a & x_3^\star & x_2^\star \\ 2x_1^\star & -1 & 0 \\ -4 & 0 & 0 \end{bmatrix} = \begin{bmatrix} 0.03 & -1.7 & 0.9 \\ -1.2 & -1 & 0 \\ -4 & 0 & 0 \end{bmatrix} \tag{19}$$

Also, the linearization of the output function (18) at $x = x^\star$ is given by

$$C = \frac{\partial h}{\partial x}(x^\star) = \begin{bmatrix} 1 & 0 & 0 \end{bmatrix} \tag{20}$$

From (19) and (20), the observability matrix for the Wei-Wang system (16) with the output (18) is given by

$$\mathbf{O}(C, A) = \begin{bmatrix} C \\ CA \\ CA^2 \end{bmatrix} = \begin{bmatrix} 1 & 0 & 0 \\ 0.03 & -1.7 & 0.9 \\ -1.5591 & 1.649 & 0.027 \end{bmatrix} \tag{21}$$

We find that

$$\det[\mathbf{O}(C, A)] = -1.53 \neq 0 \tag{22}$$

which shows that $\mathbf{O}(C, A)$ has full rank. Thus, (C, A) is completely observable [22].

Since the equilibrium $x = x^\star$ is Lyapunov stable, by Sundarapandian's theorem (Theorem 1), we obtain the following result, which gives a construction of nonlinear observer for the Wei-Wang chaotic system.

Theorem 2 *The Wei-Wang chaotic system (16) with the output (18) has a local exponential observer of the form*

$$\begin{bmatrix} \dot{z}_1 \\ \dot{z}_2 \\ \dot{z}_3 \end{bmatrix} = \begin{bmatrix} az_1 + z_2 z_3 \\ -z_2 + z_1^2 \\ 1 - 4z_1 \end{bmatrix} + K\left[y - z_1\right] \tag{23}$$

where K is a matrix chosen such that $A - KC$ is Hurwitz. Since (C, A) is observable, a gain matrix K can be found such that the error matrix $E = A - KC$ has arbitrarily assigned set of stable eigenvalues. ■

For numerical simulations, we find an observer gain matrix K so that

$$\text{eig}(A - KC) = \{-6, -6, -6\} \tag{24}$$

Using MATLAB, we get

$$K = \begin{bmatrix} 17.0300 \\ 72.3294 \\ 236.0000 \end{bmatrix} \tag{25}$$

Thus, a local exponential observer for the Wei-Wang system (16) is given by

$$\begin{bmatrix} \dot{z}_1 \\ \dot{z}_2 \\ \dot{z}_3 \end{bmatrix} = \begin{bmatrix} az_1 + z_2 z_3 \\ -z_2 + z_1^2 \\ 1 - 4z_1 \end{bmatrix} + \begin{bmatrix} 17.0300 \\ 72.3294 \\ 236.0000 \end{bmatrix}\left[y - z_1\right] \tag{26}$$

where $a = 0.03$ (as in the chaotic case).

For numerical simulations, the initial conditions are chosen as

$$x(0) = \begin{bmatrix} 1.5 \\ 2.4 \\ 1.8 \end{bmatrix} \text{ and } z(0) = \begin{bmatrix} 2.6 \\ 4.7 \\ 2.9 \end{bmatrix} \tag{27}$$

Figures 5, 6 and 7 depict the exponential convergence of the observer states z_1, z_2, z_3 of the system (26) to the plant states x_1, x_2, x_3 of the Wei-Wang system (16).

Figure 8 depicts the exponential convergence of the estimation errors e_1, e_2, e_3.

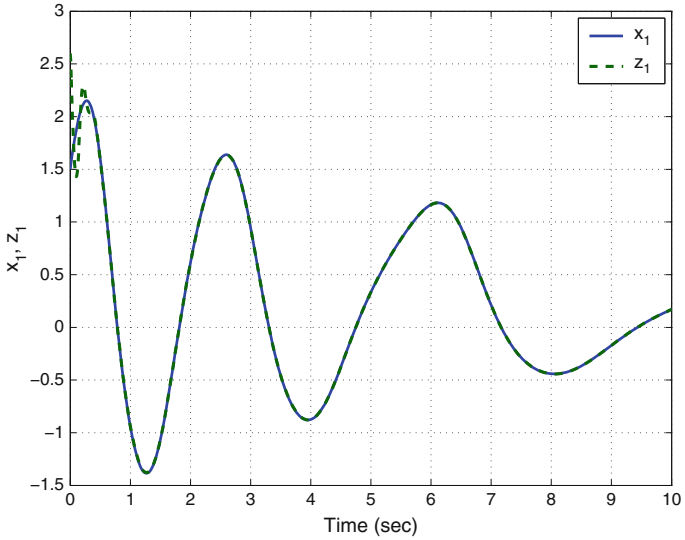

Fig. 5 Synchronization of the states x_1 and z_1

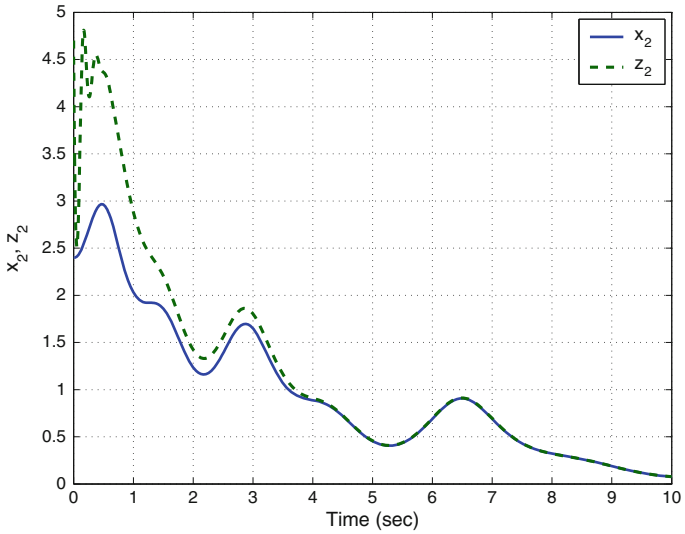

Fig. 6 Synchronization of the states x_2 and z_2

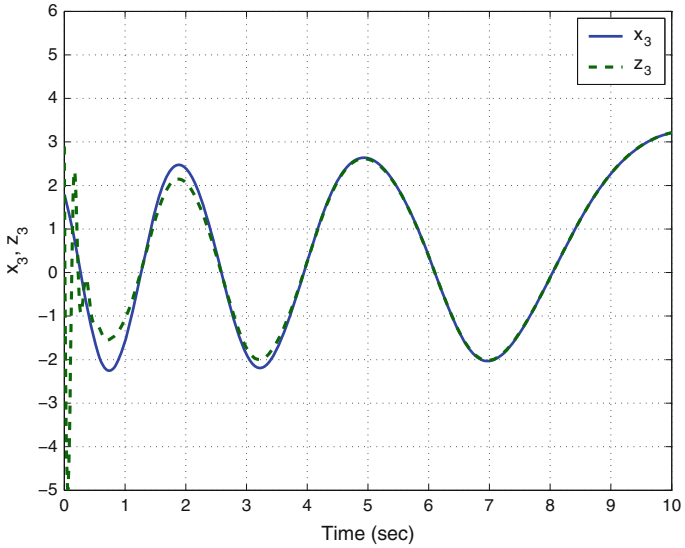

Fig. 7 Synchronization of the states x_3 and z_3

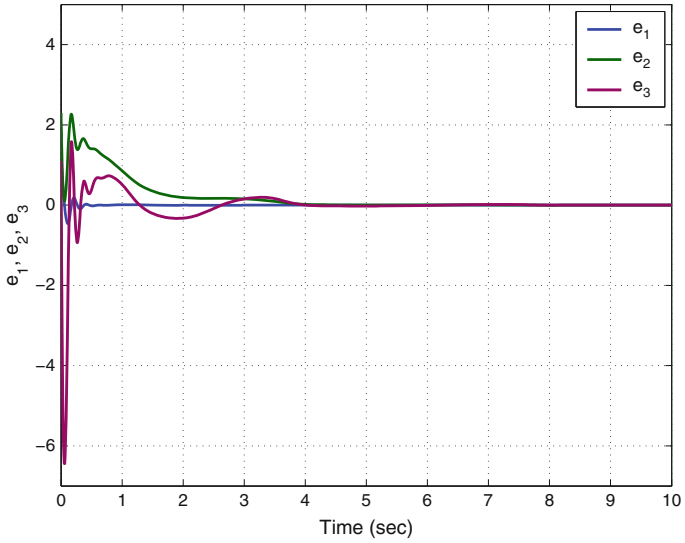

Fig. 8 Time-history of the estimation errors e_1, e_2, e_3

5 Dynamic Analysis of the Kingni-Jafari Chaotic System

The Kingni-Jafari chaotic system [13] is described by the 3-D dynamics

$$\begin{aligned} \dot{x}_1 &= -x_3 \\ \dot{x}_2 &= -x_1 - x_3 \\ \dot{x}_3 &= 3x_1 - ax_2 + x_1^2 - x_3^2 - x_2x_3 + b \end{aligned} \tag{28}$$

where a, b are constant, positive parameters.

The system (28) exhibits a chaotic attractor when $a = 1.3$ and $b = 1.01$.

For numerical simulations, we take the initial conditions as

$$x_1(0) = 0.1, \quad x_2(0) = 0.1, \quad x_3(0) = 0.1 \tag{29}$$

Figure 9 shows the 3-D phase portrait of the Kingni-Jafari chaotic system (28). Figures 10, 11 and 12 show the 2-D projections of the Kingni-Jafari chaotic system (28) on the (x_1, x_2), (x_2, x_3) and (x_1, x_3) coordinate planes respectively.

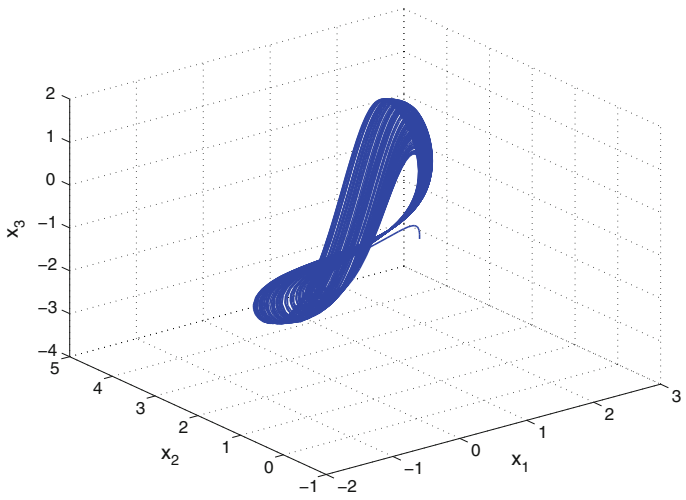

Fig. 9 3-D phase portrait of the Kingni-Jafari chaotic system

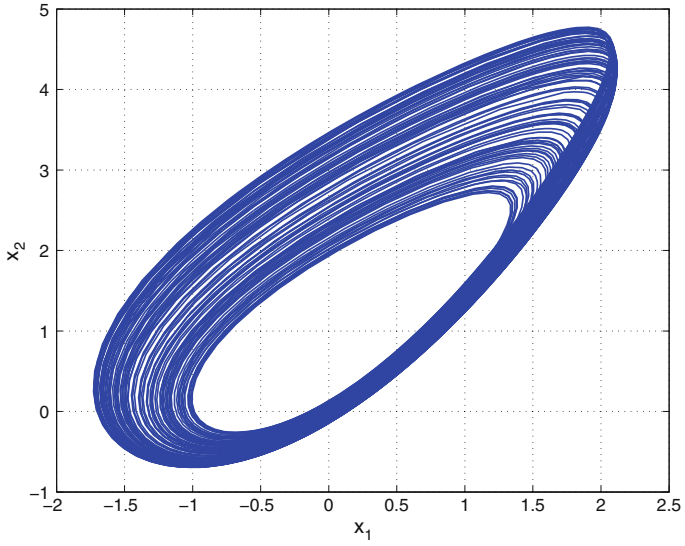

Fig. 10 2-D projection of the Kingni-Jafari chaotic system on the (x_1, x_2) plane

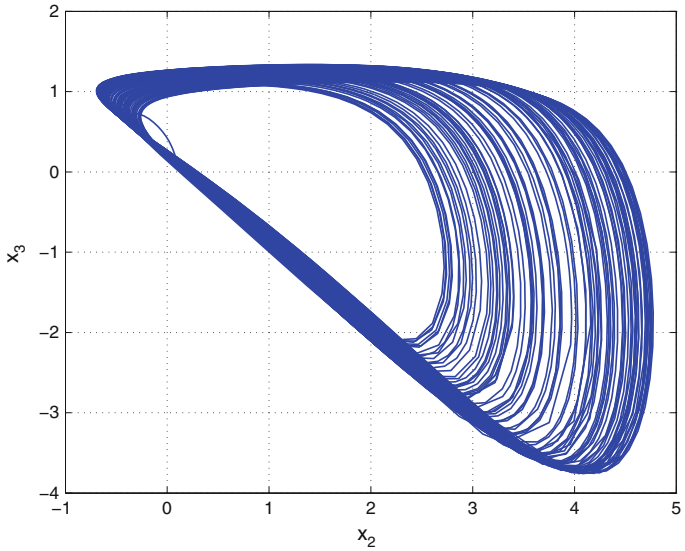

Fig. 11 2-D projection of the Kingni-Jafari chaotic system on the (x_2, x_3) plane

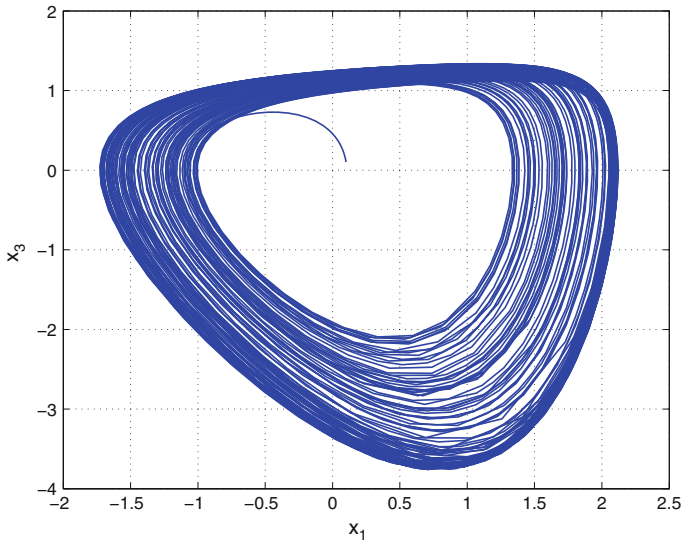

Fig. 12 2-D projection of the Kingni-Jafari chaotic system on the (x_1, x_3) plane

It is known that the Kingni-Jafari chaotic system (28) has a stable equilibrium at

$$x^\star = \begin{bmatrix} 0 \\ b/a \\ 0 \end{bmatrix} = \begin{bmatrix} 0 \\ 0.7769 \\ 0 \end{bmatrix} \tag{30}$$

Also, the Lyapunov exponents of the Kingni-Jafari chaotic system (28) for the parameter values $a = 1.3, b = 1.01$ and for the initial values (29) are numerically found as

$$L_1 = 0.0933, \quad L_2 = 0, \quad L_3 = -1.2969 \tag{31}$$

Thus, the Kaplan–Yorke dimension of the Kingni-Jafari chaotic system (28) is found as

$$D_{KY} = 2 + \frac{L_1 + L_2}{|L_3|} = 2.0719 \tag{32}$$

6 Nonlinear Observer Design for the Kingni-Jafari Chaotic System

This section investigates the problem of nonlinear observer design for the Kingni-Jafari chaotic system described by the dynamics

$$\begin{aligned}\dot{x}_1 &= -x_3\\ \dot{x}_2 &= -x_1 - x_3\\ \dot{x}_3 &= 3x_1 - ax_2 + x_1^2 - x_3^2 - x_2x_3 + b\end{aligned} \tag{33}$$

where a is a positive parameter.

The system (33) is chaotic when $a = 1.3$ and $b = 1.01$. In the chaotic case, the system (33) has a stable equilibrium point

$$x^\star = \begin{bmatrix} 0\\ 0.7769\\ 0\end{bmatrix} \tag{34}$$

We consider the output function as

$$y = x_1 \tag{35}$$

The linearization of the plant dynamics (33) at $x = x^\star$ is given by

$$A = \frac{\partial f}{\partial x}\left(x^\star\right) = \begin{bmatrix} a & x_3^\star & x_2^\star\\ 2x_1^\star & -1 & 0\\ -4 & 0 & 0\end{bmatrix} = \begin{bmatrix} 0 & 0 & -1\\ -1 & 0 & -1\\ 3 & -1.3 & -0.7769\end{bmatrix} \tag{36}$$

Also, the linearization of the output function (35) at $x = x^\star$ is given by

$$C = \frac{\partial h}{\partial x}\left(x^\star\right) = \begin{bmatrix}1 & 0 & 0\end{bmatrix} \tag{37}$$

From (36) and (37), the observability matrix for the Kingni-Jafari system (33) with the output (35) is given by

$$\mathbf{O}(C, A) = \begin{bmatrix} C\\ CA\\ CA^2\end{bmatrix} = \begin{bmatrix} 1 & 0 & 0\\ 0 & 0 & -1\\ -3 & 1.3 & 0.7769\end{bmatrix} \tag{38}$$

We find that

$$\det[\mathbf{O}(C, A)] = 1.3 \neq 0 \tag{39}$$

which shows that $\mathbf{O}(C, A)$ has full rank. Thus, (C, A) is completely observable [22].

Since the equilibrium $x = x^\star$ is Lyapunov stable, by Sundarapandian's theorem (Theorem 1), we obtain the following result, which gives a construction of nonlinear observer for the Kingni-Jafari chaotic system.

Theorem 3 *The Kingni-Jafari chaotic system (33) with the output (35) has a local exponential observer of the form*

$$\begin{bmatrix} \dot{z}_1 \\ \dot{z}_2 \\ \dot{z}_3 \end{bmatrix} = \begin{bmatrix} -z_3 \\ -z_1 - z_3 \\ 3z_1 - az_2 + z_1^2 - z_3^2 - z_2 z_3 + b \end{bmatrix} + K\left[y - z_1\right] \tag{40}$$

where K is a matrix chosen such that $A - KC$ is Hurwitz. Since (C, A) is observable, a gain matrix K can be found such that the error matrix $E = A - KC$ has arbitrarily assigned set of stable eigenvalues. ■

For numerical simulations, we find an observer gain matrix K so that

$$\text{eig}(A - KC) = \{-6, -6, -6\} \tag{41}$$

Using MATLAB, we get

$$K = \begin{bmatrix} 17.2231 \\ 182.3769 \\ -92.9194 \end{bmatrix} \tag{42}$$

Thus, a local exponential observer for the Wei-Wang system (16) is given by

$$\begin{bmatrix} \dot{z}_1 \\ \dot{z}_2 \\ \dot{z}_3 \end{bmatrix} = \begin{bmatrix} -z_3 \\ -z_1 - z_3 \\ 3z_1 - az_2 + z_1^2 - z_3^2 - z_2 z_3 + b \end{bmatrix} + \begin{bmatrix} 17.2231 \\ 182.3769 \\ -92.9194 \end{bmatrix}\left[y - z_1\right] \tag{43}$$

where $a = 1.3$ and $b = 1.01$ (as in the chaotic case).

For numerical simulations, the initial conditions are chosen as

$$x(0) = \begin{bmatrix} 3.7 \\ 5.2 \\ 2.8 \end{bmatrix} \text{ and } z(0) = \begin{bmatrix} 1.6 \\ 2.4 \\ 1.9 \end{bmatrix} \tag{44}$$

Figures 13, 14 and 15 depict the exponential convergence of the observer states z_1, z_2, z_3 of the system (43) to the plant states x_1, x_2, x_3 of the Kingni-Jafari system (33).

Figure 16 depicts the exponential convergence of the estimation errors e_1, e_2, e_3.

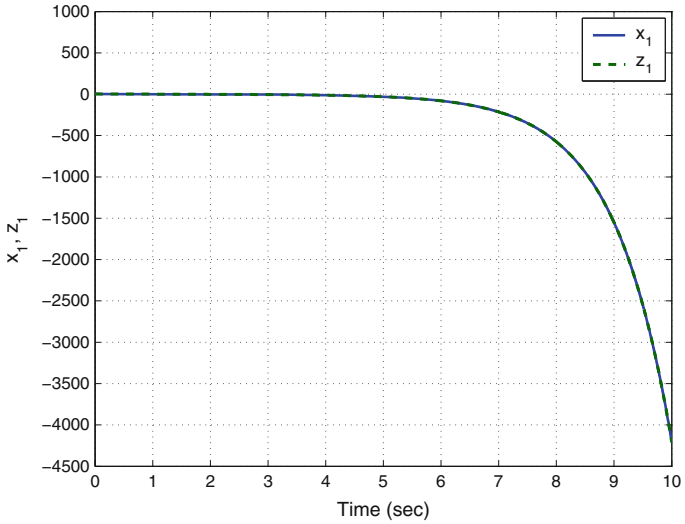

Fig. 13 Synchronization of the states x_1 and z_1

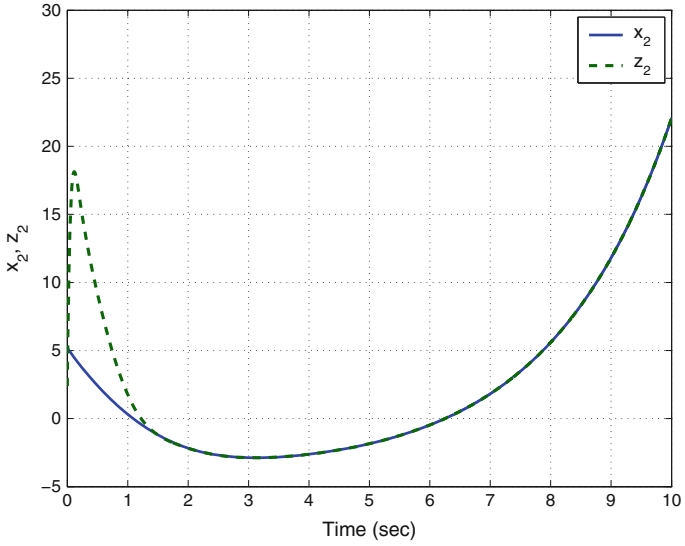

Fig. 14 Synchronization of the states x_2 and z_2

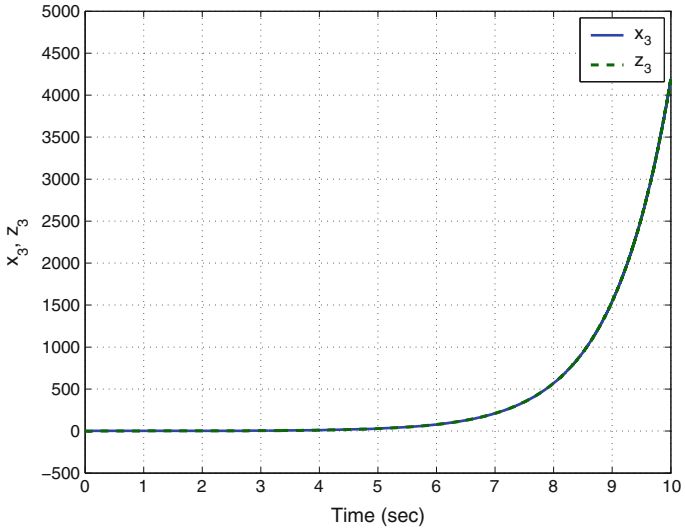

Fig. 15 Synchronization of the states x_3 and z_3

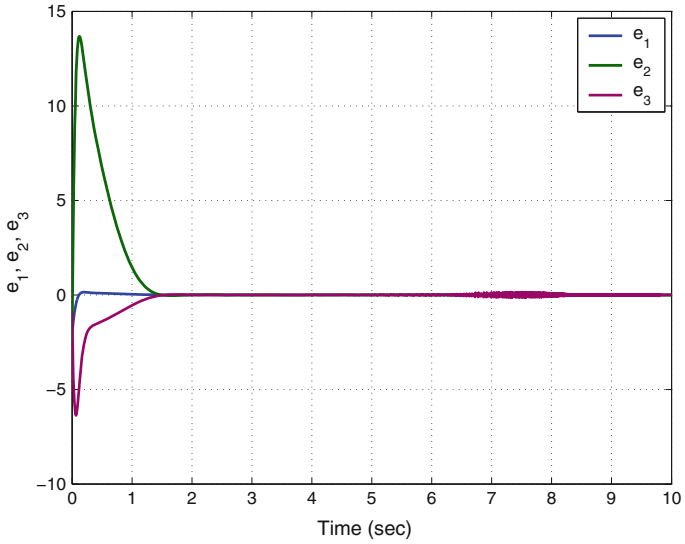

Fig. 16 Time-history of the estimation errors e_1, e_2, e_3

7 Conclusions

For many real world problems of chaotic systems, an efficient monitoring system is of great importance. In this work, the methodology based on Sundarapandian's theorem (2002) for exponential observer design is applied for the monitoring of chaotic systems with stable equilibria such as Wei-Wang system (2013) and Kingni-Jafari system (2014). MATLAB simulations have been shown to illustrate the phase portraits and nonlinear observer design for the Wei-Wang and Kingni-Jafari chaotic systems.

References

1. Arneodo A, Coullet P, Tresser C (1981) Possible new strange attractors with spiral structure. Commun Math Phys 79(4):573–576
2. Azar AT, Vaidyanathan S (2015a) Chaos modeling and control systems design, Studies in computational intelligence. Springer, Germany
3. Azar AT, Vaidyanathan S (2015b) Computational intelligence applications in modeling and control, studies in computational intelligence. Springer, Germany
4. Barrow-Green J (1997) Poincaré and the three body problem. American Mathematical Society, Providence
5. Besancon G (2007) Nonlinear observers and applications, Lecture notes in control and information sciences. Springer, Germany
6. Cai G, Tan Z (2007) Chaos synchronization of a new chaotic system via nonlinear control. J Uncertain Syst 1(3):235–240
7. Carroll TL, Pecora LM (1991) Synchronizing chaotic circuits. IEEE Trans Circuits Syst 38(4):453–456
8. Celle F, Gauthier JP, Kazakos D, Salle G (1989) Synthesis of nonlinear observers: a harmonic analysis approach. Math Syst Theory 22:291–322
9. Chen G, Ueta T (1999) Yet another chaotic attractor. Int J Bifurc Chaos 9(7):1465–1466
10. Chen HK, Lee CI (2004) Anti-control of chaos in rigid body motion. Chaos, Solitons Fractals 21(4):957–965
11. Gauthier JP, Hammouri H, Othman S (1992) A simple observer for nonlinear systems—Applications to bioreactors. IEEE Trans Autom Control 37:875–880
12. Karthikeyan R, Sundarapandian V (2014) Hybrid chaos synchronization of four-scroll systems via active control. J Electr Eng 65(2):97–103
13. Kingni ST, Jafari S, Simo H, Woafo P (2014) Three-dimensional chaotic autonomous system with only one stable equilibrium: analysis, circuit design, parameter estimation, control, synchronization and its fractional-order form. Eur Phys J Plus 129(5):1–16
14. Kou SR, Elliott DL, Tarn TJ (1975) Exponential observers for nonlinear dynamic systems. Inf Control 29(3):204–216
15. Krener AJ, Isidori A (1983) Linearization by output injection and nonlinear observers. Syst Control Lett 3:47–52
16. Krener AJ, Respondek W (1985) Nonlinear observers with linearizable error dynamics. SIAM J Control and Optim 23:197–216
17. Li D (2008) A three-scroll chaotic attractor. Phys Lett A 372(4):387–393
18. Liu C, Liu T, Liu L, Liu K (2004) A new chaotic attractor. Chaos, Solitions Fractals 22(5):1031–1038
19. Lorenz EN (1963) Deterministic periodic flow. J Atmos Sci 20(2):130–141
20. Lü J, Chen G (2002) A new chaotic attractor coined. Int J Bifurc Chaos 12(3):659–661

21. Luenberger DG (1966) Observers for multivariable linear systems. IEEE Trans Autom Control 2:190–197
22. Ogata K (2009) Modern control engineerng, 5th edn. Prentice Hall, New Jersey
23. Pecora LM, Carroll TL (1990) Synchronization in chaotic systems. Phys Rev Lett 64(8):821–824
24. Pehlivan I, Moroz IM, Vaidyanathan S (2014) Analysis, synchronization and circuit design of a novel butterfly attractor. J Sound Vib 333(20):5077–5096
25. Rasappan S, Vaidyanathan S (2012a) Global chaos synchronization of WINDMI and Coullet chaotic systems by backstepping control. Far East J Math Sci 67(2):265–287
26. Rasappan S, Vaidyanathan S (2012b) Hybrid synchronization of n-scroll Chua and Lur'e chaotic systems via backstepping control with novel feedback. Arch Control Sci 22(3):343–365
27. Rasappan S, Vaidyanathan S (2012c) Synchronization of hyperchaotic Liu system via backstepping control with recursive feedback. Commun Comput Inform Sci 305:212–221
28. Rasappan S, Vaidyanathan S (2013) Hybrid synchronization of *n*-scroll chaotic Chua circuits using adaptive backstepping control design with recursive feedback. Malays J Math Sci 7(2):219–246
29. Rasappan S, Vaidyanathan S (2014) Global chaos synchronization of WINDMI and Coullet chaotic systems using adaptive backstepping control design. Kyungpook Math J 54(1):293–320
30. Rössler OE (1976) An equation for continuous chaos. Phys Lett A 57(5):397–398
31. Sarasu P, Sundarapandian V (2011a) Active controller design for the generalized projective synchronization of four-scroll chaotic systems. Int J Syst Signal Control Eng Appl 4(2):26–33
32. Sarasu P, Sundarapandian V (2011b) The generalized projective synchronization of hyperchaotic Lorenz and hyperchaotic Qi systems via active control. Int J Soft Comput 6(5):216–223
33. Sarasu P, Sundarapandian V (2012a) Adaptive controller design for the generalized projective synchronization of 4-scroll systems. Int J Syst Signal Control Eng Appl 5(2):21–30
34. Sarasu P, Sundarapandian V (2012b) Generalized projective synchronization of three-scroll chaotic systems via adaptive control. Eur J Sci Res 72(4):504–522
35. Sarasu P, Sundarapandian V (2012c) Generalized projective synchronization of two-scroll systems via adaptive control. Int J Soft Comput 7(4):146–156
36. Sprott JC (1994) Some simple chaotic flows. Phys Rev E 50(2):647–650
37. Sundarapandian V (2002a) Global observer design for nonlinear systems. Math Comput Model 35(1–2):45–54
38. Sundarapandian V (2002b) Local observer design for nonlinear systems. Math Comput Model 35(1–2):25–36
39. Sundarapandian V (2002c) Nonlinear observer design for bifurcating systems. Math Comput Model 36(1–2):183–188
40. Sundarapandian V (2002d) Nonlinear observer design for discrete-time bifurcating systems. Math Comput Model 36(1–2):211–215
41. Sundarapandian V (2002e) Observer design for discrete-time nonlinear systems. Math Comput Model 35(1–2):37–44
42. Sundarapandian V (2003a) Exponential observer design for discrete-time nonlinear systems with real parametric uncertainty. Math Comput Model 37(1–2):191–204
43. Sundarapandian V (2003b) Exponential observer design for nonlinear systems with real parametric uncertainty. Math Comput Model 37(1–2):177–190
44. Sundarapandian V (2004a) General observers for discrete-time nonlinear systems. Math Comput Model 39(1):87–95
45. Sundarapandian V (2004b) General observers for nonlinear systems. Math Comput Model 39(1):97–105
46. Sundarapandian V (2004c) New results on general observers for discrete-time nonlinear systems. Appl Math Lett 17(12):1415–1420
47. Sundarapandian V (2004d) New results on general observers for nonlinear systems. Appl Math Lett 17(12):1421–1426

48. Sundarapandian V (2005a) Nonlinear observer design for a general class of discrete-time nonlinear systems with real parametric uncertainty. Comput Math Appl 49(7–8):1177–1194
49. Sundarapandian V (2005b) Nonlinear observer design for a general class of nonlinear systems with real parametric uncertainty. Comput Math Appl 49(7–8):1195–1211
50. Sundarapandian V (2010) Output regulation of the Lorenz attractor. Far East J Math Sci 42(2):289–299
51. Sundarapandian V (2013) Analysis and anti-synchronization of a novel chaotic system via active and adaptive controllers. J Eng Sci Technol Rev 6(4):45–52
52. Sundarapandian V, Karthikeyan R (2011a) Anti-synchronization of hyperchaotic Lorenz and hyperchaotic Chen systems by adaptive control. Int J Syst Signal Control Eng Appl 4(2):18–25
53. Sundarapandian V, Karthikeyan R (2011b) Anti-synchronization of Lü and Pan chaotic systems by adaptive nonlinear control. Eur J Sci Res 64(1):94–106
54. Sundarapandian V, Karthikeyan R (2012a) Adaptive anti-synchronization of uncertain Tigan and Li systems. J Eng Appl Sci 7(1):45–52
55. Sundarapandian V, Karthikeyan R (2012b) Hybrid synchronization of hyperchaotic Lorenz and hyperchaotic Chen systems via active control. J Eng Appl Sci 7(3):254–264
56. Sundarapandian V, Pehlivan I (2012) Analysis, control, synchronization, and circuit design of a novel chaotic system. Math Comput Model 55(7–8):1904–1915
57. Sundarapandian V, Sivaperumal S (2011) Sliding controller design of hybrid synchronization of four-wing chaotic systems. Int J Soft Comput 6(5):224–231
58. Suresh R, Sundarapandian V (2013) Global chaos synchronization of a family of *n*-scroll hyperchaotic Chua circuits using backstepping control with recursive feedback. Far East J Math Sci 73(1):73–95
59. Thau FE (1973) Observing the states of nonlinear dynamical systems. Int J Control 18:471–479
60. Tigan G, Opris D (2008) Analysis of a 3D chaotic system. Chaos, Solitons Fractals 36:1315–1319
61. Tsinias J (1989) Observer design for nonlinear systems. Syst Control Lett 13:135–142
62. Vaidyanathan S (2011) Hybrid chaos synchronization of Liu and Lü systems by active nonlinear control. Commun Comput Inform Sci 204:1–10
63. Vaidyanathan S (2012a) Analysis and synchronization of the hyperchaotic Yujun systems via sliding mode control. Adv Intell Syst Comput 176:329–337
64. Vaidyanathan S (2012b) Anti-synchronization of Sprott-L and Sprott-M chaotic systems via adaptive control. Int J Control Theory Appl 5(1):41–59
65. Vaidyanathan S (2012c) Global chaos control of hyperchaotic Liu system via sliding control method. Int J Control Theory Appl 5(2):117–123
66. Vaidyanathan S (2012d) Output regulation of the Liu chaotic system. Appl Mech Mater 110–116:3982–3989
67. Vaidyanathan S (2012e) Sliding mode control based global chaos control of Liu-Liu-Liu-Su chaotic system. Int J Control Theory Appl 5(1):15–20
68. Vaidyanathan S (2013a) A new six-term 3-D chaotic system with an exponential nonlinearity. Far East J Math Sci 79(1):135–143
69. Vaidyanathan S (2013b) Analysis and adaptive synchronization of two novel chaotic systems with hyperbolic sinusoidal and cosinusoidal nonlinearity and unknown parameters. J Eng Sci Technol Rev 6(4):53–65
70. Vaidyanathan S (2013c) Analysis, control and synchronization of hyperchaotic Zhou system via adaptive control. Adv Intel Syst Comput 177:1–10
71. Vaidyanathan S (2014a) A new eight-term 3-D polynomial chaotic system with three quadratic nonlinearities. Far East J Math Sci 84(2):219–226
72. Vaidyanathan S (2014b) Analysis and adaptive synchronization of eight-term 3-D polynomial chaotic systems with three quadratic nonlinearities. Eur Phys J: Special Top 223(8):1519–1529
73. Vaidyanathan S (2014c) Analysis, control and synchronisation of a six-term novel chaotic system with three quadratic nonlinearities. Int J Model Identif and Control 22(1):41–53

74. Vaidyanathan S (2014d) Generalized projective synchronisation of novel 3-D chaotic systems with an exponential non-linearity via active and adaptive control. Int J Model Identif Control 22(3):207–217
75. Vaidyanathan S (2014e) Global chaos synchronization of identical Li-Wu chaotic systems via sliding mode control. Int J Model Identif Control 22(2):170–177
76. Vaidyanathan S (2015) Analysis, properties and control of an eight-term 3-D chaotic system with an exponential nonlinearity. International Journal of Modelling, Identification and Control 23(2):164–172
77. Vaidyanathan S, Azar AT (2015a) Analysis and control of a 4-D novel hyperchaotic system. In: Azar AT, Vaidyanathan S (eds) Chaos modeling and control systems design, vol 581., Studies in computationali ntelligenceSpringer, Germany, pp 19–38
78. Vaidyanathan S, Azar AT (2015b) Analysis, control and synchronization of a nine-term 3-D novel chaotic system. In: Azar AT, Vaidyanathan S (eds) Chaos modelling and control systems design, vol 581., Studies in computational intelligenceSpringer, Germany, pp 19–38
79. Vaidyanathan S, Azar AT (2015c) Anti-synchronization of identical chaotic systems using sliding mode control and an application to Vaidhyanathan-Madhavan chaotic systems. Stud Computat Intell 576:527–547
80. Vaidyanathan S, Azar AT (2015d) Hybrid synchronization of identical chaotic systems using sliding mode control and an application to Vaidhyanathan chaotic systems. Stud Comput Intell 576:549–569
81. Vaidyanathan S, Madhavan K (2013) Analysis, adaptive control and synchronization of a seven-term novel 3-D chaotic system. Int J Control Theory Appl 6(2):121–137
82. Vaidyanathan S, Pakiriswamy S (2013) Generalized projective synchronization of six-term Sundarapandian chaotic systems by adaptive control. Int J Control Theory and Appl 6(2):153–163
83. Vaidyanathan S, Rajagopal K (2011a) Anti-synchronization of Li and T chaotic systems by active nonlinear control. Commun Comput Inform Sci 198:175–184
84. Vaidyanathan S, Rajagopal K (2011b) Global chaos synchronization of hyperchaotic Pang and Wang systems by active nonlinear control. Commun Comput Inform Sci 204:84–93
85. Vaidyanathan S, Rajagopal K (2011c) Global chaos synchronization of Lü and Pan systems by adaptive nonlinear control. Commun Comput Information Sci 205:193–202
86. Vaidyanathan S, Rajagopal K (2012) Global chaos synchronization of hyperchaotic Pang and hyperchaotic Wang systems via adaptive control. Int J Soft Comput 7(1):28–37
87. Vaidyanathan S, Rasappan S (2011) Global chaos synchronization of hyperchaotic Bao and Xu systems by active nonlinear control. Commun Comput Inform Sci 198:10–17
88. Vaidyanathan S, Rasappan S (2014) Global chaos synchronization of *n*-scroll Chua circuit and Lur'e system using backstepping control design with recursive feedback. Arab J Sci Eng 39(4):3351–3364
89. Vaidyanathan S, Sampath S (2011) Global chaos synchronization of hyperchaotic Lorenz systems by sliding mode control. Commun Comput Inform Sci 205:156–164
90. Vaidyanathan S, Sampath S (2012) Anti-synchronization of four-wing chaotic systems via sliding mode control. Int J Autom Comput 9(3):274–279
91. Vaidyanathan S, Volos C, Pham VT (2014a) Hyperchaos, adaptive control and synchronization of a novel 5-D hyperchaotic system with three positive Lyapunov exponents and its SPICE implementation. Arch Control Sci 24(4):409–446
92. Vaidyanathan S, Volos C, Pham VT, Madhavan K, Idowu BA (2014b) Adaptive backstepping control, synchronization and circuit simulation of a 3-D novel jerk chaotic system with two hyperbolic sinusoidal nonlinearities. Arch Control Sci 24(3):375–403
93. Vaidyanathan S, Idowu BA, Azar AT (2015a) Backstepping controller design for the global chaos synchronization of Sprott's jerk systems. Stud Comput Intell 581:39–58
94. Vaidyanathan S, Volos C, Pham VT, Madhavan K (2015b) Analysis, adaptive control and synchronization of a novel 4-D hyperchaotic hyperjerk system and its SPICE implementation. Arch Control Sci 25(1):5–28

95. Vaidyanathan S, Volos CK, Pham VT (2015c) Global chaos control of a novel nine-term chaotic system via sliding mode control. In: Azar AT, Zhu Q (eds) Advances and applications in sliding mode control systems, vol 576., Studies in computational intelligenceSpringer, Germany, pp 571–590
96. Wei Z, Wang Z (2013) Chaotic behavior and modified function projective synchronization of a simple system with one stable equilibrium. Kybernetika 49(2):359–374
97. Wei Z, Yang Q (2010) Anti-control of Hopf bifurcation in the new chaotic system with two stable node-foci. Appl Math Comput 217(1):422–429
98. Xia XH, Gao WB (1988a) Nonlinear observer design by canonical form. Int J Control 47:1081–1100
99. Xia XH, Gao WB (1988b) On exponential observers for nonlinear systems. Syst Control Lett 11:319–325
100. Zhou W, Xu Y, Lu H, Pan L (2008) On dynamics analysis of a new chaotic attractor. Phys Lett A 372(36):5773–5777
101. Zhu C, Liu Y, Guo Y (2010) Theoretic and numerical study of a new chaotic system. Intell Inform Manag 2:104–109

Nonlinear Observer Design for Population Biology Systems

Sundarapandian Vaidyanathan

Abstract This work investigates the nonlinear observer design for Lotka–Volterra population models. Explicitly, Sundarapandian's theorem (2002) for local exponential observer design for nonlinear systems is used to solve the problem of observer design for Lotka–Volterra systems. Predator-prey population models for two species and three species are studied and nonlinear observers for these multi-species models are constructed by applying Sundarapandian's theorem (2002) and using only the plant dynamics equations of the Lotka–Volterra models and the prey population sizes as the output functions. Numerical examples and MATLAB simulations are provided to demonstrate the nonlinear observer design for the multi-species Lotka–Volterra models.

Keywords Lotka–Volterra models · Nonlinear observers · Observability · Ecosystems

1 Introduction

Many control system designs are based on state vector feedback, where the input to the system is a function only of the current state vector. In many situations, the system state vector is not readily available for measurement. In these situations, it is not possible to evaluate the control function readily with the state vector, and hence either the control scheme must be abandoned, or a reasonable substitute for the state vector must be found. An observer for a plant is a system which performs the reconstruction of the state vector from the available inputs.

S. Vaidyanathan (✉)
Research and Development Centre, Vel Tech University, Avadi,
Chennai 600062, Tamil Nadu, India
e-mail: sundarvtu@gmail.com

S. Vaidyanathan and C. Volos (eds.), *Advances and Applications in Nonlinear Control Systems*, Studies in Computational Intelligence 635,
DOI 10.1007/978-3-319-30169-3_3

The problem of designing observers for linear control systems was first introduced and fully solved by Luenberger [12]. The problem of designing observers for nonlinear control systems was proposed by Thau [27]. Over the past three decades, significant attention has been paid in the control systems literature on the construction of observers for nonlinear control systems [1].

A necessary condition for the existence of a local exponential observer for nonlinear control systems was obtained by Xia and Gao [32]. On the other hand, sufficient conditions for nonlinear observers have been derived in the control literature from an impressive variety of points of view. Kou et al. [6] derived sufficient conditions for the existence of local exponential observers using Lyapunov-like method. In [4, 7, 8, 31], suitable coordinate transformations were found under which a nonlinear control systems is transferred into a canonical form, where the observer design is carried out. In [28], Tsinias derived sufficient Lyapunov-like conditions for the existence of local asymptotic observers for nonlinear systems. A harmonic analysis method was proposed in [2] for the synthesis of nonlinear observers.

A characterization of local exponential observers for nonlinear control systems was first obtained by Sundarapandian [15]. In [15], necessary and sufficient conditions were obtained for exponential observers for Lyapunov stable continuous-time nonlinear systems and an exponential observer design was provided by Sundarapandian which generalizes the linear observer design of Luenberger [12] for linear control systems. In [18], Sundarapandian obtained necessary and sufficient conditions for exponential observers for Lyapunov stable discrete-time nonlinear systems and also provided a formula for designing exponential observers for Lyapunov stable discrete-time nonlinear systems. In [14], Sundarapandian derived new results for the global observer design for nonlinear control systems.

The concept of nonlinear observers for nonlinear control systems was also extended in many ways. In [16, 17], Sundarapandian derived new results characterizing local exponential observers for nonlinear bifurcating systems. In [19, 20, 25, 26], Sundarapandian derived new results for the exponential observer design for a general class of nonlinear systems with real parametric uncertainty. In [21–24], Sundarapandian derived new results and characterizations for general observers for nonlinear systems.

This work discusses the nonlinear observer design for Lotka–Volterra population models. An important classical model of nonlinear dynamical systems is the two species population dynamics model, which was discovered independently by an Italian mathematician, Vito Volterra [30] and an American biophysicist, Alfred Lotka [11]. Recently, there has been significant interest in the application of mathematical systems theory to population biology systems [3, 9, 10, 29].

This work is organized as follows. Section 2 reviews the definition and results of local exponential observers for nonlinear systems. Section 3 details the design of local exponential observers for two species Lotka–Volterra systems. Section 4 details the design of local exponential observers for three species Lotka–Volterra systems. Section 5 provides the conclusions of this work.

2 Review of Nonlinear Observer Design for Nonlinear Systems

By the concept of a *state observer* for a nonlinear system, it is meant that from the observation of certain states of the system considered as *outputs* or *indicators*, it is desired to estimate the state of the whole system as a function of time. Mathematically, observers for nonlinear systems are defined as follows.

Consider the nonlinear system described by

$$\dot{x} = f(x) \tag{1a}$$
$$y = h(x) \tag{1b}$$

where $x \in \mathbf{R}^n$ is the *state* and $y \in \mathbf{R}^p$ is the *output*.

It is assumed that $f : \mathbf{R}^n \to \mathbf{R}^n$, $h : \mathbf{R}^n \to \mathbf{R}^p$ are C^1 mappings and for some $x^\star \in \mathbf{R}^n$, the following hold:

$$f(x^\star) = 0, \quad h(x^\star) = 0 \tag{2}$$

Remark 1 The solutions $x^\star$ of $f(x) = 0$ are called the *equilibrium points* of the plant dynamics (1a). Also, the assumption $h(x^\star) = 0$ holds without any loss of generality. Indeed, if $h(x^\star) \neq 0$, then we can define a new output function as

$$\psi(x) = h(x) - h(x^\star) \tag{3}$$

and it is easy to see that $\psi(x^\star) = 0$. ■

The linearization of the nonlinear system (1a) and (1b) at $x = x^\star$ is given by

$$\dot{x} = Ax \tag{4a}$$
$$y = Cx \tag{4b}$$

where

$$A = \left[\frac{\partial f}{\partial x}\right]_{x=x^\star} \quad \text{and} \quad C = \left[\frac{\partial h}{\partial x}\right]_{x=x^\star} \tag{5}$$

Definition 1 ([15]) A C^1 dynamical system defined by

$$\dot{z} = g(z, y), \quad (z \in \mathbf{R}^n) \tag{6}$$

is called a **local asymptotic** (respectively, **exponential**) **observer** for the nonlinear system (1a) and (1b) if the following two requirements are satisfied:

(i) If $z(0) = x(0)$, then $z(t) = x(t)$, for all $t \geq 0$.
(ii) There exists a neighbourhood V of the equilibrium $x^\star$ of $\mathbf{R}^n$ such that for all $z(0), x(0) \in V$, the estimation error

$$e(t) = z(t) - x(t) \tag{7}$$

decays asymptotically (respectively, exponentially) to zero as $t \to \infty$. ■

Theorem 1 ([15]) *Suppose that the nonlinear system dynamics (1a) is Lyapunov stable at the equilibrium $x = x^\star$ and that there exists a matrix K such that $A - KC$ is Hurwitz. Then the dynamical system defined by*

$$\dot{z} = f(z) + K[y - h(z)] \tag{8}$$

is a local exponential observer for the nonlinear system (1a) and (1b). ■

Remark 2 The estimation error is governed by the dynamics

$$\dot{e} = f(x + e) - f(x) - K[h(x + e) - h(x)] \tag{9}$$

Linearizing the error dynamics (9) at $x = x^\star$, we get the linear system

$$\dot{e} = Ee, \quad \text{where } E = A - KC \tag{10}$$

If (C, A) is observable, then the eigenvalues of $E = A - KC$ can be arbitrarily placed in the complex plane and thus a local exponential observer of the form (8) can always be found such that the transient response of the error decays quickly with any desired speed of convergence. ■

3 Nonlinear Observer Design for Two Species Lotka–Volterra Systems

In the 1920s, the Italian mathematician, Vito Volterra [30] proposed a model to describe the population dynamics of two interacting species, a predator and its prey. With this model, Volterra hoped to explain the observed increase in predator fish and corresponding decrease in the prey fish in the Adriatic Sea during the World War I.

Independently, the American biophysicist, Alfred Lotka [11] discovered the very same dynamical system to describe a hypothetical chemical reaction in which the chemical concentrations oscillate. Collectively, the two species interacting population dynamics model is referred to as *Lotka–Volterra system* or *predator–prey system*.

The two species Lotka–Volterra system is described by the following system of differential equations

$$\begin{aligned} \dot{x}_1 &= x_1(a - bx_2) \\ \dot{x}_2 &= x_2(-c + dx_1) \end{aligned} \tag{11}$$

where $x_2(t)$ and $x_1(t)$ represent, respectively, the predator and prey population as functions of time. The parameters a, b, c and d are all positive, where a represents the natural growth rate of the prey in the absence of predators, b represents the effect of predator on the prey, c represents the natural death rate of the predator in the absence of prey and d represents the efficiency and propagation rate of the predator in the presence of prey.

The equilibrium points of the Lotka–Volterra system (11) are obtained by setting $\dot{x}_1 = 0, \dot{x}_2 = 0$ and solving the resulting nonlinear equations for x_1 and x_2.

A simple calculation shows that the system (11) has two equilibrium points, *viz.*

$$\mathbf{0} = \begin{bmatrix} 0 \\ 0 \end{bmatrix} \quad \text{and} \quad x^\star = \begin{bmatrix} \frac{c}{d} \\ \frac{a}{b} \end{bmatrix} \tag{12}$$

Using Lyapunov stability theory [5], it can be easily shown that the equilibrium $x = \mathbf{0}$ is unstable, while the equilibrium $x = x^\star$ is Lyapunov stable.

Figure 1 depicts the state orbits of the two species Lotka–Volterra system (11) when $a = b = c = d = 0.5$.

Since only the stable equilibrium $x = x^\star$ pertains to problems of practical interest, we consider only the problem of nonlinear observer design for the two species Lotka–Volterra system (11) near $x = x^\star$.

Next, we suppose that the prey population is given as the output function of the Lotka–Volterra system (11), i.e.

$$y = x_1 - x_1^\star \tag{13}$$

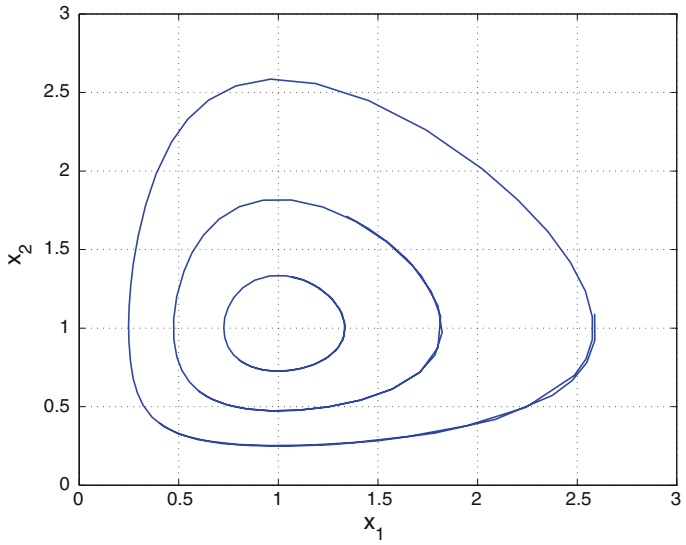

Fig. 1 State orbits of the two species Lotka–Volterra system

The linearization of the plant dynamics (11) at $x = x^\star$ is given by

$$A = \frac{\partial f}{\partial x}\left(x^\star\right) = \begin{bmatrix} 0 & -\frac{bc}{d} \\ \frac{ad}{b} & 0 \end{bmatrix} \tag{14}$$

Also, the linearization of the output function (13) at $x = x^\star$ is given by

$$C = \frac{\partial h}{\partial x}\left(x^\star\right) = \begin{bmatrix} 1 & 0 \end{bmatrix} \tag{15}$$

From (14) and (15), the observability matrix for the Lotka–Volterra system (11) with the output (13) is given by

$$\mathbf{O}(C, A) = \begin{bmatrix} C \\ CA \end{bmatrix} = \begin{bmatrix} 1 & 0 \\ 0 & -\frac{bc}{d} \end{bmatrix} \tag{16}$$

which has full rank since $a, b, c, d > 0$. Thus, (C, A) is completely observable [13].

Since the equilibrium $x = x^\star$ is Lyapunov stable, by Sundarapandian's theorem (Theorem 1), we obtain the following result, which gives a construction of nonlinear observer for the two species Lotka–Volterra system.

Theorem 2 *The two species Lotka–Volterra system (11) with the output (13) has a local exponential observer of the form*

$$\begin{bmatrix} \dot{z}_1 \\ \dot{z}_2 \end{bmatrix} = \begin{bmatrix} z_1(a - bz_2) \\ z_2(-c + dz_1) \end{bmatrix} + K\left[y - z_1 + x_1^\star\right] \tag{17}$$

where K is a matrix chosen such that $A - KC$ is Hurwitz. Since (C, A) is observable, a gain matrix K can be found such that the error matrix $E = A - KC$ has arbitrarily assigned set of stable eigenvalues. ■

Example 1 Consider a two species Lotka–Volterra system given by the dynamics

$$\begin{aligned} \dot{x}_1 &= x_1(2 - 0.4x_2) \\ \dot{x}_2 &= x_2(-2 + 0.5x_1) \end{aligned} \tag{18}$$

which has the positive equilibrium $x^\star = \begin{bmatrix} 4 \\ 5 \end{bmatrix}$.

The output function is taken as the prey population

$$y = x_1 - x_1^\star = x_1 - 4 \tag{19}$$

The linearization of the system dynamics (18) at $x = x^\star$ is

$$A = \begin{bmatrix} 0 & -\frac{bc}{d} \\ \frac{ad}{b} & 0 \end{bmatrix} = \begin{bmatrix} 0 & -1.6 \\ 2.5 & 0 \end{bmatrix} \tag{20}$$

Since (C, A) is observable, the eigenvalues of the error matrix $E = A - KC$ can be placed arbitrarily. Using the Ackermann's formula [13] for the observability gain matrix, we can choose K so that the error matrix $E = A - KC$ has the eigenvalues $\{-4, -4\}$.

A simple calculation using MATLAB yields $K = \begin{bmatrix} 8.0 \\ -7.5 \end{bmatrix}$.

By Theorem 2, a local exponential observer for the given two species Lotka–Volterra system (18) and (19) around $x^\star$ is given by

$$\begin{bmatrix} \dot{z}_1 \\ \dot{z}_2 \end{bmatrix} = \begin{bmatrix} z_1(2 - 0.4z_2) \\ z_2(-2 + 0.5z_1) \end{bmatrix} + \begin{bmatrix} 8.0 \\ -7.5 \end{bmatrix} \begin{bmatrix} y - z_1 + 4 \end{bmatrix} \tag{21}$$

For simulations, the initial conditions are chosen as $x(0) = \begin{bmatrix} 3 \\ 8 \end{bmatrix}$ and $z(0) = \begin{bmatrix} 6 \\ 2 \end{bmatrix}$.

Figures 2 and 3 depict the exponential convergence of the observer states z_1 and z_2 of the system (21) to the plant states x_1 and x_2 of the Lotka–Volterra system (18).

Figure 4 depicts the exponential convergence of the estimation errors e_1, e_2.

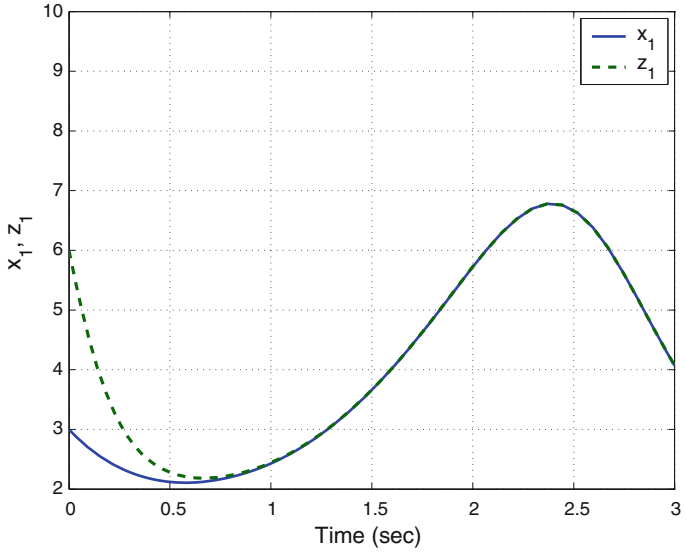

Fig. 2 Synchronization of the states x_1 and z_1

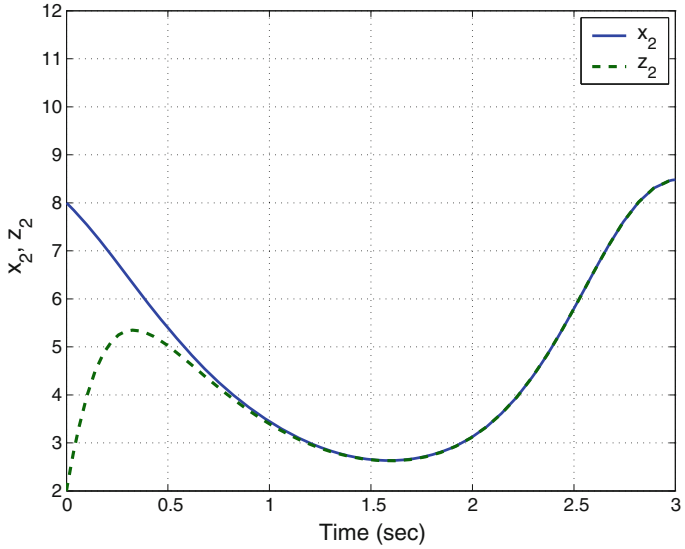

Fig. 3 Synchronization of the states x_2 and z_2

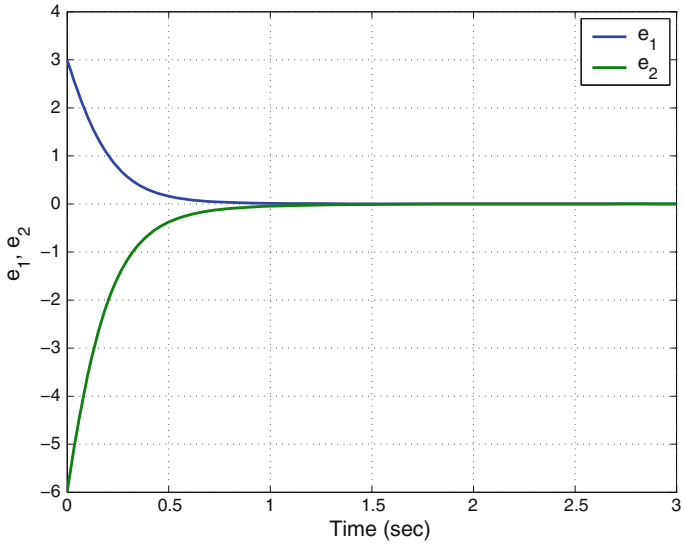

Fig. 4 Time-history of the estimation errors e_1, e_2

4 Nonlinear Observer Design for Three Species Lotka–Volterra Systems

This section investigates the problem of nonlinear observer design for three species Lotka–Volterra predator-prey system where the lowest level prey x_1 is preyed upon by a mid-level species x_2, which is, in turn, preyed upon by a top-level species x_3. Typical examples of such three species Lotka–Volterra ecosystems are mouse-snake-owl, grass-hare-lynx and worm-robin-falcon ecosystems.

The three species Lotka–Volterra system is described by the following system of differential equations

$$\begin{aligned} \dot{x}_1 &= x_1(a - bx_2) \\ \dot{x}_2 &= x_2(-c + dx_1 - \alpha x_3) \\ \dot{x}_3 &= x_3(-f + gx_2) \end{aligned} \tag{22}$$

where the parameters $a, b, c, d, \alpha, f, g > 0$.

A simple calculation shows that the three species Lotka–Volterra system (22) has two equilibrium points, *viz.*

$$\mathbf{0} = \begin{bmatrix} 0 \\ 0 \\ 0 \end{bmatrix} \quad \text{and} \quad x^\star = \begin{bmatrix} \frac{c}{d} \\ \frac{a}{b} \\ 0 \end{bmatrix} \tag{23}$$

Using Lyapunov stability theory [5], it can be easily shown that the equilibrium $x = \mathbf{0}$ is unstable, while the equilibrium $x = x^\star$ is Lyapunov stable under the assumption $ga < fb$.

Figure 5 depicts the state orbits of the three species Lotka–Volterra system (22) when $a = 2, b = 0.5, c = 1, d = 0.8, f = 4, g = 0.5, \alpha = 1$.

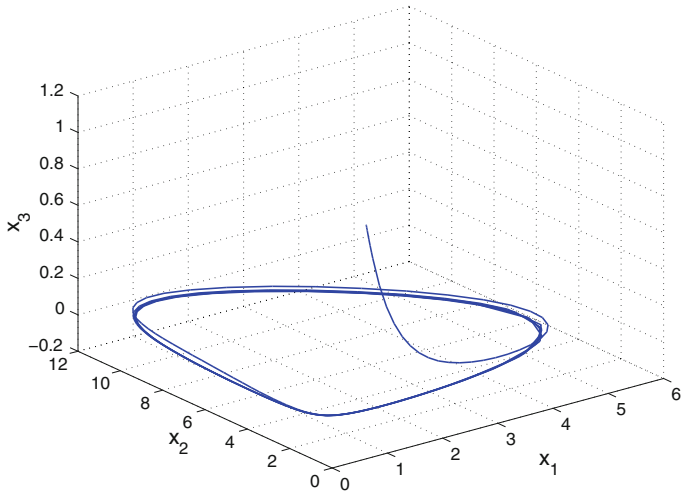

Fig. 5 State orbits of the three species Lotka–Volterra system

Since only the stable equilibrium $x = x^\star$ pertains to problems of practical interest, we consider only the problem of nonlinear observer design for the three species Lotka–Volterra system (22) near $x = x^\star$.

Next, we suppose that the prey population is given as the output function of the Lotka–Volterra system (22), i.e.

$$y = x_1 - x_1^\star \tag{24}$$

The linearization of the plant dynamics (22) at $x = x^\star$ is given by

$$A = \frac{\partial f}{\partial x}\left(x^\star\right) = \begin{bmatrix} 0 & -\frac{bc}{d} & 0 \\ \frac{ad}{b} & 0 & -\frac{\alpha a}{b} \\ 0 & 0 & -f + \frac{ga}{b} \end{bmatrix} \tag{25}$$

Also, the linearization of the output function (24) at $x = x^\star$ is given by

$$C = \frac{\partial h}{\partial x}\left(x^\star\right) = \begin{bmatrix} 1 & 0 & 0 \end{bmatrix} \tag{26}$$

From (25) and (26), the observability matrix for the Lotka–Volterra system (22) with the output (24) is given by

$$\mathbf{O}(C, A) = \begin{bmatrix} C \\ CA \\ CA^2 \end{bmatrix} = \begin{bmatrix} 1 & 0 & 0 \\ 0 & -\frac{bc}{d} & 0 \\ -ac & 0 & \frac{\alpha ac}{d} \end{bmatrix} \tag{27}$$

We find that

$$\det[\mathbf{O}(C, A)] = -\frac{\alpha abc^2}{d^2} \neq 0 \tag{28}$$

which shows that $\mathbf{O}(C, A)$ has full rank. Thus, (C, A) is completely observable [13].

Since the equilibrium $x = x^\star$ is Lyapunov stable, by Sundarapandian's theorem (Theorem 1), we obtain the following result, which gives a construction of nonlinear observer for the three species Lotka–Volterra system.

Theorem 3 *Suppose that $ga < fb$. Then the three species Lotka–Volterra system (22) with the output (24) has a local exponential observer of the form*

$$\begin{bmatrix} \dot{z}_1 \\ \dot{z}_2 \\ \dot{z}_3 \end{bmatrix} = \begin{bmatrix} z_1(a - bz_2) \\ z_2(-c + dz_1 - \alpha z_3) \\ z_3(-f + gz_2) \end{bmatrix} + K\left[y - z_1 + x_1^\star\right] \tag{29}$$

where K is a matrix chosen such that $A - KC$ is Hurwitz. Since (C, A) is observable, a gain matrix K can be found such that the error matrix $E = A - KC$ has arbitrarily assigned set of stable eigenvalues. ■

Example 2 Consider a three species Lotka–Volterra system given by the dynamics

$$\begin{aligned} \dot{x}_1 &= x_1(2 - 0.5x_2) \\ \dot{x}_2 &= x_2(-1 + 0.8x_1 - x_3) \\ \dot{x}_3 &= x_3(-4 + 0.5x_2) \end{aligned} \tag{30}$$

which has the non-trivial equilibrium $x^\star = \begin{bmatrix} 1.25 \\ 4 \\ 0 \end{bmatrix}$.

The output function is taken as the prey population

$$y = x_1 - x_1^\star = x_1 - 1.25 \tag{31}$$

The linearization of the system dynamics (30) at $x = x^\star$ is

$$A = \begin{bmatrix} 0 & -\frac{bc}{d} & 0 \\ \frac{ad}{b} & 0 & -\frac{\alpha a}{b} \\ 0 & 0 & -f + \frac{ga}{b} \end{bmatrix} = \begin{bmatrix} 0 & -0.625 & 0 \\ 3.2 & 0 & -4 \\ 0 & 0 & -2 \end{bmatrix} \tag{32}$$

Since (C, A) is observable, the eigenvalues of the error matrix $E = A - KC$ can be placed arbitrarily. Using the Ackermann's formula [13] for the observability gain matrix, we can choose K so that the error matrix $E = A - KC$ has the eigenvalues $\{-4, -4, -4\}$.

A simple calculation using MATLAB yields $K = \begin{bmatrix} 10.0 \\ -41.6 \\ 3.2 \end{bmatrix}$.

By Theorem 3, a local exponential observer for the given three species Lotka–Volterra system (30) and (31) around $x^\star$ is given by

$$\begin{bmatrix} \dot{z}_1 \\ \dot{z}_2 \\ \dot{z}_3 \end{bmatrix} = \begin{bmatrix} z_1(2 - 0.5z_2) \\ z_2(-1 + 0.8z_1 - z_3) \\ z_3(-4 + 0.5z_2) \end{bmatrix} + \begin{bmatrix} 10.0 \\ -41.6 \\ 3.2 \end{bmatrix} \begin{bmatrix} y - z_1 + 1.25 \end{bmatrix} \tag{33}$$

For simulations, the initial conditions are chosen as

$$x(0) = \begin{bmatrix} 3 \\ 12 \\ 4 \end{bmatrix} \text{ and } z(0) = \begin{bmatrix} 7 \\ 2 \\ 8 \end{bmatrix} \tag{34}$$

Figures 6, 7 and 8 depict the exponential convergence of the observer states z_1, z_2, z_3 of the system (33) to the plant states x_1, x_2, x_3 of the Lotka–Volterra system (30).

Figure 9 depicts the exponential convergence of the estimation errors e_1, e_2, e_3.

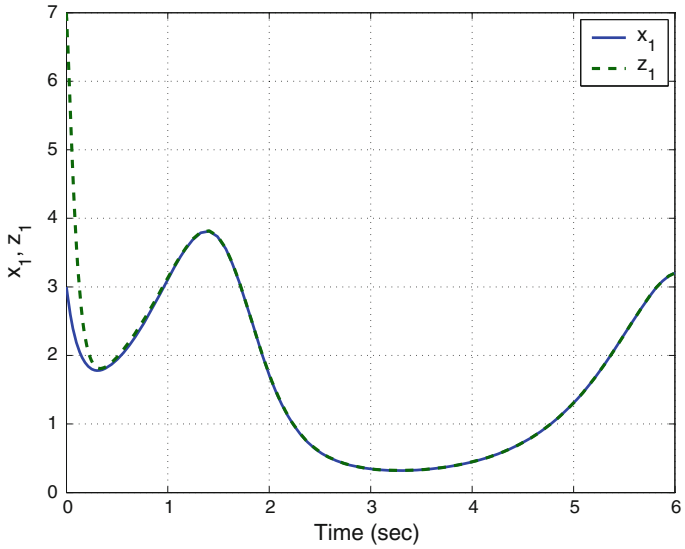

Fig. 6 Synchronization of the states x_1 and z_1

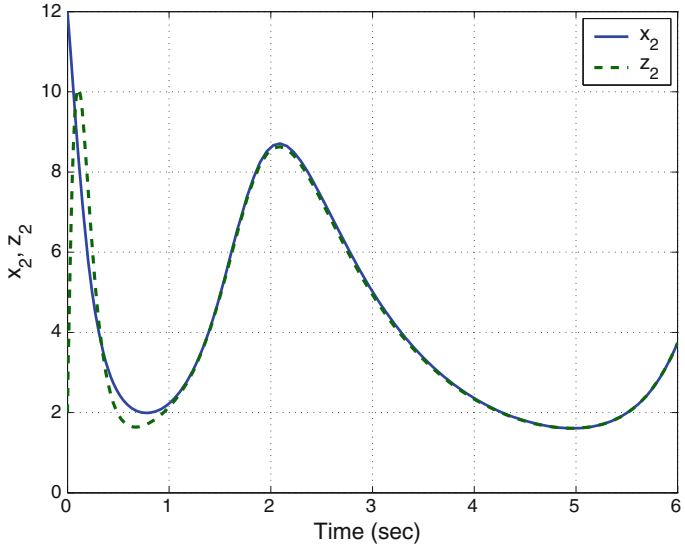

Fig. 7 Synchronization of the states x_2 and z_2

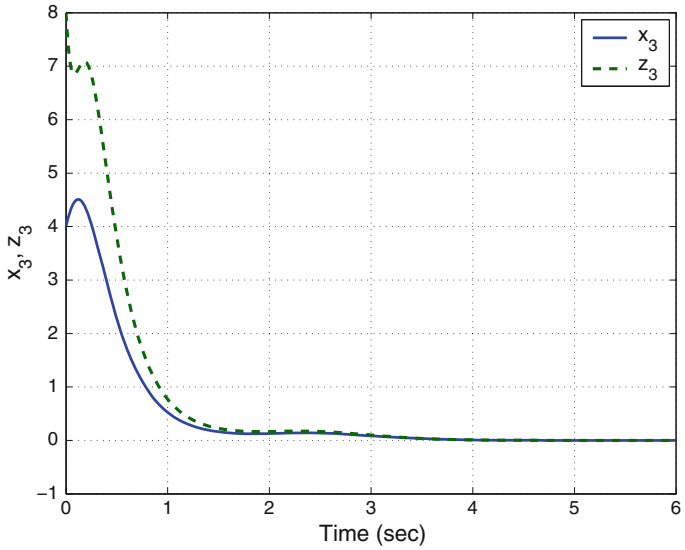

Fig. 8 Synchronization of the states x_3 and z_3

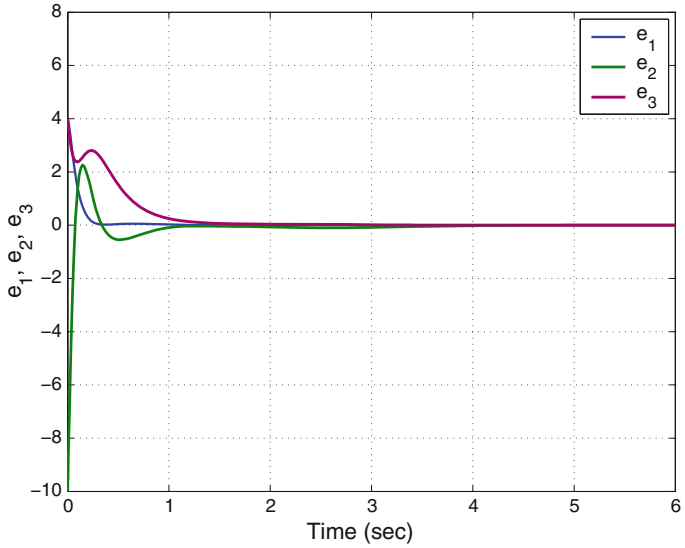

Fig. 9 Time-history of the estimation errors e_1, e_2, e_3

5 Conclusions

For many real world problems of population and conservation ecology, an efficient monitoring system is of great importance. In this work, the methodology based on Sundarapandian's theorem (2002) for exponential observer design is applied for the monitoring of two species and three species Lotka–Volterra population systems. Under the condition of stable coexistence of all the species, an exponential observer is constructed near a non-trivial equilibrium of the Lotka–Volterra population ecology system for both two species and three species Lotka–Volterra population systems using Sundarapandian's theorem (2002). Numerical examples have been illustrated in detail for the nonlinear observer design of both two species and three species Lotka–Volterra population systems. As a future work, nonlinear observer design for four species and five species Lotka–Volterra population systems may be investigated.

References

1. Besancon G (2007) Nonlinear observers and applications. Lecture notes in control and information sciences, vol 363. Springer, Berlin
2. Celle F, Gauthier JP, Kazakos D, Salle G (1989) Synthesis of nonlinear observers: a harmonic analysis approach. Math Syst Theory 22:291–322
3. Gámez M, López I, Garay J, Varga Z (2009) Observation and control in a model of a cell population affected by radiation. Biosystems 96(2):172–177
4. Gauthier JP, Hammouri H, Othman S (1992) A simple observer for nonlinear systems—applications to bioreactors. IEEE Trans Autom Control 37:875–880
5. Khalil HK (2001) Nonlinear systems, 3rd edn. Prentice Hall, New Jersey
6. Kou SR, Elliott DL, Tarn TJ (1975) Exponential observers for nonlinear dynamic systems. Inf Control 29(3):204–216
7. Krener AJ, Isidori A (1983) Linearization by output injection and nonlinear observers. Syst Control Lett 3:47–52
8. Krener AJ, Respondek W (1985) Nonlinear observers with linearizable error dynamics. SIAM J Control Optim 23:197–216
9. López I, Gámez M, Molnár S (2007) Observability and observers in a food web. Appl Math Lett 20(8):951–957
10. López I, Gámez M, Varga Z (2008) Observer design for phenotypic observation of genetic processes. Appl Math Lett 9(2):290–302
11. Lotka AJ (1925) Elements of physical biology. Williams and Wilkins, Baltimore
12. Luenberger DG (1966) Observers for multivariable linear systems. IEEE Trans Autom Control 2:190–197
13. Ogata K (2009) Modern control engineering, 5th edn. Prentice Hall, New Jersey
14. Sundarapandian V (2002) Global observer design for nonlinear systems. Math Comput Model 35(1–2):45–54
15. Sundarapandian V (2002) Local observer design for nonlinear systems. Math Comput Model 35(1–2):25–36
16. Sundarapandian V (2002) Nonlinear observer design for bifurcating systems. Math Comput Model 36(1–2):183–188
17. Sundarapandian V (2002) Nonlinear observer design for discrete-time bifurcating systems. Math Comput Model 36(1–2):211–215

18. Sundarapandian V (2002) Observer design for discrete-time nonlinear systems. Math Comput Model 35(1–2):37–44
19. Sundarapandian V (2003) Exponential observer design for discrete-time nonlinear systems with real parametric uncertainty. Math Comput Model 37(1–2):191–204
20. Sundarapandian V (2003) Exponential observer design for nonlinear systems with real parametric uncertainty. Math Comput Model 37(1–2):177–190
21. Sundarapandian V (2004) General observers for discrete-time nonlinear systems. Math Comput Model 39(1):87–95
22. Sundarapandian V (2004) General observers for nonlinear systems. Math Comput Model 39(1):97–105
23. Sundarapandian V (2004) New results on general observers for discrete-time nonlinear systems. Appl Math Lett 17(12):1415–1420
24. Sundarapandian V (2004) New results on general observers for nonlinear systems. Appl Math Lett 17(12):1421–1426
25. Sundarapandian V (2005) Nonlinear observer design for a general class of discrete-time nonlinear systems with real parametric uncertainty. Comput Math Appl 49(7–8):1177–1194
26. Sundarapandian V (2005) Nonlinear observer design for a general class of nonlinear systems with real parametric uncertainty. Comput Math Appl 49(7–8):1195–1211
27. Thau FE (1973) Observing the states of nonlinear dynamical systems. Int J Control 18:471–479
28. Tsinias J (1989) Observer design for nonlinear systems. Syst Control Lett 13:135–142
29. Varga Z (2008) Applications of mathematical system theory in population biology. Periodica Mathematica Hungarica 56:157–168
30. Volterra V (1926) Fluctuations in the abundance of species considered mathematically. Nature 118:558–560
31. Xia XH, Gao WB (1988) Nonlinear observer design by canonical form. Int J Control 47:1081–1100
32. Xia XH, Gao WB (1988) On exponential observers for nonlinear systems. Syst Control Lett 11:319–325

Output Regulation of Vaidyanathan 3-D Jerk Chaotic System

Sundarapandian Vaidyanathan

Abstract This paper investigates the problem of output regulation of the Vaidyanathan 3-D jerk chaotic system (2014). Explicitly, state feedback control laws to regulate the output of the Vaidyanathan jerk chaotic system have been derived so as to track the constant reference signals as well as to track periodic reference signals. The control laws are derived using the regulator equations of C.I. Byrnes and A. Isidori (1990), who solved the problem of output regulation of nonlinear systems involving neutrally stable exosystem dynamics. The output regulation of the Vaidyanathan jerk chaotic system has important applications in Electrical and Communication Engineering. Numerical simulations using MATLAB are shown to illustrate the phase portraits of the Vaidyanathan jerk chaotic system and the output regulation results for the Vaidyanathan jerk chaotic system.

Keywords Chaos · Chaotic systems · Output regulation · Nonlinear control systems · Feedback stabilization

1 Introduction

Output regulation of control systems is one of the very important problems in control systems theory. Basically, the output regulation problem is to control a fixed linear or nonlinear plant in order to have its output tracking reference signals produced by some external generator (the exosystem).

For linear control systems, the output regulation problem has been solved by Francis and Wonham [12]. For nonlinear control systems, the output regulation problem has been solved by Byrnes and Isidori [5] generalizing the internal model principle obtained by Francis and Wonham [12]. Byrnes and Isidori [5] have made an important assumption in their work which demands that the exosystem dynam-

S. Vaidyanathan (✉)
Research and Development Centre, Vel Tech University,
Avadi, Chennai 600062, Tamil Nadu, India
e-mail: sundarvtu@gmail.com

S. Vaidyanathan and C. Volos (eds.), *Advances and Applications in Nonlinear Control Systems*, Studies in Computational Intelligence 635,
DOI 10.1007/978-3-319-30169-3_4

ics generating reference and/or disturbance signals is a neutrally stable system (Lyapunov stable in both forward and backward time). The class of exosystem signals includes the important particular cases of constant reference signals as well as sinusoidal reference signals. Using Centre Manifold Theory [7], Byrnes and Isidori have derived regulator equations, which completely characterize the solution of the output regulation problem of nonlinear control systems.

The output regulation problem for linear and nonlinear control systems has been the focus of many studies in recent decades [48]. In [21], Mahmoud and Khalil obtained results on the asymptotic regulation of minimum phase nonlinear systems using output feedback. In [13], Fridman solved the output regulation problem for nonlinear control systems with delay using centre manifold theory [7]. In [11], Chen and Huang obtained results on the robust output regulation for output feedback systems with nonlinear exosystems. In [18], Liu and Huang obtained results on the global robust output regulation problem for lower triangular nonlinear systems with unknown control direction. In [88], Yang and Huang obtained new results on the global robust output regulation problem for nonlinear plants subject to nonlinear exosystems.

In [14], Immonen obtained results on the practical output regulation for bounded linear infinite-dimensional state space systems. In [23], Pavlov, Van de Wouw and Nijimeijer obtained results on the global nonlinear output regulation using convergence-based controller design. In [87], Xi and Ding obtained results on the global adaptive output regulation of a class of nonlinear systems with nonlinear exosystems. In [37], Serrani and Isidori obtained results on the global robust output regulation problem for a class of nonlinear systems.

In [39], Sundarapandian obtained results for the output regulation of the Lorenz attractor. In [52], Vaidyanathan obtained results for the output regulation of the unified chaotic system. In [51], Vaidyanathan derived results for the output regulation of the Arneodo-Coullet chaotic system. In [56], Vaidyanathan derived results for the output regulation of the Liu chaotic system.

Chaotic systems are defined as nonlinear dynamical systems which are sensitive to initial conditions, topologically mixing and with dense periodic orbits. Sensitivity to initial conditions of chaotic systems is popularly known as the *butterfly effect*. Small changes in an initial state will make a very large difference in the behavior of the system at future states. Chaotic behaviour was suspected well over hundred years ago in the study of three bodies problem by Henri Poincaré [4], but chaos was experimentally established by E.N. Lorenz [19] only a few decades ago in the study of 3-D weather models.

Some classical paradigms of 3-D chaotic systems in the literature are Rössler system [31], ACT system [1], Sprott systems [38], Chen system [9], Lü system [20], Liu system [17], Cai system [6], Chen-Lee system [10], Tigan system [49], etc.

Many new chaotic systems have been discovered in the recent years such as Zhou system [89], Zhu system [90], Li system [16], Wei-Yang system [86], Sundarapandian systems [40, 45], Vaidyanathan systems [58, 59, 61–64, 66, 68, 71, 82, 85], Pehlivan system [25], etc.

Synchronization of chaotic systems is a phenomenon that occurs when two or more chaotic systems are coupled or when a chaotic system drives another chaotic system. Because of the butterfly effect which causes exponential divergence of the trajectories of two identical chaotic systems started with nearly the same initial conditions, the synchronization of chaotic systems is a challenging research problem in the chaos literature [2, 3].

Major works on synchronization of chaotic systems deal with the complete synchronization of a pair of chaotic systems called the *master* and *slave* systems. The design goal of the complete synchronization is to apply the output of the master system to control the slave system so that the output of the slave system tracks the output of the master system asymptotically with time.

Pecora and Carroll pioneered the research on synchronization of chaotic systems with their seminal papers [8, 24]. The active control method [15, 32, 33, 44, 50, 73, 74, 77] is typically used when the system parameters are available for measurement. Adaptive control method [34–36, 41–43, 54, 60, 67, 72, 75, 76, 81, 84] is typically used when some or all the system parameters are not available for measurement and estimates for the uncertain parameters of the systems.

Backstepping control method [26–30, 47, 78, 83] is also used for the synchronization of chaotic systems, which is a recursive method for stabilizing the origin of a control system in strict-feedback form. Another popular method for the synchronization of chaotic systems is the sliding mode control method [46, 53, 55, 57, 65, 69, 70, 79, 80], which is a nonlinear control method that alters the dynamics of a nonlinear system by application of a discontinuous control signal that forces the system to "slide" along a cross-section of the system's normal behavior.

In this work, the output regulation problem for the Vaidyanathan jerk chaotic system [82] has been solved using the Byrnes-Isidori regulator equations [5] to derive the state feedback control laws for regulating the output of the Vaidyanathan jerk chaotic system for the important cases of constant reference signals (set-point signals) and periodic reference signals.

This work is organized as follows. In Sect. 2, a review of the solution of the output regulation for nonlinear control systems and Byrnes-Isidori regulator equations has been presented. In Sect. 3, a dynamic analysis of the Vaidyanathan jerk chaotic system [82] is detailed. In Sect. 4, output regulation problem for the Vaidyanathan jerk chaotic system is discussed and new results are derived. In Sect. 5, numerical simulations for the output regulation of the Vaidyanathan jerk chaotic system are detailed. Section 6 summarizes the main results obtained in this work.

2 Review of the Output Regulation for Nonlinear Control Systems

In this section, we consider a multi-variable nonlinear control system modelled by equations of the form

$$\dot{x} = f(x) + g(x)u + p(x)\omega \tag{1}$$

$$\dot{\omega} = s(\omega) \tag{2}$$

$$e = h(x) - q(\omega) \tag{3}$$

Here, the differential equation (1) describes the *plant dynamics* with state x defined in a neighbourhood X of the origin of $\mathbf{R}^n$ and the input u takes values in $\mathbf{R}^m$ subject to the effect of a disturbance represented by the vector field $p(x)\omega$. The differential equation (2) describes an autonomous system, known as the *exosystem*, defined in a neighbourhood W of the origin of $\mathbf{R}^k$, which models the class of disturbance and reference signals taken into consideration. The Eq. (3) defines the error between the actual plant output $h(x) \in \mathbf{R}^p$ and a reference signal $q(\omega)$, which models the class of disturbance and reference signals taken into consideration.

We also assume that all the constituent mappings of the system (1), (2) and the error Eq. (3), namely, f, g, p, s, h and q are C^1 mappings vanishing at the origin, i.e.

$$f(0) = 0,\ g(0) = 0,\ p(0) = 0,\ h(0) = 0 \text{ and } q(0) = 0.$$

Thus, for $u = 0$, the system (1), (2) has an equilibrium state $(x, \omega) = (0, 0)$ with zero error (3).

A *state feedback controller* for the composite system (1), (2) has the form

$$u = \alpha(x, \omega) \tag{4}$$

where α is a C^1 mapping defined on $X \times W$ such that $\alpha(0, 0) = 0$. Upon substitution of the feedback law (4) in the composite system (1), (2), we get the closed-loop system given by

$$\begin{aligned} \dot{x} &= f(x) + g(x)\alpha(x, \omega) + p(x)\omega \\ \dot{\omega} &= s(\omega) \end{aligned} \tag{5}$$

The purpose of designing the state feedback controller (4) is to achieve both *internal stability* and *output regulation*. Internal stability means that when the input is disconnected from (5) (i.e. when $\omega = 0$), the closed-loop system (5) has an exponentially stable equilibrium at $x = 0$. Output regulation means that for the closed-loop system (5), for all initial states $(x(0), \omega(0))$ sufficiently close to the origin, $e(t) \to 0$ asymptotically as $t \to \infty$. Formally, we can summarize the requirements as follows.

State Feedback Regulator Problem [5]:
Find, if possible, a state feedback control law $u = \alpha(x, \omega)$ such that

(OR1) *(Internal Stability)* The equilibrium $x = 0$ of the dynamics

$$\dot{x} = f(x) + g(x)\alpha(x, 0)$$

is locally asymptotically stable.

(OR2) *(Output Regulation)* There exists a neighbourhood $U \subset X \times W$ of $(x, \omega) = (0, 0)$ such that for each initial condition $(x(0), \omega(0)) \in U$, the solution $(x(t), \omega(t))$ of the closed-loop system (5) satisfies

$$\lim_{t \to \infty} [h(x(t)) - q(\omega(t))] = 0.$$

Byrnes and Isidori [5] have solved this problem under the following assumptions.

(H1) The exosystem dynamics $\dot{\omega} = s(\omega)$ is neutrally stable at $\omega = 0$, i.e. the system is Lyapunov stable in both forward and backward time at $\omega = 0$.

(H2) The pair $(f(x), g(x))$ has a stabilizable linear approximation at $x = 0$, i.e. if

$$A = \left[\frac{\partial f}{\partial x}\right]_{x=0} \quad \text{and} \quad B = \left[\frac{\partial g}{\partial x}\right]_{x=0},$$

then (A, B) is stabilizable, which means that we can find a gain matrix K so that $A + BK$ is Hurwitz. ■

Next, we recall the solution of the output regulation problem derived by Byrnes and Isidori [5].

Theorem 1 *[5] Under the hypotheses (H1) and (H2), the state feedback regulator problem is solvable if, and only if, there exist C^1 mappings $x = \pi(\omega)$ with $\pi(0) = 0$ and $u = \phi(\omega)$ with $\phi(0) = 0$, both defined in a neighbourhod of $W^0 \subset W$ of $\omega = 0$ such that the following equations (called the* Byrnes-Isidori regulator equations*) are satisfied:*

(1) $\frac{\partial \pi}{\partial \omega} s(\omega) = f(\pi(\omega)) + g(\pi(\omega))\phi(\omega) + p(\pi(\omega))\omega$
(2) $h(\pi(\omega)) - q(\omega) = 0$

When the Byrnes-Isidori regulator equations (1) and (2) are satisfied, a control law solving the state feedback regulator problem is given by

$$u = \phi(\omega) + K[x - \pi(\omega)] \tag{6}$$

where K is any gain matrix such that $A + BK$ is Hurwitz. ■

3 Dynamic Analysis of the Vaidyanathan Jerk Chaotic System

The Vaidyanathan jerk chaotic system [82] is described by the 3-D dynamics

$$\begin{aligned} \dot{x}_1 &= x_2 \\ \dot{x}_2 &= x_3 \\ \dot{x}_3 &= x_1 - a[\sinh(x_1) + \sinh(x_2)] - bx_3 \end{aligned} \tag{7}$$

In (7), a and b are constant, positive parameters.

The system (7) exhibits a chaotic attractor when the parameter values are taken as

$$a = 0.4, \quad b = 0.8 \tag{8}$$

For numerical simulations, we take the initial conditions of the Vaidyanathan jerk system (7) as

$$x_1(0) = 0.8, \quad x_2(0) = 1.2, \quad x_3(0) = 0.5 \tag{9}$$

Figure 1 shows the 3-D phase portrait of the Vaidyanathan jerk chaotic system (7). Figures 2, 3, 4 show the 2-D projections of the Vaidyanathan jerk chaotic system (7) on the (x_1, x_2), (x_2, x_3) and (x_1, x_3) coordinate planes respectively.

Also, the Lyapunov exponents of the Vaidyanathan jerk chaotic system (7) for the parameter values (8) and the initial values (9) are numerically found as

$$L_1 = 0.0771, \quad L_2 = 0, \quad L_3 = -0.8791 \tag{10}$$

Since $L_1 + L_2 + L3 = -0.802 < 0$, the Vaidyanathan jerk chaotic system (7) is dissipative and the asymptotic motion of the Vaidyanathan jerk chaotic system (7) settles onto a strange attractor of the system.

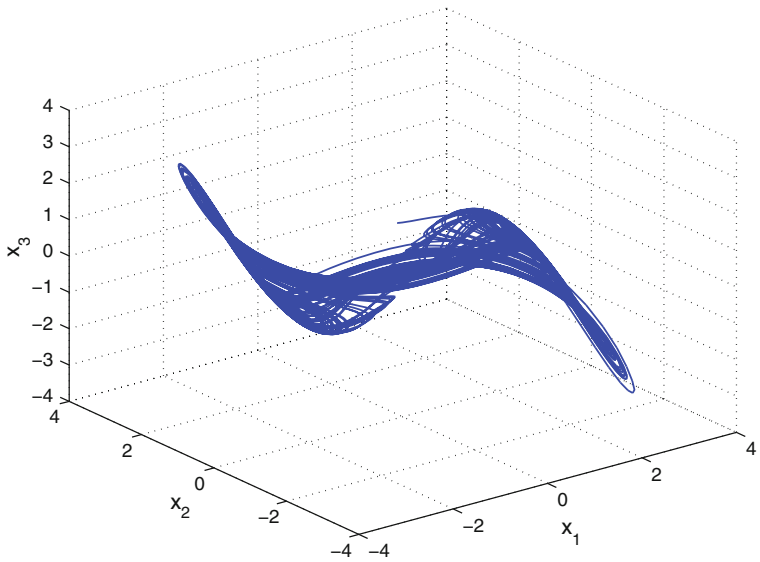

Fig. 1 3-D phase portrait of the Vaidyanathan jerk chaotic system

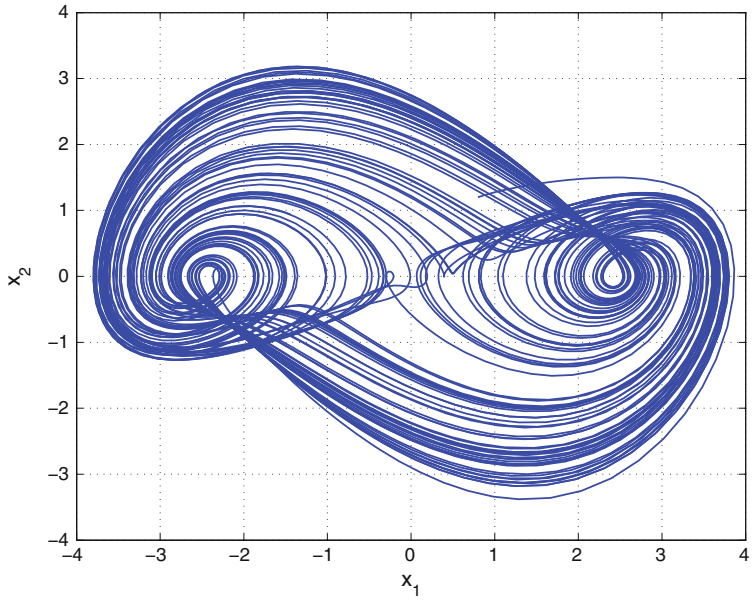

Fig. 2 2-D projection of the Vaidyanathan jerk chaotic system on the (x_1, x_2) plane

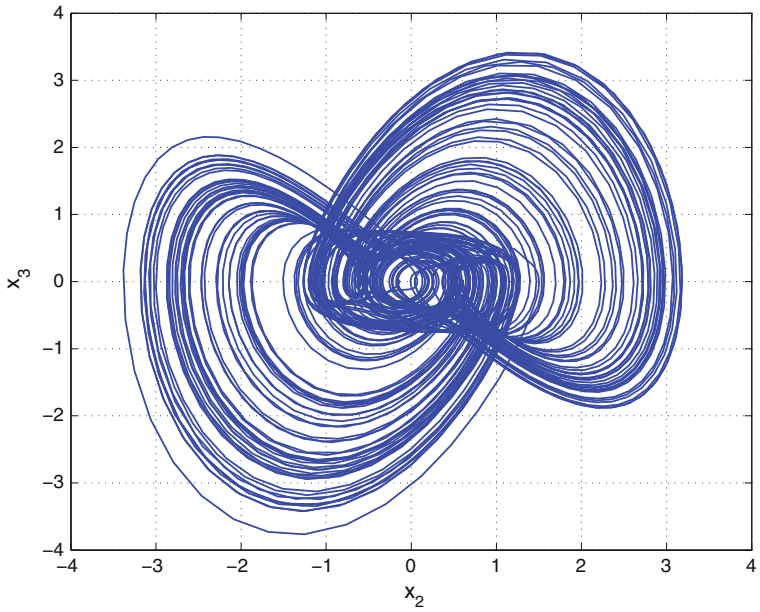

Fig. 3 2-D projection of the Vaidyanathan jerk chaotic system on the (x_2, x_3) plane

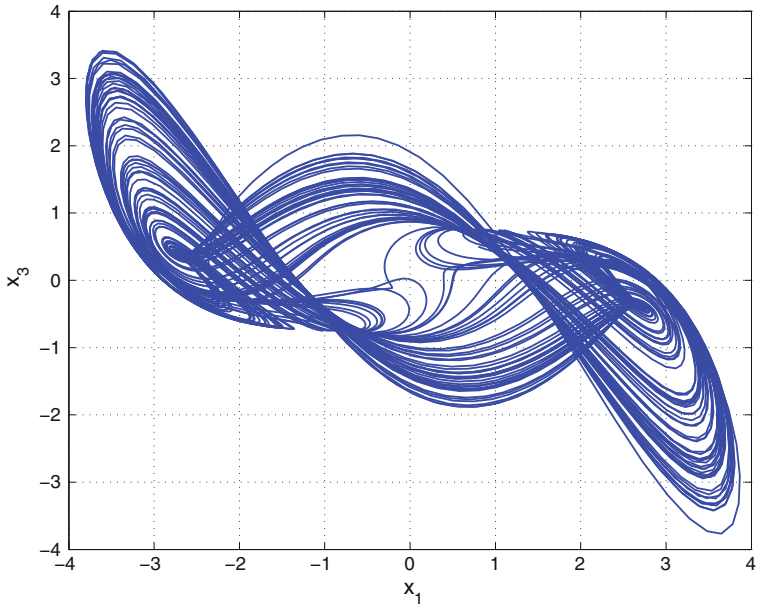

Fig. 4 2-D projection of the Vaidyanathan jerk chaotic system on the (x_1, x_3) plane

Also, the Kaplan-Yorke dimension of the Vaidyanathan jerk chaotic system (7) is calculated as

$$D_{KY} = 2 + \frac{L_1 + L_2}{|L_3|} = 2.0877, \tag{11}$$

which is fractional.

4 Output Regulation of Vaidyanathan Jerk Chaotic System

The Vaidyanathan jerk chaotic system [82] is a novel chaotic system described by the dynamics

$$\begin{aligned} \dot{x}_1 &= x_2 \\ \dot{x}_2 &= x_3 \\ \dot{x}_3 &= x_1 - a[\sinh(x_1) + \sinh(x_2)] - bx_3 + u \end{aligned} \tag{12}$$

where a, b are positive constants and u is an active feedback control.

In this work, we consider two important cases of output regulation for the Vaidyanathan jerk chaotic system [82]:

(I) Tracking of Constant Reference Signals
(II) Tracking of Periodic Reference Signals

4.1 Tracking of Constant Reference Signals

In this case, the exosystem is given by the scalar dynamics

$$\dot{\omega} = 0 \tag{13}$$

It is important to observe that the exosystem (13) is neutrally stable because the solutions of (13) are only constant trajectories, i.e.

$$\omega(t) \equiv \omega(0) = \omega_0 \quad \text{for all} \quad t$$

Thus, the assumption (H1) of Theorem 1 (Sect. 2) holds trivially.

Linearizing the dynamics of the Vaidyanathan jerk chaotic system (12) at the origin, we get the system matrices

$$A = \begin{bmatrix} 0 & 1 & 0 \\ 0 & 0 & 1 \\ 1-a & -a & -b \end{bmatrix} \quad \text{and} \quad B = \begin{bmatrix} 0 \\ 0 \\ 1 \end{bmatrix} \tag{14}$$

Using Kalman's rank test for controllability [22], it can be easily seen that the pair (A, B) is completely controllable.

Since (A, B) is in Bush companion form, the characteristic equation of $A + BK$ is given by

$$\lambda^3 + (b - k_3)\lambda^2 + (a - k_2)\lambda + (a - k_1 - 1) = 0 \tag{15}$$

where $K = \begin{bmatrix} k_1 & k_2 & k_3 \end{bmatrix}$.

By the Routh's stability criterion [22], it can be easily shown that the closed-loop system matrix $A + BK$ is Hurwitz if and only if

$$k_1 < a - 1, \quad k_2 < a, \quad k_3 < b, \quad (b - k_3)(a - k_2) > a - k_1 - 1 \tag{16}$$

Thus, the assumption (H2) of Theorem 1 (Sect. 2) also holds.

Hence, Theorem 1 can be applied to solve the output regulation problem for the Vaidyanathan jerk chaotic system (12) for the tracking of constant reference signals (*set-point signals*).

4.1.1 Constant Tracking Problem for x_1

Here, the tracking problem for the Vaidyanathan jerk chaotic system (12) is given by

$$\begin{aligned} \dot{x}_1 &= x_2 \\ \dot{x}_2 &= x_3 \\ \dot{x}_3 &= x_1 - a[\sinh(x_1) + \sinh(x_2)] - bx_3 + u \\ e &= x_1 - \omega \end{aligned} \tag{17}$$

By Theorem 1, the regulator equations of (17) are obtained as

$$\begin{cases} \pi_2(\omega) = 0 \\ \pi_3(\omega) = 0 \\ \pi_1(\omega) - a[\sinh(\pi_1(\omega)) + \sinh(\pi_2(\omega))] - b\pi_3(\omega) + \phi(\omega) = 0 \\ \pi_1(\omega) - \omega = 0 \end{cases} \tag{18}$$

Solving the regulator equation (18), we get the unique solution

$$\begin{cases} \pi_1(\omega) = \omega \\ \pi_2(\omega) = 0 \\ \pi_3(\omega) = 0 \\ \phi(\omega) = a\sinh(\omega) - \omega \end{cases} \tag{19}$$

By Theorem 1, a state feedback control law solving the output regulation problem is given by

$$u = \phi(\omega) + K[x - \pi(\omega)] = a\sinh(\omega) - \omega + k_1(x_1 - \omega) + k_2x_2 + k_3x_3 \tag{20}$$

where k_1, k_2 and k_3 satisfy the inequalities (16).

4.1.2 Constant Tracking Problem for x_2

Here, the tracking problem for the Vaidyanathan jerk chaotic system (12) is given by

$$\begin{aligned} \dot{x}_1 &= x_2 \\ \dot{x}_2 &= x_3 \\ \dot{x}_3 &= x_1 - a[\sinh(x_1) + \sinh(x_2)] - bx_3 + u \\ e &= x_2 - \omega \end{aligned} \tag{21}$$

By Theorem 1, the regulator equations of (21) are obtained as

$$\begin{cases} \pi_2(\omega) = 0 \\ \pi_3(\omega) = 0 \\ \pi_1(\omega) - a[\sinh(\pi_1(\omega)) + \sinh(\pi_2(\omega))] - b\pi_3(\omega) + \phi(\omega) = 0 \\ \pi_2(\omega) - \omega = 0 \end{cases} \tag{22}$$

The first and fourth equations in (22) contradict each other.

Thus, the regulator equation (22) are not solvable.

Hence, by Theorem 1, we conclude that the output regulation problem is not solvable for this case.

4.1.3 Constant Tracking Problem for x_3

Here, the tracking problem for the Vaidyanathan jerk chaotic system (12) is given by

$$\begin{aligned} \dot{x}_1 &= x_2 \\ \dot{x}_2 &= x_3 \\ \dot{x}_3 &= x_1 - a[\sinh(x_1) + \sinh(x_2)] - bx_3 + u \\ e &= x_3 - \omega \end{aligned} \tag{23}$$

By Theorem 1, the regulator equations of (23) are obtained as

$$\begin{cases} \pi_2(\omega) = 0 \\ \pi_3(\omega) = 0 \\ \pi_1(\omega) - a[\sinh(\pi_1(\omega)) + \sinh(\pi_2(\omega))] - b\pi_3(\omega) + \phi(\omega) = 0 \\ \pi_3(\omega) - \omega = 0 \end{cases} \tag{24}$$

The second and fourth equations in (24) contradict each other.

Thus, the regulator equation (24) are not solvable.

Hence, by Theorem 1, we conclude that the output regulation problem is not solvable for this case.

4.2 *Tracking of Periodic Reference Signals*

In this case, the exosystem is given by the planar dynamics

$$\begin{aligned} \dot{\omega}_1 &= \nu\, \omega_2 \\ \dot{\omega}_2 &= -\nu\, \omega_1 \end{aligned} \tag{25}$$

where $\nu > 0$ is any fixed constant.

Clearly, the assumption (H1) (Theorem 1) holds. Also, as established in Sect. 4.1, the assumption (H2) of Theorem 1 also holds and that the closed-loop system matrix $A + BK$ will be Hurwitz if the constants k_1, k_2 and k_3 of the gain matrix K satisfy the inequalities (16).

Hence, Theorem 1 can be applied to solve the output regulation problem for the Vaidyanathan jerk chaotic system (12) for the tracking of periodic reference signals.

4.2.1 Periodic Tracking Problem for x_1

Here, the tracking problem for the Vaidyanathan jerk chaotic system (12) is given by

$$\begin{aligned}
\dot{x}_1 &= x_2 \\
\dot{x}_2 &= x_3 \\
\dot{x}_3 &= x_1 - a[\sinh(x_1) + \sinh(x_2)] - bx_3 + u \\
\dot{\omega}_1 &= \nu\,\omega_2 \\
\dot{\omega}_2 &= -\nu\,\omega_1 \\
e &= x_1 - \omega_1
\end{aligned} \tag{26}$$

By Theorem 1, the regulator equations of (26) are obtained as

$$\begin{cases}
\frac{\partial \pi_1}{\partial \omega_1}(\nu\omega_2) + \frac{\partial \pi_1}{\partial \omega_2}(-\nu\omega_1) = \pi_2(\omega) \\
\frac{\partial \pi_2}{\partial \omega_1}(\nu\omega_2) + \frac{\partial \pi_2}{\partial \omega_2}(-\nu\omega_1) = \pi_3(\omega) \\
\frac{\partial \pi_3}{\partial \omega_1}(\nu\omega_2) + \frac{\partial \pi_3}{\partial \omega_2}(-\nu\omega_1) = \pi_1(\omega) - a[\sinh(\pi_1(\omega)) + \sinh(\pi_2(\omega))] \\
\qquad\qquad\qquad\qquad -b\pi_3(\omega) + \phi(\omega) \\
\qquad\qquad \pi_1(\omega) - \omega_1 = 0
\end{cases} \tag{27}$$

Solving the regulator equation (27), we get the unique solution

$$\begin{cases}
\pi_1(\omega) = \quad \omega_1 \\
\pi_2(\omega) = \quad \nu\omega_2 \\
\pi_3(\omega) = -\nu^2\omega_1
\end{cases} \tag{28}$$

and

$$\phi(\omega) = -\nu^3\omega_2 - \left(b\nu^2 + 1\right)\omega_1 + a[\sinh(\omega_1) + \sinh(\nu\omega_2) \tag{29}$$

By Theorem 1, a state feedback control law solving the output regulation problem is given by

$$u = \phi(\omega) + K[x - \pi(\omega)] \tag{30}$$

where $\pi(\omega)$ is given by (28), $\phi(\omega)$ is given by (29) and k_1, k_2 and k_3 satisfy the inequalities (16).

4.2.2 Periodic Tracking Problem for x_2

Here, the tracking problem for the Vaidyanathan jerk chaotic system (12) is given by

$$\begin{aligned}
\dot{x}_1 &= x_2 \\
\dot{x}_2 &= x_3 \\
\dot{x}_3 &= x_1 - a[\sinh(x_1) + \sinh(x_2)] - bx_3 + u \\
\dot{\omega}_1 &= \nu\,\omega_2 \\
\dot{\omega}_2 &= -\nu\,\omega_1 \\
e &= x_2 - \omega_1
\end{aligned} \tag{31}$$

By Theorem 1, the regulator equations of (31) are obtained as

$$\begin{cases} \frac{\partial \pi_1}{\partial \omega_1}(\nu\omega_2) + \frac{\partial \pi_1}{\partial \omega_2}(-\nu\omega_1) = \pi_2(\omega) \\ \frac{\partial \pi_2}{\partial \omega_1}(\nu\omega_2) + \frac{\partial \pi_2}{\partial \omega_2}(-\nu\omega_1) = \pi_3(\omega) \\ \frac{\partial \pi_3}{\partial \omega_1}(\nu\omega_2) + \frac{\partial \pi_3}{\partial \omega_2}(-\nu\omega_1) = \pi_1(\omega) - a[\sinh(\pi_1(\omega)) + \sinh(\pi_2(\omega))] \\ \qquad\qquad\qquad\qquad\qquad\quad -b\pi_3(\omega) + \phi(\omega) \\ \qquad\qquad \pi_2(\omega) - \omega_1 = 0 \end{cases} \tag{32}$$

Solving the regulator equation (32), we get the unique solution

$$\begin{cases} \pi_1(\omega) = -\nu^{-1}\omega_2 \\ \pi_2(\omega) = \quad \omega_1 \\ \pi_3(\omega) = \quad \nu\omega_2 \end{cases} \tag{33}$$

and

$$\phi(\omega) = \nu^2\omega_1 + \left(\nu^{-1} + b\nu\right)\omega_2 + a\left[-\sinh\left(\nu^{-1}\omega_2\right) + \sinh(\omega_1)\right] \tag{34}$$

By Theorem 1, a state feedback control law solving the output regulation problem is given by

$$u = \phi(\omega) + K[x - \pi(\omega)] \tag{35}$$

where $\pi(\omega)$ is given by (33), $\phi(\omega)$ is given by (34) and k_1, k_2 and k_3 satisfy the inequalities (16).

4.2.3 Periodic Tracking Problem for x_3

Here, the tracking problem for the Vaidyanathan jerk chaotic system (12) is given by

$$\begin{aligned} \dot{x}_1 &= x_2 \\ \dot{x}_2 &= x_3 \\ \dot{x}_3 &= x_1 - a[\sinh(x_1) + \sinh(x_2)] - bx_3 + u \\ \dot{\omega}_1 &= \nu\,\omega_2 \\ \dot{\omega}_2 &= -\nu\,\omega_1 \\ e &= x_3 - \omega_1 \end{aligned} \tag{36}$$

By Theorem 1, the regulator equations of (36) are obtained as

$$\begin{cases} \frac{\partial \pi_1}{\partial \omega_1}(\nu\omega_2) + \frac{\partial \pi_1}{\partial \omega_2}(-\nu\omega_1) = \pi_2(\omega) \\ \frac{\partial \pi_2}{\partial \omega_1}(\nu\omega_2) + \frac{\partial \pi_2}{\partial \omega_2}(-\nu\omega_1) = \pi_3(\omega) \\ \frac{\partial \pi_3}{\partial \omega_1}(\nu\omega_2) + \frac{\partial \pi_3}{\partial \omega_2}(-\nu\omega_1) = \pi_1(\omega) - a[\sinh(\pi_1(\omega)) + \sinh(\pi_2(\omega))] \\ \qquad\qquad\qquad\qquad\qquad\quad -b\pi_3(\omega) + \phi(\omega) \\ \qquad\qquad \pi_3(\omega) - \omega_1 = 0 \end{cases} \tag{37}$$

Solving the regulator equation (37), we get the unique solution

$$\begin{cases} \pi_1(\omega) = -\nu^{-2}\omega_1 \\ \pi_2(\omega) = -\nu^{-1}\omega_2 \\ \pi_3(\omega) = \quad \omega_1 \end{cases} \tag{38}$$

and

$$\phi(\omega) = \left(b + \nu^{-2}\right)\omega_1 + \nu\omega_2 - a\left[\sinh\left(\nu^{-2}\omega_1\right) + \sinh\left(\nu^{-1}\omega_2\right)\right] \tag{39}$$

By Theorem 1, a state feedback control law solving the output regulation problem is given by

$$u = \phi(\omega) + K[x - \pi(\omega)] \tag{40}$$

where $\pi(\omega)$ is given by (38), $\phi(\omega)$ is given by (39) and k_1, k_2 and k_3 satisfy the inequalities (16).

5 Numerical Simulations

For numerical simulations, we take the parameter values a and b so that the Vaidyanathan jerk system (12) is in the chaotic case, i.e.

$$a = 0.4, \quad b = 0.8 \tag{41}$$

For achieving the internal stability of the state feedback regulator problem, a gain matrix K which satisfies the inequalities (16) must be used.

With the choice

$$K = \begin{bmatrix} k_1 & k_2 & k_3 \end{bmatrix} = \begin{bmatrix} -125.6 & -74.2 & -14.2 \end{bmatrix},$$

the matrix $A + BK$ is Hurwitz with the eigenvalues $-5, -5, -5$.

In the periodic tracking output regulation problem, the value $\nu = 1$ is taken in the exosystem dynamics given by (25).

5.1 Tracking of Constant Reference Signals

5.1.1 Constant Tracking Problem for x_1

Here, the initial conditions are taken as

$$x_1(0) = 8.1, \quad x_2(0) = 5.4, \quad x_3(0) = 6.3, \quad \omega(0) = 2$$

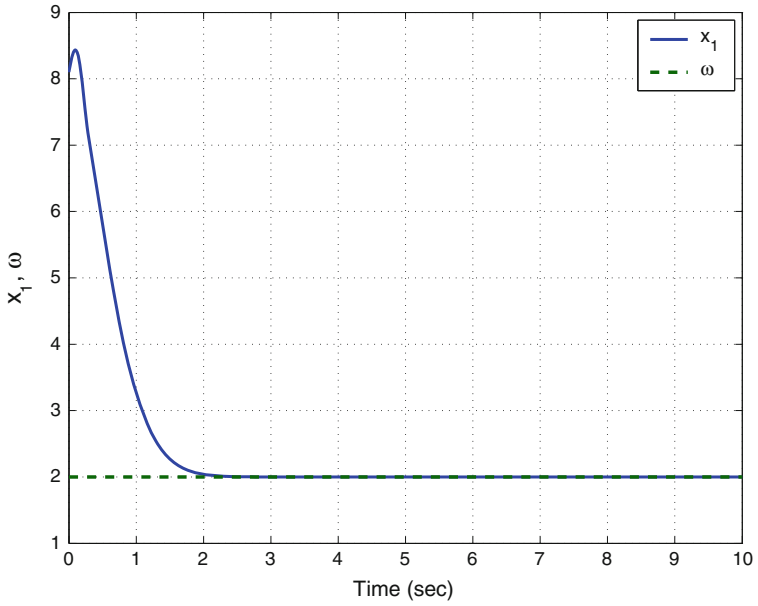

Fig. 5 Constant tracking of the state x_1

The simulation graph is depicted in Fig. 5 from which it is clear that the state trajectory $x_1(t)$ tracks the constant reference signal $\omega(t) \equiv 2$ in 3 s.

5.1.2 Constant Tracking Problem for x_2

As detailed in Sect. 4.1.2, the output regulation problem is not solvable for this case because the Byrnes-Isidori regulator equations do not admit any solution.

5.1.3 Constant Tracking Problem for x_3

As pointed out in Sect. 4.1.3, the output regulation problem is not solvable for this case because the Byrnes-Isidori regulator equations do not admit any solution.

5.2 Tracking of Periodic Reference Signals

5.2.1 Periodic Tracking Problem for x_1

Here, the initial conditions are taken as

$$x_1(0) = 5.1, \quad x_2(0) = 4.7, \quad x_3(0) = -2.5, \quad \omega_1(0) = 0, \omega_2(0) = 1$$

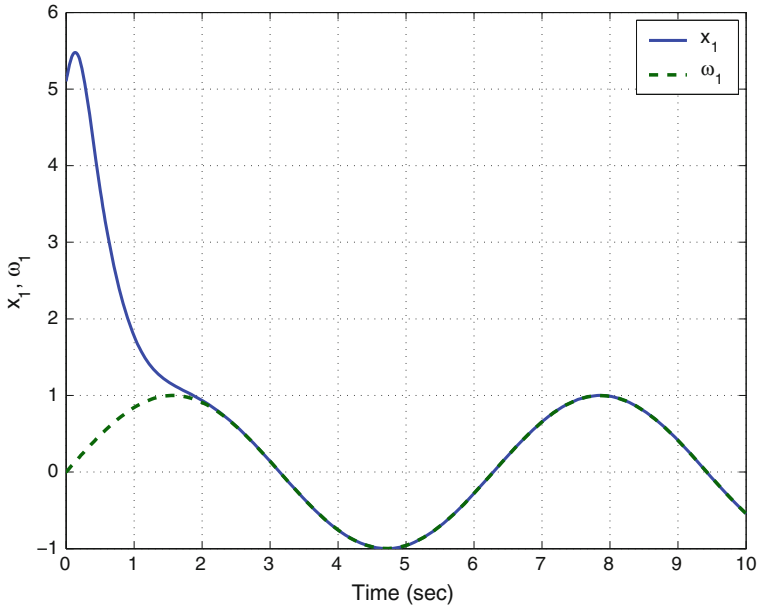

Fig. 6 Periodic tracking of the state x_1

Also, it is assumed that $\nu = 1$. The simulation graph is depicted in Fig. 6 from which it is clear that the state trajectory $x_1(t)$ tracks the periodic reference signal $\omega_1(t) = \sin t$ in 3 s.

5.2.2 Periodic Tracking Problem for x_2

Here, the initial conditions are taken as

$$x_1(0) = 8.1, \quad x_2(0) = 3.4, \quad x_3(0) = -2.7, \quad \omega_1(0) = 0, \omega_2(0) = 1$$

Also, it is assumed that $\nu = 1$. The simulation graph is depicted in Fig. 7 from which it is clear that the state trajectory $x_2(t)$ tracks the periodic reference signal $\omega_1(t) = \sin t$ in 3 s.

5.2.3 Periodic Tracking Problem for x_3

Here, the initial conditions are taken as

$$x_1(0) = 3.4, \quad x_2(0) = 2.5, \quad x_3(0) = -6.9, \quad \omega_1(0) = 0, \omega_2(0) = 1$$

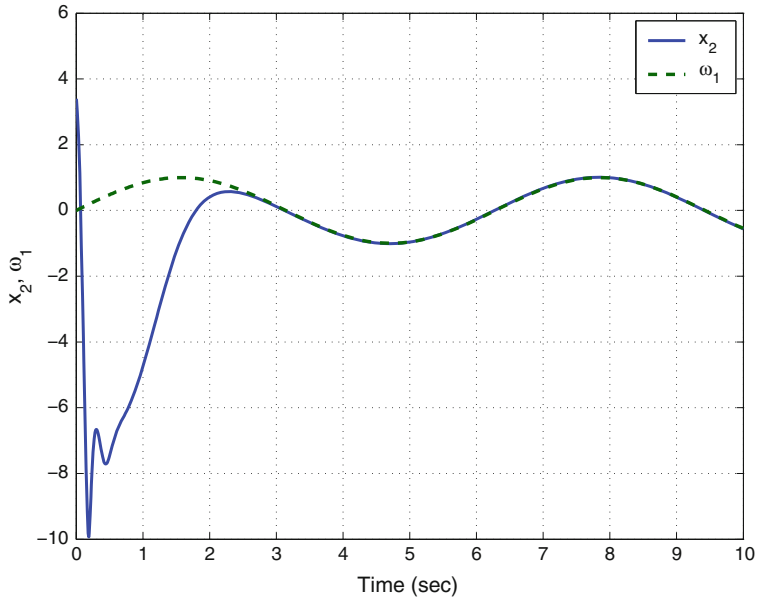

Fig. 7 Periodic tracking of the state x_2

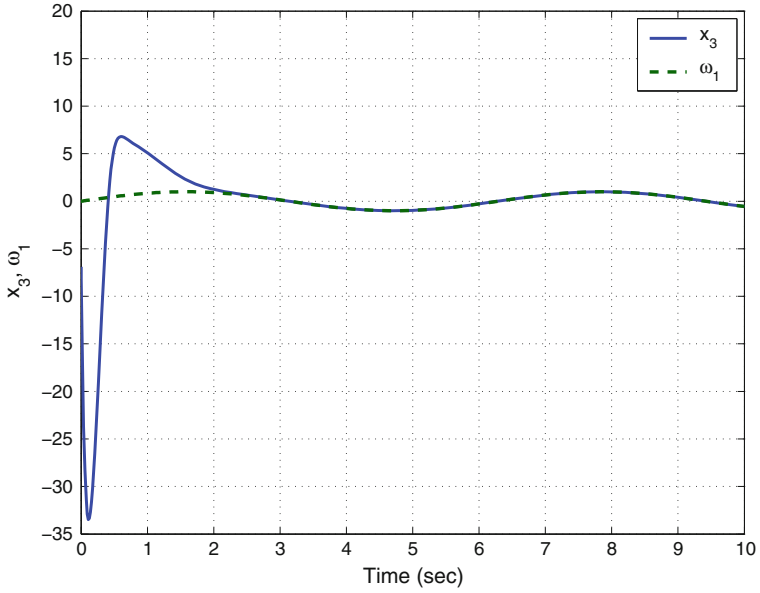

Fig. 8 Periodic tracking of the state x_3

Also, it is assumed that $\nu = 1$. The simulation graph is depicted in Fig. 8 from which it is clear that the state trajectory $x_3(t)$ tracks the periodic reference signal $\omega_1(t) = \sin t$ in 3 s.

6 Conclusions

Output regulation problem is one of the important problems in the control theory, which aims to control a fixed linear or nonlinear plant in order to have its output tracking reference signals produced by some external generator or the exosystem. Byrnes and Isidori (1990) solved the output regulation problem for a general class of nonlinear systems under some stability assumptions. In this work, the output regulation problem for the Vaidyanathan jerk chaotic system (2014)) has been studied in detail and a complete solution for the output regulation problem for the Vaidyanathan jerk chaotic system has been presented as well. Explicitly, using the Byrnes-Isidori regulator equations (1990), state feedback control laws for regulating the output of the Vaidyanathan jerk chaotic system have been derived. As tracking reference signals, constant and periodic reference signals have been considered and in each case, feedback control laws regulating the output of the Vaidyanathan chaotic system have been derived when the problem is solvable. Numerical simulations using MATLAB are shown to verify the results.

References

1. Arneodo A, Coullet P, Tresser C (1981) Possible new strange attractors with spiral structure. Commun Math Phys 79(4):573–576
2. Azar AT, Vaidyanathan S (2015a) Chaos modeling and control systems design, studies in computational intelligence, vol 581. Springer, Germany
3. Azar AT, Vaidyanathan S (2015b) Computational intelligence applications in modeling and control, studies in computational intelligence, vol 575. Springer, Germany
4. Barrow-Green J (1997) Poincaré and the three body problem. American mathematical society, providence
5. Byrnes CI, Isidori A (1990) Output regulation of nonlinear systems. IEEE Trans Autom Control 35(2):131–140
6. Cai G, Tan Z (2007) Chaos synchronization of a new chaotic system via nonlinear control. J Uncertain Syst 1(3):235–240
7. Carr J (1981) Appl Cent Manifold Theory. Springer, New York
8. Carroll TL, Pecora LM (1991) Synchronizing chaotic circuits. IEEE Trans Circuits Syst 38(4):453–456
9. Chen G, Ueta T (1999) Yet another chaotic attractor. Int J Bifurc Chaos 9(7):1465–1466
10. Chen HK, Lee CI (2004) Anti-control of chaos in rigid body motion. Chaos, Solitons and Fractals 21(4):957–965
11. Chen Z, Huang J (2005) Robust output regulation with nonlinear exosystems. Automatica 41(8):1447–1454
12. Francis BA, Wonham WM (1975) The internal model principle for linear multivariable regulators. Appl Math Optim 2(2):170–194
13. Fridman E (2003) Output regulation of nonlinear control systems with delay. Syst Control Lett 50:81–93
14. Immonen E (2007) Practical output regulation for bounded linear infinite-dimensional state space systems. Automatica 43(5):786–794
15. Karthikeyan R, Sundarapandian V (2014) Hybrid chaos synchronization of four-scroll systems via active control. J Electr Eng 65(2):97–103

16. Li D (2008) A three-scroll chaotic attractor. Phys Lett A 372(4):387–393
17. Liu C, Liu T, Liu L, Liu K (2004) A new chaotic attractor. Chaos, Solitions and Fractals 22(5):1031–1038
18. Liu L, Huang J (2008) Global robust output regulation of lower triangular systems with unknown control direction. Automatica 44(5):1278–1284
19. Lorenz EN (1963) Deterministic periodic flow. J Atmos Sci 20(2):130–141
20. Lü J, Chen G (2002) A new chaotic attractor coined. Int J Bifurc Chaos 12(3):659–661
21. Mahmoud NA, Khalil HK (1996) Asymptotic regulation of minimum phase nonlnear systems using output feedback. IEEE Trans Autom Control 41(10):1402–1412
22. Ogata K (2009) Modern Control Eng, 5th edn. Prentice Hall, New Jersey
23. Pavlov A, de Wouw NV, Nijimeijer H (2007) Global nonlinear output regulation: convergence based controller design. Automatica 43(3):456–463
24. Pecora LM, Carroll TL (1990) Synchronization in chaotic systems. Phys Rev Lett 64(8):821–824
25. Pehlivan I, Moroz IM, Vaidyanathan S (2014) Analysis, synchronization and circuit design of a novel butterfly attractor. J Sound Vib 333(20):5077–5096
26. Rasappan S, Vaidyanathan S (2012a) Global chaos synchronization of WINDMI and coullet chaotic systems by backstepping control. Far East J Math Sci 67(2):265–287
27. Rasappan S, Vaidyanathan S (2012b) Hybrid synchronization of n-scroll Chua and Lur'e chaotic systems via backstepping control with novel feedback. Arch Control Sci 22(3):343–365
28. Rasappan S, Vaidyanathan S (2012c) Synchronization of hyperchaotic Liu system via backstepping control with recursive feedback. Commun Comput Inf Sci 305:212–221
29. Rasappan S, Vaidyanathan S (2013) Hybrid synchronization of *n*-scroll chaotic Chua circuits using adaptive backstepping control design with recursive feedback. Malaysian J Math Sci 7(2):219–246
30. Rasappan S, Vaidyanathan S (2014) Global chaos synchronization of WINDMI and coullet chaotic systems using adaptive backstepping control design. Kyungpook Math J 54(1):293–320
31. Rössler OE (1976) An equation for continuous chaos. Phys Lett A 57(5):397–398
32. Sarasu P, Sundarapandian V (2011a) Active controller design for the generalized projective synchronization of four-scroll chaotic systems. Int J Syst Signal Control Eng Appl 4(2):26–33
33. Sarasu P, Sundarapandian V (2011b) The generalized projective synchronization of hyperchaotic Lorenz and hyperchaotic Qi systems via active control. Int J Soft Comput 6(5):216–223
34. Sarasu P, Sundarapandian V (2012a) Adaptive controller design for the generalized projective synchronization of 4-scroll systems. Int J Syst Signal Control Eng Appl 5(2):21–30
35. Sarasu P, Sundarapandian V (2012b) Generalized projective synchronization of three-scroll chaotic systems via adaptive control. Eur J Sci Res 72(4):504–522
36. Sarasu P, Sundarapandian V (2012c) Generalized projective synchronization of two-scroll systems via adaptive control. Int J Soft Comput 7(4):146–156
37. Serrani A, Isdori A (2000) Global robust output regulation for a class of nonlinear systems. Syst Control Lett 39(2):133–139
38. Sprott JC (1994) Some simple chaotic flows. Phys Rev E 50(2):647–650
39. Sundarapandian V (2010) Output regulation of the Lorenz attractor. Far East J Math Sci 42(2):289–299
40. Sundarapandian V (2013) Analysis and anti-synchronization of a novel chaotic system via active and adaptive controllers. J Eng Sci Technol Rev 6(4):45–52
41. Sundarapandian V, Karthikeyan R (2011a) Anti-synchronization of hyperchaotic Lorenz and hyperchaotic Chen systems by adaptive control. Int J Syst Signal Control Eng Appl 4(2):18–25
42. Sundarapandian V, Karthikeyan R (2011b) Anti-synchronization of Lü and Pan chaotic systems by adaptive nonlinear control. Eur J Sci Res 64(1):94–106
43. Sundarapandian V, Karthikeyan R (2012a) Adaptive anti-synchronization of uncertain Tigan and Li systems. J Eng Appl Sci 7(1):45–52
44. Sundarapandian V, Karthikeyan R (2012b) Hybrid synchronization of hyperchaotic Lorenz and hyperchaotic Chen systems via active control. J Eng Appl Sci 7(3):254–264

45. Sundarapandian V, Pehlivan I (2012) Analysis, control, synchronization, and circuit design of a novel chaotic system. Math Comput Model 55(7–8):1904–1915
46. Sundarapandian V, Sivaperumal S (2011) Sliding controller design of hybrid synchronization of four-wing chaotic systems. Int J Soft Comput 6(5):224–231
47. Suresh R, Sundarapandian V (2013) Global chaos synchronization of a family of *n*-scroll hyperchaotic Chua circuits using backstepping control with recursive feedback. Far East J Math Sci 73(1):73–95
48. Tarn TJ, Sanposh P, Cheng D, Zhang M (2005) Output regulation for nonlinear systems: some recent theoretical and experimental results. IEEE Trans Control Syst Technol 13(4):605–610
49. Tigan G, Opris D (2008) Analysis of a 3D chaotic system. Chaos, Solitons and Fractals 36:1315–1319
50. Vaidyanathan S (2011) Hybrid chaos synchronization of Liu and Lü systems by active nonlinear control. Commun Comput Inf Sci 204:1–10
51. Vaidyanathan S (2011b) Output regulation of the Arneodo-Coullet chaotic system. Commun Comput Inf Sci 133:98–107
52. Vaidyanathan S (2011c) Output regulation of the unified chaotic system. Commun Comput Inf Sci 198:1–9
53. Vaidyanathan S (2012a) Analysis and synchronization of the hyperchaotic Yujun systems via sliding mode control. Adv Intell Syst Comput 176:329–337
54. Vaidyanathan S (2012b) Anti-synchronization of Sprott-L and Sprott-M chaotic systems via adaptive control. Int J Control Theory Appl 5(1):41–59
55. Vaidyanathan S (2012c) Global chaos control of hyperchaotic Liu system via sliding control method. Int J Control Theory Appl 5(2):117–123
56. Vaidyanathan S (2012d) Output regulation of the Liu chaotic system. Appl Mech Mat 110–116:3982–3989
57. Vaidyanathan S (2012e) Sliding mode control based global chaos control of Liu-Liu-Liu-Su chaotic system. Int J Control Theory Appl 5(1):15–20
58. Vaidyanathan S (2013a) A new six-term 3-D chaotic system with an exponential nonlinearity. Far East J Math Sci 79(1):135–143
59. Vaidyanathan S (2013b) Analysis and adaptive synchronization of two novel chaotic systems with hyperbolic sinusoidal and cosinusoidal nonlinearity and unknown parameters. J Eng Sci Technol Rev 6(4):53–65
60. Vaidyanathan S (2013c) Analysis, control and synchronization of hyperchaotic Zhou system via adaptive control. Adv Intell Syst Comput 177:1–10
61. Vaidyanathan S (2014a) A new eight-term 3-D polynomial chaotic system with three quadratic nonlinearities. Far East J Math Sci 84(2):219–226
62. Vaidyanathan S (2014b) Analysis and adaptive synchronization of eight-term 3-D polynomial chaotic systems with three quadratic nonlinearities. Eur Phys J Spec Top 223(8):1519–1529
63. Vaidyanathan S (2014c) Analysis, control and synchronisation of a six-term novel chaotic system with three quadratic nonlinearities. Int J Model Identif Control 22(1):41–53
64. Vaidyanathan S (2014d) Generalized projective synchronisation of novel 3-D chaotic systems with an exponential non-linearity via active and adaptive control. Int J Model Identif Control 22(3):207–217
65. Vaidyanathan S (2014e) Global chaos synchronization of identical Li-Wu chaotic systems via sliding mode control. Int J Model Identif Control 22(2):170–177
66. Vaidyanathan S (2015) Analysis, properties and control of an eight-term 3-D chaotic system with an exponential nonlinearity. Int J Model Identif Control 23(2):164–172
67. Vaidyanathan S, Azar AT (2015a) Analysis and control of a 4-D novel hyperchaotic system. In: Azar AT, Vaidyanathan S (eds) Chaos Model Control Syst Des Stud Comput Intell, vol 581. Springer, Germany, pp 19–38
68. Vaidyanathan S, Azar AT (2015b) Analysis, control and synchronization of a nine-term 3-D novel chaotic system. In: Azar AT, Vaidyanathan S (eds) Chaos modelling and control systems design, studies in computational intelligence, vol 581. Springer, Germany, pp 19–38

69. Vaidyanathan S, Azar AT (2015c) Anti-synchronization of identical chaotic systems using sliding mode control and an application to Vaidhyanathan-Madhavan chaotic systems. Stud Comput Intell 576:527–547
70. Vaidyanathan S, Azar AT (2015d) Hybrid synchronization of identical chaotic systems using sliding mode control and an application to Vaidhyanathan chaotic systems. Stud Comput Intell 576:549–569
71. Vaidyanathan S, Madhavan K (2013) Analysis, adaptive control and synchronization of a seven-term novel 3-D chaotic system. Int J Control Theory Appl 6(2):121–137
72. Vaidyanathan S, Pakiriswamy S (2013) Generalized projective synchronization of six-term Sundarapandian chaotic systems by adaptive control. Int J Control Theory Appl 6(2):153–163
73. Vaidyanathan S, Rajagopal K (2011a) Anti-synchronization of Li and T chaotic systems by active nonlinear control. Commun Comput Inf Sci 198:175–184
74. Vaidyanathan S, Rajagopal K (2011b) Global chaos synchronization of hyperchaotic Pang and Wang systems by active nonlinear control. Commun Comput Inf Sci 204:84–93
75. Vaidyanathan S, Rajagopal K (2011c) Global chaos synchronization of Lü and Pan systems by adaptive nonlinear control. Commun Comput Inf Sci 205:193–202
76. Vaidyanathan S, Rajagopal K (2012) Global chaos synchronization of hyperchaotic Pang and hyperchaotic Wang systems via adaptive control. Int J Soft Comput 7(1):28–37
77. Vaidyanathan S, Rasappan S (2011) Global chaos synchronization of hyperchaotic Bao and Xu systems by active nonlinear control. Commun Comput Inf Sci 198:10–17
78. Vaidyanathan S, Rasappan S (2014) Global chaos synchronization of n-scroll Chua circuit and Lur'e system using backstepping control design with recursive feedback. Arabian J Sci Eng 39(4):3351–3364
79. Vaidyanathan S, Sampath S (2011) Global chaos synchronization of hyperchaotic Lorenz systems by sliding mode control. Commun Comput Inf Sci 205:156–164
80. Vaidyanathan S, Sampath S (2012) Anti-synchronization of four-wing chaotic systems via sliding mode control. Int J Autom Comput 9(3):274–279
81. Vaidyanathan S, Volos C, Pham VT (2014a) Hyperchaos, adaptive control and synchronization of a novel 5-D hyperchaotic system with three positive Lyapunov exponents and its SPICE implementation. Arch Control Sci 24(4):409–446
82. Vaidyanathan S, Volos C, Pham VT, Madhavan K, Idowu BA (2014b) Adaptive backstepping control, synchronization and circuit simulation of a 3-D novel jerk chaotic system with two hyperbolic sinusoidal nonlinearities. Arch Control Sci 24(3):375–403
83. Vaidyanathan S, Idowu BA, Azar AT (2015a) Backstepping controller design for the global chaos synchronization of Sprott's jerk systems. Stud Comput Intell 581:39–58
84. Vaidyanathan S, Volos C, Pham VT, Madhavan K (2015b) Analysis, adaptive control and synchronization of a novel 4-D hyperchaotic hyperjerk system and its SPICE implementation. Arch Control Sci 25(1):5–28
85. Vaidyanathan S, Volos CK, Pham VT (2015c) Global chaos control of a novel nine-term chaotic system via sliding mode control. In: Azar AT, Zhu Q (eds) Advances and applications in sliding mode control systems, studies in computational intelligence, vol 576. Springer, Germany, pp 571–590
86. Wei Z, Yang Q (2010) Anti-control of Hopf bifurcation in the new chaotic system with two stable node-foci. Appl Math Comput 217(1):422–429
87. Xi Z, Ding Z (2007) Global adaptive output regulation of a class of nonlinear systems with nonlinear exosystems. Automatica 43(1):143–149
88. Yang X, Huang J (2012) New results on robust output regulation of nonlinear systems with a nonlinear exosystem. Int J Robust Nonlinear Control 22(15):1703–1719
89. Zhou W, Xu Y, Lu H, Pan L (2008) On dynamics analysis of a new chaotic attractor. Phys Lett A 372(36):5773–5777
90. Zhu C, Liu Y, Guo Y (2010) Theoretic and numerical study of a new chaotic system. Intell Inf Manag 2:104–109

General Observer Design for Continuous-Time and Discrete-Time Nonlinear Systems

Sundarapandian Vaidyanathan

Abstract In this work, it is established that *detectability* is a necessary condition for the existence of general observers (asymptotic or exponential) for nonlinear systems. Using this necessary condition, it is shown that there does not exist any general observer (asymptotic or exponential) for nonlinear systems with real parametric uncertainty if the state equilibrium does not change with the parameter values and if the plant output function is purely a function of the state. Next, using center manifold theory, necessary and sufficient conditions are derived for the existence of general exponential observers for *Lyapunov stable* nonlinear systems. As an application of this general result, it is shown that for the existence of general exponential observers for Lyapunov stable nonlinear systems, the dimension of the state of the general exponential observer should not be less than the number of critical eigenvalues of the linearization matrix of the state dynamics of the plant. Results have been derived for both continuous-time and discrete-time nonlinear systems.

Keywords Nonlinear observers · Exponential observers · Asymptotic observers · General observers · Detectability

1 Introduction

An observer for a plant is a system which performs the reconstruction of the state vector from the available inputs. The problem of designing observers for linear control systems was first introduced and fully solved by Luenberger [9]. The problem of designing observers for nonlinear control systems was proposed by Thau [23]. Over the past three decades, significant attention has been paid in the control systems literature to the construction of observers for nonlinear control systems [1].

S. Vaidyanathan (✉)
Research and Development Centre, Vel Tech University,
Avadi, Chennai 600062, Tamil Nadu, India
e-mail: sundarvtu@gmail.com

S. Vaidyanathan and C. Volos (eds.), *Advances and Applications in Nonlinear Control Systems*, Studies in Computational Intelligence 635,
DOI 10.1007/978-3-319-30169-3_5

A necessary condition for the existence of a local exponential observer for nonlinear control systems was obtained by Xia and Gao [27]. On the other hand, sufficient conditions for nonlinear observers have been derived in the control literature from an impressive variety of points of view. Kou, Elliott and Tarn [6] derived sufficient conditions for the existence of local exponential observers using Lyapunov-like method. In [4, 7, 8, 26], suitable coordinate transformations were found under which a nonlinear control systems is transferred into a canonical form, where the observer design is carried out. In [24], Tsinias derived sufficient Lyapunov-like conditions for the existence of local asymptotic observers for nonlinear systems. A harmonic analysis method was proposed in [2] for the synthesis of nonlinear observers.

A characterization of local exponential observers for nonlinear control systems was first obtained by Sundarapandian [11]. In [11], necessary and sufficient conditions were obtained for exponential observers for Lyapunov stable continuous-time nonlinear systems and an exponential observer design was provided by Sundarapandian which generalizes the linear observer design of Luenberger [9] for linear control systems. In [14], Sundarapandian obtained necessary and sufficient conditions for exponential observers for Lyapunov stable discrete-time nonlinear systems and also provided a formula for designing exponential observers for Lyapunov stable discrete-time nonlinear systems. In [10], Sundarapandian derived new results for the global observer design for nonlinear control systems.

The concept of nonlinear observers for nonlinear control systems was also extended in many ways. In [12, 13], Sundarapandian derived new results characterizing local exponential observers for nonlinear bifurcating systems. In [15, 16, 21, 22], Sundarapandian derived new results for the exponential observer design for a general class of nonlinear systems with real parametric uncertainty. In [17–20], Sundarapandian derived new results and characterizations for general observers for nonlinear systems.

This work gives a discussion on recent results on general observers for nonlinear systems [19, 20]. This work is organized as follows. Section 2 gives a definition of general observers (asymptotic and exponential) for continuous-time nonlinear systems. Section 3 provides a necessary condition for general asymptotic observers for continuous-time nonlinear systems. Section 4 details a characterization of general exponential observers for continuous-time nonlinear systems. Section 5 gives a definition of general observers (asymptotic and exponential) for continuous-time nonlinear systems. Section 6 provides a necessary condition for general asymptotic observers for continuous-time nonlinear systems. Section 7 details a characterization of general exponential observers for continuous-time nonlinear systems. Section 8 gives a summary of the main results discussed in this work.

2 Definition of General Observers for Continuous-Time Nonlinear Systems

In this section, we consider a C^1 nonlinear plant of the form

$$\begin{aligned} \dot{x} &= f(x) \\ y &= h(x) \end{aligned} \tag{1}$$

where $x \in \mathbf{R}^n$ is the *state* and $y \in \mathbf{R}^p$, the *output* of the plant (1). We assume that the state x belongs to an open neighbourhood X of the origin of $\mathbf{R}^n$. We assume that $f : X \to \mathbf{R}^n$ is a C^1 vector field and also that $f(0) = 0$. We also assume that the output mapping $h : X \to \mathbf{R}^p$ is a C^1 map, and also that $h(0) = 0$. Let $Y \stackrel{\Delta}{=} h(X)$.

Definition 1 Consider a C^1 dynamical system described by

$$\dot{z} = g(z, y), \quad [z \in \mathbf{R}^m] \tag{2}$$

where z is defined in a neighbourhood Z of the origin of $\mathbf{R}^m$ and $g : Z \times Y \to \mathbf{R}^m$ is a C^1 map with $g(0, 0) = 0$. Consider also the map $q : Z \to \mathbf{R}^n$ described by

$$w = q(z) \tag{3}$$

Then the candidate system (2) is called a *general asymptotic* (respectively, *general exponential*) *observer* for the plant (1) corresponding to (3) if the following two requirements are satisfied:

(O1) If $w(0) = x(0)$, then $w(t) \equiv x(t)$, for all $t \geq 0$.
(O2) There exists a neighbourhood V of the origin of $\mathbf{R}^n$ such that for all initial estimation error $w(0) - x(0) \in V$, the estimation error $e(t) = w(t) - x(t)$ tends to zero asymptotically (respectively, exponentially) as $t \to \infty$. ■

Remark 1 If a general exponential observer (2) satisfies the additional properties that $m = n$ and q is a C^1 diffeomorphism, then it is called a *full-order* general exponential observer. A full-order general exponential observer (2) with the additional property that $q = \mathrm{id}_X$ is called an *identity* exponential observer, which is the same as the standard definition of local exponential observers for nonlinear systems. ■

The estimation error e is defined by

$$e = q(z) - x \tag{4}$$

Now, we consider the composite system

$$\begin{aligned} \dot{x} &= f(x) \\ \dot{z} &= g(z, h(x)) \end{aligned} \tag{5}$$

The following lemma is straightforward.

Lemma 1 ([20]) *The following statements are equivalent.*

(a) The condition (O1) in Definition 1 holds for the composite system (1) and (2).
(b) The submanifold defined via $q(z) = x$ is invariant under the flow of the composite system (5). ■

3 A Necessary Condition for General Asymptotic Observers for Continuous-Time Nonlinear Systems

In this section, we first prove a necessary condition for the plant (1) to have general asymptotic observers.

Theorem 1 ([20]) *A necessary condition for the existence of a general asymptotic observer for the plant (1) is that the plant (1) is asymptotically detectable, i.e. any state trajectory $x(t)$ of the plant dynamics in (1) with small initial condition x_0, satisfying $h(x(t)) \equiv 0$ must be such that*

$$x(t) \to 0 \quad as \quad t \to \infty \tag{6}$$

Proof Let (2) be a general asymptotic observer for the plant (1). Then the conditions (O1) and (O2) in Definition 1 are satisfied. Now, let $x(t)$ be any state trajectory of the plant dynamics in (1) with small initial condition x_0 satisfying $y(t) = h(x(t)) \equiv 0$. Then the observer dynamics (2) reduces to

$$\dot{z} = g(z, 0) \tag{7}$$

Taking $z_0 = 0$, it is immediate from (7) that $z(t) = z(t; z_0) \equiv 0$.

Hence, $w(t) = q(z(t)) \equiv 0$.

By condition (O2), we know that the estimation error trajectory $e(t) = w(t) - x(t)$ tends to zero as $t \to \infty$. Since $w(t) \equiv 0$, it follows that $x(t) \to 0$ as $t \to \infty$.

This completes the proof. ■

Using Theorem 1, we can prove the following result which says that there is no general asymptotic observer for the following plant

$$\begin{bmatrix} \dot{x} \\ \dot{\lambda} \end{bmatrix} = \begin{bmatrix} F(x, \lambda) \\ 0 \end{bmatrix} \qquad y = h(x) \tag{8}$$

if $F(0, \lambda) = 0$ (i.e. if the equilibrium $x = 0$ of the dynamics $\dot{x} = F(x, \lambda)$ does not change with the real parametric uncertainty λ).

Theorem 2 *Suppose that the plant (8) satisfies the assumption*

$$F(0, \lambda) \equiv 0 \tag{9}$$

Then there is no general asymptotic observer for the plant (8).

Proof This is an immediate consequence of Theorem 1. We show that the plant (8) is not asymptotically detectable.

This is easily seen by taking $x(0) = x_0 = 0$ and $\lambda(0) = \lambda_0 \neq 0$.

Then we have

$$y(t) = h(x(t)) \equiv 0 \quad \text{and} \quad x(t) \equiv 0 \tag{10}$$

but $\lambda(t) \equiv \lambda_0 \neq 0$. Hence, the plant (8) is not asymptotically detectable. From Theorem 1, we deduce that there is no general asymptotic observer for the plant (8).

This completes the proof. ■

4 Necessary and Sufficient Conditions for General Exponential Observers for Continuous-Time Nonlinear Systems

In this section, we establish a basic theorem that completely characterizes the existence of general exponential observers of the form (2) for Lyapunov stable nonlinear plants of the form (1).

For this purpose, we define the system linearization pair for the nonlinear plant (1) as

$$A = \frac{\partial f}{\partial x}(0) \quad \text{and} \quad h = \frac{\partial h}{\partial x}(0) \tag{11}$$

We also define

$$E = \frac{\partial g}{\partial z}(0, 0) \quad \text{and} \quad K = \frac{\partial g}{\partial y}(0, 0) \tag{12}$$

Now, we state and prove the following result, which gives a complete characterization of the general exponential observers for Lyapunov stable nonlinear systems.

Theorem 3 *Suppose that the plant dynamics in (1) is Lyapunov stable at $x = 0$. Then the system (2) is a general exponential observer for the plant (1) with respect to (3) if and only if the following conditions are satisfied:*

(a) The submanifold defined via $q(z) = x$ is invariant under the flow of the composite system (5).

(b) The dynamics

$$\dot{z} = g(z, 0) \tag{13}$$

is locally exponentially stable at $e = 0$.

Proof Necessity. Suppose that the system (2) is a general exponential observer for the plant (1). Then the conditions (O1) and (O2) in Definition 1 are readily satisfied. By Lemma 1, the condition (O1) implies the condition (a). To see that the condition (b) also holds, we take $x(0) = 0$. Then $x(t) \equiv 0$ and $y(t) = h(x(t)) \equiv 0$, for all $t \geq 0$.

Thus, the Eq. (2) simplifies into

$$\dot{z}(t) = g(z(t), y(t)) = g(z(t), 0) \tag{14}$$

By the condition (O2) in Definition 1, it is immediate that $e(t) = q(z(t)) - x(t) = q(z(t)) \to 0$ exponentially as $t \to \infty$ for all small initial conditions z_0. Hence, we must have $z(t) \to 0$ exponentially as $t \to \infty$ for the solution trajectory $z(t)$ of the dynamics (14). Hence, we conclude that the dynamics (14) is locally exponentially stable at $z = 0$. Thus, we have established the necessity of the conditions (a) and (b).

Sufficiency. Suppose that the conditions (a) and (b) are satisfied by the plant (1) and the candidate observer (2). Since the condition (a) implies the condition (O1) of Definition 1 by Lemma 1, it suffices to show that condition (O2) in Definition 1 also holds.

By hypotheses, the equilibrium $z = 0$ of the dynamics (13) is locally exponentially stable and the equilibrium $x = 0$ of the plant dynamics in (1) is Lyapunov stable. Hence, E must be Hurwitz and A must have all eigenvalues with non-negative real parts.

We have two cases to consider.

Case I: A is Hurwitz.

By Hartman–Grobman theorem [3], it follows that the composite system (5) is locally topologically conjugate to the system

$$\begin{bmatrix} \dot{x} \\ \dot{z} \end{bmatrix} = \begin{bmatrix} A & 0 \\ KC & E \end{bmatrix} \begin{bmatrix} x \\ z \end{bmatrix} \tag{15}$$

We note that

$$\text{eig} \begin{bmatrix} A & 0 \\ KC & E \end{bmatrix} = \text{eig}(A) \cup \text{eig}(E) \tag{16}$$

Since both A and E are Hurwitz matrices, it follows from (16) that the system matrix of (15) is Hurwitz. Hence, it is immediate that $x(t) \to 0$ and $z(t) \to 0$ exponentially as $t \to \infty$. Hence, it follows trivially that $e(t) = q(z(t)) - x(t) \to 0$ exponentially as $t \to \infty$ for all small initial conditions $x(0)$ and $z(0)$.

Case II: A is not Hurwitz.

Without loss of generality, we can assume that the plant dynamics in (1) has the form

$$\begin{aligned} \dot{x}_1 &= A_1 x_1 + \phi_1(x_1, x_2) \\ \dot{x}_2 &= A_2 x_2 + \phi_2(x_1, x_2) \end{aligned} \tag{17}$$

where $x_1 \in \mathbf{R}^{n_1}, x_2 \in \mathbf{R}^{n_2}$ (with $n_1 + n_2 = n$), A_1 is an $n_1 \times n_1$ matrix having all eigenvalues with zero real part, A_2 is an $n_2 \times n_2$ Hurwitz matrix and ϕ_1, ϕ_2 are C^1 functions vanishing at $(x_1, x_2) = (0, 0)$ together with all their first-order partial derivatives.

Now, $x = 0$ is a Lyapunov stable equilibrium of the dynamics in (1). Also, the equilibrium $z = 0$ of the dynamics (13) is locally exponentially stable. Hence, by a total stability result [5], it follows that $(x, z) = (0, 0)$ is a Lyapunov stable equilibrium of the composite system (5) (by its triangular structure).

Also, by the center manifold theorem for flows [25], we know that the composite system (5) has a local center manifold at $(x, z) = (0, 0)$, the graph of a C^1 map,

$$\begin{bmatrix} x_2 \\ z \end{bmatrix} = \pi(x_1) = \begin{bmatrix} \pi_1(x_1) \\ \pi_2(x_1) \end{bmatrix} \tag{18}$$

Since $q(z) = x$ is an invariant manifold for the composite system (5), it is immediate that along the center manifold, we have

$$q(\pi_2(x_1)) = \begin{bmatrix} x_1 \\ \pi_1(x_1) \end{bmatrix}. \tag{19}$$

By the principle of asymptotic phase in the center manifold theory [25], there exists a neighbourhood V of $(x, z) = (0, 0)$ such that for all $(x(0), z(0)) \in V$, we have

$$\left\| \begin{bmatrix} x_2(t) - \pi_1(x_1(t)) \\ z(t) - \pi_2(x_1(t)) \end{bmatrix} \right\| \leq M \exp(-at) \left\| \begin{bmatrix} x_2(0) - \pi_1(x_1(0)) \\ z(0) - \pi_2(x_1(0)) \end{bmatrix} \right\| \tag{20}$$

for some positive constants M and a.

Hence, it is immediate that

$$z(t) \to \pi_2(x_1(t)) \text{ exponentially as } t \to \infty \tag{21}$$

From (19) and (21), it follows that

$$q(z(t)) \to \begin{bmatrix} x_1(t) \\ \pi_1(x_1(t)) \end{bmatrix} \text{ exponentially as } t \to \infty \tag{22}$$

From (20) and (22), it follows that

$$q(z(t)) \to x(t) = \begin{bmatrix} x_1(t) \\ x_2(t) \end{bmatrix} \text{ exponentially as } t \to \infty \tag{23}$$

Thus, the condition (O2) also holds.

This completes the proof. ■

Theorem 4 *A necessary condition for the system (2) to be a general exponential observer for a Lyapunov stable plant (1) is that*

$$dim(z) \geq n_1 \tag{24}$$

where n_1 denotes the number of critical eigenvalues of the system matrix A.

Proof If the system matrix A is Hurwitz, then $n_1 = 0$ and there is nothing to prove.

If A is not Hurwitz, then by the center manifold theory, we have

$$q(\pi_2(x_1)) = \begin{bmatrix} x_1 \\ \pi_1(x_1) \end{bmatrix} \tag{25}$$

For every small $x_1 \in \mathbf{R}^{n_1}$, we know that the vector

$$\begin{bmatrix} x_1 \\ \pi_1(x_1) \end{bmatrix}$$

has a pre-image $\pi_2(x_1)$ under the mapping, q. Hence, it is immediate that the dimension of the domain of the mapping, q, cannot be lower than the dimension of the state x_1.

This completes the proof. ■

5 Definition of General Observers for Discrete-Time Nonlinear Systems

In this section, we consider a nonlinear plant of the form

$$\begin{aligned} x(k+1) &= f(x(k)), \\ y(k) &= h(x(k)) \end{aligned} \tag{26}$$

where $x \in \mathbf{R}^n$ is the *state* and $y \in \mathbf{R}^p$, the *output* of the plant (26). We assume that the state x belongs to an open neighbourhood X of the origin of $\mathbf{R}^n$. We assume that $f : X \to \mathbf{R}^n$ is a C^1 map and also that $f(0) = 0$. We also assume that the output mapping $h : X \to \mathbf{R}^p$ is a C^1 map, and also that $h(0) = 0$. Let $Y \stackrel{\Delta}{=} h(X)$.

Definition 2 Consider a discrete-time dynamical system described by

$$z(k+1) = g(z(k), y(k)), \quad [z \in \mathbf{R}^m] \tag{27}$$

where z is defined in a neighbourhood Z of the origin of $\mathbf{R}^m$ and $g : Z \times Y \to \mathbf{R}^m$ is a C^1 map with $g(0, 0) = 0$. Consider also the map $q : Z \to \mathbf{R}^n$ described by

$$w = q(z) \tag{28}$$

Then the candidate system (27) is called a *general asymptotic* (respectively, *general exponential*) *observer* for the plant (26) corresponding to (28) if the following two requirements are satisfied:

(O1) If $w(0) = x(0)$, then $w(k) \equiv x(k)$, for all $k \in \mathbf{Z}_+$, where $\mathbf{Z}_+$ denotes the set of all positive integers.

(O2) There exists a neighbourhood V of the origin of $\mathbf{R}^n$ such that for all initial estimation error $w(0) - x(0) \in V$, the estimation error $e(k) = w(k) - x(k)$ tends to zero asymptotically (respectively, exponentially) as $k \to \infty$. ■

Remark 2 If a general exponential observer (27) satisfies the additional properties that $m = n$ and q is a C^1 diffeomorphism, then it is called a *full-order* general exponential observer. A full-order general exponential observer (27) with the additional property that $q = \mathrm{id}_X$ is called an *identity* exponential observer, which is the same as the standard definition of local exponential observers for nonlinear systems. ■

The estimation error e is defined by

$$e = q(z) - x \tag{29}$$

Now, we consider the composite system

$$\begin{aligned} x(k+1) &= f(x(k)) \\ z(k+1) &= g(z(k), h(x(k))) \end{aligned} \tag{30}$$

The following lemma is straightforward.

Lemma 2 ([19]) *The following statements are equivalent.*

(a) The condition (O1) in Definition 1 holds for the composite system (26) and (27).

(b) The submanifold defined via $q(z) = x$ is invariant under the flow of the composite system (30). ■

6 A Necessary Condition for General Asymptotic Observers for Discrete-Time Nonlinear Systems

In this section, we first prove a necessary condition for the plant (26) to have general asymptotic observers.

Theorem 5 ([19]) *A necessary condition for the existence of a general asymptotic observer for the discrete-time plant (26) is that the plant (26) is asymptotically detectable, i.e. any state trajectory $x(k)$ of the plant dynamics in (26) with small initial condition x_0, satisfying $h(x(k)) \equiv 0$ must be such that*

$$x(k) \to 0 \quad as \quad k \to \infty \tag{31}$$

Proof Let (27) be a general asymptotic observer for the plant (26). Then the conditions (O1) and (O2) in Definition 2 are satisfied. Now, let $x(k)$ be any state trajectory of the plant dynamics in (26) with small initial condition x_0 satisfying $y(k) = h(x(k)) \equiv 0$. Then the observer dynamics (27) reduces to

$$z(k+1) = g(z(k), 0) \tag{32}$$

Taking $z_0 = 0$, it is immediate from (32) that $z(k) = z(k; z_0) \equiv 0$.

Hence, $w(k) = q(z(k)) \equiv 0$.

By condition (O2), we know that the error trajectory $e(k) = w(k) - x(k)$ tends to zero as $k \to \infty$. Since $w(k) \equiv 0$, it follows that $x(k) \to 0$ as $k \to \infty$.

This completes the proof. ■

Using Theorem 5, we can prove the following result which says that there is no general asymptotic observer for the following plant

$$\begin{bmatrix} x(k+1) \\ \lambda(k+1) \\ y(k) \end{bmatrix} = \begin{bmatrix} F(x(k), \lambda(k)) \\ \lambda(k) \\ = h(x(k)) \end{bmatrix} \tag{33}$$

if $F(0, \lambda) = 0$ (i.e. if the equilibrium $x = 0$ of the dynamics $x(k+1) = F(x(k), \lambda(k))$ does not change with the real parametric uncertainty λ).

Theorem 6 *Suppose that the plant (33) satisfies the assumption*

$$F(0, \lambda) \equiv 0 \tag{34}$$

Then there is no general asymptotic observer for the plant (33).

Proof This is an immediate consequence of Theorem 5. We show that the plant (33) is not asymptotically detectable.

This is easily seen by taking $x(0) = x_0 = 0$ and $\lambda(0) = \lambda_0 \neq 0$.

Then we have

$$y(k) = h(x(k)) \equiv 0 \quad \text{and} \quad x(k) \equiv 0 \tag{35}$$

but $\lambda(k) \equiv \lambda_0 \neq 0$. Hence, the plant (33) is not asymptotically detectable. From Theorem 5, we deduce that there is no general asymptotic observer for the plant (33).

This completes the proof. ■

7 Necessary and Sufficient Conditions for General Exponential Observers for Discrete-Time Nonlinear Systems

In this section, we establish a basic theorem that completely characterizes the existence of general exponential observers of the form (27) for Lyapunov stable nonlinear plants of the form (26).

For this purpose, we define the system linearization pair for the nonlinear plant (26) as

$$A = \frac{\partial f}{\partial x}(0) \quad \text{and} \quad h = \frac{\partial h}{\partial x}(0) \tag{36}$$

We also define

$$E = \frac{\partial g}{\partial z}(0, 0) \quad \text{and} \quad K = \frac{\partial g}{\partial y}(0, 0) \tag{37}$$

Now, we state and prove the following result, which gives a complete characterization of the general exponential observers for Lyapunov stable nonlinear systems.

Theorem 7 *Suppose that the plant dynamics in (26) is Lyapunov stable at $x = 0$. Then the system (27) is a general exponential observer for the plant (26) with respect to (28) if and only if the following conditions are satisfied:*

(a) The submanifold defined via $q(z) = x$ is invariant under the flow of the composite system (30).

(b) The dynamics

$$z(k + 1) = g(z(k), 0) \tag{38}$$

is locally exponentially stable at $e = 0$.

Proof Necessity. Suppose that the system (27) is a general exponential observer for the plant (26). Then the conditions (O1) and (O2) in Definition 2 are readily satisfied. By Lemma 2, the condition (O1) implies the condition (a). To see that the condition (b) also holds, we take $x(0) = 0$. Then $x(k) \equiv 0$ and $y(k) = h(x(k)) \equiv 0$, for all $k \in \mathbf{Z}_+$.

Thus, the Eq. (27) simplifies into

$$z(k + 1) = g(z(k), y(k)) = g(z(k), 0) \tag{39}$$

By the condition (O2) in Definition 2, it is immediate that $e(k) = q(z(k)) - x(k) = q(z(k)) \to 0$ exponentially as $k \to \infty$ for all small initial conditions z_0. Hence, we must have $z(k) \to 0$ exponentially as $k \to \infty$ for the solution trajectory $z(k)$ of the dynamics (39). Hence, we conclude that the dynamics (39) is locally exponentially stable at $z = 0$. Thus, we have established the necessity of the conditions (a) and (b).

Sufficiency. Suppose that the conditions (a) and (b) are satisfied by the plant (26) and the candidate observer (27). Since the condition (a) implies the condition (O1) of Definition 2 by Lemma 2, it suffices to show that condition (O2) in Definition 2 also holds.

By hypotheses, the equilibrium $z = 0$ of the dynamics (38) is locally exponentially stable and the equilibrium $x = 0$ of the plant dynamics in (26) is Lyapunov stable. Hence, E must be convergent and A must have all eigenvalues ζ with $|\zeta| \leq 1$.

We have two cases to consider.

Case I: A is convergent.

By Hartman–Grobman theorem for maps, it follows that the composite system (30) is locally topologically conjugate to the system

$$\begin{bmatrix} x(k+1) \\ z(k+1) \end{bmatrix} = \begin{bmatrix} A & 0 \\ KC & E \end{bmatrix} \begin{bmatrix} x(k) \\ z(k) \end{bmatrix} \tag{40}$$

We note that

$$\text{eig} \begin{bmatrix} A & 0 \\ KC & E \end{bmatrix} = \text{eig}(A) \cup \text{eig}(E) \tag{41}$$

Since both A and E are convergent matrices, it follows from (41) that the system matrix of (40) is convergent. Hence, it is immediate that $x(k) \to 0$ and $z(k) \to 0$ exponentially as $k \to \infty$. Hence, it follows trivially that $e(k) = q(z(k)) - x(k) \to 0$ exponentially as $k \to \infty$ for all small initial conditions $x(0)$ and $z(0)$.

Case II: A is not convergent.

Without loss of generality, we can assume that the plant dynamics in (26) has the form

$$\begin{aligned} x_1(k+1) &= A_1 x_1(k) + \phi_1(x_1(k), x_2(k)) \\ x_2(k+1) &= A_2 x_2(k) + \phi_2(x_1(k), x_2(k)) \end{aligned} \tag{42}$$

where $x_1 \in \mathbf{R}^{n_1}, x_2 \in \mathbf{R}^{n_2}$ (with $n_1 + n_2 = n$), A_1 is an $n_1 \times n_1$ matrix having all eigenvalues with unit modulus, A_2 is an $n_2 \times n_2$ convergent matrix and ϕ_1, ϕ_2 are C^1 functions vanishing at $(x_1, x_2) = (0, 0)$ together with all their first-order partial derivatives.

Now, $x = 0$ is a Lyapunov stable equilibrium of the dynamics in (26). Also, the equilibrium $z = 0$ of the dynamics (38) is locally exponentially stable. Hence, by a total stability result [5], it follows that $(x, z) = (0, 0)$ is a Lyapunov stable equilibrium of the composite system (30) (by its triangular structure).

Also, by the center manifold theorem for maps, we know that the composite system (30) has a local center manifold at $(x, z) = (0, 0)$, the graph of a C^1 map,

$$\begin{bmatrix} x_2 \\ z \end{bmatrix} = \pi(x_1) = \begin{bmatrix} \pi_1(x_1) \\ \pi_2(x_1) \end{bmatrix} \tag{43}$$

Since $q(z) = x$ is an invariant manifold for the composite system (30), it is immediate that along the center manifold, we have

$$q(\pi_2(x_1)) = \begin{bmatrix} x_1 \\ \pi_1(x_1) \end{bmatrix}. \tag{44}$$

By the principle of asymptotic phase in the center manifold theory [25], there exists a neighbourhood V of $(x, z) = (0, 0)$ such that for all $(x(0), z(0) \in V$, we have

$$\left\| \begin{bmatrix} x_2(k) - \pi_1(x_1(k)) \\ z(k) - \pi_2(x_1(k)) \end{bmatrix} \right\| \leq Ma^k \left\| \begin{bmatrix} x_2(0) - \pi_1(x_1(0)) \\ z(0) - \pi_2(x_1(0)) \end{bmatrix} \right\| \tag{45}$$

for some positive constant M and $0 < a < 1$.

Hence, it is immediate that

$$z(k) \to \pi_2(x_1(k)) \text{ exponentially as } k \to \infty \tag{46}$$

From (44) and (46), it follows that

$$q(z(k)) \to \begin{bmatrix} x_1(k) \\ \pi_1(x_1(k)) \end{bmatrix} \text{ exponentially as } k \to \infty \tag{47}$$

From (45) and (47), it follows that

$$q(z(k)) \to x(k) = \begin{bmatrix} x_1(k) \\ x_2(k) \end{bmatrix} \text{ exponentially as } k \to \infty \tag{48}$$

Thus, the condition (O2) also holds.

This completes the proof. ■

Theorem 8 *A necessary condition for the system (27) to be a general exponential observer for a Lyapunov stable plant (26) is that*

$$dim(z) \geq n_1 \tag{49}$$

where n_1 denotes the number of critical eigenvalues of the system matrix A.

Proof If the system matrix A is convergent, then $n_1 = 0$ and there is nothing to prove.

If A is not convergent, then by the center manifold theory, we have

$$q(\pi_2(x_1)) = \begin{bmatrix} x_1 \\ \pi_1(x_1) \end{bmatrix} \tag{50}$$

For every small $x_1 \in \mathbf{R}^{n_1}$, we know that the vector

$$\begin{bmatrix} x_1 \\ \pi_1(x_1) \end{bmatrix}$$

has a pre-image $\pi_2(x_1)$ under the mapping, q. Hence, it is immediate that the dimension of the domain of the mapping, q, cannot be lower than the dimension of the state x_1. This completes the proof. ■

8 Conclusions

This work has studied the problem of constructing general asymptotic and exponential observers for both continuous-time and discrete-time nonlinear systems. First, asymptotic detectability has been shown to be a necessary condition for the construction of general asymptotic observers for nonlinear systems. Next, necessary and sufficient conditions have been derived for the construction of general exponential observers for nonlinear systems. It has been established that the dimension of a general exponential observer cannot be lower than the number of critical eigenvalues of the system linearization matrix of the plant dynamics of a given nonlinear plant.

References

1. Besancon G (2007) Nonlinear observers and applications. Lecture notes in control and information sciences, vol 363. Springer, Berlin
2. Celle F, Gauthier JP, Kazakos D, Salle G (1989) Synthesis of nonlinear observers: a harmonic analysis approach. Math Syst Theory 22:291–322
3. Chicone C (1999) Ordinary differential equations with applications. Springer, New York
4. Gauthier JP, Hammouri H, Othman S (1992) A simple observer for nonlinear systems—applications to bioreactors. IEEE Trans Autom Control 37:875–880
5. Hahn W (1967) Stability of motion. Springer, New York
6. Kou SR, Elliott DL, Tarn TJ (1975) Exponential observers for nonlinear dynamic systems. Inf Control 29(3):204–216
7. Krener AJ, Isidori A (1983) Linearization by output injection and nonlinear observers. Syst Control Lett 3:47–52
8. Krener AJ, Respondek W (1985) Nonlinear observers with linearizable error dynamics. SIAM J Control Optim 23:197–216
9. Luenberger DG (1966) Observers for multivariable linear systems. IEEE Trans Autom Control 2:190–197
10. Sundarapandian V (2002) Global observer design for nonlinear systems. Math Comput Model 35(1–2):45–54
11. Sundarapandian V (2002) Local observer design for nonlinear systems. Math Comput Model 35(1–2):25–36
12. Sundarapandian V (2002) Nonlinear observer design for bifurcating systems. Math Comput Model 36(1–2):183–188

13. Sundarapandian V (2002) Nonlinear observer design for discrete-time bifurcating systems. Math Comput Model 36(1–2):211–215
14. Sundarapandian V (2002) Observer design for discrete-time nonlinear systems. Math Comput Model 35(1–2):37–44
15. Sundarapandian V (2003) Exponential observer design for discrete-time nonlinear systems with real parametric uncertainty. Math Comput Model 37(1–2):191–204
16. Sundarapandian V (2003) Exponential observer design for nonlinear systems with real parametric uncertainty. Math Comput Model 37(1–2):177–190
17. Sundarapandian V (2004) General observers for discrete-time nonlinear systems. Math Comput Model 39(1):87–95
18. Sundarapandian V (2004) General observers for nonlinear systems. Math Comput Model 39(1):97–105
19. Sundarapandian V (2004) New results on general observers for discrete-time nonlinear systems. Appl Math Lett 17(12):1415–1420
20. Sundarapandian V (2004) New results on general observers for nonlinear systems. Appl Math Lett 17(12):1421–1426
21. Sundarapandian V (2005) Nonlinear observer design for a general class of discrete-time nonlinear systems with real parametric uncertainty. Comput Math Appl 49(7–8):1177–1194
22. Sundarapandian V (2005) Nonlinear observer design for a general class of nonlinear systems with real parametric uncertainty. Comput Math Appl 49(7–8):1195–1211
23. Thau FE (1973) Observing the states of nonlinear dynamical systems. Int J Control 18:471–479
24. Tsinias J (1989) Observer design for nonlinear systems. Syst Control Lett 13:135–142
25. Vanderbauwhede A, Gils SAV (1987) Center manifolds and contraction on a scale of Banach spaces. J Funct Anal 72:209–224
26. Xia XH, Gao WB (1988) Nonlinear observer design by canonical form. Int J Control 47:1081–1100
27. Xia XH, Gao WB (1988) On exponential observers for nonlinear systems. Syst Control Lett 11:319–325

Generalized Projective Synchronization of Vaidyanathan Chaotic System via Active and Adaptive Control

Sundarapandian Vaidyanathan

Abstract Generalized projective synchronization (GPS) of chaotic systems generalizes known types of synchronization schemes such as complete synchronization (CS), anti-synchronization (AS), hybrid synchronization (HS), projective synchronization (PS), etc. In this work, we have designed active and adaptive controllers for the generalized projective synchronization (GPS) of identical Vaidyanathan chaotic systems (2014). Vaidyanathan system is an eight-term chaotic system with three quadratic nonlinearities. The Lyapunov exponents of the Vaidyanathan chaotic system are obtained as $L_1 = 6.5294$, $L_2 = 0$ and $L_3 = -26.4696$. Since the maximal Lyapunov exponent of the Vaidyanathan system is $L_1 = 6.5294$, the system exhibits highly chaotic behaviour. The Kaplan–Yorke dimension of the Vaidyanathan chaotic system is obtained as $D_{KY} = 2.2467$. The main GPS results in this work have been established using Lyapunov stability theory. MATLAB plots have been depicted to illustrate the phase portraits of the Vaidyanathan chaotic system and also the GPS results for Vaidyanathan chaotic systems using active and adaptive controllers.

Keywords Chaos · Chaotic systems · Synchronization · Active control · Adaptive control · Vaidyanathan system

1 Introduction

Chaotic systems are defined as nonlinear dynamical systems which are sensitive to initial conditions, topologically mixing and with dense periodic orbits. Sensitivity to initial conditions of chaotic systems is popularly known as the *butterfly effect*. Small changes in an initial state will make a very large difference in the behavior of the system at future states.

S. Vaidyanathan (✉)
Research and Development Centre, Vel Tech University,
Avadi, Chennai 600062, Tamil Nadu, India
e-mail: sundarvtu@gmail.com

S. Vaidyanathan and C. Volos (eds.), *Advances and Applications in Nonlinear Control Systems*, Studies in Computational Intelligence 635,
DOI 10.1007/978-3-319-30169-3_6

Some classical paradigms of 3-D chaotic systems in the literature are Lorenz system [12], Rössler system [24], ACT system [1], Sprott systems [32], Chen system [7], Lü system [13], Cai system [5], Tigan system [43], etc.

Many new chaotic systems have been discovered in the recent years such as Zhou system [97], Zhu system [98], Li system [11], Wei-Yang system [93], Sundarapandian systems [35, 40], Vaidyanathan systems [52, 53, 55–58, 60, 61, 63, 66, 70, 82, 84, 86, 87, 89], Pehlivan system [17], Sampath–Vaidyanathan system [25], etc.

The synchronization of chaotic systems is a phenomenon that occurs when two or more chaotic systems are coupled or when a chaotic system drives another chaotic system. Because of the butterfly effect which causes exponential divergence of the trajectories of two identical chaotic systems started with nearly the same initial conditions, the synchronization of chaotic systems is a challenging research problem in the chaos literature [2, 3].

Major works on synchronization of chaotic systems deal with the complete synchronization (CS) of a pair of chaotic systems called the *master* and *slave* systems. The design goal of the complete synchronization is to apply the output of the master system to control the slave system so that the output of the slave system tracks the output of the master system asymptotically with time.

Pecora and Carroll pioneered the research on synchronization of chaotic systems with their seminal papers [6, 16]. The active control method [33, 45, 50, 72, 76] is commonly used when the system parameters are available for measurement. Adaptive control method [34, 46, 54, 62, 73, 75, 81, 85, 88] is commonly used when some or all the system parameters are not available for measurement and estimates for the uncertain parameters of the systems. Memristors [18, 91, 92] are also considered for the synchronization of chaotic systems.

Backstepping control method [19–23, 42, 78, 83, 90] is also used for the synchronization of chaotic systems, which is a recursive method for stabilizing the origin of a control system in strict-feedback form. Sliding mode control method [41, 47, 49, 51, 59, 64, 65, 79, 80] is also a popular method for the synchronization of chaotic systems, which is a nonlinear control method that alters the dynamics of a nonlinear system by application of a discontinuous control signal that forces the system to "slide" along a cross-section of the system's normal behavior.

In the chaos literature, many types of synchronization schemes have been proposed such as complete synchronization [33, 45, 50, 72, 76], anti-synchronization [36–38, 48, 71], hybrid synchronization [9, 39, 44, 74, 77], generalized synchronization [4, 8, 95], projective synchronization [31, 94, 96], generalized projective synchronization [14, 15, 26–30, 67–69], etc.

Complete synchronization (CS) is characterized by the equality of state variables evolving in time, while anti-synchronization (AS) is characterized by the disappearance of the sum of relevant state variables evolving in time.

In hybrid synchronization (HS) of two chaotic systems, one part of the systems is completely synchronized and the other part is anti-synchronized. Typically, in the hybrid synchronization of two chaotic systems, the respective odd states are completely synchronized and the respective even states are anti-synchronized so that

the complete synchronization (CS) and anti-synchronization (AS) co-exist in the synchronized systems.

Projective synchronization (PS) is characterized by the fact that the master and slave systems could be synchronized up to a scaling factor. In generalized projective synchronization (GPS), the responses of the synchronized dynamical states synchronize up to a constant scaling matrix α. The complete synchronization (CS) and anti-synchronization (AS) are special cases of the generalized projective synchronization where the scaling matrix $\alpha = I$ and $\alpha = -I$, respectively.

This work derives new results for the active and adaptive controller design for the generalized projective synchronization (GPS) of the Vaidyanathan chaotic system [56], which is a novel chaotic system with highly chaotic behaviour.

This work is organized as follows. Section 2 discusses the qualitative analysis of the Vaidyanathan chaotic system [56]. Vaidyanathan system is an eight-term polynomial chaotic system with three quadratic nonlinearities. In this section, the Lyapunov exponents of the Vaidyanathan chaotic system are obtained as $L_1 = 6.5294$, $L_2 = 0$ and $L_3 = -26.4696$. Since the maximal Lyapunov exponent of the Vaidyanathan system is $L_1 = 6.5294$, the system exhibits highly chaotic behaviour. The Kaplan–Yorke dimension of the Vaidyanathan system is obtained as $D_{KY} = 2.2467$.

In Sect. 3, we derive new GPS results for the active controller design for identical Vaidyanathan chaotic systems, when the system parameters are known. In Sect. 4, we derive new GPS results for the adaptive controller design for identical Vaidyanathan chaotic systems, when the system parameters are unknown. In Sect. 5, we summarize the main results obtained in this work.

2 Analysis of the Vaidyanathan Chaotic System

Vaidyanathan–Volos system [56] is an eight-term novel chaotic system described by the 3-D dynamics

$$\begin{aligned} \dot{x}_1 &= a(x_2 - x_1) + x_2 x_3 \\ \dot{x}_2 &= b x_1 + c x_2 - x_1 x_3 \\ \dot{x}_3 &= -d x_3 + x_1^2 \end{aligned} \tag{1}$$

where x_1, x_2, x_3 are the states and a, b, c, d are constant, positive, parameters.

The system (1) exhibits a *strange chaotic attractor* when the parameter values are taken as

$$a = 25, \quad b = 33, \quad c = 11, \quad d = 6 \tag{2}$$

The Vaidyanathan chaotic system (1) is invariant under the coordinates transformation

$$(x_1, x_2, x_3) \mapsto (-x_1, -x_2, x_3) \tag{3}$$

The transformation (3) persists for all values of the system parameters. Thus, the Vaidyanathan system (3) has a rotation symmetry about the x_3-axis. As a consequence, any non-trivial trajectory of the Vaidyanathan chaotic system (3) must have a twin trajectory.

For numerical simulations, we take the initial values of the Vaidyanathan chaotic system (1) as

$$x_1(0) = 0.8, \quad x_2(0) = 1.2, \quad x_3(0) = 0.6 \tag{4}$$

For the system parameter values (2) and the initial values (4), the Lyapunov exponents of the Vaidyanathan chaotic system (1) are obtained as

$$L_1 = 6.5294, \quad L_2 = 0, \quad L_3 = -26.4696 \tag{5}$$

Also, the Kaplan–Yorke dimension of the Vaidyanathan chaotic system (1) is obtained as

$$D_L = 2 + \frac{L_1 + L_2}{|L_3|} = 2.2467 \tag{6}$$

Figure 1 shows the 3-D phase portrait of the Vaidyanathan chaotic system (1). Figures 2, 3 and 4 show the 2-D projections of the Vaidyanathan chaotic system (1) on the (x_1, x_2), (x_2, x_3) and (x_1, x_3) coordinate planes respectively.

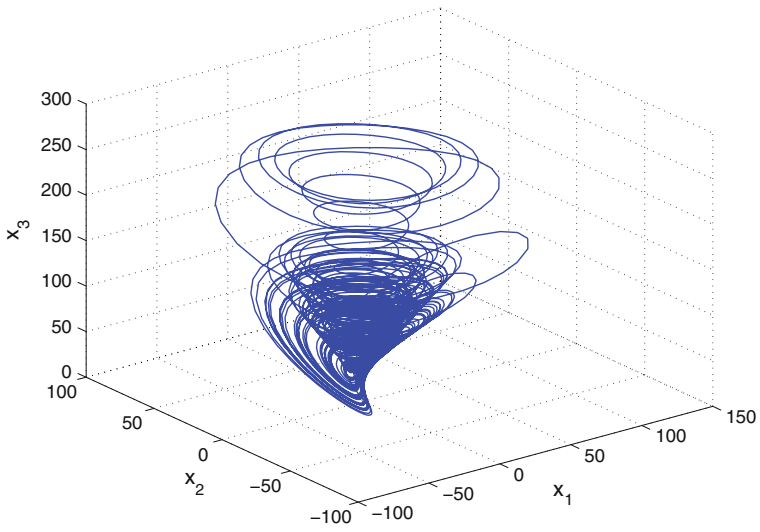

Fig. 1 3-D phase portrait of the Vaidyanathan chaotic system

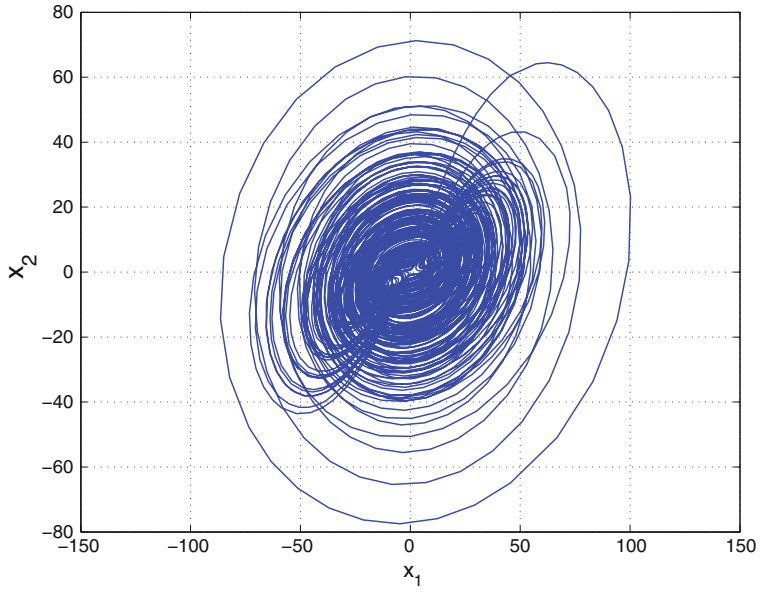

Fig. 2 2-D projection of the Vaidyanathan chaotic system on the (x_1, x_2) plane

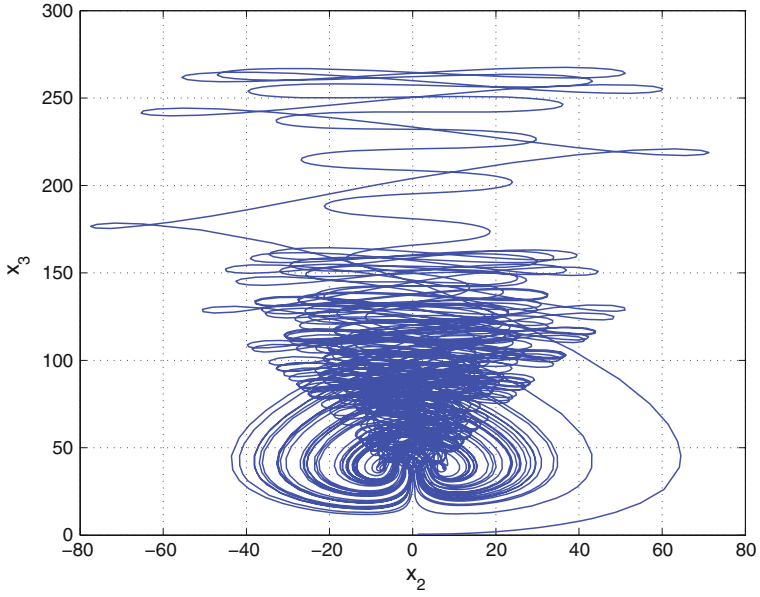

Fig. 3 2-D projection of the Vaidyanathan chaotic system on the (x_2, x_3) plane

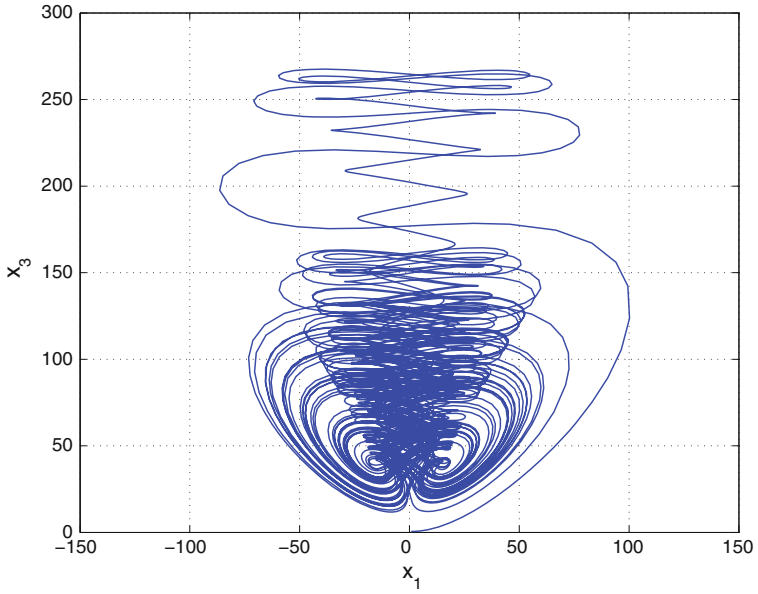

Fig. 4 2-D projection of the Vaidyanathan chaotic system on the (x_1, x_3) plane

3 Active Controller Design for the GPS of Vaidyanathan Systems

In this section, we design an active controller for the generalized projective synchronization (GPS) of identical Vaidyanathan systems [56], when the system parameters are known.

As the master system, we consider the Vaidyanathan system

$$\begin{aligned} \dot{x}_1 &= a(x_2 - x_1) + x_2 x_3 \\ \dot{x}_2 &= b x_1 + c x_2 - x_1 x_3 \\ \dot{x}_3 &= -d x_3 + x_1^2 \end{aligned} \tag{7}$$

where x_1, x_2, x_3 are the states and a, b, c, d are constant, positive, parameters.

As the slave system, we consider the controlled Vaidyanathan system

$$\begin{aligned} \dot{y}_1 &= a(y_2 - y_1) + y_2 y_3 + u_1 \\ \dot{y}_2 &= b y_1 + c y_2 - y_1 y_3 + u_2 \\ \dot{y}_3 &= -d y_3 + y_1^2 + u_3 \end{aligned} \tag{8}$$

where y_1, y_2, y_3 are the states and u_1, u_2, u_3 are active controls to be designed.

For the GPS of the identical Vaidyanathan systems (7) and (8), we define the GPS synchronization error as

$$\begin{aligned} e_1 &= y_1 - m_1 x_1 \\ e_2 &= y_2 - m_2 x_2 \\ e_3 &= y_3 - m_3 x_3 \end{aligned} \tag{9}$$

where m_1, m_2, m_3 are real scaling constants.

The error dynamics is obtained by differentiating (9) as

$$\begin{aligned} \dot{e}_1 &= a(y_2 - m_1 x_2 - e_1) + y_2 y_3 - m_1 x_2 x_3 + u_1 \\ \dot{e}_2 &= b(y_1 - m_2 x_1) + c e_2 - y_1 y_3 + m2 x_1 x_3 + u_2 \\ \dot{e}_3 &= -d e_3 + y_1^2 - m_3 x_1^2 + u_3 \end{aligned} \tag{10}$$

We consider the active controller defined by

$$\begin{aligned} u_1 &= -a(y_2 - m_1 x_2 - e_1) - y_2 y_3 + m_1 x_2 x_3 - k_1 e_1 \\ u_2 &= -b(y_1 - m_2 x_1) - c e_2 + y_1 y_3 - m2 x_1 x_3 - k_2 e_2 \\ u_3 &= d e_3 - y_1^2 + m_3 x_1^2 - k_3 e_3 \end{aligned} \tag{11}$$

where k_1, k_2, k_3 are positive gain constants.

Substituting (11) into (10), we get the closed-loop control system

$$\begin{aligned} \dot{e}_1 &= -k_1 e_1 \\ \dot{e}_2 &= -k_2 e_2 \\ \dot{e}_3 &= -k_3 e_3 \end{aligned} \tag{12}$$

Next, we establish the following main result of this section.

Theorem 1 *The active control law defined by (11) achieves global and exponential generalized projective synchronization (GPS) of the identical Vaidyanathan chaotic systems (7) and (8), where k_1, k_2, k_3 are positive gain constants.*

Proof We take the candidate Lyapunov function

$$V(e) = \frac{1}{2}\left(e_1^2 + e_2^2 + e_3^2\right) \tag{13}$$

Then V is a quadratic function and positive definite on $\mathbf{R}^3$.

Differentiating V along the trajectories of (12), we obtain

$$\dot{V} = -k_1 e_1^2 - k_2 e_2^2 - k_3 e_3^2 \tag{14}$$

which is a negative definite function on $\mathbf{R}^3$.

Thus, by Lyapunov stability theory [10], the error dynamics (12) is globally exponentially stable. ■

For numerical simulations using MATLAB, we use the classical fourth order Runge–Kutta method with $h = 10^{-8}$ for solving systems of differential equations.

The parameter values of the Vaidyanathan chaotic systems are taken as in the chaotic case (2), i.e. $a = 25$, $b = 33$, $c = 11$ and $d = 6$.

We take the gains as $k_i = 6$ for $i = 1, 2, 3$.

We the GPS scales as $m_1 = 2.3$, $m_2 = -2.9$ and $m_3 = 4.6$.

As initial values of the master system (7), we take

$$x_1(0) = 5.2, \quad x_2(0) = 4.3, \quad x_3(0) = -3.8$$

As initial values of the slave system (8), we take

$$y_1(0) = 2.7, \quad y_2(0) = 1.4, \quad y_3(0) = 4.5$$

Figures 5, 6 and 7 depict the GPS of the identical Vaidyanathan systems (7) and (8). Figure 8 depicts the time-history of the GPS synchronization errors e_1, e_2, e_3.

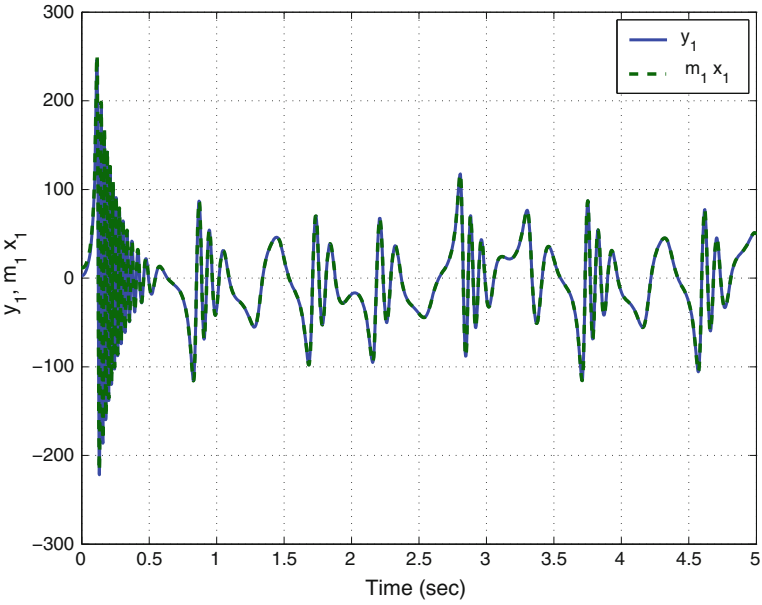

Fig. 5 Synchronization of the states y_1 and $m_1 x_1$

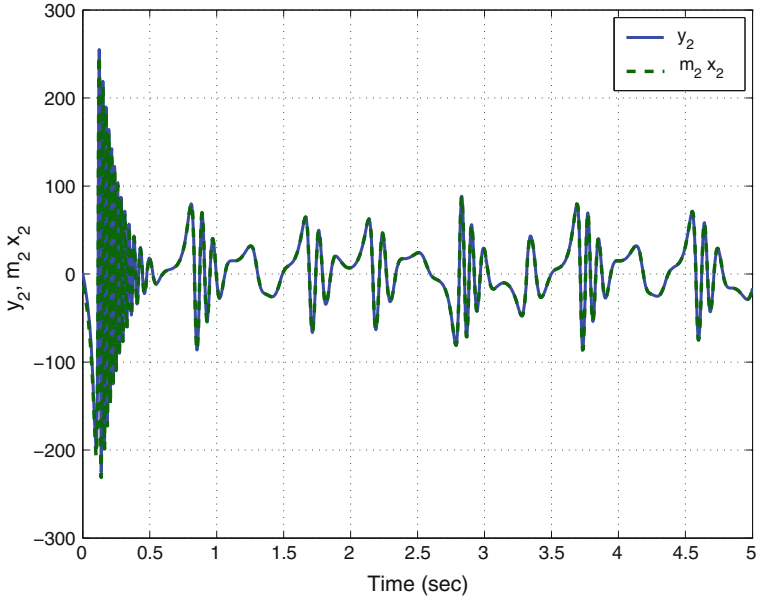

Fig. 6 Synchronization of the states y_2 and m_2x_2

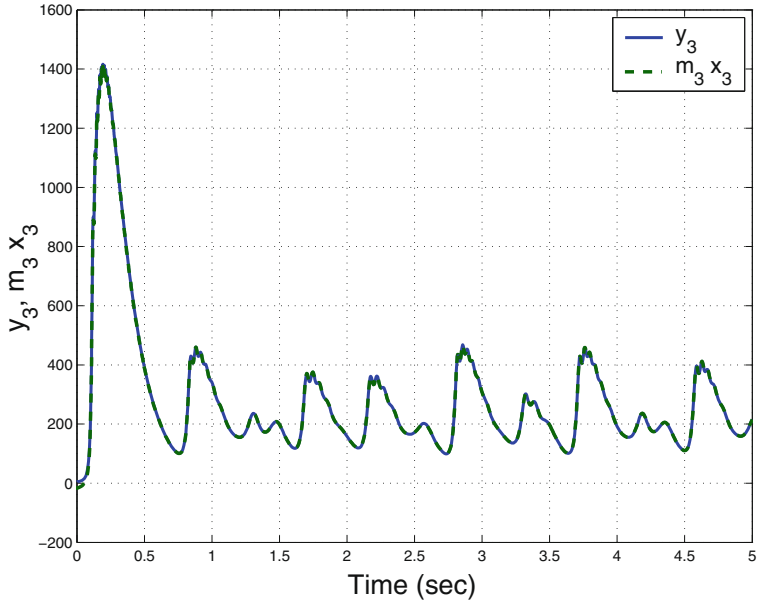

Fig. 7 Synchronization of the states y_3 and m_3x_3

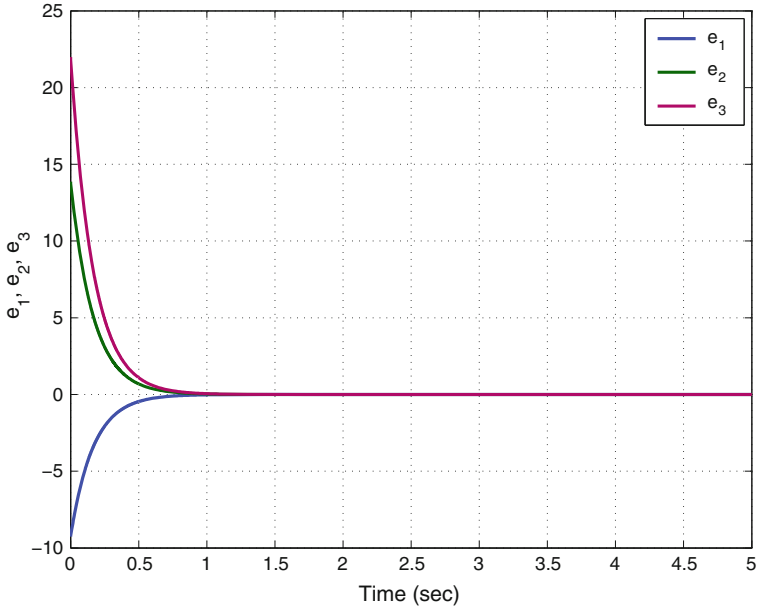

Fig. 8 Time-history of the GPS synchronization errors

4 Adaptive Controller Design for the GPS of Vaidyanathan Systems

In this section, we design an adaptive controller for the generalized projective synchronization (GPS) of identical Vaidyanathan systems [56], when the system parameters are unknown.

As the master system, we consider the Vaidyanathan system

$$\begin{aligned} \dot{x}_1 &= a(x_2 - x_1) + x_2x_3 \\ \dot{x}_2 &= bx_1 + cx_2 - x_1x_3 \\ \dot{x}_3 &= -dx_3 + x_1^2 \end{aligned} \tag{15}$$

where x_1, x_2, x_3 are the states and a, b, c, d are unknown parameters.

As the slave system, we consider the controlled Vaidyanathan system

$$\begin{aligned} \dot{y}_1 &= a(y_2 - y_1) + y_2y_3 + u_1 \\ \dot{y}_2 &= by_1 + cy_2 - y_1y_3 + u_2 \\ \dot{y}_3 &= -dy_3 + y_1^2 + u_3 \end{aligned} \tag{16}$$

where y_1, y_2, y_3 are the states and u_1, u_2, u_3 are adaptive controls to be designed using estimates for unknown parameters.

For the GPS of the identical Vaidyanathan systems (15) and (16), we define the GPS synchronization error as

$$\begin{aligned} e_1 &= y_1 - m_1 x_1 \\ e_2 &= y_2 - m_2 x_2 \\ e_3 &= y_3 - m_3 x_3 \end{aligned} \tag{17}$$

where m_1, m_2, m_3 are real scaling constants.

The error dynamics is obtained by differentiating (17) as

$$\begin{aligned} \dot{e}_1 &= a(y_2 - m_1 x_2 - e_1) + y_2 y_3 - m_1 x_2 x_3 + u_1 \\ \dot{e}_2 &= b(y_1 - m_2 x_1) + c e_2 - y_1 y_3 + m2 x_1 x_3 + u_2 \\ \dot{e}_3 &= -d e_3 + y_1^2 - m_3 x_1^2 + u_3 \end{aligned} \tag{18}$$

We consider the adaptive controller defined by

$$\begin{aligned} u_1 &= -\hat{a}(t)(y_2 - m_1 x_2 - e_1) - y_2 y_3 + m_1 x_2 x_3 - k_1 e_1 \\ u_2 &= -\hat{b}(t)(y_1 - m_2 x_1) - \hat{c}(t) e_2 + y_1 y_3 - m2 x_1 x_3 - k_2 e_2 \\ u_3 &= \hat{d}(t) e_3 - y_1^2 + m_3 x_1^2 - k_3 e_3 \end{aligned} \tag{19}$$

where k_1, k_2, k_3 are positive gain constants and $\hat{a}(t), \hat{b}(t), \hat{c}(t), \hat{d}(t)$ are estimates of the unknown parameters a, b, c, d, respectively.

Substituting (19) into (18), we get the closed-loop control system

$$\begin{aligned} \dot{e}_1 &= \left[a - \hat{a}(t)\right](y_2 - m_1 x_2 - e_1) - k_1 e_1 \\ \dot{e}_2 &= \left[b - \hat{b}(t)\right](y_1 - m_2 x_1) + \left[c - \hat{c}(t)\right] e_2 - k_2 e_2 \\ \dot{e}_3 &= -\left[d - \hat{d}(t)\right] e_3 - k_3 e_3 \end{aligned} \tag{20}$$

We define the parameter estimation errors as

$$\begin{aligned} e_a(t) &= a - \hat{a}(t) \\ e_b(t) &= b - \hat{b}(t) \\ e_c(t) &= c - \hat{c}(t) \\ e_d(t) &= d - \hat{d}(t) \end{aligned} \tag{21}$$

Using (21), we can simplify the error dynamics as

$$\begin{aligned} \dot{e}_1 &= e_a(y_2 - m_1 x_2 - e_1) - k_1 e_1 \\ \dot{e}_2 &= e_b(y_1 - m_2 x_1) + e_c e_2 - k_2 e_2 \\ \dot{e}_3 &= -e_d e_3 - k_3 e_3 \end{aligned} \tag{22}$$

Differentiating (21) with respect to t, we obtain

$$\begin{aligned} \dot{e}_a &= -\dot{\hat{a}}(t) \\ \dot{e}_b &= -\dot{\hat{b}}(t) \\ \dot{e}_c &= -\dot{\hat{c}}(t) \\ \dot{e}_d &= -\dot{\hat{d}}(t) \end{aligned} \tag{23}$$

We use adaptive control theory to find an update law for the parameter estimates. We consider the quadratic candidate Lyapunov function defined by

$$V(e_1, e_2, e_3, e_a, e_b, e_c, e_d) = \frac{1}{2}\left(e_1^2 + e_2^2 + e_3^2 + e_a^2 + e_b^2 + e_c^2 + e_d^2\right) \tag{24}$$

Differentiating V along the trajectories of (22) and (23), we obtain

$$\begin{aligned} \dot{V} = &-k_1 e_1^2 - k_2 e_2^2 - k_3 e_3^2 + e_a\left[e_1(y_2 - m_1 x_2 - e_1) - \dot{\hat{a}}\right] \\ &+ e_b\left[e_2(y_1 - m_2 x_1) - \dot{\hat{b}}\right] + e_c\left[e_2^2 - \dot{\hat{c}}\right] \\ &+ e_d\left[-e_3^2 - \dot{\hat{d}}\right] \end{aligned} \tag{25}$$

In view of Eq. (25), we take the parameter update law as

$$\begin{aligned} \dot{\hat{a}} &= e_1(y_2 - m_1 x_2 - e_1) \\ \dot{\hat{b}} &= e_2(y_1 - m_2 x_1) \\ \dot{\hat{c}} &= e_2^2 \\ \dot{\hat{d}} &= -e_3^2 \end{aligned} \tag{26}$$

Next, we state and prove the main result of this section.

Theorem 2 *The adaptive control law defined by (19) and the parameter update law (26) achieve global and exponential generalized projective synchronization (GPS) between the identical Vaidyanathan systems (15) and (16) with unknown parameters, where k_1, k_2, k_3 are positive gain constants.*

Proof We consider the quadratic Lyapunov function defined by (24), which is clearly a positive definite function on $\mathbf{R}^7$.

By substituting the parameter update law (26) into (25), we obtain the time-derivative of V as

$$\dot{V} = -k_1 e_1^2 - k_2 e_2^2 - k_3 e_3^2 \tag{27}$$

From (27), it is clear that $\dot{V}$ is a negative semi-definite function on $\mathbf{R}^7$.

Thus, we conclude that the GPS error vector $\mathbf{e}(t)$ and the parameter estimation error are globally bounded, i.e.

$$\left[e_1(t)\ e_2(t)\ e_3(t)\ e_a(t)\ e_b(t)\ e_c(t)\ e_d(t) \right]^T \in \mathbf{L}_\infty.$$

We define $k = \min\{k_1, k_2, k_3\}$.
Then it follows from (27) that

$$\dot{V} \leq -k\|\mathbf{e}(t)\|^2 \tag{28}$$

Thus, we have

$$k\|\mathbf{e}(t)\|^2 \leq -\dot{V} \tag{29}$$

Integrating the inequality (29) from 0 to t, we get

$$k\int_0^t \|\mathbf{e}(\tau)\|^2 d\tau \ \leq\ V(0) - V(t) \tag{30}$$

From (30), it follows that $\mathbf{e} \in \mathbf{L}_2$.
Using (22), we conclude that $\dot{\mathbf{e}} \in \mathbf{L}_\infty$.
Using Barbalat's lemma [10], we conclude that $\mathbf{e}(t) \to \mathbf{0}$ exponentially as $t \to \infty$ for all initial conditions $\mathbf{e}(0) \in \mathbf{R}^3$.
This completes the proof. ■

For numerical simulations using MATLAB, we use the classical fourth order Runge–Kutta method with $h = 10^{-8}$ for solving systems of differential equations.

The parameter values of the Vaidyanathan chaotic systems are taken as in the chaotic case (2), i.e.

$$a = 25,\ \ b = 33,\ \ c = 11,\ \ d = 6.$$

We take the gains as $k_i = 8$ for $i = 1, 2, 3$.
We the GPS scales as $m_1 = 1.3, m_2 = 0.4$ and $m_3 = 1.2$.
As initial values of the master system (15), we take

$$x_1(0) = 0.2,\ \ x_2(0) = 2.3,\ \ x_3(0) = 1.8$$

As initial values of the slave system (16), we take

$$y_1(0) = 2.7,\ \ y_2(0) = 1.4,\ \ y_3(0) = 2.5$$

As initial values of the parameter estimates, we take

$$\hat{a}(0) = 4.2,\ \ \hat{b}(0) = 8.1,\ \ \hat{c}(0) = 1.4,\ \ \hat{d}(0) = 2.8$$

Figures 9, 10 and 11 depict the GPS of the identical Vaidyanathan systems (15) and (16). Figure 12 depicts the time-history of the GPS synchronization errors e_1, e_2, e_3.

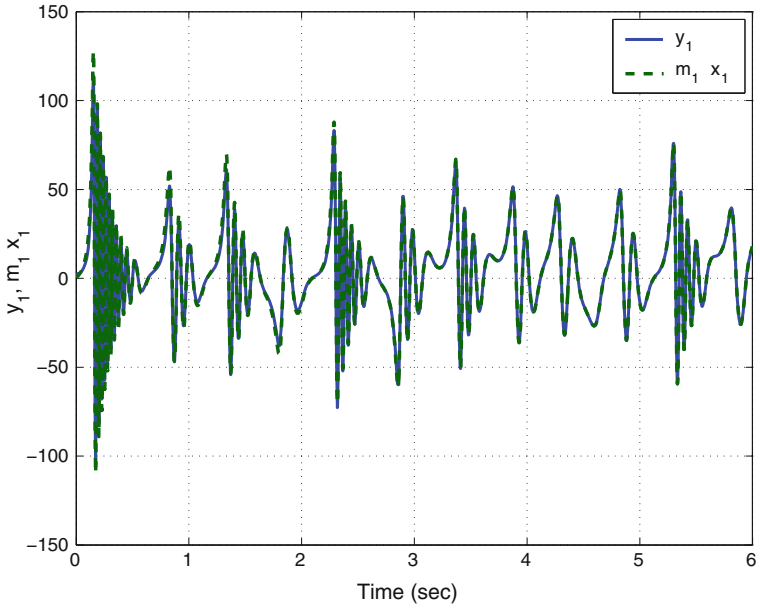

Fig. 9 Synchronization of the states y_1 and m_1x_1

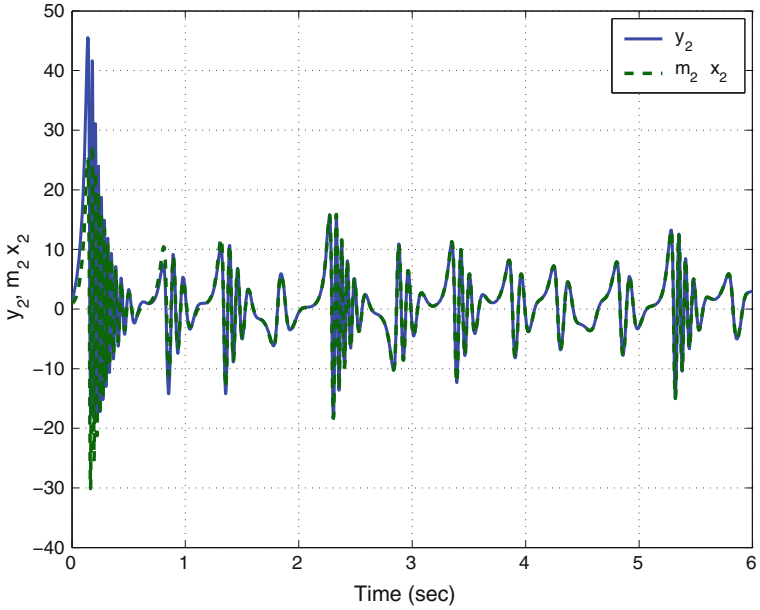

Fig. 10 Synchronization of the states y_2 and m_2x_2

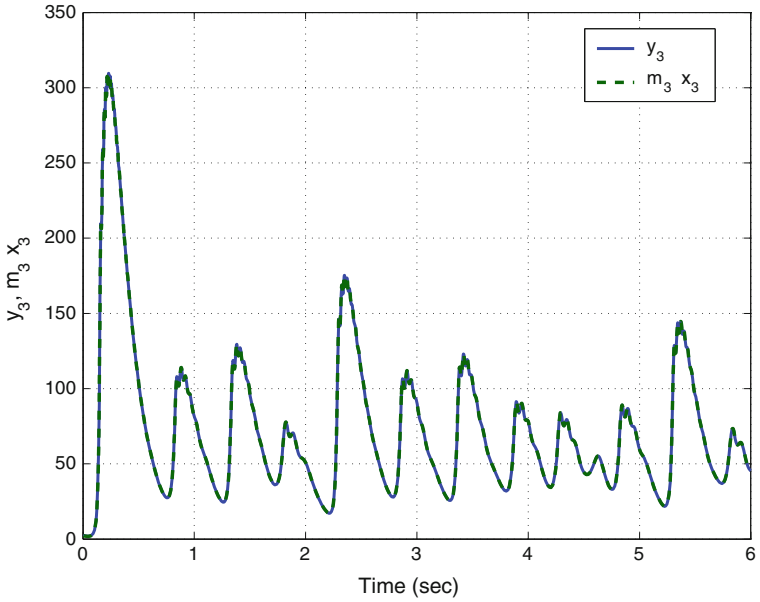

Fig. 11 Synchronization of the states y_3 and m_3x_3

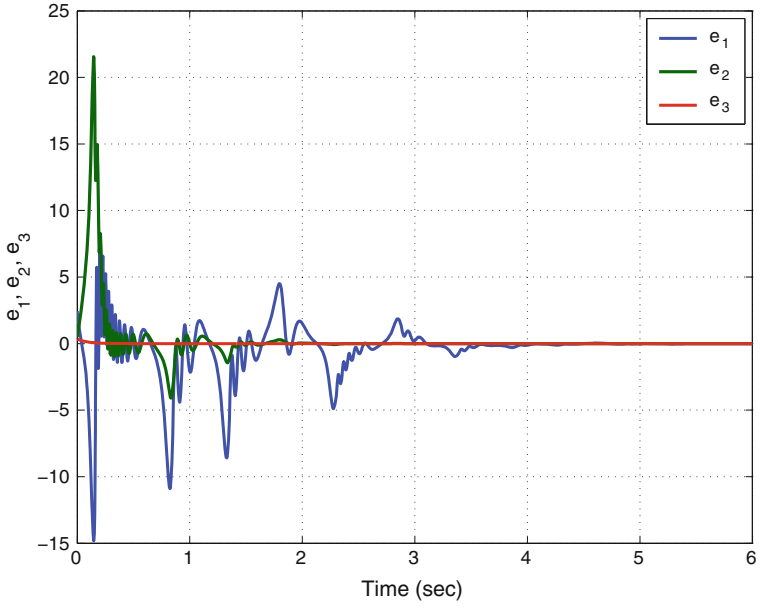

Fig. 12 Time-history of the GPS synchronization errors

5 Conclusions

In this work, we derived new results for active and adaptive controller design for the generalized projective synchronization (GPS) of identical Vaidyanathan chaotic systems (2014). Active controller design is adopted when the system parameters are known. Adaptive controller design is adopted when the system parameters are unknown. Main results were proved using Lyapunov stability theory. MATLAB plots were shown to illustrate all the main results discussed in this work.

References

1. Arneodo A, Coullet P, Tresser C (1981) Possible new strange attractors with spiral structure. Commun Math Phys 79(4):573–576
2. Azar AT, Vaidyanathan S (2015) Chaos modeling and control systems design, studies in computational intelligence, vol 581. Springer, Germany
3. Azar AT, Vaidyanathan S (2015) Computational intelligence applications in modeling and control, studies in computational intelligence, vol 575. Springer, Germany
4. Basnarkov L, Duane GS, Kocarev L (2014) Generalized synchronization and coherent structures in spatially extended systems. Chaos, Solitons and Fractals 59:35–41
5. Cai G, Tan Z (2007) Chaos synchronization of a new chaotic system via nonlinear control. J Uncertain Syst 1(3):235–240
6. Carroll TL, Pecora LM (1991) Synchronizing chaotic circuits. IEEE Trans Circuits Syst 38(4):453–456
7. Chen G, Ueta T (1999) Yet another chaotic attractor. Int J Bifurc Chaos 9(7):1465–1466
8. Hu A, Xu Z (2011) Multi-stable chaotic attractors in generalized synchronization. Commun Nonlinear Sci Numer Simul 16(8):3237–3244
9. Karthikeyan R, Sundarapandian V (2014) Hybrid synchronization of four-scroll systems via active control. J Electr Eng 65(2):97–103
10. Khalil HK (2001) Nonlinear Syst, 3rd edn. Prentice Hall, New Jersey, USA
11. Li D (2008) A three-scroll chaotic attractor. Phys Lett A 372(4):387–393
12. Lorenz EN (1963) Deterministic periodic flow. J Atmos Sci 20(2):130–141
13. Lü J, Chen G (2002) A new chaotic attractor coined. Int J Bifurc Chaos 12(3):659–661
14. Pakiriswamy S, Vaidyanathan S (2012) Generalized projective synchronization of hyperchaotic Lü and hyperchaotic Cai systems via active control. Lect Notes Inst Comput Sci Soc Inf Telecommun Eng 84:53–62
15. Pakiriswamy S, Vaidyanathan S (2012) Generalized projective synchronization of three-scroll chaotic systems via active control. Lect Notes Inst Comput Sci Soc Inf Telecommun Eng 85:146–155
16. Pecora LM, Carroll TL (1990) Synchronization in chaotic systems. Phys Rev Lett 64(8):821–824
17. Pehlivan I, Moroz IM, Vaidyanathan S (2014) Analysis, synchronization and circuit design of a novel butterfly attractor. J Sound Vib 333(20):5077–5096
18. Pham VT, Volos CK, Vaidyanathan S, Le T, Vu V (2015) A memristor-based hyperchaotic system with hidden attractors: Dynamics, synchronization and circuital emulating. J Eng Sci Technol Rev 8(2):205–214
19. Rasappan S, Vaidyanathan S (2012) Global chaos synchronization of WINDMI and Coullet chaotic systems by backstepping control. Far East J Math Sci 67(2):265–287
20. Rasappan S, Vaidyanathan S (2012) Hybrid synchronization of n-scroll Chua and Lur'e chaotic systems via backstepping control with novel feedback. Arch Control Sci 22(3):343–365

21. Rasappan S, Vaidyanathan S (2012) Synchronization of hyperchaotic Liu system via backstepping control with recursive feedback. Commun Comput Inf Sci 305:212–221
22. Rasappan S, Vaidyanathan S (2013) Hybrid synchronization of *n*-scroll chaotic Chua circuits using adaptive backstepping control design with recursive feedback. Malaysian J Math Sci 7(2):219–246
23. Rasappan S, Vaidyanathan S (2014) Global chaos synchronization of WINDMI and Coullet chaotic systems using adaptive backstepping control design. Kyungpook Math J 54(1):293–320
24. Rössler OE (1976) An equation for continuous chaos. Phys Lett A 57(5):397–398
25. Sampath S, Vaidyanathan S, Volos CK, Pham VT (2015) An eight-term novel four-scroll chaotic System with cubic nonlinearity and its circuit simulation. J Eng Sci Technol Rev 8(2):1–6
26. Sarasu P, Sundarapandian V (2011) Active controller design for generalized projective synchronization of four-scroll chaotic systems. Int J Syst Signal Control Eng Appl 4(2):26–33
27. Sarasu P, Sundarapandian V (2011) The generalized projective synchronization of hyperchaotic Lorenz and hyperchaotic Qi systems via active control. Int J Soft Comput 6(5):216–223
28. Sarasu P, Sundarapandian V (2012) Adaptive controller design for the generalized projective synchronization of 4-scroll systems. Int J Syst Signal Control Eng Appl 5(2):21–30
29. Sarasu P, Sundarapandian V (2012) Generalized projective synchronization of three-scroll chaotic systems via adaptive control. Eur J Sci Res 72(4):504–522
30. Sarasu P, Sundarapandian V (2012) Generalized projective synchronization of two-scroll systems via adaptive control. Int J Soft Comput 7(4):146–156
31. Shi Y, Zhu P, Qin K (2014) Projective synchronization of different chaotic neural networks with mixed time delays based on an integral sliding mode controller. Neurocomputing 123:443–449
32. Sprott JC (1994) Some simple chaotic flows. Phys Rev E 50(2):647–650
33. Sundarapandian V (2010) Output regulation of the Lorenz attractor. Far East J Math Sci 42(2):289–299
34. Sundarapandian V (2013) Adaptive control and synchronization design for the Lu-Xiao chaotic system. Lect Notes Electr Eng 131:319–327
35. Sundarapandian V (2013) Analysis and anti-synchronization of a novel chaotic system via active and adaptive controllers. J Eng Sci Technol Rev 6(4):45–52
36. Sundarapandian V, Karthikeyan R (2011) Anti-synchronization of hyperchaotic Lorenz and hyperchaotic Chen systems by adaptive control. Int J Syst Signal Control Eng Appl 4(2):18–25
37. Sundarapandian V, Karthikeyan R (2011) Anti-synchronization of Lü and Pan chaotic systems by adaptive nonlinear control. Eur J Sci Res 64(1):94–106
38. Sundarapandian V, Karthikeyan R (2012) Adaptive anti-synchronization of uncertain Tigan and Li systems. J Eng Appl Sci 7(1):45–52
39. Sundarapandian V, Karthikeyan R (2012) Hybrid synchronization of hyperchaotic Lorenz and hyperchaotic Chen systems via active control. J Eng Appl Sci 7(3):254–264
40. Sundarapandian V, Pehlivan I (2012) Analysis, control, synchronization, and circuit design of a novel chaotic system. Math Comput Model 55(7–8):1904–1915
41. Sundarapandian V, Sivaperumal S (2011) Sliding controller design of hybrid synchronization of four-wing chaotic systems. Int J Soft Comput 6(5):224–231
42. Suresh R, Sundarapandian V (2013) Global chaos synchronization of a family of *n*-scroll hyperchaotic Chua circuits using backstepping control with recursive feedback. Far East J Math Sci 73(1):73–95
43. Tigan G, Opris D (2008) Analysis of a 3D chaotic system. Chaos, Solitons and Fractals 36:1315–1319
44. Vaidyanathan S (2011) Hybrid chaos synchronization of Liu and Lü systems by active nonlinear control. Commun Comput Inf Sci 204:1–10
45. Vaidyanathan S (2011) Output regulatoin of Arneodo-Coullet chaotic system. Commun Comput Inf Sci 133:98–107
46. Vaidyanathan S (2012) Adaptive controller and synchronizer design for the Qi-Chen chaotic system. Lect Notes Inst Comput Sci Soc Inf Telecommun Eng 85:124–133
47. Vaidyanathan S (2012) Analysis and synchronization of the hyperchaotic Yujun systems via sliding mode control. Adv Intell Syst Comput 176:329–337

48. Vaidyanathan S (2012) Anti-synchronization of Sprott-L and Sprott-M chaotic systems via adaptive control. Int J Control Theory Appl 5(1):41–59
49. Vaidyanathan S (2012) Global chaos control of hyperchaotic Liu system via sliding control method. Int J Control Theory Appl 5(2):117–123
50. Vaidyanathan S (2012) Output regulatoin of the Liu chaotic system. Appl Mech Mat 110–116:3982–3989
51. Vaidyanathan S (2012) Sliding mode control based global chaos control of Liu-Liu-Liu-Su chaotic system. Int J Control Theory Appl 5(1):15–20
52. Vaidyanathan S (2013) A new six-term 3-D chaotic system with an exponential nonlinearity. Far East J Math Sci 79(1):135–143
53. Vaidyanathan S (2013) Analysis and adaptive synchronization of two novel chaotic systems with hyperbolic sinusoidal and cosinusoidal nonlinearity and unknown parameters. J Eng Sci Technol Rev 6(4):53–65
54. Vaidyanathan S (2013) Analysis, control and synchronization of hyperchaotic Zhou system via adaptive control. Adv Intell Syst Comput 177:1–10
55. Vaidyanathan S (2014) A new eight-term 3-D polynomial chaotic system with three quadratic nonlinearities. Far East J Math Sci 84(2):219–226
56. Vaidyanathan S (2014) Analysis and adaptive synchronization of eight-term 3-D polynomial chaotic systems with three quadratic nonlinearities. Eur Phys J Spec Top 223(8):1519–1529
57. Vaidyanathan S (2014) Analysis, control and synchronisation of a six-term novel chaotic system with three quadratic nonlinearities. Int J Model Identif Control 22(1):41–53
58. Vaidyanathan S (2014) Generalized projective synchronisation of novel 3-D chaotic systems with an exponential non-linearity via active and adaptive control. Int J Model Identif Control 22(3):207–217
59. Vaidyanathan S (2014) Global chaos synchronization of identical Li-Wu chaotic systems via sliding mode control. Int J Model Identif Control 22(2):170–177
60. Vaidyanathan S (2015) A 3-D novel highly chaotic system with four quadratic nonlinearities, its adaptive control and anti-synchronization with unknown parameters. J Eng Sci Technol Rev 8(2):106–115
61. Vaidyanathan S (2015) Analysis, properties and control of an eight-term 3-D chaotic system with an exponential nonlinearity. Int J Model Identif Control 23(2):164–172
62. Vaidyanathan S (2015) Analysis and control of a 4-D novel hyperchaotic system. Stud Comput Intell 581:3–17
63. Vaidyanathan S, Azar AT (2015) Analysis, control and synchronization of a nine-term 3-D novel chaotic system. In: Azar AT, Vaidyanathan S (eds) Chaos modelling and control systems design, studies in computational intelligence, vol 581. Springer, Germany, pp 19–38
64. Vaidyanathan S, Azar AT (2015) Anti-synchronization of identical chaotic systems using sliding mode control and an application to Vaidhyanathan-Madhavan chaotic systems. Stud Comput Intell 576:527–547
65. Vaidyanathan S, Azar AT (2015) Hybrid synchronization of identical chaotic systems using sliding mode control and an application to Vaidhyanathan chaotic systems. Stud Comput Intell 576:549–569
66. Vaidyanathan S, Madhavan K (2013) Analysis, adaptive control and synchronization of a seven-term novel 3-D chaotic system. Int J Control Theory Appl 6(2):121–137
67. Vaidyanathan S, Pakiriswamy S (2011) The design of active feedback controllers for the generalized projective synchronization of hyperchaotic Qi and hyperchaotic Lorenz systems. Commun Comput Inf Sci 245:231–238
68. Vaidyanathan S, Pakiriswamy S (2012) Generalized projective synchronization of double-scroll chaotic systems using active feedback control. Lect Notes Inst Comput Sci Soc Inf Telecommun Eng 84:111–118
69. Vaidyanathan S, Pakiriswamy S (2013) Generalized projective synchronization of six-term Sundarapandian chaotic systems by adaptive control. Int J Control Theory Appl 6(2):153–163
70. Vaidyanathan S, Pakiriswamy S (2015) A 3-D novel conservative chaotic system and its generalized projective synchronization via adaptive control. J Eng Sci Technol Rev 8(2):52–60

71. Vaidyanathan S, Rajagopal K (2011) Anti-synchronization of Li and T chaotic systems by active nonlinear control. Commun Comput Inf Sci 198:175–184
72. Vaidyanathan S, Rajagopal K (2011) Global chaos synchronization of hyperchaotic Pang and Wang systems by active nonlinear control. Commun Comput Inf Sci 204:84–93
73. Vaidyanathan S, Rajagopal K (2011) Global chaos synchronization of Lü and Pan systems by adaptive nonlinear control. Commun Comput Inf Sci 205:193–202
74. Vaidyanathan S, Rajagopal K (2011) Hybrid synchronization of hyperchaotic Wang-Chen and hyperchaotic Lorenz systems by active non-linear control. Int J Syst Signal Control Eng Appl 4(3):55–61
75. Vaidyanathan S, Rajagopal K (2012) Global chaos synchronization of hyperchaotic Pang and hyperchaotic Wang systems via adaptive control. Int J Soft Comput 7(1):28–37
76. Vaidyanathan S, Rasappan S (2011) Global chaos synchronization of hyperchaotic Bao and Xu systems by active nonlinear control. Commun Comput Inf Sci 198:10–17
77. Vaidyanathan S, Rasappan S (2011) Hybrid synchronization of hyperchaotic Qi and Lü systems by nonlinear control. Commun Comput Inf Sci 131:585–593
78. Vaidyanathan S, Rasappan S (2014) Global chaos synchronization of *n*-scroll Chua circuit and Lur'e system using backstepping control design with recursive feedback. Arabian J Sci Eng 39(4):3351–3364
79. Vaidyanathan S, Sampath S (2011) Global chaos synchronization of hyperchaotic Lorenz systems by sliding mode control. Commun Comput Inf Sci 205:156–164
80. Vaidyanathan S, Sampath S (2012) Anti-synchronization of four-wing chaotic systems via sliding mode control. Int J Autom Comput 9(3):274–279
81. Vaidyanathan S, Volos C, Pham VT (2014) Hyperchaos, adaptive control and synchronization of a novel 5-D hyperchaotic system with three positive Lyapunov exponents and its SPICE implementation. Arch Control Sci 24(4):409–446
82. Vaidyanathan S, Volos C, Pham VT, Madhavan K, Idowu BA (2014) Adaptive backstepping control, synchronization and circuit simulation of a 3-D novel jerk chaotic system with two hyperbolic sinusoidal nonlinearities. Arch Control Sci 24(3):375–403
83. Vaidyanathan S, Idowu BA, Azar AT (2015) Backstepping controller design for the global chaos synchronization of Sprott's jerk systems. Stud Comput Intell 581:39–58
84. Vaidyanathan S, Rajagopal K, Volos CK, Kyprianidis IM, Stouboulos IN (2015) Analysis, adaptive control and synchronization of a seven-term novel 3-D chaotic system with three quadratic nonlinearities and its digital implementation in LabVIEW. J Eng Sci Technol Rev 8(2):130–141
85. Vaidyanathan S, Volos C, Pham VT, Madhavan K (2015) Analysis, adaptive control and synchronization of a novel 4-D hyperchaotic hyperjerk system and its SPICE implementation. Arch Control Sci 25(1):135–158
86. Vaidyanathan S, Volos CK, Kyprianidis IM, Stouboulos IN, Pham VT (2015) Analysis, adaptive control and anti-synchronization of a six-term novel jerk chaotic system with two exponential nonlinearities and its circuit simulation. J Eng Sci Technol Rev 8(2):24–36
87. Vaidyanathan S, Volos CK, Pham VT (2015) Analysis, adaptive control and adaptive synchronization of a nine-term novel 3-D chaotic system with four quadratic nonlinearities and its circuit simulation. J Eng Sci Technol Rev 8(2):181–191
88. Vaidyanathan S, Volos CK, Pham VT (2015) Analysis, control, synchronization and SPICE implementation of a novel 4-D hyperchaotic Rikitake dynamo system without equilibrium. J Eng Sci Technol Rev 8(2):232–244
89. Vaidyanathan S, Volos CK, Pham VT (2015) Global chaos control of a novel nine-term chaotic system via sliding mode control. In: Azar AT, Zhu Q (eds) Advances and applications in sliding mode control systems, studies in computational intelligence, vol 576. Springer, Germany, pp 571–590
90. Vaidyanathan S, Volos CK, Rajagopal K, Kyprianidis IM, Stouboulos IN (2015) Adaptive backstepping controller design for the anti-synchronization of identical WINDMI chaotic systems with unknown parameters and its SPICE implementation. J Eng Sci Technol Rev 8(2):74–82

91. Volos CK, Kyprianidis IM, Stouboulos IN, Tlelo-Cuautle E, Vaidyanathan S (2015) Memristor: A new concept in synchronization of coupled neuromorphic circuits. J Eng Sci Technol Rev 8(2):157–173
92. Volos CK, Pham VT, Vaidyanathan S, Kyprianidis IM, Stouboulos IN (2015) Synchronization phenomena in coupled Colpitts circuits. J Eng Sci Technol Rev 8(2):142–151
93. Wei Z, Yang Q (2010) Anti-control of Hopf bifurcation in the new chaotic system with two stable node-foci. Appl Math Comput 217(1):422–429
94. Yu J, Hu C, Jiang H, Fan X (2014) Projective synchronization for fractional neural networks. Neural Netw 49:87–95
95. Yuan Z, Xu Z, Guo L (2012) Generalized synchronization of two bidirectionally coupled discrete dynamical systems. Commun Nonlinear Sci Numer Simul 17(2):992–1002
96. Zhang D, Xu J (2010) Projective synchronization of different chaotic time-delayed neural networks based on integral sliding mode controller. Appl Math Comput 217(1):164–174
97. Zhou W, Xu Y, Lu H, Pan L (2008) On dynamics analysis of a new chaotic attractor. Phys Lett A 372(36):5773–5777
98. Zhu C, Liu Y, Guo Y (2010) Theoretic and numerical study of a new chaotic system. Intell Inf Manag 2:104–109

Adaptive Control and Synchronization of Chlouverakis–Sprott Hyperjerk System via Backstepping Control

Sundarapandian Vaidyanathan and Babatunde A. Idowu

Abstract This work investigates the simple hyperjerk system obtained by Chlouverakis and Sprott (2006) and derives new results for the adaptive control and synchronization of Chlouverakis–Sprott hyperjerk system via backstepping control. The Chlouverakis–Sprott system is a 4-D hyperjerk system with one quadratic nonlinearity. The phase portraits of the Chlouverakis–Sprott hyperjerk system are displayed and the qualitative properties of the system are discussed. The Chlouverakis–Sprott hyperjerk system has two equilibrium points which are saddle-foci. The Lyapunov exponents of the Chlouverakis–Sprott hyperjerk system are obtained as $L_1 = 0.1885$, $L_2 = 0$, $L_3 = -0.4836$ and $L_4 = -0.7054$, which shows that the Chlouverakis–Sprott hyperjerk system is chaotic. The Kaplan–Yorke dimension of the Chlouverakis–Sprott hyperjerk system is obtained as $D_{KY} = 2.3898$. Next, an adaptive backstepping controller is designed to globally stabilize the Chlouverakis–Sprott hyperjerk system with unknown parameters. Moreover, an adaptive backstepping controller is also designed to achieve global chaos synchronization of the identical Chlouverakis–Sprott hyperjerk systems with unknown parameters. The backstepping control method is a recursive procedure that links the choice of a Lyapunov function with the design of a controller and guarantees global asymptotic stability of strict feedback systems. MATLAB simulations have been shown to illustrate the phase portraits of the Chlouverakis–Sprott hyperjerk system and also the adaptive backstepping control results.

Keywords Chaos · Chaotic systems · Backstepping control · Adaptive control · Synchronization · Hyperjerk systems

S. Vaidyanathan (✉)
Research and Development Centre, Vel Tech University,
Avadi, Chennai 600062, Tamil Nadu, India
e-mail: sundarvtu@gmail.com

B.A. Idowu
Department of Physics, Lagos State University, Ojo, Lagos, Nigeria
e-mail: babatunde.idowu@lasu.edu.ng

S. Vaidyanathan and C. Volos (eds.), *Advances and Applications in Nonlinear Control Systems*, Studies in Computational Intelligence 635,
DOI 10.1007/978-3-319-30169-3_7

1 Introduction

Chaos theory deals with the qualitative study of chaotic dynamical systems and their applications in science and engineering. A dynamical system is called *chaotic* if it satisfies the three properties: boundedness, infinite recurrence and sensitive dependence on initial conditions [2].

Some classical paradigms of 3-D chaotic systems in the literature are Lorenz system [14], Rössler system [23], ACT system [1], Sprott systems [30], Chen system [5], Lü system [15], Cai system [3], Tigan system [41], etc.

Many new chaotic systems have been discovered in the recent years such as Zhou system [89], Zhu system [90], Li system [12], Wei-Yang system [87], Sundarapandian systems [33, 38], Vaidyanathan systems [49, 50, 52–55, 57, 58, 60, 63, 65, 76, 78, 80, 82, 83], Pehlivan system [17], Sampath system [24], etc.

The study of control of a chaotic system investigates feedback controlmethods that globally or locally asymptotically stabilize or regulate the outputs of a chaotic system. Many methods have been designed for control and regulation of chaotic systems such as active control [31, 32, 43], adaptive control [74, 81, 84], backstepping control [13, 86], sliding mode control [46, 48], etc.

Synchronization of chaotic systems is a phenomenon that occurs when two or more chaotic systems are coupled or when a chaotic system drives another chaotic system. Because of the butterfly effect which causes exponential divergence of the trajectories of two identical chaotic systems started with nearly the same initial conditions, the synchronization of chaotic systems is a challenging research problem in the chaos literature [2].

Major works on synchronization of chaotic systems deal with the complete synchronization of a pair of chaotic systems called the *master* and *slave* systems. The design goal of the complete synchronization problem is to apply the output of the master system to control the slave system so that the output of the slave system tracks the output of the master system asymptotically with time.

Pecora and Carroll pioneered the research on synchronization of chaotic systems with their seminal papers [4, 16]. The active control method [10, 25, 26, 37, 42, 47, 66, 67, 70] is typically used when the system parameters are available for measurement. Adaptive control method [27–29, 34–36, 45, 51, 59, 64, 68, 69, 75, 79] is typically used when some or all the system parameters are not available for measurement and estimates for the uncertain parameters of the systems.

Sampled-data feedback control method [8, 88] and time-delay feedback control method [6, 9] are also used for synchronization of chaotic systems. Backstepping control method [18–22, 40, 71, 77, 85] is also used for the synchronization of chaotic systems. Backstepping control is a recursive method for stabilizing the origin of a control system in strict-feedback form [11]. Another popular method for the synchronization of chaotic systems is the sliding mode control method [39, 44, 56, 61, 62, 72, 73], which is a nonlinear control method that alters the dynamics of a nonlinear system by application of a discontinuous control signal that forces the system to "slide" along a cross-section of the system's normal behavior.

In the recent decades, there is some good interest in finding novel chaotic and hyperchaotic systems, which can be expressed by an explicit fourth order differential equation describing the time evolution of the single scalar variable x given by

$$\frac{d^4x}{dt} = j\left(x, \frac{dx}{dt}, \frac{d^2x}{dt^2}, \frac{d^3x}{dt^3}\right) \tag{1}$$

The differential equation (1) is called "hyperjerk system" because the fourth order time derivative in mechanical systems is called *hyperjerk*.

By defining phase variables

$$x_1 = x,\ x_2 = \frac{dx}{dt},\ x_3 = \frac{d^2x}{dt^2},\ x_4 = \frac{d^3x}{dt^3}, \tag{2}$$

the hyperjerk differential equation (1) can be expressed as a 4-D system given by

$$\begin{cases} \dot{x}_1 = x_2 \\ \dot{x}_2 = x_3 \\ \dot{x}_3 = x_4 \\ \dot{x}_4 = j(x_1, x_2, x_3, x_4) \end{cases} \tag{3}$$

In this research work, we investigate the 4-D Chlouverakis–Sprott hyperjerk system [7]. We have designed adaptive backstepping controllers for stabilization and synchronization of the 4-D Chlouverakis–Sprott hyperjerk system.

This work is organized as follows. Section 2 describes the dynamic equations and phase portraits of the 4-D Chlouverakis–Sprott hyperjerk system. Section 3 details the qualitative properties of the Chlouverakis–Sprott hyperjerk system. The Chlouverakis–Sprott hyperjerk system has two equilibrium points, which are saddle-foci. Thus, the Chlouverakis–Sprott hyperjerk system has two unstable equilibrium points.

The Lyapunov exponents of the Chlouverakis–Sprott hyperjerk system are obtained as $L_1 = 0.1885$, $L_2 = 0$, $L_3 = -0.4836$ and $L_4 = -0.7054$. Since the sum of the Lyapunov exponents is negative, the Chlouverakis–Sprott hyperjerk system is dissipative. Thus, the system limit sets are ultimately confined into a specific limit set of zero volume, and the asymptotic motion of the Chlouverakis–Sprott hyperjerk system settles onto a strange attractor of the system. The Kaplan–Yorke dimension of the Chlouverakis–Sprott hyperjerk system is obtained as $D_{KY} = 2.3898$.

In Sect. 4, we design an adaptive backstepping controller to globally stabilize the Chlouverakis–Sprott hyperjerk system with unknown parameters. In Sect. 5, an adaptive backstepping controller is designed to achieve global chaos synchronization of the identical Chlouverakis–Sprott hyperjerk systems with unknown parameters. Section 6 contains the conclusions of this work.

2 Chlouverakis–Sprott Hyperjerk System

In this section, we describe the 4-D Chlouverakis–Sprott hyperjerk system [7], which is an eight-term chaotic system with one quadratic nonlinearity. This is a simple case of a hyperjerk system showing chaotic behavior.

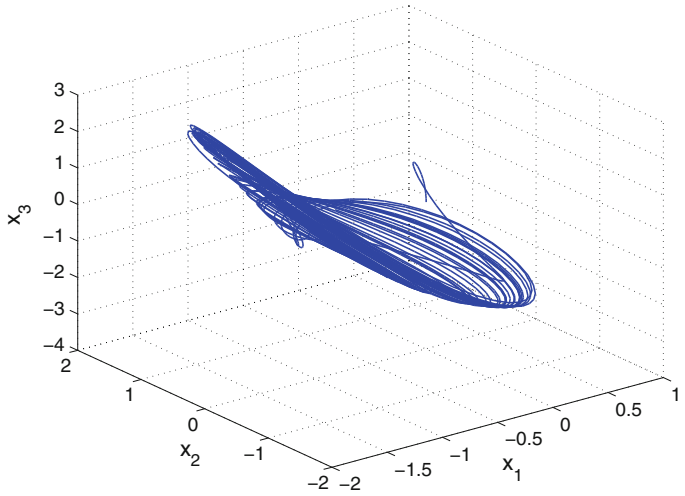

Fig. 1 3-D projection of the hyperjerk system on the (x_1, x_2, x_3) space

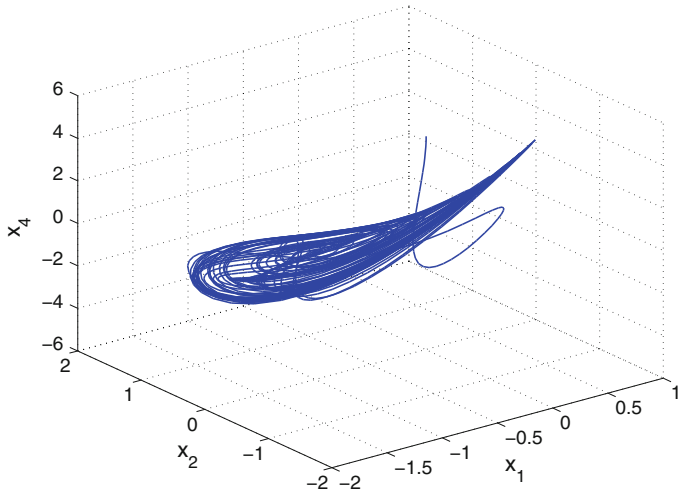

Fig. 2 3-D projection of the hyperjerk system on the (x_1, x_2, x_4) space

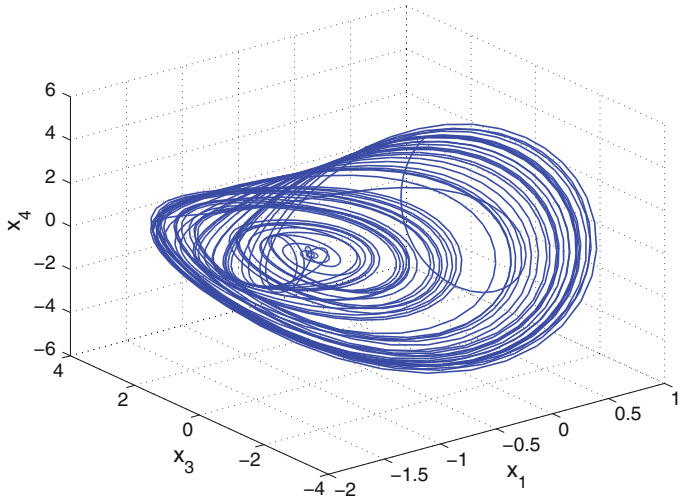

Fig. 3 3-D projection of the hyperjerk system on the (x_1, x_3, x_4) space

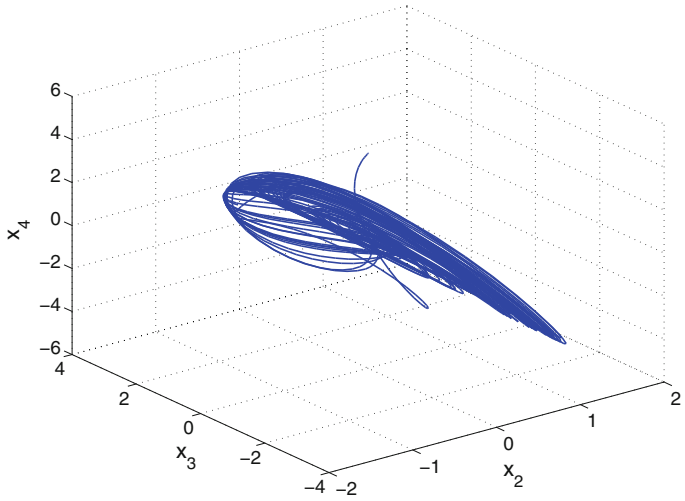

Fig. 4 3-D projection of the hyperjerk system on the (x_2, x_3, x_4) space

Chlouverakis–Sprott hyperjerk system is modeled by the 4-D dynamics

$$\begin{cases} \dot{x}_1 = x_2 \\ \dot{x}_2 = x_3 \\ \dot{x}_3 = x_4 \\ \dot{x}_4 = a\left(x_1^2 - 1\right) - bx_2 - cx_3 - x_4 \end{cases} \tag{4}$$

where x_1, x_2, x_3, x_4 are the states and a, b, c are constant positive parameters.

The system (4) exhibits a *strange chaotic attractor* for the parameter values

$$a = 4.5,\ b = 2.7,\ c = 5.2 \tag{5}$$

For numerical simulations, we take the initial conditions as

$$x_1(0) = 0.01,\ x_2(0) = 0.01,\ x_3(0) = 0.01,\ x_4(0) = 4 \tag{6}$$

Figures 1, 2, 3 and 4 show the 3-D projection of the Chlouverakis–Sprott hyperjerk system (4) on the (x_1, x_2, x_3), (x_1, x_2, x_4), (x_1, x_3, x_4) and (x_2, x_3, x_4) spaces, respectively.

3 Analysis of the Chlouverakis–Sprott Hyperjerk System

In this section, we give a dynamic analysis of the Chlouverakis–Sprott hyperjerk system (4).

3.1 Dissipativity

In vector notation, the Chlouverakis–Sprott hyperjerk system (4) can be expressed as

$$\dot{\mathbf{x}} = f(\mathbf{x}) = \begin{bmatrix} f_1(x_1, x_2, x_3, x_4) \\ f_2(x_1, x_2, x_3, x_4) \\ f_3(x_1, x_2, x_3, x_4) \\ f_4(x_1, x_2, x_3, x_4) \end{bmatrix}, \tag{7}$$

where

$$\begin{cases} f_1(x_1, x_2, x_3, x_4) = x_2 \\ f_2(x_1, x_2, x_3, x_4) = x_3 \\ f_3(x_1, x_2, x_3, x_4) = x_4 \\ f_4(x_1, x_2, x_3, x_4) = a\left(x_1^2 - 1\right) - bx_2 - cx_3 - x_4 \end{cases} \tag{8}$$

Let Ω be any region in $\mathbf{R}^4$ with a smooth boundary and also, $\Omega(t) = \Phi_t(\Omega)$, where Φ_t is the flow of f. Furthermore, let $V(t)$ denote the hypervolume of $\Omega(t)$.

By Liouville's theorem, we know that

$$\dot{V}(t) = \int\limits_{\Omega(t)} (\nabla \cdot f)\, dx_1\, dx_2\, dx_3\, dx_4 \tag{9}$$

The divergence of the hyperjerk system (7) is found as:

$$\nabla \cdot f = \frac{\partial f_1}{\partial x_1} + \frac{\partial f_2}{\partial x_2} + \frac{\partial f_3}{\partial x_3} + \frac{\partial f_4}{\partial x_4} = -1 < 0 \tag{10}$$

Inserting the value of $\nabla \cdot f$ from (10) into (9), we get

$$\dot{V}(t) = \int\limits_{\Omega(t)} (-1)\, dx_1\, dx_2\, dx_3\, dx_4 = -V(t) \tag{11}$$

Integrating the first order linear differential equation (11), we get

$$V(t) = \exp(-t)V(0) \tag{12}$$

From Eq. (12), it follows that $V(t) \to 0$ exponentially as $t \to \infty$. This shows that the Chlouverakis–Sprott hyperjerk system (4) is dissipative. Hence, the system limit sets are ultimately confined into a specific limit set of zero hypervolume, and the asymptotic motion of the Chlouverakis–Sprott hyperjerk system (4) settles onto a strange attractor of the system.

3.2 Equilibrium Points

The equilibrium points of the Chlouverakis–Sprott hyperjerk system (4) are obtained by solving the equations

$$\begin{cases} f_1(x_1, x_2, x_3, x_4) = x_2 & = 0 \\ f_2(x_1, x_2, x_3, x_4) = x_3 & = 0 \\ f_3(x_1, x_2, x_3, x_4) = x_4 & = 0 \\ f_4(x_1, x_2, x_3, x_4) = a\left(x_1^2 - 1\right) - bx_2 - cx_3 - x_4 & = 0 \end{cases} \tag{13}$$

We take the parameter values as in the chaotic case (5), i.e.

$$a = 4.5,\ b = 2.7,\ c = 5.2 \tag{14}$$

Solving the equations (13), we get two equilibrium points of the Chlouverakis–Sprott hyperjerk system (4) as

$$E_1 = \begin{bmatrix} 1 \\ 0 \\ 0 \\ 0 \end{bmatrix} \text{ and } E_2 = \begin{bmatrix} -1 \\ 0 \\ 0 \\ 0 \end{bmatrix} \tag{15}$$

To test the stability type of the equilibrium point E_1, we calculate the Jacobian matrix of the Chlouverakis–Sprott hyperjerk system (4) at any point x:

$$J(x) = \begin{bmatrix} 0 & 1 & 0 & 0 \\ 0 & 0 & 1 & 0 \\ 0 & 0 & 0 & 1 \\ 2ax_1 & -b & -c & -1 \end{bmatrix} = \begin{bmatrix} 0 & 1 & 0 & 0 \\ 0 & 0 & 1 & 0 \\ 0 & 0 & 0 & 1 \\ 9x_1 & -2.7 & -5.2 & -1 \end{bmatrix} \tag{16}$$

We find that

$$J_1 \triangleq J(E_1) = \begin{bmatrix} 0 & 1 & 0 & 0 \\ 0 & 0 & 1 & 0 \\ 0 & 0 & 0 & 1 \\ 9 & -2.7 & -5.2 & -1 \end{bmatrix} \tag{17}$$

The matrix J_1 has the eigenvalues

$$\lambda_1 = 0.9357,\ \lambda_2 = -1.4826,\ \lambda_{3,4} = -0.2356 \pm 2.5118i \tag{18}$$

This shows that the equilibrium point E_1 is a saddle-focus, which is unstable.
We also find that

$$J_2 \triangleq J(E_2) = \begin{bmatrix} 0 & 1 & 0 & 0 \\ 0 & 0 & 1 & 0 \\ 0 & 0 & 0 & 1 \\ -9 & -2.7 & -5.2 & -1 \end{bmatrix} \tag{19}$$

The matrix J_2 has the eigenvalues

$$\lambda_{1,2} = 0.2641 \pm -1.6692i,\ \lambda_{3,4} = -0.7641 \pm 1.6023i \tag{20}$$

This shows that the equilibrium point E_2 is a saddle-focus, which is unstable.

3.3 Lyapunov Exponents and Kaplan–Yorke Dimension

We take the parameter values of the Chlouverakis–Sprott hyperjerk system (4) as $a = 4.5$, $b = 2.7$ and $c = 5.2$. We take the initial state of the Chlouverakis–Sprott hyperjerk system (4) as given in (6).

Then the Lyapunov exponents of the Chlouverakis–Sprott hyperjerk system (4) are numerically obtained using MATLAB as

$$L_1 = 0.1885,\ L_2 = 0,\ L_3 = -0.4836,\ L_4 = -0.7054 \tag{21}$$

Thus, the maximal Lyapunov exponent (MLE) of the Chlouverakis–Sprott hyperjerk system (4) is positive, which means that the system has a chaotic behavior.

Since $L_1 + L_2 + L_3 + L_4 = -1.0005 < 0$, it follows that the Chlouverakis–Sprott hyperjerk system (4) is dissipative.

Also, the Kaplan–Yorke dimension of the Chlouverakis–Sprott hyperjerk system (4) is obtained as

$$D_{KY} = 2 + \frac{L_1 + L_2}{|L_3|} = 2.3898 \tag{22}$$

which is fractional.

4 Adaptive Control of the Chlouverakis–Sprott Hyperjerk System

In this section, we use backstepping control method to derive an adaptive feedback control law for globally stabilizing the 4-D Chlouverakis–Sprott hyperjerk system with unknown parameters.

Thus, we consider the 4-D Chlouverakis–Sprott hyperjerk system given by

$$\begin{cases} \dot{x}_1 = x_2 \\ \dot{x}_2 = x_3 \\ \dot{x}_3 = x_4 \\ \dot{x}_4 = a\left(x_1^2 - 1\right) - bx_2 - cx_3 - x_4 + u \end{cases} \tag{23}$$

where a, b and c are unknown constant parameters, and u is a backstepping control law to be determined using estimates $\hat{a}(t)$, $\hat{b}(t)$ and $\hat{c}(t)$ for a, b and c, respectively.

The parameter estimation errors are defined as:

$$\begin{cases} e_a(t) = a - \hat{a}(t) \\ e_b(t) = b - \hat{b}(t) \\ e_c(t) = c - \hat{c}(t) \end{cases} \tag{24}$$

Differentiating (24) with respect to t, we obtain the following equations:

$$\begin{cases} \dot{e}_a(t) = -\dot{\hat{a}}(t) \\ \dot{e}_b(t) = -\dot{\hat{b}}(t) \\ \dot{e}_c(t) = -\dot{\hat{c}}(t) \end{cases} \tag{25}$$

Next, we shall state and prove the main result of this section.

Theorem 1 *The 4-D Chlouverakis–Sprott hyperjerk system (23), with unknown parameters a, b and c, is globally and exponentially stabilized by the adaptive*

feedback control law,

$$u(t) = -5x_1 - \hat{a}(t)(x_1^2 - 1) - [10 - \hat{b}(t)]x_2 - [9 - \hat{c}(t)]x_3 - 3x_4 - kz_4 \quad (26)$$

where $k > 0$ is a gain constant,

$$z_4 = 3x_1 + 5x_2 + 3x_3 + x_4 \quad (27)$$

and the update law for the parameter estimates $\hat{a}(t), \hat{b}(t), \hat{c}(t)$ is given by

$$\begin{cases} \dot{\hat{a}}(t) = (x_1^2 - 1)z_4 \\ \dot{\hat{b}}(t) = -x_2 z_4 \\ \dot{\hat{c}}(t) = -x_3 z_4 \end{cases} \quad (28)$$

Proof We prove this result via Lyapunov stability theory [11].

First, we define a quadratic Lyapunov function

$$V_1(z_1) = \frac{1}{2} z_1^2 \quad (29)$$

where

$$z_1 = x_1 \quad (30)$$

Differentiating V_1 along the dynamics (23), we get

$$\dot{V}_1 = z_1 \dot{z}_1 = x_1 x_2 = -z_1^2 + z_1(x_1 + x_2) \quad (31)$$

Now, we define

$$z_2 = x_1 + x_2 \quad (32)$$

Using (32), we can simplify the equation (31) as

$$\dot{V}_1 = -z_1^2 + z_1 z_2 \quad (33)$$

Secondly, we define a quadratic Lyapunov function

$$V_2(z_1, z_2) = V_1(z_1) + \frac{1}{2} z_2^2 = \frac{1}{2}\left(z_1^2 + z_2^2\right) \quad (34)$$

Differentiating V_2 along the dynamics (23), we get

$$\dot{V}_2 = -z_1^2 - z_2^2 + z_2(2x_1 + 2x_2 + x_3) \quad (35)$$

Now, we define

$$z_3 = 2x_1 + 2x_2 + x_3 \tag{36}$$

Using (36), we can simplify the equation (35) as

$$\dot{V}_2 = -z_1^2 - z_2^2 + z_2 z_3 \tag{37}$$

Thirdly, we define a quadratic Lyapunov function

$$V_3(z_1, z_2, x_3) = V_2(z_1, z_2) + \frac{1}{2} z_3^2 = \frac{1}{2}\left(z_1^2 + z_2^2 + z_3^2\right) \tag{38}$$

Differentiating V_3 along the dynamics (23), we get

$$\dot{V}_3 = -z_1^2 - z_2^2 - z_3^2 + z_3(3x_1 + 5x_2 + 3x_3 + x_4) \tag{39}$$

Now, we define

$$z_4 = 3x_1 + 5x_2 + 3x_3 + x_4 \tag{40}$$

Using (40), we can simplify the equation (39) as

$$\dot{V}_2 = -z_1^2 - z_2^2 - z_3^2 + z_3 z_4 \tag{41}$$

Finally, we define a quadratic Lyapunov function

$$V(z_1, z_2, z_3, z_4, e_a, e_b, e_c) = V_3(z_1, z_2, z_3) + \frac{1}{2} z_4^2 + \frac{1}{2} e_a^2 + \frac{1}{2} e_b^2 + \frac{1}{2} e_c^2 \tag{42}$$

which is a positive definite function on $\mathbf{R}^7$.

Differentiating V along the dynamics (23), we get

$$\dot{V} = -z_1^2 - z_2^2 - z_3^2 - z_4^2 + z_4(z_4 + z_3 + \dot{z}_4) - e_a\dot{\hat{a}} - e_b\dot{\hat{b}} - e_c\dot{\hat{c}} \tag{43}$$

Equation (43) can be written compactly as

$$\dot{V} = -z_1^2 - z_2^2 - z_3^2 - z_4^2 + z_4 S - e_a\dot{\hat{a}} - e_b\dot{\hat{b}} - e_c\dot{\hat{c}} \tag{44}$$

where

$$S = z_4 + z_3 + \dot{z}_4 = z_4 + z_3 + 3\dot{x}_1 + 5\dot{x}_2 + 3\dot{x}_3 + \dot{x}_4 \tag{45}$$

A simple calculation gives

$$S = 5x_1 + a(x_1^2 - 1) + (10 - b)x_2 + (9 - c)x_3 + 3x_4 + u \tag{46}$$

Substituting the adaptive control law (26) into (46), we obtain

$$S = (a - \hat{a}(t))(x_1^2 - 1) - (b - \hat{b}(t))x_2 - (c - \hat{c}(t))x_3 - kz_4 \tag{47}$$

Using the definitions (25), we can simplify (47) as

$$S = e_a(x_1^2 - 1) - e_b x_2 - e_c x_3 - kz_4 \tag{48}$$

Substituting the value of S from (48) into (44), we obtain

$$\begin{aligned} \dot{V} = &-z_1^2 - z_2^2 - z_3^2 - (1 + k)z_4^2 + e_a((x_1^2 - 1)z_4 - \dot{\hat{a}}) + e_b(-x_2 z_4 - \dot{\hat{b}}) \\ &+ e_c(-x_3 z_4 - \dot{\hat{c}}) \end{aligned} \tag{49}$$

Substituting the update law (28) into (49), we get

$$\dot{V} = -z_1^2 - z_2^2 - z_3^2 - (1 + k)z_4^2, \tag{50}$$

which is a negative semi-definite function on $\mathbf{R}^7$.

From (50), it follows that the vector $\mathbf{z}(t) = (z_1(t), z_2(t), z_3(t), z_4(t))$ and the parameter estimation error $(e_a(t), e_b(t), e_c(t))$ are globally bounded, i.e.

$$\left[z_1(t)\ z_2(t)\ z_3(t)\ z_4(t)\ e_a(t)\ e_b(t)\ e_c(t) \right] \in \mathbf{L}_\infty \tag{51}$$

Also, it follows from (50) that

$$\dot{V} \leq -z_1^2 - z_2^2 - z_3^2 - z_4^2 = -\|\mathbf{z}\|^2 \tag{52}$$

That is,

$$\|\mathbf{z}\|^2 \leq -\dot{V} \tag{53}$$

Integrating the inequality (53) from 0 to t, we get

$$\int_0^t |\mathbf{z}(\tau)|^2 \, d\tau \leq V(0) - V(t) \tag{54}$$

From (54), it follows that $\mathbf{z}(t) \in \mathbf{L}_2$.
From Eq. (23), it can be deduced that $\dot{\mathbf{z}}(t) \in \mathbf{L}_\infty$.

Thus, using Barbalat's lemma [11], we conclude that $\mathbf{z}(t) \to \mathbf{0}$ exponentially as $t \to \infty$ for all initial conditions $\mathbf{z}(0) \in \mathbf{R}^4$.

Hence, it is immediate that $\mathbf{x}(t) \to \mathbf{0}$ exponentially as $t \to \infty$ for all initial conditions $\mathbf{x}(0) \in \mathbf{R}^4$. This completes the proof. ■

For the numerical simulations, the classical fourth-order Runge–Kutta method with step size $h = 10^{-8}$ is used to solve the system of differential equations (23) and (28), when the adaptive control law (26) is applied. The parameter values of the system (23) are taken as in the chaotic case (5), i.e. $a = 4.5$, $b = 2.7$ and $c = 5.2$.

We take the positive gain constant as $k = 8$.

As initial conditions of the Chlouverakis–Sprott hyperjerk system (23), we take

$$x_1(0) = 4.7,\ x_2(0) = -1.6,\ x_3(0) = 2.7,\ x_4(0) = -3.9 \tag{55}$$

Also, as initial conditions of the parameter estimates $\hat{a}(t)$ and $\hat{b}(t)$, we take

$$\hat{a}(0) = 3.2,\ \hat{b}(0) = 2.4,\ \hat{c}(0) = 7.5 \tag{56}$$

In Fig. 5, the exponential convergence of the controlled states is depicted, when the adaptive control law (26) is implemented.

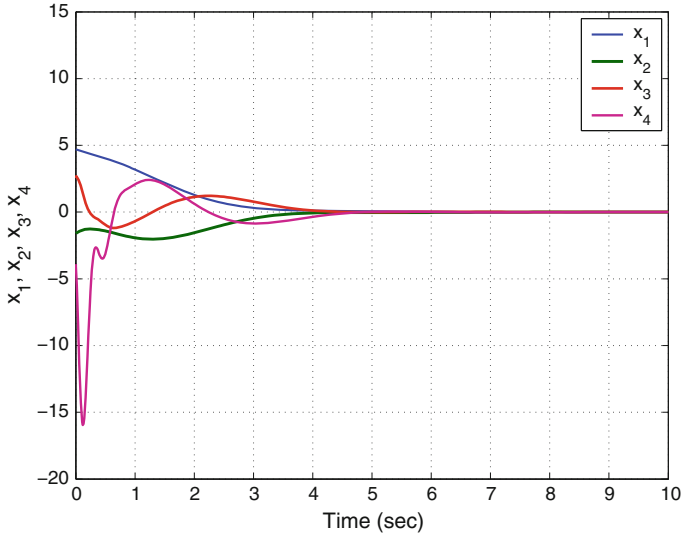

Fig. 5 Time-history of the controlled states x_1, x_2, x_3, x_4

5 Adaptive Synchronization of the Identical Chlouverakis–Sprott Hyperjerk Systems

In this section, we use backstepping control method to derive an adaptive control law for globally and exponentially synchronizing the identical Chlouverakis–Sprott hyperjerk systems with unknown parameters.

As the master system, we consider the 4-D Chlouverakis–Sprott hyperjerk system given by

$$\begin{cases} \dot{x}_1 = x_2 \\ \dot{x}_2 = x_3 \\ \dot{x}_3 = x_4 \\ \dot{x}_4 = a\left(x_1^2 - 1\right) - bx_2 - cx_3 - x_4 \end{cases} \tag{57}$$

where x_1, x_2, x_3, x_4 are the states of the system, and a, b, c are unknown constant parameters.

As the slave system, we consider the 4-D Chlouverakis–Sprott hyperjerk system given by

$$\begin{cases} \dot{y}_1 = y_2 \\ \dot{y}_2 = y_3 \\ \dot{y}_3 = y_4 \\ \dot{y}_4 = a\left(y_1^2 - 1\right) - by_2 - cy_3 - y_4 + u \end{cases} \tag{58}$$

where y_1, y_2, y_3, y_4 are the states of the system, and u is a backstepping control to be determined using estimates $\hat{a}(t), \hat{b}(t)$ and $\hat{c}(t)$ for a, b and c, respectively.

We define the synchronization errors between the states of the master system (57) and the slave system (58) as

$$\begin{cases} e_1 = y_1 - x_1 \\ e_2 = y_2 - x_2 \\ e_3 = y_3 - x_3 \\ e_4 = y_4 - x_4 \end{cases} \tag{59}$$

Then the error dynamics is easily obtained as

$$\begin{cases} \dot{e}_1 = e_2 \\ \dot{e}_2 = e_3 \\ \dot{e}_3 = e_4 \\ \dot{e}_4 = a(y_1^2 - x_1^2) - be_2 - ce_3 - e_4 + u \end{cases} \tag{60}$$

The parameter estimation errors are defined as:

$$\begin{cases} e_a(t) = a - \hat{a}(t) \\ e_b(t) = b - \hat{b}(t) \\ e_c(t) = c - \hat{c}(t) \end{cases} \tag{61}$$

Differentiating (61) with respect to t, we obtain the following equations:

$$\begin{cases} \dot{e}_a(t) = -\dot{\hat{a}}(t) \\ \dot{e}_b(t) = -\dot{\hat{b}}(t) \\ \dot{e}_c(t) = -\dot{\hat{c}}(t) \end{cases} \tag{62}$$

Next, we shall state and prove the main result of this section.

Theorem 2 *The identical 4-D Chlouverakis–Sprott hyperjerk systems (57) and (58) with unknown parameters a, b and c are globally and exponentially synchronized by the adaptive control law*

$$u = -5e_1 - \hat{a}(t)(y_1^2 - x_1^2) - \left[10 - \hat{b}(t)\right] e_2 - \left[9 - \hat{c}(t)\right] e_3 - 3e_4 - kz_4 \tag{63}$$

where $k > 0$ is a gain constant,

$$z_4 = 3e_1 + 5e_2 + 3e_3 + e_4, \tag{64}$$

and the update law for the parameter estimates $\hat{a}(t), \hat{b}(t), \hat{c}(t)$ is given by

$$\begin{cases} \dot{\hat{a}}(t) = (y_1^2 - x_1^2)z_4 \\ \dot{\hat{b}}(t) = -e_2 z_4 \\ \dot{\hat{c}}(t) = -e_3 z_4 \end{cases} \tag{65}$$

Proof We prove this result via backstepping control method and Lyapunov stability theory.

First, we define a quadratic Lyapunov function

$$V_1(z_1) = \frac{1}{2} z_1^2 \tag{66}$$

where

$$z_1 = e_1 \tag{67}$$

Differentiating V_1 along the error dynamics (60), we get

$$\dot{V}_1 = z_1 \dot{z}_1 = e_1 e_2 = -z_1^2 + z_1(e_1 + e_2) \tag{68}$$

Now, we define

$$z_2 = e_1 + e_2 \tag{69}$$

Using (69), we can simplify the equation (68) as

$$\dot{V}_1 = -z_1^2 + z_1 z_2 \tag{70}$$

Secondly, we define a quadratic Lyapunov function

$$V_2(z_1, z_2) = V_1(z_1) + \frac{1}{2} z_2^2 = \frac{1}{2} \left(z_1^2 + z_2^2\right) \tag{71}$$

Differentiating V_2 along the error dynamics (60), we get

$$\dot{V}_2 = -z_1^2 - z_2^2 + z_2(2e_1 + 2e_2 + e_3) \tag{72}$$

Now, we define

$$z_3 = 2e_1 + 2e_2 + e_3 \tag{73}$$

Using (73), we can simplify the equation (72) as

$$\dot{V}_2 = -z_1^2 - z_2^2 + z_2 z_3 \tag{74}$$

Thirdly, we define a quadratic Lyapunov function

$$V_3(z_1, z_2, x_3) = V_2(z_1, z_2) + \frac{1}{2} z_3^2 = \frac{1}{2} \left(z_1^2 + z_2^2 + z_3^2\right) \tag{75}$$

Differentiating V_3 along the error dynamics (60), we get

$$\dot{V}_3 = -z_1^2 - z_2^2 - z_3^2 + z_3(3e_1 + 5e_2 + 3e_3 + e_4) \tag{76}$$

Now, we define

$$z_4 = 3e_1 + 5e_2 + 3e_3 + e_4 \tag{77}$$

Using (77), we can simplify the equation (76) as

$$\dot{V}_2 = -z_1^2 - z_2^2 - z_3^2 + z_3 z_4 \tag{78}$$

Finally, we define a quadratic Lyapunov function

$$V(z_1, z_2, z_3, z_4, e_a, e_b, e_c) = V_3(z_1, z_2, z_3) + \frac{1}{2} z_4^2 + \frac{1}{2} e_a^2 + \frac{1}{2} e_b^2 + \frac{1}{2} e_c^2 \tag{79}$$

Differentiating V along the error dynamics (60), we get

$$\dot{V} = -z_1^2 - z_2^2 - z_3^2 - z_4^2 + z_4(z_4 + z_3 + \dot{z}_4) - e_a \dot{\hat{a}} - e_b \dot{\hat{b}} - e_c \dot{\hat{c}} \tag{80}$$

Equation (80) can be written compactly as

$$\dot{V} = -z_1^2 - z_2^2 - z_3^2 - z_4^2 + z_4 S - e_a\dot{\hat{a}} - e_b\dot{\hat{b}} - e_c\dot{\hat{c}} \tag{81}$$

where

$$S = z_4 + z_3 + \dot{z}_4 = z_4 + z_3 + 3\dot{e}_1 + 5\dot{e}_2 + 3\dot{e}_3 + \dot{e}_4 \tag{82}$$

A simple calculation gives

$$S = 5e_1 + a(y_1^2 - x_1^2) + (10 - b)e_2 + (9 - c)e_3 + 3e_4 + u \tag{83}$$

Substituting the adaptive control law (63) into (83), we obtain

$$S = -\left[a - \hat{a}(t)\right](y_1^2 - x_1^2) - \left[b - \hat{b}(t)\right]e_2 - \left[c - \hat{c}(t)\right]e_3 - kz_4 \tag{84}$$

Using the definitions (62), we can simplify (84) as

$$S = -e_a(y_1^2 - x_1^2) - e_b e_2 - e_c e_3 - kz_4 \tag{85}$$

Substituting the value of S from (85) into (81), we obtain

$$\begin{cases} \dot{V} = -z_1^2 - z_2^2 - z_3^2 - (1+k)z_4^2 + e_a\left[-z_4(y_1^2 - x_1^2) - \dot{\hat{a}}\right] \\ \qquad +e_b\left[-e_2 z_4 - \dot{\hat{b}}\right] + e_c\left[-e_3 z_4 - \dot{\hat{c}}\right] \end{cases} \tag{86}$$

Substituting the update law (65) into (86), we get

$$\dot{V} = -z_1^2 - z_2^2 - z_3^2 - (1+k)z_4^2, \tag{87}$$

which is a negative semi-definite function on $\mathbf{R}^7$.

From (87), it follows that the vector $\mathbf{z}(t) = (z_1(t), z_2(t), z_3(t), z_4(t))$ and the parameter estimation error $(e_a(t), e_b(t), e_c(t))$ are globally bounded, i.e.

$$\left[z_1(t)\ z_2(t)\ z_3(t)\ z_4(t)\ e_a(t)\ e_b(t)\ e_c(t)\right] \in \mathbf{L}_i nfty \tag{88}$$

Also, it follows from (87) that

$$\dot{V} \leq -z_1^2 - z_2^2 - z_3^2 - z_4^2 = -\|\mathbf{z}\|^2 \tag{89}$$

That is,

$$\|\mathbf{z}\|^2 \leq -\dot{V} \tag{90}$$

Integrating the inequality (90) from 0 to t, we get

$$\int_0^t |\mathbf{z}(\tau)|^2 \, d\tau \leq V(0) - V(t) \tag{91}$$

From (91), it follows that $\mathbf{z}(t) \in \mathbf{L}_2$.

From Eq. (60), it can be deduced that $\dot{\mathbf{z}}(t) \in \mathbf{L}_\infty$.

Thus, using Barbalat's lemma [11], we conclude that $\mathbf{z}(t) \to \mathbf{0}$ exponentially as $t \to \infty$ for all initial conditions $\mathbf{z}(0) \in \mathbf{R}^4$.

Hence, it is immediate that $\mathbf{e}(t) \to \mathbf{0}$ exponentially as $t \to \infty$ for all initial conditions $\mathbf{e}(0) \in \mathbf{R}^4$. This completes the proof. ■

For the numerical simulations, the classical fourth-order Runge–Kutta method with step size $h = 10^{-8}$ is used to solve the system of differential equations (57) and (58).

The parameter values of the Chlouverakis–Sprott hyperjerk system are taken as in the chaotic case, viz. $a = 4.5$, $b = 2.7$ and $c = 5.2$. The gain constant is taken as $k = 8$.

Also, as initial conditions of the master system (57), we take

$$x_1(0) = 0.5, \; x_2(0) = 0.1, \; x_3(0) = -0.2, \; x_4(0) = 0.2 \tag{92}$$

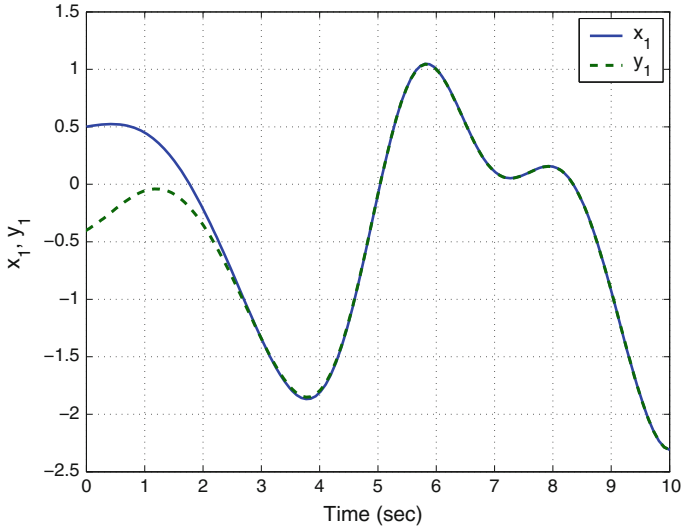

Fig. 6 Synchronization of the states x_1 and y_1

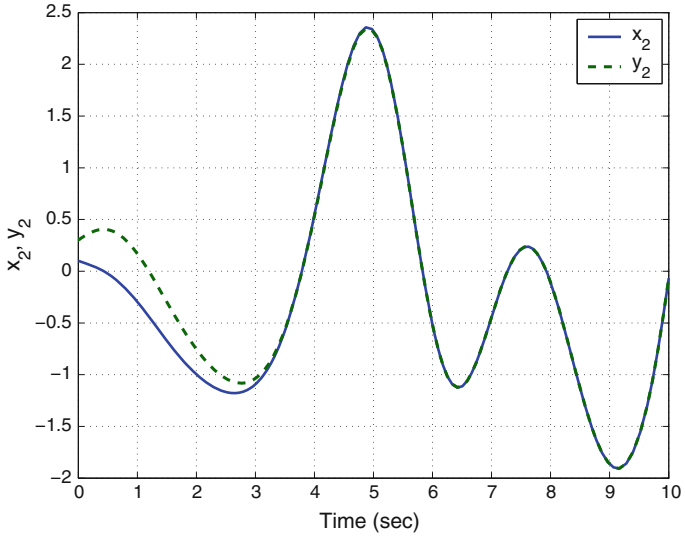

Fig. 7 Synchronization of the states x_2 and y_2

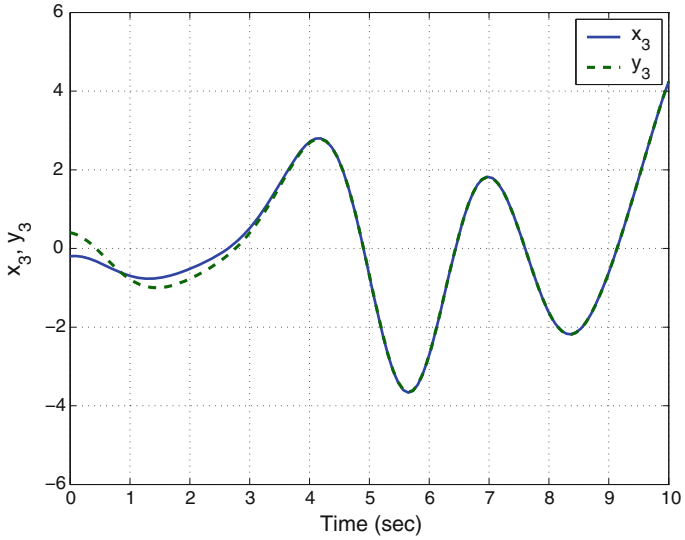

Fig. 8 Synchronization of the states x_3 and y_3

As initial conditions of the slave system (58), we take

$$y_1(0) = -0.4,\ \ y_2(0) = 0.3,\ \ y_3(0) = 0.4,\ \ y_4(0) = -0.3 \tag{93}$$

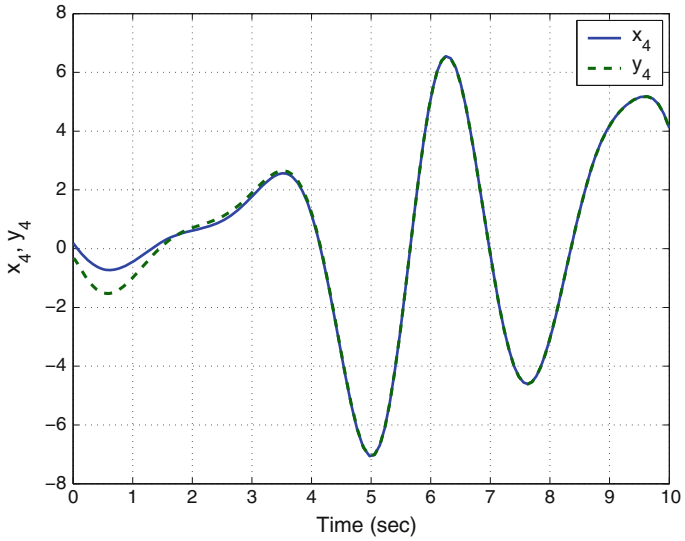

Fig. 9 Synchronization of the states x_4 and y_4

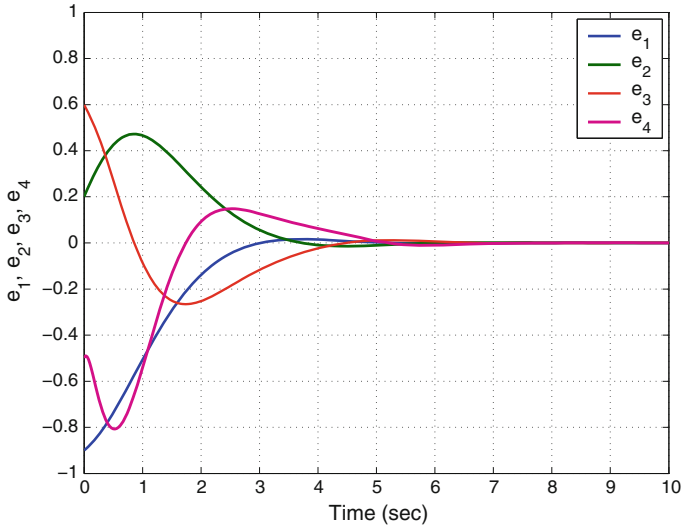

Fig. 10 Time-history of the synchronization errors e_1, e_2, e_3, e_4

Furthermore, as initial conditions of the parameter estimates $\hat{a}(t)$, $\hat{b}(t)$ and $\hat{c}(t)$, we take

$$\hat{a}(0) = 1.5,\ \hat{b}(0) = 3.8,\ \hat{c}(0) = 2.6 \tag{94}$$

In Figs. 6, 7, 8 and 9, the complete synchronization of the identical 4-D Chlouverakis–Sprott hyperjerk systems (57) and (58) is shown, when the adaptive control law and the parameter update law are implemented.

Also, in Fig. 10, the time-history of the complete synchronization errors is shown.

6 Conclusions

In this work, we derived new results for the adaptive control and synchronization of Chlouverakis–Sprott hyperjerk system (2006) via adaptive backstepping control method. The Chlouverakis–Sprott system is a 4-D hyperjerk system with one quadratic nonlinearity. We discussed the qualitative properties of the Chlouverakis–Sprott hyperjerk system. Next, an adaptive backstepping controller has been designed to globally stabilize the Chlouverakis–Sprott hyperjerk system with unknown parameters. Moreover, an adaptive backstepping controller has also been designed to achieve global chaos synchronization of the identical Chlouverakis–Sprott hyperjerk systems with unknown parameters. The backstepping control method is a recursive procedure that links the choice of a Lyapunov function with the design of a controller and guarantees global asymptotic stability of strict feedback systems. MATLAB simulations were shown to illustrate the phase portraits of the Chlouverakis–Sprott hyperjerk system and also the adaptive backstepping control results.

References

1. Arneodo A, Coullet P, Tresser C (1981) Possible new strange attractors with spiral structure. Commun Math Phys 79(4):573–576
2. Azar AT, Vaidyanathan S (2015) Chaos modeling and control systems design, vol 581. Springer, Germany
3. Cai G, Tan Z (2007) Chaos synchronization of a new chaotic system via nonlinear control. J Uncertain Syst 1(3):235–240
4. Carroll TL, Pecora LM (1991) Synchronizing chaotic circuits. IEEE Trans Circuits Syst 38(4):453–456
5. Chen G, Ueta T (1999) Yet another chaotic attractor. Int J Bifurc Chaos 9(7):1465–1466
6. Chen WH, Wei D, Lu X (2014) Global exponential synchronization of nonlinear time-delay Lure systems via delayed impulsive control. Commun Nonlinear Sci Numer Simul 19(9):3298–3312
7. Chlouverakis KE, Sprott JC (2006) Chaotic hyperjerk systems. Chaos, Solitons and Fractals 28(3):739–746
8. Gan Q, Liang Y (2012) Synchronization of chaotic neural networks with time delay in the leakage term and parametric uncertainties based on sampled-data control. J Frankl Inst 349(6):1955–1971
9. Jiang GP, Zheng WX, Chen G (2004) Global chaos synchronization with channel time-delay. Chaos, Solitons and Fractals 20(2):267–275
10. Karthikeyan R, Sundarapandian V (2014) Hybrid chaos synchronization of four-scroll systems via active control. J Electr Eng 65(2):97–103
11. Khalil HK (2001) Nonlinear Syst, 3rd edn. Prentice Hall, New Jersey

12. Li D (2008) A three-scroll chaotic attractor. Phys Lett A 372(4):387–393
13. Li GH, Zhou SP, Yang K (2007) Controlling chaos in Colpitts oscillator. Chaos, Solitons and Fractals 33:582–587
14. Lorenz EN (1963) Deterministic periodic flow. J Atmos Sci 20(2):130–141
15. Lü J, Chen G (2002) A new chaotic attractor coined. Int J Bifurc Chaos 12(3):659–661
16. Pecora LM, Carroll TL (1990) Synchronization in chaotic systems. Phys Rev Lett 64(8):821–824
17. Pehlivan I, Moroz IM, Vaidyanathan S (2014) Analysis, synchronization and circuit design of a novel butterfly attractor. J Sound Vib 333(20):5077–5096
18. Rasappan S, Vaidyanathan S (2012) Global chaos synchronization of WINDMI and Coullet chaotic systems by backstepping control. Far East J Math Sci 67(2):265–287
19. Rasappan S, Vaidyanathan S (2012) Hybrid synchronization of n-scroll Chua and Lur'e chaotic systems via backstepping control with novel feedback. Arch Control Sci 22(3):343–365
20. Rasappan S, Vaidyanathan S (2012) Synchronization of hyperchaotic Liu system via backstepping control with recursive feedback. Commun Comput Inf Sci 305:212–221
21. Rasappan S, Vaidyanathan S (2013) Hybrid synchronization of *n*-scroll chaotic Chua circuits using adaptive backstepping control design with recursive feedback. Malaysian J Math Sci 7(2):219–246
22. Rasappan S, Vaidyanathan S (2014) Global chaos synchronization of WINDMI and Coullet chaotic systems using adaptive backstepping control design. Kyungpook Math J 54(1):293–320
23. Rössler OE (1976) An equation for continuous chaos. Phys Lett A 57(5):397–398
24. Sampath S, Vaidyanathan S, Volos CK, Pham VT (2015) An eight-term novel four-scroll chaotic system with cubic nonlinearity and its circuit simulation. J Eng Sci Technol Rev 8(2):1–6
25. Sarasu P, Sundarapandian V (2011) Active controller design for the generalized projective synchronization of four-scroll chaotic systems. Int J Syst Signal Control Eng Appl 4(2):26–33
26. Sarasu P, Sundarapandian V (2011) The generalized projective synchronization of hyperchaotic Lorenz and hyperchaotic Qi systems via active control. Int J Soft Comput 6(5):216–223
27. Sarasu P, Sundarapandian V (2012) Adaptive controller design for the generalized projective synchronization of 4-scroll systems. Int J Syst Signal Control Eng Appl 5(2):21–30
28. Sarasu P, Sundarapandian V (2012) Generalized projective synchronization of three-scroll chaotic systems via adaptive control. Eur J Sci Res 72(4):504–522
29. Sarasu P, Sundarapandian V (2012) Generalized projective synchronization of two-scroll systems via adaptive control. Int J Soft Comput 7(4):146–156
30. Sprott JC (1994) Some simple chaotic flows. Phys Rev E 50(2):647–650
31. Sundarapandian V (2010) Output regulation of the Lorenz attractor. Far East J Math Sci 42(2):289–299
32. Sundarapandian V (2011) Output regulation of the Arneodo-Coullet chaotic system. Commun Comput Inf Sci 133:98–107
33. Sundarapandian V (2013) Analysis and anti-synchronization of a novel chaotic system via active and adaptive controllers. J Eng Sci Technol Rev 6(4):45–52
34. Sundarapandian V, Karthikeyan R (2011) Anti-synchronization of hyperchaotic Lorenz and hyperchaotic Chen systems by adaptive control. Int J Syst Signal Control Eng Appl 4(2):18–25
35. Sundarapandian V, Karthikeyan R (2011) Anti-synchronization of Lü and Pan chaotic systems by adaptive nonlinear control. Eur J Sci Res 64(1):94–106
36. Sundarapandian V, Karthikeyan R (2012) Adaptive anti-synchronization of uncertain Tigan and Li systems. J Eng Appl Sci 7(1):45–52
37. Sundarapandian V, Karthikeyan R (2012) Hybrid synchronization of hyperchaotic Lorenz and hyperchaotic Chen systems via active control. J Eng Appl Sci 7(3):254–264
38. Sundarapandian V, Pehlivan I (2012) Analysis, control, synchronization, and circuit design of a novel chaotic system. Math Comput Model 55(7–8):1904–1915
39. Sundarapandian V, Sivaperumal S (2011) Sliding controller design of hybrid synchronization of four-wing chaotic systems. Int J Soft Comput 6(5):224–231
40. Suresh R, Sundarapandian V (2013) Global chaos synchronization of a family of *n*-scroll hyperchaotic Chua circuits using backstepping control with recursive feedback. Far East J Math Sci 73(1):73–95

41. Tigan G, Opris D (2008) Analysis of a 3D chaotic system. Chaos, Solitons and Fractals 36:1315–1319
42. Vaidyanathan S (2011) Hybrid chaos synchronization of Liu and Lü systems by active nonlinear control. Commun Comput Inf Sci 204:1–10
43. Vaidyanathan S (2011) Output regulation of the unified chaotic system. Commun Comput Inf Sci 204:84–93
44. Vaidyanathan S (2012) Analysis and synchronization of the hyperchaotic Yujun systems via sliding mode control. Adv Intell Syst Comput 176:329–337
45. Vaidyanathan S (2012) Anti-synchronization of Sprott-L and Sprott-M chaotic systems via adaptive control. Int J Control Theory Appl 5(1):41–59
46. Vaidyanathan S (2012) Global chaos control of hyperchaotic Liu system via sliding control method. Int J Control Theory Appl 5(2):117–123
47. Vaidyanathan S (2012) Output regulation of the Liu chaotic system. Appl Mech Mat 110–116:3982–3989
48. Vaidyanathan S (2012) Sliding mode control based global chaos control of Liu-Liu-Liu-Su chaotic system. Int J Control Theory Appl 5(1):15–20
49. Vaidyanathan S (2013) A new six-term 3-D chaotic system with an exponential nonlinearity. Far East J Math Sci 79(1):135–143
50. Vaidyanathan S (2013) Analysis and adaptive synchronization of two novel chaotic systems with hyperbolic sinusoidal and cosinusoidal nonlinearity and unknown parameters. J Eng Sci Technol Rev 6(4):53–65
51. Vaidyanathan S (2013) Analysis, control and synchronization of hyperchaotic Zhou system via adaptive control. Adv Intell Syst Comput 177:1–10
52. Vaidyanathan S (2014) A new eight-term 3-D polynomial chaotic system with three quadratic nonlinearities. Far East J Math Sci 84(2):219–226
53. Vaidyanathan S (2014) Analysis and adaptive synchronization of eight-term 3-D polynomial chaotic systems with three quadratic nonlinearities. Eur Phys J Spec Top 223(8):1519–1529
54. Vaidyanathan S (2014) Analysis, control and synchronisation of a six-term novel chaotic system with three quadratic nonlinearities. Int J Model Identif Control 22(1):41–53
55. Vaidyanathan S (2014) Generalized projective synchronisation of novel 3-D chaotic systems with an exponential non-linearity via active and adaptive control. Int J Model Identif Control 22(3):207–217
56. Vaidyanathan S (2014) Global chaos synchronization of identical Li-Wu chaotic systems via sliding mode control. Int J Model Identif Control 22(2):170–177
57. Vaidyanathan S (2015) A 3-D novel highly chaotic system with four quadratic nonlinearities, its adaptive control and anti-synchronization with unknown parameters. J Eng Sci Technol Rev 8(2):106–115
58. Vaidyanathan S (2015) Analysis, properties and control of an eight-term 3-D chaotic system with an exponential nonlinearity. Int J Model Identif Control 23(2):164–172
59. Vaidyanathan S, Azar AT (2015) Analysis and control of a 4-D novel hyperchaotic system. In: Azar AT, Vaidyanathan S (eds) Chaos modeling and control systems design, studies in computational intelligence, vol 581. Springer, Germany, pp 19–38
60. Vaidyanathan S, Azar AT (2015) Analysis, control and synchronization of a nine-term 3-D novel chaotic system. In: Azar AT, Vaidyanathan S (eds) Chaos modelling and control systems design, studies in computational intelligence, vol 581. Springer, Germany, pp 19–38
61. Vaidyanathan S, Azar AT (2015) Anti-synchronization of identical chaotic systems using sliding mode control and an application to Vaidhyanathan-Madhavan chaotic systems. Stud Comput Intell 576:527–547
62. Vaidyanathan S, Azar AT (2015) Hybrid synchronization of identical chaotic systems using sliding mode control and an application to Vaidhyanathan chaotic systems. Stud Comput Intell 576:549–569
63. Vaidyanathan S, Madhavan K (2013) Analysis, adaptive control and synchronization of a seven-term novel 3-D chaotic system. Int J Control Theory Appl 6(2):121–137

64. Vaidyanathan S, Pakiriswamy S (2013) Generalized projective synchronization of six-term Sundarapandian chaotic systems by adaptive control. Int J Control Theory Appl 6(2):153–163
65. Vaidyanathan S, Pakiriswamy S (2015) A 3-D novel conservative chaotic System and its generalized projective synchronization via adaptive control. J Eng Sci Technol Rev 8(2):52–60
66. Vaidyanathan S, Rajagopal K (2011) Anti-synchronization of Li and T chaotic systems by active nonlinear control. Commun Comput Inf Sci 198:175–184
67. Vaidyanathan S, Rajagopal K (2011) Global chaos synchronization of hyperchaotic Pang and Wang systems by active nonlinear control. Commun Comput Inf Sci 204:84–93
68. Vaidyanathan S, Rajagopal K (2011) Global chaos synchronization of Lü and Pan systems by adaptive nonlinear control. Commun Comput Inf Sci 205:193–202
69. Vaidyanathan S, Rajagopal K (2012) Global chaos synchronization of hyperchaotic Pang and hyperchaotic Wang systems via adaptive control. Int J Soft Comput 7(1):28–37
70. Vaidyanathan S, Rasappan S (2011) Global chaos synchronization of hyperchaotic Bao and Xu systems by active nonlinear control. Commun Comput Inf Sci 198:10–17
71. Vaidyanathan S, Rasappan S (2014) Global chaos synchronization of n-scroll Chua circuit and Lur'e system using backstepping control design with recursive feedback. Arabian J Sci Eng 39(4):3351–3364
72. Vaidyanathan S, Sampath S (2011) Global chaos synchronization of hyperchaotic Lorenz systems by sliding mode control. Commun Comput Inf Sci 205:156–164
73. Vaidyanathan S, Sampath S (2012) Anti-synchronization of four-wing chaotic systems via sliding mode control. Int J Autom Comput 9(3):274–279
74. Vaidyanathan S, Volos C, Pham VT (2014) Hyperchaos, adaptive control and synchronization of a novel 5-D hyperchaotic system with three positive Lyapunov exponents and its SPICE implementation. Arch Control Sci 24(4):409–446
75. Vaidyanathan S, Volos C, Pham VT (2014) Hyperchaos, adaptive control and synchronization of a novel 5-D hyperchaotic system with three positive Lyapunov exponents and its SPICE implementation. Arch Control Sci 24(4):409–446
76. Vaidyanathan S, Volos C, Pham VT, Madhavan K, Idowu BA (2014) Adaptive backstepping control, synchronization and circuit simulation of a 3-D novel jerk chaotic system with two hyperbolic sinusoidal nonlinearities. Arch Control Sci 24(3):375–403
77. Vaidyanathan S, Idowu BA, Azar AT (2015) Backstepping controller design for the global chaos synchronization of Sprott's jerk systems. Stud Comput Intell 581:39–58
78. Vaidyanathan S, Rajagopal K, Volos CK, Kyprianidis IM, Stouboulos IN (2015) Analysis, adaptive control and synchronization of a seven-term novel 3-D chaotic system with three quadratic nonlinearities and its digital implementation in LabVIEW. J Eng Sci Technol Rev 8(2):130–141
79. Vaidyanathan S, Volos C, Pham VT, Madhavan K (2015) Analysis, adaptive control and synchronization of a novel 4-D hyperchaotic hyperjerk system and its SPICE implementation. Arch Control Sci 25(1):5–28
80. Vaidyanathan S, Volos CK, Kyprianidis IM, Stouboulos IN, Pham VT (2015) Analysis, adaptive control and anti-synchronization of a six-term novel jerk chaotic system with two exponential nonlinearities and its circuit simulation. J Eng Sci Technol Rev 8(2):24–36
81. Vaidyanathan S, Volos CK, Madhavan K (2015) Analysis, control, synchronization and SPICE implementation of a novel 4-D hyperchaotic Rikitake dynamo System without equilibrium. J Eng Sci Technol Rev 8(2):232–244
82. Vaidyanathan S, Volos CK, Pham VT (2015) Analysis, adaptive control and adaptive synchronization of a nine-term novel 3-D chaotic system with four quadratic nonlinearities and its circuit simulation. J Eng Sci Technol Rev 8(2):181–191
83. Vaidyanathan S, Volos CK, Pham VT (2015) Global chaos control of a novel nine-term chaotic system via sliding mode control. In: Azar AT, Zhu Q (eds) Advances and applications in sliding mode control systems, studies in computational intelligence, vol 576. Springer, Germany, pp 571–590
84. Vaidyanathan S, Volos CK, Pham VT, Madhavan K (2015) Analysis, adaptive control and synchronization of a novel 4-D hyperchaotic hyperjerk system and its SPICE implementation. Arch Control Sci 25(1):135–158

85. Vaidyanathan S, Volos CK, Rajagopal K, Kyprianidis IM, Stouboulos IN (2015) Adaptive backstepping controller design for the anti-synchronization of identical WINDMI chaotic systems with unknown parameters and its SPICE implementation. J Eng Sci Technol Rev 8(2):74–82
86. Wang X, Ge C (2008) Controlling and tracking of Newton-Leipnik system via backstepping design. Int J Nonlinear Sci 5(2):133–139
87. Wei Z, Yang Q (2010) Anti-control of Hopf bifurcation in the new chaotic system with two stable node-foci. Appl Math Comput 217(1):422–429
88. Xiao X, Zhou L, Zhang Z (2014) Synchronization of chaotic Lure systems with quantized sampled-data controller. Commun Nonlinear Sci Numer Simul 19(6):2039–2047
89. Zhou W, Xu Y, Lu H, Pan L (2008) On dynamics analysis of a new chaotic attractor. Phys Lett A 372(36):5773–5777
90. Zhu C, Liu Y, Guo Y (2010) Theoretic and numerical study of a new chaotic system. Intell Inf Manag 2:104–109

Anti-synchronization of Hyperchaotic Systems via Novel Sliding Mode Control and Its Application to Vaidyanathan Hyperjerk System

Sundarapandian Vaidyanathan and Sivaperumal Sampath

Abstract Chaos in nonlinear dynamics occurs widely in physics, chemistry, biology, ecology, secure communications, cryptosystems and many scientific branches. Anti-synchronization of chaotic systems is an important research problem in chaos theory. Sliding mode control is an important method used to solve various problems in control systems engineering. In robust control systems, the sliding mode control is often adopted due to its inherent advantages of easy realization, fast response and good transient performance as well as insensitivity to parameter uncertainties and disturbance. In this work, we derive a novel sliding mode control method for the anti-synchronization of identical chaotic or hyperchaotic systems. The general result derived using novel sliding mode control method is proved using Lyapunov stability theory. As an application of the general result, the problem of anti-synchronization of identical Vaidyanathan hyperjerk hyperchaotic systems (2015) is studied and a new sliding mode controller is derived. The Lyapunov exponents of the Vaidyanathan hyperjerk system are obtained as $L_1 = 0.1448$, $L_2 = 0.0328$, $L_3 = 0$ and $L_4 = -1.1294$. Since the Vaidyanathan hyperjerk system has two positive Lyapunov exponents, it is hyperchaotic. Also, the Kaplan–Yorke dimension of the Vaidyanathan hyperjerk system is obtained as $D_{KY} = 3.1573$. Numerical simulations using MATLAB have been shown to depict the phase portraits of the Vaidyanathan hyperjerk system and the sliding mode controller design for the anti-synchronization of identical Vaidyanathan hyperjerk systems.

Keywords Chaos · Chaotic systems · Hyperchaos · Hyperchaotic systems · Hyperjerk systems · Sliding mode control · Synchronization

S. Vaidyanathan (✉)
Research and Development Centre, Vel Tech University, Avadi, Chennai 600062, Tamil Nadu, India
e-mail: sundarvtu@gmail.com

S. Sampath
School of Electrical and Computing, Vel Tech University, Avadi, Chennai 600062, Tamil Nadu, India
e-mail: sivaperumals@gmail.com

S. Vaidyanathan and C. Volos (eds.), *Advances and Applications in Nonlinear Control Systems*, Studies in Computational Intelligence 635,
DOI 10.1007/978-3-319-30169-3_8

1 Introduction

Chaos theory describes the quantitative study of unstable aperiodic dynamic behaviour in deterministic nonlinear dynamical systems. For the motion of a dynamical system to be chaotic, the system variables should contain some nonlinear terms and the system must satisfy three properties: boundedness, infinite recurrence and sensitive dependence on initial conditions [1].

A hyperchaotic system is defined as a chaotic system with at least two positive Lyapunov exponents [1]. Thus, the dynamics of a hyperchaotic system can expand in several different directions simultaneously. Thus, the hyperchaotic systems have more complex dynamical behaviour and they have miscellaneous applications in engineering such as secure communications [3, 9, 46], cryptosystems [5, 14, 50], fuzzy logic [19, 49], electrical circuits [44, 47], etc.

The minimum dimension of an autonomous, continuous-time, hyperchaotic system is four. The first 4-D hyperchaotic system was found by Rössler [15]. Many hyperchaotic systems have been reported in the chaos literature such as hyperchaotic Lorenz system [6], hyperchaotic Lü system [2], hyperchaotic Chen system [10], hyperchaotic Wang system [43], hyperchaotic Vaidyanathan systems [28, 30, 31, 38, 40, 42], hyperchaotic Pham system [11], etc.

The synchronization of chaotic systems aims to synchronize the states of master and slave systems asymptotically with time. There are many methods available for chaos synchronization such as active control [7, 16, 17, 33, 35], adaptive control [18, 20–22, 27, 32, 34], sliding mode control [23, 29, 37, 39], backstepping control [12, 13, 24, 36], etc.

The design goal of anti-synchronization of chaotic systems is to use the output of the master system to control the slave system so that the states of the slave system have the same amplitude but opposite signs as the states of the master system asymptotically [45, 48].

In this work, we use a novel sliding mode control method for deriving a general result for the anti-synchronization of chaotic or hyperchaotic systems using sliding mode control (SMC) theory. The sliding mode control method is an effective control tool which has the advantages of low sensitivity to parameter variations in the plant and disturbances affecting the plant.

This work is organized as follows. In Sect. 2, we discuss the problem statement for the anti-synchronization of identical chaotic or hyperchaotic systems. In Sect. 3, we derive a general result for the anti-synchronization of identical chaotic or hyperchaotic systems using novel sliding mode control. In Sect. 4, we describe the Vaidyanathan hyperjerk system [41] and its dynamic properties. The Lyapunov exponents of the Vaidyanathan hyperjerk system are obtained as $L_1 = 0.1448$, $L_2 = 0.0328$, $L_3 = 0$ and $L_4 = -1.1294$, which shows that the Vaidyanathan hyperjerk system is hyperchaotic. In Sect. 5, we describe the sliding mode controller design for the anti-synchronization of identical Vaidyanathan hyperjerk systems using novel sliding mode control and its numerical simulations using MATLAB. Section 6 contains the conclusions of this work.

2 Problem Statement

This section gives a problem statement for the anti-synchronization of identical chaotic or hyperchaotic systems.

As the *master* or *drive* system, we consider the chaotic or hyperchaotic system given by

$$\dot{\mathbf{x}} = A\mathbf{x} + f(\mathbf{x}) \tag{1}$$

where $\mathbf{x} \in \mathbf{R}^n$ denotes the state of the system, $A \in \mathbf{R}^{n\times n}$ denotes the matrix of system parameters and $f(\mathbf{x}) \in \mathbf{R}^n$ contains the nonlinear parts of the system.

As the *slave* or *response* system, we consider the controlled identical system given by

$$\dot{\mathbf{y}} = A\mathbf{y} + f(\mathbf{y}) + \mathbf{u} \tag{2}$$

where $\mathbf{y} \in \mathbf{R}^n$ denotes the state of the system and $\mathbf{u}$ is the control.

The anti-synchronization error between the systems (1) and (2) is defined as

$$\mathbf{e} = \mathbf{y} + \mathbf{x} \tag{3}$$

The error dynamics is easily obtained as

$$\dot{\mathbf{e}} = A\mathbf{e} + \psi(\mathbf{x}, \mathbf{y}) + \mathbf{u}, \tag{4}$$

where

$$\psi(\mathbf{x}, \mathbf{y}) = f(\mathbf{x}) + f(\mathbf{y}) \tag{5}$$

Thus, the anti-synchronization problem between the systems (1) and (2) can be stated as follows: Find a controller $\mathbf{u}(\mathbf{x}, \mathbf{y})$ so as to render the anti-synchronization error $\mathbf{e}(t)$ to be globally asymptotically stable for all values of $\mathbf{e}(0) \in \mathbf{R}^n$, i.e.

$$\lim_{t\to\infty} \|\mathbf{e}(t)\| = 0 \ \text{ for all } \ \mathbf{e}(0) \in \mathbf{R}^n \tag{6}$$

3 A Novel Sliding Mode Control Method for Solving Anti-synchronization Problem

This section details the main results of this work, viz. novel sliding mode controller design for achieving anti-synchronization of chaotic or hyperchaotic systems.

First, we start the design by setting the control as

$$\mathbf{u}(t) = -\psi(\mathbf{x}, \mathbf{y}) + Bv(t) \tag{7}$$

In Eq. (7), $B \in \mathbf{R}^n$ is chosen such that (A, B) is completely controllable.
By substituting (7) into (4), we get the closed-loop error dynamics

$$\dot{\mathbf{e}} = A\mathbf{e} + Bv \tag{8}$$

The system (8) is a linear time-invariant control system with single input v.
Next, we start the sliding controller design by defining the sliding variable as

$$s(\mathbf{e}) = C\mathbf{e} = c_1e_1 + c_2e_2 + \cdots + c_ne_n, \tag{9}$$

where $C \in \mathbf{R}^{1\times n}$ is a constant vector to be determined.
The sliding manifold S is defined as the hyperplane

$$S = \{\mathbf{e} \in \mathbf{R}^n \ : \ s(\mathbf{e}) = C\mathbf{e} = 0\} \tag{10}$$

We shall assume that a sliding motion occurs on the hyperplane S.
In sliding mode, the following equations must be satisfied:

$$s = 0 \tag{11a}$$
$$\dot{s} = CA\mathbf{e} + CBv = 0 \tag{11b}$$

We assume that

$$CB \neq 0 \tag{12}$$

The sliding motion is influenced by the equivalent control derived from (11b) as

$$v_{\text{eq}}(t) = -(CB)^{-1}\, CA\mathbf{e}(t) \tag{13}$$

By substituting (13) into (8), we obtain the equivalent error dynamics in the sliding phase as

$$\dot{\mathbf{e}} = A\mathbf{e} - (CB)^{-1}CA\mathbf{e} = E\mathbf{e}, \tag{14}$$

where

$$E = \left[I - B(CB)^{-1}C\right]A \tag{15}$$

We note that E is independent of the control and has at most $(n-1)$ non-zero eigenvalues, depending on the chosen switching surface, while the associated eigenvectors belong to $\ker(C)$.
Since (A, B) is controllable, we can use sliding control theory [25, 26] to choose B and C so that E has any desired $(n-1)$ stable eigenvalues.
This shows that the dynamics (14) is globally asympotically stable.

Finally, for the sliding controller design, we apply a novel sliding control law, viz.

$$\dot{s} = -ks - qs^2 \operatorname{sgn}(s) \tag{16}$$

In (16), $\operatorname{sgn}(\cdot)$ denotes the *sign* function and the SMC constants $k > 0, q > 0$ are found in such a way that the sliding condition is satisfied and that the sliding motion will occur.

By combining Eqs. (11b), (13) and (16), we finally obtain the sliding mode controller $v(t)$ as

$$v(t) = -(CB)^{-1}\left[C(kI + A)\mathbf{e} + qs^2 \operatorname{sgn}(s)\right] \tag{17}$$

Next, we establish the main result of this section.

Theorem 1 *The sliding mode controller defined by (7) achieves anti-synchronization between the identical chaotic systems (1) and (2) for all initial conditions* $\mathbf{x}(0), \mathbf{y}(0)$ *in* $\mathbf{R}^n$*, where v is defined by the novel sliding mode control law (17),* $B \in \mathbf{R}^{n\times 1}$ *is such that* (A, B) *is controllable,* $C \in \mathbf{R}^{1\times n}$ *is such that* $CB \neq 0$ *and the matrix E defined by (15) has* $(n-1)$ *stable eigenvalues.*

Proof Upon substitution of the control laws (7) and (17) into the error dynamics (4), we obtain the closed-loop error dynamics as

$$\dot{\mathbf{e}} = A\mathbf{e} - B(CB)^{-1}\left[C(kI + A)\mathbf{e} + qs^2 \operatorname{sgn}(s)\right] \tag{18}$$

We shall show that the error dynamics (18) is globally asymptotically stable by considering the quadratic Lyapunov function

$$V(\mathbf{e}) = \frac{1}{2}s^2(\mathbf{e}) \tag{19}$$

The sliding mode motion is characterized by the equations

$$s(\mathbf{e}) = 0 \ \text{ and } \ \dot{s}(\mathbf{e}) = 0 \tag{20}$$

By the choice of E, the dynamics in the sliding mode given by Eq. (14) is globally asymptotically stable.

When $s(\mathbf{e}) \neq 0$, $V(\mathbf{e}) > 0$.

Also, when $s(\mathbf{e}) \neq 0$, differentiating V along the error dynamics (18) or the equivalent dynamics (16), we get

$$\dot{V}(\mathbf{e}) = s\dot{s} = -ks^2 - qs^3 \operatorname{sgn}(s) < 0 \tag{21}$$

Hence, by Lyapunov stability theory [8], the error dynamics (18) is globally asymptotically stable for all $\mathbf{e}(0) \in \mathbf{R}^n$. This completes the proof. ■

4 Vaidyanathan Hyperjerk System and Its Properties

In this section, we describe the Vaidyanathan hyperjerk system [41] and discuss its dynamic properties.

The Vaidyanathan hyperjerk system [41] is described by the 4-D dynamics

$$\begin{aligned} \dot{x}_1 &= x_2 \\ \dot{x}_2 &= x_3 \\ \dot{x}_3 &= x_4 \\ \dot{x}_4 &= -x_1 - x_2 - bx_1^2 - ax_3 - cx_1^4 x_4 \end{aligned} \tag{22}$$

where x_1, x_2, x_3, x_4 are the states and a, b, c are constant, positive, parameters.

In [41], it was shown that the system (22) is hyperchaotic when the parameters take the values

$$a = 3.7, \quad b = 0.2, \quad c = 1.5 \tag{23}$$

For numerical simulations, we take the initial values of the Vaidyanathan hyperjerk system (22) as

$$x_1(0) = 0.1, \quad x_2(0) = 0.1, \quad x_3(0) = 0.1, \quad x_4(0) = 0.1 \tag{24}$$

For the parameter values in (23) and the initial values in (24), the Lyapunov exponents of the Vaidyanathan hyperjerk system (22) are numerically obtained as

$$L_1 = 0.1448, \quad L_2 = 0.0328, \quad L_3 = 0, \quad L_4 = -1.1294 \tag{25}$$

Since there are two positive Lyapunov exponents in the LE spectrum given in (25), it follows that the Vaidyanathan hyperjerk system is *hyperchaotic*.

Since the sum of the Lyapunov exponents in (25) is negative, the Vaidyanathan hyperjerk system (22) is dissipative.

The Kaplan–Yorke dimension [4] of a chaotic system of order n is defined as

$$D_{KY} = j + \frac{L_1 + \cdots + L_j}{|L_{j+1}|} \tag{26}$$

where $L_1 \geq L_2 \geq \cdots \geq L_n$ are the Lyapunov exponents of the chaotic system and j is the largest integer for which $L_1 + L_2 + \cdots + L_j \geq 0$. (Kaplan–Yorke conjecture states that for typical chaotic systems, $D_{KY} \approx D_L$, the information dimension of the system.)

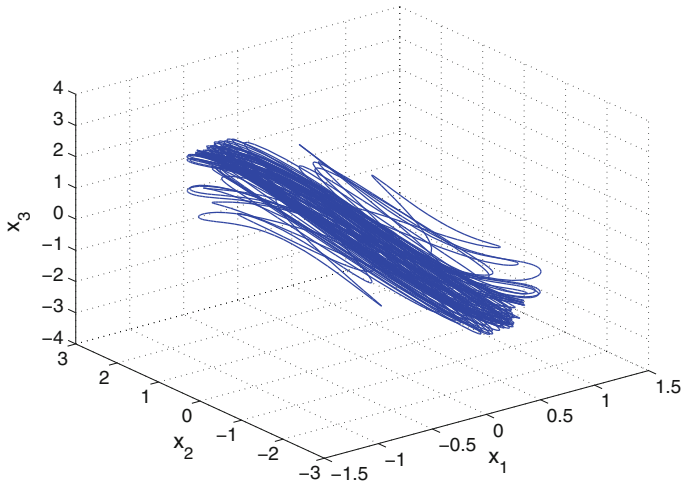

Fig. 1 3-D projection of the Vaidyanathan hyperjerk system on the (x_1, x_2, x_3) space

Thus, the Kaplan–Yorke dimension of the Vaidyanathan hyperjerk system (22) is calculated as

$$D_{KY} = 3 + \frac{L_1 + L_2 + L_3}{|L_4|} = 3.1573, \tag{27}$$

which is fractional.

It is easy to show that the Vaidyanathan hyperjerk system (22) has two equilibrium points given by

$$E_0 = \begin{bmatrix} 0 \\ 0 \\ 0 \\ 0 \end{bmatrix} \quad \text{and} \quad E_1 = \begin{bmatrix} -5 \\ 0 \\ 0 \\ 0 \end{bmatrix} \tag{28}$$

In [41], it was shown that both E_0 and E_1 are saddle-focus points, and hence they are unstable.

For the initial conditions given in (24), phase portraits of the Vaidyanathan hyperjerk system (22) are plotted using MATLAB.

Figures 1, 2, 3 and 4 show the 3-D projections of the Vaidyanathan hyperjerk system (22) in (x_1, x_2, x_3), (x_1, x_2, x_4), (x_1, x_3, x_4) and (x_2, x_3, x_4) spaces, respectively.

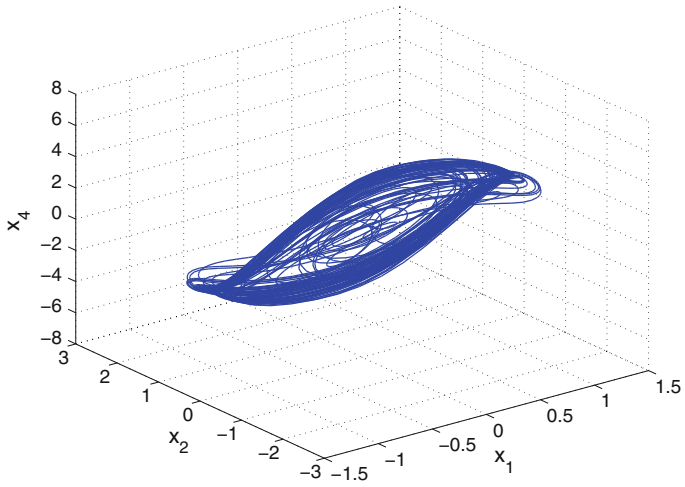

Fig. 2 3-D projection of the Vaidyanathan hyperjerk system on the (x_1, x_2, x_4) space

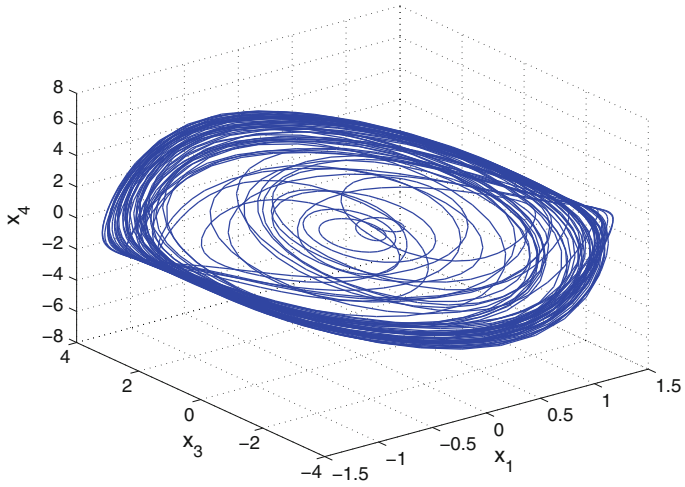

Fig. 3 3-D projection of the Vaidyanathan hyperjerk system on the (x_1, x_3, x_4) space

5 Sliding Mode Controller Design for the Anti-synchronization of Vaidyanathan Hyperjerk Systems

In this section, we describe the sliding mode controller design for the anti-synchronization of Vaidyanathan hyperjerk systems [41] by applying the novel method described by Theorem 1 in Sect. 3.

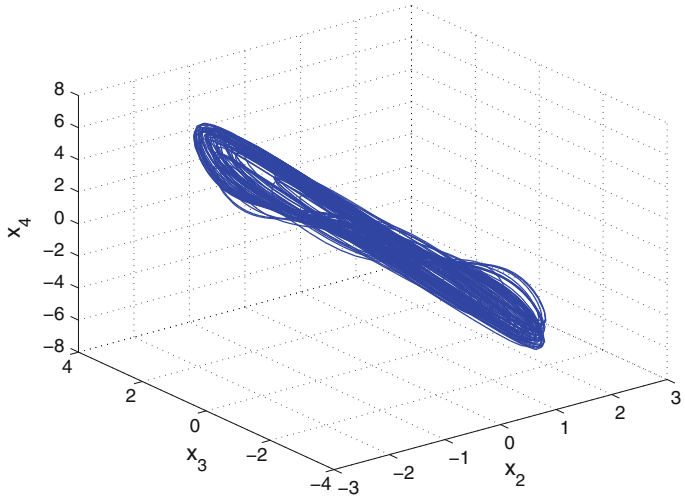

Fig. 4 3-D projection of the Vaidyanathan hyperjerk system on the (x_2, x_3, x_4) space

As the master system, we take the Vaidyanathan hyperjerk system given by

$$\begin{aligned} \dot{x}_1 &= x_2 \\ \dot{x}_2 &= x_3 \\ \dot{x}_3 &= x_4 \\ \dot{x}_4 &= -x_1 - x_2 - bx_1^2 - ax_3 - cx_1^4 x_4 \end{aligned} \tag{29}$$

where x_1, x_2, x_3, x_4 are the state variables and a, b, c are positive parameters.

As the slave system, we consider the controlled Vaidyanathan hyperjerk system given by

$$\begin{aligned} \dot{y}_1 &= y_2 + u_1 \\ \dot{y}_2 &= y_3 + u_2 \\ \dot{y}_3 &= y_4 + u_3 \\ \dot{y}_4 &= -y_1 - y_2 - by_1^2 - ay_3 - cy_1^4 y_4 + u_4 \end{aligned} \tag{30}$$

where y_1, y_2, y_3, y_4 are the state variables and u_1, u_2, u_3, u_4 are the controls.

The anti-synchronization error between the Vaidyanathan hyperjerk systems is defined by

$$\begin{aligned} e_1 &= y_1 + x_1 \\ e_2 &= y_2 + x_2 \\ e_3 &= y_3 + x_3 \\ e_4 &= y_4 + x_4 \end{aligned} \tag{31}$$

Then the error dynamics is obtained as

$$\begin{aligned}\dot{e}_1 &= e_2 + u_1\\ \dot{e}_2 &= e_3 + u_2\\ \dot{e}_3 &= e_4 + u_3\\ \dot{e}_4 &= -e_1 - e_2 - ae_3 - b\left(y_1^2 + x_1^2\right) - c\left(y_1^4 y_4 + x_1^4 x_4\right) + u_4\end{aligned} \tag{32}$$

In matrix form, we can write the error dynamics (32) as

$$\dot{\mathbf{e}} = A\mathbf{e} + \psi(\mathbf{x}, \mathbf{y}) + \mathbf{u} \tag{33}$$

The matrices in (33) are given by

$$A = \begin{bmatrix} 0 & 1 & 0 & 0\\ 0 & 0 & 1 & 0\\ 0 & 0 & 0 & 1\\ -1 & -1 & -a & 0 \end{bmatrix} \text{ and } \psi(\mathbf{x}, \mathbf{y}) = \begin{bmatrix} 0\\ 0\\ 0\\ -b(y_1^2 + x_1^2) - c(y_1^4 y_4 + x_1^4 x_4) \end{bmatrix} \tag{34}$$

We follow the procedure given in Sect. 3 for the construction of the novel sliding controller to achieve anti-synchronization of the identical Vaidyanathan hyperjerk systems (29) and (30).

First, we set $\mathbf{u}$ as

$$\mathbf{u}(t) = -\psi(\mathbf{x}, \mathbf{y}) + Bv(t) \tag{35}$$

where B is selected such that (A, B) is completely controllable.

A simple choice of B is

$$B = \begin{bmatrix} 1\\ 1\\ 1\\ 1 \end{bmatrix} \tag{36}$$

It can be easily checked that (A, B) is completely controllable.

The Vaidyanathan hyperjerk system displays a strange attractor when the parameter values are selected as

$$a = 3.7, \quad b = 0.2, \quad c = 1.5 \tag{37}$$

Next, we take the sliding variable as

$$s(\mathbf{e}) = C\mathbf{e} = \begin{bmatrix} 15 & 8 & -9 & -13 \end{bmatrix}\mathbf{e} = 15e_1 + 8e_2 - 9e_3 - 13e_4 \tag{38}$$

Next, we take the sliding mode gains as

$$k = 5, \quad q = 0.2 \tag{39}$$

From Eq. (17) in Sect. 3, we obtain the novel sliding control v as

$$v(t) = -88e_1 - 68e_2 - 11.1e_3 + 74e_4 - 0.2s^2 \operatorname{sgn}(s) \tag{40}$$

As an application of Theorem 1 to the identical Vaidyanathan hyperjerk systems, we obtain the following main result of this section.

Theorem 2 *The identical Vaidyanathan hyperjerk systems (29) and (30) are globally and asymptotically anti-synchronized for all initial conditions* $\mathbf{x}(0), \mathbf{y}(0) \in \mathbf{R}^4$ *with the sliding controller* $\mathbf{u}$ *defined by (35), where* $\psi(\mathbf{x}, \mathbf{y})$ *is defined by (34), B is defined by (36) and v is defined by (40).* ■

For numerical simulations, we use MATLAB for solving the systems of differential equations using the classical fourth-order Runge–Kutta method with step size $h = 10^{-8}$.

The parameter values of the Vaidyanathan hyperjerk systems are taken as in the hyperchaotic case, viz. $a = 3.7$, $b = 0.2$ and $c = 1.5$.

The sliding mode gains are taken as $k = 5$ and $q = 0.2$.

As an initial condition for the master system (29), we take

$$x_1(0) = 1.7, \quad x_2(0) = 0.5, \quad x_3(0) = 1.8, \quad x_4(0) = 1.2 \tag{41}$$

As an initial condition for the slave system (30), we take

$$y_1(0) = 3.1, \quad y_2(0) = 2.4, \quad y_3(0) = 0.3, \quad y_4(0) = 0.5 \tag{42}$$

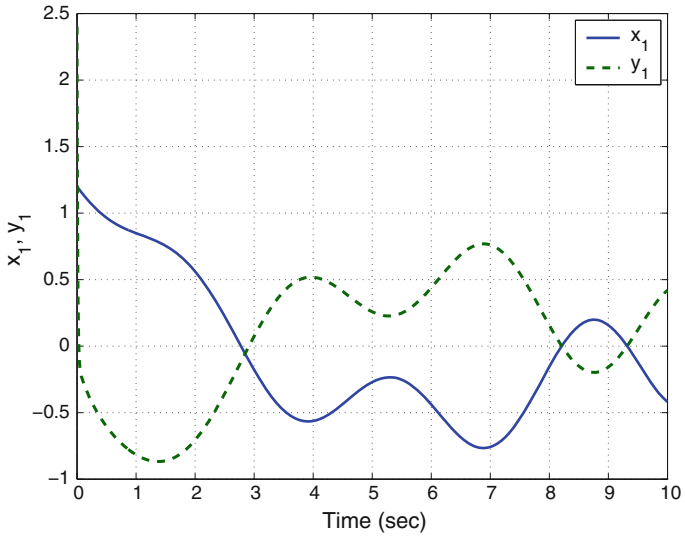

Fig. 5 Anti-synchronization of the states x_1 and y_1

Figures 5, 6, 7 and 8 show the anti-synchronization of the states of the identical Vaidyanathan hyperjerk systems (29) and (30).

Figure 9 shows the time-history of the anti-synchronization errors e_1, e_2, e_3, e_4.

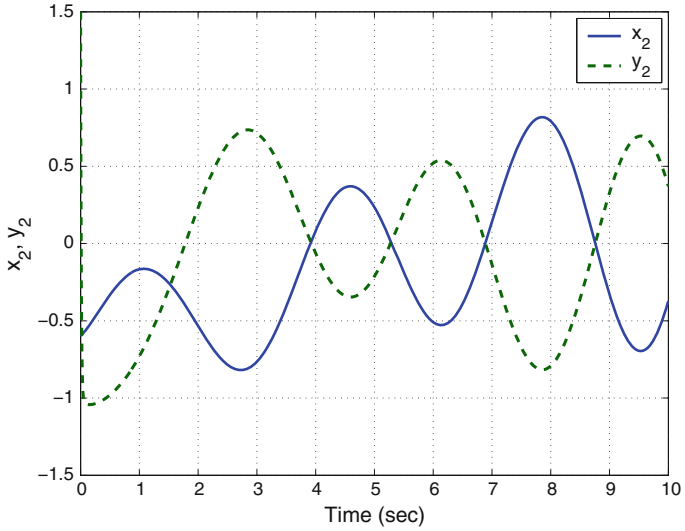

Fig. 6 Anti-synchronization of the states x_2 and y_2

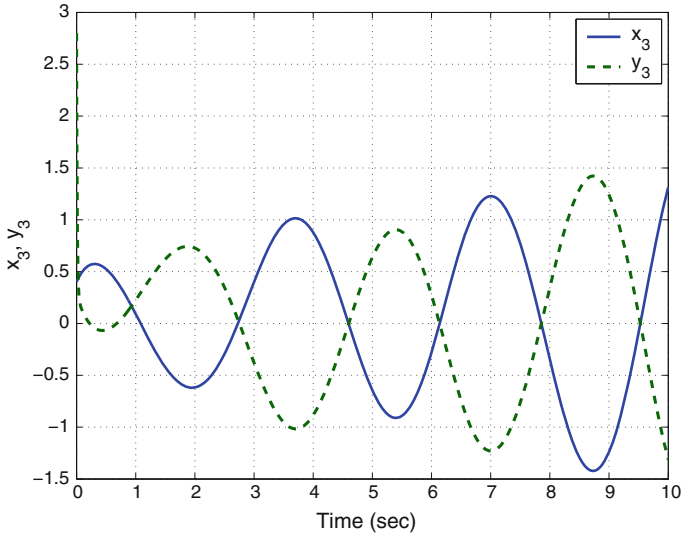

Fig. 7 Anti-synchronization of the states x_3 and y_3

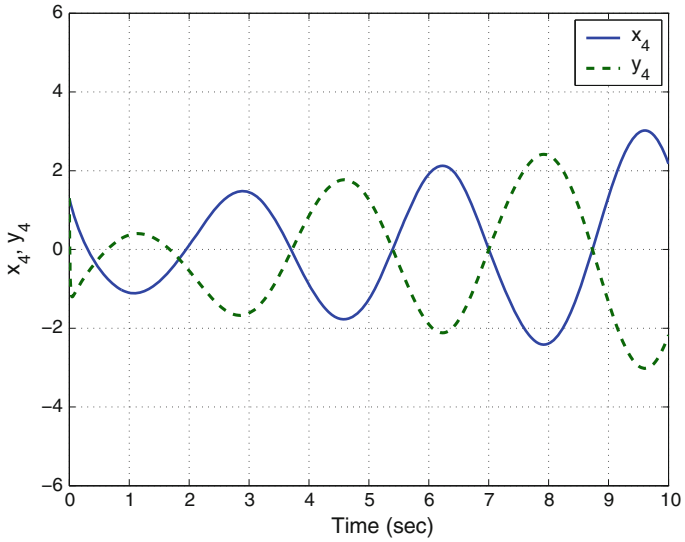

Fig. 8 Anti-synchronization of the states x_4 and y_4

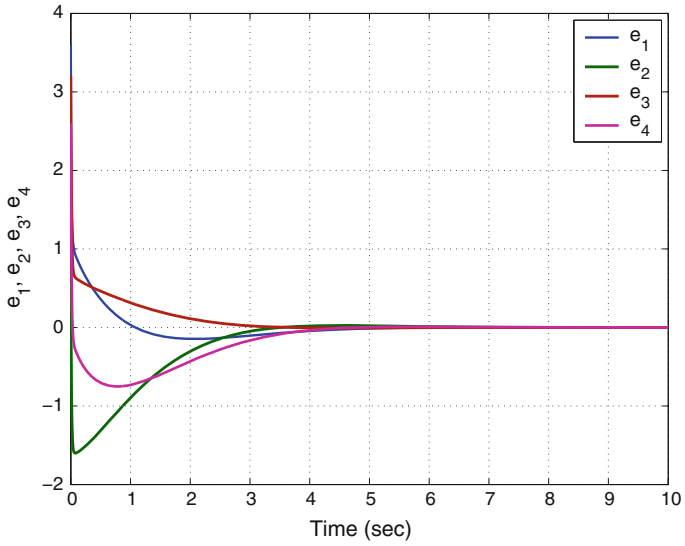

Fig. 9 Time-history of the anti-synchronization errors e_1, e_2, e_3, e_4

6 Conclusions

Chaos and hyperchaos have important applications in science and engineering. Hyperchaotic systems have more complex behaviour than chaotic systems and they have miscellaneous applications in areas like secure communications, cryptosystems, etc. In robust control systems, the sliding mode control is commonly used due to its inherent advantages of easy realization, fast response and good transient performance as well as insensitivity to parameter uncertainties and disturbance. In this work, we derived a novel sliding mode control method for the anti-synchronization of identical chaotic or hyperchaotic systems. We proved the main result using Lyapunov stability theory. As an application of the general result, the problem of anti-synchronization of identical Vaidyanathan hyperjerk hyperchaotic systems (2015) was studied and a new sliding mode controller has been derived. Numerical simulations using MATLAB were shown to depict the phase portraits of the Vaidyanathan hyperjerk system and the sliding mode controller design for the anti-synchronization of identical Vaidyanathan hyperjerk systems.

References

1. Azar AT, Vaidyanathan S (2015) Chaos modeling and control systems design, vol 581. Springer, Germany
2. Chen A, Lu J, Lü J, Yu S (2006) Generating hyperchaotic Lü attractor via state feedback control. Phys A 364:103–110
3. Filali RL, Benrejeb M, Borne P (2014) On observer-based secure communication design using discrete-time hyperchaotic systems. Commun Nonlinear Sci Numer Simul 19(5):1424–1432
4. Grassberger P, Procaccia I (1983) Measuring the strangeness of strange attractors. Phys D: Nonlinear Phenom 9:189–208
5. Hammami S (2015) State feedback-based secure image cryptosystem using hyperchaotic synchronization. ISA Trans 54:52–59
6. Jia Q (2007) Hyperchaos generated from the Lorenz chaotic system and its control. Phys Lett A 366:217–222
7. Karthikeyan R, Sundarapandian V (2014) Hybrid chaos synchronization of four-scroll systems via active control. J Electr Eng 65(2):97–103
8. Khalil HK (2001) Nonlinear systems, 3rd edn. Prentice Hall, New Jersey
9. Li C, Liao X, Wong KW (2005) Lag synchronization of hyperchaos with application to secure communications. Chaos, Solitons and Fractals 23(1):183–193
10. Li X (2009) Modified projective synchronization of a new hyperchaotic system via nonlinear control. Commun Theor Phys 52:274–278
11. Pham VT, Volos C, Jafari S, Wang X, Vaidyanathan S (2014) Hidden hyperchaotic attractor in a novel simple memristive neural network. Optoelectr Adv Mater Rapid Commun 8(11–12):1157–1163
12. Rasappan S, Vaidyanathan S (2013) Hybrid synchronization of *n*-scroll Chua circuits using adaptive backstepping control design with recursive feedback. Malays J Math Sci 73(1):73–95
13. Rasappan S, Vaidyanathan S (2014) Global chaos synchronization of WINDMI and Coullet chaotic systems using adaptive backstepping control design. Kyungpook Math J 54(1):293–320
14. Rhouma R, Belghith S (2008) Cryptanalysis of a new image encryption algorithm based on hyper-chaos. Phys Lett A 372(38):5973–5978

15. Rössler OE (1979) An equation for hyperchaos. Phys Lett A 71:155–157
16. Sarasu P, Sundarapandian V (2011a) Active controller design for generalized projective synchronization of four-scroll chaotic systems. Int J Syst Signal Control Eng Appl 4(2):26–33
17. Sarasu P, Sundarapandian V (2011b) The generalized projective synchronization of hyperchaotic Lorenz and hyperchaotic Qi systems via active control. Int J Soft Comput 6(5):216–223
18. Sarasu P, Sundarapandian V (2012) Generalized projective synchronization of two-scroll systems via adaptive control. Int J Soft Comput 7(4):146–156
19. Senouci A, Boukabou A (2014) Predictive control and synchronization of chaotic and hyperchaotic systems based on a $T - S$ fuzzy model. Math Comput Simul 105:62–78
20. Sundarapandian V, Karthikeyan R (2011a) Anti-synchronization of hyperchaotic Lorenz and hyperchaotic Chen systems by adaptive control. Int J Syst Signal Control Eng Appl 4(2):18–25
21. Sundarapandian V, Karthikeyan R (2011b) Anti-synchronization of Lü and Pan chaotic systems by adaptive nonlinear control. Eur J Sci Res 64(1):94–106
22. Sundarapandian V, Karthikeyan R (2012) Adaptive anti-synchronization of uncertain Tigan and Li systems. J Eng Appl Sci 7(1):45–52
23. Sundarapandian V, Sivaperumal S (2011) Sliding controller design of hybrid synchronization of four-wing chaotic systems. Int J Soft Comput 6(5):224–231
24. Suresh R, Sundarapandian V (2013) Global chaos synchronization of a family of n-scroll hyperchaotic Chua circuits using backstepping control with recursive feedback. Far East J Math Sci 7(2):219–246
25. Utkin VI (1977) Variable structure systems with sliding modes. IEEE Trans Autom Control 22(2):212–222
26. Utkin VI (1993) Sliding mode control design principles and applications to electric drives. IEEE Trans Ind Electr 40(1):23–36
27. Vaidyanathan S (2012) Anti-synchronization of Sprott-L and Sprott-M chaotic systems via adaptive control. Int J Control Theory Appl 5(1):41–59
28. Vaidyanathan S (2013) A ten-term novel 4-D hyperchaotic system with three quadratic nonlinearities and its control. Int J Control Theory Appl 6(2):97–109
29. Vaidyanathan S (2014a) Global chaos synchronisation of identical Li-Wu chaotic systems via sliding mode control. Int J Model Identif Control 22(2):170–177
30. Vaidyanathan S (2014b) Qualitative analysis and control of an eleven-term novel 4-D hyperchaotic system with two quadratic nonlinearities. Int J Control Theory Appl 7:35–47
31. Vaidyanathan S, Azar AT (2015) Analysis and control of a 4-D novel hyperchaotic system. Stud Comput Intell 581:3–17
32. Vaidyanathan S, Pakiriswamy S (2013) Generalized projective synchronization of six-term Sundarapandian chaotic systems by adaptive control. Int J Control Theory Appl 6(2):153–163
33. Vaidyanathan S, Rajagopal K (2011) Hybrid synchronization of hyperchaotic Wang-Chen and hyperchaotic Lorenz systems by active non-linear control. Int J Syst Signal Control Eng Appl 4(3):55–61
34. Vaidyanathan S, Rajagopal K (2012) Global chaos synchronization of hyperchaotic Pang and hyperchaotic Wang systems via adaptive control. Int J Soft Comput 7(1):28–37
35. Vaidyanathan S, Rasappan S (2011) Global chaos synchronization of hyperchaotic Bao and Xu systems by active nonlinear control. Commun Comput Inf Sci 198:10–17
36. Vaidyanathan S, Rasappan S (2014) Global chaos synchronization of n-scroll Chua circuit and Lur'e system using backstepping control design with recursive feedback. Arab J Sci Eng 39(4):3351–3364
37. Vaidyanathan S, Sampath S (2012) Anti-synchronization of four-wing chaotic systems via sliding mode control. Int J Autom Comput 9(3):274–279
38. Vaidyanathan S, Volos C, Pham VT (2014) Hyperchaos, adaptive control and synchronization of a novel 5-D hyperchaotic system with three positive Lyapunov exponents and its SPICE implementation. Arch Control Sci 24(4):409–446
39. Vaidyanathan S, Sampath S, Azar AT (2015a) Global chaos synchronisation of identical chaotic systems via novel sliding mode control method and its application to Zhu system. Int J Model Identif Control 23(1):92–100

40. Vaidyanathan S, Volos C, Pham VT, Madhavan K (2015b) Analysis, adaptive control and synchronization of a novel 4-D hyperchaotic hyperjerk system and its SPICE implementation. Nonlinear Dyn 25(1):135–158
41. Vaidyanathan S, Volos C, Pham VT, Madhavan K (2015c) Analysis, adaptive control and synchronization of a novel 4-D hyperchaotic hyperjerk system and its SPICE implementation. Arch Control Sci 25(1):135–158
42. Vaidyanathan S, Volos CK, Pham VT (2015d) Analysis, control, synchronization and SPICE implementation of a novel 4-D hyperchaotic Rikitake dynamo system without equilibrium. J Eng Sci Technol Rev 8(2):232–244
43. Wang J, Chen Z (2008) A novel hyperchaotic system and its complex dynamics. Int J Bifurc Chaos 18:3309–3324
44. Wei X, Yunfei F, Qiang L (2012) A novel four-wing hyper-chaotic system and its circuit implementation. Proc Eng 29:1264–1269
45. Wu A, Zeng Z (2013) Anti-synchronization control of a class of memristive recurrent neural networks. Commun Nonlinear Sci Numer Simul 18(2):373–385
46. Wu X, Zhu C, Kan H (2015) An improved secure communication scheme based passive synchronization of hyperchaotic complex nonlinear system. Appl Math Comput 252:201–214
47. Yujun N, Xingyuan W, Mingjun W, Huaguang Z (2010) A new hyperchaotic system and its circuit implementation. Commun Nonlinear Sci Numer Simul 15(11):3518–3524
48. Zhang G, Shen Y, Wang L (2013) Global anti-synchronization of a class of chaotic memristive neural networks with time-varying delays. Neural Netw 46:1–8
49. Zhang H, Liao X, Yu J (2005) Fuzzy modeling and synchronization of hyperchaotic systems. Chaos, Solitons Fractals 26(3):835–843
50. Zhu C (2012) A novel image encryption scheme based on improved hyperchaotic sequences. Opt Commun 285(1):29–37

Sliding Mode Control with State Derivative Feedback in Novel Reciprocal State Space Form

Yuan-Wei Tseng

Abstract This chapter introduces a novel reciprocal state space (RSS) system form. The concepts and the need of RSS form are comprehensively reviewed and explained. It shows that in RSS form, control design using state derivative related feedback is straightforward. Sliding mode control (SMC) is a nonlinear control design method and a highly active area of research. Finite-time convergence due to discontinuous control law, low sensitivity to plant parameter uncertainty and/or external perturbation, and greatly reduced-order modeling of plant dynamics are the main advantages of SMC. In the past, the majority of available SMC algorithms and the corresponding switching conditions involved only state related variables. In this chapter, the advantages of both RSS and SMC are combined to develop sliding mode control in RSS form so that state derivate related feedback can be systematically applied in SMC to handle wider range of control problems. To provide the theoretical foundation, stability analysis in RSS form is first reviewed. Next, novel switching function and approaching condition based on the derivative of sliding surface are proposed to carry out SMC design approach in RSS form with considerations of system uncertainty and disturbance. In addition, algorithm of finding upper bound of system uncertainty is developed for robustness analysis. To verify the proposed design algorithms, numerical examples are provided. Finally, conclusions are drawn.

Keywords Reciprocal state space (RSS) form · State derivate related feedback · Sliding mode control · Nonlinear control

1 Introduction

In recent years, robust control is one of the most popular topics in control area. One of the famous methods is the so-called sliding mode control (SMC) or variable structure control (VSC) [33, 35, 36] which is a nonlinear control and has been proven as an

Y.-W. Tseng (✉)
Department of Electrical Engineering, I- Shou University, Kaohsiung 84001, Taiwan, ROC
e-mail: yuanwei@isu.edu.tw

S. Vaidyanathan and C. Volos (eds.), *Advances and Applications in Nonlinear Control Systems*, Studies in Computational Intelligence 635,
DOI 10.1007/978-3-319-30169-3_9

effectively robust control technology with many practical applications. Through this chapter, the name of sliding mode control (SMC) is used for unification. The main idea of sliding mode control is to design a controller rendering the trajectory of states trapped on a predetermined sliding surface and remained on it thereafter. Sliding mode control utilizes a high-speed switching control law to drive the state trajectory staying on this sliding surface for all subsequence time such that the robust stability of the system is assured. In the present, sliding mode control is a highly active area of research. Finite-time convergence due to discontinuous control law, low sensitivity to plant parameter uncertainty and/or external perturbation, and greatly reduced-order modeling of plant dynamics are the main advantages of it. Therefore, based on SMC, many works in state space form have been developed [7, 11, 12, 20, 39].

The majority of available SMC algorithms for linear systems is developed in state space form and applies state feedback. However, in many applications, people face the problems that either cannot be handled in state space form or cannot directly apply state feedback in designs. More details are given in next section. To provide supplementary design algorithms of state derivative feedback in state space form, a direct state derivative feedback control scheme was developed in "Reciprocal state space" (RSS) form [21–26] by the author of this chapter.

In this chapter, the algorithms of SMC design utilizing state derivative feedback in RSS form are introduced [27, 28, 40]. The main purpose of this chapter is to combine the advantages of both RSS and SMC so that state derivate feedback can be systematically applied in SMC designs to handle wider range of control problems.

The rest of chapter is organized as follows. "Reciprocal state space" (RSS) form is introduced and reviewed in Sect. 2. In Sect. 3, the design approach of sliding mode control with state derivative feedback in RSS form is described and the method for finding the upper bound of system uncertainty in RSS form is also developed. The contribution of this chapter, discussion and suggested future research are given in the conclusion section.

2 Reciprocal State Space (RSS) Form and State Derivative Feedback Control Designs

The concepts and the needs of RSS form are first comprehensively reviewed and explained in this section as follows.

In general, a dynamic linear continuous time invariant system using state variables with physical meanings can be naturally expressed in the following equation under the names of generalized state space form [38] or descriptor form [42] or singular system form [2].

$$E\dot{x} = Fx + Nu \tag{1}$$

where $x_{n\times 1}$ and $u_{m\times 1}$ are state vector and control vector, respectively, and $E_{n\times n}$, $F_{n\times n}$ and $N_{n\times m}$ are known constant system matrices. Controllability and observability of

generalized state space systems have been investigated in [2, 42]. The following is the characteristic equation of open loop generalized state space system in (1).

$$\det(sE - F) = 0 \tag{2}$$

The degree r of characteristic equation in (2) is the number of system's finite eigenvalues while $n - r$ is the number of system's eigenvalues at infinity [5].
If E in (1) is nonsingular, the system has no eigenvalue at infinity but can have zero eigenvalues. Such system can be expressed in the following standard state space system form:

$$\dot{x} = E^{-1}Fx + E^{-1}Nu = \bar{A}x + \bar{B}u. \tag{3}$$

For state space system, state derivative vector can be explicitly expressed in terms of state vector and control input vector. Most of control algorithms developed for state space systems are related to state feedback such as full state feedback, state related output feedback and estimated state feedback when estimators are implemented. However, in many applications, the sensors directly measure state derivatives rather than states. For instance, accelerometers [9] in micro and nano-electro-mechanical systems (M/NEMS) and structural applications [10, 26] are such cases because acceleration signals can only be modeled as state derivatives [6, 10, 26]. Consequently, abundant control algorithms with state related feedback developed in standard state space form cannot be readily applicable in this situation. Additional integrators which may increase the cost and complexity of the implementation are needed. Mathematically speaking, state derivative related feedback designs cannot be carried out as straightforward as state related feedback for systems expressed in standard state space form. For example, if we apply the following full state derivative feedback control law

$$u = -K\dot{x} \tag{4}$$

to the state space system in (3), the closed loop system becomes

$$\dot{x} = (I + \bar{B}K)^{-1}\bar{A}x \tag{5}$$

In (5), since gain K is inside an inverse matrix $(I + \bar{B}K)^{-1}$ which is further coupled with the open loop system matrix $\bar{A}$ by multiplication, it is obvious that advanced mathematics is needed to design gain K in (4). Therefore, in the past, the developed algorithms of state derivative related feedback for systems in state space form were very few and rarely used to control the system alone [6]. In a word, standard state space system in (1) is the best system form for open loop systems without poles at infinity in designing state related feedback control algorithms. However, standard state space system is not the most suitable form to develop state derivative related feedback control algorithms and cannot handle the systems with open loop poles at infinity.

If E in (1) is singular, the system has poles at infinity and is called generalized state space system. In the past, the majority of control designs for system with poles at infinity were directly developed in the generalized state space form in (1).

Extensive applications of generalized state space systems arise in many areas of engineering such as electrical networks [16], aerospace systems [1], smart structures [26, 41] and chemical processes [18]. Generalized state space systems also exist in other areas such as the dynamic Leontief model for economic production sectors [15] and biological complex systems [14]. A comprehensive review is available in Yeh et al. [41]. In this paper, generalized state space system is used as the name to represent such systems. In previous studies, generalized state space systems are further categorized as impulse-free ones [3] and with impulse mode ones in analysis. To explain that, singular value decomposition (SVD) is performed on the original generalized state space system. This transfers the original system to the following form.

$$\begin{bmatrix} I_r & 0 \\ 0 & 0 \end{bmatrix} \begin{bmatrix} \dot{q}_1 \\ \dot{q}_2 \end{bmatrix} = \begin{bmatrix} F_{11} & F_{12} \\ F_{21} & F_{22} \end{bmatrix} \begin{bmatrix} q_1 \\ q_2 \end{bmatrix} + \begin{bmatrix} N_1 \\ N_2 \end{bmatrix} u \tag{6}$$

where I_r is an $r \times r$ identity matrix.

When F_{22}^{-1} in (6) exists, the system is impulse free, one can further obtain

$$q_2 = -F_{22}^{-1} F_{21} q_1 - F_{22}^{-1} N_2 u \tag{7}$$

Substituting (7) to (6), we have

$$\dot{q}_1 = (F_{11} - F_{12} F_{22}^{-1} F_{21}) q_1 + (N_1 - F_{12} F_{22}^{-1} N_2) u \tag{8}$$

To q_1, (8) is a standard state space system, if it is controllable, one can design a state feedback control law $u = -kq_1$ to control (8). Consequently, q_2 is stabilized through the coupling equation in (7). Therefore, control designs for impulse-free generalized state space systems can be handled and have been an active area in research. Obviously, applying state feedback methods only can control part of the states while the rest of states are just stabilized for impulse-free generalized state space systems. Therefore, the closed loop performance is limited.

For impulse-free generalized state space systems, the available control design algorithms which are usually carried out in augmented systems and require feedbacks of both state and state derivative variables [3, 4, 13, 19, 37] are much more complex than algorithms for the standard state space systems. Consequently, there are difficulties for engineers without strong mathematical background to apply those sophisticated control algorithms.

When F_{22}^{-1} in (6) does not exist, the generalized state space system has impulse mode. In this case, further investigations of impulse controllable and the impulse mode elimination [3] have to be analyzed in control designs. Therefore, this kind of generalized state space system is considered to be difficult in control designs.

As mention before, when the state derivative coefficient matrix E in (1) is nonsingular, the system can be expressed in standard state space form in (3). If the system

is controllable, applying state feedback alone is sufficient to control the system. Similarly, it is natural to ask if applying state derivative feedback alone is sufficient to control the system when the state coefficient matrix F in (1) is nonsingular. To answer this question and to provide supplementary design algorithms of state derivative feedback, a direct state derivative feedback control scheme was developed using the "Reciprocal State Space" (RSS) methodology by the author of this chapter as follows.

$$x = F^{-1}E\dot{x} - F^{-1}Nu = A\dot{x} + Bu \tag{9}$$

For above reciprocal state space (RSS) systems, state vector can be explicitly expressed in terms of state derivative vector and control input vector. The controllability and observability analyses for system in RSS form have been investigated in Tseng et al. and Tseng [24, 25]. It shows that they turn out to be the same as their counterparts in state space form. After apply full state derivative feedback control law in (4), the closed loop system becomes

$$x = (A - BK)\,\dot{x} = A_c\dot{x} \tag{10}$$

The concept of RSS is based on a fact that for a nonsingular matrix, the eigenvalues of its inverse matrix must be the reciprocals of its eigenvalues. Therefore, the eigenvalues of A_c in (10) are the reciprocals of the closed loop system poles. To address this nature, the name of reciprocal state space form was given. If state derivative feedback gain K can be designed such that real parts of all eigenvalues of A_c in (10) are strictly negative, the closed loop system in RSS form in (10) can achieve globally asymptotically stable. When a controllable system has no open loop pole at zero, it can be expressed in RSS form to carry out state derive related feedback control designs.

It also shows that state derivative feedback designs can be carried out as straightforward in RSS form as state feedback designs in standard state space form in pole placement, eigenstructure assignment, and linear quadratic regulator (LQR) designs [21–26].

The following is an example for quick understanding why expressing system in RSS form and applying state derivative feedback can easily accomplish control designs for some systems that were once thought difficult to be controlled. For the following generalized state space system with impulse mode [13], its state coefficient matrix is invertible. Therefore, the open loop system has no open loop pole at zero and the system can be expressed in RSS form.

$$\begin{bmatrix} 1 & 0 & 0 \\ 0 & 1 & 0 \\ 0 & 0 & 0 \end{bmatrix} \dot{x} = \begin{bmatrix} 0.5 & 0 & 0 \\ -1 & -1 & -1 \\ 0 & -1 & 0 \end{bmatrix} x + \begin{bmatrix} 1 \\ 1 \\ 1 \end{bmatrix} u$$

Suppose that we want to place the closed loop poles at $-2, -2.5, -5$. Using state feedback control laws in generalized state space form cannot place all of the desired closed loop poles. However, one can first express the system in RSS form as follows.

$$x = \begin{bmatrix} 2 & 0 & 0 \\ 0 & 0 & 0 \\ -2 & -1 & 0 \end{bmatrix} \dot{x} + \begin{bmatrix} -2 \\ 1 \\ 2 \end{bmatrix} u = A\dot{x} + Bu$$

Then apply the state derivative feedback law $u = -K\dot{x}$ to assign $-0.5, -0.4$ and -0.2 (the reciprocals of $-2, -2.5$ and -5, respectively) as the eigenvalues of matrix $(A - BK)$. Using "place" command of *Matlab*, one can easily get $K = \begin{bmatrix} -1.63 & -0.2 & 0.02 \end{bmatrix}$. Therefore, for the systems without open loop pole at zero, including difficult systems to be controlled such as generalized state space systems with impulse mode in this example, they can be expressed in RSS form in (9) and properly controlled by applying state derivative feedback alone. Usually, handling the same problem in generalized state space system form, both state feedback and state derivative feedback are needed [13].

Put RSS form into consideration, to streamline the design processes and keep the controller as compact as possible, the following control design procedure is suggested: For an open loop system, if it has no pole at infinity, one can express the system in state space form and apply state related feedback to control it. If it has poles at infinity but has no pole at zero, one can express the system in RSS form and apply state derivative related feedback to control it. If it has neither pole at infinity nor pole at zero, based on the type of available sensors (state related sensors or state derivative related sensors), one can make choice between state space form and RSS form to carry out control design. Generalized state space system form and control laws applying both state feedback and state derivative feedback might be considered as the last resort to handle the system with poles at both infinity and zero. In a nutshell, RSS form fills in the gap between standard state space system and generalized state space system and provides additional flexibility in control designs.

3 Sliding Mode Control with State Derivative Feedback in Reciprocal State Space Form

This section explains how sliding mode control is carried out in novel reciprocal state space (RSS) form with state derivative feedback.

Beginning with Lyapunov stability analysis in RSS form in Sects. 3.1 and 3.2 is an introduction to the proposed novel approach condition suitable for systems in RSS form. SMC design approach for a simple nominal system in RSS form and numerical examples to verify the proposed novel approach condition are presented in Sect. 3.3. Section 3.4 explains the process of finding the upper bound of system uncertainty and SMC design approach for RSS systems with both uncertainty and disturbance. Numerical example is also provided to verify the proposed methods.

3.1 Lyapunov Stability Analysis in RSS Form

Since Lyapunov stability is the fundamental of sliding mode control, in this subsection Lyapunov stability analysis in RSS form is presented.

For a linear time invariant system, it is globally asymptotically stable if the real parts of all system poles are strictly negative. Therefore, such system must have no pole at infinity or pole at zero. Consequently, a globally asymptotically stable system can be expressed in both state space form and RSS form as follows.

$$\dot{x} = \bar{A}x \tag{11}$$

$$x = A\dot{x} \tag{12}$$

where $\bar{A} = A^{-1}$ and both A and $\bar{A}$ are nonsingular. Furthermore, the eigenvalues of A are the reciprocals of the eigenvalues of $\bar{A}$ which are the system poles. If the real parts of all eigenvalues of $\bar{A}$ are strictly negative, so are all eigenvalues of A. Based on the above discussion, the following Lyapunov equation can also test the stability of RSS systems in (12).

$$PA + A^T P = -Q \tag{13}$$

The solution of P in Lyapunov equation (13) must be symmetric positive definite to ensure RSS system matrix A is globally asymptotically stable when a symmetric and positive matrix Q is used.

3.2 Novel Approaching Condition for SMC Designs in RSS Form

In general, design of sliding mode control consists of two parts. The first part involves the selection of an appropriate sliding surface and the second part is the design of a controller to meet the approaching condition. To provide the fundamentals of SMC, approaching condition and sliding mode are briefly reviewed as follows.

Approaching condition can force the system toward the predetermined sliding surface $s\,(t)$ which can stabilize the system (some studies call this "reaching condition" or "hitting condition"), and we usually consider it as follows [8, 33].

$$s^T\,(t) \cdot \dot{s}\,(t) < 0 \tag{14}$$

When the system in the predetermined sliding surface, the system will remain in the neighborhood of sliding surface therefore slip toward the target with any external disturbance.

There is a simple SMC method's moving trajectory shown in Fig. 1. From $t = 0$, the state x starts to approach the sliding surface $s = 0$ and lands on the sliding surface at

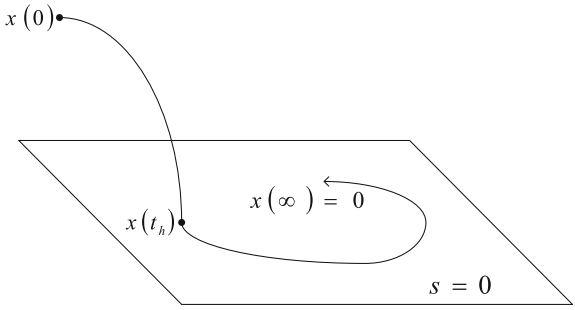

Fig. 1 The state trajectory of SMC

the finite time t_h. When $t > t_h$, this state remains on the sliding surface, and moves toward the equilibrium point $x = 0$ (i.e. $x(\infty) \to 0$).

According to the matrix sizes specified in (1), suppose that the sliding surface $s(t)$ is selected by

$$s(t) = Cx(t) = 0 \tag{15}$$

where $s \in \Re^{m\times 1}$ and $c \in \Re^{m\times n}$.

Approaching condition is briefly explained as follows. Define a Lyapunov function candidate based on the sliding surface $s(t)$ as follows.

$$V = \frac{1}{2}s^T(t)s(t) \tag{16}$$

The derivative of V with respect to time becomes

$$\dot{V} = s^T(t) \cdot \dot{s}(t) \tag{17}$$

For SMC designs in RSS form with state derivative related feedback laws, given a positive constant α, the following novel approaching condition is proposed.

$$\dot{V} = s^T(t) \cdot \dot{s}(t) < -\alpha \|\dot{s}\| < 0 \tag{18}$$

where $\|\|$ denotes norm in this chapter.

Detailed discussion will be given in the following subsections.

3.3 Sliding Model Control Design for Nominal System in RSS Form

In this subsection, sliding mode control design for nominal system in RSS form without any system uncertainty is presented for readers to easily understand the fundamental of SMC design approach carried out in RSS form. We first consider the RSS system described as follows:

$$x(t) = A\dot{x}(t) + Bu(t) + d(t) \tag{19}$$

where $x(t) \in \Re^n$, $u(t) \in \Re^m$ and $d(t) \in \Re^{n\times 1}$ are states, control inputs, and external disturbance respectively. Assuming that the pair (A, B) is known and their dimensions are $A \in \Re^{n\times n}$ and $B \in \Re^{n\times m}$.

The following assumptions are applied in this chapter.

- The nominal RSS linear system is unstable.
- The pair (A, B) is controllable; $Rank\left[B\ AB\ A^2B\ \cdots\ A^{n-1}B\right] = n$.
- The $d(t)$ is a matched external disturbance as follows.

$$d(t) = Bd_r(t) \tag{20}$$

where $d_r(t) \in \Re^{m\times 1}$ and has an upper bound δ such that $\|d_r(t)\| \leq \delta$.

So, (19) can be rewritten as

$$x(t) = A\dot{x}(t) + B(u(t) + d_r(t)) \tag{21}$$

The sliding face to be selected is

$$s(t) = Cx(t) = 0 \tag{22}$$

3.3.1 Selecting Sliding Surface with Modified Transfer Matrix Method in RSS Form

In this subsection, we present a method to select a sliding surface for developing a sliding mode controller for the system in RSS form (19). The proposed method is modified from the popular transfer matrix method [34].

If matrix B is partitioned into

$$B = \begin{bmatrix} B_1 \\ B_2 \end{bmatrix}, \tag{23}$$

where B_1 is $(n-m)\times m$ and B_2 is $m \times m$.

One can define the following transfer matrix

$$T = \begin{bmatrix} I_{(n-m)\times(n-m)} & -B_1B_2^{-1} \\ 0_{m\times(n-m)} & I_{m\times m} \end{bmatrix}, \tag{24}$$

such that $T \cdot B = \left[0\ B_2\right]^T$.

Please note that for a controllable system, one can always obtain a B matrix with an invertible sub-matrix B_2 by properly define the state variables and consequently obtain T.

Applying the following transfer,

$$q = Tx \tag{25}$$

(21) is transferred to

$$q_1 = A_{11}\dot{q}_1 + A_{12}\dot{q}_2 \tag{26}$$

$$q_2 = A_{21}\dot{q}_1 + A_{22}\dot{q}_2 + B_2 u + B_2 \cdot d_r \tag{27}$$

where

$$q = \begin{bmatrix} q_1 \\ q_2 \end{bmatrix} \in \begin{bmatrix} R^{n-m} \\ R^m \end{bmatrix}, TAT^{-1} = \begin{bmatrix} A_{11} & A_{12} \\ A_{21} & A_{22} \end{bmatrix} \tag{28}$$

Now, the sliding surface can be expressed as follows.

$$s = Cx = CT^{-1}q = \begin{bmatrix} S_1 & S_2 \end{bmatrix} q = \begin{bmatrix} S_2 k & S_2 \end{bmatrix} q = S_2 \begin{bmatrix} k & I_m \end{bmatrix} q = 0 \tag{29}$$

where $S_1 \in \Re^{m\times(n-m)}$, $S_2 \in \Re^{m\times m}$ and $k \in \Re^{m\times(n-m)}$.

In (29), S_2 can be considered as any square matrix, and if we select S_2 as an identity matrix I_m, we have sliding surface as follows.

$$s = \begin{bmatrix} k & I_m \end{bmatrix} q = kq_1 + q_2 = \begin{bmatrix} k & I_m \end{bmatrix} Tx = 0. \tag{30}$$

Solving for q_2 with (30), we have

$$q_2 = -kq_1 \tag{31}$$

Taking derivative of both sides of (31), we obtain

$$\dot{q}_2 = -k\dot{q}_1 \tag{32}$$

Substituting (32) into (26), we have:

$$q_1 = (A_{11} - A_{12}k)\,\dot{q}_1 \tag{33}$$

If (A_{11}, A_{12}) is controllable, designing k in (33) is just a pole placement problem with full state-derivative feedback in RSS framework. Note that k in (33) should be designed such that the eigenvalues of $(A_{11} - A_{12}k)$ are equal to the reciprocal of the desired closed loop poles. After k is designed, the sliding surface in (30) is obtained.

3.3.2 Sliding Mode Control Design in RSS Form

This subsection introduces a SMC control law to make the approaching condition $(s^T(t) \cdot \dot{s}(t) < 0)$ happen so that the system in (21) is guaranteed to reach and maintain on the sliding surface consequently.

After sliding surface is selected, we have to find the equivalent control $u_{eq}(t)$ which is the control law to let the system operates in the sliding mode.
Substituting (19) into (22), we have

$$s(t) = Cx(t) = C[A\dot{x}(t) + Bu(t) + d(t)] = 0 \tag{34}$$

If we let $u(t) = u_{eq}(t)$ in (34), the equivalent control can be found as

$$u_{eq}(t) = -(CB)^{-1}[CA\dot{x}(t) + Cd(t)] \tag{35}$$

Here u_{eq} is related to state derivative $\dot{x}$. Therefore, state derivative signals can be directly used in SMC design. Physically, the equivalent control $u_{eq}(t)$ cannot obtain the sliding motion if the initial state is not on the sliding surface. An ideal control law for the RSS system in (19) to generate the approaching condition of sliding mode is proposed as follows.

$$u(t) = -(CB)^{-1}CA\dot{x}(t) - (CB)^{-1} \cdot (\gamma + \alpha) \cdot sign(\dot{s}(t)) \tag{36}$$

where γ and α are all positive scalars such that $\|\gamma\| = \|C\| \cdot \|B\| \cdot \delta > \|CBd_r(t)\|$ and $\alpha > 0$.

The matrix CB is nonsingular and $sign(\dot{s}_i)$ is a novel switching function proposed as follows.

$$sign(\dot{s}_i) = \begin{cases} 1 & \dot{s}_i > 0 \\ 0 & \dot{s}_i = 0 \\ -1 & \dot{s}_i < 0 \end{cases} \tag{37}$$

Note that $sign(\dot{s}_i)$ is not a function of the sliding surface, but a function of the derivative of the sliding surface.

Proof Substituting (19) and (36) into sliding surface (22), we get the following result.

$$\begin{aligned} &s(t) = \\ &\{CA\dot{x}(t) + CB[-(CB)^{-1}CA\dot{x}(t) - (CB)^{-1}(\gamma + \alpha) \cdot sign(\dot{s}(t))] + Cd(t)\} \end{aligned} \tag{38}$$

Taking transposes and multiplying $\dot{s}(t)$ on both sides of (38) to get the equation of approaching condition, we have

$$
\begin{aligned}
s^T(t)\cdot\dot{s}(t) &= \{CA\dot{x}(t)+CB[-(CB)^{-1}CA\dot{x}(t)-(CB)^{-1}(\gamma+\alpha)\cdot sign(\dot{s}(t))] \\
&\quad + CBd_r(t)\}^T\dot{s}(t) \\
&= \left[(CBd_r)^T\dot{s}(t)-(\gamma+\alpha)^T\cdot\|\dot{s}(t)\|\right] \\
&= -\alpha\cdot\|\dot{s}(t)\|-\gamma\cdot\|\dot{s}\|\left(1-\frac{(CBd_r)^T\dot{s}(t)}{\gamma\cdot\|\dot{s}(t)\|}\right) \qquad (39)
\end{aligned}
$$

Since $-1<\frac{(CBd_r)^T\dot{s}(t)}{\gamma\cdot\|\dot{s}(t)\|}<1$, consequently, $\left(1-\frac{(CBd_r)^T\dot{s}(t)}{\gamma\cdot\|\dot{s}(t)\|}\right)>0$. We can conclude the following result.

$$
s^T(t)\cdot\dot{s}(t)=-\alpha\cdot\|\dot{s}(t)\|-\gamma\cdot\|\dot{s}(t)\|\left(1-\frac{(CBd_r)^T\dot{s}(t)}{\gamma\cdot\|\dot{s}(t)\|}\right)<-\alpha\cdot\|\dot{s}(t)\|<0 \qquad (40)
$$

Therefore, applying the ideal controller in (36), the approaching condition ($s^T(t)\cdot\dot{s}(t)<0$) holds. Consequently, the motion in the sliding mode is asymptotically stable. However, the ideal controller in (36) which using "*sign*" function may cause "Chattering Phenomenon". To avoid this problem, "*sign*" function is replaced by a novel "*sat*" saturation function in the modified control law given as follows.

$$
u(t):=-(CB)^{-1}CA\dot{x}(t)-(CB)^{-1}(\gamma+\alpha)sat(\dot{s}(t),\varepsilon) \qquad (41)
$$

where *"sat"* is a novel saturation function to handle the switching as follows.

$$
sat(\dot{s}_i,\varepsilon)=\begin{cases}1 & \dot{s}_i>\varepsilon\\ \frac{\dot{s}_i}{\varepsilon} & |\dot{s}_i|\le\varepsilon\\ -1 & \dot{s}_i<-\varepsilon\end{cases}=\begin{cases}sign(\dot{s}_i) & |\dot{s}_i|>\varepsilon\\ \frac{\dot{s}_i}{\varepsilon} & |\dot{s}_i|\le\varepsilon\end{cases} \qquad (42)
$$

Here ε is a small positive value as the bound of the differential sliding surface $\dot{s}$.

$$
|\dot{s}|\le\varepsilon \qquad (43)
$$

Although the control law (41) cannot completely eliminate the external disturbance, it still can reduce the influence of the external disturbance and can ensure the convergence of states in a boundary layer. It is still worth to avoid "Chattering Phenomenon" by paying the price of losing small accuracy.

One may wonder that if $\dot{s}$ is just bounded inside the differential sliding layer $|\dot{s}|\le\varepsilon$, can the amplitude of the sliding surface s keeps increasing as time goes by and finally become diverged? The answer is negative because when $\dot{s}=C\dot{x}$ is bounded, so is $\dot{x}$ due to the fact that C is a constant matrix. When $\dot{x}$ is bounded, from the system equation in (19) and controller in (41), x which can be expressed in term of $\dot{x}$ must be bounded, too. Consequently, $s=Cx$ must also be bounded. Similarly, through the system constraint in (19), when the approaching condition does not happen inside the differential sliding layer of $|\dot{s}|\le\varepsilon$, both $|s|$ and $|x|$ will

be increased, so will $|\dot{s}|$ and $|\dot{x}|$. When $\dot{s}$ finally reach to the condition of $|\dot{s}| > \varepsilon$, the controller will switch to (36) to push the system back to the differential sliding layer of $|\dot{s}| \leq \varepsilon$. In this manner, the controller can keep the $\dot{s}$ inside the differential sliding layer of $|\dot{s}| \leq \varepsilon$ in steady state. Consequently, through the system constraint in (19), s and x should also be bounded in steady state.

Numerical Example 1

Theoretically, if no external disturbance is considered in (19), the system should be driven toward the sliding surface and stuck on it when SMC law is applied. In the other word, one should obtain $s(\infty) \to 0$ in simulation. The following is an example to verify that the proposed SMC algorithm can achieve $s(\infty) \to 0$ for RSS systems without external disturbance. The system matrices are given as follows.

$A = \begin{bmatrix} 1 & 2 \\ 2 & 4 \end{bmatrix}$ and $B = \begin{bmatrix} 0 \\ 1 \end{bmatrix}$. Since A is singular, SMC design cannot be directly carried out in standard state space form. The initial condition is given as:

$$x_0 = \begin{bmatrix} 0 \\ 1 \end{bmatrix}.$$

The first step is to select the sliding surface by applying the presented transfer matrix method. If pole at -2 is selected, the corresponding sliding surface is found to be $s = \begin{bmatrix} 1.5 & 1 \end{bmatrix} x$. The second step is to design the controller in (41). The following parameter are used in the simulation $\varepsilon = 0.5$, $\gamma = 0$, and $\alpha = 5$.

Figures 2, 3 and 4 show the time responses of states, sliding surface, and control effort, respectively. In Fig. 2, we find that the trajectories of $x_1(t)$ and $x_2(t)$ are asymptotically stable. In Fig. 3, the sliding surface response does converge to zero when no external disturbance is considered. Therefore, the proposed approach condition in (18) and control law in (41) are successfully verified.

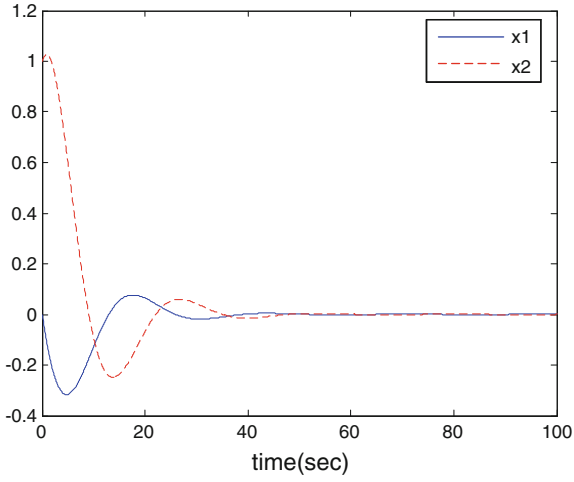

Fig. 2 The state responses of numerical example 1

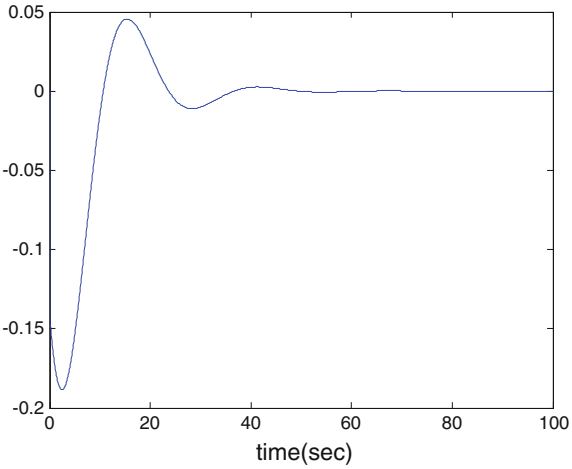

Fig. 3 The sliding surface response of numerical example 1

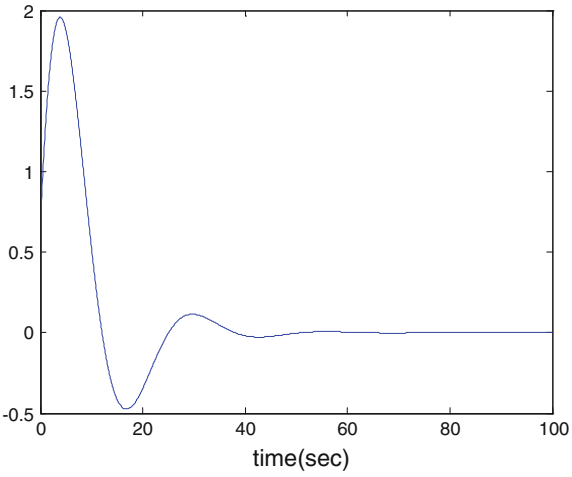

Fig. 4 The control effort of numerical example 1

From the simulation results, we conclude that the controller design in (41) as well as the proposed novel saturation switching function in (42) dose work effectively for the RSS system in (19). It also shows that SMC design can directly utilize state derivative feedback if the design is carried out in RSS framework. Furthermore, for generalized state space system in (1), if matrix E is singular but matrix F is nonsingular, it can be expressed in RSS framework to directly carry out SMC design.

Numerical Example 2

Here is another example with disturbance to verify the proposed SMC algorithm. Consider a dynamic RSS system in (19) with following parameters:

$$A = \begin{bmatrix} 1 & -0.5 & 0.25 \\ 0 & 0.5 & -0.25 \\ 0 & 0 & 0.5 \end{bmatrix}, B = \begin{bmatrix} -0.25 \\ 0.25 \\ -0.5 \end{bmatrix}, d_r(t) = 0.2 \sin(0.3333t)$$

and the initial condition is given as: $x_0 = \begin{bmatrix} 1 \\ -2 \\ 6 \end{bmatrix}$.

Using (24), the transpose matrix is constructed as follows.

$$T = \begin{bmatrix} 1 & 0 & -0.5 \\ 0 & 1 & 0.5 \\ 0 & 0 & -2 \end{bmatrix}.$$

The first step is to select the sliding surface, and the transfer matrix method is applied. If poles at -5 and -2.5 are selected, the obtained sliding surface is $s = \begin{bmatrix} -84 & -180 & 1 \end{bmatrix} x$. The second step is to design the controller given in (41). $\varepsilon = 0.5$, $\gamma = 2$ and $\alpha = 4$ are used in the simulation.

Figures 5, 6 and 7 show the time responses of states $x_1(t) - x_3(t)$, sliding surface, and control effort, respectively. As expected, in Fig. 5, under the influence of disturbance, we find that the trajectories of states are still bounded, so is the sliding surface response in Fig. 6. Therefore, the controller designed in (41) for the RSS system (19) indeed works effectively.

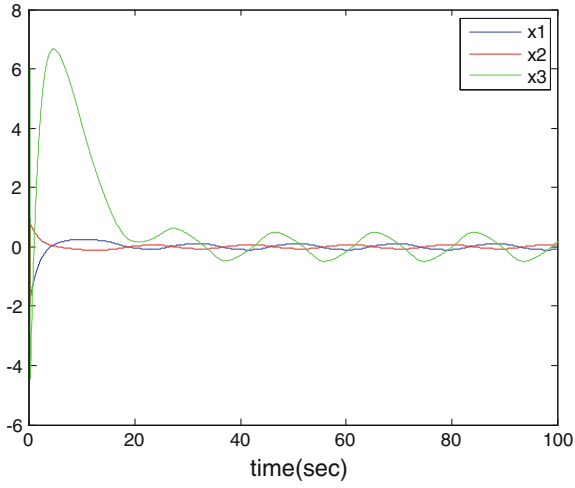

Fig. 5 The state responses of numerical example 2

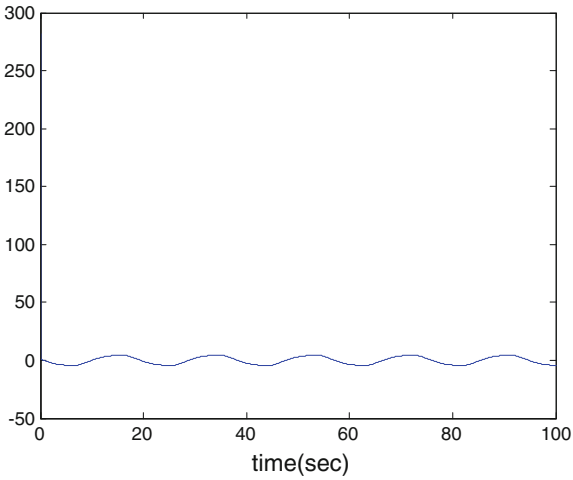

Fig. 6 Time response of the sliding surface of numerical example 2

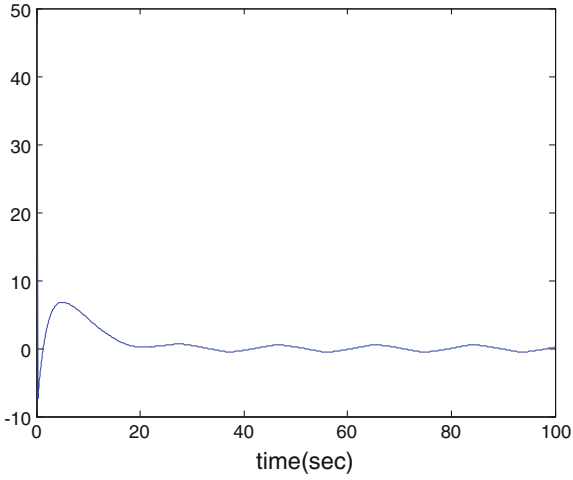

Fig. 7 Time response of control effort of numerical example 2

3.4 Sliding Model Control Design for a System with System Uncertainty and Disturbance in RSS Form

In this subsection, SMC design procedure for more realistic systems with system uncertainty and external disturbance in RSS form is presented. Consider the following RSS system:

$$x(t) = [A + \Delta A(t)]\dot{x}(t) + Bu(t) + d(t) \tag{44}$$

where $x(t) \in \Re^n$, $\Delta A(t) \in \Re^{n\times n}$, $u(t) \in R^m$ and $d(t) \in \Re^{n\times 1}$ are states, mismatched uncertainty, control inputs, and external disturbance respectively. Assuming that the nominal RSS linear system pair (A, B) is known and matrix dimensions are

$A \in \Re^{n\times n}$ and $B \in \Re^{n\times m}$. The external disturbance is a matched one and is defined as

$$d(t) = Bd_r(t) \tag{45}$$

where $d_r(t) \in \Re^{m\times 1}$.

Therefore, applying (45), (44) can be rewritten as

$$x(t) = [A + \Delta A(t)]\dot{x}(t) + B[u(t) + d_r(t)] \tag{46}$$

We assume that positive scalars, δ_A and δ_d, are the upper bounds of the uncertainty and the external disturbance, respectively.

$$\|\Delta A(t)\| \leq \delta_A, \text{ and } \|d_r(t)\| \leq \delta_d \tag{47}$$

3.4.1 Sufficient Condition for Finding the Upper Bound of System Uncertainty to Guarantee the Stability in Sliding Surface

In this subsection, we will provide a sufficient condition to determine the upper bound of uncertainty ΔA so that the stability in sliding surface is still guaranteed.

Like we mentioned in subsection 3.3.1, we can find the transfer matrix T in (25) such that $TB = \begin{bmatrix} 0 & B_2 \end{bmatrix}^T$.

Then (44) is transferred to the following equations.

$$q_1 = (A_{11} + \Delta A_{11})\dot{q}_1 + (A_{12} + \Delta A_{12})\dot{q}_2 \tag{48}$$

$$q_2 = (A_{21} + \Delta A_{21})\dot{q}_1 + (A_{22} + \Delta A_{22})\dot{q}_2 + B_2(u + d) \tag{49}$$

where every matrix with appropriate dimensions and B_2 is nonsingular.

We may neglect the uncertainty ΔA and disturbance d in (44) and apply the method in subsection 3.3.1 to design the sliding surface.

$$s = \begin{bmatrix} k & I_m \end{bmatrix} q = kq_1 + q_2 = \begin{bmatrix} k & I_m \end{bmatrix} Tx = 0 \tag{50}$$

Consequently, the derivative of sliding surface in (50) with respect to time can also be transferred to

$$\dot{s} = k\dot{q}_1 + \dot{q}_2 = 0 \tag{51}$$

Consequently, we have

$$\dot{q}_2 = -k\dot{q}_1 \tag{52}$$

Then substituting (52) into (48), we have

$$q_1 = A_e\dot{q}_1 + \Delta A_e\dot{q}_1 \tag{53}$$

where $A_e = A_{11} - A_{12}k$ and $\Delta A_e = \Delta A_{11} - \Delta A_{12}k$.

It has been proved that we also can apply Lyapunov equation to test the stability of a RSS system [24]. Based on that, the following two theorems are introduced for determining the upper bound of system uncertainty.

Theorem 1 *Assuming that A_e is a stable matrix and the time-varying uncertainty matrix ΔA_e in (53) is in a bounded value ζ such that $\|\Delta A_e\| < \zeta$, we have*

$$\|\Delta A_e\| < \zeta = \frac{\min\{\eta_i\}}{2\lambda_{\max}(P_e)}, \quad i = 1, 2, \ldots, (n-m)\,. \tag{54}$$

where η_i are all eigenvalues in a selected positive symmetric definite matrix Q_e while P_e is a positive symmetric definite matrix solved from the following Lyapunov equation.

$$A_e^T P_e + P_e A_e = -Q_e \tag{55}$$

Proof Define the Lyapunov functional:

$$V = q_1^T P_e q_1 \tag{56}$$

where P_e is symmetric positive definite matrix. It can be easily verified that V is a positive function. The time derivative of V along the trajectory of the system (53) is expressed as

$$\begin{aligned}
\dot{V} &= \dot{q}_1^T P_e q_1 + q_1^T P_e \dot{q}_1 \\
&= \dot{q}_1^T P_e \left[A_e \dot{q}_1 + \Delta A_e \dot{q}_1\right] + \left[A_e \dot{q}_1 + \Delta A_e \dot{q}_1\right]^T P_e \dot{q}_1 \\
&= \dot{q}_1^T P_e A_e \dot{q}_1 + \dot{q}_1^T P_e \Delta A_e \dot{q}_1 + \dot{q}_1^T A_e^T P_e \dot{q}_1 + \dot{q}_1^T \Delta A_e^T P_e \dot{q}_1 \\
&= \dot{q}_1^T \left[P_e A_e + A_e^T P_e\right] \dot{q}_1 + 2\dot{q}_1^T P_e \Delta A_e \dot{q}_1
\end{aligned} \tag{57}$$

Then, substituting (55) into (57), one obtains

$$\dot{V} = \dot{q}_1^T \left[-Q_e\right] \dot{q}_1 + 2\dot{q}_1^T P_e \Delta A_e \dot{q}_1 \tag{58}$$

From (58), when the following condition holds, one can conclude that $\dot{V} < 0$.

$$\dot{q}_1^T Q_e \dot{q}_1 > 2\dot{q}_1^T P_e \Delta A_e \dot{q}_1 \tag{59}$$

By Rayleigh principle, the lower bound of $\dot{q}_1^T Q_e \dot{q}_1$ in (59) can be obtained as follows.

$$\dot{q}_1^T Q_e \dot{q}_1 \geq \lambda_{\min}(Q_e) \dot{q}_1^T \dot{q}_1 = \lambda_{\min}(Q_e) \|\dot{q}_1\|^2 = \min\{\eta_i\} \|\dot{q}_1\|^2 \tag{60}$$

The following inequality can also be obtained

$$2\dot{q}_1^T P_e \Delta A_e \dot{q}_1 \leq 2 \|\Delta A_e\| \lambda_{\max}(P_e) \dot{q}_1^T \dot{q}_1 = 2 \|\Delta A_e\| \lambda_{\max}(P_e) \|\dot{q}_1\|^2 \tag{61}$$

From (60), (61) and (59), if we have

$$2\,\|\Delta A_e\|\,\lambda_{\max}(P_e)\,\|\dot{q}_1\|^2 < \min\{\eta_i\}\,\|\dot{q}_1\|^2 \tag{62}$$

and consequently,

$$\|\Delta A_e\| < \frac{\min\{\eta_i\}}{2\lambda_{\max}(P_e)} = \zeta, \quad i = 1, 2, \ldots, (n-m)\,, \tag{63}$$

it implies that (58) is negative, namely, $\dot{V} < 0$ for $t \geq 0$. Consequently, the system with mismatched time-varying uncertainty ΔA_e in (44) in the sliding surface is asymptotically stable. Next, we have to provide another condition to find the upper bound of the mismatched uncertainty ΔA.

Theorem 2 *Let the transform matrix T in (24) be partitioned as*

$$T = \begin{bmatrix} L_1 \\ L_2 \end{bmatrix} \text{ and } T^{-1} = \begin{bmatrix} R_1 & R_2 \end{bmatrix} \tag{64}$$

where $L_1 \in \Re^{(n-m)\times n}$, $L_2 \in \Re^{m\times n}$, $R_1 \in \Re^{n\times(n-m)}$, and $R_2 \in \Re^{n\times m}$.
If the following condition holds,

$$\|\Delta A\| \leq \frac{\min\{\eta_i\}}{2\left(\|L_1\| \cdot \|R_1\| + \|L_1\| \cdot \|R_2\| \cdot \|k\|\right)\lambda_{\max}(P_e)} \tag{65}$$

where P_e and Q_e are defined in (55) in Theorem 1, the RSS system with mismatched uncertainty ΔA in (44) is stable on the sliding surface.

Proof Since the transform matrix T in (24) can be partitioned as $T = \begin{bmatrix} L_1 \\ L_2 \end{bmatrix}$ and $T^{-1} = \begin{bmatrix} R_1 & R_2 \end{bmatrix}$, the uncertain matrix ΔA_{11} and ΔA_{12} in (48) can be expressed as

$$\Delta A_{11} = L_1 \Delta A R_1 \text{ and } \Delta A_{12} = L_1 \Delta A R_2. \tag{66}$$

So the uncertainty ΔA_e given in (53) can be rewritten as:

$$\Delta A_e = L_1 \Delta A R_1 - L_1 \Delta A R_2 k \tag{67}$$

Taking the norm of (67), one can obtain the following inequality.

$$\begin{aligned} \|\Delta A_e\| &\leq \|L_1 \Delta A R_1\| + \|L_1 \Delta A R_2 F C_1\| \leq \|\Delta A\|\left(\|L_1\| \cdot \|R_1\| + \|L_1\| \cdot \|R_2\| \cdot \|k\|\right) \\ &< \frac{\min\{\eta_i\}}{2\lambda_{\max}(P_e)} \end{aligned} \tag{68}$$

Consequently, the upper bound of ΔA is obtained as follow.

$$\|\Delta A\| < \frac{\min\{\eta_i\}}{2\left(\|L_1\| \cdot \|R_1\| + \|L_1\| \cdot \|R_2\| \cdot \|k\|\right)\lambda_{\max}(P_e)}, \quad i = 1, 2, \ldots, (n-m) \tag{69}$$

This concludes our proof.

From the above proof, it is clear to find that if both (54) in Theorems 1 and (65) in Theorem 2 hold, the system with the mismatched uncertainty ΔA is stable in the sliding mode. Since the presented methodology is a sufficient condition for determining the upper bound of system uncertainty, if (54) and (65) do not hold, it does not mean that the system will definitely become unstable. Above procedure is analogous to that in [17].

Remark In this remark, the procedure of finding the upper bound of the uncertainty ΔA is summarized as follows.

Step 1: Select a T such that (44) is transferred to (48) and (49).

Step 2: Neglect the uncertainty ΔA and disturbance d in (48) and (49), then select a sliding surface with the method introduced in this chapter.

Step 3: Calculate A_e in (53).

Step 4: Select a positive symmetric definite matrix Q_e, then calculate P_e using (55).

Step 5: Calculate the upper bound of ΔA_e in Theorem 1 by calculating the minimum eigenvalue of Q_e and the maximum eigenvalue of P_e.

Step 6: Finding L_1, L_2, R_1, and R_2 from T and T^{-1} in (64), then calculate the upper bound of ΔA in Theorem 2.

3.4.2 Design the SMC Controller for System with System Uncertainty and External Disturbance

When the system operates in the sliding mode, it meets the approaching condition. Applying (46), the sliding surface becomes

$$s(t) = Cx = C\left[(A + \Delta A(t))\dot{x}(t) + B(u(t) + d_r(t))\right] = 0. \tag{70}$$

If we choose $u(t) = u_{eq}(t)$ in (70), the equivalent control is found as

$$u_{eq}(t) = -(CB)^{-1}\left(CA\dot{x}(t) + C\Delta A\dot{x}(t) + CBd_r(t)\right) \tag{71}$$

Physically, the equivalent control $u_{eq}(t)$ cannot obtain the sliding motion if the initial state is not in the sliding surface. The SMC control law for the dynamic system in (44) must satisfy the approaching condition of sliding mode. Based on (71), the SMC control law is selected as

$$u(t) := -(CB)^{-1}\left(CA\dot{x}(t)\right) - (CB)^{-1}\left(\|\delta\dot{x}(t)\| + \gamma + \alpha\right) \cdot sat\left(\dot{s}(t), \varepsilon\right) \tag{72}$$

where δ, γ, and α are positive scalars such that $\delta = \|C\| \cdot \delta_A > \|C\Delta A(t)\|$, $\gamma = \|C\| \cdot \|B\| \cdot \delta_d > \|CBd_r(t)\|$, and $\alpha > 0$, respectively. Moreover, ε is a small

positive value, and sat is a saturation function of the derivative of sliding surface $\dot{s}$ and is used to handle the switching and is described as

$$sat(\dot{s}_i, \varepsilon) = \begin{cases} 1 & \dot{s}_i > \varepsilon \\ \frac{\dot{s}_i}{\varepsilon} & |\dot{s}_i| \leq \varepsilon \\ -1 & \dot{s}_i < -\varepsilon \end{cases} = \begin{cases} sign\,(\dot{s}_i) & |\dot{s}_i| > \varepsilon \\ \frac{\dot{s}_i}{\varepsilon} & |\dot{s}_i| \leq \varepsilon \end{cases} \tag{73}$$

As mention in Sect. 3.3, the control law in (72) which uses saturation function cannot completely eliminate the external disturbance, but it can reduce the influence of the external disturbance so that the states are bounded.

At first, we consider the controller as follow.

$$u\,(t) = -\,(CB)^{-1}\,(CA\dot{x}\,(t)) - (CB)^{-1}\,(\|\delta\dot{x}\,(t)\| + \gamma + \alpha) \cdot sign\,(\dot{s}\,(t)) \tag{74}$$

where $sign$ is a function of $\dot{s}$ and is described as

$$sign(\dot{s}_i) = \begin{cases} 1 & \dot{s}_i > 0 \\ 0 & \dot{s}_i = 0 \\ -1 & \dot{s}_i < 0 \end{cases} \quad i = 1..m \tag{75}$$

Then, substituting (46) and (74) into sliding surface $s\,(t)$, we have

$$s\,(t) = \{C\Delta A\dot{x}\,(t) + CBd_r\,(t) - (\|\delta\dot{x}\,(t)\| + \gamma + \alpha) \cdot sign\,(\dot{s}\,(t))\} \tag{76}$$

Applying (76), approaching condition becomes

$$s^T\,(t) \cdot \dot{s}\,(t) = \left[(C\Delta A\dot{x}\,(t) + CBd_r\,(t))^T\,\dot{s} - (\|\delta\dot{x}\,(t)\| + \gamma + \alpha)^T \cdot \|\dot{s}\,(t)\|\right]$$

$$= -\alpha \cdot \|\dot{s}\,(t)\| - (\|\delta\dot{x}\,(t)\| + \gamma) \cdot \|\dot{s}\,(t)\| \left(1 - \frac{(C\Delta A\dot{x}\,(t) + CBd_r\,(t))^T \cdot \dot{s}\,(t)}{(\|\delta\dot{x}\,(t)\| + \gamma) \cdot \|\dot{s}\,(t)\|}\right) \tag{77}$$

Since $-1 < \frac{(C\Delta A\dot{x}(t)+CBd_r(t))^T \cdot \dot{s}(t)}{(\|\delta\dot{x}(t)\|+\gamma)\cdot\|\dot{s}(t)\|} < 1$, we have

$$s^T\,(t) \cdot \dot{s}\,(t) = -\alpha \cdot \|\dot{s}\,(t)\| - (\|\delta\dot{x}\,(t)\| + \gamma)^T \cdot \|\dot{s}\,(t)\| \left(1 - \frac{(C\Delta A\dot{x}\,(t) + Cd\,(t))^T \cdot \dot{s}\,(t)}{(\|\delta\dot{x}\,(t)\| + \gamma) \cdot \|\dot{s}\,(t)\|}\right) \tag{78}$$

$$< -\alpha \cdot \|\dot{s}\,(t)\| < 0$$

Thus, the approaching condition ($s^T\,(t) \cdot \dot{s}\,(t) < 0$) satisfies the Lyapunov stability theorem. Consequently, the motion in the sliding mode is asymptotically stable. Since the controller in (74) may cause "Chattering Phenomenon", "$sign$" function is replaced by "sat" function in the applied control law given in (72).

Numerical Example 3
Consider a dynamic RSS system (44) with following parameters:

$$A = \begin{bmatrix} -0.0104 & -0.0583 & 0.1945 \\ 0.9971 & 0.0162 & 0.07715 \\ 0 & 0 & -0.1499 \end{bmatrix}, \quad \Delta A(t) = \begin{bmatrix} 0 & 0 & 0 \\ 0 & 0 & 0 \\ 0.001\sin(t) & 0.0013\sin(t) & 0 \end{bmatrix}$$

$$B = \begin{bmatrix} -0.7114 \\ -0.1969 \\ 1 \end{bmatrix}, \quad d(t) = \begin{bmatrix} -0.3557 \\ -0.0984 \\ 0.5 \end{bmatrix} \cos(2t) = \begin{bmatrix} -0.7114 \\ -0.1969 \\ 1 \end{bmatrix} \times 0.5\cos(2t) = Bd_r(t).$$

The initial condition is given as:

$$x_0 = \begin{bmatrix} -0.5 \\ 0 \\ 10 \end{bmatrix}$$

With above given matrices, the transfer matrix is then constructed as follows.

$$T = \begin{bmatrix} 1 & 0 & 0.7114 \\ 0 & 1 & 0.1969 \\ 0 & 0 & 1 \end{bmatrix}.$$

Therefore, L_1, L_2, R_1, and R_2 in (64) are then found from T.
If the poles of A_e in (53) are selected at -0.1 and -0.3, the sliding surface is selected as $s = \begin{bmatrix} 0.6179 & -0.5112 & 1 \end{bmatrix} x$.
Calculating A_e in (53), selecting $Q_e = \begin{bmatrix} 7 & 0 \\ 0 & 8 \end{bmatrix}$ and then solving P_e from (55), we have

$$P_e = \begin{bmatrix} 700.5910 & 35.5079 \\ 35.5079 & 11.9477 \end{bmatrix}.$$

Consequently, the upper bound of uncertainty $\|\Delta A\|$ is calculated using (65) and is obtained as 0.002. Since the spectral norm of given $\Delta A(t)$ is less than 0.0016, the system with $\Delta A(t)$ as uncertainty still can guarantee the stability.

The following parameters are used for controller in (72):

$\varepsilon = 0.5, \alpha = 2, \delta_A = 0.0025$ and $\delta_d = 0.25$.

In Fig. 8, we can find that the simulation trajectories of states are bounded in a boundary layer. Therefore, the proposed controller works effectively as expected.

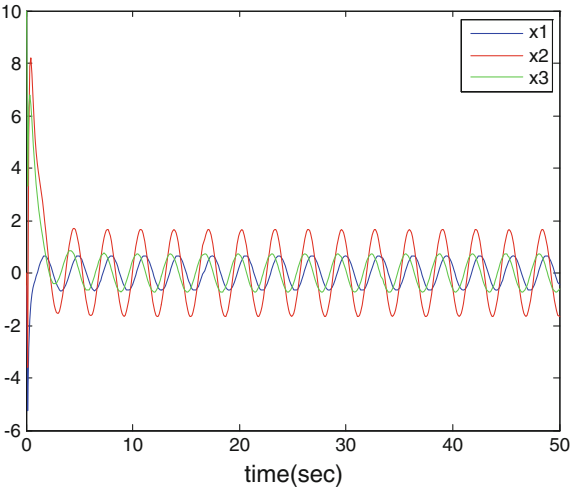

Fig. 8 State responses of example 3

4 Conclusion

In this chapter, the needs for reciprocal state space (RSS) form and state derivative related feedback control designs have been addressed. The fundamentals of state derivative feedback design in RSS form have been introduced. Basically, for controllable time invariant systems with no open loop poles at zero, the systems can be expressed in RSS form. The main advantage of RSS form is that state derivative feedback control designs can be systematically carried out in this form. Some once though tough systems to be controlled such as generalized state space system with impulse modes, can be fully controlled if it can be expressed in RSS form and apply state derivative feedback as shown in this chapter.

To better handle systems with external disturbance and system uncertainty with state derivative feedback control designs, novel sliding mode control design approach with state derivative feedback in RSS form is then presented. For systems in RSS form, nontraditional switching function utilizing the derivative of sliding surface is proposed and proven to satisfy the approaching condition of sliding mode. In addition, algorithm of finding upper bound of system uncertainty has been developed for robustness analysis. Simulation results successfully verify the proposed algorithms. State derivative output feedback algorithm for SMC design in RSS form has also been reported by author [31]. Our derivation is basically parallel to that for systems in standard state space form. Experienced engineers or researchers can be quickly familiar with the proposed design methods.

The contribution of this chapter is to provide SMC design approach by applying direct state derivative feedback in nontraditional RSS form so that people can handle more control problems without too much of mathematical overhead.

The future directions of research are suggested as follows:

- *Considering nonlinear constraint in control input*: In implementation, actuators that generate control inputs have various operating limitations such as saturation and dead zone [29]. People should develop algorithms that put actuator limits into consideration for more realistic considerations in design.
- *Using state derivative space (SDS) form in control design for nonlinear system:* State derivative space (SDS) form [30, 32] is a more general system form which can handle nonlinear systems. RSS form is a linear time invariant case of SDS form. SDS form is described as follows.

$$x = f(\dot{x}, u, t) \tag{79}$$

People may consider carrying out control design in SDS form with state derivative related feedback for some nonlinear systems. Author is working on it.

References

1. Brenan KE (1986) Numerical solution of trajectory prescribed path control problems by backward differentiation formulas. IEEE Trans Autom Control 31:266–269
2. Cobb D (1984) Controllability, observability and duality in singular systems. IEEE Trans Autom Control 29:1076–1082
3. Cobb D (2006) State feedback impulse elimination for singular systems over a hermite domain. SIAM J Control Optim 44:2189–2209
4. Cobb D (2010) Eigenvalue conditions for convergence of singularly perturbed matrix exponential functions. SIAM J Control Optim 48:4327–4351
5. Fahmy MM, O'Reilly YJ (1989) Parametric eigenstructure assignment for continuous-time descriptor systems. Int J Control 49:129–143
6. Fallah S, Khajepour A, Fidan B, Chen SK, Litkouhi B (2013) Vehicle optimal torque vectoring using state-derivative Feedback and linear matrix inequality. IEEE Trans Veh Technol 62: 1540–1552
7. Guo BZ, Jin FF (2013) Sliding mode and active disturbance rejection control to stabilization of one-dimensional anti-stable wave equations subject to disturbance in boundary input. IEEE Trans Autom Control 58:1269–1274
8. Itkis U (1976) Control systems of variable structure. Wiley, New York
9. Kulah H, Chae J, Yazdi N, Najafi K (2006) Noise analysis and characterization of a S-D capacitive silicon micro-accelerometers. IEEE J Solid-State Circuits 41:352–361
10. Kwak SK, Washington G (2001) A broadband vibration control using passive circuits in the matrix second order form. SPIE Proc Smart Struct Mater 2001(4326):14–19
11. Li H, Yu J, Hilton C, Liu H (2013) Adaptive sliding-mode control for nonlinear active suspension vehicle systems using T-S fuzzy approach. IEEE Trans Ind Electron 60:3328–3338
12. Lin FJ, Kuo LC (1997) Driving circuit for the ultrasonic motor servo drive with variable structure adaptive model-following control. IEE Proc Electr Power Appl 144:199–206
13. Liu D, Zhang G, Xie Y (2009) Guaranteed cost control for a class of descriptor systems with uncertainty. Int J Inf Syst 5:430–435
14. Liu P, Zhang Q, Yang X, Yang L (2008) Passivity and optimal control of descriptor biological complex systems. Joint Spec issue IEEE Trans Circuits Syst IEEE Trans Autom Control 53(1):122–125
15. Luenberger DG, Arbel A (1977) Singular dynamic leontief systems. Econometrica 45:991–995

16. Newcomb RW (1981) The semistate description of nonlinear time variable circuits. IEEE Trans Circuits Syst 28:28–33
17. Pai MC, Sinha A (2006) Sliding mode output feedback control of time-varying mismatched uncertain systems. IEEE international conference on systems, man, and cybernetics, pp 1355–1360
18. Pantelides CC (1988) The consistent initialization of differential-algebraic systems. SIAM J Sci Stat Comput 9:213–231
19. Saadni SM, Chaabane M, Mehdi D (2006) Robust stability and stabilization of a class of singular systems with multiple time-varying delay. Asian J Control 8:1–11
20. Shyu KK, Liu CY (1996) Variable structure controller design for robust tracking and model following. J Guid Control Dyn 19:1395–1397
21. Tseng YW (1997) Control design of linear dynamic system with matrix differential equations for aerospace applications. Ph.D. Dissertation, Department of Aerospace Engineering, The Ohio State University, Columbus, Ohio, USA
22. Tseng YW, Yedavalli RK (1997) Vibration control of a wing box via reciprocal state space framework. In: Proceedings of the IEEE conference on control applications. Hartford, Connecticut, USA, pp 854–89
23. Tseng YW, Yedavalli RK (1998) Control design via generalized state space system with state derivative measurement and reciprocal state space framework. In: Proceedings of the 1998 American control conference, Philadelphia, PA, USA, pp 2520–2521
24. Tseng YW, Kwak SK, Yedavalli RK (2003) Stability, controllability and observability criteria for the reciprocal state space framework. Proceedings of the American control conference, pp 5093–5097
25. Tseng YW (2008) Control designs of singular systems expressed in reciprocal state space framework with state derivative feedback. Int J Control Theory Appl 1:55–67
26. Tseng YW (2009) Vibration control of piezoelectric smart plate using estimated state derivatives feedback in reciprocal state space framework. Int J Control Theory Appl 2:61–71
27. Tseng YW, Wang YN (2009) Variable structure control in reciprocal state space framework. (2009) CACS international automatic control conference. Taipei, Taiwan
28. Tseng YW, Wang YN (2010) Variable structure control design and stability analysis in reciprocal state space framework. In: Proceedings of the 2nd international conference on computer and automation engineering (ICCAE) conference, vol 4, Singapore, pp 380–384,
29. Tseng YW, Wang YN (2012) Model following variable structure control design in reciprocal state space framework with dead-zone nonlinearity and lumped uncertainty. In: Proceedings of the IEEE conference on industrial electronics and applications, Singapore, pp 1627–1632
30. Tseng YW (2012) Optimal control in novel state derivative space system. In: Proceedings of the IEEE conference on industrial electronics and application, pp 371–376
31. Tseng YW, Wang YN (2013) Sliding mode control with state derivative output feedback in reciprocal state space form. special issue of switched dynamics with its applications, abstract and applied analysis, p 12. Article ID 590524. http://dx.doi.org/10.1155/2013/590524
32. Tseng YW, Hsieh JG (2013) Optimal control for a family of systems in novel state derivative space form with experiment in a double inverted pendulum system. Special issue of switched dynamics with its applications, Abstract and applied analysis. p 8, Article ID 715026. http://dx.doi.org/10.1155/2013/715026
33. Utkin VI (1977) Variable structure systems with sliding modes. IEEE Trans Autom Control 22:212–222
34. Utkin VI, Young KD (1979) Method for constructing discontinuity planes in multidimensional variable systems. Autom Remote Control 39:1466–1470
35. Utkin VI (1992) Sliding modes in control optimization. Springer, Berlin
36. Utkin VI, Guldner J, Shi J (1999) Sliding mode control in electromechanical systems. Taylor & Francis, Philadelphia
37. Varga A (2000) Robust pole assignment for descriptor systems. In: Proceeding of mathematical theory of networks and systems

38. Verghese GC, Levy BC, Kailath T (1981) A Generalized state-space for singular systems. IEEE Trans Autom Control 26:11–831
39. Wang N, Xu W, Chen F (2009) Output feedback variable structure control of uncertain linear systems in the presence of actuator dynamics. Asian J Control 11:420–426
40. Wang YN (2009) Variable structure control in reciprocal state space framework, M.S. thesis, advisor: Tseng YW Department of Electrical Engineering, I- Shou University, Kaohsiung, Taiwan, ROC
41. Yeh FB, Huang HN (2000) H infinity state feedback control of smart beam-plates via the descriptor system approach. Tunghai Sci 2:21–42
42. Yip EL, Sincovec RF (1981) Solvability, controllability and observability of continuous descriptor systems. IEEE Trans Autom Control 26:702–707

Active Controller Design for the Output Regulation of Vaidyanathan Hyperjerk System

Sundarapandian Vaidyanathan

Abstract This paper investigates the active controller design for the output regulation of the Vaidyanathan 4-D hyperjerk hyperchaotic system (2015). Explicitly, nonlinear state feedback control laws have been derived to regulate the output of the 4-D Vaidyanathan hyperjerk hyperchaotic system so as to track the constant reference signals as well as to track periodic reference signals. The active control laws are derived using the Byrnes-Isidori regulator equations (1990). Numerical simulations using MATLAB are shown to illustrate the phase portraits of the Vaidyanathan hyperjerk hyperchaotic system and the output regulation results for the Vaidyanathan hyperjerk hyperchaotic system.

Keywords Chaos · Hyperchaos · Chaotic systems · Hyperchaotic systems · Output regulation · Hyperjerk system

1 Introduction

Output regulation problem aims to control a fixed linear or nonlinear plant in order to have its output tracking reference signals produced by some external generator or the exosystem. Output regulation problem is one of the important problems in control systems which have many applications in industry.

For linear control systems, the output regulation problem has been solved by Francis and Wonham [12]. For nonlinear control systems, the output regulation problem has been solved by Byrnes and Isidori [5] generalizing the internal model principle obtained by Francis and Wonham [12]. Byrnes and Isidori [5] have made an important assumption in their work which demands that the exosystem dynamics generating reference and/or disturbance signals is a neutrally stable system (Lyapunov stable in both forward and backward time). The class of exosystem signals includes the

S. Vaidyanathan (✉)
Research and Development Centre, Vel Tech University, Avadi,
Chennai 600062, Tamil Nadu, India
e-mail: sundarvtu@gmail.com

S. Vaidyanathan and C. Volos (eds.), *Advances and Applications in Nonlinear Control Systems*, Studies in Computational Intelligence 635,
DOI 10.1007/978-3-319-30169-3_10

important particular cases of constant reference signals as well as sinusoidal reference signals. Using Centre Manifold Theory [7], Byrnes and Isidori have derived regulator equations, which completely characterize the solution of the output regulation problem of nonlinear control systems.

The output regulation problem for linear and nonlinear control systems has been the focus of many studies in recent decades [51]. In [22], Mahmoud and Khalil obtained results on the asymptotic regulation of minimum phase nonlinear systems using output feedback. In [13], Fridman solved the output regulation problem for nonlinear control systems with delay using centre manifold theory [7]. In [11], Chen and Huang obtained results on the robust output regulation for output feedback systems with nonlinear exosystems. In [19], Liu and Huang obtained results on the global robust output regulation problem for lower triangular nonlinear systems with unknown control direction. In [98], Yang and Huang obtained new results on the global robust output regulation problem for nonlinear plants subject to nonlinear exosystems.

In [14], Immonen obtained results on the practical output regulation for bounded linear infinite-dimensional state space systems. In [26], Pavlov, Van de Wouw and Nijimeijer obtained results on the global nonlinear output regulation using convergence-based controller design. In [96], Xi and Ding obtained results on the global adaptive output regulation of a class of nonlinear systems with nonlinear exosystems. In [40], Serrani and Isidori obtained results on the global robust output regulation problem for a class of nonlinear systems.

In [42], Sundarapandian obtained results for the output regulation of the Lorenz attractor. In [55], Vaidyanathan obtained results for the output regulation of the unified chaotic system. In [54], Vaidyanathan derived results for the output regulation of the Arneodo-Coullet chaotic system. In [59], Vaidyanathan derived results for the output regulation of the Liu chaotic system.

Chaotic systems are defined as nonlinear dynamical systems which are sensitive to initial conditions, topologically mixing and with dense periodic orbits. Sensitivity to initial conditions of chaotic systems is popularly known as the *butterfly effect*. Small changes in an initial state will make a very large difference in the behavior of the system at future states. Chaotic behaviour was suspected well over hundred years ago in the study of three bodies problem by Henri Poincaré [4], but chaos was experimentally established by E.N. Lorenz [20] only a few decades ago in the study of 3-D weather models.

Some classical paradigms of 3-D chaotic systems in the literature are Rössler system [34], ACT system [1], Sprott systems [41], Chen system [9], Lü system [21], Liu system [18], Cai system [6], Chen-Lee system [10], Tigan system [52], etc.

Many new chaotic systems have been discovered in the recent years such as Zhou system [99], Zhu system [100], Li system [17], Wei-Yang system [95], Sundarapandian systems [43, 48], Vaidyanathan systems [61, 63, 65–68, 71, 74, 77, 89, 93], Pehlivan system [28], etc.

Synchronization of chaotic systems is said to occur when two or more chaotic systems are coupled together or when a chaotic system drives another chaotic system. Because of the butterfly effect which causes exponential divergence of the trajectories

of two identical chaotic systems started with nearly the same initial conditions, the synchronization of chaotic systems is a challenging research problem in the chaos literature [2, 3].

Major works on synchronization of chaotic systems deal with the complete synchronization of a pair of chaotic systems called the *master* and *slave* systems. The design goal of the complete synchronization is to apply the output of the master system to control the slave system so that the output of the slave system tracks the output of the master system asymptotically with time.

Pecora and Carroll pioneered the research on synchronization of chaotic systems with their seminal papers [8, 27]. The active control method [16, 35, 36, 47, 53, 79, 80, 83] is typically used when the system parameters are available for measurement. Adaptive control method [37–39, 44–46, 57, 64, 72, 78, 81, 82, 87, 91] is typically used when some or all the system parameters are not available for measurement and estimates for the uncertain parameters of the systems.

Backstepping control method [29–33, 50, 84, 90] is also used for the synchronization of chaotic systems, which is a recursive method for stabilizing the origin of a control system in strict-feedback form. Another popular method for the synchronization of chaotic systems is the sliding mode control method [49, 56, 58, 60, 69, 75, 76, 85, 86], which is a nonlinear control method that alters the dynamics of a nonlinear system by application of a discontinuous control signal that forces the system to "slide" along a cross-section of the system's normal behavior.

Hyperchaotic systems have been defined as chaotic systems having more than one positive Lyapunov exponent. The minimum dimension of an autonomous hyperchaotic system is four. Hyperchaotic systems exhibit complex dynamics and special characteristics such as high capacity, high security and high efficiency. Some paradigms of hyperchaotic systems are hyperchaotic Rössler system [24], hyperchaotic Lorenz-Haken system [23], hyperchaotic Chua's circuit [15], hyperchaotic Chen system [97], hyperchaotic Lü system [94], hyperchaotic Vaidyanathan systems [62, 70, 73, 88, 92], etc.

In this work, the output regulation problem for the Vaidyanathan hyperjerk hyperchaotic system [92] has been solved using the Byrnes-Isidori regulator equations [5] to derive the state feedback control laws for regulating the output of the Vaidyanathan hyperjerk hyperchaotic system for the important cases of constant reference signals (set-point signals) and periodic reference signals.

This work is organized as follows. In Sect. 2, a review of the solution of the output regulation for nonlinear control systems and Byrnes-Isidori regulator equations has been presented. In Sect. 3, a dynamic analysis of the Vaidyanathan hyperjerk hyperchaotic system is detailed. In Sect. 4, output regulation problem for the Vaidyanathan hyperjerk hyperchaotic system is discussed and new results are derived. In Sect. 5, numerical simulations for the output regulation of the Vaidyanathan hyperjerk hyperchaotic system are detailed. Section 6 contains conclusions of this work.

2 Review of the Output Regulation for Nonlinear Control Systems

In this section, we consider a multi-variable nonlinear control system modelled by equations of the form

$$\dot{x} = f(x) + g(x)u + p(x)\omega \tag{1}$$
$$\dot{\omega} = s(\omega) \tag{2}$$
$$e = h(x) - q(\omega) \tag{3}$$

Here, the differential equation (1) describes the *plant dynamics* with state x defined in a neighbourhood X of the origin of $\mathbf{R}^n$ and the input u takes values in $\mathbf{R}^m$ subject to the effect of a disturbance represented by the vector field $p(x)\omega$.

The differential equation (2) describes an autonomous system, known as the *exosystem*, defined in a neighbourhood W of the origin of $\mathbf{R}^k$, which models the class of disturbance and reference signals taken into consideration.

The Eq. (3) defines the error between the actual plant output $h(x) \in \mathbf{R}^p$ and a reference signal $q(\omega)$, which models the class of disturbance and reference signals taken into consideration.

We also assume that all the constituent mappings of the system (1)–(2) and the error Eq. (3), namely, f, g, p, s, h and q are C^1 mappings vanishing at the origin, *i.e.*

$$f(0) = 0,\ g(0) = 0,\ p(0) = 0,\ h(0) = 0 \text{ and } q(0) = 0.$$

Thus, for $u = 0$, the system (1)–(2) has an equilibrium state $(x, \omega) = (0, 0)$ with zero error (3).

A *state feedback controller* for the composite system (1)–(2) has the form

$$u = \alpha(x, \omega) \tag{4}$$

where α is a C^1 mapping defined on $X \times W$ such that $\alpha(0, 0) = 0$.

Upon substitution of the feedback law (4) in the composite system (1)–(2), we get the closed-loop system given by

$$\begin{aligned} \dot{x} &= f(x) + g(x)\alpha(x, \omega) + p(x)\omega \\ \dot{\omega} &= s(\omega) \end{aligned} \tag{5}$$

State Feedback Regulator Problem [5]:
Find, if possible, a state feedback control law $u = \alpha(x, \omega)$ such that

(OR1) *(Internal Stability)* The equilibrium $x = 0$ of the dynamics

$$\dot{x} = f(x) + g(x)\alpha(x, 0)$$

is locally asymptotically stable.

(OR2) *(Output Regulation)* There exists a neighbourhood $U \subset X \times W$ of $(x, \omega) = (0, 0)$ such that for each initial condition $(x(0), \omega(0)) \in U$, the solution $(x(t), \omega(t))$ of the closed-loop system (5) satisfies

$$\lim_{t \to \infty} [h(x(t)) - q(\omega(t))] = 0.$$

Byrnes and Isidori [5] have solved this problem under the following assumptions.

(H1) The exosystem dynamics $\dot{\omega} = s(\omega)$ is neutrally stable at $\omega = 0$, i.e. the system is Lyapunov stable in both forward and backward time at $\omega = 0$.

(H2) The pair $(f(x), g(x))$ has a stabilizable linear approximation at $x = 0$, i.e. if

$$A = \left[\frac{\partial f}{\partial x}\right]_{x=0} \quad \text{and} \quad B = \left[\frac{\partial g}{\partial x}\right]_{x=0},$$

then (A, B) is stabilizable, which means that we can find a gain matrix K so that $A + BK$ is Hurwitz. ■

Next, we recall the solution of the output regulation problem derived by Byrnes and Isidori [5].

Theorem 1 *[5] Under the hypotheses (H1) and (H2), the state feedback regulator problem is solvable if, and only if, there exist C^1 mappings $x = \pi(\omega)$ with $\pi(0) = 0$ and $u = \phi(\omega)$ with $\phi(0) = 0$, both defined in a neighbourhood of $W^0 \subset W$ of $\omega = 0$ such that the following equations (called the* Byrnes-Isidori regulator equations*) are satisfied:*

(1) $\frac{\partial \pi}{\partial \omega} s(\omega) = f(\pi(\omega)) + g(\pi(\omega))\phi(\omega) + p(\pi(\omega))\omega$

(2) $h(\pi(\omega)) - q(\omega) = 0$

When the Byrnes-Isidori regulator equations (1) and (2) are satisfied, a control law solving the state feedback regulator problem is given by

$$u = \phi(\omega) + K[x - \pi(\omega)] \tag{6}$$

where K is any gain matrix such that $A + BK$ is Hurwitz. ■

3 Dynamic Analysis of the Vaidyanathan Hyperjerk Hyperchaotic System

The Vaidyanathan hyperjerk hyperchaotic system [92] is described by the 4-D dynamics

$$\begin{aligned}\dot{x}_1 &= x_2\\ \dot{x}_2 &= x_3\\ \dot{x}_3 &= x_4\\ \dot{x}_4 &= -x_1 - x_2 - bx_1^2 - ax_3 - cx_1^4 x_4\end{aligned} \tag{7}$$

In (7), a, b and c are constant, positive parameters.

The system (7) exhibits a *hyperchaotic* attractor when the parameter values are taken as

$$a = 3.7, \quad b = 0.2, \quad c = 1.5 \tag{8}$$

For numerical simulations, we take the initial conditions of the Vaidyanathan hyperjerk system (7) as

$$x_1(0) = 0.1, \quad x_2(0) = 0.1, \quad x_3(0) = 0.1, \quad x_4(0) = 0.1 \tag{9}$$

Also, the Lyapunov exponents of the Vaidyanathan hyperjerk system (7) for the parameter values (8) and the the initial values (9) are numerically found as

$$L_1 = 0.1448, \quad L_2 = 0.0328, \quad L_3 = 0, \quad L_4 = -1.1294 \tag{10}$$

Since $L_1 + L_2 + L3 + L_4 = -0.9518 < 0$, the Vaidyanathan hyperjerk hyperchaotic system (7) is dissipative. Thus the asymptotic motion of the Vaidyanathan hyperjerk hyperchaotic system (7) settles onto a strange attractor of the system.

Figures 1, 2, 3 and 4 shows the 3-D projections of the 4-D hyperchaotic hyperjerk system (7) on the (x_1, x_2, x_3), (x_1, x_2, x_4), (x_1, x_3, x_4) and (x_2, x_3, x_4) spaces, respectively.

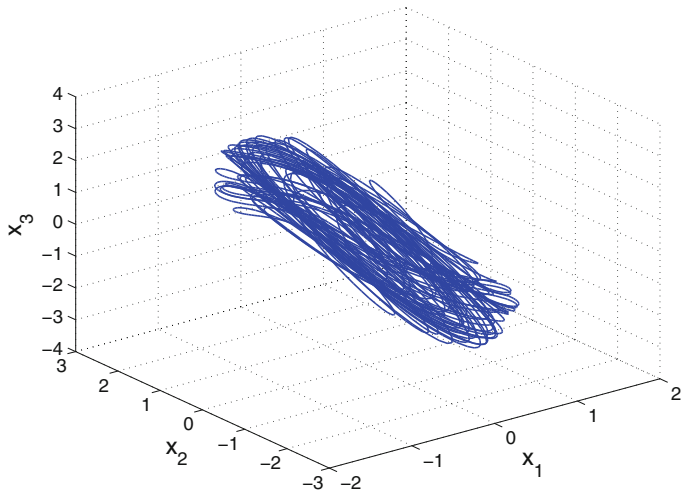

Fig. 1 3-D projection of the Vaidyanathan hyperjerk system on the (x_1, x_2, x_3) space

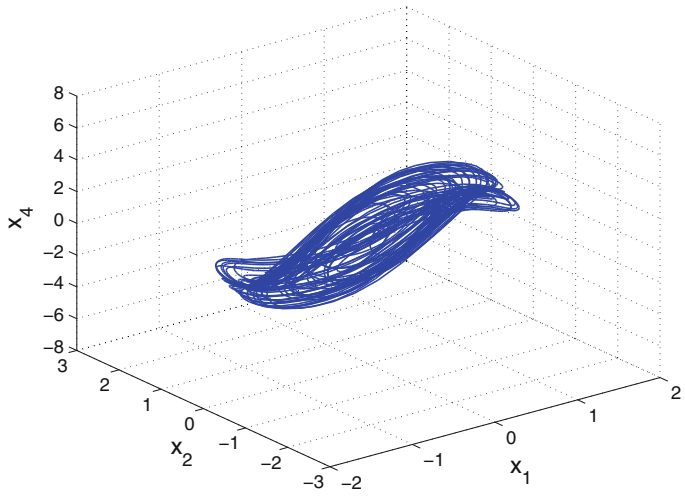

Fig. 2 3-D projection of the Vaidyanathan hyperjerk system on the (x_1, x_2, x_4) space

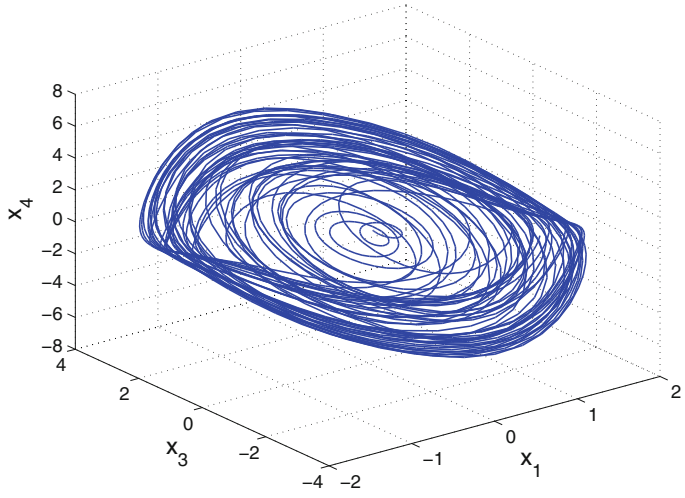

Fig. 3 3-D projection of the Vaidyanathan hyperjerk system on the (x_1, x_3, x_4) space

Also, the Kaplan-Yorke dimension of the Vaidyanathan hyperjerk hyperchaotic system (7) is calculated as

$$D_{KY} = 3 + \frac{L_1 + L_2 + L_3}{|L_4|} = 3.1573, \tag{11}$$

which is fractional.

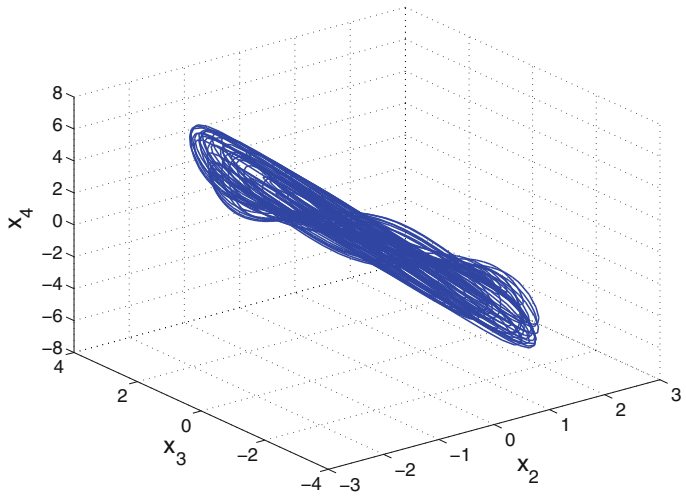

Fig. 4 3-D projection of the Vaidyanathan hyperjerk system on the (x_2, x_3, x_4) space

4 Output Regulation of Vaidyanathan Hyperjerk Hyperchaotic System

The Vaidyanathan hyperjerk hyperchaotic system [92] is a novel hyperchaotic system described by the dynamics

$$\begin{aligned} \dot{x}_1 &= x_2 \\ \dot{x}_2 &= x_3 \\ \dot{x}_3 &= x_4 \\ \dot{x}_4 &= -x_1 - x_2 - bx_1^2 - ax_3 - cx_1^4 x_4 + u \end{aligned} \tag{12}$$

where a, b, c are positive constants and u is an active feedback control.

The hyperjerk system (12) is hyperchaotic when the parameters are taken as

$$a = 3.7, \quad b = 0.2, \quad c = 1.5 \tag{13}$$

In this work, we consider two important cases of output regulation for the Vaidyanathan hyperjerk hyperchaotic system (12):

(I) Tracking of Constant Reference Signals
(II) Tracking of Periodic Reference Signals

4.1 Tracking of Constant Reference Signals

In this case, the exosystem is given by the scalar dynamics

$$\dot{\omega} = 0 \tag{14}$$

It is important to observe that the exosystem (14) is neutrally stable because the solutions of (14) are only constant trajectories, *i.e.*

$$\omega(t) \equiv \omega(0) = \omega_0 \quad \text{for all} \quad t$$

Thus, the assumption (H1) of Theorem 1 (Sect. 2) holds trivially.

Linearizing the dynamics of the Vaidyanathan hyperjerk hyperchaotic system (12) at the origin, we obtain the system matrices

$$A = \begin{bmatrix} 0 & 1 & 0 & 0 \\ 0 & 0 & 1 & 0 \\ 0 & 0 & 0 & 1 \\ -1 & -1 & -a & 0 \end{bmatrix}, \quad B = \begin{bmatrix} 0 \\ 0 \\ 0 \\ 1 \end{bmatrix} \tag{15}$$

The controllability matrix is given by

$$Q = \begin{bmatrix} B & AB & A^2B & A^3B \end{bmatrix} = \begin{bmatrix} 0 & 0 & 0 & 1 \\ 0 & 0 & 1 & 0 \\ 0 & 1 & 0 & -a \\ 1 & 0 & -a & -1 \end{bmatrix} \tag{16}$$

which has full rank.

Thus, by Kalman's rank test for controllability [25], it follows that the pair (A, B) is completely controllable.

Thus, we can easily find a controller gain matrix K such that $A + BK$ is Hurwitz with arbitrarily assigned stable eigenvalues.

Thus, the assumption (H2) of Theorem 1 (Sect. 2) also holds.

Hence, Theorem 1 can be applied to solve the output regulation problem for the Vaidyanathan hyperjerk hyperchaotic system (12) for the tracking of constant reference signals (*set-point signals*).

4.1.1 Constant Tracking Problem for x_1

Here, the tracking problem for the Vaidyanathan hyperjerk system (12) is given by

$$\begin{aligned}\dot{x}_1 &= x_2\\ \dot{x}_2 &= x_3\\ \dot{x}_3 &= x_4\\ \dot{x}_4 &= -x_1 - x_2 - bx_1^2 - ax_3 - cx_1^4 x_4 + u\\ e &= x_1 - \omega\end{aligned} \tag{17}$$

By Theorem 1, the regulator equations of (17) are obtained as

$$\begin{cases} \pi_2(\omega) = 0\\ \pi_3(\omega) = 0\\ \pi_4(\omega) = 0\\ -\pi_1(\omega) - \pi_2(\omega) - b\pi_1^2(\omega) - a\pi_3(\omega) - c\pi_1^4(\omega)\pi_4(\omega) + \phi(\omega) = 0\\ \pi_1(\omega) - \omega = 0 \end{cases} \tag{18}$$

Solving the regulator equations (18), we get the unique solution

$$\pi(\omega) = \begin{bmatrix} \pi_1(\omega)\\ \pi_2(\omega)\\ \pi_3(\omega)\\ \pi_4(\omega) \end{bmatrix} = \begin{bmatrix} \omega\\ 0\\ 0\\ 0 \end{bmatrix} \tag{19}$$

and

$$\phi(\omega) = \omega + b\omega^2 \tag{20}$$

By Theorem 1, a state feedback control law solving the output regulation problem is given by

$$u = \phi(\omega) + K[x - \pi(\omega)] \tag{21}$$

where K is chosen so that $A + BK$ is Hurwitz, $\pi(\omega)$ is given by (19) and $\phi(\omega)$ is given by (20)

4.1.2 Constant Tracking Problem for x_2

Here, the tracking problem for the Vaidyanathan hyperjerk system (12) is given by

$$\begin{aligned}\dot{x}_1 &= x_2\\ \dot{x}_2 &= x_3\\ \dot{x}_3 &= x_4\\ \dot{x}_4 &= -x_1 - x_2 - bx_1^2 - ax_3 - cx_1^4 x_4 + u\\ e &= x_2 - \omega\end{aligned} \tag{22}$$

By Theorem 1, the regulator equations of (22) are obtained as

$$\begin{cases} \pi_2(\omega) = 0 \\ \pi_3(\omega) = 0 \\ \pi_4(\omega) = 0 \\ -\pi_1(\omega) - \pi_2(\omega) - b\pi_1^2(\omega) - a\pi_3(\omega) - c\pi_1^4(\omega)\pi_4(\omega) + \phi(\omega) = 0 \\ \pi_2(\omega) - \omega = 0 \end{cases} \tag{23}$$

The first and last equations in (23) contradict each other.

Thus, the regulator equations (23) are not solvable.

Hence, by Theorem 1, we conclude that the output regulation problem is not solvable for this case.

4.1.3 Constant Tracking Problem for x_3

Here, the tracking problem for the Vaidyanathan hyperjerk system (12) is given by

$$\begin{aligned} \dot{x}_1 &= x_2 \\ \dot{x}_2 &= x_3 \\ \dot{x}_3 &= x_4 \\ \dot{x}_4 &= -x_1 - x_2 - bx_1^2 - ax_3 - cx_1^4 x_4 + u \\ e &= x_3 - \omega \end{aligned} \tag{24}$$

By Theorem 1, the regulator equations of (24) are obtained as

$$\begin{cases} \pi_2(\omega) = 0 \\ \pi_3(\omega) = 0 \\ \pi_4(\omega) = 0 \\ -\pi_1(\omega) - \pi_2(\omega) - b\pi_1^2(\omega) - a\pi_3(\omega) - c\pi_1^4(\omega)\pi_4(\omega) + \phi(\omega) = 0 \\ \pi_3(\omega) - \omega = 0 \end{cases} \tag{25}$$

The second and last equations in (25) contradict each other.

Thus, the regulator equations (25) are not solvable.

Hence, by Theorem 1, we conclude that the output regulation problem is not solvable for this case.

4.1.4 Constant Tracking Problem for x_4

Here, the tracking problem for the Vaidyanathan hyperjerk system (12) is given by

$$\begin{aligned}\dot{x}_1 &= x_2\\ \dot{x}_2 &= x_3\\ \dot{x}_3 &= x_4\\ \dot{x}_4 &= -x_1 - x_2 - bx_1^2 - ax_3 - cx_1^4 x_4 + u\\ e &= x_4 - \omega\end{aligned} \tag{26}$$

By Theorem 1, the regulator equations of (26) are obtained as

$$\begin{cases} \pi_2(\omega) = 0\\ \pi_3(\omega) = 0\\ \pi_4(\omega) = 0\\ -\pi_1(\omega) - \pi_2(\omega) - b\pi_1^2(\omega) - a\pi_3(\omega) - c\pi_1^4(\omega)\pi_4(\omega) + \phi(\omega) = 0\\ \pi_4(\omega) - \omega = 0 \end{cases} \tag{27}$$

The third and last equations in (27) contradict each other.

Thus, the regulator equations (27) are not solvable.

Hence, by Theorem 1, we conclude that the output regulation problem is not solvable for this case.

4.2 Tracking of Periodic Reference Signals

In this case, the exosystem is given by the planar dynamics

$$\begin{aligned}\dot{\omega}_1 &= \nu\,\omega_2\\ \dot{\omega}_2 &= -\nu\,\omega_1\end{aligned} \tag{28}$$

where $\nu > 0$ is any fixed constant.

Clearly, the assumption (H1) (Theorem 1) holds. Also, as established in Sect. 4.1, the assumption (H2) of Theorem 1 also holds since (A, B) is completely observable and we can easily find a controller gain matrix K so that $A + BK$ is Hurwitz.

Hence, Theorem 1 can be applied to solve the output regulation problem for the Vaidyanathan hyperjerk system (12) for the tracking of periodic reference signals.

4.2.1 Periodic Tracking Problem for x_1

Here, the tracking problem for the Vaidyanathan jerk chaotic system (12) is given by

$$\begin{aligned}
\dot{x}_1 &= x_2 \\
\dot{x}_2 &= x_3 \\
\dot{x}_3 &= x_4 \\
\dot{x}_4 &= -x_1 - x_2 - bx_1^2 - ax_3 - cx_1^4 x_4 + u \\
\dot{\omega}_1 &= \nu\,\omega_2 \\
\dot{\omega}_2 &= -\nu\,\omega_1 \\
e &= x_1 - \omega_1
\end{aligned} \tag{29}$$

By Theorem 1, the regulator equations of (29) are obtained as

$$\begin{cases}
\frac{\partial \pi_1}{\partial \omega_1}(\nu\omega_2) + \frac{\partial \pi_1}{\partial \omega_2}(-\nu\omega_1) = \pi_2(\omega) \\
\frac{\partial \pi_2}{\partial \omega_1}(\nu\omega_2) + \frac{\partial \pi_2}{\partial \omega_2}(-\nu\omega_1) = \pi_3(\omega) \\
\frac{\partial \pi_3}{\partial \omega_1}(\nu\omega_2) + \frac{\partial \pi_3}{\partial \omega_2}(-\nu\omega_1) = \pi_4(\omega) \\
\frac{\partial \pi_4}{\partial \omega_1}(\nu\omega_2) + \frac{\partial \pi_4}{\partial \omega_2}(-\nu\omega_1) = -\pi_1(\omega) - \pi_2(\omega) - b\pi_1^2(\omega) - a\pi_3(\omega) \\
\qquad\qquad\qquad\qquad -c\pi_1^4(\omega)\pi_4(\omega) + \phi(\omega) \\
\qquad\qquad \pi_1(\omega) - \omega_1 = 0
\end{cases} \tag{30}$$

Solving the regulator equations (30), we get the unique solution

$$\pi(\omega) = \begin{bmatrix} \pi_1(\omega) \\ \pi_2(\omega) \\ \pi_3(\omega) \\ \pi_4(\omega) \end{bmatrix} = \begin{bmatrix} \omega_1 \\ \nu\omega_2 \\ -\nu^2\omega_1 \\ -\nu^3\omega_2 \end{bmatrix} \tag{31}$$

and

$$\phi(\omega) = \left(1 - a\nu^2 + \nu^4\right)\omega_1 + b\omega_1^2 + \nu\left(1 - c\omega_1^4\nu^2\right)\omega_2 \tag{32}$$

By Theorem 1, a state feedback control law solving the output regulation problem is given by

$$u = \phi(\omega) + K[x - \pi(\omega)] \tag{33}$$

where K is chosen so that $A + BK$ is Hurwitz, $\pi(\omega)$ is given by (31), $\phi(\omega)$ is given by (32).

4.2.2 Periodic Tracking Problem for x_2

Here, the tracking problem for the Vaidyanathan jerk chaotic system (12) is given by

$$\begin{aligned}
\dot{x}_1 &= x_2 \\
\dot{x}_2 &= x_3 \\
\dot{x}_3 &= x_4 \\
\dot{x}_4 &= -x_1 - x_2 - bx_1^2 - ax_3 - cx_1^4 x_4 + u \\
\dot{\omega}_1 &= \nu\,\omega_2 \\
\dot{\omega}_2 &= -\nu\,\omega_1 \\
e &= x_2 - \omega_1
\end{aligned} \tag{34}$$

By Theorem 1, the regulator equations of (34) are obtained as

$$\begin{cases}
\frac{\partial \pi_1}{\partial \omega_1}(\nu\omega_2) + \frac{\partial \pi_1}{\partial \omega_2}(-\nu\omega_1) = \pi_2(\omega) \\
\frac{\partial \pi_2}{\partial \omega_1}(\nu\omega_2) + \frac{\partial \pi_2}{\partial \omega_2}(-\nu\omega_1) = \pi_3(\omega) \\
\frac{\partial \pi_3}{\partial \omega_1}(\nu\omega_2) + \frac{\partial \pi_3}{\partial \omega_2}(-\nu\omega_1) = \pi_4(\omega) \\
\frac{\partial \pi_4}{\partial \omega_1}(\nu\omega_2) + \frac{\partial \pi_4}{\partial \omega_2}(-\nu\omega_1) = -\pi_1(\omega) - \pi_2(\omega) - b\pi_1^2(\omega) - a\pi_3(\omega) \\
\qquad\qquad\qquad\qquad -c\pi_1^4(\omega)\pi_4(\omega) + \phi(\omega) \\
\qquad\qquad \pi_2(\omega) - \omega_1 = 0
\end{cases} \tag{35}$$

Solving the regulator equations (35), we get the unique solution

$$\pi(\omega) = \begin{bmatrix} \pi_1(\omega) \\ \pi_2(\omega) \\ \pi_3(\omega) \\ \pi_4(\omega) \end{bmatrix} = \begin{bmatrix} -\nu^{-1}\omega_2 \\ \omega_1 \\ \nu\omega_2 \\ -\nu^2\omega_1 \end{bmatrix} \tag{36}$$

and

$$\phi(\omega) = \left(1 - c\nu^{-2}\omega_2^4\right)\omega_1 + \left(a\nu - \nu^3 - \nu^{-1}\right)\omega_2 + b\nu^{-2}\omega_2^2 \tag{37}$$

By Theorem 1, a state feedback control law solving the output regulation problem is given by

$$u = \phi(\omega) + K[x - \pi(\omega)] \tag{38}$$

where K is chosen so that $A + BK$ is Hurwitz, $\pi(\omega)$ is given by (36), $\phi(\omega)$ is given by (37).

4.2.3 Periodic Tracking Problem for x_3

Here, the tracking problem for the Vaidyanathan jerk chaotic system (12) is given by

$$\begin{aligned}
\dot{x}_1 &= x_2 \\
\dot{x}_2 &= x_3 \\
\dot{x}_3 &= x_4 \\
\dot{x}_4 &= -x_1 - x_2 - bx_1^2 - ax_3 - cx_1^4 x_4 + u \\
\dot{\omega}_1 &= \nu\,\omega_2 \\
\dot{\omega}_2 &= -\nu\,\omega_1 \\
e &= x_3 - \omega_1
\end{aligned} \tag{39}$$

By Theorem 1, the regulator equations of (39) are obtained as

$$\begin{cases}
\frac{\partial \pi_1}{\partial \omega_1}(\nu\omega_2) + \frac{\partial \pi_1}{\partial \omega_2}(-\nu\omega_1) = \pi_2(\omega) \\
\frac{\partial \pi_2}{\partial \omega_1}(\nu\omega_2) + \frac{\partial \pi_2}{\partial \omega_2}(-\nu\omega_1) = \pi_3(\omega) \\
\frac{\partial \pi_3}{\partial \omega_1}(\nu\omega_2) + \frac{\partial \pi_3}{\partial \omega_2}(-\nu\omega_1) = \pi_4(\omega) \\
\frac{\partial \pi_4}{\partial \omega_1}(\nu\omega_2) + \frac{\partial \pi_4}{\partial \omega_2}(-\nu\omega_1) = -\pi_1(\omega) - \pi_2(\omega) - b\pi_1^2(\omega) - a\pi_3(\omega) \\
\qquad\qquad\qquad\qquad -c\pi_1^4(\omega)\pi_4(\omega) + \phi(\omega) \\
\qquad\qquad \pi_3(\omega) - \omega_1 = 0
\end{cases} \tag{40}$$

Solving the regulator equations (40), we get the unique solution

$$\pi(\omega) = \begin{bmatrix} \pi_1(\omega) \\ \pi_2(\omega) \\ \pi_3(\omega) \\ \pi_4(\omega) \end{bmatrix} = \begin{bmatrix} -\nu^{-2}\omega_1 \\ -\nu^{-1}\omega_2 \\ \omega_1 \\ \nu\omega_2 \end{bmatrix} \tag{41}$$

and

$$\phi(\omega) = \left(a - \nu^2 - \nu^{-2}\right)\omega_1 - \nu^{-1}\omega_2 + b\nu^{-4}\omega_1^2 + c\nu^{-7}\omega_1^4\omega_2 \tag{42}$$

By Theorem 1, a state feedback control law solving the output regulation problem is given by

$$u = \phi(\omega) + K[x - \pi(\omega)] \tag{43}$$

where K is chosen so that $A + BK$ is Hurwitz, $\pi(\omega)$ is given by (41), $\phi(\omega)$ is given by (42).

4.2.4 Periodic Tracking Problem for x_4

Here, the tracking problem for the Vaidyanathan jerk chaotic system (12) is given by

$$\begin{aligned}
\dot{x}_1 &= x_2 \\
\dot{x}_2 &= x_3 \\
\dot{x}_3 &= x_4 \\
\dot{x}_4 &= -x_1 - x_2 - bx_1^2 - ax_3 - cx_1^4 x_4 + u \\
\dot{\omega}_1 &= \nu\, \omega_2 \\
\dot{\omega}_2 &= -\nu\, \omega_1 \\
e &= x_4 - \omega_1
\end{aligned} \tag{44}$$

By Theorem 1, the regulator equations of (44) are obtained as

$$\begin{cases}
\frac{\partial \pi_1}{\partial \omega_1}(\nu\omega_2) + \frac{\partial \pi_1}{\partial \omega_2}(-\nu\omega_1) = \pi_2(\omega) \\
\frac{\partial \pi_2}{\partial \omega_1}(\nu\omega_2) + \frac{\partial \pi_2}{\partial \omega_2}(-\nu\omega_1) = \pi_3(\omega) \\
\frac{\partial \pi_3}{\partial \omega_1}(\nu\omega_2) + \frac{\partial \pi_3}{\partial \omega_2}(-\nu\omega_1) = \pi_4(\omega) \\
\frac{\partial \pi_4}{\partial \omega_1}(\nu\omega_2) + \frac{\partial \pi_4}{\partial \omega_2}(-\nu\omega_1) = -\pi_1(\omega) - \pi_2(\omega) - b\pi_1^2(\omega) - a\pi_3(\omega) \\
\qquad\qquad\qquad\qquad -c\pi_1^4(\omega)\pi_4(\omega) + \phi(\omega) \\
\qquad\qquad \pi_4(\omega) - \omega_1 = 0
\end{cases} \tag{45}$$

Solving the regulator equations (45), we get the unique solution

$$\pi(\omega) = \begin{bmatrix} \pi_1(\omega) \\ \pi_2(\omega) \\ \pi_3(\omega) \\ \pi_4(\omega) \end{bmatrix} = \begin{bmatrix} \nu^{-3}\omega_2 \\ -\nu^{-2}\omega_1 \\ -\nu^{-1}\omega_2 \\ \omega_1 \end{bmatrix} \tag{46}$$

and

$$\phi(\omega) = \left(c\nu^{-12}\omega_2^4 - \nu^{-2}\right)\omega_1 + \left(\nu - a\nu^{-1} + \nu^{-3}\right)\omega_2 + b\nu^{-6}\omega_2^2 \tag{47}$$

By Theorem 1, a state feedback control law solving the output regulation problem is given by

$$u = \phi(\omega) + K[x - \pi(\omega)] \tag{48}$$

where K is chosen so that $A + BK$ is Hurwitz, $\pi(\omega)$ is given by (46), $\phi(\omega)$ is given by (47).

5 Numerical Simulations

For numerical simulations, we take the parameter values a, b and c so that the Vaidyanathan hyperjerk system (12) is in the chaotic case, *i.e.*

$$a = 3.7, \quad b = 0.2, \quad c = 1.5 \tag{49}$$

With the choice

$$K = \begin{bmatrix} k_1 & k_2 & k_3 & k_4 \end{bmatrix} = \begin{bmatrix} -255 & -255 & -99.7 & -16 \end{bmatrix},$$

the matrix $A + BK$ is Hurwitz with $\text{eig}(A + BK) = \{-4, -4, -4, -4\}$.

In the periodic tracking output regulation problem, the value $\nu = 1$ is taken in the exosystem dynamics given by (28).

5.1 Tracking of Constant Reference Signals

5.1.1 Constant Tracking Problem for x_1

Here, the initial conditions are taken as

$$x_1(0) = 0.1, \quad x_2(0) = 1.4, \quad x_3(0) = 2.7, \quad x_4(0) = 3.5, \quad \omega(0) = 2$$

The simulation graph is depicted in Fig. 5 from which it is clear that the state trajectory $x_1(t)$ tracks the constant reference signal $\omega(t) \equiv 2$ in 3 s.

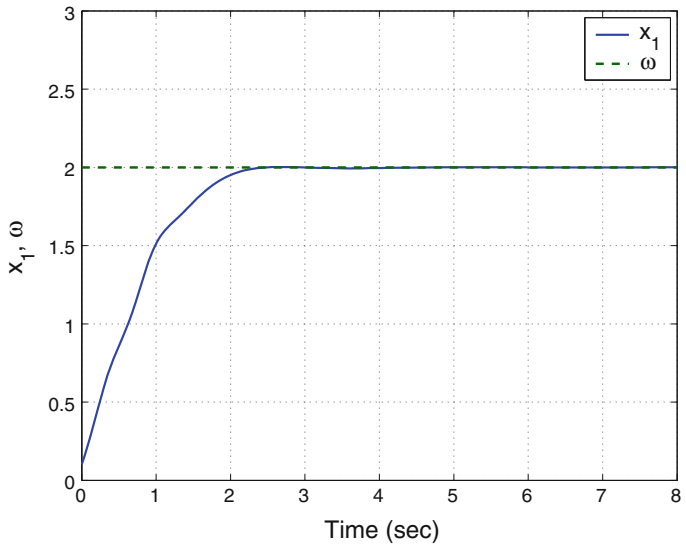

Fig. 5 Constant tracking of the state x_1

5.1.2 Constant Tracking Problem for x_2

As detailed in Sect. 4.1.2, the output regulation problem is not solvable for this case because the Byrnes-Isidori regulator equations do not admit any solution.

5.1.3 Constant Tracking Problem for x_3

As pointed out in Sect. 4.1.3, the output regulation problem is not solvable for this case because the Byrnes-Isidori regulator equations do not admit any solution.

5.1.4 Constant Tracking Problem for x_4

As pointed out in Sect. 4.1.4, the output regulation problem is not solvable for this case because the Byrnes-Isidori regulator equations do not admit any solution.

5.2 Tracking of Periodic Reference Signals

5.2.1 Periodic Tracking Problem for x_1

Here, the initial conditions are taken as

$$x_1(0) = 2.1, \;\; x_2(0) = 1.7, \;\; x_3(0) = -0.5, \;\; x_4(0) = 1.2, \;\; \omega_1(0) = 0, \omega_2(0) = 1$$

Also, it is assumed that $\nu = 1$. The simulation graph is depicted in Fig. 6 from which it is clear that the state trajectory $x_1(t)$ tracks the periodic reference signal $\omega_1(t) = \sin t$ in 5 s.

5.2.2 Periodic Tracking Problem for x_2

Here, the initial conditions are taken as

$$x_1(0) = 3.2, \;\; x_2(0) = 0.5, \;\; x_3(0) = 1.2, \;\; x_4(0) = 2.4, \;\; \omega_1(0) = 0, \omega_2(0) = 1$$

Also, it is assumed that $\nu = 1$. The simulation graph is depicted in Fig. 7 from which it is clear that the state trajectory $x_2(t)$ tracks the periodic reference signal $\omega_1(t) = \sin t$ in 5 s.

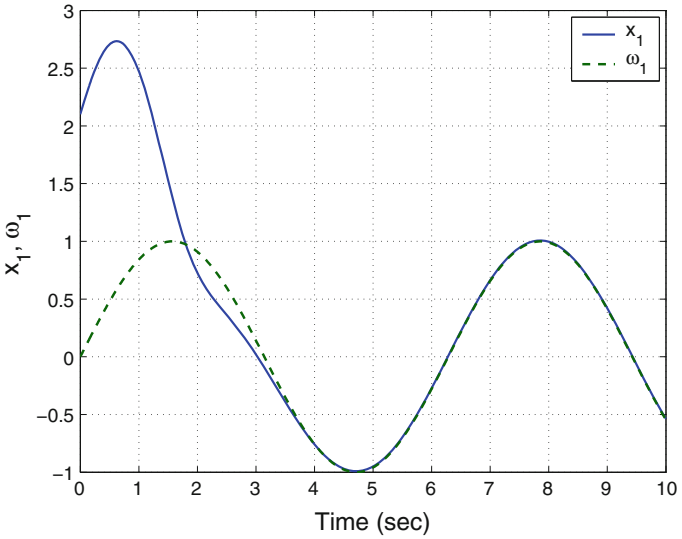

Fig. 6 Periodic tracking of the state x_1

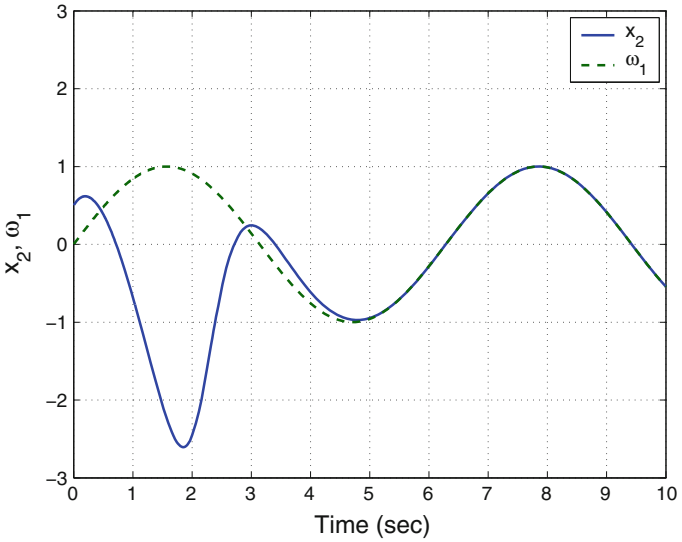

Fig. 7 Periodic tracking of the state x_2

5.2.3 Periodic Tracking Problem for x_3

Here, the initial conditions are taken as

$$x_1(0) = 1.9,\ \ x_2(0) = 2.5,\ \ x_3(0) = 0.6,\ \ x_4(0) = -0.4,\ \ \omega_1(0) = 0, \omega_2(0) = 1$$

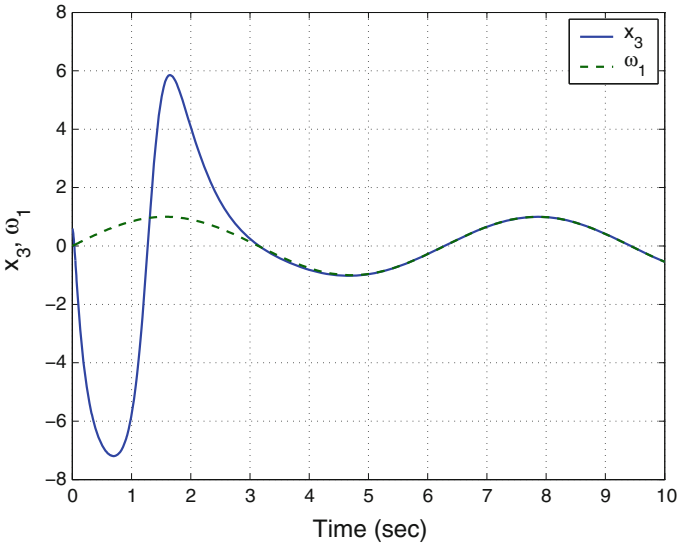

Fig. 8 Periodic tracking of the state x_3

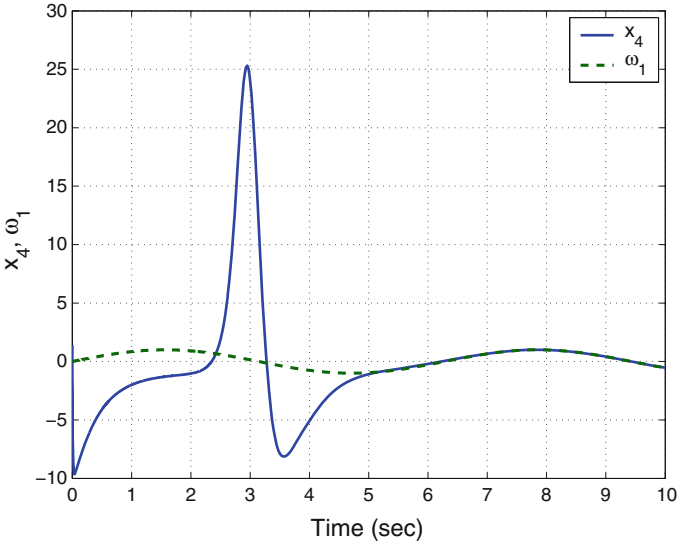

Fig. 9 Periodic tracking of the state x_4

Also, it is assumed that $\nu = 1$. The simulation graph is depicted in Fig. 8 from which it is clear that the state trajectory $x_3(t)$ tracks the periodic reference signal $\omega_1(t) = \sin t$ in 5 s.

5.2.4 Periodic Tracking Problem for x_4

Here, the initial conditions are taken as

$$x_1(0) = 2.9,\ \ x_2(0) = 1.5,\ \ x_3(0) = 2.6,\ \ x_4(0) = 1.4,\ \ \omega_1(0) = 0, \omega_2(0) = 1$$

Also, it is assumed that $\nu = 1$. The simulation graph is depicted in Fig. 9 from which it is clear that the state trajectory $x_4(t)$ tracks the periodic reference signal $\omega_1(t) = \sin t$ in 5 s.

6 Conclusions

Output regulation problem is one of the important problems in the control theory, which aims to control a fixed linear or nonlinear plant in order to have its output tracking reference signals produced by some external generator or the exosystem. Byrnes and Isidori [5] solved the output regulation problem for a general class of nonlinear systems under some stability assumptions. In this work, the output regulation problem for the 4-D Vaidyanathan hyperjerk chaotic system (2015) has been studied in detail and a complete solution for the output regulation problem for the 4-D Vaidyanathan hyperjerk hyperchaotic system has been presented as well. Explicitly, using the Byrnes-Isidori regulator equations (1990), state feedback control laws for regulating the output of the 4-D Vaidyanathan hyperjerk hyperchaotic system have been derived. As tracking reference signals, constant and periodic reference signals have been considered and in each case, feedback control laws regulating the output of the Vaidyanathan hyperchaotic system have been derived when the problem is solvable. Numerical simulations using MATLAB are shown to illustrate all the main results presented in this work.

References

1. Arneodo A, Coullet P, Tresser C (1981) Possible new strange attractors with spiral structure. Commun Math Phys 79(4):573–576
2. Azar AT, Vaidyanathan S (2015a) Chaos modeling and control systems design, studies in computational intelligence, vol 581. Springer, Germany
3. Azar AT, Vaidyanathan S (2015b) Computational intelligence applications in modeling and control, studies in computational intelligence, vol 575. Springer, Germany
4. Barrow-Green J (1997) Poincaré and the three body problem. American Mathematical Society, Providence, RI, USA
5. Byrnes CI, Isidori A (1990) Output regulation of nonlinear systems. IEEE Trans Autom Control 35(2):131–140
6. Cai G, Tan Z (2007) Chaos synchronization of a new chaotic system via nonlinear control. J Uncertain Syst 1(3):235–240
7. Carr J (1981) Applications of centre manifold theory. Springer, New York

8. Carroll TL, Pecora LM (1991) Synchronizing chaotic circuits. IEEE Trans Circuits Syst 38(4):453–456
9. Chen G, Ueta T (1999) Yet another chaotic attractor. Int J Bifurc Chaos 9(7):1465–1466
10. Chen HK, Lee CI (2004) Anti-control of chaos in rigid body motion. Chaos, Solitons Fractals 21(4):957–965
11. Chen Z, Huang J (2005) Robust output regulation with nonlinear exosystems. Automatica 41(8):1447–1454
12. Francis BA, Wonham WM (1975) The internal model principle for linear multivariable regulators. Appl Math Optim 2(2):170–194
13. Fridman E (2003) Output regulation of nonlinear control systems with delay. Syst Control Lett 50:81–93
14. Immonen E (2007) Practical output regulation for bounded linear infinite-dimensional state space systems. Automatica 43(5):786–794
15. Kapitaniak T, Chua LO (1994) Hyperchaotic attractors of unidirectionally coupled Chua's circuits. Int J Bifurc Chaos 4(2):477–482
16. Karthikeyan R, Sundarapandian V (2014) Hybrid chaos synchronization of four-scroll systems via active control. J Elect Eng 65(2):97–103
17. Li D (2008) A three-scroll chaotic attractor. Phys Lett A 372(4):387–393
18. Liu C, Liu T, Liu L, Liu K (2004) A new chaotic attractor. Chaos, Solitions Fractals 22(5): 1031–1038
19. Liu L, Huang J (2008) Global robust output regulation of lower triangular systems with unknown control direction. Automatica 44(5):1278–1284
20. Lorenz EN (1963) Deterministic periodic flow. J Atm Sci 20(2):130–141
21. Lü J, Chen G (2002) A new chaotic attractor coined. Int J Bifurc Chaos 12(3):659–661
22. Mahmoud NA, Khalil HK (1996) Asymptotic regulation of minimum phase nonlnear systems using output feedback. IEEE Trans Autom Control 41(10):1402–1412
23. Ning CZ, Haken H (1990) Detuned lasers and the complex Lorenz equations: Subcritical and supercritical Hopf bifurcations. Phys Rev A 41(7):3826–3837
24. Rössler OE (1979) An equation for hyperchaos. Phys Lett A 71(2–3):155–157
25. Ogata K (2009) Modern control engineering, 5th edn. Prentice Hall, New Jersey
26. Pavlov A, de Wouw NV, Nijimeijer H (2007) Global nonlinear output regulation: convergence based controller design. Automatica 43(3):456–463
27. Pecora LM, Carroll TL (1990) Synchronization in chaotic systems. Phys Rev Lett 64(8): 821–824
28. Pehlivan I, Moroz IM, Vaidyanathan S (2014) Analysis, synchronization and circuit design of a novel butterfly attractor. J Sound Vib 333(20):5077–5096
29. Rasappan S, Vaidyanathan S (2012a) Global chaos synchronization of WINDMI and Coullet chaotic systems by backstepping control. Far East J Math Sci 67(2):265–287
30. Rasappan S, Vaidyanathan S (2012b) Hybrid synchronization of n-scroll Chua and Lur'e chaotic systems via backstepping control with novel feedback. Archiv Control Sci 22(3):343–365
31. Rasappan S, Vaidyanathan S (2012c) Synchronization of hyperchaotic Liu system via backstepping control with recursive feedback. Commun Comput Inf Sci 305:212–221
32. Rasappan S, Vaidyanathan S (2013) Hybrid synchronization of *n*-scroll chaotic Chua circuits using adaptive backstepping control design with recursive feedback. Malays J Math Sci 7(2):219–246
33. Rasappan S, Vaidyanathan S (2014) Global chaos synchronization of WINDMI and Coullet chaotic systems using adaptive backstepping control design. Kyungpook Math J 54(1):293–320
34. Rössler OE (1976) An equation for continuous chaos. Phys Lett A 57(5):397–398
35. Sarasu P, Sundarapandian V (2011a) Active controller design for the generalized projective synchronization of four-scroll chaotic systems. Int J Syst Signal Control Eng Appl 4(2):26–33
36. Sarasu P, Sundarapandian V (2011b) The generalized projective synchronization of hyperchaotic Lorenz and hyperchaotic Qi systems via active control. Int J Soft Comput 6(5):216–223
37. Sarasu P, Sundarapandian V (2012a) Adaptive controller design for the generalized projective synchronization of 4-scroll systems. Int J Syst Signal Control Eng Appl 5(2):21–30

38. Sarasu P, Sundarapandian V (2012b) Generalized projective synchronization of three-scroll chaotic systems via adaptive control. Eur J Sci Res 72(4):504–522
39. Sarasu P, Sundarapandian V (2012c) Generalized projective synchronization of two-scroll systems via adaptive control. Int J Soft Comput 7(4):146–156
40. Serrani A, Isdori A (2000) Global robust output regulation for a class of nonlinear systems. Syst Control Lett 39(2):133–139
41. Sprott JC (1994) Some simple chaotic flows. Phys Rev E 50(2):647–650
42. Sundarapandian V (2010) Output regulation of the Lorenz attractor. Far East J Math Sci 42(2):289–299
43. Sundarapandian V (2013) Analysis and anti-synchronization of a novel chaotic system via active and adaptive controllers. J Eng Sci Technol Rev 6(4):45–52
44. Sundarapandian V, Karthikeyan R (2011a) Anti-synchronization of hyperchaotic Lorenz and hyperchaotic Chen systems by adaptive control. Int J Syst Signal Control Eng Appl 4(2):18–25
45. Sundarapandian V, Karthikeyan R (2011b) Anti-synchronization of Lü and Pan chaotic systems by adaptive nonlinear control. Eur J Sci Res 64(1):94–106
46. Sundarapandian V, Karthikeyan R (2012a) Adaptive anti-synchronization of uncertain Tigan and Li systems. J Eng Appl Sci 7(1):45–52
47. Sundarapandian V, Karthikeyan R (2012b) Hybrid synchronization of hyperchaotic Lorenz and hyperchaotic Chen systems via active control. J Eng Appl Sci 7(3):254–264
48. Sundarapandian V, Pehlivan I (2012) Analysis, control, synchronization, and circuit design of a novel chaotic system. Math Comput Modell 55(7–8):1904–1915
49. Sundarapandian V, Sivaperumal S (2011) Sliding controller design of hybrid synchronization of four-wing chaotic systems. Int J Soft Comput 6(5):224–231
50. Suresh R, Sundarapandian V (2013) Global chaos synchronization of a family of n-scroll hyperchaotic Chua circuits using backstepping control with recursive feedback. Far East J Math Sci 73(1):73–95
51. Tarn TJ, Sanposh P, Cheng D, Zhang M (2005) Output regulation for nonlinear systems: some recent theoretical and experimental results. IEEE Trans Control Syst Technol 13(4):605–610
52. Tigan G, Opris D (2008) Analysis of a 3D chaotic system. Chaos, Solitons Fractals 36: 1315–1319
53. Vaidyanathan S (2011a) Hybrid chaos synchronization of Liu and Lü systems by active nonlinear control. Communications in computer and information science, p 204
54. Vaidyanathan S (2011b) Output regulation of the Arneodo-Coullet chaotic system. Commun Comput Inf Sci 133:98–107
55. Vaidyanathan S (2011c) Output regulation of the unified chaotic system. Commun Comput Inf Sci 198:1–9
56. Vaidyanathan S (2012a) Analysis and synchronization of the hyperchaotic Yujun systems via sliding mode control. Advan Intell Syst Comput 176:329–337
57. Vaidyanathan S (2012b) Anti-synchronization of Sprott-L and Sprott-M chaotic systems via adaptive control. Int J Control Theory Appl 5(1):41–59
58. Vaidyanathan S (2012c) Global chaos control of hyperchaotic Liu system via sliding control method. Int J Control Theory Appl 5(2):117–123
59. Vaidyanathan S (2012d) Output regulation of the Liu chaotic system. Appl Mech Mater 110–116:3982–3989
60. Vaidyanathan S (2012e) Sliding mode control based global chaos control of Liu-Liu-Liu-Su chaotic system. Int J Control Theory Appl 5(1):15–20
61. Vaidyanathan S (2013a) A new six-term 3-D chaotic system with an exponential nonlinearity. Far East J Math Sci 79(1):135–143
62. Vaidyanathan S (2013b) A ten-term novel 4-D hyperchaotic system with three quadratic nonlinearities and its control. Int J Control Theory Appl 6(2):97–109
63. Vaidyanathan S (2013c) Analysis and adaptive synchronization of two novel chaotic systems with hyperbolic sinusoidal and cosinusoidal nonlinearity and unknown parameters. J Eng Sci Technol Rev 6(4):53–65

64. Vaidyanathan S (2013d) Analysis, control and synchronization of hyperchaotic Zhou system via adaptive control. Adv Intell Syst Comput 177:1–10
65. Vaidyanathan S (2014a) A new eight-term 3-D polynomial chaotic system with three quadratic nonlinearities. Far East J Math Sci 84(2):219–226
66. Vaidyanathan S (2014b) Analysis and adaptive synchronization of eight-term 3-D polynomial chaotic systems with three quadratic nonlinearities. Eur Phys J: Spec Topics 223(8):1519–1529
67. Vaidyanathan S (2014c) Analysis, control and synchronisation of a six-term novel chaotic system with three quadratic nonlinearities. Int J Modell, Identif Control 22(1):41–53
68. Vaidyanathan S (2014d) Generalized projective synchronisation of novel 3-D chaotic systems with an exponential non-linearity via active and adaptive control. Int J Modell, Identif Control 22(3):207–217
69. Vaidyanathan S (2014e) Global chaos synchronization of identical Li-Wu chaotic systems via sliding mode control. Int J Modell, Identif Control 22(2):170–177
70. Vaidyanathan S (2014f) Qualitative analysis and control of an eleven-term novel 4-D hyperchaotic system with two quadratic nonlinearities. Int J Control Theory Appl 7(1):35–47
71. Vaidyanathan S (2015) Analysis, properties and control of an eight-term 3-D chaotic system with an exponential nonlinearity. Int J Modell, Identif Control 23(2):164–172
72. Vaidyanathan S, Azar AT (2015a) Analysis and control of a 4-D novel hyperchaotic system. In: Azar AT, Vaidyanathan S (eds) Chaos modeling and control systems design, studies in computational intelligence, vol 581. Springer, Germany, pp 19–38
73. Vaidyanathan S, Azar AT (2015b) Analysis and control of a 4-D novel hyperchaotic system. Stud Comput Intell 581:3–17
74. Vaidyanathan S, Azar AT (2015c) Analysis, control and synchronization of a nine-term 3-D novel chaotic system. In: Azar AT, Vaidyanathan S (eds) Chaos modelling and control systems design, studies in computational intelligence, vol 581. Springer, Germany, pp 19–38
75. Vaidyanathan S, Azar AT (2015d) Anti-synchronization of identical chaotic systems using sliding mode control and an application to Vaidhyanathan-Madhavan chaotic systems. Stud Comput Intell 576:527–547
76. Vaidyanathan S, Azar AT (2015e) Hybrid synchronization of identical chaotic systems using sliding mode control and an application to Vaidhyanathan chaotic systems. Stud Comput Intell 576:549–569
77. Vaidyanathan S, Madhavan K (2013) Analysis, adaptive control and synchronization of a seven-term novel 3-D chaotic system. Int J Control Theory Appl 6(2):121–137
78. Vaidyanathan S, Pakiriswamy S (2013) Generalized projective synchronization of six-term Sundarapandian chaotic systems by adaptive control. Int J Control Theory Appl 6(2):153–163
79. Vaidyanathan S, Rajagopal K (2011a) Anti-synchronization of Li and T chaotic systems by active nonlinear control. Commun Comput Inf Sci 198:175–184
80. Vaidyanathan S, Rajagopal K (2011b) Global chaos synchronization of hyperchaotic Pang and Wang systems by active nonlinear control. Commun Comput Inf Sci 204:84–93
81. Vaidyanathan S, Rajagopal K (2011c) Global chaos synchronization of Lü and Pan systems by adaptive nonlinear control. Commun Comput Inf Sci 205:193–202
82. Vaidyanathan S, Rajagopal K (2012) Global chaos synchronization of hyperchaotic Pang and hyperchaotic Wang systems via adaptive control. Int J Soft Comput 7(1):28–37
83. Vaidyanathan S, Rasappan S (2011) Global chaos synchronization of hyperchaotic Bao and Xu systems by active nonlinear control. Commun Comput Inf Sci 198:10–17
84. Vaidyanathan S, Rasappan S (2014) Global chaos synchronization of n-scroll Chua circuit and Lur'e system using backstepping control design with recursive feedback. Arab J Sci Eng 39(4):3351–3364
85. Vaidyanathan S, Sampath S (2011) Global chaos synchronization of hyperchaotic Lorenz systems by sliding mode control. Commun Comput Inf Sci 205:156–164
86. Vaidyanathan S, Sampath S (2012) Anti-synchronization of four-wing chaotic systems via sliding mode control. Int J Autom Comput 9(3):274–279
87. Vaidyanathan S, Volos C, Pham VT (2014a) Hyperchaos, adaptive control and synchronization of a novel 5-D hyperchaotic system with three positive Lyapunov exponents and its SPICE implementation. Arch Control Sci 24(4):409–446

88. Vaidyanathan S, Volos C, Pham VT (2014b) Hyperchaos, adaptive control and synchronization of a novel 5-D hyperchaotic system with three positive Lyapunov exponents and its SPICE implementation. Arch Control Sci 24(4):409–446
89. Vaidyanathan S, Volos C, Pham VT, Madhavan K, Idowu BA (2014c) Adaptive backstepping control, synchronization and circuit simulation of a 3-D novel jerk chaotic system with two hyperbolic sinusoidal nonlinearities. Arch Control Sci 24(3):375–403
90. Vaidyanathan S, Idowu BA, Azar AT (2015a) Backstepping controller design for the global chaos synchronization of Sprott's jerk systems. Stud Comput Intell 581:39–58
91. Vaidyanathan S, Volos C, Pham VT, Madhavan K (2015b) Analysis, adaptive control and synchronization of a novel 4-D hyperchaotic hyperjerk system and its SPICE implementation. Arch Control Sci 25(1):5–28
92. Vaidyanathan S, Volos C, Pham VT, Madhavan K (2015c) Analysis, adaptive control and synchronization of a novel 4-D hyperchaotic hyperjerk system and its SPICE implementation. Stud Comput Intell 25(1):135–158
93. Vaidyanathan S, Volos CK, Pham VT (2015d) Global chaos control of a novel nine-term chaotic system via sliding mode control. In: Azar AT, Zhu Q (eds) Advances and applications in sliding mode control systems, studies in computational intelligence, vol 576. Springer, Germany, pp 571–590
94. Wang G, Zhang X, Zheng Y, Li Y (2006) A new modified hyperchaotic Lü system. Physica A 371(2):260–272
95. Wei Z, Yang Q (2010) Anti-control of Hopf bifurcation in the new chaotic system with two stable node-foci. Appl Math Comput 217(1):422–429
96. Xi Z, Ding Z (2007) Global adaptive output regulation of a class of nonlinear systems with nonlinear exosystems. Automatica 43(1):143–149
97. Yan Z (2005) Controlling hyperchaos in the new hyperchaotic Chen system. Physica A 168(2):1239–1250
98. Yang X, Huang J (2012) New results on robust output regulation of nonlinear systems with a nonlinear exosystem. Int J Robust Nonlinear Control 22(15):1703–1719
99. Zhou W, Xu Y, Lu H, Pan L (2008) On dynamics analysis of a new chaotic attractor. Phys Lett A 372(36):5773–5777
100. Zhu C, Liu Y, Guo Y (2010) Theoretic and numerical study of a new chaotic system. Intell Inf Manag 2:104–109

Analysis, Control and Synchronization of a Novel Highly Chaotic System with Three Quadratic Nonlinearities

Sundarapandian Vaidyanathan

Abstract In this work, we describe a novel highly chaotic system with three quadratic nonlinearities. The phase portraits of the novel highly chaotic system are illustrated and the dynamic properties of the highly chaotic system are discussed. The novel highly chaotic system has three unstable equilibrium points. We show that the equilibrium point at the origin is a saddle point, while the other two equilibrium points are saddle foci. The novel highly chaotic system has rotation symmetry about the x_3 axis. The Lyapunov exponents of the novel highly chaotic system are obtained as $L_1 = 6.34352$, $L_2 = 0$ and $L_3 = -29.26796$, while the Kaplan–Yorke dimension of the novel chaotic system is obtained as $D_{KY} = 2.2167$. Since the Maximal Lyapunov Exponent (MLE) of the novel chaotic system has a large value, viz. $L_1 = 6.34352$, the novel chaotic system is highly chaotic. Since the sum of the Lyapunov exponents is negative, the novel highly chaotic system is dissipative. Next, we derive new results for the global chaos control of the novel highly chaotic system with unknown parameters via adaptive control method. We also derive new results for the global chaos synchronization of the identical novel highly chaotic systems with unknown parameters via adaptive control method. The main adaptive control results are established using Lyapunov stability theory. MATLAB simulations are shown to depict the phase portraits of the novel highly chaotic system and also the adaptive control results derived in this work.

Keywords Chaos · Chaotic systems · Highly chaotic system · Chaos control · Adaptive control · Stability theory · Chaos synchronization

S. Vaidyanathan (✉)
Research and Development Centre, Vel Tech University,
Avadi, Chennai 600062, Tamil Nadu, India
e-mail: sundarvtu@gmail.com

S. Vaidyanathan and C. Volos (eds.), *Advances and Applications in Nonlinear Control Systems*, Studies in Computational Intelligence 635,
DOI 10.1007/978-3-319-30169-3_11

1 Introduction

Chaotic systems are defined as nonlinear dynamical systems which are sensitive to initial conditions, topologically mixing and with dense periodic orbits. Sensitivity to initial conditions of chaotic systems is popularly known as the *butterfly effect*.

Chaotic systems are either conservative or dissipative. The conservative chaotic systems are characterized by the property that they are *volume conserving*. The dissipative chaotic systems are characterized by the property that any asymptotic motion of the chaotic system settles onto a set of measure zero, i.e. a strange attractor. In this research work, we shall announce and discuss a novel 3-D dissipative highly chaotic circulant chaotic system with six sinusoidal nonlinearities.

The Lyapunov exponent of a chaotic system is a measure of the divergence of points which are initially very close and this can be used to quantify chaotic systems. Each nonlinear dynamical system has a spectrum of Lyapunov exponents, which are equal in number to the dimension of the state space. The largest Lyapunov exponent of a nonlinear dynamical system is called the *maximal Lyapunov exponent* (MLE).

In the last few decades, Chaos theory has become a very important and active research field, employing many applications in different disciplines like physics, chemistry, biology, ecology, engineering and economics, among others.

Some classical paradigms of 3-D chaotic systems in the literature are Lorenz system [31], Rössler system [44], ACT system [1], Sprott systems [51], Chen system [14], Lü system [32], Cai system [13], Tigan system [63], etc.

Many new chaotic systems have been discovered in the recent years such as Zhou system [125], Zhu system [126], Li system [27], Sundarapandian systems [56, 60], Vaidyanathan systems [71, 73, 75–78, 82, 88, 98, 99, 101, 107, 109, 112, 115, 116, 118], Pehlivan system [37], Sampath system [46], Pham system [39], etc.

Chaos theory and control systems have many important applications in science and engineering [2, 9–12, 127]. Some commonly known applications are oscillators [23, 50], lasers [28, 122], chemical reactions [17, 38, 86, 89, 91, 92, 96], biology [15, 25, 81, 83–85, 87, 90, 94, 95], ecology [18, 53], encryption [26, 124], cryptosystems [43, 64], mechanical systems [4–8], secure communications [16, 34, 123], robotics [33, 35, 120], cardiology [40, 121], intelligent control [3, 29], neural networks [20, 22, 30], finance [19, 52], etc.

The control of a chaotic system aims to stabilize or regulate the system. There are many methods available for controlling a chaotic system such as active control [54, 65, 66], adaptive control [55, 67, 72, 74, 80, 97, 108, 114, 117], sliding mode control [69, 70], backstepping control [36, 111, 119], etc.

Major works on synchronization of chaotic systems deal with the complete synchronization (CS) which has the design goal of using the output of the master system to control the slave system so that the output of the slave system tracks the output of the master system asymptotically with time.

There are many methods available for chaos synchronization such as active control [21, 47, 48, 102, 104, 110], adaptive control [45, 49, 57–59, 68, 93, 100, 103], sliding mode control [61, 79, 106, 113], backstepping control [41, 42, 62, 105], etc.

In this research work, we announce an eight-term novel highly chaotic system with three quadratic nonlinearities. Using adaptive control method, we have also derived new results for the global chaos control of the novel highly chaotic system and global chaos synchronization of the identical novel highly chaotic systems when the system parameters are unknown.

This work is organized as follows. Section 2 describes the dynamic equations and phase portraits of the eight-term novel highly chaotic system. Section 3 details the dynamic analysis and qualitative properties of the novel highly chaotic system. The Lyapunov exponents of the novel chaotic system are obtained as $L_1 = 6.34352$, $L_2 = 0$ and $L_3 = -29.26796$, while the Kaplan–Yorke dimension of the novel chaotic system is obtained as $D_{KY} = 2.2167$. Since the maximal Lyapunov exponent of the novel chaotic system has a large value, viz. $L_1 = 6.34352$, the novel chaotic system is highly chaotic.

In Sect. 4, we derive new results for the global chaos control of the novel highly chaotic system with unknown parameters. In Sect. 5, we derive new results for the global chaos synchronization of the identical novel highly chaotic systems with unknown parameters. Section 6 contains a summary of the main results derived in this work.

2 A 3-D Novel Highly Chaotic System

In this section, we describe an eight-term novel chaotic system, which is given by the 3-D dynamics

$$\begin{cases} \dot{x}_1 = a(x_2 - x_1) + x_2 x_3 \\ \dot{x}_2 = b(x_1 + x_2) - x_1 x_3 \\ \dot{x}_3 = -cx_3 + x_1^2 \end{cases} \tag{1}$$

where x_1, x_2, x_3 are the states and a, b, c are constant, positive parameters.

The novel 3-D system (1) is an eight-term polynomial system with three quadratic nonlinearities.

The system (1) exhibits a *highly chaotic attractor* for the parameter values

$$a = 32, \quad b = 18, \quad c = 9 \tag{2}$$

For numerical simulations, we take the initial conditions as

$$x_1(0) = 0.3, \quad x_2(0) = 0.2, \quad x_3(0) = 0.3 \tag{3}$$

Figure 1 depicts the 3-D phase portrait of the novel highly chaotic system (1), while Figs. 2, 3 and 4 depict the 2-D projection of the novel highly chaotic system (1) on the (x_1, x_2), (x_2, x_3) and (x_1, x_3) planes, respectively.

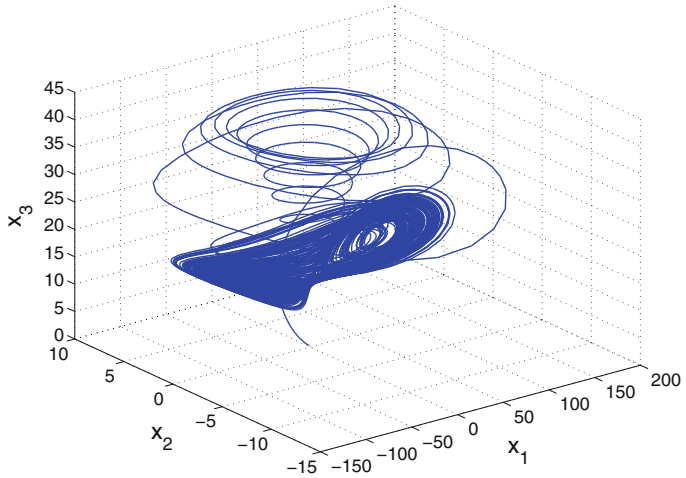

Fig. 1 3-D phase portrait of the novel highly chaotic system

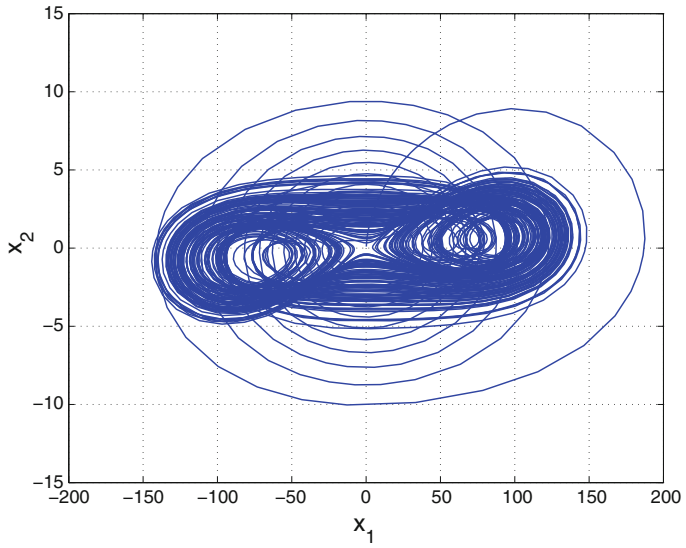

Fig. 2 2-D projection of the novel highly chaotic system on the (x_1, x_2) plane

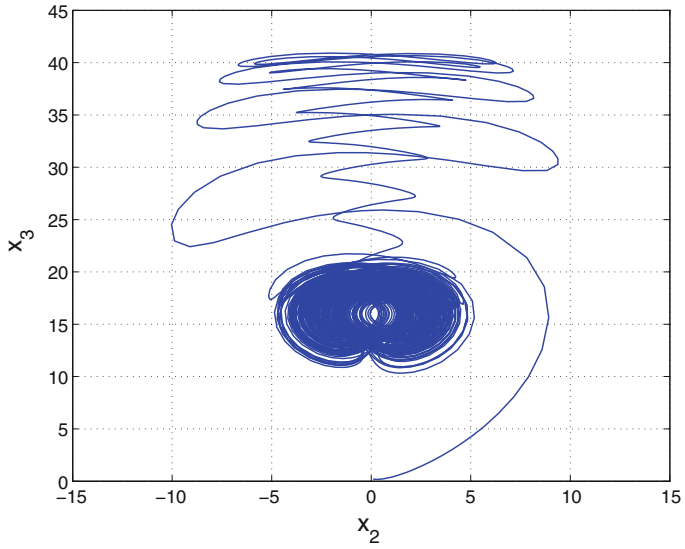

Fig. 3 2-D projection of the novel highly chaotic system on the (x_2, x_3) plane

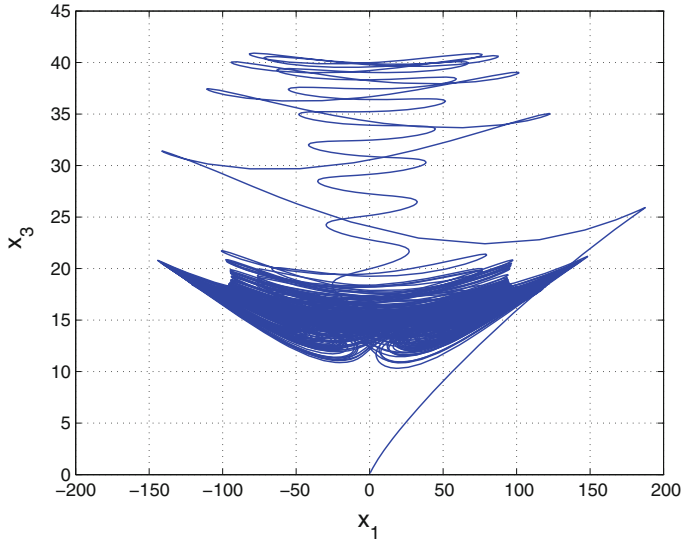

Fig. 4 2-D projection of the novel highly chaotic system on the (x_1, x_3) plane

3 Analysis of the Novel 3-D Highly Chaotic System

In this section, we give a dynamic analysis of the 3-D novel highly chaotic system (1). We take the parameter values as in the chaotic case (2), viz. $a = 32$, $b = 18$ and $c = 9$.

3.1 Dissipativity

In vector notation, the novel chaotic system (1) can be expressed as

$$\dot{\mathbf{x}} = f(\mathbf{x}) = \begin{bmatrix} f_1(x_1, x_2, x_3) \\ f_2(x_1, x_2, x_3) \\ f_3(x_1, x_2, x_3) \end{bmatrix}, \tag{4}$$

where

$$\begin{cases} f_1(x_1, x_2, x_3) = a(x_2 - x_1) + x_2 x_3 \\ f_2(x_1, x_2, x_3) = b(x_1 + x_2) - x_1 x_3 \\ f_3(x_1, x_2, x_3) = -cx_3 + x_1^2 \end{cases} \tag{5}$$

Let Ω be any region in $\mathbf{R}^3$ with a smooth boundary and also, $\Omega(t) = \Phi_t(\Omega)$, where Φ_t is the flow of f. Furthermore, let $V(t)$ denote the volume of $\Omega(t)$.

By Liouville's theorem, we know that

$$\dot{V}(t) = \int_{\Omega(t)} (\nabla \cdot f)\, dx_1\, dx_2\, dx_3 \tag{6}$$

The divergence of the novel chaotic system (4) is found as

$$\nabla \cdot f = \frac{\partial f_1}{\partial x_1} + \frac{\partial f_2}{\partial x_2} + \frac{\partial f_3}{\partial x_3} = -(a - b + c) = -\mu < 0 \tag{7}$$

since $\mu = a - b + c = 23 > 0$.

Inserting the value of $\nabla \cdot f$ from (7) into (6), we get

$$\dot{V}(t) = \int_{\Omega(t)} (-\mu)\, dx_1\, dx_2\, dx_3 = -\mu V(t) \tag{8}$$

Integrating the first order linear differential equation (8), we get

$$V(t) = \exp(-\mu t) V(0) \tag{9}$$

Since $\mu > 0$, it follows from Eq. (9) that $V(t) \to 0$ exponentially as $t \to \infty$. This shows that the novel chaotic system (1) is dissipative.

Hence, the system limit sets are ultimately confined into a specific limit set of zero volume, and the asymptotic motion of the novel chaotic system (1) settles onto a strange attractor of the system.

3.2 Equilibrium Points

We take the parameter values as in the chaotic case (2), viz. $a = 32$, $b = 18$ and $c = 9$.

It is easy to see that the system (1) has three equilibrium points, viz.

$$E_0 = \begin{bmatrix} 0 \\ 0 \\ 0 \end{bmatrix}, \quad E_1 = \begin{bmatrix} 15.7765 \\ 8.4627 \\ 27.6554 \end{bmatrix}, \quad E_2 = \begin{bmatrix} -15.7765 \\ -8.4627 \\ 27.6554 \end{bmatrix} \tag{10}$$

The Jacobian of the system (1) at any point $\mathbf{x} \in \mathbf{R}^3$ is calculated as

$$J(\mathbf{x}) = \begin{bmatrix} -a & a + x_3 & x_2 \\ b - x_3 & b & -x_1 \\ 2x_1 & 0 & -c \end{bmatrix} = \begin{bmatrix} -32 & 32 + x_3 & x_2 \\ 18 - x_3 & 18 & -x_1 \\ 2x_1 & 0 & -9 \end{bmatrix} \tag{11}$$

The Jacobian of the system (1) at the equilibrium E_0 is obtained as

$$J_0 = J(E_0) = \begin{bmatrix} -32 & 32 & 0 \\ 18 & 18 & 0 \\ 0 & 0 & -9 \end{bmatrix} \tag{12}$$

We find that the matrix $J_0 = J(E_0)$ has the eigenvalues

$$\lambda_1 = -9, \quad \lambda_2 = -41.6554, \quad \lambda_3 = 27.6554 \tag{13}$$

This shows that the equilibrium point E_0 is a saddle-point, which is unstable.

The Jacobian of the system (1) at the equilibrium E_1 is obtained as

$$J_1 = J(E_1) = \begin{bmatrix} -32 & 59.6554 & 8.4267 \\ -9.6554 & 18 & -15.7765 \\ 31.5530 & 0 & -9 \end{bmatrix} \tag{14}$$

We find that the matrix $J_1 = J(E_1)$ has the eigenvalues

$$\lambda_1 = -43.9949, \quad \lambda_{2,3} = 10.4974 \pm 25.9534i \tag{15}$$

This shows that the equilibrium point E_1 is a saddle-focus, which is unstable.
The Jacobian of the system (1) at the equilibrium E_2 is obtained as

$$J_2 = J(E_2) = \begin{bmatrix} -32 & 59.6554 & -8.4267 \\ -9.6554 & 18 & 15.7765 \\ -31.5530 & 0 & -9 \end{bmatrix} \tag{16}$$

We find that the matrix $J_2 = J(E_2)$ has the eigenvalues

$$\lambda_1 = -43.9949, \quad \lambda_{2,3} = 10.4974 \pm 25.9534i \tag{17}$$

This shows that the equilibrium point E_2 is a saddle-focus, which is unstable.

3.3 Symmetry and Invariance

It is easy to see that the system (1) is invariant under the change of coordinates

$$(x_1, x_2, x_3) \mapsto (-x_1, -x_2, x_3) \tag{18}$$

Thus, it follows that the 3-D novel chaotic system (1) has rotation symmetry about the x_3-axis and that any non-trivial trajectory must have a twin trajectory.

Next, it is easy to see that the x_3-axis is invariant under the flow of the 3-D novel chaotic system (1).

The invariant motion along the x_3-axis is characterized by

$$\dot{x}_3 = -cx_3, \quad (c > 0) \tag{19}$$

which is globally exponentially stable.

3.4 Lyapunov Exponents and Kaplan–Yorke Dimension

We take the parameter values of the novel system (1) as in the chaotic case (2), i.e.

$$a = 32, \quad b = 18, \quad c = 9 \tag{20}$$

We take the initial state of the novel system (1) as given in (3), i.e.

$$x_1(0) = 0.3, \quad x_2(0) = 0.2, \quad x_3(0) = 0.3 \tag{21}$$

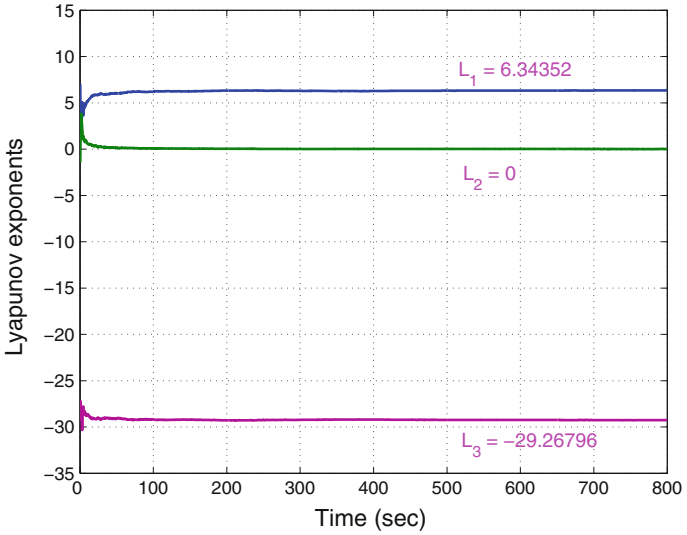

Fig. 5 Lyapunov exponents of the highly chaotic system

Then the Lyapunov exponents of the system (1) are numerically obtained as

$$L_1 = 6.34352, \quad L_2 = 0, \quad L_3 = -29.26796 \tag{22}$$

Figure 5 shows the Lyapunov exponents of the novel system (1). From Fig. 5, we note that the Maximal Lyapunov Exponent (MLE) of the novel system (1) is given by $L_1 = 6.34352$, which is a large value. This shows that the novel system (1) is *highly chaotic*.

We also note that the sum of the Lyapunov exponents in (22) is negative, i.e.

$$L_1 + L_2 + L_3 = -22.9244 < 0 \tag{23}$$

This shows that the novel chaotic system (1) is dissipative.

Also, the Kaplan–Yorke dimension of the novel chaotic system (1) is found as

$$D_{KY} = 2 + \frac{L_1 + L_2}{|L_3|} = 2.2167, \tag{24}$$

which is fractional.

Also, the relatively large value of the Kaplan–Yorke dimension of the novel chaotic system (1), i.e. $D_{KY} = 2.2167$, indicates that the system exhibits highly complex behaviour. Hence, the novel chaotic system (1) has applications in cryptosystems, secure communication devices, etc.

4 Global Chaos Control of the Novel Highly Chaotic System

In this section, we use adaptive control method to derive an adaptive feedback control law for globally stabilizing the novel 3-D highly chaotic system with unknown parameters.

Thus, we consider the novel highly chaotic system given by

$$\begin{cases} \dot{x}_1 = a(x_2 - x_1) + x_2x_3 + u_1 \\ \dot{x}_2 = b(x_1 + x_2) - x_1x_3 + u_2 \\ \dot{x}_3 = -cx_3 + x_1^2 + u_3 \end{cases} \tag{25}$$

In (25), x_1, x_2, x_3 are the states and u_1, u_2, u_3 are the adaptive controls to be determined using estimates for the unknown system parameters.

We consider the adaptive feedback control law

$$\begin{cases} u_1 = -\hat{a}(t)(x_2 - x_1) - x_2x_3 - k_1x_1 \\ u_2 = -\hat{b}(t)(x_1 + x_2) + x_1x_3 - k_2x_2 \\ u_3 = \hat{c}(t)x_3 - x_1^2 - k_3x_3 \end{cases} \tag{26}$$

where k_1, k_2, k_3 are positive gain constants.

Substituting (26) into (25), we get the closed-loop plant dynamics as

$$\begin{cases} \dot{x}_1 = \left[a - \hat{a}(t)\right](x_2 - x_1) - k_1x_1 \\ \dot{x}_2 = \left[b - \hat{b}(t)\right](x_1 + x_2) - k_2x_2 \\ \dot{x}_3 = -\left[c - \hat{c}(t)\right]x_3 - k_3x_3 \end{cases} \tag{27}$$

The parameter estimation errors are defined as

$$\begin{cases} e_a(t) = a - \hat{a}(t) \\ e_b(t) = b - \hat{b}(t) \\ e_c(t) = c - \hat{c}(t) \end{cases} \tag{28}$$

In view of (28), we can simplify the plant dynamics (27) as

$$\begin{cases} \dot{x}_1 = e_a(x_2 - x_1) - k_1x_1 \\ \dot{x}_2 = e_b(x_1 + x_2) - k_2x_2 \\ \dot{x}_3 = -e_cx_3 - k_3x_3 \end{cases} \tag{29}$$

Differentiating (28) with respect to t, we obtain

$$\begin{cases} \dot{e}_a(t) = -\dot{\hat{a}}(t) \\ \dot{e}_b(t) = -\dot{\hat{b}}(t) \\ \dot{e}_c(t) = -\dot{\hat{c}}(t) \end{cases} \tag{30}$$

We consider the quadratic candidate Lyapunov function defined by

$$V(\mathbf{x}, e_a, e_b, e_c) = \frac{1}{2}\left(x_1^2 + x_2^2 + x_3^2\right) + \frac{1}{2}\left(e_a^2 + e_b^2 + e_c^2\right) \tag{31}$$

Differentiating V along the trajectories of (29) and (30), we obtain

$$\begin{aligned}\dot{V} = &-k_1 x_1^2 - k_2 x_2^2 - k_3 x_3^2 + e_a\left[x_1(x_2 - x_1) - \dot{\hat{a}}\right] + e_b\left[x_2(x_1 + x_2) - \dot{\hat{b}}\right] \\ &+ e_c\left[-x_3^2 - \dot{\hat{c}}\right]\end{aligned} \tag{32}$$

In view of (32), we take the parameter update law as

$$\begin{cases}\dot{\hat{a}}(t) = x_1(x_2 - x_1) \\ \dot{\hat{b}}(t) = x_2(x_1 + x_2) \\ \dot{\hat{c}}(t) = -x_3^2\end{cases} \tag{33}$$

Next, we state and prove the main result of this section.

Theorem 1 *The novel 3-D highly chaotic system (25) with unknown system parameters is globally and exponentially stabilized for all initial conditions by the adaptive control law (26) and the parameter update law (33), where k_1, k_2, k_3 are positive gain constants.*

Proof We prove this result by applying Lyapunov stability theory [24].

We consider the quadratic Lyapunov function defined by (31), which is clearly a positive definite function on $\mathbf{R}^6$.

By substituting the parameter update law (33) into (32), we obtain the time-derivative of V as

$$\dot{V} = -k_1 x_1^2 - k_2 x_2^2 - k_3 x_3^2 \tag{34}$$

From (34), it is clear that $\dot{V}$ is a negative semi-definite function on $\mathbf{R}^6$.

Thus, we can conclude that the state vector $\mathbf{x}(t)$ and the parameter estimation error are globally bounded i.e.

$$\left[x_1(t)\ x_2(t)\ x_3(t)\ e_a(t)\ e_b(t)\ e_c(t)\right]^T \in \mathbf{L}_\infty.$$

We define $k = \min\{k_1, k_2, k_3\}$.

Then it follows from (34) that

$$\dot{V} \leq -k\|\mathbf{x}(t)\|^2 \tag{35}$$

Thus, we have

$$k\|\mathbf{x}(t)\|^2 \leq -\dot{V} \tag{36}$$

Integrating the inequality (36) from 0 to t, we get

$$k\int_0^t \|\mathbf{x}(\tau)\|^2\, d\tau \;\leq\; V(0) - V(t) \tag{37}$$

From (37), it follows that $\mathbf{x} \in \mathbf{L}_2$.

Using (29), we can conclude that $\dot{\mathbf{x}} \in \mathbf{L}_\infty$.

Using Barbalat's lemma [24], we conclude that $\mathbf{x}(t) \to 0$ exponentially as $t \to \infty$ for all initial conditions $\mathbf{x}(0) \in \mathbf{R}^3$.

Hence, the novel highly chaotic system (25) with unknown system parameters is globally and exponentially stabilized for all initial conditions by the adaptive control law (26) and the parameter update law (33).

This completes the proof. ■

For the numerical simulations, the classical fourth-order Runge–Kutta method with step size $h = 10^{-8}$ is used to solve the systems (25) and (33), when the adaptive control law (26) is applied.

The parameter values of the novel 3-D highly chaotic system (25) are taken as in the chaotic case (2), i.e.

$$a = 32, \quad b = 18, \quad c = 9 \tag{38}$$

We take the positive gain constants as $k_i = 8$ for $i = 1, 2, 3$.

Furthermore, as initial conditions of the novel highly chaotic system (25), we take

$$x_1(0) = 23.8, \quad x_2(0) = -16.5, \quad x_3(0) = 9.4 \tag{39}$$

Also, as initial conditions of the parameter estimates, we take

$$\hat{a}(0) = 12.7, \quad \hat{b}(0) = 5.3, \quad \hat{c}(0) = 2.6 \tag{40}$$

In Fig. 6, the exponential convergence of the controlled states of the 3-D novel highly chaotic system (25) is depicted. From Fig. 6, we see that the controlled states $x_1(t), x_2(t), x_3(t)$ converge to zero in just one second. This shows the efficiency of the adaptive controller designed in this section for the novel highly chaotic system (25).

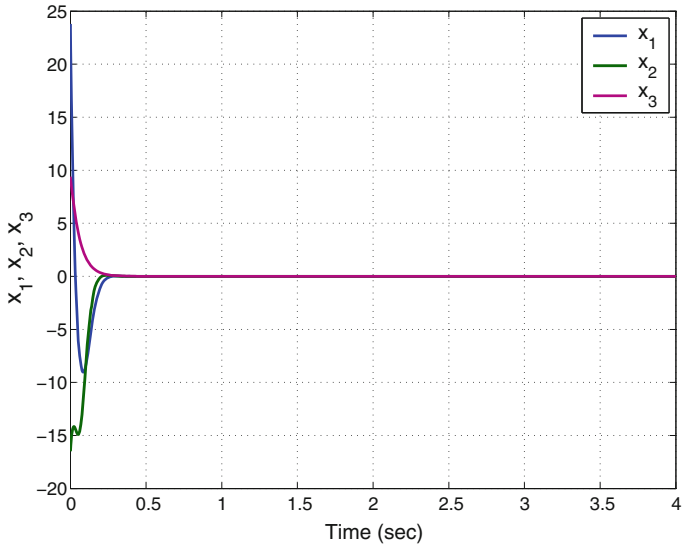

Fig. 6 Time-history of the controlled states x_1, x_2, x_3

5 Global Chaos Synchronization of the Identical Novel Highly Chaotic Systems

In this section, we apply adaptive control method to derive an adaptive feedback control law for globally synchronizing identical 3-D novel highly chaotic systems with unknown parameters. The main result is established using Lyapunov stability theory.

As the master system, we consider the novel 3-D chaotic system given by

$$\begin{cases} \dot{x}_1 = a(x_2 - x_1) + x_2 x_3 \\ \dot{x}_2 = b(x_1 + x_2) - x_1 x_3 \\ \dot{x}_3 = -cx_3 + x_1^2 \end{cases} \tag{41}$$

In (41), x_1, x_2, x_3 are the states and a, b, c are unknown system parameters.

As the slave system, we consider the novel 3-D chaotic system given by

$$\begin{cases} \dot{y}_1 = a(y_2 - y_1) + y_2 y_3 + u_1 \\ \dot{y}_2 = b(y_1 + y_2) - y_1 y_3 + u_2 \\ \dot{y}_3 = -cy_3 + y_1^2 + u_3 \end{cases} \tag{42}$$

In (42), y_1, y_2, y_3 are the states and u_1, u_2, u_3 are the adaptive controls to be determined using estimates of the unknown system parameters.

The synchronization error between the novel chaotic systems is defined by

$$\begin{cases} e_1 = y_1 - x_1 \\ e_2 = y_2 - x_2 \\ e_3 = y_3 - x_3 \end{cases} \tag{43}$$

Then the error dynamics is obtained as

$$\begin{cases} \dot{e}_1 = a(e_2 - e_1) + y_2 y_3 - x_2 x_3 + u_1 \\ \dot{e}_2 = b(e_1 + e_2) - y_1 y_3 + x_1 x_3 + u_2 \\ \dot{e}_3 = -ce_3 + y_1^2 - x_1^2 + u_3 \end{cases} \tag{44}$$

We consider the adaptive feedback control law

$$\begin{cases} u_1 = -\hat{a}(t)(e_2 - e_1) - y_2 y_3 + x_2 x_3 - k_1 e_1 \\ u_2 = -\hat{b}(t)(e_1 + e_2) + y_1 y_3 - x_1 x_3 - k_2 e_2 \\ u_3 = \hat{c}(t) e_3 - y_1^2 + x_1^2 - k_3 e_3 \end{cases} \tag{45}$$

where k_1, k_2, k_3 are positive gain constants.

Substituting (45) into (44), we get the closed-loop error dynamics as

$$\begin{cases} \dot{e}_1 = [a - \hat{a}(t)](e_2 - e_1) - k_1 e_1 \\ \dot{e}_2 = [b - \hat{b}(t)](e_1 + e_2) - k_2 e_2 \\ \dot{e}_3 = -[c - \hat{c}(t)] e_3 - k_3 e_3 \end{cases} \tag{46}$$

The parameter estimation errors are defined as

$$\begin{cases} e_a(t) = a - \hat{a}(t) \\ e_b(t) = b - \hat{b}(t) \\ e_c(t) = c - \hat{c}(t) \end{cases} \tag{47}$$

In view of (47), we can simplify the error dynamics (46) as

$$\begin{cases} \dot{e}_1 = e_a(e_2 - e_1) - k_1 e_1 \\ \dot{e}_2 = e_b(e_1 + e_2) - k_2 e_2 \\ \dot{e}_3 = -e_c e_3 - k_3 e_3 \end{cases} \tag{48}$$

Differentiating (47) with respect to t, we obtain

$$\begin{cases} \dot{e}_a(t) = -\dot{\hat{a}}(t) \\ \dot{e}_b(t) = -\dot{\hat{b}}(t) \\ \dot{e}_c(t) = -\dot{\hat{c}}(t) \end{cases} \tag{49}$$

We consider the quadratic candidate Lyapunov function defined by

$$V(\mathbf{e}, e_a, e_b, e_c, e_p, e_q) = \frac{1}{2}\left(e_1^2 + e_2^2 + e_3^2\right) + \frac{1}{2}\left(e_a^2 + e_b^2 + e_c^2\right) \tag{50}$$

Differentiating V along the trajectories of (48) and (49), we obtain

$$\begin{aligned}\dot{V} = {} & -k_1 e_1^2 - k_2 e_2^2 - k_3 e_3^2 + e_a\left[e_1(e_2 - e_1) - \dot{\hat{a}}\right] + e_b\left[e_2(e_1 + e_2) - \dot{\hat{b}}\right] \\ & + e_c\left[-e_3^2 - \dot{\hat{c}}\right]\end{aligned} \tag{51}$$

In view of (51), we take the parameter update law as

$$\begin{cases} \dot{\hat{a}}(t) = e_1(e_2 - e_1) \\ \dot{\hat{b}}(t) = e_2(e_1 + e_2) \\ \dot{\hat{c}}(t) = -e_3^2 \end{cases} \tag{52}$$

Next, we state and prove the main result of this section.

Theorem 2 *The novel highly chaotic systems (41) and (42) with unknown system parameters are globally and exponentially synchronized for all initial conditions by the adaptive control law (45) and the parameter update law (52), where k_1, k_2, k_3 are positive gain constants.*

Proof We prove this result by applying Lyapunov stability theory [24].

We consider the quadratic Lyapunov function defined by (50), which is clearly a positive definite function on $\mathbf{R}^6$.

By substituting the parameter update law (52) into (51), we obtain

$$\dot{V} = -k_1 e_1^2 - k_2 e_2^2 - k_3 e_3^2 \tag{53}$$

From (53), it is clear that $\dot{V}$ is a negative semi-definite function on $\mathbf{R}^6$.

Thus, we can conclude that the error vector $\mathbf{e}(t)$ and the parameter estimation error are globally bounded, i.e.

$$\left[e_1(t)\ e_2(t)\ e_3(t)\ e_a(t)\ e_b(t)\ e_c(t)\right]^T \in \mathbf{L}_\infty. \tag{54}$$

We define $k = \min\{k_1, k_2, k_3\}$.

Then it follows from (53) that

$$\dot{V} \leq -k\|\mathbf{e}(t)\|^2 \tag{55}$$

Thus, we have

$$k\|\mathbf{e}(t)\|^2 \leq -\dot{V} \tag{56}$$

Integrating the inequality (56) from 0 to t, we get

$$k \int_0^t \|\mathbf{e}(\tau)\|^2 \, d\tau \leq V(0) - V(t) \tag{57}$$

From (57), it follows that $\mathbf{e} \in \mathbf{L}_2$.

Using (48), we can conclude that $\dot{\mathbf{e}} \in \mathbf{L}_\infty$.

Using Barbalat's lemma [24], we conclude that $\mathbf{e}(t) \to 0$ exponentially as $t \to \infty$ for all initial conditions $\mathbf{e}(0) \in \mathbf{R}^3$.

This completes the proof. ■

For the numerical simulations, the classical fourth-order Runge–Kutta method with step size $h = 10^{-8}$ is used to solve the systems (41), (42) and (52), when the adaptive control law (45) is applied.

The parameter values of the novel chaotic systems are taken as in the chaotic case (2), i.e. $a = 32$, $b = 18$ and $c = 9$.

We take the positive gain constants as $k_i = 8$ for $i = 1, 2, 3$.

Furthermore, as initial conditions of the master system (41), we take

$$x_1(0) = 5.3, \quad x_2(0) = -6.7, \quad x_3(0) = 12.8 \tag{58}$$

As initial conditions of the slave system (42), we take

$$y_1(0) = 12.7, \quad y_2(0) = 23.5, \quad y_3(0) = 3.4 \tag{59}$$

Also, as initial conditions of the parameter estimates, we take

$$\hat{a}(0) = 6.1, \quad \hat{b}(0) = 14.3, \quad \hat{c}(0) = 7.8 \tag{60}$$

Figures 7, 8 and 9 describe the complete synchronization of the novel highly chaotic systems (41) and (42), while Fig. 10 describes the time-history of the synchronization errors e_1, e_2, e_3.

From Fig. 7, we see that the states x_1 and y_1 are synchronized in just one second.

From Fig. 8, we see that the states x_2 and y_2 are synchronized in just one second.

From Fig. 9, we see that the states x_3 and y_3 are synchronized in just one second.

From Fig. 10, we see that the errors e_1, e_2, e_3 converge to zero in just one second. This shows the efficiency of the adaptive controller developed in this section for the synchronization of identical highly chaotic systems.

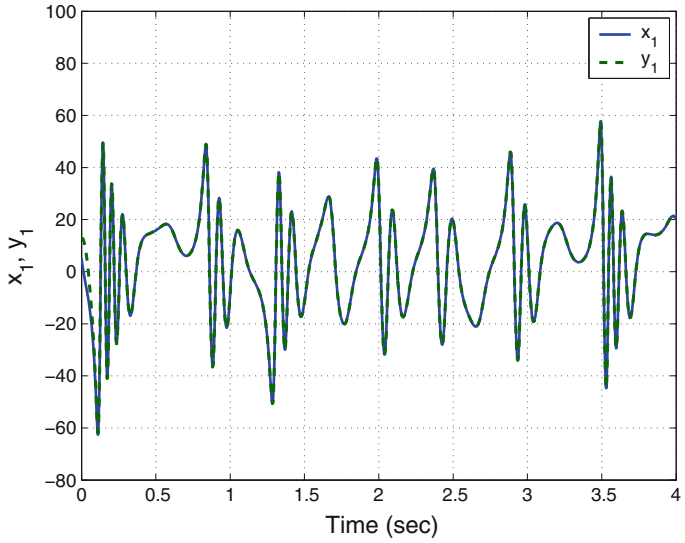

Fig. 7 Synchronization of the states x_1 and y_1

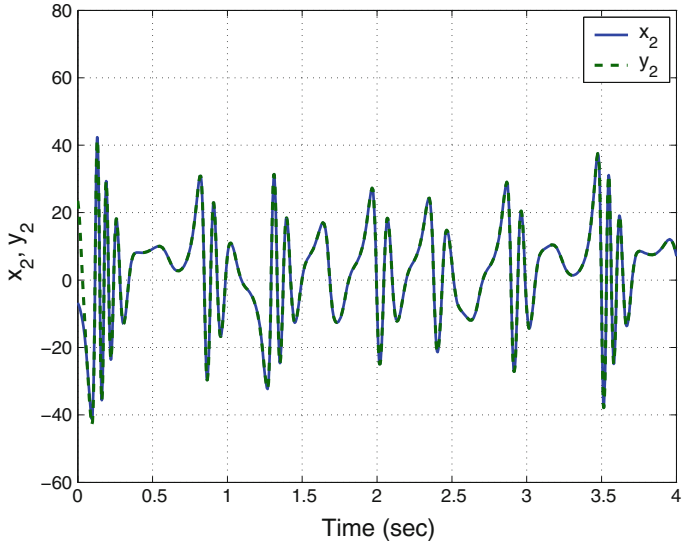

Fig. 8 Synchronization of the states x_2 and y_2

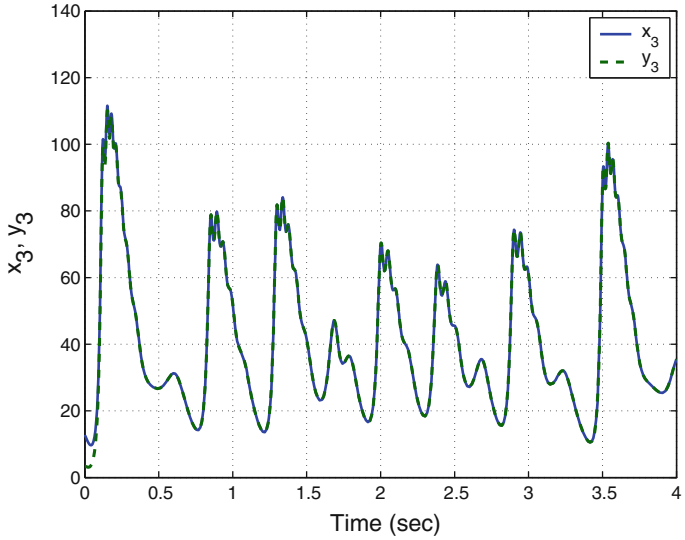

Fig. 9 Synchronization of the states x_3 and y_3

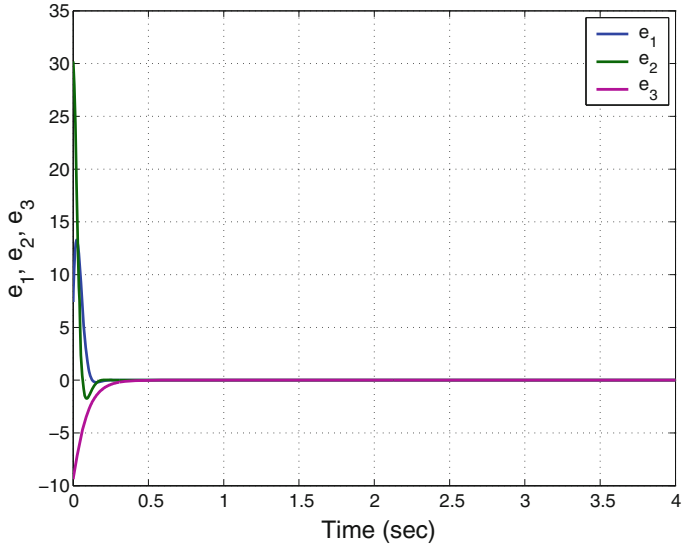

Fig. 10 Time-history of the synchronization errors e_1, e_2, e_3

6 Conclusions

In this work, we described a novel highly chaotic system with three quadratic nonlinearities. The qualitative properties and phase portraits of the highly chaotic system were discussed. The novel highly chaotic system has three unstable equilibrium points. We showed that the equilibrium point at the origin is a saddle point, while the other two equilibrium points are saddle foci. The novel highly chaotic system has rotation symmetry about the x_3 axis. The Lyapunov exponents of the novel highly chaotic system have been obtained as $L_1 = 6.34352$, $L_2 = 0$ and $L_3 = -29.26796$, while the Kaplan–Yorke dimension of the novel chaotic system has been derived as $D_{KY} = 2.2167$. Since the Maximal Lyapunov Exponent (MLE) of the novel chaotic system has a large value, viz. $L_1 = 6.34352$, we concluded that the novel chaotic system is highly chaotic. Since the sum of the Lyapunov exponents is negative, the novel highly chaotic system is dissipative. Next, we derived new results for the global chaos control and global chaos synchronization of the identical novel highly chaotic systems with unknown parameters via adaptive control method. The main adaptive control results are established using Lyapunov stability theory. MATLAB simulations have been shown to depict all the adaptive control results derived in this work.

References

1. Arneodo A, Coullet P, Tresser C (1981) Possible new strange attractors with spiral structure. Commun Math Phys 79(4):573–576
2. Azar AT (2010) Fuzzy Systems. IN-TECH, Vienna, Austria
3. Azar AT (2012) Overview of type-2 fuzzy logic systems. Int J Fuzzy Syst Appl 2(4):1–28
4. Azar AT, Serrano FE (2014) Robust IMC-PID tuning for cascade control systems with gain and phase margin specifications. Neural Comput Appl 25(5):983–995
5. Azar AT, Serrano FE (2015) Adaptive sliding mode control of the Furuta pendulum. In: Azar AT, Zhu Q (eds) Advances and applications in sliding mode control systems. Studies in computational intelligence, vol 576. Springer, Germany, pp 1–42
6. Azar AT, Serrano FE (2015) Deadbeat control for multivariable systems with time varying delays. In: Azar AT, Vaidyanathan S (eds) Chaos modeling and control systems design. Studies in computational intelligence, vol 581. Springer, Germany, pp 97–132
7. Azar AT, Serrano FE (2015) Design and modeling of anti wind up PID controllers. In: Zhu Q, Azar AT (eds) Complex system modelling and control through intelligent soft computations. Studies in fuzziness and soft computing, vol 319. Springer, Germany, pp 1–44
8. Azar AT, Serrano FE (2015) Stabilizatoin and control of mechanical systems with backlash. In: Azar AT, Vaidyanathan S (eds) Handbook of research on advanced intelligent control engineering and automation. Advances in computational intelligence and robotics (ACIR), IGI-Global, USA, pp 1–60
9. Azar AT, Vaidyanathan S (2015) Chaos modeling and control systems design. Studies in computational intelligence, vol 581. Springer, Germany
10. Azar AT, Vaidyanathan S (2015) Computational intelligence applications in modeling and control. Studies in computational intelligence, vol 575. Springer, Germany

11. Azar AT, Vaidyanathan S (2015) Handbook of research on advanced intelligent control engineering and automation. Advances in computational intelligence and robotics (ACIR), IGI-Global, USA
12. Azar AT, Zhu Q (2015) Advances and applications in sliding mode control systems. Studies in computational intelligence, vol 576. Springer, Germany
13. Cai G, Tan Z (2007) Chaos synchronization of a new chaotic system via nonlinear control. J Uncertain Syst 1(3):235–240
14. Chen G, Ueta T (1999) Yet another chaotic attractor. Int J Bifurc Chaos 9(7):1465–1466
15. Das S, Goswami D, Chatterjee S, Mukherjee S (2014) Stability and chaos analysis of a novel swarm dynamics with applications to multi-agent systems. Eng Appl Artif Intell 30:189–198
16. Feki M (2003) An adaptive chaos synchronization scheme applied to secure communication. Chaos Solitons Fractals 18(1):141–148
17. Gaspard P (1999) Microscopic chaos and chemical reactions. Phys A 263(1–4):315–328
18. Gibson WT, Wilson WG (2013) Individual-based chaos: Extensions of the discrete logistic model. J Theor Biol 339:84–92
19. Guégan D (2009) Chaos in economics and finance. Ann Rev Control 33(1):89–93
20. Huang X, Zhao Z, Wang Z, Li Y (2012) Chaos and hyperchaos in fractional-order cellular neural networks. Neurocomputing 94:13–21
21. Karthikeyan R, Sundarapandian V (2014) Hybrid chaos synchronization of four-scroll systems via active control. J Electr Eng 65(2):97–103
22. Kaslik E, Sivasundaram S (2012) Nonlinear dynamics and chaos in fractional-order neural networks. Neural Netw 32:245–256
23. Kengne J, Chedjou JC, Kenne G, Kyamakya K (2012) Dynamical properties and chaos synchronization of improved Colpitts oscillators. Commun Nonlinear Sci Numer Simul 17(7):2914–2923
24. Khalil HK (2001) Nonlinear systems, 3rd edn. Prentice Hall, New Jersey
25. Kyriazis M (1991) Applications of chaos theory to the molecular biology of aging. Exp Gerontol 26(6):569–572
26. Lang J (2015) Color image encryption based on color blend and chaos permutation in the reality-preserving multiple-parameter fractional Fourier transform domain. Opt Commun 338:181–192
27. Li D (2008) A three-scroll chaotic attractor. Phys Lett A 372(4):387–393
28. Li N, Pan W, Yan L, Luo B, Zou X (2014) Enhanced chaos synchronization and communication in cascade-coupled semiconductor ring lasers. Commun Nonlinear Sci Numer Simul 19(6):1874–1883
29. Li Z, Chen G (2006) Integration of fuzzy logic and chaos theory. Studies in fuzziness and soft computing, vol 187. Springer, Germany
30. Lian S, Chen X (2011) Traceable content protection based on chaos and neural networks. Appl Soft Comput 11(7):4293–4301
31. Lorenz EN (1963) Deterministic periodic flow. J Atmos Sci 20(2):130–141
32. Lü J, Chen G (2002) A new chaotic attractor coined. Int J Bifurc Chaos 12(3):659–661
33. Mondal S, Mahanta C (2014) Adaptive second order terminal sliding mode controller for robotic manipulators. J Franklin Inst 351(4):2356–2377
34. Murali K, Lakshmanan M (1998) Secure communication using a compound signal from generalized chaotic systems. Phys Lett A 241(6):303–310
35. Nehmzow U, Walker K (2005) Quantitative description of robot-environment interaction using chaos theory. Robot Auton Syst 53(3–4):177–193
36. Njah AN, Sunday OD (2009) Generalization on the chaos control of 4-D chaotic systems using recursive backstepping nonlinear controller. Chaos Solitons Fractals 41(5):2371–2376
37. Pehlivan I, Moroz IM, Vaidyanathan S (2014) Analysis, synchronization and circuit design of a novel butterfly attractor. J Sound Vib 333(20):5077–5096
38. Petrov V, Gaspar V, Masere J, Showalter K (1993) Controlling chaos in Belousov-Zhabotinsky reaction. Nature 361:240–243

39. Pham VT, Vaidyanathan S, Volos CK, Jafari S (2015) Hidden attractors in a chaotic system with an exponential nonlinear term. Eur Phys J - Spec Top 224(8):1507–1517
40. Qu Z (2011) Chaos in the genesis and maintenance of cardiac arrhythmias. Prog Biophys Mol Biol 105(3):247–257
41. Rasappan S, Vaidyanathan S (2013) Hybrid synchronization of *n*-scroll Chua circuits using adaptive backstepping control design with recursive feedback. Malays J Math Sci 73(1):73–95
42. Rasappan S, Vaidyanathan S (2014) Global chaos synchronization of WINDMI and Coullet chaotic systems using adaptive backstepping control design. Kyungpook Math J 54(1):293–320
43. Rhouma R, Belghith S (2011) Cryptoanalysis of a chaos based cryptosystem on DSP. Commun Nonlinear Sci Numer Simul 16(2):876–884
44. Rössler OE (1976) An equation for continuous chaos. Phys Lett A 57(5):397–398
45. Vaidyanathan S, Pham V-T, Volos CK (2015) A 5-D hyperchaotic Rikitake dynamo system with hidden attractors. Eur Phys J: Spec Top 224(8):1575–1592
46. Sampath S, Vaidyanathan S, Volos CK, Pham VT (2015) An eight-term novel four-scroll chaotic system with cubic nonlinearity and its circuit simulation. J Eng Sci Technol Rev 8(2):1–6
47. Sarasu P, Sundarapandian V (2011) Active controller design for generalized projective synchronization of four-scroll chaotic systems. Int J Syst Signal Control Eng Appl 4(2):26–33
48. Sarasu P, Sundarapandian V (2011) The generalized projective synchronization of hyperchaotic Lorenz and hyperchaotic Qi systems via active control. Int J Soft Comput 6(5):216–223
49. Sarasu P, Sundarapandian V (2012) Generalized projective synchronization of two-scroll systems via adaptive control. Int J Soft Comput 7(4):146–156
50. Sharma A, Patidar V, Purohit G, Sud KK (2012) Effects on the bifurcation and chaos in forced Duffing oscillator due to nonlinear damping. Commun Nonlinear Sci Numer Simul 17(6):2254–2269
51. Sprott JC (1994) Some simple chaotic flows. Phys Rev E 50(2):647–650
52. Sprott JC (2004) Competition with evolution in ecology and finance. Phys Lett A 325(5–6):329–333
53. Suérez I (1999) Mastering chaos in ecology. Ecol Model 117(2–3):305–314
54. Sundarapandian V (2010) Output regulation of the Lorenz attractor. Far East J Math Sci 42(2):289–299
55. Sundarapandian V (2013) Adaptive control and synchronization design for the Lu-Xiao chaotic system. Lect Notes Electr Eng 131:319–327
56. Sundarapandian V (2013) Analysis and anti-synchronization of a novel chaotic system via active and adaptive controllers. J Eng Sci Technol Rev 6(4):45–52
57. Sundarapandian V, Karthikeyan R (2011) Anti-synchronization of hyperchaotic Lorenz and hyperchaotic Chen systems by adaptive control. Int J Syst Signal Control Eng Appl 4(2):18–25
58. Sundarapandian V, Karthikeyan R (2011) Anti-synchronization of Lü and Pan chaotic systems by adaptive nonlinear control. Eur J Sci Res 64(1):94–106
59. Sundarapandian V, Karthikeyan R (2012) Adaptive anti-synchronization of uncertain Tigan and Li systems. J Eng Appl Sci 7(1):45–52
60. Sundarapandian V, Pehlivan I (2012) Analysis, control, synchronization, and circuit design of a novel chaotic system. Math Comput Model 55(7–8):1904–1915
61. Sundarapandian V, Sivaperumal S (2011) Sliding controller design of hybrid synchronization of four-wing chaotic systems. Int J Soft Comput 6(5):224–231
62. Suresh R, Sundarapandian V (2013) Global chaos synchronization of a family of *n*-scroll hyperchaotic Chua circuits using backstepping control with recursive feedback. Far East J Math Sci 7(2):219–246
63. Tigan G, Opris D (2008) Analysis of a 3D chaotic system. Chaos Solitons Fractals 36:1315–1319
64. Usama M, Khan MK, Alghatbar K, Lee C (2010) Chaos-based secure satellite imagery cryptosystem. Comput Math Appl 60(2):326–337

65. Vaidyanathan S (2011) Output regulation of Arneodo-Coullet chaotic system. Commun Comput Inf Sci 133:98–107
66. Vaidyanathan S (2011) Output regulation of the unified chaotic system. Commun Comput Inf Sci 198:1–9
67. Vaidyanathan S (2012) Adaptive controller and syncrhonizer design for the Qi-Chen chaotic system. Lect Notes Inst Comput Sci Soc-Inf Telecommun Eng 84:73–82
68. Vaidyanathan S (2012) Anti-synchronization of Sprott-L and Sprott-M chaotic systems via adaptive control. Int J Control Theory Appl 5(1):41–59
69. Vaidyanathan S (2012) Global chaos control of hyperchaotic Liu system via sliding control method. Int J Control Theory Appl 5(2):117–123
70. Vaidyanathan S (2012) Sliding mode control based global chaos control of Liu-Liu-Liu-Su chaotic system. Int J Control Theory Appl 5(1):15–20
71. Vaidyanathan S (2013) A new six-term 3-D chaotic system with an exponential nonlinearity. Far East J Math Sci 79(1):135–143
72. Vaidyanathan S (2013) A ten-term novel 4-D hyperchaotic system with three quadratic nonlinearities and its control. Int J Control Theory Appl 6(2):97–109
73. Vaidyanathan S (2013) Analysis and adaptive synchronization of two novel chaotic systems with hyperbolic sinusoidal and cosinusoidal nonlinearity and unknown parameters. J Eng Sci Technol Rev 6(4):53–65
74. Vaidyanathan S (2013) Analysis, control and synchronization of hyperchaotic Zhou system via adaptive control. Adv Intell Syst Comput 177:1–10
75. Vaidyanathan S (2014) A new eight-term 3-D polynomial chaotic system with three quadratic nonlinearities. Far East J Math Sci 84(2):219–226
76. Vaidyanathan S (2014) Analysis and adaptive synchronization of eight-term 3-D polynomial chaotic systems with three quadratic nonlinearities. Eur Phys J: Spec Top 223(8):1519–1529
77. Vaidyanathan S (2014) Analysis, control and synchronisation of a six-term novel chaotic system with three quadratic nonlinearities. Int J Model Ident Control 22(1):41–53
78. Vaidyanathan S (2014) Generalised projective synchronisation of novel 3-D chaotic systems with an exponential non-linearity via active and adaptive control. Int J Model Ident Control 22(3):207–217
79. Vaidyanathan S (2014) Global chaos synchronisation of identical Li-Wu chaotic systems via sliding mode control. Int J Model Ident Control 22(2):170–177
80. Vaidyanathan S (2014) Qualitative analysis and control of an eleven-term novel 4-D hyperchaotic system with two quadratic nonlinearities. Int J Control Theory Appl 7:35–47
81. Vaidyanathan S (2015) 3-cells cellular neural network (CNN) attractor and its adaptive biological control. Int J PharmTech Res 8(4):632–640
82. Vaidyanathan S (2015) A 3-D novel highly chaotic system with four quadratic nonlinearities, its adaptive control and anti-synchronization with unknown parameters. J Eng Sci Technol Rev 8(2):106–115
83. Vaidyanathan S (2015) Adaptive backstepping control of enzymes-substrates system with ferroelectric behaviour in brain waves. Int J PharmTech Res 8(2):256–261
84. Vaidyanathan S (2015) Adaptive biological control of generalized Lotka-Volterra three-species biological system. Int J PharmTech Res 8(4):622–631
85. Vaidyanathan S (2015) Adaptive chaotic synchronization of enzymes-substrates system with ferroelectric behaviour in brain waves. Int J PharmTech Res 8(5):964–973
86. Vaidyanathan S (2015) Adaptive synchronization of chemical chaotic reactors. Int J ChemTech Res 8(2):612–621
87. Vaidyanathan S (2015) Adaptive synchronization of generalized Lotka-Volterra three-species biological systems. Int J PharmTech Res 8(5):928–937
88. Vaidyanathan S (2015) Analysis, properties and control of an eight-term 3-D chaotic system with an exponential nonlinearity. Int J Model Ident Control 23(2):164–172
89. Vaidyanathan S (2015) Anti-synchronization of Brusselator chemical reaction systems via adaptive control. Int J ChemTech Res 8(6):759–768

90. Vaidyanathan S (2015) Chaos in neurons and adaptive control of Birkhoff-Shaw strange chaotic attractor. Int J PharmTech Res 8(5):956–963
91. Vaidyanathan S (2015) Dynamics and control of Brusselator chemical reaction. Int J ChemTech Res 8(6):740–749
92. Vaidyanathan S (2015) Dynamics and control of Tokamak system with symmetric and magnetically confined plasma. Int J ChemTech Res 8(6):795–803
93. Vaidyanathan S (2015) Hyperchaos, qualitative analysis, control and synchronisation of a ten-term 4-D hyperchaotic system with an exponential nonlinearity and three quadratic nonlinearities. Int J Model Ident Control 23(4):380–392
94. Vaidyanathan S (2015) Lotka-Volterra population biology models with negative feedback and their ecological monitoring. Int J PharmTech Res 8(5):974–981
95. Vaidyanathan S (2015) Synchronization of 3-cells cellular neural network (CNN) attractors via adaptive control method. Int J PharmTech Res 8(5):946–955
96. Vaidyanathan S (2015) Synchronization of Tokamak systems with symmetric and magnetically confined plasma via adaptive control. Int J ChemTech Res 8(6):818–827
97. Vaidyanathan S, Azar AT (2015) Analysis and control of a 4-D novel hyperchaotic system. Stud Comput Intell 581:3–17
98. Vaidyanathan S, Azar AT (2015) Analysis, control and synchronization of a nine-term 3-D novel chaotic system. In: Azar AT, Vaidyanathan S (eds) Chaos modelling and control systems design. Studies in computational intelligence, vol 581. Springer, Germany, pp 19–38
99. Vaidyanathan S, Madhavan K (2013) Analysis, adaptive control and synchronization of a seven-term novel 3-D chaotic system. Int J Control Theory Appl 6(2):121–137
100. Vaidyanathan S, Pakiriswamy S (2013) Generalized projective synchronization of six-term Sundarapandian chaotic systems by adaptive control. Int J Control Theory Appl 6(2):153–163
101. Vaidyanathan S, Pakiriswamy S (2015) A 3-D novel conservative chaotic system and its generalized projective synchronization via adaptive control. J Eng Sci Technol Rev 8(2):52–60
102. Vaidyanathan S, Rajagopal K (2011) Hybrid synchronization of hyperchaotic Wang-Chen and hyperchaotic Lorenz systems by active non-linear control. Int J Syst Signal Control Eng Appl 4(3):55–61
103. Vaidyanathan S, Rajagopal K (2012) Global chaos synchronization of hyperchaotic Pang and hyperchaotic Wang systems via adaptive control. Int J Soft Comput 7(1):28–37
104. Vaidyanathan S, Rasappan S (2011) Global chaos synchronization of hyperchaotic Bao and Xu systems by active nonlinear control. Commun Comput Inf Sci 198:10–17
105. Vaidyanathan S, Rasappan S (2014) Global chaos synchronization of *n*-scroll Chua circuit and Lur'e system using backstepping control design with recursive feedback. Arab J Sci Eng 39(4):3351–3364
106. Vaidyanathan S, Sampath S (2012) Anti-synchronization of four-wing chaotic systems via sliding mode control. Int J Autom Comput 9(3):274–279
107. Vaidyanathan S, Volos C (2015) Analysis and adaptive control of a novel 3-D conservative no-equilibrium chaotic system. Arch Control Sci 25(3):333–353
108. Vaidyanathan S, Volos C, Pham VT (2014) Hyperchaos, adaptive control and synchronization of a novel 5-D hyperchaotic system with three positive Lyapunov exponents and its SPICE implementation. Arch Control Sci 24(4):409–446
109. Vaidyanathan S, Volos C, Pham VT, Madhavan K, Idowu BA (2014) Adaptive backstepping control, synchronization and circuit simulation of a 3-D novel jerk chaotic system with two hyperbolic sinusoidal nonlinearities. Arch Control Sci 24(3):375–403
110. Vaidyanathan S, Azar AT, Rajagopal K, Alexander P (2015) Design and SPICE implementation of a 12-term novel hyperchaotic system and its synchronisation via active control. Int J Model Ident Control 23(3):267–277
111. Vaidyanathan S, Idowu BA, Azar AT (2015) Backstepping controller design for the global chaos synchronization of Sprott's jerk systems. Stud Comput Intell 581:39–58
112. Vaidyanathan S, Rajagopal K, Volos CK, Kyprianidis IM, Stouboulos IN (2015) Analysis, adaptive control and synchronization of a seven-term novel 3-D chaotic system with three

quadratic nonlinearities and its digital implementation in LabVIEW. J Eng Sci Technol Rev 8(2):130–141
113. Vaidyanathan S, Sampath S, Azar AT (2015) Global chaos synchronisation of identical chaotic systems via novel sliding mode control method and its application to Zhu system. Int J Model Ident Control 23(1):92–100
114. Vaidyanathan S, Volos C, Pham VT, Madhavan K (2015) Analysis, adaptive control and synchronization of a novel 4-D hyperchaotic hyperjerk system and its SPICE implementation. Nonlinear Dyn 25(1):135–158
115. Vaidyanathan S, Volos CK, Kyprianidis IM, Stouboulos IN, Pham VT (2015) Analysis, adaptive control and anti-synchronization of a six-term novel jerk chaotic system with two exponential nonlinearities and its circuit simulation. J Eng Sci Technol Rev 8(2):24–36
116. Vaidyanathan S, Volos CK, Pham VT (2015) Analysis, adaptive control and adaptive synchronization of a nine-term novel 3-D chaotic system with four quadratic nonlinearities and its circuit simulation. J Eng Sci Technol Rev 8(2):181–191
117. Vaidyanathan S, Volos CK, Pham VT (2015) Analysis, control, synchronization and SPICE implementation of a novel 4-D hyperchaotic Rikitake dynamo system without equilibrium. J Eng Sci Technol Rev 8(2):232–244
118. Vaidyanathan S, Volos CK, Pham VT (2015) Global chaos control of a novel nine-term chaotic system via sliding mode control. In: Azar AT, Zhu Q (eds) Advances and applications in sliding mode control systems. Studies in computational intelligence, vol 576. Springer, Germany, pp 571–590
119. Vincent UE, Njah AN, Laoye JA (2007) Controlling chaos and deterministic directed transport in inertia ratchets using backstepping control. Phys D 231(2):130–136
120. Volos CK, Kyprianidis IM, Stouboulos IN (2013) Experimental investigation on coverage performance of a chaotic autonomous mobile robot. Robot Auton Syst 61(12):1314–1322
121. Witte CL, Witte MH (1991) Chaos and predicting varix hemorrhage. Med Hypotheses 36(4):312–317
122. Yuan G, Zhang X, Wang Z (2014) Generation and synchronization of feedback-induced chaos in semiconductor ring lasers by injection-locking. Optik—Int J Light Electron Opt 125(8):1950–1953
123. Zaher AA, Abu-Rezq A (2011) On the design of chaos-based secure communication systems. Commun Nonlinear Syst Numer Simul 16(9):3721–3727
124. Zhang X, Zhao Z, Wang J (2014) Chaotic image encryption based on circular substitution box and key stream buffer. Sig Process Image Commun 29(8):902–913
125. Zhou W, Xu Y, Lu H, Pan L (2008) On dynamics analysis of a new chaotic attractor. Phys Lett A 372(36):5773–5777
126. Zhu C, Liu Y, Guo Y (2010) Theoretic and numerical study of a new chaotic system. Intell Inf Manag 2:104–109
127. Zhu Q, Azar AT (2015) Complex system modelling and control through intelligent soft computations. Studies in fuzzines and soft computing, vol 319. Springer, Germany

A No-Equilibrium Novel 4-D Highly Hyperchaotic System with Four Quadratic Nonlinearities and Its Adaptive Control

Sundarapandian Vaidyanathan

Abstract In this work, we describe an eleven-term novel 4-D highly hyperchaotic system with four quadratic nonlinearities. The phase portraits of the eleven-term novel highly hyperchaotic system are depicted and the qualitative properties of the novel highly hyperchaotic system are discussed. We shall show that the novel hyperchaotic system does not have any equilibrium point. Hence, the novel 4-D hyperchaotic system exhibits hidden attractors. The Lyapunov exponents of the novel hyperchaotic system are obtained as $L_1 = 15.06593$, $L_2 = 0.03551$, $L_3 = 0$ and $L_4 = -42.42821$. The Maximal Lyapunov Exponent (MLE) of the novel hyperchaotic system is found as $L_1 = 15.06593$, which is large. Thus, the novel 4-D hyperchaotic system proposed in this work is highly hyperchaotic. Also, the Kaplan–Yorke dimension of the novel hyperchaotic system is derived as $D_{KY} = 3.3559$. Since the sum of the Lyapunov exponents is negative, the novel hyperchaotic system is dissipative. Next, an adaptive controller is designed to globally stabilize the novel highly hyperchaotic system with unknown parameters. Finally, an adaptive controller is also designed to achieve global chaos synchronization of the identical novel highly hyperchaotic systems with unknown parameters. MATLAB simulations are depicted to illustrate all the main results derived in this work.

Keywords Chaos · Chaotic systems · Hyperchaos · Hyperchaotic systems · Adaptive control · Chaos synchronization · Stability theory

1 Introduction

In the last few decades, Chaos theory has become a very important and active research field, employing many applications in different disciplines like physics, chemistry, biology, ecology, engineering and economics, among others.

S. Vaidyanathan (✉)
Research and Development Centre, Vel Tech University, Avadi,
Chennai 600062, Tamil Nadu, India
e-mail: sundarvtu@gmail.com

S. Vaidyanathan and C. Volos (eds.), *Advances and Applications in Nonlinear Control Systems*, Studies in Computational Intelligence 635,
DOI 10.1007/978-3-319-30169-3_12

Some classical paradigms of 3-D chaotic systems in the literature are Lorenz system [35], Rössler system [50], ACT system [1], Sprott systems [59], Chen system [15], Lü system [36], Cai system [13], Tigan system [70], etc.

Many new chaotic systems have been discovered in the recent years such as Zhou system [138], Zhu system [140], Li system [31], Wei–Yang system [131], Sundarapandian systems [63, 67], Vaidyanathan systems [78, 80, 82–85, 89, 96, 106, 107, 109, 115, 117, 120, 123, 124, 126], Pehlivan system [40], Sampath system [53], Pham system [43], etc.

The Lyapunov exponent is a measure of the divergence of phase points that are initially very close and can be used to quantify chaotic systems. It is common to refer to the largest Lyapunov exponent as the *Maximal Lyapunov Exponent* (MLE). A positive maximal Lyapunov exponent and phase space compactness are usually taken as defining conditions for a chaotic system.

A hyperchaotic system is defined as a chaotic system with at least two positive Lyapunov exponents. Thus, the dynamics of a hyperchaotic system can expand in several different directions simultaneously. Thus, the hyperchaotic systems have more complex dynamical behaviour and they have miscellaneous applications in engineering such as secure communications [18, 30, 133], cryptosystems [21, 48, 139], fuzzy logic [57, 136], electrical circuits [130, 134], etc.

The minimum dimension of an autonomous, continuous-time, hyperchaotic system is four. The first 4-D hyperchaotic system was found by Rössler [51]. Many hyperchaotic systems have been reported in the chaos literature such as hyperchaotic Lorenz system [23], hyperchaotic Lü system [14], hyperchaotic Chen system [32], hyperchaotic Wang system [129], hyperchaotic Vaidyanathan systems [52, 79, 87, 101, 105, 116, 118, 122, 125], hyperchaotic Pham system [42], etc.

Chaos theory and control systems have many important applications in science and engineering [2, 9–12, 141]. Some commonly known applications are oscillators [26, 58], chemical reactions [19, 41, 93, 94, 97, 99, 100, 104], biology [16, 28, 88, 90–92, 95, 98, 102, 103], ecology [20, 60], encryption [29, 137], cryptosystems [49, 71], mechanical systems [4–8], secure communications [17, 38, 135], robotics [37, 39, 127], cardiology [45, 132], intelligent control [3, 33], neural networks [22, 25, 34], memristors [44, 128], etc.

The control of a chaotic or hyperchaotic system aims to stabilize or regulate the system with the help of a feedback control. There are many methods available for controlling a chaotic system such as active control [61, 72, 73], adaptive control [62, 74, 81], sliding mode control [76, 77], backstepping control [119], etc.

The synchronization of chaotic systems aims to synchronize the states of master and slave systems asymptotically with time. There are many methods available for chaos synchronization such as active control [24, 54, 55, 110, 112], adaptive control [56, 64–66, 75, 108, 111], sliding mode control [68, 86, 114, 121], backstepping control [46, 47, 69, 113], etc.

This work is organized as follows. Section 2 describes the dynamic equations and phase portraits of the eleven-term novel 4-D hyperchaotic system. Section 3 details the qualitative properties of the novel hyperchaotic system. In this section,

we establish that the novel hyperchaotic system does not have any equilibrium point. Thus, it follows that the novel hyperchaotic system exhibits hidden attractors.

The Lyapunov exponents of the novel hyperchaotic system are obtained as $L_1 = 15.06593$, $L_2 = 0.03551$, $L_3 = 0$ and $L_4 = -42.42821$, while the Kaplan–Yorke dimension of the novel hyperchaotic system is obtained as $D_{KY} = 3.3559$. Since the Maximal Lyapunov Exponent (MLE) of the novel hyperchaotic system is $L_1 = 15.06593$, which is a large value, we conclude that the proposed novel hyperchaotic system is highly hyperchaotic. A novel contribution of this research work is the finding of a highly hyperchaotic 4-D system with hidden attractors.

In Sect. 4, we design an adaptive controller to globally stabilize the novel highly hyperchaotic system with unknown parameters. In Sect. 5, an adaptive controller is designed to achieve global chaos synchronization of the identical novel highly hyperchaotic systems with unknown parameters. MATLAB simulations have been shown to illustrate all the main results derived in this research work. Section 6 summarizes the main results of this research work.

2 A Novel 4-D Hyperchaotic System

In this section, we describe an eleven-term novel hyperchaotic system, which is given by the 4-D dynamics

$$\begin{cases} \dot{x}_1 = a(x_2 - x_1) + x_2 x_3 + x_4 \\ \dot{x}_2 = -c x_1 x_3 + 3x_2 + p x_3^2 \\ \dot{x}_3 = x_1 x_2 - b \\ \dot{x}_4 = -q(x_1 + x_2) \end{cases} \tag{1}$$

where x_1, x_2, x_3, x_4 are the states and a, b, c, p, q are constant positive parameters.

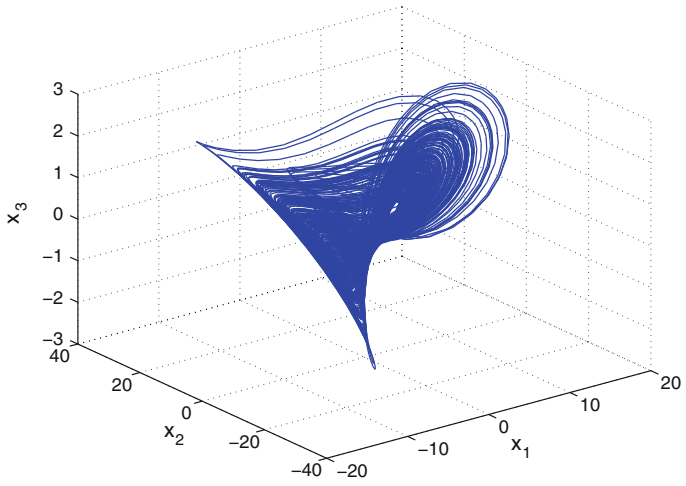

Fig. 1 3-D projection of the novel highly hyperchaotic system on the (x_1, x_2, x_3) space

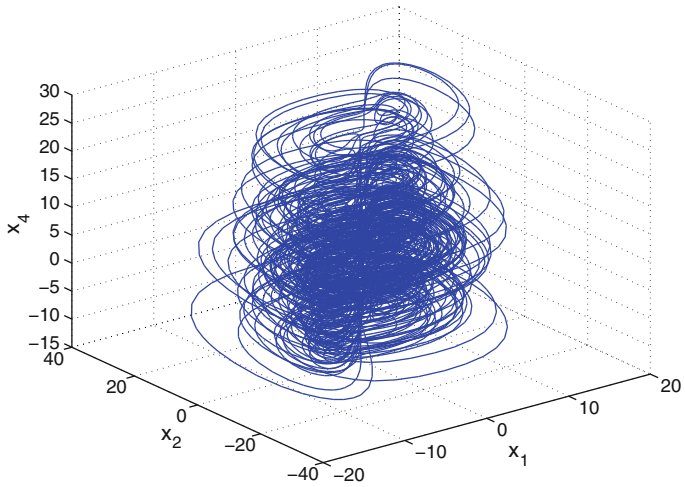

Fig. 2 3-D projection of the novel highly hyperchaotic system on the (x_1, x_2, x_4) space

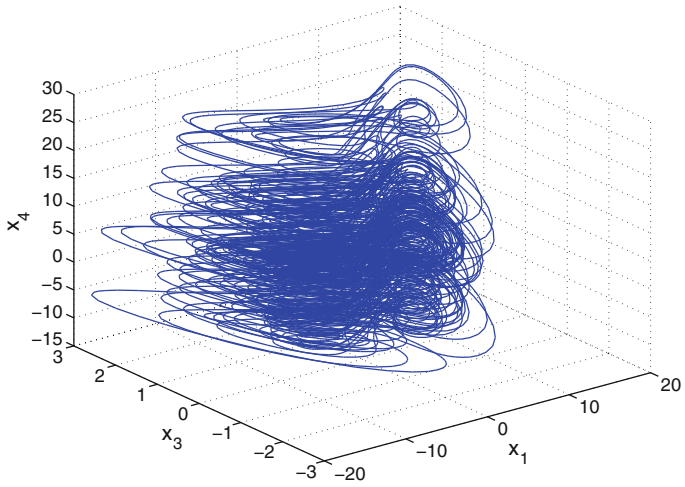

Fig. 3 3-D projection of the novel highly hyperchaotic system on the (x_1, x_3, x_4) space

The system (1) exhibits a *strange hyperchaotic attractor* for the parameter values

$$a = 62, \quad b = 36, \quad c = 160, \quad p = 0.5, \quad q = 2.8 \tag{2}$$

For numerical simulations, we take the initial conditions as

$$x_1(0) = 0.2, \quad x_2(0) = 0.8, \quad x_3(0) = 0.6, \quad x_4(0) = 0.4 \tag{3}$$

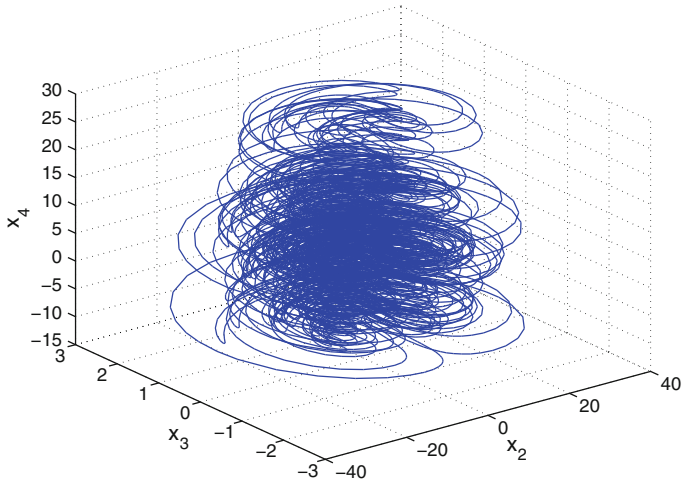

Fig. 4 3-D projection of the novel highly hyperchaotic system on the (x_2, x_3, x_4) space

Figures 1, 2, 3 and 4 show the 3-D projection of the novel hyperchaotic system (1) on the (x_1, x_2, x_3), (x_1, x_2, x_4), (x_1, x_3, x_4) and (x_2, x_3, x_4) spaces, respectively.

3 Analysis of the Novel 4-D Highly Hyperchaotic System

In this section, we study the qualitative properties of the novel 4-D highly hyperchaotic system (1). We take the parameter values as in the hyperchaotic case (2).

3.1 Dissipativity

In vector notation, the novel highly hyperchaotic system (1) can be expressed as

$$\dot{\mathbf{x}} = f(\mathbf{x}) = \begin{bmatrix} f_1(x_1, x_2, x_3, x_4) \\ f_2(x_1, x_2, x_3, x_4) \\ f_3(x_1, x_2, x_3, x_4) \\ f_4(x_1, x_2, x_3, x_4) \end{bmatrix}, \tag{4}$$

where

$$\begin{cases} f_1(x_1, x_2, x_3, x_4) = a(x_2 - x_1) + x_2 x_3 + x_4 \\ f_2(x_1, x_2, x_3, x_4) = -c x_1 x_3 + 3x_2 + p x_3^2 \\ f_3(x_1, x_2, x_3, x_4) = x_1 x_2 - b \\ f_4(x_1, x_2, x_3, x_4) = -q(x_1 + x_2) \end{cases} \tag{5}$$

Let Ω be any region in $\mathbf{R}^4$ with a smooth boundary and also, $\Omega(t) = \Phi_t(\Omega)$, where Φ_t is the flow of f.

Furthermore, let $V(t)$ denote the hypervolume of $\Omega(t)$.

By Liouville's theorem, we know that

$$\dot{V}(t) = \int_{\Omega(t)} (\nabla \cdot f)\, dx_1\, dx_2\, dx_3\, dx_4 \tag{6}$$

The divergence of the novel hyperchaotic system (4) is found as:

$$\nabla \cdot f = \frac{\partial f_1}{\partial x_1} + \frac{\partial f_2}{\partial x_2} + \frac{\partial f_3}{\partial x_3} + \frac{\partial f_4}{\partial x_4} = -a + 3 = -\mu < 0 \tag{7}$$

since $\mu = a - 3 = 59 > 0$.

Inserting the value of $\nabla \cdot f$ from (7) into (6), we get

$$\dot{V}(t) = \int_{\Omega(t)} (-\mu)\, dx_1\, dx_2\, dx_3\, dx_4 = -\mu V(t) \tag{8}$$

Integrating the first order linear differential equation (8), we get

$$V(t) = \exp(-\mu t) V(0) \tag{9}$$

Since $\mu > 0$, it follows from Eq. (9) that $V(t) \to 0$ exponentially as $t \to \infty$. This shows that the novel hyperchaotic system (1) is dissipative. Hence, the system limit sets are ultimately confined into a specific limit set of zero hypervolume, and the asymptotic motion of the novel hyperchaotic system (1) settles onto a strange attractor of the system.

3.2 Equilibrium Points

We take the parameter values as in the hyperchaotic case (2).

The equilibrium points of the 4-D system (1) are obtained by solving the system of equations

$$\begin{aligned} a(x_2 - x_1) + x_2 x_3 + x_4 &= 0 && \text{(10a)} \\ -c x_1 x_3 + 3x_2 + p x_3^2 &= 0 && \text{(10b)} \\ x_1 x_2 - b &= 0 && \text{(10c)} \\ -q(x_1 + x_2) &= 0 && \text{(10d)} \end{aligned}$$

Since $q \neq 0$, it is immediate from (10d) that

$$x_1 + x_2 = 0 \text{ or } x_1 = -x_2 \tag{11}$$

Substituting $x_1 = -x_2$ in (10c), we get

$$x_2^2 = -b \tag{12}$$

which has no solutions since $b > 0$.

Thus, we conclude that the novel highly hyperchaotic system (1) does not have any equilibrium points. Hence, the novel highly hyperchaotic system (1) exhibits hidden attractors.

3.3 Invariance

It is easy to see that the x_3-axis is invariant under the flow of the 4-D novel hyperchaotic system (1).

The invariant motion along the x_3-axis is characterized by the scalar dynamics

$$\dot{x}_3 = -b, \tag{13}$$

which is unstable.

3.4 Lyapunov Exponents and Kaplan–Yorke Dimension

We take the parameter values of the novel system (1) as in the hyperchaotic case (2), i.e.

$$a = 62, \quad b = 36, \quad c = 160, \quad p = 0.5, \quad q = 2.8 \tag{14}$$

We take the initial state of the novel system (1) as given in (3), i.e.

$$x_1(0) = 0.2, \quad x_2(0) = 0.8, \quad x_3(0) = 0.6, \quad x_4(0) = 0.4 \tag{15}$$

Then the Lyapunov exponents of the system (1) are numerically obtained using MATLAB as

$$L_1 = 15.06593, \quad L_2 = 0.03551, \quad L_3 = 0, \quad L_4 = -42.42821 \tag{16}$$

Since there are two positive Lyapunov exponents in (16), the novel system (1) exhibits *hyperchaotic* behavior.

From the LE spectrum (16), we see that the maximal Lyapunov exponent of the novel hyperchaotic system (1) is $L_1 = 15.06593$, which is large.

We find that

$$L_1 + L_2 + L_3 + L_4 = --27.32677 < 0 \tag{17}$$

Thus, it follows that the novel highly hyperchaotic system (1) is dissipative.

Also, the Kaplan–Yorke dimension of the novel hyperchaotic system (1) is calculated as

$$D_{KY} = 3 + \frac{L_1 + L_2 + L_3}{|L_4|} = 3.3559, \tag{18}$$

which is fractional.

Since the Kaplan–Yorke dimension of the novel highly hyperchaotic system (1) has a large value, it follows that the 4-D system (1) exhibits highly complex dynamics and hence, it is suitable for engineering applications like secure communication and cryptosystems.

4 Adaptive Control of the Novel Highly Hyperchaotic System

In this section, we apply adaptive control method to derive an adaptive feedback control law for globally stabilizing the novel 4-D highly hyperchaotic system with unknown parameters. We use parameter estimates in lieu of the unknown system parameters. The main control result in this section is established using Lyapunov stability theory.

Thus, we consider the controlled novel 4-D highly hyperchaotic system given by

$$\begin{cases} \dot{x}_1 = a(x_2 - x_1) + x_2x_3 + x_4 + u_1 \\ \dot{x}_2 = -cx_1x_3 + 3x_2 + px_3^2 + u_2 \\ \dot{x}_3 = x_1x_2 - b + u_3 \\ \dot{x}_4 = -q(x_1 + x_2) + u_4 \end{cases} \tag{19}$$

In (19), x_1, x_2, x_3, x_4 are the states and u_1, u_2, u_3, u_4 are the adaptive controls to be determined using estimates $\hat{a}(t), \hat{b}(t), \hat{c}(t), \hat{p}(t), \hat{q}(t)$ for the unknown parameters a, b, c, p, q, respectively.

We consider the adaptive feedback control law

$$\begin{cases} u_1 = -\hat{a}(t)(x_2 - x_1) - x_2x_3 - x_4 - k_1x_1 \\ u_2 = \hat{c}(t)x_1x_3 - 3x_2 - \hat{p}(t)x_3^2 - k_2x_2 \\ u_3 = -x_1x_2 + \hat{b}(t) - k_3x_3 \\ u_4 = \hat{q}(t)(x_1 + x_2) - k_4x_4 \end{cases} \tag{20}$$

where k_1, k_2, k_3, k_4 are positive gain constants.

Substituting (20) into (19), we get the closed-loop plant dynamics as

$$\begin{cases} \dot{x}_1 = [a - \hat{a}(t)](x_2 - x_1) - k_1 x_1 \\ \dot{x}_2 = -[c - \hat{c}(t)]x_1 x_3 + [p - \hat{p}(t)]x_3^2 - k_2 x_2 \\ \dot{x}_3 = -[b - \hat{b}(t)] - k_3 x_3 \\ \dot{x}_4 = -[q - \hat{q}(t)](x_1 + x_2) - k_4 x_4 \end{cases} \tag{21}$$

The parameter estimation errors are defined as

$$\begin{cases} e_a(t) = a - \hat{a}(t) \\ e_b(t) = b - \hat{b}(t) \\ e_c(t) = c - \hat{c}(t) \\ e_p(t) = p - \hat{p}(t) \\ e_q(t) = q - \hat{q}(t) \end{cases} \tag{22}$$

In view of (22), we can simplify the plant dynamics (21) as

$$\begin{cases} \dot{x}_1 = e_a(x_2 - x_1) - k_1 x_1 \\ \dot{x}_2 = -e_c x_1 x_3 + e_p x_3^2 - k_2 x_2 \\ \dot{x}_3 = -e_b - k_3 x_3 \\ \dot{x}_4 = -e_q(x_1 + x_2) - k_4 x_4 \end{cases} \tag{23}$$

Differentiating (22) with respect to t, we obtain

$$\begin{cases} \dot{e}_a(t) = -\dot{\hat{a}}(t) \\ \dot{e}_b(t) = -\dot{\hat{b}}(t) \\ \dot{e}_c(t) = -\dot{\hat{c}}(t) \\ \dot{e}_p(t) = -\dot{\hat{p}}(t) \\ \dot{e}_q(t) = -\dot{\hat{q}}(t) \end{cases} \tag{24}$$

We consider the quadratic candidate Lyapunov function defined by

$$V(\mathbf{x}, e_a, e_b, e_c, e_p, e_q) = \frac{1}{2}\left(x_1^2 + x_2^2 + x_3^2 + x_4^2\right) + \frac{1}{2}\left(e_a^2 + e_b^2 + e_c^2 + e_p^2 + e_q^2\right) \tag{25}$$

Differentiating V along the trajectories of (23) and (24), we obtain

$$\begin{aligned} \dot{V} = -k_1 x_1^2 - k_2 x_2^2 - k_3 x_3^2 - k_4 x_4^2 + e_a\left[x_1(x_2 - x_1) - \dot{\hat{a}}\right] + e_b\left[-x_3 - \dot{\hat{b}}\right] \\ + e_c\left[-x_1 x_2 x_3 - \dot{\hat{c}}\right] + e_p\left[x_2 x_3^2 - \dot{\hat{p}}\right] + e_q\left[-x_4(x_1 + x_2) - \dot{\hat{q}}\right] \end{aligned} \tag{26}$$

In view of (26), we take the parameter update law as

$$\begin{cases} \dot{\hat{a}}(t) = x_1(x_2 - x_1) \\ \dot{\hat{b}}(t) = -x_3 \\ \dot{\hat{c}}(t) = -x_1x_2x_3 \\ \dot{\hat{p}}(t) = x_2x_3^2 \\ \dot{\hat{q}}(t) = -x_4(x_1 + x_2) \end{cases} \tag{27}$$

Next, we state and prove the main result of this section.

Theorem 1 *The novel 4-D highly hyperchaotic system (19) with unknown system parameters is globally and exponentially stabilized for all initial conditions by the adaptive control law (20) and the parameter update law (27), where k_1, k_2, k_3, k_4 are positive gain constants.*

Proof We prove this result by applying Lyapunov stability theory [27].

We consider the quadratic Lyapunov function defined by (25), which is clearly a positive definite function on $\mathbf{R}^9$.

By substituting the parameter update law (27) into (26), we obtain the time-derivative of V as

$$\dot{V} = -k_1x_1^2 - k_2x_2^2 - k_3x_3^2 - k_4x_4^2 \tag{28}$$

From (28), it is clear that $\dot{V}$ is a negative semi-definite function on $\mathbf{R}^9$.

Thus, we can conclude that the state vector $\mathbf{x}(t)$ and the parameter estimation error are globally bounded, i.e.

$$\left[x_1(t)\ x_2(t)\ x_3(t)\ x_4(t)\ e_a(t)\ e_b(t)\ e_c(t)\ e_p(t)\ e_q(t) \right]^T \in \mathbf{L}_\infty.$$

We define $k = \min\{k_1, k_2, k_3, k_4\}$.

Then it follows from (28) that

$$\dot{V} \leq -k\|\mathbf{x}(t)\|^2 \tag{29}$$

Thus, we have

$$k\|\mathbf{x}(t)\|^2 \leq -\dot{V} \tag{30}$$

Integrating the inequality (30) from 0 to t, we get

$$k\int_0^t \|\mathbf{x}(\tau)\|^2\, d\tau \ \leq\ V(0) - V(t) \tag{31}$$

From (31), it follows that $\mathbf{x} \in \mathbf{L}_2$.

Using (23), we can conclude that $\dot{\mathbf{x}} \in \mathbf{L}_\infty$.

Using Barbalat's lemma [27], we conclude that $\mathbf{x}(t) \to 0$ exponentially as $t \to \infty$ for all initial conditions $\mathbf{x}(0) \in \mathbf{R}^4$.

Thus, the novel 4-D highly hyperchaotic system (19) with unknown system parameters is globally and exponentially stabilized for all initial conditions by the adaptive control law (20) and the parameter update law (27).

This completes the proof. ■

For the numerical simulations, the classical fourth-order Runge–Kutta method with step size $h = 10^{-8}$ is used to solve the systems (19) and (27), when the adaptive control law (20) is applied.

The parameter values of the novel 4-D hyperchaotic system (19) are taken as in the hyperchaotic case (2), i.e.

$$a = 62, \quad b = 36, \quad c = 160, \quad p = 0.5, \quad q = 2.8 \tag{32}$$

We take the positive gain constants as

$$k_1 = 8, \quad k_2 = 8, \quad k_3 = 8, \quad k_4 = 8 \tag{33}$$

Furthermore, as initial conditions of the novel 4-D highly hyperchaotic system (19), we take

$$x_1(0) = 18.5, \quad x_2(0) = -14.7, \quad x_3(0) = 24.8, \quad x_4(0) = -12.3 \tag{34}$$

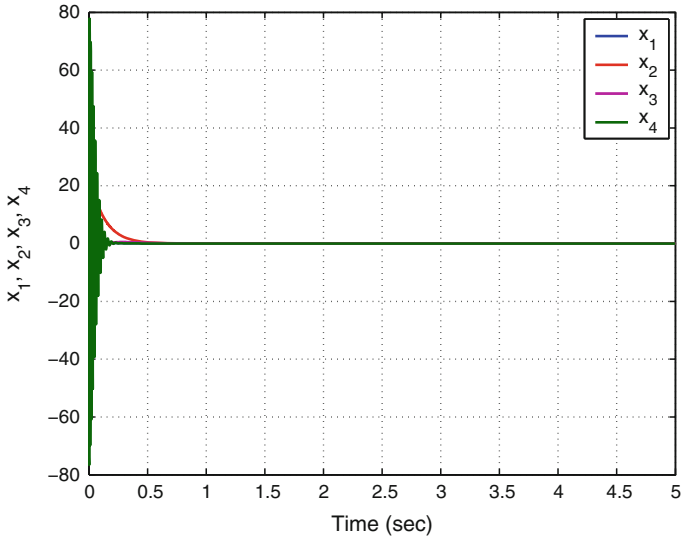

Fig. 5 Time-history of the controlled states x_1, x_2, x_3, x_4

Also, as initial conditions of the parameter estimates, we take

$$\hat{a}(0) = 15.6, \quad \hat{b}(0) = 12.4, \quad \hat{c}(0) = 22.7, \quad \hat{p}(0) = 4.8, \quad \hat{q}(0) = 19.4 \tag{35}$$

In Fig. 5, the exponential convergence of the controlled states of the novel 4-D hyperchaotic system (19) is shown.

5 Adaptive Synchronization of the Identical Novel Hyperchaotic Systems

In this section, we use adaptive control method to derive an adaptive feedback control law for globally synchronizing identical novel 4-D highly hyperchaotic systems with unknown parameters.

As the master system, we consider the novel 4-D hyperchaotic system given by

$$\begin{cases} \dot{x}_1 = a(x_2 - x_1) + x_2 x_3 + x_4 \\ \dot{x}_2 = -c x_1 x_3 + 3x_2 + p x_3^2 \\ \dot{x}_3 = x_1 x_2 - b \\ \dot{x}_4 = -q(x_1 + x_2) \end{cases} \tag{36}$$

In (36), x_1, x_2, x_3, x_4 are the states and a, b, c, p, q are unknown system parameters.

As the slave system, we consider the 4-D novel hyperchaotic system given by

$$\begin{cases} \dot{y}_1 = a(y_2 - y_1) + y_2 y_3 + y_4 + u_1 \\ \dot{y}_2 = -c y_1 y_3 + 3y_2 + p y_3^2 \\ \dot{y}_3 = y_1 y_2 - b + u_3 \\ \dot{y}_4 = -q(y_1 + y_2) + u_4 \end{cases} \tag{37}$$

In (37), y_1, y_2, y_3, y_4 are the states and u_1, u_2, u_3, u_4 are the adaptive controls to be determined using estimates $\hat{a}(t), \hat{c}(t), \hat{p}(t), \hat{q}(t)$ for the unknown parameters a, c, p, q, respectively.

The synchronization error between the novel hyperchaotic systems (36) and (37) is defined by

$$\begin{cases} e_1 = y_1 - x_1 \\ e_2 = y_2 - x_2 \\ e_3 = y_3 - x_3 \\ e_4 = y_4 - x_4 \end{cases} \tag{38}$$

Then the error dynamics is obtained as

$$\begin{cases} \dot{e}_1 = a(e_2 - e_1) + e_4 + y_2y_3 - x_2x_3 + u_1 \\ \dot{e}_2 = 3e_2 - c(y_1y_3 - x_1x_3) + p(y_3^2 - x_3^2) + u_2 \\ \dot{e}_3 = y_1y_2 - x_1x_2 + u_3 \\ \dot{e}_4 = -q(e_1 + e_2) + u_4 \end{cases} \tag{39}$$

We consider the adaptive feedback control law

$$\begin{cases} u_1 = -\hat{a}(t)(e_2 - e_1) - e_4 - y_2y_3 + x_2x_3 - k_1e_1 \\ u_2 = -3e_2 + \hat{c}(t)(y_1y_3 - x_1x_3) - \hat{p}(t)(y_3^2 - x_3^2) - k_2e_2 \\ u_3 = -y_1y_2 + x_1x_2 - k_3e_3 \\ u_4 = \hat{q}(t)(e_1 + e_2) - k_4e_4 \end{cases} \tag{40}$$

where k_1, k_2, k_3, k_4 are positive gain constants.

Substituting (40) into (39), we get the closed-loop error dynamics as

$$\begin{cases} \dot{e}_1 = \left[a - \hat{a}(t)\right](e_2 - e_1) - k_1e_1 \\ \dot{e}_2 = -\left[c - \hat{c}(t)\right](y_1y_3 - x_1x_3) + \left[p - \hat{p}(t)\right](y_3^2 - x_3^2) - k_2e_2 \\ \dot{e}_3 = -k_3e_3 \\ \dot{e}_4 = -\left[q - \hat{q}(t)\right](e_1 + e_2) - k_4e_4 \end{cases} \tag{41}$$

The parameter estimation errors are defined as

$$\begin{cases} e_a(t) = a - \hat{a}(t) \\ e_c(t) = c - \hat{c}(t) \\ e_p(t) = p - \hat{p}(t) \\ e_q(t) = q - \hat{q}(t) \end{cases} \tag{42}$$

In view of (42), we can simplify the error dynamics (41) as

$$\begin{cases} \dot{e}_1 = e_a(e_2 - e_1) - k_1e_1 \\ \dot{e}_2 = -e_c(y_1y_3 - x_1x_3) + e_p(y_3^2 - x_3^2) - k_2e_2 \\ \dot{e}_3 = -k_3e_3 \\ \dot{e}_4 = -e_q(e_1 + e_2) - k_4e_4 \end{cases} \tag{43}$$

Differentiating (42) with respect to t, we obtain

$$\begin{cases} \dot{e}_a(t) = -\dot{\hat{a}}(t) \\ \dot{e}_c(t) = -\dot{\hat{c}}(t) \\ \dot{e}_p(t) = -\dot{\hat{p}}(t) \\ \dot{e}_q(t) = -\dot{\hat{q}}(t) \end{cases} \tag{44}$$

We use adaptive control theory to find an update law for the parameter estimates.

We consider the quadratic candidate Lyapunov function defined by

$$V(\mathbf{e}, e_a, e_c, e_p, e_q) = \frac{1}{2}\left(e_1^2 + e_2^2 + e_3^2 + e_4^2\right) + \frac{1}{2}\left(e_a^2 + e_c^2 + e_p^2 + e_q^2\right) \tag{45}$$

Differentiating V along the trajectories of (43) and (44), we obtain

$$\begin{aligned}\dot{V} = &-k_1 e_1^2 - k_2 e_2^2 - k_3 e_3^2 - k_4 e_4^2 + e_a\left[e_1(e_2 - e_1) - \dot{\hat{a}}\right] \\ &+ e_c\left[-e_2(y_1 y_3 - x_1 x_3) - \dot{\hat{c}}\right] + e_p\left[e_2(y_3^2 - x_3^2) - \dot{\hat{p}}\right] \\ &+ e_q\left[-e_4(e_1 + e_2) - \dot{\hat{q}}\right]\end{aligned} \tag{46}$$

In view of (46), we take the parameter update law as

$$\begin{cases}\dot{\hat{a}}(t) = e_1(e_2 - e_1) \\ \dot{\hat{c}}(t) = -e_2(y_1 y_3 - x_1 x_3) \\ \dot{\hat{p}}(t) = e_2(y_3^2 - x_3^2) \\ \dot{\hat{q}}(t) = -e_4(e_1 + e_2)\end{cases} \tag{47}$$

Next, we state and prove the main result of this section.

Theorem 2 *The novel hyperchaotic systems (36) and (37) with unknown system parameters are globally and exponentially synchronized for all initial conditions by the adaptive control law (40) and the parameter update law (47), where k_1, k_2, k_3, k_4 are positive gain constants.*

Proof We prove this result by applying Lyapunov stability theory [27].

We consider the quadratic Lyapunov function defined by (45), which is clearly a positive definite function on $\mathbf{R}^8$.

By substituting the parameter update law (47) into (46), we obtain

$$\dot{V} = -k_1 e_1^2 - k_2 e_2^2 - k_3 e_3^2 - k_4 e_4^2 \tag{48}$$

From (48), it is clear that $\dot{V}$ is a negative semi-definite function on $\mathbf{R}^8$.

Thus, we can conclude that the error vector $\mathbf{e}(t)$ and the parameter estimation error are globally bounded, i.e.

$$\left[e_1(t)\ e_2(t)\ e_3(t)\ e_4(t)\ e_a(t)\ e_c(t)\ e_p(t)\ e_q(t)\right]^T \in \mathbf{L}_\infty. \tag{49}$$

We define $k = \min\{k_1, k_2, k_3, k_4\}$.

Then it follows from (48) that

$$\dot{V} \leq -k\|\mathbf{e}(t)\|^2 \tag{50}$$

Thus, we have

$$k\|\mathbf{e}(t)\|^2 \leq -\dot{V} \tag{51}$$

Integrating the inequality (51) from 0 to t, we get

$$k\int_0^t \|\mathbf{e}(\tau)\|^2\, d\tau \;\leq\; V(0) - V(t) \tag{52}$$

From (52), it follows that $\mathbf{e} \in \mathbf{L}_2$.

Using (43), we can conclude that $\dot{\mathbf{e}} \in \mathbf{L}_\infty$.

Using Barbalat's lemma [27], we conclude that $\mathbf{e}(t) \to 0$ exponentially as $t \to \infty$ for all initial conditions $\mathbf{e}(0) \in \mathbf{R}^4$.

This completes the proof. ■

For the numerical simulations, the classical fourth-order Runge–Kutta method with step size $h = 10^{-8}$ is used to solve the systems (36), (37) and (47), when the adaptive control law (40) is applied.

The parameter values of the novel hyperchaotic systems are taken as in the hyperchaotic case (2), i.e.

$$a = 62, \quad b = 36, \quad c = 160, \quad p = 0.5, \quad q = 2.8 \tag{53}$$

We take the positive gain constants as

$$k_1 = 8, \quad k_2 = 8, \quad k_3 = 8, \quad k_4 = 8 \tag{54}$$

Furthermore, as initial conditions of the master system (36), we take

$$x_1(0) = 12.3, \quad x_2(0) = 6.4, \quad x_3(0) = -9.7, \quad x_4(0) = -22.8 \tag{55}$$

As initial conditions of the slave system (37), we take

$$y_1(0) = 5.1, \quad y_2(0) = -18.5, \quad y_3(0) = 24.8, \quad y_4(0) = 3.7 \tag{56}$$

Also, as initial conditions of the parameter estimates, we take

$$\hat{a}(0) = 12.6, \quad \hat{c}(0) = 5.4, \quad \hat{p}(0) = 17.9, \quad \hat{q}(0) = 25.8 \tag{57}$$

Figures 6, 7, 8 and 9 describe the complete synchronization of the novel hyperchaotic systems (36) and (37), while Fig. 10 describes the time-history of the synchronization errors e_1, e_2, e_3, e_4.

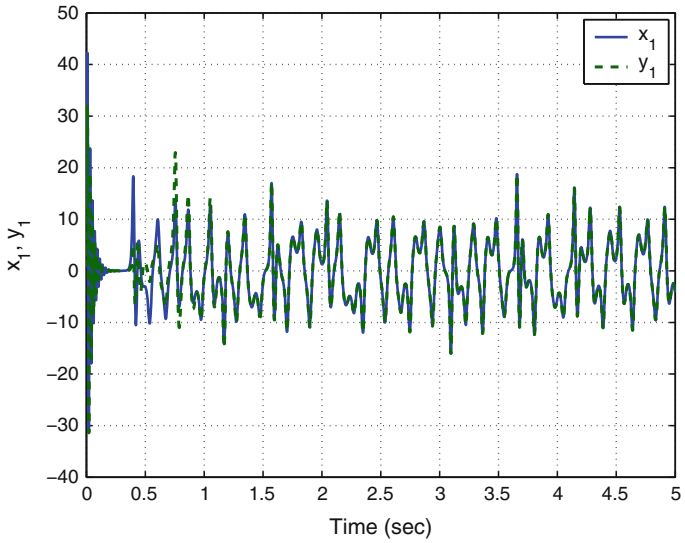

Fig. 6 Synchronization of the states x_1 and y_1

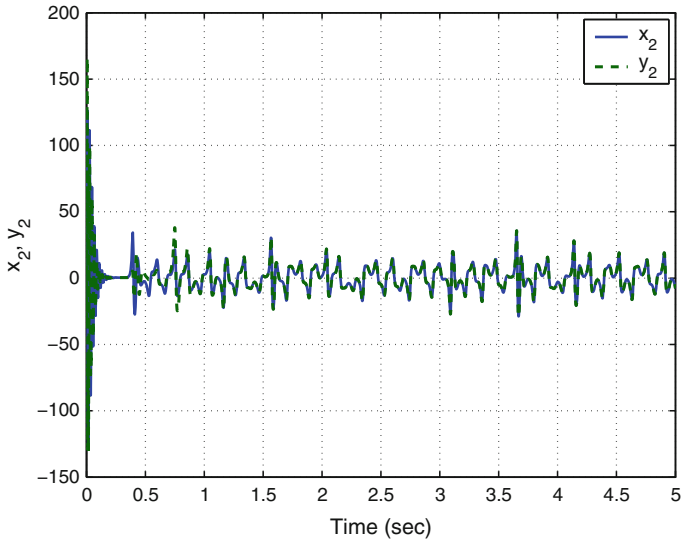

Fig. 7 Synchronization of the states x_2 and y_2

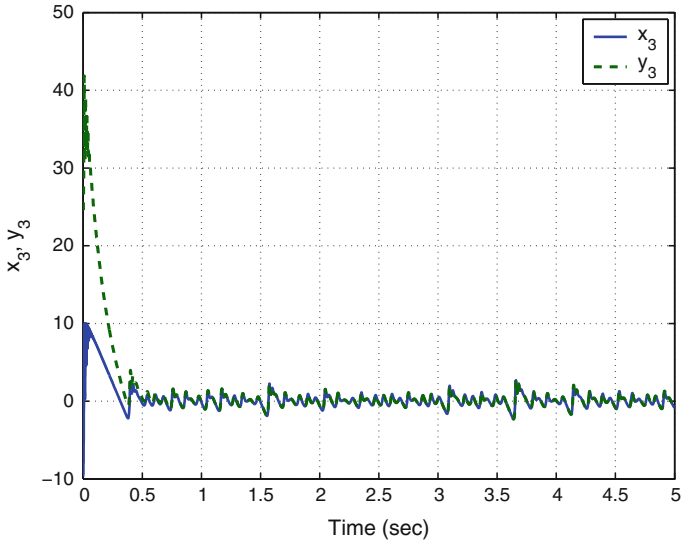

Fig. 8 Synchronization of the states x_3 and y_3

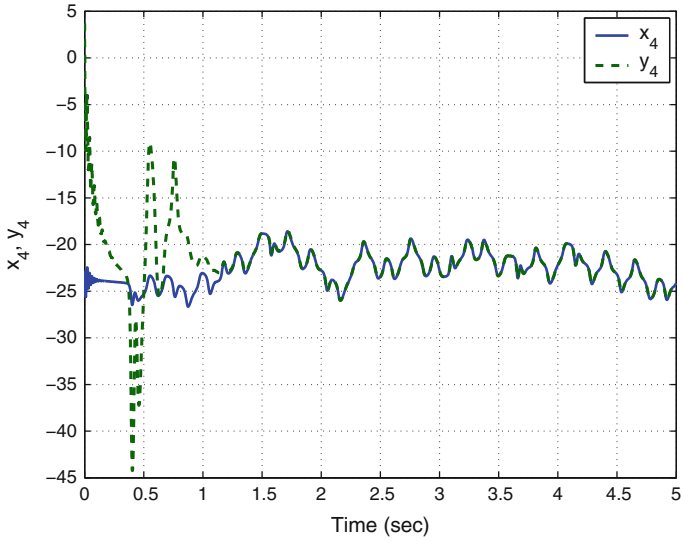

Fig. 9 Synchronization of the states x_4 and y_4

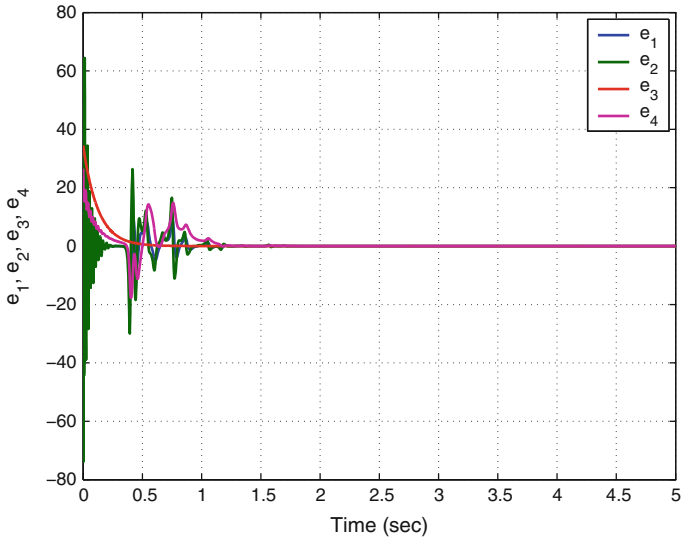

Fig. 10 Time-history of the synchronization errors e_1, e_2, e_3, e_4

6 Conclusions

In this work, we described an eleven-term novel 4-D highly hyperchaotic system with four quadratic nonlinearities. The qualitative properties of the novel highly hyperchaotic system were discussed in detail. We showed that the novel hyperchaotic system does not have any equilibrium point. Hence, the novel 4-D hyperchaotic system exhibits hidden attractors. The Lyapunov exponents of the novel hyperchaotic system have been obtained as $L_1 = 15.06593, L_2 = 0.03551, L_3 = 0$ and $L_4 = -42.42821$. The Maximal Lyapunov Exponent (MLE) of the novel hyperchaotic system is found as $L_1 = 15.06593$, which is large. Thus, the novel 4-D hyperchaotic system proposed in this work is highly hyperchaotic. Also, the Kaplan–Yorke dimension of the novel hyperchaotic system has been derived as $D_{KY} = 3.3559$. Since the sum of the Lyapunov exponents is negative, the novel hyperchaotic system is dissipative. Next, an adaptive controller was designed to globally stabilize the novel highly hyperchaotic system with unknown parameters. Finally, an adaptive controller was also designed to achieve global chaos synchronization of the identical novel highly hyperchaotic systems with unknown parameters. MATLAB simulations were shown to illustrate all the main results derived in this work.

References

1. Arneodo A, Coullet P, Tresser C (1981) Possible new strange attractors with spiral structure. Commun Math Phys 79(4):573–576
2. Azar AT (2010) Fuzzy systems. IN-TECH, Vienna, Austria
3. Azar AT (2012) Overview of type-2 fuzzy logic systems. Int J Fuzzy Syst Appl 2(4):1–28
4. Azar AT, Serrano FE (2014) Robust IMC-PID tuning for cascade control systems with gain and phase margin specifications. Neural Comput Appl 25(5):983–995
5. Azar AT, Serrano FE (2015) Adaptive sliding mode control of the Furuta pendulum. In: Azar AT, Zhu Q (eds) Advances and applications in sliding mode control systems. Studies in computational intelligence, vol 576. Springer, Germany, pp 1–42
6. Azar AT, Serrano FE (2015) Deadbeat control for multivariable systems with time varying delays. In: Azar AT, Vaidyanathan S (eds) Chaos modeling and control systems design. Studies in computational intelligence, vol 581. Springer, Germany, pp 97–132
7. Azar AT, Serrano FE (2015) Design and modeling of anti wind up PID controllers. In: Zhu Q, Azar AT (eds) Complex system modelling and control through intelligent soft computations. Studies in fuzziness and soft computing, vol 319. Springer, Germany, pp 1–44
8. Azar AT, Serrano FE (2015) Stabilizatoin and control of mechanical systems with backlash. In: Azar AT, Vaidyanathan S (eds) Handbook of research on advanced intelligent control engineering and automation. Advances in computational intelligence and robotics (ACIR), IGI-Global, USA, pp 1–60
9. Azar AT, Vaidyanathan S (2015) Chaos modeling and control systems design, Studies in computational intelligence, vol 581. Springer, Germany
10. Azar AT, Vaidyanathan S (2015) Computational intelligence applications in modeling and control. Studies in computational intelligence, vol 575. Springer, Germany
11. Azar AT, Vaidyanathan S (2015) Handbook of research on advanced intelligent control engineering and automation. Advances in computational intelligence and robotics (ACIR), IGI-Global, USA
12. Azar AT, Zhu Q (2015) Advances and applications in sliding mode control systems. Studies in computational intelligence, vol 576. Springer, Germany
13. Cai G, Tan Z (2007) Chaos synchronization of a new chaotic system via nonlinear control. J Uncertain Syst 1(3):235–240
14. Chen A, Lu J, Lü J, Yu S (2006) Generating hyperchaotic Lü attractor via state feedback control. Phys A 364:103–110
15. Chen G, Ueta T (1999) Yet another chaotic attractor. Int J Bifurc Chaos 9(7):1465–1466
16. Das S, Goswami D, Chatterjee S, Mukherjee S (2014) Stability and chaos analysis of a novel swarm dynamics with applications to multi-agent systems. Eng Appl Artif Intell 30:189–198
17. Feki M (2003) An adaptive chaos synchronization scheme applied to secure communication. Chaos Solitons Fractals 18(1):141–148
18. Filali RL, Benrejeb M, Borne P (2014) On observer-based secure communication design using discrete-time hyperchaotic systems. Commun Nonlinear Sci Numer Simul 19(5):1424–1432
19. Gaspard P (1999) Microscopic chaos and chemical reactions. Phys A 263(1–4):315–328
20. Gibson WT, Wilson WG (2013) Individual-based chaos: Extensions of the discrete logistic model. J Theor Biol 339:84–92
21. Hammami S (2015) State feedback-based secure image cryptosystem using hyperchaotic synchronization. ISA Trans 54:52–59
22. Huang X, Zhao Z, Wang Z, Li Y (2012) Chaos and hyperchaos in fractional-order cellular neural networks. Neurocomputing 94:13–21
23. Jia Q (2007) Hyperchaos generated from the Lorenz chaotic system and its control. Phys Lett A 366:217–222
24. Karthikeyan R, Sundarapandian V (2014) Hybrid chaos synchronization of four-scroll systems via active control. J Electr Eng 65(2):97–103
25. Kaslik E, Sivasundaram S (2012) Nonlinear dynamics and chaos in fractional-order neural networks. Neural Netw 32:245–256

26. Kengne J, Chedjou JC, Kenne G, Kyamakya K (2012) Dynamical properties and chaos synchronization of improved Colpitts oscillators. Commun Nonlinear Sci Numer Simul 17(7):2914–2923
27. Khalil HK (2001) Nonlinear Systems, 3rd edn. Prentice Hall, New Jersey
28. Kyriazis M (1991) Applications of chaos theory to the molecular biology of aging. Exp Gerontol 26(6):569–572
29. Lang J (2015) Color image encryption based on color blend and chaos permutation in the reality-preserving multiple-parameter fractional Fourier transform domain. Opt Commun 338:181–192
30. Li C, Liao X, Wong KW (2005) Lag synchronization of hyperchaos with application to secure communications. Chaos Solitons Fractals 23(1):183–193
31. Li D (2008) A three-scroll chaotic attractor. Phys Lett A 372(4):387–393
32. Li X (2009) Modified projective synchronization of a new hyperchaotic system via nonlinear control. Commun Theor Phys 52:274–278
33. Li Z, Chen G (2006) Integration of fuzzy logic and chaos theory. Studies in fuzziness and soft computing, vol 187. Springer, Germany
34. Lian S, Chen X (2011) Traceable content protection based on chaos and neural networks. Appl Soft Comput 11(7):4293–4301
35. Lorenz EN (1963) Deterministic periodic flow. J Atmos Sci 20(2):130–141
36. Lü J, Chen G (2002) A new chaotic attractor coined. Int J Bifurc Chaos 12(3):659–661
37. Mondal S, Mahanta C (2014) Adaptive second order terminal sliding mode controller for robotic manipulators. J Franklin Inst 351(4):2356–2377
38. Murali K, Lakshmanan M (1998) Secure communication using a compound signal from generalized chaotic systems. Phys Lett A 241(6):303–310
39. Nehmzow U, Walker K (2005) Quantitative description of robot-environment interaction using chaos theory. Robot Auton Syst 53(3–4):177–193
40. Pehlivan I, Moroz IM, Vaidyanathan S (2014) Analysis, synchronization and circuit design of a novel butterfly attractor. J Sound Vib 333(20):5077–5096
41. Petrov V, Gaspar V, Masere J, Showalter K (1993) Controlling chaos in Belousov-Zhabotinsky reaction. Nature 361:240–243
42. Pham VT, Volos C, Jafari S, Wang X, Vaidyanathan S (2014) Hidden hyperchaotic attractor in a novel simple memristive neural network. Optoelectr Adv Mater Rapid Commun 8(11–12):1157–1163
43. Pham VT, Vaidyanathan S, Volos CK, Jafari S (2015a) Hidden attractors in a chaotic system with an exponential nonlinear term. Eur Phys J - Spec Top 224(8):1507–1517
44. Pham VT, Volos CK, Vaidyanathan S, Le TP, Vu VY (2015b) A memristor-based hyperchaotic system with hidden attractors: Dynamics, synchronization and circuital emulating. J Eng Sci Technol Rev 8(2):205–214
45. Qu Z (2011) Chaos in the genesis and maintenance of cardiac arrhythmias. Prog Biophys Mol Biol 105(3):247–257
46. Rasappan S, Vaidyanathan S (2013) Hybrid synchronization of n-scroll Chua circuits using adaptive backstepping control design with recursive feedback. Malays J Math Sci 73(1):73–95
47. Rasappan S, Vaidyanathan S (2014) Global chaos synchronization of WINDMI and Coullet chaotic systems using adaptive backstepping control design. Kyungpook Math J 54(1):293–320
48. Rhouma R, Belghith S (2008) Cryptanalysis of a new image encryption algorithm based on hyper-chaos. Phys Lett A 372(38):5973–5978
49. Rhouma R, Belghith S (2011) Cryptoanalysis of a chaos based cryptosystem on DSP. Commun Nonlinear Sci Numer Simul 16(2):876–884
50. Rössler OE (1976) An equation for continuous chaos. Phys Lett A 57(5):397–398
51. Rössler OE (1979) An equation for hyperchaos. Phys Lett A 71:155–157
52. Vaidyanathan S, Pham VT, Volos CK (2015) A 5-D hyperchaotic Rikitake dynamo system with hidden attractors. Eur Phys J: Spec Top 224(8):1575–1592

53. Sampath S, Vaidyanathan S, Volos CK, Pham VT (2015) An eight-term novel four-scroll chaotic system with cubic nonlinearity and its circuit simulation. J Eng Sci Technol Rev 8(2):1–6
54. Sarasu P, Sundarapandian V (2011a) Active controller design for generalized projective synchronization of four-scroll chaotic systems. Int J Syst Signal Control Eng Appl 4(2):26–33
55. Sarasu P, Sundarapandian V (2011b) The generalized projective synchronization of hyperchaotic Lorenz and hyperchaotic Qi systems via active control. Int J Soft Comput 6(5):216–223
56. Sarasu P, Sundarapandian V (2012) Generalized projective synchronization of two-scroll systems via adaptive control. Int J Soft Comput 7(4):146–156
57. Senouci A, Boukabou A (2014) Predictive control and synchronization of chaotic and hyperchaotic systems based on a $T - S$ fuzzy model. Math Comput Simul 105:62–78
58. Sharma A, Patidar V, Purohit G, Sud KK (2012) Effects on the bifurcation and chaos in forced Duffing oscillator due to nonlinear damping. Commun Nonlinear Sci Numer Simul 17(6):2254–2269
59. Sprott JC (1994) Some simple chaotic flows. Phys Rev E 50(2):647–650
60. Suérez I (1999) Mastering chaos in ecology. Ecol Model 117(2–3):305–314
61. Sundarapandian V (2010) Output regulation of the Lorenz attractor. Far East J Math Sci 42(2):289–299
62. Sundarapandian V (2013a) Adaptive control and synchronization design for the Lu-Xiao chaotic system. Lect Notes Electr Eng 131:319–327
63. Sundarapandian V (2013b) Analysis and anti-synchronization of a novel chaotic system via active and adaptive controllers. J Eng Sci Technol Rev 6(4):45–52
64. Sundarapandian V, Karthikeyan R (2011a) Anti-synchronization of hyperchaotic Lorenz and hyperchaotic Chen systems by adaptive control. Int J Syst Signal Control Eng Appl 4(2):18–25
65. Sundarapandian V, Karthikeyan R (2011b) Anti-synchronization of Lü and Pan chaotic systems by adaptive nonlinear control. Eur J Sci Res 64(1):94–106
66. Sundarapandian V, Karthikeyan R (2012) Adaptive anti-synchronization of uncertain Tigan and Li systems. J Eng Appl Sci 7(1):45–52
67. Sundarapandian V, Pehlivan I (2012) Analysis, control, synchronization, and circuit design of a novel chaotic system. Math Comput Model 55(7–8):1904–1915
68. Sundarapandian V, Sivaperumal S (2011) Sliding controller design of hybrid synchronization of four-wing chaotic systems. Int J Soft Comput 6(5):224–231
69. Suresh R, Sundarapandian V (2013) Global chaos synchronization of a family of n-scroll hyperchaotic Chua circuits using backstepping control with recursive feedback. Far East J Math Sci 7(2):219–246
70. Tigan G, Opris D (2008) Analysis of a 3D chaotic system. Chaos Solitons Fractals 36:1315–1319
71. Usama M, Khan MK, Alghatbar K, Lee C (2010) Chaos-based secure satellite imagery cryptosystem. Comput Math Appl 60(2):326–337
72. Vaidyanathan S (2011a) Output regulation of Arneodo-Coullet chaotic system. Commun Comput Inf Sci 133:98–107
73. Vaidyanathan S (2011b) Output regulation of the unified chaotic system. Commun Comput Inf Sci 198:1–9
74. Vaidyanathan S (2012a) Adaptive controller and syncrhonizer design for the Qi-Chen chaotic system. Lect Notes Inst Comput Sci, Soc-Inf Telecommun Eng 84:73–82
75. Vaidyanathan S (2012b) Anti-synchronization of Sprott-L and Sprott-M chaotic systems via adaptive control. Int J Control Theory Appl 5(1):41–59
76. Vaidyanathan S (2012c) Global chaos control of hyperchaotic Liu system via sliding control method. Int J Control Theory Appl 5(2):117–123
77. Vaidyanathan S (2012d) Sliding mode control based global chaos control of Liu-Liu-Liu-Su chaotic system. Int J Control Theory Appl 5(1):15–20
78. Vaidyanathan S (2013a) A new six-term 3-D chaotic system with an exponential nonlinearity. Far East J Math Sci 79(1):135–143

79. Vaidyanathan S (2013b) A ten-term novel 4-D hyperchaotic system with three quadratic nonlinearities and its control. Int J Control Theory Appl 6(2):97–109
80. Vaidyanathan S (2013c) Analysis and adaptive synchronization of two novel chaotic systems with hyperbolic sinusoidal and cosinusoidal nonlinearity and unknown parameters. J Eng Sci Technol Rev 6(4):53–65
81. Vaidyanathan S (2013d) Analysis, control and synchronization of hyperchaotic Zhou system via adaptive control. Adv Intell Syst Comput 177:1–10
82. Vaidyanathan S (2014a) A new eight-term 3-D polynomial chaotic system with three quadratic nonlinearities. Far East J Math Sci 84(2):219–226
83. Vaidyanathan S (2014b) Analysis and adaptive synchronization of eight-term 3-D polynomial chaotic systems with three quadratic nonlinearities. Eur Phys J: Spec Top 223(8):1519–1529
84. Vaidyanathan S (2014c) Analysis, control and synchronisation of a six-term novel chaotic system with three quadratic nonlinearities. Int J Model Ident Control 22(1):41–53
85. Vaidyanathan S (2014d) Generalized projective synchronisation of novel 3-D chaotic systems with an exponential non-linearity via active and adaptive control. Int J Model Ident Control 22(3):207–217
86. Vaidyanathan S (2014e) Global chaos synchronisation of identical Li-Wu chaotic systems via sliding mode control. Int J Model Ident Control 22(2):170–177
87. Vaidyanathan S (2014f) Qualitative analysis and control of an eleven-term novel 4-D hyperchaotic system with two quadratic nonlinearities. Int J Control Theory Appl 7:35–47
88. Vaidyanathan S (2015a) 3-cells cellular neural network (CNN) attractor and its adaptive biological control. Int J PharmTech Res 8(4):632–640
89. Vaidyanathan S (2015b) A 3-D novel highly chaotic system with four quadratic nonlinearities, its adaptive control and anti-synchronization with unknown parameters. J Eng Sci Technol Rev 8(2):106–115
90. Vaidyanathan S (2015c) Adaptive backstepping control of enzymes-substrates system with ferroelectric behaviour in brain waves. Int J PharmTech Res 8(2):256–261
91. Vaidyanathan S (2015d) Adaptive biological control of generalized Lotka-Volterra three-species biological system. Int J PharmTech Res 8(4):622–631
92. Vaidyanathan S (2015e) Adaptive chaotic synchronization of enzymes-substrates system with ferroelectric behaviour in brain waves. Int J PharmTech Res 8(5):964–973
93. Vaidyanathan S (2015f) Adaptive control of a chemical chaotic reactor. Int J PharmTech Res 8(3):377–382
94. Vaidyanathan S (2015g) Adaptive synchronization of chemical chaotic reactors. Int J ChemTech Res 8(2):612–621
95. Vaidyanathan S (2015h) Adaptive synchronization of generalized Lotka-Volterra three-species biological systems. Int J PharmTech Res 8(5):928–937
96. Vaidyanathan S (2015i) Analysis, properties and control of an eight-term 3-D chaotic system with an exponential nonlinearity. Int J Model Ident Control 23(2):164–172
97. Vaidyanathan S (2015j) Anti-synchronization of Brusselator chemical reaction systems via adaptive control. Int J ChemTech Res 8(6):759–768
98. Vaidyanathan S (2015k) Chaos in neurons and adaptive control of Birkhoff-Shaw strange chaotic attractor. Int J PharmTech Res 8(5):956–963
99. Vaidyanathan S (2015l) Dynamics and control of Brusselator chemical reaction. Int J ChemTech Res 8(6):740–749
100. Vaidyanathan S (2015m) Dynamics and control of Tokamak system with symmetric and magnetically confined plasma. Int J ChemTech Res 8(6):795–803
101. Vaidyanathan S (2015n) Hyperchaos, qualitative analysis, control and synchronisation of a ten-term 4-D hyperchaotic system with an exponential nonlinearity and three quadratic nonlinearities. Int J Model Ident Control 23(4):380–392
102. Vaidyanathan S (2015o) Lotka-Volterra population biology models with negative feedback and their ecological monitoring. Int J PharmTech Res 8(5):974–981
103. Vaidyanathan S (2015p) Synchronization of 3-cells cellular neural network (CNN) attractors via adaptive control method. Int J PharmTech Res 8(5):946–955

104. Vaidyanathan S (2015q) Synchronization of Tokamak systems with symmetric and magnetically confined plasma via adaptive control. Int J ChemTech Res 8(6):818–827
105. Vaidyanathan S, Azar AT (2015a) Analysis and control of a 4-D novel hyperchaotic system. Stud Comput Intell 581:3–17
106. Vaidyanathan S, Azar AT (2015b) Analysis, control and synchronization of a nine-term 3-D novel chaotic system. In: Azar AT, Vaidyanathan S (eds) Chaos modelling and control systems design. Studies in computational intelligence, vol 581. Springer, Germany, pp 19–38
107. Vaidyanathan S, Madhavan K (2013) Analysis, adaptive control and synchronization of a seven-term novel 3-D chaotic system. Int J Control Theory Appl 6(2):121–137
108. Vaidyanathan S, Pakiriswamy S (2013) Generalized projective synchronization of six-term Sundarapandian chaotic systems by adaptive control. Int J Control Theory Appl 6(2):153–163
109. Vaidyanathan S, Pakiriswamy S (2015) A 3-D novel conservative chaotic system and its generalized projective synchronization via adaptive control. J Eng Sci Technol Rev 8(2):52–60
110. Vaidyanathan S, Rajagopal K (2011) Hybrid synchronization of hyperchaotic Wang-Chen and hyperchaotic Lorenz systems by active non-linear control. Int J Syst Signal Control Eng Appl 4(3):55–61
111. Vaidyanathan S, Rajagopal K (2012) Global chaos synchronization of hyperchaotic Pang and hyperchaotic Wang systems via adaptive control. Int J Soft Comput 7(1):28–37
112. Vaidyanathan S, Rasappan S (2011) Global chaos synchronization of hyperchaotic Bao and Xu systems by active nonlinear control. Commun Comput Inf Sci 198:10–17
113. Vaidyanathan S, Rasappan S (2014) Global chaos synchronization of n-scroll Chua circuit and Lur'e system using backstepping control design with recursive feedback. Arab J Sci Eng 39(4):3351–3364
114. Vaidyanathan S, Sampath S (2012) Anti-synchronization of four-wing chaotic systems via sliding mode control. Int J Autom Comput 9(3):274–279
115. Vaidyanathan S, Volos C (2015) Analysis and adaptive control of a novel 3-D conservative no-equilibrium chaotic system. Arch Control Sci 25(3):333–353
116. Vaidyanathan S, Volos C, Pham VT (2014a) Hyperchaos, adaptive control and synchronization of a novel 5-D hyperchaotic system with three positive Lyapunov exponents and its SPICE implementation. Arch Control Sci 24(4):409–446
117. Vaidyanathan S, Volos C, Pham VT, Madhavan K, Idowu BA (2014b) Adaptive backstepping control, synchronization and circuit simulation of a 3-D novel jerk chaotic system with two hyperbolic sinusoidal nonlinearities. Arch Control Sci 24(3):375–403
118. Vaidyanathan S, Azar AT, Rajagopal K, Alexander P (2015a) Design and SPICE implementation of a 12-term novel hyperchaotic system and its synchronisation via active control. Int J Model Ident Control 23(3):267–277
119. Vaidyanathan S, Idowu BA, Azar AT (2015b) Backstepping controller design for the global chaos synchronization of Sprott's jerk systems. Stud Comput Intell 581:39–58
120. Vaidyanathan S, Rajagopal K, Volos CK, Kyprianidis IM, Stouboulos IN (2015c) Analysis, adaptive control and synchronization of a seven-term novel 3-D chaotic system with three quadratic nonlinearities and its digital implementation in LabVIEW. J Eng Sci Technol Rev 8(2):130–141
121. Vaidyanathan S, Sampath S, Azar AT (2015d) Global chaos synchronisation of identical chaotic systems via novel sliding mode control method and its application to Zhu system. Int J Model Ident Control 23(1):92–100
122. Vaidyanathan S, Volos C, Pham VT, Madhavan K (2015e) Analysis, adaptive control and synchronization of a novel 4-D hyperchaotic hyperjerk system and its SPICE implementation. Arch Control Sci 25(1):135–158
123. Vaidyanathan S, Volos CK, Kyprianidis IM, Stouboulos IN, Pham VT (2015f) Analysis, adaptive control and anti-synchronization of a six-term novel jerk chaotic system with two exponential nonlinearities and its circuit simulation. J Eng Sci Technol Rev 8(2):24–36
124. Vaidyanathan S, Volos CK, Pham VT (2015g) Analysis, adaptive control and adaptive synchronization of a nine-term novel 3-D chaotic system with four quadratic nonlinearities and its circuit simulation. J Eng Sci Technol Rev 8(2):181–191

125. Vaidyanathan S, Volos CK, Pham VT (2015h) Analysis, control, synchronization and SPICE implementation of a novel 4-D hyperchaotic Rikitake dynamo system without equilibrium. J Eng Sci Technol Rev 8(2):232–244
126. Vaidyanathan S, Volos CK, Pham VT (2015i) Global chaos control of a novel nine-term chaotic system via sliding mode control. In: Azar AT, Zhu Q (eds) Advances and applications in sliding mode control systems. Studies in computational intelligence, vol 576. Springer, Germany, pp 571–590
127. Volos CK, Kyprianidis IM, Stouboulos IN (2013) Experimental investigation on coverage performance of a chaotic autonomous mobile robot. Robot Auton Syst 61(12):1314–1322
128. Volos CK, Kyprianidis IM, Stouboulos IN, Tlelo-Cuautle E, Vaidyanathan S (2015) Memristor: A new concept in synchronization of coupled neuromorphic circuits. J Eng Sci Technol Rev 8(2):157–173
129. Wang J, Chen Z (2008) A novel hyperchaotic system and its complex dynamics. Int J Bifurc Chaos 18:3309–3324
130. Wei X, Yunfei F, Qiang L (2012) A novel four-wing hyper-chaotic system and its circuit implementation. Procedia Eng 29:1264–1269
131. Wei Z, Yang Q (2010) Anti-control of Hopf bifurcation in the new chaotic system with two stable node-foci. Appl Math Comput 217(1):422–429
132. Witte CL, Witte MH (1991) Chaos and predicting varix hemorrhage. Med Hypotheses 36(4):312–317
133. Wu X, Zhu C, Kan H (2015) An improved secure communication scheme based passive synchronization of hyperchaotic complex nonlinear system. Appl Math Comput 252:201–214
134. Yujun N, Xingyuan W, Mingjun W, Huaguang Z (2010) A new hyperchaotic system and its circuit implementation. Commun Nonlinear Sci Numer Simul 15(11):3518–3524
135. Zaher AA, Abu-Rezq A (2011) On the design of chaos-based secure communication systems. Commun Nonlinear Syst Numer Simul 16(9):3721–3727
136. Zhang H, Liao X, Yu J (2005) Fuzzy modeling and synchronization of hyperchaotic systems. Chaos Solitons Fractals 26(3):835–843
137. Zhang X, Zhao Z, Wang J (2014) Chaotic image encryption based on circular substitution box and key stream buffer. Signal Process Image Commun 29(8):902–913
138. Zhou W, Xu Y, Lu H, Pan L (2008) On dynamics analysis of a new chaotic attractor. Phys Lett A 372(36):5773–5777
139. Zhu C (2012) A novel image encryption scheme based on improved hyperchaotic sequences. Opt Commun 285(1):29–37
140. Zhu C, Liu Y, Guo Y (2010) Theoretic and numerical study of a new chaotic system. Intell Inf Manag 2:104–109
141. Zhu Q, Azar AT (2015) Complex system modelling and control through intelligent soft computations. Studies in fuzzines and soft computing, vol 319. Springer, Germany

Identification, Stability and Stabilization of Limit Cycles in a Compass-Gait Biped Model via a Hybrid Poincaré Map

Hassène Gritli and Safya Belghith

Abstract This chapter focuses on identification, stability analysis and stabilization of hybrid limit cycle in the passive dynamic walking of the compass-gait biped robot as it goes down an inclined surface. The walking dynamics of such biped is described by an impulsive hybrid nonlinear system, which is composed of a nonlinear differential equation and a nonlinear algebraic equation. Under variation of the slope parameter, the passive biped robot displays symmetric (stable one-periodic) and asymmetric (unstable one-periodic and chaotic) behaviors. Then, the main objective of this chapter is to stabilize a desired asymmetric gait into a symmetric one by means of a control input, the hip torque. Nevertheless, the design of such control input using the impulsive hybrid dynamics is a complicated task. Then, to overcome this problem, we constructed a hybrid Poincaré map by linearizing the impulsive hybrid nonlinear dynamics around a desired unstable one-periodic hybrid limit cycle for some desired slope parameter. We stress that both the differential equation and the algebraic equation are linearized. The desired hybrid limit cycle is identified and analyzed first through the impulsive hybrid nonlinear dynamics via the fundamental solution matrix. We demonstrate that identification of the one-periodic fixed point of the designed hybrid Poincaré map and its stability depend only upon the nominal impact instant. We introduce a state-feedback controller in order to stabilize the linearized Poincaré map around the one-periodic fixed point. We show that the developed strategy for the design of the OGY-based controller has achieved the stabilization of the desired one-periodic hybrid limit cycle of the compass-gait biped robot.

H. Gritli (✉)
Institut Supérieur des Technologies de l'Information et de la Communication, Université de Carthage, 1164 Borj Cedria, Tunis, Tunisia
e-mail: grhass@yahoo.fr

S. Belghith
Department of Electrical Engineering, Ecole Nationale D'Ingénieurs de Tunis, Université de Tunis El-Manar, BP. 37, 1002 Le Belvédère, Tunis, Tunisia
e-mail: safya.belghith@enit.rnu.tn

S. Vaidyanathan and C. Volos (eds.), *Advances and Applications in Nonlinear Control Systems*, Studies in Computational Intelligence 635,
DOI 10.1007/978-3-319-30169-3_13

Keywords Compass-gait biped robot · Impulsive hybrid nonlinear dynamics · Hybrid Poincaré map · Hybrid limit cycle · OGY control approach

1 Introduction

The research prototypes of biped robots made under the passive dynamic walking are used mainly for investigating properties of the bipedal walking (dynamics, stability, limit cycles, etc.). The goal is to reproduce walking cycles and analyze the generated cycles. The principle meanwhile is to use the effect of gravity as an action to reproduce a stable periodic walking from some initial configurations. In this context, several works have been proposed to date showing the central utility of passive dynamic walking. There are three important motivations behind the study and design of passive dynamic walking, namely (1) The passive biped robot has a self-stabilizing mechanical walking dynamics, (2) The passive dynamic walking should significantly increase the energy efficiency of bipedal locomotion, and (3) The passive dynamic walking is studied in order to obtain an additional insight on the design principles of legged locomotion in nature. The most famous passive biped robot is the planar compass-gait biped model, which has been widely investigated in the literature (see [44] for a survey). In this chapter, we are interested in the analysis of such passive compass-gait model and its stabilization. The passive compass-gait biped robot and its impulsive hybrid nonlinear dynamics are presented in Sect. 3. The interest in the design and use of an active biped robot based on passive dynamic walking is its low power consumption. Many researches have been conducted on the development of bipedal walkers based on the observed demonstrations of passive dynamic walking (see for example [44, 47, 85] and references therein).

The model of the dynamic walking of biped robots is qualified as an impulsive hybrid nonlinear dynamics. Such dynamics is composed of nonlinear differential equations modeling the swing motion of the biped robot, and also nonlinear algebraic equations describing the impulsive transition of the state vector at the impact phase. As the periodic cyclic movement of biped robots is represented by a limit cycle, then investigation of stability of the periodic dynamic walking of biped robots is achieved by analyzing stability of the corresponding limit cycle using the concept of the Poincaré map [10, 13, 34, 44, 60, 61, 64, 73, 78, 79, 81]. Generally, stability analysis of the limit cycle of the bipedal dynamic walking is transformed into stability study of the fixed point of the corresponding limit cycle. This fixed point is identified by means of the Poincaré map. Nevertheless, because the impulsive and hybrid features of the bipedal walking dynamics, determination of an explicit expression of the Poincaré map is a complicated (if we can say impossible) task. Then, determination of the fixed point of the Poincaré map and its stability analysis was found using the concept of the shooting method and the trajectory sensitivity analysis [15, 36, 37]. Such analysis was realized using the fundamental solution matrix and the monodromy matrix. Because of the discontinuous behavior in the hybrid dynamics of the biped robot, a jump (saltation) matrix was determined for the fundamental solution matrix at the discontinuities (impacts). In Sect. 4, we revisit the investigation method for studying

stability of the hybrid limit cycle in the impulsive hybrid nonlinear dynamics of the (uncontrolled) passive compass-gait biped robot. The research method of the one-periodic hybrid limit cycle was first presented. Determination of the saltation matrix was also provided.

The passive dynamic walking has been served as an alternative point of departure for the analysis of active dynamic walking of biped robots and hence for the design of controller in order to avoid the use of high-gain control. Recently, we employed the OGY approach in order to control chaos exhibited in the passive compass-gait model [21, 22, 31] and in the semi-passive biped model with an upper body [26]. In [31], we used the hip torque as the control input in the OGY-based approach. However, in [26], the desired torso angle was employed as the accessible control parameter in the OGY method. In these two works, we linearized the impulsive hybrid nonlinear dynamics of the biped model around a desired one-periodic hybrid limit cycle. Then, we developed an analytical expression of a constrained controlled Poincaré map, a hybrid Poincaré map. Furthermore, we determined the one-periodic fixed point and we stabilized it by adopting a state-feedback controller. As a result, the unstable limit cycle was stabilized and hence chaos was controlled. We stress that only the nonlinear differential equation was linearized. However, the nonlinear algebraic equation was kept as it. It was shown that the designed OGY-based controller has permitted to obtain an active dynamic walking of the passive biped robot with a small-gain control. Hence, the OGY controller has contributed to substantially increase the energy efficiency of the biped robots as they walk down an inclined surface.

In fact, in [21, 22, 31], the impulsive hybrid nonlinear dynamics was linearized around a desired one-periodic hybrid limit cycle where the obtained linearized dynamics is affine with respect to the state vector and the control input. However, in [26], the developed linearized dynamics is affine only with respect to the state vector. The control input was found to be incorporated within different matrices defining the linearized dynamics. Then, two linearization methods have been introduced. The first linearization method is used by considering from the start the control input in the impulsive hybrid nonlinear dynamics of the passive biped robot. Thus, the nonlinear dynamics was linearized around a point defined by both the desired state vector and the desired control input. In contrast, the second linearization method does not take into account the control input from the start. Then, the impulsive hybrid nonlinear dynamics was linearized only around a desired state vector. In this chapter, we will introduce the first linearization method for the compass-gait biped model in order to derive the explicit expression of the hybrid Poincaré map. In addition, compared with [21, 22, 31], we present in this chapter (Sect. 5) a new simplified analytical expression of the hybrid Poincaré map. This simplified map was obtained by linearizing also the algebraic equation around the one-periodic fixed point of the desired one-periodic hybrid limit cycle. Then, according to this hybrid Poincaré map, we will design the control law by linearizing this map around its fixed point. Thus, we will design a state-feedback control law in order to stabilize the linearized Poincaré map. As a result, the designed control law will stabilize the one-periodic hybrid limit cycle of the impulsive hybrid nonlinear dynamics of the compass-gait biped robot.

2 Related Works

Human beings can walk in a stable and efficient manner on all kinds of terrain, seemingly without much effort. Walking on two legs implies a strongly nonlinear and multi-variable dynamics, a limited number of interaction of feet-ground and a naturally unstable dynamics (the system is an inverted pendulum pivoting at the foot). It involves also a dynamics with discrete changes (such as the impact of the heel) and a variable configuration (alternating between swing phase and support phase). In order to be able to reproduce the complex motion of walking, it is necessary to find the essential elements of the locomotive system design that make the human walks naturally and effortlessly.

In 1984, McMahon noted the similarities between the walking of the human being and a biped toy of a child [58]. When it is set on a ramp and through an initial push, the toy waddles on one side and the other and "walk" down the ramp. The most remarkable point of such toy is the absence of an external source of energy; it was driven via gravity. The toy is simple with uncontrolled walking suggested that locomotion is fundamental to a system with links and joints and requires no external power. In the past 20 years, several robotics laboratories throughout North America and Europe have been working on this phenomenon.

In 1990, McGeer showed bipedal locomotion without motor with a simple biped walker [57]. When placed on a ramp and giving a correct initial push, the biped walks on the ramp. With each step, the biped robot gains energy through the change in potential energy and kinetic energy at impact of the swing leg with the ground at the end of each step. With a good combination of initial conditions and the angle of the ramp, each successive set corresponds to the previous step and a stable passive walking is generated. This mode of bipedal locomotion became known as the "passive dynamic walking". The term "passive" comes from the fact that no external source other than gravity provides energy with every step. The advantage of such passive walking robot is its low power consumption. The term "dynamic" is linked to the stability associated with bipedal walking.

There are two kinds of bipedal walking, namely the static walking and the dynamic walking. A static walking of a biped robot is restricted by the position of its center-of-mass, which must be projected vertically inside the convex polygon of support. Despite its great efficiency, static walking is very limited and is characterized by a very slow bipedal locomotion. This will prevent the biped to reach high speeds when moving. However, unlike the static biped walking, in a dynamic walking, the biped robot is in total imbalance along a step. It recovers its balance when it rests its swing leg. Then, it is again in the imbalance by lifting the other leg. This leg transition mechanism is reflected by the fact that the center-of-mass of the biped robot leaves the convex polygon of support for periods during dynamic bipedal walking. However, such periods must be strictly short and must necessarily be controlled to avoid contingent situation of the fall of the biped.

The passive dynamic walking has been served as an alternative point of departure for the analysis of active dynamic walking of biped robots and hence for the design

of controller in order to avoid the use of high-gain control. The objective is therefore intended to the design of some control structure which could be based on performance of the passive dynamic walking of the biped robot such as using the passive limit cycle for the design of the controller. Accordingly, such controller must be designed based on the passive dynamic walking patterns of the biped robot and hence to obtain a periodic stable walk that has something of a human walking look.

Investigation of bipedal walking is difficult because it requires a complete understanding of the different characteristics of the system. Because of these characteristics, the biped robots belong to a general class of systems that make an interesting topic for the theory of dynamical systems and a challenge to the control theory. The model of dynamic walking of biped robots is qualified as an impulsive hybrid nonlinear dynamics. Such dynamics is composed of a nonlinear differential equation modeling the swing motion of the biped robot, and also a nonlinear algebraic equation describing the impulsive transition of the state vector at the impact phase. Such impulsive hybrid nonlinear dynamics can show complex, strange and attractive behaviors such as chaos and bifurcations [17, 20–25, 27–30, 32, 33, 41, 44, 48–51, 63, 67, 69, 70, 86, 89].

The most interesting and most important in the robotics community is to study and design bipedal robots, and therefore control them in order to obtain patterns of stable periodic walking. From the control point-of-view, the bipedal dynamic walking is considered as a succession of postures of walking gaits. The biped robot must follow this particular sequence of postures in order to achieve some movement allowing it to move over a given walking surface. All these walking postures can be defined as reference joint trajectories to be pursued by the joints of the biped robot. Therefore, it is necessary to find the control law obviously allows pursuing these reference trajectories in order to move the robot on the walking surface. The central objective in the problem of the control of biped robots is to have a stable periodic gait with maximum energetic efficiency.

Several methods have been designed for the identification of limit cycle walking or the corresponding fixed point of the Poincaré map. The more investigated one is based mainly on the fundamental solution matrix and then on the monodromy matrix and the saltation matrix at the discontinuities [10, 13, 15, 18, 34, 36, 37, 44, 60, 61, 64, 68, 73, 78, 79, 81]. In contrast, some approximated methods have been introduced in the literature (see for example [44] and references therein and the previous cited references). Recently, we developed an analytical expression of a constrained Poincaré map by linearizing the impulsive hybrid nonlinear dynamics of the biped robot around the one-periodic hybrid limit cycle [26, 31]. This linearization method was described in Sect. 5. The hybrid Poincaré map was used in order to design a state-feedback controller to stabilize the one-periodic fixed point of the Poincaré map and hence to stabilize the one-periodic hybrid limit cycle. However, authors in [19, 54–56, 73–75] used the transverse linearization as a fundamental tool for analysis of orbital stability of impulsive hybrid dynamics to stabilize periodic walking motions. This tool was used especially to stabilize periodic walking motions. Moreover, authors in [13] used the finite difference method to find numerically period-one gait cycles for simple passive walkers.

Usually, the design and control of biped robots have been based on the standard technologies of manipulator robots, namely solid and rigid actuators are combined with sophisticated control algorithms such that the entire system can accurately track the planned trajectories. We argue that this leads to unnecessarily complex walking machines, heavy, and inefficient energy because the pursuit of an exact trajectory is not a necessary condition for an appreciated and preferred locomotion. The key idea is that stability does not have to be achieved in a single step of biped walking (the trajectory control approach), as long as the movement of the bipedal walking is stable over several steps. In other words, the movement of the biped robot must be regarded as a cyclic movement, which only requires to be stabilized in its entirety.

Along the last two decades, many worldwide research groups have worked on the control of dynamic walking of biped robots. Because of the complexity of the dynamics of biped walking, the design of effective control strategies is a difficult task. The main goal of current research on the biped control includes many proposed control approaches, such as passivity based control [76, 77], robust sliding mode control [72, 80], computed torque method [6, 71], impedance control [65], nonlinear predictive control [8], optimal control [5, 35], speed control method with adaptive regulation [53], Lyapunov based control [9], intuitive control [4], intelligent learning control [45, 59], neural network control [43], minimalistic control [42], anti-phase synchronization control [52], hybrid-zero-dynamics control [84], feedback control [39, 40, 83], time-scaling control [11], input torque control [14], discrete-time control [7, 40], PI control [82], zero-moment-point control [12], virtual passive control [2], adaptive compliant control [88], landing force control [46], energy shaping control method [38, 87], Virtual-Slope-Walking-based control [16], 0-flat-normal-form-based control [3], among others.

Recently, we used the concept of the Poincaré map in order to design a control approach based on the OGY method [21, 22, 26, 31]. Such controller was developed in order to control chaotic motions of the compass-gait biped model [31] and also the torso-driven biped robot [26]. The design method of the OGY-based control was achieved by linearizing the impulsive hybrid nonlinear dynamics of the biped robot under consideration around a one-period limit cycle. Thus, we developed an analytical expression of a controlled constrained (hybrid) Poincaré map, which found to mimic with a reasonable error the behavior of the impulsive hybrid nonlinear dynamics of the passive dynamic walking of the planar biped robot.

3 Impulsive Hybrid Nonlinear Dynamics of the Passive Compass-Gait Model

3.1 The Compass-Gait Biped Robot

A schematic representation of the compass-gait biped robot is given in Fig. 1 [21, 22, 31]. The significant parameters in the dynamics description are provided in Table 1.

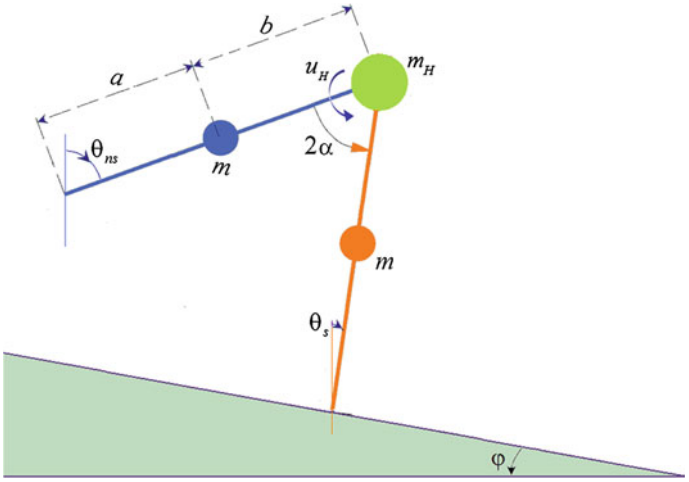

Fig. 1 The compass-gait biped robot model down an inclined surface of slope φ

Table 1 Simulation parameters for the passive compass-gait model

Symbol	Description	Value
a	Lower leg segment	0.5 m
b	Upper leg segment	0.5 m
m	Mass of leg	5 kg
m_H	Mass of hip	10 kg
g	Gravitational constant	9.8 m/s^2

The biped robot under consideration is composed of two identical legs, namely the stance leg and the swing leg, and a frictionless hip. The two legs are modeled as rigid bars without knees and feet where their masses are pinpoint. The passive walk of the compass-gait model is constrained in the sagittal plane and is divided into a swing phase and an impact phase. The swing phase describes the configuration when one leg is fixed on the ground as a pivot and the other leg swings above the ground. However, the impact phase describes the situation of the double-support of the two legs during which the swing and the stance leg are exchanged. The state configuration of the biped robot is determined by the support angle θ_s, the nonsupport angle θ_{ns}, and the corresponding angular velocities $\dot{\theta}_s$ and $\dot{\theta}_{ns}$. Positive angles are computed counterclockwise with respect to the indicated vertical lines.

The compass-gait biped robot is a non-actuated symmetric planar walker descending an inclined surface of slope φ using gravity as the only source of energy. Then, its bipedal locomotion has been known as the passive dynamic walking, where their intrinsic properties have been widely investigated from stability and dynamics points-of-view. It has been known that this kind of bipedal locomotion exhibits chaos and bifurcations as the inertial and geometrical parameters of the biped robot and as well as the slope parameter vary.

For stabilizating the passive cyclic motion of the compass-gait biped robot and hence for controlling chaos, only one control input $u = u_H$ has been introduced at the hip as shown in Fig. 1.

3.2 Impulsive Hybrid Nonlinear Dynamics

The compass-gait model consists of a nonlinear differential equation of the swing phase and nonlinear algebraic equation of the impulsive impact phase. These two equations form an impulsive hybrid nonlinear dynamics of the dynamic walking of the compass-gait biped robot on the walking surface [21, 22, 31].

Let $\boldsymbol{\theta} = \begin{bmatrix} \theta_{ns} & \theta_s \end{bmatrix}^T$ be the vector of generalized coordinates of the compass-gait model. Then, the impulsive hybrid nonlinear dynamics is described as follows:

$$\boldsymbol{\mathcal{J}}(\boldsymbol{\theta})\ddot{\boldsymbol{\theta}} + \boldsymbol{\mathcal{H}}(\boldsymbol{\theta}, \dot{\boldsymbol{\theta}}) + \boldsymbol{\mathcal{G}}(\boldsymbol{\theta}) = \boldsymbol{\mathcal{B}}u \quad \text{as long as} \quad \boldsymbol{\theta} \in \Omega \tag{1a}$$

$$\begin{cases} \boldsymbol{\theta}^+ = \boldsymbol{\mathcal{R}}_e \boldsymbol{\theta}^- \\ \dot{\boldsymbol{\theta}}^+ = \boldsymbol{\mathcal{S}}_e \dot{\boldsymbol{\theta}}^- \end{cases} \quad \text{whenever} \quad \left\{\boldsymbol{\theta}^-, \dot{\boldsymbol{\theta}}^-\right\} \in \Gamma \tag{1b}$$

$$\Omega = \left\{\boldsymbol{\theta} \in \Re^2 \ : \ \mathcal{L}_1(\boldsymbol{\theta}) = \boldsymbol{\mathcal{C}}\boldsymbol{\theta} + 2\varphi > 0\right\} \tag{1c}$$

$$\Gamma = \left\{\boldsymbol{\theta}, \dot{\boldsymbol{\theta}} \in \Re^2 \ : \ \mathcal{L}_1(\boldsymbol{\theta}) = 0 \ , \ \mathcal{L}_2(\dot{\boldsymbol{\theta}}) = \frac{\partial \mathcal{L}_1(\boldsymbol{\theta})}{\partial \boldsymbol{\theta}}\dot{\boldsymbol{\theta}} = \boldsymbol{\mathcal{C}}\dot{\boldsymbol{\theta}} < 0\right\} \tag{1d}$$

with $\boldsymbol{\mathcal{J}}$ is the inertia matrix, $\boldsymbol{\mathcal{H}}$ includes Coriolis and centrifugal terms, $\boldsymbol{\mathcal{G}}$ includes gravity forces, $\boldsymbol{\mathcal{B}}$ is the input matrix, $\boldsymbol{\mathcal{R}}_e$ is the renaming matrix and $\boldsymbol{\mathcal{S}}_e$ is the reset matrix. These matrices are defined like so:

$$\boldsymbol{\mathcal{J}}(\boldsymbol{\theta}) = \begin{bmatrix} mb^2 & -mlb\cos(\theta_s - \theta_{ns}) \\ -mlb\cos(\theta_s - \theta_{ns}) & m_H l^2 + m(l^2 + a^2) \end{bmatrix}, \boldsymbol{\mathcal{B}} = \begin{bmatrix} -1 \\ 1 \end{bmatrix},$$

$$\boldsymbol{\mathcal{H}}(\boldsymbol{\theta}, \dot{\boldsymbol{\theta}}) = \begin{bmatrix} mlb\dot{\theta}_s^2 \sin(\theta_s - \theta_{ns}) \\ -mlb\dot{\theta}_{ns}^2 \sin(\theta_s - \theta_{ns}) \end{bmatrix}, \boldsymbol{\mathcal{G}}(\boldsymbol{\theta}) = g\begin{bmatrix} mb\sin(\theta_{ns}) \\ -(m_H l + m(a+l))\sin(\theta_s) \end{bmatrix},$$

$$\boldsymbol{\mathcal{R}}_e = \begin{bmatrix} 0 & 1 \\ 1 & 0 \end{bmatrix}, \text{ and } \boldsymbol{\mathcal{S}}_e = \boldsymbol{\mathcal{Q}}_p^{-1}(\alpha)\, \boldsymbol{\mathcal{Q}}_m(\alpha), \text{ where}$$

$$\boldsymbol{\mathcal{Q}}_m(\alpha) = \begin{bmatrix} -mab & -mab + (m_H l^2 + 2mal)\cos(2\alpha) \\ 0 & -mab \end{bmatrix}, \text{ and}$$

$$\boldsymbol{\mathcal{Q}}_p(\alpha) = \begin{bmatrix} mb(b - l\cos(2\alpha)) & ml(l - b\cos(2\alpha)) + ma^2 + m_H l^2 \\ mb^2 & -mbl\cos(2\alpha) \end{bmatrix}, \text{ with}$$

$l = a + b$ (see Table 1) and α is the half-interleg angle (see Fig. 1) where $\alpha = \frac{1}{2}(\theta_s - \theta_{ns})$. Moreover, in (1c) and (1d), $\boldsymbol{\mathcal{C}} = \begin{bmatrix} 1 & 1 \end{bmatrix}$.

In (1), Ω defines the natural unilateral constraint, which corresponds to the distance between the tip of the swing leg and the ground. In other words, such unilateral

constraint represents the situation where the swing leg is above the ground. However, Γ defines constraints on the impact of the swing leg with the ground. The impact occurs when the swing leg reaches the walking surface (constraint $\mathcal{L}_1(\boldsymbol{\theta}) = 0$) and the swing leg is moving downward (constraint $\mathcal{L}_2(\dot{\boldsymbol{\theta}}) < 0$).

The nonlinear differential equation (1a) models the motion of the biped robot during the swing phase. However, the nonlinear algebraic equation (1b) describes the impulsive transition in the angular positions and the angular velocities of the two legs of the biped robot during (at) the impact phase. In (1b), subscribes $^+$ and $^-$ denote just after and just before the impact, respectively.

We emphasize that for a entirely passive dynamic walking of the compass-gait biped model, the control law $u = u_H$ in (1a) is zero. It will be designed next in order to stabilize the bipedal locomotion of the biped robot. The impulsive hybrid nonlinear dynamics (1) can be reformulated in the following state representation:

$$\dot{\boldsymbol{x}} = \boldsymbol{f}(\boldsymbol{x}) + \boldsymbol{g}(\boldsymbol{x})u \quad \text{as long as} \quad \boldsymbol{x} \in \Omega \tag{2a}$$

$$\boldsymbol{x}^+ = \boldsymbol{h}\left(\boldsymbol{x}^-\right) \quad \text{whenever} \quad \boldsymbol{x}^- \in \Gamma \tag{2b}$$

$$\Omega = \left\{\boldsymbol{x} \in \Re^4 \ : \ \mathcal{L}_1(\boldsymbol{x}) = \boldsymbol{\mathcal{C}_1}\boldsymbol{x} > 0\right\} \tag{2c}$$

$$\Gamma = \left\{\boldsymbol{x} \in \Re^4 \ : \ \mathcal{L}_1(\boldsymbol{x}) = \boldsymbol{\mathcal{C}_1}\boldsymbol{x} = 0, \ \mathcal{L}_2(\boldsymbol{x}) = \boldsymbol{\mathcal{C}_2}\boldsymbol{x} < 0\right\} \tag{2d}$$

with $\boldsymbol{x}$ is the state vector given by $\boldsymbol{x} = \left[\boldsymbol{\theta}^T \ \ \dot{\boldsymbol{\theta}}^T\right]^T$, $\boldsymbol{x}^+$ denotes the value of $\boldsymbol{x}$ right after the impact, while $\boldsymbol{x}^-$ refers to the value of $\boldsymbol{x}$ right before the impact. Moreover, in (2c) and (2d), we have $\boldsymbol{\mathcal{C}}_1 = \left[\mathcal{C} \ \ \mathcal{O}_{1\times 2}\right]$ and $\boldsymbol{\mathcal{C}}_2 = \left[\mathcal{O}_{1\times 2} \ \ \mathcal{C}\right]$, where $\mathcal{O}_{1\times 2} = \left[0 \ \ 0\right]$.

The solution of the impulsive hybrid nonlinear dynamics (2) for some desired slope parameter φ_d can be expressed in terms of flow like so:

$$\boldsymbol{x}(t) = \boldsymbol{\phi}\left(t, \boldsymbol{x}_0^-, \varphi_d\right) \tag{3}$$

where $\boldsymbol{x}_0^- = \phi\left(t_0, \boldsymbol{x}_0^-, \varphi_d\right)$ is the initial condition just before the impact phase.

4 Identification and Stability of One-Periodic Hybrid Limit Cycle in the Impulsive Hybrid Dynamics

Our objective is to identify the one-periodic hybrid limit cycle of the passive dynamic walking of the biped robot using first the impulsive hybrid nonlinear dynamics (2) and to study its stability. A passive dynamics corresponds to an uncontrolled one, i.e. for $u = 0$. Stability analysis of a one-periodic hybrid limit cycle will be based on the concept of the Poincaré map, which will be described next.

4.1 Concept of the Poincaré Map

A conventional technique for the discretization of a continuous dynamical system is the Poincaré map. It replaces the continuous flow ϕ of n-dimensional system by a $(n-1)$-dimensional discrete map. A Poincaré map samples the flow ϕ once a time in one direction. The Poincaré map is useful for reducing the order of the system [66].

For a n-dimensional autonomous system, the flow $\phi(t, \boldsymbol{x}_0)$ is defined as the trajectory Λ. When Γ is chosen to be a $(n-1)$-dimensional hyperplane such that the trajectory Λ intersects Γ transversely and $\boldsymbol{x}_0$ is a point of Λ in the hyperplane Γ, the trajectory Λ starting from $\boldsymbol{x}_0$ encounters Γ at the point $\boldsymbol{x}_1 = \boldsymbol{\mathcal{P}}(\boldsymbol{x}_0)$. Because of the continuity of the flow $\phi(t, \boldsymbol{x}_0)$, trajectories starting from Γ in a sufficiently small neighborhood of $\boldsymbol{x}_0$ will also intersect Γ in the neighborhood of $\boldsymbol{x}_1$. The hyperplane Γ is called the Poincaré section, which must be transverse to the flow $\phi(t, \boldsymbol{x}_0)$. Thus, Λ and Γ define the Poincaré map $\boldsymbol{\mathcal{P}}$ in a neighborhood $\mathcal{U} \subset \Gamma$ of $\boldsymbol{x}_0$ in a neighborhood $\mathcal{V} \subset \Gamma$ of $\boldsymbol{x}_1$.

Figure 2 shows the concept of the Poincaré map for an autonomous system. In this figure, a trajectory Λ emanated from a state $\boldsymbol{x}_k$ must meet again the Poincaré section Γ to a next state $\boldsymbol{x}_{k+1} = \boldsymbol{P}(\boldsymbol{x}_k)$ after some return time τ_r. In fact, the number of successive intersections needed for the trajectory returns to its initial state $\boldsymbol{x}_0$ gives us the period of the dynamics of the system and thus the return time $\tau_r(\boldsymbol{x}_0)$.

For example, in Fig. 2, the trajectory Λ_0 returns to its initial state $\boldsymbol{x}_0$ in only one iteration. In this case, the system response is of period 1. In general, a K-periodic limit cycle must return to its starting point after K intersections. The successive states of intersection of the flow ϕ with the Poincaré section Γ define the following Poincaré map [66]:

$$\boldsymbol{x}_{k+1} = \boldsymbol{\mathcal{P}}(\boldsymbol{x}_k) \equiv \phi(\tau_r(\boldsymbol{x}_k), \boldsymbol{x}_k) \tag{4}$$

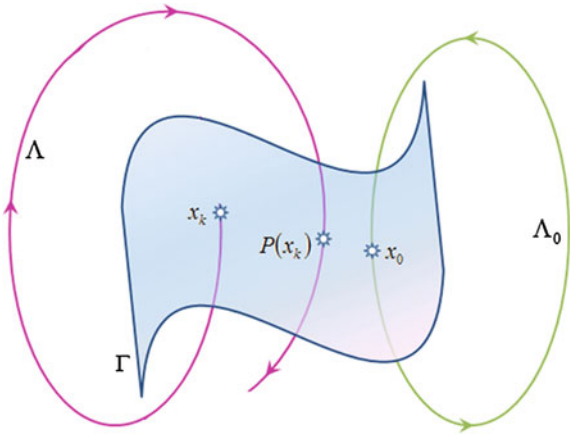

Fig. 2 Illustration of the concept of the Poincaré map for an autonomous system

This expression of the Poincaré map can be defined also for the impulsive hybrid nonlinear dynamics (2) of the passive compass-gait model.

4.2 Fundamental Solution Matrix

Let consider first the uncontrolled nonlinear differential equation (2a):

$$\dot{\boldsymbol{x}}(t) = \boldsymbol{f}(\boldsymbol{x}(t)), \boldsymbol{x}(t_0) = \boldsymbol{x}_0 \tag{5}$$

where $\boldsymbol{x}_0$ is the initial condition.

Solution of this system (5) is defined like so:

$$\boldsymbol{x}(t) = \boldsymbol{\phi}(t, \boldsymbol{x}_0), \boldsymbol{x}_0 = \phi(t_0, \boldsymbol{x}_0) \tag{6}$$

Relying on (5), we can write the following expression:

$$\dot{\boldsymbol{\phi}}(t, \boldsymbol{x}_0) = \boldsymbol{f}(\boldsymbol{\phi}(t, \boldsymbol{x}_0)), \quad \boldsymbol{\phi}(t_0, \boldsymbol{x}_0) = \boldsymbol{x}_0 \tag{7}$$

By making the derivative of (7) with respect to $\boldsymbol{x}_0$, it yields:

$$\frac{\partial \dot{\boldsymbol{\phi}}(t, \boldsymbol{x}_0)}{\partial \boldsymbol{x}_0} = \frac{\partial \boldsymbol{f}(\boldsymbol{\phi}(t, \boldsymbol{x}_0))}{\partial \boldsymbol{x}} \frac{\partial \boldsymbol{\phi}(t, \boldsymbol{x}_0)}{\partial \boldsymbol{x}_0}, \quad \frac{\partial \boldsymbol{\phi}(t_0, \boldsymbol{x}_0)}{\partial \boldsymbol{x}_0} = \boldsymbol{I}_n \tag{8}$$

where $\boldsymbol{I}_n$ is the identity matrix.

By defining

$$\boldsymbol{\Phi}(t, \boldsymbol{x}_0) = \frac{\partial \boldsymbol{\phi}(t, \boldsymbol{x}_0)}{\partial \boldsymbol{x}_0}, \tag{9}$$

expressions in (8) becomes:

$$\begin{cases} \dot{\boldsymbol{\Phi}}(t, \boldsymbol{x}_0) = \boldsymbol{\mathcal{J}}_f(\boldsymbol{x}(t)) \boldsymbol{\Phi}(t, \boldsymbol{x}_0) \\ \boldsymbol{\Phi}(t_0, \boldsymbol{x}_0) = \boldsymbol{I}_n \end{cases} \tag{10}$$

where $\boldsymbol{\mathcal{J}}_f(\boldsymbol{x}(t))$ is the Jacobian matrix and is given by $\boldsymbol{\mathcal{J}}_f(\boldsymbol{x}(t)) = \frac{\partial \boldsymbol{f}(\boldsymbol{x}(t))}{\partial \boldsymbol{x}(t)}$.

The matrix $\boldsymbol{\Phi}(t, \boldsymbol{x}_0)$ is called the fundamental solution matrix. It is called also the sensitivity matrix of a periodic trajectory with respect to the initial condition $\boldsymbol{x}_0$. More particularly, the matrix $\boldsymbol{\Phi}(T, \boldsymbol{x}_0)$ is determined after a single period T, and is called the monodromy matrix or the Floquet matrix.

The fundamental solution matrix can be obtained by integrating the following system:

$$\begin{cases} \dot{\boldsymbol{x}} = \boldsymbol{f}(\boldsymbol{x}) & \boldsymbol{x}(0) = \boldsymbol{x}_0 \\ \dot{\boldsymbol{\Phi}}(t, \boldsymbol{x}_0) = \boldsymbol{\mathcal{J}}_f(\boldsymbol{x}(t)) \boldsymbol{\Phi}(t, \boldsymbol{x}_0) & \boldsymbol{\Phi}(t_0, \boldsymbol{x}_0) = \boldsymbol{I}_n \end{cases} \tag{11}$$

For smooth (regular) continuous systems, the fundamental solution matrix is obtained elegantly by integrating the system (11). However, for non-smooth (discontinuous) dynamical systems as the impulsive hybrid nonlinear dynamics (2), the calculation is more complex. These discontinuities are provoked because of the impact event. The jump (transition) in the fundamental solution matrix can be calculated analytically as we will show in the sequel. In the next we will consider the impulsive hybrid nonlinear dynamics (2a)–(2b).

4.3 Saltation Matrix

Impulsive hybrid nonlinear dynamic systems present discontinuities in the Jacobian matrix at the transition of the state vector. The discontinuity in the Jacobian matrix accordingly causes a discontinuity (a jump) in the fundamental solution matrix $\boldsymbol{\Phi}$. The jumps in the fundamental solution matrix will be analytically calculated based on [37, 62]. According to these references, the fundamental solution matrix just after the transition $\boldsymbol{\Phi}^{+}$ is related to the fundamental solution matrix just before the transition $\boldsymbol{\Phi}^{-}$ using a saltation (jump) matrix $\boldsymbol{\mathcal{S}}$ as follows:

$$\boldsymbol{\Phi}^{+} = \boldsymbol{\mathcal{S}}\left(\boldsymbol{x}^{+}, \boldsymbol{x}^{-}\right)\boldsymbol{\Phi}^{-} \tag{12}$$

Next, we will determine an analytical expression of this saltation matrix $\boldsymbol{\mathcal{S}}\left(\boldsymbol{x}^{+}, \boldsymbol{x}^{-}\right)$.

We will assume that the transition of the state vector occurs at the instant $\tau > 0$. Then, denoting by τ^{+} (resp. τ^{-}) the instant just after (resp. before) the transition, we can note the two following notations: $\boldsymbol{x}^{+} = \boldsymbol{x}\left(\tau^{+}\right)$ and $\boldsymbol{x}^{-} = \boldsymbol{x}\left(\tau^{-}\right)$. In addition, we will assume that the initial condition $\boldsymbol{x}_0$ belongs to the region Ω. We will consider in the following two notations: $\boldsymbol{f}^{-}$ and $\boldsymbol{f}^{+}$, indicating that the vector $\boldsymbol{f}$ takes $\boldsymbol{f}^{-}$ just before the transition and further takes $\boldsymbol{f}^{+}$ just after the transition.

In fact, in the subspace Ω, and taking into account (6), solution of the corresponding differential equation in (2a)–(2b) is defined in terms of flow by expression (6). Then, relying on (6), we can derive the following relation:

$$\frac{d\boldsymbol{x}\,(t)}{d\boldsymbol{x}_0} = \frac{\partial\boldsymbol{\phi}\,(t, \boldsymbol{x}_0)}{\partial\boldsymbol{x}_0} + \frac{\partial\boldsymbol{\phi}\,(t, \boldsymbol{x}_0)}{\partial t}\frac{dt}{d\boldsymbol{x}_0} \tag{13}$$

Using this last expression and considering the fact that $\frac{\partial\boldsymbol{\phi}(t,\boldsymbol{x}_0)}{\partial t} = \frac{\partial\boldsymbol{x}(t)}{\partial t} = \boldsymbol{f}\,(\boldsymbol{x}\,(t))$, we can write:

$$\frac{d\boldsymbol{x}\left(\tau^{-}\right)}{d\boldsymbol{x}_0} = \boldsymbol{\Phi}\left(\tau^{-}, \boldsymbol{x}_0\right) + \boldsymbol{f}\left(\boldsymbol{x}\left(\tau^{-}\right)\right)\tau_{\boldsymbol{x}_0} \tag{14}$$

$$\frac{d\boldsymbol{x}\left(\tau^{+}\right)}{d\boldsymbol{x}_0} = \boldsymbol{\Phi}\left(\tau^{+}, \boldsymbol{x}_0\right) + \boldsymbol{f}\left(\boldsymbol{x}\left(\tau^{+}\right)\right)\tau_{\boldsymbol{x}_0} \tag{15}$$

with $\tau_{\boldsymbol{x}_0} = \frac{d\tau}{d\boldsymbol{x}_0}$.

In the sequel, we will consider the following notations: $\boldsymbol{\Phi}^{+} = \boldsymbol{\Phi}\left(\tau^{+}, \boldsymbol{x}_0\right)$, $\boldsymbol{\Phi}^{-} = \boldsymbol{\Phi}\left(\tau^{-}, \boldsymbol{x}_0\right)$, $\boldsymbol{f}^{+} = \boldsymbol{f}\left(\boldsymbol{x}\left(\tau^{+}\right)\right)$ and $\boldsymbol{f}^{-} = \boldsymbol{f}\left(\boldsymbol{x}\left(\tau^{-}\right)\right)$. Then, the two expressions (14) and (15) become, respectively:

$$\frac{d\boldsymbol{x}^{-}}{d\boldsymbol{x}_0} = \boldsymbol{\Phi}^{-} + \boldsymbol{f}^{-}\tau_{\boldsymbol{x}_0} \tag{16}$$

$$\frac{d\boldsymbol{x}^{+}}{d\boldsymbol{x}_0} = \boldsymbol{\Phi}^{+} + \boldsymbol{f}^{+}\tau_{\boldsymbol{x}_0} \tag{17}$$

Using the algebraic equation (2b) and the first transition condition in (2d) (i.e. $\mathcal{L}_1(\boldsymbol{x}) = 0$), we can deduce the following two relationships:

$$\frac{d\boldsymbol{x}^{+}}{d\boldsymbol{x}_0} = \frac{\partial \boldsymbol{h}\left(\boldsymbol{x}^{-}\right)}{\partial \boldsymbol{x}^{-}}\frac{d\boldsymbol{x}^{-}}{d\boldsymbol{x}_0} \tag{18}$$

$$\frac{d\mathcal{L}_1\left(\boldsymbol{x}^{-}\right)}{d\boldsymbol{x}_0} = \frac{\partial \mathcal{L}_1\left(\boldsymbol{x}^{-}\right)}{\partial \boldsymbol{x}^{-}}\frac{d\boldsymbol{x}^{-}}{d\boldsymbol{x}_0} = \boldsymbol{0} \tag{19}$$

According to (2), we have: $\frac{\partial \mathcal{L}_1(\boldsymbol{x}^{-})}{\partial \boldsymbol{x}^{-}} = \boldsymbol{\mathcal{C}_1}$. Noting $\boldsymbol{h}_{\boldsymbol{x}}^{-} = \frac{\partial \boldsymbol{h}(\boldsymbol{x}^{-})}{\partial \boldsymbol{x}^{-}}$, and using relation (16), these two last expressions, (18) and (19), become, respectively:

$$\frac{d\boldsymbol{x}^{+}}{d\boldsymbol{x}_0} = \boldsymbol{h}_{\boldsymbol{x}}^{-}\left(\boldsymbol{\Phi}^{-} + \boldsymbol{f}^{-}\tau_{\boldsymbol{x}_0}\right) \tag{20}$$

$$\boldsymbol{\mathcal{C}_1}\left(\boldsymbol{\Phi}^{-} + \boldsymbol{f}^{-}\tau_{\boldsymbol{x}_0}\right) = \boldsymbol{0} \tag{21}$$

Taking into account the second transition condition in (2d) (i.e. $\mathcal{L}_2(\boldsymbol{x}) = \frac{\partial \mathcal{L}_1(\boldsymbol{x})}{\partial \boldsymbol{x}}\dot{\boldsymbol{x}} = \boldsymbol{\mathcal{C}_1 f} < 0$) and using relation (21), we can deduce the following expression:

$$\tau_{\boldsymbol{x}_0} = -\frac{\boldsymbol{\mathcal{C}_1}}{\boldsymbol{\mathcal{C}_1 f}^{-}}\boldsymbol{\Phi}^{-} \tag{22}$$

Using the two relations (20) and (22), expression (17) becomes:

$$\boldsymbol{\Phi}^{+} = \left(\boldsymbol{h}_{\boldsymbol{x}}^{-} - \frac{\left(\boldsymbol{h}_{\boldsymbol{x}}^{-}\boldsymbol{f}^{-} - \boldsymbol{f}^{+}\right)\boldsymbol{\mathcal{C}_1}}{\boldsymbol{\mathcal{C}_1 f}^{-}}\right)\boldsymbol{\Phi}^{-} \tag{23}$$

Thus, this expression shows that there is a relationship between the fundamental solution matrix just before the transition $\boldsymbol{\Phi}^{-}$ to that just after the transition $\boldsymbol{\Phi}^{+}$ as defined by equation (12). Therefore, the saltation matrix is expressed as:

$$\boldsymbol{\mathcal{S}}\left(\boldsymbol{x}^{+},\boldsymbol{x}^{-}\right)=\boldsymbol{h}_{\boldsymbol{x}}^{-}-\frac{\left(\boldsymbol{h}_{\boldsymbol{x}}^{-}\boldsymbol{f}^{-}-\boldsymbol{f}^{+}\right)\boldsymbol{\mathcal{C}}_{\mathbf{1}}}{\boldsymbol{\mathcal{C}}_{\mathbf{1}}\boldsymbol{f}^{-}} \tag{24}$$

Computation of the fundamental solution matrix $\boldsymbol{\Phi}\left(t,\boldsymbol{x}_0\right)$ requires primarily a precise knowledge of the transition instant τ and of course the saltation matrix (24). Then, in order to calculate the fundamental solution matrix $\boldsymbol{\Phi}\left(t,\boldsymbol{x}_0\right)$ for the impulsive hybrid nonlinear dynamics (2a)–(2b), we should solve numerically the following system:

$$\begin{cases} \dot{\boldsymbol{x}}=\boldsymbol{f}(\boldsymbol{x}) & \boldsymbol{x}\left(0\right)=\boldsymbol{x}_0 \\ \dot{\boldsymbol{\Phi}}(t,\boldsymbol{x}_0)=\boldsymbol{\mathcal{J}}_{\boldsymbol{f}}(\boldsymbol{x}(t))\boldsymbol{\Phi}(t,\boldsymbol{x}_0) & \boldsymbol{\Phi}(t_0,\boldsymbol{x}_0)=\boldsymbol{I}_n \end{cases} \quad \text{if } \boldsymbol{x}\in\Omega \tag{25}$$

$$\begin{cases} \boldsymbol{x}^{+}=\boldsymbol{h}(\boldsymbol{x}^{-}) \\ \boldsymbol{\Phi}^{+}=\boldsymbol{\mathcal{S}}\left(\boldsymbol{x}^{+},\boldsymbol{x}^{-}\right)\boldsymbol{\Phi}^{-} \end{cases} \quad \text{if } \boldsymbol{x}\in\Gamma \tag{26}$$

4.4 Monodromy Matrix

The good choice of the Poincaré section is the hypersurface Γ. Emanating from the initial state $\boldsymbol{x}_0$ (which is imposed to belong to Γ), the return time to the Poincaré section Γ is $\tau_r\left(\boldsymbol{x}_0\right)$. Then, for a periodic trajectory, this return time is eventually the period of the trajectory. Hence, for a one-periodic trajectory (a one-periodic hybrid limit cycle), the monodromy matrix $\boldsymbol{\Phi}\left(\tau_r\left(\boldsymbol{x}_0\right),\boldsymbol{x}_0\right)$ is given by:

$$\boldsymbol{\Phi}\left(\tau_r\left(\boldsymbol{x}_0\right),\boldsymbol{x}_0\right)=\boldsymbol{\mathcal{S}}\left(\boldsymbol{x}^{+},\boldsymbol{x}^{-}\right)\boldsymbol{\Phi}\left(\tau_{r_{\boldsymbol{x}_0}},\boldsymbol{x}_0\right) \tag{27}$$

The eigenvalues of the monodromy matrix $\boldsymbol{\Phi}\left(\tau_r\left(\boldsymbol{x}_0\right),\boldsymbol{x}_0\right)$ are called the Floquet multipliers. Each Floquet multiplier provides a measure of the local orbital divergence/convergence of along a particular direction over a period of the periodic solution (the limit cycle). Floquet multipliers therefore determine the stability of the limit cycle. The concept of a fundamental solution matrix is important in the analysis of the stability of the periodic solutions of nonlinear dynamical systems.

4.5 Identification of a One-Periodic Hybrid Limit Cycle

Each fixed point $\boldsymbol{x}_0$ of the Poincaré map (4) corresponds to a point (state) of a limit cycle of a given dynamical system. A limit cycle corresponds to a fixed point in the Poincare section. Thus, identification of a limit cycle lies in the determination of the

fixed point $\boldsymbol{x}_0$ of the Poincaré map. The Poincaré section is also the hypersurface Γ defined in (2d).

Bu referring to (4) and in order to determine the initial condition $\boldsymbol{x}_0$ of a one-periodic hybrid limit cycle, we must solve the following equation:

$$\boldsymbol{\mathcal{F}}\left(\boldsymbol{x}_0\right) = \boldsymbol{\phi}\left(\tau_r(\boldsymbol{x}_0), \boldsymbol{x}_0\right) - \boldsymbol{x}_0 = \boldsymbol{0} \tag{28}$$

with $\tau_r\left(\boldsymbol{x}_0\right)$ is the return time of the flow $\boldsymbol{\phi}$ to the Poincaré section Γ emanating from $\boldsymbol{x}_0$ and returning to Γ after a complete cycle, which is composed of only one intersection with Γ. Thus, $\boldsymbol{x}_0 \in \Gamma$ and $\boldsymbol{\phi}\left(\tau_r(\boldsymbol{x}_0), \boldsymbol{x}_0\right) \in \Gamma$.

To find the zeros of the relation in (28), we usually choose $\boldsymbol{x}_0$, then we iterate the Poincaré map only one time to get the flow $\boldsymbol{\phi}\left(\tau_r(\boldsymbol{x}_0), \boldsymbol{x}_0\right)$, and finally we iterate the Newton–Raphson scheme [66] like so:

$$\boldsymbol{x}_0^{i+1} = \boldsymbol{x}_0^i - \left(\boldsymbol{\mathcal{D}\mathcal{F}}\left(\boldsymbol{x}_0^i\right)\right)^{-1} \boldsymbol{\mathcal{F}}\left(\boldsymbol{x}_0^i\right) \tag{29}$$

with $\boldsymbol{\mathcal{D}\mathcal{F}}$ is the Jacobian matrix of the function $\boldsymbol{\mathcal{F}}$.

According to expression (28), it follows that:

$$\boldsymbol{\mathcal{D}\mathcal{F}}\left(\boldsymbol{x}_0\right) = \frac{d\boldsymbol{\phi}\left(\tau_r(\boldsymbol{x}_0), \boldsymbol{x}_0\right)}{d\boldsymbol{x}_0} - \boldsymbol{I} \tag{30}$$

In (30), the first right term is equal to:

$$\frac{d\boldsymbol{\phi}\left(\tau_r(\boldsymbol{x}_0), \boldsymbol{x}_0\right)}{d\boldsymbol{x}_0} = \frac{\partial\boldsymbol{\phi}\left(\tau_r(\boldsymbol{x}_0), \boldsymbol{x}_0\right)}{\partial\boldsymbol{x}_0} + \frac{\partial\boldsymbol{\phi}\left(\tau_r(\boldsymbol{x}_0), \boldsymbol{x}_0\right)}{\partial\tau_r(\boldsymbol{x}_0)} \frac{d\tau_r(\boldsymbol{x}_0)}{d\boldsymbol{x}_0} \tag{31}$$

Relying on expression (9), it holds that: $\frac{\partial\boldsymbol{\phi}(\tau_r(\boldsymbol{x}_0), \boldsymbol{x}_0)}{\partial\boldsymbol{x}_0} = \boldsymbol{\Phi}\left(\tau_r(\boldsymbol{x}_0), \boldsymbol{x}_0\right)$. In fact, $\boldsymbol{\Phi}$ is the fundamental solution matrix, and the matrix $\boldsymbol{\Phi}\left(\tau_r\left(\boldsymbol{x}_0\right), \boldsymbol{x}_0\right)$ is the monodromy matrix evaluated at the return time $\tau_r\left(\boldsymbol{x}_0\right)$. Moreover, we emphasize that: $\frac{\partial\boldsymbol{\phi}(\tau_r(\boldsymbol{x}_0), \boldsymbol{x}_0)}{\partial\tau_r(\boldsymbol{x}_0)} = \boldsymbol{f}\left(\boldsymbol{x}\left(\tau_r(\boldsymbol{x}_0)\right)\right)$. Then, expression (31) becomes:

$$\frac{d\boldsymbol{\phi}\left(\tau_r(\boldsymbol{x}_0), \boldsymbol{x}_0\right)}{d\boldsymbol{x}_0} = \boldsymbol{\Phi}\left(\tau_r(\boldsymbol{x}_0), \boldsymbol{x}_0\right) + \boldsymbol{f}\left(\boldsymbol{x}\left(\tau_r(\boldsymbol{x}_0)\right)\right) \frac{d\tau_r(\boldsymbol{x}_0)}{d\boldsymbol{x}_0} \tag{32}$$

In (32), only the term $\frac{d\tau_r(\boldsymbol{x}_0)}{d\boldsymbol{x}_0}$ is unknown. To calculate it, we must consider the Poincaré section (2d). Therefore, we can note the following two conditions:

$$\mathcal{L}_1\left(\boldsymbol{\phi}\left(\tau_r(\boldsymbol{x}_0), \boldsymbol{x}_0\right)\right) = \boldsymbol{C_1}\boldsymbol{\phi}\left(\tau_r(\boldsymbol{x}_0), \boldsymbol{x}_0\right) + 2\varphi = 0 \tag{33a}$$

$$\mathcal{L}_2\left(\boldsymbol{\phi}\left(\tau_r(\boldsymbol{x}_0), \boldsymbol{x}_0\right)\right) = \boldsymbol{C_2}\boldsymbol{\phi}\left(\tau_r(\boldsymbol{x}_0), \boldsymbol{x}_0\right) = \boldsymbol{C_1}\boldsymbol{f}\left(\boldsymbol{\phi}\left(\tau_r(\boldsymbol{x}_0), \boldsymbol{x}_0\right)\right) < 0 \tag{33b}$$

Using relation (33a), we obtain:

$$\frac{d\mathcal{L}_1\left(\boldsymbol{\phi}\left(\tau_r(\boldsymbol{x}_0),\boldsymbol{x}_0\right)\right)}{d\boldsymbol{x}_0}=\frac{\partial\mathcal{L}_1\left(\boldsymbol{\phi}\left(\tau_r(\boldsymbol{x}_0),\boldsymbol{x}_0\right)\right)}{\partial\boldsymbol{x}_0}+\frac{\partial\mathcal{L}_1\left(\boldsymbol{\phi}\left(\tau_r(\boldsymbol{x}_0),\boldsymbol{x}_0\right)\right)}{\partial\tau_r(\boldsymbol{x}_0)}\frac{d\tau_r(\boldsymbol{x}_0)}{d\boldsymbol{x}_0}=\mathbf{0} \tag{34}$$

In addition, we have:

$$\frac{\partial\mathcal{L}_1\left(\boldsymbol{\phi}\left(\tau_r(\boldsymbol{x}_0),\boldsymbol{x}_0\right)\right)}{\partial\boldsymbol{x}_0}=\frac{\partial\mathcal{L}_1\left(\boldsymbol{\phi}\left(\tau_r(\boldsymbol{x}_0),\boldsymbol{x}_0\right)\right)}{\partial\boldsymbol{\phi}\left(\tau_r(\boldsymbol{x}_0),\boldsymbol{x}_0\right)}\frac{\partial\boldsymbol{\phi}\left(\tau_r(\boldsymbol{x}_0),\boldsymbol{x}_0\right)}{\partial\boldsymbol{x}_0} \tag{35}$$

$$\frac{\partial\mathcal{L}_1\left(\boldsymbol{\phi}\left(\tau_r(\boldsymbol{x}_0),\boldsymbol{x}_0\right)\right)}{\partial\tau_r(\boldsymbol{x}_0)}=\frac{\partial\mathcal{L}_1\left(\boldsymbol{\phi}\left(\tau_r(\boldsymbol{x}_0),\boldsymbol{x}_0\right)\right)}{\partial\boldsymbol{\phi}\left(\tau_r(\boldsymbol{x}_0),\boldsymbol{x}_0\right)}\frac{\partial\boldsymbol{\phi}\left(\tau_r(\boldsymbol{x}_0),\boldsymbol{x}_0\right)}{\partial\tau_r(\boldsymbol{x}_0)} \tag{36}$$

Based on the above results, expression (34) will be rewritten like so:

$$\boldsymbol{\mathcal{C}_1\Phi}\left(\tau_r(\boldsymbol{x}_0),\boldsymbol{x}_0\right)+\boldsymbol{\mathcal{C}_1 f}\left(\boldsymbol{x}\left(\tau_r(\boldsymbol{x}_0)\right)\right)\frac{d\tau_r(\boldsymbol{x}_0)}{d\boldsymbol{x}_0}=\mathbf{0} \tag{37}$$

Using expression (37) and taking into account the inequality (33b), the quantity $\frac{d\tau_r(\boldsymbol{x}_0)}{d\boldsymbol{x}_0}$ is expressed by:

$$\frac{d\tau_r(\boldsymbol{x}_0)}{d\boldsymbol{x}_0}=-\frac{\boldsymbol{\mathcal{C}_1\Phi}\left(\tau_r(\boldsymbol{x}_0),\boldsymbol{x}_0\right)}{\boldsymbol{\mathcal{C}_1 f}\left(\boldsymbol{x}\left(\tau_r(\boldsymbol{x}_0)\right)\right)} \tag{38}$$

Then, substituting this amount $\frac{d\tau_r(\boldsymbol{x}_0)}{d\boldsymbol{x}_0}$ in (32), we obtain the following relation:

$$\frac{d\boldsymbol{\phi}\left(\tau_r(\boldsymbol{x}_0),\boldsymbol{x}_0\right)}{d\boldsymbol{x}_0}=\left(\boldsymbol{I}_n-\frac{\boldsymbol{f}\left(\boldsymbol{x}\left(\tau_r(\boldsymbol{x}_0)\right)\right)\boldsymbol{\mathcal{C}_1}}{\boldsymbol{\mathcal{C}_1 f}\left(\boldsymbol{x}\left(\tau_r(\boldsymbol{x}_0)\right)\right)}\right)\boldsymbol{\Phi}\left(\tau_r(\boldsymbol{x}_0),\boldsymbol{x}_0\right) \tag{39}$$

with $\boldsymbol{I}_n$ is the identity matrix of dimension $(n\times n)$.

Therefore, the function $\boldsymbol{\mathcal{DF}}$ in (30) will be defined as follows:

$$\boldsymbol{\mathcal{DF}}\left(\boldsymbol{x}_0\right)=\left(\boldsymbol{I}_n-\frac{\boldsymbol{f}\left(\boldsymbol{x}\left(\tau_r\left(\boldsymbol{x}_0\right)\right)\right)\boldsymbol{\mathcal{C}_1}}{\boldsymbol{\mathcal{C}_1 f}\left(\boldsymbol{x}\left(\tau_r\left(\boldsymbol{x}_0\right)\right)\right)}\right)\boldsymbol{\Phi}\left(\tau_r(\boldsymbol{x}_0),\boldsymbol{x}_0\right)-\boldsymbol{I}_n \tag{40}$$

This expression can be rewritten as:

$$\boldsymbol{\mathcal{DF}}\left(\boldsymbol{x}_0\right)=\left(\boldsymbol{I}_n-\frac{\boldsymbol{f}^{-}\boldsymbol{\mathcal{C}_1}}{\boldsymbol{\mathcal{C}_1 f}^{-}}\right)\boldsymbol{\Phi}^{+}-\boldsymbol{I}_n \tag{41}$$

where $\boldsymbol{\Phi}^{+}$ is the monodromy matrix calculated just after the impact according the previous section and hence via the saltation matrix.

4.6 Stability of the One-Periodic Hybrid Limit Cycle

With a good estimate of the initial condition, the iterative scheme (29) will converge to a fixed point $\boldsymbol{x}_0$ corresponding to a one-periodic hybrid limit cycle of the impulsive hybrid nonlinear dynamics (2). This limit cycle can be stable or unstable. The stability of the limit cycle is determined via its characteristic multipliers, which are also known as the Floquet multipliers [66]. The limit cycle corresponds to a fixed point $\boldsymbol{x}_0$ in the Poincaré map. The local behavior of the Poincaré map near $\boldsymbol{x}_0$ is determined by the linearized equation of the map $\mathcal{P}$ at $\boldsymbol{x}_0$ as follows:

$$\boldsymbol{\delta x}_{k+1} = \boldsymbol{D\mathcal{P}}\left(\boldsymbol{x}_0\right)\boldsymbol{\delta x}_k \tag{42}$$

The matrix $\boldsymbol{D\mathcal{P}}$ is the Jacobian matrix of the Poincaré map $\mathcal{P}$. Referring to expression (4) and expression (39), we can deduce that the Jacobian matrix $\mathcal{DP}\left(\boldsymbol{x}_0\right)$ of the Poincaré map $\mathcal{P}$ is related to the monodromy matrix $\boldsymbol{\Phi}\left(\tau_r\left(\boldsymbol{x}_0\right), \boldsymbol{x}_0\right)$ as follows:

$$\mathcal{DP}\left(\boldsymbol{x}_0\right) = \left(\boldsymbol{I}_n - \frac{f^{-}\mathcal{C}_1}{\mathcal{C}_1 f^{-}}\right)\boldsymbol{\Phi}^{+} \tag{43}$$

The characteristics multipliers m_i, $i = 1, \ldots, n-1$, are the eigenvalues of $\mathcal{DP}\left(\boldsymbol{x}_0\right)$ and form a subset of the Floquet multipliers, which are the eigenvalues of the monodromy matrix $\boldsymbol{\Phi}\left(\tau_r\left(\boldsymbol{x}_0\right), \boldsymbol{x}_0\right)$. It is shown in [66] that an eigenvalue of this monodromy matrix is always equal to 1. The remaining eigenvalues are equal to m_i. It is shown as well as that the characteristics multipliers are independent of the choice of the Poincaré section.

Because the characteristics multipliers m_i are the eigenvalues of the Jacobian matrix of the Poincaré map, they allow to study the stability of the one-periodic hybrid limit cycle. In fact, there are two important cases:

1. if all the characteristics multipliers m_i are inside the unit circle, that is to say $|m_i| < 1$, for all $i = 1, \ldots, (n-1)$, the one-periodic hybrid limit cycle is stable.
2. while if some m_i are outside the unit circle, then one-periodic hybrid limit cycle is unstable.

5 Controller Design Based on the OGY Approach

In this section, our main objective is to design a control structure for the impulsive hybrid nonlinear dynamics (2) of the compass-gait biped model in order to stabilize the passive walking gaits. Thus, to accomplish this, the idea is to use the formalism of the OGY method, which is based mainly on the linearization of the controlled Poincaré map. Then, a mathematical expression of such Poincaré map is absolutely needed. Then, to achieve this problem, we will linearize the impulsive hybrid nonlinear dynamics (2) around a desired unstable one-periodic hybrid limit cycle. The

process of linearization and the determination of the analytical expression of the controlled Poincaré map is described in the sequel. We note that this work in this section was based on our work in [21, 22, 31]. Then, for more details about the linearization method around a desired period-1 limit cycle, we refer readers to [21, 22, 31]. We stress that our linearization method in [21, 22, 31] is done only for the nonlinear differential equation (2a). In this chapter, we will linearize also the nonlinear algebraic equation (2b).

5.1 *Linearization Procedure of the Impulsive Hybrid Nonlinear Dynamics*

Let Λ_d be the desired one-periodic hybrid limit cycle, which is defined for some desired slope φ_d. Such limit cycle is in fact identified according to the previous section and which can be either stable or unstable. It is characterized by its corresponding flow $\boldsymbol{x}_d(t) = \boldsymbol{\phi}_d\,(t, \boldsymbol{x}_d)$, the desired initial condition $\boldsymbol{x}_d^-$ and the desired impact instant τ_d. The linearization precess of the impulsive hybrid nonlinear dynamics (2) is based mainly on the specification of n points $\boldsymbol{\chi}_i$, for $i = 1, 2, \ldots, n$, of the desired flow $\boldsymbol{\phi}_d\,(t, \boldsymbol{x}_d)$. According to [21, 22, 31], each point is described by $\boldsymbol{\chi}_i = \boldsymbol{x}_d\left(\frac{t_i + t_{(i-1)}}{2}\right)$, where

$$t_i = \frac{i}{n}\tau_d \tag{44}$$

Then, the point $\boldsymbol{\chi}_i$ can be determined like so:

$$\boldsymbol{\chi}_i = \boldsymbol{x}_d\left(\frac{2i-1}{2n}\tau_d\right) \tag{45}$$

Then, linearization procedure around each point $\boldsymbol{\chi}_i$ permit us to define n submodel M_i, for $i = 1, 2, \ldots, n$. Each submodel M_i is defined in $\left[\, t_{(i-1)} \;\; t_i \,\right]$ as follows:

$$\dot{\boldsymbol{x}} = \boldsymbol{\mathcal{A}}_i \boldsymbol{x} + \boldsymbol{\mathcal{B}}_i u + \boldsymbol{\mathcal{D}}_i \quad \text{for} \quad t_{(i-1)} \leq t \leq t_i \;, \tag{46}$$

with $\boldsymbol{\mathcal{A}}_i = \frac{\partial \boldsymbol{f}(\boldsymbol{x})}{\partial \boldsymbol{x}}|_{\boldsymbol{\chi}_i}$, $\boldsymbol{\mathcal{B}}_i = \boldsymbol{g}\left(\boldsymbol{\chi}_i\right)$, and $\boldsymbol{\mathcal{D}}_i = \boldsymbol{f}\left(\boldsymbol{\chi}_i\right) - \boldsymbol{\mathcal{A}}_i \boldsymbol{\chi}_i$.

As demonstrated in [21, 22, 31], we have:

$$n < \frac{\tau_d}{\tau_d - \tau} \tag{47}$$

In addition, in this chapter, the algebraic equation in (2b) is linearized around the desired one-periodic fixed point $\boldsymbol{x}_d^-$ of the desired one-periodic hybrid limit cycle. Hence, we obtain:

$$\boldsymbol{x}^+ = \boldsymbol{\mathcal{M}} \boldsymbol{x}^- + \boldsymbol{\mathcal{N}} \quad \text{for} \quad t = \tau_d \,, \tag{48}$$

with $\mathcal{M} = \frac{\partial \boldsymbol{h}(\boldsymbol{x})}{\partial \boldsymbol{x}}_{|\boldsymbol{x}_d^-}$ and $\mathcal{N} = \boldsymbol{h}\left(\boldsymbol{x}_d^-\right) - \mathcal{M}\boldsymbol{x}_d^-$.

According to [21, 22, 31] and using expression (48), the linearization procedure of the impulsive hybrid nonlinear dynamics (2) around a one-periodic hybrid limit cycle has permitted to deduce an impulsive hybrid linear dynamics:

$$\begin{cases} \dot{\boldsymbol{x}} = \mathcal{A}_n \boldsymbol{x} + \mathcal{D}_n + \mathcal{B}_n u, & \text{as long as} \quad \boldsymbol{x} \in \Omega \\ \boldsymbol{x}^+ = \mathcal{J}_1 \boldsymbol{x}^- + \mathcal{H}_1 + \mathcal{G}_1 u & \text{whenever} \quad \boldsymbol{x}^- \in \Gamma \end{cases} \tag{49}$$

with $\mathcal{J}_1 = \left(\prod_{i=1}^{n-1} e^{\frac{\tau_d}{n}\mathcal{A}_i}\right)\mathcal{M}$, $\mathcal{H}_1 = \left(\prod_{i=1}^{n-1} e^{\frac{\tau_d}{n}\mathcal{A}_i}\right)\mathcal{N} + \sum_{i=1}^{n-1}\left(\prod_{j=i+1}^{n-1} e^{\frac{\tau_d}{n}\mathcal{A}_j}\right)\left(e^{\frac{\tau_d}{n}\mathcal{A}_i} - \mathcal{I}\right)\mathcal{A}_i^{-1}\mathcal{D}_i$, and $\mathcal{G}_1 = \sum_{i=1}^{n-1}\left(\prod_{j=i+1}^{n-1} e^{\frac{\tau_d}{n}\mathcal{A}_j}\right)\left(e^{\frac{\tau_d}{n}\mathcal{A}_i} - \mathcal{I}\right)\mathcal{A}_i^{-1}\mathcal{B}_i$. Here and in the sequel of this chapter $\mathcal{I}$ is the identity matrix of dimension 4.

5.2 Analytical Expression of the Controlled Hybrid Poincaré Map

Let define first the following notations as in [21, 22, 31]:

- $\boldsymbol{x}_k^-$ is the initial state just before the kth impact,
- τ_k is the impact instant,
- u_k is the control law applied along the kth one-periodic hybrid limit cycle,
- $\boldsymbol{x}_{k+1}^-$ is the initial state just before the $(k+1)$th impact.

According to the linear differential equation (49), we have derived the following analytical expression of a controlled hybrid Poincaré map:

$$\boldsymbol{x}_{k+1}^- = \mathcal{P}\left(\boldsymbol{x}_k^-, \tau_k, u_k\right) \tag{50a}$$

$$\begin{cases} \mathcal{L}_1\left(\mathcal{P}\left(\boldsymbol{x}_k^-, \tau_k, u_k\right)\right) = 0 \\ \mathcal{L}_2\left(\mathcal{P}\left(\boldsymbol{x}_k^-, \tau_k, u_k\right)\right) < 0 \end{cases} \tag{50b}$$

with

$$\mathcal{P}\left(\boldsymbol{x}_k^-, \tau_k, u_k\right) = \mathcal{J}\left(\tau_k\right)\boldsymbol{x}_k^- + \mathcal{H}\left(\tau_k\right) + \mathcal{G}\left(\tau_k\right)u_k \tag{51a}$$

$$\mathcal{L}_1\left(\mathcal{P}\left(\boldsymbol{x}_k^-, \tau_k, u_k\right)\right) = \boldsymbol{C_1}\mathcal{P}\left(\boldsymbol{x}_k^-, \tau_k, u_k\right) + 2\varphi = 0 \tag{51b}$$

$$\mathcal{L}_2\left(\mathcal{P}\left(\boldsymbol{x}_k^-, \tau_k, u_k\right)\right) = \boldsymbol{C_2}\mathcal{P}\left(\boldsymbol{x}_k^-, \tau_k, u_k\right) < 0 \tag{51c}$$

where $\mathcal{J}\left(\tau_k\right) = \mathcal{J}_2\left(\tau_k\right)\mathcal{J}_1$, $\mathcal{H}\left(\tau_k\right) = \mathcal{J}_2\left(\tau_k\right)\mathcal{H}_1 + \mathcal{H}_2\left(\tau_k\right)$, and $\mathcal{G}\left(\tau_k\right) = \mathcal{J}_2\left(\tau_k\right)\mathcal{G}_1 + \mathcal{G}_2\left(\tau_k\right)$, with $\mathcal{J}_2\left(\tau_k\right) = e^{\tau_k \mathcal{A}_n}$, $\mathcal{H}_2\left(\tau_k\right) = \left(\mathcal{J}_2\left(\tau_k\right) - \mathcal{I}\right)\mathcal{A}_n^{-1}\mathcal{D}_n$, and $\mathcal{G}_2\left(\tau_k\right) = \left(\mathcal{J}_2\left(\tau_k\right) - \mathcal{I}\right)\mathcal{A}_n^{-1}\mathcal{B}_n$.

5.3 Computation of the One-Periodic Fixed Point of the Hybrid Poincaré Map

Here, we look for computing the one-periodic fixed point $\boldsymbol{x}_*^-$ of the hybrid Poincaré map (50) for a passive dynamics, i.e. $u_k = u_* = 0$. Then, this fixed point $\boldsymbol{x}_*^-$ and its associated impact instant τ_* are the solutions of the following functions:

$$\boldsymbol{\mathcal{P}}\left(\boldsymbol{x}_*^-, \tau_*\right) - \boldsymbol{x}_*^- = \boldsymbol{0} \tag{52a}$$

$$\mathcal{L}_1\left(\boldsymbol{\mathcal{P}}\left(\boldsymbol{x}_*^-, \tau_*\right)\right) = 0 \tag{52b}$$

$$\mathcal{L}_2\left(\boldsymbol{\mathcal{P}}\left(\boldsymbol{x}_*^-, \tau_*\right)\right) < 0 \tag{52c}$$

Using expressions in (51), we can show that τ_* is the solution of the following two scalar constraints:

$$\boldsymbol{\mathcal{C}_1}\left(\boldsymbol{\mathcal{I}} - \boldsymbol{\mathcal{J}}\left(\tau_*\right)\right)^{-1}\boldsymbol{\mathcal{H}}\left(\tau_*\right) + 2\varphi = 0 \tag{53a}$$

$$\boldsymbol{\mathcal{C}_2}\left(\boldsymbol{\mathcal{I}} - \boldsymbol{\mathcal{J}}\left(\tau_*\right)\right)^{-1}\boldsymbol{\mathcal{H}}\left(\tau_*\right) < 0 \tag{53b}$$

Hence, the one-periodic fixed point $\boldsymbol{x}_*^-$ will be evaluated via the following expression:

$$\boldsymbol{x}_*^- = \left(\boldsymbol{\mathcal{I}} - \boldsymbol{\mathcal{J}}\left(\tau_*\right)\right)^{-1}\boldsymbol{\mathcal{H}}\left(\tau_*\right) \tag{54}$$

5.4 Linearized Hybrid Poincaré Map and Stability of the Fixed Point

As in [21, 22, 31], we pose: $\Delta\boldsymbol{x}_{k+1}^- = \boldsymbol{x}_{k+1}^- - \boldsymbol{x}_*^-$ and $\Delta\boldsymbol{x}_k^- = \boldsymbol{x}_k^- - \boldsymbol{x}_*^-$. The linearized hybrid Poincaré map around the one-periodic fixed point $\boldsymbol{x}_*^-$ is expressed like so:

$$\Delta\boldsymbol{x}_{k+1}^- = \mathcal{D}\boldsymbol{\mathcal{P}}_{\boldsymbol{x}_k^-}\left(\boldsymbol{x}_*^-, \tau_*, u_*\right)\Delta\boldsymbol{x}_k^- + \mathcal{D}\boldsymbol{\mathcal{P}}_{u_k}\left(\boldsymbol{x}_*^-, \tau_*, u_*\right)u_k \tag{55}$$

The state matrix $\mathcal{D}\boldsymbol{\mathcal{P}}_{\boldsymbol{x}_k^-}\left(\boldsymbol{x}_*^-, \tau_*, u_*\right)$ and the input matrix $\mathcal{D}\boldsymbol{\mathcal{P}}_{u_k}\left(\boldsymbol{x}_*^-, \tau_*, u_*\right)$ in the linearized hybrid Poincaré map (55) are defined, according to [21, 22, 31], as follows:

$$\mathcal{D}\boldsymbol{\mathcal{P}}_{\boldsymbol{x}_k^-}\left(\boldsymbol{x}_k^-, \tau_k, u_k\right) = \left[\boldsymbol{\mathcal{I}} - \frac{\frac{\partial\boldsymbol{\mathcal{P}}\left(\boldsymbol{x}_k^-, \tau_k, u_k\right)}{\partial\tau_k}\boldsymbol{\mathcal{C}_1}}{\boldsymbol{\mathcal{C}_2}\boldsymbol{\mathcal{P}}\left(\boldsymbol{x}_k^-, \tau_k, u_k\right)}\right]\frac{\partial\boldsymbol{\mathcal{P}}\left(\boldsymbol{x}_k^-, \tau_k, u_k\right)}{\partial\boldsymbol{x}_k^-} \tag{56a}$$

$$\mathcal{D}\boldsymbol{\mathcal{P}}_{u_k}\left(\boldsymbol{x}_k^-, \tau_k, u_k\right) = \left[\boldsymbol{\mathcal{I}} - \frac{\frac{\partial \boldsymbol{\mathcal{P}}\left(\boldsymbol{x}_k^-, \tau_k, u_k\right)}{\partial \tau_k}\boldsymbol{\mathcal{C}_1}}{\boldsymbol{\mathcal{C}_2}\boldsymbol{\mathcal{P}}\left(\boldsymbol{x}_k^-, \tau_k, u_k\right)}\right]\frac{\partial \boldsymbol{\mathcal{P}}\left(\boldsymbol{x}_k^-, \tau_k, u_k\right)}{\partial u_k} \tag{56b}$$

According to [21, 22, 31], $\frac{\partial \boldsymbol{\mathcal{P}}\left(\boldsymbol{x}_k^-, \tau_k, u_k\right)}{\partial \tau_k} = \boldsymbol{\mathcal{A}}_n\boldsymbol{\mathcal{P}}\left(\boldsymbol{x}_k^-, \tau_k, u_k\right) + \boldsymbol{\mathcal{D}}_n + \boldsymbol{\mathcal{B}}_n u_k$. Furthermore, relying on expressions in (51), it follows that: $\frac{\partial \boldsymbol{\mathcal{P}}\left(\boldsymbol{x}_k^-, \tau_k, u_k\right)}{\partial \boldsymbol{x}_k^-} = \boldsymbol{\mathcal{J}}\left(\tau_k\right)$, and $\frac{\partial \boldsymbol{\mathcal{P}}\left(\boldsymbol{x}_k^-, \tau_k, u_k\right)}{\partial u_k} = \boldsymbol{\mathcal{G}}\left(\tau_k\right)$.

It is easy to demonstrate that the state matrix $\mathcal{D}\boldsymbol{\mathcal{P}}_{\boldsymbol{x}_k^-}\left(\boldsymbol{x}_*^-, \tau_*, u_*\right)$ and the input matrix $\mathcal{D}\boldsymbol{\mathcal{P}}_{u_k}\left(\boldsymbol{x}_*^-, \tau_*, u_*\right)$ in the linearized hybrid Poincaré map (55) are described with respect to the nominal impact instant τ_* by:

$$\mathcal{D}\boldsymbol{\mathcal{P}}_{\boldsymbol{x}_k^-}\left(\tau_*\right) = \left[\boldsymbol{\mathcal{I}} - \frac{\boldsymbol{\mathcal{A}}_n\left(\boldsymbol{\mathcal{I}} - \boldsymbol{\mathcal{J}}\left(\tau_*\right)\right)^{-1}\boldsymbol{\mathcal{H}}\left(\tau_*\right)\boldsymbol{\mathcal{C}} + \boldsymbol{\mathcal{D}}_n\boldsymbol{\mathcal{C}}}{\boldsymbol{\mathcal{C}}\boldsymbol{\mathcal{A}}_n\left(\boldsymbol{\mathcal{I}} - \boldsymbol{\mathcal{J}}\left(\tau_*\right)\right)^{-1}\boldsymbol{\mathcal{H}}\left(\tau_*\right) + \boldsymbol{\mathcal{C}}\boldsymbol{\mathcal{D}}_n}\right]\boldsymbol{\mathcal{J}}\left(\tau_*\right) \tag{57a}$$

$$\mathcal{D}\boldsymbol{\mathcal{P}}_{u_k}\left(\tau_*\right) = \left[\boldsymbol{\mathcal{I}} - \frac{\boldsymbol{\mathcal{A}}_n\left(\boldsymbol{\mathcal{I}} - \boldsymbol{\mathcal{J}}\left(\tau_*\right)\right)^{-1}\boldsymbol{\mathcal{H}}\left(\tau_*\right)\boldsymbol{\mathcal{C}} + \boldsymbol{\mathcal{D}}_n\boldsymbol{\mathcal{C}}}{\boldsymbol{\mathcal{C}}\boldsymbol{\mathcal{A}}_n\left(\boldsymbol{\mathcal{I}} - \boldsymbol{\mathcal{J}}\left(\tau_*\right)\right)^{-1}\boldsymbol{\mathcal{H}}\left(\tau_*\right) + \boldsymbol{\mathcal{C}}\boldsymbol{\mathcal{D}}_n}\right]\boldsymbol{\mathcal{G}}\left(\tau_*\right) \tag{57b}$$

We emphasize that stability investigation of the one-periodic fixed point $\boldsymbol{x}_*^-$ of the hybrid Poincaré map lies in the analysis of the eigenvalues of the Jacobian matrix $\mathcal{D}\boldsymbol{\mathcal{P}}_{\boldsymbol{x}_k^-}\left(\tau_*\right)$ defined by expression (57a). It is worth noting that stability of the fixed point depends chiefly on only the impact instant τ_*. Thus, if all the eigenvalues of $\mathcal{D}\boldsymbol{\mathcal{P}}_{\boldsymbol{x}_k^-}\left(\tau_*\right)$ are inside the unit circle, then the fixed point $\boldsymbol{x}_*^-$ is stable. However, if at least one eigenvalue is outside the unit circle, then the one-periodic fixed point $\boldsymbol{x}_*^-$ is unstable. As the linearization procedure of the impulsive hybrid nonlinear dynamics was achieved around an unstable periodic-one hybrid limit cycle, then the one-periodic fixed point $\boldsymbol{x}_*^-$ is absolutely unstable.

5.5 *Stabilization of the One-Periodic Fixed Point of the Hybrid Poincaré Map*

The stabilization problem of the one-periodic fixed point $\boldsymbol{x}_*^-$ of the hybrid Poincaré map (50) is in fact the stabilization problem of the linearized hybrid Poincaré map (55). As in our work in [21, 22, 31], we introduced the state-feedback controller:

$$u_k = \boldsymbol{\mathcal{K}}\left(\boldsymbol{x}_k^- - \boldsymbol{x}_*^-\right) \tag{58}$$

where $\boldsymbol{\mathcal{K}}$ is the matrix gain.

The computation of $\boldsymbol{\mathcal{K}}$ is subject to a solving problem of the following linear matrix inequality [21, 22, 31]:

$$\begin{bmatrix} \mathcal{S} & \mathcal{DP}_{\boldsymbol{x}_k^-}(\tau_*)\,\mathcal{S} + \mathcal{DP}_{u_k}(\tau_*)\,\mathcal{R} \\ \left(\mathcal{DP}_{\boldsymbol{x}_k^-}(\tau_*)\,\mathcal{S} + \mathcal{DDP}_{u_k}(\tau_*)\,\mathcal{R}\right)^T & \mathcal{S} \end{bmatrix} > 0 \quad (59)$$

One this linear matrix inequality is solved with respect to $\mathcal{S}$ and $\mathcal{R}$, hence the matrix gain $\mathcal{K}$ is evaluated like so:

$$\mathcal{K} = \mathcal{R}\mathcal{S}^{-1} \quad (60)$$

6 Numerical Results on the Stabilization of the One-Periodic Hybrid Limit Cycle

In this section, we will verify efficiency of the developed OGY-based controller (58) for the stabilization of the one-periodic hybrid limit cycle of the impulsive hybrid nonlinear dynamics (2). Thus, we chosen three different desired slopes $\varphi_d = 4.8°$, $\varphi_d = 5.2°$ and $\varphi_d = 7°$, for which the identified passive one-periodic hybrid limit cycle of the compass-gait biped robot is unstable [25, 30]. Indeed, for the slope parameter $\varphi_d = 4.8°$, the passive steady gait is two-periodic. However, the passive gait was found to be chaotic for the second desired slope $\varphi_d = 5.2°$. In contrast, for $\varphi_d = 7°$, there is no steady gait and only an unstable limit cycle is found. As a result, the passive compass-gait biped robot falls down for any initial conditions.

For each of these three desired slopes, its corresponds a desired unstable one-periodic hybrid limit cycle, which is characterized by the desired initial condition just before the impact phase $\boldsymbol{x}_d^-$ and the desired impact instant τ_d like so:

- For $\varphi_d = 4.8°$, $\boldsymbol{x}_d^- = \begin{bmatrix} 13.4277 & -23.0277 & -130.6885 & -102.5579 \end{bmatrix}^T$, and $\tau_d = 0.7594\,\text{s}$.
- For $\varphi_d = 5.2°$, $\boldsymbol{x}_d^- = \begin{bmatrix} 13.5357 & -23.9357 & -135.9613 & -105.8478 \end{bmatrix}^T$, and $\tau_d = 0.7647\,\text{s}$.
- For $\varphi_d = 7°$, $\boldsymbol{x}_d^- = \begin{bmatrix} 13.7648 & -27.7648 & -156.8854 & -119.2884 \end{bmatrix}^T$, and $\tau_d = 0.7880\,\text{s}$.

These one-periodic hybrid limit cycles are found according to Sect. 4. Then, using the linearization procedure, discussed in Sect. 5, around these identified limit cycles for each desired slope parameter φ_d, we have computed the one-periodic fixed point $\boldsymbol{x}_*^-$ of the hybrid Poincaré map and the associated impact instant τ_*. Moreover, we have calculated the matrix gain $\mathcal{K}$ of the control law (58) by solving the linear matrix inequality (59). As a result, we obtained:

- For $\varphi_d = 4.8°$, $\boldsymbol{x}_*^- = \begin{bmatrix} 13.3806 & -22.9806 & -131.1828 & -102.4169 \end{bmatrix}^T$, $\tau_d = 0.7576\,\text{s}$, and $\mathcal{K} = \begin{bmatrix} -56.2135 & 9.0743 & 1.1929 & -10.2254 \end{bmatrix}$.
- For $\varphi_d = 5.2°$, $\boldsymbol{x}_*^- = \begin{bmatrix} 13.4855 & -23.8855 & -136.4149 & -105.7015 \end{bmatrix}^T$, $\tau_d = 0.7627\,\text{s}$, and $\mathcal{K} = \begin{bmatrix} -61.7227 & 11.5451 & 1.2807 & -10.8518 \end{bmatrix}$.

- For $\varphi_d = 7°$, $\boldsymbol{x}_*^- = \begin{bmatrix} 13.7018 & -27.7018 & -157.5949 & -119.1341 \end{bmatrix}^T$, $\tau_d = 0.7855\,\text{s}$, and $\mathcal{K} = \begin{bmatrix} -83.5237 & 22.2179 & 1.6010 & -12.8260 \end{bmatrix}$.

It is obvious that the results obtained from the hybrid Poincaré map are nearly identical to that obtained through the impulsive hybrid nonlinear dynamics. Then, by applying the control law (58) to the impulsive nonlinear dynamics (2) for each

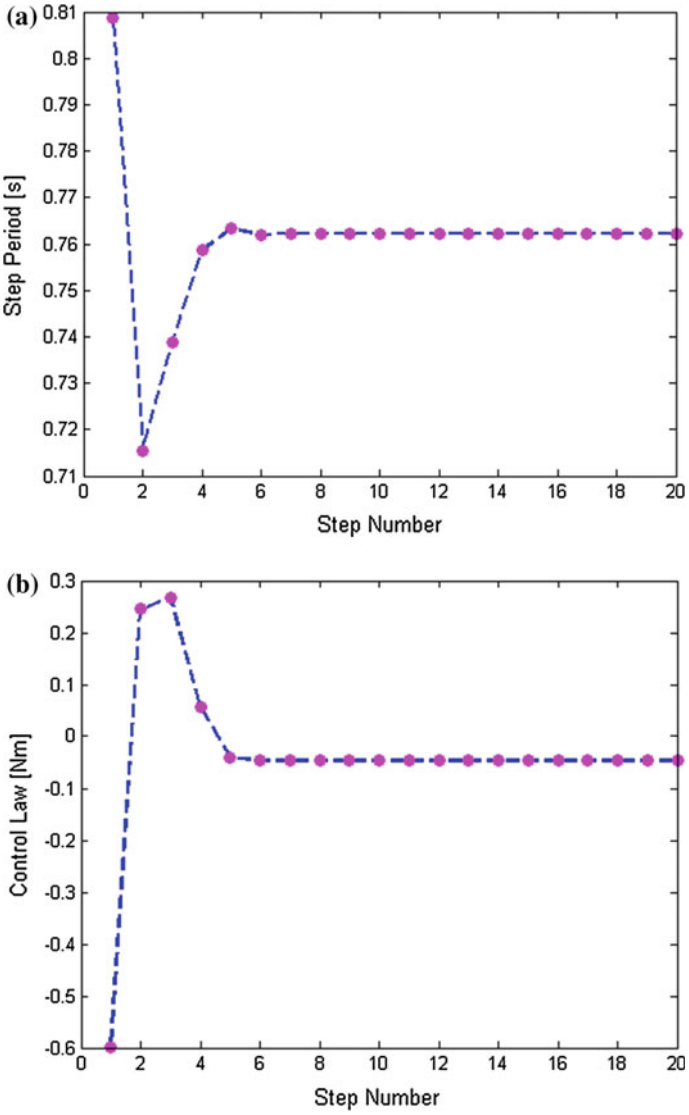

Fig. 3 Variation of walking step period **a** of the compass-gait biped model under the OGY controller **b** for the desired slope $\varphi_d = 4.8°$

desired slope parameter φ_d and for the corresponding the matrix gain $\mathcal{K}$, we obtained the numerical results presented in Figs. 3, 4 and 5. It is clear that the passive dynamic walking of the compass-gait biped robot is stabilized into the one-periodic behavior.

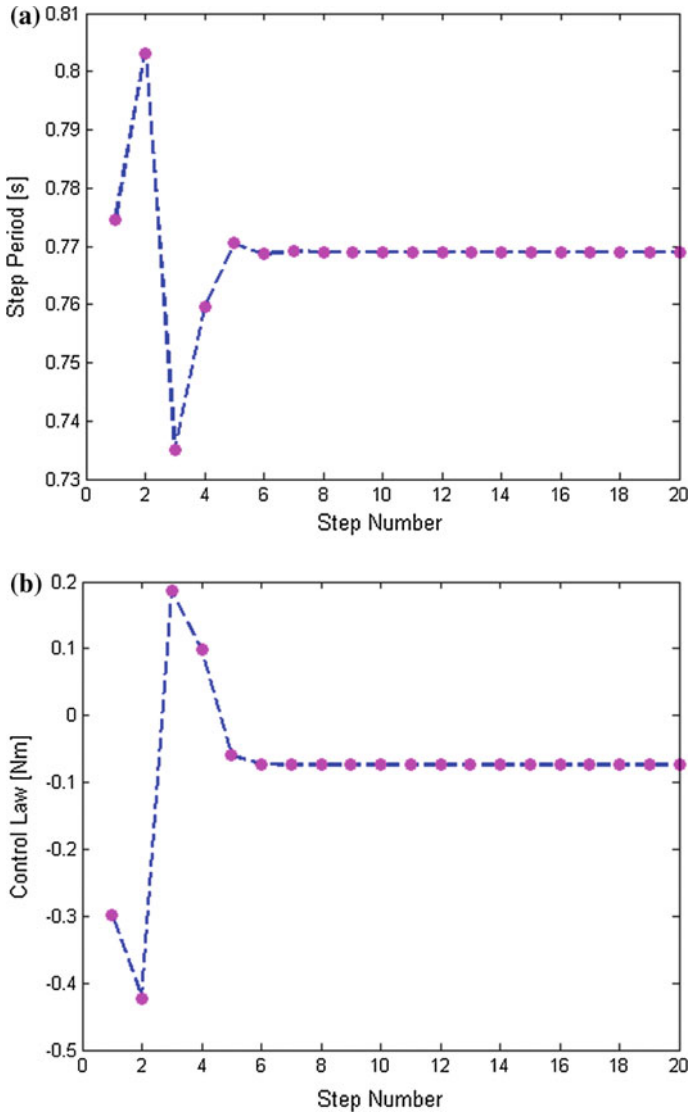

Fig. 4 Variation of walking step period **a** of the compass-gait biped model under the OGY controller **b** for the desired slope $\varphi_d = 5.2°$

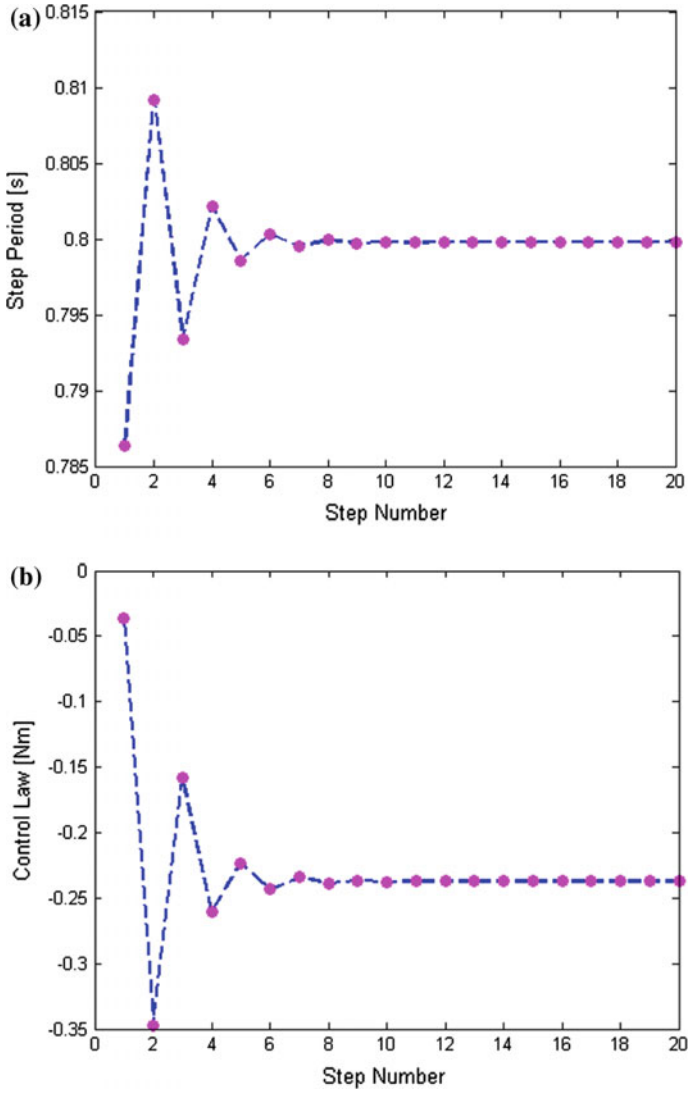

Fig. 5 Variation of walking step period **a** of the compass-gait biped model under the OGY controller **b** for the desired slope $\varphi_d = 7°$

7 Discussion

The compass-gait biped robot is the famous/popular prototype used in order to investigate the passive dynamic walking in human beings. This locomotion mode has been found to be the recommended one in order to design and build biped robots with active dynamic walking avoiding hence the use of high-gain control. The main

idea was to use the observed demonstrations of the passive dynamic walking and its performances. Then, the objective was to stabilize a one-period limit cycle walking identified in the passive dynamic walking of the compass-gait model. Such hybrid limit cycle is absolutely passive (relative to the nature of the bipedal walking). Hence, it is necessary to stabilize the identified one-periodic hybrid limit cycle by designing an intelligent controller.

To accomplish this objective, our control approach was based on the OGY method, which was based mainly (in this chapter) on the linearization of the impulsive hybrid nonlinear dynamics of the compass-gait biped robot around the desired identified one-period hybrid limit cycle. Moreover, our OGY-based control approach was based on the development of a mathematical expression of a hybrid Poincaré map ans also on its linearization around its one-periodic fixed point. The hybrid Poincaré map designed in this work is simpler enough to be amendable to analysis and also to control compared with the impulsive hybrid nonlinear dynamics where its limit cycle control is a very complicated task.

Then, using the designed hybrid Poincaré map, we achieved the stabilization of the desired one-periodic hybrid limit cycle in the impulsive hybrid nonlinear dynamics. Such limit cycle is identified for some desired slope parameter of the walking surface and also for fixed inertial and geometrical parameters of the compass-gait biped robot. Thus, each slope parameter has its own control gain. Efficiency of the designed OGY controller was observed. Indeed, the controlled passive dynamic walking of the biped robot does not need high gains. The controller was found to reach a very small value. Accordingly, this reveals the fact that our stabilization strategy of the one-periodic hybrid limit cycle based on the OGY approach has increased the energy efficiency of the bipedal locomotion.

We emphasize that, for our control approach, as the slope parameter changes, we calculated the new gain of the OGY-based controller. Hence, the main problem in our proposed control strategy is that the controller acts on the local neighborhood of the slope parameter. Indeed, for the same controller, the compass-gait biped can perform a different behavior as the slope parameter varies far away the desired one. Then, investigation of the performance of the designed OGY controller on the walking behavior of the compass-gait biped robot is needed.

Our developed method for the stabilization of the limit cycle walking can be applied also for other prototypes of biped robots like the planar under-actuated compass-like biped robot with semicircular feet [1], or other passive or semi-passive biped robots that can be found in literature, see for example [44].

8 Conclusion

In this work, a mathematical model of the passive dynamic walking of the compass-gait biped robot as it goes down an inclined surface was proposed. This walking dynamics of such biped robot is described by an impulsive hybrid nonlinear dynamics, which is composed of a nonlinear differential equation and a nonlinear algebraic

equation. We revisited the mathematical/numerical method for the identification of a one-periodic hybrid limit cycle via the impulsive hybrid nonlinear dynamics. Such method is based on the calculation of the fundamental solution matrix and the saltation matrix. A stability investigation of the hybrid limit cycle has provided also. Based on this method, a OGY-based stabilization approach of this identified one-period hybrid limit cycle was achieved. Our strategy was based firstly on the linearization of the impulsive hybrid nonlinear dynamics around the desired one-period hybrid limit cycle. Thus, the nonlinear differential equation and the nonlinear algebraic equation were both linearized. Hence, we developed an impulsive hybrid linear dynamics. Our strategy of the stabilization was based secondly on the development of an analytical expression of a hybrid (controlled constrained) Poincaré map, which was found to mimics the characteristic of the impulsive hybrid nonlinear dynamics. Determination of the one-periodic fixed point of the hybrid Poincaré map and its stability analysis were also realized. We showed that identification of such fixed point and computation of the Jacobian matrix of the Poincaré map depend together on only one variable, which is the impact instant. A linearization of the hybrid Poincaré map around its one-period fixed point was achieved. Then, we adopted a state-feedback controller in order to stabilize the linearized Poincaré map and accordingly in order to stabilize the one-periodic fixed point. Application of the designed controller to the impulsive hybrid nonlinear dynamics of he compass-gait biped model has hence achieved the stabilization of the desired one-periodic hybrid limit cycle.

References

1. Asano F (2015) Stability analysis of underactuated compass gait based on linearization of motion. Multibody Syst Dyn 33(1):93–111
2. Asano F, Luo Z-W, Yamakita M (2005) Biped gait generation and control based on a unified property of passive dynamic walking. IEEE Trans Robot 21(4):754–762
3. Bououden S, Abdessemed F (2014) Walking control for a planar biped robot using 0-flat normal form. Robot Auton Syst 62:68–80
4. Byl K, Tedrake R (1998) Intuitive control of a planar bipedal walking robot. In: Proceedings of the IEEE international conference on robotics and automation, pp 2014–2021
5. Byl K, Tedrake R (2008) Approximate optimal control of the compass gait on rough terrain. In: Proceedings of the IEEE international conference on robotics and automation, pp 1258–1263
6. Chaillet N, Abba G, Ostertag E (1994) Double dynamic modeling and computed torque control of a biped robot. In: Proceedings of the IEEE/RSJ international conference on intelligent robots and systems, pp 1149–1153
7. Chemori A (2009) A discrete-time control strategy for dynamic walking of a planar under-actuated biped robot. In: Proceedings of the IEEE/RSJ international conference on intelligent robots and systems, pp 3226–3231
8. Chemori A, Alamir M (2006) Multi-step limit cycle generation for rabbit's walking based on a nonlinear low dimensional predictive control scheme. Mechatronics 16(5):259–277
9. Chemori A, Loria A (2004) Control of a planar under-actuated biped on a complete walking cycle. IEEE Trans Autom Control 49(5):838–843
10. Cheng M-Y, Lin C-S (1996) Measurement of robustness for biped locomotion using a linearized poincaré map. Robolica 14:253–259

11. Chevallereau C (2003) Time-scaling control for an underactuated biped robot. IEEE Trans Robot Autom 19(2):362–368
12. Chevallereau C, Djoudi D, Grizzle JW (2008) Stable bipedal walking with foot rotation through direct regulation of the zero moment point. IEEE Trans Robot 24(2):390–401
13. Dardel M, Safartoobi M, Pashaei MH, Ghasemi MH, Navaei MK (2015) Finite difference method to find period-one gait cycles of simple passive walkers. Commun Nonlinear Sci Numer Simul 20(1):79–97
14. Ding CT, Yang SX, Gan CB (2013) Input torque sensitivity to uncertain parameters in biped robot. Acta Mech Sin 29(3):452–461
15. Donde V, Hiskens IA (2006) Shooting methods for locating grazing phenomena in hybrid systems. Int J Bifurc Chaos 16(3):671–692
16. Dong H, Zhao M, Zhang N (2011) High-speed and energy-efficient biped locomotion based on virtual slope walking. Auton Robots 30(2):199–216
17. Farshimi F, Naraghi M (2011) A passive-biped model with multiple routes to chaos. Acta Mech Sin 27(2):277–284
18. Flieller D, Riedinger P, Louis JP (2006) Computation and stability of limit cycles in hybrid systems. Nonlinear Anal: Theory Methods Appl 64(2):352–367
19. Freidovich LB, Shiriaev AS, Manchester IR (2008) Stability analysis and control design for an underactuated walking robot via computation of a transverse linearization. In: Proceedings of the 17th IFAC world congress, pp 10166–10171
20. Goswami A, Thuilot B, Espiau B (1998) Study of the passive gait of a compass-like biped robot: Symmetry and chaos. Int J Robot Res 17:1282–1301
21. Gritli H (2014) Analyse et Contrôle du Chaos en Robotique: Cas des Robots Bipèdes Planaires. PhD thesis, Ecole Nationale d'Ingénieurs de Tunis, Tunisia
22. Gritli H (2015) Analyse et Contrôle du Chaos dans les Systèmes Mécaniques Impulsifs. Presses Académiques Francophones, Saarbrücken, Germany, Cas des Oscillateurs avec Impact et des Robots Bipèdes Planaires
23. Gritli H, Belghith S (2015) Computation of the Lyapunov exponents in the compass-gait model under OGY control via a hybrid Poincaré map. Chaos Solitons Fractals 81:172–183
24. Gritli H, Belghith S, Khraeif N (2012) Cyclic fold bifurcation and boundary crisis in dynamic walking of biped robots. Int J Bifurc Chaos 22(10):1250257. doi:10.1142/S0218127412502574
25. Gritli H, Belghith S, Khraeif N (2012) Intermittency and interior crisis as route to chaos in dynamic walking of two biped robots. Int J Bifurc Chaos 22(3):1250056. doi:10.1142/S0218127412500563
26. Gritli H, Belghith S, Khraeif N (2015a) OGY-based control of chaos in semi-passive dynamic walking of a torso-driven biped robot. Nonlinear Dyn 79(2):1363–1384
27. Gritli H, Khraeif N, Belghith S (2011) Cyclic-fold bifurcation in passive bipedal walking of a compass-gait biped robot with leg length discrepancy. In: Proceedings of the IEEE international conference on mechatronics, pp 851–856
28. Gritli H, Khraeif N, Belghith S (2011) Falling of a passive compass-gait biped robot caused by a boundary crisis. In: Proceedings of the 4th chaotic modeling and simulation international conference, pp 155–162
29. Gritli H, Khraeif N, Belghith S (2011) Semi-passive control of a torso-driven compass-gait biped robot: Bifurcation and chaos. In: Proceedings of the international multi-conference on systems, signals and devices, pp 1–6
30. Gritli H, Khraeif N, Belghith S (2012c) Period-three route to chaos induced by a cyclic-fold bifurcation in passive dynamic walking of a compass-gait biped robot. Commun Nonlinear Sci Numer Simul 17(11):4356–4372
31. Gritli H, Khraeif N, Belghith S (2013) Chaos control in passive walking dynamics of a compass-gait model. Commun Nonlinear Sci Numer Simul 18(8):2048–2065
32. Gritli H, Khraeif N, Belghith S (2014) Further analysis of the period-three route to chaos in passive dynamic walking of a compass-gait biped robot. In: Proceedings of the copyright IPCO-2014, pp 123–130

33. Gritli H, Khraeif N, Belghith S (2015) Handbook of research on advanced intelligent control engineering and automation, chapter Further investigation of the period-three route to chaos in the passive compass-gait biped model. Advances in computational intelligence and robotics (ACIR). IGI Global, USA, pp 279–300
34. Grizzle JW, Abba G, Plestan F (2001) Asymptotically stable walking for biped robots: Analysis via systems with impulse effects. IEEE Trans Autom Control 46:51–64
35. Hardt M, Kreutz-Delgado K, Helton J (1998) Minimal energy control of a biped robot with numerical methods and a recursive symbolic dynamic model. In: Proceedings of the IEEE international conference on decision and control, pp 413–416
36. Hiskens IA (2001) Stability of hybrid system limit cycles: application to the compass gait biped robot. In: Proceedings of the IEEE international conference on decision control, pp 774–779
37. Hiskens IA, Pai MA (2000) Trajectory sensitivity analysis of hybrid systems. IEEE Trans Circuits Syst I 47:204–220
38. Holm JK, Spong MW (2008) Kinetic energy shaping for gait regulation of underactuated bipeds. In Proceedings of the IEEE International conference on control applications, part of the IEEE multi-conference on systems and control, pp 1232–1238
39. Hu Y, Yan G, Lin Z (2011a) Feedback control of planar biped robots with regulable step length and walking speed. IEEE Trans Robot 27(1):162–169
40. Hu Y, Yan G, Lin Z (2011b) Gait generation and control for biped robots with underactuation degree one. Automatica 47(8):1605–1616
41. Huang Y, Wang Q-N, Gao Y, Xie G-M (2012) Modeling and analysis of passive dynamic bipedal walking with segmented feet and compliant joints. Acta Mech Sin 28(3):1457–1465
42. Iida F, Tedrake R (2010) Minimalistic control of biped walking in rough terrain. Auton Robots 28(3):355–368
43. Ijspeert AJ (2008) Central pattern generators for locomotion control in animals and robots: A review. Neural Netw 21(4):642–653
44. Iqbal S, Zang XZ, Zhu YH, Zhao J (2014) Bifurcations and chaos in passive dynamic walking: A review. Robot Auton Syst 62(6):889–909
45. Katič D, Vukobratovič M (2003) Survey of intelligent control techniques for humanoid robots. J Intell Rob Syst 37(2):117–141
46. Kim Y-D, Lee B-J, Ryu J-H, Kim J-H (2007) Landing force control for humanoid robot by time-domain passivity approach. IEEE Trans Robot 23(6):1294–1301
47. Lee JH, Okamoto S, Koike H, Tani K (2014) Development and motion control of a biped walking robot based on passive walking theory. Artif Life Robot 19(1):68–75
48. Li Q, Guo J, Yang XS (2013) New bifurcations in the simplest passive walking model. Chaos: Interdiscip J Nonlinear Sci 23:043110
49. Li Q, Yang XS (2012) New walking dynamics in the simplest passive bipedal walking model. Appl Math Model 36(11):5262–5271
50. Li Q, Yang XS (2014) Bifurcation and chaos in the simple passive dynamic walking model with upper body. Chaos: Interdiscip J Nonlinear Sci 24:033114
51. Liu N, Li J, Wang T (2008) Passive walker that can walk down steps: simulations and experiments. Acta Mech Sin 24:569–573
52. Liu Z, Zhou C, Zhang P, Tian Y (2007) Robotic welding, intelligence and automation. Lecture notes in control and information sciences, chapter Anti-phase synchronization control scheme of passive biped robot, vol 362. Springer, pp 529–539
53. Luo X, Zhu L, Xia L (2015) Principle and method of speed control for dynamic walking biped robots. Robot Auton Syst 66:129–144
54. Manchester IR (2011) Transverse dynamics and regions of stability for nonlinear hybrid limit cycles. In: Proceedings of the 18th IFAC world congress, pp 6285–6290
55. Manchester IR, Mettin U, Iida F, Tedrake R (2009) Stable dynamic walking over rough terrain: Theory and experiment. In: Proceedings of the international symposium on robotics research, pp 1–16
56. Manchester IR, Tobenkin MM, Levashov M, Tedrake R (2011) Regions of attraction for hybrid limit cycles of walking robots. In: Proceedings of the 18th IFAC world congress, pp 5801–5806

57. McGeer T (1990) Passive dynamic walking. Int J Robot Res 9(2):62–68
58. McMahon T (1984) Mechanics of locomotion. Int J Robot Res 3(2):4–28
59. Morimoto J, Atkeson CG (2007) Learning biped locomotion. IEEE Robot Autom Mag 14(2):41–51
60. Morimoto J, Atkeson CG (2009) Nonparametric representation of an approximated poincaré map for learning biped locomotion. Auton Robots 27:131–144
61. Morris B, Grizzle JW (2005) A restricted poincaré map for determining exponentially stable periodic orbits in systems with impulse effects: application to bipedal robots. In: Proceedings of the IEEE conference on decision and control, and the european control conference, pp 4199–4206
62. Muller PC (1995) Calculation of lyapunov exponents for dynamic systems with discontinuities. Chaos Solitons Fractals 5:1671–1681
63. Ning L, Junfeng L, Tianshu W (2009) The effects of parameter variation on the gaits of passive walking models: Simulations and experiments. Robotica 27(4):511–528
64. Owaki D, Osuka K, Ishiguro A (2009) Understanding the common principle underlying passive dynamic walking and running. In: Proceedings of the IEEE/RSJ international conference on intelligent robots and systems, pp 3208–3213
65. Park JH (2001) Impedance control for biped robot locomotion. IEEE Trans Robot Autom 17(6):870–882
66. Parker TS, Chua LO (1989) Practical numerical algorithms for chaotic systems. Springer, New York
67. Qi F, Wang T, Li J (2011) The elastic contact influences on passive walking gaits. Robotica 29(5):787–796
68. Safa AT, Alasty A, Naraghi M (2015) A different switching surface stabilizing an existing unstable periodic gait: An analysis based on perturbation theory. Nonlinear Dyn 81(4):2127–2140
69. Safa AT, Naraghi M (2015) The role of walking surface in enhancing the stability of the simplest passive dynamic biped. Robotica 33(1):195–207
70. Safa AT, Saadat MG, Naraghi M (2007) Passive dynamic of the simplest walking model: Replacing ramps with stairs. Mech Mach Theory 42(10):1314–1325
71. Safartoobi M, Dardel M, Ghasemi MH, Daniali HM (2014) Stabilization and walking control for a simple passive walker using computed torque method. Int J Eng 27(11):1025–2495
72. Saglam CO, Byl K (2014) Stability and gait transition of the five-link biped on stochastically rough terrain using a discrete set of sliding mode controllers. In: Proceedings of the IEEE international conference on robotics and automation, pp 5655–5662
73. Shiriaev AS, Freidovich LB (2009) Transverse linearization for impulsive mechanical systems with one passive link. IEEE Trans Autom Control 54(12):2882–2888
74. Shiriaev AS, Freidovich LB, Manchester IR (2008) Periodic motion planning and analytical computation of transverse linearizations for hybrid mechanical systems. In: Proceedings of the IEEE conference on decision and control, pp 4326–4331
75. Song G, Zefran M (2006) Stabilization of hybrid periodic orbits with application to bipedal walking. In: Proceedings of the american control conference, pp 2504–2509
76. Spong MW, Bullo F (2005) Controlled symmetries and passive walking. IEEE Trans Autom Control 50:1025–1031
77. Spong MW, Holm JK, Dongjun L (2007) Passivity-based control of bipedal locomotion. IEEE Robot Autom Mag 14(2):30–40
78. Sugimoto Y, Osuka K (2005) Stability analysis of passive-dynamic-walking focusing on the inner structure of Poincaré map. In: Proceedings of the international conference on advanced robotics, pp 236–241
79. Sugimoto Y, Osuka K (2007) Hierarchical implicit feedback structure in passive dynamic walking. In: Proceedings of the IEEE/RSJ international conference on intelligent robots and systems, pp 2217–2222
80. Tzafestas S, Raibert M, Tzafestas C (1996) Robust sliding-mode control applied to a 5-link biped robot. Int J Intell Robot Syst 15:67–133

81. Vallejos P, del Solar JR, Swett F (2011) A new methodology for the design of passive biped robots: Determining conditions on the robot's parameters for the existence of stable walking cycles. J Intell Rob Syst 63:503–523
82. Westervelt ER, Grizzle JW, Canudas C (2003) Switching and pi control of walking motions of planar biped walkers. IEEE Trans Autom Control 48(2):308–312
83. Westervelt ER, Grizzle JW, Chevallereau C, Choi J-H, Morris B (2007a) Feedback control of dynamic bipedal robot locomotion. Taylor & Francis/CRC, London
84. Westervelt ER, Morris B, Farrell KD (2007b) Analysis results and tools for the control of planar bipedal gaits using hybrid zero dynamics. Auton Robots 23:131–145
85. Wisse M, van der Linde RQ (2007) Delft Pneumatic Bipeds. Springer, Berlin
86. Wu B, Zhao M (2014) Bifurcation and chaos of a biped robot driven by coupled elastic actuation. In: Proceedings of the world congress on intelligent control and automation, pp 1905–1910
87. Yazdi EA, Aria A (2008) Stabilization of biped walking robot using the energy shaping method. J Comput Nonlinear Dyn 3(4):1–8
88. Zhang P, Zhou C, Zhang L, Tian Y, Liu Z (2009) Adaptive compliant control of humanoid biped foot with elastic energy storage. In: Proceedings of the IEEE/ASME international conference on advanced intelligent mechatronics, pp 928–933
89. Zhao J, Wu X-G, Zang X-Z, Yan J-H (2012) Analysis of period doubling bifurcation and chaos mirror of biped passive dynamic robot gait. Chin Sci Bull 57(14):1743–1750

Explicit Delay-Dependent Stability Criteria for Nonlinear Distributed Parameter Systems

Michael Gil'

Abstract This chapter is devoted to the stability of nonlinear autonomous systems with distributed parameters and delay, governed by functional-differential equations in a Banach space with nonlinear causal mappings and bounded operators acting on the delayed state. These equations include partial differential, integro-differential and other traditional equations. Estimates for the norms of solutions are established. They give us explicit conditions for the delay-dependent Lyapunov and exponential stabilities of the considered systems. These conditions are formulated in terms of the spectra of the operator coefficients of the equations. In addition, the obtained solution estimates provide us bounds for the regions of attraction of steady states. The global exponential stability conditions are also derived. As particular cases we consider systems with discrete and distributed delays. The illustrative examples with the Dirichlet and Neumann boundary conditions are also presented. These examples show that the obtained stability conditions allow us to avoid the construction of the Lyapunov type functionals in appropriate situations. Our approach is based on a combined usage of properties of operator semigroups with estimates for fundamental solutions of the considered equations.

Keywords Nonlinear systems with distributed parameters · Systems with delay · Stability · Exponential stability · Equations in a Banach space · Partial differential equations · Causal mappings

AMS (MOS) subject classification: 93C10 · 93C20 · 93C23 · 93C25 · 93D05 · 93D20 · 34G99 · 47D06

M. Gil' (✉)
Department of Mathematics, Ben Gurion University of the Negev,
P.O. Box 653, 84105 Beer-Sheva, Israel
e-mail: gilmi@bezeqint.net

S. Vaidyanathan and C. Volos (eds.), *Advances and Applications in Nonlinear Control Systems*, Studies in Computational Intelligence 635,
DOI 10.1007/978-3-319-30169-3_14

1 Introduction and Notation

This chapter is a survey of some results from the papers [5–12] devoted to the stability analysis of nonlinear autonomous distributed parameter systems with delay, governed by functional-differential equations in a Banach space with nonlinear causal mappings. These equations include partial differential, integro-differential and other traditional equations. Time-delay naturally appears in various control systems. Recently, many papers were devoted to control systems with delay and concentrated parameters governed by ordinary differential equations with delay. It should be noted that the stability analysis of systems with distributed parameters, described by partial differential equations (PDEs) with delay is essentially more complicated and these systems are investigated considerably less than the concentrated parameter systems. As it was shown in [2, 20, 22] in the case of systems with distributed parameters, arbitrarily small delays in the feedback may destabilize the system.

The basic method for the stability analysis is the second Lyapunov method extended to time-delay equations in a Banach space, cf. [26]. By that method many very strong results were obtained. In particular, various concrete classes of nonlinear parabolic equations with variable delays were investigated in [16, 18, 21, 25]. Besides delay-dependent stability tests were established. Stability and instability conditions for delay wave equations were found in [22]. In the paper [4] the exponential stability of linear distributed parameter systems is considered. At the same time it should be noted that finding the Lyapunov type functionals for PDE is often connected with serious mathematical difficulties, especially in regard to nonlinear equations. To the contrary, the stability conditions presented in this chapter are formulated explicitly in terms of the spectra of the operator coefficients of the equations. This fact allows us to apply the well-known results from the spectral theory of operators. In addition, estimates for norms of solutions are established. These estimates provide us bounds for the regions of attraction of steady states.

Our approach is based on a combined usage of properties of operator semigroups with estimates for fundamental solutions.

A few words about the contents. The paper consists of eight sections.

In Sect. 2 we recall some well-known results from the theory of linear differential equations in a Banach space, which are used in the next sections.

The solvability of integral equations with causal mappings is explored in Sect. 3.

In Sect. 4 we prove the existence of mild solutions of the considered differential-delay equations with nonlinear causal mappings in a Banach space.

The main stability results of this paper are presented Sect. 5.

In Sect. 6 we illustrate our main results in the case of a system with one discrete delay in the linear part.

In Sect. 7 we specialize the results from Sect. 5 in the case of systems with distributed delays in linear parts.

In Sect. 8 we discuss our results.

Introduce the notations. Let Y by a Banach space with a norm $\|.\|_Y$ and the unit operator I. Then $C(J, Y)$ denotes the space of continuous Y-valued functions defined

on a finite or infinite real segment J and equipped with the sup-norm

$$\|v\|_{C(J,Y)} = \sup_{t\in J} \|v(t)\|_Y \quad (v \in C(J, Y)).$$

For $1 \le p < \infty$, $L^p(J, Y)$ means the space of Y-valued functions with the norm

$$\|w\|_{L^p(J,Y)} = \left[\int_J \|v(t)\|_Y^p dt\right]^{1/p} \quad (v \in L^p(J, Y)).$$

Denote also $R_+ = [0, \infty)$ and $R_\eta = [-\eta, \infty)$ for a finite $\eta \ge 0$.

For a linear operator A, $D(A)$ is the domain, $\sigma(A)$ is the spectrum,

$$\beta(A) := \inf \ Re\ \sigma(A)$$

and $\lambda_k(A)$ $(k = 1, 2, \ldots)$ are the eigenvalues taken with their multiplicities.

In addition, for a positive $\rho \le \infty$ we set

$$\Omega_\rho(J, Y) := \{h \in C(J, Y) : \ \|h(t)\|_Y \le \rho;\ t \in J\ \}.$$

As usually $L^2(\Omega) = L^2(\Omega, \mathbf{C})$ is the Hilbert space of complex functions defined on a set Ω with the scalar product

$$(v, w) = (v, w)_{L^2(\Omega)} := \int_\Omega v(x)\overline{w}(x)dx.$$

2 Linear Differential Equations in a Banach Space

The statements presented in this section are well-known and can be found, for instance in [3, 23, Sect. 3.1].

Let $T(t)$ for each $t \ge 0$ be a bounded linear operator in a Banach space X. Then $T(t)$ is called a C_0-semigroup (a strongly continuous semigroup) if

(i) $T(0) = I$, $T(t)T(s) = T(t + s)$ for all $t, s \ge 0$,
(ii) $T(t) \to T(s)$ as $t \to s$ for each $s \ge 0$ in the sense of the strong topology.

For any C_0-semigroup $T(t)$ $(t \ge 0)$ there exist real numbers $M \ge 1$ and α such that

$$\|T(t)\| \le Me^{\alpha t} \tag{1}$$

for all $t \ge 0$. A linear operator A is called the infinitesimal generator of a C_0-semigroup $T(t)$ if it is defined by

$$Au = \lim_{h \to +0} h^{-1}(T(h)u - u)$$

in the sense of the strong topology whenever the limit exists.

If A is the infinitesimal generator of a semigroup $T(t)$, we will sometimes write e^{At} instead of $T(t)$.

Theorem 1 *The generator A of a C_0-semigroup $T(t)$ is a closed operator. Let M and α be numbers such that (1) is satisfied. Then the half-plane $\{\lambda \in \mathbf{C} : Re\ \lambda > \alpha\}$ is contained in the resolvent set of A and therein*

$$(A - \lambda I)^{-1} = -\int_0^\infty e^{\lambda t} T(t) dt, \tag{2}$$

and the relation

$$\|(A - \lambda I)^{-n}\| \le M(Re\ \lambda - \alpha)^{-n} \tag{3}$$

is satisfied for any $n = 1, 2, \ldots$.

Theorem 2 *Let A be a densely defined closed operator. Assume that the half-plane $\{\lambda \in \mathbf{C} : Re\lambda > \alpha\}$ is contained in the resolvent set of A and that relation (3) is satisfied for any $Re\ \lambda > \alpha$, and $n = 1, 2, \ldots$. Then A generates a C_0-semigroup $T(t)$. Moreover, inequality (1) is valid.*

A semigroup $T(t)$ satisfying $\|T(t)\| \le 1$ $(t \ge 0)$ is called *a contraction semigroup*. A semigroup $T(t)$ is said to be *exponentially stable*, if inequality (1) holds with $\alpha < 0$.

Let Y be a Banach space and A be a closely-defined linear operator in Y. Consider the Cauchy (initial value) problem

$$du(t)/dt = Au(t) + f(t)\ (0 \le t \le T), \tag{4}$$

$$u(0) = u_0, \tag{5}$$

where u_0 and f are given elements of $D(A)$ and $C([0, T],\ Y)$, respectively. A function u is called *a solution* of this initial value problem if, besides satisfying (4) and (5) it is continuously differentiable and $u(t) \in D(A)$ for each $t \in [0, T]$, and $Au \in C([0, T],\ X)$.

The following result is well known (see [23, pp. 64–65]). Let A generate a C_0-semigroup e^{At}, $u_0 \in D(A)$ and f be continuously differentiable. Then the function

$$u(t) = e^{At}u_0 + \int_0^t e^{A(t-s)} f(s) ds$$

is the solution of the problem (4) and (5).

In particular the function $v(t) = e^{At}u_0$ is a solution of the homogeneous problem

$$dv(t)/dt = Av(t)\ (t \geq 0;\ v(0) = u_0 \in D(A)).$$

3 Equations with Causal Mappings

3.1 Causal Mappings

Recall that $R_+ = [0, \infty)$ and $R_\eta = [-\eta, \infty)$. Let $X(R_\eta, Z)$ be a Banach space of functions defined on $[-\eta, \infty)$ with values in a Banach space Z and $X(R_+, Y)$ be a Banach space of functions defined on $[0, \infty)$ with values in a Banach space Y. For example, $X(R_\eta, Z) = C(R_\eta, Z)$ and $X(R_+, Y) = L^p(R_+, Y)$.

For all $\tau > 0$ introduce the subspaces $X([-\eta, \tau], Z)$ of $X(R_\eta, Z)$ by

$$X([-\eta, \tau], Z) := \{f \in X(R_\eta, Z) : f(t) \equiv 0,\ t > \tau\}.$$

Similarly

$$X([0, \tau], Y) := \{f \in X(R_+, Y) : f(t) \equiv 0,\ t > \tau\}.$$

Besides, we take

$$\|f\|_{X([-\eta,\tau],Z)} = \|f\|_{X(R_\eta,Z)}\ \ (f \in X([-\eta, \tau], Z)$$

and

$$\|f\|_{X([0,\tau],Y)} = \|f\|_{X(R_+,Y)}\ \ (f \in X([0, \tau], Y).$$

Denote by P_τ $(0 < \tau < \infty)$ the projections of $X(R_+, Y)$ onto $X([0, \tau], Y)$. That is,

$$(P_\tau v)(t) = \begin{cases} v(t) & \text{if } 0 \leq t \leq \tau, \\ 0 & \text{if } t > \tau \end{cases} \quad (v \in X(R_+, Y)).$$

In addition, $P_0 = 0$, and $P_\infty w = w$.

Note that it is not always $P_\tau v \in X(R_+, Y)$. For example, it is possible that $P_\tau v \notin C(R_+, Y)$ although $v \in C(R_+, Y)$.

For a $w \in X(R_\eta, Z)$ put

$$w_\tau(t) = \begin{cases} w(t) & \text{if } -\eta \leq t \leq \tau, \\ 0 & \text{if } t > \tau. \end{cases}$$

Definition 3 Let $\Omega_X \subseteq X(R_\eta, Z)$ be a closed domain containing origin. Let F continuously map $\Omega_X \cap X([-\eta, \tau], Z)$ into $X([0, \tau], Y)$ for all $\tau > 0$. In addition, let

$$F0 = 0 \tag{6}$$

and

$$P_\tau F w = P_\tau F w_\tau \ (w \in \Omega_X, \tau > 0). \tag{7}$$

Then F will be called a (continuous) causal mapping (operator) of Ω_X into $X(R_+, Y)$.

Note that our definition is adopted from [14]. It is slightly different from the one accepted in [1, 19].

Example 1 Let $Y = Z = C(0, 1)$ and $\Omega_X = C(R_h, C(0, 1))$ $(h = const \geq 0)$. Consider the mapping defined by

$$[Fw](t, x) = \begin{cases} w^m(t - h, x) & \text{if } t \geq 0, \\ 0 & \text{if } t < 0 \end{cases}$$

$(m > 0, 0 \leq x \leq 1)$. Since $P_\tau F w(t, x) = P_\tau w^m(t - h, x) = 0 \quad (t > \tau)$ and $w_\tau(t, x) = 0 \quad (t > \tau)$ we have $w_\tau(t - h, x) = 0 \quad (t > \tau)$ and $P_\tau w^m(t - h, x) = w_\tau^m(t - h, x)$ $(0 \leq t \leq \tau)$. Therefore

$$[P_\tau F w](t, x) = P_\tau w^m(t - h, x) = P_\tau w_\tau^m(t - h, x) = [P_\tau F w_\tau](t, x).$$

So in this case the mapping is causal.

Lemma 1 *Let F be a causal mapping acting from Ω_X into $X(R_+, Y)$, and*

$$\|Fw\|_{X(R_+, Y)} \leq q \|w\|_{X(R_\eta, Z)} \quad (q = const > 0; \ w \in \Omega_X).$$

Then for all $T > 0$, one has $\|Fw\|_{X([0,T],Y)} \leq q \|w\|_{X([-\eta,T],Z)}$.

Proof Put

$$w_T(t) = \begin{cases} w(t) & \text{if } -\eta \leq t \leq T, \\ 0 & \text{if } t > T \end{cases}$$

and $F_T = P_T F$. According to (7), $F_T w = F_T w_T$. Due to the definition of P_τ we have $\|P_\tau\| = 1$. Consequently,

$$\begin{aligned} \|Fw\|_{X([0,T],Y)} &= \|F_T w\|_{X(R_+,Y)} = \|F_T w_T\|_{X(R_+,Y)} \\ &\leq \|F w_T\|_{X(R_+,Y)} \leq q \|w_T\|_{X(R_\eta,Z)} \\ &= q \|w\|_{X([-\eta,T],Z)}. \end{aligned}$$

In addition, since F is continuous on $X(R_\eta, Z)$, the continuity of F on $X([-\eta, T], Z)$ is obvious. This proves the result. □

Absolutely similarly the following result can be proved.

Lemma 2 *Let F be a causal mapping acting from Ω_X into $X(R_+, Y)$, and*

$$\|Fw - Fw_1\|_{X(R_+,Y)} \le q\|w - w_1\|_{X(R_\eta,Z)} \quad (w, w_1 \in \Omega_X).$$

Then for all $T > 0$, one has $\|Fw - Fw_1\|_{X([0,T],Y)} \le q\|w - w_1\|_{X([-\eta,T],Z)}$.

Now let

$$\Omega_\rho(R_\eta, Z) = \{w \in C(R_\eta, Z) : \|w\|_{C(R_\eta,Z)} \le \rho\}$$

for a positive $\rho \le \infty$. The following condition is often used below:

$$\|Fw\|_{C(R_+,Y)} \le q\|w\|_{C(R_\eta,Z)} \ (w \in \Omega_\rho(R_\eta, Z)). \tag{8}$$

Example 2 Let $Y = Z = C(0, 1)$. An example of a causal mapping satisfying (8) is given by the expression

$$[Fu](t, x) = \begin{cases} \psi(u(t, x), u(t - \eta, x)) & \text{if } t \ge 0, \\ 0 & \text{if } 0 < t < \eta \end{cases}$$

where $\psi : \mathbf{C}^2 \to \mathbf{C}$ is a continuous function, satisfying the condition

$$|\psi(v_1, v_2)| \le b_1|v_1| + b_2|v_2| \quad (v_1, v_2 \in \mathbf{C};\ |v_1|, |v_2| \le \rho)$$

with positive constants b_1, b_2. Simple calculations show that in this example condition (8) holds with $q = b_1 + b_2$.

Example 3 Let $Y = Z = C(0, 1)$. Another example of a causal mapping satisfying (8) is given by the expression

$$[Fu](t, x) = \int_0^\eta a(s, u(s, x))u(t - s, x)ds \quad (t \ge 0, 0 \le x \le 1),$$

where $a(., .) : [0, \eta] \times \mathbf{C} \to \mathbf{C}$ is a continuous function, and satisfying the condition

$$|a(s, v)| \le c(s)|v| \ (v \in \mathbf{C};\ |v| \le \rho;\ \ s \in [0, \eta])$$

with a positive continuous function $c(s)$. Simple calculations show that in this example condition (8) is also holds.

3.2 Integral Equations with Causal Mappings

Let $K(t,s)$ be a function defined for $t \geq s \geq 0$ whose values are bounded linear operators acting from Y into Z. Introduce the operator $\hat{K} : C(R_+, Y) \to C(R_+, Z)$ defined by

$$\hat{K}f(t) = \int_0^t K(t,s)f(s)ds \quad (t \geq 0,\ f \in C(R_+, Y))$$

assuming that it is bounded.

For given functions $z(.) \in C(R_\eta, Z)$ and $f(.) \in C(R_+, Y)$ consider the equation

$$u(t) = z(t) + \int_0^t K(t,s)[Fu + f](s)ds = z(t) + \hat{K}(Fu + f)(t) \quad (t > 0) \tag{9}$$

with a causal mapping $F : \Omega_\varrho(R_\eta, Z) \to C(R_+, Y)$ and the initial condition

$$u(t) = z(t) \quad \text{for } -\eta \leq t \leq 0. \tag{10}$$

It is supposed that

$$\|Fw - Fw_1\|_{C(R_+,Y)} \leq q\|w - w_1\|_{C(R_\eta,Z)} \quad (w, w_1 \in \Omega_\rho(R_\eta, Z)), \tag{11}$$

$$\|\hat{K}\| := \|\hat{K}\|_{C(R_+,Y)\to C(R_+,Z)} < \frac{1}{q} \tag{12}$$

and

$$\|z\|_{C(R_\eta,Z)} + \|\hat{K}f\|_{C(R_+,Z)} + q\rho\|\hat{K}\| < \rho. \tag{13}$$

If $\rho = \infty$, then (13) is automatically fulfilled.

Lemma 3 *Let conditions (11)–(13) hold. Then problem (9) and (10) has a unique solution $u(.) \in C(R_\eta, Z)$. Moreover,*

$$\|u\|_{C(R_\eta,Z)} \leq \frac{\|z\|_{C(R_\eta,Z)} + \|\hat{K}f\|_{C(R_+,Z)}}{1 - q\|\hat{K}\|}. \tag{14}$$

Proof From (13) it follows that $\|z\|_{C([-\eta,0],Z)} \leq \rho$. Define on $\Omega_\rho(R_\eta, Z)$ the mapping Φ by

$$\Phi w(t) = z(t) + \hat{K}(Fw + f)(t) \quad \text{for } t \geq 0 \ \ (w \in \Omega_\rho(R_\eta, Z)),$$

and

$$\Phi w(t) = \phi(t) \quad \text{for } -\eta \leq t \leq 0.$$

Making use (11), we have

$$\|\Phi w\|_{C(R_\eta,Z)} \le \|z\|_{X(R_\eta,Z)} + \|\hat{K}\|q\|w\|_{X(R_\eta,Z)} + l,$$

where $l = \|\hat{K} f\|_{X(R_+,Z)}$.

According to (13), Φ maps $\Omega_\rho(R_\eta, Z)$ into itself. Applying the Contraction Mapping Theorem, we prove the existence and uniqueness. Furthermore,

$$\|u\|_{C(R_\eta,Z)} \le \|z\|_{C(R_\eta,Z)} + \|\hat{K}\|q\|u\|_{C(R_\eta,Z)} + l.$$

Hence, due to (12), we obtain (14). □

Remark 1 Making use Lemma 1, by the Scauder principle, we can prove the solution existence and estimate (14), provided $\hat{K}F$ is compact on each finite interval and inequalities (8), (12) and (13) hold.

4 Mild Solutions

4.1 Fundamental Solutions

Let $E : C(R_\eta, Y) \to C(R_+, Y)$ be a linear operator defined by

$$(Ew)(t) = \int_0^\eta B(s)w(t-s)d\mu(s) \quad (w \in C(R_\eta, Y)),$$

where $\mu(s)$ is a nondecreasing function having a finite number of jumps and $B(s)$ is a bounded in Y integrable (in the Bochner-Stieltjes sense) linear operator dependent on s. That is, $\int_0^\eta \|B(s)\|_{Y\to Y} d\mu(s) < \infty$. One can take more general causal operators than E is.

Consider the problem

$$\dot{v}(t) + Sv(t) + (Ev)(t) = f(t) \quad (t > 0), \tag{15}$$

$$v(t) = 0 \quad (-\eta \le t \le 0) \tag{16}$$

where $-S$ generates a C_0-semigroup e^{-tS} in Y, is boundedly invertible and $f \in C(R_+, Y)$ is given.

Let $W(t)$ be a function defined on R_η whose values are bounded linear operators in Y, boundedly differentiable. $W(t)$ is called *the fundamental solution* to (15) if it satisfies the equation

$$\frac{W(t)}{dt} + (S+E)W(t) = 0 \quad (t > 0) \tag{17}$$

and the conditions

$$W(t) = 0 \ \ (t < 0), \quad \text{and} \quad W(0) = I \tag{18}$$

hold.

Lemma 4 *Assume that $W(t)D(S) \subseteq D(S)$ and $W'(t)S^{-1}$ $(t \geq 0)$ is bounded and integrable. In addition, let $Sf(t), t \geq 0$ be bounded and integrable. Then a solution of problem (15) and (16) can be represented as*

$$v(t) = \int_0^t W(t-s)f(s)ds \ \ (t \geq \ 0). \tag{19}$$

Proof Since S is closed and E is bounded, we obtain

$$\begin{aligned} \frac{d}{dt}\int_0^t W(t-s)f(s)ds &= W(t,t)f(t) + \int_0^t \frac{d}{dt}(W(t-s)S^{-1})Sf(s)ds \\ &= f(t) + \int_0^t (S+E)W(t-s)f(s)ds \\ &= f(t) + (S+E)\int_0^t W(t-s)f(s)ds, \end{aligned}$$

as claimed. □

Furthermore, consider the problem

$$\dot{v}_1(t) + (Ev_1)(t) = f(t) \ \ (t > 0), \tag{20}$$

$$v_1(t) = 0 \ \ (-\eta \leq t \leq 0). \tag{21}$$

Let $G(t)$ be the fundamental solution to (20). That is, it is a function defined for $t \geq -\eta$, whose values are bounded linear operators in Y, differentiable and satisfying the equation

$$\frac{dG(t)}{dt} + (EG)(t) = 0 \ \ (t > 0), \tag{22}$$

with the conditions

$$G(t) = 0 \ \ (-\eta \leq t < 0) \quad \text{and} \quad G(0) = I. \tag{23}$$

Assume that E commutes with S. Then $G(t)$ commutes with e^{-tS}. Differentiating the function $W_1(t) = G(t)e^{-tS} = e^{-tS}G(t)$ we have

$$\frac{dW_1(t)}{dt} = e^{-tS}\frac{dG(t)}{dt} - Se^{-tS}G(t) = -(S+E)W_1(t).$$

So $G(t)e^{-tS}$ is the fundamental solution to (15). Now the previous lemma implies.

Corollary 1 *Let E commute with S. In addition, let $Sf(t)$ be bounded and integrable. Then a solution of problem (15) and (16) can be represented as*

$$v(t) = \int_0^t e^{-(t-s)S} G(t-s) f(s) ds \quad (t \geq 0).$$

4.2 Existence of Mild Solutions

Let F be a causal mapping acting from $\Omega_\rho(R_\eta, Y)$ into $C(R_+, Y)$. Consider the problem

$$\dot{u}(t) + Su(t) + (Eu)(t) = [Fu](t) + f(t) \quad (t > 0), \tag{24}$$

$$u(t) = \phi(t) \quad (-\eta \leq t \leq 0) \tag{25}$$

with given $\phi \in C([-\eta, 0], Y) \cap D(S)$. Let $z(t) \in C(R_\eta, Y)$ be a solution of the linear problem

$$\dot{z}(t) + Sz(t) + (Ez)(t) = 0 \quad (t > 0) \quad \text{and} \quad z(t) = \phi(t) \quad (-\eta \leq t \leq 0). \tag{26}$$

Following Browder's terminology cf. [17, p. 55], [24, Chap. 5], according to Lemma 4 a continuous function $u(t) : R_\eta \to Y$ satisfying

$$u(t) = z(t) + \int_0^t W(t-s)((Fu)(s) + f(s))ds \quad (t \geq 0), \tag{27}$$

and (25) will be called a mild solution to problem (24) and (25).

It is again supposed that the condition

$$\|Fw - Fw_1\|_{C(R_+,Y)} \leq q\|w - w_1\|_{C(R_\eta,Y)} \quad (w, w_1 \in \Omega_\rho(R_\eta, Y)) \tag{28}$$

holds. Introduce the operator $\hat{W} : C(R_+, Y) \to C(R_+, Y)$ by

$$\hat{W} f(t) = \int_0^t W(t-s) f(s) ds \quad (t \geq 0,\ f \in C(R_+, Y))$$

Due to Lemma 3 we get

Theorem 4 *Assume that the conditions (28),*

$$\|\hat{W}\| := \|\hat{W}\|_{C(R_+,Y)\to C(R_+,Y)} < \frac{1}{q} \tag{29}$$

and

$$\|z\|_{C(R_\eta,Y)} + \|\hat{W}f\|_{C(R_+,Y)} + q\rho\|\hat{W}\| < \rho \tag{30}$$

hold. Then problem (24) and (25) has a unique (mild) solution $u \in C(R_\eta, Y)$ *and*

$$\|u\|_{C(R_\eta,Y)} \le \frac{\|z\|_{C(R_\eta,Y)} + \|\hat{W}f\|_{C(R_+,Y)}}{1 - q\|\hat{W}\|}.$$

Now assume that E commutes with S. So $W(t) = e^{-St}G(t)$. Then

$$\|\hat{W}\| \le \omega(S, G) \quad \text{where } \omega(S, G) := \int_0^\infty \|e^{-sS}G(s)\|_{Y\to Y}ds,$$

provided the integral converges. Due to the previous theorem we arrive at

Corollary 2 *Suppose* E *commutes with* S *and the conditions (28),*

$$\omega(S, G) < \frac{1}{q} \tag{31}$$

and

$$\|z\|_{C(R_\eta,Y)} + \omega(S, G)\|f\|_{C(R_+,Y)} + q\rho\omega(S, G) < \rho. \tag{32}$$

hold. Then problem (24) and (25) has a unique solution u *and*

$$\|u\|_{C(R_\eta,Y)} \le \frac{\|z\|_{C(R_\eta,Y)} + \omega(S, G)\|f\|_{C(R_+,Y)}}{1 - q\omega(S, G)}.$$

About various methods enabling us to receive existence results for evolution equations see [24] and references therein.

In the sequel the existence and uniqueness of solutions is assumed.

5 The Main Results

Consider the equation

$$\dot{u}(t) + Su(t) + (Eu)(t) = [Fu](t) \quad (t > 0) \tag{33}$$

with an initial function $\phi \in C([-\eta, 0], Y)) \cap D(S)$. F is a causal mapping acting from $\Omega_\rho(R_\eta, Y)$ into $C(R_+, Y)$. According to the definition of causal mappings one has $F0 = 0$.

The zero solution of (33) *is said to be stable (in the Lyapunov sense)* if for any $\varepsilon > 0$ there is $\delta > 0$, such that the condition $\|\phi\|_{C([-\eta,0],Y)} \leq \delta$ implies the inequality $\|u\|_{X(R_\eta,Y)} \leq \varepsilon$ for any (mild) solution $u(t)$ of (33).

The zero solution of (33) *is asymptotically stable*, if it is stable and there is a $\delta_0 > 0$, such that the condition $\|\phi\|_{C([-\eta,0],Y)} \leq \delta_0$ implies $u(t) \to 0$ as $t \to \infty$. If $\delta_0 = \infty$, then the zero solution is *globally asymptotically stable.*

Furthermore, *the zero solution of* (33) *is said to be exponentially stable*, if there are constants $m_0 \geq 1$, $\delta_0 > 0$ and $\alpha > 0$, such that $\|u(t)\|_Y \leq m_0 e^{-\alpha t}$ $(t \geq 0)$, provided $\|\phi\|_{C([-\eta,0],Y)} \leq \delta_0$. *It is globally exponentially stable if* $\delta_0 = \infty$.

From Theorem 4 we get

Theorem 5 *Suppose the conditions*

$$\|Fw\|_{C(R_+,Y)} \leq q\|w\|_{C(R_\eta,Y)} \quad (w \in \Omega_\rho(R_\eta, Y)) \tag{34}$$

and

$$q\|\hat{W}\| < 1$$

hold. Then the zero solution of (33) is stable. Moreover, any solution of (33) satisfies the inequality

$$\|u\|_{C(R_\eta,Y)} \leq \frac{\|z\|_{C(R_\eta,Y)}}{1 - q\|\hat{W}\|} \leq \rho.$$

provided the solution $z(t)$ of (26) satisfies the inequality

$$\|z\|_{C(R_\eta,Y)} < \rho(1 - q\|\hat{W}\|).$$

If, the condition

$$e^{t\varepsilon}[Fe^{-t\varepsilon}w](t) \to [Fw](t) \quad \text{as } \varepsilon \to 0 \quad (w \in C(R_d, Y))$$

holds uniformly in t in the strong topology, then we will say that F has *the ε-property*. The mappings in the above presented examples have the ε-property.

Theorem 6 *Under the hypothesis of Theorem 5, let F have the ε-property. Then the zero solution of (33) is exponentially stable. Moreover, it is globally exponentially stable if (34) holds with $\rho = \infty$.*

Proof Substitute

$$u(t) = u_\varepsilon e^{-\varepsilon t} \quad (\varepsilon > 0) \tag{35}$$

into (33). We have

$$\dot{u}_\varepsilon(t) - \varepsilon u_\varepsilon(t) = e^{t\varepsilon}[-Se^{-t\varepsilon}u_\varepsilon(t) - (Ee^{-t\varepsilon}u_\varepsilon)(t) + (Fe^{-t\varepsilon}u_\varepsilon)(t)] \quad (t > 0). \tag{36}$$

Taking ε sufficiently small and applying Theorem 5, we can assert that the zero solution of the latter equation is stable. Now (35) implies the result. □

Corollary 2 and Theorems 5 and 6 imply.

Corollary 3 *Suppose E commutes with S, and the conditions (34) and $q\omega(S, G) < 1$ hold. Then the zero solution of (33) is stable. If, in addition, F has the ε-property, then the zero solution of (33) is exponentially stable. It is globally exponentially stable, if (34) holds with $\rho = \infty$.*

Definition 7 If the condition

$$\lim_{\|w\|_{C(R_\eta, Y)} \to 0} \frac{\|Fw\|_{C(R_+, Y)}}{\|w\|_{C(R_\eta, Y)}} = 0$$

holds, then Eq. (33) will be called a quasilinear equation.

Theorem 8 (Stability in the linear approximation) *Let $\|\hat{W}\| < \infty$ and Eq. (33) be quasilinear. Then the zero solution to (33) is stable. If, in addition, F has the ε-property, then the zero solution to (33) is exponentially stable.*

Proof From (36) it follows that for any $\rho > 0$, there is a $q > 0$, such that (34) holds, and $q = q(\rho) \to 0$ as $\rho \to 0$. Take ρ in such a way that the condition $q\|\hat{W}\| < 1$ is fulfilled. Now the required result is due the to Theorems 5 and 6. □

Corollary 4 *Suppose E commutes with S, $\omega(S, G) < \infty$ and Eq. (33) is quasilinear. Then the zero solution to (33) is stable. If, in addition, F has the ε-property, then the zero solution of (33) is exponentially stable.*

Let e^{-St} be an exponentially stable C_0-semigroup in Y:

$$\|e^{-St}\|_Y \le Me^{-\beta t} \quad (\beta > 0, t \ge 0).$$

Then

$$\omega(S, G) = \int_0^\infty \|e^{-sS}G(s)\|_{Y \to Y} ds \le M \int_0^\infty e^{-s\beta}\|G(s)\|_{Y \to Y} ds \tag{37}$$

Hence we get

Corollary 5 *Suppose E commutes with S and Eq. (33) is quasilinear. If, in addition, one of the following conditions holds:*

(a) e^{-St} is exponentially stable and $G(t)$ is bounded on $[0, \infty)$;
(b) e^{-St} is bounded on $[0, \infty)$ and (20) is exponentially stable.

Then the zero solution to (33) is stable.

If, in addition, F has the ε-property, then the zero solution of (33) is exponentially stable.

Finally, let Y be densely imbedded into a Hilbert space H with a scalar product $(.,.)$ and the imbedding constant $\gamma(Y,H)$: $\|f\|_H \le \gamma(Y,H)\|f\|_Y$. Let S be a normal operator in H with an isolated spectrum:

$$S = \sum_{k=1}^{\infty} \lambda_k(S) P_k, \tag{38}$$

where $P_k = (.,e_k)e_k$ are the eigen-projections with orthogonal eigenfunctions e_k, such that $(e_k,e_k) = 1$. Then

$$e^{-tS} = \sum_{k=1}^{\infty} e^{-\lambda_k(S)t} P_k.$$

Assume that $a_k := -Re\ \lambda_k(S) > 0$ and the integrals and series considered in this section converge. Then by the Schwarz inequality

$$\begin{aligned}\|e^{-tS}f\|_Y^2 &= \|\sum_{k=1}^{\infty} e^{-\lambda_k(S)t}(f,e_k)e_k\|_Y^2 \le m_Y^2 \sum_{k=1}^{\infty} e^{-2a_k(S)t} \sum_{k=1}^{\infty} |(f,e_k)|^2 \\ &\le m_Y^2 \sum_{k=1}^{\infty} e^{-2a_k(S)t} \|f\|_H^2,\end{aligned}$$

where $m_Y = \sup_k \|e_k\|_Y$, provided the supremum is finite. So

$$\|e^{-tS}\|_{Y\to Y} \le m_Y \gamma(Y,H) \left(\sum_{k=1}^{\infty} e^{-2a_k(S)t}\right)^{1/2}. \tag{39}$$

Hence,

$$\left(\int_0^{\infty} \|e^{-tS}\|_{Y\to Y}^2 dt\right)^{1/2} \le m_Y \gamma(Y,H) \left(\sum_{k=1}^{\infty} \frac{1}{2a_k}\right)^{1/2} \tag{40}$$

and by the Schwaz inequality,

$$\int_0^{\infty} \|e^{-tS}G(t)\|_{Y\to Y} dt \le m_Y \gamma(Y,H) \left(\int_0^{\infty} \|G(t)\|_{Y\to Y}^2 dt\right)^{1/2} \left(\sum_{k=1}^{\infty} \frac{1}{2a_k}\right)^{1/2}. \tag{41}$$

In addition from (39) it follows

$$\|e^{-tS}G(t)\|^2_{Y\to Y} \le \gamma^2(Y,H)m_Y^2\sum_{k=1}^{\infty} e^{-2a_kt}\|G(t)\|^2_{Y\to Y}$$
$$\le m_Y^2\gamma^2(Y,H)\left(\sum_{k=1}^{\infty} e^{-a_kt}\|G(t)\|_{Y\to Y}\right)^2$$

and therefore

$$\int_0^{\infty}\|e^{-tS}G(t)\|_{Y\to Y}dt \le m_Y\gamma(Y,H)\sum_{k=1}^{\infty}\int_0^{\infty}\|e^{-ta_k}G(t)\|_{Y\to Y}dt. \tag{42}$$

6 Stability of a System with One Discrete Delay in the Linear Part

6.1 Equations with Positive Fundamental Solutions

Again F is a causal mapping acting from $\Omega_\rho(R_\eta, Y)$ into $C(R_+, Y)$. Recall that

$$\omega(S,G) = \int_0^{\infty}\|e^{-sS}G(s)\|_{Y\to Y}ds.$$

Consider the equation

$$\dot{u}(t) + Su(t) + bu(t-h) = [Fu](t) \quad (t > 0), \tag{43}$$

where b and h are positive constants.

So $Eu(t) = bu(t-h)$ and $G(t) = k(t)I$, where $k(t)$ is a fundamental solution of the scalar equation.

$$\dot{v}(t) + bv(t-h) = 0 \quad (t > 0). \tag{44}$$

Assume that

$$\|e^{-St}\| \le m_0e^{-at} \quad (t \ge 0; a \ge 0) \tag{45}$$

and

$$ebh < 1. \tag{46}$$

Then $k(t) \geq 0$ and (44) is exponentially stable, cf. [13, Lemma 11.4.1]. So we have

$$\omega(S, G) \leq m_0 \int_0^\infty k(t)e^{-at}dt.$$

Recall that $k(.)$ is a solution of (44), $k(0) = 1$ and $k(t) = 0$ $(t < 0)$; then with $a > 0$, integrating by parts, we have

$$\begin{aligned}\int_0^\infty k(t)e^{-at}dt - \frac{1}{a} = \frac{1}{a}\int_0^\infty k'(t)e^{-at}dt = -\frac{b}{a}\int_0^\infty k(t-h)e^{-at}dt \\ = -\frac{b}{a}e^{-ah}\int_0^\infty k(t-h)e^{-a(t-h)}dt \\ = \frac{b}{a}e^{-ah}\int_{-h}^\infty k(t-h)e^{-a(t-h)}dt \\ = -\frac{b}{a}e^{-ah}\int_0^\infty k(t)e^{-at}dt.\end{aligned}$$

Hence

$$\int_0^\infty k(t)e^{-at}dt = \frac{1}{a}\left(1 + \frac{b}{a}e^{-ah}\right)^{-1} = \frac{1}{a + be^{-ah}} \quad (a > 0). \tag{47}$$

Hence (see also Lemma 4.6.5 from [13]), we have

$$\int_0^\infty k(t)dt = \frac{1}{b},$$

and consequently,

$$\omega(S, G) \leq \frac{m_0}{a + be^{-ah}} \quad (a \geq 0).$$

Now Corollary 3 yields

Corollary 6 *Suppose the conditions (45) and (46),*

$$\|Fw\|_{C(R_+,Y)} \leq q\|w\|_{C(R_\eta,Y)} \quad (w \in \Omega_\rho(R_\eta, Y)) \tag{48}$$

and

$$qm_0 < a + be^{-ah}$$

hold. Then the zero solution to (43) is stable in Lyapunov's sense. If, in addition, F has the ε-property, then the zero solution is exponentially stable. Moreover, it is globally exponentially stable, provided (48) holds with $\rho = \infty$.

Let Y be densely imbedded into a Hilbert space H and S be a normal operator in H with an isolated spectrum. Due to (42), the equality $G(s) = k(s)I$ and positivity of $k(t)$ we get

$$\omega(S, G) \le m_Y \gamma(Y, H) \sum_{k=1}^{\infty} \int_0^{\infty} e^{-ta_k} k(t) dt$$

provided $a_k = -Re\ \lambda_k(S) > 0$. Now (47) implies

$$\omega(S, G) \le m_Y \gamma(Y, H) \sum_{k=1}^{\infty} \int_0^{\infty} e^{-a_k s} k(s) ds.$$
$$\le m_Y \gamma(Y, H) \sum_{k=1}^{\infty} \frac{1}{a_k + be^{-a_k h}},$$

provided the series converges. Making use Corollary 3, we arrive at

Corollary 7 *Let Y be densely imbedded into a Hilbert space H and S be a normal operator in H with an isolated spectrum. Suppose the conditions (45), (46), (48) and*

$$q m_Y \gamma(Y, H) \sum_{k=1}^{\infty} \frac{1}{a_k + be^{-a_k h}} < 1$$

hold. Then the zero solution to (43) is stable in Lyapunov's sense. If, in addition, F has the ε-property, then the zero solution is exponentially stable. In particular, it is globally exponentially stable, provided if (48) holds with $\rho = \infty$.

Example 4 In space $C(0, 1)$ of the continuous functions defined on $[0, 1]$ consider the equation

$$\frac{\partial u(t, x)}{\partial t} = \frac{\partial^2 u(t, x)}{\partial x^2} + cu(t, x) + bu(t - h, x) + (Fu)(x, t) \quad (0 < x < 1,\ t > 0) \tag{49}$$

with a real constant $c < \pi$ and the Dirichlet boundary conditions

$$u(t, 0) = u(t, 1) = 0 \quad (t > 0). \tag{50}$$

Take $Sv = -d^2v/dx^2 - cv$ $(v \in D(S))$. Besides, $D(S)$ is the closure of the set

$$\{v \in C(0, 1) : d^2v/dx^2 \in C(0, 1); v(0) = v(1) = 0\}.$$

This operator is selfadjoint in $L^2(0, 1)$ with $\lambda_k(S) = \pi^2 k^2 - c > 0$ and

$$(P_k v)(x) = \int_0^1 v(s) e_k(s) ds\ \ e_k(x), \quad \text{where } e_k(x) = \sqrt{2}\, sin(\pi x) \quad (k = 1, 2, \ldots).$$

So $m_Y = \sqrt{2}$. Since

$$\int_0^1 |f(x)|^2 dx \le \sup_x |f(x)|^2,$$

the imbedding constant is 1. Therefore,

$$\int_0^\infty \|e^{-sS} G(s)\|_{C(0,1)\to C(0,1)} ds \le \sqrt{2} \sum_{k=1}^\infty \frac{1}{\pi^2 k^2 - c + be^{-\pi^2 k^2 + c}}.$$

Thus we can apply the previous corollary. For example, take

$$(Fu)(x,t) = d_1 e^{d_2 u(x,t)} u(t-h) \quad (d_1, d_2 = const \ge 0). \tag{51}$$

Hence, it follows that (48) holds with $q = q(\rho) = d_1 e^{d_2 \rho}$. Suppose the relation (51) and

$$d_1 \sqrt{2} \sum_{k=1}^\infty \frac{1}{\pi^2 k^2 - c + be^{-(\pi^2 k^2 - c)h}} < 1, \tag{52}$$

then there is a constant $\rho > 0$, such that

$$d_1 \sqrt{2} e^{d_2 \rho} \sum_{k=1}^\infty \frac{1}{\pi^2 k^2 - c + be^{-(\pi^2 k^2 - c)h}} < 1.$$

Thus by Corollary 7 the zero solution to (49) and (50) is exponentially stable, provided conditions (51) and (52) are fulfilled.

Furthermore, instead of (51) take

$$(Fu)(x,t) = \ d_1 \cos(u(x,t))\, u(t-h). \tag{53}$$

Then (48) holds with $\rho = \infty$ and $q = d_1$. In this case the zero solution to (49) is globally exponentially stable, provided (52) holds.

Example 5 Consider Eq. (49) with $c = 0$, the boundary conditions (50), $Y = C(0, 1)$ and F satisfying (48).

Take $Sv = -d^2 v/dx^2$ with the domain as in the previous example. This operator is dissipative [3, p. 88] and therefore generates a contracting semigroup: $\|e^{-St}\| \le 1$. As it was above mentioned $\int_0^\infty k(t)dt = 1/b$. Now Corollary 6 implies that the considered equation under condition (46) is stable, provided

$$q \int_0^\infty k(t)dt = \frac{q}{b} < 1. \tag{54}$$

Example 6 Consider Eq. (49) with $c = 0$, $Y = C(0, 1)$, F satisfying (48) and the Neumann boundary conditions:

$$\frac{\partial u(t, 0)}{\partial x} = \frac{\partial u(t, 1)}{\partial x} = 0 \quad (t > 0). \tag{55}$$

Take $Sv = -d^2v/dx^2$ ($v \in D(S)$). Besides, $D(S)$ is the closure of the set

$$\{v \in C(0, 1) : d^2v/dx^2 \in C(0, 1); v'(0) = v'(1) = 0\}.$$

This operator generates a semigroup satisfying: $\|e^{-St}\| = 1$ [3, p. 75 and p. 87] . Now Corollary 6 implies that the considered equation under conditions (46), (54) and (55) is stable.

6.2 Equations with Non-positive Fundamental Solutions

Again consider Eq. (43) assuming now that instead of (46) the condition

$$bh < \pi/4 \tag{56}$$

holds. Then due to Lemma 4.7.1 from [13],

$$\|k\|_{L^2(R_+)} \le \sqrt{\frac{2}{\tau(b, h)}\left(\frac{b}{\tau(b, h)} + 1\right)}$$

where $\tau(b, h) = inf_s|is + be^{-ish}|$. By Lemma 4.6.4 [13] $\tau(b, h) \ge bcos(2bh)$. Thus,

$$\|k\|_{L^2(R_+)} \le w(b, h) := \frac{1}{cos(2bh)}\sqrt{2(cos(2bh) + 1)/b}. \tag{57}$$

Under condition (45), the Cauchy inequality implies

$$\omega(G, S) \le \|e^{-St}\|_{L^2(R_+, Y)} w(b, h) \le \frac{m_0}{\sqrt{2a}} w(b, h).$$

Now Corollary 3 yields

Corollary 8 *Suppose the conditions (45), (48), (56) and*

$$qm_0 w(b, h) < \sqrt{2a}$$

hold. Then the zero solution to (43) is stable in Lyapunov's sense. If, in addition, F has the ε-property, then the zero solution is exponentially stable. Moreover, it is globally exponentially stable, provided (48) holds with $\rho = \infty$.

Let Y be densely imbedded into a Hilbert space H and S be a normal operator in H with an isolated spectrum. Due to (40) and (57) and the equality $G(s) = k(s)I$ we get

$$\omega(S, G) = \int_0^\infty \|e^{-tS}G(t)\|_{Y\to Y}dt \le m_Y\gamma(Y, H)w(b, h)\left(\sum_{k=1}^{\infty}\frac{1}{2a_k}\right)^{1/2}.$$

Now Corollary 3 implies

Corollary 9 *Let Y be densely imbedded into H and S be a normal operator in H with an isolated spectrum. Then the zero solution to (43) is stable in Lyapunov's sense, provided.*

$$qm_Y\gamma(Y, H)w(b, h)\left(\sum_{k=1}^{\infty}\frac{1}{2a_k}\right)^{1/2} < 1. \tag{58}$$

If, in addition, F has the ε-property, then the zero solution is exponentially stable. In particular, it is globally exponentially stable, provided $\rho = \infty$ in (48).

Example 7 Consider Eq. (49) with the boundary condition (50) and condition (55).

Define S as in Example 4. Then as it was pointed in that example $\gamma(Y, H) = \gamma(C, L^2) = 1$, $m_Y = \sqrt{2}$ and $\lambda_k(S) = \pi^2k^2 - c$. Now we can directly apply inequality (58).

Furthermore, due to Lemma 4.4.10 [13],

$$\|k\|_{L^1(R_+)} \le \|k\|_{L^2(R_+)}\sqrt{\pi(1 + bh)/\tau(b, h)} \le \zeta(b, h),$$

where

$$\begin{aligned}\zeta(b, h) &= w(b, h)\sqrt{\pi(1 + bh)/bcos(2bh)}\\ &= \frac{1}{bcos^{3/2}(2bh)}\sqrt{2\pi(1 + bh)(cos(2bh) + 1)}\\ &\le \frac{2}{b\,cos^{3/2}(2bh)}\sqrt{\pi(1 + bh)}.\end{aligned}$$

Now Corollary 3 implies.

Corollary 10 *Suppose the conditions (45), (48), (56) and*

$$qm_0\zeta(b, h) < 1$$

hold. Then the zero solution to (43) is stable in Lyapunov's sense. If, in addition, F has the ε-property, then the zero solution is exponentially stable. Moreover, it is globally exponentially stable, provided (48) holds with $\rho = \infty$.

Suppose now that (43) is quasilinear and

$$hb < \frac{\pi}{2}. \tag{59}$$

Then Eq. (44) is exponentially stable, cf. [15, Appendix 1]. Thus the zero solution to (43) is stable due to Corollary 5, provided e^{-St} is bounded.

7 Stability of Systems with Distributed Delays in Linear Parts

Consider the equation

$$\dot{u}(t) + Su(t) + \int_0^\eta u(t-s)d\mu(s) = [Fu](t) \quad (t > 0), \tag{60}$$

where $\mu(s)$ is a nondecreasing function having a finite number of jumps and F is the same as in the previous section. So $Eu(t) = \int_0^\eta u(t-s)d\mu$ and $G(t) = k_\mu(t)I$, where $k_\mu(t)$ is the fundamental solution of the scalar equation.

$$\dot{v}(t) + \int_0^\eta v(t-s)d\mu = 0 \quad (t > 0). \tag{61}$$

Assume that relations (45) and

$$e\,\eta var(\mu) < 1 \tag{62}$$

are fulfilled. Then $k_\mu(t) \geq 0$, and (61) is exponentially stable [13, Lemmas 4.6.5 and 11.4.2]. So we have

$$\omega(S, G) \leq m_0 \int_0^\infty k_\mu(t)e^{-at}dt,$$

where a and m_0 are taken from (45). Recall that k_μ is a solution of (61), $k_\mu(0) = 1$ and $k_\mu(t) = 0$ $(t < 0)$; With $a > 0$, integrating by parts, we have

$$\begin{aligned}\int_0^\infty k_\mu(t)e^{-at}dt - \frac{1}{a} &= \frac{1}{a}\int_0^\infty k'_\mu(t)e^{-at}dt \\ &= -\frac{1}{a}\int_0^\infty \int_0^\eta k_\mu(t-s)d\mu e^{-at}dt \\ &= -\frac{1}{a}\int_0^\eta e^{-as}\int_0^\infty k_\mu(t-s)e^{-a(t-s)}dtd\mu \\ &= \frac{1}{a}\int_0^\eta e^{-as}\int_{-\eta}^\infty k_\mu(t-s)e^{-a(t-s)}dtd\mu \\ &= -\frac{1}{a}\int_0^\eta e^{-as}d\mu\int_0^\infty k_\mu(t)e^{-at}dt.\end{aligned}$$

Hence for $a > 0$.

$$\int_0^\infty k_\mu(t)e^{-at}dt = \left(a + \int_0^\eta e^{-as}d\mu\right)^{-1}. \tag{63}$$

Letting $a \to 0$ we get

$$\int_0^\infty k_\mu(t)dt = \left(\int_0^\eta d\mu\right)^{-1} = \frac{1}{var(\mu)}.$$

Thus (63) is valid for $a \geq 0$ and

$$\omega(S, G) \leq \frac{m_0}{a + \int_0^\eta e^{-as}d\mu} \quad (a \geq 0).$$

Now Corollary 3 yields

Corollary 11 *Suppose the conditions (45), (48), (62) and*

$$qm_0 < a + \int_0^\eta e^{-as}d\mu \tag{64}$$

hold. Then the zero solution to (60) is stable in Lyapunov's sense. If, in addition, F has the ε-property, then the zero solution is exponentially stable. Moreover, it is globally exponentially stable, provided (48) holds with $\rho = \infty$,

Again consider Eq. (60) assuming now that instead of (62) the condition

$$\eta var(\mu) < \pi/4 \tag{65}$$

holds. Then due to Lemma 4.7.1 [13]

$$\|k_\mu\|_{L^2(R_+)} \leq \sqrt{\frac{2}{\tau(\mu)}\left(\frac{var(\mu)}{\tau(\mu)} + 1\right)}$$

where $\tau(\mu) = inf_s|is + \int_0^\eta e^{-is\tau}d\mu|$. By Lemma 4.6.2 [13],

$$\tau(\mu) \geq \tau_1(\mu) := \int_0^\eta cos(2var(\mu)\tau)d\mu(\tau).$$

Consequently,

$$\|k_\mu\|_{L^2(R_+)} \leq w(\mu) := \sqrt{\frac{2}{\tau_1(\mu)}\left(\frac{var(\mu)}{\tau_1(\mu)} + 1\right)}.$$

Under condition (45), the Cauchy inequality implies

$$\omega(G, S) \leq \|e^{-St}\|_{L^2(R_+,Y)}w(\mu) \leq \frac{m_0}{\sqrt{2a}}w(\mu),$$

where a and m_0 are taken from (45). Now Corollary 3 yields

Corollary 12 *Suppose the conditions (45), (48), (65) and*

$$qm_0w(\mu) < \sqrt{2a}$$

hold. Then the zero solution to (60) is stable in Lyapunov's sense. If, in addition, F has the ε-property, then the zero solution is exponentially stable. Moreover, it is globally exponentially stable, provided (48) holds with $\rho = \infty$.

8 Discussion

We have derived explicit delay-dependent stability tests for autonomous nonlinear distributed parameter systems, governed by functional differential equations in a Banach space with nonlinear causal mappings. These equations include partial differential, integro-differential and other traditional equations. This fact enables us to consider various classes of distributed retarded systems from the unified point of view.

As the examples show, the obtained stability conditions allow us to avoid the construction of the Lyapunov type functionals.

Concluding remarks

It should be very interesting to extend our results to non-autonomous nonlinear distributed parameter systems, especially to systems with time-variable delays.

References

1. Corduneanu C (2002) Functional equations with causal operators. Taylor and Francis, London
2. Datko R (1988) Not all feedback stabilized hyperbolic systems are robust with respect to small time delays in their feedbacks. SIAM J Control Optim 26:697–713
3. Engel K-J, Nagel R (2006) A short course on operator semigroups. Springer, New York
4. Fridmana E, Orlov Y (2009) Exponential stability of linear distributed parameter systems with time-varying delays. Automatica 45:194–201
5. Gil' MI (1998) On global stability of parabolic systems with delay. Appl Anal 69:57–71
6. Gil' MI (1998) On the generalized Wazewski and Lozinskii inequalities for semilinear abstract differential-delay equations. J Inequal Appl 2:255–267
7. Gil' MI (2000) Stability of linear time-variant functional differential equations in a Hilbert space. Funcialaj Ekvasioj 43:31–38
8. Gil' MI (2002) Solution estimates for abstract nonlinear time-variant differential delay equations. J Math Anal Appl 270:51–65
9. Gil' MI (2002) Stability of solutions of nonlinear nonautonomous differential-delay equations in a Hilbert space. Electron J Differ Equ 2002(94):1–15
10. Gil' MI (2003) The generalized Aizerman - Myshkis problem for abstract differential-delay equations. Nonlinear Anal TMA 55:771–784
11. Gil' MI (2003) On the generalized Aizerman - Myshkis problem for retarded distributed parameter systems. IMA J Math Control 20:129–136
12. Gil' MI (2005) Stability of abstract nonlinear nonautonomous differential-delay equations with unbounded history-responsive operators. J Math Anal Appl 308:140–158
13. Gil' MI (2013) Stability of vector differential delay equations. Birkhäuser Verlag, Basel
14. Gil' MI (2014) Stability of neutral functional differential equations. Atlantis Press, Amsterdam
15. Hale JK (1977) Theory of functional differential equations. Springer, New York
16. He Y, Wang Q-G, Lin C, Wu M (2007) Delay-range-dependent stability for systems with time-varying delay. Automatica 43(2):371–376
17. Henry D (1981) Geometric theory of semilinear parabolic equations. In: Lectures notes in mathematics, vol 840. Springer, New York
18. Ikeda K, Azuma T, Uchida K (2001) Infinite-dimensional LMI approach to analysis and synthesis for linear time-delay systems. Special issue on advances in analysis and control of time-delay systems. Kybernetika (Prague) 37(4):505–520
19. Lakshmikantham V, Leela S, Drici Z, McRae FA (2009) Theory of causal differential equations, Atlantis studies in mathematics for engineering and science, vol 5. Atlantis Press, Paris
20. Logemann H, Rebarber R, Weiss G (1996) Conditions for robustness and nonrobustness of the stability of feedback systems with respect to small delays in the feedback loop. SIAM J Control Optim 34(2):572–600
21. Luo YP, Deng FQ (2006) LMI-based approach of robust control for uncertain distributed parameter control systems with time-delay. Control Theory Appl 23:318–324
22. Nicaise S, Pignotti C (2006) Stability and instability results of the wave equation with a delay term in the boundary or internal feedbacks. SIAM J Control Optim 45(5):1561–1585
23. Tanabe H (1997) Functional analytic methods for partial differential equations. Marcel Dekker, Inc., New York
24. Vrabie II (1987) Compactness methods for nonlinear evolutions. Pitman, New York
25. Wang L, Yangfan W (2009) LMI-based approach of global exponential robust stability for a class of uncertain distributed parameter control. Systems with time-varying delays. J Vib Control 15(8):1173–1185
26. Wu J (1996) Theory and applications of partial functional differential equations. Springer, New York

The Case of Bidirectionally Coupled Nonlinear Circuits Via a Memristor

Ch.K. Volos, V.-T. Pham, S. Vaidyanathan, I.M. Kyprianidis and I.N. Stouboulos

Abstract The realization of a physical model of memristor by HP's researchers revealed a number of applications in which memristor can be used. Probably the most interesting of these, is in neuromorphic computing circuits, in which this new element could be used as an artificial synapse. So, in this work, a first step to this approach by studying the effect of using an HP memristor in the coupling branch of two nonlinear circuits is made. As a circuit, the Chua's oscillator is chosen. The two identical circuits are coupled bidirectionally via the proposed memristor, in which two different window functions have been used. Simulation results show an interesting dynamic behavior, which, among others confirm the complete chaotic synchronization achieved through the memristor, depending on system's initial conditions, the chosen window function and the memristor's parameters.

Keywords Memristor · Nonlinear circuit · Chua oscillator · Bidirectional coupling · Complete chaotic synchronization

Ch.K. Volos (✉) · I.M. Kyprianidis · I.N. Stouboulos
Physics Department, Aristotle University of Thessaloniki, GR-54124 Thessaloniki, Greece
e-mail: volos@physics.auth.gr

I.M. Kyprianidis
e-mail: imkypr@auth.gr

I.N. Stouboulos
e-mail: stouboulos@physics.auth.gr

V.-T. Pham
School of Electronics and Telecommunications, Hanoi University of Science and Technology, 01 Dai Co Viet, Hanoi, Vietnam
e-mail: pvt3010@gmail.com

S. Vaidyanathan
Research and Development Centre, Vel Tech University, Avadi, Chennai 600062, Tamil Nadu, India
e-mail: sundarvtu@gmail.com

S. Vaidyanathan and C. Volos (eds.), *Advances and Applications in Nonlinear Control Systems*, Studies in Computational Intelligence 635,
DOI 10.1007/978-3-319-30169-3_15

1 Introduction

The electronic circuit theory, until the beginning of seventies, has been spinning around the three known, fundamental two-terminal circuit elements, which are known as: resistor (R), capacitor (C) and inductor (L). These elements reflect the relations between pairs of the four basic electrical quantities of charge (q), current (i), voltage (v) and magnetic flux (φ) that mathematically can be written as:

$$\begin{aligned} dv &= R(i)di \\ dq &= C(v)dv \\ d\varphi &= L(i)di \end{aligned} \tag{1}$$

However, as it can be derived from the previous equations, a relation between the charge (q) and the flux (φ) is missing.

Professor Leon Chua of the University of California at Berkley, in 1971, was the first person who defined this missing link, by introducing the fourth fundamental element based on symmetry arguments [10]. This fourth circuit element was named Memristor (M), an acronym for **mem**ory res**istor**, which its existence was conjectured due to the following missing relation between the charge (q) and the flux (φ).

$$d\varphi = M(q)dq \tag{2}$$

The multiplicative term $M(\cdot)$ is called the memristance function. Dividing both sides of Eq. (2) by dt one obtains:

$$v = M(q)i \tag{3}$$

This element proved to have a very interesting behavior. As it can be shown from Eqs. (1) and (3), if M is constant, the previous equation presents nothing else, but the defining relation of a linear resistor (R). However, Chua has proved theoretically that a memristor is a nonlinear element because its v-i characteristic is similar to that of a Lissajous pattern. So, a memristor with a non-constant M describes a resistor with a memory, more precisely a resistor which resistance depends on the amount of charge that has passed through the device.

Another interesting feature of a memristor is its response to a sinusoidal input (Fig. 1). The "pinched hysteresis loop current-voltage characteristic" is a fingerprint of this new element. So, if any element or device has a current-voltage hysteresis curve of this kind, then it is either a memristor or a memristive device. Also, the memristor has as a signature that the "pinched hysteresis loop" shrinks as the frequency of the input signal is increased. The fundamentality of the memristor can also be deduced from this figure, as it is impossible to make a network of capacitors, inductors and resistors with a v-i behavior forming a pinched hysteresis curve [12].

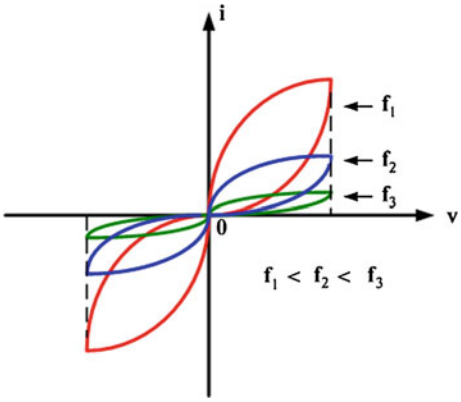

Fig. 1 A typical *v*-*i* characteristic curves of a memristor driven by a sinusoidal voltage input

Summarizing, the memristor has the following properties [10]:

- Non-linear relationship between current (i) and voltage (v).
- Does not store energy.
- Similar to classical circuit elements, a system of memristors can also be described as a single memristor.
- Behaves like a linear resistor for high frequencies as it is evident from the *v*-*i* characteristic curve.
- Memory capacity based on different resistances produced by the memristor.
- Non-volatile memory possible if the magnetic flux and charge through the memristor have a positive relationship ($M > 0$).

Furthermore, in 1976 Chua introduced a more generalized class of systems, in regard to the original definition of a memristor, which were called "memristive systems" [12]. An nth-order current-controlled memristive one-port is represented by

$$\begin{aligned} v &= R(w, i, t)i \\ \frac{dw}{dt} &= f(w, i, t) \end{aligned} \tag{4}$$

where $x \in R^n$ is the n-dimensional state variable of the system.

In the same way, the nth-order voltage-controlled memristive one-port is defined as:

$$\begin{aligned} i &= G(w, v, t)v \\ \frac{dw}{dt} &= f(w, v, t) \end{aligned} \tag{5}$$

After Chua's pioneering work, only a few works appeared in the literature for a long time since it was thought that the memristor was only a theoretical element and it could not be realized in the laboratory. So, until recently, the memristor had

received little attention even though a working device made from op-amps and discrete nonlinear resistors had been built and demonstrated in the seminal paper of Chua [10].

However, in 2008, Hewlett-Packard researchers, working at its laboratories in Palo Alto-California, announced in Nature [32] that a physical model of memristor has been realized. In their scheme, a memory effect is achieved in solid-state thin film two-terminal device.

This announcement brought a revolution in various scientific fields, as many phenomena in systems, such as in thermistors, which internal state depends on the temperature [31], spintronic devices which resistance varies according to their spin polarization [26] and molecules which resistance changes according to their atomic configuration [9], could be explained now with the use of the memristor. Also, electronic circuits with memory circuit elements could simulate processes typical of biological systems, such as learning and associative memory [27] and the adaptive behavior of unicellular organisms [28].

Furthermore, neuromorphic computing circuits, which are designed by borrowing principles of operation typical of the human (or animal) brain, can potentially solve problems that are cumbersome (or outright intractable) by digital computation. Therefore, certain realizations of memristors can be very useful in such circuits because of their intrinsic properties which mimic to some extent the behavior of biological synapses. Just like a synapse, which is essentially a programmable wire used to connect neighboring neurons, the memristor changes its resistance in varying levels. Many research teams [8, 11, 22, 23, 36] found that memristors can simulate synapses because electrical synaptic connections between two neurons can seemingly strengthen or weaken depending on when the neurons fire. Furthermore, memristors have been used in a cellular neural network [1, 6, 18, 29], for performing a number of applications, such as logical operations, image processing operations, complex behaviors and higher brain functions, or in designing stateful Boolean logic gates for the AND, OR and NOT operations [14]. Also, in many well-known nonlinear circuits, the nonlinear element has been replaced by memristors and various interesting dynamical phenomena have been observed [3, 7, 15, 17, 19, 20, 24, 25].

So, in this direction, this chapter presents the study of the effect of using the HP memristor in the coupling branch of two nonlinear circuits. Despite the fact that a memristor of smooth continuous cubic function of charge (q) versus flux (φ) has been used as a coupling element between coupled chaotic circuits [33, 34], it is the first time that the specific memristor model proposed by the researchers of HP is used for such an application. This is a very interesting approach, especially for using, in next stage, the HP's memristor as an artificial synapse in neuromorphic computing circuits.

For the need of this work, the most well-known nonlinear circuit, the Chua oscillator, is used. The two identical circuits are coupled bidirectionally (mutually) via the proposed memristor, in which two different window functions have been used. The simulation results show the achievement of complete (or full) chaotic synchronization, when some conditions are fulfilled, depending on system's initial conditions and the chosen window function. The phenomenon of full chaotic synchronization,

according to which the interaction between two identical coupled chaotic systems leads to a perfect coincidence of their chaotic trajectories ($x_1(t) = x_2(t)$, as $t \to \infty$), plays an important role, especially in the case of coupling via a synapse [2, 5, 30].

The rest of the chapter is organized as follows. The next section provides a brief description of the memristor proposed by HP researchers, which consists the base of this work. Section 3 presents the mutual coupling scheme, via the proposed memristor, between two identical coupled Chua oscillators. The simulation results of systems' dynamic behavior are presented in details in Sect. 4. Finally, Sect. 5 outlines the conclusions of this research study and some thoughts for future work.

2 Structure, Properties and Formulas of HP's Memristor

After 36 years of Chua's hypothesis about memristor, this element came into life, as it is mentioned, when researchers of HP's lab reported the first ever solid state version of memristor in their famous article [32]. This memristor, is made of a titanium dioxide layer which is located between two platinum electrodes (Fig. 2). This layer is of the dimension of several nanometers and if an oxygen dis-bonding occurs, its conductance will rise instantaneously. However, without doping, the layer behaves as an isolator. The area of oxygen dis-bonding is referred to as space-charge region and changes its dimension if an electrical field is applied. This is done by a drift of the charge carriers. The smaller the insulating layer, the higher the conductance of the memristor. Also, the tunnel effect plays a crucial role. Without an external influence the extension of the space-charge region does not change.

The internal state (ω) is the extent of the space-charge region, which is restricted in the interval [0, 1] and can be described by the equation:

$$\omega = \frac{w}{D}, 0 \leq \omega \leq 1, \omega \in R \tag{6}$$

where (w) is the absolute extent of the space-charge region and (D) is the absolute extent of the titanium dioxide layer. The memristance can be described by the following equation:

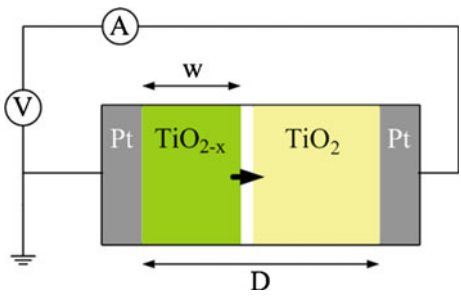

Fig. 2 Structure of TiO_2 memristor, in which TiO_{2-x} and TiO_2 layers are sandwiched between two platinum electrodes

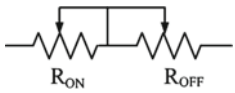

Fig. 3 The equivalent circuit of the memristor

$$M(\omega) = R_{ON}\omega + R_{OFF}\,(1-\omega) \tag{7}$$

where (R_{ON}) is the resistance of the maximum conducting state and (R_{OFF}) represents the opposite case (Fig. 3). So, when $\omega = 0$, $R = R_{OFF}$, and when $\omega = 1$, $R = R_{ON}$. The vector containing the internal states of the memristor is one dimensional. For this reason scalar notation is used. The state equation is:

$$\frac{d\omega}{dt} = \frac{\mu_v R_{ON}}{D^2} i(t) \tag{8}$$

where (μ_v) is the oxygen vacancy mobility and $i(t)$ is the current through the device. By using the Eq. (6) the previous equation can be rewritten as:

$$\frac{dw}{dt} = \frac{m_n R_{ON}}{D} i(t) \tag{9}$$

So, the dynamics of the memristor can therefore be modeled through the time dependence of the width (w) of the doped region. Integrating Eq. (9) with respect to time,

$$w = w_0 + \frac{\mu_v R_{ON}}{D} q(t) \tag{10}$$

where (w_0) is the initial width of the doped region at $t = 0$ and (q) is the amount of charges that have passed through the device. Substituting Eqs. (6), (10) into Eq. (7) gives:

$$M(q) = R_0 - \frac{\mu_v R_{ON} \Delta R}{D^2} q(t) \tag{11}$$

where

$$R_0 = R_{ON}\frac{w_0}{D} + R_{OFF}\left(1 - \frac{w_0}{D}\right) \tag{12}$$

and $\Delta R = R_{OFF} - R_{ON}$. The term ($R_0$) refers to the net resistance at $t = 0$ that serves as the device's memory. This term is associated with the memristive state, which is essentially established through a collective contribution, i.e. it depends directly on the amount of all charges that have flown through the device. That's why, we can say that the memristor has the feature to "remember" whether it is "ON" or "OFF" after its power is turned on or off.

The model of memristor which has been presented by HP scientists, does not take into consideration the boundary effects as the speed of the boundary between doped

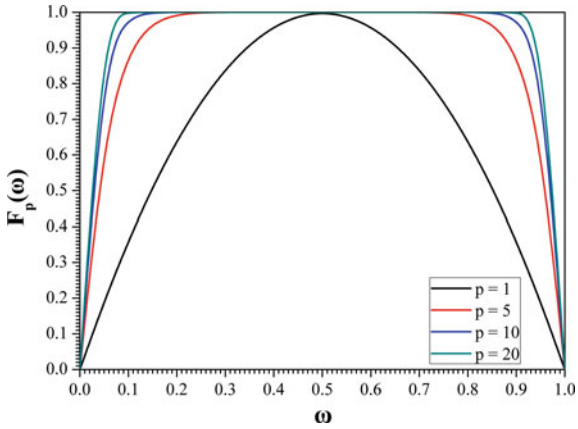

Fig. 4 The window functions of Eq. (14)

and undoped regions get suppressed at either edge. For this reason, Joglekar and Wolf accounted this suppression by proposing a new window function $F(\omega)$ and so Eq. (9) is modified as [21]:

$$\frac{dw}{dt} = \eta \frac{\mu_v R_{ON} i(t)}{D} F\left(\frac{w}{D}\right) \tag{13}$$

where $\eta = \pm 1$ depending on the polarity of the memristor. The function $F(\omega)$ is symmetric to $\omega = 1/2$ and $F(0) = F(1) = 0$, for restricting ion drifting at the edge. In the interval, for $0 < \omega < 1/2$ the function $F(\omega)$ is monotonically increasing, while for $1/2 < \omega < 1$ is monotonically decreasing. Also, Joglekar and Wolf defined a parameter p to constitute a family of windows functions of the form (Fig. 4):

$$F_p(\omega) = 1 - (2\omega - 1)^{2p} \tag{14}$$

As the parameter p increases the function $F(\omega)$ becomes linear, while for $p = 1$ the Eq. (13) reduces to the HP model.

In 2009, Biolek et al. proposed an alternative window function which considers the boundary speeds of the approaching and receding from the thin film edge [4]. This function (Fig. 5) is given as:

$$F_p(\omega) = 1 - \left[\omega - stp(-i)\right]^{2p} \tag{15}$$

where (p) is a positive integer, (i) is the memristor's current, which is considered to be positive if it increases the width of the doped layer, or $\omega \to 1$ and

$$stp(i) = \begin{cases} 1, & if\ i \geq 0 \\ 0, & if\ i < 0 \end{cases} \tag{16}$$

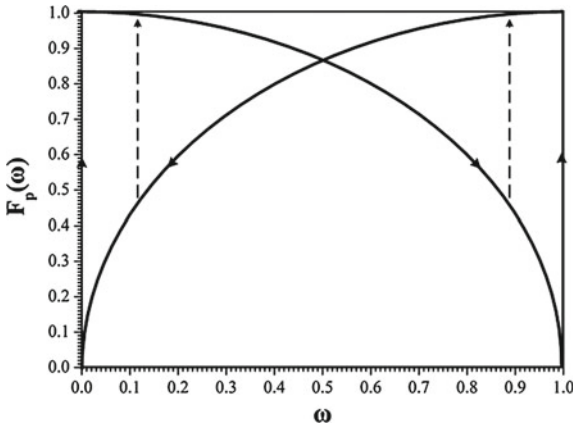

Fig. 5 The window functions of Eq. (15)

Fig. 6 The symbol of the memristor

In this chapter, the two different approaches of Eqs. (14) and (15) for the windows function have been adopted for being used in the HP's memristor model as an artificial synapse in the coupling branch between two bidirectionally coupled nonlinear systems. In Fig. 6 the symbol of the memristor is shown.

3 The Coupling Scheme

For studying the effect of the HP's memristor as an artificial synapse between coupled chaotic systems, the bidirectional or mutual coupling scheme has been used. In this coupling scheme both the coupled systems are connected and each system's behavior influences the dynamics of the other. This case of coupling, which is even the simplest, is very interesting because displays many of the phenomenology that is observed in more complex networks. The case of bidirectional or mutual coupling between two coupled chaotic oscillators is described by the following set of differential equations:

$$\begin{cases} \dot{x}_1 = F(x_1) + C\,(x_2 - x_1) \\ \dot{x}_2 = F(x_2) + C\,(x_1 - x_2) \end{cases} \tag{17}$$

where $F(x)$ is a vector field in a phase space of dimension n, i.e. $x \in R^n$, and C a symmetric matrix of constants which describes the nature and strength of the coupling between the oscillators [16].

In this work, as a nonlinear system, the Chua's oscillator, which is structurally the simplest and dynamically the most complex member of the Chua's circuit family, is chosen [13, 35]. Until now, a great number of nonlinear phenomena concerning

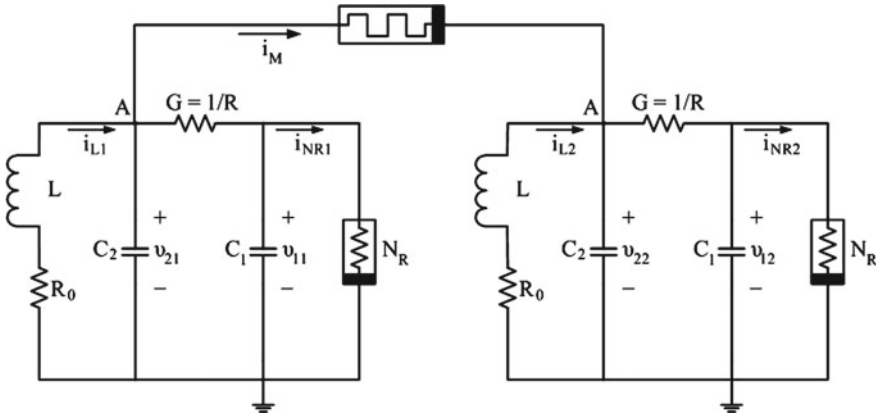

Fig. 7 Mutually coupled Chua oscillators via an HP memristor

chaos theory have been discovered by using the specific circuit. This is the reason for choosing the Chua oscillator as a nonlinear system in this work.

The dynamics of the mutually coupled Chua oscillators via an HP memristor (Fig. 7) is described by the following set of normalized differential equations:

$$\begin{cases} \frac{dx_1}{d\tau} = \frac{C_0}{C_1}\left[\frac{R_{ON}}{R}(y_1 - x_1) - f(x_1)\right] \\ \frac{dy_1}{d\tau} = \frac{C_0}{C_2}\left[\frac{R_{ON}}{R}(x_1 - y_1) + z_1 - \frac{1}{\hat{R}(\omega)}(y_1 - y_2)\right] \\ \frac{dz_1}{d\tau} = \frac{L_0}{L}\left[-y_1 - \frac{R_0}{R_{ON}}z_1\right] \\ \frac{dx_2}{d\tau} = \frac{C_0}{C_1}\left[\frac{R_{ON}}{R}(y_2 - x_2) - f(x_2)\right] \\ \frac{dy_2}{d\tau} = \frac{C_0}{C_2}\left[\frac{R_{ON}}{R}(x_2 - y_2) + z_2 + \frac{1}{\hat{R}(\omega)}(y_1 - y_2)\right] \\ \frac{dz_2}{d\tau} = \frac{L_0}{L}\left[-y_2 - \frac{R_0}{R_{ON}}z_2\right] \\ \frac{d\omega}{d\tau} = \eta F(\omega)\frac{1}{\hat{R}(\omega)}(y_1 - y_2) \end{cases} \tag{18}$$

where $\hat{R}(\omega) = \omega + \frac{R_{OFF}}{R_{ON}}(1 - \omega)$ and $\eta = 1$.

In system's equations, the first three equations describe the first of the two coupled Chua's oscillator, while the other three describe the second one and the last one is the state equation of the proposed memristor model.

The dimensionless form of the nonlinear function $f(x_i)$, with $i = 1, 2$ of the Chua's diode N_R (Fig. 8) is given by the following equation:

$$\begin{aligned} f(x_i) = {} & m_c x_i + 0.5(m_a - m_b)(|x_i + 1| - |x_i - 1|) \\ & + 0.5(m_b - m_c)(|x_i + E_2/E_1| - |x_i - E_2/E_1|) \end{aligned} \tag{19}$$

where, $m_a = RG_a$, $m_b = RG_b$ and $m_c = RG_c$, while G_a, G_b, G_c the slopes of the five segments and $E_{1,2}$ the breakpoints.

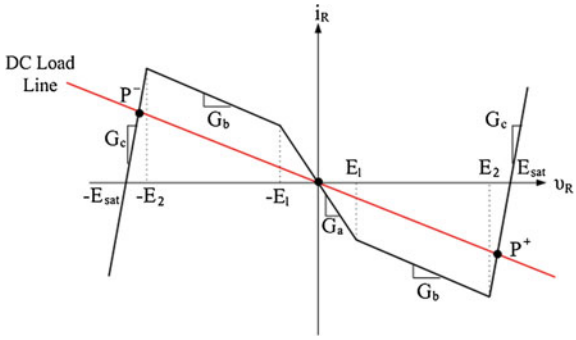

Fig. 8 Five-segment υ-i characteristic of the nonlinear element N_R of the Chua oscillator

Furthermore, x_i, y_i, z_i and ω are the normalized state variables which are given by the following equations:

$$x_i = \frac{\upsilon_{C1i}}{\upsilon_0}, \qquad y_i = \frac{\upsilon_{C2i}}{\upsilon_0}, \qquad z_i = \frac{i_{Li}}{i_0}, \qquad \omega = \frac{w}{D}, \qquad \tau = \frac{t}{t_0}$$

with

$$\upsilon_0 = 1V, \quad i_0 = \frac{\upsilon_0}{R_{ON}}, \qquad t_0 = \frac{D^2}{\mu\upsilon_0}, \qquad C_0 = \frac{D^2}{\mu\upsilon_0 R_{ON}}, \qquad L_0 = \frac{D^2 R_{ON}}{\mu\upsilon_0}$$

In this work, the following values for the HP memristor have been used: $R_{ON} = 100\,\Omega$, $D = 10\,\text{nm}$, $\mu = 10^{-14}\,\text{cm}^2\text{s}^{-1}\text{V}^{-1}$. Also, the values of the identical coupled Chua's oscillators parameters are chosen, so that each coupled circuit demonstrates double-scroll chaotic attractors (Fig. 9), which is a sign of generating chaotic behavior [20]: $L/L_0 = 1/18$, $C_1/C_0 = 1/10$ $C_2/C_0 = 1$, $G = 1/R = 555\,\mu\text{S}$, $R_0/R_{ON} = 1/140$, while the parameter (R_{OFF}) varies. Also, Chua's oscillator has three equilibrium points. One of these equilibria is the origin $(x, y, z) = (0, 0, 0)$, while the other two are usually referred as P^+, P^- (Fig. 8). So, a typical trajectory of this kind of attractor rotates "randomly" around one of these equilibrium points (P^+ or P^-), getting away from it until it goes back to a point closer to the equilibrium and either repeats the process or goes to the other equilibrium point and repeats the process around it (Fig. 9).

4 Simulation Results

For studying the effect of the HP memristor as a coupling element in mutual coupling system's dynamic behavior, the two aforementioned window functions have been used with different values of the parameter (p), while the parameter (R_{OFF}) varies

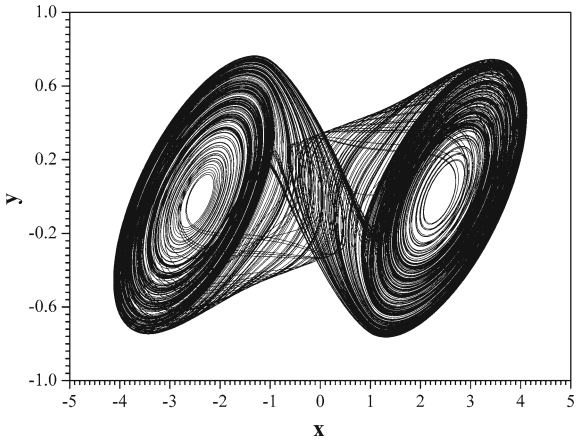

Fig. 9 Projection on the x–y plane of the double-scroll chaotic attractor of the Chua oscillator

from 1 to 100 kΩ, in order to see the dynamics behavior of the coupling system. The value of memristor's parameters and especially of (R_{OFF}) plays a crucial role in the design of the physical model of the memristor. So, it is important to know memristor's behavior in regard to (R_{OFF}) values. The system of differential equations (18) has been solved numerically by using the fourth order Runge–Kutta algorithm, while the initial conditions of the system are: $(x_{10}, y_{10}, z_{10}, x_{20}, y_{20}, z_{20}, \omega_0) = (0.8, -0.2, 0.4, -0.5, 0.1, 0.2, 0.5)$.

4.1 First Approach

At the beginning the window function of Eq. (14) introduced by Joklegar and Wolf, is adopted in the memristor model. The chosen value of the parameter (p) is equal to one ($p = 1$), so the window function will give a nonlinear drift model with $F_{p=1}(\omega) = 4\omega(1-\omega)$. Also, the resistance ($R_{OFF}$) is chosen to be equal to 1 kΩ.

As it can be shown in Fig. 10, the state variable (ω) of the memristor increases from the initial value ($\omega_0 = 0.5$) and gradually reaches its upper limit ($\omega \to 1$) for $t_1 > 1.229$ s. From a physical point of view, this means, that the space-charge region (w) expands and tends to cover the entire titanium dioxide layer. So, as it is previously mentioned, for $t > t_1$, the state variable (ω) remains equal to one ($\omega = 1$) and the resistance of the maximum conducting state is $R = R_{ON}$. In this case, each one of the coupled circuits starts from a chaotic double-scroll state and under the influence of the memristor, especially for $t > t_1$, this behavior is suppressed into single-scroll attractors around the two different equilibrium points (Fig. 14). Finally, after a long transition time ($t > 64.738$ s), the system results in full chaotic synchronization (Fig. 11 and 15), in which each of the two coupled circuits returning again in a chaotic double-scroll state. In Figs. 12 and 13 the time-series of the signals

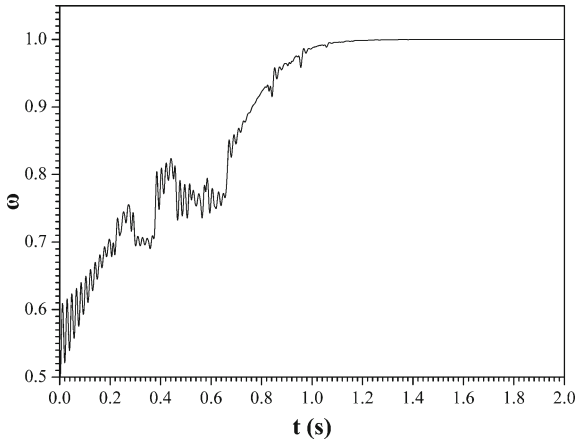

Fig. 10 Time-series of the normalized variable (ω) of the width of the doped region, for $R_{OFF} = 1\,\mathrm{k}\Omega$ and $p = 1$, using the first approach

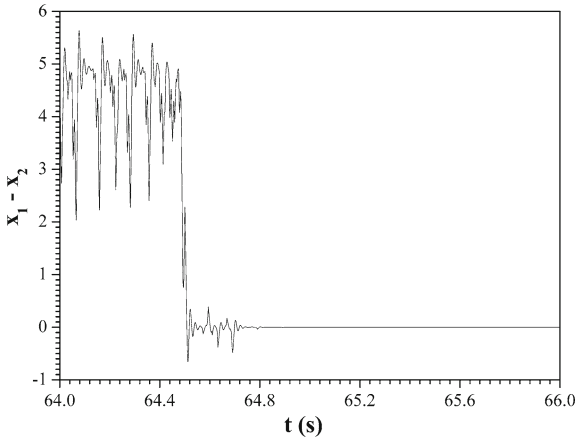

Fig. 11 Time-series of the difference signal ($x_1 - x_2$), for $R_{OFF} = 1\,\mathrm{k}\Omega$ and $p = 1$, using the first approach

x_1 and x_2 are displayed, in which the transition from a single-scroll to a double-scroll is shown for $t > 64.738\,\mathrm{s}$.

For $R_{OFF} = 10\,\mathrm{k}\Omega$ and $p = 1$, the system presents the same behavior as in the previous case, but the time in which the state variable (ω) become equal to one has been increased significantly ($t > 35.723\,\mathrm{s}$), as it can be shown in Fig. 16. Also, Fig. 20 displays the single-scroll attractors of the two coupled circuits around the two different equilibrium points. Respectively, the transient time, in order to observe full chaotic synchronization (Fig. 21), is also increased, $t_2 = 275.652\,\mathrm{s}$, (Fig. 17). For $t > t_2$, each oscillator is in a double-scroll chaotic state, (Figs. 18 and 19).

Finally, for $R_{OFF} = 100\,\mathrm{k}\Omega$ and $p = 1$, the state variable (ω) of the memristor oscillates chaotically (Fig. 22), and the system remains always in a chaotic desynchronization mode, (Figs. 23 and 26), in which each oscillator is in a double-scroll chaotic state, (Figs. 24 and 25).

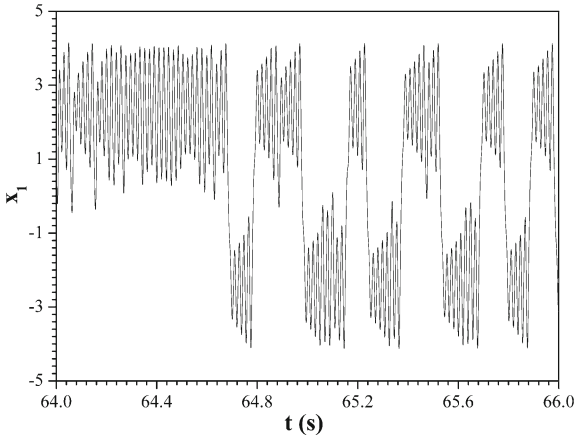

Fig. 12 Time-series of the signal (x_1), for $R_{OFF} = 1\,\text{k}\Omega$ and $p = 1$, using the first approach

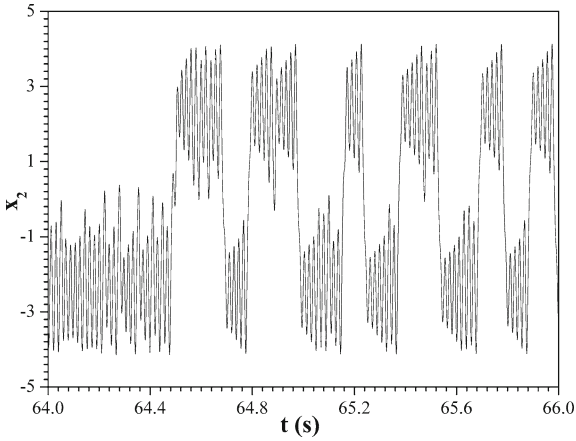

Fig. 13 Time-series of the signal (x_2), for $R_{OFF} = 1\,\text{k}\Omega$ and $p = 1$, using the first approach

For greater values of the parameter (p), i.e. for $R_{OFF} = 1\,\text{k}\Omega$ and $p = 10$, the memristor has the same behavior and so the coupled system reacts with the same way. The state variable (ω) gradually increases from the initial value ($\omega_0 = 0.5$) and after a long time (0.218–1.249 s) of oscillations around the value of $\omega = 0.712$ the variable ω with an almost sudden jump results to the maximum value of $\omega = 1$, for $t > 1.389\,\text{s}$, which is slightly greater than in the case of $p = 1$ (Fig. 27).

Furthermore, each one of the coupled circuits begins from a chaotic double-scroll behavior and under the influence of the memristor, this behavior is suppressed into a single-scroll attractors for $t > 1.389\,\text{s}$ (Fig. 31). Finally, after a long transition time ($t > 28.101\,\text{s}$), the system results in full chaotic synchronization (Figs. 28 and 32), in which each of the two coupled circuits returns again in a chaotic double-scroll state (Figs. 29 and 30).

For $R_{OFF} = 100\,\text{k}\Omega$ and $p = 10$, the system shows the same behavior as in the previous case for $p = 1$ (Figs. 12, 13, 14, 15, 16, 17, 18, 19, 20, 21, 22, 23, 24,

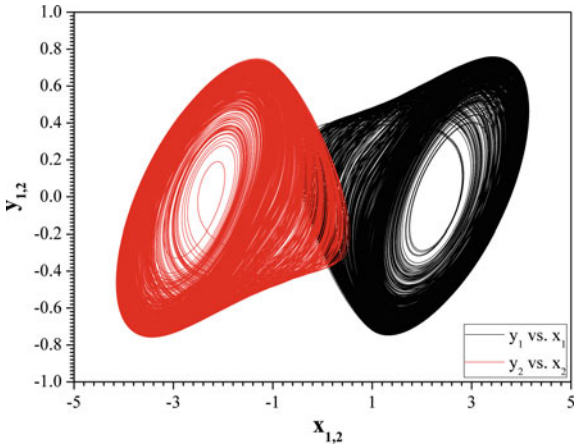

Fig. 14 Phase portraits of $(y_{1,2})$ versus $(x_{1,2})$, for $t <$ 64.738 s while $R_{OFF} = 1\,\text{k}\Omega$ and $p = 1$, using the first approach

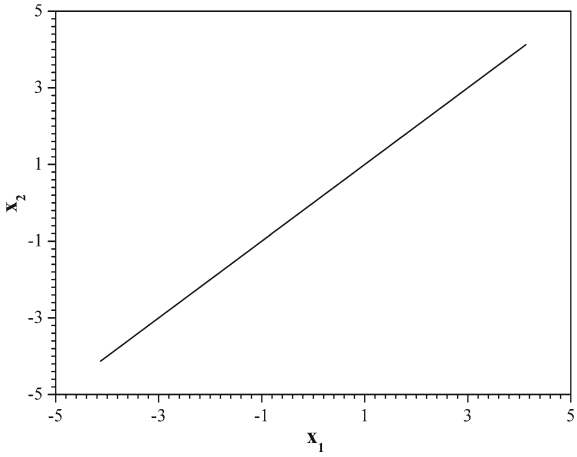

Fig. 15 Phase portraits of (x_2) versus (x_1), for $t >$ 64.738 s while $R_{OFF} = 1\,\text{k}\Omega$ and $p = 1$, using the first approach

25 and 26). The state variable (ω) of the memristor oscillates chaotically (Fig. 33) without reaching the boundaries and so the system remains always in a chaotic desynchronization mode (Fig. 34), in which each one of the coupled circuits presents the expected behavior of double-scroll chaotic attractor (Figs. 35 and 36).

4.2 Second Approach

In the second case, the window function of Eq. (15) introduced by Biolek et al., has been adopted. At the beginning the parameter (p) is chosen to be equal to one $(p = 1)$. For various values of the resistance R_{OFF}, the variable (ω) is likely to reach its limits without remaining therein. This is the advantage of the use of the window

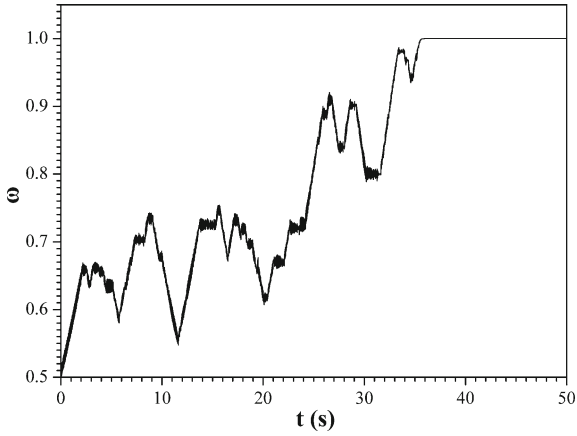

Fig. 16 Time-series of the normalized variable (ω) of the width of the doped region, for $R_{OFF} = 10\,\text{k}\Omega$ and $p = 1$, using the first approach

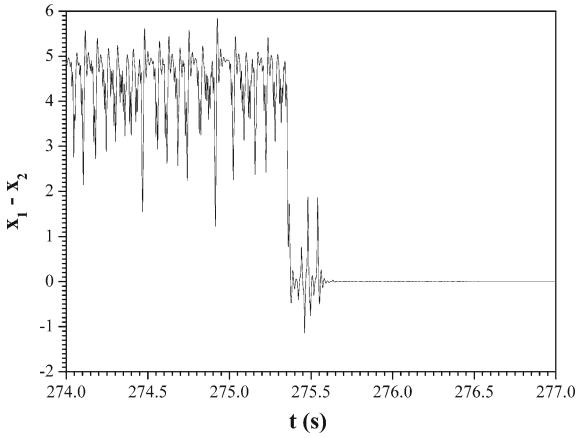

Fig. 17 Time-series of the difference signal ($x_1 - x_2$), for $R_{OFF} = 10\,\text{k}\Omega$ and $p = 1$, using the first approach

function of Eq. (15). So the system remains always in a chaotic desynchronization mode. However, even in this case some interesting phenomena can be mentioned.

The aforementioned system's behavior, for $R_{OFF} = 1\,\text{k}\Omega$, is displayed in Figs. 37, 38, 39 and 40. The state variable (ω) of the memristor through Sudden Jumps (SJ), either is increased or decreased, as shown in Fig. 37. In this figure, seven such jumps in the range of [347s, 350s] are depicted. These jumps are a consequence of the sudden change of the equilibrium point around which each one of the variables (x_1) and (x_2) of the two coupled systems oscillates (Figs. 39 and 40). As a result, the difference signal ($x_1 - x_2$) may oscillates in a chaotic way around three levels, a high, $x_1 - x_2 > 0$, a low, $x_1 - x_2 < 0$, and a level around $x_1 - x_2 = 0$), in which the system switches through sudden jumps (Fig. 38). The aforementioned dynamical behavior is confirmed by the phase portraits of $y_{1,2}$ versus $x_{1,2}$ of Figs. 41, 42, 43, 44, 45 and 46, for the six ranges between the sudden jumps which are shown in Fig. 37.

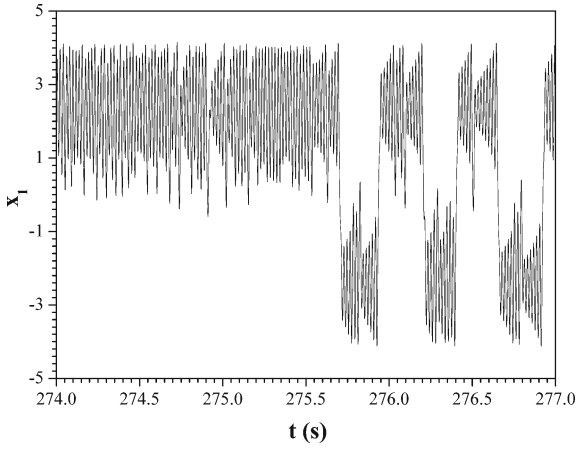

Fig. 18 Time-series of the signal (x_1), for $R_{OFF} = 10\,\text{k}\Omega$ and $p = 1$, using the first approach

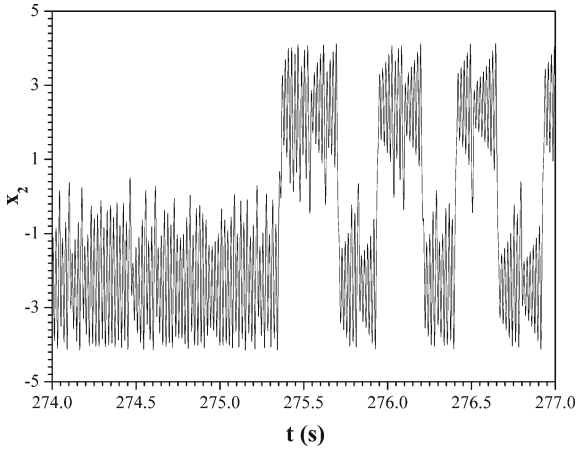

Fig. 19 Time-series of the signal (x_2), for $R_{OFF} = 10\,\text{k}\Omega$ and $p = 1$, using the first approach

In Figs. 47 and 48 the effect of the resistance (R_{OFF}) in the state variable's (ω) behavior is shown. From this figure deducted, that when (ω) varies, the range around its initial value reduces by increasing the (R_{OFF}). So, for $R_{OFF} = 10\,\text{k}\Omega$ this range is $\Delta\omega = 0.089$ ($\omega \in [0.454, 0.543]$) while for $R_{OFF} = 100\,\text{k}\Omega$ this range is $\Delta\omega = 0.012$ ($\omega \in [0.4946, 0.5066]$) significantly lower in regards to the previous one.

Finally, by increasing the value of the parameter (p) of the window function two phenomena have been observed. Firstly, the range of variation of the state variable (ω) is increased, (Figs. 49, 50, 51 and 52). This means that the space-charge region (w) of the memristor tends to cover all the range (D) of the titanium dioxide layer ($w = D$). Secondly, as it is previously mentioned, using this window function, the variable (ω) reaches the upper limit ($\omega = 1$) without remaining therein, but oscillates chaotically around a mean value of 0.95. Also, by increasing the value of the parameter (p), the

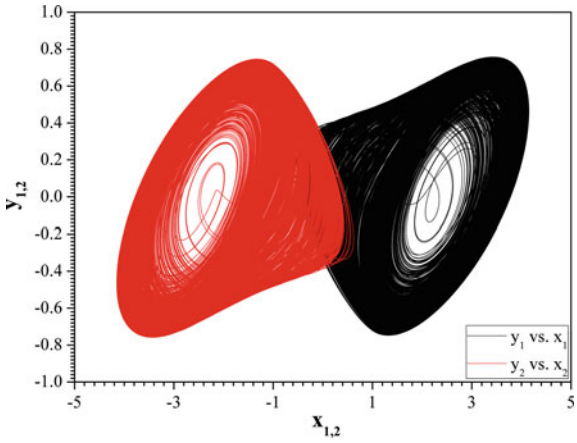

Fig. 20 Phase portraits of $(y_{1,2})$ versus $(x_{1,2})$, for 40 s $< t <$ 275 s while $R_{OFF} =$ 10 kΩ and $p = 1$, using the first approach

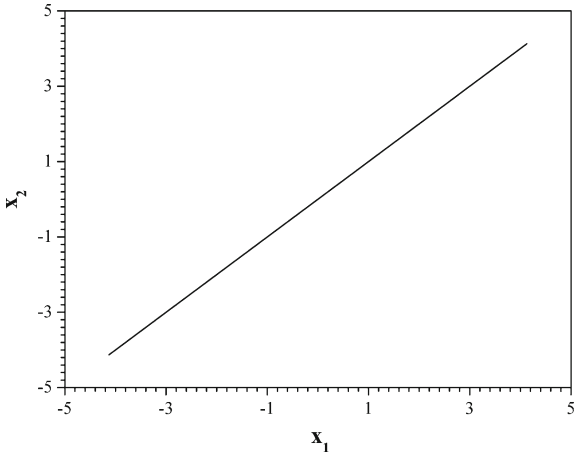

Fig. 21 Phase portraits of (x_2) versus (x_1), for $t >$ 275.652 s while $R_{OFF} =$ 10 kΩ and $p = 1$, using the first approach

memristor remains for a longer time in this state, as it is clearly shown in Figs. 50, 51 and 52. In Figs. 53 and 54 the phase portraits of (x_2) versus (x_1), in the case of $R_{OFF} = 1\,\text{k}\Omega$ and $p = 8$, for $t < 308$ s and $t > 310$ s, are displayed.

4.3 The Effect of Initial Conditions on System's Behavior

In this section, the effect of initial conditions on system's behavior by using the two different window functions is studied. For this reason different sets of initial conditions of coupled circuits and values of the parameter (ω) have been chosen.

In the first case, by using the first window function with $p = 1$ and $R_{OFF} =$ 1 kΩ, only the signs of some of the initial conditions of the coupled systems have

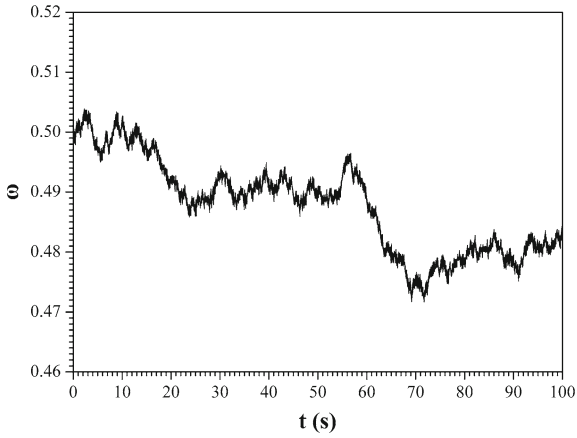

Fig. 22 Time-series of the normalized variable (ω) of the width of the doped region, for $R_{OFF} = 100\,\mathrm{k}\Omega$ and $p = 1$, using the first approach

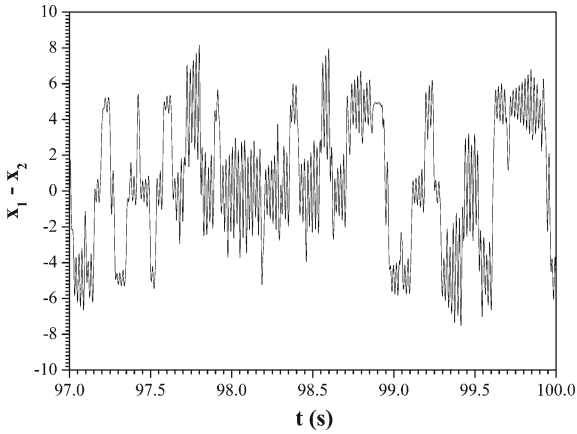

Fig. 23 Time-series of the difference signal ($x_1 - x_2$), for $R_{OFF} = 100\,\mathrm{k}\Omega$ and $p = 1$, using the first approach

been changed, while the initial value of the parameter (ω) remains the same as in the previous simulations, (x_{10}, y_{10}, z_{10}, x_{20}, y_{20}, z_{20}, ω_0) = (−0.8, 0.2, 0.4, 0.5, −0.1, 0.2, 0.5). Figure 55 shows the time-series of the normalized variable (ω). From the comparison of this figure with the respective diagram of Fig. 10, one could say that the system is driven to the same dynamical behavior (full chaotic synchronization for $\omega = 1$). However, for this set of initial conditions the variable (ω) presents a significant time delay until it reaches the aforementioned final state in regard to the other set of initial conditions, by following also a different route. Furthermore, by changing the initial condition of (ω) in the value of 0.1, the variable approaches its lower limit ($\omega \to 0$), remaining there for a long period of time, and after a sudden "shock", it is immediately driven again to the upper limit, which is the final state (Fig. 56).

In Figs. 57, 58, 59 and 60 the time-series of the variable (ω), in the second approach, for different set of initial conditions and system's parameters (p, R_{OFF}) are shown. In more detail, Figs. 57 and 58 display the variation of the variable (ω),

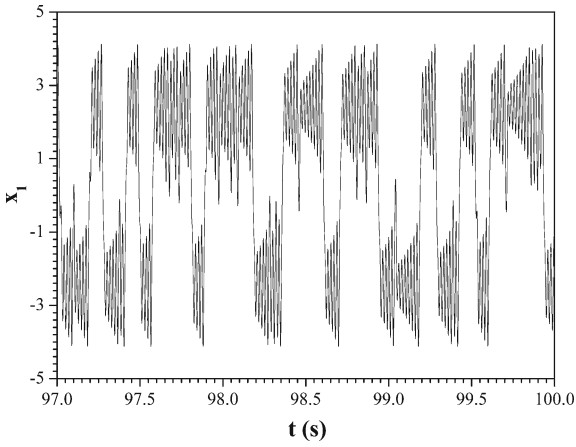

Fig. 24 Time-series of the signal (x_1), for $R_{OFF} = 100\,\text{k}\Omega$ and $p = 1$, using the first approach

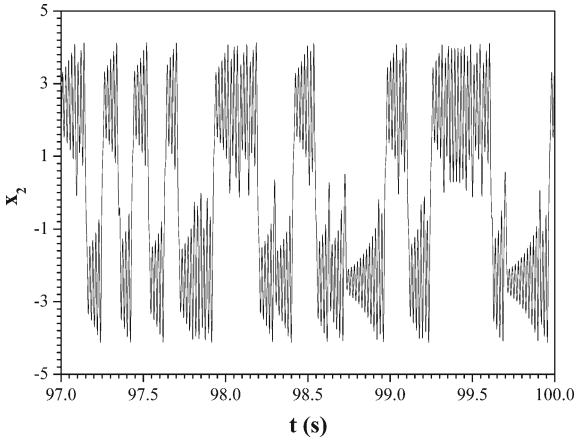

Fig. 25 Time-series of the signal (x_2), for $R_{OFF} = 100\,\text{k}\Omega$ and $p = 1$, using the first approach

for (x_{10}, y_{10}, z_{10}, x_{20}, y_{20}, z_{20}) = (–0.8, 0.2, 0.4, 0.5, –0.1, 0.2), while $\omega_0 = 0.2$ and $\omega_0 = 0.8$, respectively. Furthermore, the system follows the same behavior as in the previous set of initial conditions. However, an important conclusion can be exported. The variable (ω), independent of its initial value, oscillates chaotically around its middle value ($\omega = 0.5$), which means that the boundary between the doped and undoped regions inside the titanium dioxide layer oscillates chaotically around the middle point. The same conclusion can be drawn for (x_{10}, y_{10}, z_{10}, x_{20}, y_{20}, z_{20}, ω_0) = (–0.8, 0.2, 0.4, 0.5, –0.1, 0.2, 0.8) but for $R_{OFF} = 100\,\text{k}\Omega$, $p = 1$ from Fig. 59 and $R_{OFF} = 1\,\text{k}\Omega$, $p = 5$ from Fig. 60, with different range of variation around the middle value of (ω) according to the conclusions of the previous section.

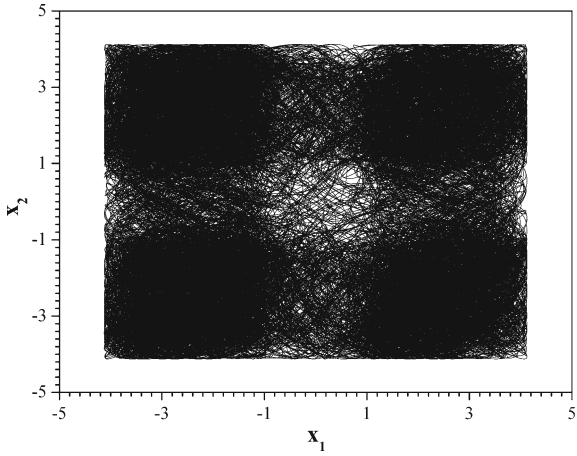

Fig. 26 Phase portrait of (x_2) versus (x_1), for $R_{OFF} = 100\,\mathrm{k}\Omega$ and $p = 1$, using the first approach

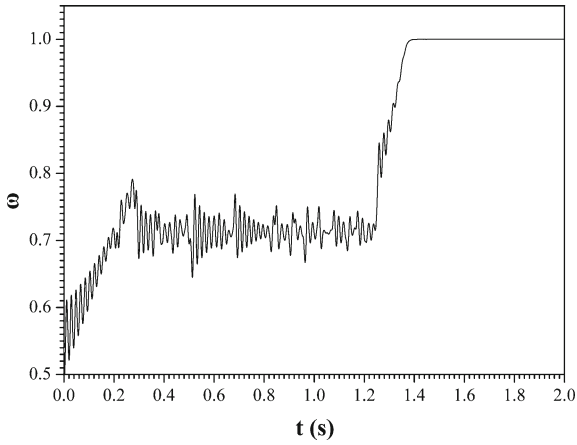

Fig. 27 Time-series of the normalized variable (ω) of the width of the doped region, for$R_{OFF} = 1\,\mathrm{k}\Omega$ and $p = 10$, using the first approach

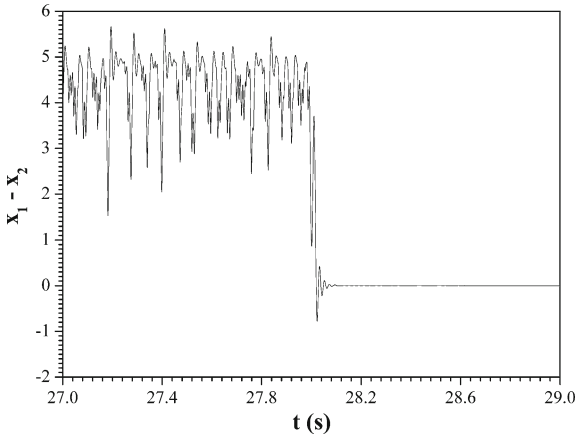

Fig. 28 Time-series of the difference signal $(x_1 - x_2)$, for $R_{OFF} = 1\,\mathrm{k}\Omega$ and $p = 10$, using the first approach

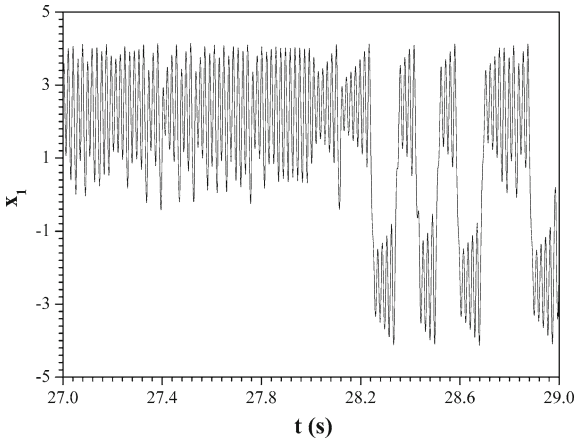

Fig. 29 Time-series of the signal (x_1), for $R_{OFF} = 1\,\text{k}\Omega$ and $p = 10$, using the first approach

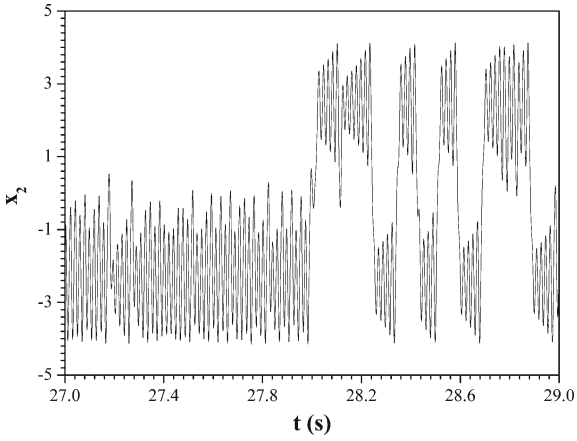

Fig. 30 Time-series of the signal (x_2), for $R_{OFF} = 1\,\text{k}\Omega$ and $p = 10$, using the first approach

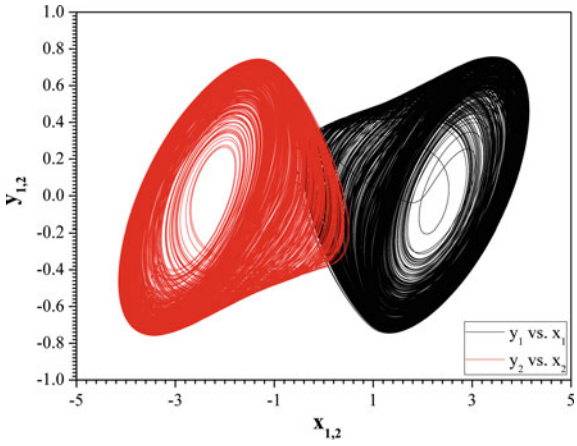

Fig. 31 Phase portraits of ($y_{1,2}$) versus ($x_{1,2}$), for $1.389\,\text{s} < t < 27.8\,\text{s}$ while $R_{OFF} = 1\,\text{k}\Omega$ and $p = 10$, using the first approach

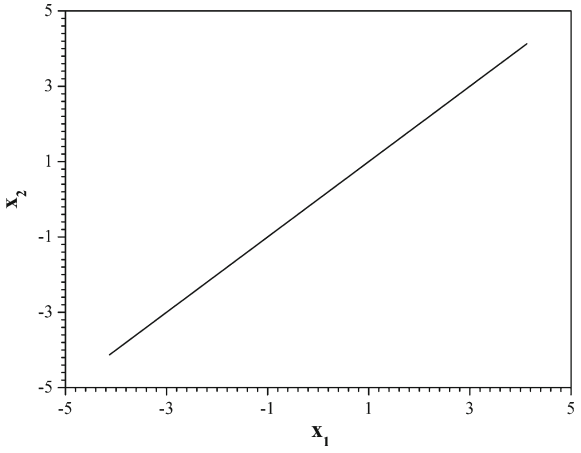

Fig. 32 Phase portraits of (x_2) versus (x_1) for $t >$ 28.101 s, for $R_{OFF} = 1\,\mathrm{k}\Omega$ and $p = 10$, using the first approach

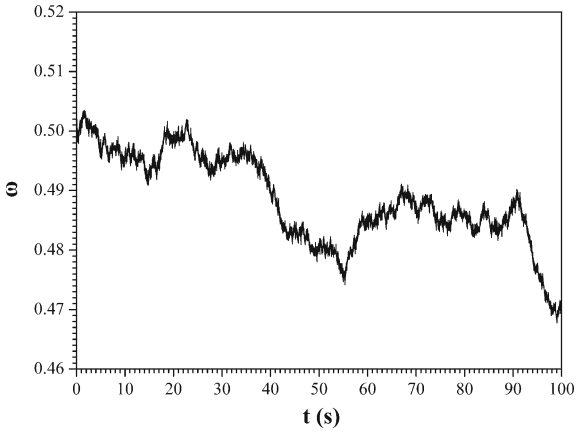

Fig. 33 Time-series of the normalized variable (ω) of the width of the doped region, for $R_{OFF} = 100\,\mathrm{k}\Omega$ and $p = 10$, using the first approach

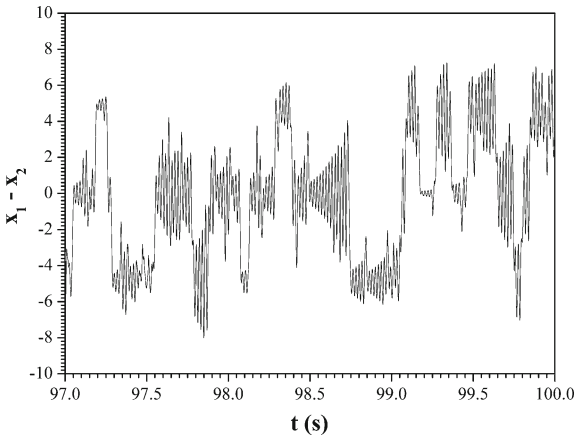

Fig. 34 Time-series of the difference signal $(x_1 - x_2)$, for $R_{OFF} = 100\,\mathrm{k}\Omega$ and $p = 10$, using the first approach

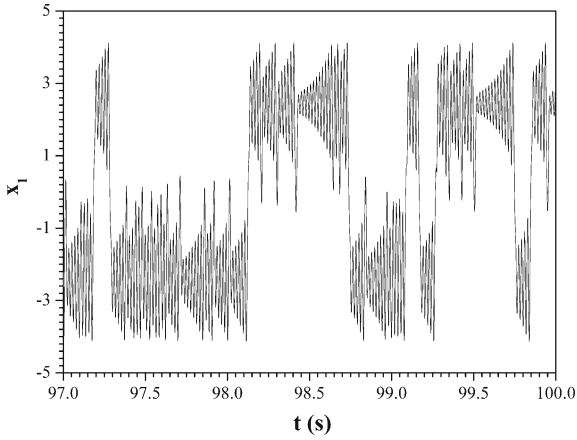

Fig. 35 Time-series of the signal (x_1), for $R_{OFF} = 100\,\text{k}\Omega$ and $p = 10$, using the first approach

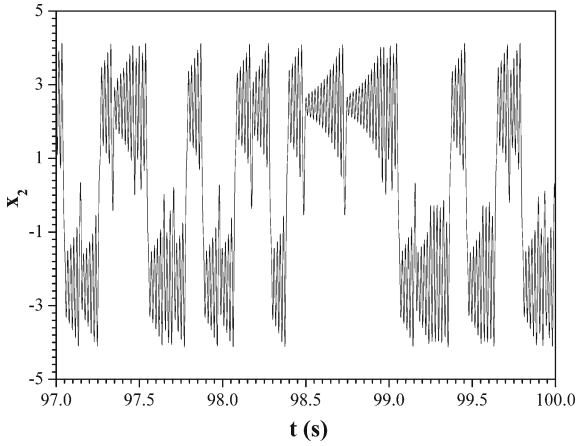

Fig. 36 Time-series of the signal (x_2), for $R_{OFF} = 100\,\text{k}\Omega$ and $p = 10$, using the first approach

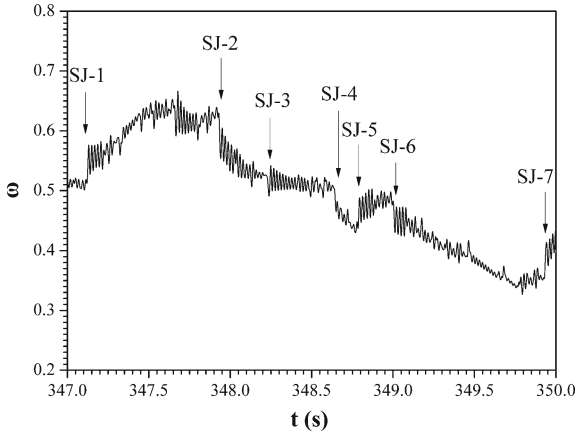

Fig. 37 Time-series of the normalized variable (ω) of the width of the doped region, for $R_{OFF} = 1\,\text{k}\Omega$ and $p = 1$, using the second approach

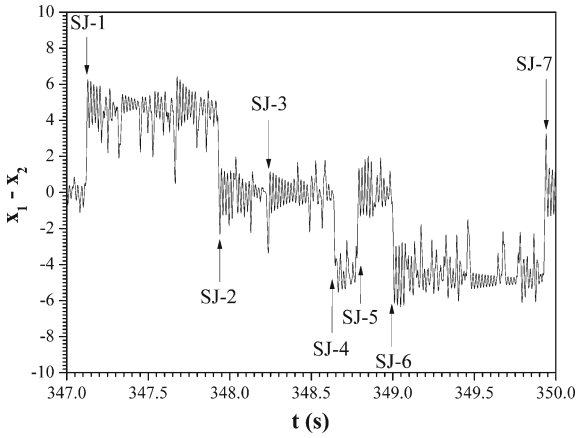

Fig. 38 Time-series of the difference signal $(x_1 - x_2)$, for $R_{OFF} = 1\,\mathrm{k}\Omega$ and $p = 1$, using the second approach

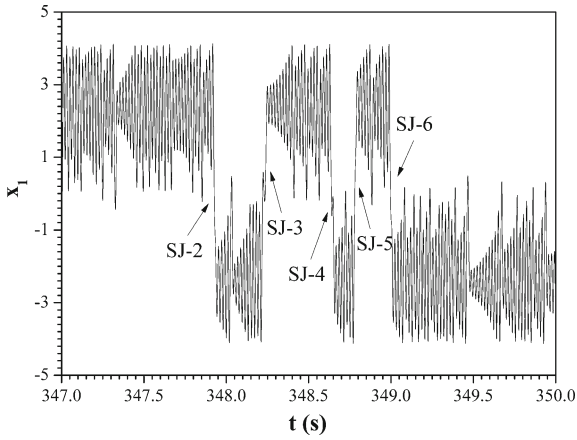

Fig. 39 Time-series of the signal (x_1), for $R_{OFF} = 1\,\mathrm{k}\Omega$ and $p = 1$, using the second approach

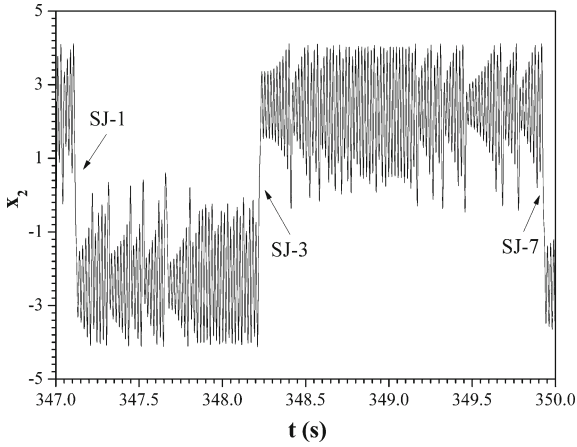

Fig. 40 Time-series of the signal (x_2), for $R_{OFF} = 1\,\mathrm{k}\Omega$ and $p = 1$, using the second approach

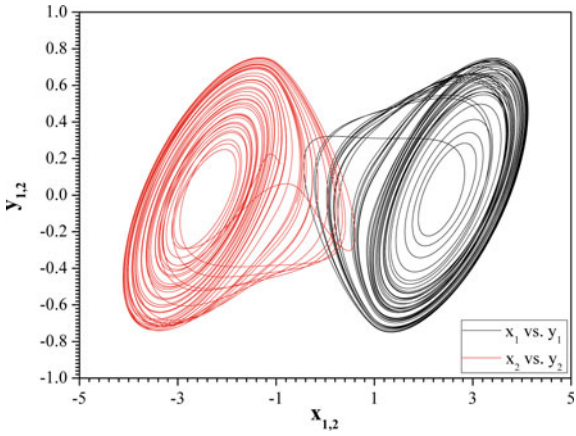

Fig. 41 Phase portraits of $y_{1,2}$ versus $x_{1,2}$ in the time interval between (SJ-1) and (SJ-2), for $R_{OFF} = 1\,\text{k}\Omega$ and $p = 1$, using the second approach

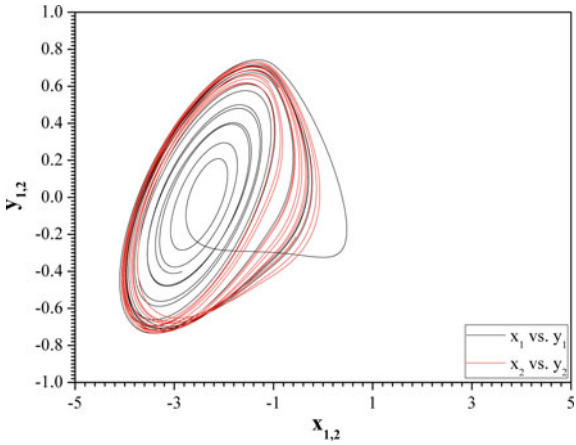

Fig. 42 Phase portraits of $y_{1,2}$ versus $x_{1,2}$ in the time interval between (SJ-2) and (SJ-3), for $R_{OFF} = 1\,\text{k}\Omega$ and $p = 1$, using the second approach

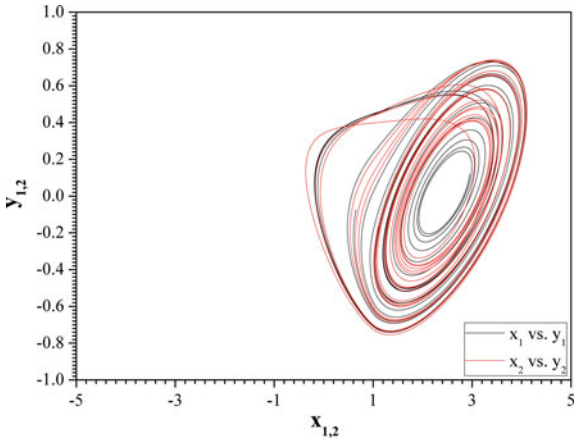

Fig. 43 Phase portraits of $y_{1,2}$ versus $x_{1,2}$ in the time interval between (SJ-3) and (SJ-4), for $R_{OFF} = 1\,\text{k}\Omega$ and $p = 1$, using the second approach

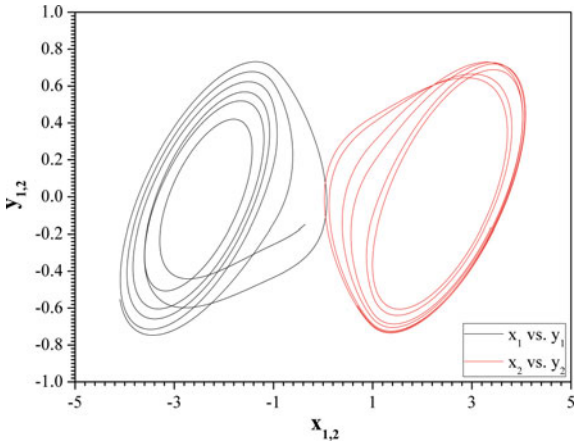

Fig. 44 Phase portraits of $y_{1,2}$ versus $x_{1,2}$ in the time interval between (SJ-4) and (SJ-5), for $R_{OFF} = 1\,\text{k}\Omega$ and $p = 1$, using the second approach

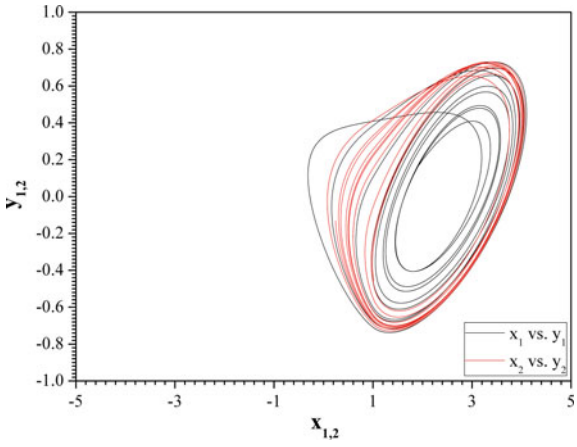

Fig. 45 Phase portraits of $y_{1,2}$ versus $x_{1,2}$ in the time interval between (SJ-5) and (SJ-6) for $R_{OFF} = 1\,\text{k}\Omega$ and $p = 1$, using the second approach

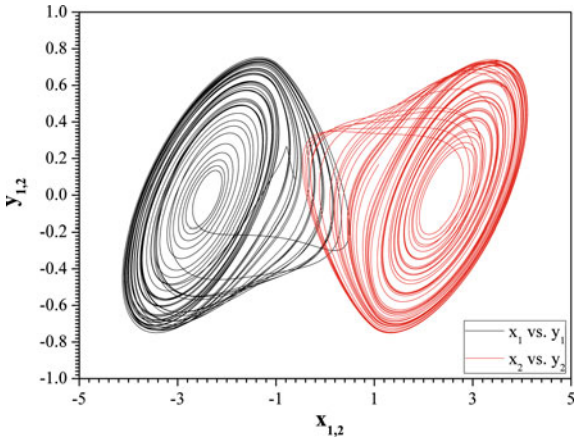

Fig. 46 Phase portraits of $y_{1,2}$ versus $x_{1,2}$ in the time interval between (SJ-6) and (SJ-7), for $R_{OFF} = 1\,\text{k}\Omega$ and $p = 1$, using the second approach

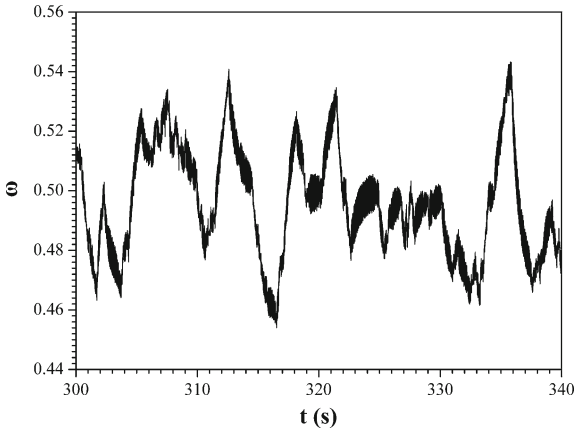

Fig. 47 Time-series of the normalized variable (ω) of the width of the doped region, for $p = 1$ and $R_{OFF} = 10\,\mathrm{k}\Omega$, using the second approach

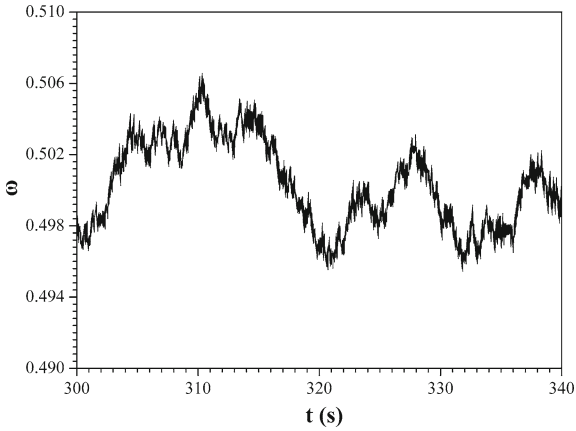

Fig. 48 Time-series of the normalized variable (ω) of the width of the doped region, for $p = 1$ and $R_{OFF} = 100\,\mathrm{k}\Omega$, using the second approach

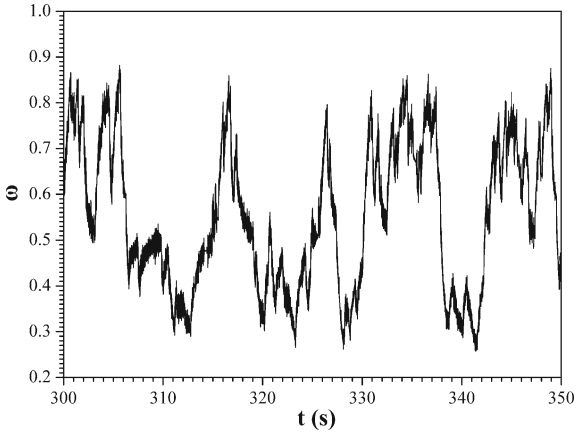

Fig. 49 Time-series of the normalized variable (ω) of the width of the doped region, for $p = 2$ and $R_{OFF} = 1\,\mathrm{k}\Omega$ using the second approach

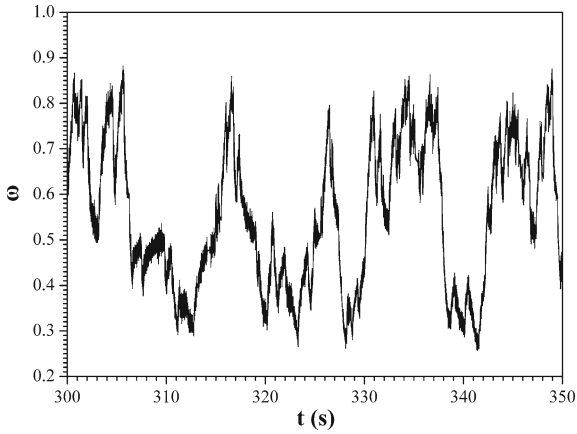

Fig. 50 Time-series of the normalized variable (ω) of the width of the doped region, for $p = 5$ and $R_{OFF} = 1\,\mathrm{k}\Omega$ using the second approach

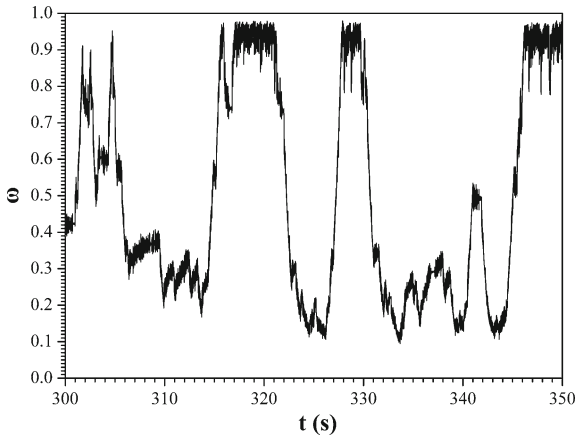

Fig. 51 Time-series of the normalized variable (ω) of the width of the doped region, for $p = 8$, and $R_{OFF} = 1\,\mathrm{k}\Omega$ using the second approach

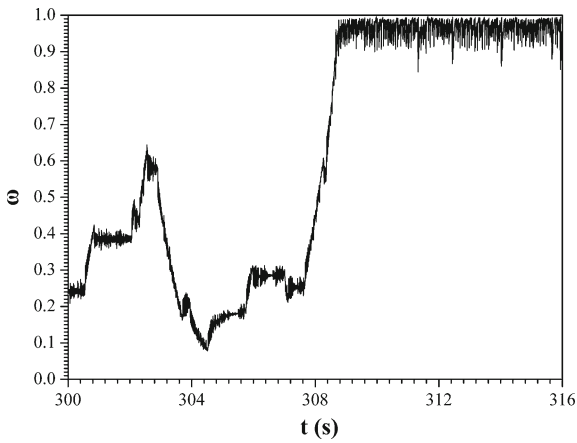

Fig. 52 Time-series of the normalized variable (ω) of the width of the doped region, for $p = 10$ and $R_{OFF} = 1\,\mathrm{k}\Omega$ using the second approach

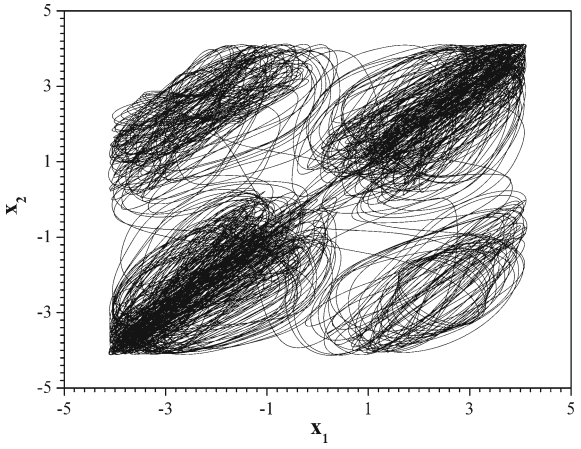

Fig. 53 Phase portraits of (x_2) versus (x_1), in the case of $p = 8$, for $t < 308\,\mathrm{s}$ and $R_{OFF} = 1\,\mathrm{k}\Omega$ using the second approach

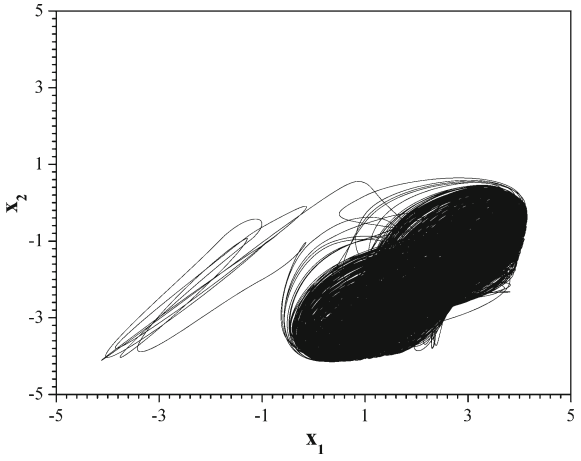

Fig. 54 Phase portraits of (x_2) versus (x_1), in the case of $p = 8$, for $t > 310\,\mathrm{s}$ and $R_{OFF} = 1\,\mathrm{k}\Omega$ using the second approach

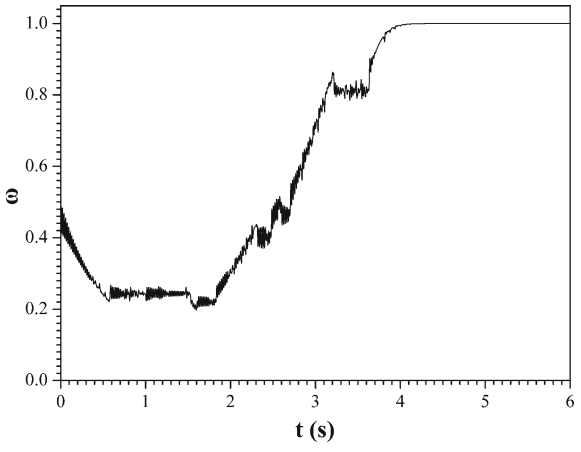

Fig. 55 Time-series of the normalized variable (ω) of the width of the doped region, with the following sets of initial conditions: $(x_{10}, y_{10}, z_{10}, x_{20}, y_{20}, z_{20}, \omega_0) = (-0.8, 0.2, 0.4, 0.5, -0.1, 0.2, 0.5)$, for $R_{OFF} = 1\,\mathrm{k}\Omega$ and $p = 1$, using the first approach

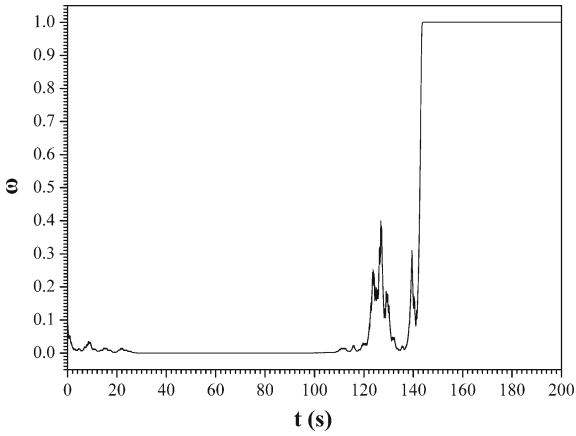

Fig. 56 Time-series of the normalized variable (ω) of the width of the doped region, with the following sets of initial conditions: (x_{10}, y_{10}, z_{10}, x_{20}, y_{20}, z_{20}, ω_0) = (−0.8, 0.2, 0.4, 0.5, −0.1, 0.2, 0.1), for $R_{OFF} = 1\,\mathrm{k}\Omega$ and $p = 1$, using the first approach

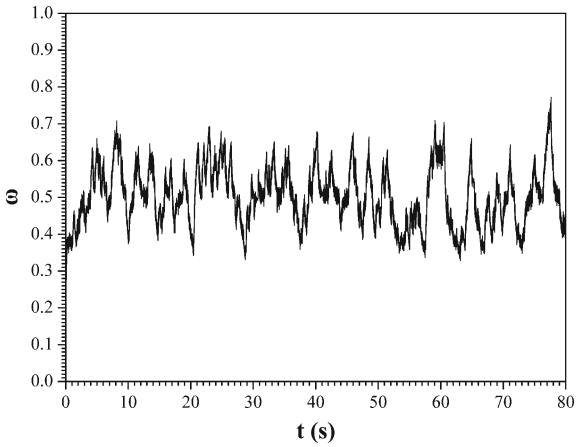

Fig. 57 Time-series of the normalized variable (ω) of the width of the doped region, with the following sets of initial conditions and parameters: (x_{10}, y_{10}, z_{10}, x_{20}, y_{20}, z_{20}, ω_0) = (−0.8, 0.2, 0.4, 0.5, −0.1, 0.2, 0.2), for $R_{OFF} = 1\,\mathrm{k}\Omega$ and $p = 1$

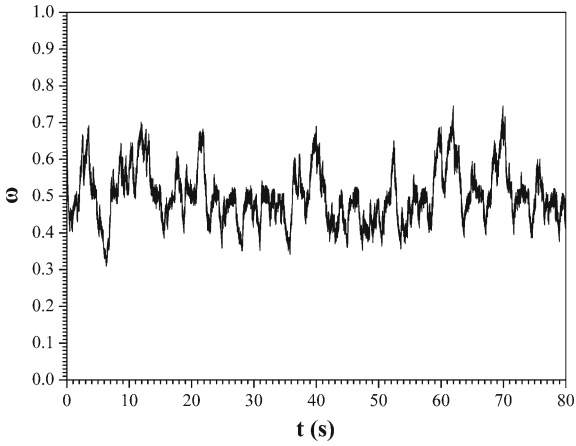

Fig. 58 Time-series of the normalized variable (ω) of the width of the doped region, with the following sets of initial conditions and parameters: (x_{10}, y_{10}, z_{10}, x_{20}, y_{20}, z_{20}, ω_0) = (–0.8, 0.2, 0.4, 0.5, –0.1, 0.2, 0.8), for $R_{OFF} = 1\,\mathrm{k}\Omega$ and $p = 1$

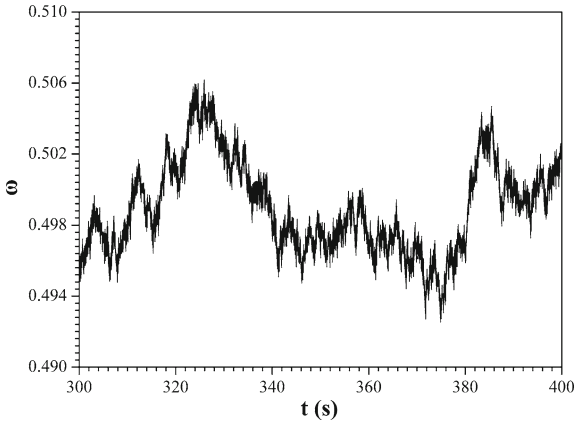

Fig. 59 Time-series of the normalized variable (ω) of the width of the doped region, with the following sets of initial conditions and parameters: (x_{10}, y_{10}, z_{10}, x_{20}, y_{20}, z_{20}, ω_0) = (–0.8, 0.2, 0.4, 0.5, –0.1, 0.2, 0.8), for $R_{OFF} = 100\,\text{k}\Omega$ and $p = 1$

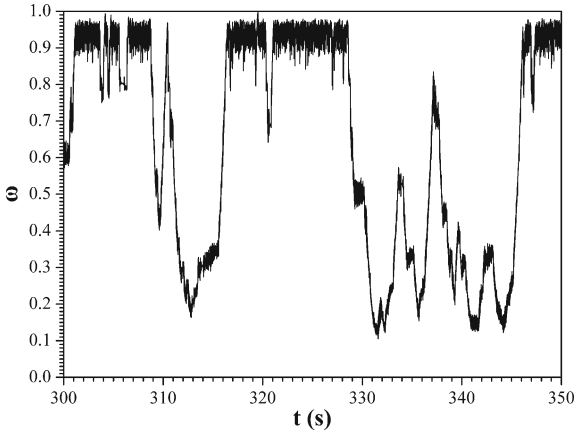

Fig. 60 Time-series of the normalized variable (ω) of the width of the doped region, with the following sets of initial conditions and parameters: (x_{10}, y_{10}, z_{10},x_{20},y_{20}, z_{20}, ω_0) = (–0.8, 0.2, 0.4, 0.5, –0.1, 0.2, 0.8), for R_{OFF} = 1kΩ and $p = 5$

5 Conclusion

In this work the case of two mutually coupled identical nonlinear systems via the proposed HP memristor was presented. As a nonlinear system, the most well-known, the Chua's oscillator, was chosen due to its properties. For studying the effect of the HP memristor as a coupling element in mutual coupling system's dynamic behavior, two different window functions have been used with different values of parameter (p), while the parameter (R_{OFF}) of the memristor varied from 1 to 100 kΩ, in order to study the dynamical behavior of the coupling system.

By using the first window function, which was presented by Joglekar and Wolf, for taking into consideration the boundary effects, the coupling system could be in two different dynamical states, depending mainly on the values of the parameter (R_{OFF}). In more detail, for low values of the resistance (R_{OFF}) the state variable (ω) increased from its initial value and gradually reached its upper limit ($\omega \rightarrow 1$), which

means that the space-charge region (w) was expanded and had the tension to cover the entire titanium dioxide layer of the memristor. As a consequence the resistance of the maximum conducting state was $R = R_{ON}$ and after a long transition time the system resulted in full chaotic synchronization mode. However, before the system resulted in this state, each one of the coupled circuits had started from a chaotic double-scroll state and under the influence of the memristor, this behavior was suppressed into single-scroll attractors around the two circuits' equilibrium points. For greater values of (R_{OFF}) the system presented the same route from chaotic desynchronization to full chaotic synchronization. The only difference was the significant greater time in which the variable (ω) became equal to one. Finally, for extreme high value of (R_{OFF}) in regards to (R_{ON}) the system remained always in a chaotic desynchronization mode, in which each one of the coupled circuits were in a double-scroll chaotic state.

In the second approach, by using the window function, which was proposed by Biolek et al., the coupling system had not shown synchronization but many other interesting dynamical phenomena. Firstly, for low values of (R_{OFF}) the state variable (ω) was increased or decreased through sudden jumps that were consequence of the sudden change of the equilibrium point around which each one of the coupled circuits oscillated. With the increase of the resistance (R_{OFF}), the range of values ($\Delta\omega$) in which the state variable (ω) took values, was decreasing. In contrary, with the increase of the parameter's (p) value the range of variation of (ω) also increased and the space-charge region (w) had the tension to cover all the range (D) of the memristor's layer. Furthermore, the state variable (ω) reached the upper limit ($\omega = 1$) and oscillated chaotically in the region near to this value. Further increase of the value of the parameter (p) had as a consequence the system to remain for longer time in the aforementioned state.

Also, the initial conditions of the system could change the time duration and the route through which the system was driven in the chaotic synchronization mode in the first case, or the way with which the variable (ω) oscillated chaotically around its middle value.

So, as a future work, the most extensive study of the system's behavior regarding its various dynamic behaviors, depending on different sets of initial conditions and values of memristor's parameters (p) and (R_{OFF}), should be done. Also, the use of the HP memristor as a coupling element, in the case of unidirectionally coupled nonlinear circuits, could be studied next. Finally, the use of other memristor's model in the coupling branch between coupled nonlinear circuits may has a great research interest, especially as an artificial synapse, because of the nature of this fourth circuit fundamental element.

References

1. Adamatzky A, Chua LO (2011) Memristive excitable cellural automata. Int J Bifurc Chaos 21:3083–3102
2. Banerjee S (2010) Chaos synchronization and cryptography for secure communications: applications for encryption. IGI Global, USA

3. Bao B, Ma Z, Xu J, Liu Z, Xu QA (2011) Simple memristor chaotic circuit with complex dynamics. Int J Bifurc Chaos 21:2629–2645
4. Biolek Z, Biolek D, Biolkova V (2009) Spice model of memristor with nonlinear dopant drift. Radioengineering 18:210–224
5. Boccaletti S, Kurths J, Osipov G, Valladares DL, Zhou CS (2002) The synchronization of chaotic systems. Phys Rep 366:1–101
6. Buscarino A, Fortuna L, Frasca M, Gambuzza V, Sciuto G (2012) Memristive chaotic circuits based on cellural nonlinear networks. Int J Bifurc Chaos 22:250070/1-13
7. Buscarino A, Fortuna L, Frasca M, Gambuzza LV (2013) A gallery of chaotic oscillators based on HP memristor. Int J Bifurc Chaos 23:1330015/1-14
8. Chang T, Jo S-H, Kim K-H, Sheridan P, Gaba S, Lu W (2011) Synaptic behaviors and modeling of a metal oxide memristive device. Appl Phys A 102:857–863
9. Chen Y, Jung GY, Ohlberg DAA, Li XM, Stewart DR, Jeppesen JO, Nielsen KA, Stoddart JF, Williams RS (2003) Nanoscale molecular-switch crossbar circuits. Nanotechology 14:462–468
10. Chua LO (1971) Memristor-the missing circuit element. IEEE Trans Circuit Theory CT-18(5):507–519
11. Chua LO (2013) Memristor, Hodgkin-Huxley, and edge of chaos. Nanotechnology 24:383001/1-14
12. Chua LO, Kang SM (1976) Memristive devices and systems. Proc IEEE 64:209–223
13. Chua LO, Wu CW, Huang A, Zhong GQ (1993) A universal circuit for studying and generating chaos—part I: routes to chaos. IEEE Trans Circuits Syst CAS-40:732–744
14. Erokhin V, Howard GD, Adamatzky A (2012) Organic memristor devices for logic elements with memory. Int J Bifurc Chaos 22:1250283/1-9
15. Fitch AL, Yu D, Iu HC, Sreeram V (2012) Hyperchaos in a memristor-based modified canonical Chua's circuit. Int J Bifurc Chaos 22:1250133/1-8
16. Fortuna L, Frasca M, Xibilia MG (2009) Chua's circuit implementations: yesterday, today and tomorrow. World Scientific, Singapore
17. Itoh M, Chua LO (2008) Memristor oscillators. Int J Bifurc Chaos 18:3183–3206
18. Itoh M, Chua LO (2009) Memristor cellural automata and memristor discrete-time cellural neural networks. Int J Bifurc Chaos 19:3605–3656
19. Itoh M, Chua LO (2011) Memristor Hamiltonian circuits. Int J Bifurc Chaos 21:2395–2425
20. Itoh M, Chua LO (2013) Duality of memristor circuits. Int J Bifurc Chaos 23:1330001/1-50
21. Joglekar YN, Wolf SJ (2009) The elusive memristor: properties of basic electrical circuits. Eur J Phys 30:661–675
22. Laiho M, Lehtonen E (2010) Cellular nanoscale network cell with memristors for local implication logic and synapses. In: Proceedings of the IEEE of international symposium on circuits and systems (ISCAS 2010), pp 2051–2054
23. Linares-Barranco B, Serrano-Gotarredona T (2009) Memristance can explain spike-time-dependentplasticity in neural synapses. Nature Proceedings, pp 1–4
24. Muthuswamy B, Kokate PP (2009) Memristor based chaotic circuits. IETE Tech Rev 26:415–426
25. Muthuswamy M (2010) Implementing memristor based chaotic circuits. Int J Bifurc Chaos 20:1335–1350
26. Pershin YV, Di Ventra M (2008) Spin memristive systems: spin memory effects in semiconductor spintronics. Phys Rev B 78:113309/1-4
27. Pershin YV, Di Ventra M (2010) Experimental demonstration of associative memory with memristive neural networks. Neural Netw 23:881
28. Pershin YV, La Fontaine S, Di Ventra M (2009) Memristive model of amoeba learning. Phys Rev E 80:021926/1-6
29. Pham V-T, Buscarino A, Fortuna L, Frasca M (2012) Autowaves in memristive cellural neural networks. Int J Bifurc Chaos 22:230027/1-9
30. Pikovsky A, Rosenblum M, Kurths J (2001) Synchronization: a universal concept in nonlinear sciences. Cambridge University Press, New York

31. Sapoff M, Oppenheim RM (1963) Theory and application of self-heated thermistors. Proc IEEE 51:1292–1305
32. Strukov D, Snider G, Stewart G, Williams R (2008) The missing memristor found. Nature 453:80–83
33. Volos ChK, Kyprianidis IM, Stouboulos IN (2011) The memristor as an electric synapse - synchronization phenomena. In: Proceedings of IEEE conference of digital signal processing (DSP11)
34. Volos ChK, Kyprianidis IM, Stouboulos IN, Stavrinides SG, Anagnostopoulos AN, Ozer M (2012) The concept of unidirectionally coupled nonlinear circuits via a memristor. Acta Phys Pol A 121:268–270
35. Wu CW, Pivka L (1994) From Chua's circuit to Chua's oscillator: a picture book of attractors. World Scientific, Singapore
36. Yang C, Sah MP, Adhikari SP, Park D, Kim H (2012) Highly accurate doublet generator for memristor-based analog memory. Int J Bifurc Chaos 22:1250153/1-4

Fuzzy Adaptive Sliding-Mode Control Scheme for Uncertain Underactuated Systems

Soumia Moussaoui, Abdesselem Boulkroune and Sundarapandian Vaidyanathan

Abstract This chapter proposes a fuzzy approximation-based adaptive sliding-mode control scheme for uncertain nonlinear perturbed underactuated systems. The underactuated system under study can be modeled by two subsystems. In the controller design, a sliding surface for each subsystem is defined and adaptive fuzzy systems are utilized to online estimate the unknown nonlinear functions. To estimate the fuzzy system parameters, a set of adaptation laws are appropriately designed. The boundedness of all signals of the closed-loop system as well as the asymptotic convergence of the underlying tracking errors to the origin are established based on a Lyapunov analysis. The main contributions of this chapter with respect to the existing works lie in the following: (1) The controller designed is free of model. (2) The stability analysis of the corresponding closed-loop system is rigorously proven by using some mild assumptions. (3) The uncertain interconnected terms are eliminated by appropriately designing a novel dynamic robust compensator. The effectiveness and robustness of the proposed adaptive fuzzy adaptive controller is illustrated through two simulation case studies taken from the underactuated system control literature.

Keywords Adaptive fuzzy control · Sliding-mode control · Uncertain underactuated system · Acrobot systems · Overhead-crane system

S. Moussaoui · A. Boulkroune (✉)
LAJ, University of Jijel, BP. 98, Ouled-Aissa, 18000 Jijel, Algeria
e-mail: boulkroune2002@yahoo.fr

S. Moussaoui
e-mail: soumia_moussaoui@yahoo.com

S. Vaidyanathan
R & D Centre, Vel Tech University, Chennai, India
e-mail: sundarvtu@gmail.com

S. Vaidyanathan and C. Volos (eds.), *Advances and Applications in Nonlinear Control Systems*, Studies in Computational Intelligence 635,
DOI 10.1007/978-3-319-30169-3_16

1 Introduction

The control literature has shown a growing attention in study and control of underactuated systems, which are characterized by the fact that they have fewer actuators than degree of freedom to be controlled, [18, 20, 30]. These systems have very important applications such as free-flying space robots, underwater robots, manipulators with structural flexibility, and overhead crane. The underactuated systems own some advantages which include: the decreasing of the actuators number can decrease the cost, the volume and the weight of system.

Recently, many control techniques have been developed for underactuated nonlinear systems [13–18, 20–22, 24, 25, 27, 29, 30]. Nevertheless, a general theory for control of these systems is not yet available. The obtained results are generally for some specific classes. In [30], an adaptive controller based on hierarchical sliding mode approach has been designed for an underactuated spherical robot. An optimal control for underactuated nonholonomic mechanical systems has been studied in [18]. Using incremental sliding mode approach, a robust controller has been proposed in [15] for a class of underactuated mechanical systems with mismatched uncertainties. A sliding-mode control of double-pendulum crane systems has been designed in [27]. An adaptive multiple-surface sliding controller based on function approximation techniques (FAT) for a class of underactuated mechanical systems with disturbances and mismatched uncertainties has been proposed in [16]. A motion planning-based adaptive control method of underactuated crane systems has been investigated in [14]. A sliding-mode control based on adaptive fuzzy systems has been developed in [20] for a class underactuated systems. The considered systems have been modeled as two subsystems, and a sliding surface has been respectively defined for each subsystem. The fuzzy systems have been used to estimate some uncertain functions. Shine et al. have designed a robust adaptive control system to achieve a globally asymptotic stability for a class of uncertain underactuated mechanical systems [25]. A direct adaptive fuzzy sliding-mode decoupling control for a class of underactuated mechanical systems has been developed in [22]. A stable sliding-mode controller has been designed in [29] for a class of second-order underactuated systems. In [21], based on hierarchical sliding-mode technology, a disturbance adaptive control for an under-actuated spherical robot has been investigated. In [17], a disturbance observer-based sliding mode control has been proposed for a class of underactuated systems. The incorporation of this disturbance observer in the controller allows to reduce the effect of the disturbances. In [24], a hierarchical sliding mode control to swing up a pendubot has been designed. In [13], a fuzzy sliding mode control for uncertain nonlinear underactuated systems has been proposed. However, the stability analysis of the corresponding closed-loop system is not rigorously proven.

In this chapter, motivated by the previous works mentioned above, we will propose a fuzzy approximation-based adaptive sliding-mode controller for a class of uncertain underactuated systems. In the control design, the considered underactuated system is divided into two subsystems, and then a sliding surface is defined for each subsystem.

The adaptive fuzzy systems are adequately incorporated in the controller to online approximate uncertain nonlinear functions. The adaptive sliding-mode control law is designed to derive the subsystems toward their corresponding sliding surfaces and to achieve their desired values. The asymptotic stability of the sliding surfaces is rigorously established and theoretically proved in Lyapunov sense.

The main contributions of this chapter with respect to the existing works [13–18, 20–22, 24, 25, 27, 29, 30] are emphasized below:

(**1**) A novel fuzzy adaptive sliding-mode controller for a class of underactuated systems with the presence of both uncertain dynamics and external disturbances is proposed.

(**2**) The controller designed is free of model.

(**3**) Unlike many previous works [13, 20, 21, 29, 30], the stability analysis of the corresponding closed-loop system is rigorously proven using a Lyapunov approach and with mild assumptions.

(**4**) The uncertain interconnected terms are eliminated by appropriately designing a novel dynamic robust compensator.

2 System Description and Problem Formulation

Consider a class of uncertain underactuated nonlinear systems which can be expressed in the following form:

$$\begin{aligned} \dot{x}_1 &= x_2 \\ \dot{x}_2 &= f_1(x) + b_1(x)\,u + d_1(t,x) \\ \dot{x}_3 &= x_4 \\ \dot{x}_4 &= f_2(x) + b_2(x)\,u + d_2(t,x) \end{aligned} \tag{1}$$

where $x = [x_1, x_2, x_3, x_4]^T \in \Re^4$ is the overall state vector of the system, $u \in \Re$ is the control input, $f_i(x)$ and $b_i(x)$, $i = 1, 2$, are unknown continuous nonlinear functions. $d_1(t, x)$ and $d_2(t, x)$ are the external disturbances.

In the subsequent, we need the following mild assumptions, which are quite standard in the adaptive control literature.

Assumption 1 ([10, 26]) There exists an unknown positive constants $\bar{d}_i$ such that $|d_i(t, x)| \leq \bar{d}_i$, for $i = 1, 2$.

Assumption 2 ([10, 26]) The sign of the function $b_i(x)$ is assumed to be known. Without loss of generality, we assume that $b_i(x)$ is strictly positive. Thus, there exists an unknown positive constant b_{0i} such that $0 < b_{0i} < b_i(x)$.

Assumption 3 The desired trajectory vector $x_d(t) = \left[x_{d1}\ x_{d2}\ x_{d3}\ x_{d4}\right]^T$ $\left[x_{d1}\ \dot{x}_{d1}\ x_{d3}\ \dot{x}_{d3}\right]^T \in \Re^4$ is supposed to be continuous, bounded and available for measurement.

Our objective consists in designing a fuzzy adaptive sliding-mode controller for a class of uncertain underactuated systems described by (1) that guarantees the stability of the closed-loop system and the tracking error convergence to zero.

3 Control System Design and Stability Analysis

Now, let us define the tracking error vector as follows:

$$e = \begin{bmatrix} e_1 \\ e_2 \\ e_3 \\ e_4 \end{bmatrix} = \begin{bmatrix} x_{d1} - x_1 \\ x_{d2} - x_2 \\ x_{d3} - x_3 \\ x_{d4} - x_4 \end{bmatrix} \tag{2}$$

where $x_{d2} = \dot{x}_{d1}$ and $x_{d4} = \dot{x}_{d3}$.

The sliding surfaces are selected as follows:

$$\begin{cases} s_1 = \dot{e}_1 + c_1 e_1 \\ s_2 = \dot{e}_2 + c_2 e_2 \end{cases} \tag{3}$$

where c_1 and c_2 are positive design constants.

Differentiating (3) with respect to time yields:

$$\begin{cases} \dot{s}_1 = c_1 \dot{e}_1 + \dot{x}_{2d} - f_1(x) - b_1(x)u - d_1(t, x) \\ \dot{s}_2 = c_2 \dot{e}_2 + \dot{x}_{4d} - f_2(x) - b_2(x)u - d_2(t, x) \end{cases} \tag{4}$$

We can rewrite the dynamics (4) as follows:

$$\begin{cases} \frac{1}{2}\frac{db_1^{-1}(x)}{dt}s_1 + \frac{\dot{s}_1}{b_1(x)} = \frac{1}{2}\frac{db_1^{-1}(x)}{dt}s_1 + \frac{c_1\dot{e}_1 + \dot{x}_{2d} - f_1(x)}{b_1(x)} - u - \frac{d_1(t,x)}{b_1(x)} \\ \frac{1}{2}\frac{db_2^{-1}(x)}{dt}s_2 + \frac{\dot{s}_2}{b_2(x)} = \frac{1}{2}\frac{db_1^{-1}(x)}{dt}s_2 + \frac{c_2\dot{e}_2 + \dot{x}_{4d} - f_2(x)}{b_2(x)} - u - \frac{d_2(t,x)}{b_2(x)} \end{cases} \tag{5}$$

Now, let's denote

$$\alpha_1(x) = \frac{1}{2}\frac{db_1^{-1}(x)}{dt}s_1 + \frac{c_1\dot{e}_1 + \dot{x}_{2d} - f_1(x)}{b_1(x)}$$

$$\alpha_2(x) = \frac{1}{2}\frac{db_2^{-1}(x)}{dt}s_2 + \frac{c_2\dot{e}_2 + \dot{x}_{4d} - f_2(x)}{b_2(x)}.$$

By multiplying both expressions in (5) by s_1 and s_2 respectively, we get

$$\begin{cases} \frac{1}{2}\frac{db_1^{-1}(x)}{dt}s_1^2 + \frac{s_1\dot{s}_1}{b_1(x)} = (\alpha_1(x) - u)s_1 - \frac{s_1 d_1(t,x)}{b_1(x)}. \\ \frac{1}{2}\frac{db_2^{-1}(x)}{dt}s_2^2 + \frac{s_2\dot{s}_2}{b_2(x)} = (\alpha_2(x) - u)s_2 - \frac{s_2 d_2(t,x)}{b_2(x)}. \end{cases} \tag{6}$$

Because the nonlinear functions $\alpha_1(x)$ and $\alpha_2(x)$ are unknown, the design of a stable controller for (1) is difficult. To solve this problem, we will use an adaptive fuzzy system to online estimate these unknown nonlinear functions.

3.1 Description of Fuzzy Logic System

The fuzzy logic system performs a mapping for $U \subset \Re^4$ to $V \subset \Re$. Let $U = U_1 \times \cdots \times U_4$ where $U_i \subset \Re, i = 1, 2, 3, 4$. The fuzzy logic system is characterized by a set of IF-THEN rules in the following form:

$$R^{(l)}: \text{IF } x_1 \text{ is } F_1^l \text{ and} \ldots x_4 \text{ is } F_4^l \text{ THEN } y \text{ is } G^l \tag{7}$$

with $l = 1, 2, \ldots, N$, N is the number of fuzzy rules for each the fuzzy model, and $x = [x_1, x_2, x_3, x_4] \in U$ and $y \in V$ are the input and output of the fuzzy systems respectively, F_i^l and G^l are fuzzy sets in U and V, respectively.

As shown in Fig. 1, the fuzzifier maps a crisp point x into a fuzzy set and the inference engine uses the fuzzy If-Then rules to perform a mapping from fuzzy sets in U to fuzzy sets in V.

By using the singleton fuzzifier, product inference, and center-average defuzzifier, the output of the fuzzy system can be expressed as follows:

$$\hat{y}(x) = \theta^T \psi(x) \tag{8}$$

where $\theta^T = \left[\theta^1\ \theta^2 \ldots \theta^N\right] \in \Re^N$ is the adjustable parameters vector (composed of consequent parameters), and $\psi^T(x) = \left[\psi^1(x)\ \psi^2(x) \ldots \psi^N(x)\right] \in \Re^N$ is the

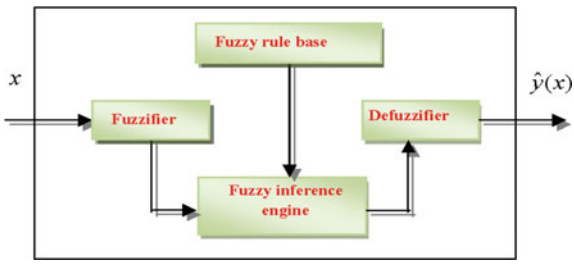

Fig. 1 Basic configuration of a fuzzy logic system

fuzzy basis function (FBF) with $\psi^l(X)$ expressed as follows:

$$\psi^l(x) = \prod_{i=1}^{4} \mu_{F_i^l}(x_i) / \sum_{l=1}^{N} \left(\prod_{i=1}^{4} \mu_{F_i^l}(x_i) \right) \tag{9}$$

$\mu_{F_i^l}(x_i)$ is the membership function of fuzzy set.

It is worth nothing that the fuzzy system (8) is commonly used in control applications [1–9, 11, 12, 28]. Following the universal approximation theorem, the fuzzy system (8) is able to approximate any nonlinear smooth function y on compact operating space to an arbitrary degree of accuracy. Of particular importance, it is assumed that the structure of the fuzzy system, namely the pertinent inputs, the number of membership functions for each input and the number of rules, and the membership function parameters are properly specified beforehand. The consequent parameters are then determined by some appropriate parameter adaptation algorithms [1–9, 11, 12, 28].

3.2 *Design of Adaptive Fuzzy Sliding-Mode Controller*

To facilitate the control system design, the following assumption will be used in the subsequent developments.:

Assumption 4 There exists an unknown continuous positive function $\bar{\alpha}_2(x)$, such as:

$$|\alpha_2(x) - \alpha_1(x)| \leq \bar{\alpha}_2(x), \quad \forall x \in \Omega_x \subset \Re^4. \tag{10}$$

The unknown nonlinear function $\alpha_1(X)$ and $\bar{\alpha}_2(X)$ can be approximated by the linearly parameterized fuzzy systems (8), as follows::

$$\hat{\alpha}_1(x) = \theta_1^T \psi_1(x) \tag{11a}$$

$$\hat{\bar{\alpha}}_2(x) = \theta_2^T \psi_2(x) \tag{11b}$$

where $\psi_1(x)$ and $\psi_2(x)$ are fuzzy basis functions, and θ_1 and θ_2 are the adjustable parameters vector of the fuzzy systems.

Let's define the following optimal parameter vectors::

$$\begin{aligned} \theta_1^* &= \arg_{\theta_1} \min \left[\sup_{x \in \Omega_x} \left| \alpha_1(x) - \hat{\alpha}_1(x, \theta_1) \right| \right] \\ \theta_2^* &= \arg_{\theta_2} \min \left[\sup_{x \in \Omega_x} \left| \bar{\alpha}_2(x) - \hat{\bar{\alpha}}_2(x, \theta_2) \right| \right] \end{aligned} \tag{12}$$

Note that θ_1^* and θ_2^* are artificial constant quantities introduced only for analysis purposes, and their values are not needed when implementing the controller. Define $\tilde{\theta}_1 = \theta_1 - \theta_1^*$ and $\tilde{\theta}_2 = \theta_2 - \theta_2^*$ as the parameter estimation error, and $\varepsilon_1(x) =$

$\alpha_1(x) - \hat{\alpha}_1\left(x, \theta_1^*\right)$ and $\varepsilon_2(x) = \bar{\alpha}_2(x) - \hat{\bar{\alpha}}_2\left(x, \theta_2^*\right)$ as the fuzzy approximation errors, where

$$\hat{\alpha}_1\left(x, \theta_1^*\right) = \theta_1^{*T} \psi_1(x) \tag{13a}$$

$$\hat{\bar{\alpha}}_2\left(x, \theta_2^*\right) = \theta_2^{*T} \psi_2(x) \tag{13b}$$

As in [3–9, 11, 12, 28], we assume that the used fuzzy systems do not violate the universal approximator property on the compact set Ω_x, which is assumed large enough so that the input vector of the fuzzy system remains in Ω_x under closed-loop control system. So it is logical that the fuzzy approximation error is bounded for all $x \in \Omega_x$, i.e. $|\varepsilon_i(x)| \leq \bar{\varepsilon}_i$, where $\bar{\varepsilon}_i$ is an unknown constant.

From the above analysis, we can write the following relations

$$\begin{aligned} \hat{\alpha}_1(x, \theta_1) - \alpha_1(x) &= \hat{\alpha}_1(x, \theta_1) - \hat{\alpha}_1(x, \theta_1^*) + \hat{\alpha}_1(x, \theta_1^*) - \alpha_1(x) \\ &= \hat{\alpha}_1(x, \theta_1) - \hat{\alpha}_1(x, \theta_1^*) - \varepsilon_1(x) \\ &= \tilde{\theta}_1^T \psi_1(x) - \varepsilon_1(x) \end{aligned} \tag{14a}$$

$$\begin{aligned} \hat{\bar{\alpha}}_2(x, \theta_2) - \bar{\alpha}_2(x) &= \hat{\bar{\alpha}}_2(x, \theta_2) - \hat{\bar{\alpha}}_2(x, \theta_2^*) + \hat{\bar{\alpha}}_2(x, \theta_2^*) - \bar{\alpha}_2(x) \\ &= \hat{\bar{\alpha}}_2(x, \theta_2) - \hat{\bar{\alpha}}_2(x, \theta_2^*) - \varepsilon_2(x) \\ &= \tilde{\theta}_2^T \psi_2(x) - \varepsilon_2(x) \end{aligned} \tag{14b}$$

To meet our control objective, a suitable adaptive fuzzy sliding mode controller is proposed as follows:

$$u = k_1(s_1 + s_2) + \beta_1 sign(s_1 + s_2) + \theta_1^T \psi_1(x) + v_r \tag{15}$$

The associated adaptive laws are given by

$$\dot{v}_r = -\gamma_v v_r + \gamma_v \left[(s_1 + s_2) - v_r \left(\frac{\theta_2^T \psi_2(x) |s_2| + \beta_2 |s_2| + k_2 s_2^2}{v_r^2 + \delta^2} \right) \right] \tag{16}$$

$$\dot{\delta} = -\gamma_\delta \delta \left(\frac{\theta_2^T \psi_2 |s_2| + \beta_2 |s_2| + k_2 s_2^2}{v_r^2 + \delta^2} \right) \tag{17}$$

$$\dot{\theta}_1 = \gamma_{\theta_1}(s_1 + s_2)\psi_1(X) \tag{18}$$

$$\dot{\theta}_2 = \gamma_{\theta_2} |s_2| \psi_2(X) \tag{19}$$

$$\dot{\beta}_1 = \gamma_{\beta_1} |s_1 + s_2| \tag{20}$$

$$\dot{\beta}_2 = \gamma_{\beta_2} |s_2| \tag{21}$$

where k_1, k_2, γ_v, γ_δ, γ_{θ_1}, γ_{θ_2}, γ_{β_1} and γ_{β_2} are positive design constants.

Theorem 1 *Consider the system (1) and suppose that Assumptions 1–4 are valid. Then, the proposed control scheme (15)–(21) guarantees the following properties.*

- *all signals in the closed-loop system are bounded, and*
- *the tracking errors asymptotically converge to zero.*

Proof of Theorem 1: Let us consider the following Lyapunov function candidate:

$$V = \frac{1}{2b_1(x)}s_1^2 + \frac{1}{2b_2(x)}s_2^2 + \frac{1}{2\gamma_v}v_r^2 + \frac{1}{2\gamma_\delta}\delta^2 + \frac{1}{2\gamma_{\theta_1}}\tilde{\theta}_1^T\tilde{\theta}_1 + \frac{1}{2\gamma_{\theta_2}}\tilde{\theta}_2^T\tilde{\theta}_2 + \frac{1}{2\gamma_{\beta_1}}\tilde{\beta}_1^2 + \frac{1}{2\gamma_{\beta_2}}\tilde{\beta}_2^2 \tag{22}$$

with $\tilde{\beta}_1 = \beta_1 - \beta_1^*$ and $\tilde{\beta}_2 = \beta_2 - \beta_2^*$, where $\beta_1^* = \bar{\varepsilon}_1 + \bar{d}_1/b_{01}$ and $\beta_2^* = \bar{\varepsilon}_2 + \left(\bar{d}_1/b_{01} + \bar{d}_2/b_{02}\right)$.

Differentiating (22) with respect to time yields

$$\begin{aligned}\dot{V} = {} & \frac{d}{dt}\left(b_1^{-1}(x)\right)\frac{s_1^2}{2} + \frac{1}{b_1(x)}s_1\dot{s}_1 + \frac{d}{dt}\left(b_2^{-1}(x)\right)\frac{s_2^2}{2} + \frac{1}{b_2(x)}s_2\dot{s}_2 + \frac{1}{\gamma_v}v_r\dot{v}_r + \frac{1}{\gamma_\delta}\delta\dot{\delta} \\ & + \frac{1}{\gamma_{\theta_1}}\tilde{\theta}_1^T\dot{\theta}_1 + \frac{1}{\gamma_{\theta_2}}\tilde{\theta}_2^T\dot{\theta}_2 + \frac{1}{\gamma_{\beta_1}}\tilde{\beta}_1\dot{\beta}_1 + \frac{1}{\gamma_{\beta_2}}\tilde{\beta}_2\dot{\beta}_2\end{aligned} \tag{23}$$

Using (6) and (23) becomes

$$\begin{aligned}\dot{V} = {} & (s_1 + s_2)\,\alpha_1(x) + (\alpha_2 - \alpha_1)\,s_2 - (s_1 + s_2)\,u - \frac{(s_1 + s_2)d_1(t,x)}{b_1(x)} + \frac{s_2 d_1(t,x)}{b_1(x)} \\ & - \frac{s_2 d_2(t,x)}{b_2(x)} + \frac{1}{\gamma_v}v_r\dot{v}_r + \frac{1}{\gamma_\delta}\delta\dot{\delta} + \frac{1}{\gamma_{\theta_1}}\tilde{\theta}_1^T\dot{\theta}_1 + \frac{1}{\gamma_{\theta_2}}\tilde{\theta}_2^T\dot{\theta}_2 + \frac{1}{\gamma_{\beta_1}}\tilde{\beta}_1\dot{\beta}_1 + \frac{1}{\gamma_{\beta_2}}\tilde{\beta}_2\dot{\beta}_2\end{aligned} \tag{24}$$

Substituting (14a) and (15) into (24), we obtain

$$\begin{aligned}\dot{V} \leq {} & -(s_1 + s_2)\,\tilde{\theta}_1^T\psi_1(x) + \beta_1^*|s_1 + s_2| + \beta_2^*|s_2| - \varepsilon_2(x)|s_2| + \bar{\alpha}_2(x)|s_2| \\ & - k_1(s_1 + s_2)^2 - \beta_1|s_1 + s_2| - (s_1 + s_2)\,v_r + \frac{1}{\gamma_v}v_r\dot{v}_r + \frac{1}{\gamma_\delta}\delta\dot{\delta} + \frac{1}{\gamma_{\theta_1}}\tilde{\theta}_1^T\dot{\theta}_1 \\ & + \frac{1}{\gamma_{\theta_2}}\tilde{\theta}_2^T\dot{\theta}_2 + \frac{1}{\gamma_{\beta_1}}\tilde{\beta}_1\dot{\beta}_1 + \frac{1}{\gamma_{\beta_2}}\tilde{\beta}_2\dot{\beta}_2\end{aligned} \tag{25}$$

Using (14b), (18) and (20), we have

$$\begin{aligned}\dot{V} \leq {} & -\tilde{\beta}_2|s_2| + \beta_2|s_2| - |s_2|\,\tilde{\theta}_2^T\psi_2(x) - k_1(s_1 + s_2)^2 + |s_2|\,\theta_2^T\psi_2(x) - (s_1 + s_2)\,v_r \\ & + \frac{1}{\gamma_v}v_r\dot{v}_r + \frac{1}{\gamma_\delta}\delta\dot{\delta} + \frac{1}{\gamma_{\theta_2}}\tilde{\theta}_2^T\dot{\theta}_2 + \frac{1}{\gamma_{\beta_2}}\tilde{\beta}_2\dot{\beta}_2\end{aligned} \tag{26}$$

Substituting (16), (17), (19) and (21) into (26), we get

$$\dot{V} \leq -k_1 (s_1 + s_2)^2 - v_r^2 - k_2 s_2^2 \tag{27}$$

Therefore, all signals $s_1, s_2, s_1 + s_2, v_r, \delta, \theta_1, \theta_2, x$ and u are bounded. Then, from (4), we can conclude about the boundedness of $\dot{s}_1, \dot{s}_2$ and $\dot{s}_1 + \dot{s}_2$. Also, we can demonstrate from (27) that s_2 and $s_1 + s_2 \in L_2$. By using the Barbalat's lemma [19], we can obtain the asymptotic convergence to zero of the signals s_2 and $s_1 + s_2$. Hence, the signal s_1 asymptotically converges to zero. The convergence of e_1 and e_2 follows that of the surfaces s_1 and s_2.

4 Numerical Examples

In this section, we will test our proposed controller for the stabilization of two underactuated systems, namely acrobot and overhead crane.

Example 1 In this subsection, the acrobot in Fig. 2 is used to verify the performance of the proposed controller. Its model can be given by [17]:

$$\begin{aligned} m_{11}\ddot{q}_1 + m_{22}\ddot{q}_2 + h_1 + \varphi_1 &= d_1 \\ m_{12}\ddot{q}_1 + m_{22}\ddot{q}_2 + h_2 + \varphi_2 &= \tau + d_2 \end{aligned} \tag{28}$$

with $q_1(t) \in \Re$ and $q_2(t) \in \Re$, τ is the control input, and

$$\begin{aligned} &m_{11} = a + b\cos(q_2), \quad m_{12} = c + 0.5b\cos(q_2), \quad m_{12} = m_{21} \quad , m_{22} = c, \\ &a = m_1 l_{c1}^2 + m_2\left(l_1^2 + l_{c2}^2\right) + I_1 + I_2, \quad c = m_2 l_{c2}^2, \quad b = 2m_2 l_1 l_{c2}. \\ &h_1 = -m_2 l_1 l_{c2}\sin(q_2)\,\dot{q}_2^2 - 2m_2 l_2 l_{c2}\sin(q_2)\,\dot{q}_1\dot{q}_2, \quad h_2 = m_2 l_1 l_{c2}\sin(q_2)\,\dot{q}_1^2, \end{aligned}$$

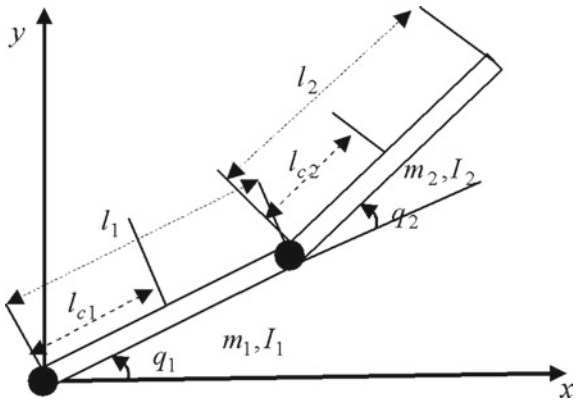

Fig. 2 The mechanical structure of acrobot

Table 1 The parameters of acrobot

m_1	1	kg	l_{c2}	1	m
m_2	1	kg	I_1	0.083	kg.m
l_1	1	m	I_2	0.33	kg.m
l_2	2	m	g	9.8	m/s^2
l_{c1}	0.5	m			

$$\varphi_1 = (m_1 l_{c1} + m_2 l_1)\, g \cos(q_1) + m_2 l_{c2} g \cos(q_1 + q_2)\,, \quad \varphi_2 = m_2 l_{c2} g \cos(q_1 + q_2)\,.$$

The parameters of this acrobot system are given in Table 1, [17].

The initial conditions are chosen as $q_1 = \pi/2 + 0.2$, $q_2 = -0.5$, $\dot{q}_1 = 0$, $\dot{q}_2 = 0$. The desired output vector is selected as follows $x_d = \left[\pi/2\ 0\ 0\ 0\right]^T$.

The adaptive fuzzy systems, $\theta_i^T \psi_i(x)$, with $i = 1, 2$, have the state vector as input. For each input variable of these fuzzy systems, as in [10], we define three (one triangular and two trapezoidal) membership functions uniformly distributed on the intervals $[-2, 2]$.

The design parameters are chosen as follows: $\gamma_{\theta_1} = 1, \gamma_{\theta_2} = 1, \gamma_{\beta_1} = 0.01$, $\gamma_{\beta_2} = 0.01, \gamma_v = 0.5, \gamma_\delta = 0.005, k_1 = k_2 = 1, c_1 = 1, c_2 = 2$. The initial conditions of the adaptive parameters are selected as $\delta(0) = 1, \theta_1(0) = \theta_2(0) = 0, \beta_1(0) = 1, \beta_2(0) = 4$, and $v_r(0) = 2$.

When the input disturbances are not considered (i.e. when $d_1 = 0$ and $d_2 = 0$), the simulation results of acrobot are given in Figs. 3 and 4. Obviously, from Fig. 3, the states of this system asymptotically converge to their desired values. Figure 4 clearly illustrates the convergence towards zero of the sliding mode surfaces and the tracking errors as well as the boundedness of the control signal.

When the input disturbances are considered (i.e. when $d_1 = 0.1\sin(0.5t + \pi/2)$ and $d_2 = 0.5\sin(2t)$), the simulation results are given in Figs. 5 and 6. From these figures, it is clear that the system states oscillate near the equilibrium with small range. Compared to results obtained by applying the classical sliding mode controller in [17], our results are improved.

Example 2 In this subsection, the validity of the proposed controller is demonstrated on an overhead crane system, given by Fig. 7. This system consists of a trolley subsystem and a load subsystem. The dynamic model of this system is [23]:

$$\begin{aligned} &(m_c + m_L)\,\ddot{x} + m_L\left(\ddot{q}\cos q - \dot{q}^2 \sin q\right) + m_L \ddot{l} \sin q + 2m_L \dot{l}\dot{q}\cos q + w_1 = u \\ &m_L l \ddot{x}\cos q + m_L l^2 \ddot{q} + 2m_L l \dot{l}\dot{q} + m_L g l \sin q + w_2 = 0 \end{aligned} \tag{29}$$

Let us select the state variables as $q_1 = x, q_2 = \dot{x}, q_3 = q$, and $q_4 = \dot{q}$. So, if l is constant, we have:

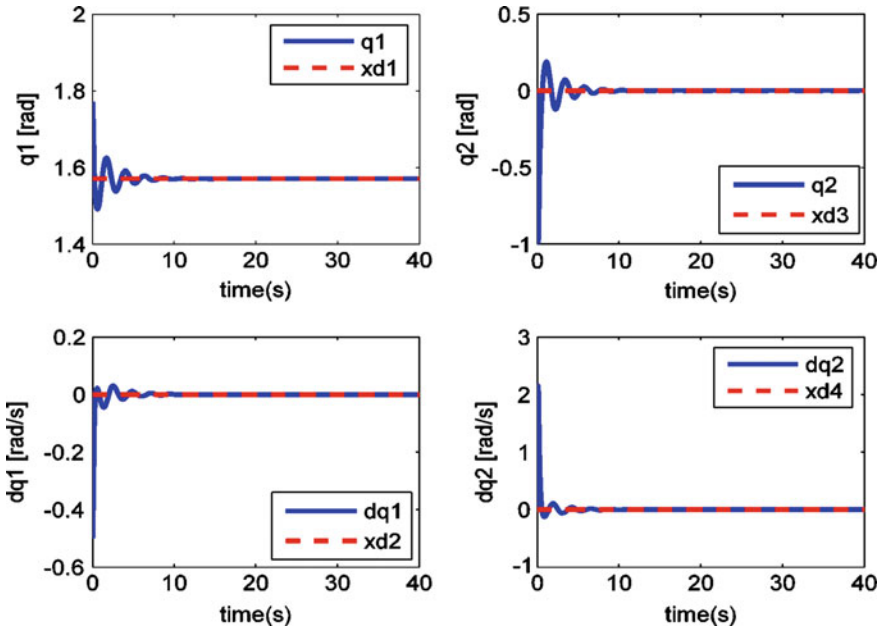

Fig. 3 States of acrobot (without disturbances)

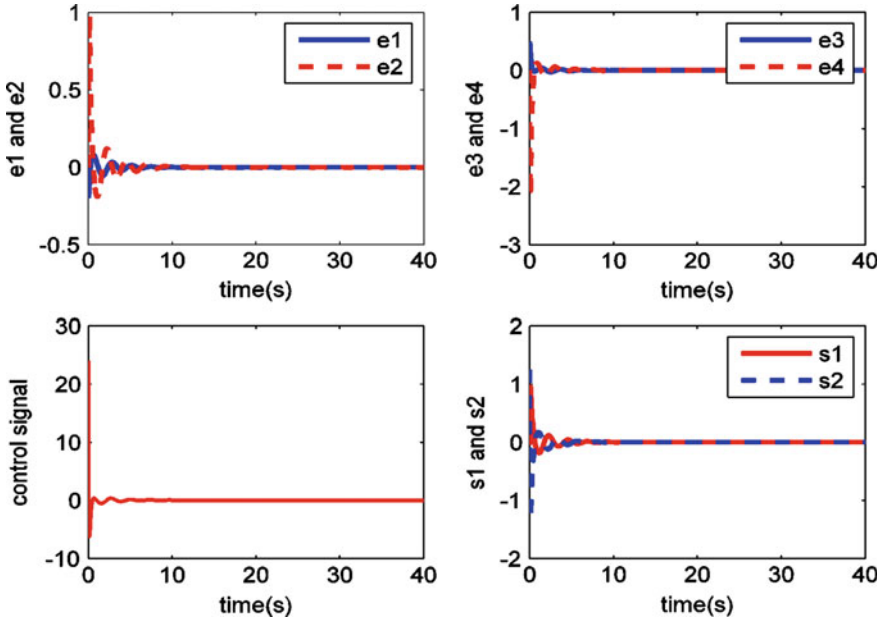

Fig. 4 Curves of trajectories errors, control signal and sliding surfaces, respectively (without disturbances)

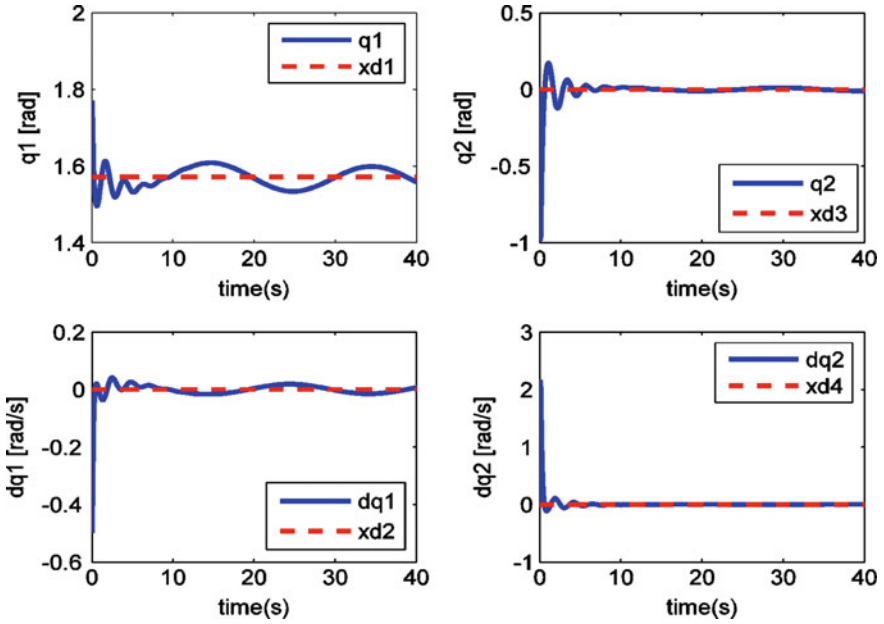

Fig. 5 States of acrobot (with disturbances)

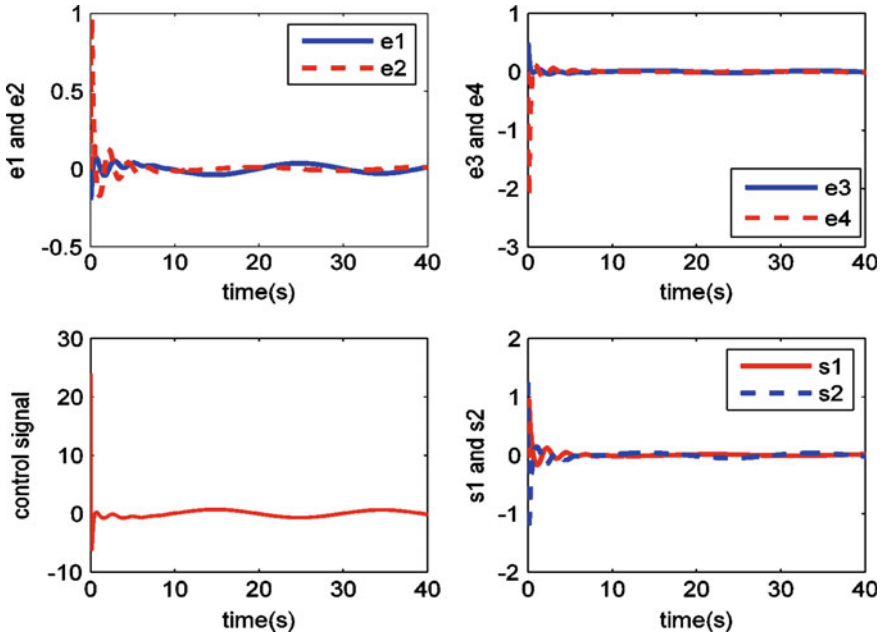

Fig. 6 Curves of trajectories errors, control signal and sliding surfaces, respectively (with disturbances)

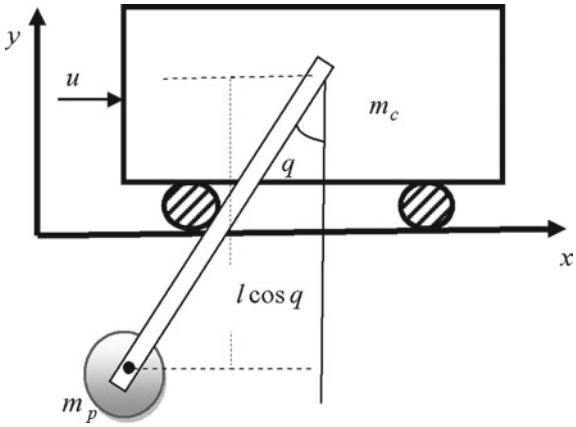

Fig. 7 Overhead crane system

Table 2 Overhead crane physical parameters

Variable	Value used
m_c	24 (kg)
m_L	5 (kg)
l	1 (m)
g	9.81 (m/s^2)

$$\begin{aligned}
\dot{q}_1 &= q_2 \\
\dot{q}_2 &= f_1\left(\underline{q}\right) + b_1\left(\underline{q}\right)u + d_1\left(t, \underline{q}\right) \\
\dot{q}_3 &= q_4 \\
\dot{q}_4 &= f_2\left(\underline{q}\right) + b_2\left(\underline{q}\right)u + d_2\left(t, \underline{q}\right)
\end{aligned}$$

where $\underline{q} = [q_1, q_2, q_3, q_4]^T$ is the state vector, and

$$f_1 + d_1 = \left(m_L\left(-q_4^2 l - g\cos q_3\right)\sin q_3 + l w_1 - \frac{\cos q_3}{l} w_2\right) / \left(m_L \cos^2 q_3 - (m_L + m_c)\, l\right),$$

$$g_1 = \frac{-l}{m_L \cos^2 q_3 - (m_L + m_c)\, l}, \quad g_2 = \frac{\cos q_3}{m_L \cos^2 x_3 - (m_L + m_c)\, l}, \text{ and}$$

$$\begin{aligned}
f_2 + d_2 = &\left(\left(\left((m_c + m_L)\, g + m_L q_4^2 \cos q_3\right)\sin q_3\right)\right. \\
&\left. + \left(\left((m_L + m_c)/m_L l\right) w_2 - w_1 \cos q_3\right)\right) / \left(m_L \cos^2 q_3 - (m_L + m_c)\, l\right)
\end{aligned}$$

The external disturbance are chosen as: $w_1 = 0.2\cos(t)$, $w_2 = 0.2\sin(t)$. Its physical parameters are summarized in Table 2, [23].

The initial state and desired state vector are assumed $q(0) = \begin{bmatrix} 0 & 0 & 0 & 0 \end{bmatrix}$ and $x_d(t) = \begin{bmatrix} 1 & 0 & 0 & 0 \end{bmatrix}$, respectively. The design parameters used in this simulation are chosen as follows $k_1 = k_2 = 1, c_1 = 2, c_2 = 1$. $\gamma_{\theta_1} = 1, \gamma_{\theta_2} = 2, \gamma_v = 0.5$,

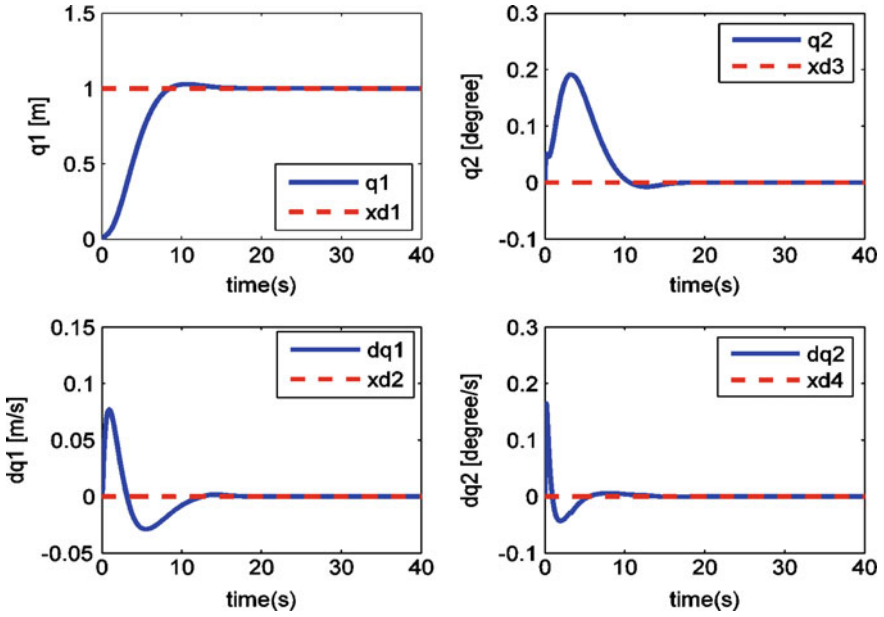

Fig. 8 States of overhead crane (without disturbances)

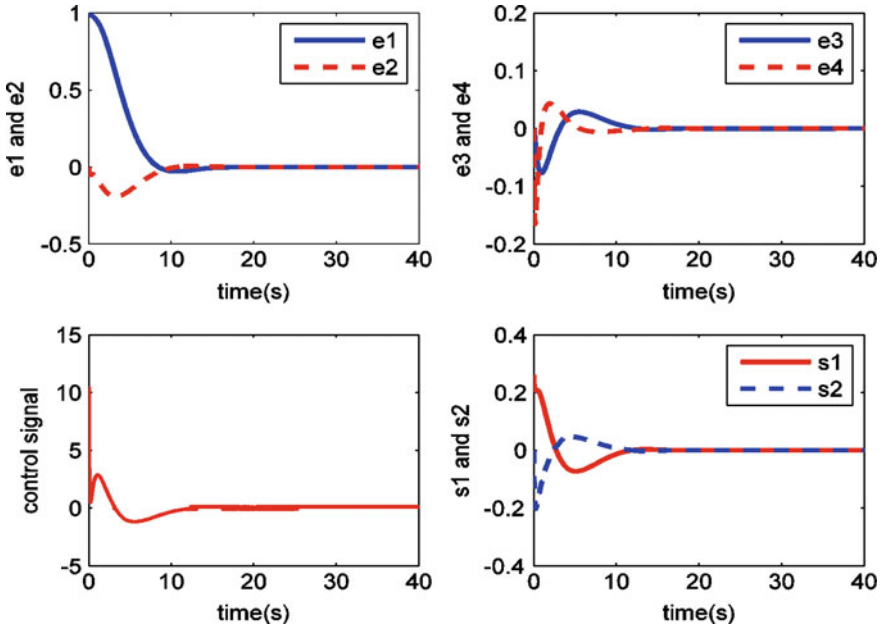

Fig. 9 Curves of trajectories errors, control signal and sliding surfaces, respectively (without disturbances)

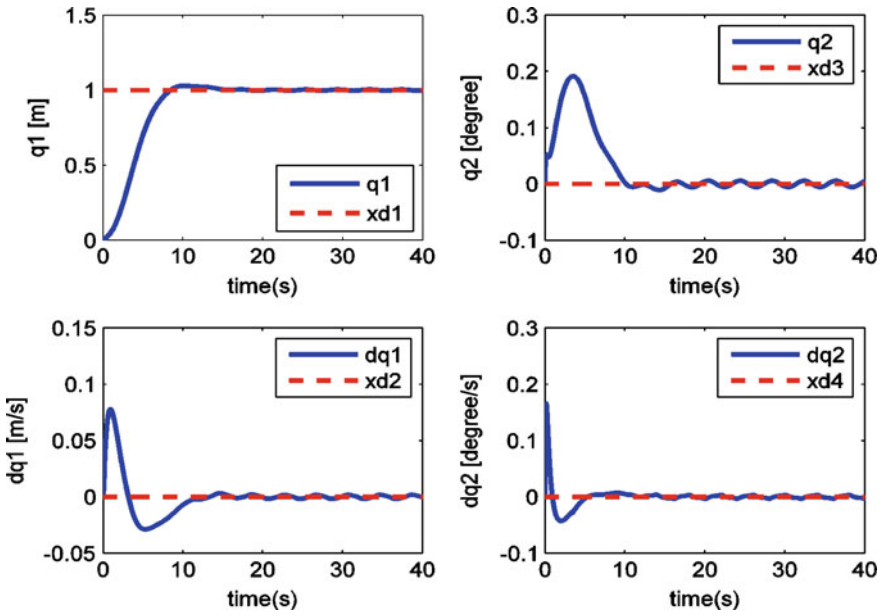

Fig. 10 States of overhead crane (with disturbances)

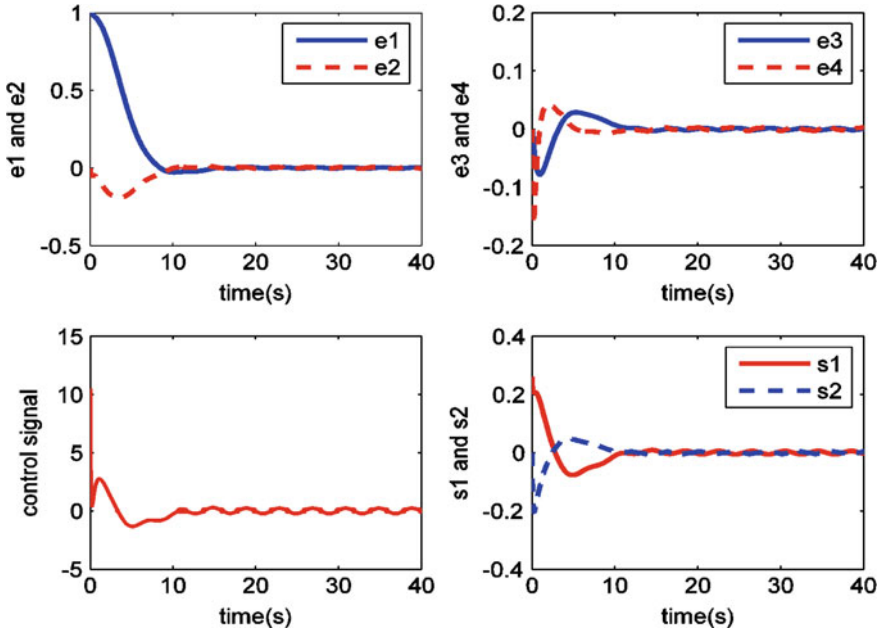

Fig. 11 Curves of trajectories errors, control signal and sliding surfaces, respectively (with disturbances)

$\gamma_\delta = 0.5, \gamma_{\beta_1} = 0.01, \gamma_{\beta_2} = 0.01, \gamma_\delta = 0.005, k_1 = k_2 = 1$. The initial conditions of the adaptive parameters are selected as $\delta(0) = 1, \theta_1(0) = \theta_2(0) = 0.002, \beta_1(0) = 1, \beta_2(0) = 4$, and $v_r(0) = 1$.

For each input variable of the used fuzzy systems, we defined three (triangular and trapezoidal) membership functions uniformly distributed on the following intervals: $[-0.5, 2]$ for q_1, $[-0.1, 0.2]$ for q_2, and $[-0.5, 0.5]$ for q_3 and q_4. Therefore, the number of fuzzy rules used in each fuzzy system is 81.

In the case without disturbances, the simulation results of overhead crane system are given in Figs. 8 and 9. It is clear, from Fig. 8, that the states of this system asymptotically converge to their desired values. Figure 9 shows the convergence towards zero of the sliding mode surfaces and the tracking errors as well as the boundedness of the control signal.

When the disturbances w_1, w_2 are considered, the obtained simulation results are given in Figs. 10 and 11. From these figures, it is clear that the system states oscillate near the equilibrium with small range as in the first example.

5 Conclusion

Exploiting the intrinsic approximation ability of the fuzzy systems for the continuous uncertain nonlinear functions, an adaptive sliding-mode controller for a class of underactuated systems has been investigated in this chapter. A Lyapunov based analysis has been carried out to conclude about the asymptotic stability as well as the convergence of the tracking errors towards zero, and to derive the adaptive laws. The numerical simulations have been carried out to evaluate the performance of the proposed control scheme.

References

1. Azar AT, Vaidyanathan S (2015) Computational intelligence applications in modeling and control, vol 576. Springer, Germany
2. Azar AT, Vaidyanathan S (2015) Handbook of research on advanced intelligent control engineering and automation. IGI Global, USA
3. Boulkroune A, M'saad M (2011) A fuzzy adaptive variable-structure control scheme for uncertain chaotic MIMO systems with sector nonlinearities and dead-zones. Expert Syst Appl 38:4744–4750
4. Boulkroune A, M'saad M (2012) On the design of observer-based fuzzy adaptive controller for nonlinear systems with unknown control gain sign. Fuzzy Sets and Syst 201:71–85
5. Boulkroune A, M'saad M (2012) Fuzzy adaptive observer-based projective synchronization for nonlinear systems with input nonlinearity. J Vib Control 18:437–450
6. Boulkroune A, M'saad M, Farza M (2012) Adaptive fuzzy tracking control for a class of MIMO nonaffine uncertain systems. Neurocomptiung 93:48–55
7. Boulkroune A, M'saad M, Farza M (2012) Fuzzy approximation-based indirect adaptive controller for multi-input multi-output non-affine systems with unknown control direction. IET Control Theory Appl 17:2619–2629

8. Boulkroune A, M'saad M, Farza M (2014) State and output feedback fuzzy variable structure controllers for multivariable nonlinear systems subject to input nonlinearities. Int J Adv Manuf Technol 71:539–556
9. Boulkroune A, Bounar N, M'saad M, Farza M (2014) Indirect adaptive fuzzy control scheme based on observer for nonlinear systems: a novel SPR-filter approach. Neurocomputing 135:378–387
10. Boulkroune A, Tadjine M, M'saad M, Farza M (2008) How to design a fuzzy adaptive control based on observers for uncertain affine nonlinear systems. Fuzzy Sets Syst 159:926–948
11. Boulkroune A, Tadjine M, M'Saad M, Farza M (2014) Design of a unified adaptive fuzzy observer for uncertain nonlinear systems. Inf Sci 265:139–153
12. Boulkroune A, Bouzeriba A, Hamel S, Bouden T (2014) A projective synchronization scheme based on fuzzy adaptive control for unknown multivariable chaotic systems. Nonlinear Dyn 78(1):433–447
13. Chaing C, Yeh Y (2014) Hierarchical fuzzy sliding mode control for uncertain nonlinear underactuated systems. In: Proceedings of the international conference on fuzzy systems (FUZZ-IEEE). Beijing, China, pp 662–669
14. Fang Y, Ma B, Wang P, Zhang X (2012) A motion planning-based adaptive control method for an under-actuated crane system. IEEE Trans Autom Control 20(1):241–248
15. Hao Y, Yi J, Zhao D, Qian D (2008) Robust control using incremental sliding mode for underactuated systems with mismatched uncertainties. In: Proceedings of the American control conference. Seattle, Washington, USA, pp 532–537
16. Huang A-C, Chen Y-F (2010) Adaptive control for a class of underactuated system with mismatched uncertainties. In: Proceedings of the IEEE Chinese control conference. Beijing, China, pp 2053–2059
17. Huang J, Ding F, Wang Y (2013) Sliding mode control with nonlinear disturbance observer class of underactuated system. In: Proceedings of the Chinese control conference. Xi'an, China, pp 541–546
18. Hussein II, Bloch M (2008) Optimal control of underactuated nonholonomic mechanical systems. IEEE Trans Autom Control 53(3):668–682
19. Khalil HK (2001) Nonlinear systems, 3rd edn. Prentice Hall, New Jersey
20. Kung CC, Chen T-H, Huang LC (2009) Adaptive fuzzy sliding mode control for a class underactuated systems. In: Proceedings of the FUZZ-IEEE Conference. Korea, pp 1791–1795
21. Ming Y, Baoyin L (2012) Disturbance adaptive control for an under-actuated spherical robot based on hierarchical sliding-mode technology. In: Proceedings of the Chinese control conference. Hefei, China, pp 4787–4791
22. Nafa F, Labiod S, Chekireb H (2013) Direct adaptive fuzzy sliding mode decoupling control for a class of underactuated mechanical systems. Turk J Electr Eng Comput Sci 21(6):1615–1630
23. Pezeshki S, Badamchizadeh MA, Ghiasi MA, Ghaemi S (2014) Control of overhead crane system Using adaptive model-free and adaptive fuzzy sliding mode controllers. J Control Autom Electr Syst 26:1–15
24. Qian D, Yi J, Zhao D (2007) Hierarchical sliding mode control to swing up pendubot. In: Proceedings of the American control conference. New-York city, pp 5254–5258
25. Shine K, Yang Y, Cheng C (2012) Robust adaptive controller design for second-order underactuated mechanical systems. In: Proceedings of the international conference in electric, communication and automatic control, pp 711–719
26. Slotine JJE, Li W (1991) Applied nonlinear control. Prentice-Hall, Englewood Cliffs
27. Tuan L, Lee S (2013) Sliding mode controls of double-pendulum crane systems. J Mech Sci Technol 23(10):1863–1873
28. Wang LX (1994) Adaptive fuzzy systems and control: design and stability analysis. Prentice-Hall, Englewood Cliffs
29. Wang W, Zhao J, Liu D (2004) Design of a stable sliding-mode controller for class of second-order under-actuated systems. IEE Proc Control Theory Appl 151(6):683–690
30. Yue M, Liu B (2014) Adaptive control of an under-actuated spherical robot with a dynamic stable equilibrium point using hierarchical sliding mode approach. Int J Adapt Control Signal Process 28(6):523–535

Unstable PLL-Controller as FM Modulator and Detection of Modulating Self-Oscillations

Bishnu Charan Sarkar, Suvra Sarkar and Saumen Chakraborty

Abstract Phase locked loops are well known nonlinear feedback control circuits extensively used in different electronic systems, particularly in communication and control. Generally they are used in stable mode of operation where loop error magnitude is small and system nonlinearity can be replaced by linear approximation. However, PLL designers over the years observed that due to variation of signal and loop parameters, dynamics of a PLL enters in a region which is not stable in conventional sense, even though predictable and controllable through parameter tuning. Hence attention has been given to explore so called unstable mode of PLL dynamics. PLLs operating in such mode produce periodic or chaotic self-oscillatory signals. In this chapter we focus on generation of self-oscillations in PLLs operating in their unstable mode and examine the possibilities of using these PLLs as modulators of periodic as well as chaotic oscillations. We consider a third order PLL with resonant type loop filter since in continuous time domain third order system is susceptible to chaotic self oscillations and gain as well as phase shift of a resonant filter could be tuned through a single parameter. We estimate the influence of loop design parameters in determining stable operating zone and hence find conditions of self-oscillation of third order PLL. With the variation of a design parameter, PLL is found to undergo a sequence of period doubling oscillations and ultimately chaotic oscillation of control signal results. In this condition, PLL is treated as an FM modulator of self-generated chaotic signal. We also report the effectiveness of PLL-based demodulators in detecting chaotically modulated signals. We consider second order and third order PLLs as chaos detecting loops for this purpose and obtain their relative responses. Detection of chaotically self-modulated signal is found to be difficult compared to that with

B.C. Sarkar (✉)
Physics Department, Burdwan University, Burdwan 713104, West Bengal, India
e-mail: bcsarkar_phy@yahoo.co.in

S. Sarkar
Electronics Department, Burdwan Raj College, Burdwan 713104, West Bengal, India
e-mail: suvrabrc@gmail.com

S. Chakraborty
Physics Department, Bidhan Chandra College, Asansol 713304, West Bengal, India
e-mail: saumenbcc@gmail.com

S. Vaidyanathan and C. Volos (eds.), *Advances and Applications in Nonlinear Control Systems*, Studies in Computational Intelligence 635,
DOI 10.1007/978-3-319-30169-3_17

periodically self modulated signal. We describe a circuit modification algorithm to PLL in order to enhance its response as a demodulator. Modified loop is shown to have increased stable zone of operation and faster transient response which makes it a better FM demodulator. Besides analytical and numerical simulation results, we have reported hardware experimental results on this problem.

1 Introduction

Phase locked loop (PLL) is a well known nonlinear feedback control system used in different areas of electronic technology. Its dynamics has different complexities and has been discussed in the literature in details during last several decades [7, 11, 17, 45]. In simple words, the purpose of a PLL is to acquire the instantaneous phase of a reference input signal and in steady state operation, to get the loop voltage control oscillator (VCO) synchronized to the input signal. Performing these activities, PLLs have become indispensable parts of synchronous signal processors like angle modulators and demodulators, carrier regenerators, frequency synthesizers etc. [24, 33, 35, 46]. However the dynamics of this simple looking system becomes immensely complicated because of inherent nonlinearities of loop constituents [16, 23]. Phase-error detector (PD), employed to detect the phase difference (ϕ) between input and VCO signals, produces a signal which is a nonlinear odd-periodic function of ϕ [17, 35]. Loop filter introduces frequency dependent amplitude response and additional phase shift to detected error signal. Moreover loop VCO has, in general, a nonlinear sensitivity to control signal applied to it [41]. All these features, separately or jointly, complicate PLL dynamics. Like any other control system, the operating mode of a PLL is of two types, namely, transient or acquisition mode and steady state or tracking mode [5, 30]. In transient mode, loop VCO tries to acquire input signal phase and in steady state mode, loop VCO follows input signal phase. Over the years, design objectives of a PLL are to have acquisition time (i.e., the time required to acquire input signal phase) as small as possible and to have tracking range (i.e., the frequency shift of input signal up to which VCO can track it) as large as possible [17, 45]. PLL designers have suggested several techniques to reach this goal through different techniques. In the following, we first briefly discuss different aspects of PLL study undertaken by researchers and then focus on the problem of self-oscillation of PLLs in their unstable mode of operation [15, 21, 25]. Examination of consequences of self-oscillation in a PLL-based modulator is the main interest of this work.

Conventionally, phase detector used in an analog PLL is a multiplier followed by hard filtering arrangement to suppress double frequency ripple term. As such its output is modeled as a sinusoidal function of phase error. Studies on responses of sinusoidal and other analog PDs are reported in literature [9, 26]. However, with predominant introduction of digital circuits in electronic systems, flip-flop based PDs or tri-state phase/frequency detectors (PFDs) having triangular, saw-tooth or extended linear characteristics have become very popular [2, 24, 35]. Logic states of a PFD output are converted into continuous VCO control signal with the help of a special

class of filters called charge pump (CP) filters [17, 20, 34]. This design methodology has led to charge pump PLLs (CP-PLLs) whose dynamics needs discrete time domain analysis [12, 47]. Besides hybrid type CP-PLLs, digital PLLs based on digitally controlled oscillators, digital filters and edge sensitive PDs have been designed and their dynamics have been extensively studied in discrete time domain. [2, 26, 27, 49]. Different techniques to enhance responses of digital PLLs are studied in literature [2, 3, 28, 37, 40]. Studies on nonlinear dynamics and chaotic oscillations in digital PLLs are topics of increasing interest [4, 6, 38, 43]. However in our present study we would concentrate on time continuous dynamics of analog PLLs based on sinusoidal PDs and continuously tunable VCOs. These systems have practical applications as well as analytical importance in the context of modern communication technology.

Dynamics of a PLL is heavily dependent on type and response of loop filters. A PLL with nth order filter is of $(n + 1)$th order. Thus a second order PLL (SO-PLL) is designed using first order filters which are passive or active in respect of transfer gain. SO-PLLs are extensively studied analytically in literature and predominantly employed in practical systems [17]. However, in some cases, use of a third order PLL (TO-PLL) is a must. Among several reasons, TO-PLLs are used to suppress the effects of double frequency error signals and to track a frequency ramp type input signal phase with zero steady state tracking error [7]. Several authors have examined the dynamics of third order analog and digital PLLs [10, 29, 31, 32, 43] following various techniques. Since third order feedback control systems are conditionally stable, the knowledge of parameter range ensuring stable system operation is required by a system designer. Further in unstable zone of operation, TO-PLLs show bifurcation and chaos which deserve special attention. The choice of loop LPF structure depends on the purpose for which PLL is being applied. Requirements of a carrier tracking loop are obviously different from those of an FM demodulator loop. So it is necessary to have flexibility in controlling loop gain, natural frequency and damping [17, 35]. In this respect a Sallen-Key type active resonant second order LPF is often used in the design of TO-PLLs [31, 43]. The closed loop response of a second order PLL becomes seriously affected because of additional time delay of IF amplifiers used in heterodyne PLLs [13, 17, 18, 41, 44]. Effectively time delay causes an uplift of in the order of PLL and adverse effects of higher order loops are observed in time delayed SO-PLLs. A good amount of studies on delayed SO-PLLs could be found in the literature. The inclusion of nonlinear amplifiers in a PLL is also suggested either to enhance the speed of convergence or to broaden the tracking range of operation. For these purposes, nature of nonlinearities of loop amplifiers could be cubic type or limiter type [14]. However, these additional nonlinearities lead to nonlinear dynamical behavior in PLLs.

In practical applications, response of a PLL becomes even more complicated because of unwanted signals accompanying input reference signal. These additional signals could be of discrete frequency or broad band noise signals. Loop phase error becomes a random variable because of the presence of interference and noisy signals [36, 42]. This obviously disturbs acquisition as well as tracking performance of PLL. In order to combat deleterious effects of these unwanted signals careful design of loop filter has been suggested. In the analysis of the loop dynamics, one has to take

time averaged loop phase error to estimate loop response. Statistical characterization of loop response in this situation has drawn the attention of researchers and to this end, selection of an optimum loop filter has become an important design problem. A good amount of research has been published on these problems.

In conventional application oriented studies, PLL is approximated as a linear feedback loop by considering loop phase error a small quantity. Further in most of these studies, time averaged analysis is found to provide reasonably satisfactory results. But in general it is not always possible to linearize the effects of nonlinearities in loop response. Also instantaneous time response has to be taken into account to obtain transient behavior of a PLL. In this respect, characteristics of PD and order of loop filter play vital roles. Like any other feedback control system, higher order loop filters cause additional phase shift of control signal applied to loop VCO. This additional phase shift affects loop stability and dynamics of the system becomes unstable and complicated. As such one can observe features of non linear dynamics like bifurcation and chaos in a deterministic PLL. The nonlinearity of PD and loop amplifier (included to amplify the loop error signal) has pronounced effects in non linear dynamics of a PLL. A higher order PLL operating in nonlinear mode is conditionally stable and in unstable condition, produces periodic as well as chaotic oscillations of control signal. In the context of increased interests on chaos based communication during recent years, generation and synchronization of chaotic oscillations have become very attractive topic of research [8, 22]. A PLL operating in unstable self-oscillatory mode is capable of generating chaotically modulated FM signals. Moreover, PLL-based demodulators could be used to recover the modulating chaos. On the other hand, in some cases, suppressing the possibilities of chaotic self oscillations in PLLs is primarily needed. These reasons have motivated PLL designers to study chaotic dynamics of PLLs in general and in PLL-based modulators and demodulators in particular.

Present chapter deals with problems of chaotic self oscillations in TO-PLL having resonant loop LPFs. We estimate the influence of loop design parameters in stable operating condition and hence find conditions of self-oscillation of TO-PLL. It is observed that in unstable mode of operation TO-PLL undergoes a process of period doubling oscillation with the variation of suitable design parameter and chaotic oscillation of control signal ultimately results. In this condition, PLL is treated as an FM modulator of self-generated chaotic signal. Problem of demodulating this chaotically modulated signal has practical importance and we report the effectiveness of PLL-based demodulators in this respect. We consider SO-PLL and TO-PLL as chaos detecting loops and obtain their response through numerical analysis and experimental study. We describe a circuit modification algorithm to TO-PLL in order to enhance its response as a PLL-demodulator. Modified TO-PLL has increased stable zone of operation and faster transient response which makes it a better FM demodulator. The chapter is organized in the following way. We discuss self-oscillation problem of a TO-PLL in Sect. 2. Process of bifurcation of stable state and periodic oscillation with variation of loop design parameter and period doubling route to chaos have been narrated. Numerical simulation establishes the difference between stable frequency zones of operation of TO-PLL in tracking and acquisition modes. In Sect. 3, we study

demodulation capabilities of a conventional SO-PLL and a TO-PLL with resonant filter operating in stable condition. We compare generalized auto-correlation functions of modulating chaos and demodulated chaos to establish faithful detection of chaos. A modified TO-PLL is described in Sect. 4 and enhanced performance of modified PLL is studied analytically and numerically. We describe hardware experimental results performed to estimate responses of PLL-based chaotic modulator and demodulator in Sect. 5. Obtained results fairly agree with analytical predictions. Section 6 discusses the outcome of the study reported in the chapter and a few conclusions are given in Sect. 7.

2 FM Modulator with Self-Generated Modulating Signal

In this section we discuss the dynamics of a TO-PLL and obtain the conditions of self-oscillation in the loop. With the variation of design parameters, stable state of PLL operation bifurcates and VCO control signal becomes periodically oscillating one. With further change in design parameter, bifurcation process continues and control signal becomes chaotic in a period doubling route. In this situation VCO output signal would be frequency modulated by self generated periodic or chaotic signals and can be used for communication related applications. First we would study loop dynamics analytically and then examine the same numerically. We would formulate the system equation in terms of some measurable quantities for a TO-PLL and these equations could be suitably modified for other forms of PLLs.

2.1 Analytical Considerations on Self-Oscillation

The structure of a basic PLL consisting of a PD, a LPF and a VCO is shown in Fig. 1. We take for simplicity a single un-modulated signal at PLL input. The signal at PD output is a function of instantaneous phase error ϕ between the phases of input signal $A\sin((\omega_r + \Omega)t)$ and VCO signal $2\cos(\omega_r t + \theta)$. Averaging PD output in

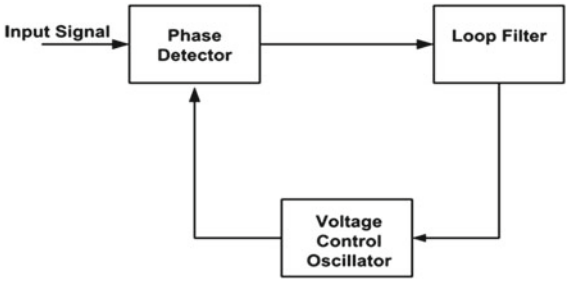

Fig. 1 Basic block diagram of phase locked loop

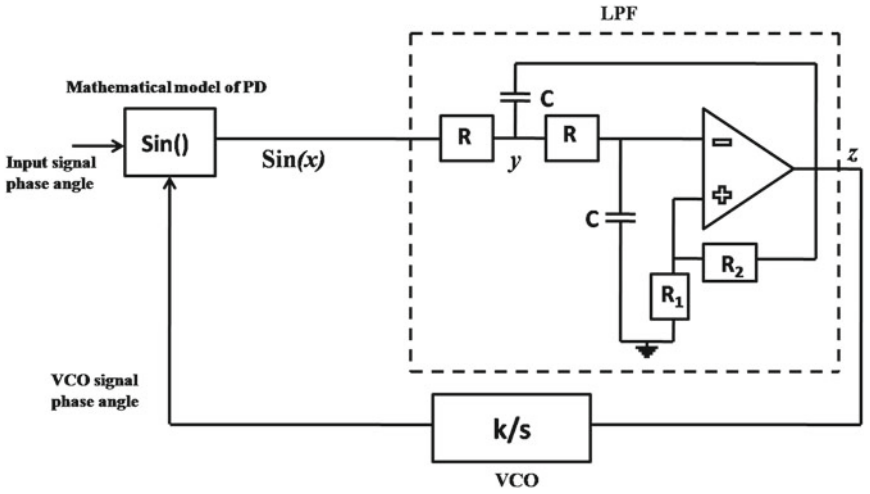

Fig. 2 Mathematical model of third order PLL with resonant filter

loop LPF, it is applied to VCO to force its phase to become phase locked to input signal.

A second order loop filter could be realized in different ways, for example, cascading two first order filters [19]. Here we take a resonant type second order LPF and an analog multiplier as PD to design a third order PLL. Figure 2 shows mathematical model of PD and hardware structure of loop filter. It is a Sallen-Key type resonant LPF of gain g determined by resistors R_1 and R_2. The transfer function of resonant LPF in the complex frequency (s) domain is as follows [43],

$$F(s) = \frac{g}{s^2T^2 + (3-g)sT + 1} \tag{1}$$

where $g(=1 + R_2/R_1)$ and $T = RC$ are gain and time constant of LPF respectively. Frequency and phase transfer characteristics of $F(s)$ play important role in PLL dynamics. Introduction of discontinuous phase shift and nonlinearly varying gain by the filter around its characteristics frequency would influence the stability of PLL. The phase governing equation of PLL written in terms of instantaneous phase error ϕ, frequency offset Ω between input signal and VCO signal, overall loop gain parameter k and LPF transfer function $F(p)$ in operator form is,

$$\frac{d\phi}{dt} = \Omega - kF(p)\sin\phi \tag{2}$$

Here $p(\equiv \frac{d}{dt})$ is the Heaviside operator and $k(=Ak_Dk_v)$ takes care of VCO sensitivity k_v, PD gain k_D, input signal amplitude (A) etc. The system equation can be rewritten in terms of three state variables $x(t)$, $y(t)$ and $z(t)$ as shown in Fig. 2. These variables are related to ϕ as follows [43],

$$x(t) = \phi(t),\ \ \phi(t) \in [-\pi, \pi] \tag{3a}$$

$$y(t) = \left[\frac{1 + Tp}{T^2p^2 + (3-g)Tp + 1}\right] \sin(\phi(t)) \tag{3b}$$

$$z(t) = \left[\frac{g}{T^2p^2 + (3-g)Tp + 1}\right] \sin(\phi(t)) \tag{3c}$$

Here $y(t)$ is the voltage at the input capacitor of LPF and filter output $z(t)$ acts as control signal to loop VCO. We derive three normalized state equations describing the dynamics of conventional TO-PLL in terms of these state variables as,

$$\frac{dx}{d\tau} = \Omega_n - k_n z \tag{4a}$$

$$\frac{dy}{d\tau} = \sin(x) + (g-2)y - (g - 1/g)\, z \tag{4b}$$

$$\frac{dz}{d\tau} = gy - z \tag{4c}$$

Here Ω_n, k_n and τ denote normalized frequency offset, loop gain and time respectively. The normalization has been done with respect to the time constant T of the filter. Note that the time evolution of x is dependent on control signal z as given in (4a). Dynamics of PLL is examined with the help of these equations.

Steady state values or fixed points of x, y and z are obtained by equating their time variations to zero and these values are $\sin^{-1}\mu$, μ and μg respectively, where, $\mu = (\Omega_n / k_n g)$. The parameter zone for stable loop operation has been obtained in the literature [31]. Note that steady state value of x is $x_s = \sin^{-1}\mu$, where $\mu = (\Omega_n / k_n g)$ and the argument of arcsin must be less than or equal to one in magnitude. So we get for stable operation of TO-PLL, the upper limit of Ω_n is given by,

$$\Omega_n \leq k_n g \tag{5}$$

However Ω_n cannot be arbitrarily increased by increasing g or k_n. By examining the stability of fixed points of state variables we derive another limiting condition. The said condition connecting Ω_n and g for a particular k_n is,

$$\Omega_n > \sqrt{(k_n g)^2 - (3-g)^2} \tag{6}$$

It is obtained from the linear transformation Jacobian J of the system described by set of Eqs. (4a)–(4c), evaluated at the fixed point of stability. The characteristic equation of steady state Jacobian J_s is a cubic equation of Eigen value λ and it is as given below:

$$\lambda^3 + (3-g)\lambda^2 + \lambda + k_n g \cos(x_s) = 0 \tag{7}$$

Replacing the term $\cos(x_s)$ by $\sqrt{(1-(\Omega_n/k_n g)^2)}$, we get characteristic Eq. (7) in terms of loop parameters. The stability condition of fixed point is obtained by applying Routh–Hurwitz array technique to this equation. This gives the limiting value of g for achieving stable state as less than 3 and the limiting relation (6). If, for given values of Ω_n and k_n, we take g beyond the limits specified by (5) and (6), the stable state of the loop is disturbed and periodic oscillations of PLL control signal is obtained. At this condition the variation of y and z shown in y–z plane would be a closed trajectory indicating limit cycle oscillation of the loop.

With further increase of g, limit cycle again bifurcates and control signal becomes a combination of two sinusoidal signals, one the original periodic signal and the other is its double period harmonic. This is known as period doubling phenomenon and process of period doubling continues with increasing values of g until control signal becomes a chaotic oscillation. The critical value of g leading to bifurcation of first oscillatory steady state can be predicted in terms of other loop parameters. This is done by finding the Jacobian matrix J_0 at a point on the limit cycle trajectory of oscillatory steady state and constructing the characteristic equation of this Jacobian J_0. As before we apply Routh Hurwitz technique to characteristic equation and find the conditions of stability of limit cycle in terms of the roots of characteristic equation. Predicted values of critical g required for bifurcation of fixed point and limit cycle are 2.16 and 2.54 respectively calculated for $k_n = 0.4$ and $\Omega_n = 0.3$. These values have been verified through numerical simulation and reported in following sub-section. Chaotic self-oscillation of control signal in TO-PLL causes frequency modulation of loop VCO and as such VCO output can be used as a chaos modulated signal for communication applications.

So far we have examined the stable zone of TO-PLL in terms of conditions of stability of the fixed point of loop state variables. The zone of stability is thus so called tracking range of PLL which gives the limiting range of parameters up to which an already synchronized loop would remain locked. But another range of stability, called acquisition range, is equally important. This gives the parameter zone for which a PLL, not in locked condition initially, would become synchronized. This range in terms of Ω_n for same values of k_n and g is less than tracking range. This is shown through numerical simulation in next subsection.

2.2 Numerical Simulation

We have studied the dynamics of a TO-PLL by numerical integration of Eqs. (4a)–(4c) using fourth order Runge–Kutta technique. Dynamics of the system is examined by noting the time series data of state variable z and phase plane plot of state variables y and z. For each simulation run, a large number of initial time series data are discarded to avoid primary transients in loop dynamics and thus to get steady state response. For example, in a set of 100,000 time series data, about 60 % data are not stored and the rest data are used to draw phase-plane plot or to calculate frequency spectrum. This method of simulation study has been followed for other loops reported in this chapter.

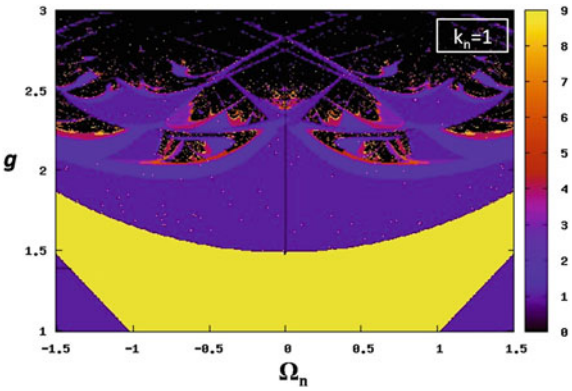

Fig. 3 Dynamical states of TO-PLL in parameter space denoted by color shades; 9 indicates stable state and 0 indicates chaotic state in two extremes

Figure 3 shows dynamical states of the PLL for different values of initial frequency off-sets (Ω_n) and loop filter gain (g) at a fixed value of parameter k_n ($k_n = 1$). Dividing ($\Omega_n - g$) parameter space in closely spaced grid points, we obtain the steady state dynamical state of the PLL at each of these points. Different colour shades are used to indicate various stable states like synchronous state, period-1 limit cycle, period-2, period-4 etc. oscillations and finally chaotic state. The boundaries of the parameter space indicating the stable synchronous state indicated by Eqs. (5) and (6) are also plotted in the same figure.

The simulation results agree very well with analytically predicted results. To find the limiting range of stable zone of operation in the simulation study, we start computation with parameter values, Ω_n, k_n and g, inside the predicted stable range and vary any one of them at a time in higher and lower directions of magnitude. The convergence of the state variables to a steady value ensures the existence of the stable state. This method obviously gives the range of parameters where the synchronous state is stable. The system dynamics is symmetrical about zero value of frequency offset.

We plot the bifurcation diagram of the loop with g as control parameter. Figure 4 shows one such diagram obtained through numerical integration of system Eqs. (4a)–(4c) for fixed values of other loop parameters. We find instantaneous peaks in time variation of z for a particular g. Increase in number of peaks from one to two, four, etc. with increasing g is due to period doubling process of z. Critical values of g where bifurcation occur are noted and compared with analytically predicted values for fixed point bifurcation or limit cycle bifurcation etc. A close agreement between predicted and simulated values are obtained. For example with increasing g, we get chaotic oscillation of z which is shown by all possible instantaneous peak values of z. So, chaotic self-oscillation of TO-PLL is observed. To get a conclusive evidence of chaotic state, we evaluate the maximum Lyapunov exponent (MLE) of numerically obtained time series data for state variable z when $g = 2.64$, with k_n and Ω_n as 0.4 and 0.3 respectively. We adopt the method suggested in [48] to find MLE. The obtained value of MLE is 0.469. Since the value is positive, it is a strong evidence of

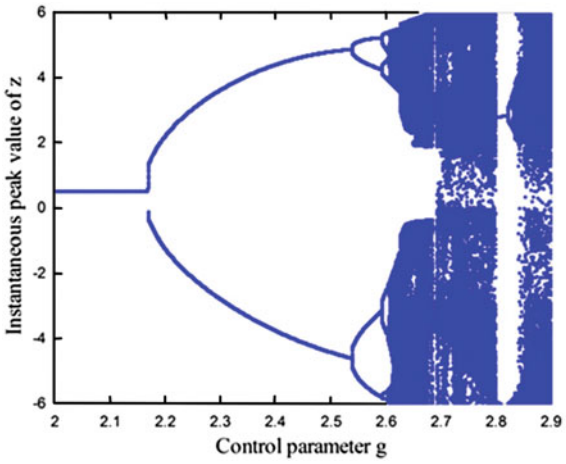

Fig. 4 Bifurcation diagram of 3rd order PLL for fixed values of $\Omega_n = 0.3$ and $k_n = 0.4$

chaotic oscillation. Figure 5a, b show the $y - z$ diagram for two different values of g, one at the period-1 limit cycle range and the other in chaotic range of oscillation.

In the simulation study we have obtained the range of frequency offset between input signal and VCO signal leading to synchronized condition in steady state starting from an unsynchronized state. The frequency range thus obtained is called acquisition range (AR). This zone is compared with that obtained by examining the stability of synchronized state, called tracking range (TR). Simulation results show that AR is less than TR for a TO-PLL. Simulation results are shown in Fig. 6. We note the appearance of hysteresis zone at the synchronization boundaries and the loop is susceptible to self-oscillations in this.

Frequency spectrum of the modulating signal is an important parameter for any modulator or demodulator. Frequency spectrum of self-generated chaotic oscillations in TO-PLL is obtained from the Fourier transform of time series data set of signal z. We represent the same in Fig. 7a, b and compare it with closed loop transfer function of modulator PLL. The same would be required to examine performance of demodulator.

3 PLL-Based Demodulator Response

We examine the problem of demodulation of *chaotically* modulated signal obtained from an unstable TO-PLL in a PLL-based demodulator. For this purpose, responses of demodulators designed with conventional SO-PLL and resonant filter based TO-PLL are studied. The modification of TO-PLL-based demodulator is discussed in Sect. 4. From basic PLL theory, it is known that the output of filter of PLL is demodulated version of modulating signal present in input FM signal [17]. In complex frequency domain, the output of loop filter is given by $Z(s)$, where,

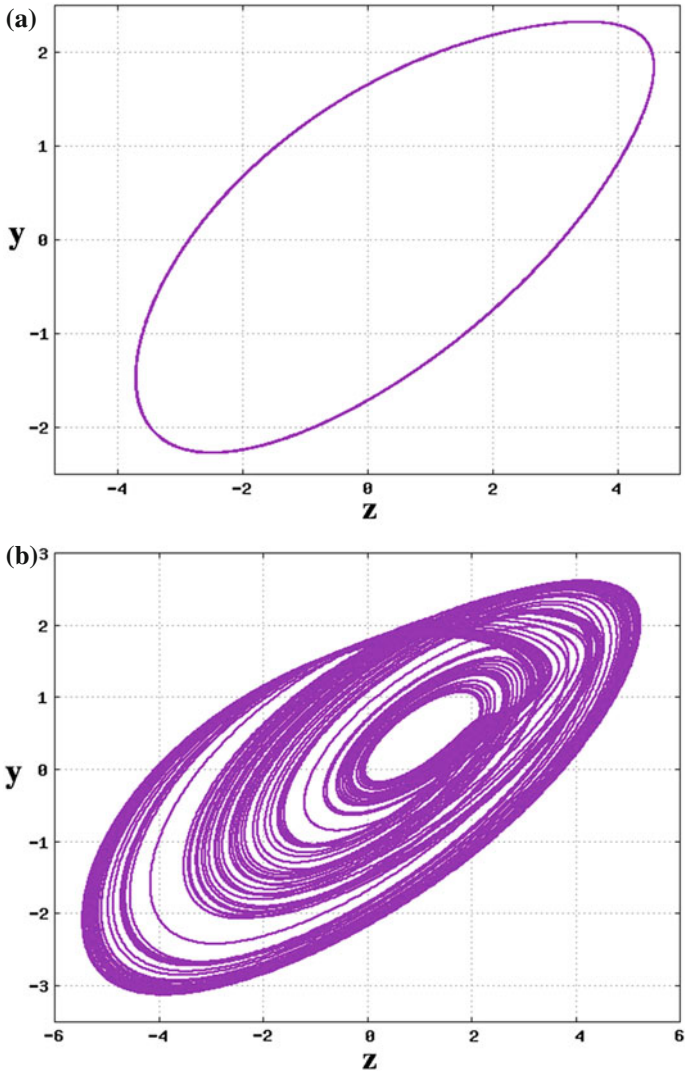

Fig. 5 Phase space plot of modulator PLL; **a** periodic self oscillation, **b** chaotic self oscillation

$$Z(s) = \frac{H(s)}{k_n g} M(s) \tag{8}$$

Here, $M(s)$ is frequency spectrum of modulating signal and $H(s)$ is closed loop transfer function of PLL. $H(s)$ is related to loop filter $F(s)$ and un-normalized parameter k by following equation:

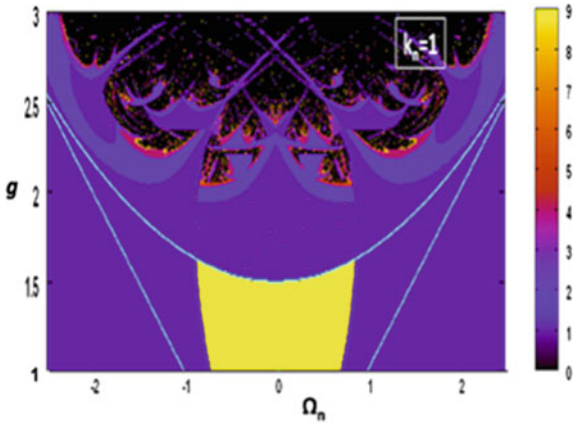

Fig. 6 Parameter space showing different dynamical states of modulator PLL computed in reverse direction of Ω_n variation (unstable to stable zone) compared to Fig. 3; reduced stable zone indicates lesser acquisition than tracking range

$$H(s) = \frac{kF(s)}{s + kF(s)} \tag{9}$$

It shows that the nature of loop filter has important effect in demodulation characteristics of PLL. $H(s)$ of PLL used should ideally have constant transfer gain and linear phase shift in the frequency band of modulating signal to provide undistorted demodulated signal. We examine different demodulators on the basis of this requirement.

In cascaded configuration of modulator and demodulator PLLs (Fig. 8), VCO output of modulator PLL (M-PLL) is taken as input of demodulator PLL (Dm-PLL). System equations of M-PLL are those given in (4a)–(4c), with suffix 1 to state variables and loop parameters. The equations are as follows:

$$\frac{dx_1}{d\tau} = \Omega_{n1} - k_{n1} z_1 \tag{10a}$$

$$\frac{dy_1}{d\tau} = \sin(x_1) + (g_1 - 2) y_1 - (g_1 - 1/g_1)\, z_1 \tag{10b}$$

$$\frac{dz_1}{d\tau} = g_1 y_1 - z_1 \tag{10c}$$

We take normalized design parameters for two PLLs as k_{ni}, g_i and Ω_{ni} (where $i = 1$ for M-PLL and $i = 2$ for Dm-PLL). Filter time constant T of M-PLL is normalizing parameter. Note that for M-PLL, frequency offset Ω_{n1} is defined with respect to input reference frequency and that for Dm-PLL Ω_{n2} with respect to M-PLLs VCO

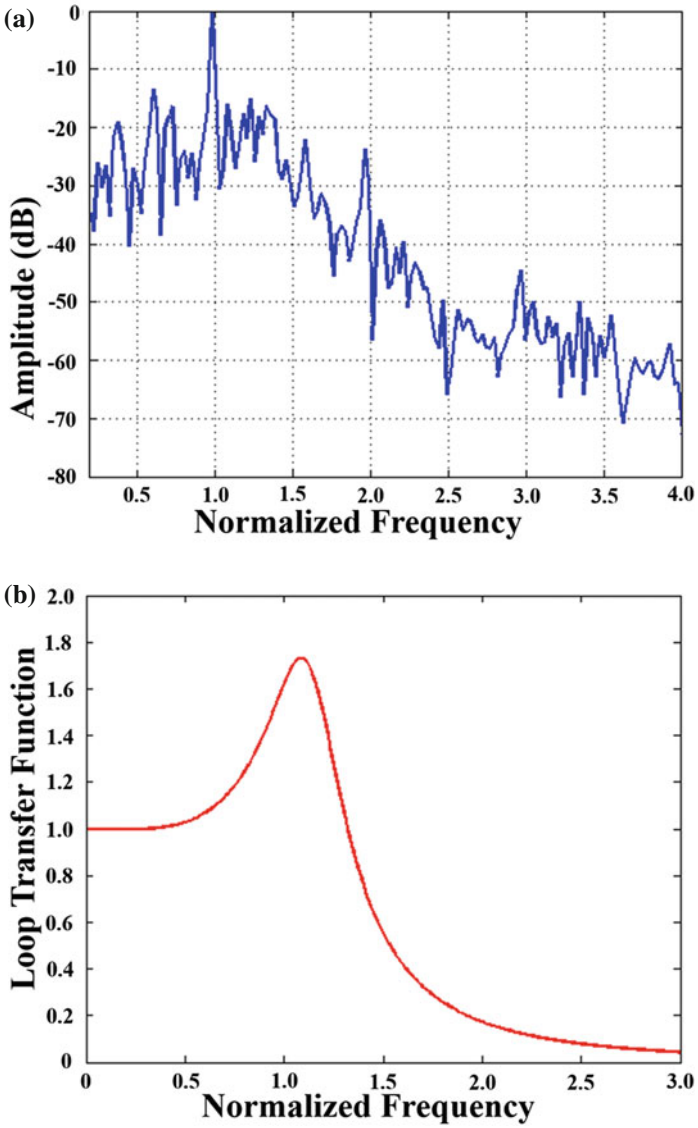

Fig. 7 **a** Frequency spectrum of chaotic control signal of modulator TO-PLL due to self oscillation; **b** Amplitude transfer function of closed loop TO-PLL in that condition

free running frequency. In synchronized condition, M-PLLs VCO frequency is equal to input reference signal frequency. Hence effective frequency off-set (Ω_{eff}) of Dm-PLL with respect to main reference signal frequency is an algebraic sum of Ω_{n1} and Ω_{n2}.

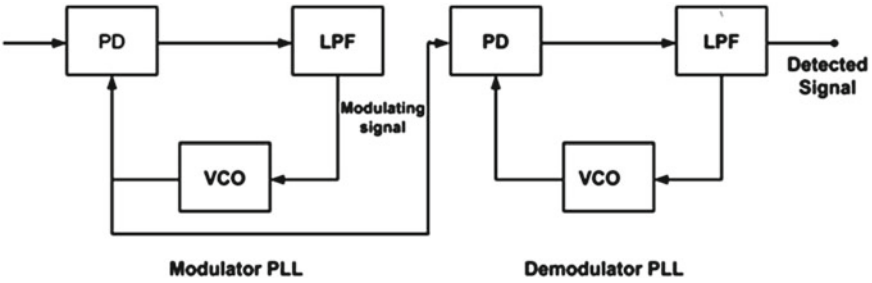

Fig. 8 Block diagram showing modulator-demodulator configuration

Response of a demodulator is examined by noting the similarity between waveforms and spectrum of modulating (z_1) and demodulated (z_2) signals. To examine similarity in time domain, we plot instantaneous values of z_1 and z_2 along X and Y axes in Cartesian plane. Similarity in two waveforms is indicated by a closed loop elliptical curve obtained in such plotting. This curve becomes a straight line when two waveforms are of same phase. For periodic modulation, inference can be easily made. But for chaotic modulating signals, tracing would be complex and inference of demodulation is to be made from frequency domain presentations.

3.1 Second Order PLL Based Demodulator

We take a first order lag-lead type filter in SO-PLL (Fig. 9a). Frequency domain transfer function of filter is given by,

$$F(s) = g_2 \left(\frac{1 + F_0 sT}{1 + sT} \right) \tag{11}$$

Here g_2 and F_0 are dc gain and high frequency gain normalized to g_2 of filter respectively. For a SO-PLL we have two state variables $x_2(t)$ and $z_2(t)$ which are loop phase error and filter output respectively. Remembering that input to demodulator is frequency modulated by state variable z_1 of M-PLL, we get state equations for Dm-PLL as,

$$\frac{dx_2}{d\tau} = \Omega_{n2} + k_{n1} z_1 - k_{n2} z_2 \tag{12a}$$

$$\frac{dy_2}{d\tau} = g_2 \sin(x_2) + g_2 F_0 \cos(x_2)(\Omega_{n2} + k_{n1} z_1 - k_{n2} z_2) - z_2 \tag{12b}$$

Note that when input to SO-PLL is zero we can estimate the steady state values of by equating RHS of (12a) and (12b) to 0. Steady state values of x_2 and z_2 (for

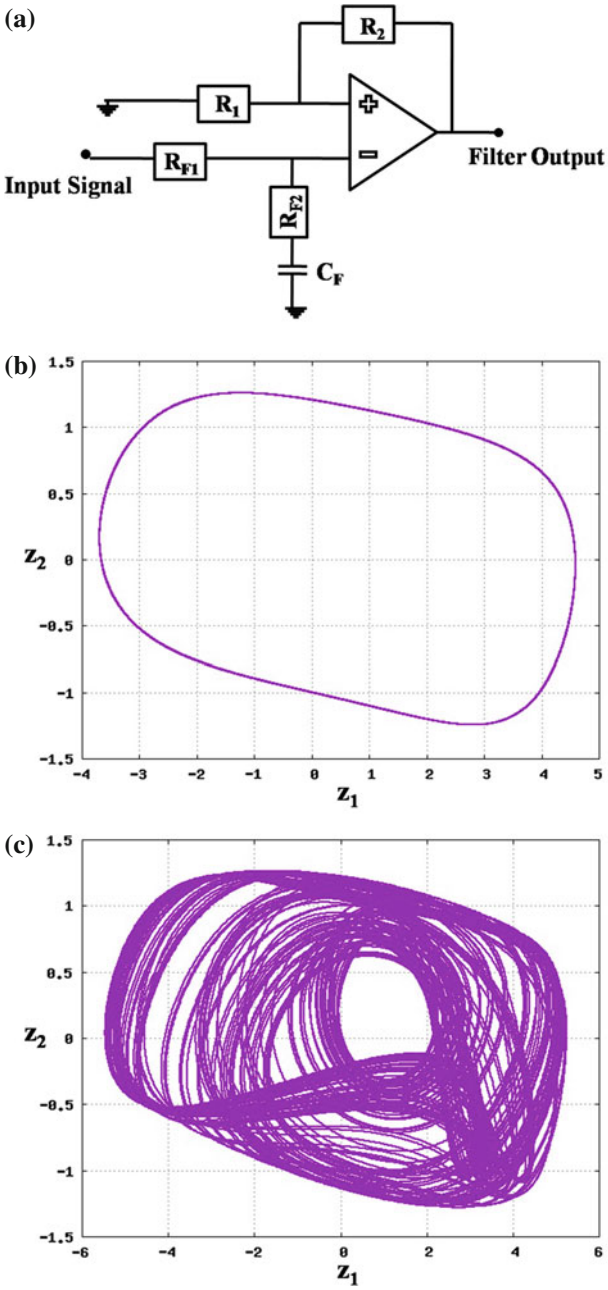

Fig. 9 **a** Lag-lead loop filter used in SO-PLL. SO-PLL based demodulator response through $z_1 - z_2$ plot for **b** periodic self oscillation, **c** for chaotic self oscillation

un-modulated input i.e., $z_1 = 0$), are $\sin^{-1}(\Omega_{n2}/k_{n2}g_2)$ and Ω_{n2}/k_{n2} respectively. Thus loop parameters are to be chosen satisfying the condition:

$$\Omega_{n2} \leq k_{n2}g_2 \tag{13}$$

If M-PLL is in steady state, z_1 is a nonzero time invariant quantity given by Ω_{n1}/k_{n1}. Then steady state value of x_2 is calculated in terms effective frequency off-set as $(\Omega_{n1} + \Omega_{n2})/k_{n2}$. When input to SO-PLL is an FM signal obtained from M-PLL modulated by self generated z_1 signal, for synchronized operation of demodulator, z_2 is related to z_1. Closed loop transfer function SO-PLL considered here we have as,

$$H_2(s) = \frac{k_{n2}g_2 + sTk_{n2}g_2F_0}{k_{n2}g_2 + sT(1 + k_{n2}g_2F_0) + s^2T^2} \tag{14}$$

Amplitude transfer function of $H_2(s)$ and spectrum of z_2 are to be estimated to examine the response of demodulator.

3.2 Third Order PLL Based Demodulator

Since modulated signal is generated in a self-oscillating TO-PLL, we are interested to examine the response of a demodulator based on a similar type TO-PLL. However this TO-PLL is to be operated in stable zone by suitably choosing design parameters. State equations for TO-PLL based demodulator with FM input signal would be written as,

$$\frac{dx_2}{d\tau} = \Omega_{n2} + k_{n1}z_1 - k_{n2}z_2 \tag{15a}$$

$$\frac{dy_2}{d\tau} = \sin(x_2) + (g_2 - 2)y_2 - (g_2 - 1/g_2)\,z_2 \tag{15b}$$

$$\frac{dz_2}{d\tau} = g_2y_2 - z_2 \tag{15c}$$

Here z_1 represents modulating signal. When M-PLL is in steady state, input signal to Dm-PLL is not modulated by time varying signal. Then, taking steady state value of z_1 as Ω_{n1}/k_{n1} from Sect. 2.1, we obtain steady state values of x_2, y_2 and z_2 as $\sin^{-1}(\mu_2)$, μ_2 and μ_2g_2 respectively where $\mu_2 = (\Omega_{n1} + \Omega_{n2})/k_{n2}g_2$. The range of the stable dynamics of Dm-PLL can be obtained by applying the conditions obtained in (5) and (6), by putting Ω_{eff}, as $(\Omega_{n1} + \Omega_{n2})$. Closed loop frequency transfer function of TO-PLL is obtained as,

$$H_3(s) = \frac{k_{n2}g_2}{k_{n2}g_2 + sT + (3 - g_2)s^2T^2 + s^3T^3} \tag{16}$$

In this case also amplitude transfer function of $H_3(s)$ and spectrum of z_2 are to be estimated to examine the response of demodulator. These are described in following section.

3.3 Numerical Simulation

To study Dm-PLL response numerically, we take M-PLL described by (10) and adjust loop parameters to get periodic or chaotic self oscillations of control signal. State equations of SO-PLL-based demodulator are given in (12). Modulator-demodulator response is obtained by solving these five equations, simultaneously. Thus we get time series data for z_1 and z_2 for given set of design parameters. Figure 9b shows response of the system with periodic modulation through plot of z_1 and z_2 ($\Omega_{eff} = 0$) in the Cartesian XY plane. One closed elliptic curve indicates demodulation of modulating signal. But with chaotic modulation, plot of z_1 and z_2 shown in Fig. 9c is a complicated trajectory containing number of elliptic curves. A chaos is a combination of huge number of sinusoids having different frequencies and amplitudes and this results complex curve. We represent amplitude transfer characteristic of $H_2(s)$ in Fig. 10, with selected values of design parameters. We observe that response is not flat in the band of modulating chaos (shown in Fig. 7a) and so demodulated chaos would be distorted. Spectrum of z_2 obtained from SO-PLL is shown in Fig. 11a, and distorted output is evident. Thus demodulation of chaos with SO-PLL is not satisfactory.

We study response of TO-PLL-based demodulator in a similar way. Here we take six state equations (three from (10) and three from (15)) for modulator demodulator system. We take parameters for M-PLL as taken before and choose Dm-PLL parameters as $g_2 = 1.5$, with $k_{n2} = 0.6$ and $\Omega_{n2} = -0.3$. We estimate amplitude transfer function Dm-PLL from $H_3(s)$ given in (16). It is shown in Fig. 10 for two different time constants (T_2) of Dm-PLL. The difference in response is evident in figure.

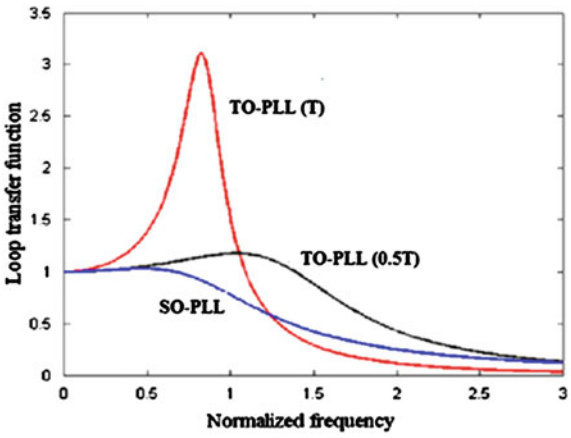

Fig. 10 Amplitude transfer function of closed loop PLL of different orders shown in same frequency scale normalized to time constant T

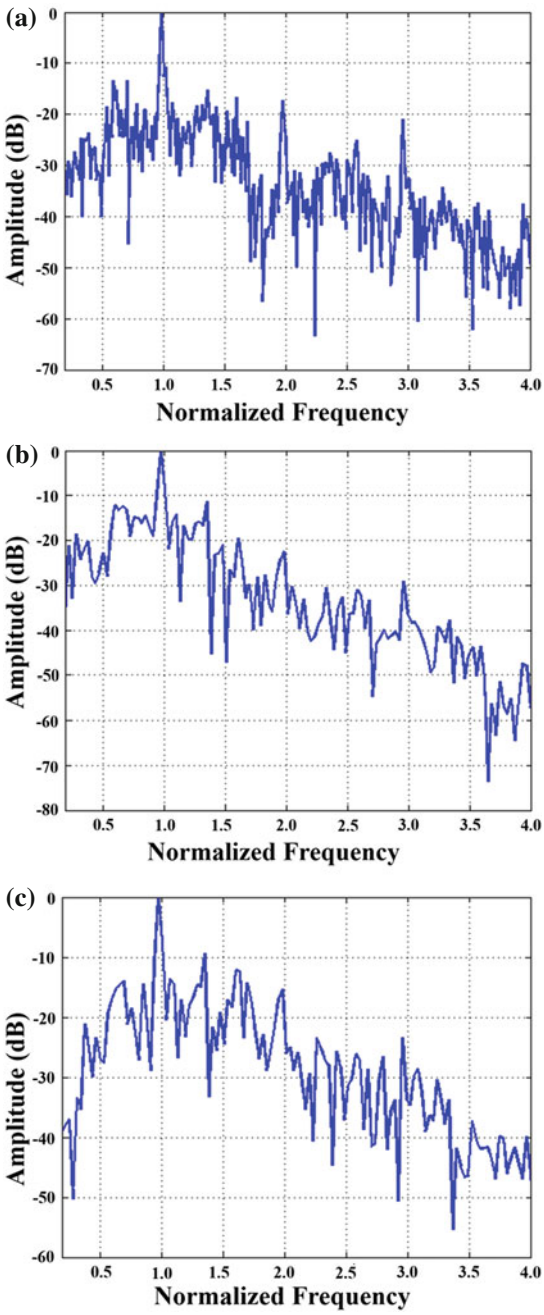

Fig. 11 Frequency spectrum of demodulated chaotic oscillations by different demodulators in same normalized frequency. **a** SO-PLL (filter time constant T); **b** TO-PLL (filter time constant T); **c** TO-PLL (filter time constant $0.5T$)

When T_2 is equal to that of M-PLL, response is not flat in the frequency band of modulating chaos and it emphasizes some higher frequency components of chaos around characteristic frequency. Thus demodulated chaos would be different from modulating chaos. However with T_2 equal to $0.5T$, the flat zone extends; but still there is greater gain for higher frequency components of z_1. This introduces distortion in demodulated signal. Spectrum of demodulated chaos is shown in Fig. 11b, c, for two values of time constants of TO-PLL demodulator.

4 Modified TO-PLL-Based Demodulator

Motivation behind modifying TO-PLL structure is to have larger tracking and acquisition zones which would lead to better response of demodulator. For this purpose VCO control signal is modified such that VCO modulation becomes phase as well as frequency modulation type.

4.1 Design Algorithm and System Equation

Figure 12 shows proposed design algorithm of modified TO-PLL (MTO-PLL) [39]. Here, VCO control signal is taken as a sum of $z(t)$ and time derivative of $y(t)$. Thus, VCO control signal, $z_m(t)$, is written as:

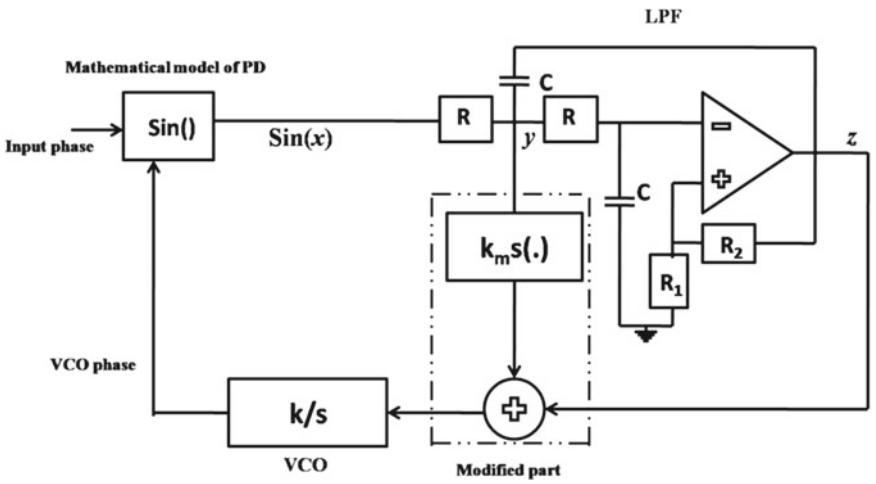

Fig. 12 Block diagram of modified TO-PLL

$$z_m(t) = z(t) + k_m \frac{dy}{dt} \tag{17}$$

Here k_m is a new design parameter. Using the expressions of $y(t)$ and $z(t)$ given in (4b) and (4c), we write time derivative of $y(t)$ as,

$$\frac{dy}{dt} = \frac{dz}{dt} + T\frac{d^2z}{dt^2} \tag{18}$$

This means that $z_m(t)$ is proportional to $z(t)$, dz/dt and d^2z/dt^2, where $z(t)$ is conventional control signal. In effect VCO output signal of MTO-PLL is frequency as well as phase modulated by signals proportional to loop phase error. Due to proposed circuit modification effective transfer function of loop filter in complex frequency (s) domain, written as $F_m(s)$, is obtained as,

$$F_m(s) = \frac{k_m(s^2T^2 + sT) + g}{s^2T^2 + (3-g)sT + 1} \tag{19}$$

Normalized time evolution equation for x_2 in MTO-PLL is obtained as,

$$\frac{dx_2}{d\tau} = \Omega_{n2} - k_{n2}z - k_{n2}k_m\frac{dy_2}{d\tau} \tag{20}$$

Using Eqs. (17)–(19), we get the normalized state equations for MTO-PLL-based demodulator as,

$$\begin{aligned}\frac{dx_2}{d\tau} &= \Omega_{n2} - k_{n2}k_m\sin(x_2) - k_{n2}k_m(g_2-2)y_2 \\ &\quad - k_{n2}\left[1 - k_m\left(\frac{g_2-1}{g_2}\right)\right] + k_{n1}z_1 \end{aligned} \tag{21a}$$

$$\frac{dy_2}{d\tau} = \sin(x_2) + (g_2-2)y_2 - (g_2 - 1/g_2)\,z_2 \tag{21b}$$

$$\frac{dz_2}{d\tau} = g_2y_2 - z_2 \tag{21c}$$

For, steady state values of x_2, y_2 and z_2 for $z_1 = 0$ are $\sin^{-1}\mu$, μ and μg respectively, where, $\mu = \frac{\Omega_{n2}}{k_{n2}g_2}$. These values are identical to those of TO-PLL-based demodulator indicating that steady state response of MTO-PLL would not change. However, the additional control term in MTO-PLL would influence its transient response. For a non-zero time invariant z_1, effective frequency off-set has to taken as described earlier. Closed loop frequency transfer function of TO-PLL is obtained as,

$$H_{3m}(s) = \frac{k_{n2}g_2 + k_mk_{n2}sT + k_mk_{n2}s^2T^2}{k_{n2}g_2 + sT(1 + k_mk_{n2}) + (3 - g_2 + k_mk_{n2})s^2T^2 + s^3T^3} \tag{22}$$

We obtain amplitude transfer function of $H_{3m}(s)$ and spectrum of z_2 to examine the response of demodulator.

4.2 Numerical Simulation

Dynamics of MTO-PLL with modulation-free input signal is studied numerically by putting $z_1 = 0$ in (21a). Stability of fixed point of state variables are obtained and shown in Fig. 13a. While compared to basic TO-PLL ($k_m = 0$), increased stable zone for MTO-PLL ($k_m = 1$) is evident. Further the ability of MTO-PLL to acquire a stable state from unlocked state is estimated by performing simulation with suitable initial values of effective frequency offset. Results are shown in Fig. 13b which shows increased range of acquisition range. These observations indicate better transient response as well as tracking ability of modified loop.

To study response of MTO-PLL-based demodulator we take a total of six state equations, three from (10) and three from (21), for modulator demodulator system.

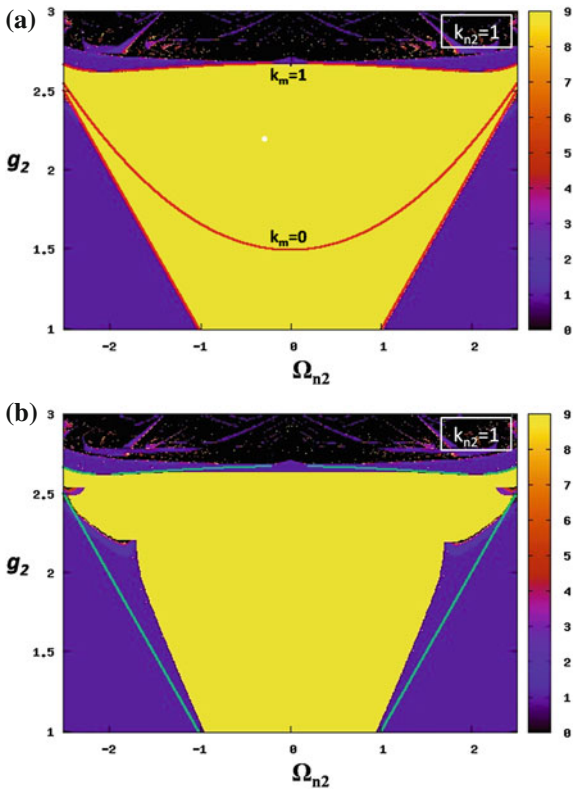

Fig. 13 Parameter space showing different dynamical states of MTO-PLL in different colors. 9 indicates stable state and 0 indicates chaotic state. **a** For tracking and **b** for acquisition modes of operation of MTO-PLL

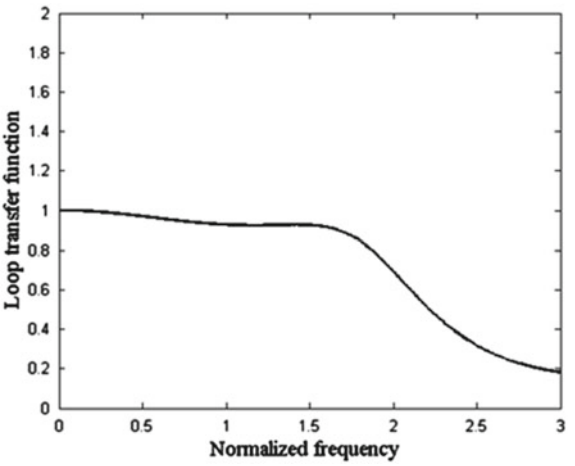

Fig. 14 Amplitude transfer function of closed loop MTO-PLL in same normalized frequency as given in Fig. 11

We choose parameters for M-PLL as taken before for self-generation of periodic and chaotic oscillations. For Dm-PLL parameters are taken as $g_2 = 2.1$, $k_{n2} = 0.6$ and $\Omega_{n2} = -0.3$. We estimate amplitude transfer function Dm-PLL from $H_3(s)$ given in (16). It is shown in Fig. 14 for time constant of Dm-PLL filter taken half of that of M-PLL filter. This has been done to increase the flat zone of amplitude response and it extends even though we have enhanced filter gain value. Spectrum of demodulated chaos is shown in Fig. 15b, and it has fair similarity with modulating chaos spectrum shown in Fig. 7a. We plot $z_1 - z_2$ curve for MTO-PLL (Fig. 15a) and observe it has structural similarity with $z_1 - y_1$ plot of M-PLL with chaotic modulation. We note that z_1 and y_1 are signals with phase shift between them because of the integrating action. Similarly in a synchronized demodulation condition z_1 and z_2 are phase shifted versions of one another. This is the reason of similar structures of attractor shown Fig. 5a, b.

Next we estimate parameter zone for possible detection of chaos using the concept of generalized synchronization (GS) [1]. Concept of GS is well documented in literature. We consider more than one demodulators having identical design parameters but operating with different initial conditions. They are operating in the face of a common input FM signal. If in steady state, error between two corresponding state variables of two demodulators be zero or constant of time, we conclude GS has taken place between modulator and demodulator. Mathematically in this situation z_2 would be a function of z_1. Detection of modulating chaos would be possible for a range of parameter values used to design Dm-PLLs. In Fig. 16 the shaded regions of parameter space where GS would take place [43]. Figure 16a shows the region for TO-PLL based demodulators and Fig. 16b shows the same for MTO-PLL based demodulator. It shows increased range of design parameters where GS is possible in MTO-PLL-based demodulator.

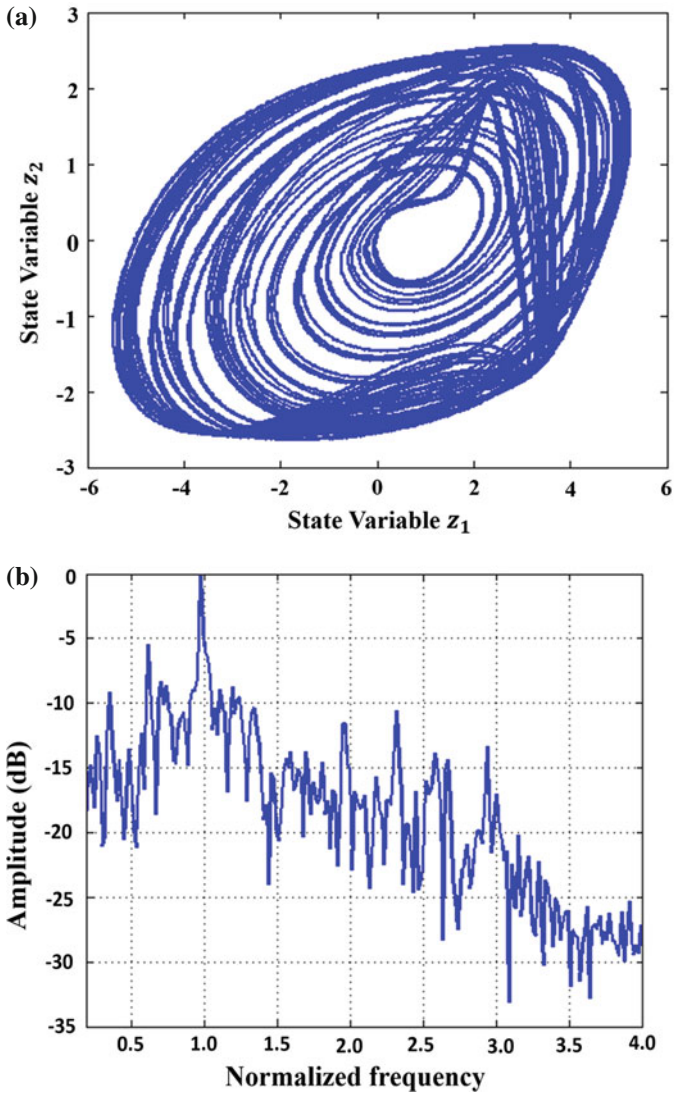

Fig. 15 Response of MTO-PLL based demodulator. **a** $z_1 - z_2$ plot of demodulator; **b** Frequency spectrum of demodulated signal

5 Hardware Experiment

This section describes results of experimental verification of responses of PLL-based modulators and demodulators under study. Prototype hardware circuits are fabricated using some off-the-shelf ICs in RF frequency range. Signal generators, having external frequency modulation facility, are used as loop VCOs. Frequency

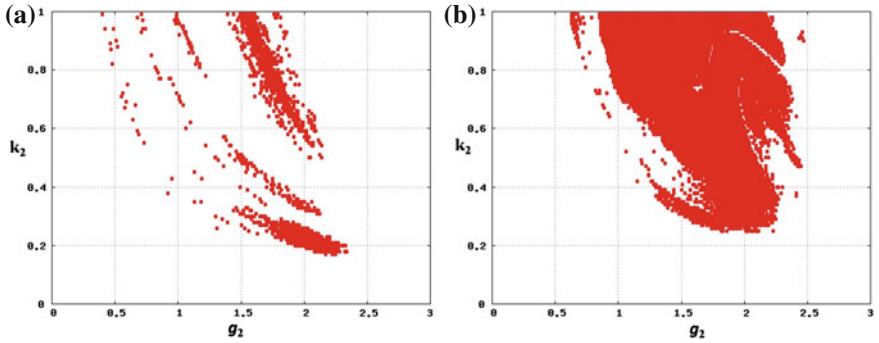

Fig. 16 Parameter space showing state of generalized synchronization (shaded zone) between modulating and demodulated chaos. **a** TO-PLL, **b** MTO-PLL

modulation sensitivity of these VCO are experimentally determined. Time constant of PLLs, amplitude and frequency of input reference signal and VCO signals are suitably chosen. With these values of signal and loop parameters, experimental values of the normalized frequency offset and the loop gain are calculated. We perform experiments to examine following properties of the system:

- Conditions of self-oscillation of TO-PLL and MTO-PLL are verified;
- Periodic and chaotic attractors of unstable TO-PLL are experimentally obtained;
- Demodulation capability of TO-PLL based demodulator is experimentally verified;
- Response of MTO-PLL-based demodulator is examined and its capability is compared with that of TO-PLL-based demodulator.

Adjusting Ω_{n1} and k_{n1} at 0.22 and 0.38, we vary g_1 from 1.0 in the increasing direction and observe that the control signal in the feedback path of the Modulator PLL breaks into self-oscillation in period-1 mode at $g_1 = 2.1$. This observation is consistent with analytical prediction. Next we go on increasing g_1 and note that the control signal bifurcates in period doubling route and ultimately becomes chaotic. Figure 17a shows experimentally obtained periodic attractor and power spectrum of corresponding frequency modulated VCO output. Observations for chaotic condition of control signal is shown in Fig. 17b where we have depicted chaotic attractor and frequency modulated VCO output in this situation.

We study demodulation capability of TO-PLL-based demodulator with normalized parameters as, $\Omega_{n2} = 0.33$, $k_{n2} = 0.53$ and $g_2 = 2.33$. With these values Dm-PLL is in stable zone of operation. The demodulator response in this situation is shown in Fig. 18a for period-1 type self-oscillation in modulator ($\Omega_{n1} = -0.27$, $k_{n1} = 0.36$). Obtained traces indicate that two signals are in a state of constant phase difference and so TO-PLL based demodulator is able to detect periodic modulation.

Then we study the response of proposed MTO-PLL and its demodulation capability. We measure stable zone of operation of the loop with $\Omega_{n2} = 0.33$, $k_{n2} = 0.53$

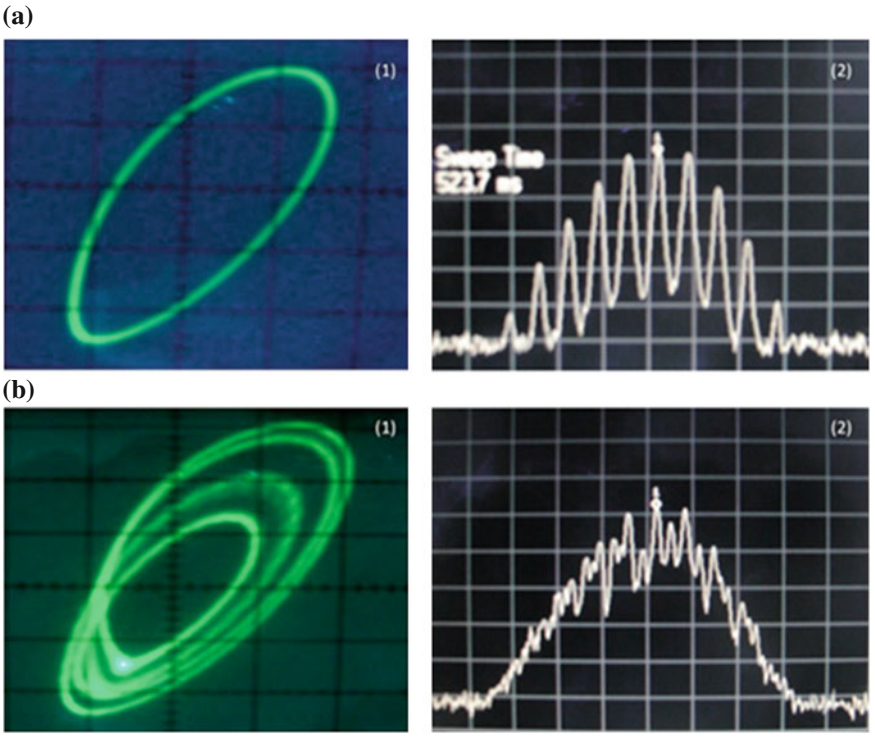

Fig. 17 Experimental results for TO-PLL-based modulator. **a** Periodic self oscillation, **b** chaotic self oscillation

and increasing g_2. It is found that MTO-PLL remains stable for g_2 up to 2.070, but unmodified TO-PLL becomes oscillatory at $g_2 = 1.794$. Observations are similar for other loop parameters also. Demodulated signals obtained from MTO-PLL demodulator with time constant T and $0.5T$ are shown in Fig. 18b, c for periodic self-modulation. Here T is time constant of modulator PLL. An improved response is evident in Fig. 18c, as compared to that shown in Fig. 18a, b. For chaotic modulation signal, obtained traces for MTO-PLL are better than TO-PLL because of better transient response and larger tracking zone MTO-PLL. But we have not included them for poor photographs.

6 Discussion

In this work we discuss unstable dynamics of resonant second order filter based TO-PLL and generation of self oscillations in periodic and chaotic modes. Consequences of oscillations in feedback control path are discussed in details to design PLL-based

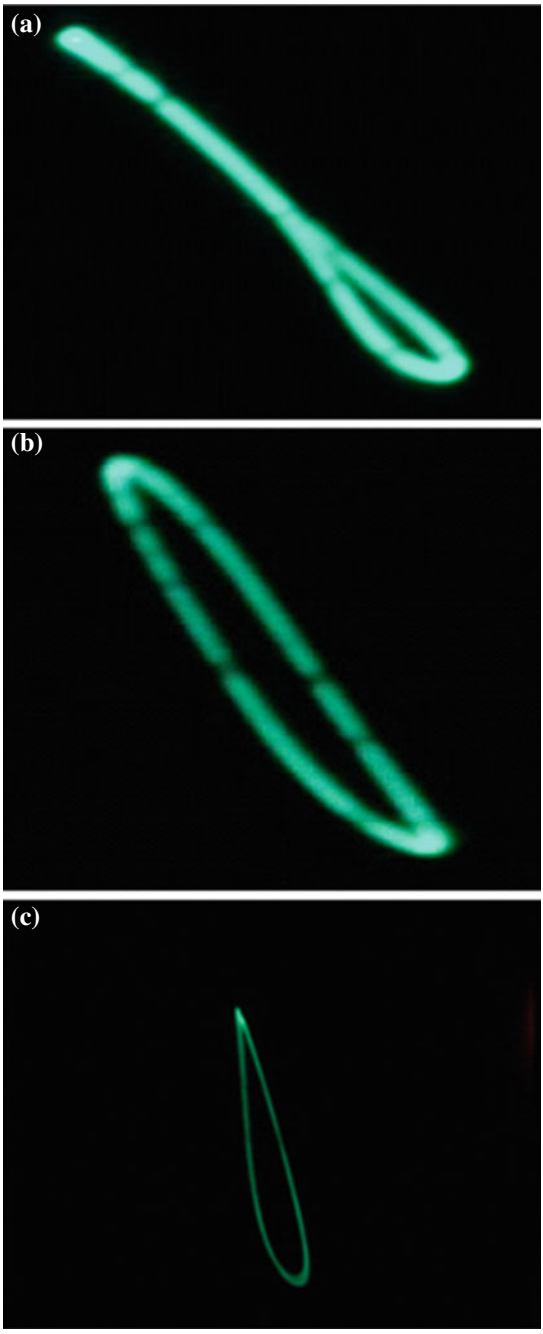

Fig. 18 Experimental results showing response of demodulators based on different PLLs for periodic modulation. **a** TO-PLL, **b** MTO-PLL **c** MTO-PLL with reduced time constant

FM modulators. By tuning a single design parameter, PLL can be driven to chaotic mode in a period doubling route. Additional gain and phase shift of loop filter around characteristic frequency is the cause of unstable dynamics of TO-PLL. We have discussed stability of fixed point and obtained tracking range of a locked PLL and also acquisition range has been obtained by numerical simulation when loop is initially unlocked and then goes to locked state. Difference between these two ranges has been shown and hysteresis around transition boundary confirms the possibility of chaos generation in this range. Unstable TO-PLL could be used as a FM demodulator but modulation index as well as frequency of modulating signal would be dependent on loop design parameters. Availability of multiple design parameters would be of much help for a system designer.

Applicability of PLL-based demodulators to detect self-generated oscillation modulated FM signal is examined in details. In general responses of demodulators degrade for chaotic modulating signals. Large number of component signals in broad bandwidth of a chaotic signal is main cause of degradation. Demodulator PLLs frequency pass band should be flat and as wide as modulating signals bandwidth. With this motivation of design a modified TO-PLL is used as demodulator and better responses are obtained. Physically, loop filter of MTO-PLL becomes effectively proportional integrating and derivative (PID) control type due to proposed structure modification and leads to improved response of demodulator. We have examined performances of modulator and demodulator through prototype hardware experiment. Obtained results agree well with analytical and numerical observations.

7 Conclusion

The study reported in this chapter leads to following conclusions.

1. Unstable mode dynamics of a resonant filter based TO-PLL is rich in complexities but predictable and reproducible. It transits from single period oscillation to chaotic oscillation through period doubling route. As long as the PLL remains in a locked condition to its input reference signal, VCO output can be treated as a frequency modulated signal by self generated oscillations of VCO control signal.
2. Inherent phase shift in the resonant filter is primarily responsible for in-stability in loop operation. A zone of hysteresis is found in the region of transition from stable state to unstable state. This gives acquisition range of loop less than tracking range. During acquisition process loop may go into an oscillatory state, mentioned as “false lock” in literature.
3. Detection of self-generated oscillations of an unstable PLL is possible in a PLL-based FM demodulator. Frequency modulated VCO output of unstable PLL is taken as input of demodulator PLL. While detection is easy for periodic self modulation, for chaotic self-modulation undistorted detection is a bit difficult. Bandwidth of PLL demodulator is to be large having flat amplitude response in the frequency band of modulating chaos. Conventional SO-PLL or a TO-

PLL introduces unavoidable distortions to detected chaos; hence proper detection becomes difficult.
4. Modified TO-PLL is studied which has larger acquisition and tracking zones as well as wide flat amplitude response band width. MTO-PLL has better demodulation capability and can be used for detection of self generated chaos modulated signals.
5. MTO-PLLs loop filter has the properties of proportional-integrating-and-derivative controller. This is the reason of its improved performance. Hardware required for MTO-PLL implementation is not much complex from that of a conventional TO-PLL. So it will be an attractive demodulator of FM signals in general.

Present study suggests that self oscillatory PLLs can be employed in chaos based communication systems. It has potential of controlled chaos generation as well as it provides chaos modulated signals. Changing a gain parameter of the loop electrically, one can map zero-one bit stream of a data sequence into different type of oscillatory signals either periodic or chaotic having different attractors. This can be used in secure communications. Moreover demodulation capability of PLL is studied in this chapter and it is shown that modified TO-PLL could be a useful detector of FM signals. Further studies are required in this direction.

Acknowledgments Authors thankfully acknowledge the infrastructural support provided by Physics department, Burdwan University to carry out this work. They also acknowledge the assistance of Mr. Debdeep Sarkar in different ph1ases of preparation of manuscript.

References

1. Abarbanel HDI, Rulkov NF, Sushchik MM (1996) Generalized synchronization of chaos: the auxiliary system approach. Phys Rev E 53(5):4528
2. AI-Araji SR, Hussain ZM, AI-Qutairi MA (2006) Digital phase locked loops, architecture and applications. Springer, Berlin
3. Banerjee T, Sarkar BC (2006) A new dynamic gain control technique for speed enhancement of digital phase locked loops. Signal Process 86(7):1426–1434
4. Banerjee T, Sarkar BC (2008) Chaos and bifurcation in a third-order digital phase locked loop. AEU: Int J Electron Commun 62(6):459–463
5. Benjamin CK (1995) Automatic control systems. Prentice Hall, Englewood Cliffs
6. Bernstein GM, Liberman MA, Lichtenberg AJ (1989) Nonlinear dynamics of a digital phase locked loops. IEEE Trans Commun 37(3):1062
7. Best RE (2003) Phase-locked loops: design, simulation and applications. McGraw-Hill, New York
8. Best RE, Kuznetsov NV, Leonov GA, Yuldashev MV, Yuldashev RV (2014) Nonlinear analysis of phase-locked loop-based circuits, discontinuity and complexity in nonlinear physical systems. Springer, Berlin
9. Biswas BN (1988) Phase lock theories and applications. Oxford and IBH Publishers, New Delhi
10. Bueno AM, Rigon AG, Ferreira AA, Piqueira JRC (2010) Design constraints for third-order PLL nodes in master-slave clock distribution networks. Commun Nonlinear Sci Numer Simul 15(9):2565–2574

11. Crawford JA (2008) Advanced phase-lock techniques. Artech House, Boston
12. Curran PF, Chuang B, Feely O (2013) Dynamics of charge-pump phase-locked loops. Int J Circuit Theory Appl 41(11):1109
13. Dandapathak M, Sarkar S, Sarkar BC (2014) Nonlinear dynamics of an optical phase locked loop in presence of additional loop time delay. Int J Light Electron Opt Optik 125:7007–7012
14. De B, Sarkar BC (2008) Nonlinear dynamics of nonlinear amplifier based delayed PLL incorporating additional phase modulator. Int J Electron 95(9):939–949
15. Dmitriev AS, Kletsov AV, Kuzmin LV (2008) Generation of RF chaos with PLL circuit. Uspekhi Sovremennoy Radioelektroniki (in Russian) 46
16. Endo T (1994) A review of chaos and nonlinear dynamics in phase locked loops. J Frankl Inst 331(6):859–902
17. Gardner FM (2005) Phase lock techniques. Wiley, Hoboken
18. Harb BA (2014) Effect of time delay on the pull-in range of phase locked loops. J Vibroeng 16(1):369–377
19. Harb BA, Harb MA (2004) Chaos and bifurcation in third-order phase-locked loop. Chaos Solitons Fractals 19(3):463–698
20. Hati A, Sarkar BC (1999) Pump current modulated charge pump PLL. Electron Lett 35(18):1498–1499
21. Kennedy MP, Rovatti R, Setti G (eds) (2000) Chaotic electronics in telecommunications. CRC Press, Boca Raton
22. Korsinova MV, Matrosov VV, Shalfeev VD (1999) Communications using cascade coupled phase-locked loop chaos. Int J Bifurc Chaos 9(5):963–973
23. Kudrewicz J, Wasowicz S (2007) Equations of phase locked loops: dynamics on the circle, torus and cylinder. World Scientific, Singapore
24. Lee T (1998) The design of CMOS radio frequency integrated circuits. Cambridge University Press, Cambridge
25. Leonov GA, Kuznetsov NV, Seledzhi SM (2009) Nonlinear analysis and design of phase-locked loops. Automation control theory and practice. In-Tech
26. Leonov GA, Kuznetsov NV, Yuldashev MV, Yuldashev RV (2012) Analytical method for computation of phase-detector characteristic. IEEE Trans Circuits Syst Part II 10:633
27. Lindsey WC (1972) Synchronization systems in communication and control. Prentice Hall, Englewood Cliffs
28. Lindsey WC, Chie CM (1981) A survey of digital phase lock loops. Proc IEEE 69(4):410–431
29. Matrosov VV (2006) Nonlinear dynamics of phase-locked loop with the second-order filter. Radio phys Quantum Electron 49(4):322–332
30. Ogata K (2002) Modern control engineering. Prentice Hall, Upper Saddle River
31. Piqueira JRC (2009) Using bifurcations in the determination of lock in ranges for third-order phase-locked loops. Commun Nonlinear Sci Numer Simul 14:2328
32. Qananwah QM, Malkawi SR, Harb A (2008) Chaos synchronization of the third-order phase-locked loop. Int J Electron 95:799–803
33. Razavi B (1996) Monolithic phase locked loops and clock recovery circuits. IEEE Press, New York
34. Razavi B (2005) Design of analog CMOS integrated circuits. Tsinghua University Press, Beijing
35. Rohde UL (1983) Digital PLL frequency synthesizers theory and design. Prentice Hall, Englewood Cliffs
36. Sarkar BC (1990) Phase error dynamics of a first order Phase Locked Loop in the presence of co-channel tone interference and additive noise. IEEE Trans Commun 38(7):962–965
37. Sarkar BC, Banerjee T (2006) Speed enhancement of a class of digital phae locked loops by dynamic gain control technique. Int J Electron Commun (AEU) 60:539–544
38. Sarkar BC, Chakraborty S (2014) Self-oscillations of a third order PLL in periodic and chaotic mode and its tracking in a response PLL. Commun Nonlinear Sci Numer Simul 19(3):738–749
39. Sarkar BC, Chakraborty S (2015) Chaotic oscillations in a third order PLL in the face of two co-channel signals and its control. Spec Issue J Eng Sci Technol Rev (JESTR) 8(2):68–73

40. Sarkar BC, Chattopadhyay S (1988) Novel quick response digital phase locked loops. Electron Lett 24(20):1263–1264
41. Sarkar BC, De B (1998) Effect of additional loop time delay on the performance of a nonlinear amplifier-based PLL with and without phase modulator. Int J Electron 84(4):321
42. Sarkar BC, Hati R (1999) Chaos from a second order PLL in the presence of CW interference. Electron Lett 35(15):1217–1218
43. Sarkar BC, Sarkar SSD, Banerjee T (2014) Nonlinear dynamics of a class of symmetric lock range DPLLs with an additional derivative control. Signal Process 94:631–641
44. Schanz MI, Pelster AX (2005) Analytical and numerical investigation of the phaselocked loop with time delay. J Chaos Solitons Fractals 11
45. Stensby JL (1997) Phase-locked loops: theory and applications. CRC Press, USA
46. Stephens DR (1998) Phase locked loops for wireless communications. Kluwer Academic Publishers, Boston
47. Wiegand C, Hedayat C, Hilleringmann U (2010) Non-linear behaviour of charge-pump phase-locked loops. Adv Radio Sci 8:161
48. Wolf A, Swift JB, Swinney HL, Vastano JA (1985) Determining Lyapunov exponents from a time series. Physica D 16:285
49. Zoltowski M (2001) Some advances and refinements in digital phase locked loops. Signal Process 81:735–789

Application of Time-Delayed Feedback Control Techniques in Digital Phase-Locked Loop

Tanmoy Banerjee and B.C. Sarkar

Abstract In this chapter we investigate how time-delayed feedback control (TDFC) techniques can be exploited in controlling chaos and bifurcation in a digital phase-locked loop (DPLL) and thus improve its system response. We use both the TDFC techniques: The conventional one and its extended version. Using local stability analysis, two parameter bifurcation studies and two parameter Lyapunov exponent spectrum we explore the nonlinear dynamics of conventional and controlled DPLLs. A condition for the optimum value of the system control parameter is derived analytically for a TDFC based DPLL. We describe the implementation of the extended time-delayed feedback control (ETDFC) technique in a DPLL. It is observed that the application of the delayed feedback control technique on the sampled values of the incoming signal results in the *nonlinear* time-delayed feedback control on the phase error dynamics. We establish that, for some suitably chosen control parameters, an ETDFC based DPLL has a broader stability zone in comparison with a DPLL and its TDFC version.

1 Intoduction

Control of chaos and bifurcation has been an active field of research for the last two decades [9, 10, 19, 25]. By controlling chaos and bifurcation one can suppress the chaotic behavior where it is unwanted (e.g., in power electronics [14, 24] and mechanical systems [9]), and on the other hand in electronic systems one can exploit chaos in chaos-based electronic communication systems [15]. The methodology of controlling chaos in dynamical systems was first introduced in [21] and is well known as the OGY method. In the OGY method, a physically accessible parameter is perturbed to stabilize a desired unstable periodic orbit (UPO) embedded in the phase

T. Banerjee (✉) · B.C. Sarkar
Department of Physics, University of Burdwan, Burdwan 713104, West Bengal, India
e-mail: tbanerjee@phys.buruniv.ac.in

B.C. Sarkar
e-mail: bcsarkar_phy@yahoo.co.in

S. Vaidyanathan and C. Volos (eds.), *Advances and Applications in Nonlinear Control Systems*, Studies in Computational Intelligence 635,
DOI 10.1007/978-3-319-30169-3_18

space. In practical applications the OGY-method lacks the robustness as it requires accurate sampling of a variable at discrete times in order to compare it with a reference value and involves discontinuous adjustments of the control parameter. A second method, known as the time-delayed feedback control (TDFC) algorithm, proposed by Pyragas [22] is more suitable for practical applications, because in this case no precise knowledge of either the form of the periodic orbit or the system of equations is required. Taking into account only the period of the unstable orbit, the system under control automatically settles on the target periodic motion, and the stability of this motion is maintained with only small perturbations [23]. Later, in Ref. [27] the idea of the TDFC algorithm has been modified by introducing the Extended Time-Delayed Feedback Control (ETDFC) algorithm, which is more effective than the original one because it can stabilize the UPOs of higher periods.

In this chapter we show how time-delayed feedback control techniques are useful in a real engineering system, namely Digital Phase-Locked Loop (DPLL). In general phase locked loops (PLLs) are one of the important building blocks in synchronous communication systems. A PLL is a nonlinear feedback controlled system [12, 16] that is widely used in electronic communication systems as in the form of noise filter, frequency demodulator, frequency synthesizer, etc. PLLs have attracted much attention in the research community owing to their application potentiality and rich nonlinear behavior. At the advent of digital communication systems, digital phase-locked loops (DPLLs) have rapidly replaced the conventional analogue PLLs because DPLLs overcome some of the problems associated with its analog counterpart [18]. DPLLs are commonly used in frequency demodulators, frequency synthesizers, data and clock synchronizers, modems, digital signal processors, hard disk drives, etc. [28]. Many studies on DPLL reveal that the following variants of DPLLs show chaos and bifurcations: positive zero-crossing DPLL (ZC1-DPLL) [1, 3, 5, 7, 17], uniform sampling DPLL [28], bang-bang DPLL [11], dual sampler-based zero crossing DPLL (ZC2-DPLL) [4] and tanlock DPLL [6, 13]. Although several variants of DPLLs exist in the literature but zero-crossing DPLL (ZC-DPLL), which is a non-uniform sampling DPLL, is the most popular one due to their less circuit complexity.

Exploring the time-delayed control technique on DPLLs have two-fold goals; from a designer's point of view, using the control techniques one can design an optimum DPLL system. An optimum DPLL is one that has the fastest convergence behavior, and at the same time a broader frequency acquisition range (FAR). From the view point of electronic communication system, by generating and characterizing the chaos from DPLLs in a controlled manner, one can explore the possibility of using DPLLs in chaos-based electronic communication systems. To simultaneously achieve both of these goals, one has to apply the techniques of control of chaos and bifurcation in DPLLs. But a little work has been reported on the control of chaos and bifurcation of DPLLs.

The present chapter investigates the effect of the delayed feedback control (DFC) techniques on a first-order positive zero-crossing DPLL (ZC1-DPLL). We consider both the ETDFC technique of chaos control and its original version, namely, the TDFC technique. To proceed in a systematic manner, we start by exploring the nonlinear dynamics of a ZC1-DPLL in the parameter space using two parameter bifurcation

diagrams and two parameter Lyapunov exponent spectrum. Next, the TDFC algorithm on a ZC1-DPLL is explored in the parameter space. Also, an estimate of the optimum value of the control parameter is derived analytically. Finally, we describe the controller design algorithm for an ETDFC based ZC1-DPLL (ETDFC-DPLL). A stable zone of operation is identified with the help of local stability analysis, two parameter bifurcation diagrams and two-parameter Lyapunov exponent spectrum. It is found that, for some suitably chosen control parameters, an ETDFC-DPLL has an extended stability zone in comparison with a conventional ZC1-DPLL and a TDFC-DPLL, which will make the ETDFC-DPLL more superior for practical applications.

This chapter is organized in the following manner: The next section describes the structure, system equation formulation and stability analysis of a ZC1-DPLL. Also, the system dynamics in the parameter space is reported here. In Sect. 3, the TDFC algorithm is described and a local stability analysis is performed. The two parameter bifurcation diagram and Lyapunov exponent spectrum are explored. Also, the condition of optimality is derived analytically. Section 4 describes the ETDFC algorithm on a ZC1-DPLL. The stability analysis is followed by the parameter space exploration of the system; numerical search for the optimum control parameter is carried out in this section. Finally, Sect. 5 summarizes the outcome and importance of the study.

2 ZC1-DPLL

2.1 Structure and System Equation Formulation

The functional block diagram of a ZC1-DPLL is shown in Fig. 1. A ZC1-DPLL consists of a sample and hold (S/H) block, a loop digital filter (LDF) and a digitally controlled oscillator (DCO). The incoming signal $e(t)$ is given by: $e(t) = s(t) + n(t)$, where $s(t)$ is the sinusoidal reference signal and $n(t)$ is a noise or unwanted continuous wave interference signal. Let us consider a noise free and interference free (i.e., $n(t) = 0$) unmodulated incoming signal of amplitude A_0, written in term of the angular frequency (ω_0) of the DCO as,

$$e(t) = A_0 \sin(\omega_0 t + \theta(t)). \tag{1}$$

Here we make the substitution $\theta(t) = (\omega_i - \omega_0)t + \theta_0$. Where ω_i is the angular frequency of the incoming signal and θ_0 is a constant phase part. $e(t)$ is sampled by the sampler at the positive zero crossing edges of the incoming signal at the time instants t_k. The time elapsed between the $(k-1)$th and kth instants is given by $T_k = t_k - t_{k-1}$. The sampled value of $e(t)$ at t_k is given by $x_k = e(t_k)$. The sequence of the samples $\{x_k\}$ is filtered by the LDF, which produces the control signal $\{y_k\}$ that in turn controls the period of the DCO at the $(k+1)$th instant with the following algorithm [1]:

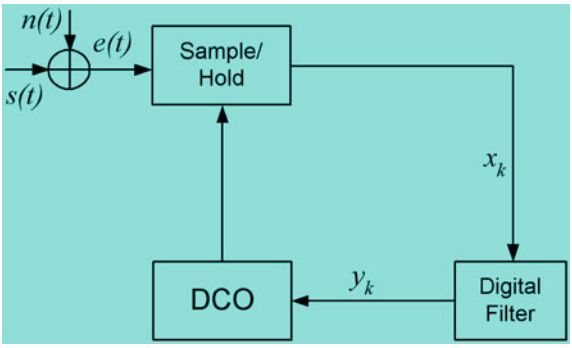

Fig. 1 Functional block diagram of a ZC1-DPLL

$$T_{k+1} = T - y_k, \tag{2}$$

where $T(= 2\pi/\omega_0)$ is the nominal period of the DCO. Taking $t(0) = 0$, one can get the sampling instants t_k as,

$$t_k = kT - \sum_{0}^{k-1} y(i). \tag{3}$$

We define the phase error ϕ_k at the kth instant as:

$$\phi_k = \theta_k - \omega_0 \sum_{0}^{k-1} y(i). \tag{4}$$

where $\theta_k = \theta(t_k)$. Now, for a first-order ZC1-DPLL the LDF is a zeroth order digital filter having only a memory less gain element of gain G_0. Thus the control signal y_k is simply given by: $y_k = G_0 x_k$. This in turn gives the following phase error equation of a first-order ZC1-DPLL,

$$\phi_{k+1} = \Lambda_0 + \phi_k - K_1 \xi \sin(\phi_k) \tag{5}$$

where we define $\xi = \omega_i/\omega_0$ (normalized frequency of the incoming signal), $\Lambda_0 = 2\pi(\xi - 1)$; K_1 is substituted in place of $A_0\omega_0 G_0$, which is defined as the closed loop gain of a 1st-order ZC1-DPLL.

2.2 *Stability Analysis*

We study the dynamics of Eq. (5) near the fixed point, which is a stable phase-locked state, ϕ_s given by

$$\phi_s = \arcsin(\Lambda_0/\xi K_1) \tag{6}$$

For a stable loop operation the condition $\Lambda_0 \leq \xi K_1$ should be obeyed. The system will converge to the fixed point ϕ_s if the condition $|f^{'}(\phi_s)| < 1$ is satisfied, which in turn gives,

$$|1 - \xi K_1 \cos(\phi_s)| < 1. \tag{7}$$

For a phase step input (i.e., if the incoming signal frequency and DCO frequency coincide) $\xi = 1$ and one has two stationary solutions, $\phi_s = 2j\pi$ and $\phi_s = (2j + 1)\pi$ ($j = 0, 1, 2, \ldots$). The former solution is asymptotically stable and the latter solution is Lyapunov unstable [17]. Also, the behavior of the orbits generated by Eq. (5) is bounded by only those ϕ_ks that do not leave the segment $[-\pi, \pi]$ as k grows larger. So, the stability condition of a ZC1-DPLL in the face of a phase step input is given by [20],

$$0 < K_1 < 2 \tag{8}$$

Also, for a frequency step input (i.e., $\omega_i \neq \omega_0$ or $\xi \neq 1$), the stability condition of the loop can be obtained as:

$$0 < (K_1\xi)^2 - \Lambda_0^2 < 4 \tag{9}$$

If the system and signal parameters are restricted within the region given by Eqs. (8) and (9), the loop will converge asymptotically to the period-1 fixed point. The optimum loop operation can be achieved by making $|f^{'}(\phi_s)| = 0$, which gives the condition of fastest convergence as: $\xi K_1 = 1$.

Following observations can be made from the above results: ϕ_s is small for a large K_1 (Eq. (6)). Since ξ is a measure of the FAR, thus to get a large FAR, one has to make K_1 large. But K_1 can not be increased beyond a certain limit, otherwise the system becomes unstable. Also, a larger K_1 results in a poorer convergence behavior of the system. These are the inherent limitations of a ZC1-DPLL. A designer's goal is to design a ZC1-DPLL that will be stable even for a large K_1, which ensures a small ϕ_s and a large FAR; subsequently, it has to be ensured that the system response should not get slower even for a large K_1.

2.3 Two Parameter Bifurcation and Lyapunov Exponent Spectrum

Figure 2 shows the two parameter (2-D) bifurcation diagram in the $K_1 - \xi$ parameter space. It shows that with the deviation of ξ from unity, K_1 has to be made large in order to get a stable locked state (i.e., period-1 state). Further, with an increasing K_1, beyond a certain value of K_1, the system losses its locked state through a period doubling bifurcation. For a quantitative measure we compute the Lyapunov exponent (LE) [26] of the system, which is defined by:

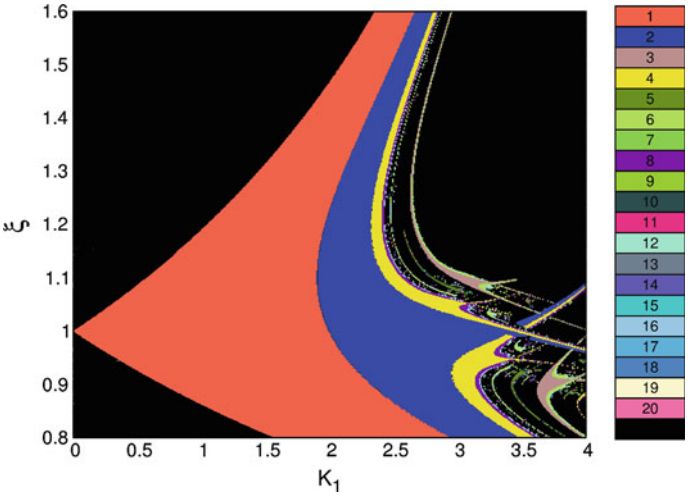

Fig. 2 Two parameter bifurcation diagram in the $K_1 - \xi$ parameter space. *Black zone* indicates the chaotic or higher periodic solutions. Numbers in the *color-box* indicate the period of oscillations

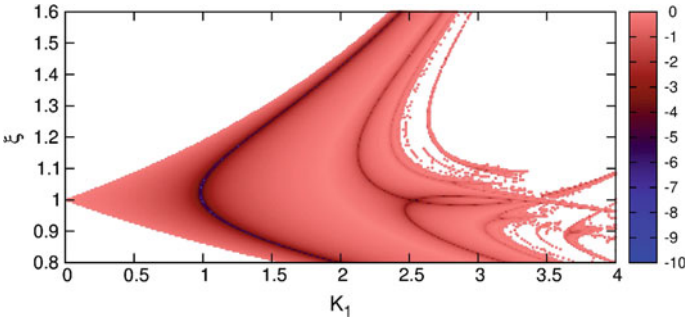

Fig. 3 Two parameter Lyapunov exponent spectrum in the $K_1 - \xi$ parameter space, *white zone* indicates the chaotic region

$$\lambda = lim_{N\to\infty}\frac{1}{N}\sum_{i=1}^{N}\ln|1 - \xi K_1\cos(\phi_i)| \tag{10}$$

We take the number of iterations $N = 20{,}000$ skipping the first 5000 iteration to allow the transients to settle down. The spectrum of negative LEs in the parameter space is shown in Fig. 3, which agrees with the 2-D bifurcation diagram. Note that, for $\xi = 1$ and $K_1 = 1$, the LE is minimum (from the color code of Fig. 3) that indicates the optimum (i.e., fastest) loop operation. White zone corresponds to the positive LE, which ensures the occurrence of chaos in the system. Figure 4 shows the single parameter (1-D) bifurcation diagram of ϕ_k with K_1 as the control parameter for $\xi = 1.1$. It shows that the period-1 locked state losses its stability through a period

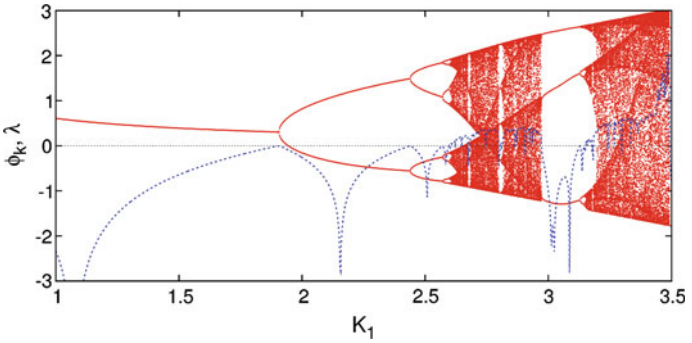

Fig. 4 Bifurcation diagram (*red*) and Lyapunov exponent (λ) (*blue*) with K_1 as the control parameter ($\xi = 1.1$)

doubling bifurcation at $K_1 = 1.906$; with increasing K_1 the system enters into the chaotic zone through a cascade of period doubling bifurcations. The corresponding LE is also shown in the same figure that is in accordance with the 1-D bifurcation diagram. Further, we can see that the 1-D and 2-D bifurcation diagrams agree with each other.

3 Time-Delayed Feedback Controlled ZC1-DPLL (TDFC-DPLL)

3.1 Controller Design

Figure 5 shows a ZC1-DPLL with the TDFC algorithm (TDFC-DPLL). The TDFC algorithm is realized on the sampled values x_k of the ZC1-DPLL. In a TDFC-DPLL a time-delayed feedback controlled signal is generated by subtracting the sampled value at the $(k-1)$th instant (i.e., x_{k-1}) from that at the kth instant (i.e., x_k) with some weight factor β; that is, the TDFC signal is given by: $x_k^{td} = \beta(x_k - x_{k-1})$. The LDF input signal x_k^c at the kth sampling instant is the sum of x_k and x_k^{td} (unlike a ZC1-DPLL, where the LDF input signal is simply x_k); that is,

$$x_k^c = x_k + x_k^{td}. \tag{11}$$

x_k^c is filtered by a zeroth order LDF and its output, $y_k^c = G_0 x_k^c$, is used to control the period of the DCO. Using the similar arguments of the previous section one can easily arrive at the following phase error equation of a TDFC-DPLL:

$$\phi_{k+1} = \Lambda_0 + \phi_k - K_1\xi \sin(\phi_k) - K_1\xi\beta(\sin(\phi_k) - \sin(\phi_{k-1})) \tag{12}$$

If we put $\beta = 0$, system Eq. (12) reduces to that of a ZC1-DPLL, i.e., Eq. (5).

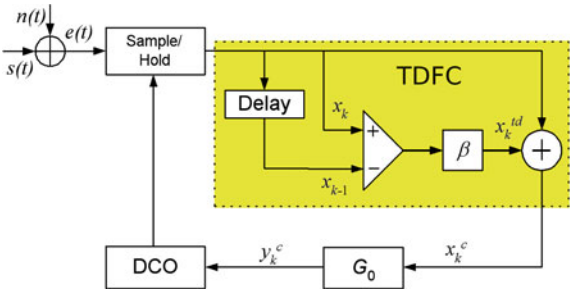

Fig. 5 Block diagram of a TDFC-DPLL. The *delay block* indicates a unit delay

An interesting observation can be made from Eq. (12), the application of the TDFC algorithm on the sampled values x_k finally results in the *nonlinear* time-delayed feedback control (NL-TDFC) algorithm on the system phase error dynamics. One can expect that the exact analytical solution for the ZC1-DPLL based on this NL-TDFC algorithm is difficult, and where impossible, we have to resort to numerical tools.

3.2 Stability Analysis

For the local stability analysis of Eq. (12) around the fixed point ϕ_s we define two new state variables as $p_k = \phi_k$ and $q_k = \phi_{k+1}$, and we can write the following relations:

$$\begin{pmatrix} p_{k+1} \\ q_{k+1} \end{pmatrix} = \begin{pmatrix} q_k \\ \Lambda_0 + q_k - K_1\xi \sin(q_k) - K_1\xi\beta(\sin(q_k) - \sin(p_k)) \end{pmatrix} \tag{13}$$

As can be seen from Eq. (12), a TDFC-DPLL and a ZC1-DPLL have the same steady state phase error ϕ_s. To investigate the local stability, one has to define the Jacobian near ϕ_s:

$$J = \begin{pmatrix} 0 & 1 \\ K_1\xi\beta\cos(\phi_s) & 1 - K_1\xi(1+\beta)\cos(\phi_s) \end{pmatrix} \tag{14}$$

The characteristic equation is given by:

$$z^2 - J_2 z - J_1 = 0. \tag{15}$$

where we use the following substitutions: $J_1 = K_1\xi\beta\cos(\phi_s)$ and $J_2 = 1 - K_1\xi(1+\beta)\cos(\phi_s)$. The Jury stability criteria for the stable loop operation are:

$$|-J_1| < 1 \tag{16a}$$
$$1 - J_2 - J_1 > 0 \tag{16b}$$
$$1 + J_2 - J_1 > 0 \tag{16c}$$

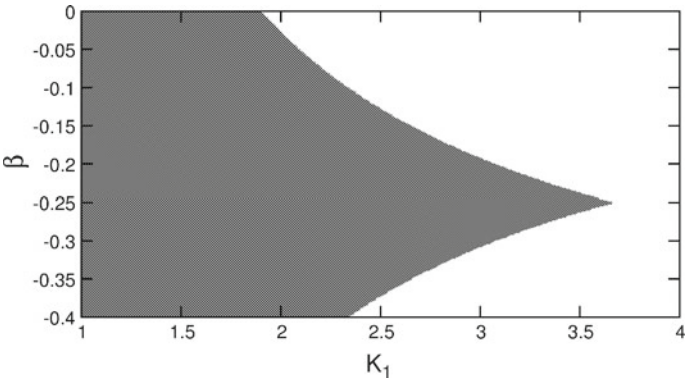

Fig. 6 Analytical stability zone (*shaded region*) in $K_1 - \beta$ space with $\xi = 1.1$

Using the above criteria, the following stability conditions for a TDFC-DPLL can be derived:

$$0 < (K_1\xi)^2 - \Lambda_0^2 < \frac{4}{(1+2\beta)^2} \tag{17a}$$

$$|\beta^2((K_1\xi)^2 - \Lambda_0^2)| < 1. \tag{17b}$$

Equation (17) is graphically shown in Fig. 6, which shows the stable locked state of the system in the $K_1 - \beta$ parameter space for $\xi = 1.1$. It can be seen that, a negative value of β has to be chosen such that for a given ξ, K_1 can be made large without making the system unstable. For example, if we take $\beta = -0.246$, for $\xi = 1.1$ one has $K_1^{\max} = 3.624$, where $K_1^{\max}$ is the largest possible value of K_1 in a stable locked condition (at this condition $K_1^{\max}$ for a ZC1-DPLL is 1.906). Thus, for a TDFC-DPLL we have a larger K_1 value compared to that of a ZC1-DPLL in the stable locked state of operation.

3.3 Two Parameter Bifurcation and Lyapunov Exponent Spectrum

To explore the dynamics of a TDFC-DPLL we employ bifurcation diagrams in the two-dimensional parameter space. In practical cases frequency of the incoming signal does not coincide with the DCO frequency, i.e., most of the signal inputs are frequency step in nature (i.e., $\xi \neq 1$); the phase step input ($\xi = 1$) is only a special case. So, in our numerical exploration, we consider the frequency step input with $\xi = 1.1$. Two-parameter bifurcation diagram in the $K_1 - \beta$ parameter space is shown in Fig. 7, which shows that there exists a certain value of β for which a TDFC-DPLL allows the

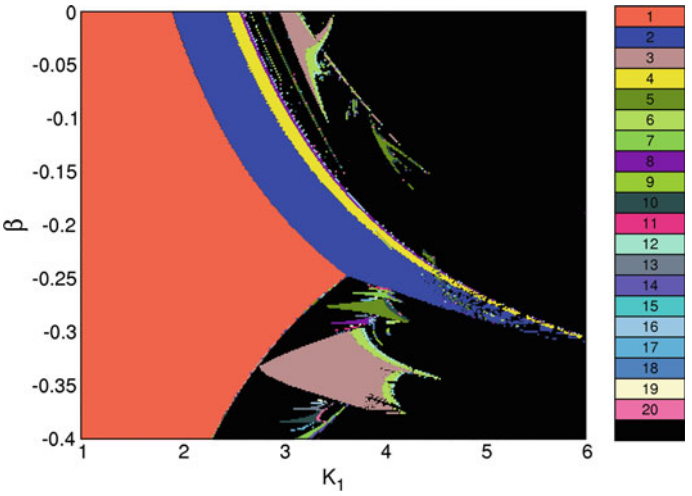

Fig. 7 Two parameter bifurcation diagram in the $K_1 - \beta$ parameter space with $\xi = 1.1$. *Black zone* indicates the chaotic or higher periodic solutions

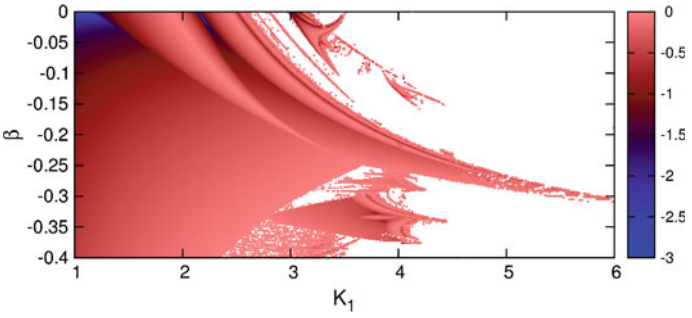

Fig. 8 Two parameter largest Lyapunov exponent (LE) spectrum, *white zone* indicates the chaotic region. ($\xi = 1.1$)

largest loop gain K_1 (say $K_1^{\max}$) under the stable locked state, i.e., period-1 state. For example, in this figure one has $K_1^{\max} = 3.624$ for $\beta = -0.246$, which agrees with the stability analysis of the previous subsection. For a quantitative support to the 2-D bifurcation diagram, we compute the largest Lyapunov exponent (LE) spectrum in the $K_1 - \beta$ space; Fig. 8 depicts the negative largest LE spectrum. White zone indicates the zone of positive LEs, i.e., the chaotic zone of the system. It agrees with the 2-D bifurcation diagram.

Bifurcation diagram with K_1 as the control parameter, with $\beta = -0.246$, is shown in Fig. 9, which shows that the system losses the locked state through a period doubling bifurcation at $K_1 > 3.624$ that is in accordance with the 2-D bifurcation diagram and the stability analysis. The same figure shows the variation of the largest LEs with

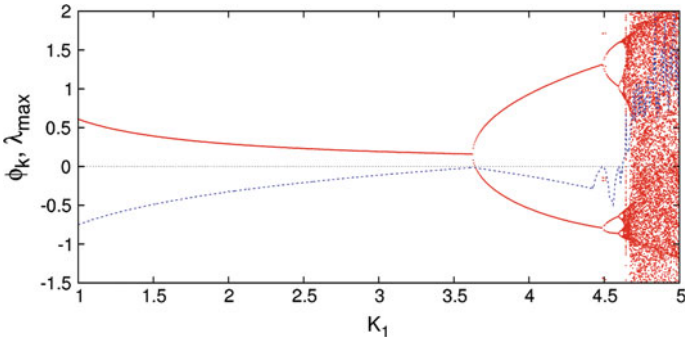

Fig. 9 Bifurcation diagram (*red*) and largest LE (λ_{max}) (*blue*) with K_1 as the control parameter ($\xi = 1.1$, $\beta = -0.246$)

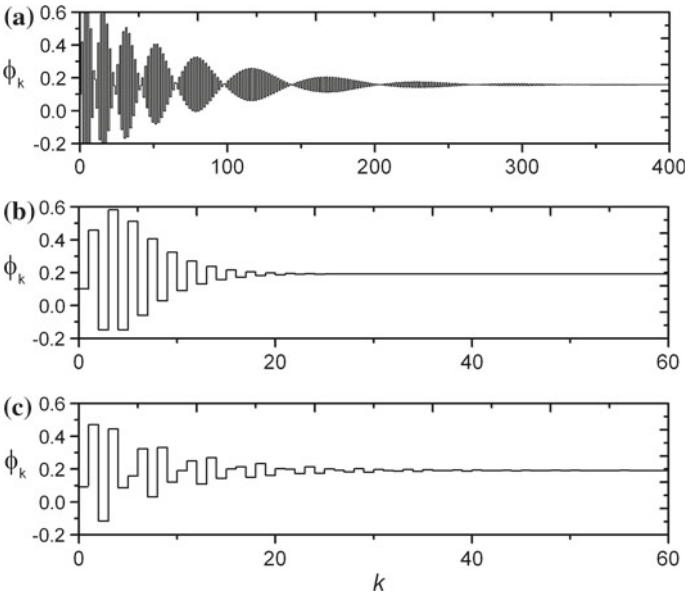

Fig. 10 Real time variation of phase error (with $\xi = 1.1$) **a** $K_1 = 3.62$, $\beta = -0.246$ **b** $K_1 = 3$, optimum value $\beta = -0.198$ **c** $K_1 = 3$, non-optimum value $\beta = -0.24$

K_1, that also agrees with the 2-D LE spectrum in the parameter space (i.e., Fig. 8). Time variation of ϕ_k is shown in Fig. 10a for $K_1 = 3.62$ and $\beta = -0.246$, which shows that the system converges to a locked state (i.e., period-1 state), whereas at this large value of K_1 a conventional ZC1-DPLL becomes chaotic.

3.4 Optimum Value of β

Two parameters are commonly used to characterize the performance of a ZC1-DPLL, one is the frequency acquisition range (FAR) and the other one is the convergence time (CT) of the system to the steady state. In a practical situation it is necessary that a ZC1-DPLL must have a large FAR, and at the same time a small CT. It has been observed that, for a conventional ZC1-DPLL, the FAR increases with increasing loop gain parameter K_1, but the CT is minimum for $K_1\xi = 1$; the CT increases with increase of K_1 [2]. Thus, a faster transient response and a broader acquisition range can not be achieved simultaneously in a ZC1-DPLL. Since in a TDFC-DPLL one can extend the largest possible value of K_1 in the stable locked zone, then at this large value of K_1, the CT will be increased. Thus, in a TDFC-DPLL we have to search for an optimum value of β for which the response of the system is fastest even for a large K_1. It has been shown in Refs. [8, 24] that to achieve the optimum condition we have to find out the parameter values for which the spectral radius of J of Eq. (14) is minimum, which is equivalent to make the discriminant of J equal to zero, i.e.,

$$J_2^2 + 4J_1 = 0 \tag{18}$$

That gives the optimum value of β as:

$$\beta = -\frac{1}{\sqrt{L}}((\sqrt{L}+1) - 2L^{\frac{1}{4}}), \tag{19}$$

where, $L = (\xi K_1)^2 - \Lambda_0^2$.

For example, according to Eq. (19), for $\xi = 1.1$ and $K_1 = 3$, the optimum value of β is -0.198. Figure 10 b, c shows the real time convergence behavior of a TDFC-DPLL for an optimum and non-optimum value of β, respectively. It can be seen that the CT is lesser for the optimum value of β. Using Eq. (19) we plot Fig. 11 that shows

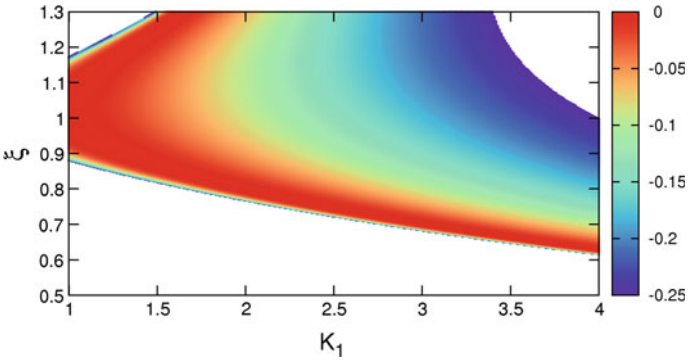

Fig. 11 Optimum value of β in the $K_1 - \xi$ parameter space. *White region* indicates the out of locked states

the optimum values of β in the $K_1 - \xi$ parameter space. From the color map it can be observed that, for a particular value of ξ, if we increase K_1, the optimum value of $|\beta|$ increases; also, this increasing nature is observed for a value of ξ far from unity with a fixed K_1.

4 Extended Time-Delayed Feedback Controlled ZC1-DPLL (ETDFC-DPLL)

4.1 Controller Design

Figure 12 shows the Extended Time-Delayed Feedback Controlled ZC1-DPLL (ETDFC-DPLL) along with the controller design algorithm. The ETDFC technique extends the effect of many previous states to the present output with a decaying weight as we go further in the past [27]. Note that, to achieve this goal only two unit delay elements are used. The controller output x_k^{etd} is defined as:

$$x_k^{etd} = \beta\left(x_k - (1-r)\sum_{l=1}^{k} r^{(l-1)} x_{k-l}\right) \tag{20}$$

Note the limit of the new control parameter r: $0 \leq r < 1$. For $r = 0$, an ETDFC-DPLL reduces to a TDFC-DPLL. Here the input to the LDF is,

$$x_k^c = x_k + x_k^{etd}, \tag{21}$$

For convenience, let us redefine x_k^{etd} as: $x_k^{etd} = \zeta_k$. Then one can write,

$$\zeta_k = \beta(x_k - x_{k-1}) + r\zeta_{k-1} \tag{22}$$

i.e., the input to the LDF can be written as

$$x_k^c = x_k + \beta(x_k - x_{k-1}) + r\zeta_{k-1} \tag{23}$$

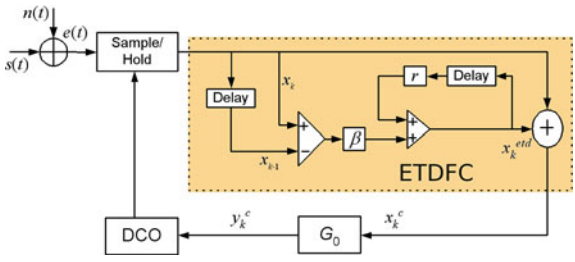

Fig. 12 Block diagram of an ETDFC-DPLL. *Delay blocks* indicate unit delay

The control signal is achieved from the output of the LDF as: $y_k^c = G_0 x_k^c$; after simplifications one can arrive at the phase error equation of the system:

$$\phi_{k+1} = \Lambda_0 + \phi_k - K_1\xi\sin(\phi_k) - K_1\xi\beta(\sin(\phi_k) - \sin(\phi_{k-1})) - r\xi\omega_0 G_0\zeta_{k-1} \quad (24)$$

Now, let us define $\psi_k = \omega_0 G_0 \zeta_k$. Thus, finally we get the following phase error equations that describe the system:

$$\phi_{k+1} = \Lambda_0 + \phi_k - K_1\xi\sin(\phi_k) - K_1\xi\beta\left(\sin(\phi_k) - \sin(\phi_{k-1})\right) - r\xi\psi_{k-1} \quad (25a)$$

$$\psi_{k+1} = \beta\left(\sin(\phi_{k+1}) - \sin(\phi_k)\right) + r\psi_k \quad (25b)$$

Here also, the application of the ETDFC algorithm on the sampled values x_k finally results in the *nonlinear* extended time-delayed feedback control (NL-ETDFC) algorithm on the system phase error dynamics. One can see that, by putting $r = 0$ in Eq. (25), one gets the phase governing equation of a TDFC-DPLL (i.e., Eq. 12), also $r = 0$ along with $\beta = 0$ reduce Eqs. (25)–(5), i.e., the phase error equation for a conventional ZC1-DPLL.

4.2 Stability Analysis

To analyze the stability criteria of an ETDFC-DPLL, let us define $\alpha_k = \phi_k$, $\eta_k = \phi_{k+1}$. Thus, one gets

$$\begin{pmatrix} \alpha_{k+1} \\ \eta_{k+1} \\ \psi_{k+1} \end{pmatrix} = \begin{pmatrix} \eta_k \\ \Lambda_0 + \eta_k - K_1\xi\sin(\eta_k) - K_1\xi\beta(\sin(\eta_k) - \sin(\alpha_k)) - r\xi\psi_k \\ \beta(\sin\eta_k - \sin\alpha_k) + r\psi_k \end{pmatrix} \quad (26)$$

The steady state phase error is same as ϕ_s of Eq. (6). The Jacobian of the system around the fixed point ϕ_s is:

$$J = \begin{pmatrix} 0 & 1 & 0 \\ J_1 & J_2 & J_3 \\ -\beta K_1\cos(\phi_s) & \beta K_1\cos(\phi_s) & r \end{pmatrix}. \quad (27)$$

Here we define $J_3 = -\xi r$. The characteristic equation is given by:

$$z^3 - (J_2 + r)z^2 - (J_1 - J_2 r + J_3\beta K_1\cos(\phi_s))z = 0 \quad (28)$$

Using the Jury stability analysis, one gets the following stability conditions:

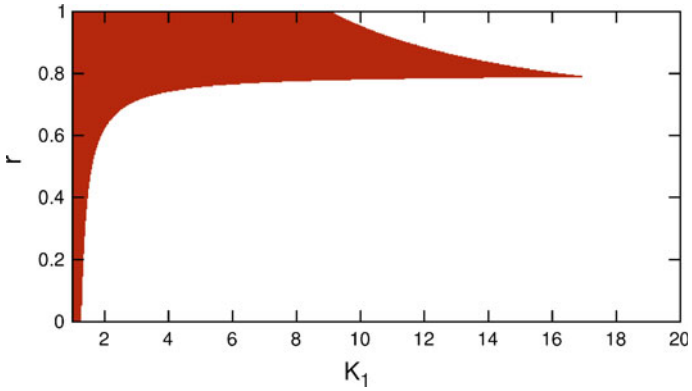

Fig. 13 Analytical stability zone (*colored region*) in $K_1 - r$ space with $\beta = -0.8$ and $\xi = 1.1$

$$0 < (K_1\xi)^2 - \Lambda_0^2 < \frac{4(r+1)^2}{(1+r+2\beta)^2} \tag{29a}$$

$$|(\beta + r)\sqrt{(K_1\xi)^2 - \Lambda_0^2} - r| < 1. \tag{29b}$$

It is noteworthy that if we put $r = 0$ in Eq. (29), it reduces to the stability condition of a TDFC-DPLL (i.e., Eq. (17)). Figure 13 shows the analytically obtained stable locked zone of an ETDFC-DPLL (with $\xi = 1.1$ and $\beta = -0.8$), which shows that one can have a much larger value of K_1 (e.g., $K_1^{\max} = 16.67$ for $r = 0.796$) in comparison with a ZC1-DPLL and a TDFC-DPLL.

4.3 Two Parameter Bifurcation and Lyapunov Exponent Spectrum

Extensive numerical simulation is carried out on an ETDFC-DPLL to explore the system dynamics in the parameter space. As before, in the numerical simulations we have chosen a more general input condition, i.e., a frequency step input with $\xi = 1.1$. Figure 14 shows the two parameter bifurcation diagram in the $K_1 - r$ parameter space with $\beta = -0.8$. Numerically obtained period-1 zone agrees with the analytically obtained stable locked zone (Fig. 13). It can be seen from the figures that for $\beta = -0.8$ at $r = 0.796$ we get $K_1^{\max} = 16.67$, which is more than eight (four) times the value of that of a conventional (TDFC-) ZC1-DPLL. It is found that as β is decreased $K_1^{\max}$ increases with increasing r, which is in accordance with the stability analysis. Further, to give a quantitative support to the 2-D bifurcation result we have computed the largest Lyapunov exponent (LE) spectrum in the $K_1 - r$ space using time series analysis. Figure 15 shows the region of negative largest LEs (i.e., the non chaotic region) in the $K_1 - r$ parameter space that agrees with the 2-D bifurcation diagram.

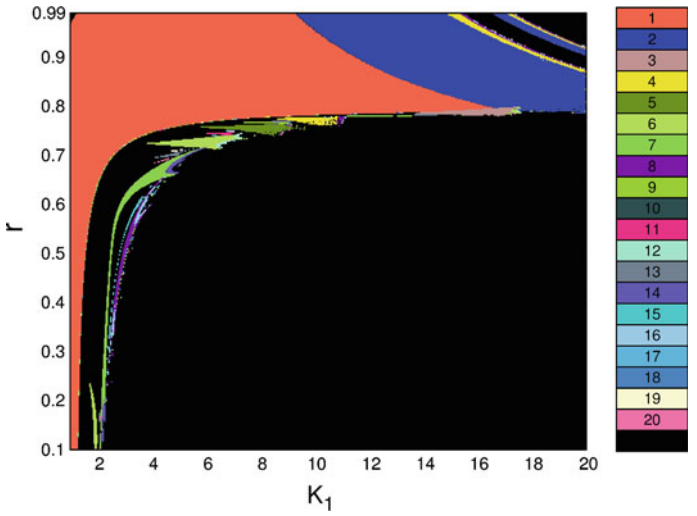

Fig. 14 Two parameter bifurcation diagram in the $K_1 - r$ parameter space with $\xi = 1.1$ and $\beta = -0.8$. *Black zone* indicates the chaotic or higher periodic solutions

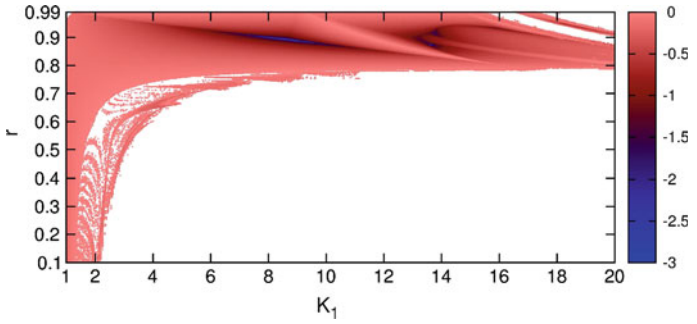

Fig. 15 Two parameter largest Lyapunov spectrum in the $K_1 - r$ parameter space ($\xi = 1.1$), $\beta = -0.8$. *White zone* indicates the chaotic zone

White zone represents the region of positive LEs that indicates the occurrence of chaos. 2-D bifurcation diagrams in the $\beta - r$ parameter space (with $K_1 = 6$) and $K_1 - \beta$ parameter space (with $r = 0.5$) are shown in Fig. 16 a and b, respectively. From Fig. 16a we can see that for a large K_1 one can choose a broad range of parameter values from the $\beta - r$ parameter space to get a phase-locked state. The same is true for the $K_1 - \beta$ parameter space, also. Thus, we can draw an inference that the ETDFC technique provides options to choose a suitable parameter values to achieve a stable phase-locked state.

Figure 17 shows the bifurcation diagram and largest LE ($\lambda_{\max}$) of the system with K_1 as the control parameter for $\beta = -0.8$ and $r = 0.796$. It shows that the stable locked state losses its stability through a period doubling bifurcation at $K_1 > 16.67$

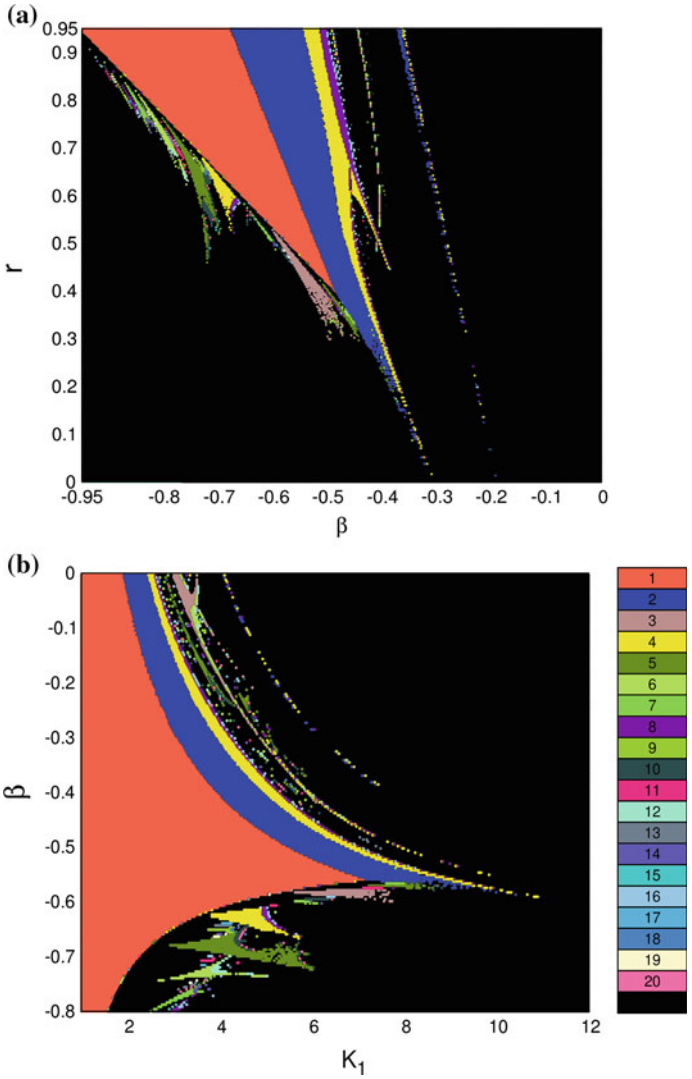

Fig. 16 Two parameter bifurcation diagram in **a** $\beta - r$ parameter space, $\xi = 1.1$, $K_1 = 6$ **b** $K_1 - \beta$ parameter space, $\xi = 1.1$, $r = 0.5$. *Black zone* indicates the chaotic or higher periodic solutions

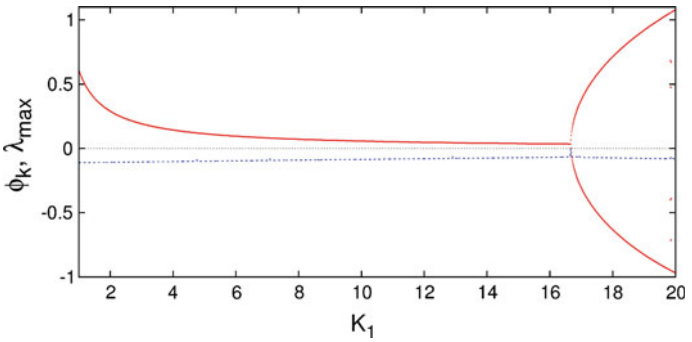

Fig. 17 Bifurcation diagram (*red*) and largest LE (λ_{max}) (*blue*) with K_1 as the control parameter ($\xi = 1.1$, $\beta = -0.8$, $r = 0.796$)

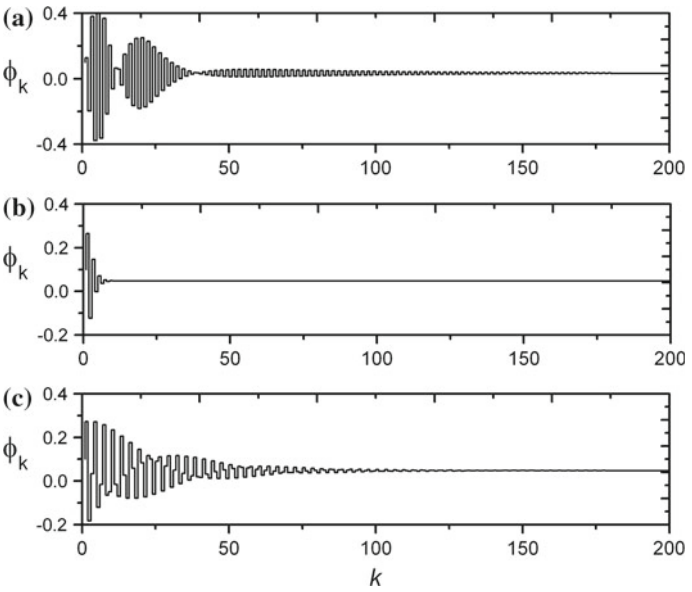

Fig. 18 Real time variation of phase error (with $\xi = 1.1$, $\beta = -0.8$) **a** $K_1 = 16.60$, $r = 0.796$ **b** $K_1 = 12$, optimum value $r = 0.853$ **c** $K_1 = 12$, non-optimum value $r = 0.79$

that agrees with the 2-D bifurcation diagram and clearly proves the extension of stability range (i.e., K_1^{max}) with the proper choice of the control parameter. From the figure it is important to note that the steady state phase error (ϕ_s) decreases with increasing K_1, e.g., at $K_1 = 16$, $\phi_s = 0.035$, whereas at $K_1 = 1$ we have $\phi_s = 0.570$. Small ϕ_s is essential for application of a ZC1-DPLL in the coherent communication systems. Figure 18a shows the time variation of ϕ_k for $\xi = 1.1$, $K_1 = 16.60$, $\beta = -0.8$ and $r = 0.796$ that shows the convergence of an ETDFC-DPLL to the stable

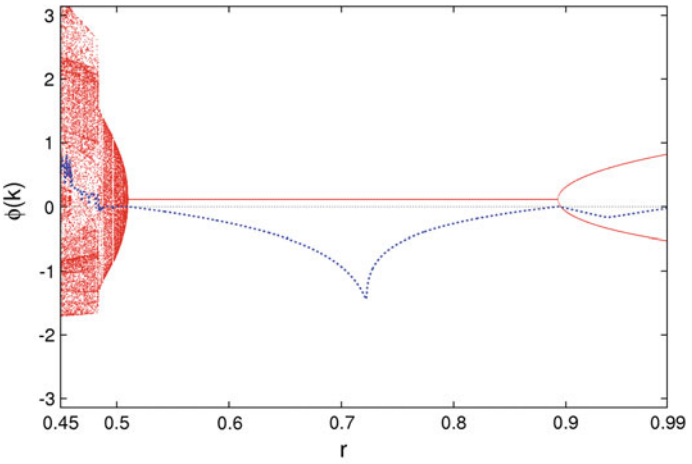

Fig. 19 Bifurcation diagram with r. Other parameters are: $\xi = 1.1$, $K_1 = 5$ and $\beta = -0.6$

locked state; whereas at this large value of K_1 a TDFC-DPLL or a conventional ZC1-DPLL become unstable.

Further, we explore the effect of variation of r for fixed K_1 and β. We observed many complex behaviors: An exemplary result is shown in Fig. 19 for $\xi = 1.1$, $K_1 = 5$ and $\beta = -0.6$. One can see that the increasing r destabilizes the phase-locked condition (at $r \approx 0.9$) through a period doubling bifurcation. But in the low r regime the system goes into chaotic mode through a quasiperiodic route (at $r \approx 0.52$). It can be seen that in the quasiperiodic region the value of Lyapunov exponent becomes zero, which indeed quantify the quasiperiodic behavior.

5 Conclusion

In this chapter we have studied the effect of the ETDFC algorithm and its original version, the TDFC algorithm, on a ZC1-DPLL. At first we have explored the nonlinear dynamics of a ZC1-DPLL in the parameter space. Next, we have investigated the stability criteria of a TDFC and an ETDFC based ZC1-DPLL using local stability analysis, 2-D bifurcation analysis and 2-D Lyapunov exponent spectrum. Subsequently, we have identified the optimal condition of operation of the controlled system. Let us summarize the results obtained in our study and also discuss their importance from the perspective of practical communication systems:

- We have proved that for some suitably chosen system parameters, the largest possible value of loop gain under the stable locked condition of an ETDFC-DPLL is larger than that of a ZC1-DPLL and a TDFC-DPLL (see Eqs. (29), (17) and (9)).

Thus, by wisely choosing the system control parameters one can extend the stable locked zone of operation in an ETDFC-DPLL.

- We have identified the optimality condition for which the system can have the fastest convergence even for a large loop gain parameter K_1. Large value of K_1 means a large frequency acquisition range (FAR). Thus in an ETDFC-DPLL one can obtain a large FAR simultaneously with a small CT by choosing the proper design parameters.
- The inherent disadvantage of a first-order ZC1-DPLL is that, it has a non-zero steady state phase error for a frequency step input. This nonzero steady-state phase error gives rise to a phase offset between the input and recovered carrier that precludes the use of ZC1-DPLLs in a coherent demodulation application. In an ETDFC-DPLL one can operate in a large K_1 value, which ensures a very small (almost zero) steady state phase error that is advantageous in the coherent or synchronous communication systems.
- Another inherent limitation of a ZC1-DPLL is that the loop gain depends upon the incoming signal power (as can be seen from the definition, $K_1 = A_0\omega_0 G_0$). Thus, the variation of signal power may make the system unstable [1]. To alleviate this problem an automatic gain control arrangement is used in the practical ZC1-DPLL that increases the design complexity and at the same time affects the phase part of the incoming signal. But as an ETDFC-DPLL can withstand a large K_1, thus the variation of input signal power will be less effective for this loop.

Since all the time delay techniques discussed here can be implemented in hardware level using the FPGA based systems, thus we believe that the control algorithms can be tested in real experimental set up.

References

1. Banerjee T, Sarkar BC (2005) Phase error dynamics of a class of modified second order digital phase-locked loops in the background of co channel interference. Signal Process 85:1611–1622
2. Banerjee T, Sarkar BC (2006) A new dynamic gain control technique for speed enhancement of digital phase locked loops (DPLLs). Signal Process 86:1426–1434
3. Banerjee T, Sarkar BC (2008) Chaos and bifurcation in a third-order digital phase locked loop. Int J Electron Commun 62:86–91
4. Banerjee T, Sarkar BC (2009) Chaos, intermittency and control of bifurcation in a ZC2-DPLL. Int J Electron 96:717–732
5. Banerjee T, Sarkar BC (2012) Conventional and extended time delayed feedback controlled zero-crossing digital phase locked loop. Int J Bifurc Chaos 22:1230044
6. Banerjee T, Paul B, Sarkar BC (2013) Bifurcation, chaos and their control in a time-delay tanlock loop. Int J Bifurc Chaos 23:1330029
7. Bernstein GM, Liberman MA, Lichtenberg AJ (1989) Nonlinear dynamics of a digital phase locked loop. IEEE Trans Commun 37:1062–1070
8. Callier F, Desoer C (1991) Linear system theory. Springer, London
9. Chen G, Hill DJ, Yu XH (2003) Bifurcation control: theory and applications. Springer, Germany
10. Collado A, Suarez A (2005) Application of bifurcation control to practical circuit design. IEEE Trans Microw Theory Tech 53:2777–2788

11. Dalt ND (2005) A design oriented study of the nonlinear dynamics of a digital bang-bang PLLs. IEEE Trans Circuit Syst—I 52:21–31
12. Gardner FM (1979) Phaselock techniques, 2nd edn. Wiley, New york
13. Hussain ZM, Boashash B (2002) The time-delay digital tanlock loop: Performance analysis in additive gaussian noise. J Frankl Inst 399:43–60
14. Iu HHC, Robert B (2003) Control of chaos in a PWM current-mode H-bridge inverter using time-delayed feedback. IEEE Trans Circuits Syst—I 50:1125–1129
15. Kennedy MP, Rovatti R, Setti G (2000) Chaotic electronics in telecommunications. CRC Press, Florida
16. Kudrewicz J, Wasowicz S (2007) Equations of phase-locked loops: dynamics on the circle, torus and cylinder. World Scientific Publishing, Singapore
17. Leonov GA, Seledzhi SM (2005) Stability and bifurcations of phase locked loops for digital signal processors. Int J Bifurc Chaos 15:1347–1360
18. Lindsey WC, Chie CM (1981) A survey of digital phase lock loops. Proc IEEE 69:410–431
19. Ling BWK, Iu HHC, Lam HK (2009) Control of chaos in nonlinear circuits and systems, volume 64 of world scientific series on nonlinear science, Series A. World Scientific
20. Osborne HC (1980) Stability analysis of an N-th power digital phase-locked loop. I and II. first order second and third order DPLLs. IEEE Trans Commun COM–28:1343–1364
21. Ott E, Grebogi C, Yorke JA (1990) Controlling chaos. Phys Rev Lett 64:1196–1199
22. Pyragas K (1992) Continuous control of chaos by self-controlling feedback. Phys Lett A 170:421–428
23. Pyragas K (2006) Delayed feedback control of chaos. Phil Trans R Soc A 364:2309–2334
24. Robert B, Feki M, Iu HHC (2006) Control of a PWM inverter using proportional plus extended time-delayed feedback. Int J Bifurc Chaos 16:113–128
25. Schöll E, Schuster HG (eds) (2007) Handbook of chaos control. Willey, Germany
26. Schuster HG, Just W (2005) Deterministic chaos: an introduction. Wiley, VCH Weinheim
27. Socolar JES, Sukow DW, Gauthier DJ (1994) Stabilizing unstable periodic orbits in fast dynamical systems. Phy Rev E 50:3245–3248
28. Zoltowski M (2001) Some advances and refinements in digital phase locked loops (DPLLs). Signal Process 81:735–789

Modeling and Predictive Control of Nonlinear Hybrid Systems Using Mixed Logical Dynamical Formalism

K. Halbaoui, M.F. Belazreg, D. Boukhetala and M.H. Belhouchat

Abstract This work deals with the modeling and the control of hybrid systems by using Mixed Logical Dynamical (MLD) system framework described by interdependent physical laws, logic rules, and operating constraints. These are describe by linear dynamic equations subject to linear inequalities involving real and integer variables. The changes which may appear over such dynamics, are modeled by using the auxiliary variables which take into account the interconnections effects. The MLD model is used to synthesize the model predictive control law (MPC). The discrete-time equivalent of the model predicts the hybrid system behavior over a prediction horizon. The controller requires solution of on line mixed integer quadratic or linear program to solve an optimization problem. Simulation was performed using HYSDEL compiler and APROS software to illustrate performances and efficiently of these tools using the model of a three-tank COSY benchmark.

Keywords Hybrid system · Non-linear systems · Mixed logical and dynamical · Model predictive control · Mixed integer quadratic programming · APROS

K. Halbaoui (✉) · M.F. Belazreg · M.H. Belhouchat
Nuclear Research Centre of Birine, Djelfa, Algeria
e-mail: khalbaoui@ieee.org

M.F. Belazreg
e-mail: faouzi.belazreg@gmail.com

M.H. Belhouchat
e-mail: bmohdz@hotmail.com

D. Boukhetala
National Polytechnic School, Algiers, Algeria
e-mail: djamel.boukhetala@g.enp.edu.dz

S. Vaidyanathan and C. Volos (eds.), *Advances and Applications in Nonlinear Control Systems*, Studies in Computational Intelligence 635,
DOI 10.1007/978-3-319-30169-3_19

1 Introduction

The term "hybrid systems" refers to categories of systems that explicitly involve simultaneously phenomena or dynamic type models continuous and event type. These systems are typically composed of continuous processes interacting with or supervised by discrete processes. They are also the result of the hierarchical organization of complex/control systems or interaction between discrete planning algorithms and control algorithms continuous [17, 18].

In conventional automatic, the control problem is treated differently depending on the nature of the system to be studied: continuous or discrete. The study and analysis of the system is based on a set of theories and concepts lead to making methods and development of effective solutions to the problem of adjustment in its homogeneous in nature without resorting to solutions and contribution of the other domain. A general unified theory to model, analyze and design controls for such systems is not currently available. However, many researchers are working on subclasses of hybrid systems for which such approaches have been developed [2, 3, 14, 18]. Knowing that industrial processes are complex in nature and are difficult to control, the engineers use supervision and control systems by sequential controllers coupled with control loop in the different modes of operation. This operating dynamic aspect is characterized by a continuous and event nature.

For this purpose, the study of hybrid systems has attracted the attention of the automation community, as well as that of the IT community. The objectives can be assigned to the study of SDH hybrid systems are to provide a solution in terms of models, methods, performance and quality to problems improperly addressed by the homogeneous or conventional approaches. Indeed, the researcher community has focused these efforts in three areas: modeling, analysis and control [17].

The concept of hybrid dynamic system HDS appeared first time in [10] in 1987 where the author insists on the need to develop a theory combining continuous and discrete signals. This need can be applied in many areas:

- The simulation of complex processes composed of several units and continuous operating modes
- Supervision processes and safe operation of multiple-model systems
- The development of smart controllers, that is to say, continuous controllers but adapting their response following a discrete logic
- Scheduling and task management for real-time systems
- Modeling the dynamic behavior of the response time systems constrained by their environment
- The air traffic control
- Robotics,

The hybrid term that refers to the essential coupling continuous and discrete phenomena in a system such as is shown in Fig. 1. A hybrid dynamic system allows globally represent the interdependence of continuous/discrete dynamic elements in

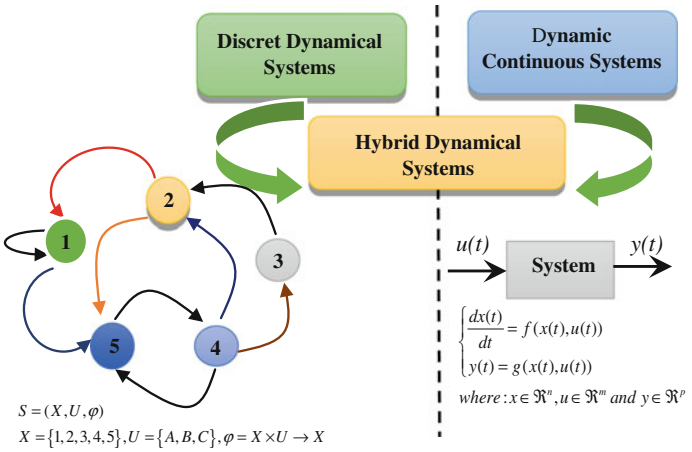

Fig. 1 Coupling of continuous and discrete phenomena in a hybrid dynamic system

the classical sense of differential equations or difference equations, subject to discrete decision points deterministic or discrete event systems DES.

For modeling hybrid dynamic systems, several formalisms have been proposed to establish a uniform model for the interaction between the continuous and discrete part. Various formalisms are available, the best known are linear automata [19] the piecewise affine systems PWA [12] linear complementarity systems LC [11], linear complementarity systems extended ELC [7] the Max-Min-Plus Scaling systems MMPS [8] dynamics and logic mixed systems 'MLD' [2, 3].

The approaches developed in this chapter adopt the MLD formalism proposed by Bemporad [3]. It allows modeling of hybrid systems, including continuous and discrete dynamics with interactions and constraints. Furthermore, the predictive control based model (MPC) is widely distributed in as simple and efficient control for industry. The MLD model is used to control a hybrid system in terms of trajectory tracking. Predictive control structure developed under the receding horizon with MLD formalism is based on a mixed integer quadratic optimization technic.

2 MLD Formalism

The control problem of a hybrid system is to lead the process in one or more desired states and prevent other states, all of the functionality described by rules. In this way, we can consider the interference that can occur in the models of continuous systems, but also non-controlled events such defects that may occur in discrete models.

For analysis of the system, it is necessary to define the interface between the continuous and discrete systems. The structure adopted for the definition is very important in the formalization of the control law.

In this chapter, the work is oriented to modeling and control systems, described by interdependent physical laws, logical rules and operating constraints, systems called MLD (mixed logical dynamical). These are described by linear dynamic equations, including linear inequalities involving continuous or logical variables.

For hybrid systems, MLD modelling allows to translate the logical rules in linear inequalities. To this effect, the MLD systems include a set of classes of systems namely: linear hybrid systems, finite state machines, discrete event systems, linear systems with constraints, and nonlinear systems whose non-linearity can be expressed by piecewise affine function.

2.1 Description of the Modeling Formalism MLD

In the study presented in [2, 3, 13] we express a logical proposition as linear constraints on logical variables provides a powerful modeling structure using the MLD form. This formalism is used to describe a number of important classes of systems, such as piecewise linear systems, systems with inputs and mixed states continuous/discrete. This framework includes constraints, and incorporates heuristic rules in the description of the model, by the description of interacting physical laws, logical rules, and operating constraints. The techniques described by, [5, 15, 21] allows to transforming propositional logic to linear inequalities involving continuous and binary variables. This produces an MLD system described by linear dynamic equations and linear inequalities involving continuous and binary variables, which included continuous/discrete states, continuous/logical input and auxiliary continuous/binary variables.

2.2 Propositional Calculus

We will adopt later X_1 as capital letters to represent relations. Variable X_1 is commonly referred literal name can have a truth value 'T' 'true' or 'F' "false". We can also associate a literal X_1 a logical variable $\delta_i \in \{0, 1\}$ that has a value of 1 if $X_i = T$ or 0 otherwise [5, 21].

The linear integer programming is an effective method to calculate a systematic transformation of logical relations in linear inequalities on binary variables [15] The propositional logic problem for a set of literal statements denoted $X_1, X_2, \ldots, X_n$, can be solved using linear integer programming [21].

This can be achieved by appropriately reflecting the initial declarations to linear inequalities involving logical variables δ_i. Thus, the following proposals and linear constraints can easy to be shown as equivalent.

$$\begin{cases} X_1 \vee X_2 \textit{ is equivalent to } \delta_1 + \delta_2 \geq 1 \\ X_1 \wedge X_2 \textit{ is equivalent to } \delta_1 = 1, \delta_2 = 1 \\ \sim X_1 \textit{ is equivalent to } \delta_1 = 0 \\ X_1 \rightarrow X_2 \textit{ is equivalent to } \delta_1 - \delta_2 \leq 1 \\ X_1 \leftrightarrow X_2 \textit{ is equivalent to } \delta_1 - \delta_2 = 0 \\ X_1 \oplus X_2 \textit{ is equivalent to } \delta_1 + \delta_2 = 1 \end{cases} \tag{1}$$

Other alternative methods and formulations to perform the transformation of logic proportional to equivalent entire programming exist.

This technique inference calculation will later be used to model the logical parts of the process (switches On/Off' mechanisms networks combinational and sequential networks) and heuristic knowledge related to the operation of the entire linear inequality systems. The study of the dynamics and logic mixed systems needed to establish a link between the two parts.

For this purpose, it is necessary to establish a link between the two modes; which results in the relations between the input events and the physical dynamics, one using linear inequalities involving continuous variables $x \in \Re^n$ and logical variables (indicators) $\delta \in \{0, 1\}$ ("Mixed-Integer Linear Inequalities").

Consider $X = \left[f(x) \leq 0\right]$, *where* $f : \Re^n \rightarrow \Re$ is linear and $x \in \chi$, where χ is a bounded set, such as:

$$\begin{cases} M = \max\limits_{x \in X} f(x) \\ m = \min\limits_{x \in X} f(x) \end{cases} \tag{2}$$

By associating a binary variable δ to the literal relations X, one can deduce the relation:

$$\left[f(x) \leq 0\right] \leftrightarrow [\delta = 1] \textit{ is true if and only if } \begin{cases} f(x) \geq \varepsilon + (m - \varepsilon)\delta \\ f(x) \leq M(1 - \delta) \end{cases} \tag{3}$$

where ε is a tolerance (the machine precision), beyond which the constraint is considered violated.

Furthermore, the term $\delta f(x)$, where $f : \Re^n \mapsto \Re$ et $\delta \in \{0, 1\}$, may be replaced with an auxiliary variable $z = \delta f(x)$, which satisfies: $[\delta = 0] \rightarrow [z = 0]$, $[\delta = 1] \rightarrow \left[z = f(x)\right]$. Therefore, by defining M, m as in Eq. (2), $z = \delta f(x)$ is equivalent to:

$$\begin{cases} z \leq M\delta \\ z \geq m\delta \\ z \leq f(x) - m(1 - \delta) \\ z \geq f(x) - M(1 - \delta) \end{cases} \tag{4}$$

All of these tools will be used to transform logical facts involving continuous variables in linear inequalities and also express relationships describing the

evolution of systems where physical laws, logical rules and operating constraints are interdependent.

2.3 The Steps of MLD Formalism Modelling

The MLD modelling of a hybrid system is based on the combination of the three main ideas:

1. Represent logical relations of linear inequalities on binary variables.
2. Associate logical and continuous variables by linear inequalities on binary and continuous variables.
3. Include binary variables in the differential equations.

The logic part is transformed into a system of inequalities involving binary variables. These proposals will be transcribed into equations translating an evolution, as the continuous part, but with additional constraints of logical variables.

2.3.1 Architecture of the MLD Formalism

A hybrid system is generally composed of two parts, a party related to the continuous dynamics and the other to discrete/digital dynamics. The diagram below shows the MLD model for a hybrid system and the associated transfer: continuous/discrete.

Auxiliary variables used to model the relations between the continuous and discrete parts (Fig. 2). Thus, the transition from discrete part to the continuous part requires the addition of logic variables. In general, an auxiliary logic variable is set to translate a switching phenomenon. A proposal form can represent such a phenomenon we saw previously $[\delta = 1] \Leftrightarrow [f(x) \leq 0]$. For the part corresponding to the discrete/continuous transformation continuous auxiliary variables are added, such that if $\delta = 1$, *then* $z = f_1(x)$, *else* $z = f_2(x)$.

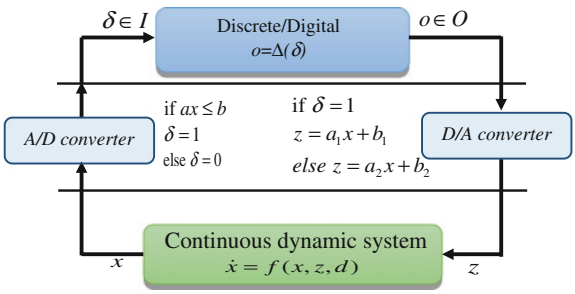

Fig. 2 A hybrid system structure

2.3.2 Modelling by the MLD Formalism

We have seen earlier that all auxiliary continuous and binary variables and logical relations can be translate into linear inequalities on binary and continuous variables:

$$\left[f(x) \leq 0\right] \leftrightarrow [\delta = 1] \Leftrightarrow \begin{cases} f(x) \leq M(1-\delta) \\ f(x) \geq \varepsilon + (m-\varepsilon)\delta \end{cases} \tag{5a}$$

$$z = \delta f(x) \Leftrightarrow \begin{cases} z \leq M\delta \\ z \geq m\delta \\ z \leq f(x) - m(1-\delta) \\ z \geq f(x) - M(1-\delta) \end{cases} \tag{5b}$$

The system under **MLD** formalism resulting from the continuous/discrete association is therefore describe by the following linear relationship:

$$\begin{cases} x(k+1) = Ax(k) + B_1 u(k) + B_2 \delta(k) + B_3 z(k) \\ x(k) = Cx(k) + D_1 u(k) + D_2 \delta(k) + D_3 z(k) \\ E_2 \delta(k) + E_3 z(k) \leq E_1 u(k) + E_4 x(k) + E_5 \end{cases} \tag{6}$$

These relations involves the following variables, mixed continuous/binary, binary and continuous:

State: $x = \begin{bmatrix} x_c \\ x_l \end{bmatrix}$, $x_c \in \Re^{n_c}$, $x_l \in \{0,1\}^{n_l}$, $n = n_n + n_l$

Output: $y = \begin{bmatrix} y_c \\ y_l \end{bmatrix}$, $y_c \in \Re^{p_c}$, $y_l \in \{0,1\}^{p_l}$, $p = p_n + p_l$

Input: $u = \begin{bmatrix} u_c \\ u_l \end{bmatrix}$, $u_c \in \Re^{m_c}$, $u_l \in \{0,1\}^{m_l}$, $m = m_n + m_l$

$\delta \in \{0,1\}^{r_l}$ are the auxiliary binary variables

$z \in \Re^{r_c}$ are the auxiliary continuous variables

The MLD model represents the hybrid system by linear equations with linear inequalities on continuous and binary variables. All the inequalities of the MLD model thus collects firstly the constraints of the system, secondly inequalities resulting from logical propositions and auxiliary variables. A problem called "well-posed" if the solution δ and z is unique for a given pair (x, u), and therefore $x(k+1)$ is uniquely defined, allowing find unique trajectory of the states.

3 Predictive Control of a Hybrid System in the MLD Form

The prediction is a concept that is important for any activity in which one seeks to anticipate a predefined path. In fact, many human activities such as walking, driving a car or sport seek to anticipate a trajectory to predict the actions and switching

operations. It is this intuitive and natural concept that is based predictive control. Industrial processes, for a large part of them must also follow certain guidelines.

The first theoretical and practical results related to predictive control have been achieved in the late 1970s, including the work done by [16]. In the 1980s, several methods based on the same predictive concepts were developed. Among, these include generalized predictive control GPC, developed by [6], which proved the most widely used technology in the future. A historical introduction to the various predictive control methods can be found in the book of [4] .This diversity in the predictive control is the origin of the birth of predictive control model based: Model Predictive Control "MPC".

The predictive control based model MPC has been very well received in the industry because it proves a technique of simple and effective control. Predictive control has been implemented in a number of industrial applications, including chemical processes, which were the first to use this type of control, distillation processes, the oil industry and electromechanical systems. These industrial applications all have a common denominator: knowing of the trajectory to be followed by the system in the future, at least over a certain horizon. Finally, these techniques are capable of controlling a wide variety of processes.

The goal to be achieved by the use of predictive control is to create an anticipatory effect exploiting explicit knowledge about the evolution of the trajectory to be followed in the future (explicit knowledge on the horizon of a few points beyond the moment). This constraint takes advantage of all the resources of the method which necessarily limited the scope of the control system for which the trajectory to be followed is well known and stored point by point in the calculator (Fig. 3).

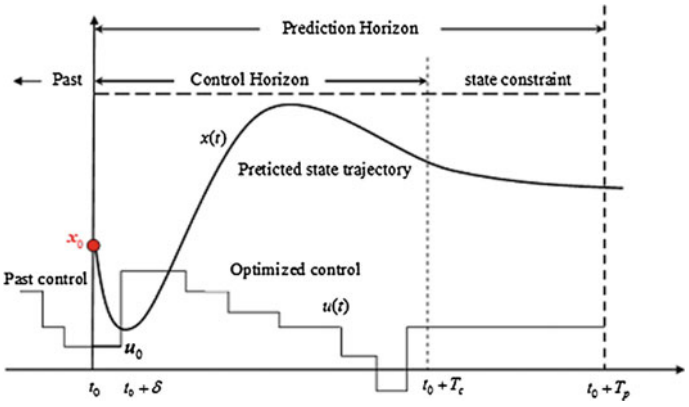

Fig. 3 Principles of predictive control

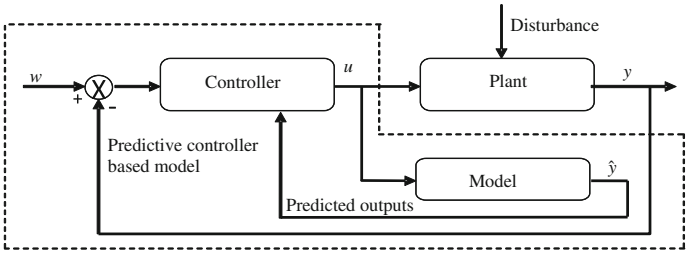

Fig. 4 Scheme characterized predictive control

Four points are common to all methods:

1. Definition of a numerical model of the system to make the prediction of future behavior of the system. This discrete model most often results of prior identification offline.
2. Minimization of a quadratic criterion for finite horizon on future prediction errors, differences between the predicted output of the system and the following trajectory (Fig. 4).
3. Calculating a future optimal control sequence, only the first value is applied to the system and the model.
4. Repetition of the previous steps to the next sampling period according to the principle of receding horizon.

Predictive control, based on the use of a model and the principle of moving horizon (RHC), can be seen as a strategy to which the control at time t is obtained by solving online, every at each sampling time an optimal control problem in open loop finite horizon, using the current state of the system as initial state.

The optimization algorithm provides an optimal sequence of future control, which only the first is apply to the input of the process. There is interest in this type of control when the trajectory to be following by the system it is well known.

The model used is CARIMA (Controlled Auto Regressive Integrated Moving Average). The GPC control law is obtained by minimizing a quadratic criterion on future errors with a weighting term on the control or control increment. Constraints on the output signals may be taken into account in the criterion.

3.1 Prediction Model for MPC

In this section a brief description of the prediction model used with the generalized predictive control to be later reintroduced for application to hybrid systems.

Calculating the predicted output in the future requires the use of a digital model of the system, as used in GPC. The model is a model conventionally used input/output type CARIMA in the form:

$$A(q^{-1})y(k) = B(q^{-1})u(k-1) + \frac{C(q^{-1})}{\Delta(q^{-1})}\xi(k) \tag{7}$$

$y(k)$, $u(k-1)$ *et* $\xi(k)$ are respectively the output, input and the system disturbance signal. The $\xi(k)$ signal is considered random and with zero mean. The polynomial $C(q^{-1})$ models the influence of noise on the system. The introduction of $\Delta(q^{-1}) = 1 - q^{-1}$ in the noise model aims to reason about the signals increments, and then to provide integrated action corrector, to cancel the static errors against input or a step change.

The overall aim is to reach the mistake of future output to zero, with minimal control effort. Thus, the GPC control law is obtained by minimizing a quadratic criterion on future mistakes with a weighting term on command increments.

$$J(N_1, N_2, N_u) = \sum_{j=N_1}^{N_2} \beta(j)(\hat{y}(k+j|k) - w(k+j))^2 + \sum_{j=1}^{N_u} \lambda(j)(u(k+j-1))^2 \tag{8}$$

where: N_1, N_2 are the horizons of lower and upper prediction on the output, Nu is the prediction horizon on the command, $\beta(j)$, $\lambda(j)$ are the weights on the order. The prediction horizon enables the user to reduce the number of future orders calculated since we assume the following relationship:

$$\Delta u(k+j) = 0 \; pour \; j \geq N_u \tag{9}$$

$w(k+j)$ is the set point or the reference trajectory imposing rallying of the output at set point.

The constraints on the control and output may be added in the cost function:

$$\begin{cases} u_{\min} \leq u(k) \leq u_{\max} \\ y_{\min} \leq y(k) \leq y_{\max} \end{cases} \tag{10}$$

In this case, the minimization becomes complex, which requires the use of quadratic programming methods *MIQP*.

3.2 Structure of the Optimization Criterion

For a system as MLD, MPC predictive control strategy developed by [2] can be summarized as follows:

Let $\boldsymbol{k}$ be the current time, $x(k)$ the current state, (x_e, u_e) an equilibrium point or reference value to reach, $\boldsymbol{k+N}$ the final time prediction, we seek to develop the sequence future control $u_k^{k+N+1} = \{u(k), \ldots, u(k+N-1)\}$ go from the state $x(k)$ to x_e by minimizing the following cost function:

$$\begin{aligned}\min_{\{u_k^{k+N-1}\}} J(u_k^{k+N-1}, x(k)) = \sum_{i=0}^{N-1} &\|u(k+i) - u_e\|_{Q_1}^2 + \|\delta(k+i/k) - \delta_e\|_{Q_2}^2 \\ &+ \|z(k+i/k) - z_e\|_{Q_3}^2 + \|x(k+i/k) - x_e\|_{Q_4}^2 \\ &+ \|y(k+i/k) - y_e\|_{Q_5}^2\end{aligned} \tag{11}$$

$$\text{subject to constraints} \begin{cases} x(k+N/k) = x_e \\ x(k+i+1/k) = Ax(k+i/k) + B_1u(k+i) \\ +B_2\delta(k+i/k) + B_3z(k+i/k) \\ y(k+i/k) = Cx(k+i/k) + D_1u(k+i) \\ +D_2\delta(k+i/k) + D_3z(k+i/k) \\ E_2\delta(k+i/k) + E_3z(k+i/k) \leq E_1u(k+i) \\ +E_4x(k+i/k) + E_5 \end{cases}$$

N is the prediction horizon on the output, δ_e *and* z_e the values of the auxiliary variables to the reference point, calculated by resolution of a problem for equation MIQP on inequality.
Let: $x(k+i+1/k) \approx x(k+i, x(k), u_k^{k+i})$. Furthermore, it is assumed that $Q_i = Q_i^T \succ 0$, pour $i = 1, 4$ and $Q_i = Q_i^T \geq 0$, for $i = 2, 3, 5$.

Assume that the optimal solution $\left\{u_k^{k+N-1}(j)\right\}_{j=0,\ldots,N-1}$ exists. According to the philosophy of moving horizon, only the first $u(k)$ of this sequence is applied to the system.

The following optimal control $u(k+1), \ldots, u(k+N-1)$: are then neglected and the complete optimization process is repeated at time $k+1$.

To be able examine in more detail this control strategy, it is first necessary to reformulate the problem of quadratic optimization (12) originally proposed by **Bemporad and Morari** [2] in a form similar to the problem GPC, to as follows:

$$\begin{aligned}&\min_{\{u_k^{k+N-1}\}} J(u_k^{k+N-1}, x(k)) \\ &= \sum_{i=0}^{N-1} \|u(k+i) - u_e\|_{Q_1}^2 + \|\delta(k+i/k) - \delta_e\|_{Q_2}^2 + \|z(k+i/k) - z_e\|_{Q_3}^2 \\ &+ \|x(k+i/k) - x_e\|_{Q_4}^2 + \|y(k+i/k) - y_e\|_{Q_5}^2\end{aligned} \tag{12a}$$

Subject to relations:

$$\begin{cases} x(k+i+1/k) = Ax(k+i/k) + B_1u(k+i) + B_2\delta(k+i/k) + B_3z(k+i/k) \\ y(k+i/k) = Cx(k+i/k) + D_1u(k+i) + D_2\delta(k+i/k) + D_3z(k+i/k) \\ E_2\delta(k+i/k) + E_3z(k+i/k) \leq E_1u(k+i) + E_4x(k+i/k) + E_5 \end{cases} \tag{12b}$$

Follows the same steps for the development of the GPC control (CARIMA), as follows:

$$H(z) = \frac{C}{z}(I + \frac{A}{z} + \frac{A^2}{z^2} + \frac{A^3}{z^3} + \cdots)B_1 + \frac{D_1}{z}(I + \frac{A}{z} + \frac{A^2}{z^2} + \frac{A^3}{z^3} + \cdots)B_2 + \frac{D_2}{z}(I + \frac{A}{z} + \frac{A^2}{z^2} + \frac{A^3}{z^3} + \cdots)B_2 + \frac{D_3}{z}(I + \frac{A}{z} + \frac{A^2}{z^2} + \frac{A^3}{z^3} + \cdots)B_3$$

We substitute the operator Z in the following equation; we have:

$$\begin{aligned} y(k) = {} & D_1u(k) + CB_1u(k-1) + CAB_1u(k-2) + CA^2B_1u(k-3) + \cdots + \\ & D_2\delta(k) + CB_2\delta(k-1) + CAB_2\delta(k-2) + CA^2B_2\delta(k-3) + \cdots + \\ & D_3z(k) + CB_3z(k-1) + CAB_3z(k-2) + CA^2B_3z(k-3) + \cdots + \end{aligned}$$

The future outputs can ben then calculated as:

$$\begin{aligned} y(k+1) = {} & D_1u(k+1) + CB_1u(k) + CAB_1u(k-1) + CA^2B_1u(k-2) + \cdots + \\ & D_2\delta(k+1) + CB_2\delta(k) + CAB_2\delta(k-1) + CA^2B_2\delta(k-2) + \cdots + \\ & D_3z(k+1) + CB_3z(k) + CAB_3z(k-1) + CA^2B_3z(k-2) + \cdots + \end{aligned}$$

$$\begin{aligned} y(k+2) = {} & D_1u(k+2) + CB_1u(k+1) + CAB_1u(k) + CA^2B_1u(k-1) + \cdots + \\ & D_2\delta(k+2) + CB_2\delta(k+1) + CAB_2\delta(k) + CA^2B_2\delta(k-1) + \cdots + \\ & D_3z(k+2) + CB_3z(k+1) + CAB_3z(k) + CA^2B_3z(k-1) + \cdots + \end{aligned}$$

For a prediction horizon N, one obtains:

$$\begin{aligned} y(k+N) = {} & D_1u(k+N) + CB_1u(k+N-1) + CAB_1u(k+N-2) \\ & + CA^2B_1u(k+N-3) + \cdots + \\ & D_2\delta(k+N) + CB_2\delta(k+N-1) + CAB_2\delta(k+N-2) \\ & + CA^2B_2\delta(k+N-3) + \cdots + \\ & D_3z(k+N) + CB_3z(k+N-1) + CAB_3z(k+N-3) \\ & + CA^2B_3z(k+N-3) + \cdots + \end{aligned}$$

More generally, the term $y(k+j)(j = 1, 2, \ldots, N)$, the previous equation can be written as :

$$\begin{aligned} y(k+j) = {} & \sum_{i=1}^{\infty} CA^{i-1}B_1u(k+j-i) + D_1u(j+1) + \sum_{i=1}^{\infty} CA^{i-1}B_2\delta(k+j-i) \\ & + D_2\delta(j+1) + \sum_{i=1}^{\infty} CA^{i-1}B_3z(k+j-i) + D_3z(j+1) \end{aligned}$$

$$y(k+j) = \sum_{i=1}^{j} CA^{i-1}B_1u(k+j-i) + \sum_{i=j+1}^{\infty} CA^{i-1}B_1u(k+j-i) + D_1u(j+1)$$
$$+ \sum_{i=1}^{j} CA^{i-1}B_2\delta(k+j-i) + \sum_{i=j+1}^{\infty} CA^{i-1}B_2\delta(k+j-i) + D_2\delta(j+1)$$
$$+ \sum_{i=1}^{j} CA^{i-1}B_3z(k+j-i) + \sum_{i=j+1}^{\infty} CA^{i-1}B_3z(k+j-i) + D_3z(j+1)$$

$$y(k+j) = \sum_{i=1}^{j} CA^{i-1}B_1u(k+j-i) + \sum_{m=0}^{\infty} CA^{m+j}B_1u(k-m-1) + D_1u(j+1)$$
$$+ \sum_{i=1}^{j} CA^{i-1}B_2\delta(k+j-i) + \sum_{m=0}^{\infty} CA^{m+j}B_2\delta(k-m-1) + D_2\delta(j+1)$$
$$+ \sum_{i=1}^{j} CA^{i-1}B_3z(k+j-i) + \sum_{m=0}^{\infty} CA^{m+j}B_3z(k-m-1) + D_3z(j+1)$$

$$y(k+j) = \sum_{i=1}^{j} CA^{i-1}B_1u(k+j-i) + \sum_{i=1}^{j} CA^{i-1}B_2\delta(k+j-i)$$
$$+ \sum_{i=1}^{j} CA^{i-1}B_3z(k+j-i)$$
$$+D_1u(j+1) + D_2\delta(j+1) + D_3z(j+1)$$
$$+ \sum_{m=0}^{\infty} CA^{m+j}(B_1u(k-m-1)) + B_2\delta(k-m-1)) + B_3z(k-m-1))$$

$$y(k+j) = \sum_{i=1}^{j} CA^{i-1}B_1u(k+j-i) + \sum_{i=1}^{j} CA^{i-1}B_2\delta(k+j-i)$$
$$+ \sum_{i=1}^{j} CA^{i-1}B_3z(k+j-i)$$
$$+D_1u(j+1) + D_2\delta(j+1) + D_3z(j+1)$$
$$+ \sum_{m=0}^{\infty} CA^{m+j}(x(k-m) - Ax(k-m-1))$$

After simplification, one obtains:

$$y(k+j) = \sum_{i=1}^{j} CA^{i-1}(B_1u(k+j-i) + B_2\delta(k+j-i) + B_3z(k+j-i))$$
$$+D_1u(j+1) + D_2\delta(j+1) + D_3z(j+1) + CA^jx(k) \tag{13}$$

We set: $Y = \left[y(k)\ y(k+1)\ y(k+2)\ \cdots y(k+N-1)\right]$ and $U = [u(k)\ \cdots u(k+N-1),\ z(k)\ \cdots z(k+N-1), z(k)\ \cdots z(k+N-1)]$, we obtain the following compact form:

$$Y = GU + F \tag{14}$$

With:

$$F = \begin{bmatrix} C \\ CA \\ CA^2 \\ \vdots \\ CA^{N-1} \end{bmatrix} x(k), \quad G = \begin{bmatrix} D_1 & \cdots & 0 & D_2 & \cdots & 0 & D_3 & \cdots & 0 \\ CB_1 & & & CB_2 & & & CB_3 & & \\ CAB_1 & \ddots & \vdots & CAB_2 & & \vdots & CAB_3 & & \vdots \\ CA^2B_1 & & & CA^2B_2 & & & CA^2B_3 & & \\ \vdots & & & \vdots & & \vdots & \vdots & & \vdots \\ CA^{N-1}B_1 & & D1 & CA^{N-1}B_2 & & D_2 & CA^{N-1}B_3 & & D_3 \end{bmatrix} \tag{15}$$

We use this formulation in the quadratic optimization criterion:

$$\begin{cases} F(\chi, x(k)) = \min\limits_{x} \ \frac{1}{2}\chi^T H\chi + f^T\chi \\ \text{subject to constraints : c}\,\chi \begin{Bmatrix} = \\ \leq \end{Bmatrix} b \end{cases} \tag{16}$$

We have the following matrices: $H = P^T QP, f = Y_e^T QP$ with:

$$c = \begin{bmatrix} -\mathrm{E}_1 & \cdots & 0 & E_2 & \cdots 0 & E_3 & \cdots & 0 \\ -E_4B_1 & & & -E_4B_2 & & -E_4B_3 & & \\ -E_4AB_1 & \ddots & & -E_4AB_2 & \ddots & -E_4AB_3 & \ddots & \\ -E_4A^2B_1 & & & -E_4A^2B_2 & & -E_4A^2B_3 & & \\ \vdots & & \vdots & \vdots & \vdots & \vdots & & \vdots \\ -E_4A^{N-2}B_1 & \cdots & -E_1 & -E_4A^{N-2}B_2 & \cdots & E_2 - E_4A^{N-2}B_3 & & E_3 \end{bmatrix}$$

$$b^T = \left[(E_4x(k)+E_5)^T \ (E_4Ax(k)+E_5)^T \cdots (\mathrm{E}_4A^{N-1}x(k)+\mathrm{E}_5)^T\right]$$

$$Y_e^T = \begin{bmatrix} (Ax(k) - x_e)^T \ (Ax(k) - x_e)^T \ \cdots \ (A^N x(k)\text{-}x_e)^T \ , \\ (Cx(k) - y_e)^T \ (CAx(k) - y_e)^T \ \cdots \ (CA^{N-1}x(k)\text{-}y_e)^T , \\ \underbrace{-u_e^T, -u_e^T, ..., -u_e^T}_{N}, \ \underbrace{-\delta_e^T, -\delta_e^T, ..., -\delta_e^T}_{N}, \ \underbrace{-z_e^T, -z_e^T, ..., -z_e^T}_{N} \end{bmatrix}$$

$$Q^T = diag\left[diag(Q_4)_N \ diag(Q_5)_N diag(Q_1)_N diag(Q_2)_N diag(Q_3)_N\right]$$

where $diag(Q_i)_N$ is a diagonal matrix with elements Q_i and dimension N.

The number of binary variables relevant to the optimization is then equal to $L = N^*(m_l + r_l)$.

Where m_l is the number of binary control variable (logical/Discrete) and r_l is the number of auxiliary binary variables.

$$
P = \begin{bmatrix}
B_1 & \cdots & 0 & B_2 & \cdots & 0 & B_3 & \cdots & 0 & \\
AB_1 & & & & & & & & & \\
\vdots & & \vdots & \vdots & & \vdots & \vdots & & \vdots & \\
A^{N-1}B_1 & \cdots & \mathrm{B}_1 & A^{N-1}B_2 & \cdots & \mathrm{B}_2 & A^{N-1}B_3 & \cdots & & \mathrm{B}_3 \\
\mathrm{D}_1 & \cdots & 0 & \mathrm{D}_2 & \cdots & 0 & \mathrm{D}_3 & \cdots & 0 & \\
CB_1 & & & CB_2 & & & CB_3 & & & \\
CAB_1 & & & CAB_2 & & & CAB_3 & & & \\
CA^2B_1 & & & CA^2B_2 & & & CA^2B_3 & & & \\
\vdots & & & \vdots & & \vdots & \vdots & & \vdots & \\
CA^{N-1}B_1 & \cdots & \mathrm{D1} & CA^{N-1}B_2 & \cdots & \mathrm{D}_2 & CA^{N-1}B_3 & \cdots & & \mathrm{D}_3 \\
I_{m\times m} & & & & & & & & & \\
 & I_{m\times m} & & & & & & & & \\
 & & \cdots & & & & & & & \\
 & & & I_{m\times m} & & & & & & \\
 & & & & I_{r_l\times r_l} & & & & & \\
 & & & & & \cdots & & & & \\
 & & & & & & I_{r_l\times r_l} & & & \\
 & & & & & & & I_{r_c\times r_c} & & \\
 & & & & & & & & \cdots & \\
 & & & & & & & & & I_{r_l\times r_l}
\end{bmatrix}
$$

With: $m = m_c + m_l$

3.3 *Formulation of the Optimization Criterion for the Method of Bemporad [2, 14]*

For the formulation of MIQP optimization criterion if the prediction horizon is different from the control, it follows the same previous approach to reformulating the following criteria as a MIQP problem:

$$
\min_{u,\delta,z} J\left(\left\{\begin{matrix} u_k^{k+N_m-1}, \\ \delta_k^{k+N_p-1}, \\ z_k^{k+N_p-1} \end{matrix}\right\}, x(k)\right) = \sum_{i=0}^{N_p-1} \|y(k+i/k) - y_e\|_{Q_5}^2 + \|\delta(k+i/k) - \delta_e\|_{Q_2}^2 + \|z(k+i/k) - z_e\|_{Q_3}^2 + \sum_{i=0}^{N_u-1} \|u(k+i) - u_e\|_{Q_1}^2 \tag{17}
$$

$$
Q_M = 2^* \begin{bmatrix}
H_{M1}^T Q_5 H_{M11} & H_{M1}^T Q_5 H_{M2} & H_{M1}^T Q_5 H_{M3} \\
H_{M2}^T Q_5 H_{M1} & H_{M2}^T Q_5 H_{M2} + Q_2 & H_{M2}^T Q_5 H_{M3} \\
H_{M3}^T Q_5 H_{M1} & H_{M3}^T Q_5 H_{M2} & H_{M3}^T Q_5 H_{M3} + Q_3
\end{bmatrix}
$$

$$H_{Mi} = \begin{bmatrix} CB_i & 0 & \cdots & 0 \\ CAB_i & CB_i & \cdots & 0 \\ CA^2B_i & CAB_i & \cdots & 0 \\ \vdots & & \vdots & \vdots \\ CA^{(p-2)}B_1 & CA^{(p-3)}B_1 & \cdots\ CB_i & 0 \\ CA^{(p-1)}B_1 & CA^{(p-2)}B_1 & \cdots\ CAB_i & CB_i \end{bmatrix}$$

where i = 2, 3

$$H_{M1} = \begin{bmatrix} CB_1 & \boldsymbol{0} & \cdots & \cdot & \boldsymbol{0} \\ CAB_1 & CB_1 & \cdots & & \boldsymbol{0} \\ \boldsymbol{CA}^2B_1 & CAB_1 & \cdots & & \boldsymbol{0} \\ \vdots & & \vdots & & \vdots \\ \boldsymbol{CA}^{(m-1)}B_1 & CA^{(m-2)}B_1 & \cdots & \boldsymbol{CAB}_1 & \boldsymbol{CB}_1 \\ \boldsymbol{CA}^mB_1 & CA^{(m-1)}B_1 & \cdots & \boldsymbol{CA}^2\boldsymbol{B}_1 & \boldsymbol{CB}_1 + CAB_1 \\ \vdots & \vdots & \vdots & & \\ CA^{(p-1)}B_1 & CA^{(p-2)}B_1 & \cdots\ \boldsymbol{CA}^{(p-m-1)} & \sum_{i=0}^{p-m} & CA^iB_1 \end{bmatrix}$$

$$E_{Mi} = \begin{bmatrix} E_i & 0 & \cdots & 0 \\ -E_4B_i & E_i & \cdots & 0 \\ -E_4AB_i & -E_4B_i & \cdots & 0 \\ \vdots & \vdots & \ddots & \vdots \\ -E_4A^{(p-3)}B_i & -E_4A^{(p-4)}B_i & \cdots\ E_i & 0 \\ -E_4A^{(p-2)}B_i & -E_4A^{(p-3)}B_i & \cdots\ -E_4B_i & E_i \end{bmatrix}$$

where i=2, 3

$$E_{M4} = \begin{bmatrix} -E_4 \\ -E_4A \\ -E_4A^2 \\ \vdots \\ \\ \\ \vdots \\ -E_4A^{(p-1)} \end{bmatrix} \quad E_{M5} = \begin{bmatrix} -E_5 \\ -E_5 \\ -E_5 \\ \vdots \\ p\ times \\ \vdots \\ -E_5 \end{bmatrix}$$

$$E_{M1} = \begin{bmatrix} -E_1 & 0 & \cdots & . & 0 \\ -E_4B_1 & -E_1 & \cdots & & 0 \\ -E_4A^2B_1 & -E_4B_1 & & \cdots & 0 \\ \vdots & \vdots & -E_1 & & \vdots \\ -E_4A^{(m-2)}B_1 & -E_4A^{(m-3)}B_1 & \cdots & -E_4B_1 & -E_1 \\ -E_4A^{(m-1)}B_1 & -E_4A^{(m-2)}B_1 & \cdots & -E_4AB_1 & -E_1 - E_4B_1 \\ -E_4A^mB_1 & -E_4A^{(m-1)}B_1 & \cdots & -E_4A^2B_1 & -E_1 - E_4B_1 - -E_4AB_1 \\ \vdots & \vdots & & & \vdots \\ -E_4A^{(p-2)}B_1 - E_4A^{(p-3)}B_1 & \cdots & -E_4A^{(p-m)}B_1 & -E_1 + \sum_{i=0}^{p-m-1} -E_4A^iB_1 & \end{bmatrix}$$

$$E_{M1} = \begin{bmatrix} -E_1 & 0 & \ldots & \cdot & 0 \\ -E_4B_1 & -E_1 & \ldots & & 0 \\ -E_4A^2B_1 & -E_4B_1 & \ldots & & 0 \\ \vdots & \vdots & -E_1 & & \vdots \\ -E_4A^{(m-2)}B_1 & -E_4A^{(m-3)}B_1 \ldots & -E_4B_1 & & -E_1 \\ -E_4A^{(m-1)}B_1 & -E_4A^{(m-2)}B_1 \ldots & -E_4AB_1 & & -E_1 - E_4B_1 \\ -E_4A^mB_1 & -E_4A^{(m-1)}B_1 \ldots & -E_4A^2B_1 & & -E_1 - E_4B_1 - -E_4AB_1 \\ & \vdots & \vdots & & \vdots \\ -E_4A^{(p-2)}B_1 & -E_4A^{(p-3)}B_1 \ldots & -E_4A^{(p-m)}B_1 & -E_1 + \sum_{i=0}^{p-m-1} & -E_4A^iB_1 \end{bmatrix}$$

$$\Phi_M = \begin{bmatrix} CA \\ CA^2 \\ CA^3 \\ \vdots \\ \\ \vdots \\ CA^p \end{bmatrix}$$

$$f_M = 2^* \begin{bmatrix} x_k^T \Phi_M^T Q_5 H_{M1} - \psi_{sp}^T Q_5 H_{M1} - \mu_{sp}^T \Lambda_{su} + d_k^T S_d^T \Lambda_y H_{M1} \\ x_k^T \Phi_M^T Q_5 H_{M2} - \psi_{sp}^T Q_5 H_{M2} - \delta_{sp}^T Q_2 + d_k^T S_d^T Q_5 H_{M2} \\ x_k^T \Phi_M^T Q_5 H_{M3} - \psi_{sp}^T Q_5 H_{M3} - z_{sp}^T Q_2 + d_k^T S_d^T Q_5 H_{M3} \end{bmatrix} S_1 = \begin{bmatrix} E_{M1} & E_{M2} & E_{M3} \end{bmatrix}$$

$$S_2 = \begin{bmatrix} H_{M1} & H_{M2} & H_{M3} \end{bmatrix}$$

$$S_3^T = \begin{bmatrix} eye(m(size(B_1, 2))) \\ zeros(size(B_1, 2)), p(size(B_2, 2))) \\ zeros(m(size(B_1, 2)), p(size(B_3, 2))) \end{bmatrix}$$

$$A_{in} = \begin{bmatrix} S_1 \\ S_2 \\ -S_2 \\ S_3 \\ -S_3 \end{bmatrix}, \quad \begin{cases} b_1 = E_{M5} - E_{M4} x_k \\ b_{21} = \psi_{max} - \Phi_M x_k - S_d d_k \\ b_{22} = -\psi_{max} + \Phi_M x_k + S_d d_k \\ b_{31} = \mu_{max} \\ b_{32} = -\mu_{\min} \end{cases} \Rightarrow b_{in} = \begin{bmatrix} b_1 \\ b_{21} \\ b_{22} \\ b_{31} \\ b_{32} \end{bmatrix}$$

MIQP
Optimization Problem !

$$\begin{cases} min \dfrac{1}{2} \chi^T Q_m \chi + f_m^T \chi \\ \text{subject to: } A_m \chi \le b_m \end{cases}$$

$$\psi_k = \left[y_{k+1} y_{k+2} .... y_{k+p} \right]^T \begin{cases} \mu_k = \left[u_k \; u_{k+1} ..... u_{k+m-1} \right]^T \\ \bar{\delta}_k = \left[\delta_k \; \delta_{k+1} ..... \delta_{k+p-1} \right]^T \\ \bar{z}_k = \left[z_k \; z_{k+1} ..... z_{k+p-1} \right]^T \end{cases} \Rightarrow \chi = \left[\mu_k \; \bar{\delta}_k \; \bar{z}_k \right]^T$$

3.4 *Programming of the Quadratic Optimization Algorithm MIQP*

The establishment of the MPC for the problem (12) requires the solution of a mixed quadratic programming problem (MIQP), that is to say, an optimization problem including a quadratic cost function, for which the optimization vector consists of mixed variables (continuous and binary), and linear constraints. The optimization problem (12) can actually be transcribed in the generic form Eq. (16). Where the optimization vector is:

$$\chi = \left[u^T(k), \ldots, u^T(k+N-1), \delta^T(k), \ldots, \delta^T(k+N-1), z^T(k), \ldots, z^T(k+N-1) \right. \\ \left. x^T(k), \ldots, x^T(k+N), y(k), \ldots, y^T(k+N-1) \right]^T \tag{18}$$

Techniques of type "Branch and Bound" were successfully applied during criteria optimization phases (5) [2]. Several authors agree on the fact that B & B methods are most effective for solving problems MIQP [9]. The following section provides a summary of the technique B&B:

3.5 *Description of the Optimization Algorithm MIQP "Branch and Bound" (B&B)*

All control laws that can be applied to hybrid systems as MLD require the use of an integer optimization solver. Two major problems may be encountered "Mixed integer Linear Problems" (MILP) and "Mixed Integer Quadratic Problems" (MIQP).

In the literature, these types of problems are solved not only for binary variables, but also to a larger area of values. Our limiting case these general problems at the particular logical variables case. The algorithm "Branch and Bound" is then a general

framework for solving combinatorial problems and integers. The combinatorial part of the problem (determining the integer optimal part) is resolved by searching a tree during which the relaxations QP problem MIQP are produced and non-integer QP solutions are eliminated by adding simple limits ("Branch").Using the lower and upper limits to the optimal value of the objective ("Bound"), it is possible to limit the search in the tree, thus avoiding the complete enumeration.

To describe the strategy of B&B, it is necessary to clarify some notations and terminologies. Let P' the problem obtained from P by relaxing all integer restrictions. The problem P' is then an ordinary QP problem.

The two authors [9] showed that the algorithm B&B within the MIQP problems is to generate and solve new problems QP in a search tree, where the nodes of the tree correspond to the QP sub-problems. The operation called "branch" is to produce child nodes from parent nodes according branching rules.

A node that has been fully explored is referred to as: probed. A standby node is a node that was produced by branching but has not yet been resolved. The algorithm "B&B" explores the tree until all nodes waiting disappeared. It is not always necessary to explore the complete tree and the success of "B&B" is partly due to the fact that integer sub-trees can be excluded from the search if the node to the root produces an infeasible integer solution. The problem "MIQP" to solve has the following form:

$$\begin{cases} \min\ x^T Q x + b^T x \\ \text{subject to constraints :} \begin{cases} Cx + d \leq 0 \\ x = \begin{bmatrix} x_c \\ x_l \end{bmatrix},\ x_c \in \Re^{n_c},\ x_l \in \{0,1\}^{n_l} \end{cases} \end{cases} \tag{19}$$

The idea of solving this MIQP with methods "B&B" is based on the relaxation of the whole constraints, variables may be in the continuous interval [0, 1].

Let ξ be a vector of dimension n_d and the symbol "*" meaning that the entry of ξ is relaxed, i.e. may be in continuous interval. Consider the following initial problem MIQP without full constraints:

$$\xi_0 = \underbrace{[*, *, \ldots, *]}_{n_d} \tag{20}$$

The vector ξ_0 will be assigned to the root of the tree. Separating the initial ***MIQP*** problem sub-problem ***QP*** relaxed is performed by assigning **0 or 1** to integer variables. New problems resulting ***QP*** are assigned to children of the node.

If the component of the element $\xi^i = 0$(ou $\xi^i = 1$), then the ***QP*** corresponding to that node is solved by placing the ith binary variable to 0 (or 1).

The tree of ***MIQP*** problem can be explored in several ways. The choice of the separation of the problem and the procedure for consideration of sub-problems affect the average volume calculation. A good "Branch & Bound" algorithm aims to quickly search the integer's sub-trees by reducing the number of sub-problems resolutions. Two choices determine the order of sub-problems: (1) the branching rule, and (2) the exploration of the tree strategy.

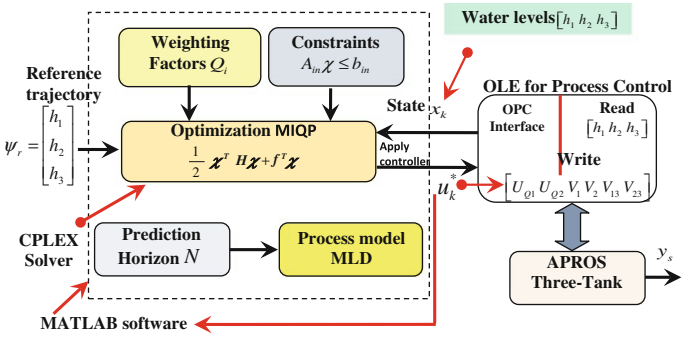

Fig. 5 Hybrid Model predicted control strategy applied on-line to the three-tank system under APROS environmental Software

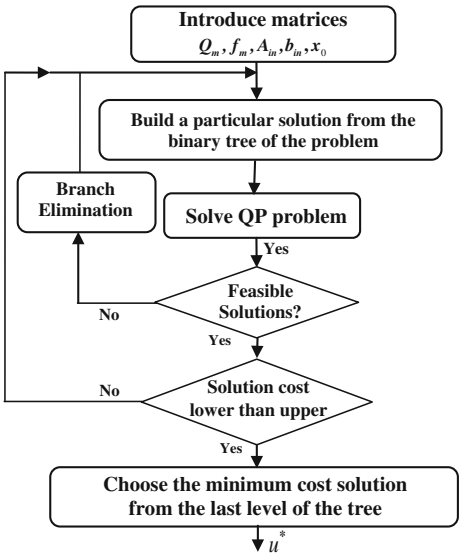

Fig. 6 Branch and bound algorithm [20]

The solver used to solve the problem ***MIQP*** developed under the **MATLAB** environment based on a strategy of "B&B" (Fig. 5) and includes the tree exploration strategy and the selection rule branching variables (Fig. 6). The problem solved by this program takes the quadratic formulation ***MIQP*** following:

$$\begin{cases} \min \frac{1}{2}\chi^T H\chi + f^T\chi \\ \\ \text{subject to constraints :} \begin{cases} A\chi \le b \\ A_{eq}\chi \le b_{eq} \\ v_{lb} \le \chi \le v_{ub} \\ \chi \in \Re^{m_c} \times \{0,1\}^{nt_d} \\ \chi\left(i\text{var}_{type}\right) \in \{0,1\}^{nt_d} \end{cases} \end{cases} \tag{21}$$

The length of vector optimization is $nt = nt_c + nt_d$. The variables are stored by the index "$i_{\text{var } type}$" subset of $\{1, \ldots, nt_c + nt_d\}$, are binary constraints. The matrix $H \in \Re^{nt \times nt}$ is positive semi-definite. The special case where $H = 0$ corresponds to mixed integer program (***MILP***) and can also be treated by this optimization program. The matrix $A \in \Re^{mt \times nt}$ and vector $b \in \Re^{mt}$ define linear constraints inequality type of optimization variables. Linear constraints equal type are given by $A_{eq} \in \Re^{mt \times nt}$ and $b_{eq} \in \Re^{mt}$ and while limits on optimization vector may be indicated by the v_{lb}, $v_{ub} \in \Re^{nt}$ vectors.

4 Application

4.1 Description of the Modeling Tool APROS

This section discusses the modeling and simulation environment under the APROS (Advanced Process Simulation Software). This tool is multifunctional software used by various methods such as power plants and nuclear reactors. It was developed by VTT Technical Research Centre of Finland. The APROS software was primarily used in nuclear power plants and combustion power plants. It can simulate and examine the thermal-hydraulic behavior of processes in transient and steady. It is based on an inhomogeneous hydrodynamic model and not balanced for the two-phase flow system solved by implicit, semi expressed or implied numerical methods. The development and enrichment is constantly growing meets the requirements of users in different areas. The latest version has undergone a mutation to Simantics platform that includes tools for modeling and simulation as Fluent and Modelica.

The modeling is to use a set of predefined process component models that are conceptually one-to-one with a concrete form (pumps, valves, tanks ... etc.). The setting of the components is achieved by the introduction of physical properties. Then we connect the components by Connections to establish the link between the various elements constituting the process (http://www.Apros.fi) [1].

The database structure APROS is subject to a hierarchical model. We acting on the component level by using components of predefined processes, such as pipes, valves, heat exchangers, automatically generate objects of calculation levels.

The modeling process is organized around a set of models. Each model is composed of one or more sub-model contained in Grades net pages. The net form contains the basic components of the process. Each component has an interface for introducing the initialization data, which later will be used to simulate the dynamic behavior. The components defined in the simulation are out of data determining the boundary conditions.

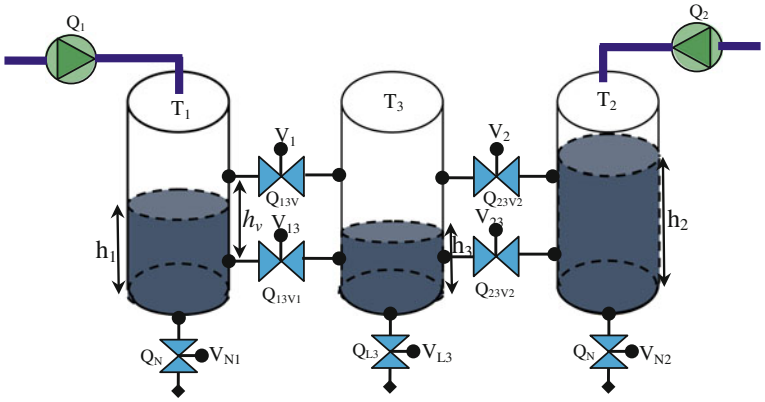

Fig. 7 Benchmark three-tank 'COSY'

4.2 Description of the Benchmark Three Tanks 'COSY'

The hydraulic system with three tanks is governed by a set of mathematical equations that describe the transient and steady dynamic behavior. The benchmark COSY (Control of Complex Systems) shown in Fig. 7 is, in fact, a model designed for control problems and detection failures of hybrid systems [18].

The system consists of three tank filled by two independent pumps Q_1 *et* Q_2 flow into the tanks T1 and T2 respectively. Both pumps are operated in a continuous manner from 0 to a maximum flow rate $Q_{\max}$. The four valves V_1, V_2, V_{13} et V_{23} control the flow between the reservoirs as shown in Fig. 8. These four valves are all or nothing (open if $V_i = 1$, else closed). The manual valve V_{N3} control the nominal flow rate output of the central tank. It is assumed throughout the rest of our study that the manual valves and V_{N1} et V_{N2} are still closed and V_{N3} open. Water levels to control are denoted h_1, h_2 et h_3 respectively.

4.3 Modeling of Three-Tank System

Conservation of mass in the tanks provides differential equations:

$$\begin{cases} \dot{h}_1 = \frac{1}{A}(Q_1 - Q_{13V_1} - Q_{13V_{13}} - Q_{N_1}) \\ \dot{h}_2 = \frac{1}{A}(Q_2 - Q_{23V_2} - Q_{23V_{23}} - Q_{N_2}) \\ \dot{h}_3 = \frac{1}{A}(Q_{13V_1} + Q_{13V_{13}} + Q_{23V_2} + Q_{23V_{23}} - Q_{N_3}) \end{cases} \tag{22}$$

where Q_i represents the flow variables and A section of each of the tanks. Torricelli's law provides the expressions flow in valves:

$$Q_{13V_{13}} = V_{13} a S_{13} sign(h_1 - h_3)\sqrt{|2g(h_1 - h_3)|} \tag{23}$$

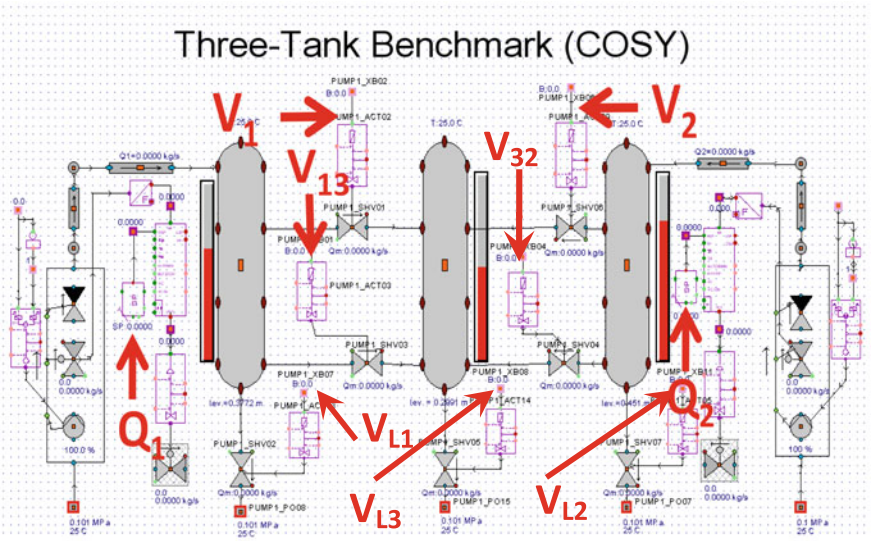

Fig. 8 Modeling the three tanks system by APROS software

$$Q_{23V_{23}} = V_{23} a S_{23} sign(h_2 - h_3)\sqrt{|2g(h_2 - h_3)|} \tag{24}$$

$$Q_{13V_1} = V_1 a S_1 sign(\max(h_1 - h_v) - \max(h_3 - h_v))\sqrt{|2g(\max(h_1 - h_v) - \max(h_3 - h_v))|} \tag{25}$$

$$Q_{23V_2} = V_2 a S_2 sign(\max(h_2 - h_v) - \max(h_3 - h_v))\sqrt{|2g(\max(h_2 - h_v) - \max(h_3 - h_v))|} \tag{26}$$

$$Q_{N3} = V_{N3} a S_{N3}\sqrt{2gh_3} \tag{27}$$

where S_i represents the surface of the valve V_i and a is a constant dependent on the liquid (Table 1).

Table 1 Three-tank benchmark parameters

Symbol	Meaning	Value
A	Tank section	$0.0154\,\mathrm{m}^2$
S_h	Cross-section of valve V_h	$2 \times 10^{-5}\,\mathrm{m}^2$
g	Gravity constant	$9.81\,\mathrm{m/S}^2$
$h_{\max}$	Upper level water	$0.62\,\mathrm{m}$
h_v	Height of valve V_1 *et* V_2	$0.30\,\mathrm{m}$
$Q_{i\max}$	Maximum inflow through pump $i(i = 1, 2)$	$10^{-4}\,\mathrm{m}^3/\mathrm{s}$
T_s	Sampling time	$5\,\mathrm{s}$

In order to model the entire test bed in the MLD form should be to approximate the non-linear relationships giving flows through the following linearized equations:

$$Q_{i3V_{i3}} \approx k_{i3} V_{i3}(h_i - h_3) \tag{28}$$

$$Q_{i3V_i} \approx k_i V_i(\max(h_v - h_i) - \max(h_v - h_3)) \tag{29}$$

$$Q_{N3} \approx k_{N3} V_{N3} h_3 \tag{30}$$

With: $i = 1, 2$.

$$k_{i3} \approx aS_{i3}\sqrt{\frac{2g}{h_{\max}}} \tag{31}$$

$$k_i \approx aS_i\sqrt{\frac{2g}{h_{\max} - h_v}} \tag{32}$$

$$k_{N3} \approx aS_{N3}\sqrt{\frac{2g}{h_{\max}}} \tag{33}$$

4.4 Modelling Three-Tank System Under APROS

The modeling of the system under the COSY APROS environment (Fig. 8) requires the use of certain components namely: pipes, valves discrete control by pneumatic actuators, reservoirs, check valves, pumps and boundary conditions with analog and digital inputs.

The open loop simulation performed on our model "three-tanks" mathematics and APROS, for flow control levels with gradual variation between the maximum and Qmax zero. For binary commands from the valves of interconnections between the tanks and output each. The results shows some differences between the response of the mathematical model and APROS model that is partly due to numerical calculations following the discretization of the mathematical model and hydraulic parameters declared in the environment of APROS is height hydraulic pressure losses caused by the valves, the other hand pipes. This modeling aspect in the APROS environment takes into account all the physical and hydraulic considerations (temperature, pressure, viscosity coefficient,... etc.) That are not included in a mathematical model.

4.5 Processed into MLD Model

From these expressions, an MLD model can be obtained by conventional techniques described in [3, 13, 14, 18] by introducing the auxiliary continuous and binary variables required by the interface translation, so that we will involves the following vectors:

$$x = [h_1\ h_2\ h_3]^T \tag{34}$$

$$u = [Q_1\ Q_2\ V_1\ V_2\ V_{13}\ V_{23}\ V_{L1}\ V_{L2}\ V_{N3}]^T \tag{35}$$

$$\delta = [\delta_{01}\ \delta_{02}\ \delta_{03}]^T \tag{36}$$

$$z = [z_{01}\ z_{02}\ z_{03}\ z_1\ z_2\ z_{13}\ z_{23}\ z_{L1}\ z_{L2}\ z_{N3}\ ]^T \tag{37}$$

With:

$$[\delta_{0i}(k) = 1] \leftrightarrow [h_i(k) \geq h_v]\ \ i = 1, 2, 3 \tag{38}$$

$$z_{0i}(k) = \delta_{0i}(k)(h_i(k) - h_v)\ \ i = 1, 2, 3 \tag{39}$$

$$z_i(k) = V_i(k)(z_{0i}(k) - z_{03}(k))\ \ i = 1, 2 \tag{40}$$

$$z_{i3}(k) = V_{i3}(k)(h_i(k) - h_3(k))\ \ i = 1, 2 \tag{41}$$

From the relations (14)–(32), using the discretization technique to first order (Euler) $\dot{h}(t) \rightarrow h(k+1) - h(k)/T_s$, we obtain the following discrete form:

$$\begin{cases} h_1(k+1) = h_1(k) + \frac{1}{A}(Q_1 - k_1 z_1(k) - k_{13} z_{13}(k) - k_{L1} z_{L1}(k)) \\ h_2(k+1) = h_2(k) + \frac{1}{A}(Q_2 - k_1 z_2(k) - k_{23} z_{23}(k) - k_{L2} z_{L2}(k)) \\ h_3(k+1) = h_3(k) + \frac{1}{A}(k_1 z_1(k) + k_{13} z_{13}(k) + k_2 z_2(k) + k_{23} z_{23}(k) - k_{N3} z_{N3}(k)) \end{cases} \tag{42}$$

The MLD structure therefore requires the addition of three (03) binary auxiliary variables and seven (07) continuous auxiliary variables, it is reminder that the control vector includes two (02) continuous variables and four (04) binary variables and the vector state contains only three (03) continuous variables because the system does not have discrete dynamics. The HYSDEL File MLD model for this system is as Fig. 9.

The hybrid approach was applied initially on the model APROS three tanks with the following configuration: the control vector with the outlet valve on the tank T3 is kept fully open by against the two outlet valves on the T1 and T2 tanks are completely closed (see Fig. 10). The MLD model developed for the synthesis of MPC is composed of two continuous variables, 4 binary variables, 3 auxiliary binary variables and 7 auxiliary continuous variables with 44 linear mixed integer constraints. The **MPC** control problem is transformed into a linear optimization problem with constraints whole mixed giving on a prediction horizon selected equal to the order

```
SYSTEM Three Tanks {

INTERFACE {
STATE {
        REAL h1,h2,h3;
}
INPUT {
        REAL Q1,Q2;
        BOOL
V1,V2,V13,V23;
}
PARAMETER
{
REAL Su = 0.0154;
REAL Ts = 5;
/* constant for valves V13, V23,
VL1 and VN3 */
REAL k1 = 0.0001125;
REAL k2 = 0.0001566;
 /* constant for valves V1 and V2
*/
REAL hmax = 0.62;
REAL hv = 0.30;
REAL Qmax = 0.0001;
REAL VL1 = 0;
REAL VL2 = 0;
REAL VN3 = 1;
}
}
IMPLEMENTATION {
AUX {
REAL z01,z02,z03,z1,z2,z13,z23;
BOOL d01,d02,d03;
}
```

```
AD
{d01 = hv-h1 <= 0;
        d02 = hv-h2 <= 0;
        d03 = hv-h3 <= 0;
}
DA
{z01={ IF d01 THEN h1-hv  ELSE 0};
        z02={ IF d02 THEN h2-hv  ELSE 0};
        z03={ IF d03 THEN h3-hv  ELSE 0};
        z1={ IF V1 THEN z01-z03 ELSE 0};
        z2={ IF V2 THEN z02-z03 ELSE 0};
z13={ IF V13 THEN h1-h3 ELSE 0};
z23={ IF V23 THEN h2-h3 ELSE 0};
}
CONTINUOUS
{ h1=h1+(Ts/Su)*(Q1-k1*z13-k2*z1-
k1*h1*VL1);
h2=h2+(Ts/Su)*(Q2-k1*z23-k2*z2);
h3=h3+(Ts/Su)*(k1*z13+k1*z23+k2*z1+k2*z2-
k1*h3*VN3);
}
MUST
{h1<=hmax;
        h2<=hmax;
        h3<=hmax;
        -h1<=0;
        -h2<=0;
        -h3<=0;
        Q1<=Qmax;
        Q2<=Qmax;
 -Q1<=0;
-Q2<=0;}
}
}
```

Fig. 9 The HYSDEL File MLD model of the three tanks system

N = 3 to 48 continuous and binary variables with 132 mixed integer linear constraints. Controls calculated by ***MIQP*** optimization program with **CPLEX** solver are applied via the **OPC** interface (**OLE for Process Control**) on the model to achieve the water level specifications h1 = 0.45 m; h2 = 0.35 and h3 = 0.1 m. Three tanks being initially empty (level = 0). Note that the level of the third tank exhibits oscillations around the name, as the level h3 = 0.1 m does not correspond to an equilibrium point level for these instructions, the outflow of the third tank Q_{N3} is equal to any combination of inflows (Q_{13V1}, Q_{23v2}, Q_{13V13} et Q_{23V23}). The level h_2 does not present oscillations and that the two valves are kept closed after reaching the set point h_{r2}=0.35 m. Against by the level of the tank T1 exhibits oscillations induced by the opening and closing of the two valves [V_1 V_{13}] for the h_1 and h_3 level adjustment around their instructions. For the choice of weights in the optimization criterion, our choice is particularly intended for the penalization of tracking error between levels and set points affected by the matrix Qy = 6000.

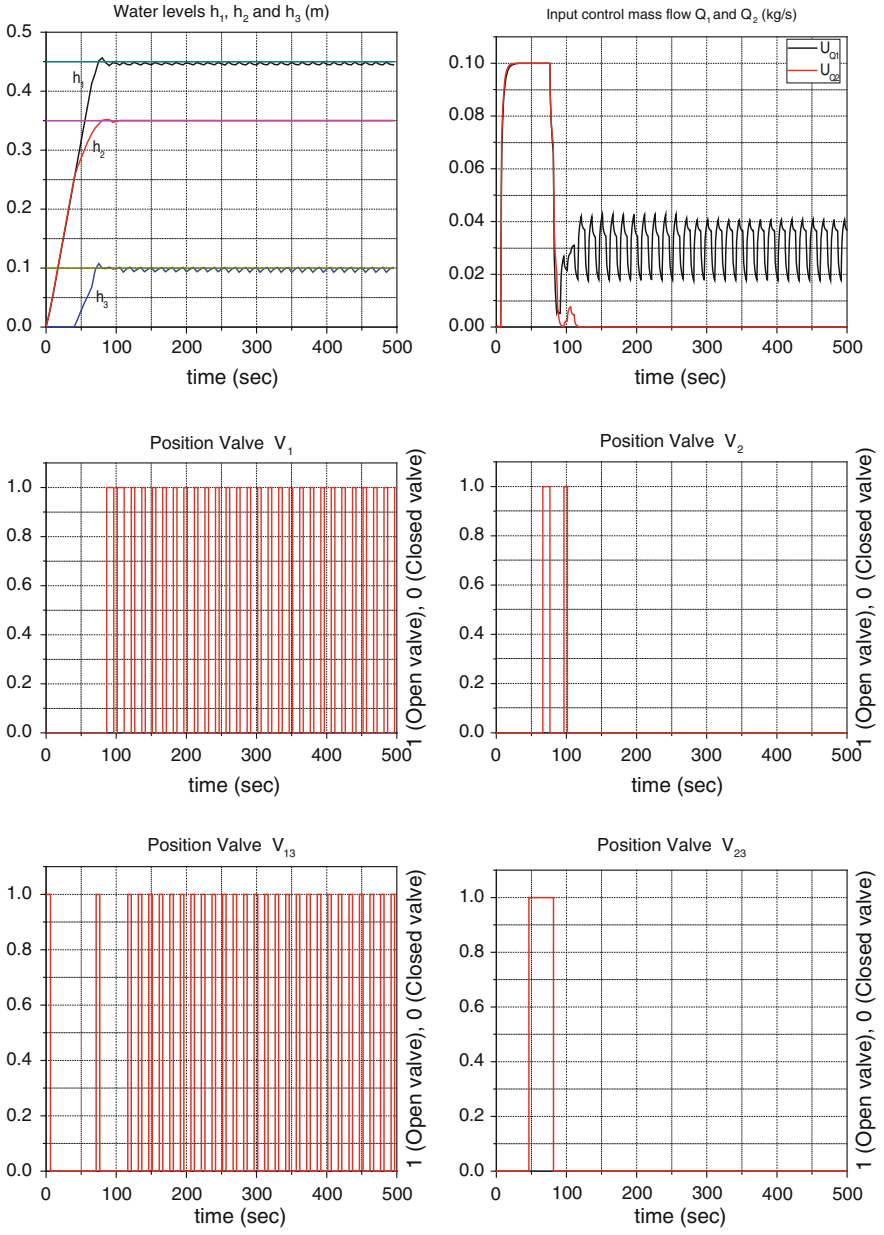

Fig. 10 Predictive control of fluid levels h_1, h_2 and h_3 (Prediction horizon N = 3, $Q_u = 610^3$, $Q_d = Q_z = 10^{-2}$, valve V_{L3} (=1) is held open)

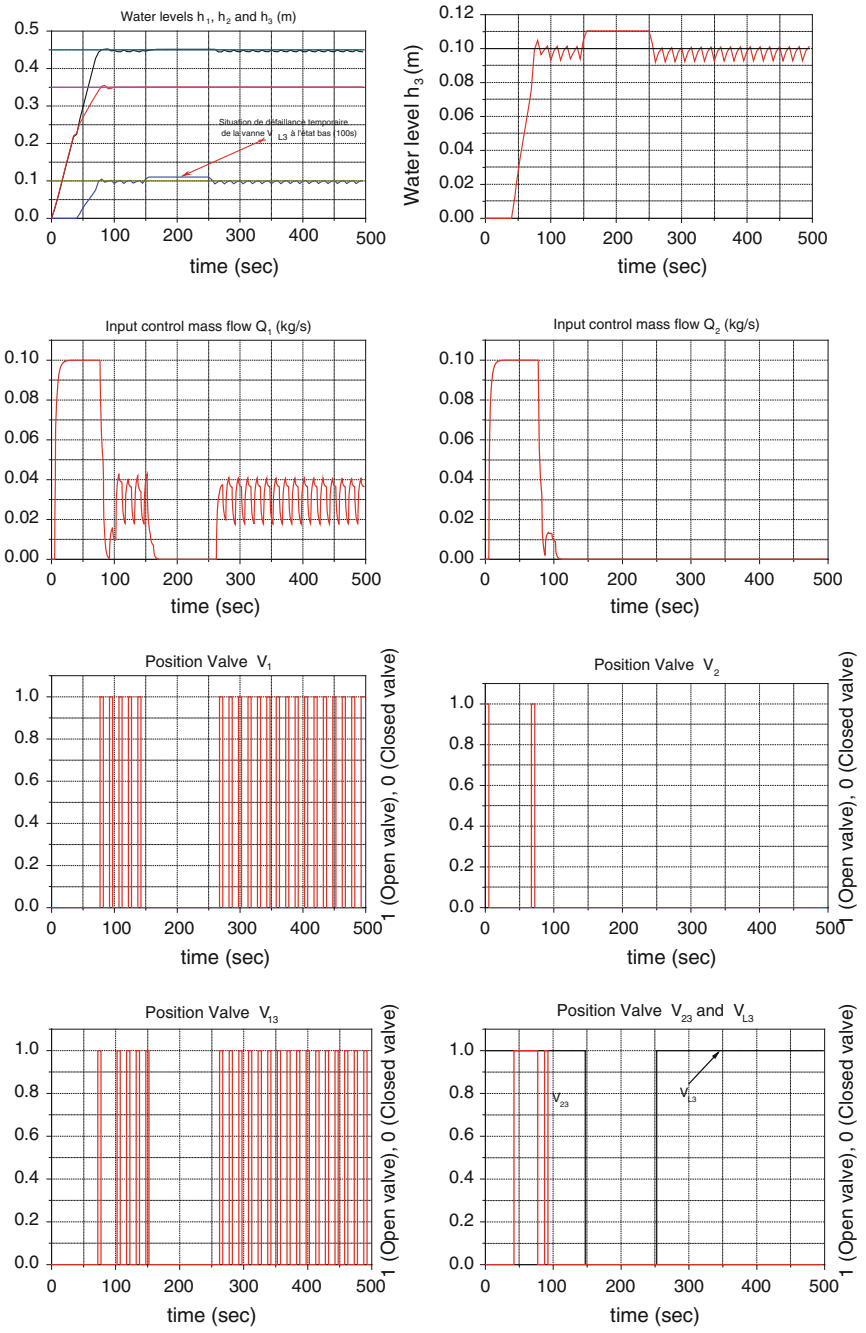

Fig. 11 Predictive control of the leves h_1, h_2 and h_3 (Prediction horizon N=3, Q_u=610^3, Q_d=Q_z=10^{-2}, valve V_{rmL3} (=1) is held open with deadlock in the low state for 100 s)

In order to test the robustness of the control algorithm vis-à-vis a blocking position of the outlet valve VL3 on the third tank R3. The same previous configuration is reused with the situation following locking at time t = 150 s, the VL3 valve is kept closed for 100 s (end of blocking at time 250 s).

The predictive controller responds quickly to this situation after one sampling period with an overshoot less than 10 % of the value of the h3 set point. This disturbance in the functioning of the system is rejected by the regulator acting on the state of the two valves $[V_1, V_2]$ leading them to the closure and flow Q_1 to a total shutdown (see Fig. 11). From time t = 250 s, the system resumes operation correctly by acting on the valves between the tank R1 and R3 by performing the emptying and oscillations around the level h1 and h3 appear again to maintain the set around their set points references.

5 Conclusion

In this chapter we presented definitions hybrid dynamic systems, and applications in the field of industry. We also flew review the models and work performed mainly affecting the control of hybrid dynamic systems. Subsequently, there is described the various steps necessary for the modeling with the MLD formalism. MLD model is used for the development of an MPC predictive control strategy.

The so-called MLD representation of a hybrid system is particularly well suited to the implementation of predictive control strategy for these systems. Nevertheless, the combinatorial explosion resulting from a large number of binary variables from the MLD formalism restricts online application possibilities of this structure for low sampling period systems.

The application of this strategy in the three-tank benchmark under the APROS environment, brings interesting for the implementation of a predictive control strategy for hybrid systems in the form MLD in real time.

References

1. Apros—Dynamic Process Simulation Software. http://www.apros.fi
2. Bemporad A, Morari M (1999) Control of systems integrating logic, dynamics and constraints. Automatica 35:407–427
3. Bemporad A, Mignone D, Morari M (1999) Moving horizon estimation for hybrid systems and fault detection. In: International proceedings of the american control conference, SanDiego
4. Camacho EF, Bordons C (2007) Model predictive control. Springer, London
5. Cavalier TM, Pardalos PM, Soyster AL (1990) Modeling and integer programming techniques applied to propositional calculus. J Oper Res 17:561–570 (Pergamon Press)
6. Clarke DW, Mohtadi C, Tuffs PS (1987) Generalized predictive control—part I. and II. Automatica 23:137–160 (Pergamon Journal)
7. De Schutter B, de Moor B (1999) The extended linear complementarity problem and the modeling and analysis of hybrid systems. In: Antsaklis P, Kohn W, Lemmon M, Nerode A,

Sastry S (eds) Hybrid systems. Volume 1567 of lecture notes in computer science, pp 70–85. Springer, Berlin
8. De Schutter B, van den Boom T (2000) On model predictive control for maxmin-plus-scaling discrete event systems. Technical Report, The Netherlands
9. Fletcher R, Leyffer S (1995) Numerical experience with lower bounds for MIQP branch and bound. Technical report, department of mathematics, University of Dundee, Scotland
10. Levis AH et al (1987) Challenges to control: a collective view. IEEE Trans Autom Control AC-32:275–285
11. Heemels WPMH (1999) Linear complementarity Systems: A Study in hybrid dynamics. Ph.D. thesis, Department of Electrical Engineering, Eindhoven University of Technology, The Netherlands
12. Leenaerts DMW, van Bokhoven WMG (1998) Piecewise linear modeling and analysis. Kluwer Academic Publishers, Dordrecht (Springer science)
13. Mignone D (2002) Control and estimation of hybrid systems with mathematical optimization. Swiss federal institute of technology (ETH), thesis for the degree of Dr. Science, Italy
14. Nareshkumar NN (2009) A Multiple model approch for modeling, identification and control of nonlinear hybrid systems. Indian Institute of technology Bombay
15. Raman R, Grossmann IE (1992) Integration of logic and heuristic knowledge in MINLP optimization for process synthesis. Comput Chem Eng 16:155–171
16. Richalet J, Rault A, Testud JL, Papon J (1978) Model predictive heuristic control: applications to industrial processes. Automatica 14:413–428
17. Riedinger P (2000) Contribution à la commande optimale des systèmes dynamiques hybrides. PhD thesis, Centre de recherche en Automatique de Nancy & Institut National Polytechnique de Lorraine, France
18. Thomas J (2004) Estimation et commande prédictive à horizon glissant de systèmes hybrides. Ph.D. thesis, University Paris XI Orsay, Supelec
19. Torrisi FD, Bemporad A (2004) HYSDEL—a tool for generating computational hybrid models for analysis and synthesis problems. IEEE Trans Control Syst Technol 12:235–249
20. Villa JL, Duque M, Gauthier A, Rakoto-Ravalontsalama N (2003) MLD control of hybrid systems: application to the three-tank benchmark problem. In: IEEE International, conference on systems, man & cybernetics (SMC2003), USA, pp 666–671. Accessed 5–8 Oct 2003
21. Williams HP (2013) Model building in mathematical programming. 3rd edn. Wiley, New York

A Non-linear Decentralized Control of Multimachine Power Systems Based on a Backstepping Approach

M. Ouassaid, M. Maaroufi and M. Cherkaoui

Abstract Power system requires high-performance control techniques due to their elevated complexity, high nonlinearity and almost continuously time-varying nature. Also, power systems are often subjected to small and large disturbances. To enhance the multimachine power system stability, a new approach to designing decentralized nonlinear control scheme is proposed. The approach seeks first build a novel mathematical model of multimachine power systems. The main characteristic of this model is that interactions between generators and changes in operating conditions are represented by time-varying parameters. More important, those parameters are update online, using only local measurements. Second, it develops a decentralized controller for the transient stabilization and voltage regulation. The controller consists of two controllers, known as the terminal voltage regulator and rotor speed stabilizer. The methodology adopted is based on backstepping design strategy. The proposed stabilizing feedback laws for the power system are shown to be globally asymptotically stable in the context of Lyapunov theory. Case studies are achieved in a two-area four machine power system to verify the effectiveness of the approach. Numerical results are presented to illustrate the usefulness and the performance of the proposed control scheme, under different contingencies.

Keywords Modeling of a multimachine power system · Backstepping design · Voltage regulation · Transient stability · Nonlinear decentralized control

M. Ouassaid (✉) · M. Maaroufi · M. Cherkaoui
Ecole Mohammadia d'Ingénieurs, Mohammed V University, Rabat, Morocco
e-mail: ouassaid@emi.ac.ma

M. Maaroufi
e-mail: maaroufi@emi.ac.ma

M. Cherkaoui
e-mail: cherkaoui@emi.ac.ma

S. Vaidyanathan and C. Volos (eds.), *Advances and Applications in Nonlinear Control Systems*, Studies in Computational Intelligence 635,
DOI 10.1007/978-3-319-30169-3_20

1 Introduction

Modern Electrical Power Systems (EPS) are increasingly operated closer to their transfer power and stability limits. The control systems, accordingly, will have to regulate the system, to improve its global stability including inter-area transfer capability and dynamic performance under a diversity of operating conditions. Traditionally, conventional controllers such as the Automatic Voltage Regulator (AVR), the Power System Stabiliser (PSS) and Speed Governor (SG), are mainly designed by using linear models of the power systems [16]. Those linear controllers, based mainly on classical control algorithms, can be used to insure asymptotic stability of the equilibrium following a small perturbation. Unfortunately, in the event of a large disturbance, the operating point of the system may vary significantly and a linear controller may not be able to guarantee asymptotic stability.

Therefore, the high complexity and nonlinearity of power systems together with their almost continuously time varying nature require candidate controllers to be able to take into account the important non linearities of the power system model and to be independent of the equilibrium point [16]. To meet this challenge, a lot of interest has been considered in the application of the nonlinear control theory for the control of power systems and consequently to enhance the power systems stability. Most of these controllers are based on feedback linearization [8, 34], Hamiltonian techniques [35, 37], sliding-mode control [4, 5, 9, 11, 17, 24, 25] have been successfully applied to improve the transient stability. New approaches have been proposed for power stability designs according to other sophisticated schemes such as fuzzy logic control [1, 6, 19], adaptive control [7, 10, 12, 13, 29, 36], and neurocontrol [18, 26, 32]. Combinations of the above techniques are also proposed in order to exploit the advantages of each method at the cost of the increase in complexity [2, 28, 33].

The backstepping is one of the most important techniques, which provides a powerful design tool to solve many design problems under restrictive conditions than those encountered in the other methods [15, 27]. Further, the adaptive backstepping approach is capable of guaranteeing almost all robustness properties of the mismatched uncertainties [30, 31]. This technique has been successfully applied for power system in [14, 22, 23].

Generally, the design of the controllers, for power system, is based on two main modeling approaches:

- The Single-Machine, Infinite-Bus (SMIB) approach is simple but it does not take into account dynamic phenomena in the rest of the electrical network. Therefore, controllers may not perform well when inter-area oscillations occur.
- The Multimachine Power System (MPS) approach is based on the global N-generator modeling [9, 34]. The controllers based on this model dampen inter-machine and inter-area oscillations very well.

A new approach for modelling the EPS combines the advantages of both previous modelling approaches [20, 21]. The approach consists of partitioning the power system into the generator to be controlled and the rest of the network viewed as dynamic load. The time-varying parameters of the resulting model encapsulate operating-condition variations and interactions between generators. Nevertheless, wide area control laws are derived from a reformulation of the multimachine model, generator terminal voltages are used as state variables instead of internal field voltages, through complex transformations. In addition, time varying parameters of the model are unknown and must be estimated online by an adaptation process.

The main aim of this study is the design of controllers to guarantee the voltage regulation and enhance transient stability for multimachine power systems. These controllers are proposed to replace the traditional speed governor (SG), automatic voltage regulator (AVR) plus the power system stabilizer control structure (PSS). To this end, a novel modelling of multimachine power system is proposed. Contrary to the model proposed in Okou et al. [20, 21] which is based on a third order simplified model, in the resulting modelling, the model of synchronous machine is based on a seventh order model which takes into account both field effects and damper winding effects introduced by different rotor circuits. In addition, time varying parameters of the model, which depend on the steady-state active and reactive power delivered by each generator, and the interactions between generators, are update continuously online.

Furthermore, a backstepping control system is designed to control the rotor speed and terminal voltage, simultaneously, in order to enhance the transient stability and ensure good post-fault voltage regulation for power system. The theoretical bases of the proposed control technique are derived in detail where the feedback system is shown to be globally asymptotically stable in the sense of the Lyapunov's stability theory.

Finally, the decentralized proposed controller requires only local measurement, which owns highly desirable advantages in cost, reliability and can be easily implemented.

The rest of this chapter is organized as follows. In Sect. 2, a new dynamic mathematical model of a multimachine power system is developed. Section 3 is devoted to a design of a backstepping control for the multimachine power system to ensure the voltage regulation and enhance the transient stability of the system. The stability of this controller is proven. In Sect. 4, simulation results are given to validate the proposed model and illustrate the performance of the proposed scheme. Also, the performances of the developed controller are compared to the performance of a standard AVR/PSS and SG. Conclusions are finally made in Sect. 5.

2 New Dynamic Power System Model

2.1 Mathematical Model of Synchronous Generator

The synchronous generator is described by a 7th order nonlinear mathematical model which comprises three stator windings, one field winding and two damper windings. The model takes into account both field effects and damper windings effects introduced by the different rotor circuits. The synchronous machine equations in terms of Park's d-q axis are expressed as follows [3, 16]

$$\begin{cases} v_d = -R_s i_d + L_q \omega i_q - L_{mq} \omega i_{kq} - L_d \frac{di_d}{dt} + L_{md} \left(\frac{di_{fd}}{dt} + \frac{di_{kd}}{dt} \right) \\ v_q = -R_s i_q + -L_d \omega i_d + L_{md} \omega (i_{fd} + i_{kd}) - L_q \frac{di_q}{dt} + L_{mq} \frac{di_{kq}}{dt} \\ v_{fd} = R_s i_{fd} - L_{md} \frac{di_d}{dt} + L_{fd} \frac{di_{fd}}{dt} + L_{md} \frac{di_{kd}}{dt} \\ 0 = R_{kd} i_{kd} - L_{md} \frac{di_d}{dt} + L_{md} \frac{di_{fd}}{dt} + L_{kd} \frac{di_{kd}}{dt} \\ 0 = R_{kq} i_{kq} - L_{mq} \frac{di_d}{dt} + L_{kq} \frac{di_{kq}}{dt} \end{cases} \tag{1}$$

where v_d and v_q are direct and quadrature axis stator terminal voltage components, respectively; v_{fd} excitation control input; v_t terminal voltage; i_d, i_q direct and quadrature axis stator current components, respectively; i_{fd} field winding current; i_{kd}, i_{kq} direct and quadrature axis damper winding current components, respectively; R_s stator resistance; R_{fd} field resistance; R_{kd}, R_{kq} damper winding resistances; L_d, L_q direct and quadrature self inductances, respectively; L_{fd} rotor self inductance; L_{kd}, L_{kq} direct and quadrature damper winding self inductances, respectively; L_{md}, L_{mq} direct and quadrature magnetizing inductances, respectively.

Mechanical equations are as follows

$$2H \frac{d\omega}{dt} = T_m - T_e - D\omega \tag{2}$$

$$\frac{d\delta}{dt} = \omega - 1 \tag{3}$$

where ω is angular speed of the generator; δ rotor angle of the generator; T_m mechanical torque, T_e electromagnetic torque; D damping constant; H inertia constant.

The electromagnetic torque is

$$T_e = \left(L_q - L_d \right) i_d i_q + L_{mfd} i_{fd} i_q + L_{md} i_{kd} i_q - L_{mq} i_d i_{kq} \tag{4}$$

The steam turbine dynamics and valve are represented by the following equations [8].

$$\begin{cases} \frac{dP_m}{dt} = -\frac{1}{T_t} P_m + \frac{K_m}{T_t} X_e \\ \frac{dX_e}{dt} = -\frac{1}{T_g} X_e + \frac{K_g}{T_g} \left(u_g - \frac{1}{R\omega_R} \omega \right) \end{cases} \tag{5}$$

where X_e is the steam valve opening of the system; u_g the input power of control system; T_t the time constant of the turbine; K_t the gain of the turbine; R the regulation constant of the system; T_g the time constant of the speed governor; K_g the gain of the speed governor and ω_R is the power system frequency.

2.2 Mathematical Model of the Rest of the Network

The modelling of the rest of network is made by using the concept introduced in [20]. In this approach, each generator views the rest of the grid as a dynamic load. This load is represented by an instantaneous effective impedance and is given by the following equation in per-unit

$$v(t) = R_L(t)i(t) + X_L(t)\frac{di(t)}{dt} \tag{6}$$

where v and i are the generator's instantaneous terminal voltage and stator current, respectively. The time dependent parameters $R_L(t)$ and $X_L(t)$ summarize the dynamic exchange of active and reactive powers, respectively.

In the d-q reference frame, after applying a Park transformation, we obtain

$$\begin{cases} v_d = R_L(t)i_d - X_L(t)\omega i_q + X_L(t)\frac{di_d}{dt} \\ v_q = R_L(t)i_q + X_L(t)\omega i_d + X_L(t)\frac{di_q}{dt} \end{cases} \tag{7}$$

2.3 New Dynamic Mathematical Model of Multimachine Power System

The mathematical model is obtained by combining equations of the synchronous generator (1) with equation of the rest of the network (7). After some lengthy but straightforward algebraic manipulations, the resulting model has the following form

$$\begin{cases} \frac{di_d}{dt} = h_{11}(t)i_d + h_{12}(t)i_{fd} + h_{13}(t)\omega i_q + h_{14}(t)i_{kd} + h_{15}(t)i_{kq}\omega + g_1(t)u_{fd} \\ \frac{di_{fd}}{dt} = h_{21}(t)i_d + h_{22}(t)i_{fd} + h_{23}(t)\omega i_q + h_{24}(t)i_{kd} + h_{25}(t)i_{kq}\omega + g_2(t)u_{fd} \\ \frac{di_q}{dt} = h_{31}(t)i_d\omega + h_{32}(t)i_{fd}\omega + h_{33}(t)i_q + h_{34}(t)i_{kd}\omega + h_{35}(t)i_{kq} \\ \frac{di_{kd}}{dt} = h_{41}(t)i_d + h_{42}(t)i_{fd} + h_{43}(t)i_q\omega + h_{44}(t)i_{kd} + h_{45}(t)i_{kq}\omega + g_3(t)u_{fd} \\ \frac{di_{kq}}{dt} = h_{51}(t)i_d\omega + h_{52}(t)i_{fd}\omega + h_{53}(t)i_q + h_{54}(t)i_{kd}\omega + h_{55}(t)i_{kq} \\ \frac{d\omega}{dt} = h_{61}(t)\omega + h_{62}(t)\frac{P_m}{\omega} - h_{62}(t)T_e \end{cases} \tag{8}$$

The time-varying parameters $h_{ij}(t)$ and $g_i(t)$ depend on $R(t)$ and $X(t)$ and hence on the operating conditions of the power system. Their expressions are given as follow

$$h_{11}(t) = -(R_s + R_L(t))(L_{fd}L_{kd} - L_{md}^2)\omega_R D_d^{-1} \quad h_{12}(t) = -R_{fd}(L_{mq}L_{kd} - L_{md}^2)\omega_R D_d^{-1}$$
$$h_{13}(t) = (L_q + X_L(t))(L_{md}L_{kd} - L_{md}^2)\omega_R D_d^{-1} \quad h_{14}(t) = R_{kd}((L_d + X_L(t))L_{md} - L_{md}^2)\omega_R D_d^{-1}$$
$$h_{15}(t) = -L_{mq}(L_{fd}L_{kd} - L_{md}^2)\omega_R D_d^{-1}$$

$$h_{21}(t) = -(R_s + R_L(t))(L_{md}L_{kd} - L_{md}^2)\omega_R D_d^{-1} \quad h_{22}(t) = -R_{fd}((L_d + X_L(t))L_{kd} - L_{md}^2)\omega_R D_d^{-1}$$
$$h_{23}(t) = (L_q + X_L(t))(L_{md}L_{kd} - L_{md}^2)\omega_R D_d^{-1} \quad h_{24}(t) = R_{kd}((L_d + X_L(t))L_{md} - L_{md}^2)\omega_R D_d^{-1}$$
$$h_{25}(t) = -L_{mq}(L_{md}L_{kd} - L_{md}^2)\omega_R D_d^{-1}$$

$$h_{31}(t) = (L_d + X_L(t))L_{kq}\omega_R D_q^{-1} \quad h_{32}(t) = L_{md}.L_{kq}\omega_R D_q^{-1}$$
$$h_{33}(t) = -(R_s + R_L(t))L_{kq}\omega_R D_q^{-1} \quad h_{34}(t) = L_{md}L_{kq}\omega_R D_q^{-1}$$
$$h_{35}(t) = -L_{mq}.R_{kq}\omega_R D_q^{-1}$$

$$h_{41}(t) = -(R_s + R_L(t))(L_{fd}L_{md} - L_{md}^2)\omega_R D_d^{-1} \quad h_{42}(t) = R_{fd}((L_d + X_L(t))L_{md} - L_{md}^2)\omega_R D_d^{-1}$$
$$h_{43}(t) = (L_q + X_L(t))(L_{md}L_d - L_{md}^2)\omega_R D_d^{-1} \quad h_{44}(t) = -R_{kd}((L_d + X_L(t))L_{fd} - L_{md}^2)\omega_R D_d^{-1}$$
$$h_{45}(t) = -L_{md}(L_{mq}.L_{fd} - L_{md}^2)\omega_R D_d^{-1}$$

$$h_{51}(t) = -(L_d + X_L(t))L_{mq}\omega_R D_q^{-1} \quad h_{52}(t) = L_{md}L_{mq}\omega_R D_q^{-1}$$
$$h_{53}(t) = -(R_s + R_L(t))L_{mq}\omega_R D_q^{-1} \quad h_{54}(t) = L_{md}L_{mq}\omega_R D_q^{-1}$$
$$h_{55}(t) = -R_{kq}(L_q + X_L(t))\omega_R D_q^{-1}$$

$$h_{61}(t) = 1/2H \quad h_{62}(t) = -D/2H$$

$$g_1(t) = (L_{md}L_{kd} - L_{md}^2)\omega_R D_d^{-1} \quad g_2(t) = ((L_d + L_{fd})L_{kd} - L_{md}^2)\omega_R D_d^{-1}$$
$$g_3(t) = ((L_d + X_L(t))L_{md} - L_{md}^2)\omega_R D_d^{-1}$$

These parameters encapsulate the interactions between the generator to be controlled and the rest of the grid.

In order to reduce the controller complexity and hence to increase its reliability, we consider the two-axis model assumption, by neglecting the stator current dynamics. Hence, equations (7) have the following form

$$\begin{pmatrix} v_d \\ v_q \end{pmatrix} = \begin{pmatrix} R_L(t) & -X_L(t)\omega \\ X_L(t)\omega & R_L(t) \end{pmatrix} \begin{pmatrix} i_d \\ i_q \end{pmatrix} \tag{9}$$

Therefore, the expressions of $R_L(t)$ and $X_L(t)$ in terms of the d-q axis voltage and current are derived of the forms

$$\begin{cases} R_L(t) = \frac{v_d i_d + v_q i_q}{i_d^2 + i_q^2} \\ X_L(t) = \frac{1}{\omega} \frac{v_q i_d - v_d i_q}{i_d^2 + i_q^2} \end{cases} \tag{10}$$

From (10), it is evident that, $R_L(t)$ and $X_L(t)$ are proportional to, respectively, the active and reactive power delivered by the generator and give information about the operating conditions of the rest of the grid. More important, they are update online using only local measurement.

The terminal voltage is defined by

$$v_t = \sqrt{v_d^2 + v_q^2} \tag{11}$$

The expressions of v_d and v_q as a function of the state variables can be expressed, by combining Eqs. (1) and (7), as follow

$$\begin{cases} v_d = \partial_{11}(t) i_d + \partial_{12} i_{fd} + \partial_{13} \omega i_q + \partial_{14} i_{kd} + \partial_{15} i_{kq} \omega + \partial_{16}(t) u_{fd} \\ v_q = \partial_{21}(t) i_d \omega + \partial_{22}(t) i_{fd} \omega + \partial_{23}(t) i_q + \partial_{24}(t) i_{kd} \omega + \partial_{25}(t) i_{kq} \end{cases} \tag{12}$$

where the time-varying parameters ∂_{ij} depend on $h_{ij}(t)$ and $g_i(t)$ and hence on the operating conditions of the power system. Their expressions are given as follows

$$\begin{aligned} \partial_{11}(t) &= R_L + h_{11}(t) X_L(t) \omega_R^{-1} & \partial_{12}(t) &= h_{12}(t) X_L(t) \omega_R^{-1} \\ \partial_{13}(t) &= X_L(t)(h_{13}(t) \omega_R^{-1} - 1) & \partial_{14}(t) &= h_{14}(t) X_L(t) \omega_R^{-1} \\ \partial_{15}(t) &= h_{15}(t) X_L(t) \omega_R^{-1} & \partial_{16}(t) &= g_1(t) X_L(t) \omega_R^{-1} \end{aligned}$$

$$\begin{aligned} \partial_{21}(t) &= X_L(t) + h_{31}(t) X_L(t) \omega_R^{-1} & \partial_{22}(t) &= h_{32}(t) X_L(t) \omega_R^{-1} \\ \partial_{23}(t) &= h_{33}(t) X_L(t) \omega_R^{-1} + R_L(t) & \partial_{24}(t) &= h_{34}(t) X_L(t) \omega_R^{-1} \\ \partial_{25}(t) &= h_{35}(t) X_L(t) \omega_R^{-1} \end{aligned}$$

Then, combining Eqs. (8), (11) and (12) with mechanical equation (2), and the equations of the turbine (5), we can formulate the new mathematical model of the power system in the following nonlinear state-space form

$$\frac{dv_t}{dt} = \partial_{16}(t) \frac{v_d}{v_t} \frac{du_{fd}}{dt} + g_3(t) \partial_{14}(t) \frac{v_d}{v_t} u_{fd} + f(t) \tag{13}$$

$$\frac{d\omega}{dt} = h_{61}(t) \omega + h_{62}(t) \frac{P_m}{\omega} - h_{62}(t) T_e \tag{14}$$

$$\frac{dP_m}{dt} = h_{81}(t) P_m + h_{82}(t) X_e \tag{15}$$

$$\frac{dX_e}{dt} = h_{91}(t) X_e + h_{92}(t) \omega + g_4(t) u_g \tag{16}$$

where

$$f(t) = \frac{v_d}{v_t} \left[\partial_{11}(t) \frac{di_d}{dt} + \partial_{12}(t) \frac{di_{fd}}{dt} + \partial_{13}(t) \left(\omega \frac{di_q}{dt} + i_q \frac{d\omega}{dt} \right) \right] + \frac{v_d}{v_t} \partial_{15}(t) \left[\omega \frac{di_{kq}}{dt} + i_{kq} \frac{d\omega}{dt} \right]$$
$$+ \partial_{14}(t) \frac{v_d}{v_t} \left[h_{41}(t) i_d + h_{42}(t) i_{fd} + h_{43}(t) i_q \omega + h_{44}(t) i_{kd} + h_{45}(t) i_{kq} \omega \right] + \frac{v_q}{v_t} \frac{dv_q}{dt}$$

$$\begin{aligned} h_{81}(t) &= -(T_m)^{-1} & h_{82}(t) &= K_m (T_m)^{-1} \\ h_{91}(t) &= -(T_g)^{-1} & h_{92}(t) &= -K_g (T_g R \omega_R)^{-1} \\ g_4(t) &= K_g (T_g)^{-1} \end{aligned}$$

3 Backstepping Terminal Voltage and Rotor Speed Controllers Design

The control objectives are the terminal voltage magnitude v_t regulation and rotor speed ω stability enhancement. The form of the nonlinear system, described by (13)–(16), allows the use of the recursive backstepping procedure for the controller design. The basic idea of backstepping design is to select recursively some appropriate functions of state variables as pseudo-control inputs for lower dimension subsystems of the overall system. Each backstepping stage results in a new pseudocontrol design, expressed in terms of the pseudocontrol designs from preceding design stages. When the procedure terminates, a feedback design for the true control input results which achieves the original design objective by virtue of a final Lyapunov function, which is formed by summing up the Lyapunov functions associated with each individual design stage [15]. In the rest of this section, this idea is adopted to design a nonlinear controller for terminal voltage and rotor speed tracking of the power system.

3.1 Backstepping Control Design

To satisfy the first control objective, the terminal voltage control error is defined as

$$z_1 = v_t - v_t^{ref} \tag{17}$$

where v_t^{ref} is the desired trajectory. The time derivative of the z_1 , using (13), is

$$\frac{dz_1}{dt} = \partial_{16}\frac{v_d}{v_t}\frac{du_{fd}}{dt} + g_3\partial_{14}\frac{v_d}{v_t}u_{fd} + f(t) \tag{18}$$

The design procedure starts by defining the following Lyapunov-like function:

$$V_1 = \frac{1}{2}z_1^2 \tag{19}$$

Its time derivative can be written as

$$\frac{dV_1}{dt} = \left[\partial_{16}\frac{v_d}{v_t}\frac{du_{fd}}{dt} + g_3\partial_{14}\frac{v_d}{v_t}u_{fd} + f(t)\right]z_1 \tag{20}$$

To ensure the global asymptotic stability, we impose

$$\frac{dV_1}{dt} = -K_1 z_1^2 \tag{21}$$

where K_1 is a positive constant feedback gain. Then (20) can be rewritten as

$$\frac{dV_1}{dt} = -K_1 z_1^2 + \left[K_1 z_1 + \partial_{16} \frac{v_d}{v_t} \frac{du_{fd}}{dt} + g_3 \partial_{14} \frac{v_d}{v_t} u_{fd} + f(t) \right] z_1 \tag{22}$$

From the above expression, we can define the following control function

$$\frac{du_{fd}}{dt} = -\frac{v_t}{\partial_{16} v_d} \left[K_1 z_1 + g_3 \partial_{14} \frac{v_d}{v_t} u_{fd} + f(t) \right] \tag{23}$$

The second control objective is to keep the rotor speed tracks the desired trajectory $\omega_{ref} = 1$ p.u.

Step 1: To reach the control objective, the rotor speed error is defined as

$$z_2 = \omega - \omega_{ref} \tag{24}$$

From (14), the derivative of the rotor speed error is given as

$$\frac{dz_2}{dt} = h_{61}\omega + h_{62}\frac{P_m}{\omega} - h_{62} T_e \tag{25}$$

Consider the second Lyapunov function

$$V_2 = \frac{z_1^2}{2} + \frac{z_2^2}{2} \tag{26}$$

Using (21) and (25), the derivative of (26) can be derived as follows

$$\frac{dV_2}{dt} = -K_1 z_1^2 + \left(h_{61}\omega + h_{62}\frac{P_m}{\omega} - h_{62} T_e \right) z_2 \tag{27}$$

The P_m can be viewed as a virtual control in the above equation. Define the following stabilizing function

$$\alpha_1 = \frac{\omega}{h_{62}} \left(h_{62} T_e - h_{61}\omega - K_2 z_2 \right) \tag{28}$$

where K_2 is a positive constant feedback gain. Since the mechanical power P_m is not our control input, we define

$$z_3 = P_m - \alpha_1 \tag{29}$$

which is the stabilizing error between P_m and its desired trajectory α_1. When a fault occurs, large currents and torque are produced. This electrical perturbation may destabilize the operating conditions. Hence, it becomes necessary to account for these uncertainties by designing a higher performance controller.

In (28), as electromagnetic load T_e is unknown, when fault occurs, it has to be estimated adaptively. Thus, let us define

$$\hat{\alpha}_1 = \frac{\omega}{h_{62}}\left(h_{62}\hat{T}_e - h_{61}\omega - K_2 z_2\right) \tag{30}$$

where $\hat{T}_e$ is the estimated value of the electromagnetic load. Thus from (25), (29) and (30), the following rotor speed error dynamics is obtained

$$\frac{dz_2}{dt} = -K_2 z_2 + h_{62}\frac{z_3}{\omega} - h_{62}\tilde{T}_e \tag{31}$$

where $\tilde{T}_e = T_e - \hat{T}_e$.

Step 2: To stabilize the mechanical power P_m, one defines the following derivative of z_3 using (15), (29) and (30) as

$$\frac{dz_3}{dt} = h_{81}P_m + h_{82}X_e - \frac{d\hat{\alpha}_1}{dt} \tag{32}$$

Now, we can define a new Lyapunov function including the mechanical power error variable z_3 as

$$V_3 = \frac{1}{2}z_1^2 + \frac{1}{2}z_2^2 + \frac{1}{2}z_3^2 + \frac{1}{2\mu}\tilde{T}_e^2 \tag{33}$$

where μ is a positive adaptive gain. Its derivative, using (21), (31) and (32), is given as follows

$$\begin{aligned}\dot{V}_3 = &-K_1 z_1^2 - K_2 z_2^2 - K_3 z_3^2 + \tilde{T}_e\left(\tfrac{1}{\mu}\dot{\tilde{T}}_e - h_{62}z_2\right)\\ &+\left(h_{81}P_m + h_{82}X_e - \tfrac{d\hat{\alpha}_1}{dt} + h_{62}\tfrac{z_2}{\omega} + K_3 z_3\right)z_3\end{aligned} \tag{34}$$

Similarly, if we consider X_e as a second virtual control, one easily obtains the following stabilizing function

$$\alpha_2 = \frac{1}{h_{82}}\left(\frac{d\hat{\alpha}_1}{dt} - K_3 z_3 - h_{62}\frac{z_2}{\omega} - h_{81}P_m\right) \tag{35}$$

where K_3 is a positive constant feedback gain. And the following update law can be derived as

$$\dot{\tilde{T}}_e = \mu h_{62} z_2 \tag{36}$$

Step 3: Define the steam valve opening error as

$$z_4 = X_e - \alpha_2 \tag{37}$$

Its derivative along the trajectory, using (16), is

$$\frac{dz_4}{dt} = h_{91}X_e + h_{92}\omega + g_4 u_g - \frac{d\alpha_2}{dt} \tag{38}$$

By substituting (37) into (32), one can get

$$\frac{dz_3}{dt} = h_{82}z_4 - K_3z_3 - h_{62}\frac{z_2}{\omega} \tag{39}$$

Finally, let us define a Lyapunov function for the closed-loop system as follows

$$V_4 = V_3 + \frac{1}{2}z_4^2 = \frac{1}{2}z_1^2 + \frac{1}{2}z_2^2 + \frac{1}{2}z_3^2 + \frac{1}{2\mu}\tilde{T}_e^2 + \frac{1}{2}z_4^2 \tag{40}$$

By differentiating the Lyapunov function V_4 in (40) one obtains

$$\dot{V}_4 = -K_1z_1^2 - K_2z_2^2 - K_3z_3^2 + z_4\left(h_{82}z_3 + h_{91}X_e + h_{92}\omega + g_4u_g - \dot{\alpha}_2\right) \tag{41}$$

From (41), a backstepping control law is designed as follows

$$u_g(t) = \frac{1}{g_4}\left(\frac{d\alpha_2}{dt} - K_4z_4 - h_{82}z_3 - h_{91}X_e - h_{92}\omega\right) \tag{42}$$

where K_4 is a positive constant feedback gain.
By substituting (42) into (41), one can get

$$\dot{V}_4 = -K_1z_1^2 - K_2z_2^2 - K_3z_3^2 - K_4z_4^2 \leq 0 \tag{43}$$

3.2 Stability Analysis

Theorem *The globally asymptotic stability of the system defined by (13)–(16), is guaranteed, if the control laws and the adaptive control are given by (23), (42) and (36), respectively.*

Proof The system error dynamics of the resulting closed loop adaptive system can be written as

$$\begin{aligned}
\tfrac{dz_1}{dt} &= -K_1z_1 \\
\tfrac{dz_2}{dt} &= -K_2z_2 + h_{62}\tfrac{z_3}{\omega} - h_{62}\overset{\sim}{T_e} \\
\tfrac{dz_3}{dt} &= h_{82}z_4 - K_3z_3 - h_{62}\tfrac{z_2}{\omega} \\
\tfrac{dz_4}{dt} &= -K_4z_4 - h_{82}z_3 \\
\tfrac{dT_e}{dt} &= h_{62}\mu z_2
\end{aligned} \tag{44}$$

This system has an equilibrium at $z_1 = z_2 = z_3 = z_4 = 0$.

It is then clear that a Lyapunov function (40) for the system defined by (13)–(16), the control laws (23), (42) and the adaptive law (36) make it derivative negative semi-definite. So, define the following equation

$$W(t) = K_1 z_1^2 + K_2 z_2^2 + K_3 z_3^2 + K_4 z_4^2 \geq 0$$

Using Lasalle–Yoshizawa's principle [15], it can be shown that $W(t)$ tend to zero as $t \to \infty$. Therefore, the tracking errors which include terminal voltage, rotor speed, mechanical power and steam valve opening will converge to zero asymptotically as $t \to \infty$.

4 Validation and Discussion

The developed dynamic model and control strategy were tested on the two-area four-machine interconnected power system [16] whose schematic is shown in Fig. 1. At the steady state of the full load case, about 700 MW power is generated from each of the generators. The loads on buses LD7 and LD9 are 967 and 1767 MW, respectively. About 400 MW power is transferred from area 1 to area 2 through the parallel tie lines. The numerical values of the studied system parameters are presented in the Tables 1, 2 and 3. The Matlab/Simulink software is used for the time-domain simulations. Nonlinearities were taken into account incorporating both exciter ceilings, control signal limiters and rate of opening and closing in the turbine valve.

Figure 2 shows the decentralized control system configuration of the multimachine power system. In order to prove the usefulness and supremacy robustness of the proposed modelling and controllers, the results are compared with those of the conventional AVR + PSS and SG. Simulation studies are carried out for the power system under different contingencies.

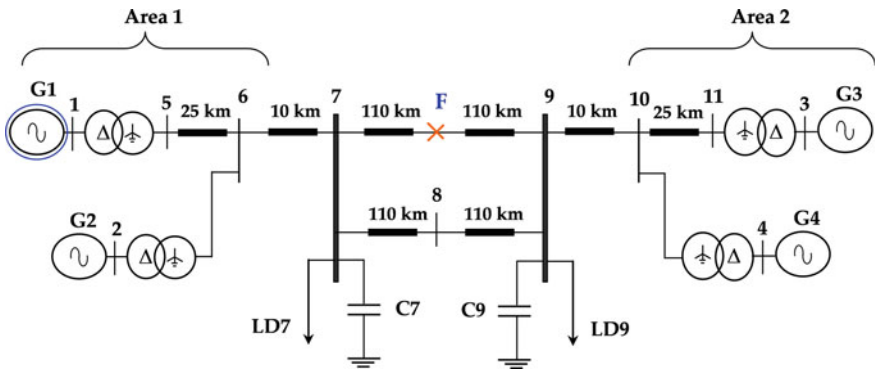

Fig. 1 Single-line diagram of the two-area four-machine power system

Table 1 Parameters of the power synchronous generator (# 1) in p.u.

Parameter	Value
S_{base}	900 MVA
R_s, stator resistance	1.096×10^{-3}
R_{fd}, field resistance	7.42×10^{-4}
R_{kd}, direct damper winding resistance	13.1×10^{-3}
R_{kq}, quadrature damper winding resistance	54×10^{-3}
L_d, direct self-inductance	1.700
L_q quadrature self-inductances	1.640
L_{fd}, rotor self inductance	1.650
L_{kd},direct damper winding self inductance	1.605
L_{kq}, quadrature damper winding self inductance	1.526
L_{md}, direct magnetizing inductance	1.550
L_{mq}, quadrature magnetizing inductance	1.490
$V^{\propto}$, infinite bus voltage	1
D,damping constant	0
H, inertia constant	2.37 s

Table 2 Parameters of the power synchronous generators (# 2, 3, 4) in p.u.

Parameter	Value
S_{base}	900 MVA
x_l leakage reactance	0.2 p.u.
r_{a} resistance	0.0025 p.u.
x_{d} d-axis synchronous reactance	1.8 p.u.
x'_{d} d-axis synchronous transient reactance	0.25 p.u.
T'_{d0} d-axis open circuit time constant	8 s
x_{q} q-axis synchronous reactance	1.7 p.u.
x'_{q} q-axis synchronous transient reactance	0.25 p.u.
T'_{q0} q-axis open circuit time constant	0.4 s
H inertia constant	6.5 s

4.1 Effect of Severe Disturbance on the Dynamic Performance of the System

A symmetric three-phase short circuit fault occurs at location F (in the middle of the transmission line between bus B7 and bus B9), see Fig. 1, at 3 s. The transmission line subject to a fault is cut off at 3.1 s. The original system is restored after the fault clearance. Figure 3 illustrates terminal voltage and rotor speed. According to this figure, the trajectories command can be well tracked and the tracking error

Table 3 Parameters of the steam turbine and speed governor

Parameter	Value
T_t, time constant of the turbine	0.35 s
K_t, gain of the turbine	1
R regulation constant of the system	0.05
T_g, time constant of the speed governor	0.2 s
K_g, gain of the speed governor	1

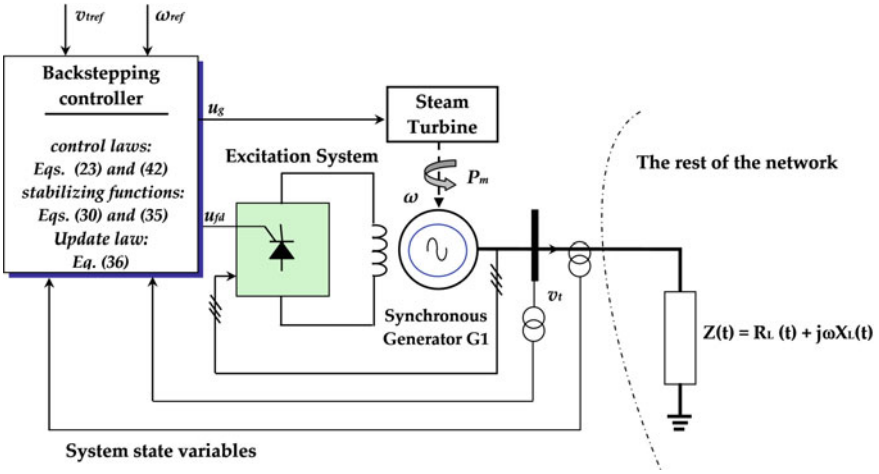

Fig. 2 Decentralized control system configuration

converged to zero. The electrical power of controlled generator and tie-line power flow are shown in Fig. 4. It is seen how dynamics of the terminal voltage, rotor speed and electrical power exhibit large overshoots during post fault state before they settle to their steady state values with the standard controllers (AVR + PSS + SG) rather than with the nonlinear decentralized scheme. It is quite evident that the developed decentralized controller achieves very good voltage regulation and transient stability.

Also, Fig. 5 shows the variations of the inter-area and local mode of oscillation. From these figures, it can be seen that, the inter-area modes of oscillations are very quickly damped out with the application of the proposed controller. Further, the proposed approach is also effective in suppressing the local mode of oscillations.

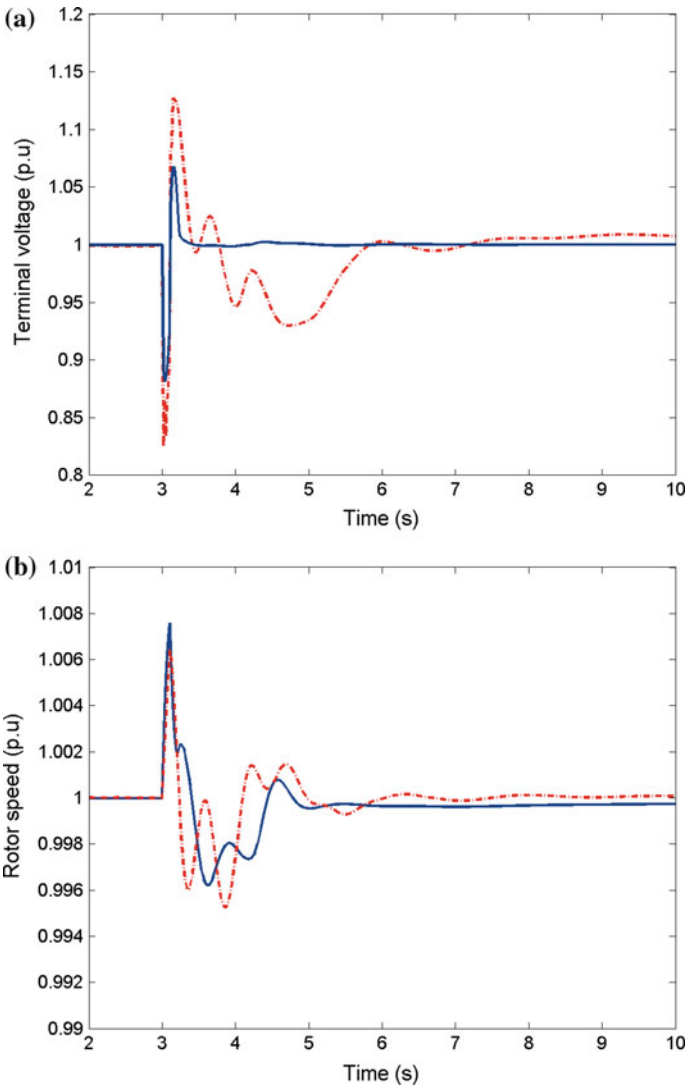

Fig. 3 Dynamic performance tracking of generator G1, following temporary three-phase short circuit fault. *Solid* proposed nonlinear control scheme; *dot* conventional controllers

4.2 Effect of Small Disturbance on the Dynamic Performance of the System

In any power system, the operating load varies over a wide range. It is extremely important to investigate the effect of variation of the loading condition on the dynamic performance of the system. In order to examine the robustness of the

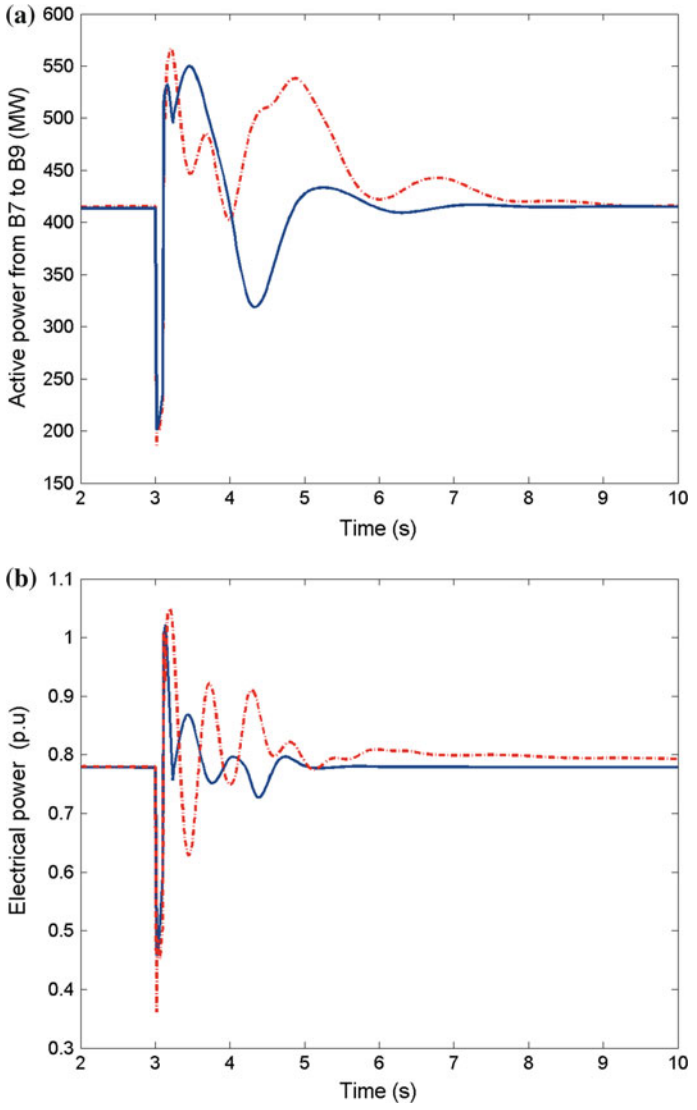

Fig. 4 Tie-line power flow (**a**) and electrical power of generator G1 (**b**) following temporary three-phase short circuit fault. *Solid* proposed nonlinear control scheme; *dot* conventional controllers

damping controllers to wide variation in the loading condition, the load at bus 7 (LD7 = 967 MW) is disconnected at $t = 5$ s for 100 ms.

Figures 6 and 7 show the tracking performance of the proposed controller. As it can be seen, the state variables reach a steady state condition, exhibiting the stability of the closed-loop system.

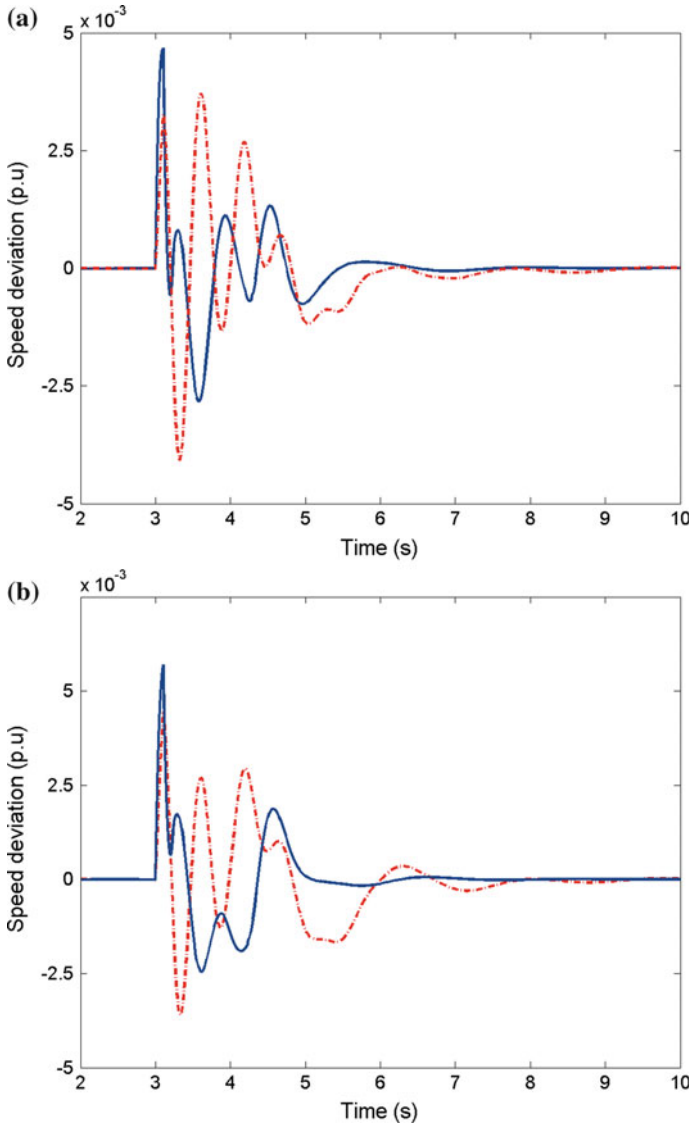

Fig. 5 Local mode of oscillation $\omega 1$-$\omega 2$ (**a**) and inter-area mode of oscillation $\omega 1$-$\omega 3$ (**b**) following temporary three-phase short circuit fault. *Solid* proposed nonlinear control scheme; *dot* conventional controllers

Figure 8 shows the variations of the inter-area and local mode of oscillation. It can be seen that, the transient response of the classical controllers (PSS/AVR and SG) is more oscillatory than the response given by the designed nonlinear controller. The developed decentralized controller provides significantly better damping enhance-

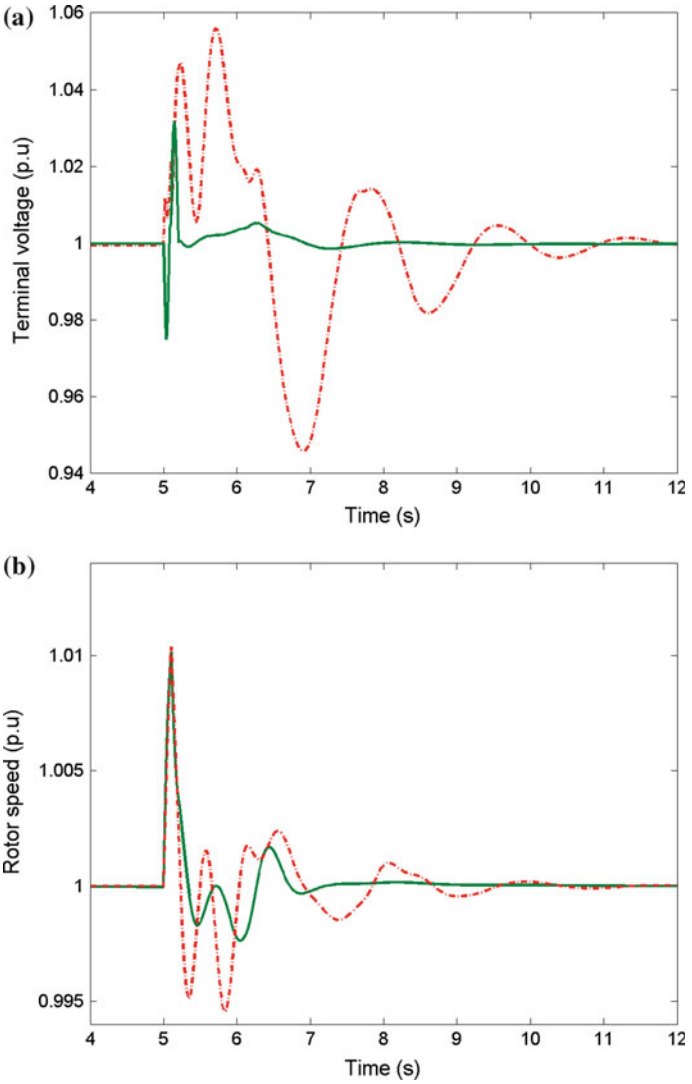

Fig. 6 Dynamic performance tracking of generator G1, following load variation *Solid* proposed nonlinear control scheme; *dot* conventional controllers

ment in the power system oscillations. It is possible to observe that the overshoot and settling time are reduced as well.

It is evident that the proposed controller is robust to this type of disturbance and provides efficient damping to power system oscillations even under small disturbance.

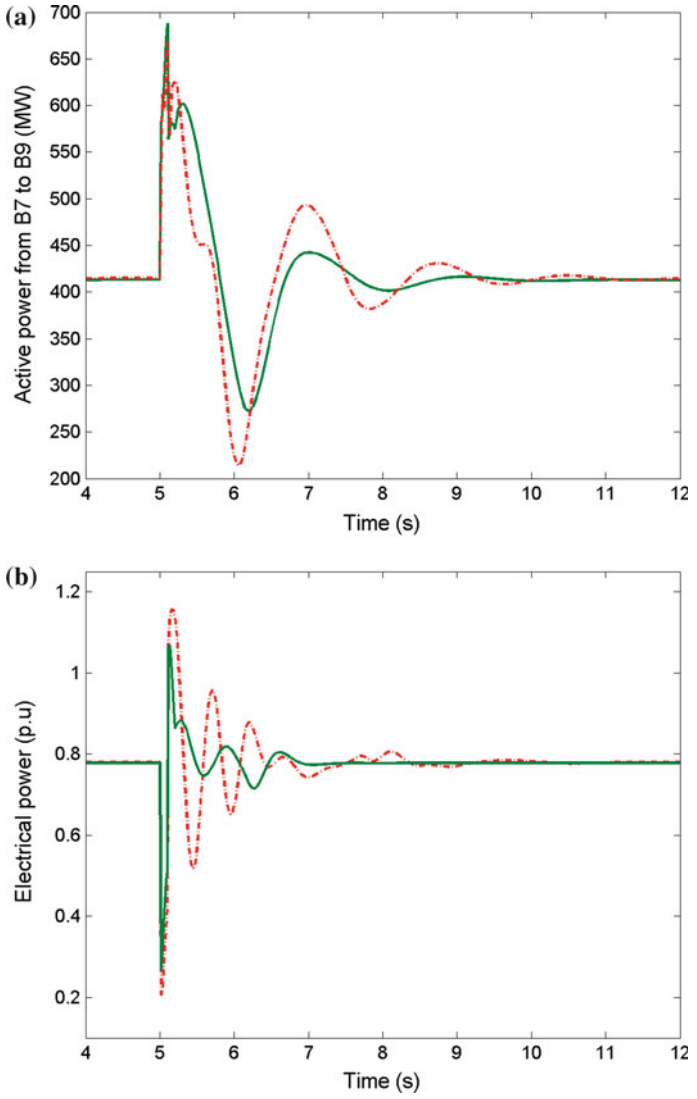

Fig. 7 Tie-line power flow (**a**) and electrical power of generator G1 (**b**) following load variation. *Solid* proposed nonlinear control scheme; *dot* conventional controllers

4.3 Robustness to Parameters Uncertainties and Modelling Errors

The variation of system parameters and model errors are considered for robustness evaluation of the proposed controller. In fact, an accurate model of power system is

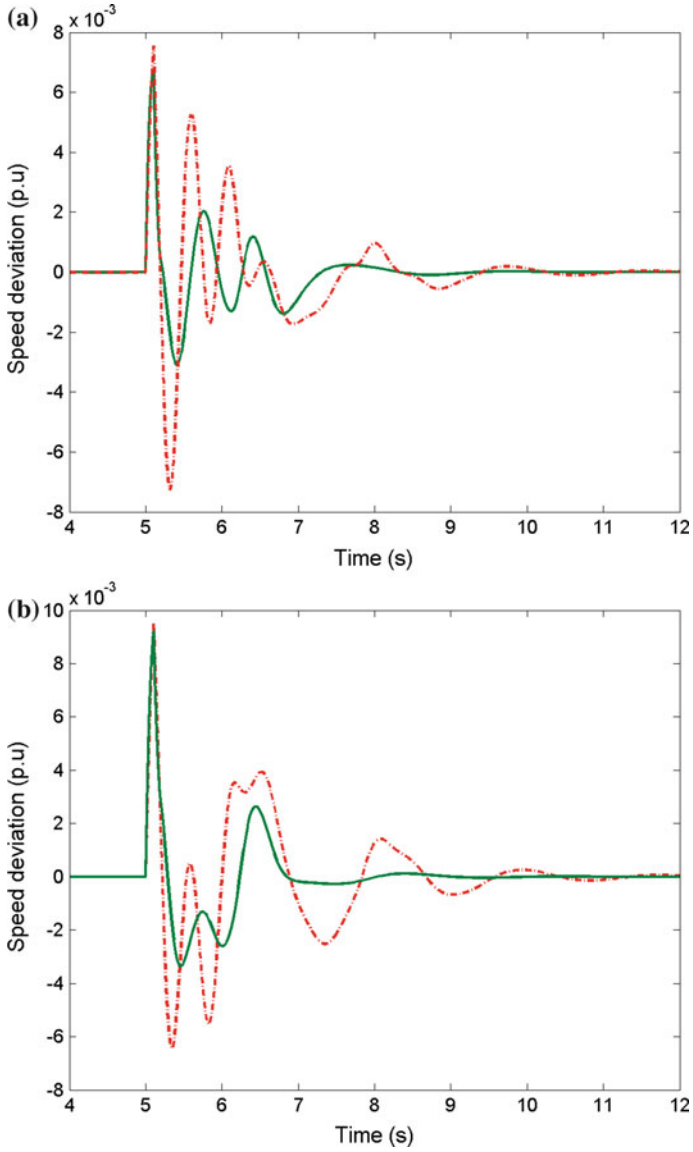

Fig. 8 Local mode of oscillation $\omega 1$-$\omega 2$ (**a**) and inter-area mode of oscillation $\omega 1$-$\omega 3$ (**b**) following load variation *Solid* proposed nonlinear control scheme; *dot* conventional controllers

not available. Therefore, it is required to investigate the robustness of the proposed controller with system parameter variation and model errors.

A robustness test has been carried out by changing the controlled generator parameters from their nominal values. Two cases are examined in the following:

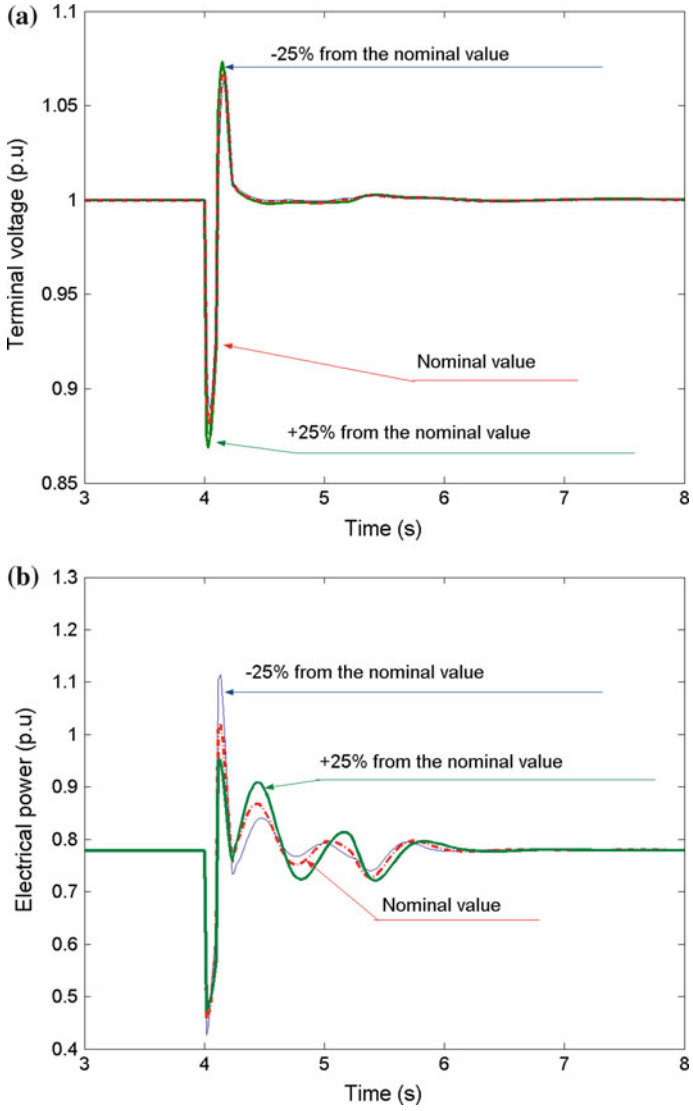

Fig. 9 Terminal voltage (**a**) and Electrical power of generator G1 (**b**) under parameter variations

- Case 1: The parameters of the controlled generator have +25 % perturbations of the nominal values.
- Case 2: The parameters of the controlled generator have −25 % perturbations of the nominal values.

In addition to the abrupt and permanent variation of the power system parameters a three-phase short-circuit is simulated at t = 4 s. It can be seen in Figs. 9 and 10 that

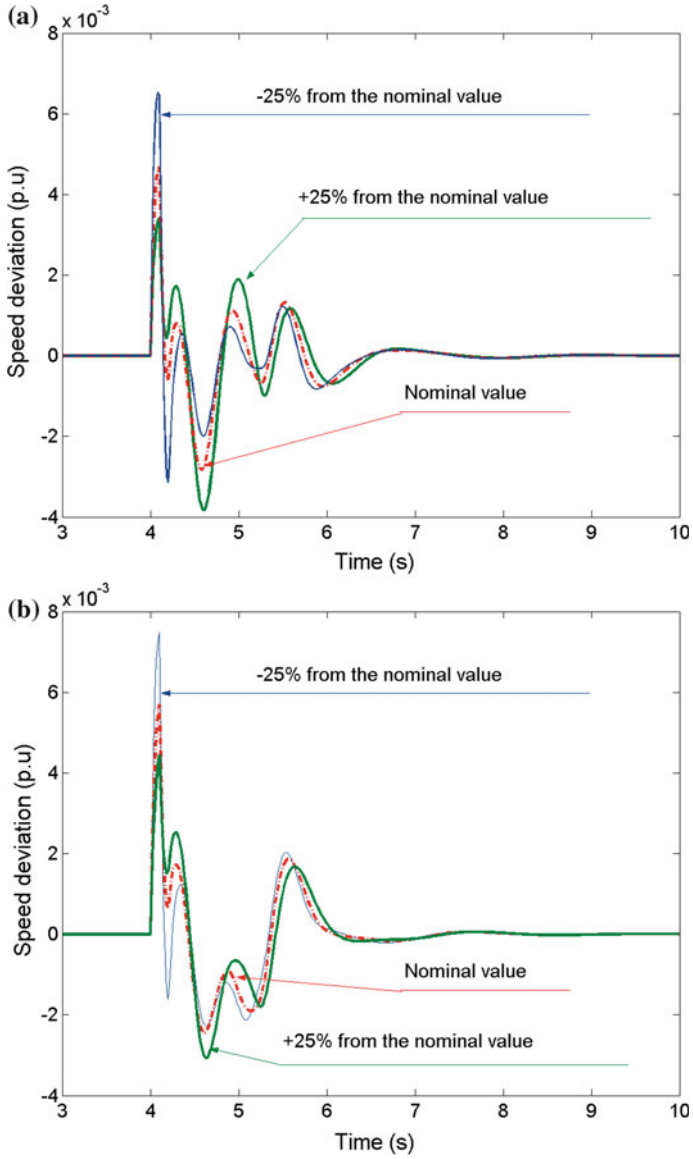

Fig. 10 Local mode of oscillation $\omega 1$-$\omega 2$ (**a**) and inter-area mode of oscillation $\omega 1$-$\omega 3$ (**b**) under parameter variations

the proposed scheme can still provide consistent control performance even if system parameters have changed and furthermore the controller is not sensitive to the model errors.

5 Conclusion

A nonlinear decentralized controller based on a new dynamic model of multimachine power systems is developed. In our solution a nonlinear nine order model for synchronous generator, driven by steam turbine and connected to EPS was used. This novel model, with time-varying parameters representing intermachine interactions, takes into account all interactions in EPS between the electrical and mechanical dynamics and load constraints. The only local information is required; therefore, the proposed control scheme can be implemented in a decentralized way.

The proposed nonlinear decentralized controllers, of terminal voltage and speed rotor, are constructed using adaptive backstepping design. The feedback system is globally asymptotically stable in the sense of Lyapunov method despite the nature of the contingencies.

The designed nonlinear controller is tested through simulation under the most important perturbations in the power systems: (a) load variation, (b) large fault (a 100 ms short circuit) and (c) generator parameter variations. Digital simulation results confirm that the developed decentralized control gains much priority over conventional controllers (AVR/PSS and speed governor) in damping oscillation, improving voltage regulation and enhancing transfer capability.

References

1. Abbadi A, Nezli L, Boukhetala D (2013) A nonlinear voltage controller based on interval type 2 fuzzy logic control system for multi-machine power systems. Int J Electr Power Energy Syst 45(1):456–467
2. Alkhatib H, Duveau J (2013) Dynamic genetic algorithms for robust design of multi-machine power system stabilizers. Int J Electr Power Energy Syst 45(1):242–245
3. Anderson PM, Fouad AA (1994) Power system control and stability. IEEE Press, New York
4. Bandal V, Bandyopadhyay B, Kulkarni AM (2005) Decentralized sliding mode control technique based power system stabilizer (PSS) for multimachine power system. In: Proceedings of the conference on control applications, Toronto, Canada
5. Colbia-Vega A, de Léon-Morales J, Fridman L, Salas-Péna O, Mata-Jiménez MT (2008) Robust excitation control design using sliding-mode technique for multimachine power systems. Electr Power Syst Res 78:1627–1643
6. El-Metwally KA, Malik OP (1995) Fuzzy logic power system stabilizer. IEE Proc Gener, Transm Distrib 142(3):277–281
7. Ghandakly A, Dai J (2000) An adaptive synchronous generator stabilizer design by generalized multivariable pole shifting (GMPS) technique. IEEE Trans Power Syst 7(3):436–446
8. Hill DJ, Wang Y (2000) Nonlinear decentralized control of large scale power systems. Automatica 36:1275–1289
9. Huerta H, Alexander G, Loukianov Cañedo JM (2010) Decentralized sliding mode block control of multimachine power systems. Int J Electr Power Energy Syst 32(1):1–11
10. Hui L, Wechu H, Song Y (2012) Lyapunov-based decentralized excitation control for global asymptotic stability and voltage regulation of multi-machine power systems. IEEE Trans Power Syst 27(4):2262–2270
11. Leonid M Fridman, Soto-Cota A (2011) High-order block sliding-mode controller for a synchronous generator with an exciter system. IEEE Trans Ind Electr 58(1):337–347

12. Jiao X, Sun Y, Shen T (2005) Adaptive controller design for a synchronous generator with unknown perturbation in mechanical power. Int J Control Autom Syst 3(2):308–314
13. Jiawei Y, Zhu C, Chengxiong M, Dan W, Jiming L, Jianbo S, Miao L, Dah L, Xiaoping L (2014) Analysis and assessment of VSC excitation system for power system stability enhancement. Int J Electr Power Energy Syst 7(5):350–357
14. Karimi A, Feliachi A (2008) Decentralized adaptive backstepping of electric power systems. Electr Power Syst Res 78(3):484–493
15. Krstić M, Kanellakopoulos I, Kokotović P (1995) Nonlinear and adaptive control design. Wiley Interscience Publication, New York
16. Kundur GP (1994) Power system stability and control. McGraw-Hill, NewYork
17. Loukianov AG, Cañedo JM, Huerta H (2006) Decentralized sliding mode block control of power systems. In: Proceedings of the of PES general meeting, Montreal, Quebec, Canada
18. Mohagheghi S, Valle Y, Venayagamoorthy GK, Harley RG (2007) A proportional-integrator type adaptive critic design-based neuro-controller for a static compensator in a multimachine power system. IEEE Trans Ind Electr 54(1):86–96
19. Mrad F, Karaki S, Copti B (2000) An adaptive fuzzy-synchronous machine stabilizer. IEEE Trans Syst Man Cybern-Part C 30(1):131–137
20. Okou F, Akhrif O, Dessaint L-A (2003) A novel modelling approach for decentralised voltage and speed control in multimachine power systems. Int J Control 76(8):845–857
21. Okou F, Dessaint L-A, Akhrif O (2005) Power systems stability enhancement using a wide-area signals based hierarchical controller. IEEE Trans Power Syst 2(3):1465–1477
22. Ouassaid M, Nejmi A, Cherkaoui M, Maaroufi M (2008) A nonlinear backstepping controller for power systems terminal voltage and rotor speed controls. Int Rev Autom Control 3(1):355–363
23. Ouassaid M, Maaroufi M, Cherkaoui M (2010) Decentralized nonlinear adaptive control and stability analysis of multimachine power system. Int Rev Electr Eng 5(6):2754–2763
24. Ouassaid M, Maaroufi M, Cherkaoui M (2012) Observer based nonlinear control of power system using sliding mode control control strategy. Electr Power Syst Res 84(1):135–143
25. Ouassaid M, Maaroufi M, Cherkaoui M (2015) Transient stability enhancement of power systems using observer-based sliding mode control. Stud Comput Intell 581:435–462
26. Park JW, Harley RG, Venayagamoorthy GK (2003) Adaptive-critic-based optimal neurocontrol for synchronous generators in a power system using MLP/RBF neural networks. IEEE Trans Ind Appl 39(5):1529–1540
27. Rasappan S, Vaidyanathan S (2012) Hybrid synchronization of n-scroll Chua and Lur'e chaotic systems via backstepping control with novel feedback. Arch Control Sci 22(3):343–364
28. Segal R, Kothari ML, Madnani S (2000) Radial basis function (RBF) network adaptive power system stabilizer. IEEE Trans Power Syst 15(2):722–727
29. Shen T, Mei S, Lu Q, Hu W, Tamura K (2003) Adaptive nonlinear excitation control with L2 disturbance attenuation for power systems. Automatica 39(1):81–89
30. Vaidyanathan S, Rasappan S (2014) Global chaos synchronization of n-scroll Chua circuit and Lur'e system using backstepping control design with recursive feedback. Arabian J Sci Eng 39(4):3351–3364
31. Vaidyanathan S, Idowu BA, Azar AT (2015) Backstepping controller design for the lobal chaos synchronization of Sprott's jerk systems. Stud Comput Intell 581:39–58
32. Venayagamoorthy GK, Harley RG, Wunsch DC (2003) Dual heuristic programming excitation neurocontrol for generators in a multimachine power system. IEEE Trans Ind Appl 39(2):382–394
33. Wang SK (2013) A novel objectif function and algorithm for optimal PSS parameter design in a multi-machine power System. IEEE Trans Power Syst 28(1):522–531
34. Wang Y, Guo G, Hill D (1997) Robust decentralized nonlinear controller design for multimachine power systems. Automatica 33(9):1725–1734
35. Wang Y, Cheng D, Li C, Ge Y (2003) Dissipative Hamiltonian realization and energybased L2-disturbance attenuation control of multimachine power systems. IEEE Trans Autom Control 48(8):1428–1433

36. Wu B, Malik OP (2006) Multivariable adaptive control of synchronous machines in a multi-machine power system. IEEE Trans Power Syst 21(2):1772–1787
37. Xi Z, Cheng D, Lu Q, Mei S (2002) Nonlinear decentralized controller design for multimachine power systems using Hamiltonian function method. Automatica 38(2):527–534

Diving Autopilot Design for Underwater Vehicles Using an Adaptive Neuro-Fuzzy Sliding Mode Controller

G.V. Lakhekar, L.M. Waghmare and Sundarapandian Vaidyanathan

Abstract In general, the diving dynamics of an autonomous underwater vehicle (AUV) has been derived under various assumptions on the motion of the vehicle in vertical plane. Usually, pitch angle of AUV is assumed to be small in maneuvering, so that the nonlinear dynamics in the depth motion of the vehicle could be linearized. However, a small-pitch-angle is a somewhat strong restricting condition and may cause serious modeling inaccuracies of AUV's dynamics. For this reason, many researchers concentrated their interests on the applications of adaptive control methodology to the motion control of underwater vehicle. In this chapter, we directly resolve the nonlinear equation of the AUV's diving motion without any restricting assumption on the pitch angle in diving model. The proposed adaptive neuro-fuzzy sliding mode controller (ANFSMC) with a proportional + integral + derivative (PID) sliding surface is derived so that the actual depth position tracks the desired trajectory despite uncertainty, nonlinear dynamics and external disturbances. In the proposed control structure, the corrective term is approximated by a continuous fuzzy logic control and the equivalent control is determined by a feedforward neural network. The weights of the neural network are updated such that the corrective control term of the ANFSMC goes to zero. The adaptive laws are employed to adjust the output scaling factor and to compute PID sliding surface coefficients. Finally, the lyapunov

G.V. Lakhekar (✉)
Department of Electrical Engineering, G. H. Raisoni Institute
of Engineering and Technology, Pune, India
e-mail: gv_lakhekar@rediffmail.com

L.M. Waghmare
Department of Instrumentation Engineering, S. G. G. S. Institute
of Engineering and Technology, Nanded, India
e-mail: lmwaghmare@yahoo.com

S. Vaidyanathan
Vel Tech University, Chennai, India
e-mail: sundarvtu@gmail.com

S. Vaidyanathan and C. Volos (eds.), *Advances and Applications in Nonlinear Control Systems*, Studies in Computational Intelligence 635,
DOI 10.1007/978-3-319-30169-3_21

theory is employed to prove the stability of the ANFSMC for trajectory tracking of diving behaviors. Simulation results show that this control strategy can attain excellent control performance.

Keywords Autonomous underwater vehicle · Adaptive neuro-fuzzy sliding mode control · Fuzzy logic control and Neural network

1 Introduction

Underwater robotic vehicles (URV's) have experienced remarkable growth in their emerging applications, such as scientific inspection of deep sea, oceanographic mapping, long range survey, underwater structure maintenance, oil and gas exploration, underwater pipelines tracking, rescue operation, underwater precision-guided munitions and so on. The area of URV's currently falls into two basic categories such as Manned Underwater Vehicles and Unmanned Underwater Vehicles (UUVs). Again, UUVs is classified in to Remotely Operated Underwater Vehicles (ROVs) and Autonomous Underwater Vehicles (AUVs). ROV is a physically linked vehicle via the tether to the surface and are remotely operated by a human pilot. AUV is an unmanned, untethered and underactuated, underwater vehicle that carries its own power source and relies on an on-board computer along with machine intelligence to execute a mission. However, AUV's dynamics are highly nonlinear, time varying and hydrodynamic coefficients of vehicles are difficult to be accurately estimated a prior, because of the variations of these coefficients with different operating conditions. These types of difficulties cause modeling inaccuracies as parametric uncertainty and unstructured uncertainty in AUV's dynamics. In order to deal with the uncertainties in the AUV's dynamics, most control related researchers on URV are mainly focused on the applications of robust control methodology to the motion control of underwater vehicles.

In the existing literatures, several different studies have been done in order to design autopilots for controlling the AUV's such as PD/PID controllers are designed in [16, 22, 23, 31, 33, 48, 50, 61, 79] as model based controllers most dynamically used in dynamic positioning and motion control. The adaptive control law is developed with estimation of uncertain parameters associated with the hydrodynamic damping co-efficients, which is used to generate appropriate control for the AUV mentioned in [2, 4, 11, 53, 76–78]. Recent progress in the design of robust control schemes has resulted in the linear quadratic gaussian (LQG) methodology with loop transfer recover (LTR), gain scheduling and H^{∞} control method employed in control of AUV, as described in [15, 40, 47, 51, 54, 56, 57, 59, 60, 64–66]. As compared to robust methods, adaptive control is better for plants with uncertainties because it can improve it's performance by adaptation with little or no information of the bounds on uncertainties and it is difficult for higher order system.

Sliding mode approach introduced in [9–12, 17, 18, 21, 24, 42, 49, 68, 71, 72] as an effective means of controlling an AUV, mainly due to its ability to tolerate imprecision in the dynamics of undersea robots. A fuzzy logic framework is used for navigation and control of underwater vehicles as discussed in [1, 3, 14, 26, 34, 36, 41, 62, 69]. This control technique dealing with problems characterized by the presence of uncertainty and nonlinearity; in this case the vehicle's movement and sensing actions depend on a number of environment conditions that are impossible to model. Another intelligent control technique as neural networks (NNs) have an inherent capability of approximating uncertain nonlinear dynamics of the AUV without explicit knowledge of its dynamic structure and it is an attractive tool for steering and diving motion control depicted in [5, 27–30, 44–46, 52, 67, 70, 73–76, 80]. The controllers for AUV should be robust to suppress the uncertain effects from nonlinearity, modeling error and the interferences from complicated external environment.

Usually, it is difficult to derived or identify an accurate dynamic model of a complicated AUV system for designing autopilots. So that, an intelligent control method as fuzzy logic control (FLC) law can be designed based on some knowledge or without any knowledge about the system. In addition, an appropriate FLC can overcome the parameter variation and environmental disturbance during operation. But, there is still lacking of theoretical modeling and analysis for the FLC stability and robustness problems. Hence, the robustness feature of a sliding mode control (SMC) was introduced into the fuzzy controller in current researches. More recently, several studies have been done in order to combine the advantages of SMC and FLC. Kim and Lee [37] proposed a fuzzy controller with fuzzy sliding surface for reducing tracking error and eliminating chattering problem due to that stability and robustness is improved. Song and Smith [63] introduced a sliding mode fuzzy controller that uses pontryagins maximum principle for time optimal switching surface design and uses fuzzy logic to this surface. Guo et al. [19] applied a sliding mode fuzzy controller to motion control and line of sight guidance of an AUV. The parameters of FSMC algorithm are non-adaptive in nature, which could be adapted by intelligent techniques for improving output response. Balasuriya and Cong [6] proposed adaptive fuzzy controller can approximate the unknown system and sliding mode approach provide strong robustness against model uncertainties and external disturbances. Its parameters will be adapted online to utilize control energy more efficiently. Kim and Shin [38] developed autopilot for depth control of an underwater flight vehicle (UFV) based on adaptive fuzzy sliding mode control (AFSMC) with a fuzzy basis function expansion (FBFE) is employed with a proportional integral augmented sliding signal. Afterwards, Kim and Shin [39] proposed an expanded adaptive fuzzy sliding mode controller (EAFSMC), is based on the decomposition method designed by using an expert knowledge and the decoupled sub-controllers and composition method designed by using the FBFE's. Sebastion et al. (2007) address the kinematic variables controller based on pioneering algorithm, is utilized in control of underactuated snorkel vehicle. In proposed methodology, adaptive capabilities are provided by several fuzzy estimators, while robustness is provided by the SMC law.

In the further development, Bessa et al. [7] presented an adaptive fuzzy control algorithm based on sliding mode for depth control of an ROV, which is employed for uncertainty and disturbance compensation with completely eliminating chattering effect. Later, Bessa et al. [8] applied AFSMC for identification of external disturbances to control the dynamic positioning of underwater vehicles with four controllable degrees of freedom. Javadi-Moghaddam and Bagheri [32] introduced an adaptive neuro-fuzzy sliding-mode-based genetic algorithm (ANFSGA) control system for a ROV with four degrees of freedom (DOF)s. Since, the dynamic of ROVs are highly nonlinear and time varying, an ANFSGA control system is investigated according to direction-based genetic algorithm (GA) with the spirit of sliding mode control and adaptive neuro-fuzzy sliding mode (ANFS) based evolutionary procedure. Guo et al. [20] presented AFSMC to deal with the depth and heading regulation of spherical underwater robots. Furthermore, the designed controller can't only tolerate actuator stuck faults, but also compensate the disturbances with constant components. Lakhekar and Waghmare [43] designed dynamic fuzzy sliding mode control (DFSMC) for heading angle control in horizontal turn to track desired command, under the influence of disturbances and parameter variations. In this control technique, two fuzzy supervisory systems are employed to determine the value of boundary layer width and hitting gain as the base values of input-output membership functions of FSMC control structure. From the literatures, it can be observed that many approaches in FSMC algorithms have been taken to address the control aspect of the AUV's.

To accomplish the mentioned motivation in controlling of undersea robots, an ANFSMC designed as diving autopilot for trajectory tracking of AUV's. This is a cooperative control that is based on the concept of combining NN, FLC and SMC, where the equivalent control is determined by a feed forward NN and the corrective control is approximated by a continuous FLC. At first, we design PID sliding surface and their coefficients are estimated with the help of adaptive control law. In order to reduce the chattering phenomenon, a FLC is used to approximate the corrective control term and the equivalent control is computed by a feed-forward NN. The weights of the NN are adopted by the gradient descent method and adaptive PID sliding surface. This approach can achieve asymptotic stability and converge faster. The rest of this chapter is organized as follows. In Sect. 2, we shall briefly describe diving model of an AUV. The design of ANFSMC applied to AUV for tracking periodic command is described in Sect. 3. Then, Sect. 4 presented, MATLAB/Simulink based numerical simulations for diving motion control for AUV. Finally, conclusions are summarized in Sect. 5.

2 Mathematical Model of AUV

Generally, AUV has a streamlined torpedo-like body propelled by a single thruster and it's dynamics is highly nonlinear, coupled and time-varying. In addition to these, the hydrodynamic parameters are often poorly known and the vehicle may be

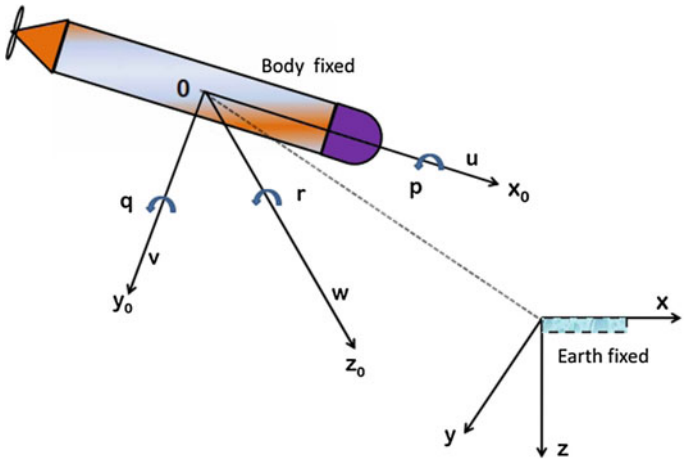

Fig. 1 Body-fixed frame and earth-fixed frame for AUV

subjected to unknown forces due to ocean currents.For vehicle maneuvering, two stern planes and two stern rudder underneath the hull are used. Dynamical behavior of an AUV can be described in a common way through six degree of freedom (DOF) nonlinear equations suggested by Fossen [16], in the two co-ordinate frames such as *Body fixed frame* and *Earth fixed frame* as indicated in Fig. 1.
The nonlinear underwater vehicle's motion equation expressed in the *Body fixed frame* is given as,

$$M(\nu)\dot{\nu} + C_D(\nu)\nu + g(\eta) + d = \tau, \qquad \dot{\eta} = J(\eta)\nu, \tag{1}$$

where, $\eta = [x, y, z, \phi, \theta, \psi]^T$ is the position and orientation vector in earth fixed frame, $\nu = [u, v, w, p, q, r]^T$ is the velocity and angular rate vector in body-fixed frame. $M(\nu) \in \Re^{6\times6}$ the inertia matrix (including added mass), $C_D(\nu) \in \Re^{6\times6}$ denotes the matrix of Coriolis, centripetal and damping term, $g(\eta) \in \Re^6$ the gravitational forces and moments vector, d is the disturbances, τ is the input torque vector and $J(\eta)$ is the transformation matrix. In vertical plane, we can assume that the roll and yaw angular velocities are close to zeros. This can be achieved by properly adjusting the RPM of propeller and the rudders' angles. Under these assumptions, the heave dynamics of AUVs could be represented as,

$$\dot{z} = -u\sin\theta + v\cos\theta\sin\phi + \omega\cos\theta\cos\phi \approx -u_0\sin\theta \tag{2}$$

where $u_0 > 0$ is a forward constant speed, and the pitch kinematics could be written as

$$\dot{\theta} = q\cos\phi - r\sin\phi \approx q\cos\phi \tag{3}$$

The roll angle ϕ is nearly constant, since $p \approx 0$. Without any loss of generality, we assume that $\phi = 0$. Therefore, above equation could be rewritten as

$$\dot{\theta} \approx q \tag{4}$$

Consequently, the diving equation of an AUV can be certain modified as

$$\dot{z} = -u_0 \sin\theta \tag{5}$$

$$\dot{\theta} = q \tag{6}$$

$$m_q \dot{q} = \Phi^T \Theta + F_q u_0^2 \delta_q + d_q \tag{7}$$

where, $\Phi = [q, \dot{u}, u, u^2, \omega q, rq, \cos\phi \sin\Psi]^T$, $\Theta = [\theta_1, \theta_2, \theta_3, \theta_4, \theta_5, \theta_6, \theta_7]^T$, m_q is the inertia term including added mass, F_q is the fin moment coefficient and δ_q denotes the stern plane angle and d_q is the disturbance term. The main focus of this chapter is taken on an attempt to break a conventional restricting condition, which is typically added to the AUV's motion behavior while in maneuvering. Mostly, the pitch angle of the vehicle is assumed to be small in maneuvering so that the nonlinear dynamics in the depth motion of the vehicle could be linearized. Here, small-pitch-angle is a strong restricting condition and may cause difficulty in many practical applications. In this work, we directly resolve the nonlinear equation of the vehicle's depth motion without any restricting assumption on the pitch angle of the vehicle. In fact, robustness has become one of the important aspect related to nonlinear depth control problems, and attention have been taken in to guarantee the stabilities of the proposed control algorithm under various assumptions on the unstructured uncertainties. An ANFSMC was proposed for diving control of an AUV with the nonlinear depth dynamics and their unstructured uncertainties were assumed to be unknown and unbounded.

3 Design of Adaptive Neuro-Fuzzy Sliding Mode Controller

3.1 Proposed Control Structure

The derivation of the proposed ANFSMC scheme for diving control of an AUV is discussed in this section. The control problem is to synthesize an adaptive control law, so that it can provide direct solution to the nonlinear depth dynamics without any restricting assumption on the AUV's pitch angle, during diving motion behavior. The overall control scheme for motion behavior of undersea robot in vertical plane is depicted in Fig. 2, in which reaching mode control law or switching law means discontinuous control part is approximated by a continuous fuzzy logic control and a feedback control law as equivalent control is to be designed to provide convergence of a system's trajectory to the sliding surface, within finite time period is computed

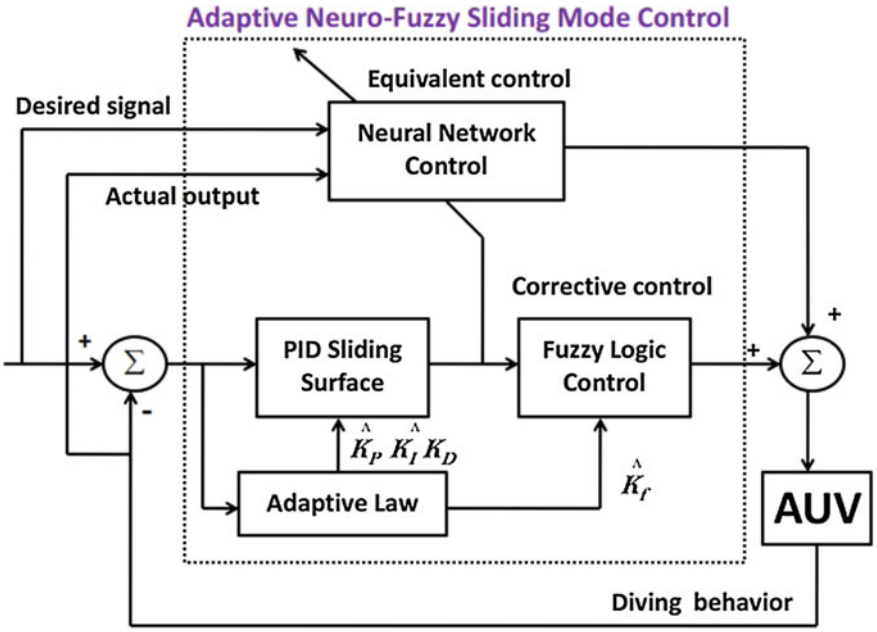

Fig. 2 The structure of ANFSMC

by a NN. The output of the NN is added with fuzzy logic based corrective control to form the control signal. In the overall control structure, fuzzy logic control is applied to eliminate chattering phenomenon by smoothing the switching signal and the equivalent control effort computed by a feed-forward neural network. The design procedure of the ANFSMC includes the following steps.

Step(1): Design PID sliding surface with adaptation scheme
Step(2): Determine corrective control u_{fe} using e or S
Step(3): Determine equivalent control u_{eq} with the help of NN
Step(4): Estimate output scaling factor k_f of fuzzy logic control
Step(5): Calculate the overall control signal for diving control

In this work, a NN controller with the learning rule based on sliding mode algorithm, is employed to assure computation of unknown part in the equivalent control under the influence of parametric uncertainties and the second one is chattering free smooth switching law based on fuzzy logic control. The weights of the NN are updated by using iterative gradient algorithm, due to which reaching time is shorten and gain factor of fuzzy inference system along with sliding surface coefficients are computed using adaptive laws.

3.2 PID Sliding Surface

At the first step, let us define a PID sliding surface $S(t)$ in the state space $\Re^2$ by the equation $S(q, \theta, \tilde{z})$ with following equation

$$S = K_p(z_{(t)} - z_d) + K_i\theta_{(t)} + K_d q_{(t)} \tag{8}$$

where, $\tilde{z}$ is the tracking error, z is the depth parameter and z_d is desired vertical position. An integral term included in the PD type sliding surface expression that resulted in a type of PID sliding surface as hyperbolic function. PID sliding surface coefficients K_p, K_i and K_d are designed such that the sliding mode on $S = 0$ is stable ie convergence of S to zero in turn guarantees that $\tilde{z}$ converge to zero. The coefficients of PID based sliding surface are strictly positive constant K_p, K_i and $K_d \in \Re^T$. The coefficients of PID sliding surface can be obtained by adaptive laws as,

$$\dot{K}_p = -\eta_1 Se \tag{9}$$

$$\dot{K}_i = -\eta_2 S \int edt \tag{10}$$

$$\dot{K}_d = -\eta_3 S\dot{e} \tag{11}$$

where, $\eta_i > 0$ is the learning rate i = 1, 2, 3, …, The control law based on a continuous time varying PID sliding surface, here coefficients are systematically obtained according to the adaptive law.

3.3 Corrective Control

An advantage of using fuzzy logic in the controller design is that the dynamics of system need not be fully known. On the other hand, the linguistic expression of the fuzzy controller makes it difficult to guarantee the stability and robustness of the control system. Therefore, their designing based on the sliding mode theory assures performance and stability, while simultaneously reducing the number of fuzzy rules. Sliding mode control (SMC) produces a serious chattering phenomenon, which is avoided by smoothing the switch signal. Therefore, a fuzzy logic controller is used to replace the switching control or discontinuity in the signum function at the reaching phase in the SMC design.

A principal diagram for ANFSMC includes NN module and fuzzy inference system for combined action of equivalent and corrective control algorithm. In fuzzy inference engine, generalized fuzzy sliding mode based rule is designed as follows

Equivalently, R^i: If s is $F_s^{'i}$ then u_f is $F_{uf}^{'i}$, i = 1, 2, . . . 5.

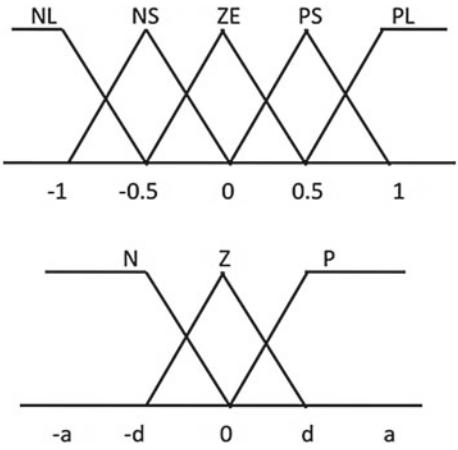

Fig. 3 Membership functions for corrective control as fuzzy logic control

Table 1 Rule base for FSMC algorithm

Sliding surface (S)	NL	NS	ZE	PS	PL
Control signal (u_f)	P	P	Z	N	N

where, NL is *Negative Large*, NM is *Negative Medium*, ZE is *Zero*, PM is *Positive Medium*, PL is *Positive Large*, P is Positive, N is Negative and Z is Zero. NL, NM, …P, N, Z are labels of fuzzy sets and their corresponding membership functions are depicted in Fig. 3, respectively. Let X and Y are the input and output space of the fuzzy rules, respectively. For any arbitrary fuzzy F_x in X, each rule R_i can determine a fuzzy set $F_x * R_i$ in Y. The reduced rule base table for corrective control part in proposed control scheme as stated in Table 1.

The corrective control part is based on single input single output (SISO) mamdani type fuzzy inference system with minimum If-Then rules. Here, reaching law or corrective control is defined as,

$$u_{fe} = k_f \, u_{fuzzy} \tag{12}$$

where, k_f is the output scaling factor and u_{fuzzy} is the output of fuzzy inference system, which is determined by the sliding surface S. The fuzzy control rules can be represented as mapping of the input linguistic variable S to the output linguistic variable as u_f.

According to the following the sup-min compositional rule of inference

$$\mu_{\tilde{F}_x \circ R^i}(u_f) = \underset{s \in X}{Sup} \left[min \left(\mu_{\tilde{F}_x}(s), min \left(\mu_{\tilde{F}_s^i}(s), \mu_{\tilde{F}_{u_f}^i}(u_f) \right) \right) \right] \tag{13}$$

It can be further simplified by supposing $\tilde{F}_x$ be a fuzzy singleton, then

$$\mu_{F_x \circ R^i}(u_f) = min[\mu_{F_s^i}(\alpha), \mu_{F_{uf}^i}(u_f)] \tag{14}$$

the deduced MF $F_u^{'d}$ of the consequence of all rules is,

$$\mu^d_{\tilde{F}^d_{uf}}(u_f) = max[\mu_{\tilde{F}_x \circ R^i}(u_f), \ldots \mu_{\tilde{F}_x \circ R^s}(u_f)] \tag{15}$$

the output variable in above equation is fuzzified output. For the defuzzifier, the center of area defuzzification method is used to find the crisp output is given as.

$$u_{fuzzy} = \frac{\int u_f \quad \mu^d_{\tilde{F}^d_{uf}}(u_f) du_f}{\int \mu^d_{\tilde{F}^d_{uf}}(u_f) du_f} \tag{16}$$

The crisp control signal from extended fuzzy controller is applied to the system model for achieving stabilized diving motion behavior. Other task is to update output scaling factor on line, which depends on sliding surface variable S and its number of fuzzy partitions. The gain updating factor k_f is calculated using following relation

$$k_f = k_1[1/\tilde{p} + |S|] \tag{17}$$

Here, k_f is nonfuzzy adapted output normalization gain, $\tilde{p}$ is the number of fuzzy partitions of S ie. $(\tilde{p} = 5)$, k_1 is a positive constant, that will bring appropriate variations in k_f, which is formulated according to the rule-base of fuzzy inference system with the following strategy: when the state is moving fast towards its set-point, control action needs to be reduced to prevent possible large overshoot and/or undershoot; on the other hand, when the state is rapidly moving away from the set-point, control action needs to be increased to restrict such deviations for a good recovery of the process. In this way, corrective control part is designed to provide smooth switch signal.

3.4 Equivalent Control

The computation of equivalent control is based on fully connected neural network structure, which is consists of an input layer with two neurons (n), one hidden layer with four neurons (h) and a single neuron in output layer (m). The structure of NN presented in control configuration as depicted in Fig. 4 with x is the $n \times 1$ input vector and y is a $m \times 1$ diagonal vector. Here, ω and ϑ denotes the input-to-hidden layer and hidden -to-output layer weights respectively in feed forward NN structure. In forward propagation, response of NN is expressed as follows:
The input of the jth hidden layer is specified as

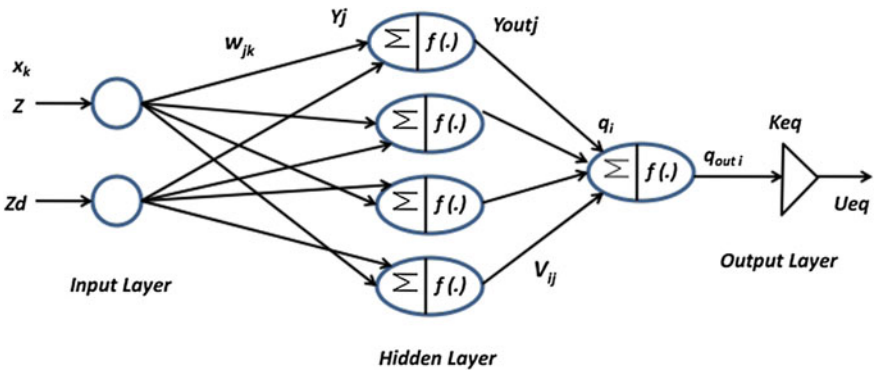

Fig. 4 NN structure for estimation of equivalent control

$$y_j = \sum_{k=1}^{n} \omega_{jk}\, x_k \tag{18}$$

The output of the *j*th hidden unit is represented as

$$y_{out_j} = f(y_j) \tag{19}$$

where, f is the sigmoidal transfer function

$$f(\sigma) = \frac{2}{1 + e^{-\sigma}} - 1 \tag{20}$$

In above activation function, $\sigma = y_j$ is output of first layer in NN. Afterwards, the input to the *i*th output unit is

$$q_i = \sum_{j=1}^{h} \vartheta_{ij}\, y_{out_j} \tag{21}$$

The output of NN is given as

$$q_{out_i} = f(q_i) \tag{22}$$

The estimated value of equivalent control is obtained as

$$\hat{u}_{eq} = k_{eq}\, q_{out_i} \tag{23}$$

In backward propagation, the weight adaptation of NN for equivalent control estimation is expressed as follows:

The error back propagation algorithm is derived on the basis of simple gradient principle for minimizing mean square error between the actual output and the desired output. That is, to minimize the cost function selected as the difference between

the desired and the estimated equivalent control. Hence, a simple cost function is described as follows

$$E = \frac{1}{2}[u_{eq} - \hat{u}_{eq}]^2 \tag{24}$$

The weights are updated by using

$$\triangle \vartheta_{ij} = -\alpha \frac{\partial E}{\partial \vartheta_{ij}} \tag{25}$$

Similarly, another weights between input and hidden layer is updated as

$$\triangle \omega_{jk} = -\alpha \frac{\partial E}{\partial \omega_{jk}} \tag{26}$$

Here, α is the learning rate of the back propagation algorithm and it is constant. Moreover, the two factor as $\partial E/\partial \vartheta_{ij}$ and $\partial E/\partial \omega_{jk}$ can be expressed as follows

$$\frac{\partial E}{\partial \vartheta_{ij}} = -\frac{1}{2} k_{eq}(u_{eq} - \hat{u}_{eq})(1 - q^2_{out_i})\, y_{out_j} \tag{27}$$

$$\frac{\partial E}{\partial \omega_{jk}} = -\frac{1}{4} k_{eq}(u_{eq} - \hat{u}_{eq})\vartheta_{ij}(1 - q^2_{out_i})(1 - y^2_{out_j})\, x_k \tag{28}$$

In above equation, u_{eq} is the unknown term. So that, $\partial \vartheta_{ij}$ can not be determined. In order to solve this problem, we have to use the value of adapted PID sliding surface S to replace the $u_{eq} - \hat{u}_{eq}$. The reason is that S is given by the designer and characteristics of $u_{eq} - \hat{u}_{eq}$ and S are similar.

$$\frac{\partial E}{\partial \vartheta_{ij}} = -\frac{1}{2} k_{eq}\, S\, (1 - q^2_{out_i})\, y_{out_j} \tag{29}$$

$$\frac{\partial E}{\partial \omega_{jk}} = -\frac{1}{4} k_{eq}\, S\, \vartheta_{ij}(1 - q^2_{out_i})(1 - y^2_{out_j})\, x_k \tag{30}$$

The structure of NN that estimate the equivalent control action, is a standard two layer feed-forward NN with the back propagation adaptation algorithm. The error between the desired and estimated equivalent control is adjusted by the PID sliding surface based on adaptive law. The overall output of the neural network structure is given as

$$\hat{u}_{eq} = u_{nn} = \Gamma(\vartheta(\Gamma(\omega x_k))) \tag{31}$$

where, u_{nn} is the output of NN structure, employed to estimate equivalent control and Γ is a nonlinear operator. According to the neural network function approximation property, a smooth function u_n is a compact set based on hidden layer neurons with

weights matrices as ω and ϑ such that,

$$u_n(X) = \vartheta^T g(\omega^T, X) + \varepsilon(X) \tag{32}$$

where, $\varepsilon(X)$ represent NN approximation of error satisfying $\|\varepsilon(X)\| < \varepsilon_n$ for some $\varepsilon_n > 0$. Then, estimate of u_n can be given as

$$\hat{u}_n(X) = \hat{\vartheta}^T g(\hat{\omega}^T, X) \tag{33}$$

where, $\hat{\vartheta}^T$ and $\hat{\omega}^T$ are the estimations of ϑ and ω respectively obtained by updating weights of NN. The proof of the convergence of E to zero is given

Theorem 1 *Using the back propagation algorithm with a proper learning rate, it is guaranteed that E defined in Eq. (24) converges to zero, without bonding to local minimum. Means that, for a bounded disturbance $D_{(t)}$ and unknown dynamics, it is guaranteed that system is stable with zero steady state error.*

Proof According to Lyapunov stability criteria, we have to show that $\dot{E} < 0$. The derivative of the error function with respect to time is given by

$$\frac{dE}{dt} = \frac{\partial E}{\partial \omega}\frac{\partial \omega}{\partial t} + \frac{\partial E}{\partial \vartheta}\frac{\partial \vartheta}{\partial t} \tag{34}$$

We know that updated weights in Eqs. (25) and (26) utilized in NN structure and substituted in above Eq. (34),

$$\frac{dE}{dt} = -\alpha\left[\left(\frac{\partial E}{\partial \omega}\right)^2 + \left(\frac{\partial E}{\partial \vartheta}\right)^2\right] \tag{35}$$

Substituting Eqs. (29) and (30) into Eq. (35),

$$\begin{aligned}\frac{dE}{dt} = -\alpha\Bigg\{&\left(-\frac{1}{4}k_{eq}S\vartheta_{ij}(1-q_{out_i}^2)(1-y_{out_j}^2)\,x_k\right)^2 \\ &+\left(-\frac{1}{2}k_{eq}\,S\,(1-q_{out_i}^2)\,y_{out_j}\right)^2\Bigg\}\end{aligned} \tag{36}$$

Due to squaring operation inner terms become positive as $\tilde{H}$ is given as

$$\frac{dE}{dt} = -\alpha\,[H_1 + H_2] = -\alpha\tilde{H} \tag{37}$$

Note that Eq. (37) is a negative definite function, which completes the proof.

4 The Parameter Adaptive Method

The ANFSMC structure proposed in the previous section has substantially improved the performance of the fuzzy control (corrective control) by adaptation of dead band width as width of output membership function, while in neural network (equivalent control), learning rate is also adapted by using Lyapunov function.

4.1 Tuning of Output Membership Function in Corrective Control

The response time due to corrective control is minimized, based on the initial condition of system and dead band $\pm d$. These two factors were considered as the tuning parameter to achieve minimum time response. In this work, it is demonstrated that, the settling time can be significantly reduced by on line tuning of the universe of discourse of the output membership function range $\pm a$ with no a prior information of the initial condition is required. Here, problem is that to tune the base value of output membership function defined by three fuzzy sets such as negative, zero and positive with universe of discourse $\{-a, a\}$. In order to accomplish a better performance and devise a systematic method to obtain optimal membership functions. So that, we employ following algorithm for tuning of dead zone parameter as base value of output fuzzy variable, which can significantly minimize settling time of output response.

Determine the universe of discourse $\pm a$ for output fuzzy variable
Initialize dead band d value of output fuzzy variable as d = a/2
Initialize integral absolute function and integral time absolute function
For i = 1 to maximum number of epochs to refinement all d
For j = 1 to minimum number of epochs to refinement one d
Run the experiment and get new values of IAF and ITAF
If ((new IAF $<$ IAF) and (new ITAF $<$ ITAF))
IAF = new IAF;
ITAF = new ITAF;
Save d;
End If
If ((new IAF $\leq$ IAF) and (new ITAF $\leq$ ITAF))
d = d $\times$ increase ratio
Else
d = d $\times$ decrease ratio
End if
End for
End for

Here, multi variable unconstrained optimization algorithm is employed to determine the minimum state trajectory θ as function of $f(a)$ of the range $\pm a$ of output membership function in corrective control part. We use decrease ratio and increase ratio as 0.8 and 1.25 respectively. IAF and ITAF are defined as follows:

$$IAF: \quad minimize \quad f(a) = \int_0^\infty |\theta(a)| d\theta \tag{38}$$

$$ITAF: \quad minimize \quad f(a) = \int_0^\infty t|\theta(a)| d\theta \tag{39}$$

IAF accounts mainly for state at the beginning of the response and to a lesser degree for the steady state duration. ITAF keeps account of state at the beginning but also emphasizes the steady state. Due to this tuning method, response time is significantly reduced with non oscillatory behavior.

4.2 Adaptive Learning Rate

A simple feed-forward NN has a single output with nonlinear activation function for neurons. The network is parameterized in terms of its weights which is represented as a weight vector $\mathbf{W} \in \Re^m$. For a specific function approximation problem, the training data consists of N patterns, $\{x^p, y^p\}$.
Let us consider a specific pattern p for the input vector is x^p, then the network output is given as,

$$y^p = f(W, x^p) \tag{40}$$

In this work, usual quadratic cost function seen in Eq. (24), which is minimized to train the weight vector $W = \{\omega, \vartheta\}$ is mentioned in Eqs. (25) and (26).
We consider a Lyapunov function candidate as

$$V = \frac{1}{2}(\tilde{y}^T, \tilde{y}) \tag{41}$$

where, $\tilde{y} = [y_d^1 - y^1, \ldots, y_d^p - y^p, \ldots, y_d^N - y^N]^T$
it's time derivative is given as

$$\dot{V} = -\tilde{y}^T \frac{\partial y}{\partial W} \dot{W} = -\tilde{y}^T J \dot{W} \tag{42}$$

where, $J = \partial y / \partial W \in \Re^{N \times m}$

In back propagation algorithm, weights are updated as follows

$$W(t+1) = W(t) + \alpha \left(\frac{\partial E}{\partial W} \right) \tag{43}$$

Here, α is the fixed learning rate, which is replaced by its adaptive version α_a is given by

$$\alpha_a = \left(\mu \frac{\|\tilde{y}\|^2}{\|J_p^T \tilde{y}\|^2} \right) \tag{44}$$

In earliest stage, there have been more contribution concerning the adaptive learning rate and it is the most remarkable factor for determination purpose. However, the computation of adaptive learning rate using the Lyapunov function approach is the key part in neural network based control.

5 Stability Analysis

Lyapunov stability analysis is the most popular approach to prove and to evaluate the stable convergence property of proposed control algorithm as ANFSMC. Here, direct Lyapunov stability approach is employed to investigate the stability property of the proposed controller and to derive the adaptive robust control.

Theorem 2 *Let the underwater vehicle represented by Eqs. (5)–(7) in vertical plane. Then subject to required assumptions in diving motion is considered, the proposed controller is combination of corrective control defined by Eq. (12) and equivalent control as in Eq. (23) ensures the convergence of state to the sliding surface S and having desired trajectory tracking response.*

Proof Let a Lyapunov function V_L be defined as

$$V_L = \frac{1}{2} S^2 \tag{45}$$

The time derivative of Lyapunov function is,

$$\dot{V}_L = S\dot{S} \tag{46}$$

$$\dot{V}_L = S\left[K_p(\dot{z} - \dot{z}_d) + K_i\dot{\theta} + K_d\dot{q} \right] \tag{47}$$

$$\dot{V}_L = S\left[K_p(-u_0 \sin\theta) + K_i q + \frac{K_d}{m_q}(\Phi^T \Theta) + \frac{K_d F_q u_0^2 \delta_q}{m_q} - K_p \dot{z}_d \right] \tag{48}$$

Here, control input to the underwater vehicle is $u = \delta_q$ as an ANFSMC control signal,

$$\dot{V}_L = S\left[f(z,\theta,q) + D_{(t)} + B_0 u - K_p \dot{z}_d\right] \tag{49}$$

$$\dot{V}_L = S\left[f(z,\theta,q) + D_{(t)} + B_0(\hat{u}_{eq} + u_{fe}) - K_p \dot{z}_d\right] \tag{50}$$

$$\dot{V}_L = S\left[f(z,\theta,q,D) + B_0((K_p \dot{z}_d - \hat{f}(z,\theta,q))B_0^{-1} + u_{fe}) - K_p \dot{z}_d\right] \tag{51}$$

$$\dot{V}_L = S\left[B_0 u_{fe} + D_{(t)}\right] = S\left[B_0 K_f fuzz(S) + D_{(t)}\right] \tag{52}$$

$$\dot{V}_L \leq -\left[B_0 K_f - D_{(t)}\right]|S| \tag{53}$$

$$\dot{V}_L \leq -\|S\|\left[\|B_0\|\|K_f\| - \|D_{(t)}\|\right] \tag{54}$$

From the above analysis, the global asymptotic stability is guaranteed since the derivative of the Lyapunov function is a negative definite $\dot{V}_L = S\dot{S} < 0$.

6 Simulation Results

In order to demonstrate the effectiveness and robustness of the proposed ANFSMC approach for diving motion control of AUV has been simulated using MATLAB/ Simulink. The main focus of this work is to design adaptive diving autopilot for nonlinear depth dynamics control of AUV. In this case, the diving equation of an AUV can be expressed as

$$\dot{z} = -u_0 \sin\theta \tag{55}$$

$$\dot{\theta} = q \tag{56}$$

$$\dot{q} = \frac{1}{I_y - C_{M_{\dot{q}}}}\left(B_{z_{CB}} \sin\theta + C_{M_q} u_0 q + u_0^2 C_{M_{\delta_q}} \delta_q\right) \tag{57}$$

The parameter values are given as follows:
Length of AUV = 1.8 m
Weight of AUV = $m * g = 53 * 9.81 = 519.93$ kg.m/s^2
Density of sea water = $\rho = 1025$ kg/m^3
Forward Speed = $u_0 = 1.5$ m/s
Vehicle's mass moment of inertia = $I_y = 9.921$ kg.m^2
Vertical distance between center of gravity and center of buoyancy
$B_{z_{CB}} = -(z_g - z_b) * W = -3.5942$

Non-dimensional hydrodynamic coefficient expressed in body frame B
$M_q = -0.000641877$
$M_{\dot{q}} = -0.00190690$
$M_{\delta_s} = -0.00786620$

Non-dimensional hydrodynamic coefficient = $C_{(.)}$
$C_{M_q} = 0.5\rho M_q L^4 = -34.5331$
$C_{M_{\dot{q}}} = 0.5\rho M_{\dot{q}} L^5 = -18.4665$
$C_{M_{\delta_s}} = 0.5\rho M_{\delta_s} L^5 = -23.5113$

The performance of the traditional FSMC and ANFSMC has been compared in terms of the set point control, sinusoidal trajectory tracking control, phase portrait and control signal. Moreover, suppose the AUV has some disturbance effect, then tracking capabilities among these controller are also compared for analysis purpose. In order to evaluate the control system performance, three different numerical simulations were performed. In first stage, constant input signal applied to underwater robot, afterwards sinusoidal trajectory tracking of AUV was carried out through simulation and in last simulation disturbance and uncertainties are included in operation of undersea robot.

6.1 Set Point Control

In set point control, the initial conditions of the AUV in diving motion behavior are considered as $\{q_0, \theta_0, z_0\}$. The simulation response of three parameter with control signal in vertical plane are shown in Fig. 5, which demonstrates that the ANFSMC provides the shortest reaching time, no overshoot and smooth tracking response.
The developed control algorithm employed for regulating diving motion behavior based on combined control action of fuzzy logic control as corrective control and NN control as equivalent control. In this controller design, output fuzzy variable was tuned using multi variable unconstrained optimization method, while learning rate of NN was adopted using Lyapunov function. The weights of NN adapted using back propagation algorithm and adaptive PID sliding surface, while output scaling factor of fuzzy logic control was determined with the help of non fuzzy adaptation technique.

6.2 Sinusoidal Trajectory Tracking Control

In second stage of simulation, sinusoidal reference signal $z_d = 2\sin(\pi t)$ applied to diving model of AUV gives corresponding results of tracking as seen in Fig. 6, with considering that the initial state coincides with the initial desired state. As observed

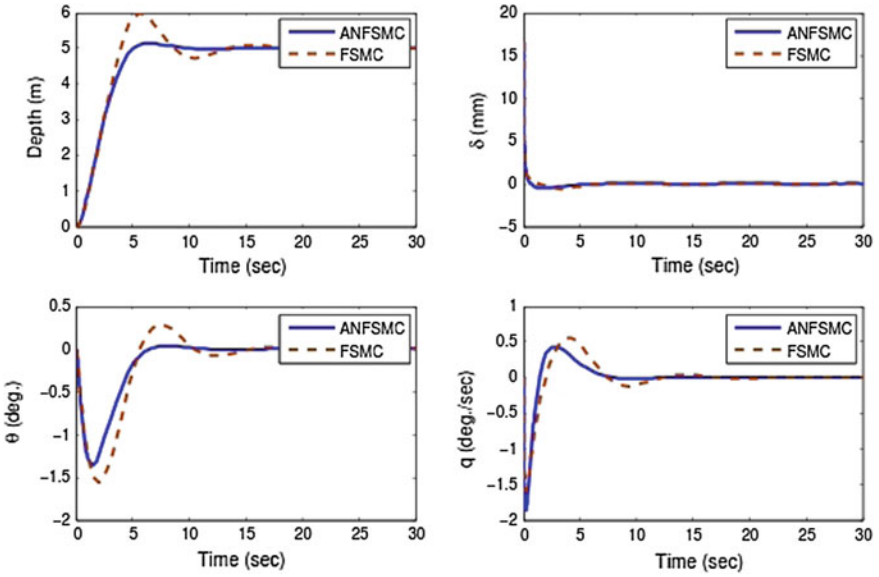

Fig. 5 Set point tracking response of AUV in diving motion behavior

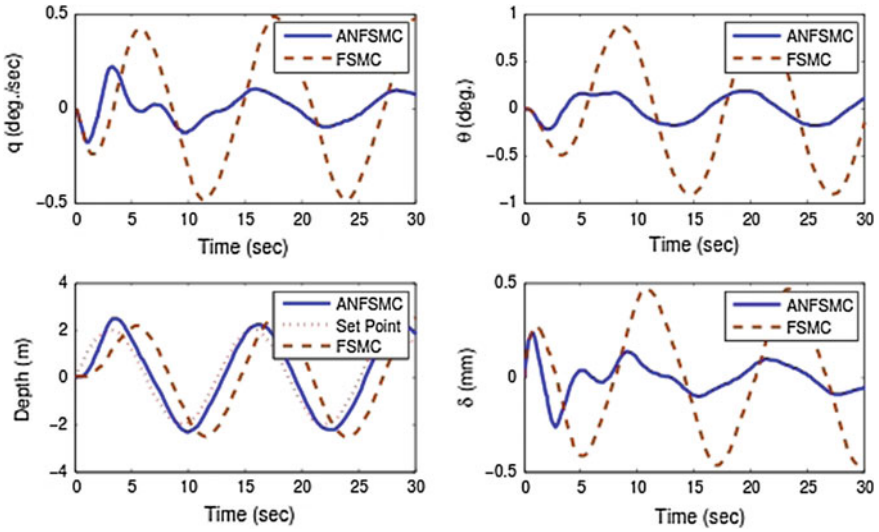

Fig. 6 Sinusoidal trajectory tracking response of AUV

in sine wave trajectory tracking, ANFSMC is able to provide trajectory tracking with a small associated error and no chattering at all. It can be also verified that proposed method provides a minimum tracking error, when compared with the traditional FSMC. Despite the external disturbance forces and parameter variation with respect

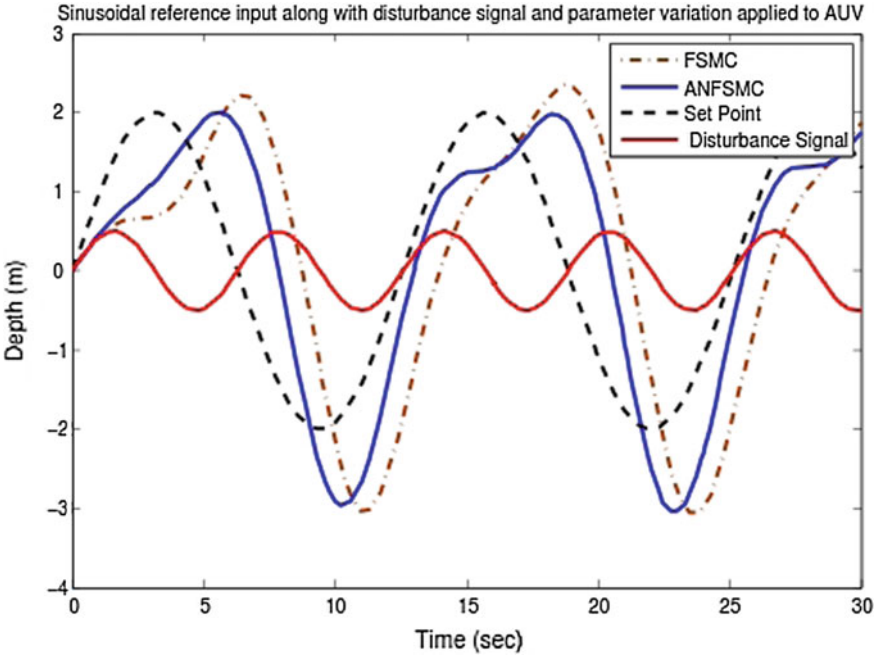

Fig. 7 Sinusoidal trajectory tracking response under the influence of disturbance effect and parameter variation

to diving model parameters, the ANFSMC allows the underwater robotic vehicle to track the desired trajectory with a less tracking error and undesirable chattering effect was not observed in Fig. 7, the disturbance signal employed in simulation as $d_{(t)} = 0.5\sin(\pi t)$

As observed phase portrait in Fig. 8, reaching time of proposed control algorithm was better than other control technique such as FSMC, without any chattering effect. Due to the adaptation scheme employed in NN module and fuzzy logic control, reaching time get significantly reduced with smoother response.

As performance measure for a quantitative comparison, we use integral square of error (ISE) and integral absolute of error (IAE) which are defined as

$$ISE = \int_0^t e^2 \cdot dt \tag{58}$$

$$IAE = \int_0^t |e| \cdot dt \tag{59}$$

In performance comparison, three conditions are considered as set point tracking and disturbance rejection as shown in Figs. 9 and 10, respectively. Here, a piecewise constant reference positions were employed, which reports that ANFSMC gives

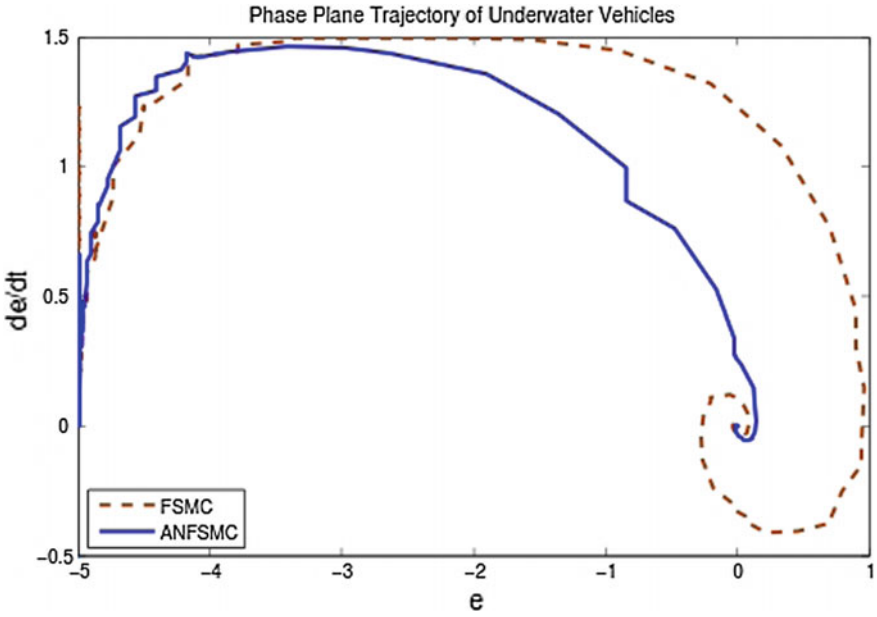

Fig. 8 Phase portrait of AUV in vertical plane

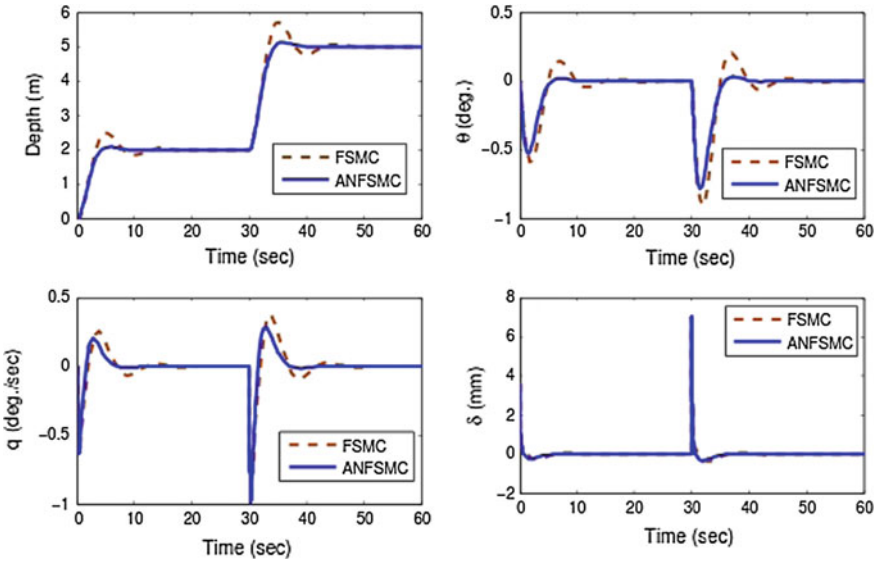

Fig. 9 Response of AUV under set point variation

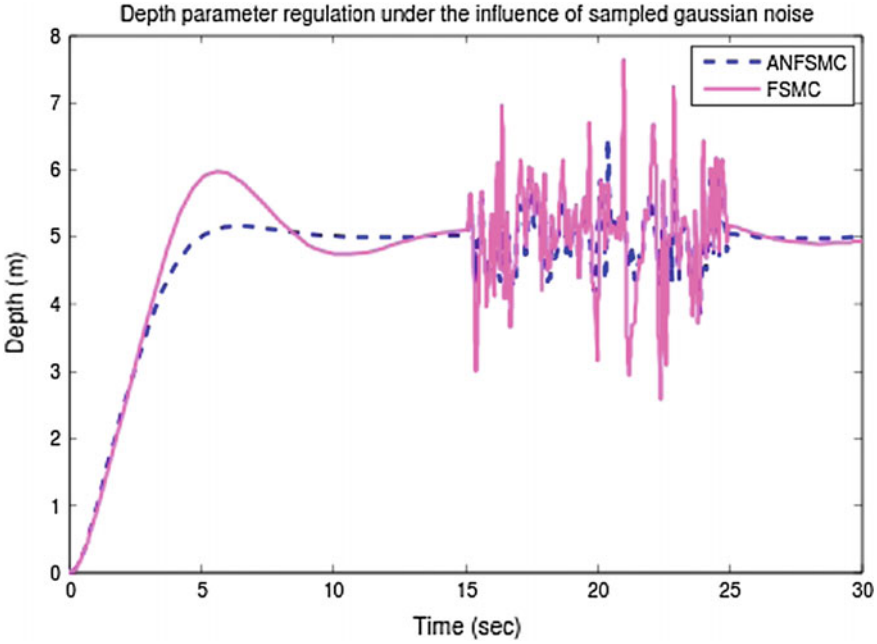

Fig. 10 Response of AUV under influence of sampled gaussian noise

better performance than traditional FSMC, due to the adaptation of corrective and equivalent control by selecting parameters like PID sliding surface, output scaling factor, width of output fuzzy variable and learning rate of NN module. In disturbance rejection condition, effect of sampled gaussian noise is less as compared with FSMC on depth parameter regulation by ANFSMC. Time integral performance indices are used such as ISE and IAE for comparison between the controllers. The smaller value of performance measures shows that good controller performance characteristics. It is observed that, ISE and IAE values for above mentioned conditions are considerably reduced in magnitude than other techniques dealt within this chapter. The values of different errors for various control strategies and under the influences of different conditions are tabulated in Table 2.

The proposed controller is more robust in sense that, under the conditions of set point variation, sinusoidal trajectory tracking, parameter variation and disturbance effects leads to small tracking error and minimum settling time in output response.

Table 2 Performance comparison of controllers

Case(I): Set point tracking				
	ISE		IAE	
Depth (m)	FSMC	EDFSMC	FSMC	EDFSMC
2	0.5243	0.3425	3.248	1.541
5	0.4123	0.2513	2.832	1.216
Case(II): Under the influence of gaussian noise				
	ISE		IAE	
Depth (m)	FSMC	EDFSMC	FSMC	EDFSMC
5	3.878	1.985	5.875	3.752

7 Conclusion

In this work, we have presented an ANFSMC for diving motion behavior of AUV in vertical plane. It basically consists of equivalent and corrective control, in which fuzzy logic control is employed for approximating discontinuous control action, while NN module is used to estimate equivalent control, because AUV's parameters are uncertain in nature. In the adaptation scheme, PID sliding surface coefficients, width of output fuzzy variable, scaling factor, weights and learning rate of NN structure are adapted for improving response of depth parameters of AUV in vertical plane. We found that the performance of the proposed ANFSMC is superior to that of conventional FSMC. The attractive features of the controller are mentioned as follows:

- The exact knowledge of AUV's diving model and their parameter estimation of upper bounds on uncertainties of the AUV are not required in autopilot design. The necessary information to the design of the diving autopilot is the qualitative knowledge of the system such as operating ranges and the form of its nominal model.
- The fuzzy logic controller is designed to provide smooth control by approximating switching control action. The problem of chattering effect in sliding mode approach is effectively eliminated by given corrective control law
- In fuzzy inference engine, width of output fuzzy variable is tuned by multivariable unconstrained optimization method based on integral absolute function and integral time absolute function for minimizing reaching time.
- In NN module, weights are updated using gradient descent method and their learning rate adopted by Lyapunov function based approach

It is significant to point out that proposed control algorithm assure its validity, effectiveness and its superiority to the conventional FSMC method as demonstrated in simulation results. Further research can be done on adaptation scheme to enhance the

output response of AUV in vertical plane by using simplified adaptation algorithm as genetic algorithm, modified particle swarm optimization and other bio-inspired optimization algorithm.

References

1. Akkizidis S, Roberts GN, Ridao P, Batlle J (2003) Designing a Fuzzy-like PD controller for an underwater robot. Control Eng Pract 11(4):471–480
2. Antonelli G, Chiaverini S, Sarkar N, West M (2001) Adaptive control of an autonomous underwater vehicle: experimental results on ODIN. IEEE Trans Control Syst Technol 9(5):756–765
3. Antonelli G, Chiaverini S (2003) A fuzzy approach to redundancy resolution for underwater vehicle-manipulator systems. Control Eng Pract 11(4):445–452
4. Antonelli G, Caccavale F, Chiaverini S, Fusco G (2003) A novel adaptive control law for underwater vehicles. IEEE Trans Control Syst Technol 11(2):221–232
5. Bagheri A, Karimi T, Amanifard N (2010) Tracking performance control of a cable communicated underwater vehicle using adaptive neural network controllers. Appl Soft Comput 10(3):908–918
6. Balasuriya A, Cong L (2003) Adaptive fuzzy sliding mode controller for underwater vehicles. In: Proceeding of international conference on control and automation, 12 June 2003, Montreal, Quebec, Canada, pp 917–921. doi:10.1109/ICCA.2003.1595156
7. Bessa WM, Dutra MS, Kreuzer E (2008) Depth control of remotely operated underwater vehicles using an adaptive fuzzy sliding mode controller. J Robot Auton Syst 56(8):670–677
8. Bessa WM, Dutra MS, Kreuzer E (2010) An adaptive fuzzy sliding mode controller for remotely operated underwater vehicles. Robot Auton Syst 58(1):16–26
9. Choi SK, Yuh J (1996) Experimental study on a learning control system with bound estimation for underwater vehicles. Int J Auton Robots 3(2):187–194
10. Chu ZZ, Zhang MJ (2014) Fault reconstruction of thruster for autonomous underwater vehicle based on terminal sliding mode observer. J Ocean Eng 88:426–434
11. Cristi R, Papoulias FA, Healey AJ (1990) Adaptive sliding mode control of autonomous underwater vehicles in the dive plane. IEEE J Ocean Eng 15(3):152–160
12. Da Cunha JPVS, Costa RR, Hsu L (1995) Design of high performance variable structure control of ROV's. IEEE J Ocean Eng 20(1):42–55
13. DeBitetto PA (1994) Fuzzy logic for depth control of unmanned undersea vehicles. In: Proceedings of IEE of AUV symposium, 19–20 July 1994, Cambridge, pp 233–241. doi:10.1109/AUV.1994.518630
14. DeBitetto PA, (1995) Fuzzy logic for depth control of Unmanned Undersea Vehicles. In:IEEE J Ocean Eng 20(3):242–248
15. Doyle JC, Stein G (1981) Multivariable feedback design concepts for a classical/modern synthesis. IEEE Trans Autom Control 26(1):4–16
16. Fossen T (1994) Guidance and control of ocean vehicles. Wiley, New York
17. Fossen TI, Sagatun S (1991) Adaptive control of nonlinear systems: a case study of underwater robotic systems. J Robot Syst 8(3):393–412
18. Goheen KR, Jefferys ER (1990) Multivariable self tuning autopilots for autonomous underwater vehicles. IEEE J Ocean Eng 15(3):144–151
19. Guo J, Chiu FC, Huang CC (2003) Design of a sliding mode fuzzy controller for the guidance and control of an autonomous underwater vehicle. J Ocean Eng 30(16):2137–2155
20. Guo S, Du J, Lin X, Yue C (2012) An adaptive neuro-fuzzy sliding mode based genetic algorithm control system for under water remotely operated vehicle. Int Conf Mech Autom 3:1681–1685
21. Healey AJ, Lienard D (1993) Multivariable sliding mode control for autonomous diving and steering of unmanned underwater vehicles. IEEE J Ocean Eng 18(3):327–339

22. Herman P (2009) Decoupled PD set-point controller for underwater vehicles. Control Eng Pract 36(6–7):529–534
23. Hoang NQ, Kreuzer E (2007) Adaptive PD-controller for positioning of a remotely operated vehicle close to an underwater structure: theory and experiments. Control Eng Pract 15(4):411–419
24. Hoang NQ, Kreuzer E (2008) A robust adaptive sliding mode controller for remotely operated vehicles. Tech Mech 28(3):185–193
25. Ishaque K, Abdullah SS, Ayob SM, Salam Z (2010) Single input fuzzy logic controller for unmanned underwater vehicle. J Intell Robot Syst 59(1):87–100
26. Ishaque K, Abdullah SS, Ayob SM, Salam Z (2011) A simplified approach to design fuzzy logic controller for an underwater vehicle. Ocean Eng 38(1):271–284
27. Ishii K, Fujii T, Ura T (1995) An on-line adaptation method in a neural network based control system for AUVs. IEEE J Ocean Eng 20(3):221–228
28. Ishii K, Fujii T, Ura T (1998) Neural network system for online controller adaptation and its application to underwater robot. Proc IEEE Int Conf Robot Autom 1:756–761
29. Ishii K, Ura T (2000) An adaptive neural-net controller system for an underwater vehicle. Control Eng Pract 8(2):177–184
30. Jagannathan S, Galan G (2003) One-layer neural-network controller with preprocessed inputs for autonomous underwater vehicles. IEEE Trans Veh Technol 52(5):1342–1355
31. Jalving B (1994) The NDRE-AUV flight control system. IEEE J Ocean Eng 19(4):497–501
32. Javadi-Moghaddam J, Bagheri A (2010) An adaptive neuro-fuzzy sliding mode based genetic algorithm control system for under water remotely operated vehicle. Expert Syst Appl 37:647–660
33. Jimenez TS, Jouvencel B (2003) Using a Higher order sliding modes for diving control a torpedo autonomous underwater vehicle. In MTS/IEEE OCEANS:03 conference, vol 2, pp 56–62
34. Kanakakis V, Valavanis KP, Tsourveloudis NC (2004) Fuzzy logic based navigation of underwater vehicles. J Intell Robot Syst 40(1):45–88
35. Kato N, Ito Y, Kojjma J, Asakawa K, Shirasaki Y (1994) Guidance and control of autonomous underwater vehicle AQUA EXPLORER 1000 for inspection of underwater cables. In: International Symp. on unmanned untethered submersible technology, Brest, pp 195–211. 1994, doi:10.1109/OCEANS.1994.363845. Accessed 13-16 Sept
36. Kato N, Yuh J (1995) Underwater robotic vehicles: Design and control. TSI Press, Albuquerque
37. Kim SW, Lee JJ (1995) Design of a fuzzy controller with fuzzy sliding surface. J Fuzzy Sets Syst 71(3):359–367
38. Kim HS, Shin YK (2005) Design of adaptive fuzzy sliding mode controller based on fuzzy basis function expansion for UFV depth control. Int J Control Autom Syst 3(2):217–224
39. Kim HS, Shin YK (2007) Expanded adaptive fuzzy sliding mode controller using expert knowledge and fuzzy basis function expansion for UFV depth control. J Ocean Eng 34:1080–1088
40. Kim JH, Lee KR, Cho YC, Lee HH, Park HB (2000) Mixed H2/ H-infinity control with regional pole placements for underwater vehicle systems. In: Proceedings of the 2000 American control conference, pp 82–87
41. Kim TW, Yuh J (2001) A novel neuro-fuzzy controller for autonomous underwater vehicles. IEEE Int Conf Robotic Autom 3:2350–2355
42. Lam WC, Ura T (1996) Nonlinear controller with switched control law for tracking control of non-cruising AUV. In: AUV' 96 symposium on autonomous underwater vehicle technology, vol 4, pp 75–85
43. Lakhekar GV, Waghmare LM (2014) Dynamic fuzzy sliding mode control of underwater vehicles. Springer book publication book chapter: advances and applications in sliding mode control systems (studies in computational intelligence, vol 576, p 280. ISBN 978-3-319-11172-8 (XIV, 628)
44. Li JH, Lee PM (2005) A neural network adaptive controller design for free-pitch-angle diving behavior of an autonomous underwater vehicle. Robot Auton Syst 52(3):132–147

45. Li JH, Lee PM (2005) Design of an adaptive nonlinear controller for depth control of an autonomous underwater vehicle. Ocean Eng 32(17):2165–2181
46. Li JH, Lee PM, Hong SW, Lee SJ (2007) Stable nonlinear adaptive controller for an autonomous underwater vehicle using neural networks. Int J Syst Sci 38(4):327–337
47. Liceaga-Castro E, van der Molen GM, Grimble M (1994) Submarine H/sup Infinity/depth control wave disturbances. In: Proceedings of 1994 American control conference–ACC '94, pp 121–127
48. Lee J, Roh M, Lee J, Lee D (2007) Clonal selection algorithms for 6-DOF PID control of autonomous underwater vehicles. Lect Notes Comput Sci 4628:182–190
49. Lee PM, Hong SW, Lim YK, Lee CM, Jeon BH, Park JW (1999) Discrete-time quasi-sliding mode control of an autonomous underwater vehicle. IEEE J Ocean Eng 24(3):388–395
50. Lee SK, Sohn KH, Byun SW, Kim JY (2009) Modeling and controller design of manta-type unmanned underwater test vehicle. J Mech Sci Technol 23:987–990
51. Logan CL (1994) A comparison between h-infinity/mu-synthesis control and sliding-mode control for robust control of a small autonomous underwater vehicle, In: Proceedings of the 1994 symposium on autonomous underwater vehicle technology, AUV '94. Accessed 19–20 July 399–416
52. Lorentz J, Yuh J (1996) A survey and experimental study of neural network AUV control. Proc Symp Auton Underw Veh Technol AUV '96. 20(3):109–116
53. Narasimhan M, Singh SN (2006) Adaptive optimal control of an autonomous underwater vehicle in the dive plane using dorsal fins. Ocean Eng 33:404–416
54. Petrich J, Stilwell DJ (2011) Robust control for an autonomous underwater vehicle that suppresses pitch and yaw coupling. Ocean Eng 38(1):197–204
55. Riedel JS, Healey AJ (1998) Shallow water station keeping of AUVs using multi-sensor fusion for wave disturbance prediction and compensationIn: Proceedings of IEEE oceanic engineering society. OCEANS'98. Conference, pp 212–218
56. Riedel J, Healey A (1998) Model based predictive control of AUV's for station keeping in a shallow water wave environment, In: Proc Int Adv Robot Prog. New Orleans, LA. 77–102
57. Ruth MJ, Humphreys DE (1990) A robust depth and speed control system for a low-speed undersea vehicle. Int Symp Auton Underw Veh Technol. AUV '90. 51–58
58. Sebastian E, Sotelo MA (2007) Adaptive fuzzy sliding mode controller for the kinematic variables of an underwater vehicle. J Intell Robot Syst 49(2):189–215
59. Silvestre C, Pascoal A (2004) Control of the INFANTE AUV using gain scheduled static output feedback. Control Eng Pract 12(12):1501–1509
60. Silvestre C, Pascoal A (2007) Depth control of the INFANTE AUV using gain-scheduled reduced order output feedback. Control Eng Pract 15(7):883–895
61. Smallwood DA, Whitcomb LL (2004) Model based dynamic positioning of underwater robotic vehicles: theory and experiments. IEEE J Ocean Eng 29(1):169–186
62. Smith SM, Rae GJS, Anderson DT, Shien AM (1994) Fuzzy logic control of an autonomous underwater vehicle. Control Eng Pract 2(2):321–331
63. Song F. Smith SM (2000) Design of sliding mode fuzzy controllers for an autonomous underwater vehicle without system model. In: Proceeding of MTS/IEEE ocean conference, Providence, pp 835–840. 2000, doi:10.1109/OCEANS.2000.881362. Accessed 14 Sept
64. Soylu S, Buckham BJ, Podhorodeski RP (2009) MIMO sliding-mode and H-Infinity controller design for dynamic coupling reduction in underwater-manipulator systems. Trans Can Soc Mech Eng 33(4):731–743
65. Stein G, Athans M (1987) The LQG-LTR procedure for multivariable feedback control design. IEEE Trans Autom Control 32:105–114
66. Triantafyllou MS, Grosenbaugh MA (1991) Robust control for underwater vehicle systems with time delays. IEEE J Ocean Eng 16(1):146–151
67. Venugopal KP, Sudhakar R, Pandya AS (1992) On-line learning control of autonomous underwater vehicles using feedforward neural networks. IEEE J Ocean Eng 17(4):308–319
68. Walchko KJ, Nechyba MC (2003) Development of a sliding mode control system with extended Kalman filter estimation for Subjugator. In: Proceeding of Florida conference on recent advances in robotics, Florida, pp 185–191. Accessed 18–20 June 2003

69. Wang JS, Lee CSG, Yuh J (2000) Self-adaptive neuro-fuzzy systems with fast parameter learning for autonomous underwater vehicle control. In: Proceedings 2000 ICRA. Millennium conference. IEEE international conference on robotics and automation, pp 110–116
70. Wang JS, Lee CSG (2003) Self-adaptive recurrent neuro-fuzzy control of an autonomous underwater vehicle. IEEE Trans Robot Autom 19(2):283–295
71. Yoerger DR, Slotine JJE (1991) Adaptive sliding control of an experimental underwater vehicle. Proc IEEE Conf Robot Autom 5:2746–2751
72. Yoerger D, Slotine J (1985) Robust trajectory control of underwater vehicles. IEEE J Ocean Eng 10(4):462–470
73. Yuh J (1990) A neural net controller for underwater robotic vehicles. IEEE J Ocean Eng 15(3):161–166
74. Yuh J (1990) Modeling and control of underwater robotic vehicles. IEEE Trans Syst Man Cybern 20:1475–1483
75. Yuh J, Lakshmi R (1993) An intelligent control system for remotely operated vehicles. IEEE J Ocean Eng 18(1):55–62
76. Yuh J (1994) Learning control for underwater robotic vehicles. IEEE Control Syst 14(2):39–46
77. Yuh J (1995) Underwater Robotic Vehicles: Design and Control. TSI Press
78. Yuh J, Nie J (2000) Application of Nonregressor-based adaptive control to underwater robots: experiment. Int J Comput Electron Eng 26:169–179
79. Zhao S, Yuh J (2005) Experimental study on advanced underwater robot control. IEEE Trans Robot 21(4):695–703
80. Zhang LJ, Qi X, Pang YJ (2009) Adaptive output feedback control based on DRFNN for AUV. Ocean Eng 36(9):716–722

Variable Structure Sensorless Control of PMSM Drives

Lucio Ciabattoni, Maria Letizia Corradini, Massimo Grisostomi, Gianluca Ippoliti, Sauro Longhi and Giuseppe Orlando

Abstract In this chapter has been proposed a robust sensorless cascade control scheme for a Permanent Magnet Synchronous Motor (PMSM) drive. A Discrete Time Variable Structure Control (DTVSC) is considered and the rotor position and speed are obtained through an Adaptive Extended Kalman Filter (AEKF). The performance of the filter is improved by an on line adjustment of the input and measurement noise covariances obtained by a suitably defined estimation algorithm. The proposed solution is experimentally tested on a commercial PMSM drive equipped with a control system based on a floating point Digital Signal Processor (DSP).

Keywords Adaptive Kalman filtering · Permanent magnet motors · Digital control · Variable structure control · Sensorless control · Robust control

L. Ciabattoni · M. Grisostomi · G. Ippoliti (✉) · S. Longhi · G. Orlando
Dipartimento di Ingegneria dell'Informazione, Università Politecnica
delle Marche,Via Brecce Bianche, 60131 Ancona, Italy
e-mail: gianluca.ippoliti@univpm.it

L. Ciabattoni
e-mail: l.ciabattoni@univpm.it

M. Grisostomi
e-mail: m.grisostomi@univpm.it

S. Longhi
e-mail: sauro.longhi@univpm.it

G. Orlando
e-mail: giuseppe.orlando@univpm.it

M.L. Corradini
Scuola di Scienze e Tecnologie, Università di Camerino,
via Madonna delle Carceri, 62032 Camerino, MC, Italy
e-mail: letizia.corradini@unicam.it

S. Vaidyanathan and C. Volos (eds.), *Advances and Applications in Nonlinear Control Systems*, Studies in Computational Intelligence 635,
DOI 10.1007/978-3-319-30169-3_22

1 Introduction

Electric motors are the single biggest consumer of electricity in modern society. According to an analysis of the International Energy Agency [43], more than 45 % of the global electrical energy is consumed by industrial and domestic motors. With a share of 64 %, the industrial sector consumes the most power for electric motorized applications. The next most important sectors are the commercial (accounting for 20 %) and the residential one (accounting for about 13 %). To better understand these data, it can be useful to highlight that the second consumer of electricity, i.e. lighting, is responsible of less than 15 % of consumptions.

In this scenario the demand of inexpensive and reliable drives is pushing applied research towards the elimination of mechanical sensors, in particular for mass-produced motors in the kW range, see e.g. [4, 5, 16, 21, 25, 31, 47, 57]. Indeed, in most applications, these sensors present several disadvantages in terms of reliability, susceptibility to noise, additional cost and weight contemporarily increasing the complexity of the drive system and observer-based solutions are needed [12, 18, 19]. High performance control of PMSM drives typically requires the knowledge of the rotor shaft position and speed in order to synchronize the phase excitation pulses to the rotor position, as described in [55]. This implies the need for speed or position sensors such as an encoder or a resolver attached to the shaft of the motor. The position and velocity sensorless control of PMSM drive may overcome these difficulties. Therefore, sensorless control of motors based on algorithms simple enough to be real-time executed in low-cost industrial DSP appears susceptible of industrial interest due to its cost-effective nature and wide applicability to a large class of motors, see e.g. [1, 24, 29]. A comprehensive overview of methods developed to obtain rotor position and angular speed from measurements of electric quantities is reported in [6, 8, 9].

In this chapter, an Adaptive Extended Kalman Filter (AEKF), which is a simple and efficient state estimator for nonlinear systems with inherent robustness against parameter variations, is proposed for the estimation of rotor position and speed of PMSM drives from measurements of electric quantities. Recent advances in digital technology allow nowadays adequate data processing on cost-effective DSP-based platforms, and the EKF can be now considered a viable and computationally efficient tool for position and speed estimation, as reported in [6, 56]. Theoretical issues and digital implementation of the EKF have been deeply investigated in the past by [3, 7, 26, 34, 41] and a novel procedure for the offline tuning of covariance matrices in EKF-based PMSM drives has been presented in [8]. Application examples reported in [9, 10, 30] seem to prove that some well-known pitfalls (such as the starting from unknown rotor position and the filter matrices tuning) have been successfully fixed.

Nonetheless, at least one major drawback of the EKF application to sensorless drives is still unsolved. Indeed, the use of Kalman filtering techniques requires to derive a stochastic state-space representation of the system model and of the measure process, and the design and the online tuning of the covariance matrices appearing in the EKF equations are still an open problem. Most of the EKF techniques proposed

in the literature for state estimation are based on some fixed values of the input and measurement noise covariance matrices, as in [3, 6, 8, 9, 33, 41]. In many practical applications an a priori information of this kind is often unavailable and it is necessary to allow the filter to properly weight online the incoming observations. On the other hand it is well known how poor estimates of noise statistics may seriously degrade the Kalman filter performance.

The main feature of the Adaptive Extended Kalman Filter (AEKF) here adopted is its capability of online adaptively estimating such unknown statistical parameters. This adaptive solution should reduce customization required by each application that makes most of the EKF-based drives incompatible with an off-the-shelf market strategy. It is worth noticing that particular attention has been paid, in developing the algorithm, to prevention of filter divergence and to the simplicity of implementation, in view of its implementation on commercial DSP.

Considering control issues requiring specific attention in electric drive systems, it is well known that electromechanical parameters are subject to significant variations. A nonlinear control strategy widely recognized and successfully applied in recent years is the Variable Structure Control (VSC), adopted by [11, 27, 44, 45, 53, 54, 58, 59]. Indeed, VSC methods provide robustness to matched uncertainties (see e.g. [17, 20, 52, 60]), and are computational simpler with respect to other robust control approaches, thus well suited for low-cost DSP implementation. VSC schemes are typically affected by chattering of the control signal but, as discussed in [2, 54], this well-known implementation drawback of VSC does not cause difficulties for electric drives since the on-off operation mode is the only admissible one for power converters.

For PMSM, the cascade control structure of the Field Oriented Control (FOC) is often usefully applied to achieve fast four quadrant operation, smooth starting and acceleration, as described in [38–40, 42]. FOC is implemented with two current controllers in inner control loops and a speed controller in an outer control loop. The speed controller provides the reference current for one of the two inner current control loops; this reference current corresponds to the required motor torque. As argued in [54], VSC techniques cannot be applied for the outer speed control loop, since the reference input of the inner control loop should have bounded time derivatives. To overcome this problem, different approaches have been followed, such as, for instance, the ‘direct speed control’ in [54] and the ‘second-order sliding-mode technique’ in [44]. Both techniques, however, share a formulation in the continuous time framework, while the practical implementation on a low-cost DSP of a real motor drive claims for a more appropriate formulation of the problem in a sampled-data systems context.

In particular in the present study, a control policy based on Discrete-Time VSC (DTVSC) [13–15, 22, 32], endowed with a AEKF for the estimation of the rotor position and speed, is developed and experimentally tested. The introduction of a DTVSC is motivated by the need of taking directly into account the issue of control law digitalization. Reported experimental evidences seem to show that it is actually able to cope with electromechanical disturbances.

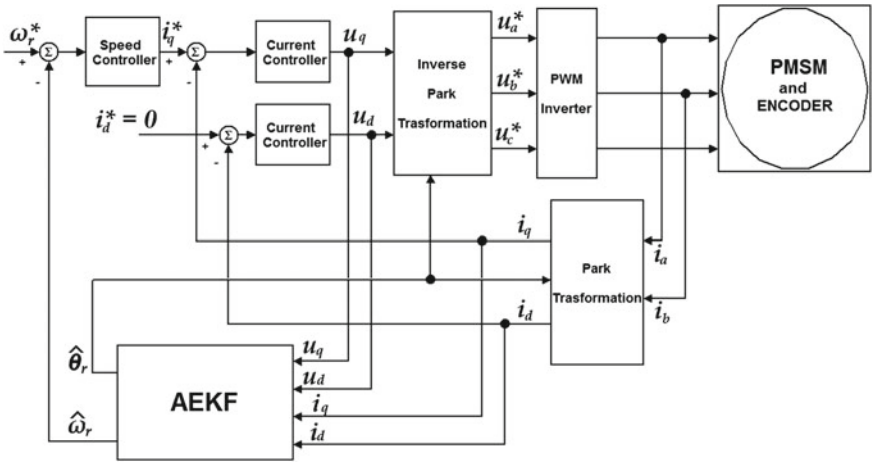

Fig. 1 Block scheme of the proposed cascade controller (FOC)

Summing up, the features of the DTVSC technique combined with the AEKF-based rotor position and speed estimator are exploited in this work to design the cascade control architecture shown in Fig. 1. In this scheme, the external velocity DTVS control loop, two internal current DTVS control loops and the AEKF-based rotor position and speed estimator can be identified. The task is to make the speed error $\omega_r^* - \hat{\omega}_r$ to tend to zero as close as possible. As well known, the discrete-time sliding mode condition can be imposed exactly only outside a given sector. This issue has been addressed using the approach known as Time Delay Control [23, 50].

The chapter is organized as follows. The nonlinear state space model of the PMSM dynamics is presented in Sect. 2. The AEKF algorithm is reported in Sect. 3. In Sect. 4 details on the considered DTVS controller are discussed. Results on experimental tests are reported in Sect. 5. The chapter ends with comments on the performance of the proposed solution.

2 Motor Dynamics

In the $(d,\ q)$ reference frame, synchronously rotating with the motor rotor, the electrical equations of motion of a permanent-magnet synchronous motor can be written as [46, 54]:

$$\frac{di_d}{dt} = -\frac{R}{L}i_d + \omega_e i_q + \frac{1}{L}u_d \tag{1}$$

$$\frac{di_q}{dt} = -\frac{R}{L}i_q - \omega_e i_d - \frac{1}{L}\lambda_0\omega_e + \frac{1}{L}u_q \tag{2}$$

where i_d and i_q are the $d\text{-}axis$ and $q\text{-}axis$ stator currents, respectively; u_d and u_q are the $d\text{-}axis$ and $q\text{-}axis$ stator voltages, respectively; R is the winding resistance and $L = L_d = L_q$ is the winding inductance on axis d and q; λ_0 is the flux linkage of the permanent magnet and ω_e is the electrical angular speed of the motor rotor.

The electrical torque τ_e and the mechanical power P of the motor are given by $\tau_e = K_t i_q$ and $P = \tau_e \omega_r$ in which $K_t = \frac{3}{2}\lambda_0 N_r$ is the torque constant with N_r the number of pole pairs and ω_r is the mechanical angular speed of the motor rotor. The developed torque of the motor is proportional to the i_q current because of the assumption that there is no reluctance torque in the considered PMSM.

The mechanical motion equation of the motor is described by:

$$J\frac{d\omega_r}{dt} + B\omega_r = \tau_e - \tau_\ell; \quad \frac{d\theta_r}{dt} = \omega_r \tag{3}$$

where J is the mechanical inertia of the motor and load, B is the coefficient of viscous friction, τ_ℓ is the load torque and θ_r denotes the mechanical angular position of the motor rotor.

For the electrical angular position/speed and the mechanical angular position/speed, these relations hold: $\omega_e = N_r \omega_r$ and $\theta_e = N_r \theta_r$.

3 Adaptive Estimation of Rotor Position and Speed

The proposed AEKF providing online estimates of rotor position and speed is derived in this section. Denote with $X(t) := \left[\, \omega_r(t)\ i_d(t)\ i_q(t)\ \vartheta_r(t) \,\right]$ the motor state and with $U(t) := \left[\, u_d(t)\ u_q(t) \,\right]$ the motor control input. The motor nonlinear dynamic state space model can be written in the compact form of the following stochastic differential equation:

$$dX(t) = F(X(t), U(t))dt + \eta(t), \tag{4}$$

where $F(X(t), U(t))$, obtained by (1)–(3), is given by:

$$F\left(X(t), U(t)\right) = \begin{bmatrix} -\frac{B}{J}\omega_r(t) + \frac{K_t}{J} i_q(t) - \frac{\tau_\ell}{J} \\ -\frac{R}{L} i_d(t) + \omega_e(t) i_q(t) + \frac{1}{L} u_d(t) \\ -\frac{R}{L} i_q(t) - \omega_e(t) i_d(t) - \frac{1}{L}\lambda_0 \omega_e(t) + \frac{1}{L} u_q(t) \\ \omega_r(t) \end{bmatrix}$$

and $\eta(t)$, is a white noise process $\sim N(0,\, Q(t))$ representing the model inaccuracies. Assuming a constant sampling period $\Delta t_k = T_c$ and denoting t_{k+1} by $(k+1)T_c$, the following sampled nonlinear measure equation can be associated to Eq. (4):

$$Z((k+1)T_c) = G(X((k+1)T_c)) + v(kT_c), \tag{5}$$

where $Z(kT_c)$ is the vector containing measures of motor phase currents and $v(kT_c)$ is a white sequence $\sim N(0, R(kT_c))$. The measure vector $Z(kT_c)$ is composed of two elements, i.e. $Z(kT_c) = [z_1(kT_c)\ z_2(kT_c)]^T$, where $z_1(kT_c) = i_d(kT_c) + v_1(kT_c)$ and $z_2(kT_c) = i_q(kT_c) + v_2(kT_c)$.

By definition of the measurement vector one has that the output function $G(X((k+1)T_c))$ has the following form:

$$G(X(kT_c)) = \left[i_d(kT_c)\ i_q(kT_c) \right]^T = C(kT_c)X(kT_c) \tag{6}$$

where

$$C(kT_c) = \begin{bmatrix} 0\ 1\ 0\ 0 \\ 0\ 0\ 1\ 0 \end{bmatrix} \tag{7}$$

and $v(kT_c) = [v_1(kT_c)\ v_2(kT_c)]^T$. Assume $U(t) = U(kT_c)$ for $t \in [kT_c, (k+1)T_c)$. To obtain an extended Kalman filter with an effective state prediction equation in a simple form, model (1) and (2) has been linearized about the current state estimate $\hat{X}(kT_c, kT_c)$ and the control input $U((k-1)T_c)$ applied until the linearization instant. Subsequent discretization with period T_c of the linearized model results in the following EKF (where explicit dependence on T_c has been dropped for simplicity of notation),

$$\hat{X}(k+1,k) = A_d(k)\hat{X}(k,k) + L(k)U(k) + D(k) \tag{8}$$

$$P(k+1,k) = A_d(k)P(k,k)A_d^T(k) + Q_d(k) \tag{9}$$

$$K(k+1) = P(k+1,k)C^T(k+1)[C(k+1)P(k+1,k)C^T(k+1) + R(k+1)]^{-1} \tag{10}$$

$$\hat{X}(k+1,k+1) = \hat{X}(k+1,k) + K(k+1)[Z(k+1 - G(\hat{X}(k+1,k))] \tag{11}$$

$$P(k+1,k+1) = [I - K(k+1)C(k+1)]P(k+1,k) \tag{12}$$

where

$$A_d(k) = e^{A(k)T_c} \simeq I + A(k)T_c$$
$$= \begin{bmatrix} 1 - \frac{B}{J}T_c & 0 & \frac{K_t}{J}T_c & 0 \\ \hat{i}_q(k,k)T_c & 1 - \frac{R}{L}T_c & N_r\hat{\omega}_r(k,k)T_c & 0 \\ -\left(\frac{\lambda_0}{L} + \hat{i}_d(k,k)\right)T_c & -N_r\hat{\omega}_r(k,k)T_c & 1 - \frac{R}{L}T_c & 0 \\ 1 & 0 & 0 & 0 \end{bmatrix} \tag{13}$$

with

$$A(k) := \left[\frac{\partial F(X(t), U(t))}{\partial X(t)}\right]_{\substack{X(t)=\hat{X}(k,k) \\ U(t)=U(k-1)}} \tag{14}$$

and

$$L(k) = \begin{bmatrix} 0 & 0 \\ \frac{T_c}{L} & 0 \\ 0 & \frac{T_c}{L} \\ 0 & 0 \end{bmatrix} \tag{15}$$

$$D(k) = T_c\bar{D}(k) = \begin{bmatrix} -\frac{\tau_\ell T_c}{J} \\ -\hat{i}_q(k,k)N_r\hat{\omega}_r(k,k)T_c \\ \hat{i}_d(k,k)N_r\hat{\omega}_r(k,k)T_c \\ 0 \end{bmatrix} \tag{16}$$

$$\bar{D}(k) := F\left(\hat{X}(k,k), U(k-1)\right) - A(k)\hat{X}(k,k) - L(k)U(k-1) \tag{17}$$

$$Q_d(k) = \sigma_\eta^2(k)\bar{Q}(k). \tag{18}$$

The elements of the matrix $\bar{Q}(k)$ have been reported in the Appendix. The form of $Q_d(k)$ expressed by (18) derives by the hypothesis that $Q(\tau) = \sigma_\eta^2(k)I_4$, $\tau \in [kT_c, (k+1)T_c)$. This simplification assumption has been introduced to obtain a $Q_d(k)$ which is completely known up to the unknown multiplicative scaling factor $\sigma_\eta^2(k)$. Moreover, the covariance matrix $R(k)$ is assumed to have the following diagonal form:

$$R(k) = diag\left[\sigma_{v,1}^2(k), \sigma_{v,2}^2(k)\right]; \tag{19}$$

this means that no correlation is assumed between the measurement errors introduced by the sensors. As $R(k)$ is diagonal, the components of $Z(k)$ may be processed one by one by reducing the inversion of the 2×2 matrix in (3) to the two inversions

of scalars [35], thus saving much computation time. The sequential processing of each component $z_1(k)$ and $z_2(k)$ must be performed in a period of time (typically the sampling period) such that no significant change occurs in the state estimate and in its covariance matrix due to dynamics (4) [35].

The EKF can be implemented once estimates of $Q_d(k)$ and $R(k)$ are available. In general, a complete and reliable information about these matrices is not available; on the other hand it is well known how poor knowledge of noise statistics may seriously degrade the Kalman filter performance. This problem is here dealt with introducing an adaptive adjustment mechanism of $Q_d(k)$ and $R(k)$ values in the EKF equations.

3.1 Adaptive Estimation of $Q_d(k)$ and $R(k)$

A considerable amount of research has been carried out in the adaptive Kalman filtering area [35–37, 48], but in practice it is often necessary to redesign the adaptive filtering scheme according to the particular characteristics of the problem faced. Following [36], in view of real time applications, a particular attention has been here devoted to simplicity of implementation and to prevention of filter divergence, moreover, the particular structure of the input noise covariance matrix $Q_d(k)$, which is completely known save that for a multiplicative scalar, has been suitably taken into account.

The following nearly stationarity assumption is made: the parameters $\sigma^2_{v,i}(k)$, $i = 1, 2$, and $\sigma^2_\eta(k)$ are nearly constant over $n_v \geq 2$ and $n_\eta \geq 2$ samples respectively [36].

Define $\gamma_i(k+1) = z_i(k+1) - G_i(\hat{X}(k+1,k))$, where $z_i(k+1)$ and $G_i(\hat{X}(k+1,k))$ are the ith component of $Z(k+1)$ and $G(\hat{X}(k+1,k))$, respectively. For analogy with the linear case, residuals $\gamma_i(k+1)$, $i = 1, 2$, are called the innovation process samples and are assumed to be well described by a white sequence $\sim N(0, s_i(k+1))$, where $s_i(k+1)$, $i = 1, 2$ can be expressed as

$$\begin{aligned} s_i(k+1) &= C_i(k+1)P(k+1,k)C_i^T(k+1) + \sigma^2_{v,i}(k+1) \\ &= C_i(k+1)[A_d(k)P(k,k)A_d^T(k) + \sigma^2_\eta(k)\bar{Q}(k)]C_i^T(k+1) \\ &\quad + \sigma^2_{v,i}(k+1). \end{aligned} \tag{20}$$

This simplifying assumption is as more valid as discretization and linearization of (4) is more accurate and makes it possible to apply the methods of the adaptive filtering theory developed for the linear case.

The two above assumptions will allow us to define a simple and efficient estimation algorithm based on the condition of consistency, at each step, between the observed innovation process samples $\gamma_i(k+1)$, $i = 1, 2$ and their predicted statistics $E\{\gamma_i^2(k+1)\} = s_i(k+1)$. Imposing such a condition, one stage estimates $\hat{\sigma}^2_\eta(k)$ and $\hat{\sigma}^2_{v,i}(k+1)$, $i = 1, 2$, of $\sigma^2_\eta(k)$ and $\sigma^2_{v,i}(k+1)$, $i = 1, 2$, respectively are obtained at each step. To increase their statistical significance, the one stage estimates $\hat{\sigma}^2_\eta(k)$ and

$\hat{\sigma}^2_{v,i}(k+1)$, $i=1,2$, are averaged obtaining the relative smoothed versions $\bar{\hat{\sigma}}^2_{\eta}(k)$ and $\bar{\hat{\sigma}}^2_{v,i}(k+1)$, $i=1,2$.

From (20) it is apparent that the statistical information carried by each $\gamma_i(k+1)$, $i=1,2$, depends, at the same time, on the two unknown parameters $\sigma^2_{\eta}(k)$ and $\sigma^2_{v,i}(k+1)$.

This indeterminateness is here dealt with using a number (say n'_{η}) of innovation process samples $\gamma_i(k+1)$, $i=1,2$, to estimate $\sigma^2_{\eta}(k)$ and the others (say n'_{v}) to estimate $\sigma^2_{v,i}(k+1)$. In the light of the nearly stationarity assumption, the two integers n'_{η} and n'_{v} are chosen such that $n'_{\eta}/n'_{v}=n_v/n_{\eta}$.

Assume $n_v \geq n_{\eta}$, let α and β two coprime integers such that $\alpha/\beta=n_v/n_{\eta}$ and let q and r two integers such that $\alpha=\beta q+r$; then, the innovation process sequence is subdivided into intervals $I_{\alpha+\beta}$ composed of $\alpha+\beta$ samples. Each interval contains β sequences of q samples used to estimate $\sigma^2_{\eta}(k)$ (the faster varying parameter), the ensembles of q samples are separated by β sequences of one sample used to estimate $\sigma^2_{v,i}(k+1)$, $i=1,2$ (the more slowly varying parameter), the last r samples of each $I_{\alpha+\beta}$ interval are used to estimate $\sigma^2_{\eta}(k)$. This scheme minimizes the interval of time over which either one step estimate is not updated. A symmetric situation holds if $n_{\eta} \geq n_v$.

When the one step estimate $\hat{\sigma}^2_{\eta}(k)(\hat{\sigma}^2_{v,i}(k+1), i=1,2)$ is updated, the other single stage estimate $\hat{\sigma}^2_{v,i}(k+1)$, $i=1,2$, $(\hat{\sigma}^2_{\eta}(k))$ is kept constant, so that the symbol $\hat{\sigma}^2_{\eta}(k)(\hat{\sigma}^2_{v,i}(k+1))$ does not necessarily imply that this estimate has been computed using the last observed innovation process sample $\gamma_i(k+1)$, $i=1,2$.

Because of the particular form (18) of $Q_d(k)$ and of the sequential scalar processing of measures, two one stage estimates $\hat{\sigma}^2_{\eta,i}(k)$ of the unknown $\sigma^2_{\eta}(k)$, $i=1,2$ can be determined maximizing the probability of observing the corresponding ith component of the predicted residual $\gamma_i(k+1)$, $i=1,2$ [35]. Namely, each $\hat{\sigma}^2_{\eta,i}(k)$ is determined by the operation

$$\max \text{prob}_{\sigma^2_{\eta,i}(k+1)\geq 0}\gamma_i(k+1).$$

The maximizing $\hat{\sigma}^2_{\eta,i}(k)$ is obtained by imposing the condition of consistency between residuals and their predicted statistics, namely $\gamma_i^2(k+1)=E\{\gamma_i^2(k+1)\}=s_i(k+1)$. Using (20) and replacing $\sigma^2_{v,i}(k+1)$ with $\bar{\hat{\sigma}}^2_{v,i}(k+1)$ one has

$$\hat{\sigma}^2_{\eta,i}(k)=\max\Big\{(C_i(k+1)\bar{Q}(k)C_i^T(k+1))^{-1}[\gamma_i(k+1)^2 - C_i(k+1)A_d(k)P(k,k)A_d^T(k)C_i^T(k+1)\bar{\hat{\sigma}}^2_{v,i}(k+1)],0\Big\}. \quad (21)$$

To obtain a unique estimate of $\sigma^2_{\eta}(k)$ and to increase the statistical significance of estimators (21), which are based on only one component $\gamma_i(k+1)$, the following smoothed estimate is computed

$$\bar{\hat{\sigma}}^2_{\eta}(k) = \frac{1}{2(l_\eta + 1)} \sum_{j=0}^{l\eta} \sum_{i=1}^{2} \hat{\sigma}^2_{\eta,i}(k-j), \tag{22}$$

where l_η denotes the number of one-stage estimates $\hat{\sigma}^2_{\eta,i}(\cdot)$ yielding the smoothed estimate.

In a recursive form the proposed estimate of $\sigma^2_\eta(k)$ is

$$\bar{\hat{\sigma}}^2_{\eta}(k) = \bar{\hat{\sigma}}^2_{\eta}(k-1) + \frac{1}{2(l_\eta + 1)} \left[\sum_{i=1}^{2} \left(\hat{\sigma}^2_{\eta,i}(k) - \hat{\sigma}^2_{\eta,i}(k-(l_\eta+1)) \right) \right]. \tag{23}$$

Analogously, the operation

$$\max \text{prob}_{\sigma^2_{v,i}(k+1)\geq 0} \gamma_i(k+1)$$

and (20) give the following one stage estimate of $\sigma^2_{v,i}(k+1)$, $i = 1, 2$,

$$\begin{aligned} \hat{\sigma}^2_{v,i}(k+1) = \ & \max\{\gamma_i^2(k+1) - [C_i(k+1)A_d(k)P(k,k)A_d^T(k)C_i^T(k+1) \\ & + C_i(k+1)\bar{\hat{\sigma}}^2_{\eta,i}(k)\bar{Q}(k)C_i^T(k+1)], 0\}, \end{aligned} \tag{24}$$

the smoothed version $\bar{\hat{\sigma}}^2_{v,i}(k+1)$ is

$$\bar{\hat{\sigma}}^2_{v,i}(k+1) = \frac{1}{l_v + 1} \sum_{j=0}^{l_v} \hat{\sigma}^2_{v,i}(k+1-j), \tag{25}$$

where l_v denotes the number of one-stage estimates $\hat{\sigma}^2_{v,i}(\cdot)$ yielding the smoothed estimate.

In a recursive form the proposed estimates of $\sigma^2_{v,i}(k+1)$ becomes

$$\bar{\hat{\sigma}}^2_{v,i}(k+1) = \bar{\hat{\sigma}}^2_{v,i}(k) + \frac{1}{l_v + 1}(\hat{\sigma}^2(k+1) - \hat{\sigma}^2(k-l_v)). \tag{26}$$

The proposed adaptive estimation algorithm is given by Eqs. (23) and (26) and is able to prevent filter divergence. In fact, as long as the innovation samples $\gamma_i(k+1)$, $i = 1, 2$ are sufficiently small and consistent with their statistics, the filter operates satisfactorily and the noise model is kept small (or null) by (21). If a sudden increase of the absolute value of the innovation process samples is observed, Eq. (21) provides an increased $\hat{Q}_d(k) = \bar{\hat{\sigma}}^2_{\eta}(k)\bar{Q}(k)$, and hence an augmented filter gain, thus preventing filter divergence.

Parameters l_η and l_v of estimators (23) and (26) are chosen on the basis of two antagonist considerations: low values would produce noise estimators which are not statistically significant, large values would produce estimators which are scarcely

sensitive to possible rapid fluctuations of the true $\sigma_\eta^2(k)$ and $\sigma_{v,i}^2(k)$, $i = 1, 2$. During filter initialization, the starting values $\hat{\sigma}_\eta^2(0)$ and $\hat{\sigma}_{v,i}^2(0)$, $i = 1, 2$, of $\hat{\sigma}_\eta^2(k)$ and $\hat{\sigma}_{v,i}^2(k)$ respectively, must be chosen on the basis of the a priori available information. In the case of a lack of such information, a large value of $P(0, 0)$ is useful to prevent divergence.

Remark 3.1 As stated in [6], to reduce the computational effort for a real time implementation of the EKF an acceptable approximation is to use a diagonal covariance matrix $Q_d(k)$.

4 Control Design

The discretization of Eqs. (1)–(3) with a sampling time T_c according to standard techniques gives:

$$\omega_e(k+1) = A_\omega \omega_e(k) + B_\omega(K_t i_q(k) - \tau_\ell) \tag{27}$$

$$i_d(k+1) = A_i i_d(k) + B_i u_d(k) + f_1(\omega_e, i_q, k) \tag{28}$$

$$i_q(k+1) = A_i i_q(k) + B_i u_q(k) - f_2(\omega_e, i_d, k) \tag{29}$$

with

$$A_\omega = e^{-\frac{B}{J}T_c}, \quad B_\omega = \frac{1}{J}\int_0^{T_c} e^{-\frac{B}{J}\tau} d\tau$$

$$A_i = e^{-\frac{R}{L}T_c}, \quad B_i = \frac{1}{L}\int_0^{T_c} e^{-\frac{R}{L}\tau} d\tau$$

$$f_1(\omega_e, i_q, k) = \int_{kT_c}^{(k+1)T_c} \omega_e(\tau) i_q(\tau) d\tau \simeq \omega_e(k) i_q(k) T_c;$$

$$f_2(\omega_e, i_d, k) = \int_{kT_c}^{(k+1)T_c} \omega_e(\tau)(i_d(\tau) + \frac{\lambda_0}{L}) d\tau \simeq \omega_e(k)(i_d(k) + \frac{\lambda_0}{L}) T_c.$$

To account for possible model uncertainties, it is assumed that model parameters may differ from their nominal values for some unknown but bounded quantities:

$$\begin{aligned} A_\omega &= \bar{A}_\omega + \Delta A_\omega; \quad B_\omega = \bar{B}_\omega + \Delta B_\omega; \\ |\Delta A_\omega| &\le \rho_{A\omega}; \quad |\Delta B_\omega| \le \rho_{B\omega} \\ A_i &= \bar{A}_i + \Delta A_i; \quad B_i = \bar{B}_i + \Delta B_i; \\ |\Delta A_i| &\le \rho_{Ai}; \quad |\Delta B_i| \le \rho_{Bi}. \end{aligned} \tag{30}$$

Define the following discrete-time sliding surfaces:

$$s_\omega(k) = (\hat{\omega}_e(k) - \omega_e^*(k)) + \lambda_\omega(\hat{\omega}_e(k-1) - \omega_e^*(k-1)) = 0 \tag{31}$$

$$s_{iq}(k) = (i_q(k) - i_q^*(k)) + \lambda_q(i_q(k-1) - i_q^*(k-1)) = 0 \tag{32}$$

$$s_{id} = i_d(k) + \lambda_d i_d(k-1) = 0 \tag{33}$$

where $\lambda_\omega, \lambda_q, \lambda_d \in (-1, 1)$, $\hat{\omega}_e(k)$ is the estimate of $\omega_e(k)$ provided by the AEKF, $\omega_e^*(k)$ is the given reference value for the angular velocity, and $i_q^*(k)$ will be defined in the following of this section.

As well known, a quasi sliding motion on the surface $s_\omega(k) = 0$ can be achieved imposing the following discrete time sliding mode existence condition [22, 28]:

$$s_\omega(k)\Delta s_\omega(k+1) < -\frac{1}{2}[\Delta s_\omega(k+1)]^2 \tag{34}$$

being $\Delta s_\omega(k+1) = s_\omega(k+1) - s_\omega(k)$. It can be easily verified that condition (34) is ensured by the control law $i_q^*(k) = i_q^{eq}(k) + i_q^n(k)$, where the equivalent control is given by:

$$i_q^{eq}(k) = \frac{1}{\bar{B}_\omega K_t}(\omega_e^*(k+1) - \bar{A}_\omega\hat{\omega}_e(k) - \lambda_\omega(\hat{\omega}_e(k) - \omega_e^*(k))). \tag{35}$$

As usual, the discontinuous control i_q^n is such that the sliding condition can be imposed exactly only outside a given sector. Inside such sector the sliding condition can be imposed only approximately. To this purpose we made resort to the approach known as time delay control [23], obtaining

$$i_q^n(k) = \begin{cases} \theta_\omega \dfrac{|s_\omega(k)| - \rho_\omega}{\bar{B}_\omega K_t} & if\ |s_\omega(k)| > \rho_\omega \\ -\dfrac{s_\omega(k) - \bar{B}_\omega i_q^n(k-1)}{\bar{B}_\omega K_t} & if\ |s_\omega(k)| \le \rho_\omega \end{cases} \tag{36}$$

with $|\theta_\omega| \le 1$, and with

$$\rho_\omega = (|\bar{B}_\omega| + \rho_{B\omega})\rho_\tau + \rho_{A\omega}\omega_e^{max} + K_t\rho_{B\omega}i_q^{max}$$

ρ_τ being the constant bound of the unknown load which can affect the motor, i.e. $|\tau_\ell| \le \rho_\tau$. Note that ω_e^{max} and i_q^{max} are the largest speed achievable by the motor and the largest current which can be supplied, respectively, according to its constructive limits.

The control law $i_q^*(k)$ is fed as reference value, which is the required motor torque, to one of the two inner current control loops. The tracking of such reference is ensured by the imposition of a quasi sliding motion of the surface $s_{iq}(k) = 0$. Following the same lines as before, it can be easily verified that the sliding condition on $s_{iq}(k) = 0$

is ensured by the control law $u_q(k) = u_q^{eq}(k) + u_q^n(k)$, where:

$$u_q^{eq}(k) = \frac{1}{\bar{B}_i}\left[i_q^*(k) - \bar{A}_i i_q(k) - \lambda_q(i_q(k) - i_q^*(k))\right] \tag{37}$$

$$u_q^n(k) = \begin{cases} \theta_q \dfrac{|s_{iq}(k)| - \rho_q}{\bar{B}_i} & if \quad |s_{iq}(k)| > \rho_q \\ -\dfrac{s_{iq}(k) - \bar{B}_i u_q^n(k-1)}{\bar{B}_i} & if \quad |s_{iq}(k)| \leq \rho_q \end{cases} \tag{38}$$

where $|\theta_q| \leq 1$, $\rho_q = \rho_{Ai} i_q^{max} + \rho_{Bi} u_q^{max} + \rho + \omega_e^{max}(i_d^{max} + \frac{\lambda_0}{L})T_c$, ρ being the bound of $\Delta i_q^*(k) = |i_q^*(k+1) - i_q^*(k)|$.

Finally, the achievement of a quasi sliding motion on $s_{id}(k) = 0$ guarantees the vanishing of the variable $i_d(k)$, and is ensured by the control law:

$$u_d^{eq}(k) = -\frac{(\bar{A}_i + \lambda_d) i_d(k)}{\bar{B}_i} \tag{39}$$

$$u_d^n(k) = \begin{cases} \theta_d \dfrac{|s_{id}(k)| - \rho_d}{\bar{B}_i} & if \quad |s_{id}(k)| > \rho_d \\ -\dfrac{s_{id}(k) - \bar{B}_i u_d^n(k-1)}{\bar{B}_i} & if \quad |s_{id}(k)| \leq \rho_d \end{cases} \tag{40}$$

where $|\theta_d| \leq 1$ and $\rho_d = \rho_{Ai} i_d^{max} + \rho_{Bi} u_d^{max} + \omega_e^{max} i_q^{max} T_c$.

5 Experimental Implementation

The proposed DTVS controller and AEKF-based rotor position and speed estimator have been implemented on the Technosoft MCK28335-Pro DSP motion control kit [49], available in the Robotics Laboratory at the Dipartimento di Ingegneria dell'Informazione of the Università Politecnica delle Marche. The experimental setup is shown in Fig. 2. It is a combination of hardware and software and includes a DSP-based controller board, a power module, a PMSM equipped with a 500-line quadrature encoder (4 is the multiplication ratio of the position resolution done in the encoder interface) and a software platform to develop motion control applications. All communication between PC and DSP board is done through the RS-232 interface using a real-time serial communication monitor resident in the DSP flash.

In this section, the drive structure, the experimental setup and the results are discussed.

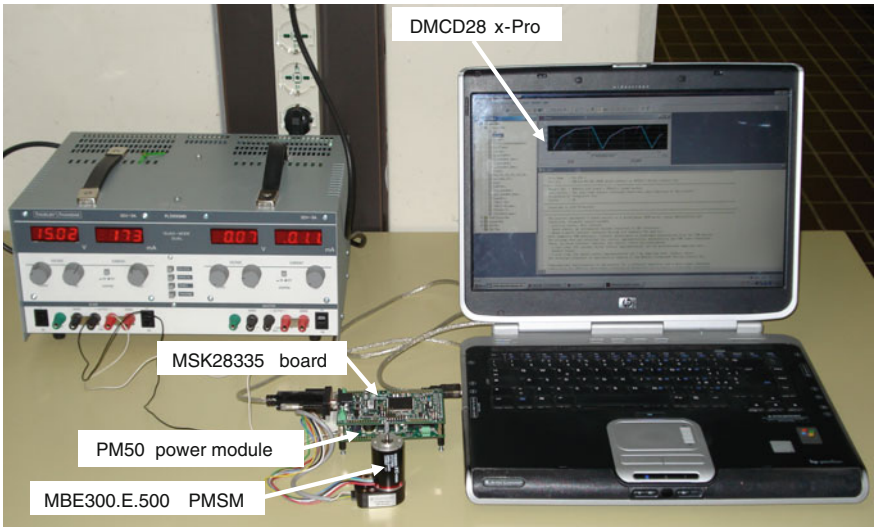

Fig. 2 Experimental setup

5.1 Drive Structure

Control design methods performed in the $(d,\ q)$ coordinates are called field-oriented control which consists of controlling the stator currents represented by a vector (vector control). This approach uses a state transformation after which the decoupling and linearization tasks can be performed [55]. In particular, FOC-based schemes exploit the fact that in the $(d,\ q)$ rotating reference frame the torque and the flux dynamics are linear and decoupled and independent torque and flux control loops can be implemented. PI controllers are commonly used in both loops to produce the 'd' and 'q' voltage vector components, affecting the flux and torque dynamics, respectively. Recently, high-speed DSP has become very common in electric drive systems and FOC has been implemented in many drive systems of AC machines. The FOC scheme of Fig. 1 is based on the measure of two phase currents (i_a and i_b) and the AEKF-based estimator is designed to estimate the rotor position and speed from measurements of electric quantities. The measured phase currents, i_a and i_b, are transformed, based on the rotor position information and the Park coordinate transformation, into the rotor frame direct and quadrature components, i_d and i_q. The inverse Park coordinate transformation is used for the computation of the three-phase voltage references, u_a^*, u_b^* and u_c^*, applied to the inverter starting from the values of voltage references computed by the current controllers in the (d, q) reference frame, i.e. u_d and u_q. Thus, 6 PWM outputs of the DSP controller are directly driven by the implemented control algorithm, based on these reference voltages.

The remaining problem is robustness associated with disturbances in both the electrical and mechanical subsystems which deteriorate the drive performance. Therefore in this chapter the application of the VSC methodology provides advantages over conventional PI-based control design due to the robustness property of the VSC principle. In particular, the motion control of Fig. 1, uses a cascade control structure where the inner loops for the current control and the outer loop for the speed control are DTVSCs.

In the proposed solution the reference (i_d^*) of the direct current component is set to zero (see Fig. 1). This case corresponds to the motion of the motor in the normal speed range, without considering possible field weakening operations [46].

The sampling frequency is selected as 1 kHz for the velocity control loop and 10 kHz for the current control loops.

As proposed in [6], Fig. 1 shows that the AEKF is fed with the reference voltages u_d and u_q instead of the measured ones. In fact, taking into account saturation phenomena in the current controller implementation, it is possible to use the voltage references instead of the actual voltages because of the inverter switching period is small with respect to the electrical time constant of the motor [6].

5.2 Experimental Setup

Experiments have been carried out on the Technosoft MBE.300.E500 PMSM. The motor catalog electric and mechanical parameters are given in Table 1. The Technosoft PM50 power module includes a three-phase inverter, the protection circuits and the measurement circuits for the DC-bus voltage and the motor currents. The three-phase inverter uses MOSFET transistors with switching frequency up to 50 kHz. The PM50 interface includes six PWM command inputs (TTL/CMOS compatible) through which the control unit can drive each transistor of the inverter. The PM50 electrical specifications are given in Table 2. The control unit is the Technosoft MSK28335 board based on the high-performance Texas Instruments Delfino™ TMS320F28335 DSP motion controller [51]. The three-phase voltage commands are generated using the PWM unit of the DSP. The PWM outputs are applied to the six transistors of the power inverter, based on sinusoidal reference values for the motor phase voltage, as generates after computation in (d, q) rotor coordinates frame at the output of the current controllers, and transformation to stator coordinates frame by the inverse Park transformation (see Fig. 1). The DSP has a 150-MIPS, 32 bit single-precision floating-point DSP core and operates at a 150-MHz frequency. The MSK28335 board is equipped also with 128-kWords 0-wait state external RAM, 2 channels of 12-bit accuracy D/A outputs, 16 channels of 12-bit accuracy and 80 ns conversion time A/D inputs, RS-232, CAN-bus and JTAG interfaces.

The motor phase current measurement scheme of the MCK28335 kit is based on shunts mounted on each lower leg of the inverter. The voltage drop on a shunt is amplified and sent to the TMS320F28335 A/D channels. This current measure-

Table 1 Technosoft MBE.300.E500 PMSM parameters [49]

Coil dependent parameters		
Phase-phase resistance	ohm	8.61
Phase-phase inductance	mH	07.13
Back-EMF constant	V/1000 rpm	3.86
Torque constant	mNm/A	36.8
Pole pairs	–	1
Dynamic parameters		
Rated voltage	V	36
Max. voltage	V	58
No-load current	mA	73.2
No-load speed	rpm	9170
Max. cont. current (at 5000 rpm)	mA	913
Max. cont. torque (at 5000 rpm)	mNm	30
Max. permissible speed	rpm	15000
Peak torque (stall)	mNm	154
Mechanical parameters		
Rotor inertia	$\text{Kgm}^2 \times 10^{-7}$	11
Mechanical time constant	ms	7

ment scheme, simple and cost-effective from the hardware point of view, requires some special care from the software implementation. The A/D conversion have to be synchronized with the PWM command of the inverter transistors, for a proper

Table 2 Technosoft PM50 power module electrical specifications [49]

Parameter	Cond.	Min.	Typ.	Max.	Units
DC input power					
Mot. supply volt.	–	9	–	36	V
Mot. supply cur.	–	–	–	2.1	Arms
Mot. supply cur.	–	–	–	6.33	Apeak
Output power					
Voltage	Set by external	0	–	36	Vrms
	PWM control				
Nom. Mot. Power	$V_{in} = 36\,\text{V}$,	–	–	75	W
	$f_{pwm} = 20\,\text{kHz}$,				
	$T_A = 40\,^\circ\text{C}$				
Nom. Mot. Cur.	$T_A = 40\,^\circ\text{C}$	–	–	1.7	Arms
PWM frequency	–	0.1	20	100	kHz

measurement of the currents on each phase of the motor. In fact a ripple in the motor currents exists and its value is relative to the motor parameters (electrical time constant), PWM frequency, and current controller bandwidth. Consequently, due to this inherent current ripple, in order to get the closest measured value of the current, the measurements have been performed at the middle of the PWM period [49].

The MCK28335-Pro kit includes the DMCD28x-Pro, the Technosoft software platform, which allows the development of motor control applications. The code is developed in C language using a modular approach providing flexibility for further system integration.

5.3 Experimental Results

Some of the performed speed-tracking experiments considering the proposed DTVSC equipped with the AEKF-based rotor position and speed estimator are shown in Figs. 3 and 5. The numerical values of the control scheme parameters have been selected as in Table 3. Achieved performance has been compared to a conventional PI-based FOC equipped with a conventional backward-difference method for speed estimation, using sampled position measurements provided by a digital incremental encoder. This PI-based FOC has a cascade control structure with inner loops for current control and an outer loop for speed control (see Fig. 1). Standard PI controllers have been designed for each control loop following the directions reported in the user manual of the MCK28335-Pro kit [49]. The controller design has been done under the assumption that the outer loop pass band is much smaller than that of inner loops and the torque regulation is much faster than the speed reference achievement. In particular, current control is performed by two identical PI regulators that have been designed and tuned to get a bandwidth of 400 Hz. Similarly, the parameters of the PI speed regulator have been set considering a bandwidth of 40 Hz. PI constants are related to both the electrical and mechanical system parameters (see Table 1) and the required bandwidth; the proportional gain and the integral action factor are 0.0001 and 0.9618, respectively, for the two current controllers and 171.2532 and 31.4921, respectively, for the speed controller.

Figures 3 and 4 show performance considering a reference trajectory given by a rectangular velocity profile. In particular, the DTVSC equipped with the AEKF-based rotor position and speed estimator (Fig. 3a—black continuous line) shows a better tracking performance with respect to the PI-based FOC equipped with the encoder and the backward-difference based speed estimator (Fig. 3a—blue dashed line). The speed-tracking errors are reported in Fig. 3b; in particular the black continuous line is the tracking error for the DTVSC with the AEKF-based rotor position and speed estimator and the blue dashed line is the tracking error for the PI-based FOC with the encoder and the backward-difference based speed estimator.

In Fig. 4a, the AEKF-based estimated rotor position (blue continuous line) is compared with the encoder-based measured one (red dashed line); the estimated position shows good correspondence to the measured rotor position.

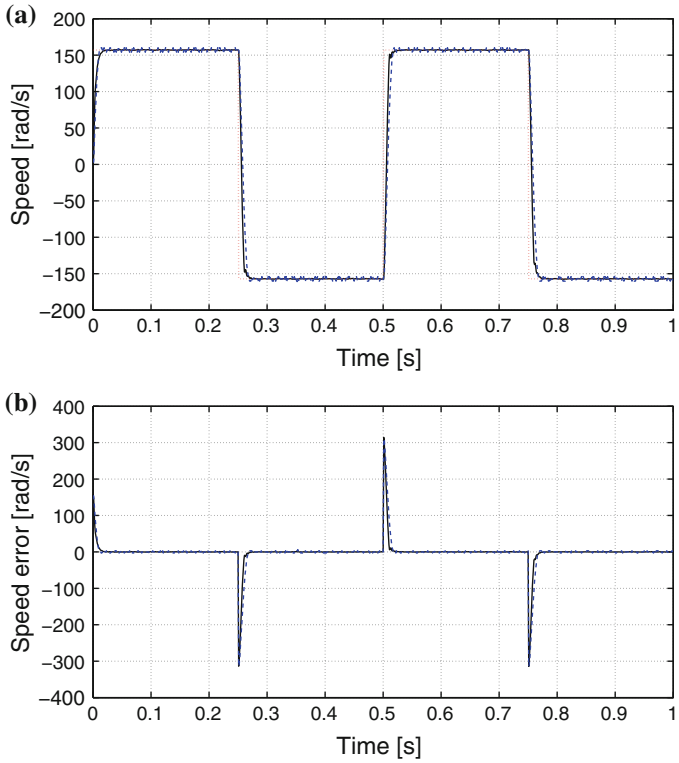

Fig. 3 Rectangular velocity profile. **a** DTVSC-based FOC with the AEKF-based rotor position and speed estimator (*black continuous line*), PI-based FOC with the encoder and the backward-difference based speed estimator (*blue dashed line*) and reference velocity (*red dotted line*) **b** Speed error: DTVSC-based FOC with the AEKF-based rotor position and speed estimator (*black continuous line*) and PI-based FOC with the encoder and the backward-difference based speed estimator (*blue dashed line*)

Figures 5 and 6 depict a sample of the tests performed with a time-varying disturbance affecting the i_q current for the rectangular reference velocity profile. Such picture proves that, in response to disturbances acting in the electrical subsystem, the actual velocity deviates significantly from the reference with the PI-based FOC with the encoder and the backward-difference based speed estimator (Fig. 5b),

Table 3 Control scheme parameters

$\bar{A}_\omega = 0.9999$	$\bar{B}_\omega = 909.0877$	$\lambda_\omega = -0.74$	$\theta_\omega = -0.02$
$\bar{A}_i = 0.2988$	$\bar{B}_i = 0.1630$	$\theta_q = -0.04$	$\rho_q = 1.3604$
$\rho_d = 0.9776$	$\theta_d = -0.07$	$K_t = 0.0368$	$\rho_\omega = 10.7816$
$\lambda_q = -0.7$	$\lambda_d = -0.6$		

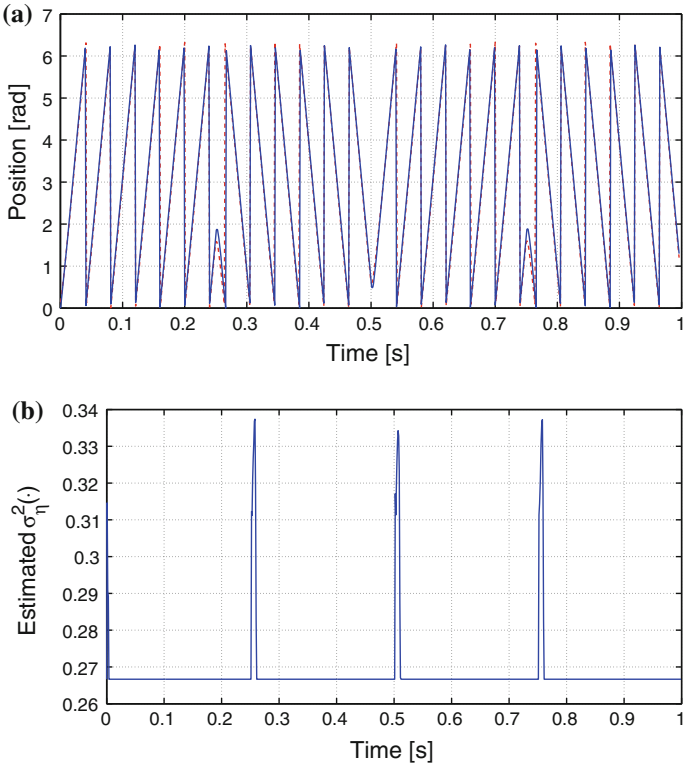

Fig. 4 Rectangular velocity profile. **a** AEKF-based estimated rotor position (*blue continuous line*) and encoder-based measured rotor position (*red dashed line*); **b** Behavior of the estimated $\bar{\hat{\sigma}}_\eta^2(\cdot)$ assuming $l_\eta = 5$ and $\bar{\hat{\sigma}}_\eta^2(0) = 0.3$

while the DTVSC-based FOC with the AEKF-based rotor position and speed estimator performs a more accurate tracking (Fig. 5a). The DTVSC-based controller reacts to the disturbance producing a small peak in the angular velocity and quickly re-approaching the reference velocity. On the contrary, the PI-based controller seems unable to compensate for the disturbance, and produces an evident offset with respect to the reference in the angular velocity.

In Fig. 6a, the AEKF-based estimated rotor position (blue continuous line) is compared with the encoder-based measured one (red dashed line); the estimated position shows good correspondence to the measured rotor position.

The IAE criterion, i.e. the integral of the absolute value of the speed-tracking error and of the error between the estimated and the encoder-based measured rotor position, is used to summarize the above experimental results (see Table 4). In Table 4 are also reported results for the motor following speed trajectories chosen with trapezoidal and sinusoidal shapes. Figures 4b and 6b show the behavior of the estimated $\bar{\hat{\sigma}}_\eta^2(k)$ assuming $l_\eta = 5$ and the initial value $\bar{\hat{\sigma}}_\eta^2(0) = 0.3$ for the rectangular velocity profile.

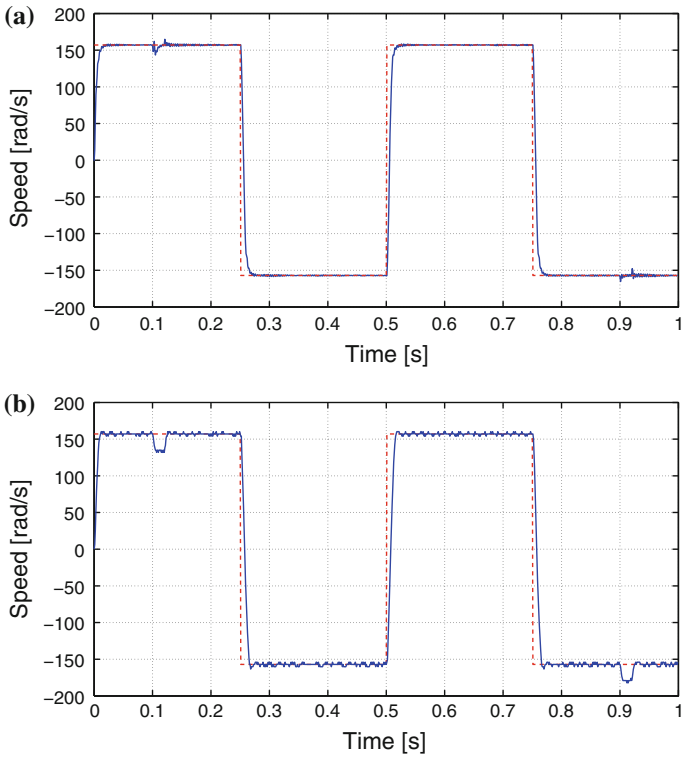

Fig. 5 Rectangular velocity profile; a time-varying disturbance acts on the i_q current. Actual (*blue continuous line*) and reference (*red dashed line*) velocities: **a** DTVSC-based FOC with the AEKF-based rotor position and speed estimator; **b** PI-based FOC with the encoder and the backward-difference based speed estimator

These figures evidence increases of $\bar{\hat{\sigma}}^2_\eta(k)$ in correspondence of the initial time instant, time instants when step changes of the reference trajectory occur and in Fig. 6b also when electrical disturbances act on the motor drive. At these time instants the effects of these sharp trajectory changes and disturbances is a rapid increase of residuals $\gamma_i(k)$ and, by Eq. (22), $\bar{\hat{\sigma}}^2_\eta(k)$ increases too. As a consequence also the filter gain increases and this allows the filter to properly weight the incoming observations. The estimated motor state is rapidly corrected and this provokes a decrease of residual samples and hence of the estimated $\bar{\hat{\sigma}}^2_\eta(k)$. On the basis of experimental tests, the adaptive estimation of $\bar{\hat{\sigma}}^2_{v,i}(k)$ did not produce very significant changes with respect to the initial values and for this reason the relative figures are not reported. In all the experiments the values $n_\eta = n_v = 2$ have been assumed; this means that the innovation process vector samples $\Gamma(k+1)$ have been alternately used to estimate $\sigma^2_\eta(k)$ and $\sigma^2_{v,i}(k+1)$, $i = 1, 2$ according to the algorithm described in Sect. 3.1.

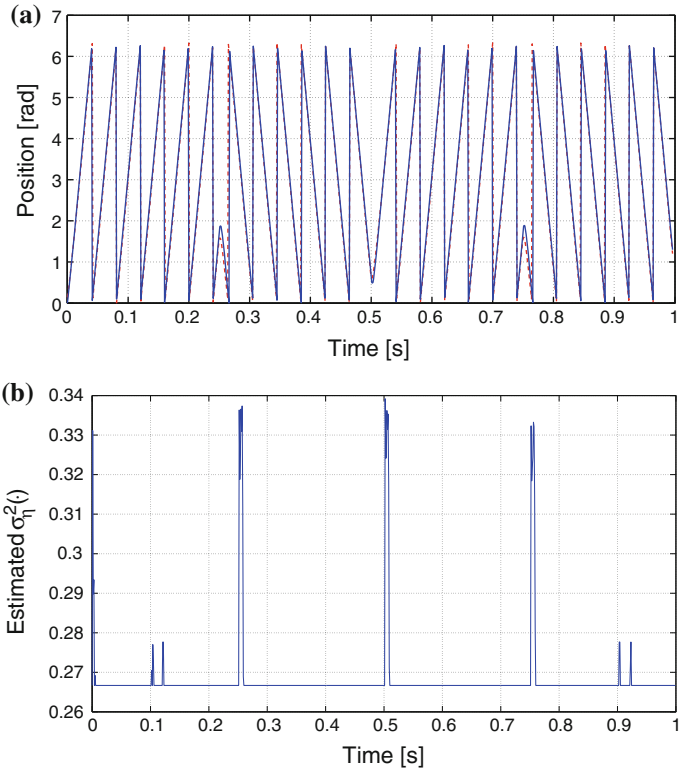

Fig. 6 Rectangular velocity profile; a time-varying disturbance acts on the i_q current. **a** AEKF-based estimated rotor position (*blue continuous line*) and encoder-based measured rotor position (*red dashed line*); **b** Behavior of the estimated $\bar{\tilde{\sigma}}^2_\eta(\cdot)$ assuming $l_\eta = 5$ and $\bar{\tilde{\sigma}}^2_\eta(0) = 0.3$

Table 4 Performance comparison at high speed (157 rad/s)

No disturbance	AEKF-speed	Backward-difference	AEKF-position
Rectangular	1.98	2.90	0.16
Trapezoidal	0.35	1.01	0.14
Sinusoidal	0.35	2.19	0.30
Disturbance	AEKF-speed	Backward-difference	AEKF-position
Rectangular	2.12	3.04	0.18
Trapezoidal	0.39	1.23	0.15
Sinusoidal	0.43	2.29	0.31

Experimental tests at low speed have been also performed with trapezoidal, rectangular and sinusoidal velocity profiles. In particular, velocities of 78.5 rad/s and 31.4 rad/s have been considered; results have been summarized in Table 5. The reported index IAE shows an improvement of the proposed solution based on the

Table 5 Performance comparison at low speed

78.5 rad/s	AEKF-speed	Backward-difference	AEKF-position
Rectangular	0.76	0.95	0.30
Trapezoidal	0.19	0.37	0.35
Sinusoidal	0.36	0.78	0.13
31.4 rad/s	AEKF-speed	Backward-difference	AEKF-position
Rectangular	0.31	0.42	0.16
Trapezoidal	0.20	0.24	0.34
Sinusoidal	0.36	0.40	0.05

AEKF-based rotor position and speed estimator with respect to the PI-based FOC equipped with the encoder and the standard backward-difference method for speed estimation.

6 Concluding Remarks

This chapter has proposed a DSP-based discrete time VSC equipped with an AEKF for the accurate rotor position and speed estimation of a PMSM from measurements of electric quantities. The approach is based on a linearized Kalman filter endowed with an adaptive algorithm for the adjustment of the input and measurement noise covariance matrices. The adaptation mechanism has been introduced to allow the filter to cope with realistic operating conditions. The introduction of an adaptive algorithm seems to be the most efficient and simple remedy to prevent filter divergence. Experiments on a commercial PMSM drive reported in the chapter have confirmed that high performance of the rotor position and speed estimation algorithm are really obtainable in a wide range of experimental situations. Moreover experimental evidence shows good speed trajectory tracking performance as well as robustness in the presence of disturbances acting on the system. In particular, the tests have shown superior robustness of the proposed DTVSC-based FOC with respect to a conventional PI-based FOC.

7 Q-Matrix Elements

$$\bar{Q}(k)_{1,1} = T_c - \frac{{T_c}^2}{2}\frac{B}{J} + \frac{{T_c}^3}{2}\left[\left(\frac{B}{J}\right)^2 + \left(\frac{K_t}{J}\right)^2\right]$$

$$\bar{Q}(k)_{1,2} = \hat{i}_q(k,k)\frac{T_c}{2}^2 + \frac{T_c}{2}^3\left[\frac{B}{J}\hat{i}_q(k,k) + \frac{K_t}{J}N_r\hat{\omega}_r(k,k)\right]$$

$$\bar{Q}(k)_{1,3} = \frac{T_c^2}{2}\left(\frac{\lambda_0}{L} + \hat{i}_d(k,k)\right)\left(\frac{BT_c}{J} - 1\right) + \frac{K_t}{J}\frac{T_c^2}{2}\left(1 - \frac{RT_c}{L}\right)$$

$$\bar{Q}(k)_{1,4} = \frac{T_c^2}{2}\left(\frac{B}{J}T_c - 1\right)$$

$$\bar{Q}(k)_{2,1} = \bar{Q}(k)_{1,2}$$

$$\bar{Q}(k)_{2,2} = \hat{i}_q^2(k,k)\frac{T_c^3}{2} + T_c\left(1 - \frac{RT_c}{L} + \frac{T_c^2}{2}\left(\frac{R}{L}\right)^2\right) + \frac{T_c^3}{2}N_r\hat{\omega}_r^2(k,k)$$

$$\bar{Q}(k)_{2,3} = -\frac{T_c^3}{2}\left(\frac{\lambda_0}{L} + \hat{i}_d(k,k)\right) + N_r\hat{\omega}_r(k,k)\frac{T_c^2}{2}\left(1 - \frac{RT_c}{L}\right)$$

$$\bar{Q}(k)_{2,4} = \frac{T_c^3}{2}\hat{i}_q(k+1/k)$$

$$\bar{Q}(k)_{3,1} = \bar{Q}(k)_{1,3}$$

$$\bar{Q}(k)_{3,2} = \bar{Q}(k)_{2,3}$$

$$\bar{Q}(k)_{3,3} = \frac{T_c^3}{2}\left(\frac{\lambda_0}{L} + \hat{i}_d(k,k)\right) + N_r\hat{\omega}_r(k,k)\frac{T_c^3}{2} + \left[1 - \frac{RT_c}{L} + \left(\frac{R}{L}\right)^2\frac{T_c^2}{2}\right]T_c$$

$$\bar{Q}(k)_{3,4} = -\left(\frac{\lambda_0}{L} + \hat{i}_d(k+1/k)\right)\frac{T_c^3}{2}$$

$$\bar{Q}(k)_{4,1} = \bar{Q}(k)_{1,4}$$

$$\bar{Q}(k)_{4,2} = \bar{Q}(k)_{2,4}$$

$$\bar{Q}(k)_{4,3} = \bar{Q}(k)_{3,4}$$

$$\bar{Q}(k)_{4,4} = \frac{T_c^2}{2}(1 + T_c) + T_c$$

References

1. Aller J, Habetler T, Harley R, Tallam R, Lee S (2002) Sensorless speed measurement of AC machines using analytic wavelet transform. IEEE Trans Ind Appl 38(5):1344–1350
2. Bartolini G, Orani N, Pisano A, Usai E (2006) Higher-order sliding mode approaches for control and estimation in electrical drives. In: Edwards C, Colet EF, Fridman L (eds) Advances in variable structure and sliding mode control. Lecture notes in control and information sciences. Springer, Berlin, pp 423–445
3. Barut M, Bogosyan S, Gokasan M (2007) Speed-sensorless estimation for induction motors using extended Kalman filters. IEEE Trans Ind Electron 54(1):272–280
4. Bianchi N, Bolognani S, Jang J-H, Sul S-K (2007) Comparison of PM motor structures and sensorless control techniques for zero-speed rotor position detection. IEEE Trans Power Electron 22(6):2466–2475

5. Boldea I, Paicu M, Andreescu G-D (2008) Active flux concept for motion-sensorless unified AC drives. IEEE Trans Power Electron 23(5):2612–2618
6. Bolognani S, Oboe R, Zigliotto M (1999) Sensorless full-digital PMSM drive with EKF estimation of speed and rotor position. IEEE Trans Ind Electron 46(1):184–191
7. Bolognani S, Tubiana L, Zigliotto M (2003) EKF-based sensorless IPM synchronous motor drive for flux-weakening applications. IEEE Trans Ind Appl 39(3):768–775
8. Bolognani S, Tubiana L, Zigliotto M (2003) Extended Kalman filter tuning in sensorless PMSM drives. IEEE Trans Ind Appl 39(6):1741–1747
9. Bolognani S, Zigliotto M, Zordan M (2001) Extended-range PMSM sensorless speed drive based on stochastic filtering. IEEE Trans Power Electron 16(1):110–117
10. Boussak M (2005) Implementation and experimental investigation of sensorless speed control with initial rotor position estimation for interior permanent magnet synchronous motor drive. IEEE Trans Power Electron 20(6):1413–1422
11. Ciampichetti S, Corradini M, Ippoliti G, Orlando G (2011) Sliding mode control of permanent magnet synchronous generators for wind turbines. In: IECON proceedings (industrial electronics conference), pp 740–745
12. Ciccarelli O, Corradini M, Cucchieri G, Ippoliti G, Orlando G (2012) Sliding mode control based robust observer of aerodynamic torque for variable-speed wind turbines. In: IECON proceedings (industrial electronics conference), pp 4332–4337
13. Cimini G, Corradini M, Ippoliti G, Malerba N, Orlando G (2013) Control of variable speed wind energy conversion systems by a discrete-time sliding mode approach. In: 2013 IEEE international conference on mechatronics, ICM 2013, pp 736–741
14. Corradini M, Fossi V, Giantomassi A, Ippoliti G, Longhi S, Orlando G (2012) Discrete time sliding mode control of robotic manipulators: development and experimental validation. Control Eng Pract 20(8):816–822
15. Corradini M, Fossi V, Giantomassi A, Ippoliti G, Longhi S, Orlando G (2012) Minimal resource allocating networks for discrete time sliding mode control of robotic manipulators. IEEE Trans Ind Inf 8(4):733–745
16. Corradini M, Ippoliti G, Longhi S, Marchei D, Orlando G (2013) A quasi-sliding mode observer-based controller for PMSM drives. Asian J Control 15(2):380–390
17. Corradini M, Ippoliti G, Orlando G (2012) An aerodynamic torque observer for the robust control of variable-speed wind turbines. In: Proceedings of the IEEE conference on decision and control, pp 2483–2488
18. Corradini M, Ippoliti G, Orlando G (2013) Fully sensorless robust control of variable-speed wind turbines for efficiency maximization. Automatica 49(10):3023–3031
19. Corradini M, Ippoliti G, Orlando G (2013) Robust control of variable-speed wind turbines based on an aerodynamic torque observer. IEEE Trans Control Syst Technol 21(4):1199–1206
20. Corradini M, Ippoliti G, Orlando G, Pettinari S (2009) Robust control of hybrid plants in the presence of quantization errors. In: 2009 IEEE international conference on control and automation, ICCA 2009, pp 234–239
21. Corradini M, Ippoliti G, Orlando G, Pettinari S (2011) Speed estimation and fault detection for PMSM via quasi sliding modes. In: IFAC proceedings volumes (IFAC-PapersOnline), vol 18, part 1, pp 6142–6147
22. Corradini ML, Orlando G (1997) A discrete adaptive variable-structure controller for MIMO systems, and its application to an underwater ROV. IEEE Trans Control Syst Technol 5(3):349–359
23. Corradini ML, Orlando G (1998) Variable structure control of discretized continuous-time systems. IEEE Trans Autom Control 43(9):1329–1334
24. De Belie F, Sergeant P, Melkebeek J (2010) A sensorless drive by applying test pulses without affecting the average-current samples. IEEE Trans Power Electron 25(4):875–888
25. De Kock H, Kamper M, Kennel R (2009) Anisotropy comparison of reluctance and PM synchronous machines for position sensorless control using HF carrier injection. IEEE Trans Power Electron 24(8):1905–1913

26. Dhaouadi R, Mohan N, Norum L (1991) Design and implementation of an extended Kalman filter for the state estimation of a permanent magnet synchronous motor. IEEE Trans Power Electron 6(3):491–497
27. Foo G, Rahman M (2010) Direct torque control of an IPM-synchronous motor drive at very low speed using a sliding-mode stator flux observer. IEEE Trans Power Electron 25(4):933–942
28. Furuta K (1993) VSS type self-tuning control. IEEE Trans Ind Electron 40(1):37–44
29. Han Y, Song Y (2003) Condition monitoring techniques for electrical equipment a literature survey. IEEE Trans Power Deliv 18(1):4–13
30. Haque M, Zhong L, Rahman M (2003) A sensorless initial rotor position estimation scheme for a direct torque controlled interior permanent magnet synchronous motor drive. IEEE Trans Power Electron 18(6):1376–1383
31. Hu J, Liu J, Xu L (2008) Eddy current effects on rotor position estimation and magnetic pole identification of PMSM at zero and low speeds. IEEE Trans Power Electron 23(5):2565–2575
32. Hung C-W, Lin C-T, Liu C-W, Yen J-Y (2007) A variable-sampling controller for brushless DC motor drives with low-resolution position sensors. IEEE Trans Ind Electron 54(5):2846–2852
33. Ippoliti G, Jetto L, La Manna A, Longhi S (2005) Improving the robustness properties of robot localization procedures with respect to environment features uncertainties. Proc IEEE Int Conf Robot Autom 2005:1451–1458
34. Ippoliti G, Jetto L, Longhi S (2005) Localization of mobile robots: development and comparative evaluation of algorithms based on odometric and inertial sensors. J Robot Syst 22(12):725–735
35. Jazwinsky A (1970) Stochastic processes and filtering theory. Academic Press, New-York
36. Jetto L, Longhi S, Venturini G (1999) Development and experimental validation of an adaptive extended Kalman filter for the localization of mobile robots. IEEE Trans Robot Autom 15:119–129
37. Kim KH, Lee JG, Park CG (2009) Adaptive two-stage extended Kalman filter for a fault-tolerant INS-GPS loosely coupled system. IEEE Trans Aerosp Electron Syst 45:125–137
38. Konghirun M, Xu L (2006) A fast transient-current control strategy in sensorless vector-controlled permanent magnet synchronous motor. IEEE Trans Power Electron 21(5):1508–1512
39. Lidozzi A, Solero L, Crescimbini F, Di Napoli A (2007) SVM PMSM drive with low resolution hall-effect sensors. IEEE Trans Power Electron 22(1):282–290
40. Lin F-J, Hwang J-C, Chou P-H, Hung Y-C (2010) FPGA-based intelligent-complementary sliding-mode control for PMLSM servo-drive system. IEEE Trans Power Electron 25(10):2573–2587
41. Liu Y, Zhu ZQ, Howe D (2006) Instantaneous torque estimation in sensorless direct-torque-controlled brushless DC motors. IEEE Trans Ind Appl 42(5):1275–1283
42. Mattavelli P, Tubiana L, Zigliotto M (2005) Torque-ripple reduction in PM synchronous motor drives using repetitive current control. IEEE Trans Power Electron 20(6):1423–1431
43. Walde P, Brunner C (2011) IEA (International energy agency). Energy-efficiency policy opportunities for electric motor-driven systems. http://www.iea.org/publications/freepublications/publication/ee_for_electricsystems.pdf. Accessed 15 Feb 2014
44. Pisano A, Davila A, Fridman L, Usai E (2008) Cascade control of PM DC drives via second-order sliding-mode technique. IEEE Trans Ind Electron 55(11):3846–3854
45. Sabanovic A, Jezernik K, Sabanovic N (2002) Sliding modes applications in power electronics and electrical drives. In Yu X, Xu J-X (eds) Variable structure systems: towards the 21st Century, vol 274. Springer, Berlin, pp 223–251
46. Shi J, Lu Y (1996) Field-weakening operation of cylindrical permanent-magnet motors. In: Proceeding of IEEE international conference on control applications, pp 864–869, Dearborn
47. Solsona J, Valla M, Muravchik C (1996) A nonlinear reduced order observer for permanent magnet synchronous motors. IEEE Trans Ind Electron 43(4):492–497
48. Szabat K, Orlowska-Kowalska T (2008) Performance improvement of industrial drives with mechanical elasticity using nonlinear adaptive Kalman filter. IEEE Trans Ind Electron 55:1075–1084

49. Technosoft SA (2011) http://www.technosoftmotion.com/. Accessed 15 Feb 2014
50. Tesfaye A, Tomizuka M (1995) Robust control of discretized continuous systems using the theory of sliding modes. Int J Control 62:209–226
51. Texas Instruments Incorporated (2011) http://www.ti.com/. Accessed 15 Feb 2014
52. Utkin VI (1992) Sliding modes in control and optimization. Springer, Berlin
53. Utkin VI (1993) Sliding modes control design principles and applications to electric drives. IEEE Trans Ind Electron 40(1):23–35
54. Utkin VI, Guldner J, Shi J (1999) Sliding mode control in electromechanical systems. Systems and control. CRC Press LLC, Florida
55. Vas P (1990) Vector control of AC machines. Oxford University Press, London
56. Vas P (1993) Parameter estimation, condition monitoring, and diagnosis of electrical machines. Oxford Science, Oxford
57. Wu R, Slemon G (1991) A permanent magnet motor drive without a shaft sensor. IEEE Trans Ind Appl 27(5):1005–1011
58. Xu Z, Rahman M (2007) Direct torque and flux regulation of an IPM synchronous motor drive using variable structure control approach. IEEE Trans Power Electron 22(6):2487–2498
59. Yan Z, Jin C, Utkin VI (2000) Sensorless sliding-mode control of induction motors. IEEE Trans Ind Electron 47(6):1286–1297
60. Zinober ASI (1994) Variable structure and Lyapunov control. Springer, New York

Sliding Mode Control of Induction Generator Wind Turbine Connected to the Grid

M. Ouassaid, K. Elyaalaoui and M. Cherkaoui

Abstract Conventional fossil fuels such as coal, oil and natural gas are being reduced and become more and more a source of serious undesirable effects on the environment. Wind power is playing a major role in the effort to augment the share of renewable energy sources in the world energy mix with a continuously increasing penetration into the grid. Wind turbine generators can be divided into two basic categories: fixed speed and variable speed. Variable-speed wind energy systems are presently favored than fixed-speed wind turbines thanks to their higher wind power extraction, improved efficiency, reactive power support and voltage control. This study addresses the problem of control of Wind Energy Conversion System (WECS) in variable speed. To this end, two simultaneous control objectives, namely the maximization of the energy conversion efficiency based on Squirrel Cage Induction Generator (SCIG) wind turbine and the regulation of the active and reactive power feed to the grid, to guarantee Unit Power Factor (UPF), have been established. To deal with the complexity and nonlinearity of the system, the sliding mode control is adopted. Indeed, this technique provides an efficient tool for controller design and presents attractive features such as robustness to parametric uncertainties of the different components of the system. In this way, sliding-mode control laws are developed using Lyapunov stability analysis, to guarantee the reaching and sustaining of sliding mode and stability of the system control. Evaluation of the reliability and performance of the proposed sliding mode control approach has been established on a 3MW three-blade wind turbine. Simulation results demonstrate that the proposed control strategy is effective in terms of MPPT control strategy, active and reactive power tracking trajectories and robustness against system parameter variations.

M. Ouassaid (✉) · K. Elyaalaoui · M. Cherkaoui
Ecole Mohammadia d'Ingénieurs, Mohammed V University, Rabat, Morocco
e-mail: ouassaid@emi.ac.ma

K. Elyaalaoui
e-mail: k.elyaalaoui@gmail.com

M. Cherkaoui
e-mail: cherkaoui@emi.ac.ma

S. Vaidyanathan and C. Volos (eds.), *Advances and Applications in Nonlinear Control Systems*, Studies in Computational Intelligence 635,
DOI 10.1007/978-3-319-30169-3_23

Keywords Induction generator · Wind energy · Sliding mode control · Unity power factor · MPPT · Laypunov stability

1 Introduction

Currently, the demand for electric energy is growing rapidly. On the other hand, the conventional energy sources are depleting fast, their costs are going up, and they are causing the environment contamination. To meet these challenges, the attention has focused to renewable and clean energy sources, like wind, solar, fuel cell, etc. [6, 39].

Wind energy is an important renewable green energy resource. Indeed, it is omnipresent, environmentally friendly, and freely available [8]. Further, it is characterized by its high reliability and cost effectiveness. Thanks to all these features, the wind power generation capacity has been growing rapidly, with an average annual growth around 30 %, in the world, over the last decade.

Electric energy is generated from wind using a wind turbine and an electric generator. It can be used either for standalone loads or fed into the electric network through a suitable power electronic converters.

A wind turbine operates either at a fixed or variable speed.

- A fixed-speed wind turbine generator generally uses a squirrel-cage induction generator to convert the mechanical energy from the wind turbine into electrical energy (Fig. 1). The generator is connected directly to the electric network. The system operates almost at constant speed even if the wind speed varies. This topology is simple, less expensive and effective. But, it suffers from the low energy capture, mechanical stress and mediocre power quality [8, 20, 21, 25].
- Variable-speed wind turbine generator provides high efficiency in capturing the energy from wind over a wider range of wind speeds, along with better power quality. Also this scheme is capable to regulate the power factor, by either consuming

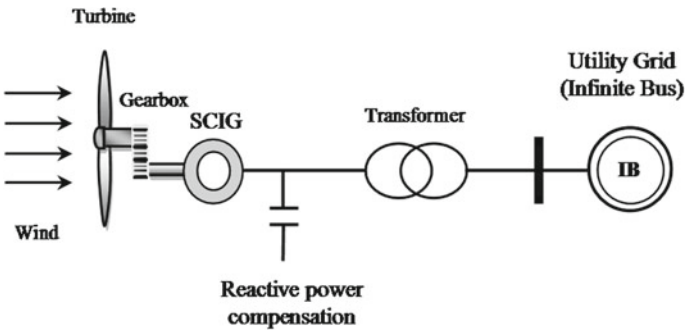

Fig. 1 Cage induction generator-based fixed speed wind turbine

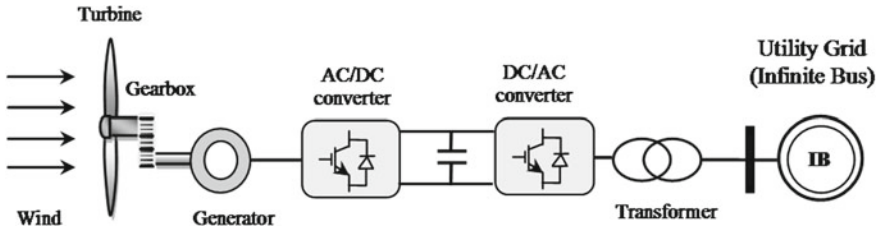

Fig. 2 Variable speed wind turbine connected to a grid

or producing reactive power, and ensure lower mechanical stress. The power electronic converters are incorporated between the electrical machine and the power system as shown in Fig. 2 [22, 24, 33].

Most of the major wind turbine manufacturers are developing new megawatt scale wind turbines based on variable-speed operation with pitch control.

1.1 Wind Turbine Generators Technologies

Different types of electric machines are used for the generation of electric energy from wind:

- **Permanent Magnets Synchronous Generator (PMSG)**: The PM generators can be divided into radial-flux and axial-flux generators. The advantages of a PMSG configuration are gearless construction, the elimination of a dc excitation system, full controllability of the system for maximum wind power extraction and grid interface; and straightforward in accomplishing fault-ride through and grid support [7, 20, 21]. However, the major drawback of the PMSG is the high cost of the PM material and power converter [28].
- **Doubly-Fed Induction Generator (DFIG)—**wounded rotor: With this topology, the stator is connected directly to the grid whereas the rotor is linked to the grid via a bidirectional converter [27, 32]. The main characteristics of the DFIG are (i) limited operating speed range (ii) small scale power electronic converter (iii) reduced power losses and cost (vi) complete control of active and reactive power exchanged with the grid. However the most important disadvantages are necessity of gear and use of slip-rings which involve maintenance.
- **Squirrel Cage Induction Generator (SCIG)**: Induction generators were used for a long time for constant speed wind turbines. In this operating mode, the pitch control or active stall control are imposed for power limitation and protection. Currently, it is used for variable-speed wind energy systems which guarantee superior wind power extraction and better efficiency. In comparison with the DFIG, this configuration offers extended speed operating range, and complete decoupling between the generator and the network (Fig. 2), which results in higher power

extraction at different wind speeds and improved capability to realize the low-voltage ride-through. Indeed, SCIG provides some advantages when compared with the PMSG and DFIG such as light weight, small size, high reliability, maintenance less, high efficiency, low cost and operational simplicity [19, 36].

1.2 Control Technique Strategies of WECS

Wind generator and its control is a very complex electromechanical system. Linear controllers have been widely used in the engineering field for their reliability and simplicity. However, their parameters are usually tuned with the approximately linearized model. Consequently, the dynamic control performance may not be guaranteed during the transients of the wind turbine with WECS. To overcome these disadvantages, many methods for the design of controllers for the WECS have been investigated in order to ensure better control performance in terms of transient stability and robustness to parameter uncertainties or disturbances. These methods are summarized as follow:

- **Field Oriented Control (FOC)**. Common control of grid-connected WECS is based on FOC [1, 5]. The scheme decouples the stator current into active and reactive components in the synchronous reference frame. In this technique, the control of the system is accomplished by regulating the decoupled stator currents, using proportional-integral controllers [3]. However, the major disadvantage for this linear control scheme is that the performance may demean in the case of deviation of the machine parameters, such as stator and rotor inductances and resistances, from values used in the control system.
- **Feedback linearization**. The control based on this technique has been the subject of several investigations [14]. The aim of this method is to make the model of the system to be controlled exactly linearized by coordinate transformation using differential geometry theory. The obtained linearized system allows the synthesis of the control laws based on the linear optimal control principles. However, these control designs require precise models and often cancel some useful nonlinearities. Therefore, it does not guarantee the robustness in the presence of parameter uncertainties or disturbances. To overcome this drawback, numerous adaptive versions of the feedback linearizing techniques are then proposed [15, 38]. References [26, 41] present an application of this approach.
- **Backstepping technique**. This method offers an efficient tool for controller synthesis through building step by step the Lyapunov functions which can guarantee the asymptotic stability of the overall closed-loop system [17]. Indeed, the backstepping is less restrictive compared to the feedback linearization control which cancels the nonlinearities that might be useful. Unlike the adaptive controllers, based on certain equivalence, which separate the design of the controller and the terms of adaptation, adaptive backstepping has emerged as an alternative. This technique has been successfully applied for control of power system and wind power generator system in [3, 29, 30].

- **Direct Torque Control (DTC)**. In contrast to vector control with linear controllers (PI), DTC technique presents advantages such as simple structure and insensitivity to the parameters disturbances. The DTC technique directly controls machine torque and flux by selecting voltage vectors from a look-up-table using the stator flux and torque information. The problems with the DTC method is that (i) performances are very mediocre during starting and low-speed operation; (ii) converter switching frequency variation complicates the power circuit design; (iii) ripples in flux and torque [34]. This is due to the use of predefined switching table and hysteresis regulator. To deal with those drawbacks modified DTC strategies, incorporating space vector modulation, have been used to obtain constant switching frequency [16]. Nevertheless, further drawbacks were introduced, such as additional PI controller parameters, and sensitivity to system parameter variations [13, 18].
- **Direct Power Control (DPC)**. More recently, direct power control was developed based on the principles of DTC strategy. In [42], it was demonstrated that the control system is less complicated and robust against parameters machine variation. Nevertheless, switching frequency varies significantly with active and reactive power variations, rotor slip, and hysteresis bandwidth of power controllers. References [12, 34, 42] present an application of this technique.
- **Sliding-Mode Control (SMC)**. It is the most robust control techniques for systems with uncertainties and parameter variations. It dates back to the 70 s with the work of Utkin [40]. SMC features simple implementation, disturbance rejection, strong robustness, and fast responses. Nevertheless, the problems of chattering inherent in this type of discontinuous control appear quickly and may excite the highfrequency dynamics neglected sometimes leading to instability. Methods to tackle this phenomenon have been developed [35]. More recently, This technique has been successfully applied for wind power system in [10, 11, 23, 37].

In this study, a SMC strategy, for a variable speed wind turbine equipped with SCIG connected to the grid through power converters is developed:

- The prime control objective of the WECS is to capture the maximum wind power through MPPT control strategy. To this end, the turbine tip-speed ratio should be kept at its optimum value despite wind variations.
- The second objective consists of maintaining the DC bus voltage constant and to achieve the grid-side Unity Power Factor (UPF).

In the sections that follow, the chapter first introduces the mathematical model of different components of wind energy conversion system in Sect. 2. Then, Sect. 3 presents the synthesis of the control laws of the SCIG in order to maximize the wind energy conversion efficiency. Control design, of active and reactive power injected into the grid, is developed in Sect. 4. Section 5 presents the simulation results to demonstrate the performance of the proposed SMC strategy. Finally, the conclusions are made in Sect. 6.

2 Mathematical Model of Wind Energy Conversion System

The complete wind energy conversion system consists mainly of three parts: a wind turbine drive train, a SCIG, and two back-to back Voltage Source Converters (VSC). The system considered is shown in Fig. 3.

2.1 Model of Wind Turbine

The wind turbine basic principle is to convert the linear action of the wind into rotational energy. The converted energy is used to drive an electrical generator. Hence, the kinetic energy of the wind is transformed to electric power.

The wind power acting on the swept area of the blade A is a function of the air density ($1.225\,\mathrm{kg/m^2}$) and the wind speed V_w (m/s). The transmitted power Pw (w) is generally deduced from the wind power using the power coefficient C_p as [9]

$$P_w = \frac{1}{2}.C_p(\lambda, \beta) \cdot \rho \cdot A \cdot V_w^3 \tag{1}$$

The power coefficient is a nonlinear function of the tip speed-ratio λ, which depends on the wind velocity and the rotation speed of the shaft ω_t.

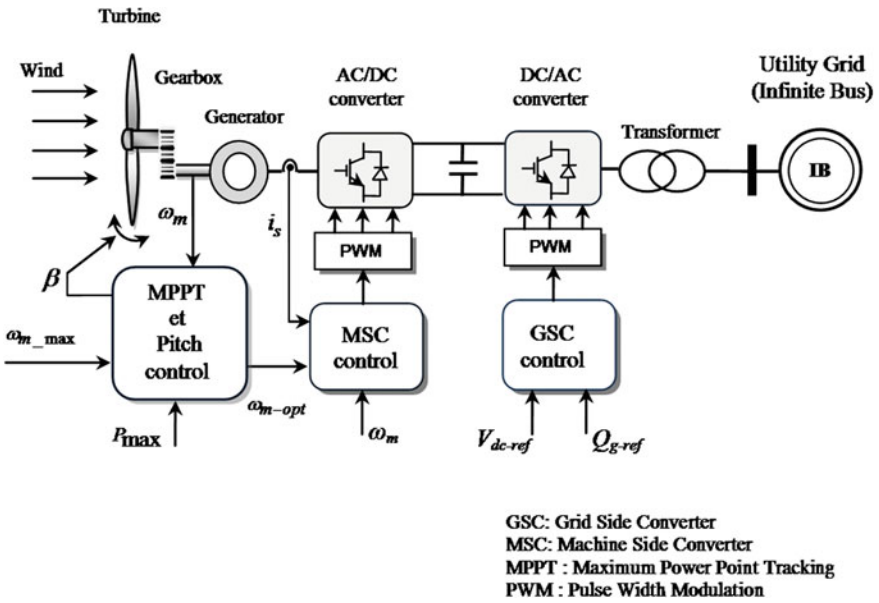

Fig. 3 Control scheme of wind turbine based-SCIG connected to a grid

Table 1 Parameters of the coefficient of power

Symbole	C1	C2	C3	C4	C5	C6
Value	0.5109	116	0.4	5	21	0.0068

$$\lambda = \frac{R \cdot \omega_m}{V_w} \tag{2}$$

where R is the blade radius (m). The coefficient of power is expressed as

$$\begin{aligned} C_p(\lambda, \beta) &= C_1 \left(\frac{C_2}{\lambda_i} - C_3 \cdot \beta - C_4 \right) \cdot \exp\left(\frac{-C_5}{\lambda_i} - C_6 \cdot \lambda \right) \\ \frac{1}{\lambda_i} &= \frac{1}{\lambda + 0.08 \cdot \beta} - \frac{0.035}{\beta^3 + 1} \end{aligned} \tag{3}$$

The parameters of coefficient of power are defined in Table 1.

Then, the input torque in the transmission mechanical system is given as

$$T_w = \frac{P_w}{\omega_t} = \frac{C_p(\lambda, \beta) \cdot \rho \cdot A \cdot V_w^3}{2\omega_t} \tag{4}$$

The maximum value of C_p (λ, β) is $C_{pmax} = 0.47$ and obtained for $\lambda_{opt} = 8.1$ and for $\beta = 0°$. If the parameters are in pet unit, λ_{pu} and C_{p_pu} can be computed as

$$\begin{aligned} \lambda_{pu} &= \frac{\lambda}{\lambda_{opt}} \\ C_{p\_pu} &= \frac{C_p}{C_{p-opt}} \end{aligned} \tag{5}$$

Both mechanical shafts are linked by the gearbox. The equation is expressed as [2]

$$2H \frac{d\omega_m}{dt} = T_m - T_e - F\omega_m \tag{6}$$

where $H = H_b + H_h + H_g$ is the inertia constant of the single rotating mass (which includes the blades, hub and generator rotor), ω_m is the rotor speed and F is the damping coefficient of a single mass.

2.2 Model of the Induction Generator

The generator, converting mechanical energy into electrical energy, is a SCIG with its stator windings connected to the grid through a frequency converter. The induction generator is described by 5th nonlinear mathematical model, in the space vector by the following state-space form [3, 20, 21]

$$\frac{1}{\omega_b}\frac{di_{sd}}{dt} = -\partial_1 i_{sd} + \omega_s i_{sq} - \partial_2 \phi_{rd} - \frac{V_{sd}}{\sigma L_s} \tag{7}$$

$$\frac{1}{\omega_b}\frac{di_{sq}}{dt} = -\partial_1 i_{sq} - \omega_s i_{sd} + \partial_3 \phi_{rd} - \frac{V_{sq}}{\sigma L_s} \tag{8}$$

$$\frac{1}{\omega_b}\frac{d\phi_{rd}}{dt} = -\frac{R_r \phi_{rd}}{L_r} - \frac{R_r L_m}{L_r} i_{sd} \tag{9}$$

$$\frac{1}{\omega_b}\frac{d\phi_{rq}}{dt} = -\frac{R_r L_m}{L_r} i_{sq} - (\omega_s - \omega_m)\,\phi_{rd} \tag{10}$$

$$2H\frac{d\omega_m}{dt} = -\frac{L_m}{L_r}\phi_{rd} i_{sq} + T_m - F\omega_m \tag{11}$$

where

$$\partial_1 = \frac{R_s L_r^2 + R_r L_m^2}{\sigma L_s L_r^2},\ \partial_2 = \frac{R_r L_m}{\sigma L_s L_r^2},\ \partial_3 = \frac{L_m \omega_m}{\sigma L_s L_r},\ L_r = L_{\sigma r} + L_m \quad \text{and} \quad L_s = L_{\sigma s} + L_m$$

$L_{\sigma r}$ and $L_{\sigma r}$ are the leakage inductances of stator and rotor, L_m is the mutual inductance. $\omega_b = 2\pi f$ is the system base frequency, ω_s is the synchronous electrical speed, ω_m is the rotor speed of the SCIG.

Remark The nonlinear control is applied to orient rotor flux on d-axis of the rotating reference frame, therefore, $\Phi_{rq} = 0$ and $\Phi_{rd} = \Phi_{ref}$.

2.3 Model of the Converters

The frequency converter is built by two current-regulated voltage-source pulse width modulation (PWM) converters: a Machine Side Converter (MSC) and a Grid Side Converter (GSC), with a dc voltage link in between.

The modeling of the converters is made by using the concept of instantaneous average value. The converter is equivalent to a matrix topology as given in (12).

$$\begin{bmatrix} V_{sa} \\ V_{sb} \\ V_{sc} \end{bmatrix} = \frac{V_{dc}}{3}\begin{bmatrix} 2 & -1 & -1 \\ -1 & 2 & -1 \\ -1 & -1 & 2 \end{bmatrix}\begin{bmatrix} S_a \\ S_b \\ S_c \end{bmatrix} \tag{12}$$

S_a, S_b, S_c are variables which represent the switching status and take the value 1 when the switch is closed (on) and 0 when it is opened (off).

The model of DC link voltage is given as [4]

$$Cv_{dc}\frac{dv_{dc}}{dt} = P_{ge} - P_{gr} \tag{13}$$

where C is the capacitance, P_{ge} is the active power of generator and P_{gr} is the active power injected into AC network.

2.4 The Model of the Filter

The SCIG is connected to the grid through a filter. The model of the filter is given by [20, 21]

$$v_{fd} = L_f\frac{di_{fd}}{dt} + R_f i_{fd} - L_f\omega_e i_{fq} + e_d \tag{14}$$

$$v_{fq} = L_f\frac{di_{fq}}{dt} + R_f i_{fq} + L_f\omega_e i_{fd} + e_q \tag{15}$$

where L_f and R_f are the filter inductance and filter resistance respectively; v_{fd} and v_{fq} are the filter voltage components of d-axis and q-axis respectively, e_d and e_q are the grid voltage components of d-axis and q-axis respectively, i_{fd} and i_{fq} are the values of the current of d axis and q-axis respectively, and $\omega_e = 2\pi f$ where f is the grid frequency.

3 Nonlinear Control of SCIG

A generator side converter connected to the stator of the SCIG effectively decouples the generator from the grid. Hence, the generator rotor speed depends only on the wind conditions.

The first control objective is to track the optimum generator speed ω_{m_opt} and to orient the rotor flux on the d-axis.

3.1 Control of Generator Speed

The optimum generator speed ω_{m_opt} is generated by a MPPT technique to determine the stabilizing function. The tracking error between speed and its reference is given as

$$e_1 = \omega_{m\_opt} - \omega_m \tag{16}$$

The sliding surface is chosen as follow

$$S_1(t) = K_1 e_1(t) \tag{17}$$

where K_1 is a positive constant feedback gain.

In order to satisfy the sliding mode existence law, the control input is chosen to have the following structure

$$u(t) = u_{eq}(t) + u_n(t) \tag{18}$$

where $u_{eq}(t)$ is an equivalent control-input that determines the system's behavior on the sliding surface and $u_n(t)$ is a non-linear switching input, which drives the state to the sliding surface and maintains the state on the sliding surface in the presence of the parameter variations and disturbances [31, 40]. The equivalent control-input is obtained from the invariance condition and is given by the following condition $S_1 = 0$ and $\frac{dS}{dt} = 0 \Rightarrow u(t) = u_{eq}(t)$.

Hence the derivative of the sliding surface (17) is given as

$$\begin{aligned} \frac{dS_1(t)}{dt} &= K_1 \left(\frac{d\omega_{m\_opt}}{dt} - \frac{d\omega_m}{dt} \right) \\ &= K_1 \frac{d\omega_{m\_opt}}{dt} + \frac{K_1}{2H} \left(\frac{L_m \phi_{ref}}{L_r} i_{sq} - T_m + F\omega_m \right) \end{aligned} \tag{19}$$

The i_{sq} can be viewed as a virtual control in the above equation. It is derived to ensure the SCIG speed convergence to the optimum speed. To ensure the Lyapunov stability criteria i.e. $\frac{dS_1}{dt} S_1 \prec 0$, the nonlinear control input i_{sq_eq} is defined as

$$i_{sq\_eq} = \left(-2H \frac{d\omega_{m\_opt}}{dt} + T_m - F\omega_m \right) \frac{L_r}{L_m \varphi_{ref}} \tag{20}$$

The nonlinear switching input i_{sq-n} can be chosen as follows

$$i_{sq-n} = -\alpha_1 \frac{2HL_r}{L_m \varphi_{ref}} \operatorname{sgn}(e_1) \tag{21}$$

where α_1 is a positive constant and the sign function is defined to reduce the phenomenon of charting as

$$\operatorname{sgn}(S(t)) = \frac{S(t)}{|S(t)| + \varepsilon} \tag{22}$$

where ε is a small positive number. Then, the reference of q-axis current is expressed as

$$i_{sq\_ref} = \left(-2H \frac{d\omega_{m\_opt}}{dt} + T_m - F\omega_m - 2H\alpha_1 \operatorname{sgn}(e_1) \right) \frac{L_r}{L_m \phi_{ref}} \tag{23}$$

Substituting (23) in (19), the q-axis current sliding surface dynamics becomes

$$\frac{dS_1(t)}{dt} = -K_1\alpha_1 \operatorname{sgn}(e_1) \tag{24}$$

3.2 Control of d-Axes Rotor Flux

The d-axis rotor flux Φ_{rd} can be estimated from Eq. (9) as

$$\phi_{rd-estim} = -\frac{L_m}{1 + T_r \cdot s} i_{sd} \tag{25}$$

where $T_r = \frac{\omega_b L_r}{R_r}$ is the time constant.

The stabilizing error between ϕ_{rd} and its desired trajectory ϕ_{ref} is defined as

$$e_2(t) = \phi_{ref} - \phi_{rd} \tag{26}$$

To stabilize the d-axis rotor flux Φ_{rd}, the new sliding surface is selected as

$$S_2(t) = K_2 e_2(t) \tag{27}$$

where K_2 is a positive constant. The derivative of $S_2(t)$ using (9) and (27) is given as

$$\frac{dS_2(t)}{dt} = K_2 \frac{d\phi_{ref}}{dt} + K_2\omega_b \frac{R_r}{L_r}\left[\phi_{rd} + L_m i_{sd}\right] \tag{28}$$

Then, the equivalent control i_{sd_eq} (29) is obtained as the solution of the equation $\frac{dS_2(t)}{dt} = 0$.

$$i_{sd\_eq} = -\frac{L_r}{\omega_b L_m R_r}\frac{d\phi_{ref}}{dt} - \frac{1}{L_m}\phi_{rd} \tag{29}$$

As a result, the stabilizing function of the control current is defined as

$$i_{sd\_ref} = -\frac{L_r}{\omega_b L_m R_r}\frac{d\phi_{ref}}{dt} - \frac{1}{L_m}\phi_{rd} - \frac{L_r}{\omega_b L_m R_r}\alpha_2 \operatorname{sgn}(e_2) \tag{30}$$

where α_2 is a positive constant. Using (30), the d-axis current sliding surface dynamics (28) becomes

$$\frac{dS_2(t)}{dt} = -K_2\alpha_2 \operatorname{sgn}(e_2) \tag{31}$$

Since the d-axis current and the q-axis current are not our control inputs, the stabilizing errors between i_{sd_ref} and i_{sq_ref} and their desired trajectories, respectively, are defined as

$$e_3(t) = i_{sd\_ref}(t) - i_{sd}(t) \tag{32}$$

$$e_4(t) = i_{sq\_ref}(t) - i_{sq}(t) \tag{33}$$

To stabilize $i_{sd}(t)$ and $i_{sq}(t)$, the new sliding surfaces are selected as

$$\begin{cases} S_3(t) = K_3 e_3(t) \\ S_4(t) = K_4 e_4(t) \end{cases} \tag{34}$$

where K_3 and K_4 are a positive constants. Then, the derivative of sliding surfaces are defined as

$$\frac{dS_3(t)}{dt} = K_3 \left(\frac{di_{sd\_ref}}{dt} - \frac{di_{sd}}{dt} \right) \tag{35}$$

$$\frac{dS_4(t)}{dt} = K_4 \left(\frac{di_{sq\_ref}}{dt} - \frac{di_{sq}}{dt} \right) \tag{36}$$

when replacing (7) in (35) and (8) in (36), then track the same steps used to obtain the control currents, the control voltage laws are obtained as

$$V_{sd\_ref} = \sigma L_s \left(-\frac{1}{\omega_b} \frac{di_{sd\_ref}}{dt} - \partial_1 i_{sd} + \omega_s i_{sq} - \partial_2 \phi_{rd} - \frac{\alpha_3}{\omega_b} \operatorname{sgn}(e_3(t)) \right) \tag{37}$$

$$V_{sq\_ref} = \sigma L_s \left(-\frac{1}{\omega_b} \frac{di_{sq\_ref}}{dt} - \partial_1 i_{sq} - \omega_s i_{sd} + \partial_3 \phi_{rd} - \frac{\alpha_4}{\omega_b} \operatorname{sgn}(e_4(t)) \right) \tag{38}$$

3.3 Stability Analysis

Theorem 1 *The dynamic sliding mode control laws (37) and (38) with stabilizing functions (23) and (30) when applied to the SCIG side converter, guarantee the asymptotic convergence of the generator speed ω_m and the d-axis rotor flux Φ_{rd} to their desired values ω_{m_opt} and ϕ_{ref}, respectively.*

Proof Consider the following positive definite Lyapunov function

$$V_1 = \frac{1}{2} S_1^2 + \frac{1}{2} S_2^2 + \frac{1}{2} S_3^2 + \frac{1}{2} S_4^2 \tag{39}$$

By considering (24), (31), (35) and (36), the derivative of (39) can be derived as follows

$$\begin{aligned}\frac{dV_1}{dt} &= \frac{dS_1}{dt}S_1 + \frac{dS_2}{dt}S_2 + \frac{dS_3}{dt}S_3 + \frac{dS_4}{dt}S_4 \\ &= -K_1^2\alpha_1 e_1 \operatorname{sgn}(e_1) - K_2^2\alpha_2 e_2 \operatorname{sgn}(e_2) \\ &\quad + K_3^2 e_3\left(\frac{di_{sd\_ref}}{dt} - \frac{di_{sd}}{dt}\right) + K_4^2 e_4\left(\frac{di_{sq\_ref}}{dt} - \frac{di_{sq}}{dt}\right)\end{aligned} \tag{40}$$

Substituting the control laws (37) and (38) in (40) gives

$$\begin{aligned}\frac{dV_1}{dt} &= -K_1^2\alpha_1 e_1 \operatorname{sgn}(e_1(t)) - K_2^2\alpha_2 e_2 \operatorname{sgn}(e_2(t)) \\ &\quad - K_3^2\alpha_3 e_3 \operatorname{sgn}(e_3(t)) - K_4^2\alpha_4 e_4 \operatorname{sgn}(e_4(t)) \\ &= -\sum_{i=1}^{4}\alpha_i K_i^2 |e_i| < 0\end{aligned} \tag{41}$$

From the above analysis, it is evident that the reaching condition of sliding mode is guaranteed.

4 Sliding Mode Control of Grid Side Converter

The aim of the grid side converter control is to maintain the dc link voltage constant, thereby ensuring that the active power generated by the SCIG is fed to the grid. Also this control must be able to provide perfect tracking performance of the reactive power fed to the network to its reference trajectory.

4.1 Control Laws of Reactive and Active Powers

By orienting the grid voltage space vector on the d axis, we obtain

$$\begin{aligned} e_d &= V \\ e_q &= 0 \end{aligned} \tag{42}$$

Substituting (42) in (14) and (15) gives the following equations of the filter

$$\frac{di_{fd}}{dt} = \frac{1}{L_f}\left(v_{fd} - R_f i_{fd} + L_f \omega_e i_{fq} - V\right) \tag{43}$$

$$\frac{di_{fq}}{dt} = \frac{1}{L_f}\left(v_{fq} - R_f i_{fq} - L_f \omega_e i_{fd}\right) \tag{44}$$

The reactive power and active power of grid can be expressed as

$$P_{gr} = i_{fd} V \tag{45}$$

$$Q_{gr} = i_{fq} V \tag{46}$$

From (45) and (46), it can be seen that the active and reactive power of grid can be controlled by the direct and quadrature components current, respectively. Then, let's define

$$e_5(t) = i_{fd\_ref} - i_{fd} \tag{47}$$

$$e_6(t) = i_{fq\_ref} - i_{fq} \tag{48}$$

where i_{fd_ref} and i_{fq_ref} are the desired values of the i_{fd} and i_{fq}. The current i_{fd_ref} is derived directly from the control loop of the DC bus voltage, while i_{fq_ref} is computed by (48). Q_{gr} is set to zero in order to ensure unit power factor $i_{fq\_ref} = 0$. The sliding surface for i_{fd} and i_{fq} can be expressed as

$$S_5(t) = K_5 e_5(t) \tag{49}$$

$$S_6(t) = K_6 e_6(t) \tag{50}$$

The DC bus voltage is regulated by using the proportional integral (PI) regulator. The derivative of (49) and (50) using (43) and (44) gives

$$\frac{dS_5(t)}{dt} = K_5\left(\frac{di_{fd\_ref}}{dt} - \frac{1}{L_f}\left(v_{fd} - R_f i_{fd} + L_f \omega_e i_{fq} - V\right)\right) \tag{51}$$

$$\frac{dS_6(t)}{dt} = K_6\left(\frac{di_{fq\_ref}}{dt} - \frac{1}{L_f}\left(v_{fq} - R_f i_{fq} - L_f \omega_e i_{fd}\right)\right) \tag{52}$$

To ensure the reaching condition $\frac{dS_5}{dt} S_5 \prec 0$, the equivalent control $v_{fd-eq}(t)$ is obtained as

$$v_{fd-eq} = L_f \frac{di_{fd\_ref}}{dt} + R_f i_{fd} - L_f \omega . i_{fq} + V \tag{53}$$

Subsequently, the control law is written as follows

$$v_{fd} = L_f \frac{di_{fd\_ref}}{dt} + R_f i_{fd} - L_f \omega . i_{fq} + V + \alpha_5 \operatorname{sgn}\left(e_5(t)\right) \tag{54}$$

In the same way, the control voltage law for the reactive power tracking is given as

$$v_{fq} = L_f \frac{di_{fq\_ref}}{dt} + R_f i_{fq} + L_f \omega . i_{fd} + L_f \alpha_6 \operatorname{sgn}(e_6(t)) \tag{55}$$

4.2 Stability Analysis

Theorem 2 *The dynamic sliding mode control laws (54) and (55) when applied to the grid side converter, guarantee the asymptotic convergence of the reactive and active powers to their reference trajectories P_{gr} and $Q_{gr} = 0$, respectively.*

Proof Consider the following positive definite Lyapunov function

$$V_2 = \frac{1}{2} S_5^2 + \frac{1}{2} S_6^2 \tag{56}$$

By considering (51) and (52) the derivative of (56) can be derived as follows

$$\begin{aligned} \frac{dV_2}{dt} &= \frac{dS_5}{dt} S_5 + \frac{dS_6}{dt} S_6 \\ &= K_5^2 e_5 \left(\frac{di_{fd\_ref}}{dt} - \frac{1}{L_f} \left(v_{fd} - R_f i_{fd} + L_f \omega_e i_{fq} - V \right) \right) \\ &\quad + K_6^2 e_6 \left(\frac{di_{fq\_ref}}{dt} - \frac{1}{L_f} \left(v_{fq} - R_f i_{fq} - L_f \omega_e i_{fd} \right) \right) \end{aligned} \tag{57}$$

Substituting the control laws (54) and (55) in (57) gives

$$\begin{aligned} \frac{dV_2}{dt} &= -\alpha_5 K_5^2 e_5 \operatorname{sgn}(e_5(t)) - \alpha_6 K_6^2 e_6 \operatorname{sgn}(e_6(t)) \\ &= -\alpha_5 K_5^2 |e_5| - \alpha_6 K_6^2 |e_6| \\ &\leq 0 \end{aligned} \tag{58}$$

Therefore the condition of sliding mode of the system is guaranteed.

5 Simulation Results and Discussion

A 3 MW, 690 V SCIG wind turbine system is simulated in the MATLAB/Simulink software environment to demonstrate the effectiveness of the proposed control scheme. The SCIG wind turbine is modeled by 5th nonlinear mathematical model.

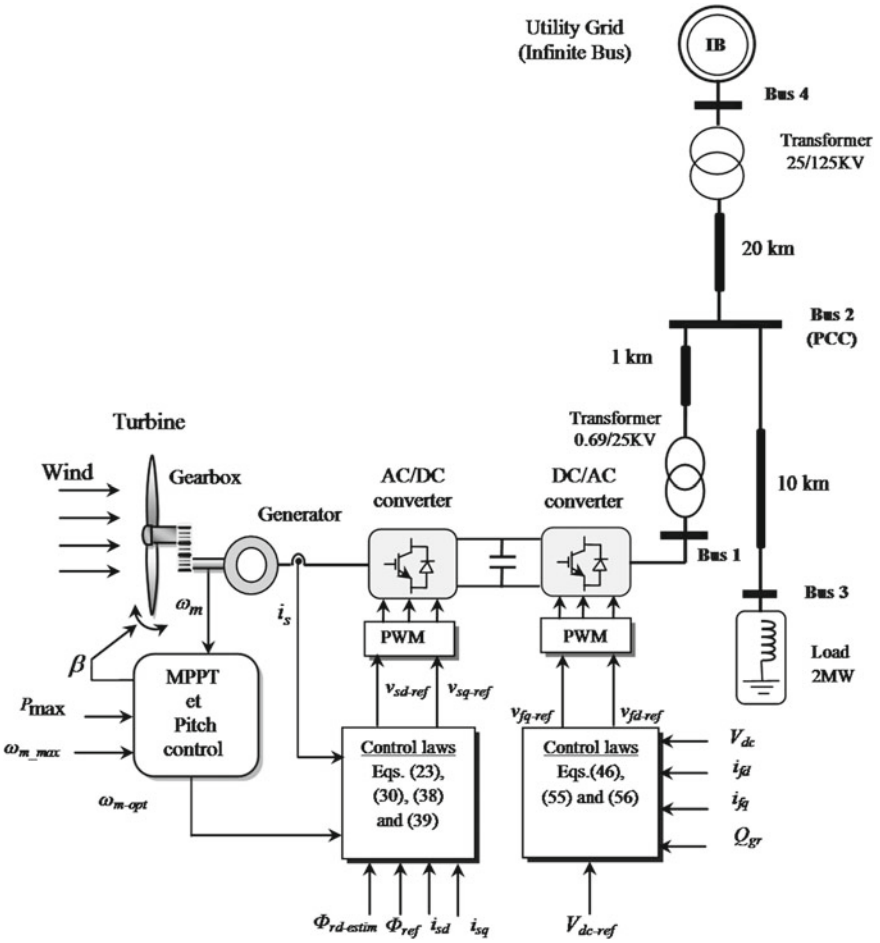

Fig. 4 Schematic diagram of the proposed control of SCIG wind turbine

The MSC and the GSC are represented by a switch-level model in which the operation of each individual switch is fully represented. Figure 4 shows the scheme of the implemented system. The parameters of the SCIG wind turbine are given in the Table 2.

The power reference is generated by a maximum power point tracking (MPPT) algorithm that searches for the peak power on the power–speed curve.

Table 2 Parameters of the wind turbine SCIG

Symbol	Quantity	Value
P_r	Rated power	3 (MW)
V_s	Rated voltage	690 (V)
F	Rated frequency	50 (Hz)
R_s	Stator resistance	0.004843 (pu)
L_s	Stator leakage Inductance	0.1248 (pu)
R_r	Rotor resistance	0.004347 (pu)
L_r	Rotor leakage Inductance	0.1791 (pu)
L_m	Mutual inductance	6.77 (pu)
H	Per unit Inertia constant	3.04 (pu)

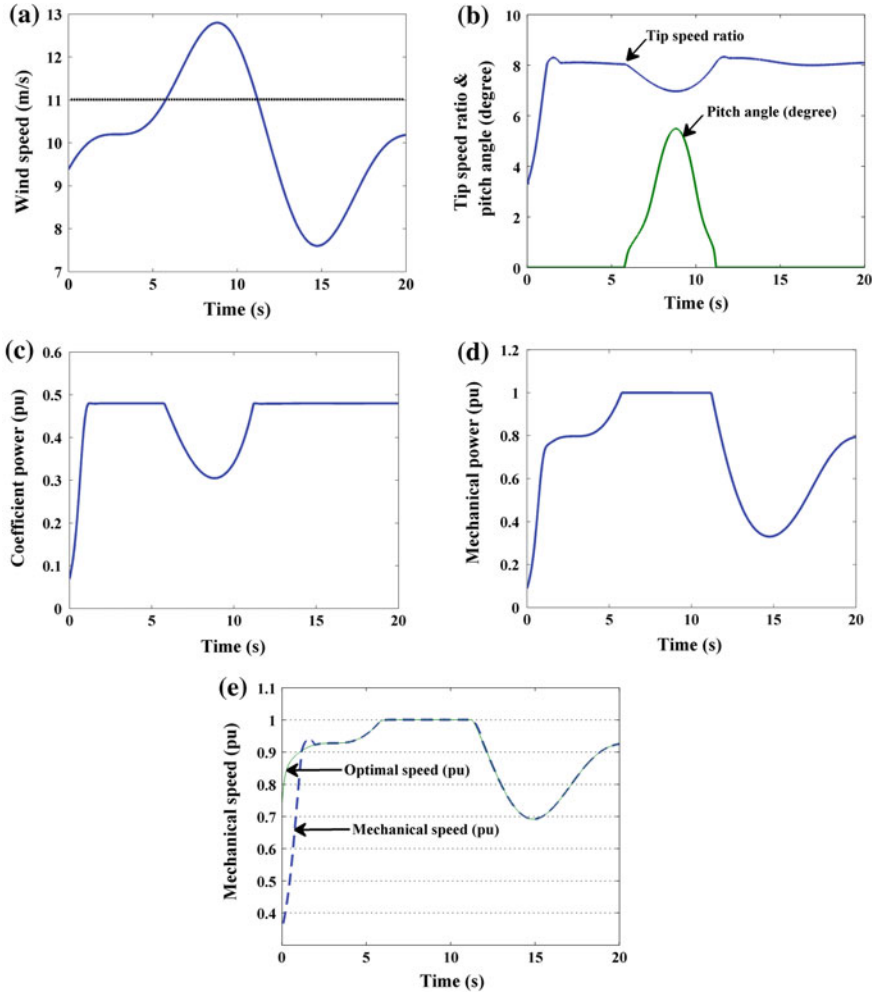

Fig. 5 Simulation results of MPPT control of SCIG wind turbine

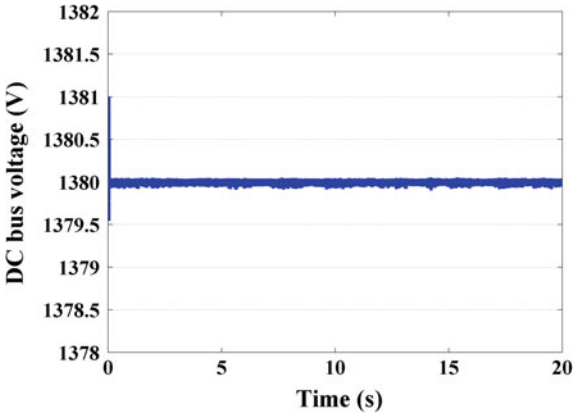

Fig. 6 Illustration of tracking performance of DC link voltage

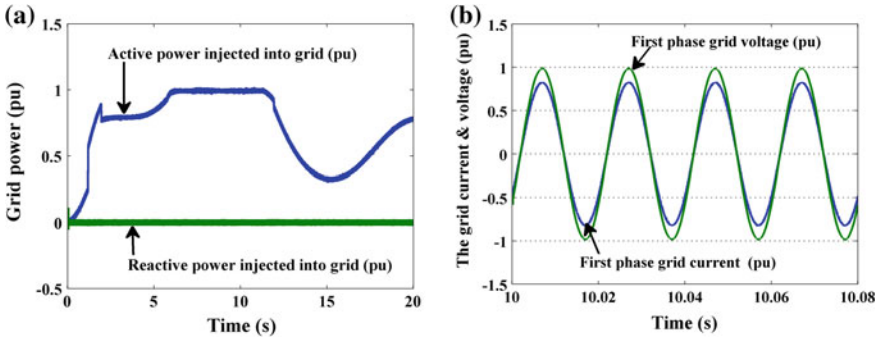

Fig. 7 Performance tracking of power and wave forms of grid voltage and current

5.1 Responses of MPPT Control

To extract maximum power corresponding to a specified wind velocity, the frequency at the terminals of the SCIG is adjusted in such a way that the machine rotates at a speed corresponding to the MPP. The objective of this case is to show the overall performance of the proposed controller under varied conditions of operation. With this purpose, the simulation was carried out considering the wind speed profile and rated wind speed presented in Fig. 5.

In this figure, it's also represented the pitch angle, the tip speed ratio, the coefficient of power conversion, the aerodynamic power, the generator speed and the optimum speed. It is shown that the pitch angle value is set at 0°, the tip speed ratio is equal to 8.1, and the power coefficient Cp is around of 0.47 when the wind speed is lower than 11 m/s. Once the rated speed is greater than 11m/s, the rated power 1 p.u (3 MW) is obtained.

5.2 Tracking Performance of DC Link Voltage and Powers

The Fig. 6 depicts the response of the DC bus voltage. It is noticeable that is regulated at 1380 V. Figure 7 presents the simulation results concerning the grid side: the voltage, the current, the reactive and active powers, respectively. It can be seen that the measured active power tracks very well the reference. Also, the reactive power is equal to its reference which is set to 0. Consequently, the unity power factor is achieved, since the current and the voltage of the grid are in phase.

5.3 Robustness to Parameter Disturbances

In this section, simulation results of the wind turbine SCIG under parameter variation is considered, in order to confirm the robustness of the proposed control. While the variations of the stator and rotor leakage inductances during operation are insignificant, mutual inductance variation should be taking into account due to possible variation of the magnetic permeability of the stator and rotor cores under different operating conditions. Figure 8 shows the simulation results with inductances used in the controller with increase of +50 % from their original values. Besides,

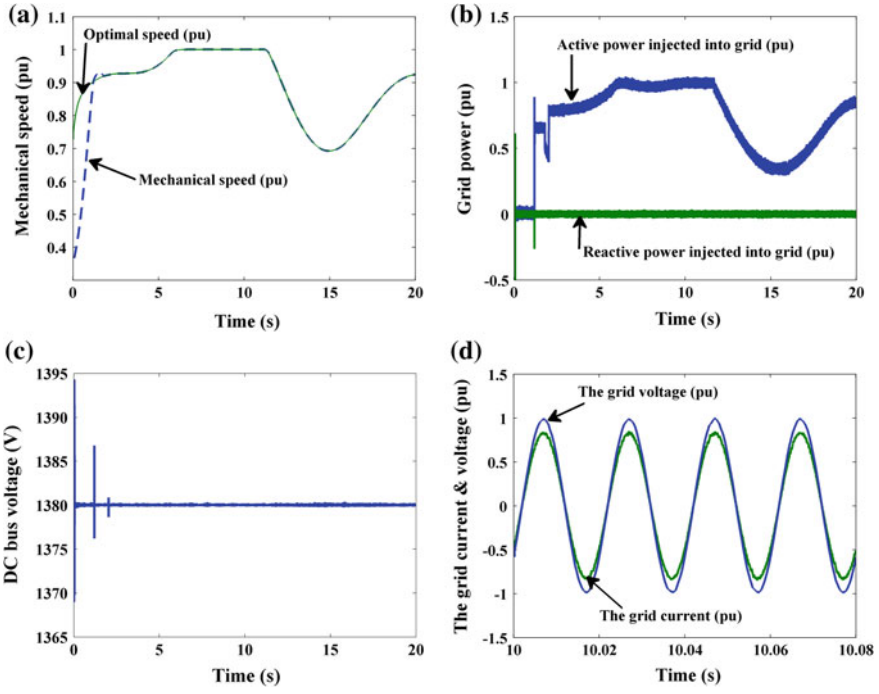

Fig. 8 Performance of the system under +50 % change in inductance values

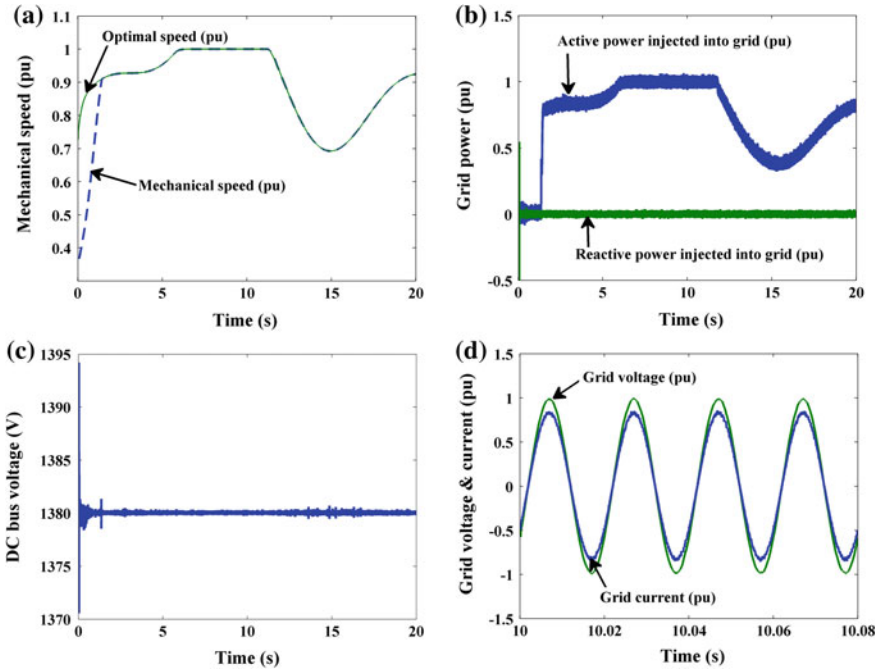

Fig. 9 Performance of the system under +50 % change in resistances of stator and rotor

variations of stator and rotor resistances should also be considered. Simulation results with change of resistances of stator and rotor (with the range of +50 %) are shown in Fig. 9. As a result, it can be seen that the proposed scheme can still provide consistent performance even if system parameters have changed.

6 Conclusion

Compared to other types of renewable energy, wind energy system has become a fast increasing energy source in the world; mainly as a consequence of its environmentally friendly, high reliability and cost effectiveness.

WECS based on SCIG is one of promising topology to reduce maintenance costs and to increase mechanical robustness and versatility. Further, it guarantees superior wind power extraction, better efficiency in variable-speed of the wind and improved quality of the energy feed to the grid.

In this context, two simultaneous control objectives have been investigated:

- the maximization of the energy conversion efficiency based SCIG wind turbine
- the regulation of the active and reactive power injected into the grid, to ensure UPF,

To this end, a sliding-mode control strategy, which presents attractive features such as robustness to parametric uncertainties of the different components of the system, has been adopted. The globally and exponentially stability of the derived control laws has been proven by applying Lyapunov stability analysis.

Simulation results have been performed to illustrate successful mathematical analysis and prove the effectiveness of the proposed nonlinear control laws. It can be observed from the simulation study that proposed controllers guarantee good performance in terms of (i) tracking of maximum power, (ii) reactive power regulation to guarantee unity power factor and (iii) robust feedback control solution despite parameter uncertainties and disturbances.

References

1. Alepuz S, Calle A, Busquets-Monge S, Kouro S (2013) Use of stored energy in PMSG rotor inertia for low-voltage ride-through in back-to-back npc converter-based wind power systems. IEEE Trans Indus Electron 60(5):1787–1796
2. Benchagra M, Errami Y, M. Hilal, Maaroufi M, Cherkaoui M, Ouassaid M (2012) New control strategy for inductin generator-wind turbine connected grid. In: International conference on multimedia computing and systems (IEEE-ICMCS), pp 1043–1048
3. Benchagra M, Maaroufi M, Ouassaid M (2014) A performance comparison of linear and nonlinear control of a SCIG-wind farm connecting to a distribution network. Turkish J Electr Eng Comput Sci 22(1):1–11
4. Caliao ND (2011) Dynamic modeling and control of fully rated converter wind turbines. Renew Energy 36:2287–2297
5. Cardenas R, Pena R (2004) Sensorless vector control of induction machines for variable-speed wind energy applications. IEEE Trans Energy Convers 19(1):196–205
6. Chou S, Chia-Tse L, Hsin-Cheng K, Po-Tai C (2014) A low-voltage ride-through method with transformer flux compensation capability of renewable power grid-side converters. IEEE Trans Power Electron 29(4):1710–1719
7. Chen Z, Guerrero JM, Blaabjerg F (2009) A review of the state of the art of power electronics for wind turbines. IEEE Trans Power Electron 24(8):1859–1875
8. Chen J, Jie C, Chunying G (2013) New overall power control strategy for variable-speed fixed-pitch wind turbines within the whole wind velocity range. IEEE Trans Ind Electron 60(7):2652–2660
9. Errami Y, Ouassaid M, Maaroufi M (2013) Modeling and variable structure power control of PMSG based variable speed wind energy conversion system. J Optoelectron Adv Mater 15(12):1248–1255
10. Evangelista C, Fernando V, Paul P (2013) Active and reactive power control for wind turbine based on a MIMO 2-sliding mode algorithm with variable gains. IEEE Trans Energy Convers 28(3):682–689
11. Huang N, He J, Nabeel A, Demerdash O (2013) Sliding Mode observer based position self-sensing control of a direct-drivePMSGwind turbine system fed by NPC converters. In: IEEE international electric machines drives conference (IEMDC), pp 919–925
12. Hu J, Nian H, He BHY, Zhu ZQ (2010) Direct active and reactive power regulation of dfig using sliding-mode control approach. IEEE Trans Energy Convers 25(4):1028–1039
13. Idris NRN, Yatim AHM (2004) Direct torque control of induction machines with constant switching frequency and reduced torque Ripple. IEEE Trans Ind Electron 51(4):758–767
14. Isidori A (1995) Nonlinear control systems, 3rd edn. Springer, New York

15. Jain S, Khorrami F, Fardanesh B (1994) Adaptive nonlinear excitation control of power system withunknown interconnections. IEEE Trans Control Syst Technol 2(4):436–446
16. Kang J, Sul S (1999) New direct torque control of induction motor for minimum torque ripple and constant switching frequency. IEEE Trans Ind Appl 35(5):1076–1082
17. Krstić M, Kanellakopoulos I, Kokotović P (1995) Nonlinear and adaptive control design. Wiley Interscience Publication, New York
18. Lai YS, Chen JH (2001) A new approach to direct torque control of inductionmotor drives for constant inverter switching frequency and torque ripple reduction. IEEE Trans Energy Convers 16(3):220–227
19. Ledesma P, Usaola J (2005) Doubly fed induction generator model for transient stability analysis. IEEE Trans Energy Convers 20(2):388–397
20. Li H, Zhao B, Yang C, Chen HW, Chen Z (2012) Analysis and estimation of transient stability for a grid-connected wind turbine with induction generator. Renew Energy 36:1469–1476
21. Li S, Haskew TA, Swatloski RP, Gathings W (2012) Optimal And Direct-current Vector Control Of Direct-driven Pmsg Wind Turbines. IEEE Trans Power Electron 27(5):2325–2337
22. Li R, Dianguo X (2013) Parallel operation of full power converters in permanent-magnet direct-drive wind power generation system. IEEE Trans Ind Electron 60(4):1619–1629
23. Martinez MI, Susperregui A, Tapia G (2013) Sliding-mode control of a wind turbine-driven doublefed induction generator under non-ideal grid voltages. IET Renew Power Gener 7(4):370–379
24. Melo DFR, Chang-Chien L-R (2014) Synergistic control between hydrogen storage system and offshore wind farm for grid operation. IEEE Trans Sustain Energy 5(1):18–27
25. Meng W, Yang Q, Ying Y, Sun Y, Yang Z, Sun Y (2013) Adaptive power capture control of variablespeed wind energy conversion systems with guaranteed transient and steady-state performance. IEEE Trans Energy Convers 28(3):716–725
26. Mullane A, Lightbody G, Yacamini R (2005) Wind-turbine fault ridethrough enhancement. IEEE Trans Power Syst 20(4):1929–1937
27. Nian H, Song Y (2014) Direct power control of doubly fed induction generator under distorted grid voltage. IEEE Trans Power Electron 29(2):894–905
28. Oliveira DS, Reis MM, Silva CEA, Colado Barreto HS, Antunes FLM, Soares BL (2010) A three-phase high-frequency semicontrolled rectifier for PM WECS. IEEE Trans Power Electron 25(3):677–685
29. Ouassaid M, Nejmi A, Cherkaoui M, Maaroufi M (2008) A Nonlinear backstepping controller for power systems terminal voltage and rotor speed controls. Int Rev Autom Control 3(1):355–363
30. Ouassaid M, Maaroufi M, Cherkaoui M (2010) Decentralized nonlinear adaptive control and stability analysis of multimachine power system. Int Rev Electr Eng 5(6):2754–2763
31. Ouassaid M, Maaroufi M, Cherkaoui M (2012) Observer based nonlinear control of power system using sliding mode control control strategy. Electr Power Syst Res 84(1):135–143
32. Peresada S, Tilli A, Tonielli A (2004) Power control of a doubly fed induction machine via output feedback. Control Eng Prac 12(1):41–57
33. Patil NS, Bhosle YN (2013) A review on wind turbine generator topologies. In: IEEE international conference on power, energy and control (ICPEC), pp 625–629
34. Rajaei AH, Mohamadian M, Varjani AY (2013) Vienna-rectifier-based direct torque control of PMSG for wind energy application. IEEE Trans Ind Electron 60(7):2919–2929
35. Slotine JJE, Li W (1991) Applied nonlinear control. Prentice-Hall, Englewoods Cliffs
36. Souza CL et al (2001) Power system transient stability analysis including synchronous and induction generator. Proc IEEE Porto Power Tech 2:6
37. Susperregui A, Martinez MI, Tapia G, Vechiu I (2013) Second-order sliding-mode controller design and tuning for grid synchronisation and power control of a wind turbine-driven doubly fed induction generator. IET Renew Power Gener 7(5):540–551
38. Tan Y, Wang Y (1998) Augmentation of transient stability using a supperconduction coil and adaptive nonlinear control. IEEE Trans Power Syst 13(2):361–366

39. Tseng K, Huang C-C (2014) High step-up high-efficiency interleaved converter with voltage multiplier module for renewable energy system. IEEE Trans Ind Electron 61(3):1311–1319
40. Utkin VI (1977) Variable structure systems with sliding modes. IEEE Trans Autom Control AC–22:212–222
41. Wu F, Zhang X, Ju P, Sterling MJH (2008) Decentralized nonlinear control of wind turbine with doubly fed induction generator. IEEE Trans Power Syst 23(2):613–621
42. Xu L, Cartwright P (2006) Direct active and reactive power control of DFIG for wind energy generation. IEEE Trans Energy Convers 21(3):750–758

Iterative Learning Control for Affine and Non-affine Nonlinear Systems

Farah Bouakrif

Abstract This chapter deals with Iterative Learning Control ILC schemes to solve the trajectory tracking problem of affine and non-affine nonlinear systems performing repetitive tasks. Two ILC laws are presented; the first law is a simple on-line 2D-type learning control for affine nonlinear systems. In addition, an initial condition algorithm is generated to provide the initial state value at each iteration automatically. To prove the asymptotic stability of the closed loop system over the whole finite time interval when the iteration number tends to infinity, λ-norm is used, as the topological measure. The second law is the on-line P-type ILC applied to non affine nonlinear systems. The asymptotic stability of the closed loop system is guaranteed upon the use of a Lyapunov-like positive definite sequence, which is shown to be monotonically decreasing under the proposed control scheme. Finally, simulation results on nonlinear system are provided to illustrate the effectiveness of the two controllers.

Keywords Asymptotic stability · Iterative learning control · Lyapunov theory · λ-norm

1 Introduction

The design of a controller for dynamical system is typically divided into two different design problems: The first design problem is a regulation problem which consists of finding a control law that manipulates the input variable so that the system automatically holds the output at a constant value even when unknown disturbances try to move output away from this constant set point. The second one is the trajectory tracking problem which consists of forcing the output response to follow a desired trajectory as close as possible, for example Proportional-Integral-Derivative PID control [17], adaptive control [20], variable structure control [21], fuzzy control [26]

F. Bouakrif (✉)
Laboratoire d'Automatique de Jijel, University of Jijel, Jijel, Algeria
e-mail: f.bouakrif@gmail.com

S. Vaidyanathan and C. Volos (eds.), *Advances and Applications in Nonlinear Control Systems*, Studies in Computational Intelligence 635,
DOI 10.1007/978-3-319-30169-3_24

and passivity-based control [2, 3]. In many cases, this desired trajectory is repeated over a given operation time, i.e., these nonlinear systems are used for repetitive tasks. The use of conventional control algorithms with such systems will result in the same level of tracking error being repeated time and time again. Iterative Learning Control ILC is a relatively new addition to the toolbox of control algorithms. It is concerned with the performance of systems that operate in a repetitive manner and includes examples such as robot arm manipulators. The basic idea of this method is to use information from previous operation in an attempt to improve performance from repetition to repetition in the sense that the tracking error (between the output and a specified reference trajectory) is sequentially reduced to zero. Since the early works of Arimoto et al. [1], Casalino and Bartolini [12], Craig [13], this technique has been the centre of interest of many researchers over the last decade (see, for instance, Bouakrif [4–6, 9] and Tayebi [25]).

In these works, the structures of ILC appeared as D-type, P-type, PD-type and PID-type. In addition, and for the sake of convergence speed, the forgetting factors have been introduced in ILC by Bouakrif [7]. From these works, it should be noted that ILC can be further classified into two kinds: off-line learning and on-line learning. In the case of off-line learning control, information in the controlled torque in the current iteration comes from the previous iteration. Philosophically, the learning in this case is shifted to the off-line mode. In the case of the on-line learning control, information in the controlled torque in the current iteration comes from the current iteration. Thus, the feedback control decision incorporates ILC at real-time.

Although, using ILC, the system should be started with the same initial condition at the beginning of each iteration [15, 16, 19], there have many works on ILC without identical initial condition [8, 18, 23, 27]. The first control law presented in this chapter is an ILC scheme without identical condition.

The most useful and general approach for studying the stability of nonlinear control systems is the theory introduced by the Russian mathematician Alexander Mikhailovich Lyapunov. Lyapunov's work includes two methods for stability analysis, the linearization method and direct method. The first one draws conclusions about a nonlinear system's local stability around an equilibrium point from the stability properties of its linear approximation. The second method is not restricted to local motion, and determines the stability properties of a nonlinear system by constructing a scalar energy-like function for the system and examining the function's time variation. This last method has become the most important tool for nonlinear system analysis and design. Recently, another type of ILC algorithms has been developed using a positive definite Lyapunov-like sequence which is made monotonically decreasing along the iteration axis via a suitable choice of the control input. In fact, [14] utilized Lyapunov-based techniques to develop an ILC that is combined with a robust control design to achieve global uniformly ultimately bounded link position tracking for robot manipulators. Using Lyapunov-like function, [10, 24] derived an adaptive ILC and a velocity observer based ILC, respectively, to solve the trajectory tracking problem of robot manipulators.

Using another proof of the stability for such controller (iterative learning controller), λ-norm defined firstly by Arimoto et al. [1], is used as the topological

measure, to prove the asymptotic stability of the closed loop system over the whole finite time interval when the iteration number tends to infinity. Using this norm and to solve the trajectory tracking problem for nonlinear systems with arbitrary relative degree and no state measurement, a state observer based iterative learning controller has been presented by Bouakrif [11].

In this chapter, we present two ILC schemes to solve the trajectory tracking problem of affine and non affine nonlinear systems performing repetitive tasks. The first law is a simple on-line 2D-type learning control for affine nonlinear systems with an initial condition algorithm to provide the initial state value at each iteration automatically. Using λ-norm, the asymptotic stability of such controller is guaranteed, over the whole finite time interval when the iteration number tends to infinity. The second law is an on-line P-type ILC of non affine nonlinear systems. To prove the asymptotic stability of the closed loop system, a Lyapunov-like positive definite sequence is used. It is shown to be monotonically decreasing under the proposed control scheme. Finally, simulation results on nonlinear system are provided to illustrate the effectiveness of the two controllers.

2 Iterative learning control design

2.1 General Form of Iterative Learning Controller

In general case, the ILC scheme is presented as follows

$$u_{k+1}(t) = f(u_k(t), e_{k+1}(t), e_k(t), \ldots, e_{k-m}(t)),\ m \geq 1. \tag{1}$$

We note that f depends on errors, and/or on derivative errors, and/or on integral errors obtains from different cycles. The fundamental problem resides to determine a simple recursive form of f ensuring the error convergence and a satisfactory rate convergence. Indeed, the Eq. (1) can be written as

$$u_{k+1}(t) = u_k(t) + \phi_{k+1}e_{k+1}(t) + \phi_k e_k(t) + \cdots + \phi_{k-m}e_{k-m}(t) \quad m \geq 1. \tag{2}$$

Figure 1 shows the block diagram of Eq. (2).
From this block, the following can be easily obtained

$$u_{k+1}(t) = u_{ff}(t) + u_{fb}(t). \tag{3}$$

$u_{ff}(t)$: is the feedforword controller.
$u_{fb}(t)$: is the current cycle feedback controller.

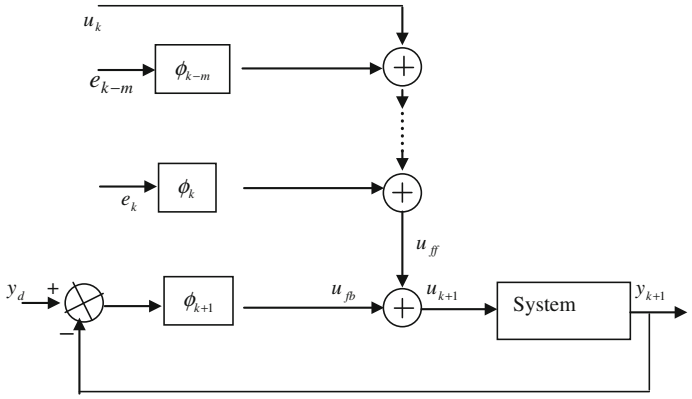

Fig. 1 Block diagram of ILC

2.2 Off-Line Iterative Learning Control Scheme

The off-line ILC scheme is obtained when ϕ_{k+1} equals to zero. It is important to note that this scheme in open loop via iterations domain. The off-line ILC scheme is given by:

$$u_{k+1}(t) = u_{ff}(t) = u_k(t) + \phi_k e_k(t) + \cdots + \phi_{k-m} e_{k-m}(t). \tag{4}$$

The original off-line ILC scheme was proposed firstly by Arimoto et al. [1], and it applied mainly in robotics. This scheme is as follows:

$$u_{k+1}(t) = u_k(t) + \phi \frac{d}{dt} e_k(t) \tag{5}$$

where ϕ is the learning gain and $\frac{d}{dt} e_k(t)$ is the derivative error.

2.3 On-Line Iterative Learning Control Scheme

Adding a current cycle feedback controller to open loop ILC scheme, the on-line ILC scheme is obtained. Thus, the form of this scheme is given by:

$$u_{k+1}(t) = u_{ff}(t) + u_{fb}(t) = u_k(t) + \phi_{k+1} e_{k+1}(t) + \phi_k e_k(t) + \cdots + \phi_{k-m} e_{k-m}(t). \tag{6}$$

3 On-Line 2D-Type Iterative Learning Control for Affine Non Linear Systems

3.1 System Description

Consider the following affine non linear system

$$\begin{cases} \dot{x}(t) = f(x(t), t) + B(t)u(t) \\ y(t) = h(x(t), t). \end{cases} \tag{7}$$

where k denotes the iteration index or the operation number, $x_k \in R^n$, $u_k \in R^r$ and $y_k \in R^m$ are the state, control input and output of the system, respectively. The function $f(*) = [f_1(*), \ldots . f_n(*)] \in R^n$ is strictly unknown. The functions $f(*) = [f_1(*), \ldots . f_n(*)] \in R^n$ and $h(*) = [h_1(*)...h_m(*)]^T \in R^m$ are smooth in their domain of definition, and let the associated time interval be $t \in [0, T]$.

The Jacobi of $h(x(t), t)$ is given by

$$h_x(x_k) = \left[\left(\frac{\partial h_1}{\partial x_1} \cdots \frac{\partial h_1}{\partial x_n} \right) \cdots \left(\frac{\partial h_m}{\partial x_1} \cdots \frac{\partial h_m}{x_n} \right) \right]^T \tag{8}$$

The following assumption is needed.

Assumption A1 The function $f(x(t), t)$ satisfies the Lipschitz condition with respect x over the time interval t∈[0, T]. Thus $\exists \alpha$ for $x_1(t), x_2(t) \in R \times [0, T]$ such as

$$\| f(x_1, t) - f(x_2, t) \| \leq \alpha \| x_1 - x_2 \| . \tag{9}$$

The following lemmas are used.

Lemma 1 *Let* $z(t) = [z_1(t), z_2(t), \ldots . z_n(t)]^T \in R^n$ *is defined for t∈[0, T], then we have*

$$\left(\int_0^t \| z(s) \| \, ds \right) \cdot e^{-\lambda t} \leq \frac{1}{\lambda} \| z(t) \|_\lambda . \tag{10}$$

Lemma 2 (Gronwall-Bellman) [22] *Suppose that* $f(t)$ *and* $g(t) \geq 0$ *are real and locally integrable scalar functions in [a, b], and L is a constant. If the real scalar function* $f(t)$ *satisfies the integral equation*

$$f(t) \leq L + \int_0^t g(\tau) f(\tau) d\tau \quad t \in [a, b]. \tag{11}$$

Then, on the same interval, $f(t)$ *satisfies*

$$f(t) \leq L \exp\left(\int_0^t g(\tau)d\tau\right). \tag{12}$$

Lemma 3 *Letting $\xi(t)$, $\eta_1(t)$, $\eta_2(t)$ the continuous functions in [0, T]. If*

$$\|\xi(t)\| \leq \Gamma \int_0^t \|\xi(s)\| ds + \Gamma_1 \int_0^t \|\eta_1(s)\| ds + \Gamma_2 \|\eta_2(t)\| \tag{13}$$

then

$$\|\xi(t)\|_\lambda \leq \left(\frac{1}{\lambda}\Gamma_1 \|\eta_1(t)\|_\lambda + \Gamma_2 \|\eta_2(t)\|_\lambda\right) \exp\left(\frac{\Gamma}{\lambda}\right) \tag{14}$$

with $\Gamma \geq 0$, Γ_1 and Γ_2 are constants.

Proof Multiplying (13) by $e^{-\lambda t}$, we have

$$\|\xi(t)\| e^{-\lambda t} \leq \Gamma \int_0^t \|\xi(s)\| e^{-\lambda s} e^{-\lambda(t-s)} ds + (\Gamma_1 \int_0^t \|\eta_1(s)\| ds) e^{-\lambda t} + \Gamma_2 \|\eta_2(t)\| e^{-\lambda t}. \tag{15}$$

Applying the Lemma 1, we obtain

$$\|\xi(t)\| e^{-\lambda t} \leq \left(\frac{1}{\lambda}\Gamma_1 \|\eta_1(t)\|_\lambda + \Gamma_2 \|\eta_2(t)\|_\lambda\right) + \Gamma \int_0^t \|\xi(s)\| e^{-\lambda s} e^{-\lambda(t-s)} ds. \tag{16}$$

Using Lemma 2, it comes

$$\|\xi(t)\| e^{-\lambda t} \leq \left(\frac{1}{\lambda}\Gamma_1 \|\eta_1(t)\|_\lambda + \Gamma_2 \|\eta_2(t)\|_\lambda\right) \exp\left(\int_0^t \Gamma e^{-\lambda(t-s)} ds\right). \tag{17}$$

Thus

$$\|\xi(t)\| e^{-\lambda t} \leq \left(\frac{1}{\lambda}\Gamma_1 \|\eta_1(t)\|_\lambda + \Gamma_2 \|\eta_2(t)\|_\lambda\right) \exp\left(\frac{\Gamma}{\lambda}\right). \tag{18}$$

3.2 Iterative Learning Control Design

Objective

Our objective is to design a controller that is updated iteratively such that the output trajectory $y_k(t)$ follows a desired trajectory $y_d(t)$, for $t \in [0, T]$ and $k \to \infty$.

In this section, we consider a simple on-line 2D-type learning control and an initial condition algorithm. This algorithm provides the initial state value at each iteration automatically. Using λ-norm defined firstly by Arimoto et al. [1], as the topological measure, the asymptotic stability of the closed loop system is guaranteed over the whole finite time interval when the iteration number tends to infinity. More specifically, the output system is proved to be convergence to the desired output by showing that the inequality

$$\|e_{k+1}(t)\|_\lambda \leq \varpi \, \|e_k(t)\|_\lambda \tag{19}$$

holds if $\varpi \prec 1$. With $e_k(t) = y_d(t) - y_k(t)$.

The formal definition of the λ-norm for a function $f : [0, T] \to R^n$ is given by

$$\|f(t)\|_\lambda = \sup_{t\in[0,T]}(e^{-\lambda t} \, \|f(t)\|_\infty) \tag{20}$$

Throughout the paper, we will use the following norms.

$$\|f(t)\|_\infty = \sup_{t\in[0,T]} \|f(t)\|, \|M\| = \max_{1\leq i\leq n} \left(\sum_{j=1}^{m} |m_{ij}| \right),$$

$\|V\| = \max_{1\leq i\leq n} |V_i|$, where

$M = (m_{ij}), V = (V_i), 1 \leq i \leq n$ and $1 \leq j \leq m$.

The asymptotic stability conditions for such controller are given in the following theorem.

Theorem 1 *Given the affine nonlinear system (7), and let assumption A1 be satisfied. For any initial state $x_1(0)$, any admissible control $u_1(t)$, and applying the following on-line 2D-type iterative learning control and initial state algorithm*

$$u_{k+1}(t) = u_k(t) + L(t)\dot{e}_k(t) + K(t)\dot{e}_{k+1}(t) \tag{21}$$

$$x_{k+1}(0) = (I_n + B(0)K(0)h_x(x(0)))^{-1}(x_k(0) + B(0)K(0)y_d(0)) + B(0)L(0)e_k(0) \tag{22}$$

If

1—$h_x(x, t)$ is bounded in $R^n \times [0, T]$,

2—$I_m + h_x(x(t), t)B(t)K(t)$ is non-singular,

3— $\sup_{(x,t)\in R^n\times[0,T]} \left\| (I_m - h_x(x, t)B(t)L(t)).(I_m + h_x(x, t)B(t)K(t))^{-1} \right\| < 1.$

Then

$$\lim_{k\to\infty} y_k(t) = y_d(t) \quad . \tag{23}$$

where $e_k(t) = y_d(t) - y_k(t)$. $K(t) \in R^{r\times m}$ and $L(t) \in R^{r\times m}$ are the gain matrices, with $I_n + B(0)K(0)h_x(x(0))$ is non singular.

Proof From (7), (21) and (22), we have

$$\begin{aligned} x_{k+1}(t) &= x_{k+1}(0) + \int_0^t (f(x_{k+1}(s), s) + B(s)u_{k+1}(s))ds \\ &= x_k(0) + B(0)K(0)e_{k+1}(0)B(0)L(0)e_k(0) + \int_0^t f(x_{k+1}(s), s)ds \\ &\quad + \int_0^t B(s)(u_k(s) + L(s)\dot{e}_k(s) + K(s)\dot{e}_{k+1}(s))ds \\ &= x_k(0) + \int_0^t [f(x_k(s), s) + B(s)u_k(s)]ds \\ &\quad + \int_0^t [f(x_{k+1}(s), s) - f(x_k(s), s)]ds + B(t)L(t)e_k(t) \\ &\quad - \int_0^t \frac{d(B(s)L(s))}{ds} e_k(s)ds + B(t)K(t)e_{k+1}(t) - \int_0^t \frac{d(B(s)K(s))}{ds} e_{k+1}(s)ds \end{aligned} \tag{24}$$

consequently

$$\begin{aligned} x_{k+1}(t) - x_k(t) &= \int_0^t [f(x_{k+1}(s), s) - f(x_k(s), s)]ds + B(t)L(t)e_k(t) \\ &\quad - \int_0^t \frac{d(B(s)L(s))}{ds} e_k(s)ds \\ &\quad + B(t)K(t)e_{k+1}(t) - \int_0^t \frac{d(B(s)K(s))}{ds} e_{k+1}(s)ds \end{aligned} \tag{25}$$

Using assumption A1, Lemmas 1 and 2, we find

$$\|x_{k+1}(t) - x_k(t)\|_\lambda \leq \gamma_1 \exp(\frac{\alpha}{\lambda}) \|e_k(t)\|_\lambda + \gamma_2 \exp(\frac{\alpha}{\lambda}) \|e_{k+1}(t)\|_\lambda \tag{26}$$

with $a = \max_{t\in[0,T]} \|B(t)L(t)\|$, $b = \max_{t\in[0,T]} \left\| \frac{dB(t)L(t))}{dt} \right\|$, $\gamma_1 = a + \frac{b}{\lambda}$, $\gamma_2 = c + \frac{d}{\lambda}$, $c = \max_{t\in[0,T]} \|B(t)K(t)\|$ and $d = \max_{t\in[0,T]} \left\| \frac{dB(t)K(t))}{dt} \right\|$.

Using the theorem of differential mean value, it exists $\xi_k(t)$, such that

$$\begin{aligned} e_{k+1}(t) - e_k(t) &= y_k(t) - y_{k+1}(t) \\ &= h_x(\xi_k(t), t)(x_k(t) - x_{k+1}(t)). \end{aligned} \tag{27}$$

From (25) and (27), it comes

$$\begin{aligned} [I_m + h_x(x_k(t), t)B(t)K(t)]e_{k+1}(t) &= [I_m - h_x(x_k(t), t)B(t)L(t)]e_k(t) \\ &- h_x(x_k(t), t)\int_0^t [f(x(s), s) - f(x(s), s)]ds \\ &- h_x(x_k(t), t)\left[\int_0^t \frac{d(B(s)L(s)}{ds} e_k(s)ds + \int_0^t \frac{d(B(s)K(s)}{ds} e_{k+1}(s)ds\right] \end{aligned} \tag{28}$$

From (26), (28) and using assumption A1, we have

$$\left\|e_{k+1}(t)\right\|_\lambda \leq \left[\frac{\max\limits_{t\in[0,T]} \|(I_m - h_x(x(t), t)B(t)L(t))\| + \frac{\delta}{\lambda}\left[\alpha\gamma_1 \exp(\frac{\alpha}{\lambda}) + b\right]}{\max\limits_{t\in[0,T]} \|(I_m + h_x(x(t), t)B(t)K(t))\| - \frac{\delta}{\lambda}\left[\alpha\gamma_{21} \exp(\frac{\alpha}{\lambda}) + d\right]}\right] \|e_k(t)\|_\lambda \tag{29}$$

Choosing $\lambda(\lambda > 0)$ widely great, we obtain

$$\|e_{k+1}(t)\|_\lambda \leq \max_{t\in[0,T]} \left\{\left\|(I_m - h_x(x(t), t)B(t)L(t))(I_m + h(x(t), t)B(t)K(t))^{-1}\right\|\right\} \|e_k(t)\|_\lambda. \tag{30}$$

If

$$\max_{t\in[0,T]} \left\{\left\|(I_m - h_x(x(t), t)B(t)L(t))(I_m + h(x(t), t)B(t)K(t))^{-1}\right\|\right\} < 1. \tag{31}$$

Then $y_k(t)$ converges uniformly to $y_d(t)$, when $k \to \infty$ and t∈[0, T].

3.3 Simulation Results

Consider the dynamic model of robot manipulator given by

$$J_m\ddot{q}(t) + Sg\sin(q(t)) = u(t) \tag{32}$$

g is the gravitational acceleration, $u(t)$ is the input control, $q(t)$ is the rotation angle of the robot.

We takes $x_1 = q$ and $x_2 = \dot{q}$, thus we obtain

$$\begin{bmatrix} \dot{x}_1 \\ \dot{x}_2 \end{bmatrix} = \begin{bmatrix} x_2 \\ -J_m^{-1} Sg \sin x_1 \end{bmatrix} + \begin{bmatrix} 0 \\ J_m^{-1} \end{bmatrix} \cdot u. \tag{33}$$

The output is $y = \frac{2}{5}x_2$. $J_m = 14\,\text{kgm}^2$, $S = 6\,\text{kg} \cdot \text{m}$, $g = 9.8\,\text{m/s}^2$, T=2 s, $h_x = \left[0, \frac{2}{5}\right]$.

The ILC laws is given by

$$\begin{aligned} u_{k+1}(t) &= u_k(t) + 10\dot{e}_k(t) + 14\dot{e}_{k+1}(t) \\ x_{k+1}(0) &= \begin{bmatrix} 1 & 0 \\ 0 & \frac{5}{7} \end{bmatrix} x_k(0) + \begin{bmatrix} 0 \\ \frac{5}{7} \end{bmatrix} y_d(0) + \begin{bmatrix} 0 \\ 1 \end{bmatrix} e_k(0) \end{aligned} \tag{34}$$

with $L(t) = 10$ and $K(t) = 14$.

For a continuous function $y_d(t)$ in [0, T], it exists $u(t) \in U$, such that $y_d(t) = h(x_d(t), t)$, with $x_d(t)$ is generated by $u_d(t)$, given as

$$u_d(t) = 35 - 70t - 58.8 \sin\left(\frac{5t^2(2t-3)}{12}\right) \tag{35}$$

with $x_1(0) = [0, 1]$, and $u_1(t) = 1$.

Applying the ILC law, we obtain the following results.

The simulation results are given in Figs. 2, 3, 4 and 5. These figures present the simulation results of the real and desired trajectories for 1st, 3rd, 7th and 10th iteration. We can see that the real trajectory follows the desired one through learning iteration. Thus, the system executes 10 iterations so that the real output system follows the desired trajectory without error.

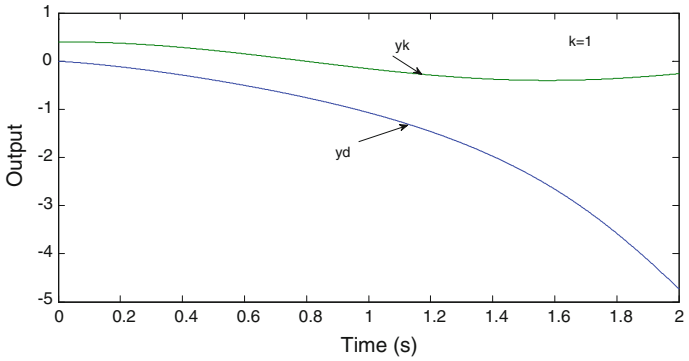

Fig. 2 Real and desired trajectories for k = 1

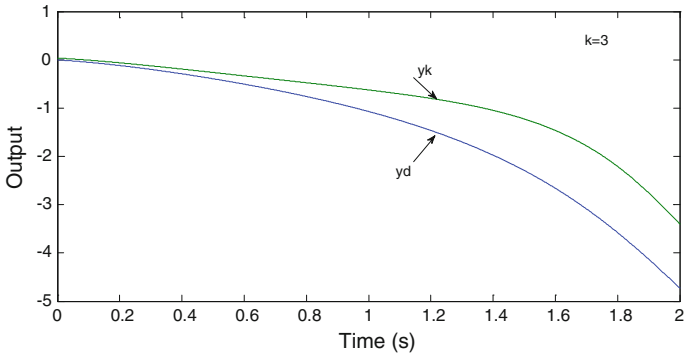

Fig. 3 Real and desired trajectories for k = 3

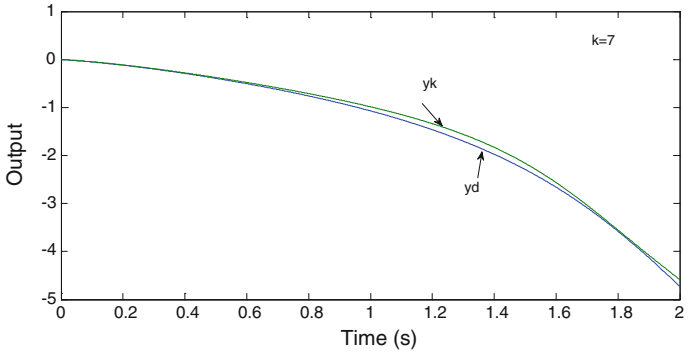

Fig. 4 Real and desired trajectories for k = 7

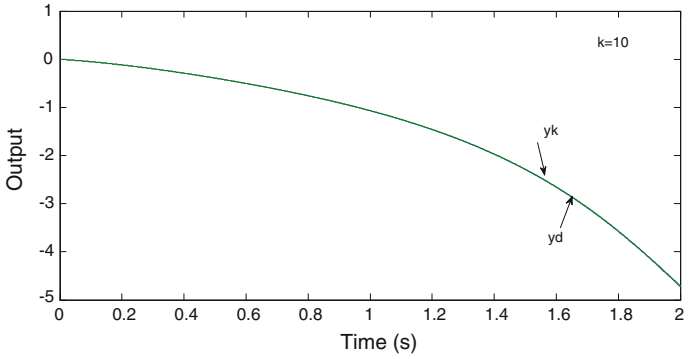

Fig. 5 Real and desired trajectories for k = 10

4 On-Line P-Type Iterative Learning Control for a Class of Non affine Nonlinear Systems

4.1 System Description

Consider the non-affine time-varying nonlinear systems described by

$$\begin{cases} \dot{x}_k(t) = f(x_k(t), u_k(t), t) + w_k(t) \\ y_k(t) = h(x_k(t), t) \end{cases} \tag{36}$$

where k denotes the iteration index or the operation number, $x_k \in R^n$, $u_k \in R^r$ and $y_k \in R^m$ are the state, control input and output of the system, respectively. $w_k(t)$ is the external disturbance of the system. The functions $f(*) = [f_1(*), \ldots . f_n(*)] \in R^n$ and $h(*) = [h_1(*) \ldots h_m(*)]^T \in R^m$ are smooth in their domain of definition, and let the associated time interval be $t \in [0, T]$.

4.2 Iterative Learning Control Design

In order to design a controller that is updated iteratively such that the system output (36) can follow the desired output, one presents the following on-line P-type ILC law:

$$u_{k+1}(t) = u_k(t) + L_1 e_{k+1}(t) \tag{37}$$

where $e_k(t) = y_d(t) - y_k(t)$ is the trajectory tracking error, L_1 is diagonal positive definite matrix.

It is important to note here that the asymptotic stability is proved using a positive definite Lyapunov-like sequence which is made monotonically decreasing along the iteration axis.

Theorem 2 *Given the unknown nonlinear systems (36) under the iterative learning control law (37), the closed loop system is asymptotically stable, i.e.,*

(i) $\lim_{k \to \infty} e_k(t) = 0 \quad t \in [0, T]$.
(ii) $u_k(t)$ *is uniformly convergent on* $[0, T]$.

Proof Letting

$$\Phi_k(t) = \begin{pmatrix} e_k(t) \\ \Delta u_k(t) \end{pmatrix} \tag{38}$$

where $\Delta u_k(t) = u_k(t) - u_{k-1}(t)$.

It is clear that

$$\begin{cases} e_k(t) = y_d(t) - y_k(t) = y_d(t) - h(x_k(t), t) \\ e_{k+1}(t) = y_d(t) - y_{k+1}(t) = y_d(t) - h(x_{k+1}(t), t). \end{cases} \tag{39}$$

Thus

$$e_{k+1}(t) = e_k(t) - (h(x_{k+1}(t), t) - h(x_k(t), t)). \tag{40}$$

From (37), the control law at k^{th} iteration is as follows

$$u_k(t) = u_{k-1}(t) + L_1 e_k(t). \tag{41}$$

From (37), (40) and (41), we have

$$\Delta u_{k+1}(t) = \Delta u_k(t) - L_1 (h(x_{k+1}(t), t) - h(x_k(t), t)). \tag{42}$$

From (38) and (42), we obtain

$$\Phi_{k+1}(t) = \Phi_k(t) + B F_k(t) \tag{43}$$

where $B = \begin{pmatrix} -I_n \\ -L_2 \end{pmatrix}$ and $F_k(t) = (h(x_{k+1}(t), t) - h(x_k(t), t))$.

Stability analysis: The proof of the theorem 2 is in three parts. The first part consists of taking a positive definite Lyapunov-like composite energy function, namely $V_k(t)$, and show that this sequence is non-increasing with respect to k and hence bounded if $V_0(t)$ is bounded. In the second part, one shows that $V_0(t)$ is bounded for all $t \in [0, T]$. In the third part, one shows that $\lim_{k\to\infty} e_k(t) = 0$ and $u_k(t)$ is uniformly convergent $\forall t \in [0, T]$.

Part 1: Let us consider the following Lyapunov-like sequence

$$V_k(e_k(t), \Delta u_k(t)) = \sum_{j=k}^{\infty} \Phi_j^T(t) P \Phi_j(t) \tag{44}$$

where P is symmetric, positive definite matrix.

At $(k+1)$th iteration, we have

$$V_{k+1}(e_{k+1}(t), \Delta u_{k+}(t)) = \sum_{j=k+1}^{\infty} \Phi_j^T(t) P \Phi_j(t). \tag{45}$$

In the sequel, since the time t does not have any impact on the stability analysis, it is removed for the sake of simplicity.

Let's define

$$\Delta V_k = V_{k+1} - V_k. \tag{46}$$

From (43), (44), (45) and (46), we can write

$$\Delta V_k = -\Phi_k^T P \Phi_k. \tag{47}$$

Since P is symmetric, we can apply the theorem of Rayleigh-Ritz. It becomes

$$\Delta V_k \leq -\lambda_{\min}(P) \left\| \Phi_k \right\|^2. \tag{48}$$

where $\lambda_{\min}(P)$ denotes the minimum eigenvalue of P.

It is clear that

$$\Delta V_k \leq 0. \tag{49}$$

Hence V_k is non-increasing sequence. Thus if V_0 is bounded, we can conclude that V_k is bounded.

Part 2: Now, we will show that V_0 is bounded over the time interval $[0, T]$. In fact, from (44) V_0 is given by

$$V_0 = \sum_{j=0}^{\infty} \Phi_j^T P \Phi_j. \tag{50}$$

with $\Phi_j = \begin{pmatrix} e_j \\ \Delta u_j \end{pmatrix}$.

From (40) and (42), Δu_0 and Δu_1 are given by

$$\Delta u_0 = \Delta u_{-1} + L_1 (e_0 - e_{-1}). \tag{51}$$

and

$$\begin{aligned} \Delta u_1 &= u_1 - u_0 \\ &= \Delta u_0 + L_1 (e_1 - e_0). \end{aligned} \tag{52}$$

Before applying the control at the first iteration, it is logical to suppose that $e_{-1} = e_0 = 0$ and $u_{-1}(t) = u_0(t) = 0$. Hence, it becomes

$$\begin{cases} \Delta u_0 = 0 \\ \Phi_0 = 0 \end{cases} \tag{53}$$

and

$$u_1 = L_1 e_1 \tag{54}$$

Since the control at the first iteration is bounded, we can conclude from (54) that e_1 is bounded.

We note that

$$V_\infty = f(e_\infty) \tag{55}$$
$$V_{\infty-1} = f(e_{\infty-1}, e_\infty) \tag{56}$$
$$\vdots$$
$$V_2 = f(e_2, \ldots, e_{\infty-1}, e_\infty) \tag{57}$$
$$V_1 = f(e_1, e_2, \ldots, e_{\infty-1}, e_\infty). \tag{58}$$

Knowing that $V_{k+1} \leq V_k$ for $k \geq 1$, we can use the following reasoning:

$$e_\infty \text{ is bounded if } e_{\infty-1} \text{ is bounded}$$
$$e_{\infty-1} \text{ is bounded if } e_{\infty-2} \text{is bounded}$$
$$\vdots$$
$$e_2 \text{ is bounded if } e_1 \text{ is bounded}$$

Since e_1 is bounded and using this reasoning, we can conclude that e_∞ is bounded. This implies that all Φ_j, $j = 1, \ldots, \infty$ are bounded. Finally and knowing that Φ_0 is bounded, we can conclude from (50) that V_0 is bounded over $[0, T]$.

Part 3: We note that V_k can be written as follows

$$V_k = V_0 + \sum_{j=1}^{k} \Delta V_j. \tag{59}$$

Thus, from (48), we have

$$V_k \leq V_0 - \lambda_{\min}(P) \|\Phi_k\|^2. \tag{60}$$

This implies that

$$\lambda_{\min}(P) \|\Phi_k\|^2 \leq 2 (V_0 - V_k). \tag{61}$$

Since $V_k(t)$ is bounded $\forall k \in N$ and $\forall t \in [0, T]$, this implies that Φ_k disappears when $k \to \infty$. Therefore, $\lim_{k\to\infty} e_k(t) = 0$ for $t \in [0, T]$ and $u_k(t)$ is uniformly convergent. This completes the proof.

4.3 Simulation Results

Consider the dynamical model of a nonlinear system given as follows

$$\begin{bmatrix} \dot{x}_{1k}(t) \\ \dot{x}_{2k}(t) \end{bmatrix} = \begin{bmatrix} x_{2k}(t) \\ -J_m^{-1} Sg \sin x_{1k}(t) \end{bmatrix} + \begin{bmatrix} 0 \\ J_m^{-1} \end{bmatrix} u_k(t) \tag{62}$$

where $t \in [0, 2](s)$, $J_m = 14\,\mathrm{kgm}^2$, $S = 6\,\mathrm{kg} \cdot \mathrm{m}$, $g = 9.8\,\mathrm{m/s}^2$ (gravitational acceleration), and $u_k(t)$ is the control.

Adding the disturbances, we have

$$\begin{bmatrix} \dot{x}_{1k}(t) \\ \dot{x}_{2k}(t) \end{bmatrix} = \begin{bmatrix} x_{2k}(t) \\ -J_m^{-1} Sg \sin x_{1k}(t) \end{bmatrix} + \begin{bmatrix} 0 \\ J_m^{-1} \end{bmatrix} u_k(t) + \begin{bmatrix} w_{1k}(t) \\ w_{2k}(t) \end{bmatrix}. \tag{63}$$

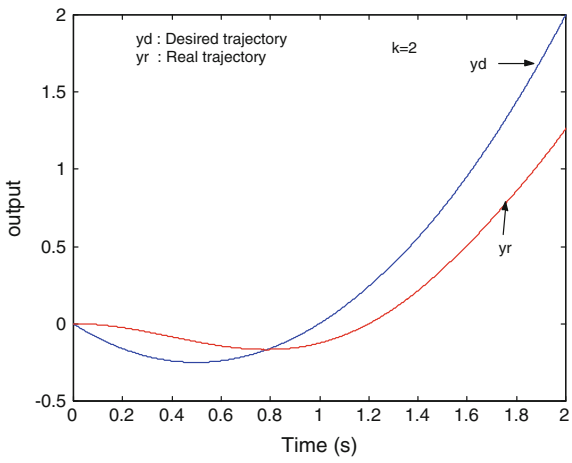

Fig. 6 Real and desired trajectories after 2 iterations

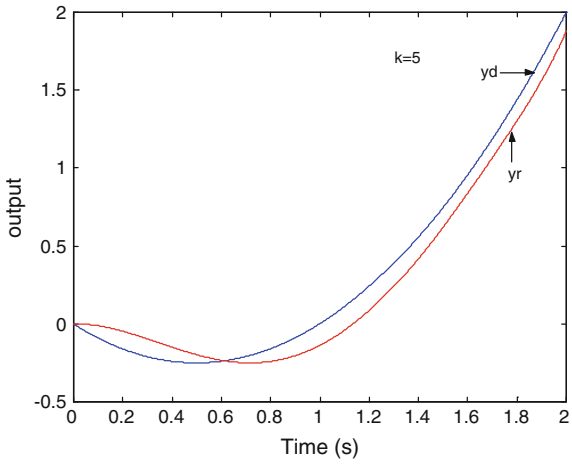

Fig. 7 Real and desired trajectories after 5 iterations

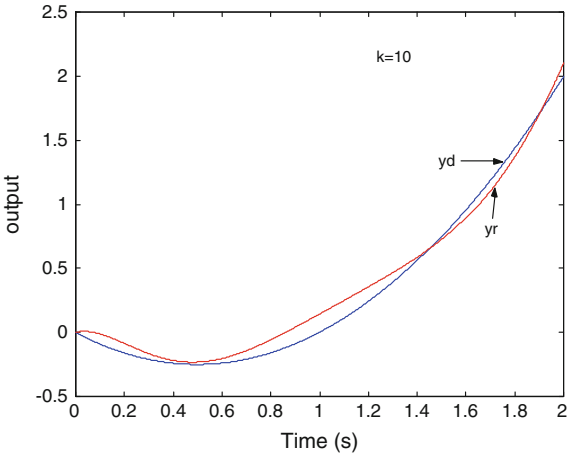

Fig. 8 Real and desired trajectories after 10 iterations

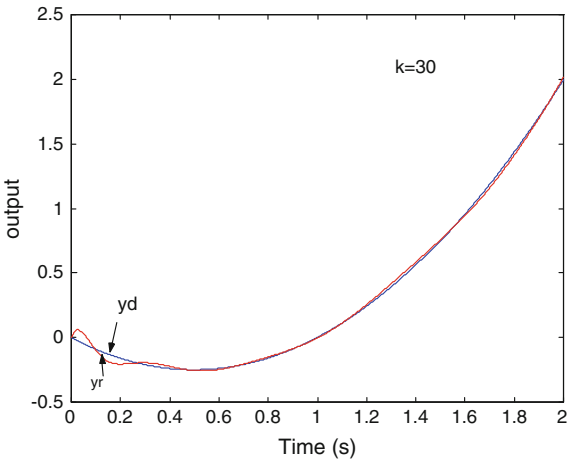

Fig. 9 Real and desired trajectories after 30 iterations

where the disturbances are given by

$$\begin{bmatrix} w_{1k}(t) \\ w_{2k}(t) \end{bmatrix} = a \begin{bmatrix} \cos(2\pi\ f_0\ t\ ) \\ 2\cos(4\pi\ f_0\ t\ ) \end{bmatrix} \tag{64}$$

with $f_0 = 1/(20h)$ and $a = 0.1$. The output is chosen as: $y = \frac{1}{4}x_2$. The desired trajectory is chosen as: $y_d(t) = t^2 - t$, and $u_1(t) = 1$.

Simulation parameters: $L_1 = diag\,\{90, 90\}$.

Applying the control law (37), the simulation results for real and desired trajectories for 2nd, 5th, 10th, 30th and 40th iteration are shown in Figs. 6, 7, 8, 9 and 10. We can see that the real trajectory follows the desired trajectory through learning iteration. Thus, the system executes 40 iterations so that the real trajectory follows

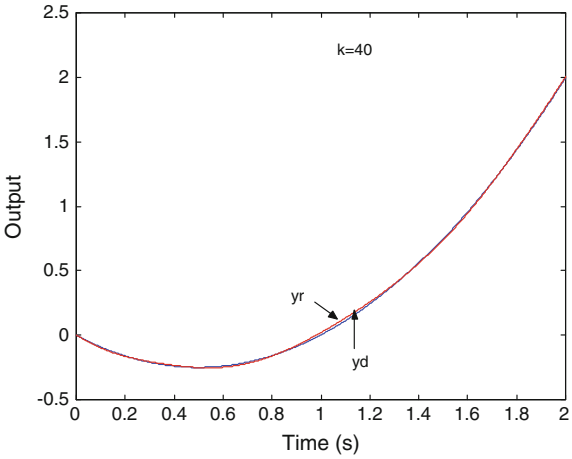

Fig. 10 Real and desired trajectories after 40 iterations

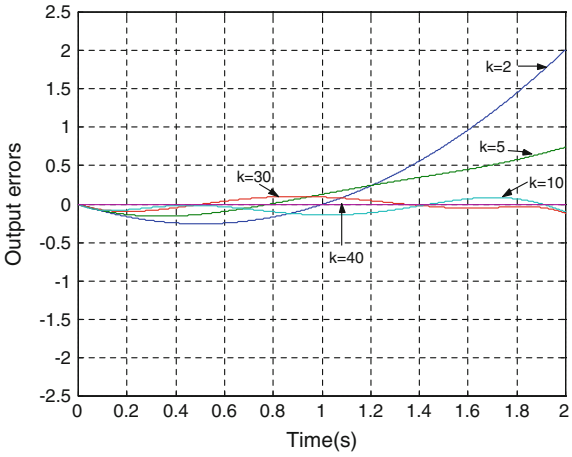

Fig. 11 Output errors for 2nd , 5th, 10th, 30th and 40th iteration

the desired trajectory without error. Figure 11 shows the trajectory tracking error for different number of iterations. It is clear that the trajectory tracking error decrease through the iterations. Therefore, we can conclude that the control algorithm works well.

5 Conclusion

In this chapter, two ILC schemes have been presented to solve the trajectory tracking problem of affine and non affine nonlinear systems performing repetitive tasks. The first law is a simple on-line 2D-type learning control applied to affine nonlinear systems. In this control scheme, the initial state value at each iteration is provided

automatically via an initial condition algorithm. Using λ-norm, the asymptotic stability of such controller is guaranteed, over the whole finite time interval when the iteration number tends to infinity. The second law is an on-line P-type ILC of non affine nonlinear systems. To prove the asymptotic stability of the closed loop system, a Lyapunov-like positive definite sequence is used. It is shown to be monotonically decreasing under the proposed control scheme. Finally, simulation results on nonlinear system are provided to illustrate the effectiveness of the two controllers. It is important to note that, the control laws here are very simple in the sense that there is no dependence with the system.

References

1. Arimoto S, Kawamura S, Miyazaki F (1984) Bettering operation of robots by learning. J Robot Syst 1:123–140
2. Berghuis H, Nijmeijer H (1993) A passivity approach to controller observer design for robots. IEEE Trans Robot Autom 9:740–754
3. Bouakrif F, Boukhetala D, Boudjema F (2010) Passivit based controller-observer for robot manipulators. Int J Robot Autom 25:1–8
4. Bouakrif F (2010a) Reference model iterative learning control for nonlinear systems. Int J Adv Manuf Tech 51:1159–1169
5. Bouakrif F (2010b) Reference model iterative learning control for linear systems. Proceedings, MED'2010, IEEE mediterranean conference on control and automation, 18:1637–1642
6. Bouakrif F (2011a) Iterative learning control for strictly unknown nonlinear systems subject to external disturbances. Int J Control Autom Syst 9:642–648
7. Bouakrif F (2011b) Iterative learning control with forgetting factor for robot manipulators with strictly unknown model. Int J Robot Autom 26:264–271
8. Bouakrif F (2011c) D-type iterative learning control without resetting condition for robot manipulators. Robotica 29:975–980
9. Bouakrif F (2012) Commande par apprentissage itératif des robots manipulateurs, pour résoudre le problème de poursuite de trajectoires. Editions Universitaires Européennes, Germany
10. Bouakrif F, Boukhetala D, Boudjema F (2013) Velocity observer based iterative learning control for robot manipulators. Int J Syst Sci 42:214–222
11. Bouakrif F (2013) Iterative learning control for MIMO nonlinear systems with arbitrary relative degree and no states measurement. Complexity 19:37–45
12. Casalino G, Bartolini G (1984) A Learning Procedure for the Control of Movements of Robotic Manipulators. IASTED Symposium on Robotics and Automation, Amsterdam, pp 108–111
13. Craig J. J. (1984). Adaptive Control of Manipulators Through Repeated Trials. Proceedings of the American Control Conference, San Diego, pp. 1566–1574
14. Ham C, Qu Z, Johnson R (2000) A nonlinear iterative learning control for robot manipulators in the presence of actuator dynamics. Int J Robot Autom 15:119–130
15. Jang T, Choi C, Ahn H (1995) Iterative learning control in feedback systems. Automatica 31:243–248
16. Lee KH, Bien Z (1991) Initial condition problem of learning control. IEE Proceedings D (Control Theory and Applications) 138:525–528
17. Li Y, Ang KH, Chong GCY (2006) PID control system analysis and design. IEEE Control Syst Mag 26:32–41
18. Park KH, Bien Z (2000) A generalized iterative learning controller against initial state error. Int J Control 73:871–881

19. Porter B, Mohamed SS (1991) Iterative learning control of partially irregular multivariable plants with initial state shifting. Int J Syst Sci 22:229–235
20. Sastry S, Bodson M (1989) Adaptive control: stability convergence and robustness. Prentice Hall, New Jersey
21. Sira-Ramirez H (1992) On the sliding mode control of nonlinear systems. Syst Control Lett 19:303–312
22. Sontag ED (1998) Mathematical control theory, 2nd edn. Springer, New York
23. Sun M, Wang D (2002) Iterative learning control with initial rectifying action. Automatica 38:1177–1182
24. Tayebi A (2004) Adaptive iterative learning control for robot manipulators. Automatica 40:1195–1203
25. Tayebi A (2007) Analysis of two particular iterative learning control schemes in frequency and time domains. Automatica 43:1565–1572
26. Wang HO, Tanaka K, Griffin MF (1996) An approach to fuzzy control of nonlinear systems: stability and design issues. IEEE Trans Fuzzy Syst 4:14–23
27. Xu JX, Yan R (2005) On initial conditions in iterative learning control. IEEE Trans Autom Control 50:1349–1354

On Nonlinear Robust Adaptative Control: Application on Electro-Hydraulic Valve System

Lilia Sidhom, Ines Chihi, Xavier Brun, Eric Bideaux and Daniel Thomasset

Abstract In this work, a robust adaptive control (RAC) of electro-hydraulic servo-system is investigated. The dynamics of hydraulic systems are highly nonlinear and the system may be subjected to some discontinuous nonlinearity due principally to servo-valve characteristics. Aside from the nonlinear nature of hydraulic dynamics, our test bench presents an intermediate interface between the actuator and the servo-valve, which leads to have some pressure drop between the servo-valve and the cylinder chambers. This pressure drop depends on some operating conditions. Therefore, the system may possess both parametric uncertainties and unknown nonlinear functions that may represent modelling errors. To address these challenging issues, the robust adaptive control (RAC) is applied. Based on adaptive update techniques, the parametric uncertainties are compensated. Moreover, a robust method is used to solve the problem derived from the modelling errors. The proposed controller ensure that the position tracking errors of the system remains bounded and can be made arbitrarily small. Simulation studies on the control of hydraulic servo-actuator show the effectiveness of the proposed scheme.

Keywords Electro-hydraulic system · Nonlinear system · Uncertainties model · Adaptive control · Lyapunov method · Robust control

L. Sidhom (✉) · I. Chihi
LARA Laboratory ENIT, Tunis, Tunisia
e-mail: lilia.sidhom@gmail.com

I. Chihi
e-mail: chihi4ines@hotmail.fr

X. Brun · E. Bideaux · D. Thomasset
AMPERE Laboratory UMR CNRS 5005, INSA-Lyon, Lyon, France
e-mail: xavier.brun@insa-lyon.fr

E. Bideaux
e-mail: freric.bideaux@insa-lyon.fr

D. Thomasset
e-mail: daniel.thomasser@insa-lyon.fr

S. Vaidyanathan and C. Volos (eds.), *Advances and Applications in Nonlinear Control Systems*, Studies in Computational Intelligence 635,
DOI 10.1007/978-3-319-30169-3_25

1 Introduction

Hydraulic actuators are widely utilized in industry, ranging from heavy-duty applications such as hydraulic manipulators to precision machine tool control and ground base simulators. Moreover, the compactness, the high force-to-mass ratio and the reliable performance of hydraulic actuators are factors that could potentially be exploited in sophisticated manipulator design. However, the dynamic behaviour of hydraulic systems is highly nonlinear. These nonlinearities depend on the servo-valve flow-pressure characteristics, change of the control volumes and the friction force equation [1]. Furthermore, the electro-hydraulic system has many uncertainties models, which are generated by both parametric uncertainties and uncertain nonlinearities. Parametric uncertainties consist to the large variations in the hydraulic parameters, due generally to the change of the operating conditions such as oil temperature and supply pressure. The other uncertainties include uncertain dynamics such as leakage flow, dry friction which can be described by some unknown functions.

The complexity of the electro-hydraulic systems and the important range of control laws are a real industrial problem where the target is to choose the best control strategy for an application. For this reason, some research efforts have been directed toward meeting this requirement. Most of them have been based on the linear control theory [2, 3]. But in such works, some important dynamic information may be lost when the hydraulic servo system is linearized around some operating point, during the design.

Therefore, it is important to choose a nonlinear control method that is reasonably suitable for hydraulic servo systems. Some numbers of investigations have been conducted on feedback linearization techniques [4–6]. But these methods did not account for model uncertainties and also require exact knowledge of the system dynamics. To overcome this problem, nonlinear robust control techniques are essentially used for controlling this kind of systems with a good performance. In this way, a sliding mode variable structure controller is adopted in electro-hydraulic systems in some research works [7–9]. A specific drawback associated with implementation of such technique is the chattering phenomenon, which is essentially a high frequency switching of the control. In effect, the presence of a discontinuous function in a controller design can affected the performance of the controlled system [10].

For an electro-hydraulic system, the adaptive control is considered as one valid method that can maintain consistent performances in the presence of some variations in plant parameters. There exists relatively little general theory for the adaptive control of nonlinear systems. In the previous research, some kinds of nonlinear robust adaptive control (RAC) laws have been investigated and applied for some application. For example, a feedback linearization adaptive control [6] and a nonlinear robust adaptive control based on backstepping technique are employed on [11–13]. In these latter works, the backstepping design procedures [14] are presented in order to design a global stable controller for a class of nonlinear systems transformable to a strict-feedback form. Some alternative approach is based on both sliding mode and an adaptive technique, which is defined by the integral-type adaptation law, [15]. In [16],

the authors applied nonlinear RAC in single-rod cylinder hydraulic system based on backstepping technique to compensate the uncertainties. A systematic design procedure to combine the adaptive control and the smoothed sliding mode control for tracking objectives of robot manipulators is presented in [17], where the control designer is described for a multi-input multi-output (MIMO) nonlinear system. In [18, 19] the authors consider that the original total control volumes are uncertain unknown nonlinear parameters. This kind of consideration can be useful when the dynamic system is affected by a small variation of the original control volumes.

In this work, we address the RAC of electro-hydraulic system with nonlinear and parametric uncertainties. The major contribution of this work concerns the effectiveness of the controller design on the real system. This system is a symmetric double acting electro-hydraulic servo-drive is considered. This system disposes of some interface block between the actuator and the servo-valve. The presence of this interface generates some pressure drop between the servo-valve and the cylinder chambers. This derived pressure decrease depends on the geometrical characteristics of the different pipes constituting this block, the velocity of the fluid and also the input exciting signal. In order to obtain a good performance, with presence of an intermediary interface, a RAC is applied. Effectively, this kind of technique can successfully solve the control problem, particularly in the presence of unknown parameters. Such control law gives an idea about the evolution of some unknown parameters, for example the value of the pressure drop caused by the intermediate block, in each operating conditions.

The RAC of single-input single-output (SISO) nonlinear system in a strict-feedback form is considered with allowing both parametric uncertainties and unknown nonlinear functions, with assuming a prior knowledge of some bounds. By introducing the projection technique to the integral-type adaptation law and based on the Lyapunov method, a simpler control law and adaptive mechanism are designed. We combine a defined adaptive controller with a conventional robust control method to obtain a RAC.

The outline of the work is as follows. In Sect. 2, the detailed nonlinear model is presented. In Sect. 3, the designed robust adaptive control for the electro-hydraulic system is given. The following section is dedicated to the simulation results and discussion.

2 Electro-Hydraulic Servo-System Model First Heading

Table 1 illustrates descriptions and units of several parameters used in this work.

The considered system Fig. 1 is a symmetric double acting electro-hydraulic servo-drive using a double-rod cylinder with a stroke of 330 mm, controlled by a five two-way servo-valve.

The intermediary interface is specifically produced for our test bench to implement two servo-valves in order to ensure different operating mode of the system. However

Table 1 List of notation

Parameter	Description	Unit
b	Viscous friction coefficient	N/m/s
M	Total load mass	kg
p	Pressure in the cylinder chamber	Pa
S	Area of the piston cylinder	m^2
V	Volume	m^3
y, v, a	Position, velocity, acceleration	m, m/s, m/s^2
ρ	Fluid density	kg/ m^3
$h(t)$	Dry friction function	N
l	Length of stroke	m
x_t	Spool valve displacement	m
ϕ	Pressure drop caused by the intermediary interface	Pa

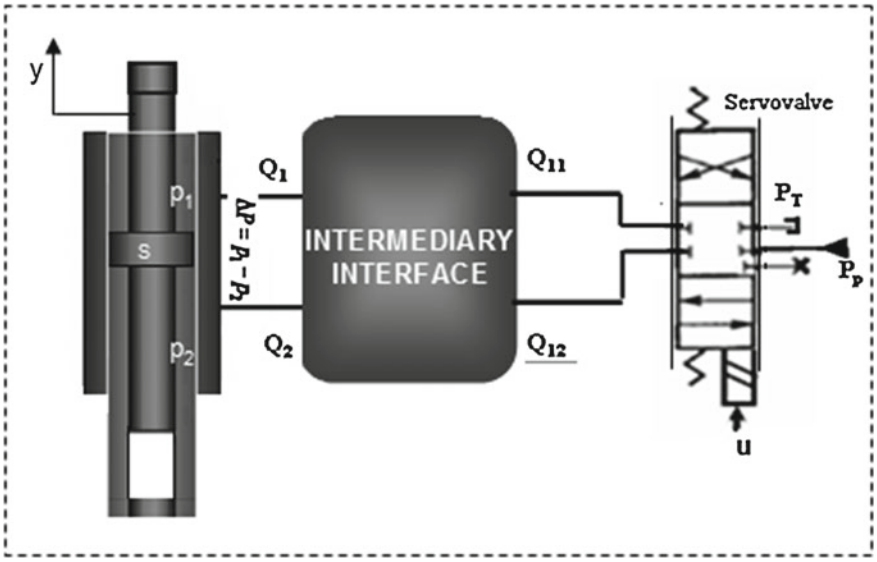

Fig. 1 Schematic diagram of the studied hydraulic system

the presence of this block, let to have output flow of servo-valve (Q_{11}, Q_{12}) is different than the input flow of the actuator (Q_1, Q_2), see Fig. 1.

In this work, the intermediate block is just approximated to a resistive component which is described by some pipes. The simulation model of the system is designed on the AMESim software, by the Fig. 2. This model introduces some components which are neglected on the control model. The added components in the simulation

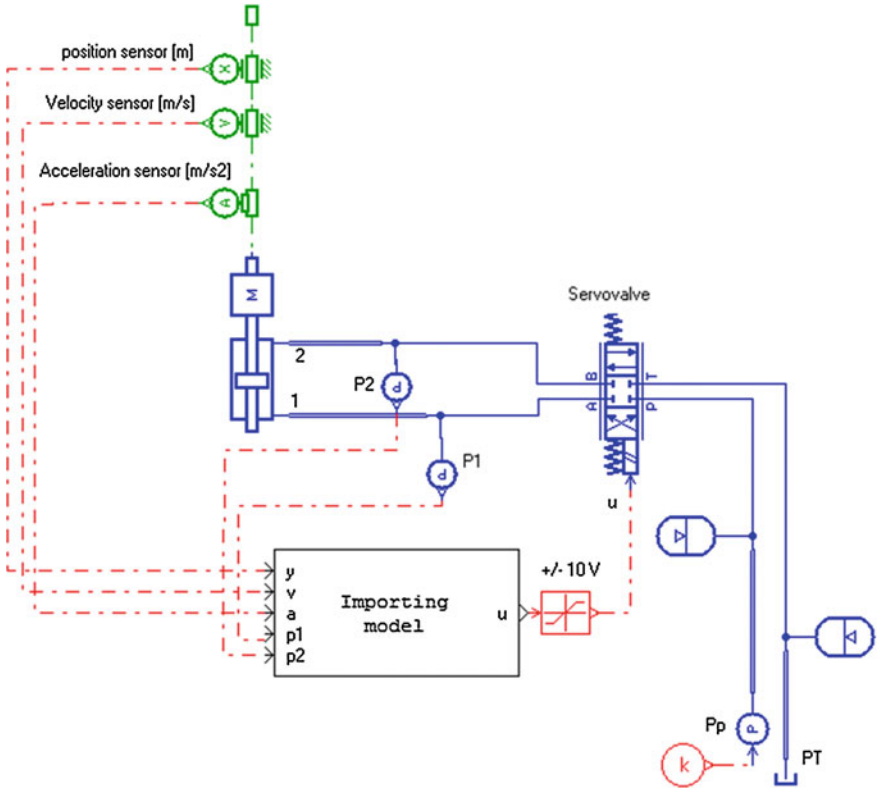

Fig. 2 Simulation model of the studied system

model include two pipes between the cylinder chambers and the servovalve in order to represent the intermediary block in a simplified way, two accumulators, and some lines respectively on the supply and exhaust pressure way. In this model, the dynamic of the servovalve is described by a second-order model. The pulsation of this model is fixed in order to be higher than the actuator. The viscous, stiction and coulomb friction forces are taken into account in this model.

As a first step, the control law defined in this work is designed by a more simplified model denoted by control model. The used equations of the control model are explained as below. The dynamic of the inertia load is:

$$Ma = S\Delta P - Mg - bv - h(t). \tag{1}$$

where M is the mass of the moving part, $\Delta P = p_1 - p_2$ is the drop across load piston, S is the effective area of the two chambers, b represents the coefficient of the viscous friction force, v, a are respectively the velocity and the acceleration of the load. Dry friction force is represented by the function $h(t)$. This function must be a nonlinear and a differentiable one with bounded value. For this reason, the dry friction force

is defined around null velocity by a smooth function such as a "tanh" instead of the "sign" function.

The governing nonlinear equations that describe the fluid flow distribution in the valve can be written in their simplest forms [1]:

$$\begin{cases} Q_1 = \frac{V_1(y)}{\beta}\frac{dp_1}{dt} + \frac{dV_1}{dt} \\ Q_2 = \frac{V_2(y)}{\beta}\frac{dp_2}{dt} + \frac{dV_2}{dt} \end{cases} \tag{2}$$

where β is the effective bulk modulus, V_1 and V_2 are the total volumes of the cylinder, defined respectively by $V_1(y) = V_0 + Sy$ and $V_2(y) = V_0 - Sy$, with: $V_0 = V_D + S\frac{l}{2}$ is the piping volume of the chambers for the zero position, V_D is a dead volume present on each extremities of the cylinder, y is the displacement of the load and l is the cylinder stroke. With D notes a subscript of the dead volume in the cylinder chamber, S and T are respectively a subscript denote a supply and an exhaust pressure.

In this present work, some assumptions are considered. Firstly consider that the spool valve displacement x is related to the control voltage u by a given equation: $x_t = K_{sv}u$. This type of assumption can be used in control [19] for some operating mode.

The flow laws can be written as follows:

$$\begin{cases} Q_1 = \eta \cdot \psi_1(p_1, p_P, p_T, \text{sign}(u))u \\ Q_2 = -\eta \cdot \psi_2(p_2, p_P, p_T, \text{sign}(u))u \end{cases} \tag{3}$$

where:

$$\begin{cases} \psi_1(p_1, p_p, p_T, \text{sign}(u)) = \alpha[\gamma(u)\sqrt{|p_P - p_1|}\text{sign}(p_P - p_1) \\ \qquad\qquad + \gamma(-u)\sqrt{|p_1 - p_T|}\text{sign}(p_1 - p_T)] \\ \psi_2(p_2, p_p, p_T, \text{sign}(u)) = [\alpha\gamma(u)\sqrt{|p_2 - p_T|}\text{sign}(p_2 - p_T) \\ \qquad\qquad + \gamma(-u)\sqrt{|p_P - p_2|}\text{sign}(p_P - p_2)] \end{cases} \tag{4}$$

with: $\gamma(u) = \frac{1+\text{sign}(u)}{2}$ and the function $\text{sign}(u)$ is defined by:

$$\text{sign}(u) = \begin{cases} 1 & u \geq 0 \\ -1 & u < 0 \end{cases}$$

p_P, p_T are respectively the supply pressure and the exhaust pressure of the fluid. The servo-valve is supposed a symmetric one, which justify the presence of the same variable gain η in the two flow laws. The flow gain η is defined by a given expression $\eta = C_q\omega\phi$, C_q is the flow coefficient of each restriction, ω is the spool valve area gradient, and ϕ is the pressure drop caused by the intermediary interface. Let us define the known variable α by $\alpha = K_{sv}\sqrt{\frac{2}{\rho}}$, where$\rho$ is a fluid density.

Note that under normal practical working condition, the domain of the pressure is defined by:

$$p_1, p_2 \in \Omega_p \triangleq \left]p_T, p_P\right[, \tag{5}$$

with the assumption (5), the term $\text{sign}(p_P - p_j)$ and $\text{sign}(p_j - p_T)$ introduced in (4) can be deleted, with $j = \{1, 2\}$.

Define the state variable $X = \left[y, v, a\right]^T$. The system can be expressed in state space form as:

$$\begin{cases} \dot{y} = v, \\ \dot{v} = a, \\ \dot{a} = \frac{\beta \cdot S}{M(V_0 + Sy)} \left(\eta \psi_1(p_1, p_p, p_T, \text{sign}(u))u - Sv\right) \\ \quad - \frac{S \cdot \beta}{M(V_0 - Sy)} \left(-\eta \psi_2(p_2, p_p, p_T, \text{sign}(u))u + Sv\right) - \frac{b}{M}a - \frac{\dot{h}(t)}{M}. \end{cases} \tag{6}$$

Given the desired trajectories y_d, v_d, a_d our work aims to synthesize a control input u such that the position tracking error of the system remains as closely as possible to zero in spite of various model uncertainties.

The desired trajectories are assumed to be all bounded and y_d must be chosen in order to respect the required differentiability.

3 Controller Design

The system is subjected to parametric uncertainties due to the variations of b, ω, C_q, ϕ and β in the work process for different environments conditions, as the influence of bulk modulus due to entrapped air or temperature. In this work, the parametric uncertainties of important parameters β, b and the coefficient flow gain η are taken into account. Moreover S, M, V_0 are considered as fixed and known parameters.

In this section we describe one class of SISO system to design a RAC for the considered nonlinear system. From the system (6), some conditions can be satisfied such that the nonlinear plant dynamics shall be linearly parameterized [19] and we suppose that the full state is measurable.

Let $c = \frac{V_0}{S}$, so the third equation of the system (6) can be rewritten:

$$\begin{aligned} \dot{a} = \frac{1}{(c+y)(c-y)} \Bigg[& (c-y)\left(\frac{\beta}{M}\eta\psi_1(p_1, p_p, p_T, \text{sign}(u))u - \frac{\beta}{M}Sv\right) \\ & -(c+y)\left(-\frac{\beta}{M}\eta\psi_2(p_2, p_p, p_T, \text{sign}(u))u + \frac{\beta}{M}Sv\right)\Bigg] - \frac{b}{M}a - \frac{\dot{h}(t)}{M} \end{aligned} \tag{7}$$

The above equation can be transformed in terms of unknown parameters θ_i as:

$$\dot{a} = \frac{1}{(c^2 - y^2)}[\theta_1 \psi\ (p_1, p_2, p_P, p_T, \text{sign}(u))\, u - 2\theta_2 v] - \theta_3 a - d(t). \tag{8}$$

where:

$$\begin{aligned}\psi(p_1, p_2, p_P, p_T, \text{sign}(u)) = (c - y)\psi_1(p_1, p_p, p_T, \text{sign}(u)) \\ +\ (c + y)\psi_2(p_2, p_p, p_T, \text{sign}(u))\end{aligned}$$

Thus

$$\begin{aligned}\psi(p_1, p_2, p_P, p_T, \text{sign}(u)) = c\psi_1(p_1, p_p, p_T, \text{sign}(u)) + c\psi_2(p_2, p_p, p_T, \text{sign}(u)) \\ -y\psi_1(p_1, p_p, p_T, \text{sign}(u)) + y\psi_2(p_2, p_p, p_T, \text{sign}(u))\end{aligned} \tag{9}$$

Define the unknown parameters as $\theta_1 = \frac{\beta\eta}{M}$, $\theta_2 = \frac{V_0\beta}{M}$, $\theta_3 = \frac{b}{M}$ and $d(t) = \frac{\dot{h}(t)}{M}$.

Before starting the controller design, some practical assumptions on the system must be made.

The first one is that all uncertain parameters are bounded such as:

$$\theta_i \in \left[\theta_{i_{\min}}, \theta_{i_{\max}}\right], i = \{1, 2, 3\}. \tag{10}$$

Physically, all θ_i are positives parameters. So we assume that $\theta_{i_{\min}} > 0$. The second assumption is described by the inequality $|d(t)| < H$, where H is a positive constant, defined by some maximum bound on the function $\dot{h}(t)$.

The displacement y satisfies this expression $-\frac{l}{2} \leq y \leq \frac{l}{2}$. So we have: $c = \frac{V_D}{S} + \frac{l}{2} > \frac{l}{2}$.

Remark that in spite of the simplifications already made, the system dynamics remains highly nonlinear such as the nonlinear functions $\psi_1(p_1, p_P, p_T, \text{sign}(u))$, $\psi_2(p_2, p_P, p_T, \text{sign}(u))$ and the change of control volumes represented by $V_1(y)$ and $V_2(y)$.

Consider now the position error as: $e_y = y - y_d$.

Let a function error $\sigma(t)$ described by (11). This function, introduced in [6], includes the integral term of e_y in order to cancel a static error:

$$\begin{aligned}\sigma(t) &= \left(k + \frac{d}{dt}\right)^3 \int_0^t e_y(\tau)d\tau, \\ &= k^3 \int_0^t e_y(\tau)d\tau + 3k^2 e_y + 3k e_v + e_a.\end{aligned} \tag{11}$$

where e_v, e_a are respectively a velocity and an acceleration error. A Hurwitz polynomial can be associated to the function $\sigma(t)$, if the parameter k is chosen as a positive one. Then the time derivative of $\sigma(t)$ along the trajectories system is given by:

$$\begin{aligned}\dot{\sigma}(t) &= \dot{e}_a + 3ke_a + 3k^2e_v + k^3e_y,\\ &= \dot{a} + \chi(t)\end{aligned} \tag{12}$$

With: $\chi(t) = -\dot{a}_d + \sum_{i=0}^{2} \varpi_i e_y^{(i)}(t)$.

Where $\varpi_0 = k^3$, $\varpi_1 = 3k^2$, $\varpi_2 = 3k$.

Basing on the Lyapunov approach, both a control law and an update mechanism is constructed in order to guarantee that the derivative of a suitable Lyapunov candidate function is non-positive. With the chosen function error $\sigma(t)$, a controller designer with a Lyapunov theory is easily applied. This is justified by the relative degree of $\sigma(t)$ with respect to the tracking errors, which it equal to one. Otherwise, the recursive design procedure must be used [12, 16, 17].

Let $\hat{\theta}_i$ the estimates of the parameters θ_i and denote $\tilde{\theta}_i$ the errors of parameters estimations defined by $\tilde{\theta}_i = \theta_i - \hat{\theta}_i$, for each $i = \{1, 2, 3\}$.

The integral-type update law is generally defined by some function which incorporate a tracking error and the estimated parameters. Indeed, the adaptive law can be written by $\dot{\hat{\theta}}_i = \tau_i(X, \hat{\theta}_i)$. So the aim consists to select a control input u which can be expressed by $u = \varphi(X, \hat{\theta}_i)$ and the adaptation functions τ_i to ensure a global stability of the whole system. To achieve the required purpose, a Lyapunov function candidate $V(X, \tilde{\theta}_i)$ is defined. This function is described by a quadratic term in the parameter estimation errors and the tracking error, which is given by:

$$V = \frac{1}{2}\sigma^2(t) + \frac{1}{2}\sum_{i=1}^{3} \tilde{\theta}_i^T \Gamma^{-1} \tilde{\theta}_i. \tag{13}$$

$\Gamma \in \mathbf{R}^{(3\times 3)}$ is a positive symmetric matrix.

The time derivative of the defined Lyapunov function V along the system trajectories is obtained as:

$$\begin{aligned}\dot{V} &= \sigma\dot{\sigma}(t) - \sum_{i=1}^{3} \tilde{\theta}_i^T \Gamma^{-1} \dot{\hat{\theta}}_i,\\ &= \sigma\left[\frac{1}{(c^2 - y^2)}\left(\theta_1 \psi(p_1, p_2, p_P, p_T, \text{sign}(u))u - 2\theta_2 v\right) - \theta_3 a - d(t) + \chi\right]\\ &\quad - \sum_{i=1}^{3} \tilde{\theta}_i^T \Gamma^{-1} \dot{\hat{\theta}}_i.\end{aligned} \tag{14}$$

In order to design a controller and adaptation laws, it is sufficient to replace θ_i by $\hat{\theta}_i + \tilde{\theta}_i$, in the Eq. (15). Then the control law can be structured as:

$$u = \frac{(c^2 - y^2)}{\hat{\theta}_1 \psi(p_1, p_2, p_P, p_T, \text{sign}(u))}\left[u_1 + u_2 + u_3\right]. \tag{15}$$

where $u_1 = -\chi$ is the controller part which allows the compensation of certain known components, $u_2 = \frac{2\hat{\theta}_2 v}{(c^2-y^2)} + \hat{\theta}_3 a$ is an adaptive part used to overcome the problem from uncertain parameters, u_3 is a robust part of controller defined in order to compensate the function $d(t)$ related to the poorly modelled dynamics of dry friction. Indeed, the robust controller is designed by $u_3 = -k_1\sigma - \frac{H}{\varepsilon}$. This choice is explained below. k_1, H and ε are positive constants.

It is clear that the singularity of the Eq. (15) happens when $\psi(p_1, p_2, p_P, p_T, \text{sign}(u)) = 0$, which can be occur when the pressure in the two chambers are equal respectively to the supply and the exhaust pressure. Or according to the assumption (5), this problem is avoided.

Substituting (15) into (14) $\dot{V}$ becomes:

$$\begin{aligned}\dot{V} = -k_1\sigma^2 - \tilde{\theta}_1 \frac{\psi(p_1, p_2, p_P, p_T, \text{sign}(u))}{(c^2 - y^2)}\sigma u - \frac{2v}{(c^2 - y^2)}\tilde{\theta}_2\sigma \\ - \tilde{\theta}_3 a\sigma - \sigma d(t) - \frac{H}{\varepsilon}\sigma - \sum_{i=1}^{3} \tilde{\theta}_i^T \Gamma^{-1}\dot{\hat{\theta}}_i\end{aligned} \tag{16}$$

To make sure that $\dot{V}$ is semi-definite negative, the adaptation laws can be chosen as:

$$\begin{cases} \dot{\hat{\theta}}_1 = \tau_1 = \Gamma_{11}\sigma \frac{\psi(p_1, p_2, p_P, p_T, \text{sign}(u))}{(c^2-y^2)} u, \\ \dot{\hat{\theta}}_2 = \tau_2 = -\Gamma_{22}\frac{2v}{(c^2-y^2)}\sigma \\ \dot{\hat{\theta}}_3 = \tau_3 = -\Gamma_{33}\sigma a. \end{cases}, \tag{17}$$

where Γ_{11}, Γ_{22}, Γ_{33} are the components of the matrix Γ.

With the knowledge of the set values of estimated parameters, it is interesting to use this information for the adaptation mechanism designer. Indeed, the knowledge of $\theta_{i_{\min}}$ and $\theta_{i_{\max}}$ for each parameters helps to speed up the convergence of adaptive mechanism, reduce the transition effect and prevent $\hat{\theta}_1$ from tacking the value zero.

For meeting this requirement, a simple modification is introduced at the equations of adaptation law (18):

$$\dot{\hat{\theta}}_i = \text{Proj}\{\tau_i\}, i = \{1, 2, 3\}.$$

So this modification is just described by the discontinuous projection [11]:

$$\text{Proj}(\tau_i) = \begin{cases} 0 & \text{if } \hat{\theta}_i = \theta_{i_{\max}} \text{ and } \tau_i > 0, \\ 0 & \text{if } \hat{\theta}_i = \theta_{i_{\min}} \text{ and } \tau_i < 0, \\ \tau_i & \text{Otherwise.} \end{cases} \tag{18}$$

The projection method presented in [18] guarantees the condition (10) and always holds the following equation $\tilde{\theta}_i^T(\Gamma^{-1}\text{Proj}(\tau_i) - \tau_i) \leq 0$.

Thus, from the system (18) the system (17) can be rewritten as:

$$\dot{\hat{\theta}}_i = \text{Proj}\left\{\Gamma\sigma\left[\frac{\psi(p_1, p_2, p_P, p_T, \text{sign}(u))}{(c^2 - y^2)}u, -\frac{2v}{(c^2 - y^2)}, -a\right]^T\right\}. \tag{19}$$

Substituting the adaptation laws defined by (19) into the Eq. (16):

$$\dot{V} \leq -k_1\sigma^2 - \sigma \cdot d(t) - \frac{H}{\varepsilon}\sigma. \tag{20}$$

In order to ensure the non-positiveness of $\dot{V}$, we must impose some positive bound value ε on σ, which is chosen arbitrarily. The proof is done by the contraposition.

Supposed that $|\sigma| \geq \varepsilon$ and we know that $|d(t)| \leq H$, so in this sense two cases can be presented. If $\sigma \geq \varepsilon$ and $d(t) \geq -H$ the following equation can be written:

$$\frac{\sigma^2}{\varepsilon} \geq \sigma \Rightarrow \frac{H\sigma^2}{\varepsilon} \geq H\sigma, \tag{21}$$

$$H\sigma \geq -\sigma d(t). \tag{22}$$

With both Eqs. (21) and (22), the following inequality is checked:

$$\sigma \cdot d(t) + \frac{H}{\varepsilon}\sigma \geq 0. \tag{23}$$

In the same manner, the Eq. (23) is obtained for $\sigma \leq -\varepsilon$ and $d(t) \leq H$.

Then, we have $\dot{V} \leq 0$ which implies that $|\sigma| \leq \varepsilon$ and the parameter estimation errors remain bounded and also can be made arbitrarily small.

Based on the work done in [20], the function $\delta(t) = e_y(t)e^{kt}$ can be defined. So we can obtain:

$$\dddot{\delta}(t) = \dot{\sigma}(t)e^{kt}. \tag{24}$$

Integrating (24), the following equation holds:

$$\ddot{\delta}(t) - \ddot{\delta}(0) = \sigma(t)e^{kt} - \sigma(0) - k\int_0^t \sigma(\tau)e^{k\tau}d\tau.$$

Then we can write,

$$\left|\ddot{\delta}(t) - \ddot{\delta}(0) + \sigma(0)\right| \leq |\sigma(t)|\, e^{kt} + k\int_0^t |\sigma(\tau)|\, e^{k\tau}d\tau.$$

And we have $|\sigma(t)| \leq \varepsilon$.

Then,

$$\begin{cases} \dddot{\delta}(t) \leq 2\varepsilon e^{kt} + \xi_1, \\ \dddot{\delta}(t) \geq -2\varepsilon e^{kt} + \xi_1'. \end{cases} \tag{25}$$

where

$$\begin{cases} \xi_1 = \ddot{\delta}(0) - \sigma(0) - \varepsilon, \\ \xi_1' = \ddot{\delta}(0) - \sigma(0) + \varepsilon. \end{cases}$$

Integrate the first equation of system (25) at three times, so these following inequalities are:

$$\begin{aligned} \delta(t) &\leq \frac{2\varepsilon}{k^2} e^{kt} + (\xi_1 t^2 + \xi_2 t + \xi_3) \\ &\Rightarrow e_y(t) \leq \frac{2\varepsilon}{k^2} + (\xi_1 t^2 + \xi_2 t + \xi_3) e^{-kt} \end{aligned} \tag{26}$$

With ξ_2, ξ_3 are constants which include the initial condition of $\dot{\delta}(0), \delta(0)$ where:

$$\begin{cases} \xi_2 = \dot{\delta}(0) - \frac{2\varepsilon}{k}, \\ \xi_3 = \delta(0) - \frac{2\varepsilon}{k^2}. \end{cases}$$

Thus when time tends to infinity, the inequality (26) becomes

$$e_y(t) \leq \frac{2\varepsilon}{k^2}.$$

From the second equation of system (25), we can show in the same manner the following inequality:

$$e_y(t) \geq -\frac{2\varepsilon}{k^2}.$$

So we can deduce that for a bounded function error, $\sigma(t)$ the absolute value of the error dynamics $e_y(t)$ is bounded by $\frac{2\varepsilon}{k^2}$.

Finally we have that $\sigma(t)$, the tracking position error $e_y(t)$ and all state variables of system (6) are bounded. Moreover with the discontinuous projection included in the adaptation law, we ensure that all estimated parameters are always bounded and satisfy the Eq. (10). The fact that the Lyapunov function V is semi-negative implies:

$$\sum_{i=1}^{3} \tilde{\theta}_i^T(t) \Gamma^{-1} \tilde{\theta}_i(t) \leq 2V(t) \leq 2V(0).$$

then

$$\sum_{i=1}^{3} \tilde{\theta}_i^T(t) \Gamma^{-1} \tilde{\theta}_i(t) \leq \sigma^2(0) + \sum_{i=1}^{3} \tilde{\theta}_i^T(0) \Gamma^{-1} \tilde{\theta}_i(0).$$

This bound shows that the possibility for reducing the estimation parameters errors lies in $\sigma(0)$, that could be chosen as small as possible.

So we can conclude that the synthesized controller permit a global stability of the closed loop system with a bounded position error.

4 Simulation Results

To illustrate the above controller design, a simulation results are obtained for a hydraulic cylinder. The control model of system and the controller design are both developed on the Simulink software. The sampling frequency of the control loop is equal to 1 Khz.

The value of position tracking error is related to controller parameter k and ε, with the last one can be chosen arbitrarily. As the placement of poles, the value of the gain k can be computed taking into account the natural frequency of the tangent linearized model for the central position. This pulsation is about 1000(rad/s). So we can impose the closed-loop dynamics system by acting on the gain k. For example, we can choose the value of k in order to obtain the closed-loop system twice faster than the open-loop one. On the other hand, when k is so high, the performance of the control system and the update laws will be affected by some chattering phenomenon. Therefore, it is important to select an appropriate k.

Note that the stability and convergence of the RAC is guaranteed for any positive Γ_{11}, Γ_{22}, Γ_{33}. However, the performance of the controller will depend critically on these gains. If small gains are chosen the adaptation will be slow and the transient tracking error will be large. Conversely, when the magnitudes of the gains are too large will lead to very oscillatory parameters. Therefore, the choice of these parameters is a difficult task.

The desired trajectory is a sinusoidal curve given by $y_d(t) = 0.01\sin(10t)$. The true system parameters that are used in the control model are set as follows: $b = 400\,(\mathrm{N/m} \cdot \mathrm{s}^{-1})$, $\beta = 17{,}000\,(\mathrm{bars})$ and $\eta = 2.545 \times 10^{-7}\,(\mathrm{Kg/s} \cdot \mathrm{Pascal} \cdot \mathrm{V})$.

A direct validation is carried out to the control model. It consists in comparing respectively the actual position, velocity and acceleration to their desired one (Figs. 3, 5, 7). These figures show the effectiveness of the control schema. Figures 4, 6 and 8 illustrate that the errors of position, of velocity and of acceleration are very small.

Figures 9, 10 and 11 shows the evolution and the convergence of the dynamic parameters along the tracking trajectory and the control law is presented in Fig. 12.

The identified parameters correspond to the a priori values of the model system with small relative standard deviations which can due to the features of the reference signals.

With appropriate chosen of adaptation gains, the parameter convergence has the smallest transient tracking error.

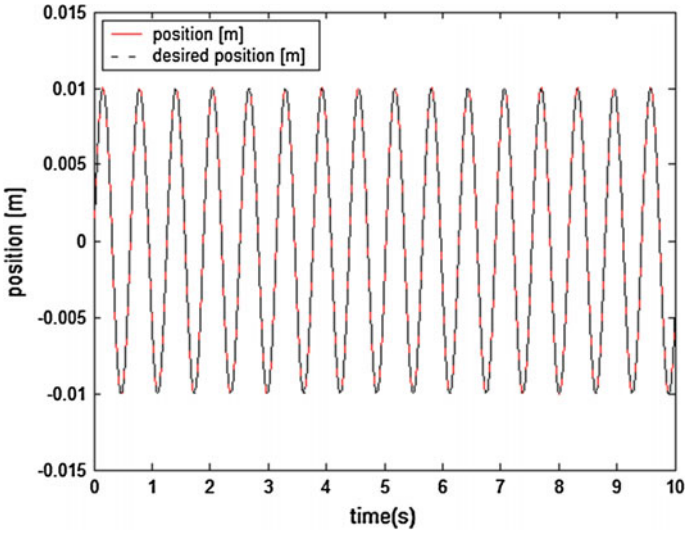

Fig. 3 Position and desired position

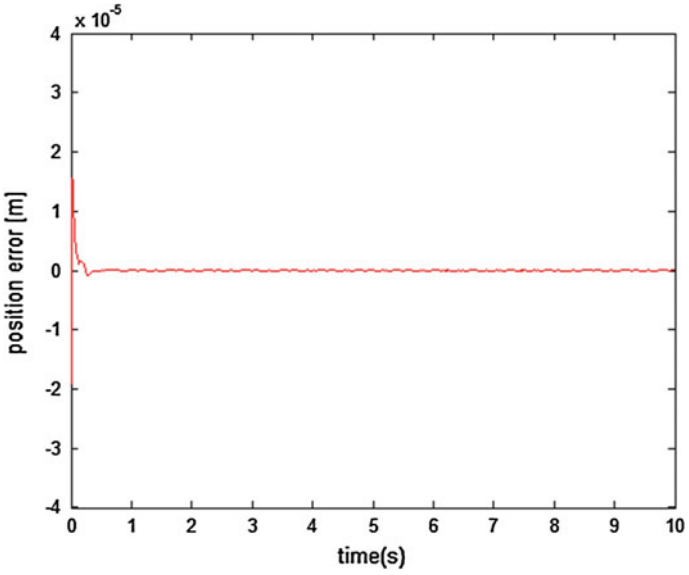

Fig. 4 Error position

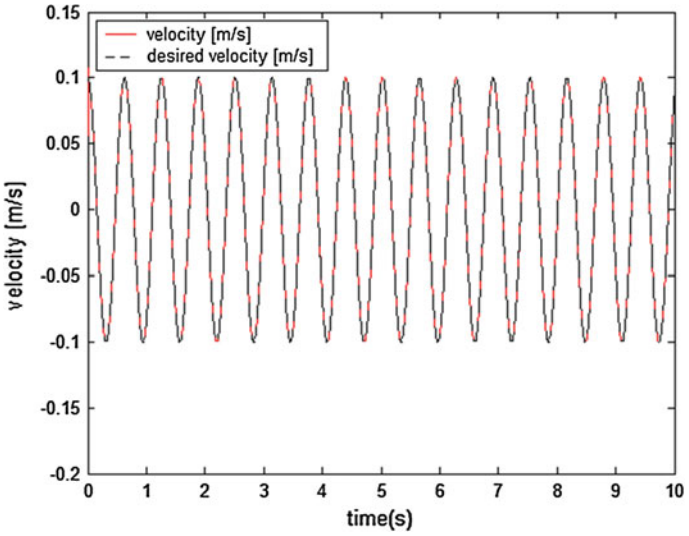

Fig. 5 Velocity and desired velocity

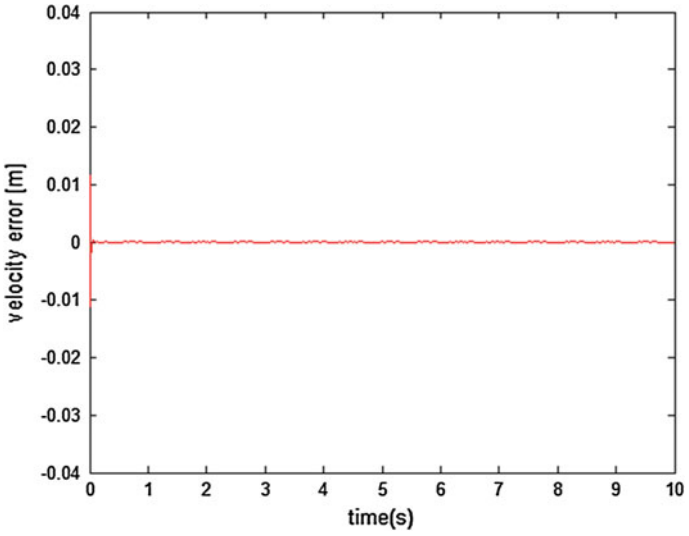

Fig. 6 Error velocity

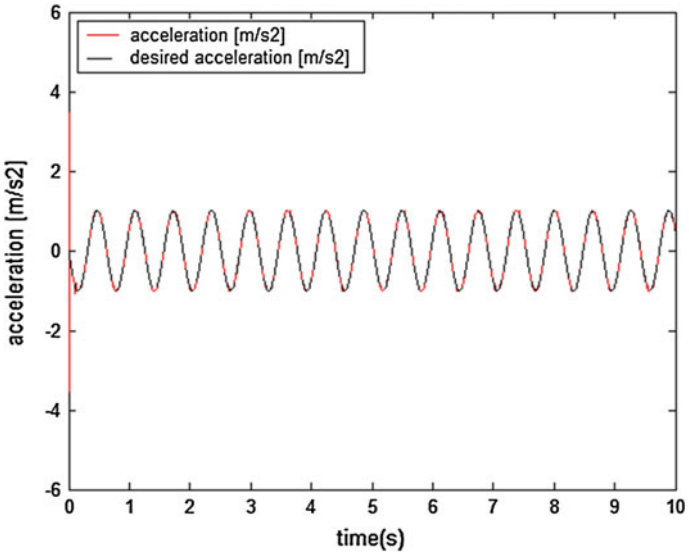

Fig. 7 Acceleration and desired acceleration

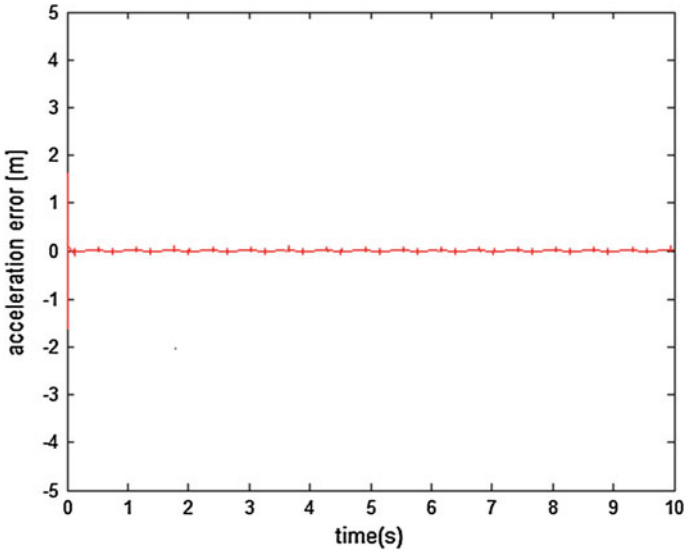

Fig. 8 Error acceleration

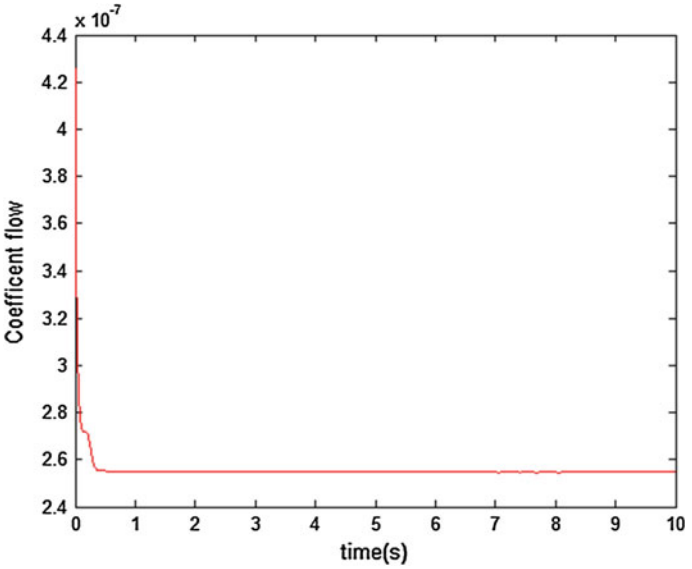

Fig. 9 Evolution of parameter $\hat{\eta}$

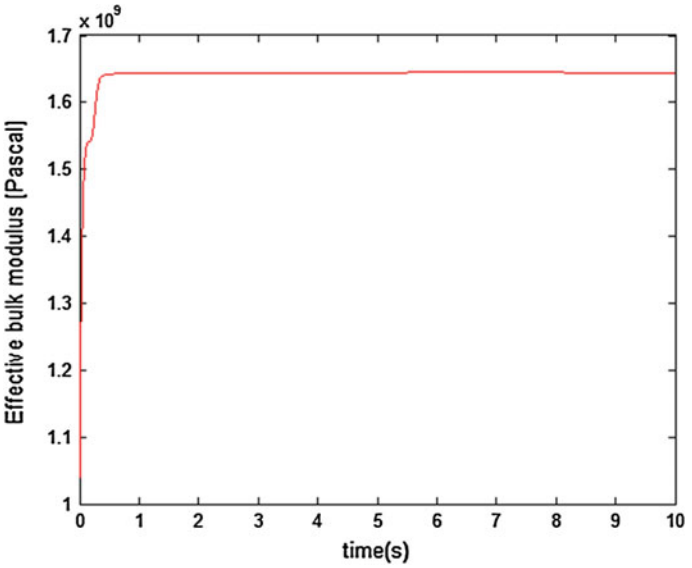

Fig. 10 Evolution of parameter $\hat{\beta}$

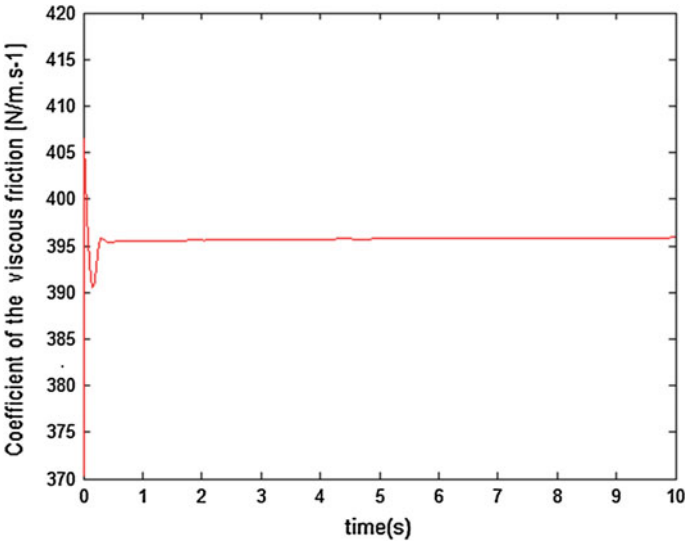

Fig. 11 Evolution of parameter $\hat{b}$

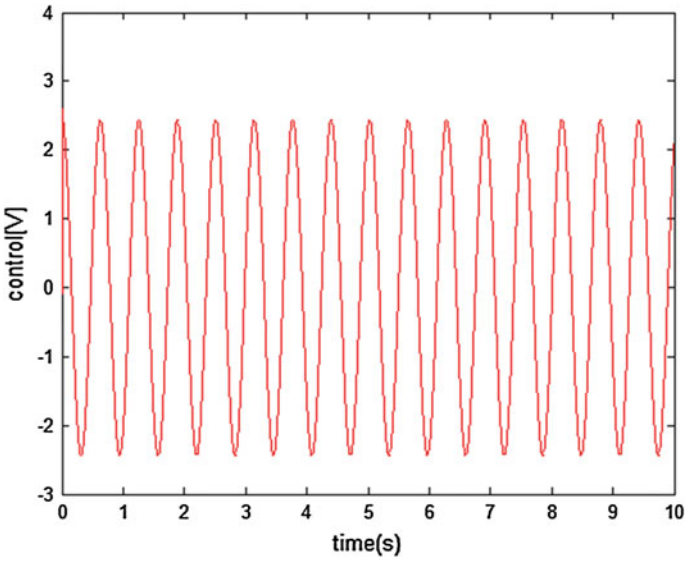

Fig. 12 Control law

5 Conclusion and Perspectives

In this work, an RAC controller based on discontinuous projection method is applied for the high performance robust motion control of a special electro-hydraulic servo-system. The controller which is based on the Lyapunov theory takes into account the particular nonlinearities associated with hydraulic dynamics and allows parametric uncertainties as well as uncertain nonlinearities coming from uncompensated friction dry forces. Simulation results show that the proposed scheme achieves a better tracking performance. The basic idea in this application of this controller is especially to estimate on-line the coefficient of flow gain, based on the measured system signals and using the estimated parameters in the control input computation.

From this study we can consider several future works. One is to show the effectiveness of the presented controller on the simulation model already presented and also on the test bench. Another is the consideration of the partial measured of the state. So in this case, the study of an estimator is required. The third one consists to replace the actually robust method by a sliding integral smoothing technique.

References

1. Alleyne A, Hedrick JK (1995) Nonlinear adaptive control of active suspensions. IEEE Trans Control Syst Technol 1:94–101. doi:10.1109/87.370714
2. Bobrow JE, Lum K (1996) Adaptive, high bandwidth control of a hydraulic actuator. ASME J Dyn Syst Meas Contr 4:714–720. doi:10.1115/1.2802347
3. Bonchis A, Corke PI, Rye DC, Ha QP (2001) Variable structure methods in hydraulic servo systems control. Automatica 37:589–595. doi:10.1016/S0005-1098(00)00192-8
4. Bu F, Yao B (2001) Integrated direct/Indirect adaptive robust motion control of single-rod hydraulic actuators with time-varying unknown inertia. In: IEEE/ASME international conference on advanced intelligent mechatronics proceedings, Como, Italy
5. Bouri M, Thomasset D (2001) Sliding control of an electropneumatic actuator using an integral switching surface. IEEE Trans Control Syst Technol 9(2):368. doi:10.1109/87.911388
6. Guan C, Pan S (2008) Adaptive sliding mode control of electro-hydraulic system with nonlinear unknown parameters. Control Eng Pract 11:1275–1284. doi:10.1016/j.conengprac.2008.02.002
7. Guan C, Pan S (2008) Nonlinear adaptive robust control of single-rod electro-hydraulic actuator with unknown nonlinear parameters. IEEE Trans Control Syst Technol 16:434. doi:10.1109/TCST.2007.908195
8. Hisseine D (2005) Robust tracking control for a hydraulic actuation system. IEEE Conf Control Appl 1:422–427
9. Isidori A (1989) Nonlinear control systems design. Springer, New York, p 479
10. Krstiçacute M, Kanellakopoulos L, Kokotoviçcute P (1995) Nonlinear and adaptive control design. Wiley, New York, p 563
11. Merritt HE (1967) Hydraulic control systems. Wiley, New York, p 368
12. Li D, Salcuden SE (1997) Modeling, simulation, and control of a hydraulic stewart platform. IEEE Int Conf Robot Autom 4:3360–3366
13. Liu Y, Handroos H (1999) Technical note sliding mode control for a class of hydraulic position servo. Mechatronics 1:111–123
14. Slotine JE, Li W (1991) Applied nonlinear control. Prentice-Hall, Englewood Cliffs, p 461

15. Plummer AR, Vaughan ND (1996) Robust adaptive control for hydraulic servosystems. ASME J Dyn Syst Meas Control 118:237–244. doi:10.1115/1.2802309
16. Re LD, Isidori A (1995) Performance enhancement of nonlinear drives by feedback linearization of linear-bilinear cascade models. IEEE Trans Control Syst Technol 2:299–308. doi:10.1109/87.406977
17. Yao B, Bu F, Chiu GTC (1998) Nonlinear adaptive robust control of electro-hydraulic servo systems with discontinuous projections. IEEE Conf Decis Control pp. 2265–2270
18. Yao B, Bu F, Reedy J, Chiu GTC (2000) Adaptive robust motion control of single-rod hydraulic actuators: theory and experiments. IEEE/ASME Trans Mechatron 5(1):79–91. doi:10.1109/3516.828592
19. Yao B, Bu F, Chiu GTC (2001) Non-linear adaptive robust control of electro-hydraulic systems driven by double-rod actuators. Int J Control 8:761–775. doi:10.1080/002071700110037515
20. Yao B, Tomizuka M (1997) Adaptive robust control of SISO nonlinear systems in a semi-strict feedback form. Automatica 33:893–900. doi:10.1016/S0005-1098(96)00222-1

Nonlinear Discrete Time Sliding Mode Control Applied to Pumping System

Asma Chihi and Anis Sellami

Abstract In this chapter, a discrete time Indirect Field Oriented Control (IFOC) by sliding mode applied to pumping system is studied. The main contribution of this work is to design a novel form of switching surfaces which presented by an addition of an integral term into the considered sliding surfaces. First, an overview of pumping system is presented. Second, sliding mode controllers are designed by using the new concept of proposed switching surfaces. Then, the stability of digitized sliding mode control pumping system is investigated. After that, a comparative study is given to validate the proposed control. To illustrate the effectiveness of the proposed controllers, simulation results is developed and discussed.

Keywords Discrete time sliding mode control (DSMC) · Pumping system · Switching surfaces · Stability analysis

1 Introduction

Nonlinear control theory have been developed in the last decades both in continuous time and in discrete time with respect to their nonlinearity. The sampled dynamical model is performed in two methods: the first one is a simple digital implementation of the continuous control using the zero order hold. But, this techniques allows a small sampling time compared with the dynamical process. Using this methods we cannot maintained the control objectives because some dynamical performances change into the passage of the continuous case to the discrete one. The second method is to develop the digitized control to the sampled process. This technique includes the calculation of the numerical control. So, the control objectives is achieved.

A. Chihi (✉) · A. Sellami
Unit C3S, High School of Sciences and Techniques of Tunis (ENSIT),
5 Av. Taha Hussein, BP 56, 1008 Tunis, Tunisia
e-mail: asma.chihi@live.fr

A. Sellami
e-mail: anis.sellami@esstt.rnu.tn

S. Vaidyanathan and C. Volos (eds.), *Advances and Applications in Nonlinear Control Systems*, Studies in Computational Intelligence 635,
DOI 10.1007/978-3-319-30169-3_26

The industrial applications [1, 6, 8, 10, 15] (such as: the induction motor, pumping system, robotics, etc.) recourse to different form of control such as: Indirect Field Oriented Control (IFOC), Direct Torque Control (DTC), Fuzzy Logic Control (FLC) and Sliding Mode Control (SMC). All these one are designed both in continuous time and discrete time [11]. The development of the microprocessor makes frequent the utilization of the discrete time. For this reason, we choose to use the SMC in discrete time.

In [3, 4], Castillo define the switching surfaces as the error between the selected variable and its references. But, in some different application we are interested by the system performances especially when it comes to a pumping system, it must specify with accuracy the pressure and flow when pumping wants. For that, the objectives of this work is to develop a novel switching surfaces witch presents an addition of an integral term into the surfaces defining the proposed control. The aims of this methods is the control of torque and speed respectively the head (H) and le flow (Q) with more performances for the complete pump unit. This work is organized into seven sections. After introduction, the problem statement is designed. Then, an overview of pumping system is presented. The third section develop the discrete time sliding mode control with defining the novel switching surfaces. The forth section gives the stability analysis. Section five, allows the simulation results. The last section, gives a comparative study. Finally, a conclusion is drawn.

2 Overview of Pumping System

Pumping, ventilation and compression systems are shown in many industrials applications. For example, in water sector the pump is used for irrigation, distribution and processing. In oil and gas sector, the pump is used for transportation and extraction. The recourse of this type of system is frequently used because the model of pump is simple to use, robust and relatively inexpensive to produce. Specially, the centrifugal pump occurs a wide range of power, flow and pressure. The significant value used in the pumping systems are: the flow (Q) and the Head (H): the flow represents the volume of transported fluid per unit time; it's expressed in m3/s. The head represents the pressure in a given point of the circuit, expressed as a column height of the transported fluid in (m). The relation between the head and the pressure is given by Eq. (1):

$$\mathrm{Pr} = \rho g H \tag{1}$$

with
Pr = pressure (Pa)
ρ = volumetric fluid mass
g = acceleration of gravity.
In water the volumetric fluid mass is equal to 1000 Kg/m^3.

The pump is characterized by a nominal operating point which is defined as a point where the efficiency of the pump is maximum. It exists a similitude law which can helped in determining the pressure and flow in different operating point. There is presented by:

$$\begin{aligned} Q_{N'} &= Q_N{}^* \frac{N'}{N} \\ H_{N'} &= H_N{}^* \left(\frac{N'}{N}\right)^2 \\ P_{N'} &= P_N{}^* \left(\frac{N'}{N}\right)^3 \end{aligned} \tag{2}$$

3 Problem Statement

The proposed system is constituted by an induction motor coupled to pump. The aims of this work is to design a control law based on Indirect Field Oriented Control (IFOC) by sliding mode in discrete time. The objective is to control the torque and speed respectively pressure and flow [5]. Figure 1 present a strategy of this control system.

The main problem of this type of system is to maintain a robustness and accuracy in the same time. But, the recourse of both present an important task.

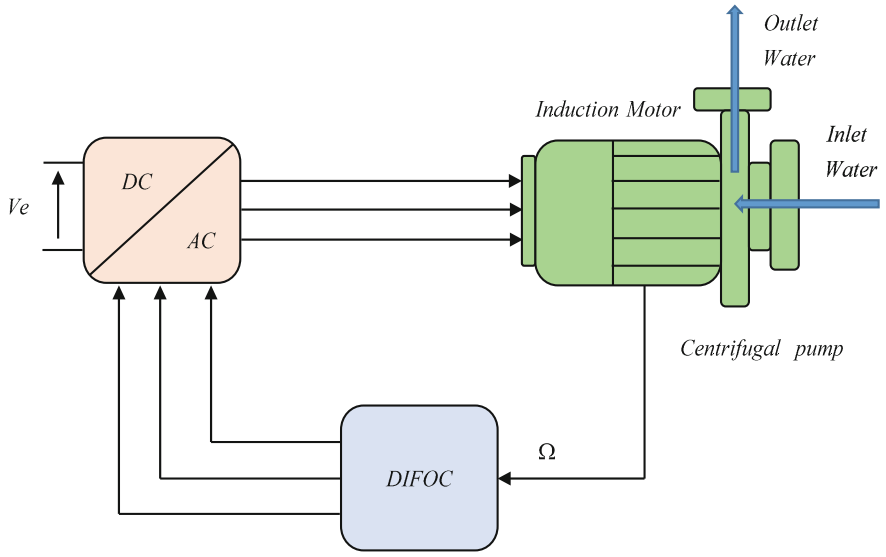

Fig. 1 Dynamical system strategy

Consider a mathematical model defining the induction motor with discrete time approach by applying a zero order hold sampled that the control law $u(t) = u(k)$ for to time $t \in$ [kTe, (k + 1)Te], where: Te is the sampled period. So, referring to Euler's discretization, the system defining induction motor is written by [12, 17]:

$$\begin{cases} a) \;\; i_{sd}(k+1) = i_{sd}(k) - Te\left(\frac{1}{\sigma\tau_s} + \frac{1-\sigma}{\sigma\tau_r}\right) i_{sd}(k) + \frac{Te(1-\sigma)}{\sigma M_{sr}\tau_r}\varphi_{rd}(k) \\ \qquad\qquad + \frac{Te(1-\sigma)}{\sigma M_{sr}}\varphi_{rq}(k)w(k) + \frac{Te}{\sigma L_s}V_{sd}(k) \\ b) \;\; i_{sq}(k+1) = i_{sq}(k) - Te\, w_{dq} i_{sd} - Te\left(\frac{1}{\sigma\tau_s} + \frac{1-\sigma}{\sigma\tau_r}\right) i_{sq}(k) \\ \qquad\qquad - \frac{1-\sigma}{\sigma M_{sr}} w(k)\varphi_{rd}(k) + \frac{Te(1-\sigma)}{\sigma M_{sr}\tau_r}\varphi_{rq}(k) + \frac{Te}{\sigma L_s}V_{sq}(k) \\ c) \;\; \varphi_{rd}(k+1) = \varphi_{rd}(k) + Te\frac{M_{sr}}{\tau_r} i_{sd}(k) - \frac{Te}{\tau_r}\varphi_{rd}(k) - w(k)\varphi_{rq}(k) \\ d) \;\; \varphi_{rq}(k+1) = \varphi_{rq}(k) + Te\frac{M_{sr}}{\tau_r} i_{qs}(k) + w(k)\varphi_{dr}(k) - \frac{Te}{\tau_r}\varphi_{qr}(k) \\ e) \;\; w(k+1) = w(k) + Te\frac{3}{2}\frac{np^2}{j}\frac{M_{sr}}{L_r}(\varphi_{rd}(k) i_{sq}(k) \\ \qquad\qquad - \varphi_{rq}(k) i_{sd}(k)) - Te\frac{np}{j}(C_r(k) - C_f(k)) \end{cases} \tag{3}$$

where:

$Ids, Iqs =$ d-, q-axis stator current components,
$\varphi_{dr}, \varphi_{qr} =$ d-, q-axis rotor flux components,
$wsl =$ slip angular speed (wdq-wr),
$wdq =$ synchronous angular speed,
$Rr, Rs =$ rotor and stator resistances,
$Msr =$ cyclic mutual inductance stator-rotor,
$Lr, Ls =$ rotor and stator self-inductions,
$\tau_s, \tau_r =$ stator and rotor time constant,
$\sigma =$ leakage coefficient,
$np =$ pole-pair number,
$j =$ inertia,
$Cf =$ friction torque,
$Cr =$ load torque,
$k =$ Continuous time,
$Te =$ sampling time.

Same to the continuous case, the switching surfaces is presented by:

$$s_k = Cx_k \tag{4}$$

where $C \in \Re^{1Xn}$ is such that the system is maintain the switching manifold.

$$s = \{x_k / Cx_k = 0\} \tag{5}$$

Definition 1 System (1) is said to be in a Quasi Sliding Mode (QSM) in the Δ vicinity of the switching manifold (4), if a motion of the system (3) satisfies $\{x_k / |Cx_k| \leq \Delta\}$ for all $k \geq k^*$(k^* is a constant integer). The specified space domain where the QSM occurs is called the QSMD and the positive constant Δ called the width of the QSMD.

Definition 2 System (3) is said to satisfy the reaching condition of the QSM in the Δ vicinity of the switching manifold (4) in the following condition hold: when $s_k > \Delta$, then $-\Delta \leq s_{k+1} < s_k$; when $s_k < -\Delta$, then $s_k < s_{k+1} \leq \Delta$; and when $|s_k| \leq \Delta$, then $|s_{k+1}| \leq \Delta$, [16].

4 Discrete Sliding Mode Control

The design of the Discrete Sliding Mode Control (DSMC) is constitute by two tasks [2, 9, 16]: The first one, establish a sliding mode controller u_k that the closed loop system (3) satisfies the reaching law conditions in Definition 2. The second one, design a switching surfaces (4) such that the closed loop system (3) is stable. The discrete IFOC based on sliding control is constituted by three regulators such as: speed controller, direct stator current controller and quadratic stator current controller. The induction motor is modeled in (d–q) stationary reference frame. That is $\varphi_{rd} = \varphi_r$ and $\varphi_{rq} = 0$. The control strategy is defined by Fig. 2.

4.1 Switching Surfaces Design

Several investigator defined the switching surfaces as the error between the selected variable and its reference Eq. (6), [3, 4]:

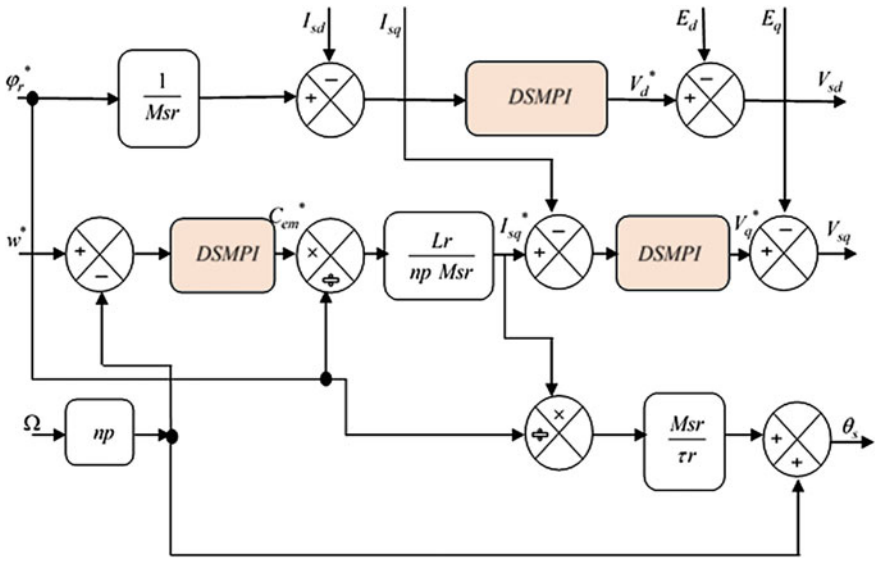

Fig. 2 Discrete sliding mode control design

$$\begin{cases} \mathrm{s}_w = \mathrm{c}_1 e_w \quad with \quad e_w = w^* - w \\ \mathrm{s}_d = \mathrm{c}_2 e_d \quad with \quad e_\mathrm{d} = \mathrm{I}^*_{sd} - \mathrm{I}_{sd} \\ \mathrm{s}_q = \mathrm{c}_3 e_q \quad with \quad e_\mathrm{q} = \mathrm{I}^*_{sq} - \mathrm{I}_{sq} \end{cases} \tag{6}$$

Due to ameliorate the performance of the system, that obtained a faster response time and zero steady state error, we added an integral term to the switching surfaces. The novel proposed sliding surfaces are defined is continuous time as:

$$\begin{cases} \mathrm{s}_w = \mathrm{c}_1 \varepsilon_w + \mathrm{c}_4 \int \varepsilon_w \mathrm{dt} \\ \mathrm{s}_d = \mathrm{c}_2 \varepsilon_d + \mathrm{c}_5 \int \varepsilon_d \mathrm{dt} \\ \mathrm{s}_q = \mathrm{c}_3 \varepsilon_q + \mathrm{c}_6 \int \varepsilon_q \mathrm{dt} \end{cases} \tag{7}$$

The Euler discretization for the system Eq. (7) is as follows:

$$\begin{cases} \mathrm{s}_w(k+1) - s_w(k) = \mathrm{c}_1(\varepsilon_w(k+1) - \varepsilon_w(k)) + Te\, \mathrm{c}_4 \varepsilon_w(k) \\ \mathrm{s}_d(k+1) - s_d(k) = \mathrm{c}_2(\varepsilon_d(k+1) - \varepsilon_d(k)) + Te\, \mathrm{c}_5 \varepsilon_d(k) \\ \mathrm{s}_q(k+1) - s_q(k) = \mathrm{c}_3(\varepsilon_q(k+1) - \varepsilon_q(k)) + Te\, \mathrm{c}_6 \varepsilon_q(k) \end{cases} \tag{8}$$

4.2 Control Law Design

After the determination of the sliding surfaces, we developed the control strategy.

4.2.1 Speed Controller

The switching surface relative to the speed controller is defined by:

$$\mathrm{s}_w(k+1) - \mathrm{s}_w(k) = Te \left[\mathrm{c}_1 \left(\frac{(w^*(k+1) - w^*(k))}{Te} - \frac{(w(k+1) - w(k))}{Te} \right) + \mathrm{c}_4 (w^*(k) - w(k)) \right] \tag{9}$$

Substituting the equation (3-e) in Eq. (9), we get:

$$\begin{aligned} \mathrm{s}_w(k+1) - \mathrm{s}_w(k) = {} & c_1 w^*(k+1) - c_1 w^*(k) - c_1 w(k) \\ & - c_1 Te \frac{3}{2} \frac{np^2}{j} \frac{M_{sr}}{L_r} (\varphi_{rd}(k) i_{sq}(k)) \\ & + c_1 Te \frac{np}{j} (C_r(k) - C_f(k)) + c_1 w(k) \\ & + Te\, \mathrm{c}_4\, w^*(k) - Te\, \mathrm{c}_4\, w(k) \end{aligned} \tag{10}$$

The nonlinear component is defined by:

$$s_w(k+1) - s_w(k) = -Q\,Te\,s_w(k) - K_w Te\,sign(s_w(k)) \tag{11}$$

The global control is the sum of equivalent component and nonlinear component:

$$i_{sq}(k) = \frac{2jL_r}{3c_1 Te\,np^2 M_{sr}\varphi_{rd}(k)} \begin{bmatrix} c_1 w^*(k+1) - c_1 w^*(k) + c_1 Te\frac{np}{j}(C_r(k) \\ - C_f(k))] + Te\,c_4 w^*(k) - Te\,c_4\,w(k) \\ + Q\,Te\,s(k) + K\,Te\,sign(s(k)) \end{bmatrix} \tag{12}$$

4.2.2 Direct Stator Current Controller

The sliding surfaces defining the direct stator current controller is presented by:

$$\mathrm{s}_d(k+1) - \mathrm{s}_d(k) = Te\left[\mathrm{c}_2\left(\frac{{I_{sd}}^*(k+1) - {I_{sd}}^*(\mathrm{k})}{Te}\right) - \left(\frac{I_{sd}(k+1) - I_{sd}(\mathrm{k})}{Te}\right) + \mathrm{c}_5({I_{sd}}^*(k) - I_{sd}(\mathrm{k}))\right] \tag{13}$$

Replacing the equation (3-a) in the Eq. (13), we get:

$$\mathrm{s}_d(k+1) - \mathrm{s}_d(k) = \mathrm{c}_2 {I_{sd}}^*(k+1) - \mathrm{c}_2 {I_{sd}}^*(\mathrm{k}) - \mathrm{c}_2 \begin{bmatrix} I_{sd}(\mathrm{k}) - Te\left(\frac{1}{\sigma\tau_s} + \frac{1-\sigma}{\sigma\tau_r}\right) I_{sd}(k) \\ + \frac{Te(1-\sigma)}{\sigma M_{sr}\tau_r}\varphi_r(k) + \frac{Te}{\sigma L_s} V_{sd}(k) \end{bmatrix} + \mathrm{c}_2 I_{sd}(\mathrm{k}) + Te\,\mathrm{c}_5 {I_{sd}}^*(k) - Te\,\mathrm{c}_5 I_{sd}(\mathrm{k}) \tag{14}$$

The nonlinear control is presented by:

$$s_d(k+1) - s_d(k) = -Q\,Te\,s_d(k) - K_d Te\,sign(s_d(k)) \tag{15}$$

From Eq. (14), we determine the control law relative to the direct stator current controller:

$$V_{sd}(k) = \frac{\sigma L_s}{\mathrm{c}_2 Te} \begin{bmatrix} \mathrm{c}_2 {I_{sd}}^*(k+1) - \mathrm{c}_2 {I_{sd}}^*(\mathrm{k}) + \mathrm{c}_2 Te\left(\frac{1}{\sigma\tau_s} + \frac{1-\sigma}{\sigma\tau_r}\right) I_{sd}(\mathrm{k}) \\ - \mathrm{c}_2 \frac{Te(1-\sigma)}{\sigma M_{sr}\tau_r}\varphi_r(k) - \mathrm{c}_2 \frac{Te}{\sigma L_s} + \mathrm{c}_2 I_{sd}(\mathrm{k}) + Te\,\mathrm{c}_5 {I_{sd}}^*(k) \\ - Te\,\mathrm{c}_5 I_{sd}(\mathrm{k}) + Q\,Te\,s_d(k) + K\,Te\,sign(s_d(k)) \end{bmatrix} \tag{16}$$

4.2.3 Quadratic Stator Current Controller

The equation defined the quadratic stator current controller is presented by:

$$\begin{aligned} \mathrm{s}_q(k+1) - \mathrm{s}_q(k) = {} & \mathrm{c}_3 {I_{sq}}^*(k+1) - \mathrm{c}_3 {I_{sq}}^*(\mathrm{k}) - \mathrm{c}_3 I_{sq}(k+1) + \mathrm{c}_3 I_{sq}(\mathrm{k}) \\ & + Te \mathrm{c}_6 {I_{sq}}^*(k) - T e \mathrm{c}_6 I_{sq}(\mathrm{k}) \end{aligned} \tag{17}$$

Replacing the equation (3-b) in the Eq. (17), we get:

$$\begin{aligned} \mathrm{s}_q(k+1) - \mathrm{s}_q(k) = {} & \mathrm{c}_3 {I_{sq}}^*(k+1) - \mathrm{c}_3 {I_{sq}}^*(k) \\ & - \mathrm{c}_3 \begin{bmatrix} I_{sq}(\mathrm{k}) - Te\, w_{dq} I_{sq}(k) - Te \left(\frac{1}{\sigma \tau_s} + \frac{1-\sigma}{\sigma \tau_r} \right) I_{sq}(k) \\ - \frac{1-\sigma}{\sigma M_{sr}} w(k) \varphi_r(k) - \frac{Te}{\sigma L_s} V_{sq}(k) \end{bmatrix} \\ & + \mathrm{c}_3 I_{sq}(k) + Te\, \mathrm{c}_6 {I_{sq}}^*(k) - Te\, \mathrm{c}_6 I_{sq}(k) \end{aligned} \tag{18}$$

The nonlinear component is defined by:

$$s_q(k+1) - s_q(k) = -Q\, Te\, s_q(k) - K_q Te\, sign(s_q(k)) \tag{19}$$

The global control is:

$$V_{sq}(k) = \frac{\sigma L_s}{c_3 Te} \begin{bmatrix} -\mathrm{c}_3 {I_{sq}}^*(k+1) + \mathrm{c}_3 {I_{sq}}^*(k) + \mathrm{c}_3 I_{sq}(\mathrm{k}) - \mathrm{c}_3 Te\, w_{dq} I_{sq}(k) \\ -\mathrm{c}_3 Te \left(\frac{1}{\sigma \tau_s} + \frac{1-\sigma}{\sigma \tau_r} \right) I_{sq}(k) - \mathrm{c}_3 \frac{1-\sigma}{\sigma M_{sr}} w(k) \varphi_r(k) \\ -\mathrm{c}_3 I_{sq}(k) - Te\, \mathrm{c}_6 {I_{sq}}^*(k) + Te\, \mathrm{c}_6 I_{sq}(k) + QTe\, s_q(k) \\ + K_q Te\, sign(s_q(k)) \end{bmatrix} \tag{20}$$

5 Stability Analysis

To satisfy discrete time sliding mode control, it is necessary to involve the system stability [13, 14]. We consider the constraint $|u(k)| \leq u_{\max}$ the control is defined by:

$$u(k) = \begin{cases} u(k)_{\mathrm{eq}} & for \quad \left\| u(k)_{\mathrm{eq}} \right\| \leq u(k)_{\max} \\ \frac{u(k)_{\mathrm{eq}}}{\|u(k)\|} u(k)_{\max} & for \quad \left\| u(k)_{\mathrm{eq}} \right\| > u(k)_{\max} \end{cases} \tag{21}$$

In [7], we present the QSM reaching conditions with the Lyapunov function candidate.

5.1 Speed Controller

The Eq. (10) can be rewritten as follows:

$$s_v(k+1) = s_v(k) + \mathrm{G}(k) + \mathrm{A}(k) u(k) \tag{22}$$

where

$$\mathrm{G}(k) = c_1 w^*(k+1) - c_1 w^*(k) - c_1 w(k) + c_1 Te \frac{np}{j}(C_r(k) - C_f(k)) + c_1 w(k) + Te\, \mathrm{c}_4 w^*(k) - Te\, \mathrm{c}_4 w(k) \tag{23}$$

And

$$A(k) = -c_1 Te \frac{3}{2} \frac{np^2}{j} \frac{M_{sr}}{L_r} \varphi_{rd}(k) \tag{24}$$

The stability analysis will be carried out under the assumption.
(A.1) the value $u_{\max}$ is such that

$$u_{\max} \geq -\frac{1}{A(k)} \|G(k)\| (1+\varepsilon) \tag{25}$$

for a $\varepsilon > 0$ *for all* $w(k)$, $\varphi(k)$ *and for all admissible functions* $w(k)$.
The increasing of Lyapunov function $\mathrm{V}(k) = \|s_v(k)\|$ is as follows:

$$\Delta \mathrm{V}(k) = \|s_v(k+1)\| - \|s_v(k)\| \tag{26}$$

$$= \left\| (s_v(k) + G(k)) \left(1 - \frac{I_{sq,k}}{I_{sq,\mathrm{eq}}}\right) \right\| - \|s_v(k)\| \tag{27}$$

$$\leq \|s_v(k) + G(k)\| \left(1 - \frac{I_{sq,\max}}{\left\|I_{sq,\mathrm{eq}}\right\|}\right) - \|s_v(k)\| \tag{28}$$

$$\leq \|s_v(k) + G(k)\| - \mathrm{A}(k) I_{sq,\max} - \|s_v(k)\| \tag{29}$$

From above we get:

$$0 \leq 1 - \frac{I_{sq,k}}{I_{sq,\mathrm{eq}}} \leq 1 - \frac{I_{sq,\max}}{\left\|I_{sq,\mathrm{eq}}\right\|}; \textit{where } \left\|I_{sq,\mathrm{eq}}\right\| = -\frac{1}{A(k)} \|s_v(k) + G(k)\| \tag{30}$$

Under assumption (A.1), it is possible to determine

$$\|s_v(k) + G(k)\| - A(k) I_{sq,\max} \leq \|s_v(k)\| - \varepsilon \|G(k)\| < \|s_v(k)\| \tag{31}$$

After the condition above, when the decreases monotonically. The decreases monotonically. It exists a time k_1 that $\left\|I_{sq,\mathrm{eq}}\right\|$ for all $k \geq k_1$ which the equivalent controllers is applied. $\left\|I_{sq,\mathrm{eq}}\right\| \leq I_{sq,\max}$

5.2 Direct Stator Current Controller

The Eq. (19) is defined by

$$s_d(k+1) = s_d(k) + H(k) + B(k)u(k) \tag{32}$$

where

$$H(k) = \mathrm{c}_2 {I_{sd}}^*(k+1) - \mathrm{c}_2 {I_{sd}}^*(k) - \mathrm{c}_2 \left[\begin{array}{l} I_{sd}(\mathrm{k}) - Te \left(\frac{1}{\sigma \tau_s} + \frac{1-\sigma}{\sigma \tau_r} \right) I_{sd}(\mathrm{k}) \\ + \frac{Te(1-\sigma)}{\sigma M_{sr} \tau_r} \varphi_r(k) \end{array} \right] + \mathrm{c}_2 I_{sd}(\mathrm{k}) + Te\, \mathrm{c}_5 {I_{sd}}^*(k) - Te\, \mathrm{c}_5 I_{sd}(\mathrm{k}) \quad (33)$$

And

$$B(k) = c_2 \frac{Te}{\sigma L_s} \quad (34)$$

From assumption (A.1), the Lyapunov function is given by $\mathrm{V}(k) = \|s_d(k)\|$

$$\Delta \mathrm{V}(k) = \|s_d(k+1)\| - \|s_d(k)\| \quad (35)$$

$$= \left\| (s_d(k) + H(k)) \left(1 - \frac{V_{sd,k}}{V_{sd,\mathrm{eq}}} \right) \right\| - \|s_d(k)\| \quad (36)$$

$$\leq \|s_d(k) + H(k)\| \left(1 - \frac{V_{sd,\max}}{\left\| V_{sd,\mathrm{eq}} \right\|} \right) - \|s_d(k)\| \quad (37)$$

$$\leq \|s_d(k) + G(k)\| - H(k) V_{sd,\max} - \|s_d(k)\| \quad (38)$$

From Eq. (38), we define

$$0 \leq 1 - \frac{V_{sd,k}}{I_{sd,\mathrm{eq}}} \leq 1 - \frac{V_{sd,\max}}{\left\| V_{sd,\mathrm{eq}} \right\|}; \textit{where} \quad \left\| V_{sd,\mathrm{eq}} \right\| = -\frac{1}{\mathrm{B}(k)} \|s_d(k) + H(k)\| \quad (39)$$

On the basis of (A.1), it is possible to write

$$\|s_d(k) + H(k)\| - B(k) V_{sd,\max} \leq \|s_d(k)\| - \varepsilon \|\mathrm{H}(k)\| < \|s_d(k)\| \quad (40)$$

The $\|s_d(k)\|$ decreases monotonically. Then, the $\left\| V_{sd,\mathrm{eq}} \right\|$ decreases monotonically. It exists a time k_2 that $\left\| V_{sd,\mathrm{eq}} \right\| \leq V_{sd,\max}$ for all $k \geq k_2$ which the equivalent controllers is applied.

5.3 Quadratic Stator Current Controller

The Eq. (17) is rewritten as follows:

$$s_q(k+1) = s_q(k) + I(k) + C(k) u(k) \quad (41)$$

where

$$\begin{aligned} \mathrm{I}(k) &= \mathrm{c}_3 {I_{sq}}^*(k+1) - \mathrm{c}_3 {I_{sq}}^*(k) - \mathrm{c}_3 I_{sq}(\mathrm{k}) + \mathrm{c}_3 Te\, w_{dq} I_{sq}(k) \\ &+ \mathrm{c}_3 Te \left(\frac{1}{\sigma \tau_s} + \frac{1-\sigma}{\sigma \tau_r} \right) I_{sq}(k) + \mathrm{c}_3 \frac{1-\sigma}{\sigma M_{sr}} w(k) \varphi_r(k) + \mathrm{c}_3 I_{sq}(k) \\ &+ Te\, \mathrm{c}_6 {I_{sq}}^*(k) - Te\, \mathrm{c}_6 I_{sq}(k) \end{aligned} \tag{42}$$

and

$$\mathrm{C}(k) = \mathrm{c}_3 \frac{Te}{\sigma L_s} V_{sq}(k) \tag{43}$$

Considering the Lyapunov function candidate:

$$\Delta \mathrm{V}(k) = \left\| s_q(k+1) \right\| - \left\| s_q(k) \right\| \tag{44}$$

$$= \left\| (s_q(k) + I(k)) \left(1 - \frac{V_{sq,k}}{V_{sq,\mathrm{eq}}} \right) \right\| - \left\| s_q(k) \right\| \tag{45}$$

$$\leq \left\| s_q(k) + I(k) \right\| \left(1 - \frac{V_{sq,\max}}{\left\| V_{sq,\mathrm{eq}} \right\|} \right) - \left\| s_q(k) \right\| \tag{46}$$

$$\leq \left\| s_q(k) + I(k) \right\| - I(k) V_{sq,\max} - \left\| s_q(k) \right\| \tag{47}$$

Referring to Eq. (47), we get

$$0 \leq 1 - \frac{V_{sq,k}}{I_{sq,\mathrm{eq}}} \leq 1 - \frac{V_{sq,\max}}{\left\| V_{sq,\mathrm{eq}} \right\|}; \textit{where} \quad \left\| V_{sq,\mathrm{eq}} \right\| = -\frac{1}{C(k)} \left\| s_q(k) + I(k) \right\| \tag{48}$$

Under assumption (A.1), it is possible to write:

$$\left\| s_q(k) + I(k) \right\| - C(k) V_{sq,\max} \leq \left\| s_q(k) \right\| - \varepsilon \left\| I(k) \right\| < \left\| s_q(k) \right\| \tag{49}$$

We concluded that the $\left\| s_q(k) \right\|$ decreases monotonically. Then, the $\left\| V_{sq,\mathrm{eq}} \right\|$ decreases monotonically. It exists a time k_3 that $\left\| V_{\mathrm{sq,eq}} \right\| \leq V_{sq,\max}$ for all $k \geq k_3$ which the equivalent controllers is applied.

6 Results and Discussions

We considered an induction motor with the following characteristics: three phase, two pole, 85/140 V; 3.5/6 A; $f = 50$ Hz $R_s = 3.45\,\Omega$; $R_r = 2.95\,\Omega$; $L_s = 0.1442$ H; $L_r = 0.1442$ H; $M_{sr} = 0.1342$ H; $j = 0.01$ Kgm^2; $np = 2$. The coefficients c_1, c_2, c_3, c_4, c_5, c_6 and the gains k_v, k_d, k_q associated in the control law, are adjusted to values: $c_1 = 0.00018, c_2 = 0.0099, c_3 = 0.00000009, c_4 = 0.000000002, c_5 = 0.0000003$, $c_6 = 0.0000000009$, $k_v = 115$, $k_d = 3000$ and $k_v = 115, k_d = 3000, k_q = 3000$. These coefficients and gains have been tuned until the obtain of the validate results.

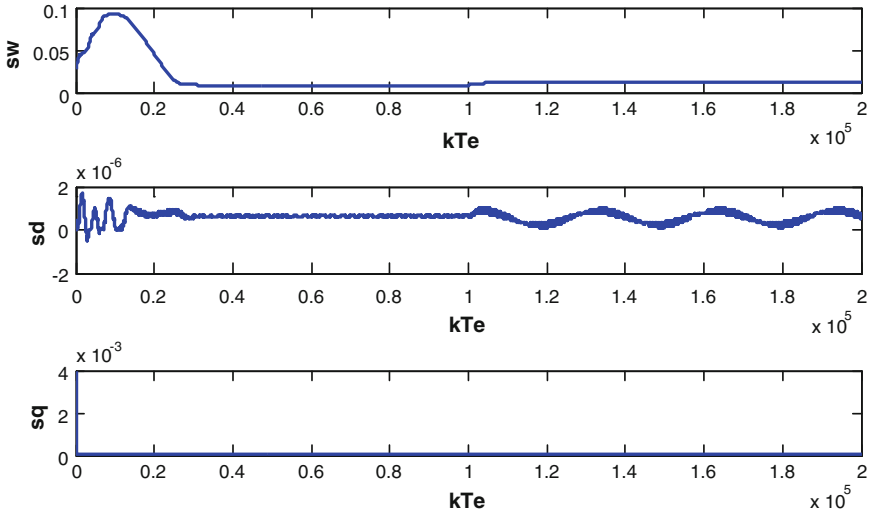

Fig. 3 Switching surfaces

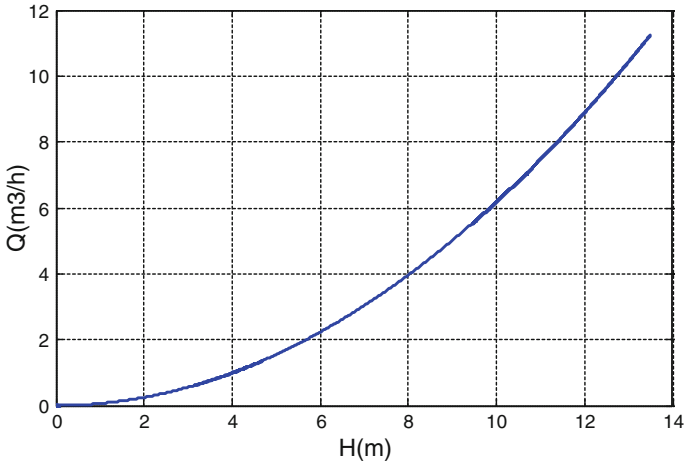

Fig. 4 Pumping characteristics Q = f(H)

Figure 3 presents the evolution of the three sliding surfaces relative to three controller such as: speed controller, direct stator current controller and quadratic stator current controller. We remark that all the surfaces converge to zero in a minimal band. That satisfy the criteria of the sliding mode control.

Figure 4 shows the characteristics of the pump, it presents a parabolic form. If the head (H) increasing so, the flow (Q) increase. This characteristic is verified by the system equation given by Eq. (2).

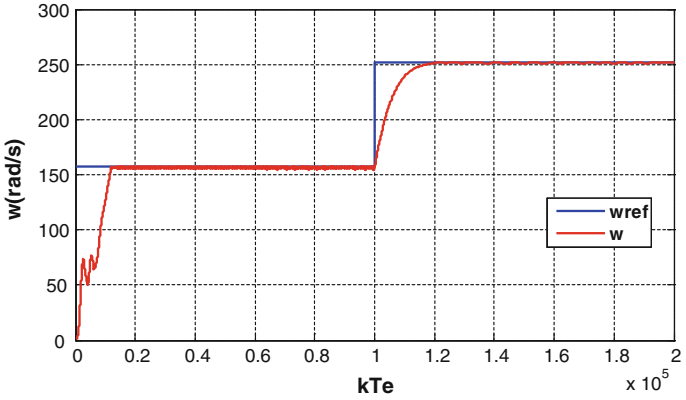

Fig. 5 Evolution of the speed

The speed started with a nominal value equal to 157 rad/s, and in the instant 1 s, it increases in the value 250 rad/s. We remark that this curve will follow the reference without overshoot and admits a settling time equal to 0.9 s. This test is achieved with unloaded torque and reference flux equal to 0.8 Wb, Fig. 5.

7 Comparative Study

For testing the robustness of the proposed control, it is necessary to know the degree of confidence that we can fix some control and the reliability that brings. For this reason, we make a comparison between the classical Proportional Integral (PI) and Proportional Integral Sliding Mode Control (PISMC).

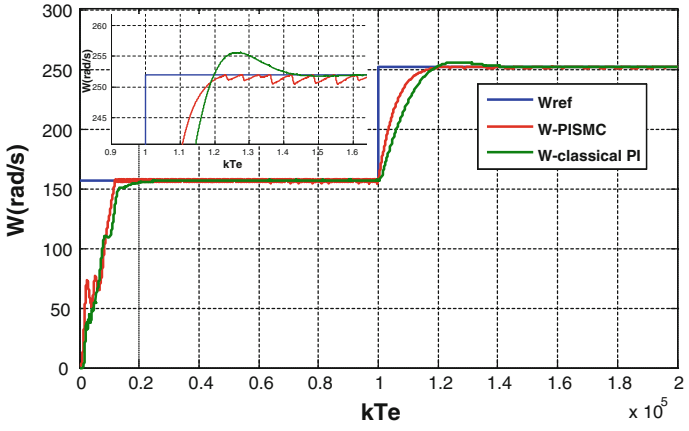

Fig. 6 Comparison results with PISM and conventional PI

Figure 6 allows the evolution of the speed with two methods: the first one presents the conventional PI and the second one presents the PISM. The characteristic with PISM is faster than the conventional PI. The response time in the case of unloaded system is about 0.2 s for the conventional PI and 0.18 s for PISM. During the insertion of the load, the response time is 0.4 s in the case of the conventional PI and 0.18 s in the case of the PISM. We conclude that the PISM give the best performances than the conventional PI.

8 Conclusion

The work presented in this chapter is about analysis and evaluation of discretization behavior for pumping system. The control design is the indirect field oriented control by sliding mode in discrete time. The principle becomes in choice of switching function which an integral action is added into the considered function. This addition provides a satisfactory results regardless uncertainties and robustness. In fact, the studied system is presented. Then, the control strategy is developed. This kind of control synthetize three control loops in discrete time related to speed controller, direct stator current controller and quadratic stator current controller. Yet, the proposed control is compared with conventional PI and shows a good results.

References

1. Argha A, Li L, Su SW, Hung N (2013) The application of discrete sliding mode control inparabolic PDE dynamics. In: Australian control conference, 4–5 November
2. Bartoszewicz A (1998) Discrete-time quasi-sliding-mode control strategies. IEEE Trans Ind Electron 45:633–637
3. Castillo-Toledo B, Gennarro DS, Loukianov AG, Rivera J (2004) On the discrete-time modelling and control of induction motors with sliding modes. In: Proceeding of the 2004 American control conference Boston, 30 June– 02 July
4. Castillo-Toledo B, Gennaro DS, Galicia MI, Loukianov AG, Rivera J (2010) Indirect discrete-time sliding mode torque control of induction motors. In: XIX international conference on electrical machines - ICEM
5. Chihi A, Chbeb A, Sellami A (2015) Switching function optimization of sliding mode control to a photovoltaic pumping system. Advances and applications in sliding mode control systems. Springer, New York, pp 463–493
6. Ching-Tsai P, Ting-Yu C, Chin-Ming H (1994) A fixed structure discrete-time sliding mode controller for induction motor drives. IEEE Trans Energy Convers 9:645–651
7. Furuta K, Morisada M (1988) Implementation of sliding mode control by a digital computer. In: 14 annual conference of industrial electronics society IECON'88, vol 2, pp 453–458
8. Galicia M, Castillo-Toledo B, Gennaro DD, Loukianiv A (2010) Discrete time sliding mode torque control of induction motor. World Automation Congress TS1 Press
9. Gao W, Yufu W, Homaifa A (1995) Discrete-time variable structure control systems. IEEE Trans Ind Electron 42:117–122
10. Lim K-W, Teck-Seng L, Rahman MF, Liang-Boon W (1991) A discrete time variable structure controller for brushless DC motor drive. IEEE Trans Ind Electron 38:102–107

11. Monaco S (1984) On the realization of nonlinear discrete time systems. Syst Control Lett 5:145–152
12. Monaco S, Noramand-Cyrot D (1977) A unified representation for nonlinear discrete time and sampled dynamics. J Math Syst Estim Control 7:477–503
13. Monaco S, Normand-Cyrot D (2010) Nonlinear average passivity and stabilizing controllers in discrete time. Syst Control Lett 60:431–439
14. Monaco S, Normand-Cyrot D (2012) Nonlinear optimal stabilizing control in discrete time. In: American conference Fairmont Queen Elizabeth
15. Pan S, Edelberg K, Hedrick KJ (2014) Discrete adaptive sliding control of automotive powertrains. In: American control conference (ACC)
16. Shaocheng Q, Xiaohua X, Jiangfeng Z (2014) Dynamics of discrete-time sliding-mode-control uncertain systems with a disturbance compensator. IEEE Trans Ind Electron 61:3502–3510
17. Shihua L, Haibo D, Xinghuo Y (2014) Discrete-time terminal sliding mode control systems based on Euler's discretization. IEEE Trans Autom Control 59:546–552

Design of a Controller of Switched Nonlinear Systems Based on Multiple Lyapunov Functions

Khalil Jouili, Arwa Abdelkarim and Naceur Benhadj Braiek

Abstract In this work, we focus on the stabilization issue of a class of non-minimum phase switched nonlinear systems where the internal dynamics of each mode may be unstable and uncontrollable. We develop a hybrid nonlinear control technique based on the coupling between bounded nonlinear feedback controllers and the switching laws designed to stabilize the transitions between the stability regions associated to each modes arising from the limitations imposed by the input constraints. The key feature of the proposed approach is based on the formalism of the input–output feedback linearization. The performed developments largely rely on Hauser's approximation and multiple Lyapunov functions. In summary, the synthesized controllers can guarantee the stability of individual modes while switching law that will be generating ensures overall system stability. The differences between the switching strategies, and their implications on the switching logic, are discussed. A non-minimum phase Continuously Stirred Tank Reactor (CSTR) illustrates the efficiency of the proposed approach

Keywords Switched nonlinear systems · Non-minimum phase · Multiple Lyapunov functions · Input–output feedback linearization · Stabilization

K. Jouili (✉) · A. Abdelkarim · N.B. Braiek
Laboratory of Advanced Systems Polytechnic School of Tunisia (EPT),
B.P. 743, 2078 Marsa, Tunisia
e-mail: khalil.jouili@gmail.com

A. Abdelkarim
e-mail: abdelkrimarwa@gmail.com

N.B. Braiek
e-mail: naceur.benhadj@ept.rnu.tn

S. Vaidyanathan and C. Volos (eds.), *Advances and Applications in Nonlinear Control Systems*, Studies in Computational Intelligence 635,
DOI 10.1007/978-3-319-30169-3_27

1 Introduction

There are numerous examples of chemical processes include both continuous dynamics and discrete events. Continuous behavior of a process caused by some factors, such as momentum, mass, and energy conservation, can be modeled more conveniently as discrete events by continuous-time differential equations.

However discrete phenomena is ubiquitously multifaceted and can originate from physical constraints or manufacturing distinct phases such as discontinuous actuators, phase changes, flow reversals, shocks, and transitions; the use of measurement sensors and control actuators with discrete settings/positions or filling/emptying a reactor [7, 14].

The overall process behavior in all of these instances is characterized by the interaction of continuous and discrete dynamics that they cannot be decoupled effectively, and is modeled by hybrid systems.

A class of hybrid systems that have drawn considerable attention in the past decade is the class of switched systems which consists of a family of subsystems and a switching signal, which defines a specific subsystem that is active at each instant of time. For a survey on switched systems we refer to [6, 10, 11, 18, 21, 23, 24].

The study of stability analysis and stabilization of switched systems is an important problem that has been the subject of significant research works in control theory [1–4, 20, 22, 28, 29, 32, 35]. In this framework one of these problems is the stabilization of non-minimum phase nonlinear switched systems.

This system control, however, is a delicate task. Some contributions have been devoted to non-minimum phase switched nonlinear systems where each nonlinear mode may be non-minimum phase. In [34], H∞ control goal is achieved for a class of non-minimum phase cascade switched nonlinear systems where the internal dynamics of each mode is assumed to be asymptotically stabilizable. Output tracking of non-minimum phase switched nonlinear systems has been considered in [26], where an approximated minimum phase model is utilized. The same problem is also investigated in [8] by means of an inversion based control strategy. In [33], a switching control methodology for non-minimum phase nonlinear switched systems with the control law which has singularities was developed. However, it is well known that the stabilization of non-minimum phase nonlinear systems is quite difficult, and is even impossible to achieve if the unstable zero dynamics is uncontrollable.

Motivated by these considerations, we present in this work a nonlinear control methodology for a class of non-minimum phase nonlinear switched systems with input constraints.

The main feature of the proposed approach is not only to synthesize the bounded nonlinear feedback controllers of the individual subsystems, but also to design an appropriate switching scheme that organizes the transitions between the different non-minimum phase modes and keeps all the system stable. The controller synthesis procedure yields also an explicit characterization that coupling the switching strategy and the stability regions associated for each mode arising from the limitations imposed by the input constraints.

The proposed method involves the integration of Input–output feedback linearization control and Hauser's approximation [17] in the particular case where the relative degree coincides with the system order.

To this end, we Use Multiple Lyapunov Functions [13, 36], one for each mode, a family of feedback controllers was synthesized for the individual closed-loop approximate modes and has provided an explicit characterization of the corresponding stability regions in terms of the input constraints. Then for the synthesis of a family of feedback controllers that enforce the desired stability and performance properties within each individual dynamical mode in the presence of input constraints. Finally we derive a set of switching rules that organize stabilizing transitions between the output feedback stability regions of the non-minimum phase modes.

The outline of this chapter is as follows: In Sect. 2, we introduce a motivating example. Section 3 provides the system description and preliminaries. The problem formulated is solved in Sect. 4. The proposed method is successfully applied to the switched exothermic chemical reactor [27] example in spite of to the fact that it is a nonlinear non-minimum phase system and that it is also characterized by a dynamic that leads to the instability of the dynamic of zero. Finally, a conclusion is drawn in Sect. 6.

2 Motivating Example: A Continuously Stirred Tank Reactor with Two Modes

Chemical reactors are known to be ones of the most important plants in chemical industry. The process in the reactor is usually exhibit complex behavior, so it is necessary to control their operation. In recent years, various nonlinear design tools have been proposed to provide global stabilization [5, 15, 16, 30]. One of the major control problems which has attracted the attention of researchers for a long time deal with the temperature regulation under input constraints of exothermic irreversible reaction in a continuously stirred tank reactor (CSTR).

Consider a general class of a constant-volume, non-isothermal CSTR system with a hybrid behavior, in which the reaction $A \rightarrow B$ takes place in the liquid phase. The reactor has two inlet streams: the first continuously feeds pure A at flow rate $F_r = 0.45\,\mathrm{m}^3/\mathrm{min}$, concentration $C_{A_0} = 12\,\mathrm{kmol\,m}^{-3}$ and $T_{A_0} = 300\,\mathrm{K}$, while the second can be turned on or off (by means of an on/off valve) during reactor operation. When turned on, the second stream feeds pure A at flow rate $F_r^* = 0.7\,\mathrm{m}^3/\mathrm{min}$, concentration $C_{A_0}^* = 14\,\mathrm{kmol\,m}^{-3}$ and $T_{A_0}^* = 320\,\mathrm{K}$. For the parameters given in Table 1 under standard modeling assumptions, the mathematical model of the process takes the following form:

Table 1 Parameter values of the non-isothermal reactor

Parameter	Value	Unit
Z_r	Reaction rate pre-exponential factor	$5 \times 10^8\,\mathrm{S}^{-1}$
V_0	Reactor volume	$0.1\,\mathrm{m}^3$
E_a	Activation energy	49.884 kJ/mol
R_r	Ideal gas constant	8.31×10^{-3} kJ/mol °C
C_{A_0}	Inlet concentration of reactant A	$12\,\mathrm{kmol/m}^{-3}$
γ	Reactor model parameter	3.9

$$\begin{cases} \dfrac{dC_A}{dt} = -Z_r\, exp\left(-\dfrac{E_a}{R_r T}\right) C_A + \left(C_{A_0} - C_A\right) \dfrac{F_r}{V_0} + (i-1)\left(C^*_{A_0} - C_A\right) \dfrac{F^*_r}{V_0} \\ \dfrac{dT}{dt} = \gamma_r Z_r\, exp\left(-\dfrac{E_a}{R_r T}\right) C_A + \left(T_{A_0} - T\right) \dfrac{F_r}{V_0} + (i-1)\left(T^*_{A_0} - T\right) \dfrac{F^*_r}{V_0} + Q_r \end{cases} \tag{1}$$

If the variable i is equal to *1* then the second inlet stream is turned off and it is turned on when i has the value of *2*. Initially, it is assumed that $i = 1$. The control objectives are to stabilize the reactor temperature at the unstable steady state of mode *1* ($x_e = 302.0\,\mathrm{K}$), and to maintain this temperature at this steady state when the reactor switches to mode *2* subject to the constraint $|Q_r| \leq 10 \times 10^{-2}\,\mathrm{K\,s}^{-1}$.

3 System Description and Preliminaries

We consider a class of single-input single-output switched nonlinear systems of the following state-space equation:

$$\begin{cases} \dot{x} = f_i(x) + g_i(x)\, u_i \\ y = h(x) \\ i \in I = \{1, 2, \ldots, N\} \end{cases} \tag{2}$$

where $x = [x_1 \ldots x_n]^T \in \Re^n$ denote the vector of continuous state variables, $u_i = \left[u_i^1 \ldots u_i^m\right]^T$ is the vector of manipulated inputs taking values in a nonempty compact convex subset $U = \left\{u_i \in \Re^m : \|u_i\| \leq u_i^{max}\right\}$ with $u^i_{\max} \geq 0$ denotes the bound on the manipulated inputs, the notation $\|\cdot\|$ will be used to denote the standard Euclidean norm of a vector u_i. The nonlinear vector functions $f_i(.)$, $g_i(.)$ and the scalar function $h(x)$ are assumed to be sufficiently smooth which gives rise to the switched nonlinear system (2). The index i represent a discrete state that takes values in a finite index set I which specifies the active subsystem. The number N of the switches is finite on every bounded time interval. Throughout the paper, we use the notations t_i^k

and t_i^{k+1} to denote the tth times that the ith subsystem is switched in and out. We can assume, in the rest of the study, that the continuous state of the ith active mode evolves according to the state equation and the output equation governed for each $t_i^k < t < t_i^{k+1}$.

In order to provide the necessary background for our main results in Sect. 3, we will briefly review in the remainder of this section the stability properties of the system viewed as a finite collection of continuous-time nonlinear systems with discrete events that direct the transition between them. One of the main tools for stability analysis of switched systems is Multiple Lyapunov Functions (MLFs). In fact, its principle lies in the use of a family of functions named pseudo-Lyapunov functions $\{V_i : i \in I\}$ associated with each field of vectors $\dot{x} = f_i(x)$, to demonstrate stability.

Definition 1 ([19] *Pseudo-Lyapunov function*) A pseudo Lyapunov function for the system (2), around an operating point in a stability region of the space ($x_n \in \Omega_i \subset \Re^n$) is a real-valued function $V_i(x)$ defined in a region Ω_i satisfying the following conditions:

- Positive definite: $V_i(x_n) = 0$ and $V_i(x) > 0$ for $x_n \neq x \in \Omega_i$
- Derivative defined non-positive: for all x included in the stability region Ω_i

$$\frac{dV(x)}{dt} = (\partial V_i(x)/\partial x)\,[f_i(x) + g_i(x)\,u_i] \leq 0 \tag{3}$$

We can, then, write the following result proving the sufficient conditions for stability:

Theorem 1 *([9, 11]) Suppose that* $\cup\Omega_i = \Re^n$ *and each vector field* f_i *has an associated Lyapunov like function* V_i *in the region* Ω_i*, neighborhood* x_n*.*

For the N switched nonlinear system (1), with $u_i \equiv 0, i \in I$, the switching sequence can take the value of i only if $x \in \Omega_i$, then the value of V_i decreases on each interval when the ith subsystem is active, more specifically

$$V_i\left(x\left(t_i^k\right)\right) \leq V_i\left(x\left(t_i^{k-1}\right)\right) \tag{4}$$

We pose t_i^k the kth switching instant for the sequence. Then, the adjacent of the operating point x_e of the system (2), is Lyapunov stable.

As shown above in Theorem 1, The Multiple Lyapunov Function approach, usually one for each of the individual subsystems being switched, can be used to determine the stability of switched systems without input signals; such that if for every i the value of V_i, at the end of each such interval exceeds the value at the end of the next interval on which the ith subsystem is active, the switched system can be shown to be asymptotically stable. However it cannot inquire about the existence of a stabilizing feedback law for the switched control system (2). Here we introduce the notion of control Lyapunov function for feedback controller synthesis. The idea is to expect the MLFs method to play an important role for designing the feedback controllers.

Referring to the system (2), the concept of Control Lyapunov Function (CLF) introducing as follows:

Definition 2 ([31] *Control Lyapunov Function*) A smooth, proper, and Positive-Definite function $V : \Re^n \rightarrow \Re_+$ is called a CLF for a nonlinear control system of the form $\dot{x} = f(x) + g(x)u$ when there is an admissible value $u^1, \ldots, u^m$ for the controls such that:

$$inf\left\{L_f V + L_{g_1} V u^1 + \cdots + L_{g_m} V u^m\right\} < 0 \tag{5}$$

where $L_f V = [\partial V / \partial x] f(x)$, g_k is the kth column of the matrix g.

We can generalize the Definition 1 to a switched nonlinear system as shown in this assumption:

Assumption 1 For every $i \in I = \{i = 1, \ldots, N\}$, a Control Lyapunov Function, V_i, exists for system (2).

By Assumption 1; if we can find a family of CLF for the switched System (2), one for each subsystem, then for the solution of (2) we can derive a control signal u such that family of CLF monotonically decreases.

4 Main Results

4.1 Problem Formulation

In order to clear presentation of the main results of this paper, we will start in this section by reviewing the state feedback control problem.

Consider the class of nonlinear systems that has been represented by Eq. (2). We need to assume that for all $i \in I$, there exists an integer r (this assumption is made only to simplify notations and can be readily relaxed to allow a different relative degree r_i for each subsystem) and a set of coordinates (see [19] for a detailed treatment of feedback linearizable nonlinear systems)

$$\Phi_i(x) = \begin{bmatrix} \Phi_{\mathrm{i},1}(x) \\ \Phi_{\mathrm{i},2}(x) \\ \vdots \\ \Phi_{\mathrm{i},r_i}(x) \\ \Phi_{\mathrm{i},r_i+1}(x) \\ \vdots \\ \Phi_{\mathrm{i},n}(x) \end{bmatrix} = \begin{bmatrix} h(x) \\ L_{f_i} h(x) \\ \vdots \\ L_{f_i}^{r_i} h(x) \\ \chi_{i,1}(x) \\ \vdots \\ \chi_{i,n-r_i}(x) \end{bmatrix} \tag{6}$$

where $\chi_{i,1}(x), \ldots, \chi_{i,n-r_i}(x)$ are nonlinear scalar functions of x.

The coordinate change $\phi_i(x)$ allows transforming the subsystem of Eq. (1) into a partially linear form such that the system takes the form:

$$\begin{cases} \begin{cases} \dot{\xi}_1 = \xi_2 \\ \vdots \\ \dot{\xi}_{r_i-1} = \xi_{r_i} \\ \dot{\xi}_{r_i} = L_{f_i}^{r_i} h(x) + L_{g_i} L_{f_i}^{r_i-1} h(x) u_i \\ \dot{\eta}_{i,1} = Q_{i,1}(x) \\ \vdots \\ \dot{\eta}_{i,n-r_i} = Q_{i,n-r_i}(x) \end{cases} \\ y = \xi_1 \end{cases} \tag{7}$$

where $L_{g_i} L_{f_i}^{r-1} h(x) \neq 0$ for all $x \in \Re^n$, $i \in I$ and $Q_{1,i}(x), \ldots, Q_{(n-r),i}(x)$ are nonlinear functions of their arguments describing the evolution of the inverse dynamics of the ith mode.

4.2 Theory and Design

In this section, we present a technique that combines the multiple Lyapunov functions and Hauser's [17] approximation to develop a nonlinear control strategy for the stabilization of a switched nonlinear system where each mode may be non-minimum phase. The key component of this methodology is to use a family of control Lyapunov functions, one for each subsystem, to:

1. Synthesize the bounded nonlinear feedback controllers of the individual subsystems.
2. Design an appropriate switching scheme that organizes the transitions between the different modes and keeps all the system stable.

Owing to the presence of the unstable zero dynamics, the problem becomes more challenging not only in the synthesizes of the control laws but also in the design of an appropriate switching scheme that guarantees stability in the presence of non-minimum phase modes. To present the solution, we will first define the notion of robust relative degree.

Consider the system (2), we assume that $x = x_e$ is an equilibrium point, that is $f_i(x_e) = 0$, and without loss of generality we assume that $h(x_e) = 0$.

If we will also assume the following "controllability" rank condition: *Rank* $\left\{g_i, ad(f_i g_i), \ldots, ad^{n-1}(f_i g_i)\right\} = n$ for each mode $i \in I = \{i = 1, \ldots, N\}$ at $x = x_e$, we will impose the following assumptions on the system (2).

Assumption 2 The nonlinear system (7) has a robust relative degree γ_i, for all for each mode $i (i \in I)$, in the neighborhood of x_e if there is a set of smooth functions $\hat{\Phi}_{i,j}(x)$ as the following one:

$$\begin{cases} y = h(x) = \hat{\Phi}_{i,1}(x) + \psi_{i,0}(x, u_i) \\ y^{(j)} = \hat{\Phi}_{i,j+1}(x) + \psi_{i,j}(x, u_i) \\ \vdots \\ y^{(\gamma_i - 1)} = \hat{\Phi}_{i,\gamma_i}(x) + \psi_{i,\gamma_i - 1}(x, u_i) \\ y^{(\gamma_i)} = L_{f_i}^{\gamma_i} h(x) + L_{g_i} L_{f_i}^{\gamma_i} h(x) u_i \\ i = 1, \ldots, N \\ j = 0, \ldots, \gamma_i \end{cases} \tag{8}$$

where the functions $\psi_{i,j}(x, u_i)$, are sums of terms $O(x)^2$, $O(x, u_i)$, or $O(u_i)^2$, $L_{f_i}^{\gamma_i} h(x)$ and $L_{g_i} L_{f_i}^{\gamma_i} h(x)$ are smooth, and $L_{g_i} L_{f_i}^{\gamma_i} h(x_e) \neq 0$.

Let us note that that a function $\delta(x)$ is $O(x)^n$ if $\lim_{|x| \to 0} (|\delta(x)| / |x|^n) \neq 0$. Moreover, the functions known as $O(x)^0$ will be indicated by $O(1)$.

The determination of the robust relative degree γ_i of a nonlinear system shows that the latter arises in a way similar to the case of the classic relative degree r_i. Indeed, one also obtains: $\gamma_i < n$.

The study of the properties of the approximately linearized system on a parameterized family of operating envelopes can be defined as follows:

Definition 1 For all $i \in I$, we call $B_{\varepsilon_i}^i \subset \Re^n$ for some $\varepsilon_i > 0$, a family of operating envelopes provided that $B_{\delta_i}^i \subset B_{\varepsilon_i}^i$, whenever $\delta_i < \varepsilon_i$ and $\sup \left\{ \delta : B_{\delta_i}^i \subset B_{\varepsilon_i}^i \right\} = \varepsilon_i$ where $B_{\delta_i}^i$, is a ball of radius δ_i centered at the origin.

Then, for the approximation in a larger region, we will impose following assumption

Assumption 3 For all $i \in I$, a function $\psi_i : \Re^n \times \Re \to \Re$ is said to be of uniformly high order on $B_{\varepsilon_i}^i \times B_{\sigma_i}^i$ if for some $\varepsilon_i > 0$, $\sigma_i > 0$ there exists a monotone increasing function of ε_i, $\lambda_i(\varepsilon_i)$, such that:

$$\begin{cases} |\psi_i(x, u_i)| \leq \varepsilon_i \lambda_i(\varepsilon_i)(|x| + |u_i|) \\ \forall x \in B_{\varepsilon_i}^i, \forall u_i \in B_{\sigma_i}^i \end{cases} \tag{9}$$

where $B_{\varepsilon_i}^i$ is a ball of radius ε_i centered at x_e, and $B_{\varepsilon_i}^i$ is a ball of radius σ_i centered at the origin.

Now, we return to the original problem. We assume that system (1) has robust relative degree γ_i. Adopting the notation of [17], we define new coordinates ξ with $\xi_j = \hat{\Phi}_{i,j}(x)$, $j = 0, \ldots, \gamma_i$. Thus, we obtain the new representation of the system (1) which is written in mixed ξ and x coordinates as follows:

$$\begin{cases} \dot{\xi}_1 = \xi_2 + \psi_{i,1}(x, u_i) \\ \vdots \\ \dot{\xi}_{\gamma_i - 1} = \xi_{\gamma_i} + \psi_{i,\gamma_i - 1}(x, u_i) \\ \dot{\xi}_{\gamma_i} = L_{f_i}^{\gamma_i} h(x) + L_{g_i} L_{f_i}^{\gamma_i - 1} h(x) u_i \end{cases} \tag{10}$$

Consider the switched nonlinear system of Eq. (10). Our Objective now is twofold. The first is to synthesize an output feedback controller from where the requested closed-loop properties for each mode Then the second objective is to design an appropriate set of switching scheme that organizes the transitions between constituent modes and their respective controllers and keeps all the system stable.

In order to proceed with the controller synthesis task, we will impose the following assumption on the on the process of Eq. (10). This assumption allows constructing bounded controls using the Lyapunov function [12, 25].

Assumption 4 For each $i \in I$, there exists a family of N bounded nonlinear state feedback controllers of the form:

$$u_i = -k_i(x)\left(L_{g_i} V_i(x)\right)^T, i = 1, \ldots, N \tag{11}$$

where V_i is a CLF for the ith mode and $L_{g_i} V_i$ is the Lie derivatives of the control Lyapunov function V_i for the ith mode along the column vectors of the matrix g_i.

Theorem 2 that follows provides the explicit synthesis formula for the desired bounded nonlinear state feedback controllers and states precise switching conditions that guarantee closed-loop stability.

Theorem 2 *Consider the switched nonlinear system (10), for which a family of CLFs $V_i, i = 1, \ldots, N$ has been founds, using each control Lyapunov function, we construct the following family of bounded nonlinear feedback controllers:*

$$u_i = -k_i\left(x, u_i^{max}\right)\left(L_{g_i} V_i(x)\right)^T, i = 1, \ldots, N \tag{12}$$

where

$$k_i\left(V_i, u_i^{\max}\right) = \begin{cases} \dfrac{\beta_i(x)+\left(\beta_i^2(x)+\left(u_i^{\max}\left\|\left(\left(L_{g_i} V_i\right)^T(x)\right)\right\|\right)^4\right)^{\frac{1}{2}}}{\left\|\left(\left(L_{g_i} V_i\right)^T(x)\right)\right\|^2\left(1+\left(1+\left(u_i^{\max}\left\|\left(\left(L_{g_i} V_i\right)^T(x)\right)\right\|\right)^2\right)^{\frac{1}{2}}\right)} & \left(L_{g_i} V_i\right)^T(x) \neq 0 \\ 0 & \left(L_{g_i} V_i\right)^T(x) = 0 \end{cases}$$

with $\beta_i(x) = L_{f_i} V_i(x) + \rho_i V_i(x), \rho_i > 0.$

Let $\Upsilon_i\left(u_i^{max}\right)$ be the largest set of x, containing the origin, such that $\beta_i(x) \leq u_i^{max}\left\|\left(L_{g_i} V_i(x)\right)^T\right\|$. Also, let $\Omega_i^*\left(u_i^{max}\right) := \left\{x \in \Re^n : V_i(x) \leq \varsigma_{x,i}\right\}$ be a level set of V_i, completely contained in Υ_i, for some $\varsigma_{x,i} > 0$, and assume, without loss of generality, that $x(0) \in \Omega_i^*\left(u_i^{max}\right)$ for some $i \in I$. If, at any given time, T, the following conditions hold:

$$\begin{cases} x(T) \in \Omega_l^*\left(u_l^{max}\right) \\ V_l(x(T)) < V_l(x(t_{l*})) \end{cases} \tag{13}$$

For some $l \in I, l \neq i$, where $t_{l*} < T$ is the time when the lth subsystem was last switched in, i.e., for $t \geq T^+$, guarantees that the origin of the switched closed-loop system is asymptotically stable.

The stability requirement of Theorem 2, on the other hand, the behavior is globally input–output linearized according to the previous design as it is allowed to synthesize controllers ensuring the stability of the closed loop system. For this reason, we adopt the following notation $e_k = \xi_k - x_e^k = \left[e_1 \; e_2 \; \ldots \; e_k \right]^T$, $\bar{x}_e = \left[x_e \; x_e^{(1)} \; \ldots \; x_e^{(\gamma_i - 1)} \right]^T$, where $\bar{x}_e^k$, kth time derivative of the reference input x_e which is assumed to be a smooth function of time. Consequently, one may prove that the ξ-subsystem of Eq. (10) will be equivalent to the following more compact form:

$$\dot{e} = \bar{f}_i \left(e, \bar{x}_e \right) + \bar{g}_i \left(e, \bar{x}_e \right) u_i, i = 1, \ldots, N \tag{14}$$

where $\bar{f}_i \left(e, \bar{x}_e \right) = A_i e + b_i L_{f_i}^{\gamma_i} h \left(x \right)$, $\bar{g}_i \left(e, \bar{x}_e \right) = b_i L_{g_i} L_{f_i}^{\gamma_i - 1} h \left(x \right)$ are $\gamma_i \times 1$ vector functions, and

$$A_i = \begin{bmatrix} 0 \; 1 \; 0 \ldots 0 \\ 0 \; 0 \; 1 \ldots 0 \\ \vdots \qquad \vdots \\ 0 \; 0 \; 0 \ldots 0 \\ 0 \; 0 \; 0 \ldots 0 \end{bmatrix}, \; \mathrm{b}_i = \begin{bmatrix} 0 \\ 0 \\ \vdots \\ 0 \\ 1 \end{bmatrix} \tag{15}$$

are $\gamma_i \times \gamma_i$ matrix and $\gamma_i \times 1$ vector, respectively.

We use the above normal form to construct a control Lyapunov Function for each mode of the switched system. A sufficient condition to construct CLF is provided in the following theorem.

Theorem 3 *Consider the system (2) with the form (14), a simple choice for a Control Lyapunov Function is a quadratic function:*

$$\overline{V_i} = e^T P_i e \tag{16}$$

where P_i is a positive definite matrix chosen so that $A_i^T P_i + P_i A_i - P_i b_i b_i^T P_i < 0$.

We must note that the Lyapunov functions $\bar{V}_i$ used in designing the controllers are equal to the Lyapunov functions V_i used in implementing the switching rules because the robust relative degree γ_i is equal to order n of the system.

Using these quadratic CLFs, a controller can be designed for each mode using (12) applied to the system (14). By means of a standard Lyapunov argument, it can be shown that each controller asymptotically stabilizes the e-states in each mode. This result with the Assumptions 3 and 4 can then show that the closed-loop system (14), for each individual mode, is asymptotically stable.

5 Results and Discussion

In this section, we show the applicability and effectiveness of our approach on the CSTR example illustrating the main results of the paper. Let's revisit the CSTR system (1) presented in Sect. 2.

Defining $x = \begin{bmatrix} x_1 & x_2 \end{bmatrix} = \begin{bmatrix} C_A & T \end{bmatrix}$, $u = [Q_r]$, and $y = [T]$. The model of CSTR (1) can be written under the same form of system (2). Hence, we have:

$$f_i(x) = \begin{bmatrix} -Z_r \, exp\left(-\frac{E_a}{R_r x_2}\right) x_1 + \left(C_{A_0} - x_1\right) \frac{F_r}{V_0} + (i-1)\left(C^*_{A_0} - x_1\right) \frac{F^*_r}{V_0} \\ \gamma_r Z_r \, exp\left(-\frac{E_a}{R_r x_2}\right) x_1 + \left(T_{A_0} - x_2\right) \frac{F_r}{V_0} + (i-1)\left(T^*_{A_0} - x_2\right) \frac{F^*_r}{V_0} \end{bmatrix},$$

$$g_i(x) = \begin{bmatrix} 0 \\ \\ 1 \end{bmatrix} \text{ and } h(x) = x_2$$

We apply the approach presented in Sect. 3, the system given by (1) satisfying the Assumptions 2 and 3 is transformed by the two following modes:

- Mode 1:

$$\begin{cases} \dot{\xi}_1 = \underbrace{\gamma_r Z_r \, exp\left(-\frac{E_a}{R_r x_2}\right) x_1 + \left(T_{A_0} - x_2\right) \frac{F_r}{V_0}}_{\xi_2} + \underbrace{u_1}_{\psi_{1,1}(x,u_1)} \\ \dot{\xi}_2 = L^2_{f_1} h(x) + L_{g_1} L_{f_1} h(x) \, u_1 \end{cases} \tag{17}$$

where $\begin{cases} L^2_{f_1} h(x) = \left[\gamma_r Z_r \, exp\left(-\frac{E_a}{R_r x_2}\right)\right] \times \left[Z_r x_1 \, exp\left(-\frac{E_a}{R_r x_2}\right) + \left(C_{A_0} - x_1\right) \frac{F_r}{V_0}\right] \\ + \left[\left(\frac{\gamma_r Z_r E_a x_1}{R_r x_2^2}\right) exp\left(-\frac{E_a}{R_r x_2}\right) + \frac{F_r}{V_0}\right] \times \left[\gamma_r Z_r x_1 \, exp\left(-\frac{E_a}{R_r x_2}\right) - \left(T_{A_0} - x_2\right) \frac{F_r}{V_0}\right] \end{cases}$

and $L_{g_1} L_{f_1} h(x) = \left(\frac{\gamma_r Z_r E_a x_1}{R_r x_2^2}\right) exp\left(-\frac{E_a}{R_r x_2}\right) + \frac{F_r}{V_0}$

- Mode 2:

$$\begin{cases} \dot{\xi}_1 = \underbrace{\gamma_r Z_r \, exp\left(-\frac{E_a}{R_r x_2}\right) x_1 + \left(T_{A_0} - x_2\right) \frac{F_r}{V_0} + \left(T^*_{A_0} - x_2\right) \frac{F^*_r}{V_0}}_{\xi_2} + \underbrace{u_2}_{\psi_{2,1}(x,u_2)} \\ \dot{\xi}_2 = L^2_{f_2} h(x) + L_{g_2} L_{f_2} h(x) \, u_2 \end{cases} \tag{18}$$

where $\begin{cases} L^2_{f_1} h(x) = \left[\gamma_r Z_r \, exp\left(-\frac{E_a}{R_r x_2}\right)\right] \times \left[Z_r x_1 \, exp\left(-\frac{E_a}{R_r x_2}\right) + \left(C_{A_0} - x_1\right) \frac{F_r}{V_0} + \left(C^*_{A_0} - x_1\right) \frac{F^*_r}{V_0}\right] \\ + \left[\left(\frac{\gamma_r Z_r E_a x_1}{R_r x_2^2}\right) exp\left(-\frac{E_a}{R_r x_2}\right) + \frac{F_r}{V_0} + \frac{F^*_r}{V_0}\right] \times \left[\gamma_r Z_r x_1 \, exp\left(-\frac{E_a}{R_r x_2}\right) - \left(T_{A_0} - x_2\right) \frac{F_r}{V_0} + \left(T^*_{A_0} - x_2\right) \frac{F^*_r}{V_0}\right] \end{cases}$

and

$$L_{g_2}L_{f_2}h\,(x) = \left(\frac{\gamma_r Z_r E_a x_1}{R_r x_2^2}\right)\ exp\left(-\frac{E_a}{R_r x_2}\right) + \frac{F_r}{V_0} + \frac{F_r^*}{V_0}$$

with $e = \left[\, e_1 = \xi_1 - x_e \;\; e_2 = \xi_2 - \dot{x}_e \,\right]^T$, a scalar system under the same form of system (14), describing the approximate input–output dynamics, can be obtained for controller design:

- For mode 1:

$$\dot{e} = \bar{f_1}\,(e, \bar{x}_e) + \bar{g}_1\,(e, \bar{x}_e)\,u_1 \tag{19}$$

where $\bar{f_1}\,(e, \bar{x}_e) = A_1 e + b_1 L_{f_1}^2 h(x)$, $\bar{g}_i\,(e, \bar{x}_e) = b_1 L_{g_1} L_{f_1} h(x)$,

$$A_1 = \begin{bmatrix} 0 & 1 \\ 0 & 0 \end{bmatrix} \text{ and } \mathrm{b}_1 = \begin{bmatrix} 0 \\ 1 \end{bmatrix}$$

- For mode 2:

$$\dot{e} = \bar{f_2}\,(e, \bar{x}_e) + \bar{g}_2\,(e, \bar{x}_e)\,u_2 \tag{20}$$

where $\bar{f_2}\,(e, \bar{x}_e) = A_2 e + b_2 L_{f_2}^2 h(x)$, $\bar{g}_2\,(e, \bar{x}_e) = b_2 L_{g_2} L_{f_2} h(x)$, $A_2 = \begin{bmatrix} 0 & 1 \\ 0 & 0 \end{bmatrix}$ and $b_2 = \begin{bmatrix} 0 \\ 1 \end{bmatrix}$.

For each mode $i\,(i = 1, 2)$ the relative degree $\gamma_i = 2$, then the choice $V_i = \bar{V}_i$ is sufficient.

We construct the controllers and for each mode $i\,(i = 1, 2)$ under the same form of Eq. (14) satisfying the Theorem 3, we choose the following quadratic Lyapunov functions:

- $V_1 = \bar{V}_1$ for mode 1:

$$V_1 = \bar{V}_1 = \frac{1}{2}c_1 e_1^2 + \frac{1}{2}c_2 e_2^2 \tag{21}$$

- $V_2 = \bar{V}_2$ for mode 2:

$$V_2 = \bar{V}_2 = \frac{1}{2}c_3 e_1^2 + \frac{1}{2}c_4 e_2^2 \tag{22}$$

The stabilizing controller u_1 is:

$$u_1 = -\left(L_{\bar{g}_1}\bar{V}_1\right) \times \left(\frac{L_{\bar{f}_1}\bar{V}_1 + 1.2V_1 + \left(\left(L_{\bar{f}_1}\bar{V}_1 + 1.2\bar{V}_1\right)^2 + \left(u_1^{max} L_{\bar{g}_1}\bar{V}_1\right)^4\right)^{\frac{1}{2}}}{\left(L_{\bar{g}_1}\bar{V}_1\right)^2\left(1 + \left(u_1^{max} L_{\bar{g}_1}\bar{V}_1\right)^2\right)^{\frac{1}{2}}}\right) \tag{23}$$

The stabilizing controller u_2 is:

$$u_2 = -\left(L_{\bar{g}_2}\bar{V}_2\right) \times \left(\frac{L_{\bar{f}_2}\bar{V}_2 + 2.3V_2 + \left(\left(L_{\bar{f}_2}\bar{V}_2 + 2.3\bar{V}_2\right)^2 + \left(u_2^{max} L_{\bar{g}_2}\bar{V}_2\right)^4\right)^{\frac{1}{2}}}{\left(L_{\bar{g}_2}\bar{V}_2\right)^2 \left(1 + \left(u_2^{max} L_{\bar{g}_2}\bar{V}_2\right)^2\right)^{\frac{1}{2}}} \right) \tag{24}$$

In order to validate the performance of the proposed approach, we have performed the simulations on Matlab.

A first simulation study is shown in Figs. 1 and 2. In these figures (solid lines) we respectively represent the evolution of the reaction temperature and the evolution of the control variable when the reactor is initialized at $x(0) = x_0 = \left[13\,\text{kmol m}^{-3}\ 293\,\text{K}\right]$ and is operating in mode1 for all times (without switching). We observe that for this mode the controller successfully stabilizes the reactor temperature at the desired steady-state ($x_e = 302.0\,\text{K}$).

Figures 1 and 2 (dashed lines) depict the result when the reactor (initialized at x_0 within) switches to mode 2 at a randomly chosen time t = *1.1* min. It is clear that in this case the controller is unable to stabilize the temperature at the desired steady-state. The reason is the fact that at $t = 1.1$ min, the state of the system lies

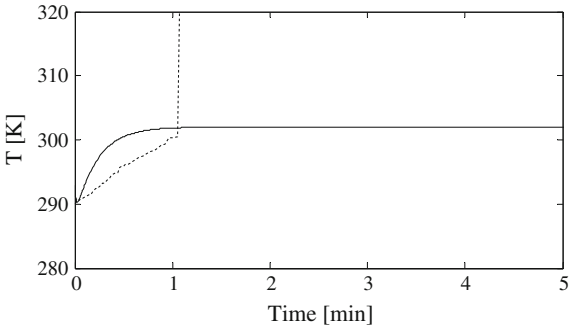

Fig. 1 Evolution of the reactor temperature when the reactor is initialized and operates in mode 1 (*solid*), when the reactor switches to mode 2 at t = 1.1 min (*dashed*)

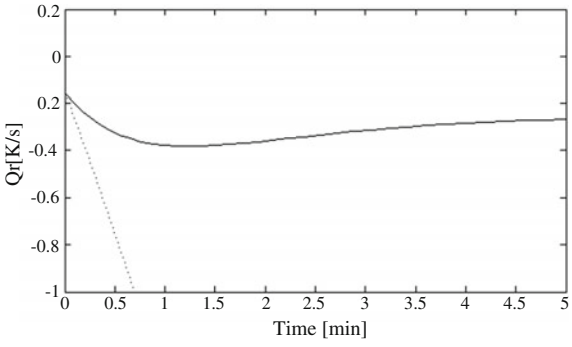

Fig. 2 Evolution of the controller when the reactor is initialized and operates in mode 1 (*solid*), when the reactor switches to mode 2 at $t = 1.1$ min (*dashed*)

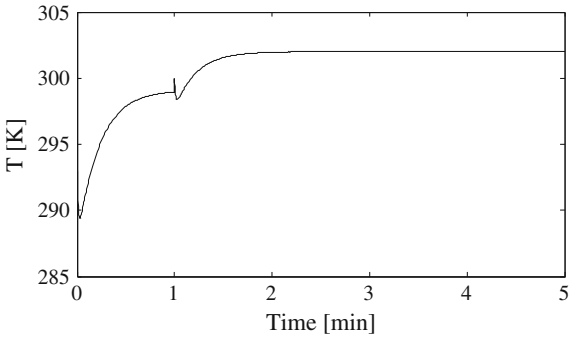

Fig. 3 Evolution of the reactor temperature while applying the Theorem 2

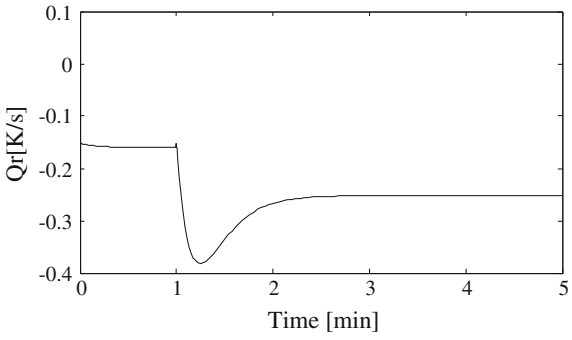

Fig. 4 Evolution of the controller while applying the Theorem 2

outside the stability region of mode 2 and, therefore, the available control action is insufficient to achieve stabilization.

To avoid this instability, we used the switching scheme proposed in Theorem 2 in a second study. The simulation results representing the evolution of the reaction temperature and the evolution of the control variable are respectively given by Figs. 3 and 4. It appears in these figures that the controllers successfully drive the reactor temperature to the desired steady-state ($x_e = 302.0$ K) and maintain it there with the available control action.

6 Conclusions

In this chapter, we have considered the global stabilization problem of a class of non-minimum phase switched nonlinear systems where the global stabilization problem of individual subsystems is not assumed to be solvable when applying the formalism of the input–output feedback linearization.

Based on the MLFs method and the Hauser's approximation, we have designed state feedback controllers of subsystems and constructed a switching law, which guarantees global asymptotic stability of the corresponding closed-loop system.

The main idea is the coupling between the switching strategy and the stability regions arising from the limitations imposed by the input constraints. A set of switching rules is designed to stabilize the transitions between the stability regions associated for each mode. We demonstrated the efficiency of the proposed approach through a non-minimum phase CSTR example.

References

1. Abdelkrim A, Jouili K (2014) Input-state feedback control of switched nonlinear systems using multiple Lyapunov functions. In: Proceedings of the international conference on control, engineering and information technology: (CEIT'14). Copyright IPCO-2014 ISSN 2356–5608
2. Abdelkrim A, Jouili K, Benhadj Braeik N (2013) An advanced linearization control for a class of switched nonlinear systems. In: 14th IEEE international conference on sciences and techniques of automatic control and computer engineering: (STA'13), pp 14–19
3. Abdelkrim A, Jouili K, Benhadj Braiek N (2015) Synthesis of a switching control approach based on the input-output feedback linearization. In: International of automatic control. I.RE.A.CO 8:1–8
4. Abdelkrim A, Jouili K, Benhadj Braeik N (2015) Stabilization of CSTR with arbitrary switchings using backstepping approach. In: Proceedings of engineering and technology, international conference on automation, control, engineering and computer science (ACECS'15), in press
5. Adesina AA, Adewale KEP (1991) Steady-state cubic autocatalysis in an isothermal stirred tank. Ind Eng Chem Res 30:430–434
6. Barkhordari MY, Jahed-Motlagh MR (2009) Stabilization of a CSTR with two arbitrarily switching modes using modal state feedback linearization. Chem Eng J 155:838–843
7. Barton PI, Lee CK (2002) Modeling, simulation, sensitivity analysis, and optimization of hybrid systems. ACM Trans Model Comput Simul 12:256–289
8. Benosman M, Lum KY (2007) Output trajectory tracking for a switched nonlinear non-minimum phase system. In: Proceedings of the 16th IEEE international conference on control applications. Singapore, pp 262–269
9. Branicky SM (1998) Lyapunov multiple, functions and other analysis tools for switched and hybrid systems. IEEE Trans Autom Control 43:475–482
10. Chesi G (2009) On, the minimum stable commutation time for switching nonlinear systems. IEEE Trans Autom Control 54:1284–1289
11. Decarlo AR, Branicky MS, Petterson S, Lennartson B (2000) Perspectives and results on the stability and stabilizability of hybrid systems. IEEE Proc 88:1069–1082
12. El-Farra NH, Christofides PD (2002) Switching and feedback laws for control of constrained switched nonlinear systems. In: Tomlin CJ, Greenstreet MR (eds) Lecture notes in computer science, vol 2289. Springer, Berlin, pp 164–178
13. El-Farra NH, Mhaskar P, Christofides PD (2005) Output feedback control of switched nonlinear systems using multiple Lyapunov functions. Syst Control Lett 54:1163–1182
14. Engell S, Stursberg O (2005) Hybrid control techniques for the design of industrial controllers. In: Proceedings of the 44th IEEE conference on decision and control, and the European control conference. Seville, Spain
15. Fissore D (2008) Robust control in presence of parametric uncertainties: observer-based feedback controller design. Chem Eng Sci 63:1890–1900
16. Ge SS, Hang CC, Zhang T (1998) Nonlinear adaptive control using neural networks and its application to CSTR systems. J Process Control 9:313–323
17. Hauser J, Sastry S, Kokotovic PV (1992) Nonlinear control via approximate input-output linearization: the ball and beam example. IEEE Trans Autom Control 37:392–398

18. Hu T, Ma L, Lin Z (2008) Stabilization of switched systems via composite quadratic functions. IEEE Trans Autom Control 53:2571–2585
19. Isidori A (1995) Nonlinear control systems: an introduction, 3rd edn. Springer, Heidelberg
20. Jouili K, Benhadj Braeik N (2015) Stabilization of non-minimum phase switched nonlinear systems with the concept of multi-diffeomorphism. Comm Nonlinear Sci Numer Simulat 23:282–293
21. Jouili K, Abdelkrim A, Benhadj Braeik N (2015) Control of non-minimum phase switched nonlinear systems using multiple Lyapunov functions. In: Proceedings of engineering and technology, international conference on automation, control, engineering and computer science (ACECS'15), in press
22. Lee CT, Jiang PZ (2008) Uniform asymptotic stability of nonlinear switched systems with an application to mobile robots. IEEE Trans Autom Control 53:1235–1252
23. Liberzon D, Morse AS (1999) Basic problems in stability and design of switched systems. IEEE Control Syst Mag 19:59–70
24. Lin H, Antsaklis PJ (2009) Stability and stabilizability of switched linear systems: a survey of recent results. IEEE Trans Autom Control 54:308–322
25. Lin Y, Sontag ED (1991) A universal formula for stabilization with bounded controls. Syst Control Lett 16:393–397
26. Oishi M, Tomlin C (2000) Switching in non-minimum phase systems: applications to a VSTOL aircraft. In: Proceedings of American control conference. Chicago, USA'2000, pp 487–491
27. Panjapornpon C, Soroush M (2006) Control of non-minimum-phase nonlinear systems through constrained input–output linearization. In: Proceedings of the 2006 American control conference. Minneapolis, Minnesota, USA, pp 14–16
28. Peleties P, Decarlo R (1991) Asymptotic stability of m-switched systems using Lyapunov-like functions. In: Proceedings of American control conference. Boston, pp 1679–1684
29. Shorten R, Wirth F, Mason O, Wulff K, King C (2007) Stability criteria for switched and hybrid systems. SIAM Rev 49:545–592
30. Salehi S, Shahrokhi M (2009) Adaptive fuzzy backstepping approach for temperature control of continuous stirred tank reactors. Fuzzy Sets Syst 160:1804–1818
31. Sontag DE (1983) A Lyapunov-like characterization of asymptotic controllability. SIAM J Control Opt 21:462–471
32. Sun Z, Ge SS (2005) Switched linear systems: control and design, 1st edn. Springer, Berlin
33. Tomlin CJ, Sastry SS (1998) Switching through singularities. Syst Control Lett 35:145–154
34. Wang M, Dimirovski GM, Zhao J (2008) H∞ control for a class of non-minimum phase cascade switched nonlinear systems. In: Proceedings of American control conference. Seattle, USA, pp 5080–5085
35. Yanga H, Jianga B, Zhangb H (2012) Stabilization of non-minimum phase switched nonlinear systems with application to multi-agent systems. Syst Control Lett 61:1023–1031
36. Ye H, Michel N, Hou AL (1998) Stability theory for hybrid dynamical systems. IEEE Trans Autom Control 43:461–474

Nonlinear Sliding Mode Observer for Tire Pressure Monitoring

Nada Ouasli and Lilia El Amraoui

Abstract The tire is an essential element for road holding, comfort and safety of a vehicle. Nevertheless, under inflation will cause rapid tire wear and increases fuel consumption. It is therefore important to develop Tire pressure Monitoring Systems (TPMS). One approach, called "direct", consisting in using pressure sensors proves to be expensive and unreliable (possibility of breakdowns). New generations of TPMS favor "indirect" methods without pressure sensor. Supervision is carried from physical quantities related to the pressure. The drop in pressure results a decrease in effective radius of wheel and an increase in rolling resistance force. We study in the context of this chapter, the possibility to use the models of longitudinal and rotational dynamics of the two front wheels and the vehicle for the implementation of nonlinear observer, which variables depend on the pressure. The observer is based on a higher order sliding mode approach, allowing finite time convergence of the estimation error and robustness face disturbance. The originality of the presented results consists in providing a joint estimation of three variables, namely, the effective radii of wheels and rolling resistance force of the front axle, without use of additional sensors.

Keywords Wheels' effective radii · High order sliding mode observer · Rolling resistance force · Tire monitoring system

1 Introduction

The tires are the only physical link between the vehicle and the road, their impact on safety is crucial. Their physical properties that affect its dynamic behavior are largely related to its pressure. A drop in pressure has a direct impact on characteristics

N. Ouasli (✉) · L. El Amraoui (✉)
National Engineering School of Carthage, Research Unit Signals and Mechatronic Systems, University of Carthage, 2035 Tunis-Carthage, Tunisia
e-mail: nada.ouasli.esti@gmail.com

L. El Amraoui
e-mail: lilia.elamraoui@esti.rnu.tn

S. Vaidyanathan and C. Volos (eds.), *Advances and Applications in Nonlinear Control Systems*, Studies in Computational Intelligence 635,
DOI 10.1007/978-3-319-30169-3_28

such as damping, stiffness and rigidity of the tire. Any unsuitable inflation leads to increase fuel consumption, accentuate the risk of explosion and cause rapid wear of the tire. In addition, the chassis configuration of current vehicles, designed to provide optimum road holding, tends to mask the effects of inflation problem. For the driver, the behavior of the car seems to remain in a normal situation until it is faced with an emergency or more radically to an incident [7]. It is therefore important to inform the driver of any anomaly by displaying a message on the dashboard. It is the vocation of the tire pressure monitoring system.

The tire pressure monitoring system is intended to improve the safety of the equipped vehicle. Over the years, various statistics have shown that over 40 % of vehicles are driven with tires under inflated by an average 0.6 bars and that many accidents are due to a failure primarily caused by pressure loss [5].

These accidents have led to the development of Tire Pressure Monitoring Systems (TPMS) to supervise permanently the pressure. A European regulation which comes into force in 2012 requires the presence of such systems on all new vehicles. The constraint is that the minimum pressure loss that these systems must be able to detect, is 25 % of the hot pressure. In addition, a pressure drop on a wheel must be detected in less than 10 min and more wheels in less than 1 h [5].

Many research aims to improve the performance of existing systems and to design innovative solutions (especially without pressure sensors) corresponding to new regulations. Two techniques are proposed to measure the physical parameters of tires: The first strategy (direct approach) is to directly measure the pressure in each tire, thanks to pressure sensors installed at the inflation valve [25]. Nevertheless, the presence of the sensors may have disadvantages such as a reduction in the reliability of the system caused by the risk of damage of sensors in case of shock intervening during rolling or when the wheels are removed, furthermore, the need to add additional cabling thus a significant price increase. To overcome these disadvantages, an alternative is to favor methods without pressure sensor for reasons of economy and reliability, and also for monitoring in case of sensor failure in a direct approach.

The indirect approach can detect a fall pressure from physical measurements already used by the central computer of the vehicle (angular wheels speeds, acceleration, useful torque, steering wheel angle) without adding sensors for measuring the tire pressure. The underlying idea is to use the effect of pressure on certain physical variables to detect its variations. Indeed, the drop in tire pressure leads for example by a decreased in effective radii of wheels, an increase in their angular velocities and an increase in rolling resistance force. It would be sufficient, thanks to appropriate tools, using these physical quantities as indicators of the state of the pressure [21].

2 Motivation, Related Work, and Objectives

A variation in the pressure in the tire leads to decrease in its effective radius and increase in rolling resistance force. Thus, first key information related to the wheel is its effective radius. In fact, knowledge of effective radius has several advantages:

the estimated effective radius in real time can be used to inform the driver of tire pressure level and its evolution in order to emit an alarm [19]. There is therefore a great interest in trying to estimate the effective radius. An assessment of the value of this radius may be obtained from the vehicle speed, the angular velocity of the wheel and the slip-ratio [22].

Another feature providing information about the tire pressure is the rolling resistance force. The variation of this force is in fact indicative of the general state of the vehicle in terms of load, tire pressure or road type. Moreover, the rolling resistance force acts not only on the longitudinal dynamics of the vehicle, but also, and very significantly, on the fuel consumption [26]. As it will be seen later in this chapter, the rolling resistance force is much more sensitive to pressure variation than the radius (larger relative variations) but the vehicles are not equipped with rolling resistance sensor, so there is a real interest in assessing this force. In addition to detect pressure loss, the estimation of rolling resistance force can detect a vehicle overload and improve vehicle control strategies in this type of situation.

Studies have already focused on the estimator design for vehicle wheels radii [19] and have proposed to use this estimation for the diagnosis of pressure in tires [3]. The used models consider that the rolling resistance force can be measured a priori under normal driving conditions, and then connected to the vehicle speed and the load by using empirical models. Nevertheless, according to [8], the rolling resistance force is heavily dependent on the tire parameters, e.g., pressure and temperature, type of road and the vehicle speed. Consequently, such approaches cannot be used in driving conditions and online estimation of the rolling resistance force is necessary. Note that in [27], the longitudinal stiffness and the effective radius assumed as being constant are identified from the correction terms of a sliding mode observer. An estimation of the pressure in the tire is deduced from the identified value of the radius. This observer considers the angular position, angular velocity of the wheel and the vehicle speed as state variables. It uses the measurement of the angular position of the wheel provided by the ABS encoders and the measuring speed vehicle. The unknown terms of the observation model are written as a function of the longitudinal stiffness and the effective radius in order to identify those parameters.

The work on the assessment of the rolling resistance force has been, to our knowledge, mainly based on tests using laboratory measurement benches and static models of finite elements [1]. This allows establishing the characteristic curves of the rolling resistance based on road type, vehicle load and tire temperature. The rolling resistance force is determined offline. In addition, these tests are carried out in very specific experimental conditions versus actual driving conditions. Note finally that much work has also been made on the synthesis of observers for the purpose to estimate other variables of the wheel or the vehicle (longitudinal stiffness coefficient of adhesion between tire and the soil and lateral speed of the vehicle; forces and parameters required for controlling the vehicle [27]; differential between the useful torque and braking torque applied to the wheel [24]; tire-soil friction).

The contribution of this chapter is to apply an online evaluation of effective radii of the front wheels and the rolling resistance of the whole axle, in order to analyze the unknown variations of the pressure. The originality is located in:

- observation model using nonlinear dynamics and consideration of the effective radius and the rolling resistance force as state variables,
- observation strategy "by sliding mode" which main features are the robustness opposite to uncertainty and disturbance and convergence in finite time.

In this chapter is proposed the synthesis of a nonlinear observer based on technical of high order sliding mode [4]: an observer, applied on the front axle, the effective radii of the wheels and the global rolling resistance force of the whole axle. As will be seen later in this chapter, these estimated values are all dependent on the pressure; their variations, thus, allows to evaluate the variation of the pressure. This observer is designed to reconstruct unmeasured variables (effective radii and the rolling resistance force) of the wheels based on available measurements of mechanical quantities (angular speeds provided by ABS encoders and useful torque).

The remaining parts of this chapter are structured as follows. Section 3 presents the notions of observability of nonlinear systems, and the canonical form of observability of such systems. Section 4 presents solutions for the observation of nonlinear systems, with particular emphasis on high order sliding mode observer. Section 5 presents the physical model of longitudinal and rotational dynamics of a vehicle coupled with the model of the vertical dynamics. From this model will be carried out, in Sect. 6, a study of the influence of the pressure drop in the front tires on three parameters: the effective radius of each wheel and the rolling resistance force of the whole axle, being based on the synthesis of a nonlinear sliding mode observer. Section 7 presents conclusions and future research directions of the work presented in this chapter.

3 Observability and Observers

The synthesis of an observer for a physical system begins by the following question: Is it the system observable, that means, is it possible to estimate the overall state of the system from the measurements performed? The corollary to this question is: which outputs measured use to make the system observable? In addition, in the case where the systems are represented by nonlinear models, analysis of observability should highlight the presence of possible singularities. Indeed, a notable difference between the observability of nonlinear and linear dynamic systems lies in the fact that the observability of nonlinear systems potentially depends of the input of the system and the state and it may therefore be losses observability according borrowed trajectories.

3.1 Observability: Concept and Criteria

Consider the nonlinear system of the form:

$$\begin{cases} \dot{x} = f(x, u) \\ y = h(x) \end{cases} \tag{1}$$

where $x \in \mathbb{R}^n$ represents the state, $u \in \mathbb{R}^m$ the input and $y \in \mathbb{R}^p$ the output. $f(:;:)$ and $h(:)$ are analytic functions. It is assumed that the functions $f(:;:)$ and $h(:)$ are meromorphic functions of x and u. We also assume that $u(t)$ is admissible, that is to say, measurable and bounded. According to [10], observability is defined from the notion of indistinguishability.

Definition 3.1.1 Two initial states $x(t_0) = x_1$ and $x(t_0) = x_2$ are indistinguishable for the system (1) if, $\forall t \in [t_0, t_1]$ the corresponding outputs $y_1(t)$ and $y_2(t)$ are the same regardless of the allowable input $u(t)$ of the system.

Definition 3.1.2 The nonlinear system (1) is said observable, if it does not admit indistinguishable pair. This means that the system is said observable if there is no distinct initial state that cannot be separated by review of the system output.

Definition 3.1.3 Considering the system (1), space observability H, is defined by the smallest vector space containing the outputs; $h_1, h_2, \ldots, h_p$ and closed under the operation of the derivation Lie to the vector field $f(x, u)$, u being fixed. We denote dH the space of differential elements H.

Definition 3.1.4 The space $dH(x_0)$ characterizes the local low observability x_0 of system (1).

System (1) is said to satisfy the observability rank condition x_0 if : $\dim(dH(x_0)) = n$.

The system (1) satisfies the rank condition of observability if $\forall x \in \mathbb{R}^n$, $\dim(dH(x)) = n$.

Definition 3.1.5 For system (1), the space generic observability [23] is defined by $O = X \cap (Y + U)$, with:

$$\begin{cases} X = Span_K \{d_x\} \\ Y = Span_K \left\{ d_u^{(j)} \right\}, j \geq 0 \\ U = Span_K \left\{ d_y^{(q)} \right\}, q \geq 0 \end{cases} \tag{2}$$

or K is the set of meromorphic functions and $Span_K$ is the space generated on K of meromorphic functions of x and of a finite number of derivatives of u. System (1) is said generically observable if:

$$\dim O = n \tag{3}$$

A property is generically satisfied when it is locally satisfied around a point $x_0 \in M \subset \mathbb{R}^n$. An equivalent algebraic definition can also be given. A system is generically observable if the whole state can be expressed as a function of y, of u and a finite number of their derivatives (with $j \in \mathbb{N}$, $q \in \mathbb{N}$):

$$x = X(y, \dot{y}, \ldots, y^{(j)}, u, \dot{u}, \ldots, u^{(j)}) \tag{4}$$

In the nonlinear context, observability depends clearly of u and state x. The generic aspect is that we are not interested in any singularities.

Suppose that condition (3) is satisfied, and then we can check the equivalent condition of this definition. This ultimately amounts to analyzing the observability of a local perspective that is to say in an area defined by physical constraints.

Definition 3.1.6 System (1) is said locally observable if for any $x \in M \subset \mathbb{R}^n$ and $u \in U \subset \mathbb{R}^p$ (M and U being respectively open in $\mathbb{R}^n$ and $\mathbb{R}^p$):

$$Rang_K \left[dy \; d\dot{y} \ldots dy^{(n-1)} \right]^T = n \tag{5}$$

An equivalent criterion focuses on the analysis of vector Ψ

$$\Psi = \left[dy \; d\dot{y} \ldots dy^{(n-1)} \right]^T \tag{6}$$

Definition 3.1.7 **S**ystem (1) is said locally observable if for $x \in M$ and $u \in U$:

$$\det \left(\frac{\partial \Psi}{\partial x} \right) \neq 0 \tag{7}$$

The last property implies that Ψ defines a transformation of state on this consider field. In the following, the term "observable" will mean "locally observable". If there is a singularity of observability, it obviously causes problems for the proper functioning of the observers. A first solution is to pass the observer, in estimator mode (this means to putting the observer in "open loop": there are no correction term). Another solution is to switch to another observer structure, e.g. by using different indices of observability [17].

3.2 Canonical Forms of Observability and Observer

Based on the form of the dynamic system of the tire used in the rest of this chapter, we consider the following nonlinear system:

$$\begin{cases} \dot{x} = f(x) + \Delta f(x, t) + \chi(y, u) \\ y = h(x) \end{cases} \tag{8}$$

with $x \in M$ and $u \in U$ the additive uncertainty term $\Delta f(x,t)$ sufficiently derivable and the additive terms which only depends on well-known variables (measurements and control) grouped in the vector called "input–output injection" $\chi(y,u)$.

Consider the following assumptions:

Assumption 3.2.1 The additive uncertainty term $\Delta f(x,t)$ does not change the observability of (8):

i.e. $\|\Delta f\| \leq F_H < \infty, \forall x \in M$ and $t \geq 0$.

Like the goal is to synthesize an observer, and Δf is unknown and verified this assumption, therefore consider the nonlinear system (8) without any uncertainty ($\Delta f = 0$).

$$\begin{cases} \dot{x} = f(x) + \chi(y,u) \\ y = h(x) \end{cases} \tag{9}$$

Assumption 3.2.2 The input–output injection $\chi(y,u)$ does not change the observability of the system [2].

The main idea is simple: for the purpose to analyze the observability, then to synthesize the observer, the system (8) is transformed into a simple system and well known from which observability will be analyzed, and observer designed. Adding to the observer the input–output injection term, we obtain an observer for (9). Remains to propose an adequate solution for that this observation is sufficiently robust to provide a good estimate of the uncertain system (8). Via an input–output injection defined by $\chi(y,u)$, the nonlinear system (9) can be transformed into:

$$\begin{cases} \dot{x} = f(x) \\ y = h(x) \end{cases} \tag{10}$$

Assumption 3.2.3 Consider the system (10) and p integers $\{k_1, k_2, \ldots, k_p\}$ defined such that [14]:

$\sum_{i=1}^{p} k_i = n$ and $k_1 \geq k_2 \geq \cdots \geq k_p$ after numbering of output components if necessary.

The function $\Psi(x)$ defined by:

$$\Psi(x) = \begin{bmatrix} [y_1(x) \cdots y_1^{(k_1-1)}(x)]^T \\ \vdots \\ [y_p(x) \cdots y_p^{(k_p-1)}(x)]^T \end{bmatrix}_{x \in M} \tag{11}$$

verifies:

$$\det\left(\frac{\partial \psi(x)}{\partial x}\right) \neq 0 \tag{12}$$

The function $\zeta = \Psi(x)$ is thus a state transformation. The integers $\{k_1, k_2, \ldots, k_p\}$ are called observability indices.

Proposition 3.2.1 *Given the Assumptions 3.2.1; 3.2.2 and 3.2.3, the system (8) is observed for $x \in M$ and $u \in U$.*

Consider again the system (8) verifying the Assumptions 3.2.1 and 3.2.3. By asking $\zeta = \left[y\ \dot{y} \cdots y^{(n-1)} \right]^T$, is obtained by:

$$\begin{aligned} \dot{\zeta} &= A\zeta + \begin{bmatrix} 0 \\ 0 \\ 0 \\ \vdots \\ \Phi(\zeta) \end{bmatrix} \\ y &= C\zeta \end{aligned} \tag{13}$$

with:

$$A = \begin{bmatrix} 0\,1\,0\,0 \cdots 0 \\ 0\,0\,1\,0 \cdots 0 \\ \vdots\ \vdots\ \vdots\ \vdots\ \ \vdots\ \ \vdots \\ 0\,0\,0\,0 \cdots 1 \\ 0\,0\,0\,0 \cdots 0 \end{bmatrix}, C = \begin{bmatrix} 1\,0\,0 \cdots 0 \end{bmatrix} \text{ and } \Phi(\zeta) = y^{(n)} \tag{14}$$

The representation (13) is called "canonical form of observability". Given system (8), it is clear that the term $\Phi(\zeta)$ is uncertain; is assumed to be written:

$$\Phi(\zeta) = \Phi_n + \Delta\Phi \tag{15}$$

with Φ_n the "nominal" part (composed of parameters and dynamics known derived from the term $f(x)$) and "uncertain" part $\Delta\Phi$ (derived from $\Delta f(x,t)$). Is thus obtained:

$$\dot{\zeta} = A\zeta + \begin{bmatrix} 0 \\ 0 \\ 0 \\ \vdots \\ \Phi_n(\zeta) \end{bmatrix} + \begin{bmatrix} 0 \\ 0 \\ 0 \\ \vdots \\ \Delta\Phi \end{bmatrix} \tag{16}$$

Proposition 3.2.2 *An observer for the system (16) is written in the form:*

$$\dot{\hat{\zeta}} = A\hat{\zeta} + \begin{bmatrix} 0 \\ 0 \\ 0 \\ \vdots \\ \Phi_n(\zeta) \end{bmatrix} + k(y, \hat{\zeta}) \tag{17}$$

The function k is the correction term which ensures convergence of the estimated state to the actual state $\hat{\zeta} \to \zeta$.

The term $k(y, \zeta)$ can be obtained by various methods (high gains, sliding mode,…) and must ensure convergence (exponentially or in finite time) of the observer to the real system, i.e., it ensures that $\hat{\zeta} \to \zeta$ exponentially or in finite time despite the presence of uncertain term $\Delta\Phi$. In addition, it depends only on the measured output y and the estimated state vector $\hat{\zeta}$. To summarize, knowing that the dynamics of the estimation error is written:

$$\dot{e} = Ae + \begin{bmatrix} 0 \\ 0 \\ 0 \\ \vdots \\ \Phi_n(\hat{\zeta}) - \Phi_n(\zeta) \end{bmatrix} - \begin{bmatrix} 0 \\ 0 \\ 0 \\ \vdots \\ \Delta\Phi \end{bmatrix} + k(y, \hat{\zeta}) \tag{18}$$

with $e = (\zeta - \hat{\zeta}) \to 0$

It is necessary to choose that the correction term $k(y, \zeta)$ such that the observer converges to the real system despite the initial error $e(0)$ and the uncertain term $\Delta\Phi$. From (17), two methods can be used to obtain the vector $\hat{x}$, representing the estimated x.

- When the inverse of the transformation Ψ, i.e. Ψ^{-1}, can be analytically calculate, the estimated state $\hat{x}$ is deduced from $\hat{\zeta}$ by:

$$\hat{x} = \Psi^{-1}(\zeta) \tag{19}$$

- In many cases of applications [17], it is very difficult to calculate the inverse of Ψ (including with formal calculation software). In this case, using an approach based on the calculation of the inverse Jacobian of Ψ. As $\hat{\zeta} = \Psi(\hat{x})$, we can write:

$$\dot{\hat{\zeta}} = \frac{\partial \Psi}{\partial \hat{x}} \dot{\hat{x}} \to \dot{\hat{x}} = \left[\frac{\partial \Psi}{\partial \hat{x}}\right]^{-1} \dot{\hat{\zeta}} \tag{20}$$

According to (17) and (20), is obtained

$$\dot{\hat{x}} = \left[\frac{\partial \Psi}{\partial \hat{x}}\right]^{-1} \left(A\hat{\zeta} + \begin{bmatrix} 0 \\ 0 \\ 0 \\ \vdots \\ \Phi_n(\hat{\zeta}) \end{bmatrix} + k(y, \hat{\zeta}) \right) \tag{21}$$

Then, from (17) and (21), an observer for the system (10) can be written by:

$$\dot{\hat{x}} = f(\hat{x}) + \left[\frac{\partial \Psi}{\partial x}\right]^{-1} k(y, \hat{x}) \tag{22}$$

Applying the inverse transform of the input–output injection $\chi(y, u)$ allows to obtain the observer for the system (9):

$$\dot{\hat{x}} = f(\hat{x}, y) + \chi(y, u) + \left[\frac{\partial \Psi}{\partial \hat{x}}\right]^{-1} k(y, \hat{x}) \tag{23}$$

In the following section, an observer of the type (23) is proposed to estimate "sufficiently" a precise state x of the system (8) despite the uncertain term Δf, and this thanks to a judicious choice of k. In the following, we consider:

Assumption 3.2.4 For every $\zeta \in M_\zeta$(M_ζ being the area of application in the state space ζ, corresponding to M in which evolves x):

$$|\Phi_n(\zeta)| \leq L_\Phi \tag{24}$$

with L_Φ being known Lipschitz positive constant. Furthermore:

$$|\Delta\Phi| \leq L_{\Delta\Phi} \tag{25}$$

with $0 < L_{\Delta\Phi} < \infty$.

4 Observation Technique Using Sliding Mode

Many techniques of observation of nonlinear systems exist: the observers based on linearization by input–output injection [23], high gains observers [9], continuous observer with finite time convergence [20], and sliding mode observers [4]. Each of these observation strategies is applied to a more or less broad class of nonlinear systems. In this section sliding mode observers are studied and then applied for tire pressure monitoring.

4.1 Sliding Mode Observers

One of the known classes of nonlinear robust observers is that of sliding mode observer. Among the different observation methods, sliding mode observers have been widely studied for their robust qualities [12]. The main features of observer type are:

- finite time convergence of the estimation error,
- robustness face to disturbances and uncertainties.

Sliding mode observer is characterized by discontinuous functions in their correction terms. The principle of sliding mode observer involves to constrain the

dynamics of the estimation error, of dimension n, to evolve in finite time on a variety S, corresponding to a null estimation error. The attractiveness and the invariance of this surface are ensured by conditions called sliding conditions. If these conditions are satisfied, the observer converges to S and remains there.

In the next section, will be presented an observation solution based on sliding mode approach of first order and high order [16].

4.2 First Order Sliding Mode Observer

The first solutions were based on the approach of the first order sliding mode. In this case, the variety S is defined $S = \left\{ y - \hat{y} = 0 \right\}$ with $\hat{y}$ the estimate of the measure. The discontinuous corrective terms depend on the estimation error of y. This observer is applicable for systems with observability indices equal to 1. For observability indices 2, this observer does not allow to perfectly cancel the estimation error of x_2. Another drawback is the phenomenon of "chattering". This phenomenon is not desirable as it deteriorates the accuracy of the observation. Many studies have been work done in order to reduce or eliminate this problem. One solution is the introduction of new dynamics to act on higher order derivatives of the estimation error of y. This technique is the basic concept of higher order sliding mode which reduces the "chattering" retaining the qualities of robustness and finite time convergence of the approach first order sliding mode [11].

4.3 High Order Sliding Mode Observer

The concept of high order sliding mode was introduced in the 80s by Emelyanov [6], the principle involves acting via discontinuous corrective terms, on higher order derivatives of the measurement error y. The main advantages are:

- improving robustness and convergence in finite time,
- reducing the effects of chattering,
- improving the observer performance (precision), the application to systems with indices of observability higher than 1.

4.3.1 Second Order Sliding Mode Differentiation

The problem here is to constrain the estimation error to evolve in finite time on the sliding surface:

$$S = \begin{cases} y - \hat{y} = 0 \\ \dot{y} - \dot{\hat{y}} = 0 \end{cases} \tag{26}$$

In this way, the estimation error is now continuous and the chattering is eliminated. In this framework: The "Super Twisting algorithm" is proposed. This algorithm has been developed, to the base, for control systems (output feedback sliding mode of order 2) and is based on the technique of differentiation, hence its adequacy in observing systems written under canonical form of observability. This method is robust and does require only knowledge of it (no derivative calculation) but its use is limited to an index of observability equal to 2 [15].

4.3.2 High Order Sliding Mode Differentiation

For a given observability indices k, the objective here is to force the quantity $(y - \hat{y})$ and its first $(k - 1)$ derivatives to zero in finite time [16]. Observers based on differentiation technique of high order sliding mode are offered in this context. This technique will be presented in detail since it was adopted in this chapter. In fact, according to its robustness and convergence in finite time it can be applied to a wide class of observable nonlinear systems. Considering system (16) with $\zeta = \left[\, \zeta_1 \;\; \zeta_2 \;\; \zeta_3 \;\; \zeta_4 \;\; \ldots \;\; \zeta_n \,\right]^T$ in this case, a single output y is measured; the observability indices k then being equal to k_1. Is obtained:

$$\begin{aligned} \dot{\zeta}_1 &= \zeta_2 \\ \dot{\zeta}_2 &= \zeta_3 \\ \dot{\zeta}_3 &= \zeta_4 \\ &\vdots \\ \dot{\zeta}_n &= \Phi(\zeta) \\ y &= \zeta_1 \end{aligned} \tag{27}$$

When assumptions of Sect. 3.2 are satisfied, the observer is described by form (17). The correction term k must ensure the convergence of e to 0, despite the initial error $e(0)$ and the uncertain term $\Delta\Phi$. A possible choice of observer based on the differentiation of higher order [16]:

$$\begin{aligned} \dot{\hat{\zeta}}_1 &= \hat{\zeta}_2 + a_1 L^{\frac{1}{n+1}} \left|\zeta_1 - \hat{\zeta}_1\right|^{\frac{n}{n+1}} sign(\zeta_1 - \hat{\zeta}_1) \\ \dot{\hat{\zeta}}_2 &= \hat{\zeta}_3 + a_2 L^{\frac{1}{n}} |\gamma_1|^{\frac{n-1}{n}} sign(\gamma_1) \\ \dot{\hat{\zeta}}_3 &= \hat{\zeta}_4 + a_3 L^{\frac{1}{n-1}} |\gamma_2|^{\frac{n-2}{n-1}} sign(\gamma_2) \\ &\vdots \\ \dot{\hat{\zeta}}_i &= \hat{\zeta}_{i+1} + a_i L^{\frac{1}{n+2-i}} |\gamma_{i-1}|^{\frac{n+1-i}{n+2-i}} sign(\gamma_{i-1}) \\ &\vdots \\ \dot{\hat{\zeta}}_n &= \Phi(\hat{\zeta}) + a_n L sign(\gamma_{n-1}) \end{aligned} \tag{28}$$

with $L > L_\Phi + L_{\Delta\Phi}$ and $a_1 \ldots a_n$ coefficients fixed according to Table 1 [16].

Table 1 a_i coefficients a_i for sliding modes order 2 and 3

Coefficient	n = 2	n = 3
a_1	1.5	2
a_2	1.1	1.5
a_3	–	1.1

Thus, from (23) a finite time convergence observer is developed for the initial system (8). It can be written:

$$\dot{\hat{x}} = f(\hat{x}, y) + \chi(y, u) + \left[\frac{\partial \Psi}{\partial \hat{x}}\right]^{-1} \begin{bmatrix} \gamma_1 \\ \gamma_2 \\ \gamma_3 \\ \vdots \\ \gamma_n \end{bmatrix} \tag{29}$$

with:

$$\begin{bmatrix} \gamma_1 \\ \gamma_2 \\ \vdots \\ \gamma_i \\ \vdots \\ \gamma_n \end{bmatrix} = \begin{bmatrix} a_1 L^{\frac{1}{n+1}} \left| y - \hat{x}_1 \right|^{\frac{n}{n+1}} sign(y - \hat{x}_1) \\ a_2 L^{\frac{1}{n}} \left| \gamma_1 \right|^{\frac{n-1}{n}} sign(\gamma_1) \\ \vdots \\ a_i L^{\frac{1}{n+2-i}} \left| \gamma_{i-1} \right|^{\frac{n+1-i}{n+2-i}} sign(\gamma_{i-1}) \\ \vdots \\ a_n L sign(\gamma_{n-1}) \end{bmatrix} \tag{30}$$

5 Vehicle Front Axle Modeling

This section presents the model of longitudinal and rotational dynamics of the vehicle front axle wheels. This model and its coupling with the vertical vehicle dynamic are the basis of wheels behavior description. With consideration of rolling resistance force and effective radii of the wheels.

5.1 Dynamics of the Front Axle

The suspension system is composed of mechanical components that connect the wheels to the main structure of the vehicle. The suspension provides an elastic connection to absorb and transmit smoothly the irregularities. There are several types of suspension, the most common are steel suspensions (called mechanical) and pneumatic suspensions. Currently the vehicles are equipped, in most cases, with pneumatic

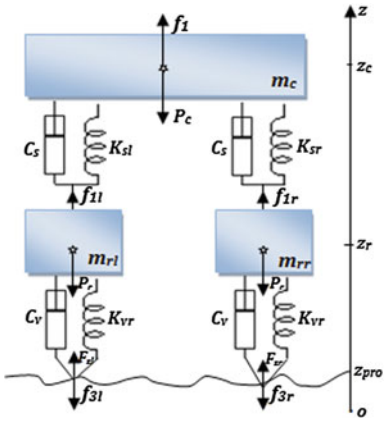

Fig. 1 Vertical vibration model of a half vehicle

suspension that provide better dynamic stability and are less aggressive for the road [28]. This study considers a simplified air suspension mechanism described by a mass-spring-damper system. The front axle model of the vehicle is used to describe the vertical dynamics of the vehicle and those of the wheels shown in Fig. 1.
with

m_c : suspended mass brought on two wheels,
m_r : unsprung mass,
K_{sr} : stiff right suspension,
K_{sl} : stiff left suspension,
K_{vr} : vertical stiffness of the right tire,
K_{vl} : vertical stiffness of the left tire,
C_s : suspension damping,
C_v : vertical pneumatic damping,
R_0 : nominal radius,
R : tire radius,
C_f : viscous friction coefficient,
z_c : vertical position of the suspended mass,
z_r : vertical position of the unsprung mass,
z_{pro} : profile of the wheel surface,
d_{pro} : road profile.

Referring to a fixed vertical position referenced by o, Z_{pro_0} on the initial contact (between the wheel and the ground) is located by vertical axis z shown on Fig. 1. Z_{c_0} is the vertical distance in the static state of the vehicle body and Z_{r_0} the vertical distance in the static state from the center of the wheel.

The relative positions of wheel-ground contact z_{pro}, wheel center z_r and vehicle body z_c given by:

$$d_{pro} = z_{pro} - Z_{pro_0} \tag{31}$$
$$d_r = z_r - Z_{r_0} \tag{32}$$
$$d_c = z_c - Z_{c_0} \tag{33}$$

The application of the second Newton's law can write the equations of the vertical dynamics of a half vehicle and of the wheel [29] according to:

$$\begin{cases} m_c\ddot{d}_c = -K_{sl}(d_c - d_r) - C_{sl}(\dot{d}_c - \dot{d}_r) - K_{sr}(d_c - d_r) - C_{sr}(\dot{d}_c - \dot{d}_r) \\ m_r\ddot{d}_r = K_{sl}(d_c - d_r) + C_{sl}(\dot{d}_c - \dot{d}_r) + K_{sr}(d_c - d_r) + C_{sr}(\dot{d}_c - \dot{d}_r) \\ \qquad -K_{vl}(d_r - d_{prol}) - K_{vr}(d_r - d_{pror}) - C_v(\dot{d}_r - \dot{d}_{pro}) \end{cases} \tag{34}$$

The damping of the tires is assumed to be negligible compared to other variables ($C_v = 0$).
Thus, taking as a state vector $(x_1, x_2, x_3, x_4)^T = (d_c, \dot{d}_c, d_r, \dot{d}_r)^T$ and as input $u = (d_{prol}, d_{pror})$, the state model of the pneumatic is written in the form:

$$\begin{bmatrix} \dot{d}_c \\ \ddot{d}_c \\ \dot{d}_r \\ \ddot{d}_r \end{bmatrix} = \begin{bmatrix} 0 & 1 & 0 & 0 \\ -a_1 & -a_2 & a_1 & a_2 \\ 0 & 0 & 0 & 1 \\ a_3 & a_4 & -a_5 & -a_4 \end{bmatrix} \begin{bmatrix} d_c \\ \dot{d}_c \\ d_r \\ \dot{d}_r \end{bmatrix} + \begin{bmatrix} 0 & 0 \\ 0 & 0 \\ 0 & 0 \\ a_6 & a_7 \end{bmatrix} \begin{bmatrix} d_{prol} \\ d_{pror} \end{bmatrix} \tag{35}$$

$$\text{with} \begin{cases} a_1 = \frac{K_{sl}+K_{sr}}{m_c} \\ a_2 = \frac{C_{sl}+C_{sr}}{m_c} \\ a_3 = \frac{K_{sl}+K_{sr}}{m_r} \\ a_4 = \frac{C_{sl}+C_{sr}}{m_r} \\ a_5 = \frac{K_{vl}+K_{vr}}{m_r} \\ a_6 = \frac{K_{vl}}{m_r} \\ a_7 = \frac{K_{vr}}{m_r} \end{cases} \tag{36}$$

Tire/road contact forces are obtained from the tire model, which we will present in the next section. These forces are transmitted to the chassis (sprung mass) via the suspension. They depend on the characteristics of the latter and axle configuration.

5.2 *Dynamics of Wheels*

The application of the second Newton's law to the forces acting on two wheels of front axle allows writing their rotational and longitudinal dynamics as (Fig. 2):

$$\begin{cases} J_l\dot{\Omega}_l = T_l - R_lF_{xl} - C_f\Omega_l \\ J_r\dot{\Omega}_r = T_r - R_rF_{xr} - C_f\Omega_r \\ M_{1/2}\dot{v}_x = F_{xl} + F_{xr} - F_{d1/2} - F_{rg} \end{cases} \tag{37}$$

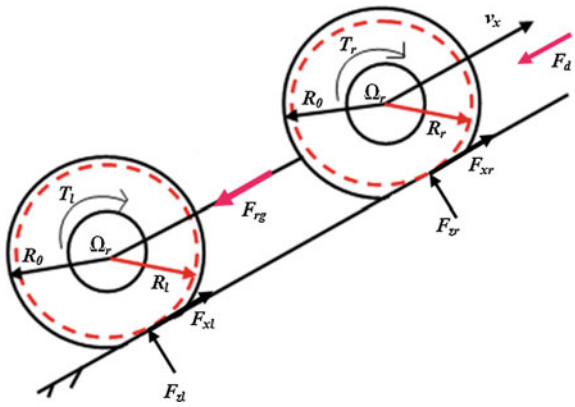

Fig. 2 Forces and torques acting on the front wheels

where indexes l and r respectively refer to the front left and rights wheels, Ω is the wheel angular velocity, R is the effective radius, v_x the vehicle's linear velocity, C_f the viscous friction coefficient of the wheel, J and $M_{1/2}$ are respectively the inertia and the half-vehicle mass. T is the torques applied to the wheel.
The complete model of the front axle of a vehicle can be obtained from the model (37) coupled to the model of the vertical dynamics (34). The coupling is done through the normal force F_z (38).

• **Normal force**: This force depends mainly on the half-vehicle mass and the vertical displacement of the tire-road point contact [5], it is defined by the following relationship:

$$F_{zi} = Mg - K_{vi}(R_{lib} - (d_r - d_{proi})) - C_v(\dot{d}_r - \dot{d}_{proi}) \tag{38}$$

where $i \in \{l, r\}$ and g the gravitational acceleration.

A simplifying assumption may be considered to reduce the model of normal force. This assumption is formulated by Eq. (39):

$$K_{vi}(R_{lib} - (d_r - d_{proi})) - C_v(\dot{d}_r - \dot{d}_{proi}) \langle\langle Mg \tag{39}$$

The expression of the normal force becomes:

$$F_{zi} = Mg \tag{40}$$

• **Aerodynamic drag force**: This force is proportional to the square of the vehicle's velocity [8].

$$F_{d1/2} = \frac{1}{2}(\rho A_{d1/2} C_{d1/2} v_x^2) \tag{41}$$

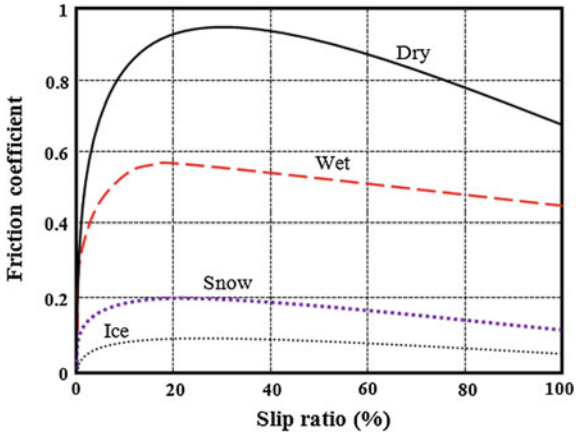

Fig. 3 Friction coefficient versus slip ratio

with ρ the air density, $A_{d1/2}$ the frontal area of the half-vehicle and $C_{d1/2}$ the drag coefficient.

• **Tractive forces**: These forces are expressed according to friction wheel-ground coefficient $\mu(\lambda_i)$ [8] as:

$$F_x(\lambda_i) = F_{zi}\mu(\lambda_i) \tag{42}$$

with λ_i the slip ratio defined by:

$$\lambda_i = -\frac{(\nu_x - R_i\Omega_i)}{R_i\Omega_i} = -\frac{\nu_x}{R_i\Omega_i} + 1 \tag{43}$$

Figure 3 shows the friction coefficient evolution slip ratio for different road types.

The friction coefficient μ_i is theoretically given by semi-empirical formulas. An acceptable approximation [13] is expressed as a function of λ_i by:

$$\mu_i(\lambda) = 2\mu_0 \left(\frac{\lambda_0 \lambda_i}{\lambda_0^2 + \lambda_i^2} \right) \tag{44}$$

where λ_0 is the optimal slip ratio, leading to the maximum friction value $\mu_0 = \mu(\lambda_0)$. The tractive forces are then given by:

$$F_{xi} = 2\mu_0 \frac{\lambda_0 \left(1 - \frac{\nu_x}{\Omega_i R_i}\right)}{\lambda_0^2 + \left(1 - \frac{\nu_x}{\Omega_i R_i}\right)^2} M_{1/2} g \tag{45}$$

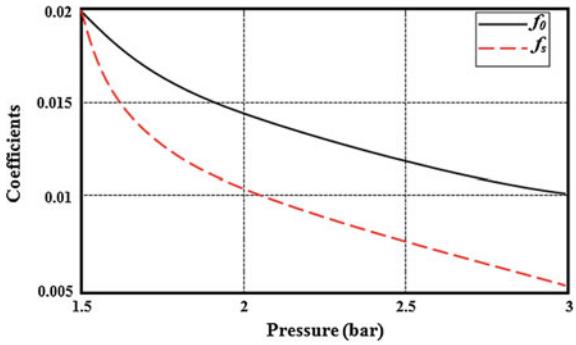

Fig. 4 f_0 and f_s evolution of according to pressure

- **Global rolling resistance force**: It is related to the normal force F_z by:

$$F_{rg}(v_x) = F_{rl}(v_x) + F_{rr}(v_x) = 2F_{zi}f_r(v_x) \tag{46}$$

with f_r the rolling resistance coefficient. This coefficient depends mainly on the tire inflation pressure, temperature, velocity, and road surface type then this assumption can be made for heavy vehicles and is valid on light vehicles only for low speeds [8].

In the case of light vehicles with higher speeds, another equation must be considered by:

$$f_r(\nu_x) = f_0 + 3.24f_s\,(3.6v_x/100)^{5/2} \tag{47}$$

This expression will be used for the model of half vehicle. The coefficients f_0 and f_s of the rolling resistance force vary for a given tire, with the pressure according to the characteristic shown in Fig. 4.

5.3 Global Model Coupling

The complete model of the vehicle front axle is elaborated from association of the vertical axle and wheels dynamic modeling. The considered state variables are expressed as:

$$\left[x_1\ x_2\ x_3\ x_4\ x_5\ x_6\ x_7\right]^T = \left[\Omega_l\ \Omega_r\ v_x\ d_c\ \dot{d}_c\ d_r\ \dot{d}_r\right]^T$$

Then, the global model, is written as follows:

$$\dot{x} = \begin{bmatrix} \frac{1}{J_l}[T_l - R_l F_x - C_f \Omega_l] \\ \frac{1}{J_r}[T_r - R_r F_x - C_f \Omega_r] \\ \frac{1}{M_{1/2}}[F_{xl} + F_{xr} - F_{d1/2} - F_{rg}] \\ x_5 \\ \frac{1}{m_c}[-K_{sl}(x_4 - x_6) - C_{sl}(x_5 - x_7) - K_{sr}(x_4 - x_6) - C_{sr}(x_5 - x_7)] \\ x_7 \\ \frac{1}{m_r}[K_{sl}(x_4 - x_6) + C_{sl}(x_5 - x_7) + K_{sr}(x_4 - x_6) + C_{sr}(x_5 - x_7) \\ -K_{vl}(x_6 - d_{prol}) - K_{vr}(x_6 - d_{pror})] \end{bmatrix} \quad (48)$$

6 Observer of Wheels' Effective Radii and Rolling Resistance Force of the Front Axle

In this section, will first be developed the sliding mode observer for only estimation of wheel effective radii and rolling resistance force. This observer uses, in addition, measures of the angular velocity of each wheel and the wheel applied torque.

The physical area of work is defined by:

$$M = \left\{ 0 < \Omega \leq 175\,\mathrm{rds}^{-1};\ 0 < \nu_x \leq 200\,\mathrm{kmh}^{-1};\ 0.29 \leq R \leq 0.32\,\mathrm{m};\ 80 \leq F_{rg} \leq 800\,\mathrm{N} \right\}$$

Since the aim is pressure drop detection, the knowledge of the two wheels radii gives information about pressure state in the tire of each wheel and the rolling resistance force. Therefore it seems to be judicious to develop joint estimation observers using the effective radius and the rolling resistance force.

6.1 Observation Model

In order to simplify the study, only the longitudinal dynamics of the front axle and the rotational dynamics of the two front wheels are considered. The state variables considered in this case are $x = \begin{bmatrix} \Omega_l & \Omega_r & v_x \end{bmatrix}^T$, with:

$$\dot{x} = \begin{bmatrix} \frac{1}{J_l}\left(T_l - R_l F_{xl}(x) - C_f x_1\right) \\ \frac{1}{J_r}\left(T_r - R_r F_{xr}(x) - C_f x_2\right) \\ \frac{1}{M_{1/2}}\left(F_{xl}(x) + F_{xr}(x) - F_{d1/2}(x) - F_{rg}\right) \end{bmatrix} \quad (49)$$

with $M_{1/2}$ the mass of the two wheels, $F_{d1/2}(x)$ the aerodynamic drag force on the train, T_l and T_r couples applied to each wheel. $F_{rg} = F_{rl} + F_{rr}$ is the global rolling resistance force on the train. The force $F_{xl}(x)$ and $F_{xl}(x)$ are written:

$$F_{xl} = 2\mu_0 \frac{\lambda_0 \left(1 - \frac{x_3}{x_1 R_l}\right)}{\lambda_0^2 + \left(1 - \frac{x_3}{x_1 R_l}\right)^2} Mg \tag{50}$$

$$F_{xr} = 2\mu_0 \frac{\lambda_0 \left(1 - \frac{x_3}{x_2 R_r}\right)}{\lambda_0^2 + \left(1 - \frac{x_3}{x_2 R_r}\right)^2} Mg \tag{51}$$

The aerodynamic drag force for the half of vehicle is written:

$$F_{d1/2} = \frac{1}{2}(\rho A_{d1/2} C_{d1/2} x_3^2) \tag{52}$$

The effective radii R_l and R_r and the global rolling resistance force F_{rg} of the front axle are unknown and may change due to loss of pressure in both wheels.

$$\begin{cases} \dot{R}_l = \eta_l(t) \\ \dot{R}_r = \eta_r(t) \\ \dot{F}_{rg} = \eta_g(t) \end{cases} \tag{53}$$

with $\eta_l(t)$, $\eta_r(t)$ and $\eta_F(t)$: unknown and bounded functions,

$u = \begin{bmatrix} u_1 \ u_2 \end{bmatrix}^T = \begin{bmatrix} T_l \ T_r \end{bmatrix}^T$: control input,

$x = \begin{bmatrix} x_1 \ x_2 \ x_3 \ x_4 \ x_5 \ x_6 \end{bmatrix}^T = \begin{bmatrix} \Omega_l \ \Omega_l \ v_x \ F_{rg} \ R_l \ R_r \end{bmatrix}^T$: state vector of the observation model.

The dynamic behavior of the whole axle is given by:

$$\dot{x} = \begin{bmatrix} -\frac{1}{J_l}\left(x_5 F_{xl}(x) + C_f x_1\right) \\ -\frac{1}{J_r}\left(x_6 F_{xr}(x) + C_f x_2\right) \\ \frac{1}{M_{1/2}}\left(F_{xl}(x) + F_{xr}(x) - F_{d1/2}(x) - x_4\right) \\ \eta_l \\ \eta_l \\ \eta_g \end{bmatrix} + \begin{bmatrix} \frac{1}{J_l} & 0 \\ 0 & \frac{1}{J_r} \\ 0 & 0 \\ 0 & 0 \\ 0 & 0 \\ 0 & 0 \end{bmatrix} u \tag{54}$$

with measurements $y = \begin{bmatrix} y_1 \ y_2 \ y_3 \end{bmatrix}^T = \begin{bmatrix} x_1 \ x_2 \ x_3 \end{bmatrix}^T$. The structure of the effective radii of the observer and the global force of rolling resistance, from the knowledge

of the angular velocities Ω_l and Ω_r and torques applied to each wheels T_l and T_r, is based on the observation model and the strategy of higher order sliding modes [16]. The terms $-\frac{C_f}{J_l}x_1 + \frac{1}{J_l}u_1$, $-\frac{C_f}{J_l}x_2 + \frac{1}{J_l}u_2$ depend only of known variables. Thus, system (54) can be written as:

$$\dot{x} = f(x) + \Delta f + \chi(y, u) \tag{55}$$

where

$$f(x) = \begin{bmatrix} -\frac{1}{J_l}x_5 F_{xl}(x) \\ -\frac{1}{J_r}x_6 F_{xr}(x) \\ \frac{1}{M_{1/2}}(F_{xl}(x) + F_{xr}(x) - F_{d1/2}(x) - x_4) \\ 0 \\ 0 \\ 0 \end{bmatrix} \tag{56}$$

$$\Delta f = \begin{bmatrix} 0 & 0 & 0 & \eta_l(t) & \eta_r(t) & \eta_F(t) \end{bmatrix}^T \tag{57}$$

$$\chi(y, u) = \begin{bmatrix} -\frac{C_f}{J_l}x_1 + \frac{1}{J_l}u_1 & -\frac{C_f}{J_r}x_2 + \frac{1}{J_r}u_2 & 0 & 0 & 0 & 0 \end{bmatrix}^T \tag{58}$$

Assumptions 3.2.1 and 3.2.2 are satisfied for this system.

6.2 *Observability Analysis*

In order to analysis the observability of the studied system, the function $\psi(x)$ is defined by:

$$\psi(x) = \begin{bmatrix} y_1 \\ \dot{y}_1 \\ y_2 \\ \dot{y}_2 \\ y_3 \\ \dot{y}_3 \end{bmatrix} = \begin{bmatrix} x_1 \\ -\frac{1}{J_l}x_5 F_{xl}(x) \\ x_2 \\ -\frac{1}{J_r}x_5 F_{xr}(x) \\ x_3 \\ \frac{1}{M_{1/2}}(F_{xl}(x) + F_{xr}(x) - F_{d1/2}(x) - x_4) \end{bmatrix} \tag{59}$$

The measured variables are the wheels' velocities and the vehicle's longitudinal speed $y = \left[x_1\ x_2\ x_3\right]^T$. If the determinant of the Jacobian of the function $\psi(x)$ is in all cases different from 0 on the operating trajectories, this implies that the transformation ψ is invertible and the system (54) is locally observable [5]. In this case, the observability indices vector is equal to $[2\,2\,2]^T$.

6.3 Observer Design

According to Sect. 3, the application of the inverse input–output injection transformation $\chi(y, u)$ allows the observer synthesis for system (54). The observer proposed as part of this problem is based on differentiation of a second order sliding mode. Thus, an observer of (54) is written as:

$$\dot{\hat{x}} = f(\hat{x}, y) + \chi(y, x) + \left[\frac{\partial \psi}{\partial x}\right]^{-1} \begin{bmatrix} 1.5L_1^{1/2} \left|y_1 - \hat{x}_1\right|^{1/2} sign(y_1 - \hat{x}_1) \\ 1.1L_1 sign(\gamma_1) \\ 1.5L_2^{1/2} \left|y_2 - \hat{x}_2\right|^{1/2} sign(y_2 - \hat{x}_2) \\ 1.1L_2 sign(\gamma_3) \\ 1.5L_3^{1/2} \left|y_3 - \hat{x}_3\right|^{1/2} sign(y_3 - \hat{x}_3) \\ 1.1L_3 sign(\gamma_5) \end{bmatrix} \tag{60}$$

$L_1 = 6, L_2 = 5$ and $L_3 = 4$ are observer gains.

6.4 Simulation Results and Discussion

To verify and validate the effectiveness of the observer in more general case, simulation are carried out with full model (48) of the vehicle front axle based on the coupling between the vertical dynamic and front axle wheels modeling. The initial state of the system $x(0)$ is given by:

$$\begin{aligned} x(0) &= \left[\Omega_l\ \Omega_r\ v_x\ d_c\ \dot{d}_c\ d_r\ \dot{d}_r\right]^T \\ &= \left[\tfrac{17}{0.3}\ \tfrac{17}{0.3}\ 17\ 0\ 0\ 0\ 0\right]^T \end{aligned} \tag{61}$$

From (61) it is assumed that at starting time, the vehicle vertical displacements d_c and d_r as well as wheels positions with their first derivatives are null. The parameters used for the front axle provided by Renault of the system (48) and the observer (60) are summarized in Table 2 [5].

Table 2 Wheels and vehicle model parameters for the axle model

Coefficient	n = 2	n = 3
J_l	1.6	Kg.m^2
J_r	1.6	Kg.m^2
R_0	0.32	m
$M_{1/2}$	880	Kg
$A_{d1/2}$	0.65	m^2
ρ_0	1.205	Kg/m^3
g	9.807	m/s2
C_f	0	Kg.m^2/s
$C_{d1/2}$	0.25	–
C_s	7722	Kg/s
K_s	19,960	Kg/s^2
μ_0	0.9	–
λ_0	0.25	–
R	0.3	m
v_x	17	m/s
d_{pro}	1	mm

The Observer (60) allowing joint estimation of the two wheel effective radii the global rolling resistance forces is initialized by:

$$\begin{aligned}\hat{x}(0) &= \left[\,\hat{\Omega}_l\ \hat{\Omega}_r\ \hat{v}_x\ \hat{F}_{rg}\ \hat{R}_l\ \hat{R}_r\,\right]^T \\ &= \left[\,\tfrac{17}{0.3}\ \tfrac{17}{0.3}\ 17\ 128\ 0.302\ 0.302\,\right]^T\end{aligned} \tag{62}$$

A case of pneumatic pressure fall of 40 % according to nominal value of 2.3 bar between instants $t_1 = 20$ s and $t_2 = 30$ s is simulated. It is therefore assumed, at the initial time, that there is an error of 8 mm between actual and estimated radii and an error of 2.6 rad/s between actual and estimated angular velocities of each wheel. The control strategy imposes low variable speed.

$$v_x^d = v^d(1 + 0.01sin(\omega t)) \tag{63}$$

with: $f = \frac{2\pi}{\omega} = 0.05$ Hz and $v^d = 40$ km/h

The controller output is then:

$$z = R_i\Omega_i - \upsilon_x^d(t) \tag{64}$$

From (49) and (64) it comes:

$$\begin{aligned}\dot{z} &= \tfrac{R_i}{J_i}(T_i - R_i F_x - C_f \Omega_i) + \dot{R}_i \Omega_i - \dot{v}_x^d \\ &= \underbrace{-\frac{R_i}{J_i}(R_i F_x + C_f \Omega_i) + \dot{R}_i \Omega_i - \dot{v}_x^d}_{\alpha(x,t)} + \underbrace{\frac{R_i}{J_i}}_{\beta(x,t)} T_i \\ &= -k\, z\end{aligned} \tag{65}$$

where $i \in \{l, r\}$.

Therefore the torque applied to each wheels can be written as follow:

$$T_i = \frac{1}{\beta_i}\left[-\alpha_i(x,t) - (R_i \Omega_i - v_x^d(t))\right] \tag{66}$$

Figure 5 shows the schematic diagram for the simulation of the system and the observer effective radii and the rolling resistance force of the front axle.

The estimation of the left wheel radius, the right wheel radius and the rolling resistance force of the front axle are respectively shown in Figs. 6, 7 and 8. The designed observer ensures a simultaneous control of the two front wheels. It appears that when the pressure is decreased in the tire of the front left wheel, the observer gives a lower value of the left wheel radius and a very high value of rolling resistance force of the whole axle.

It also presents a convergence time (around 10 s) compatible with the objectives of Automobile Manufacturers (European standard requires the pressure fall detection on a wheel in less than 10 min). The radius of the right front wheel is also estimated, this estimation is constant (Fig. 7).

The increase in the global rolling resistance force can detect a pressure drop; however, this information alone does not allow us to establish which tire presents a pressure fall. The radii of the both wheels are directly connected to their pressure. These graphical representations allow us to establish that the pressure fall comes from the left wheel.

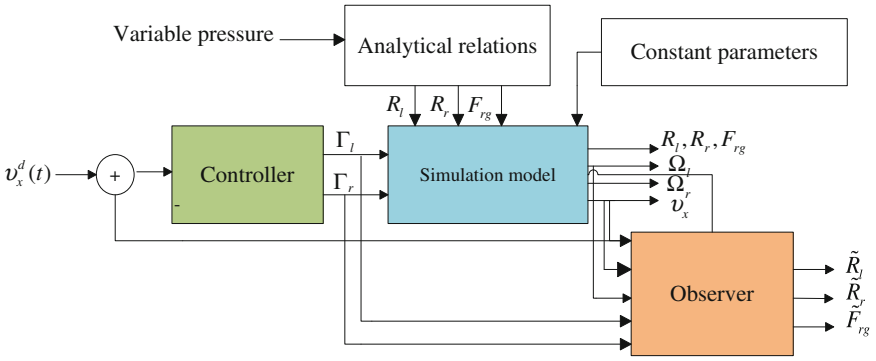

Fig. 5 Simulation diagram

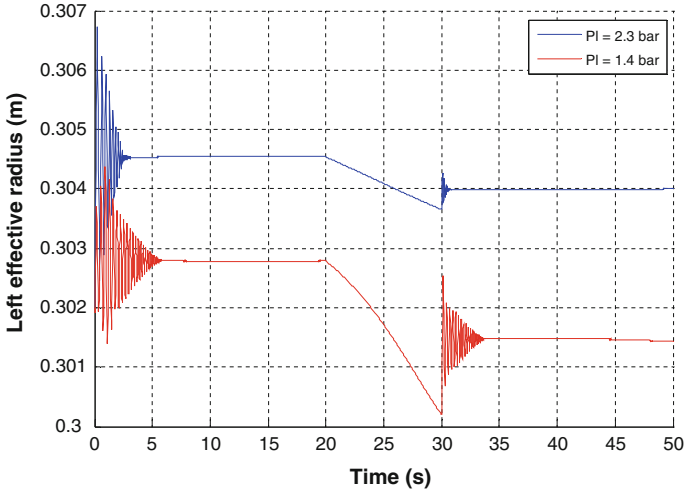

Fig. 6 Estimated left wheel radius for two tire pressure

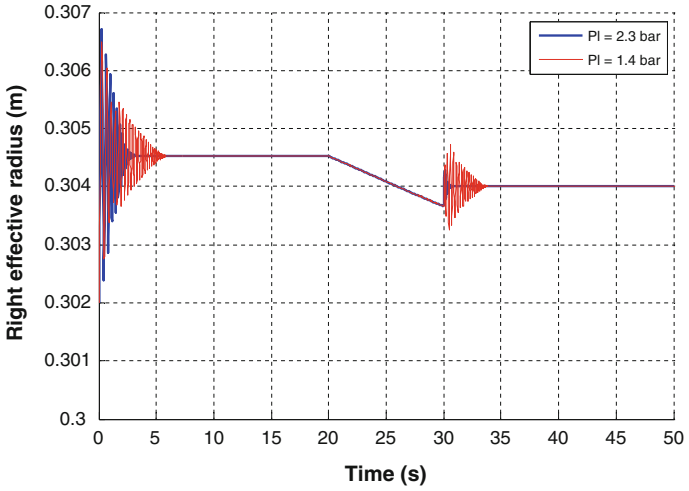

Fig. 7 Estimated right wheel radius for two tire pressures

Consequently, the joint estimation of three parameters: left effective radius, right effective radius and rolling resistance force appears to be an adequate tool for monitoring tire pressure.

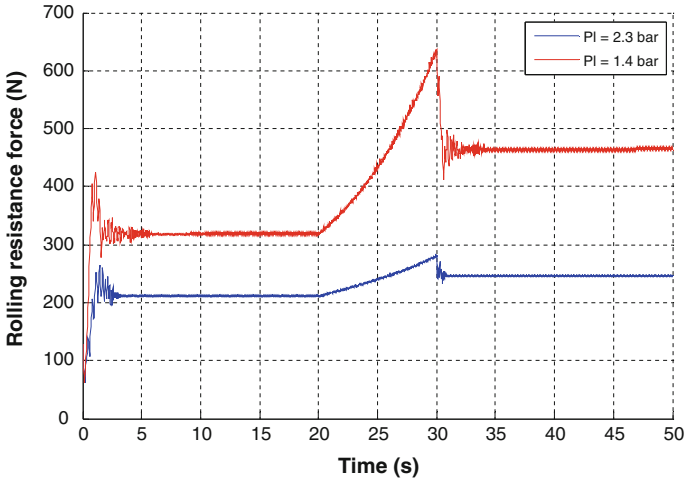

Fig. 8 Estimated rolling resistance force of the front axle for two tire pressures

7 Conclusions

In this chapter, different notions of observability have been recalled, emphasizing mainly on nonlinear systems. Then, the longitudinal and rotational dynamics of the wheels and their coupling with the vertical dynamics of the front axle of the vehicle were studied. This coupling model is used for validation of observer design. The model of longitudinal and rotational dynamics was used for nonlinear observer design which constitutes a major contribution of our work.

The synthesis of a sliding mode observer seeks on non-measurable quantities estimation (left effective radius, right effective radius and rolling resistance force of the whole axle) using only measured quantities (angular speed of each wheel, vehicle speed and useful torque) was designed. The choice of high order sliding modes observer was made for its well-known characteristics of robustness and precision. The results show a satisfactory estimation of effective radii and rolling resistance force for the vehicle front axle.

The future directions of research include:

- Real-time implementation of the observer studied taking into account the various constraints, in particular the complexity and computation time.
- Suggest of adequate strategy for observer gain determination or design of adaptive sliding mode observer.
- Elaboration of a global model of the complete vehicle for the extension of the study to an observation model taking into account simultaneous operation of the 4 wheels.
- Use of one or two pressure sensors for indirect approach elaboration [18].

References

1. Atsushi M (2010) Method for evaluating rolling resistance of tire, system for evaluating tire using the same, and program for evaluating rolling resistance of tire. Patent JP, 249527
2. Bestle D, Zeitz M (1983) Canonical form observer design for non-linear time-variable systems. Int J control 38(2):419–431
3. Carlson CR, Gerdes JC (2005) Consistent nonlinear estimation of longitudinal tire stiffness and effective radius. IEEE Trans Control Syst Technol 13(6):1010–1020
4. Davila J, Fridman L, Poznyak A (2006) Observation and identification of mechanical systems via second order sliding modes. Int J Control 79(10):1251–1262
5. El Tannoury C, Moussaoui S, Plestan F, Romani N, Gil GP (2013) Synthesis and application of nonlinear observers for the estimation of tire effective radius and rolling resistance of an automotive vehicle. IEEE Trans Control Syst Technol 21(6):2408–2416
6. Emelyanov SV, Korovin SK, Levantovskiy LV (1986) A drift algorithm in control of uncertain processes. Prob Control Inf Theory 15(6):425–438
7. Greenwood J, Clarke C (2011) Tire pressure monitoring. U.S. Patent Application 13/578,482
8. Gillespie TD (1992) Fundamentals of vehicle dynamics, vol 400. Society of Automotive Engineers, Warrendale
9. Gauthier JP, Hammouri H, Othman S (1992) A simple observer for nonlinear systems applications to bioreactors. IEEE Trans Autom Control 37(6):875–880
10. Hermann R, Krener AJ (1977) Nonlinear controllability and observability. IEEE Trans Autom Control 22(5):728–740
11. Hedrick JK, Misawa EA (1987) On sliding observers for nonlinear systems1. J Dyn Syst Meas Control 109:245
12. Imine H, Fridman L, Shraim H, Djemai M (2011) Sliding mode based analysis and identification of vehicle dynamics. Springer Science & Business Media, New York
13. Jazar RN (2008) Vehicle dynamics. Theory and applications. Springer Science & Business Media, Riverdale
14. Krener AJ, Respondek W (1985) Nonlinear observers with linearizable error dynamics. SIAM J Control Optim 23(2):197–216
15. Kamal S, Chalanga A, Moreno JA, Fridman L, Bandyopadhyay B (2014) Higher order super-twisting algorithm. In: 13th international workshop on variable structure systems (VSS). IEEE, pp 1–5
16. Levant A (2003) Higher-order sliding modes, differentiation and output-feedback control. Int J Control 76(9–10):924–941
17. Lebastard V, Aoustin Y, Plestan F (2011) Estimation of absolute orientation for a bipedal robot: experimental results. IEEE Trans Robot 27(1):170–174
18. Mayer H (1994) Comparative diagnosis of tyre pressures. In: Proceedings of the third IEEE conference on control applications. IEEE, pp 627–632
19. M'Sirdi NK, Rabhi A, Fridman L, Davila J (2008) Second order sliding-mode observer for estimation of vehicle dynamic parameters. Int J Veh Des 48(3):190–207
20. Menold PH, Findeisen R, Allgower F (2003) Finite time convergent observers for nonlinear systems. In: Proceedings of the 42nd IEEE conference on decision and control, vol 6. IEEE, pp. 5673–5678
21. Ouasli N, Ben Mehrez R, El Amraoui L (2014) Parameter estimation of one wheel vehicle using nonlinear observer. In: International conference on electrical sciences and technologies in Maghreb (CISTEM). IEEE, pp 1–8
22. Pacejka H (2005) Tire and vehicle dynamics, 2nd edn. SAE International and Elsevier, Butterworth
23. Plestan F, Glumineau A (1997) Linearization by generalized input–output injection. Syst Control Lett 31(2):115–128
24. Ribbens WB, Fredricks RJ (2005) Antilock brake systems employing a sliding mode observer based estimation of differential wheel torque. U.S. Patent No. 6,890,041

25. Schimetta G, Dollinger F, Weigel R (2000) A wireless pressure-measurement system using a SAW hybrid sensor. IEEE Trans Microw Theory Tech 48(12):2730–2735
26. Schuring DJ (1994) Effect of tire rolling loss on vehicle fuel consumption. Tire Sci Technol 22(3):148–161
27. Shraim H, Ananou B, Ouladsine M, Fridman L (2007) A new diagnosis strategy based on the online estimation of the tire pressure. In: European Control conference (ECC). IEEE, pp 3437–3443
28. Sammier D, Sename O, Dugard L (2000) H∞ control of active vehicle suspensions. In: Proceedings of the IEEE international conference on control applications. IEEE, pp 976–981
29. Ting WE, Lin JS (2004) Nonlinear control design of anti-lock braking systems combined with active suspensions. In: 5th Asian control conference, vol 1. IEEE, pp 611–616

Global Stabilization of Switched Nonlinear Systems Using Backstepping Approach: Applications to Chemical Processes

Arwa Abdelkarim, Khalil Jouili and Naceur BenHadj Braiek

Abstract This work presents a hybrid control methodology for a broad class of switched nonlinear systems in strict-feedback form under arbitrary switching. Thus, the focus of this chapter is to devise controller design based on the formalism of backstepping and simultaneous domination assumption it is shown that, a classes of state feedback controllers and a common Lyapunov function (CLF) are simultaneously constructed in a way that switched system can be globally uniformly asymptotically stabilized under arbitrary switching. Finally a global stabilization problem for a Continuous Stirred Tank Reactor (CSTR) in strict-feedback form with arbitrary switching between two modes is discussed to demonstrate effectiveness of the proposed approach.

Keywords Switched nonlinear systems · Common lyapunov function · Backstepping · Arbitrary switching · Global stabilization

1 Introduction

Studying of switched systems in control is motivated by the fundamentally hybrid nature of many modern-day control systems.

A switched system is a dynamical system made up of a family of subsystems and a rule that orchestrate the switching between them. Such systems can be used to describe a wide range of physical and engineering systems, see for example [26].

A. Abdelkarim (✉) · K. Jouili · N.B. Braiek
Laboratory of Advanced Systems, Polytechnic School of Tunisia (EPT),
B.P. 743, 2078 Marsa, Tunisia
e-mail: abdelkrimarwa@gmail.com

K. Jouili
e-mail: khalil.jouili@gmail.com

N.B. Braiek
e-mail: naceur.benhadj@ept.rnu.tn

S. Vaidyanathan and C. Volos (eds.), *Advances and Applications in Nonlinear Control Systems*, Studies in Computational Intelligence 635,
DOI 10.1007/978-3-319-30169-3_29

The motivation grows in importance for studying switched systems because it exists a class of system that cannot be asymptotically stabilized by a single smooth feedback control law [1, 3, 16, 17]. One of these problems is the stabilization of a switched system under arbitrary switching signal [9, 21, 22]. It is well established that, the existence of a Common Lyapunov Function CLF [2, 27]; the constituent systems of a switched system, was shown to be a necessary and sufficient condition for switched systems to be asymptotically stable under arbitrary switching signal.

Furthermore, some linearization techniques based on the theory of Lyapunov were successively developed [4, 20]. In particular, Multiple Lyapunov Functions (MLFs) [3, 12, 13, 18]; switched Lyapunov functions [11]; and the concept of dwell-time [25].

On the other hand, for nonlinear systems in lower triangular form, both feedback controllers and associated Lyapunov functions can be constructed systematically by backstepping [19, 23, 30], which constitutes one of the most important controller design methods for switched systems. The key idea of this technique is to synthesize the control law in a recursive manner.

Continuous stirred tank reactors (CSTRs) are known to be one of the systems that exhibit a very complicated dynamics behavior. Unfortunately, the stabilization of chemical reactors meets a serious problem owing to their nonlinearity and the existence of several stable and unstable operating points [28]. Some nonlinear methods resting on the linearization techniques have been used to provide a global stabilization [9]. Therefore, nonlinear design tools such as feedback linearization have been used to ensure global stabilization [6, 7, 10]. Also, various auxiliary solutions have been brought into play so as to reduce the drawbacks of the feedback linearization approach [9]. Moreover, the input constraints and the multivariable behavior of CSTRs encourage the utilization of other advanced controllers based on the Common Control Lyapunov Function (CCLF) [29] and the backstepping approaches [14]. In this context, we consider, in this paper, a CSTR with hybrid behavior as a case study. It is described by switched nonlinear systems model.

The main idea of this work is to design stabilizing state feedback controller for switched nonlinear systems in lower triangular form under arbitrary switching. The proposed method involves the integration of Modal feedback linearization, to make the system in strict-feedback form, and the backstepping algorithm where both feedback controllers and associated CCLF can be constructed systematically [24]. Note also that finding common control Lyapunov functions (CCLFs) is a necessary and sufficient condition to guarantee the stability in the case when the switching law is not generated by the controller.

The remainder of the manuscript is organized as follows. In Sect. 2, we present the class of switched systems considered and briefly review CCLF stability analysis, also the modal feedback linearization which is addressed in Sect. 3 to obtain a switched system in strict feedback form, and it will be combined with backstepping approach to implement a controller design based on construction of CCLFs. In Sect. 4, the proposed methodology is used to solve the global stabilization problem of a second order continuously stirred tank reactor (CSTR) with two modes. Finally, a conclusion is drawn in Sect. 5.

2 Theoretical Background

2.1 Class of Systems, Useful Definition and Theorem

A simple expression version of SISO switched nonlinear system is shown in Eq. (1):

$$\dot{x} = F^{\sigma(t)}(x) + G^{\sigma(t)}(x)u \tag{1}$$

where $x = [x_1 \dots x_n]^T \in \Re^n$, $u \in \Re$ are the state variables and the control input of the system, respectively $\sigma(t)$ is the set of switching signals consisting of all right-continuous piecewise constant functions from $\Re^+$to $M = \{1, 2, \dots, m\}$. In this paper, we consider the case when the switching signal is arbitrary. $F(x)$, $G(x)$ are smooth functions describing the system dynamics.

Definition 1 ([29]) Consider the system given by Eq. (1).

A Common Control Lyapunov Function (CCLF) for the subsystems of (1) is a smooth function $V(x) : \Re^n \to \Re^+$, satisfying $\forall k \in M, x \neq 0$ the conditions:

$$\frac{\partial V(x)}{\partial x} G_k(x) = 0 \Rightarrow \frac{\partial V(x)}{\partial x} F_k(x) < 0 \tag{2}$$

Definition 2 ([29]) A CCLF of the subsystems of (1) satisfies the common small control property (CSCP) if $\forall \varsigma < 0$, $\exists \delta > 0$ such that, if $x \neq 0$ satisfies $\|x\| < \delta$ then there exist u with $\|u\| < \varsigma$ such that and

$$\frac{\partial V(x)}{\partial x} [F_k(x) + G_k(x)u] < 0 \quad \text{k} = 1, \dots, \text{m} \tag{3}$$

From the definition of a Common Control Lyapunov function $V(x)$, the existence of $V(x)$ is the necessary and sufficient conditions for the stabilizability of switched nonlinear systems with arbitrary switching signals. Therefore, once we construct the CCLF for all subsystems of (1), then, we can select an explicit form of the stabilizing control law.

The idea of Theorem 1 below is that if there exists such a CCLF exists for all closed-loop subsystems of (1). In fact, it is possible to construct if a simultaneous domination condition, holds. Then, a stabilizing feedback law can be established by the obtained CCLF.

Theorem 1 ([30]) *Switched system is globally uniformly asymptotically stable under arbitrary switching if and only if, there exists a common control Lyapunov function CCLF $V(x)$ for all subsystems in a way that all the subsystems are simultaneously dominatable, and then a continuous feedback law u exists.*

2.2 Modal State Feedback Linearization

For the switched nonlinear system modal feedback linearization [5, 8, 9] can transform the switched nonlinear system into a controlled switching linear system using a common coordinate transformation.

In general, this case of problem is described and formulated from some classes of second-order switching nonlinear system.

The switching nonlinear system (1) is one of these classes, without loss of generality we suppose that

$$k = 2, x \in \Re^2, g^i(x) = \begin{bmatrix} 0 \\ g_2^i(x_1, x_2) \end{bmatrix} \text{and } f^i(x) = \begin{bmatrix} f_1^i(x_1, x_2) \\ f_2^i(x_1, x_2) \end{bmatrix}$$

and the model can be described by this state space representation:

$$\begin{cases} \dot{x}_1 = f_1^i(x_1, x_2) \\ \dot{x}_2 = f_2^i(x_1, x_2) + g_2^i(x_1, x_2)u \end{cases} \tag{4}$$

where $\begin{cases} f_1^i = c_1^i f_{11}(x_1) + c_2^i f_{12}(x_1, x_2) \\ f_2^i = f_2^i(x_1, x_2) \\ g_2^i = g_2^i(x_1, x_2) \end{cases}$

$c_2^i, c_1^i \in \Re$ are the parameter of the system, f_{11}, f_{12} are linearly independent and f_2^i, g_2^i are sufficiently smooth real-valued function.

To implement modal feedback linearization strategy for Switched Nonlinear System (4), let us state the following theorem.

Theorem 2 ([15])

- $f_{12}(x_1, x_2)$ *can be written as* $f_{12}(x_1, x_2) = f_{12a}(x_2) \cdot f_{12b}(x_1, x_2)$ *where*
  - *Assumption 1.*

    $$\frac{\partial f_{11}}{\partial x_1} - \frac{\partial f_{12b}}{\partial x_1} \cdot \frac{f_{11}}{f_{12b}} = p_1 \quad p_1 \in \Re/\{0\}$$

  - *Assumption 2.*

    $$f_{12a}(0) = 0$$

  - *Assumption 3.*

    $$\| f_{12b}(0) \| < \infty$$

  - *Assumption 4.*

    $$\frac{\partial f_{12a}}{\partial x_2}(0) \neq 0$$

- *Define* $h_1(x_1, x_2) = \frac{f_{11}}{f_{12b}}$. *So the Assumption 5*
  - *Assumption 4.*

$$h(0) = 0$$

Then a local diffeomorphism in a neighborhood of the $\dot{x} = F^{\sigma(t)}(x) + G^{\sigma(t)}(x)uU_0 \in \Re^2$ *origin denote by:*

$$T(x) = \begin{bmatrix} p_2 h_1(x_1, x_2) \\ f_{12a}(x_1) \end{bmatrix} \tag{5}$$

$T(x)$ *transforms the switched nonlinear system* (4) *to a switched linear system of the form:*

$$\begin{cases} \dot{z}_1 = a_1^i z_1 + a_2^i z_2 \\ \dot{z}_2 = f_z^i(z_1, z_2) + g_z^i(z_1, z_2)\, u \end{cases} \tag{6}$$

3 Main Result

3.1 Motivation

The main objective of this section can be summed up as a presentation of a technique to synthesis of a nonlinear stabilizing control to ensure a regulation around a desired operating point and the stability of the nonlinear controlled system by backstepping.

This technique is based on the combination between Modal feedback linearization formalism and the backstepping approach in a way that guarantees asymptotic stability of the overall switched closed-loop system under arbitrary switching signal.

The basic motivation for developing this approach is the serious drawbacks of the Modal feedback linearization, which may not stabilize system (1) when the switching between the controllers and the subsystems are asynchronous.

To confront this challenge, we have taken into consideration in references [4, 20], that we cannot guarantee the stability of a global switched system by the use of stability of each mode individual under arbitrary switching. It is to be noted here that the design of a stabilizing controller for each mode is not sufficient to achieve our control objectives. To solve this problem, auxiliary techniques should be developed to guarantee the stability under a randomly chosen switching signal. The design of the present study consists of two main stages. We plan to apply, in the first step, the concept of modal state feedback linearization [9], in order to transform the switched nonlinear model system into an equivalent switched linear system in the strict feedback form (Pavlichkov et al. 2009). Then, in the second stage is to synthesize the stabilizing control law in a recursive manner using the technique of backstepping. To achieve our goal, we must found a CCLF for all closed loop subsystems, necessary and sufficient condition to design continuous state feedback law u.

3.2 Description Design

3.2.1 System in Strict Feedback Form

This problem requires the setting into the strict feedback or triangular form, of the state Eq. (1).

Referring to the Theorem 2, we first exploit the formalism of modal feedback method so as to construct a suitable change of coordinates, to transform the model to the desired class of system.

Now we can obtain the strict feedback form:

$$\begin{cases} \dot{x}_j = x_{j+1} + f_{j,\sigma(t)}(x_1, \ldots, x_j) \quad 1 \leq j \leq n-1 \\ \dot{x}_n = f_{\sigma(t)}(x) + g_{\sigma(t)}(x)u \end{cases} \tag{7}$$

Our objective is to find a continuous feedback law u, which will stabilize the following form of (7):

$$\begin{cases} \dot{x}_1 = x_2 + f_{1,\sigma(t)}(x_1) \\ \vdots \\ \dot{x}_i = x_{i+1} + f_{i,\sigma(t)}(X_i) \\ \vdots \\ \dot{x}_{n-1} = x_n + f_{n,\sigma(t)}(X_{n-1}) \\ \dot{x}_n = f_{\sigma(t)}(x) + g_{\sigma(t)}(x)u. \end{cases} \tag{8}$$

where $\dot{x} = F^{\sigma(t)}(x) + G^{\sigma(t)}(x)u$, $i \in I = \{1, \ldots, n-1\}$ and $X_i = [x_1\, x_2\, \ldots \quad x_i]$. For all $i \in I$ and $k \in M$, $f_{1,\sigma(t)}(x)$, $f_k(x)$ and $g_k(x)$ are smooth.

3.2.2 The Backstepping Approach

To establish the main results of this paper, we will frequently employ backstepping to construct controllers for subsystems and a switching law to achieve global asymptotically stabilization for the system (8) under arbitrary switching.

Our goal is to globally uniformly asymptotically stabilize a switched nonlinear system in strict-feedback form by a continuous state feedback controller.

The detailed design procedure is based on the following main steps:

Step 1: Let us define the first variable of the procedure:

$$z_1(x_1) = x_1 \tag{9}$$

Then, we construct a candidate Lyapunov Function:

$$V_1(x_1) = \frac{1}{2}x_1^2 \tag{10}$$

This is called the auxiliary first-order subsystems which are represented by:

$$\dot{z}_1 = x_2 + f_{1,k}(x_1) \qquad \mathrm{k} = 1, \ldots, \mathrm{m} \tag{11}$$

By treating x_2 as a virtual control input of the system (8), the first order subsystem is simultaneously dominatable if there is a continuous feedback law $x_2 = \theta_1(x_1)$.

Thus, the derivative of the Lyapunov function is definite negative so:

$$\dot{V}_1(x_1) = x_1 \left(\theta_1(x_1) + f_{1,k}(x_1)\right) < 0 \tag{12}$$

If we found a simultaneously dominating feedback law $x_2 = \theta_1(x_1)$we can achieve the first step.

Step i (for i = 2… n − 1):

After different algebraic manipulations of the derivative of the variable of the procedure, we define:

$$z_i(X_i) = x_i - \phi_{i-1}(X_{i-1}) \tag{13}$$

We also define the augmented candidate Lyapunov function:

$$V_i(X_i) = V_{i-1}(X_{i-1}) + \frac{1}{2}\left(x_i - \theta_{i-1}(X_{i-1})\right)^2 \tag{14}$$

Consider the auxiliary ith order subsystems given by:

$$\begin{cases} \dot{z}_1 = z_2(X_2) + \phi_1(x_1) + f_{1,k}(x_1) \\ \qquad\qquad \vdots \\ \dot{z}_i = x_{i+1} + f_{i,k}(X_i) - \sum_{j=1}^{i-1} \dfrac{\partial \theta_{i-1}(X_{i-1})}{\partial x_j}\left(x_{j+1} + f_{i,k}(X_i)\right) \end{cases} \tag{15}$$

In a similar fashion, we can design a virtual controller With by taking x_{i+1}as a virtual control input of the system (12), and we consider the ith order subsystems as a simultaneously dominatable if there exists continuous feedback law: $x_{i+1} = \theta_i(X_i)$.

In this respect, the derivative along the trajectory is:

$$\dot{V}_i(X_i) = \sum_{j=1}^{i} z_j(X_j)\dot{z}_j(X_j) < 0 \qquad \forall X_i \neq 0 \text{ and } \mathrm{k} = 1, \ldots, \mathrm{m} \tag{16}$$

The goal here is to check the n − 1 step in order to affirm that the subsystems of Eq. 5 are simultaneously dominatable, and, hence, one can build a CCLF.

Step n: It is the last step of the design of CCLF. As soon as the final control u appears in the derivative of $\dot{V}_n$, we define $z_n(x) = x_n - \theta_{n-1}(X_{n-1})$ and V_n in a way that it is defined negative:

$$V(x) = V_{n-1}(X_{n-1}) + \frac{1}{2}\left(x_n - \theta_{n-1}(X_{n-1})\right)^2 \tag{17}$$

Thus, the Lyapunov derivative,

$$\begin{aligned}\dot{V}(x) &= \frac{\partial V(x)}{\partial x}(F_k(x) + G_k(x)u) = \sum_{i=1}^{n} z_i(X_i)\dot{z}_i(X_i) \\ &= \sum_{i=1}^{n-1} z_i(X_i)\dot{z}_i(X_i) + z_n(x)\left(\begin{array}{l} z_{n-1}(X_{n-1}) + f_k(x) + g_k(x)\cdot u - \\ \sum_{j=1}^{n-1}\frac{\partial \theta_{n-1}(X_{n-1})}{\partial x_j}\cdot(x_{j+1} + f_{i,k}(X_j)\end{array}\right) \\ &= \alpha_k(x) + \beta_k(x)\cdot u\end{aligned} \tag{18}$$

where:

$$\alpha_k(x) = \sum_{i=1}^{n-1} z_i(X_i)\dot{z}_i(X_i) + z_n(x)\left(\begin{array}{l} z_{n-1}(X_{n-1}) + f_k(x) - \\ \sum_{j=1}^{n-1}\frac{\partial \theta_{n-1}(X_{n-1})}{\partial x_j}.(x_{j+1} + f_{i,k}(X_j)\end{array}\right)$$

$$\beta_k(x) = z_n(x)\,(g_k(x).u)$$

Because of $g_k(x) \neq 0\ \forall x$, it is obvious that $\beta_k(x) = 0$ if and only if $z_n(x) = 0$, and $\alpha_k(x)\Big|_{\beta_k(x)=0}$ and $x \neq 0 = \sum_{i=1}^{n-1} z_i(\tilde{x}_i)\dot{z}_i(\tilde{x}_i) < 0$

Therefore, $V(x)$ is a CCLF for the subsystems given by Eq. 8. Moreover, it is easy to verify that satisfies the CSCP condition.

As shown above in Theorem 2, The Common Lyapunov Function approach, for all subsystems being switched, can be used to determine the stability of switched systems without input signals; such that the constructed positive definite and radially unbounded smooth function $V(x)$, so the subsystems of (8) are simultaneously dominatable, then a continuous feedback law u is established by the obtained CCLF So the switched system (8) is globally uniformly asymptotically stabilize under arbitrary switching.

4 Application to Control of Nonlinear Switched CSTR Example

In this section we will design a controller for the below CSTR based on backstepping technique and synthesize of CCLF. A backstepping design is combined with a modal feedback linearization to develop a controller of switched model of CSTR under arbitrary switching.

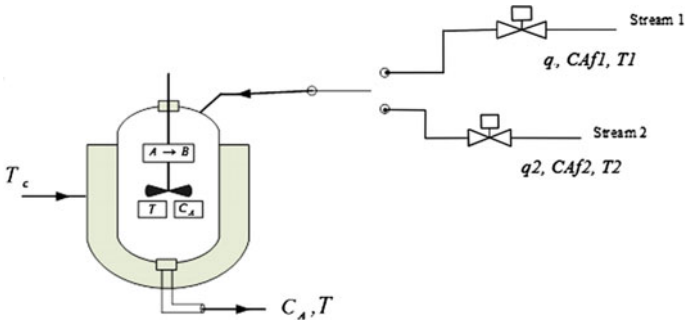

Fig. 1 Schematic diagram of the process

4.1 Mathematical Model of the Reactor

The process, shown schematically in Fig. 1, consists of a standard nonlinear second order model of a continuous stirred tank reactor (CSTR), with constant volume fed by a single input flow manipulated by a selector valve connected to two different source streams. In the reactor an exothermic, irreversible first-order reaction in reactant A, of the form $A \rightarrow B$ takes place. B is the product specie. At each time you change the position of the selector, and this allows changing instantaneously the excitation parameters of the reactor to obtain a two reactor mode according to the flow q^{σ} and concentration C_{Af}^{σ}. In this paper we consider an arbitrary signal which determines the position of the selector valve, and then the mode of operation of the reactor at any time. We named $\sigma = \{1, 2\}$ the switching signal.

Source 1 feeds pure species A at the flow rate $q^1 = 50(\mathrm{L\,min^{-1}})$, concentration $C_{Af}^{1} = 1.5(\mathrm{mol\,L^{-1}})$ and temperature $T_f^{1} = 350\mathrm{K}$. Source 2 allows feed the pure species A at the flow rate $q^2 = 200(\mathrm{L\,min^{-1}})$, concentration $C_{Af}^{2} = 0.75(\mathrm{mol\,L^{-1}})$ and temperature $T_f^{2} = 350\mathrm{K}$.

The dynamical model of the reactor obtained from mass and energy balances can be molded as a switched nonlinear system in the following form:

$$\begin{cases} \frac{dC_A}{dt} = \frac{q^{\sigma}}{V}\left(C_{Af}^{\sigma} - C_A\right) - k_0 exp\left(-\frac{E}{RT}\right) C_A \\ \frac{dT}{dt} = \frac{q^{\sigma}}{V}\left(T_f^{\sigma} - T\right) + \frac{(-\Delta H)}{\rho C_p} k_0 exp\left(-\frac{E}{RT}\right) C_A + \frac{UA}{\rho C_p V}\left(T_c - T\right) \end{cases} \tag{19}$$

where C_A [mol/l] is the concentration of the A component in the reactor [K] is the reactor temperature, while the input of the process is the T_j [K]: temperature of the reactor jacket.

The considered controlled output y of the process is the reactor temperature T. The nominal operating conditions can be found in [9]. Consider, then, the representation of the state vector of the model of the reactor:

$$x = [x_1 = C_A \quad x_2 = T]^T \tag{20}$$

In this state space, the model will be described, at each mode, by an equation of the state such as [16]:

$$\begin{cases} \dot{x}_1 = \frac{q^\sigma}{V}\left(C^\sigma_{Af} - x_1\right) - k_0 exp\left(-\frac{E}{RX_2}\right) x_1 \\ \dot{x}_2 = \frac{q^\sigma}{V}\left(T^\sigma_f - x_2\right) - \frac{\Delta H}{\rho C_p} k_0 exp\left(-\frac{E}{Rx_2}\right) x_1 + \frac{UA}{\rho C_p V}\left(U - x_2\right) \end{cases} \tag{21}$$

The position of the selector valve at each time is determined by our objective. In other words, the control objectives are to stabilize the reactor temperature T and the concentration C_{Af} by manipulating the control temperature T_c and the valve position, also to ensure global asymptotic stability when the reactor switches between mode *1* and mode *2* under arbitrary switching

4.2 CSTR in Strict Feedback Form

The system (3) can be represented by the model:

$$\begin{cases} \dot{x}_1 = c^\sigma_1 f_{11}(x_1) + c^\sigma_2 f_{12}(x_1, x_2) \\ \dot{x}_2 = f^\sigma_2(x_1, x_2) + g^\sigma_2(x_1, x_2)u \end{cases} \tag{22}$$

where $c^\sigma_1 = -q^\sigma / V$, $c^\sigma_2 = 1$, $f_{11} = x_1$ and $f_{12} = \frac{q^\sigma}{V}\left(C^\sigma_{Af} - x_1\right) - k_0 exp\left(-\frac{E}{Rx_2}\right) x_1$.

In [16] the system can be modal state feedback linearizable using the diffeomorphism $\xi(x)$:

$$\xi(x) = \begin{bmatrix} x_1 \\ \frac{q^\sigma}{V}\left(C^\sigma_{Af} - x_1\right) - k_0 exp\left(-\frac{E}{Rx_2}\right) x_1 \end{bmatrix}$$

According to the procedure described in (Barkordaroi), one can easily obtain the strict feedback form of the CSTR given by:

$$\begin{cases} \dot{x}_1 = f_1^{\sigma(t)}(x_1) - x_1 \\ \dot{x}_2 = u^{\sigma(t)} \end{cases} \tag{23}$$

where $f_{11} = 0.5x_1$ and $f_{12} = 2x_2$.

4.3 Synthesis of Control Law

Drawing on the algebraic developments presented in Sect. 3, we will synthesize a CCLF and a control law u using the backstepping algorithm, such that the closed-loop of the reactor is globally asymptotically stable.

Firstly, we define:

$$z_1(x_1) = x_1 \tag{24}$$

with the Lyapunov control function,

$$V_1(x_1) = \frac{1}{2}x_1^2 \tag{25}$$

The Lyapunov function is defined positive and the derivative is defined negative, so

$$\begin{cases} \dot{V}_1(x_1) = x_1\left(\theta_1(x_1) + f_{1,1}(x_1)\right) < 0 & \text{k} = 1 \\ \dot{V}_1(x_1) = x_1\left(\theta_1(x_1) + f_{1,2}(x_1)\right) < 0 & \text{k} = 2 \end{cases}$$

We can choose $\theta_1(x_1) = -3x_1$.

Secondly, we define our second variable:

$$z_2(x_1) = x_2 - \theta_1(x_1) \tag{26}$$

with the candidate CCLF for both subsystems:

$$V = \frac{1}{2}\sum_{i=1}^{2} z_1^2(\bar{x}) \tag{27}$$

According to the theory we can design the individual controller:

$$\begin{cases} u_1 = 27x_1\text{-}7x_2 & \text{k} = 1 \\ u_2 = 14x_1\text{-}4x_2 & \text{k} = 2 \end{cases} \tag{28}$$

4.4 Simulation and Discussion

The control objectives are to:

1. Stabilize the reactor temperature at the open-loop unstable steady state of mode 1.
2. Maintain the temperature at this steady-state when the reactor switches to mode 2.

As mentioned in our motivation in Sect. 3, we must overcome the problem of instability of the system (22), when switching between controllers and subsystems are asynchronous. The temperature and concentration profiles for this case are given in Fig. 2 (dotted lines and dashed line respectively), which show that the controllers fail to drive the reactor temperature to the desired steady-state.

We now consider the case when the backstepping algorithm is applied and, therefore, a feedback controller of the form of Eq. (28) is designed for each mode.

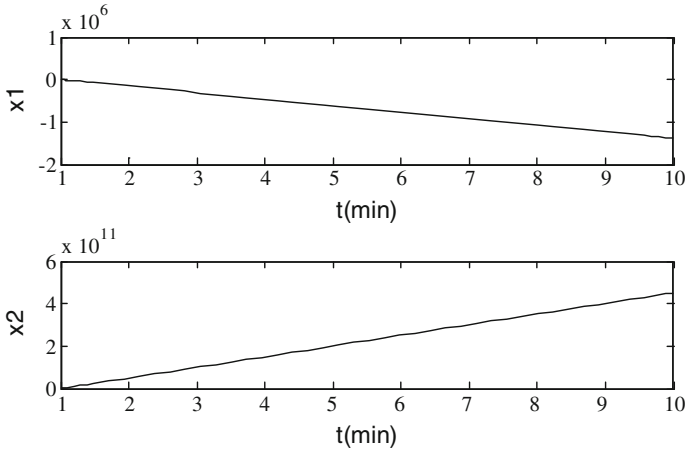

Fig. 2 Evolution of the reaction temperature T_A following the application of an arbitrary switching signal and backstepping design

The results are outlined in Figs. 3 and 4. In these figures, we are respectively representing the two state of the reactor: the concentration of the A component and the reaction temperature.

The simulation results show that the controller can achieve the desired control objective in a short time interval, and the controlled system remains stable under the switching signal.

It can be seen that the switched system (3) is globally uniformly asymptotically stabilize under a randomly chosen switching signal.

Fig. 3 Evolution of the reaction temperature T_A following the application of an arbitrary switching signal and backstepping design

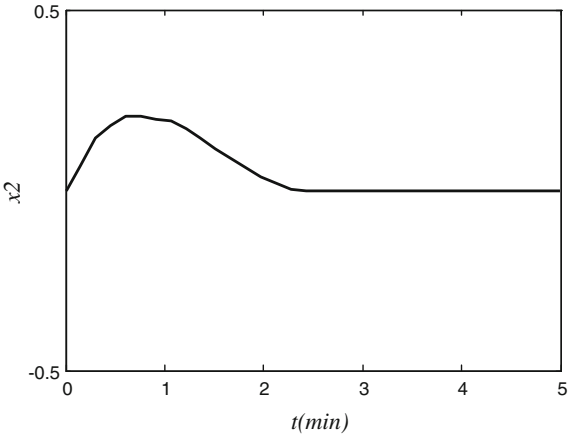

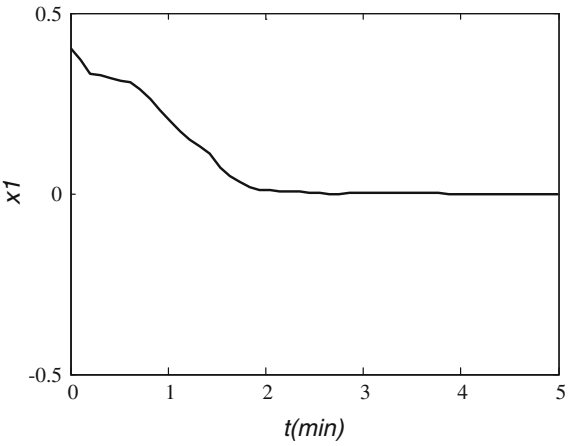

Fig. 4 Evolution of the concentration C_A following the application of an arbitrary switching signal and backstepping design

5 Conclusion

In this work, we have considered the global stabilization problem of switched nonlinear systems in strict-feedback form, as well as its application, where the global stabilization problem of individual subsystems is not assumed to be solvable when applying modal feedback linearization with some arbitrary switching.

Based on the Backstepping technique, we have designed feedback controllers of subsystems and constructed a Common Control Lyapunov Function, which guarantees global asymptotic stability of the corresponding closed-loop system.

The Construction of CCLFs for all subsystems plays a very important role in the method. This can be effective tool to guarantee the global stability. Moreover, the applications of the proposed control schemes have been illustrated by a CSTR system.

Future works will concentrate on generalize the study to a system having order higher than two.

References

1. Adebekun AK, Schork FJ (1991) On the robust global stabilization of nth order reactions. Chem Eng Commun 101:1–15
2. Abdelkrim A, Jouili K, Benhadj Braeik N (2013) An advanced linearization control for a class of switched nonlinear systems. In: 14th IEEE international conference on sciences and techniques of automatic control and computer engineering: (STA'13), pp 14–19
3. Abdelkrim A, Jouili K, (2014) Input-state feedback control of switched nonlinear systems using multiple lyapunov functions. In: Proceedings of the international conference on control, engineering & information technology: (CEIT'14), Copyright IPCO-2014 ISSN 2356–5608
4. Abdelkrim A, Jouili K, Benhadj Braiek N (2015) Synthesis of a switching control approach based on the Input-Output Feedback Linearization. In: International of Automatic Control. I.RE.A.CO 8:1–8

5. Abdelkrim A, Jouili K, Benhadj Braeik N (2015). Stabilization of CSTR with arbitrary switchings using backstepping approach. In: Proceedings of engineering & technology international conference on automation, control, engineering and computer science (ACECS'15) (in press)
6. Alvarez J (1994) Stability of a class of uncertain continuous stirred chemical reactors with a nonlinear feedback. Chem Eng Sci 49:1743–1748
7. Alvarez J, Gonzales E (1989) Global nonlinear control of a continuous stirred reactor. Chem Eng Sci 44:1147–1160
8. Barkhordari MY, Jahed-Motlagh MR (2009) Stabilization of a CSTR with two arbitrarily switching modes using modal state feedback linearization. Chem Eng J 155:838–843
9. Barkhordari Yazdi M, Jahed-Motlagh MR, Attia SA, Raisch J (2009) Switched feedback equivalence of a class of planar switched nonlinear systems. In: Proceedings of the 48th IEEE conference on decision and control/the 2009 28th Chinese control conference, pp 4264–4269
10. Daoutidis P, Kravaris C (1992) Dynamic output feedback control of minimum-phase nonlinear processes. Chem Eng Sci 47:837–849
11. Du D, Jiang B, Shi P, Zhou S (2007) H∞ filtering of discrete-time switched systems with state delays via switched Lyapunov function approach. IEEE Trans Autom Control 52:1520–1525
12. El-Farra NH, Mhaskar P, Christofides PD (2005) Output feedback control of switched nonlinear systems using multiple Lyapunov functions. Syst Control Lett 54:1163–1182
13. Freeman RA, Kokotović P (1996) Robust nonlinear control design: state-spaceand Lyapunov techniques. Birkhäuser, Boston
14. Goebel R, Sanfelice RG, Teel AR (2009) Hybrid dynamical systems. IEEE Control Syst Mag 29:28–93
15. Isidori A (1995) Nonlinear control systems, 3rd edn. Springer-Verlag, New York
16. Jouili K, Jerbi H, Benhadj Braiek N (2010) An advanced fuzzy logic gain scheduling trajectory control for nonlinear systems. J Process Control 20:426–440
17. Jouili K, Benhadj Braeik N (2015). Stabilization of non-minimum phase switched nonlinear systems with the concept of multi-diffeomorphism. Comm Nonlinear Sci Numerical Simulat 23:282–293
18. Jouili K, Abdelkrim A, Benhadj Braeik N (2015) Control of non-minimum phase switched nonlinear systems using multiple Lyapunov functions. In: Proceedings of engineering & technology international conference on automation, control, engineering and computer science (ACECS'15) (in press)
19. Khalil HK (2002) Nonlinear systems, 3rd edn. Prentice-Hall, New Jersey
20. Liberzon D (2003) Switching in systems and control. Birkhauser, Switzerland
21. Liberzon D, Morse AS (1999) Basic problems in stability and design of switched systems. IEEE Control Syst Mag 19:59–70
22. Lin H, Antsaklis PJ (2009) Stability and stabilizability of switched linear systems: a survey of recent results. IEEE Trans Autom Control 54:308–322
23. Long L, Zhao J (2011) Global stabilization for a class of switched nonlinear feedforward systems. Syst Control Lett 60:734–738
24. Ma R, Zhao J (2010) Backstepping design for global stabilization of switched nonlinear systems in lower triangular form under arbitrary switchings. Automatica 46:1819–1823
25. Mitra, S., Lynch, N., Liberzon, D. (2006). Verifying average dwell time by solving optimization problems, J. Hespanha, A. Tiwari (Eds.), Hybrid Systems: Computation and Control, in: LNCS, Springer-Verlag, Berlin, 3927: 476–490
26. Ozkan L, Kothare MV (2006) Stability analysis of a multi-model predictive control algorithm with application to control of chemical reactors. J Process Control 16:81–90
27. Shorten R, Wirth F, Mason O, Wulff K, King C (2007) Stability criteria for switched and hybrid systems. SIAM Rev 49:545–592
28. Viel F, Jadot F, Bastin G (1997) Robust feedback stabilization of chemical reactors. IEEE Trans Autom Control 42:473–481
29. Wu JL (2008) Feedback stabilization for multi-input switched nonlinear systems: two subsystems case. IEEE Trans Autom Control 53:1037–1042
30. Wu J (2009) Stabilizing controllers design for switched nonlinear systems in strict-feedback form. Automatica 45:1092–1096

Second Order Sliding Mode Based Synchronization Control for Cooperative Robot Manipulators

Fatma Abdelhedi, Yassine Bouteraa and Nabil Derbel

Abstract This work develops a modern controller design, combining reformulated second order sliding mode conception with the cross-coupling synchronizing approach. The goal behind the developed control architecture is to synchronize a group of robot manipulators while guaranteeing a performant trajectory tracking motion control. The developed robust approach allows not only to deal with sudden disturbances but also to avoid chattering phenomena yielded by acute discontinuous control signals. The Lyapunov-based analysis has been utilized to establish the multi-robot system asymptotic stability. Simulation results have been provided to demonstrate the performance of the adopted control schemes.

Keywords Trajectory tracking · Synchronization · Cross coupling technical · Sliding mode control · Second order sliding mode control · Robot manipulators

1 Introduction

Nowadays, in the modern industry, there exist enormous pressure to realize great and rapid developments, especially with the notable increasing exigency for greater productivity. Modern manufacturing devices are consequently intended to be organized such as all machine axes progress simultaneously aiming to reduce the time of work-in-progress, in such a way that a number of specific operations can be combined into only one. Such integration can be successfully guaranteed by the motion synchronization, which represents an interesting research field and becomes increasingly

F. Abdelhedi (✉) · Y. Bouteraa · N. Derbel
Control and Energy Management Laboratory (CEM-Lab),
Sfax Engineering School, University of Sfax, Sfax, Tunisia
e-mail: fatma.abdelhedi@live.com

Y. Bouteraa
e-mail: yassinebouteraa@gmail.com

N. Derbel
e-mail: n.derbel@enis.rnu.tn

S. Vaidyanathan and C. Volos (eds.), *Advances and Applications in Nonlinear Control Systems*, Studies in Computational Intelligence 635,
DOI 10.1007/978-3-319-30169-3_30

needed mainly in the industrial area [6]. In fact, the interest in synchronization of multiple motion axes and motors has recently grown worldwide. As an illustration, large applications of the motion synchronization lie in the industrial assembling, where the multi-axis system proceeds in coordinated behaviors [4, 5]. Furthermore, there has been a great interest in the methodological development for robotic manipulation where each robot operates cooperatively in order to realize a common goal. Besides, real systems are mostly non-linear. They have variable parameters and are constantly subject to external disturbances. The modeling of these systems is often an approximation of involved physical phenomena. It is from this systems approximate representation that it is required to build a robust control, in the sense that it can afford a low sensitivity to parameters uncertainties and to external disturbances.

1.1 Previous Works

While treating a specific process where the controlled part is slightly disturbed, conventional controls such as Proportional, Integral and Derivative actions [7] can be sufficient in cases where precision requests and system performances are not unduly required. Otherwise, it is needed to design more control designs ensuring robustness of behavior, regarding parameters uncertainties and their variations. There may be mentioned in this context, the H_∞ control [14], the adaptive control [16], the sliding modes control [2, 3, 8, 13] etc.

The problem faced by the type of variable structure approach is the control limitation by the chattering phenomenon [10]. Such problems are produced by residual vibrations at high frequencies, that occur on slaved magnitudes and on control variables. As solutions, various smoothing functions have been proposed in the literature to overcome this major drawback, but at the expense of system performances [1]. For this reason, several control laws based on higher order sliding modes has been recently proposed to generalize the basic sliding mode concept and to ensure high-order accuracy [9, 12, 15], these controllers are supposed sufficiently smooth to eliminate the chattering phenomenon.

1.2 Contribution

The object we have set in the present research lies in determining robust and effective controls, relatively simple to implement and to be adapted with rapid robotic systems. Then, we are interested as a first step, in the second order sliding mode approach to control robot manipulators systems, that we combine in a second step with the cross coupling technique in order to realize robot manipulators synchronization tasks.

The intended targets are the elimination of the chattering phenomenon, guaranteeing asymptotic convergence to zero of both tracking and synchronization errors, in order to impose to each manipulator joint to track its desired trajectory, while synchronizing behavior with those of other robot joints.

The first step in the present work is to provide a brief introduction to the sliding mode theory, and to clearly represent main features and abilities of higher order sliding modes. Thus, the main characteristic of sliding mode control lies in its variable structure that switches under certain predefined conditions upon synthesis of the sliding surface.

The proposed approaches are detailed and illustrated in a "SCARA" robot manipulator example.

2 Preliminaries

2.1 Modeling of a SCARA Robot

In this study, simulations are based on a SCARA robot manipulator model with rigid links and having three degrees of freedom (DOF), where the system includes two revolute articulations and a prismatic one related to the end effector. Figure 1 demonstrates one of the current SCARA manipulator representations with three DOF.

The corresponding dynamic equation of robot "i" is expressed as:

$$M_i(q_i)\ddot{q}_i + C_i(q_i, \dot{q}_i)\dot{q}_i + G_i(q_i) = \tau_i \tag{1}$$

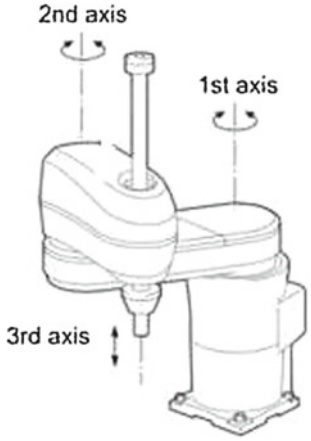

Fig. 1 Example of a three DOF "SCARA" robot representation

Table 1 Model parameters values

Parameters	m_0 (kg)	m_1 (kg)	m_2 (kg)	m_3 (kg)	l_0 (m)	l_1 (m)	l_2 (m)	l_3 (m)
Values	19.5	8	6	0.5	0.65	0.4	0.3	0.3

where:

- $q_i(t) \in \mathbb{R}^n$ denotes measured displacements vector,
- $\dot{q}_i \in \mathbb{R}^n$ is the measured velocity vector,
- $\ddot{q}_i \in \mathbb{R}^n$ is the articulatory acceleration vector,
- $M_i(q_i) \in \mathbb{R}^{n\times n}$ is the inertia matrix, which is symmetric uniformly bounded and positive definite,
- $C_i(q_i, \dot{q}_i)\dot{q}_i \in \mathbb{R}^n$ is the vector expressing the Coriolis and the centrifugal forces,
- $G_i(q_i) \in \mathbb{R}^n$ is the gravitational forces vector,
- $\tau_i \in \mathbb{R}^n$ denotes the external torques and forces vector, applied at each joint.

Dynamic parameters values corresponding to the adopted SCARA robot manipulator model are presented in Table 1.

2.2 Sliding Mode Control

Sliding mode control has long revealed its profits, reflecting special impact in controls of independent motion, through several operational methods, such as trajectory control [5], observation [11].

Fundamentally, such variable structure control results from the discontinuous control phenomenon. Especially, it involves discontinuous feedback control laws in order to force system states to reach, and then to remain on the specified surface in the state space known by switching or sliding surface. When confined by the sliding surface, the system dynamic is considered as an ideal sliding motion that represent the controlled system behavior.

Thus, there are two major methods that deal in a detailed manner with the sliding mode strategies: The 'Filippov' method and the 'equivalent control' method [17].

In this study, the proposed control law is developed exploiting the equivalent control method, which admits that in sliding mode everything happens as if the system is driven by an "equivalent control" denoted by u_{eq}. This control method allows to system states to reach and to maintain on the sliding surface S.

- **Equivalent control theory**:

Consider the nonlinear affine system used in the following control:

$$\dot{x}(t) = f(x) + g(x)u(t) \tag{2}$$

where $x \in \mathbb{R}^n$, $u \in \mathbb{R}^m$, $f(x) \in \mathbb{R}^n \times \mathbb{R}^m$, and $g(x) \in \mathbb{R}^n \times \mathbb{R}^m$, and S is a set of m switching surfaces chosen in such away x goes to x_d, while remaining on the sliding surface. Defining the generalized error vector $S(x)$, the sliding surface is described by:

$$S = \{x \in \mathbb{R}^n / s(x) = [s_1(x), ..., s_m(x)]^T = 0\} \tag{3}$$

In order to satisfy the control objective, the controller can be expressed as:

$$u = u_{eq} + \Delta u \tag{4}$$

where the equivalent control u_{eq} represents the required term to reach and to remain on the sliding surface. The corrected term Δu is intended to guarantee the remaining on the surface defined by $s(x) = 0$.

As results from the previous expressions we can obtain that:

1. Based on the sliding mode expression,

$$\dot{s}(x) = \frac{\partial s}{\partial x} [f(x) + g(x)\, u(t)] = 0 \tag{5}$$

Assuming that matrix $\dfrac{\partial s}{\partial x} g(x)$ is regular, which represents the intrinsic condition for the existence of the sliding mode control, the associated equivalent control is written as:

$$u_{eq} = -\left(\frac{\partial s}{\partial x} g(x)\right)^{-1} \frac{\partial s}{\partial x} f(x) \tag{6}$$

2. The resulting dynamics:

$$\dot{x} = \left[I - g(x) \left(\frac{\partial s}{\partial x} g(x)\right)^{-1} \frac{\partial s}{\partial x}\right] f(x) \tag{7}$$

3. By adopting the simple sliding mode approach, the discontinuous term can be chosen as:

$$\Delta u = -\left(\frac{\partial s}{\partial x} g(x)\right)^{-1} W \operatorname{sign}(s) \tag{8}$$

where W is a positive definite matrix.

2.3 High Order Sliding Mode Control

Generally, the dynamics smoothness degree is characterized by the sliding order, in the vicinity of the mode. If we need to maintain a constraint determined by equability of the smooth function $s(x)$ to zero, then the sliding order is specified by a number of continuous derivatives of $s(x)$, including the zero one, in the proximity of the sliding mode. Thus, the rth order sliding mode is established by the successive equalities:

$$s = \dot{s} = \ddot{s} = \cdots = s^{(r-1)} = 0 \tag{9}$$

The standard sliding surface expression (10) is defined in the state space $\mathbb{R}^n$ as follows:

$$s(x) = \left(\frac{d}{dt} + \lambda\right)^{n-1} \tilde{x}(t) \tag{10}$$

where, λ is a strict positive scalar, taken to be the bandwidth of the system, and $\tilde{x}(t) = q(t) - q_d(t)$ represents the error in the output state.

Thus, high order sliding mode control aims for keeping the main advantages of the original method, and seems to be able to remove the chattering effect and provide at the same time to further higher accuracy in realization.

3 Control Design

We consider decentralized control laws for three manipulator robots, taking into account the status of each neighbor, all agents 'follower' synchronize their positions while tracking the 'leader' robot trajectory.

Specifically, the purpose of each torque controller is to ensure the convergence to zero of position, velocity and synchronization errors.

3.1 Cross Coupling Technical

To achieve a coordinated control motion, a cross-coupled control approach is applied where the whole multi-agent system is considered as a single generalized system.

In order to achieve this goal, we define the tracking error as follows:

$$\varepsilon_{1i}(t) = q_i(t) - q_M(t) \tag{11}$$

where $q_M(t) \in \mathbb{R}^n$ denotes the position of the leader robot.

The 'cross-coupling' technique consists in presenting a synchronization error that is presented as follows:

$$\begin{aligned}\varepsilon_{2i}(t) &= \sum_{j\neq i}^{p} K_{ij}[(q_i - q_M) - (q_j - q_M)] \\ &= \sum_{j\neq i}^{p} K_{ij}[(q_i - q_j)] \end{aligned} \tag{12}$$

where K_{ij} is a symmetric positive-definite matrix that reveals an idea about the communication quality between the ith and the jth agents. Finally, the global error concerning each agent of the system, which contains both trajectory tracking error and synchronization error is given by:

$$e_i = \varepsilon_{1i} + \int_{t_0}^{t} \varepsilon_{2i}\ (\tau)\ d\tau \tag{13}$$

Consider the standard sliding surface (10) that can be written as:

$$s_i = \dot{e}_i + \lambda_i e_i, \quad i = 1, 2, \ldots \tag{14}$$

where λ_i are positive scalars.

3.2 Second Order Sliding Mode Concept

The main problem in the implementation of higher order sliding modes is the increasing information demand. For this reason the second order sliding mode controllers are the most widely used in practice among higher order sliding mode controllers because of their simplicity and their low information demand.

In this context, and as it is mentioned above, the sliding surface derivative doesn't reach zero values anymore, it rather has new expression presented in (15), that follows the general sliding system (9). Then:

$$\dot{s}_i = \sigma_i \quad \Rightarrow \quad u = u_{eq} + \left[\frac{\partial s}{\partial x} g(x)\right]^{-1} \sigma \tag{15}$$

Consider now the following representation of the system described by:

$$\begin{cases} \dot{s}_i = \sigma_i \\ \dot{\sigma}_i = -a_0\ s_i - a_1\ \sigma_i + v_i \end{cases} \tag{16}$$

where a_0 and a_1 are positive scalars. This representation considers single-input single-output systems. However, the present study can be easily generalized to multi-

input multi-output systems. Besides, the following polynomial $A(p)$ in (17) is a Hurwitz one, i.e. its roots have negative real parts.

$$A(p) = a_1\ p + a_0 = 0 \tag{17}$$

Then, the previous polynomial can be chosen as:

$$A(p) = (p + \mu)^2 \tag{18}$$

where μ is a positive scalar. System (16) can be represented by the following form:

$$\dot{S}_i = \phi S_i + \Gamma v_i \tag{19}$$

where:

$$S_i = \begin{bmatrix} s_i \\ \sigma_i \end{bmatrix},\ \phi = \begin{bmatrix} 0 & 1 \\ -a_0 & -a_1 \end{bmatrix},\ \Gamma = \begin{bmatrix} 0 \\ 1 \end{bmatrix} \tag{20}$$

Note that ϕ clearly represents a Hurwitz matrix. Therefore, there exist two positive definite matrices P and Q such that:

$$P\phi + \phi^T P = -Q \tag{21}$$

Here, v_i is defined by:

$$v_i = -v_{0i}\ \text{sign}\ (w_i) \tag{22}$$

where w_i is a linear combination of S_i, and v_{0i} is a diagonal positive matrix. This yields that:

$$w_i = LS_i \tag{23}$$

where:

$$L = \Gamma^T P \tag{24}$$

Remembering that $\dot{s}_i = \sigma_i$, and taking into consideration Eq. (14) we obtain:

$$\ddot{q}_i - \ddot{q}_d + \sum_{j \neq i} K_{ij}(\dot{q}_i - \dot{q}_j) + \lambda_i \left[\dot{q}_i - \dot{q}_d + \sum_{j \neq i} K_{ij}(q_i - q_j) \right] = \sigma_i \tag{25}$$

Retaking dynamic model representation, (1), and substituting it in (25) gives:

$$\begin{aligned} \sigma_i = {M_i}^{-1}[\tau_i - C_i(q_i, {q_i}^{-1}) - g_i(q_i)] + \sum_{j \neq i} K_{ij}(\dot{q}_i - \dot{q}_j) \\ + \lambda_i \left[(\dot{q}_i - \dot{q}_d) + \sum_{j \neq i} K_{ij}(q_i - q_j) \right] - \ddot{q}_d \end{aligned} \tag{26}$$

This produces:

$$\tau_i = C_i(q_i, \dot{q}_i) + g_i(q_i) + M_i \left[\ddot{q}_d - \sum_{j \neq i} K_{ij}(\dot{q}_i - \dot{q}_j) - \lambda_i \left[(\dot{q}_i - \dot{q}_d) + \sum_{j \neq i} K_{ij}(q_i - q_j) \right] + \sigma_i \right] \tag{27}$$

Theorem 1 *Control laws (22), (23), (24) and (27) stabilize the global system (1).*

Proof We consider the positive Lyapunov function candidate:

$$V = \sum_i V_i = \sum_i {S_i}^T P S_i, \tag{28}$$

Differentiating the previous Lyapunov expression (28) with respect to time, gives:

$$\begin{aligned} \dot{V} &= \sum_i \dot{S}_i^T P S_i + \sum_i {S_i}^T P \dot{S}_i \\ &= \sum_i (\phi S_i + \Gamma v_i)^T P S_i + \sum_i {S_i}^T P(\phi S_i + \Gamma v_i) \\ &= \sum_i {S_i}^T (\phi^T P + P\phi) S_i + 2 \sum_i v_i \Gamma^T P S_i \end{aligned} \tag{29}$$

Consequently, the final $\dot{V}$ expression is given by (30):

$$\dot{V} = \sum_i -{S_i}^T Q S_i - 2 \sum_i v_{0i} |w_i| < 0 \tag{30}$$

This demonstration illustrates the Lyapunov theorem and guarantees the stability of the closed loop system.

4 Simulation Results

Consider the SCARA robot controlled by the second order SMC law applied on the robot for the motion control. The desired trajectory is noted $q_d(t)$, and its desired velocities and accelerations are noted $\dot{q}_d(t)$ and $\ddot{q}_d(t)$ respectively.

Besides, q is the position vector of the manipulator, $\dot{q}$ its speed vector, $\ddot{q}$ its acceleration vector, and τ is the torque vector applied to joints of the manipulator:

Table 2 Initial conditions

Articulation	Leader	Follower	Unit
$q_1(0)$	$\pi/3.5$	$\pi/5$	rad
$q_2(0)$	$\pi/3.5$	$\pi/5$	rad
$q_3(0)$	0.4	0	m
$\dot{q}_1(0)$	0	0	rad/s
$\dot{q}_2(0)$	0	0	rad/s
$\dot{q}_3(0)$	0	0	m/s

Table 3 Control parameters

Control parameters	Values
λ	6
K_{ij}	0.03
μ	4

$$q = \begin{bmatrix} q_1 \\ q_2 \\ q_3 \end{bmatrix}, \ \dot{q} = \begin{bmatrix} \dot{q}_1 \\ \dot{q}_2 \\ \dot{q}_3 \end{bmatrix}, \ \ddot{q} = \begin{bmatrix} \ddot{q}_1 \\ \ddot{q}_2 \\ \ddot{q}_3 \end{bmatrix}, \ \tau = u = \begin{bmatrix} \tau_1 \\ \tau_2 \\ \tau_3 \end{bmatrix} \tag{31}$$

State equations of a SCARA robot are presented as:

$$\frac{d}{dt}\begin{bmatrix} q \\ \dot{q} \end{bmatrix} = \begin{bmatrix} \dot{q} \\ M(q)^{-1}[\tau - C(q,\dot{q})\dot{q} - G(q)] \end{bmatrix} \tag{32}$$

The robot initially at rest has initial conditions as mentioned in Table 2. Control parameters values have been chosen as indicated in Table 3.

We consider the desired trajectory defined by:

$$q_d(t) = \begin{bmatrix} q_{d1}(t) \\ q_{d2}(t) \\ q_{d3}(t) \end{bmatrix} = \begin{bmatrix} \frac{\pi}{6}\sin(1.5\pi t) \\ \frac{\pi}{4}\sin \pi t \\ 0.2\,\text{sign}\,(0.8 - t) \end{bmatrix} \tag{33}$$

We have considered two cases:

- Simulation results without external disturbances are presented in Figs. 2a, b, 3 and 4.
- Simulation results in the presence of external disturbances are presented in Figs. 5, 6 and 7. In this case, the follower position state vector is afflicted by 10 % measured errors.

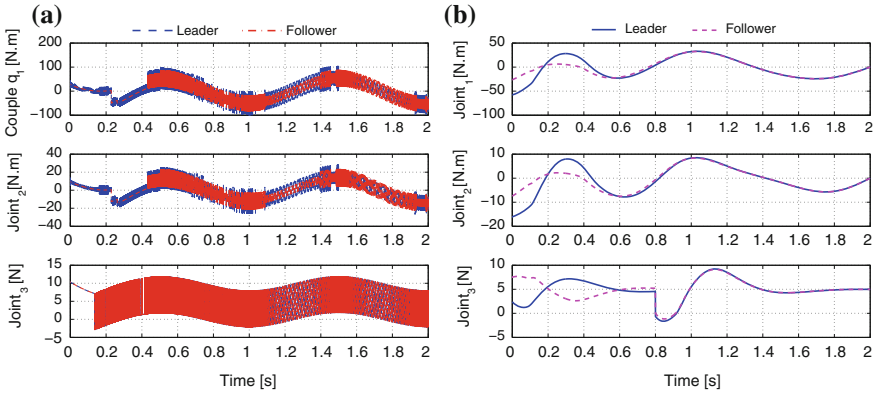

Fig. 2 **a** Simple SMC torques. **b** Second order SMC torques

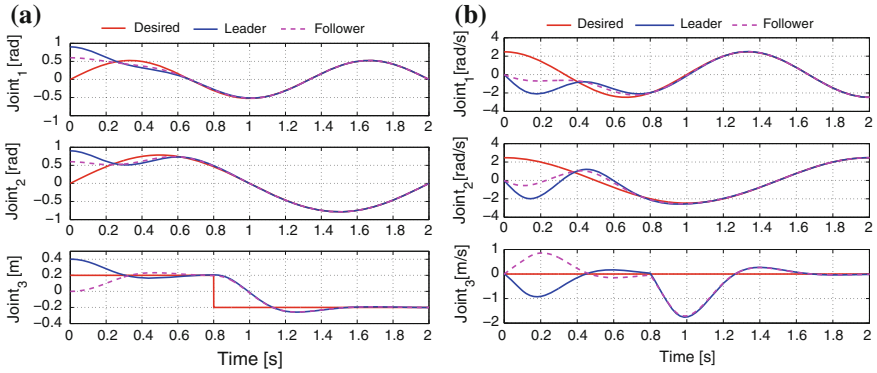

Fig. 3 **a** Trajectory tracking and positions synchronization. **b** Velocity synchronizing behavior

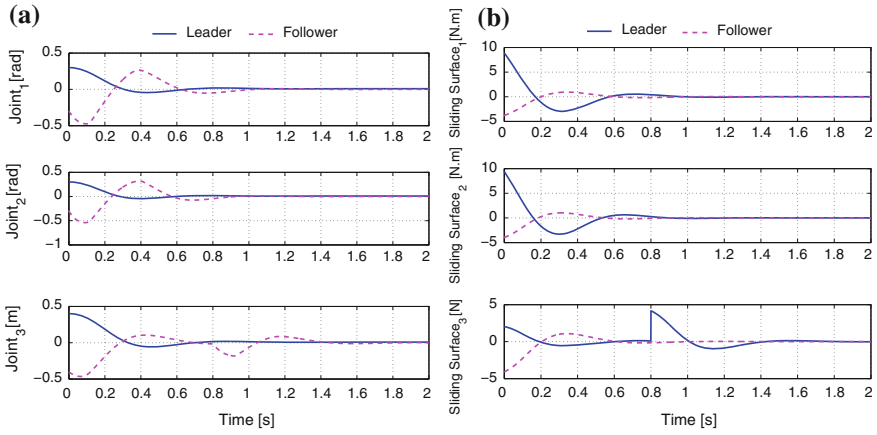

Fig. 4 **a** Synchronization and trajectory tracking errors. **b** Evolution of the generalized error vector $s(x)$

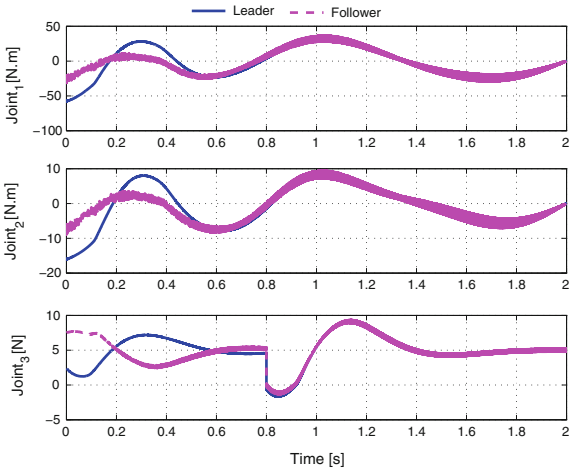

Fig. 5 Second order sliding mode control torques behaviors in presence of external disturbances

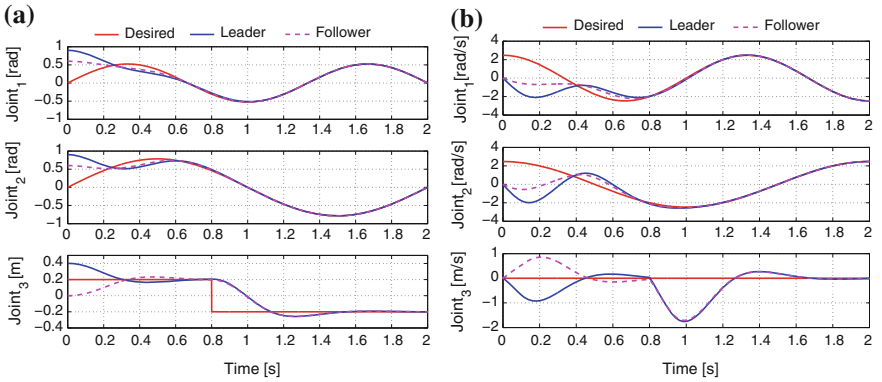

Fig. 6 Simulations in presence of external disturbances: **a** Trajectory tracking and positions synchronization. **b** Velocity synchronizing behavior

5 Discussion

Simulation results demonstrate the evolution of the trajectory tracking motion with respect to time, where the first and the second order SMC torques are shown in Fig. 2a and b respectively, whereas the positions and velocities tracking behavior of the second order SMC are presented in Fig. 3.

Concerning the simple SMC torques in Fig. 2a, it is clearly noted that the imperfections impact and the finite switching frequencies are obviously significant, whose

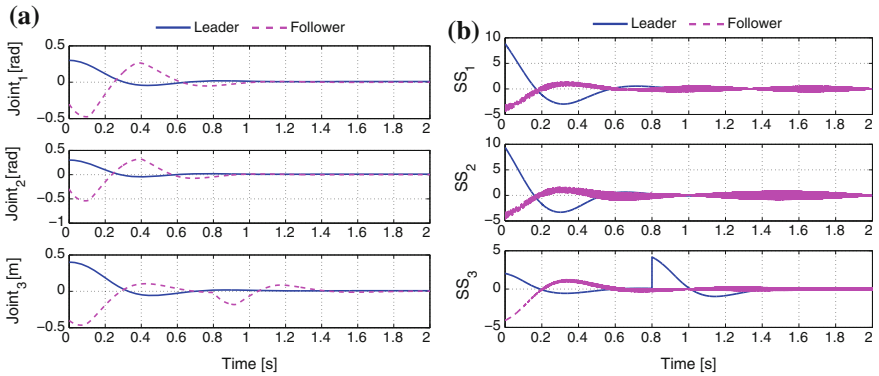

Fig. 7 Simulations in presence of external disturbances: **a** Synchronization and trajectory tracking errors. **b** Evolution of the generalized error vector $s(x)$

effect appears through the strong oscillations. Compared to that produced by the simpler controller in Fig. 2a, second order SMC produces smooth control torques behavior in Fig. 2b, where the chattering effect is attenuated, even thoroughly eliminated.

Sliding surface representations and trajectory tracking and synchronization errors are reflected through Fig. 4, where resulted errors curves have low values and attain zero nearly in 1.5 s, as indicated in Fig. 4a. Generalized error vector representations in Fig. 4b reflect the rapidity and the smoothness of the convergence behavior.

Otherwise, obtained results of the disrupted process analysis yield clear dissimilarities with those of the ideal system, depending on torques and the generalized error behavior. In fact, Figs. 5 and 7b show parasitic effects presented as small disrupting oscillations attaining second order SMC torques and the generalized error vector smoothness of the follower robot. In addition, trajectory tracking motions and joints velocity behaviors retain same behaviors of those described by the ideal system controller. Besides, this proves the follower controller robustness in spite of the sudden apparition of external disturbances. Consequently, the trajectory tracking task of the second order SMC is insensitive to changes in environmental conditions, and resists such fluctuating situations.

Thus, simulations show major advantages of the second order order SMC, which proves its superior ability to eliminate the chattering phenomenon, and to clearly minimize input values comparing to the simple SMC torques, even in the presence of external disturbances. So it seems to be a better solution that enables the controller response to be suitable with high performances of the closed-loop control system.

6 Conclusion

This work develops a second order SMC design combined with the cross-coupling control strategy for a robots synchronization task. The objective is to deal with external disturbances and uncertain parameters, by eliminating the chattering phenomenon, while solving problems of the inaccurate communication during the information exchange between cooperative manipulator robots. Depending on the proposed controller, the synchronization of a multi-agent system in a trajectory tracking task is optimally achieved, and synchronization errors and tracking errors rapidly converge to zero even in the presence of external measured errors affecting the state position vector. Simulation results illustrate good performances, high tracking precision and robustness in the face of parameter variations and mainly external disturbances affecting the developed controller.

Acknowledgments Authors would like to thank the University of Sfax, the National Engineering School of Sfax and the Control and Energy Management Laboratory, for their support to the success of this work.

References

1. Abera A, Bandyopadhyay B, Janardhanan S (2006) Digital redesign of sliding mode control algorithms using saturation function: state and multirate output feedback approach. In: Proceedings of the 45th IEEE conference on decision and control, pp 1594–1598
2. Acob J, Pano V, Ouyang P (2013) Hybrid PD sliding mode control of a two degree of freedom parallel robotic manipulator. In: Proceedings of the 10th IEEE international conference on control and automation (ICCA), pp 1760–1765
3. Azar AT, Zhu Q (2015) Advances and applications in sliding mode control systems. Springer, Cham
4. Bouaziz F, Bouteraa Y, Derbel N (2015) Distributed second order sliding mode control for synchronization of robot manipulators. In: Proceedings of the second international conference on automation, control, engineering and computer science, systems, signals devices (SSD), pp 1–7
5. Bouaziz FA, Bouteraa Y, Medhaffar H (2013) Distributed sliding mode control of cooperative robotic manipulators. In: Proceedings of the 10th international multi-conference on systems, signals and devices (SSD), pp 1–7
6. Bouteraa Y, Ghommam J, Poisson G, Derbel N (2011) Distributed synchronization control to trajectory tracking of multiple robot manipulators. J Robot 2011:1–10
7. Chunqing H, Weiyao L (2009) Modified scheme of PID controllers for robot manipulators with an uncertain Jacobian matrix. In: Proceedings of the IEEE international conference on control and automation, ICCA 2009. pp 1925–1930
8. Fei J, Wang S (2013) Feedback linearization-based adaptive fuzzy sliding mode control of mems triaxial gyroscope. Int J Robot Autom 28:72–80
9. Feng Y, Zhou M, Yu X (2013) High-order sliding-mode based energy saving control of induction motor. In: Proceedings of the 25th Chinese control and decision conference (CCDC), pp 4657–4660
10. Levant A (2010) Chattering analysis. IEEE Trans Autom Control 55(6):1380–1389
11. Ligang Wua CW, Zengb Q (2008) Observer-based sliding mode control for a class of uncertain nonlinear neutral delay systems. J Frankl Inst 345:233–253

12. Msaddek A, Gaaloul A, M'sahli F (2013) A novel higher order sliding mode control: application to an induction motor. Int J Control Eng Inf Technol 31:13–21
13. Perruquetti W (2002) Sliding mode control in engineering. Marcel Dekker, New York
14. Rigatos G, Siano P (2014) An H-infinity feedback control approach to autonomous robot navigation. In: Proceedings of the 40th annual conference of the IEEE industrial electronics society, IECON, pp 2689–2694
15. Tagne G, Talj R, Charara A (2013) Higher-order sliding mode control for lateral dynamics of autonomous vehicles, with experimental validation. In: Proceedings of the IEEE intelligent vehicles symposium (IV), pp 678–683
16. Taleb M, Plestan F, Bououlid B (2013) High order integral sliding mode control with gain adaptation. In: Proceedings of the European control conference (ECC), pp 890–895
17. Utkin V, Parnakh A (1978) Sliding modes and their application in variable structure systems. MIR, Moscow